

# INDIAN JOURNAL OF PHYSICS

VOL. 35

AND

## PROCEEDINGS

OF THE

Indian Association for the Cultivation of Science, Vol. 43

*(Published in Collaboration with the Indian Physical Society)*

---

( With Eleven Plates )

---

Printed by Kalipada Mukherjee, Eka Press, 204/1, B. T. Road, Calcutta  
and published by the Registrar, Indian Association for the Cultivation  
of Science, Jadavpur, Calcutta 32

**1961**

## BOARD OF EDITORS

K. BANERJEE	D. S. KOTHARI
D. M. BOSE	S. K. MITRA
S. N. BOSE	K. R. RAO
P. S. GILL	D. B. SINHA
S. R. KHASTOIR	S. C. SIRKAR ( <i>Secretary</i> )
B. N. SRIVASTAVA	

## EDITORIAL COLLABORATORS

PROF. R. K. ASUNDI, PH.D., F.N.I.
PROF. D. BASU, PH.D.
PROF. J. N. BHAR, D.Sc., F.N.I.
PROF. A. BOSE, D.Sc., F.N.I.
PROF. S. K. CHAKRABARTY, D.Sc., F.N.I.
DR. J. S. CHATTERJEE.
DR. K. DAS GUPTA, PH.D.
PROF. N. N. DAS GUPTA, PH.D., F.N.I.
PROF. A. K. DUTTA, D.Sc., F.N.I.
PROF. S. GHOSH, D.Sc., F.N.I.
PROF. S. N. GHOSH, D.Sc.
PROF. S. GUPTA, M.Sc., F.N.I.
PROF. D. N. KUNDU, PH.D., F.N.I.
PROF. R. C. MAJUMDER, PH.D., F.N.I.
PROF. B. D. NAG CHAUDHURI, PH.D.
PROF. S. R. PALIT, D.Sc., F.R.I.C., F.N.I.
DR. H. RAKSHIT, D.Sc., F.N.I.
PROF. A. SAINI, D.Sc., F.N.I.
DR. VIKRAM A. SARABHAI, M.A., PH.D.
DR. A. K. SENGUPTA, D.Sc.
DR. M. S. SINHA, D.Sc., F.N.I.
PROF. N. R. TAWDE, PH.D., F.N.I.
DR. P. VENKATESWARLU

### ASSISTANT EDITOR

SRI J. K. ROY, M.Sc.

### Annual Subscription—

Inland Rs. 25.00

Foreign £ 2-10-0 or \$ 7.00

## NOTICE

### TO INTENDING AUTHORS

1. Manuscripts for publication should be sent to the Assistant Editor, Indian Journal of Physics, Jadavpur, Calcutta-32.

2. The manuscripts submitted must be type-written with double space on thick foolscap paper with sufficient margin on the left and at the top. The original copy, and not the carbon copy, should be submitted. Each paper must contain an ABSTRACT at the beginning.

3. All REFERENCES should be given in the text by quoting the surname of the author, followed by year of publication, e.g., (Mazumder, 1959). The full REFERENCE should be given in a list at the end, arranged alphabetically, as follows; MAZUMDER, M. 1959, *Ind. J. Phys.*, **33**, 346.

4. Line diagrams should be drawn on white Bristol board or tracing paper with black Indian ink, and letters and numbers inside the diagrams should be written neatly in capital type with Indian ink. The size of the diagrams submitted and the lettering inside should be large enough so that it is legible after reduction to one-third the original size. A simple style of lettering such as gothic, with its uniform line width and no serifs should be used, e.g.

A·B·E·F·G·M·P·T·W·

5. Photographs submitted for publication should be printed on glossy paper with somewhat more contrast than that desired in the reproduction.

6. Captions to all figures should be typed in a separate sheet and attached at the end of the paper.

7. The mathematical expressions should be written carefully by hand. Care should be taken to distinguish between capital and small letters and superscripts and subscripts. Repetition of a complex expression should be avoided by representing it by a symbol. Greek letters and unusual symbols should be identified in the margin. Fractional exponents should be used instead of root signs.



## CONTENTS

### No. 1. January

	PAGE
1. Effects of Coulomb Friction on the Performance of a Servomechanism having Backlash. Part II—Transient Response Consideration—A. K. Mahalanobis ... ..	1
2. Raman Spectra of Para Fluorotoluene and Phenyl Acetonitrile in the Solid State at - 180°C - Krishna Kumar Deb ... ..	16
3. Dynamics of the Longitudinal Propagation of Elastic Disturbance Through a Medium Exhibiting Gradient of Elasticity—S. K. Ghosh	22
4. Dispersion of Microwaves in Oxygen—Prem Swarup and S. K. Garg	28
5. A Minimisation Method of Boolean Functions—Amarendra Mukhopadhyay ... ..	34

### No. 2. February

6. Various Approximations for the Isotopic Thermal Diffusion Factor. I. Application to Helium Isotopes—S. C. Saxena and P. A. Pardeshi	55
7. X-Ray Thermal Diffuse Scattering in Azelaic and Pimelic Acids—R. L. Banerjee, M. L. Canut and J. L. Amoros ... ..	62
8. Investigations into the Low Energy Gamma Ray Background and its Variations—Bijon Roy, Probir K. Sandell and Ajoy K. Choudhury	77
9. Determination of Unlike Interactions from Binary Viscosity—I. B. Srivastava ... ..	86
10. A Low Pressure Expansion Cloud Chamber—M. Rama Rao ...	92

#### LETTERS TO THE EDITOR

1. Equivalent Pressure Concept in Crossed Electric and Magnetic field in Electrodeless Discharge—S. N. Sen and A. K. Ghosh ...	107
--	-----

### No. 3. March

11. A Note on the Problem of Introducing Sphericity Correction to Conservative Scattering Stellar Atmosphere Model—K. K. Sen ...	105
12. Theory of Indirect Exchange Interaction in Spinel-like Systems—K. P. Sinha ... ..	111
13. A Note on the Cross-Section of the Luminous Discharge Channel in a Glow Discharge—Kumari D. V. Nagamani and V. T. Chiplonkar	128
14. Light Scattering in Cellulose Acetate Solutions—N. K. Subramanian and S. R. Sivarajan ... ..	135
15. A Comparative Study of Singlet→Triplet Absorption in some Halogenated Toluenes in the Vapour and Liquid States—J. K. Roy ...	143
16. Infrared Spectra of <i>o</i> -Bromophenol in the Liquid State and in Solutions in Different Solvents—S. B. Banerjee and A. K. Chakraborty	150

	PAGE
17. On the Absorption of 3.18 cm Microwaves in some Aliphatic Alcohols and their Solutions—T. J. Bhattacharyya ... ..	156

#### No. 4. April

18. Scattering of Electron by Thomas-Fermi Potential—S. C. Mukherjee	165
19. A Simple Study of the Nuclear Self-Consistent Field Problem—N. V. V. J. Swamy ... ..	170
20. Potential Constants and Calculated Thermodynamic Properties of Nitryl Fluoride and Nitryl Chloride—P. G. Puranik and E. V. Rao	177
21. A Study of Development Defects and Track Structures in Nuclear Emulsions using Amidol Developers—O. N. Kaul ... ..	183
22. Interpenetration of two Ionized Gas Clouds—J. N. Tandon ...	193
23. Growth of Hydromagnetic Shock Waves—I. J. Singh and K. P. Chopra ... ..	199
24. Electronic Spectra of <i>m</i> -Chlorophenol and <i>o</i> -Bromoanisole in Different States—T. N. Misra and S. B. Banerjee ... ..	203
BOOK REVIEW ... ..	211

#### No. 5. May

25. Effect of World-Wide Changes of Isotropic Cosmic Ray Intensity on the Daily Variation of Cosmic Rays—R. P. Kane ... ..	213
26. F <sup>19</sup> Nuclear Magnetic Resonance in Polycrystalline MgF <sub>2</sub> —S. K. Ghosh, J. Lahiri and S. K. Sinha ... ..	236
27. Decay of Ionization below the F-layer at Night—P. Bandyopadhyay and S. K. Chatterjee ... ..	240
28. Transmission Characteristics of Pulse-Slope-Modulated Signals Through Band Limited Systems—J. Das ... ..	245
29. Space Groups of Crystals of $\alpha$ -, $\beta$ - and $\gamma$ -Picoline at -180°C—S.G. Biswas ... ..	261
BOOK REVIEW ... ..	269

#### No. 6. June

30. Thermodynamic Properties of Fluid Flow Across a Magnetic Field—I. J. Singh and K. P. Chopra ... ..	271
31. Scattering of Electrons by a Screened Coulomb Field in Higher Born Approximation—T. K. Mitra ... ..	278
32. Fluorescence Spectra of Some Uranyl Salts—K. V. Narasimham ...	282
33. A General Treatment of Penetration Factor in Alpha-decay—S. K. Dutta ... ..	299
34. Intensity Measurements in Molecular Bands—N. R. Tawde, B. G. Jyoti and M. I. Savadatti ... ..	307
35. On the Superheat of liquids—D. B. Sinha and A. K. Jalaluddin ...	311

	PAGE
<b>LETTERS TO THE EDITOR</b>	
2. A New Method for Measuring Absolute Magnetic Susceptibilities —P. K. Ghosh ... ..	319
3. Intermolecular Potentials of H <sub>2</sub> and D <sub>2</sub> —I. B. Srivastava and A. K. Barua ... ..	320
<b>BOOK REVIEW</b> ... ..	323

**No. 7. July**

36. Microwave Analogue for X-Ray Diffraction Part II. Size of the Scatterers—G. S. Sanyal and G. B. Mitra ... ..	325
37. Potential Function of Helium-like Atoms and Electron Scattering by the Born Approximation—S. C. Mukherjee ... ..	333
38. Determination of Photoelastic Constants in the Presence of Tilt of the Axes—K. V. Krishna Rao ... ..	341
39. Study of Ultrasonic Velocity in Liquids—P. R. K. L. Padmini and B. Ramachandra Rao ... ..	346
40. Gas Properties at High Temperatures on the Exponential Model —P. K. Chakraborti ... ..	354
41. An Internal Counter Controlled Low Pressure Cloud Chamber —M. Rama Rao ... ..	361

**LETTERS TO THE EDITOR**

4. The Crystal Structure of Benzalazine—U. C. Sinha ... ..	374
--	-----

**No. 8. August**

42. Wing of the Rayleigh Line Recorded with a Self-Recording Grating Spectrophotometer—S. C. Sirkar, S. B. Roy and D. K. Ghosh ... ..	377
43. Structure of the Spectrum of Doubly Ionised Bromine—Y. Bhupola Rao ... ..	386
44. Topotactic Transformations in Iron Oxides and Oxyhydroxides —D. R. Dasgupta ... ..	401
45. On the Electronic Spectra of 2-Aminopyridine and 3-Aminopyridine in Different States and in Solutions—T. N. Misra ... ..	420

**LETTERS TO THE EDITOR**

5. On the Evaluation of the Coefficients of Thermal Expansion of Crystals from X-ray Data—V. T. Deshpande and V. M. Mudholker ... ..	434
---	-----

**No. 9. September**

46. Light Absorption in Paramagnetic Ions in State of Solution. Part III Cr <sup>+++</sup> Ion—A Mookherjee and N. S. Chhonkar ... ..	437
47. Anelastic Measurements of Diffusion in $\alpha$ -AgCd Alloys —M. A. Quader ... ..	446

	PAGE
17. On the Absorption of 3.18 cm Microwaves in some Aliphatic Alcohols and their Solutions—T. J. Bhattacharyya ... ..	156
<b>No. 4. April</b>	
18. Scattering of Electron by Thomas-Fermi Potential—S. C. Mukherjee	165
19. A Simple Study of the Nuclear Self-Consistent Field Problem—N. V. V. J. Swamy ... ..	170
20. Potential Constants and Calculated Thermodynamic Properties of Nitryl Fluoride and Nitryl Chloride—P. G. Puranik and E. V. Rao	177
21. A Study of Development Defects and Track Structures in Nuclear Emulsions using Amidol Developers—O. N. Kaul ... ..	183
22. Interpenetration of two Ionized Gas Clouds—J. N. Tandon ...	193
23. Growth of Hydromagnetic Shock Waves—I. J. Singh and K. P. Chopra ... ..	199
24. Electronic Spectra of <i>m</i> -Chlorophenol and <i>o</i> -Bromoanisole in Different States—T. N. Misra and S. B. Banerjee ... ..	203
BOOK REVIEW ... ..	211

#### No. 5. May

25. Effect of World-Wide Changes of Isotropic Cosmic Ray Intensity on the Daily Variation of Cosmic Rays—R. P. Kane ... ..	213
26. F <sup>19</sup> Nuclear Magnetic Resonance in Polycrystalline MgF <sub>2</sub> —S. K. Ghosh, J. Lahiri and S. K. Sinha ... ..	236
27. Decay of Ionization below the F-layer at Night—P. Bandyopadhyay and S. K. Chatterjee ... ..	240
28. Transmission Characteristics of Pulse-Slope-Modulated Signals Through Band Limited Systems—J. Das ... ..	245
29. Space Groups of Crystals of $\alpha$ -, $\beta$ - and $\gamma$ -Picoline at -180°C—S. G. Biswas ... ..	261
BOOK REVIEW ... ..	269

#### No. 6. June

30. Thermodynamic Properties of Fluid Flow Across a Magnetic Field—I. J. Singh and K. P. Chopra ... ..	271
31. Scattering of Electrons by a Screened Coulomb Field in Higher Born Approximation—T. K. Mitra ... ..	278
32. Fluorescence Spectra of Some Uranyl Salts—K. V. Narasimham ...	282
33. A General Treatment of Penetration Factor in Alpha-decay—S. K. Dutta ... ..	299
34. Intensity Measurements in Molecular Bands—N. R. Tawde, B. G. Jyoti and M. I. Savadatti ... ..	307
35. On the Superheat of liquids—D. B. Sinha and A. K. Jalaluddin ...	311

	PAGE
<b>LETTERS TO THE EDITOR</b>	
2. A New Method for Measuring Absolute Magnetic Susceptibilities —P. K. Ghosh           ...           ...           ...           ...	319
3. Intermolecular Potentials of H <sub>2</sub> and D <sub>2</sub> —I. B. Srivastava and A. K. Barua           ...           ...           ...           ...	320
<b>BOOK REVIEW</b> ...           ...           ...           ...	323

**No. 7. July**

36. Microwave Analogue for X-Ray Diffraction Part II. Size of the Scatterers—G. S. Sanyal and G. B. Mitra   ...           ...           ...	325
37. Potential Function of Helium-like Atoms and Electron Scattering by the Born Approximation—S. C. Mukherjee   ...           ...	333
38. Determination of Photoelastic Constants in the Presence of Tilt of the Axes—K. V. Krishna Rao   ...           ...           ...           ...	341
39. Study of Ultrasonic Velocity in Liquids—P. R. K. L. Padmini and B. Ramachandra Rao           ...           ...           ...           ...	346
40. Gas Properties at High Temperatures on the Exponential Model —P. K. Chakraborti           ...           ...           ...           ...	354
41. An Internal Counter Controlled Low Pressure Cloud Chamber —M. Rama Rao           ...           ...           ...           ...	361

**LETTERS TO THE EDITOR**

4. The Crystal Structure of Benzalazine—U. C. Sinha   ...           ...	374
---	-----

**No. 8. August**

42. Wing of the Rayleigh Line Recorded with a Self-Recording Grating Spectrophotometer—S. C. Sirkar, S. B. Roy and D. K. Ghosh   ...           ...	377
43. Structure of the Spectrum of Doubly Ionised Bromine—Y. Bhupola Rao           ...           ...           ...           ...	386
44. Topotactic Transformations in Iron Oxides and Oxyhydroxides —D. R. Dasgupta   ...           ...           ...           ...	401
45. On the Electronic Spectra of 2-Aminopyridine and 3-Aminopyridine in Different States and in Solutions—T. N. Misra   ...           ...	420

**LETTERS TO THE EDITOR**

5. On the Evaluation of the Coefficients of Thermal Expansion of Crystals from X-ray Data—V. T. Deshpande and V. M. Mudholker   ...	434
--	-----

**No. 9. September**

46. Light Absorption in Paramagnetic Ions in State of Solution. Part III Cr <sup>+++</sup> Ion—A Mookherjee and N. S. Chhonkar   ...           ...	437
47. Anelastic Measurements of Diffusion in $\alpha$ -AgCd Alloys —M. A. Quader           ...           ...           ...           ...	446

	PAGE
48. On the Processing of Nuclear Emulsions—O. N. Kaul. ...	459
49. Studies on Binary Diffusion of the Gas Pairs $O_2$ -A, $O_2$ -Xe and $O_2$ -He—R. Paul and I. B. Srivastava ... ..	465
50. Periodic Fading in Oblique Incidence Shortwave Transmissions —B. Ramachandra Rao, M. G. Seshagiri Rao and D. Satyanarayana Murty ... ..	475
51. The Role of Empty Orbitals in Superexchange Interaction —K. P. Sinha ... ..	484

### No. 10. October

52. Application of the Urey-Bradley and the Orbital Valency Force Fields to some Tetrahedral Ions—T. A. Hariharan ... ..	493
53. X-ray Study of a Dehydrated Phase of Copper Ammonium Sulphate Hexahydrate—Gouri Bhowmik ... ..	499
54. The Crystallite Orientation in Mesta Fibre—Subhrendu Kar and R. K. Basu ... ..	505
55. The Dielectric Properties of Rosin-Maleic Anhydride Resin—A. K. Sen and G. N. Bhattacharya ... ..	509
56. Vibrational Spectra of Thioglycollic Acid—P. G. Puranik, K. Venkata Ramiah and Vijay Kumar ... ..	517
57. Studies on Binary Diffusion of the Gas Pairs $N_2$ -A, $N_2$ -Xe and $N_2$ -He—R. Paul and I. B. Srivastava ... ..	523
58. Electron Microscope Studies on the Cotton Cellulose—D. K. Saha ...	530

### No. 11. November

59. Influence of Environment on the Raman and Infrared Spectra of Quinoline and Tetralin—Krishna Kumar Deb ... ..	535
60. On the Calculation of low-energy Neutron Scattering by a Complex Potential—Arundhati Ghosh and S. K. Dutta ... ..	550
61. The Spectrum of CoCl in the Photographic Infrared and the Visible —S. V. Krishna Rao and P. Tiruvenganna Rao ... ..	556
62. Role Played by Ammonium Salts in the Clearing of Nuclear Emulsions—O. N. Kaul ... ..	562
63. Directional Properties of Extensive Air Shower Arrays—A. Bhaskara Rao and P. S. Gill ... ..	568
64. Unlike Molecular Interactions for $CO_2$ - $N_2$ and a few other Gas Mixtures—H. K. Sahoo and M. N. Sharma ... ..	573
65. Raman and Infrared Spectra of 1-Fluoro-2, 4-Dinitrobenzene and 1-Chloro-2, 4-Dinitrobenzene—K. C. Medhi ... ..	583

### LETTERS TO THE EDITOR

6. Periodicity in Nuclear Binding Energy and Correlation Between the Isotopes of Different Nuclei—A. K. Dutta ... ..	591
--	-----

	PAGE
7. On the Applicability of Debye's Theory in the Determination of the Time of Relaxation in the case of Pure Liquids—Dilip Kumar Ghosh	594
8. Cohesive Energies and other Properties of Ionic Crystals—M. N. Sharma and M. P. Madan	596
<b>No. 12. December</b>	
66. Emission Band Spectrum of $\text{ScO}_2$ Molecule—P. B. V. Haranath and V. Sivaramamurty	599
67. The Shape of the Target Molecule and the Diffusion Distance of Radicals Formed by Ionizing Radiation—S. B. Bhattacharjee and N. N. Das Gupta	604
68. Studies in K-Capture Positron Branching Ratios— $\text{Co}^{58}$ —M. K. Ramaswamy	610
69. Scattering of Electron by Excited Helium Atom—Mrs. Tara Bhattacharyya	623
70. On the Singlet→Triplet Absorption in a few Polysubstituted Benzenes in the Vapour State—J. K. Roy	628
71. Amplitude of Thermal Vibrations in $\text{PCl}_3$ , $\text{AsCl}_3$ and $\text{SbCl}_3$ Molecules—T. A. Hariharan	637

LETTERS TO THE EDITOR

9. Refined Molecular Structure of Naphthazarin—P. Srivastava	640
10. On the Optical Absorption Spectra of $\text{Ni}^{2+} \cdot 6\text{H}_2\text{O}$ Complex in Crystals—A. S. Chakravarty and R. Chatterjee	643





# AUTHOR INDEX

Author	Subject	Page
Amoros, J. L.	See, Banerjee, R. L.	
Bandyopadhyay, P. and Chatterjee, S. K.	Decay of ionization below the F-layer at night	240
Banerjee, R. L., Canut, M.L. and Amoros, J. L.	X-ray thermal diffuse scattering to azelaic and pimelic acids	62
Banerjee, S. B. and Chakraborty, A. K.	Infrared spectra of o-bromophenol in the liquid state and in solutions in different solvents	150
Banerjee, S. B.	See, Misra, T. N.	
Barua, A. K.	See, Srivastava, I. B.	
Basu, R. K.	See, Kar, Subhrendu	
Bhattacharyya, T. J.	On the absorption of 3.18 cm micro-waves in some aliphatic alcohols and their solutions	156
Bhattacharya, G. N.	See, Sen, A. K.	
Bhattacharjee, S. B. and Das Gupta, N. N.	The shape of target molecule and the diffusion distance of radicals formed by ionizing radiation	604
Bhattacharyya, Mrs. Tara	Scattering of electron by excited helium atom	623
Bhowmik, Gouri	X-ray study of a dehydrated phase of copper ammonium sulphate hexahydrate	499
Biswas, S. G.	Space groups of crystals of $\alpha$ - $\beta$ - and $\gamma$ -picoline at $-180^{\circ}\text{C}$	261
Canut, M. L.	See Banerjee, R. L.	
Chakraborty, A. K.	See Banerjee, S. B.	
Chakravarty, A. S. and Chatterjee, R.	On the optical absorption spectra of $\text{Ni}^{2+} \cdot 6\text{H}_2\text{O}$ complex in crystals (L)	643
Chakraborti, P. K.	Gas properties at high temperature on the exponential model	354
Chatterjee, R.	See Chakravarty, A. S.	
Chatterjee, S. K.	See Bandyopadhyay, P.	
Chhonkar, N. S.	See Mookherjee, A.	
Chiplonkar, V. T.	See Nagamani, Kumari D. V.	
Chopra, M. P.	See Sinha, I. J.	
"    "	See Sinha, I. J.	
Choudhury, Ajoy K.	See Roy, Bijon	

Author	Subject	Page
Das, J.	Transmission characteristics of pulse-slope-modulated signals through band limited systems	245
Das Gupta, N. N.	See Bhattacharjee, S. B.	
Dasgupta, D. R.	Topotactic transformations in iron oxides and dyhydroxides	401
Deb, Krishna Kumar	Influence of environment on the Raman and infrared spectra of quinoline and tetralin	535
	Raman spectra of para fluorotoluene and phenyl acetonitrile in the solid state at $-180^{\circ}\text{C}$ .	16
Deshpande, V. T. and Mudholker, V. M.	On the evaluation of the coefficients of thermal expansion of crystals from X-ray data (L)	434
Dutta, A. K.	Periodicity in nuclear binding energy and correlation between the isotopes of different nuclei (L)	591
Dutta, S. K.	A general treatment of penetration factor in alpha-decay	299
	See Ghosh, Arundhati	
Garg, S. K.	See Swarup, Prem	
Ghosh, A. K.	See Sen, S. N.	
Ghosh, Arundhati and Dutta, S. K.	On the calculation of low-energy neutron scattering by a complex potential	550
Ghosh, P. K.	A new method for measuring absolute magnetic susceptibilities (L)	319
Ghosh, D. K.	See Sirkar, S. C.	
Ghosh, Dilip Kumar	On the applicability of Debye's theory in the determination of the time of relaxation in the case of pure liquids (L)	594
Ghosh, S. K.	Dynamics of the longitudinal propagation of elastic disturbance through a medium exhibiting gradient of elasticity	22
Ghosh, S. K., Lahiri, J. and Sinha, S. K.	$\text{F}^{19}$ nuclear magnetic resonance in polycrystalline $\text{MgF}_2$	236
Gill, P. S.	See Rao, Bhaskara A.	
Haranath, P. B. V. and Sivaramamutty, V.	Emission band spectrum of $\text{ScO}_2$ molecule	599

Author	Subject	Page
Hariharan, T. A.	Application of the Urey-Bradley and the orbital valency force fields to some tetrahedral ions	493
	Amplitude of thermal vibrations in $\text{PCl}_3$ , $\text{AsCl}_3$ , and $\text{SbCl}_3$	637
Jalaluddin, A. K.	See Sinha, D. B.	
Jyoti, D. G.	See Tawde, N. R.	
Kane, R. P.	Effect of world-wide changes of isotropic cosmic ray intensity on the daily variation of cosmic rays	213
Kar, Subhrendu and Basu, R. K.	The crystallite orientation in mesta fibre	505
Kaul, O. N.	A study of development defects and track structures in nuclear emulsions using amidol developers	183
	On the processing of nuclear emulsions	459
	Role played by ammonium salts in the clearing of nuclear emulsions	562
Kumar, Vijay	See Puranik, P. G.	
Lahiri, J.	See Ghosh, S. K.	
Madan, M. P.	See Sharma, M. N.	
Mahalanobis, A. K.	Effect of Coulomb friction on the performance of a servomechanism having backlash. Part II—transient response considerations	1
Medhi, K. C.	Raman and infrared spectra of 1-fluoro-, 2,4-dinitrobenzene and 1-chloro- 2,4-dinitrobenze	583
Misra, T. N. and Banerjee, S. B.	Electronic spectra of <i>m</i> -chlorophenol and <i>o</i> -bromoanisole in different states.	203
Misra, T. N.	On the electronics spectra of 2-aminopyridine and 3-aminopyridine in different states and in solutions	420
Mitra, G. B.	See Sanyal, G. S.	
Mitra, T. K.	Scattering of electrons by a screened Coulomb field in higher Born approximation	278
Mookherjee, A. and Chhonkar, N. S.	Light absorption in paramagnetic ions in state of solution. Part III $\text{Cr}^{+++}$ ion	437

Author	Subject	Page
Das, J.	Transmission characteristics of pulse-slope-modulated signals through band limited systems	245
Das Gupta, N. N.	See Bhattacharjee, S. B.	
Dasgupta, D. R.	Topotactic transformations in iron oxides and dyhydroxides	401
Deb, Krishna Kumar	Influence of environment on the Raman and infrared spectra of quinoline and tetralin	535
	Raman spectra of para fluorotoluene and phenyl acetonitrile in the solid state at $-180^{\circ}\text{C}$ .	16
Deshpande, V. T. and Mudholker, V. M.	On the evaluation of the coefficients of thermal expansion of crystals from X-ray data (L)	434
Dutta, A. K.	Periodicity in nuclear binding energy and correlation between the isotopes of different nuclei (L)	591
Dutta, S. K.	A general treatment of penetration factor in alpha-decay	299
	See Ghosh, Arundhati	
Garg, S. K.	See Swarup, Prem	
Ghosh, A. K.	See Sen, S. N.	
Ghosh, Arundhati and Dutta, S. K.	On the calculation of low-energy neutron scattering by a complex potential	550
Ghosh, P. K.	A new method for measuring absolute magnetic susceptibilities (L)	319
Ghosh, D. K.	See Sirkar, S. C.	
Ghosh, Dilip Kumar	On the applicability of Debye's theory in the determination of the time of relaxation in the case of pure liquids (L)	594
Ghosh, S. K.	Dynamics of the longitudinal propagation of elastic disturbance through a medium exhibiting gradient of elasticity	22
Ghosh, S. K., Lahiri, J. and Sinha, S. K.	$\text{F}^{19}$ nuclear magnetic resonance in polycrystalline $\text{MgF}_2$	236
Gill, P. S.	See Rao, Bhaskara A.	
Haranath, P. B. V. and Sivaramamutty, V.	Emission band spectrum of $\text{ScO}_2$ molecule	599

Author	Subject	Page
Hariharan, T. A.	Application of the Urey-Bradley and the orbital valency force fields to some tetrahedral ions	493
	Amplitude of thermal vibrations in $\text{PCl}_3$ , $\text{AsCl}_3$ , and $\text{SbCl}_3$	637
Jalaluddin, A. K.	See Sinha, D. B.	
Jyoti, D. G.	See Tawde, N. R.	
Kane, R. P.	Effect of world-wide changes of isotropic cosmic ray intensity on the daily variation of cosmic rays	213
Kar, Subhrendu and Basu, R. K.	The crystallite orientation in mesta fibre	505
Kaul, O. N.	A study of development defects and track structures in nuclear emulsions using amidol developers	183
	On the processing of nuclear emulsions	459
	Role played by ammonium salts in the clearing of nuclear emulsions	562
Kumar, Vijay	See Puranik, P. G.	
Lahiri, J.	See Ghosh, S. K.	
Madan, M. P.	See Sharma, M. N.	
Mahalanobis, A. K.	Effect of Coulomb friction on the performance of a servomechanism having backlash. Part II—transient response considerations	1
Medhi, K. C.	Raman and infrared spectra of 1-fluoro-, 2,4-dinitrobenzene and 1-chloro- 2,4-dinitrobenze	583
Misra, T. N. and Banerjee, S. B.	Electronic spectra of <i>m</i> -chlorophenol and <i>o</i> -bromoanisole in different states.	203
Misra, T. N.	On the electronics spectra of 2-aminopyridine and 3-aminopyridine in different states and in solutions	420
Mitra, G. B.	See Sanyal, G. S.	
Mitra, T. K.	Scattering of electrons by a screened Coulomb field in higher Born approximation	278
Mookherjee, A. and Chhonkar, N. S.	Light absorption in paramagnetic ions in state of solution. Part III $\text{Cr}^{+++}$ ion	437

Author	Subject	Page
Mukherjee, S. C.	Scattering of electrons by Thomas-Fermi potential	165
	Potential function of helium-like atoms and electron scattering by the Born approximation	333
Mukhopadhyay, Amarendra	A minimisation method of Boolean functions	24
Murty, Satyanarayana D.	See Rao, Ramachandra B.	
Nagamani, Kumari D. V. and Chiplonkar, V. T.	A note on the cross-section of the luminous discharge channel in a glow discharge	128
Narasimham, K. V.	Fluorescence spectra of some uranyl salts	282
Padmini, P. R. K. L. and Rao, Ramachandra B.	Study of ultrasonic velocity in liquids	346
Pardeshi, P. A.	See Saxena, S. C.	
Paul, R. and Srivastava, I. B.	Studies on binary diffusion of the gas pairs $O_2$ -A, $O_2$ -Xe, and $O_2$ -He	465
	Studies on binary diffusion of the gas pairs $N_2$ -A, $N_2$ -Xe and $N_2$ -He	523
Puranik, P. G., and Rao, E. V.	Potential constants and calculated thermodynamic properties of nitril fluoride and nitril chloride	177
Puranik, P. G. Venkata Ramiah, K. and Kumar, Vijay	Vibrational spectra of thioglycolic acid	517
Quader, M. A.	Anelastic measurements of diffusions in $\alpha$ -AgCd alloys	446
Ramaswamy, M. K.	Studies in K-capture positron branching ratios-Co <sup>58</sup>	610
Rao, Bhaskara A. and Gill, P. S.	Directional properties of extensive air shower arrays	568
Rao, Bhupala, Y.	Structure of the spectrum of doubly ionised bromine	386
Rao, E. V.	See Puranik, P. G.	
Rao, Krishna K. V.	Determination of photoelastic constants in the presence of tilt of the axes	341
Rao, Krishna S. V. and Rao, Tiruvenganna P.	The spectrum of CoCl in the photographic infrared and the visible	556
Rao, Ramachandra B.	See Padmini, P. R. K. L.	

Author	Subject	Page
Rao., Ramachandra B., Rao, Seshagiri M. G. and Murty, Satyanarayana D.	Periodic fading in oblique incidence showtwave transmissions	475
Rao, Rama M.	A low pressure expansion cloud chamber	92
	An internal counter controlled low pressure cloud chamber	361
Rao, Seshagiri, M. G.	See Rao, Ramachandra B.	
Rao, Tiruvenganna P.	See Rao Krishna S. V.	
Roy, Bijon, Sandell, Probir K. and Choudhury, Ajoy K.	Investigations into the low energy gamma ray background and its variations	77
Roy, J. K.	A comparative study of singlet→ triplet absorption in some halo- genated toluenes in the vapour and liquid states	143
	On the singlet→triplet absorption in a few polysubstituted benzenes in the vapour state	628
Roy, S. B.	See Sirkar, S. C.	
Saha, D. K.	Electron microscope studies on the cotton cellulose	530
Sahoo, H. K. and Sharma, M. N.	Unlike molecular interactions for CO <sub>2</sub> -N <sub>2</sub> and a few other gas mixtures	573
Sandell, Probir K.	See Roy, Bijon	
Sanyal, G. S. and Mitra, G. B.	Microwave analogue for X-ray dif- fraction Part II. Size of the scatters	325
Saxena, S. C. and Pardeshi, P. A.	Various Approximations for the iso- topic thermal diffusion factor. I. application to helium isotopes	55
Savadatti, M. I.	See Tawde, N. R.	
Sen, A. K. and Bhattacharya, G. N.	The dielectric properties of rosin- maleic anhydride resin	509
Sen, K. K.	A note on the problem of introduc- ing sphericity correction to con- servative scattering stellar at- mosphere model	105
Sen, S. N. and Ghosh, A. K.	Equivalent pressure concept in crossed electric and magnetic field in electrodeless discharge (L)	101

Author	Subject	Page
Sharma, M. N.	See Sahoo, H. K.	
Sharma, M. N. and Madan, M.P.	Cohesive energies and other properties of ionic crystal (L)	596
Singh, I. J. and Chopra, K. P.	Thermodynamic properties of fluid flow across a magnetic field	271
Singh, I. J. and Chopra, K. P.	Growth of hydromagnetic shock-wave	199
Sinha, D. B. and Jalaluddin, A. K.	On the superheat of liquids	311
Sinha, K. P.	Theory of indirect exchange interaction in spinel-like systems	111
	The role of empty orbitals in superexchange interaction	484
Sinha, S. K.	See Ghosh, S. K.	
Sinha, U. C.	The crystal structure of benzalazine (L)	374
Sirkar, S. C., Roy, S. B. and Ghosh, D. K.	Wing of the Rayleigh line recorded with a self-recording grating spectrophotometer	377
Srivastava, I. B.	Determination of unlike interactions from binary viscosity	86
Srivastava, I. B. and Barua, A. K.	Intermolecular potentials of H <sub>2</sub> and D <sub>2</sub> (L)	320
Srivastava, I. B. " "	See Paul, R. See Paul, R.	
Srivastava, P.	Refined molecular structure of naphthazarin (L)	640
Sivarajan, S. R.	See Subramanian, N. K.	
Sivaramamurty, V.	See Haranath, P. B. V.	
Subramanian, N. K. and Sivarajan, S. R.	Light scattering in cellulose acetate solutions	135
Swamy, N. V. V. J.	A simple study of the nuclear self-consistent field problem	170
Swarup, Prem and Garg, S. K.	Dispersion of microwaves in oxygen	28
Tandon, J. N.	Interpenetration of two ionized gas clouds	193
Tawde, N. R., Jyoti, B. G. and Savadatti, M. I.	Intensity measurements in molecular bands	307
Venkata Ramiah, K.	See Puranik, P. G.	



# SUBJECT INDEX

Subject	Author	Page
Absolute magnetic susceptibilities. A new method for measuring (L)	P. K. Ghosh	319
Absorption of 3.18 cm microwaves in some aliphatic alcohols and their solutions	T. J. Bhattacharyya	156
Absorption spectra of $\text{Ni}^{2+} \cdot 6\text{H}_2\text{O}$ complex in crystals. On the optical (L)	A. S. Chakravarty and R. Chatterjee	643
Binary diffusion of the gas pairs $\text{O}_2\text{—A}$ , $\text{O}_2\text{—Xe}$ and $\text{O}_2\text{—He}$ . Studies on	R. Paul and I. B. Srivastava	465
Binary diffusion of the gas pairs $\text{N}_2\text{—A}$ , $\text{N}_2\text{—Xe}$ and $\text{N}_2\text{—He}$ . Studies on	R. Paul and I. B. Srivastava	523
Clearing of nuclear emulsions. Role played by ammonium salts	O. N. Kaul	562
Coefficients of thermal expansion of crystals from X-ray data. On the evaluation of (L)	V.T. Deshpande and V. M. Mudholkar	434
Coulomb friction on the perfor- mance of a servo mechanism having backlash. Effects of. Part II. Transient response considerations	A. K. Mahalanobis	11
Crossed electric and magnetic field in electrodeless discharge. Equi- valent pressure concept in (L)	S. N. Sen and A. K. Ghosh	101
Cross-section of the luminous discharge channel in a glow dis- charge. A note on the	Kumari D. V. Nagamani and V. T. Chimponkar	128
Crystal structure of benzalazine. The (L)	U. C. Sinha	374
Crystallite orientation in mesta fibre. The	Subhrendu Kar and R. K. Basu	505
Daily variation of cosmic rays. Effect of world-wide changes of isotopic cosmic ray intensity on the	R. P. Kane	213

Subject	Author	Page
Decay of ionization below the F-layer at night	P. Bandyopadhyay and S. K. Chatterjee	240
Development defects and track structures in nuclear emulsions using amidol developers. A study of	O. N. Kaul	183
Dielectric properties of rosinmaleic anhydride resin. The	A. K. Sen and G. N. Bhattacharya	509
Diffusion distance of radicals formed by ionizing radiation. The shape of the target molecule and the	S. B. Bhattacharjee and N. N. Das Gupta	604
Diffusion in $\alpha$ -AgCd alloys. An elastic measurements of	M. A. Quader	446
Dispersion of microwaves in oxygen	Prem Swarup and S. K. Garg	28
Dynamics of the longitudinal propagation of elastic disturbance through a medium exhibiting gradient of elasticity	S. K. Ghosh	22
Electron microscope studies on the cotton cellulose	D. K. Saha	530
Electron scattering by the Born approximation. Potential function of helium-like atoms	S. C. Mukherjee	333
Extensive air shower arrays. Directional properties of	A. Bhaskara Rao and P. S. Gill	568
F <sup>19</sup> nuclear magnetic resonance in polycrystalline MgF <sub>2</sub>	S. K. Ghosh, J. Lahiri and S. K. Sinha	236
Gas properties at high temperatures on the exponential model	P. K. Chakraborti	354
Growth of hydromagnetic shock waves	I. J. Sinha and K. P. Chopra	199
Indirect exchange interaction in spinel-like systems. Theory of	K. P. Sinha	111
Intensity measurements in molecular bonds	N. R. Tawde, B. G. Jyoti and M. I. Savadathi	307
Intermolecular potentials of H <sub>2</sub> and D <sub>2</sub> (L)	I. B. Srivastava and A. K. Barua	320
Internal counter controlled low pressure cloud chamber. An	M. Rama Rao	361

Subject	Author	Page
Interpenetration of two ionized gas clouds	J. N. Tandon	193
Ionic crystals. Cohesive energies and other properties of (L)	M. N. Sharma and M. P. Madan	596
Isotopic thermal diffusion factor. I. Various approximations for the application to helium isotopes	S. C. Saxena and P. A. Pardeshi	55
K-capture positron branching ratios—Co <sup>58</sup> . Studies in	M. K. Ramaswamy	610
Light scattering in cellulose acetate solutions	N. K. Subramanian and S. R. Sivarajan	135
Low energy gamma ray background and its variations. Investigations into the	Bijon Roy, Probir K. Sandell and Ajoy K. Choudhury	77
Low energy neutron scattering by a complex potential. On the calculation of	Arundhati Ghosh and S. K. Dutta	550
Low pressure expansion cloud chamber. A	M. Rama Rao	92
Minimisation method of Boolean functions. A	Amarendra Mukhopadhyay	34
Molecular structure of naphthazarin refined (L)	P. Srivastava	640
Nuclear binding energy and correlation between the isotopes of different nuclei periodicity in (L)	A. K. Dutta	591
Nuclear self-consistent field problem. A simple study of the	N. V. V. J. Swamy	170
Oblique incidence shortwave transmissions. Periodic fading in	B. Ramachandra Rao, M. G. Seshagiri Rao and D. Satyanarayana Murty	475
Paramagnetic ions in state of solution. Light absorption in. Part III Cu <sup>+++</sup> ion	A. Mookherjee and N. S. Chhonkar	437
Penetration factor in alpha-decay. A general treatment of	S. K. Dutta	299
Photoelastic constants in the presence of tilt of the axes. Determination of	K. V. Krishna Rao	341
Potential function of helium-like atoms and electron scattering by the Born approximation	S. C. Mukherjee	331

Subject	Author	Page
Potential constants and calculated thermodynamic properties of nitril fluoride and nitril chloride	P. G. Puranik and E. V. Rao	177
Problem of introducing sphericity correction to conservative scattering stellar atmosphere model. A note on the	K. K. Sen	105
Processing of nuclear emulsions. On the	O. N. Kaul	459
Scattering of electrons by a screened Coulomb field in higher Born approximation	T. K. Mitra	278
Scattering of electrons by excited helium atom	Mrs. Tara Bhattacharya	623
Scattering of electrons by Thomas-Fermi potential	S. C. Mukherjee	165
Singlet→triplet absorption in a few polysubstituted benzenes in the vapour state. On the	J. K. Roy	628
Singlet→triplet absorption in some halogenated toluenes in the vapour and liquid states. A comparative study of	J. K. Roy	143
Space groups of crystals of $\alpha$ -, $\beta$ - and $\gamma$ -picoline at $-180^{\circ}\text{C}$	S. G. Biswas	261
SPECTRA		
Self-recording grating spectrophotometer. Wing of the Rayleigh line recorded with	S. C. Sirkar, S. B. Roy and D. K. Ghosh	377
Electronic spectra of <i>m</i> -chlorophenol and <i>o</i> -bromoanisole in different states	T. N. Misra and S. B. Banerjee	203
Electronic spectra of 2-aminopyridine and 3-aminopyridine in different states and in solutions. On the	T. N. Misra	420
Emission band spectrum of $\text{SeO}_2$ molecule	P. B. V. Haranath and V. Sivaramamurty	599
Fluorescence spectra of some uranyl salts	K. V. Narasimham	282

Subject	Author	Page
Infrared spectra of <i>o</i> -bromophenol in the liquid state and in solutions in different solvents	S. B. Banerjee and A. K. Chakraborty	150
Raman and infrared spectra of 1- fluoro, 2, 4-dinitrobenzene and 1-chloro 2, 4-dinitrobenzene	K. C. Medhi	583
Raman and infrared spectra of quinolino and tetralin. Influence of environment on the	Krishna Kumar Deb	535
Raman spectra of parafluorotoluene and phenyl acetonitrile in the solid state at $-180^{\circ}\text{C}$	Krishna Kumar Deb	16
Spectrum of $\text{CoCl}$ in the photo- graphic infrared and the visible. The	S. V. Krishna Rao and P. Tiruvenganna Rao	556
Spectrum of doubly ionised bro- mine. Structure of the	Y. Bhupala Rao	386
Vibrational spectra of thioglycollic acid	P. G. Puranik, K. Venkata Ramiah and Vijay Kumar	517
Superheat of liquids. On the Superexchange interaction. The role of empty orbitals in	D. B. Sinha and A. K. Jalaluddin K. P. Sinha	311 484
Tetrahedral ions. Application of the Urey-Bradley and the orbital velency force fields to some	T. A. Hariharan	493
Topotactic transformations in iron oxides and oxyhydroxides	D. R. Dasgupta	401
Thermal vibrations in $\text{PCl}_3$ , $\text{AsCl}_3$ and $\text{SbCl}_3$ molecules. Amplitude of	T. A. Hariharan	637
Time of relaxation in the case of pure liquids. On the applica- bility of Debye's theory in the determination of the (L)	Dilip Kumar Ghosh	594
Thermodynamic property of fluid flow across a magnetic field	I. J. Singh and K. P. Chopra	271
Transmission characteristic of pulse- slope-modulated signals through band limited systems	J. Das	245

Subject	Author	Page
Unlike molecular interactions for CO <sub>2</sub> -N <sub>2</sub> and a few other gas mixtures	H. K. Sahoo and M. N. Sharma	573
Ultrasonic velocity in liquids. Study of	P. R. K. L. Padmini and B. Ramachandra Rao	346
Unlike interactions from binary viscosity. Determination of	I .B. Srivastava	86
X-ray diffraction. Microwave ana- logue for. Part II size of the scatterers	G. S. Sanyal and G. B. Mitra	325
X-ray thermal diffuse scattering in azelaic and pimelic acids.	R. L. Banerjee, M. L. Canut and J. L. Amoros	62
X-ray study of a dehydrated phase of copper ammonium sulphate hexahydrate.	Gouri Bhowmik	499

# EFFECTS OF COULOMB FRICTION ON THE PERFORMANCE OF A SERVOMECHANISM HAVING BACKLASH.

## PART II—TRANSIENT RESPONSE CONSIDERATIONS

A. K. MAHALANOBIS

INSTITUTE OF RADIOPHYSICS AND ELECTRONICS, UNIVERSITY COLLEGE  
OF TECHNOLOGY, CALCUTTA

(Received, October 9, 1960)

**ABSTRACT.** The paper gives results of analysis of the effects of coulomb friction on the transient response of a servo system containing backlash in the output coupling. First, the qualitative aspects of the transient response characteristics are discussed with the help of frequency response methods; next, a quantitative discussion of the same is provided with the help of a piece-wise linear solution of the characteristic differential equations. Simulator results in support of the theoretical observations are also given.

### INTRODUCTION

In a previous paper the effects of coulomb friction on the stability of sustained oscillations in a second order servomechanism having backlash in the output coupling was discussed (Mahalanabis, 1960). The coulomb friction has been taken to be present in the driving member. A describing function was developed for the motor under the action of the nonlinear friction; it was discussed how presence of coulomb friction helps to avoid sustained oscillations that are otherwise produced by the system backlash.

Beside the question of the stability of sustained oscillations the stability of the response of a system in the transient state is also of considerable interest to servo designers. In the present paper the relative stability of a servo system affected by the two nonlinearities under consideration viz. backlash and coulomb friction has been analysed.

It is to be mentioned that the discussions that follow have been based on the results of application of two methods. First, the results of application of the frequency response method are presented. These are necessarily of approximate nature but are nevertheless of interest since this is perhaps the most nearly generalised approach available at present for nonlinear systems analysis. More accurate data on the transient response of the system concerned are provided by solution of the piece-wise linear differential equations that characterise the system.

Finally, the response of a system simulated on an electronic analogue computer for step displacement inputs is presented as an experimental aid to the understanding of the system transient behaviour.

### SYSTEM UNDER CONSIDERATION

The system under consideration has been described in part I (Mahalanobis, 1960) in some details and will be only briefly outlined here for the sake of convenience. The system is shown in Fig. 1 in the schematic form. Nonlinearities

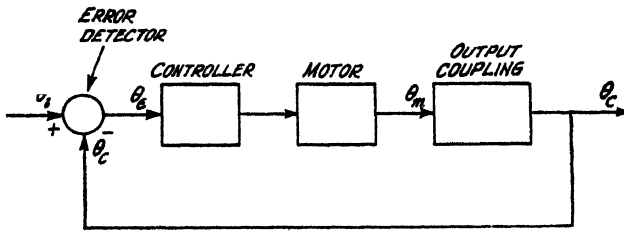


Fig. 1. System under consideration

are assumed in (i) the motor shaft whose motion is taken to be subject to both viscous and coulomb frictions and (ii) the output coupling unit which is taken to have backlash. The load is assumed to be a resistive one so that the nonlinear characteristics resulting from the coupling-unit backlash is as shown in Fig. 2. In Fig. 3 is depicted the composite friction characteristics of the motor.

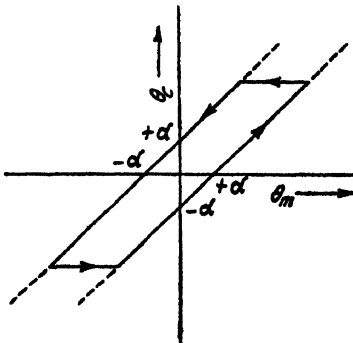


Fig. 2. Coupling unit characteristics.

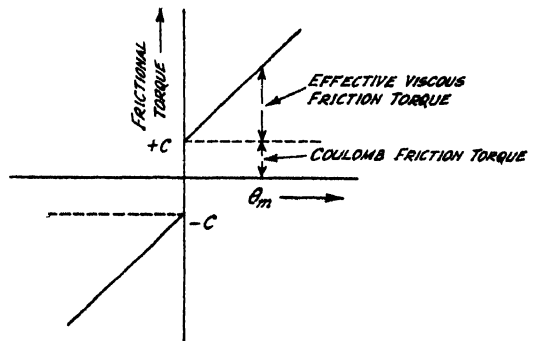


Fig. 3. Motor friction characteristics.

As has been derived in appendix I of part I the dynamics of the system in Fig. 1 is described by the following equations:

$$T_m \ddot{\theta}_m + \dot{\theta}_m + F = k\theta_s \quad \dots (1)$$

$$\theta_s = \theta_i - \theta_c \quad \dots (2)$$



where,  $\theta_m$ —motor shaft position  
 $\theta_i$ —input shaft position  
 $\theta_o$ —output shaft position  
 $T_m$ —motor time constant  
 $F$ —coulomb friction torque,  
 and  $K$ —a constant, being the velocity-constant of the system that results if the nonlinearities in Fig. 1 are neglected.

The backlash characteristics shown in Fig. 2 relates the motor shaft position  $\theta_m$  and the load shaft position  $\theta_o$  and can be represented mathematically as

$$\left. \begin{aligned} \theta_o &= \theta_m - \alpha \frac{\dot{\theta}_o}{|\dot{\theta}_o|}; \dot{\theta}_o \neq 0 \\ |\theta_m - \theta_o| &< \alpha; \dot{\theta}_o = 0 \end{aligned} \right\} \quad \dots (3)$$

$\alpha$  being the backlash half width.

And, the coulomb friction torque  $F$  is given by

$$\left. \begin{aligned} F &= C \frac{\dot{\theta}_m}{|\dot{\theta}_m|}; \dot{\theta}_m \neq 0 \\ -C &< F < C; \dot{\theta}_m = 0 \end{aligned} \right\} \quad \dots (4)$$

$C$  being the coulomb friction torque constant.

Eqs. (1) to (4) completely describe the system in Fig. 1.

#### SYSTEM TRANSIENT RESPONSE FROM FREQUENCY RESPONSE DATA

##### (a) General

If the nonlinearities in Fig. 1 are assumed absent the time response of the system has definite relationships with its frequency response. In presence of the nonlinearities there is of course no basis for such relationship (the superposition principle being no longer valid). However, in the describing function method the nonlinearity is replaced by a slowly varying quasi-linear transfer function and it is still possible to obtain the transient response from the frequency response data, though such deductions are necessarily of approximate nature (Kochenburger 1950 and 1953). For this purpose the system in Fig. 1 is represented in the block diagram form in Fig. 4. The block  $G_c(\theta_m)$  represents the describing function of the coulomb friction device and is given by (Hass 1953)

$$G_c(\theta_m) = \frac{4C}{\pi} \frac{1}{|\dot{\theta}_m|} \quad \dots (5)$$

The block  $G_B(\theta_m)$  represents the describing function of the coupling unit having backlash and is given by (Nichols 1953)

$$G_B(\theta_m) = [\beta^2 + \gamma^2]^{\frac{1}{2}} ; / -\tan^{-1}(\gamma/\beta) \quad \dots (6)$$

$$\beta = \frac{1}{\pi} [\cos^{-1}(2n-1) + 2(1-2n)\sqrt{n(1-n)}] \quad \dots (7)$$

and 
$$\gamma = \frac{4}{\pi} n(1-n) \quad \dots (8)$$

where  $n = \alpha/\hat{\theta}_m$ , the normalised backlash width.

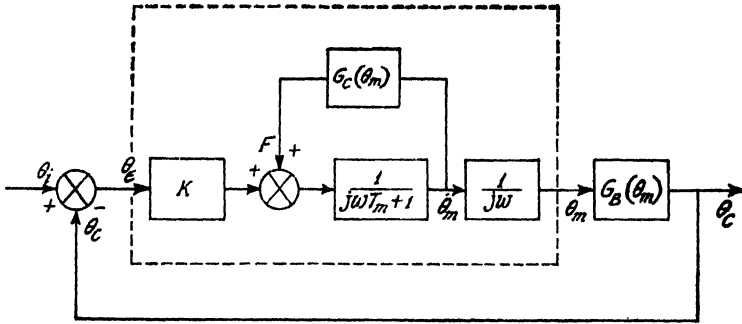


Fig. 4. Frequency response representation of the system.

The frequency response transfer function of the portion in Fig. 4 shown within the dotted box representing the motor with the coulomb friction is easily seen to be given by

$$G(j\omega, \theta_m) = \frac{K}{j\omega(j\omega T_m + 1) + j \frac{4B}{\pi}} ; \quad \dots (9)$$

$$B = \frac{C}{\hat{\theta}_m} \quad \dots (10)$$

The total forward-loop transference of the system is then

$$\frac{\theta_c}{\theta_i}(j\omega, \theta_m) = G(j\omega, \theta_m) \times G_B(\theta_m) ; \quad \dots (11)$$

and the closed-loop transference is accordingly,

$$\frac{\theta_c}{\theta_i}(j\omega, \theta_m) = \frac{G_B(\theta_m)}{G(j\omega, \theta_m)^{-1} + G_B(\theta_m)} \quad \dots (12)$$

The right-hand side of Eq. (12) incorporates the effects of the nonlinearities on the system frequency response. This is clearly dependent on both amplitude and frequency of the input signal. It is most convenient to assume the input signal to be a periodic function of time such that  $\theta_m(t)$  varies sinusoidally i.e.  $\theta_m(t) = \hat{\theta}_m \sin \omega t$ . Then, using Eqs. (6) to (10) and Eq. (12) the closed-loop transfer function can be computed as a function of the frequency for a number of assumed values of the amplitude  $\hat{\theta}_m$ . These computations are conveniently carried out graphically in the manner outlined below:

The describing function  $-G_B(\theta_m)$  is plotted in the complex plane as an amplitude locus. On the same plane are superposed plots of the frequency loci of  $G(j\omega, \theta_m)^{-1}$  each locus being drawn for a specific value of  $\hat{\theta}_m$ . In Fig. 5 are shown these plots for the system in Fig. 4 for the assumed values of  $K = 10$  and  $T_m = 1$ , using the normalised signal parameters  $n$  and  $B$ .

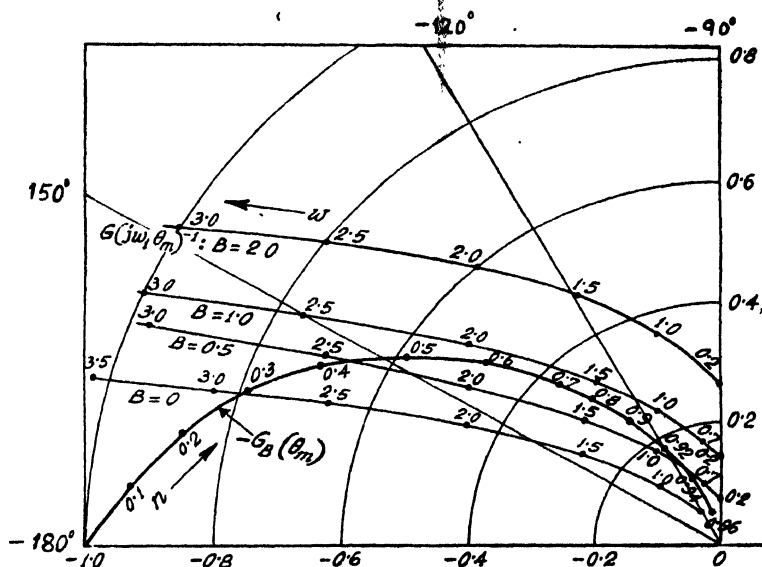


Fig. 5. Plots of  $G(j\omega, \theta_m)^{-1}$  and  $-G_B(\theta_m)$  in the complex plain.

Let us assume that the frequency response of the system corresponding to a signal amplitude  $\hat{\theta}_m = \hat{\theta}_{m1}$  is desired. This is easily done by locating the point  $G_B(\theta_{m1})$  on the amplitude locus (marked  $P$  in Fig. 5) and considering the frequency locus  $G(j\omega, \theta_{m1})^{-1}$ . Then at any frequency  $\omega_1$  (corresponding to the point  $Q$  in Fig. 5) the frequency response modulus is given by the ratio

$$\left| \frac{\theta}{\theta_i} \right| = \left| \frac{OP}{PQ} \right| \quad \dots (13)$$

$$\hat{\theta}_m = \hat{\theta}_{m1}$$

$$\omega = \omega_1$$

This ratio, if evaluated for a number of frequencies over the range of interest gives, when plotted against the frequency, the system frequency response corresponding to the signal amplitude  $\hat{\theta}_m = \hat{\theta}_{m1}$ . If this whole procedure is repeated for a number of values of  $\hat{\theta}_m$  the frequency response of the system is evaluated as a function of amplitude and frequency. This can be done for different amounts of coulomb friction.

In Figs. 6(a), (b) and (c) are shown the frequency response curves of the system in Fig. 4 as obtained from the loci of Fig. 5 for three different cases corresponding

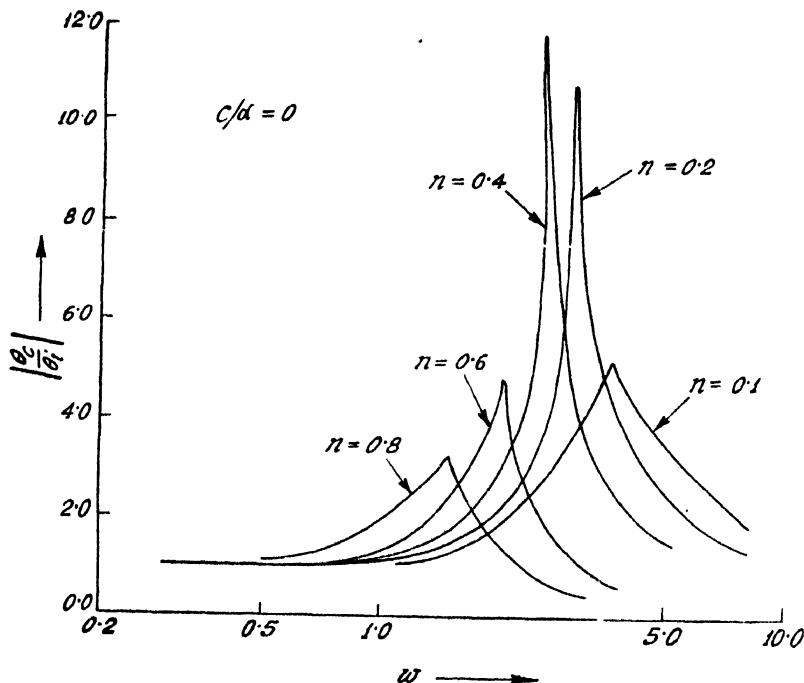


Fig. 6. (a) Frequency response plots:  $C/\alpha = 0$

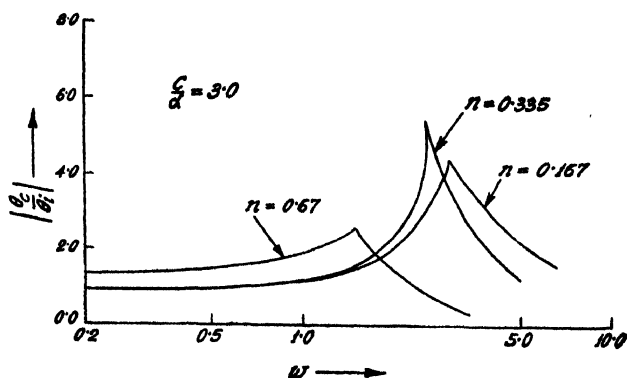


Fig. 6(b)  $C/\alpha = 3.0$

to  $C/\alpha = 0, 3.0$  and  $5.0$ . The peak value of the ratio  $|\theta_o/\theta_i|$  gives a measure of the system's relative stability and the frequency  $\omega_r$  at which this peak occurs gives a measure of the system's speed of response.

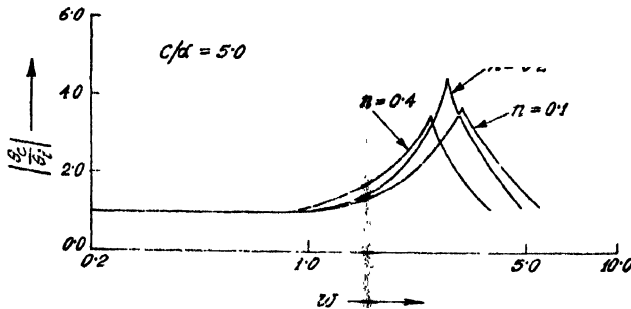


Fig. 6(c)  $C/\alpha = 5.0$

### (b) Effects of the nonlinearities

The effects of the two nonlinearities viz. backlash and coulomb friction, on the degree of stability as well as the speed of the response of the system can be seen from the frequency response curves of Fig. 6. In order to bring out the effects of the coulomb friction we proceed as follows :

Let us first assume that the motor is characterised by a truly linear friction characteristics so that instead of the quasilinear describing function  $G(j\omega, \theta_m)$  given by Eq. (9) the motor is characterised by linear transfer function

$$G(j\omega) = \frac{K}{j\omega(j\omega T_m + 1)} \quad (14)$$

The resultant frequency response curves are shown in Fig. 6(a). These curves incorporate the effects of backlash alone. The values of  $|\theta_o/\theta_i|$  ( $\theta_m$ ) and  $\omega_r(\theta_m)$  obtained from these curves are plotted against the normalised amplitude  $n$  in Figs. 7(a) and (b) respectively (curves marked  $C/\alpha = 0$ ). It is seen that the magnitude of the ratio  $|\theta_o/\theta_i|$  increases with falling signal amplitude (i.e. with  $n$  increasing) until it reaches an infinitely large value (at a signal amplitude corresponding to  $n = .3$  in Fig. 8). This indicates a possibility of sustained oscillation (of this amplitude) in the system. The reduction of the magnitude of the response amplitude at still smaller values of the signal amplitude is of course to be expected since the effective gain approaches zero due to the backlash dead-zone. The region of instability (round about the signal amplitude of about 3.3 in the present case) is of the order of backlash width. It can be concluded therefore that the presence of backlash causes the system stability to be impaired primarily at comparatively small signal levels. Also there is a slight reduction in the values of  $\omega_r(\theta_m)$  at smaller signal amplitudes thus reducing the system's speed of response.

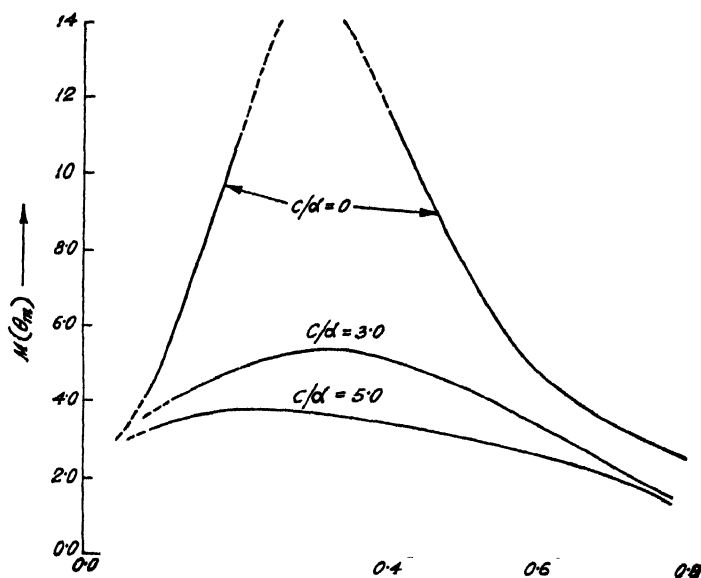


Fig. 7. Plots of (a) frequency-response peak  $M(\theta_m)$

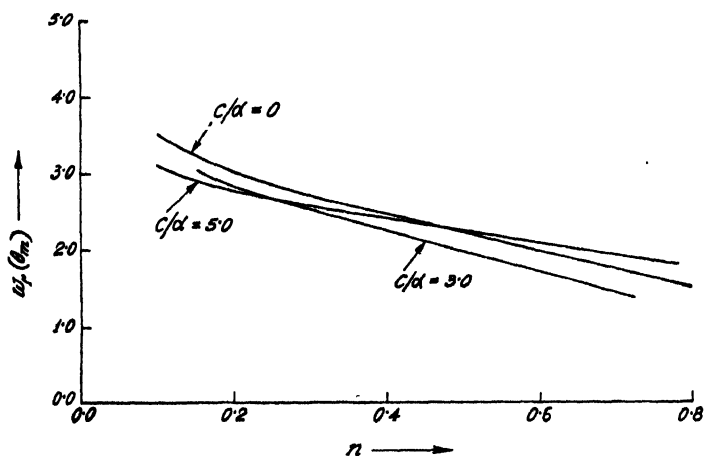


Fig. 7(b). frequency of occurrence of the peak  $\omega_r(\theta_m)$  against  $n$ .

If now the same parameters  $|\theta_e/\theta_i|(\theta_m)$  and  $\omega_r(\theta_m)$  are evaluated from the response curves of Figs. 6(b) and (c) the results of addition of the coulomb friction becomes evident. These also are plotted in Fig. 7 against  $n$  (curves marked  $C/\alpha = 3.0$  and  $C/\alpha = 5.0$ ) in order to emphasize the effects of the coulomb friction. It is seen that for the conditions specified the value of the frequency response peak as also the frequency show much less dependence on the signal amplitude; not only are the sustained oscillations avoided but addition of adequate coulomb friction can effectively improve the system's damping at small signal levels.

These results are in fact to be expected from the form of the describing function  $G(j\omega, \theta_m)$  as given by Eq. (9). It is seen that the effect of considering only the fundamental component of the coulomb friction torque for an assumed sinusoidal motor speed is to replace the nonlinear friction by an equivalent amplitude-dependent viscous friction  $4C/\pi |\dot{\theta}_m|$ , a quantity which is predominant at comparatively smaller values of  $\hat{\theta}_m$ .

#### TIME RESPONSE FROM THE SOLUTION OF THE CHARACTERISTIC EQUATIONS

The discussions in the previous sections give a qualitative picture of the effects of coulomb friction on the stability and the speed of the response of a servo system having backlash in the output coupling. A more quantitative analysis of the problem is, however, possible by following a method suggested by Oldenburg and Sartorius (1948). This consists of solving certain piecewise linear differential equations which characterise the system under the stipulated conditions. To set up these equations we start with a typical step response of a system which has low damping. This is indicated in Fig. 8; a response which exhibits some oscillations before attaining the steady state value. Taking  $t = 0$  at the instant at which

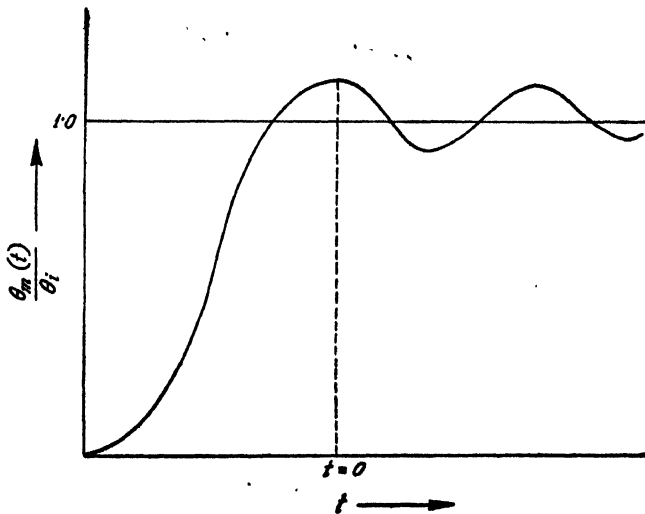


Fig. 8. A typical step input response of the system.

the first overshoot occurs the function  $\theta_m(t)$  in Fig. 8 can be considered as a damped sinusoid, at least during the first few oscillations. The relationship between the motor shaft and outputshaft positions can then be set up as

$$\left. \begin{aligned} \theta_o &= \hat{\theta}_{m0} - \alpha; & 0 \leq \omega t \leq \theta_2 \\ &= \theta_m + \alpha; & \theta_2 \leq \omega t \leq \pi \end{aligned} \right\} \quad \dots \quad (15)$$

$$\left. \begin{array}{l} \text{where } \hat{\theta}_{m0} = \text{the initial amplitude of oscillation} \\ \text{and} \end{array} \right\} \quad \theta_2 = \cos^{-1}(1 - 2\alpha/\hat{\theta}_{m0}) \quad \dots (16)$$

These quantities are defined as in Fig. 9. Now substituting for  $\theta_c$  in Eq. (1) and setting  $\theta_i = 0$  we get the two following equations which are valid for the two sections of the half period of  $\theta_m(t)$  defined in Eq. (15). Thus, for

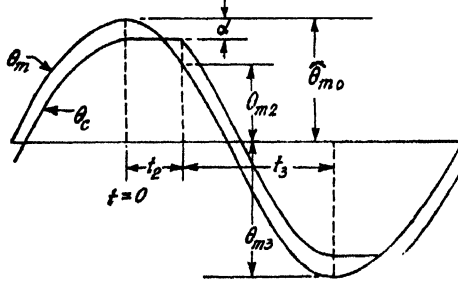


FIG. 9. Waveforms illustrating the boundary conditions.

$$0 \leq t \leq \theta_2/\omega,$$

$$T_m \frac{d^2\theta_m}{dt^2} + \frac{d\theta_m}{dt} = C - K(\hat{\theta}_{m0} - \alpha) \quad \dots (17)$$

the boundary conditions being

$$t = 0, \quad \theta_m = \hat{\theta}_{m0} \quad \text{and} \quad \dot{\theta}_m = 0$$

$$\text{and} \quad t = t_2(\text{say}) = \theta_2/\omega, \quad \theta_m = \hat{\theta}_{m0} - 2\alpha = \theta_{m2}(\text{say})$$

$$\text{and} \quad \dot{\theta}_m = [\dot{\theta}_m]_2(\text{say}), \text{ which is a negative quantity.}$$

For the other section using a new independent variable  $t_1$  i.e. for

$$0 \leq t_1 \leq \theta_3/\omega (\text{say}),$$

$$T_m \frac{d^2\theta_m}{dt_1^2} + \frac{d\theta_m}{dt_1} + K\theta_m = C - K\alpha \quad \dots (18)$$

—the boundary conditions being

$$t_1 = 0, \quad \theta_m = \theta_{m2} \quad \text{and} \quad \dot{\theta}_m = [\dot{\theta}_m]_2, \text{ as obtained from the previous section,}$$

$$\text{and} \quad t_1 = t_3 = \theta_3/\omega, \quad \theta_m = \theta_{m3}(\text{say}) \quad \text{and} \quad \dot{\theta}_m = 0.$$



Eqs. (17) and (18), subject to the specified boundary conditions, can now be solved to give the nature of the system response during the half period in question. The solution can then be used to compute such transient response parameters as the half period decrement and the half period of the transient oscillations. The results of these computations involve the nonlinearities and bring out their effects on the system response. In terms of the symbols used above these two parameters require evaluation of  $\theta_{m3}$  and  $(t_2+t_3)$ . The procedure for the purpose is outlined below :

Solution of Eq. (17) gives

$$\theta_m(t) = \hat{\theta}_{m0} - k(t - T_m + T_m) e^{-t/T_m} \quad \dots (19)$$

where  $k = K(\hat{\theta}_{m0} - \alpha) - C \quad \dots (20)$

Substituting  $t = t_2 = \theta_2/\omega$ ,

$$\theta_{m2} = \hat{\theta}_{m0} - 2\alpha = \hat{\theta}_{m0} - k(t_2 - T_m D) \quad \dots (21)$$

where  $D = 1 - e^{-t_2/T_m} \quad \dots (22)$

Eqs. (21) and (22), when solved, gives  $t_2$ .

Solution of Eq. (18) gives

$$\begin{aligned} \theta_m(t_1) = & \frac{C}{K} - \alpha + \left( \alpha - \frac{C}{K} + \theta_{m2} \right) e^{-\rho t_1} \cos \lambda t_1 \\ & + \frac{1}{\lambda} \left[ \rho \left( \alpha - \frac{C}{K} + \theta_{m2} \right) \right] e^{-\rho t_1} \sin \lambda t_1 \quad \dots (23) \end{aligned}$$

where  $\rho$  and  $\lambda$  are two parameters given by

$$\rho = \frac{1}{2T_m} ; \quad \rho^2 + \lambda^2 = K/T_m \quad \dots (24)$$

Substitution of the terminating condition in (23) leads to

$$\tan \lambda t_3 = \frac{\lambda D / \rho}{D - 2} \quad \dots (25)$$

This gives  $t_3$ .

Also putting  $t_1 = t_3$  in (23) we get

$$\theta_{m3} = \frac{C}{K} - \alpha + \frac{\left( \hat{\theta}_{m0} - \alpha - \frac{C}{K} \right) (1 - D + D^2 K T_m)}{1 - D/2} e^{-\rho t_3} \cos \lambda t_3 \quad \dots (26)$$

From (26) we have

$$\frac{\theta_{m3} + \alpha}{\hat{\theta}_{m0} - \alpha} = \frac{C}{K(\hat{\theta}_{m0} - \alpha)} + \frac{\hat{\theta}_{m0} - \alpha - \frac{C}{K}}{\hat{\theta}_{m0} - \alpha} \cdot \frac{1 - D + D^2 K T_m}{1 - D/2} e^{-\rho t_3} \cos \lambda t_3 \dots (27)$$

Noting (Fig. 9) that  $\theta_{m3}$  has a negative value, Eq. (27) can be rewritten as

$$\begin{aligned} \Delta = \frac{|\theta_{m3}| - \alpha}{\hat{\theta}_{m0} - \alpha} &= \frac{\theta_{m0} - \alpha - \frac{C}{K}}{\hat{\theta}_{m0} - \alpha} \cdot \frac{1 - D + D^2 K T_m}{D/2 - 1} e^{-\rho t_3} \cos \lambda t_3 \\ &\quad - \frac{C}{K(\hat{\theta}_{m0} - \alpha)} \\ &= \left[ 1 - \frac{C/\alpha}{K(\phi_{m0} - 1)} \right] H - \frac{C/\alpha}{K(\phi_{m0} - 1)} \dots (28) \end{aligned}$$

where  $\phi_{m0} = \hat{\theta}_{m0}/\alpha$ —the normalised amplitude.

The left hand side of this equation is easily identified as the half period decrement of  $\theta_O(t)$ , the load motion. On the right hand side of (28) the factor  $H$  represents the half-period decrement of the load motion when the coulomb friction constant  $C$  is zero. This factor has been worked out by Nichols (1953) who studied the effects of backlash in a servo system. The effect of the coulomb friction is obviously to reduce this value thus indicating a stabilising action.

For given values of the system constants the half period decrement given by (28) and the half period given by  $T/2 = t_2 + t_3$  as obtained from Eqs. (21) and (22) and Eq. (25) respectively, can be computed. The results are plotted in Fig. 10 against the normalised signal amplitude  $\phi_{m0} - 1 = (\hat{\theta}_{m0} - \alpha)/\alpha$  using the normalised coulomb friction constant  $C/\alpha$  as a parameter. The curves of Fig. 10 point out that the effects of the coulomb friction predominate when the signal amplitude is small. In general an increase in the value of  $C$  results in a reduction of  $\Delta$  and slight increase of the half-period. The results are in agreement with the earlier conclusions of the qualitative discussions.

## RESULTS OF SIMULATOR STUDIES

The arrangement of the simulator has been discussed in reference 1 and is shown in Fig. 11. The simulator is capable of varying the normalised coulomb friction constant  $C/\alpha$  as well as the gain  $K$ . The response  $\theta_m(t)$  for step displacement inputs under different conditions of gain and the constant  $C/\alpha$  have been

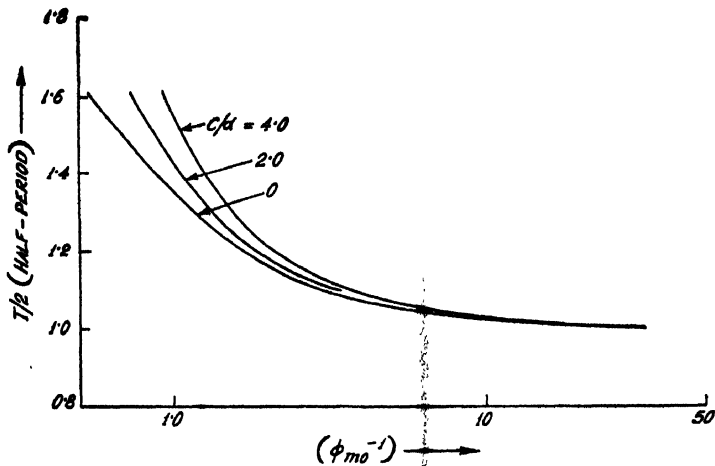


Fig. 10(a). Plots of the half-period decrement  $\Delta$  against  $\phi_{m_0}^{-1}$ .

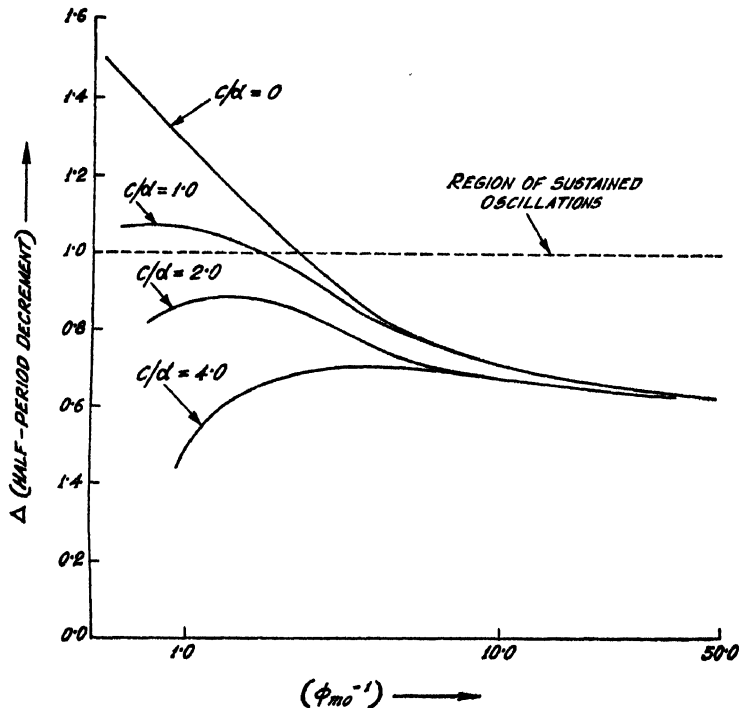


Fig. 10(b). Plots of half period  $T/2$  against  $\phi_{m_0}^{-1}$ .

obtained and are displayed in the traces of Figs. 12(a) and (b). In Fig. 12(a) are shown traces of response for a gain  $K = 4.0$  and  $C/\alpha = 0, 2.5$  and  $4.0$ . In Fig. 12(b) are shown traces of the response for  $K = 2.0$  and  $C/\alpha = 0, 2.5$  and  $4.0$ . The stabilising actions of the coulumb friction are clearly displayed by these traces.

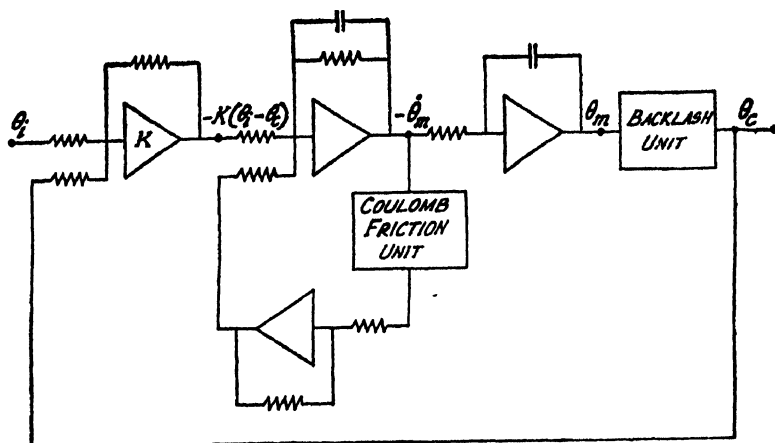
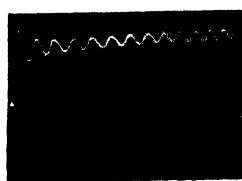


FIG. 11. Simulator set up for the system.



a (i)



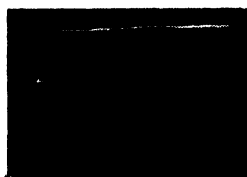
a (ii)



a (iii)



b (i)



b (ii)



b (iii)

FIG. 12. Traces of step responses obtained with the help of the simulator :

(a)  $K=4.0$  ;  $C/\alpha=0, 2.5$  and  $4.0$ (b)  $K=2.0$  ;  $C/\alpha=0, 2.5$  and  $4.0$ 

## CONCLUSIONS

The frequency response data indicate that the presence of coulomb friction in a servomechanism results in an increase of the effective system damping at relatively low signal amplitudes. If the servo system has backlash in the output coupling, coulomb friction can accordingly provide a proper compensation for the backlash effects. Solutions of the piece-wise linear differential equations which characterise the system having the two nonlinearities can be obtained to provide with quantitative data regarding the effects of the two nonlinearities on such transient response parameters as the half period decrement and the half period.

Conclusions drawn from these computations are corroborated by the results of analogue computer studies.

#### ACKNOWLEDGMENT

The author is grateful to Prof. J. N. Bhar for his guidance and to Dr. A. K. Choudhury for discussions. The award of a scholarship by the Government of India is also thankfully acknowledged.

#### REFERENCES

- Haas, V. B., 1953, *Trans. A. I. E. E.*, **72**, Part 2, pp. 119-123.  
Kochenburger, R. J., 1950, *Trans. A.I.E.E.*, **69**, Part 1, 270.  
Kochenburger, R. J., 1953, *Trans. A.I.E.E.* **72**, Part 2, 180.  
Mahalanobis, A. K., 1960, A.I.E.E. paper No. DP 60-667.  
Nichols, N. B., 1953, *Trans. A.I.E.E.*, **72**, Part 2, 492.  
Oldenbourg, R. C. and Sartorius, H., 1948, *Dynamics of Automatic Controls* (book), Transaction by A.S.M.E., New York, N.Y., pp. 168-173.

# RAMAN SPECTRA OF PARA FLUOROTOLUENE AND PHENYL ACETONITRILE IN THE SOLID STATE AT $-180^{\circ}\text{C}^*$

KRISHNA KUMAR DEB

OPTICS DEPARTMENT, INDIAN ASSOCIATION FOR THE CULTIVATION OF  
SCIENCE, CALCUTTA-32

(Received, December 12, 1960)

## PLATE I

**ABSTRACT.** The Raman spectra of para fluorotoluene and phenyl acetonitrile have been studied in the liquid state and in the solid state at  $-180^{\circ}\text{C}$  and the results have been compared with those reported by previous workers for a few compounds having similar molecules. In the case of para fluorotoluene a strong and broad new Raman line of Raman shift  $103\text{ cm}^{-1}$  has been observed. The lines  $152\text{ cm}^{-1}$  and  $333\text{ cm}^{-1}$  are found to shift considerably with the solidification of the liquid.

In the case of phenyl acetonitrile the Raman line  $361\text{ cm}^{-1}$  due to  $\text{C}\equiv\text{N}$  deformation oscillation is found to become very weak but the line  $2250\text{ cm}^{-1}$  due to  $\text{C}\equiv\text{N}$  stretching oscillation remains almost unchanged when the liquid is solidified. Further, this compound in the solid state also produces only one new Raman line at  $95\text{ cm}^{-1}$ . A strong and broad luminescence band at about  $21198\text{ cm}^{-1}$  has also been observed in the spectrum due to the crystals in the solid state at  $-180^{\circ}\text{C}$ . The significance of these changes has been discussed.

## INTRODUCTION

Raman spectra of some substituted toluenes (Biswas, 1954; Sanyal, 1953) and a few nitriles (Bishui, 1948) in different states were studied in this laboratory and some interesting changes were observed in the spectra with solidification of the substances. In continuation of these investigations the Raman spectra of para fluorotoluene and phenyl acetonitrile in the liquid state and in the solid state at  $-180^{\circ}\text{C}$  have been investigated and the results have been discussed in the light of the assignment of the lines made by previous workers.

## EXPERIMENTAL

The chemicals used in the present investigation were of chemically pure quality. Para fluorotoluene was supplied by Eastman Kodak Co., U.S.A. and phenyl acetonitrile by Fischer Scientific Co., New York. The liquids were subjected to distillation under reduced pressure before each exposure. The spectro-

\* Communicated by Prof. S. C. Sirkar.

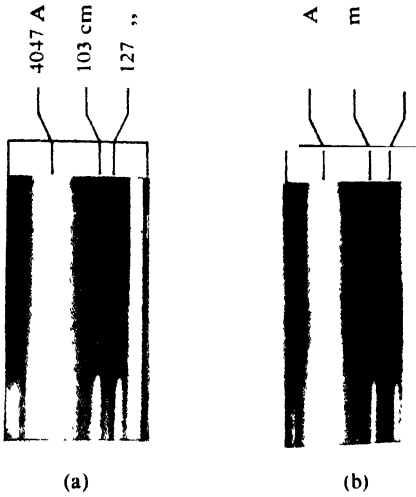
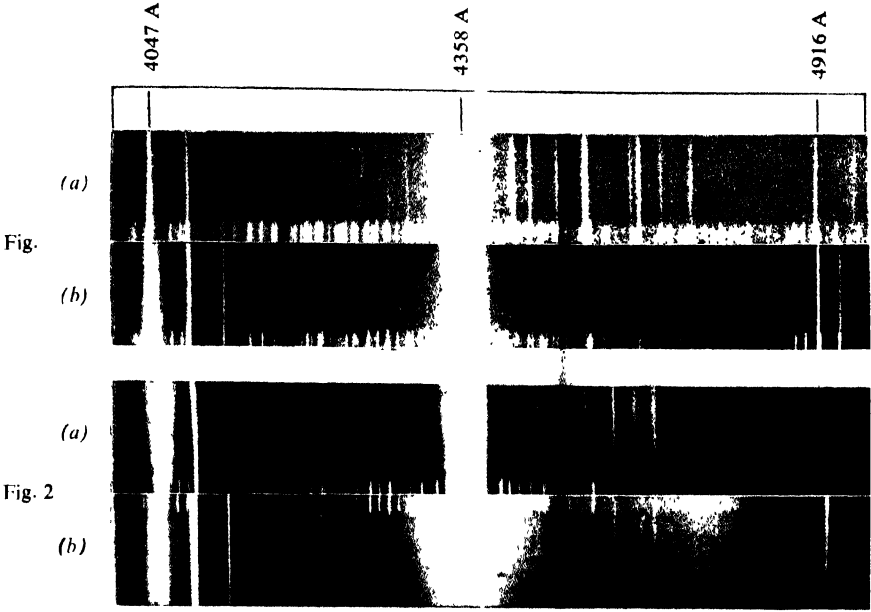


Fig. 3.

Fig. 1. (a) Raman spectra of para fluorotoluene liquid with filter at 28°C  
(b) " " " " " " solid at -180°C  
Fig. 2. (a) Raman spectra of phenyl acetonitrile liquid at 28°C  
(b) " " " " " " solid at -180°C  
Fig. 3. (a) Low frequency Raman lines of para fluorotoluene at -180°C  
(b) " " " " " " phenyl acetonitrile at -180°C





grams of the substances in the liquid and solid states and the polarised spectra were recorded with the same arrangements as those used previously (Deb, 1960). The spectra were photographed on Ilford Zenith plates using a Fuess glass spectrograph giving a dispersion of about 11 Å per mm in the 4046 Å region. The wavelengths were measured with the help of iron arc spectrum recorded on the same plate as a comparison.

## RESULTS AND DISCUSSION

The spectrograms are reproduced in Plate I. The observed Raman frequencies together with those reported for the compounds in the liquid state by previous workers are tabulated in Table I and Table II. The polarised and totally depolarised lines are indicated by the letters P and D respectively.

### *Parafluorotoluene*

#### (a) *Low-frequency lines*

It can be seen from Figs. 1(a) and 1(b) and Table I that in the solid state at  $-180^{\circ}\text{C}$ , para fluorotoluene yields two new low frequency Raman lines with Raman frequencies  $103\text{ cm}^{-1}$  and  $127\text{ cm}^{-1}$  respectively. It was previously observed by Sanyal (1953) and Biswas (1954) that para chlorotoluene yields four such lines of Raman frequencies  $30\text{ cm}^{-1}$ ,  $50\text{ cm}^{-1}$ ,  $85\text{ cm}^{-1}$  and  $129\text{ cm}^{-1}$  respectively and para bromotoluene yields only three such lines of Raman frequencies  $52\text{ cm}^{-1}$ ,  $94\text{ cm}^{-1}$  and  $133\text{ cm}^{-1}$  respectively. A comparison of these results shows that the frequency about  $130\text{ cm}^{-1}$  is present in all these three molecules in the solid state and the other two frequencies 50 and  $85\text{ cm}^{-1}$  shown by para chlorotoluene do not change very much when the chlorine atom is replaced by the bromine atom. This shows that the atomic weight of the substituent halogen atoms has very little influence on the frequencies and therefore, they may not belong to any intermolecular vibration in which the adjacent molecules oscillate against each other in the lattice. It also appears that the number of low frequency lines is related very much to the chemical affinity of the molecules. Similar results were observed in the case of halogen substituted benzenes (Mukherjee, 1960). It has been suggested by some previous workers (Sirkar and Bishui, 1946; Sirkar, 1951) that these lines might be due to vibrations in groups of associated molecules in the solid state, but no attempt has been made to indicate the nature of such modes. The analysis of the results obtained with a large number of such compounds is necessary before such modes can be visualised.

#### (b) *Changes in the position of the other Raman lines with solidification.*

Ferguson *et al.* (1953) have reported the Raman and infrared spectra of para fluorotoluene and have analysed the vibrational bands assuming a point group  $D_{2h}$  for the molecule, because the effective mass of the fluorine atom is

nearly the same as that of the  $\text{CH}_3$  group taken as a point mass. It can be seen from Table I that the line at  $152\text{ cm}^{-1}$  of the liquid, assigned by them to a

TABLE I  
Raman spectrum of *p*-fluorotoluene

Liquid		Solid at $-180^\circ\text{C}$
Ferguson <i>et al.</i> (1953)	Present author	Present author
		103 (8b) 127 (4)
152	152 (1b)D	
312	310 (1)P	
341	333 (10)D	353 (6)
425		
454	450 (10)P	456 (6)
502	498 (1)D	
638	638 (10)D	638 (6)
695	692 (2)P	
728	722 (2)P	
740		
825	819 (10)P	826 (5)
842	840 (10)P	844 (3)
908	910 (0)	
929		
1003	997.(1)	
1017		
1040		
1061		
1099		
1157	1153 (6)P	1153 (5)
1178		
1214	1214 (10)P	1219 (8)
1221		
1278		
1299	1298 (4) P	1296 (3)
1351		
1382	1380 (6) P	1383 (3)
1404		
1433		
1455	1455 (1b)P	
1495		
1508	1510 (0b)	
1601	1597 (6b)P	1597 (2)
1614		
1858		
1906		
1940		
2385		
2416		
2454		
2740	2736 (2)P	
2871	2876 (4)	
2928	2922 (6) P	2922 (2)
3071	3069 (8)P	3069 (3)

$b_{3u}$  mode of the molecule representing probably an out-of-plane carbon bending vibration shifts to  $127\text{ cm}^{-1}$  when the substance is solidified and cooled to  $-180^\circ\text{C}$ . Also the line at  $333\text{ cm}^{-1}$  due to a  $b_{3u}$  mode shifts under similar conditions to  $353\text{ cm}^{-1}$ . In place of two lines at  $1601\text{ cm}^{-1}$  and  $1614\text{ cm}^{-1}$  observed by the above authors in the case of the liquid, a broad unresolved band at  $1597\text{ cm}^{-1}$  is observed in the present investigation. This band, however, becomes sharp when the liquid is frozen. Further, the lines  $450\text{ cm}^{-1}$ ,  $819\text{ cm}^{-1}$  and  $840\text{ cm}^{-1}$  of the liquid shift respectively to  $456\text{ cm}^{-1}$ ,  $826\text{ cm}^{-1}$  and  $844\text{ cm}^{-1}$  when the liquid is frozen. All these changes suggest some sort of intermolecular association which affects the frequencies of some of the modes of vibration of the single molecule.

### *Phenyl acetonitrile*

#### (a) *Low-frequency lines*

This compound yields only one low frequency Raman line at  $95\text{ cm}^{-1}$  when the liquid is solidified and cooled to  $-180^\circ\text{C}$ . Bishui (1948) studied Raman spectrum of benzonitrile at low temperature and he also observed only one such line at  $94\text{ cm}^{-1}$ . A similar compound benzyl chloride, on the other hand, produces four such new lines of Raman shifts  $46\text{ cm}^{-1}$ ,  $62\text{ cm}^{-1}$ ,  $82\text{ cm}^{-1}$  and  $88\text{ cm}^{-1}$  respectively in the solid state at  $-180^\circ\text{C}$  (Ray, 1951). These results again show that the number of low frequency lines produced by these compounds cannot be satisfactorily explained on the hypothesis of the angular oscillations of the molecules in the crystal lattice, because the number seems to depend on the nature of the individual substituents and not on their masses.

#### (b) *Changes in the other Raman lines*

In the solid state at  $-180^\circ\text{C}$ , the line  $361\text{ cm}^{-1}$  due to  $\text{C} \equiv \text{N}$  deformation oscillation of the molecule in the liquid becomes very weak, but the line  $2250\text{ cm}^{-1}$  due to  $\text{C} \equiv \text{N}$  stretching oscillation remains almost unchanged. These changes are similar to those observed in the case of benzonitrile by Bishui (1948) who suggested that  $\text{C} \equiv \text{N}$  deformation oscillation might be restricted in the solid state due to association of the molecules. The results of the present investigation thus confirm this view. The lines  $3059\text{ cm}^{-1}$  and  $3065\text{ cm}^{-1}$  in the liquid state reported in Tables by Landolt-Börnstein (1951) are not resolved in the spectrograms obtained in the present case, but they appear as a broad band with its centre at  $3065\text{ cm}^{-1}$ . With the solidification of the liquid, the band remains broad. Besides these changes mentioned above, frequencies of some other Raman lines of the single molecules are also affected slightly. All these changes again appear to point to the formation of associated groups of molecules in the frozen state of the nitrile compound at the low temperature.

(c) *Luminescence spectra*

In the Raman spectrum of phenyl acetonitrile in the solid state at  $-180^{\circ}\text{C}$  a strong and broad luminescence band with its centre at  $21198\text{ cm}^{-1}$  has been observed. It is well known now that some substituted benzenes at low temperatures produce such bands in the visible region (Kasha, 1952; Sirkar and Biswas,

TABLE I  
Raman spectrum of phenyl acetonitrile

Liquid		Solid at $-180^{\circ}\text{C}$
Landolt-Bornstein (1951)	Present author	Present author
126 (6)	132 (8b)D	95 (6b)
216 (2sb)		132 (4)
235 (3b)	238 (4b)D	243 (3)
322 (4)	324 (2)P	
358 (5)	361 (5)D	361 (0)
428 (3b)	432 (1b)P	
468 (1b)	482 (2b)P	482 (2)
618 (7)	621 (6)D	623 (3)
744 (2)	752 (0b)P	752 (2)
798 (6)	808 (6) P	
812 (6b)	820 (6)P	812 (4)
849 (1)		
991 (1)		
1003 (10)	1008 (12)P	1008 (8)
1031 (8)	1032 (6)P	1032 (2)
1157 (4)	1160 (2) P	
1188 (4)		
1192 (7)	1192 (8)P	1205 (4b)
1414 (5)	1419 (3)P	1416 (0)
1499 (0)		
1589 (5)	1591 (3)P	
1602 (6)	1602 (4)D	1599 (3b)
2252 (6)	2250 (10)P	2249 (6)
2914 (5b)	2920 (10)P	2923 (6)
2984 (3)		
3011 (3)		
3046 (3)		
3059 (9)		
3065 (8b)	3065 (10b)P	3062 (8b)

1956; Biswas, 1956a, 1956b) by triplet→singlet transition, but all disubstituted benzenes do not necessarily produce such luminescence in the visible region. Probably the wavelength of singlet→triplet absorption band of phenyl acetonitrile is longer than 3650 Å group of mercury lines, and in other nitriles not showing such luminescence the absorption band may be at wavelengths shorter than the 3650 Å group.

## ACKNOWLEDGMENT

The author is grateful to Professor S. C. Sarkar, D.Sc., F.N.I., for his kind interest and helpful guidance during the progress of the work. The author's thanks are also due to Dr. S. B. Banerjee for his valuable discussions.

## REFERENCE

- Bishui, B. M., 1948, *Ind. J. Phys.*, **22**, 167.  
Biswas, D. C., 1954, *Ind. J. Phys.*, **28**, 423.  
Biswas, D. C., 1956a, *Ind. J. Phys.*, **30**, 143.  
Biswas, D. C., 1956b, *Ind. J. Phys.*, **30**, 407.  
Deb, K. K., 1960, *Ind. J. Phys.*, **34**, 247.  
Ferguson *et al.*, 1953, *J. Chem. Phys.*, **21**, 1736.  
Kasha, M., 1952, *J. Chem. Phys.*, **20**, 71.  
Landolt-Börnstein, 1951, *Zahlenwerte und Funktionen, I Band Atom-und Molekular Physik Teil (2)*, p. 545.  
Mukherjee, D. K., 1960, *Ind. J. Phys.*, **34**, 402.  
Ray, A. K., 1951, *Ind. J. Phys.*, **25**, 131.  
Sanyal, S. B., 1953, *Ind. J. Phys.*, **27**, 447.

# DYNAMICS OF THE LONGITUDINAL PROPAGATION OF ELASTIC DISTURBANCE THROUGH A MEDIUM EXHIBITING GRADIENT OF ELASTICITY

S. K. GHOSH

DEPARTMENT OF PHYSICS, JADAVPUR UNIVERSITY, CALCUTTA-32

(Received July 6, 1960)

**ABSTRACT.** Extensional vibration in an isotropic medium for linear variation of elastic parameters has been considered. The problem is worked out following Operational methods. Two distinct cases have been worked from the general solution, namely, (1) for a source having impulsive force at one end, the other end remaining free, and (2), impulsive force at one end, the other end being fixed. Solution obtained in the form of modified Bessel functions have further been simplified for small variations of the parameter using method of steepest descents as adopted by Debye.

## INTRODUCTION

The general problem of the extensional vibration of a bar excited by the impact of an elastic load has already been solved for a number of cases by the author, following Operational method. The theory has been further extended to include dynamics of plastic deformations in a bar exhibiting strain-rate effect and subjected to (1) impact stress, (2) alternating stress.

In the present paper, an isotropic elastic medium of uniform density  $\rho$  is considered, where the elastic parameters  $\lambda, \mu$ , are supposed to vary linearly.

Explanations of the symbols used:

$l$  = Length of the medium

$t$  = Variable time

$x$  = Variable length, measured in the direction of propagation of the disturbance, the medium being free at  $x = 0$  and impacted at  $x = l$  (as in sec. I). But in section II, the medium is supposed fixed at  $x = 0$  and impacted at  $x = l$ .

$U$  = Displacement at any section.

$U_l$  = Displacement at  $x = l$ .

$\rho$  = Density of the medium (supposed uniform)

$\lambda, \mu$  = Elastic parameters whose linear variations are supposed in accordance with the relations,

$$\left. \begin{aligned} \lambda &= \lambda_0 + \lambda_1 x \\ \mu &= \mu_0 + \mu_1 x \end{aligned} \right\} (\lambda_1, \mu_1 > 0)$$

where  $\lambda_0, \mu_0$  are the values at the origin,  $x = 0$

$v_0$  = Velocity of impact.

$a_0$  = Compressional wave velocity at  $x = 0$

$J$  = Impulse per unit area.

$P$  = Pressure of impact.

$D$  = Operator  $d/dt$ .

The differential equation governing motion in one dimension in an isotropic elastic medium of uniform density  $\rho$  is given by

$$\frac{d}{dx} \left[ (\lambda + 2\mu) \frac{du}{dx} \right] = \rho \frac{d^2u}{dt^2} \quad \dots (1)$$

Using transformation

$$Z = \lambda_0 + 2\mu_0 + (\lambda_1 + 2\mu_1)x \quad \dots (2)$$

Eq. (1) reduces to

$$Z \frac{d^2u}{dz^2} + \frac{du}{dz} = C^2 \frac{d^2u}{dt^2} \quad \dots (1.1)$$

which is equivalent to

$$Z \frac{d^2u}{dz^2} + \frac{du}{dz} - C^2 D^2 u = 0 \quad \dots (1.2)$$

where

$$C^2 = \rho / (\lambda_1 + 2\mu_1)^2. \quad \dots (3)$$

The substitution

$$y = 2C[D(\lambda_0 + 2\mu_0 + (\lambda_1 + 2\mu_1)x)]^{1/2} \quad \dots (4)$$

reduces Eq. (1.2) to

$$\frac{d^2u}{dy^2} + \frac{1}{y} \frac{du}{dy} - u = 0 \quad \dots (1.3)$$

which is modified Bessel's equation of Zero order and has the solution,

$$U(x, t) = AI_0(y) + BK_0(y) \quad \dots (5)$$

where  $I_0$ ,  $K_0$  are modified Bessel Functions of zero order.

For large values of  $y$  (since  $C$  is large for small values of  $\lambda_1$ ,  $\mu_1$ ), Eq. (5) can be approximately written, using the method of steepest descents, as adopted by Debye, as

$$U(x, t) = y^{-1/2} [A_1 e^y + B_1 e^{-y}] \quad \dots (6)$$

## SECTION I.

The terminal conditions are :

$$\text{at the free end } x = 0, \quad \frac{du}{dx} = 0 \quad \dots \quad (6.1)$$

$$\text{and at the end } x = l, \quad u = U_l \quad \dots \quad (6.2)$$

Conditions (6.1) and (6.2) reduce equation (6) to

$$U(x, t) = (Z/Z_l)^{-1/4} \cdot \frac{\cosh 2CD(Z_l^4 - Z_0^4)}{\cosh 2CD(Z_l^4 - Z_0^4)} \cdot U_l \quad \dots \quad (7)$$

$$\begin{aligned} \text{where} \quad & Z_l = \lambda_0 + 2\mu_0 + (\lambda_1 + 2\mu_1)l \\ \text{and} \quad & Z_0 = \lambda_0 + 2\mu_0 \end{aligned} \quad \dots \quad (7.1)$$

Now the pressure of impact on the medium at  $x = l$  is given by

$$P = - \left( Z \frac{du}{dx} \right)_{x=l} \quad \dots \quad (8)$$

An impulse  $J$  per unit area is given to the medium, at  $x = l$ , and the subsequent equation of motion is given by

$$J/v_0 \cdot \frac{d^2 U_l}{dt^2} = - \left( Z \frac{du}{dx} \right)_{x=l} \quad \dots \quad (9)$$

Now substituting the value of  $\left( Z \frac{du}{dx} \right)_{x=l}$  as obtained from Eq. (7) in

Eq. (9) and imposing the boundary conditions, we have

$$D\rho a_0 \left[ 1 + \frac{1}{2} \frac{(\lambda_1 + 2\mu_1)l}{\lambda_0 + 2\mu_0} \right] U_l \tanh \frac{Dl}{a_0} + J/v_0 D^2 U_l = JD. \quad \dots \quad (10)$$

retaining up to first power of  $\lambda_1, \mu_1$  and using the condition

$$l < (\lambda_0 + 2\mu_0)/(\lambda_1 + 2\mu_1)$$

Eq. (10) yields,

$$U_l = v_0/F(D). \quad \dots \quad (11)$$



$$\begin{aligned} \text{where } F(D) &= D + \frac{\rho a_0 v_0}{J} \left\{ 1 + \frac{1}{2} \frac{(\lambda_1 + 2\mu_1)l}{\lambda_0 + 2\mu_0} \right\} \tanh \frac{Dl}{a_0} \\ &= D + q \cdot \frac{1 - e^{-2Dl/a_0}}{1 + e^{-2Dl/a_0}} \end{aligned} \quad \dots \quad (12)$$

$$\text{where} \quad q = \frac{\rho a_0 v_0}{J} \left\{ 1 + \frac{1}{2} \frac{(\lambda_1 + 2\mu_1)l}{\lambda_0 + 2\mu_0} \right\} \quad \dots \quad (12.1)$$

Eq. (11) with the help of (12) becomes

$$\begin{aligned} U_t &= \left[ \frac{1}{D+q} + \left\{ \frac{1}{D+q} - \frac{D-q}{(D+q)^2} \right\} e^{-2Dl/a_0} \right. \\ &\quad \left. \left\{ \frac{(D-q)^2}{(D+q)^3} - \frac{D-q}{(D+q)^2} \right\} e^{-4Dl/a_0} + \dots + \dots \right] v_0 \\ &= [f_1(t) + 2f_1(t_1) - 2f_2(t_1) + 4f_3(t_2) - 6f_2(t_2) + 2f_1(t_1) + \dots + \dots] \end{aligned} \quad \dots \quad (13)$$

where  $f(t_n)$  denotes  $f(t - n\theta_1) = f(t - n.2l/a_0)$ .

The values of the functions are similar to those obtained by the author earlier (Ghosh and Ghosh, 1951).

#### DISPLACEMENT AT ANY SECTION

Eq. (7) when expanded in terms of its equivalent exponential and simplified using small values of  $\lambda_1, \mu_1$  up to first power gives with the help of Eq. (13),

$$\begin{aligned} U(x, t) &= \left\{ 1 + \frac{1}{4} \frac{(\lambda_1 + 2\mu_1)(l-x)}{\lambda_0 + 2\lambda_0} \right\} \sum_{r=1}^n \left[ e^{D/a_0 \{x-l-r-1.2l\}} \right. \\ &\quad \left. + e^{-D/a_0 \{x-l+r.2l\}} \right] U_t \end{aligned} \quad \dots \quad (14)$$

where  $r$  is an integer.

Eq. (14) is the general form, giving the displacement at any section at any instant during impact.

Now substituting the value of  $U_t$  from Eq. (13) in Eq. (14) and collecting only the useful terms occurring during the desired interval of time, we get for the displacement at any section during  $0 < t < 2l/a_0$ ,

$$U(x, t) = \left\{ 1 + \frac{1}{4} \frac{(\lambda_1 + 2\mu_1)(l-x)}{\lambda + 2\mu_0} \right\} \left[ e^{\frac{D}{a_0}(x-l)} + e^{-\frac{D}{a_0}(x+l)} \right] f_1(t) \quad \dots \quad (14.1)$$

$$= \frac{J}{\rho a_0} \left[ 1 - \frac{1}{4} \frac{(\lambda_1 + 2\mu_1)(x+l)}{\lambda_0 + 2\mu_0} \right] \left[ 1 - e^{-\frac{q}{a_0} (a_0 t - l - x)} \right] \quad \dots \quad (14.2)$$

Since  $a_0 \times v_0$  is large (when  $v_0$  is large),  $q$  is large and at  $t = l/a_0$  equation (14.2) reduces to

$$U(x, t) = \frac{Jt}{\rho l} \left[ 1 - \frac{1}{4} \frac{(\lambda_1 + 2\mu_1)(l+x)}{\lambda_0 + 2\mu_0} \right] \quad \dots \quad (14.3)$$

Eq. (14.3) is similar to that obtained by A. N. Dutta (1956) and is a particular case derived from the general solution given by Eq. (14.2).

It is clear that Eq. (14.3) fails to give general displacement  $U(x, t)$  for time  $t < l/a_0$  i.e., until the waves have reached the far end. Further, the displacement Eq. (13) shows that the wave train does not return after reflection, as shown by the second term of Eq. (15) below.

#### PRESSURE AT THE IMPACTED END

Combining Eq. (8) with (7), the pressure of impact on the medium at  $x = l$ , i.e. impacted end is numerically given by

$$\begin{aligned} P &= \rho a_0 \left[ 1 + \frac{1}{2} \frac{(\lambda_1 + 2\mu_1)l}{\lambda_0 + 2\mu_0} \right] \tanh \frac{Dl}{a_0} \cdot U_l \\ &= \rho a_0 \left[ 1 + \frac{1}{2} \frac{(\lambda_1 + 2\mu_1)l}{\lambda_0 + 2\mu_0} \right] \left[ f_1'(t) - 2f_2'(t_1) + 4f_3'(t_2) - 2f_2'(t_2) + \dots \right] \quad \dots \quad (15) \end{aligned}$$

Thus during  $0 < t < 2l/a_0$ ,

$$P_1 = \rho a_0 \left[ 1 + \frac{1}{2} \frac{(\lambda_1 + 2\mu_1)l}{\lambda_0 + 2\mu_0} \right] \cdot v_0 e^{-qt}. \quad \dots \quad (15.1)$$

#### SECTION II

The terminal conditions are:

$$\text{at the fixed end, } x = 0, \quad U = 0 \quad \dots \quad (16.1)$$

$$\text{and at the end, } x = l, \quad U = U_l \quad \dots \quad (16.2)$$

Conditions (16.1) and (16.2) reduce equation (6) to

$$U(x, t) = \left( \frac{Z}{Z_l} \right)^{-1/4} \cdot \frac{\sinh \frac{2CD(Z_l - Z_0)}{2}}{\sinh \frac{2CD(Z_l - Z_0)}{2}} \cdot U_l \quad \dots \quad (17)$$

Now substituting the value of  $\left( Z \frac{du}{dx} \right)_{x=l}$  from Eq. (17) in Eq. (9) and imposing the boundary conditions we have,

$$D\rho a_0 \left[ 1 + \frac{1}{\lambda} \frac{(\lambda_1 + 2\mu_1)l}{\lambda_0 + 2\mu_0} \right] U_l \coth \frac{Dl}{a_0} + J/v_0 D^2 U_l = JD \quad \dots (18)$$

retaining up to first power of  $\lambda_1, \mu_1$  and subject to the condition that  $l < \frac{\lambda_0 + 2\mu_0}{\lambda_1 + 2\mu_1}$

Eq. (18) yields

$$U_l = \frac{v_0}{F(D)} \quad (19)$$

where 
$$F(D) = D + \frac{\rho a_0 v_0}{J} \left\{ 1 + \frac{1}{2} \frac{(\lambda_1 + 2\mu_1)l}{\lambda_0 + 2\mu_0} \right\} \coth \frac{Dl}{a_0}$$

$$= D + q \coth \frac{Dl}{a_0} \quad (20)$$

where 
$$q = \frac{\rho a_0 v_0}{J} \left\{ 1 + \frac{1}{2} \frac{(\lambda_1 + 2\mu_1)l}{\lambda_0 + 2\mu_0} \right\} \text{ as before.}$$

Eq. (19) with the help of Eq.(20) becomes

$$\begin{aligned} U_l = & f_1(t) + 2f_2(t_1) - 2f_1(t_1) + 4f_3(t_2) - 6f_2(t_2) + 2f_1(t_2), \\ & + \dots + 2 \left[ 2^{n-1}f_{n+1}(t_n) - 2^{n-2} \cdot \frac{n+1}{n} {}^nC_1 f_n(t_n) + 2^{n-3} \cdot \frac{n+2}{n} {}^nC_2 f_{n-1}(t_n) \right. \\ & \left. \dots + \dots + (-1)^n f_1(t_n) \right] . \end{aligned}$$

The values of the functions are the same as those in Section I.

## REFERENCES

- Datta, A. N., 1956, *Ind. J. Theo. Phys.*, **4**, No. 2.  
 Ghosh, M. and Ghosh, S. K., 1951, *Ind. J. Phys.*, **25**, 153.

# DISPERSION OF MICROWAVES IN OXYGEN

PREM SWARUP AND S. K. GARG

INSTITUTE OF APPLIED PHYSICS, UNIVERSITY OF ALLAHABAD, ALLAHABAD

(Received, February 7, 1960)

**ABSTRACT.** Dispersion of microwaves has been theoretically calculated in the case of gaseous oxygen on the basis of Van Vleck-Weisskopf expressions for the collision broadened microwave spectral lines. Curves are plotted at pressures of  $\frac{1}{2}$ , 1, 2, 10, 25 and 50 atmospheres in a wide frequency band both for resonant and nonresonant cases. The calculated value of static magnetic susceptibility agrees with the known experimental value.

## INTRODUCTION

Oxygen molecule presents an interesting case in the microwave region. The molecule is electrically nonpolar and the absorption and dispersion of microwaves is attributed to it being magnetically polar. Analysis of the band spectrum has shown that oxygen molecule has a  $^3\Sigma$  ground state. It has the spin quantum number unity and the Lande  $g$  factor two and, hence, the molecule has the magnetic dipole moment of 2 Bohr magnetons; which interacts with the 'end over end' rotation of the molecule to form a 'rho type triplet'. The resolved fine structure of the microwave spectrum has been studied by a number of workers in the vicinity of 60 kMcps.<sup>1,2</sup> The transitions involved here are between  $J = K$  and  $J = K-1$  (negative transition) and  $J = K$  and  $J = K+1$  (positive transitions). Selection rule prohibits the transition between  $J = K-1$  and  $J = K+1$ . These states nearly coincide and differ from  $J = K$  by about  $2\text{ cm}^{-1}$  and hence all the lines are clustered about  $2\text{ cm}^{-1}$ . There is, however, a subsidiary resonance at  $4\text{ cm}^{-1}$  involving the single transition  $J = K$  to  $J = K-1$  for  $K = 1$ . In addition to this resonance absorption, oxygen molecule also shows a nonresonant or Debye type of absorption and dispersion which is attributed to the diagonal part of the matrix element of the magnetic moment i.e. projection of the Spin vector  $S$  parallel to the resultant angular momentum vector  $J$  about which  $S$  precesses. On the average it is found that one third of the total mean squared moment is of the diagonal variety while the other two third being consumed by the nondiagonal type of absorption i.e. the resonance absorption. The study of the resolved oxygen spectrum in the low pressure has shown about 29 absorption lines. The measurement of the line width parameter (Artman, 1953) has shown that it is very nearly constant for all the lines. At a higher pressure, all the lines merge to form a single broad line with centroid frequency at  $2\text{ cm}^{-1}$ . An average value of the line width parameter weighted for line intensity has been found to

be 1.94 Mc/mm Hg. In case of air, allowing for difference in collision cross section between oxygen and air, the average value is 18% lower i.e. 0.039 cm<sup>-1</sup>/atm. The value of the line width parameter for the 'nonresonant' line at zero frequency is still uncertain for lack of any experimental absorption data at wavelengths above 1 cm. Van Vleck (1947) predicted the attenuation offered by oxygen in the millimeter region due to the nonresonant line taking two likely values of the line width parameter i.e.  $\Delta\bar{\nu} = 0.02$  and 0.05 cm<sup>-1</sup>/atmos. the former being the most probable value and the latter being the upper limit.

### CALCULATIONS

Van Vleck's and later Artman's calculations predicting the amount of attenuation offered by oxygen in the mm region at atmospheric pressure of air were based on the quantum mechanical expressions of Van Vleck and Weisskopf (1945) for the collision broadened microwave spectral lines. The expression for the absorption coefficient is:

$$\frac{\alpha'}{\bar{\nu}^2} = \frac{4\pi^2 \sum N_{ij} |\mu_{ij}|^2}{3kT} \left[ \frac{\Delta\bar{\nu}^2}{\Delta\bar{\nu}^2 + (\bar{\nu} + \bar{\nu}_0)^2} + \frac{\Delta\bar{\nu}^2}{\Delta\bar{\nu}^2 + (\bar{\nu} - \bar{\nu}_0)^2} \right] \quad \dots (1)$$

$$= 2\pi I.p \left[ \frac{\Delta\bar{\nu}^2}{\Delta\bar{\nu}^2 + (\bar{\nu} + \bar{\nu}_0)^2} + \frac{\Delta\bar{\nu}^2}{\Delta\bar{\nu}^2 + (\bar{\nu} - \bar{\nu}_0)^2} \right] \quad \dots (2)$$

where  $\alpha$  is the absorption coefficient (per cm);  $\bar{\nu}$  is the frequency (cm<sup>-1</sup>);  $\bar{\nu}_0$  is the resonance frequency;  $\Delta\bar{\nu}$  is the line width parameter (cm<sup>-1</sup>);  $I$  is the intensity factor and  $p$  is the pressure in cm of Hg.

The contribution of the nonresonant line with the line width parameter  $\Delta\bar{\nu}_0$  to the absorption at a frequency  $\bar{\nu}$  is obtained by putting  $\bar{\nu}_0 = 0$  and using half the value of  $I.p$ , since one third of the squared moment contributes to the non-resonant absorption while two thirds to the resonant absorption, in the expression (2) above:

$$\frac{\alpha''}{\bar{\nu}^2} = 2\pi \left( \frac{I.p}{2} \right) \left[ \frac{2\Delta\bar{\nu}_0^2}{\Delta\bar{\nu}^2 + \bar{\nu}^2} \right] \quad \dots (3)$$

$$= 2\pi I.p [\Delta\bar{\nu}_0^2 / (\Delta\bar{\nu}^2 + \bar{\nu}^2)]$$

Hence the net absorption at a frequency comes out to be:

$$\frac{\alpha}{\bar{\nu}^2} = \frac{\alpha' + \alpha''}{\bar{\nu}^2} = 2\pi I.p \left[ \frac{\Delta\bar{\nu}^2}{\Delta\bar{\nu}^2 + (\bar{\nu} + \bar{\nu}_0)^2} + \frac{\Delta\bar{\nu}^2}{\Delta\bar{\nu}^2 + (\bar{\nu} - \bar{\nu}_0)^2} + \frac{\Delta\bar{\nu}_0^2}{\Delta\bar{\nu}^2 + \bar{\nu}^2} \right] \quad \dots (4)$$

The associated dispersion of the microwaves due to the magnetic dipole moment can be calculated by the quantum mechanical Van Vleck-Weisskopf expression

for dispersion. The case is parallel to the calculation of the electric susceptibility in  $\text{ND}_3$  by the author (1956). In this case the magnetic susceptibility  $(\mu' - 1)$  or  $\delta_m$  at a frequency  $\bar{\nu}$  due to a resonance line at  $\bar{\nu}_0$  of line width parameter  $\Delta\bar{\nu}$

$$\delta_m'' = I.p \left[ \frac{\Delta\bar{\nu}^2 + \bar{\nu}_0(\bar{\nu} + \bar{\nu}_0)}{\Delta\bar{\nu}^2 + (\bar{\nu} + \bar{\nu}_0)^2} + \frac{\Delta\bar{\nu}^2 - \bar{\nu}_0(\bar{\nu} - \bar{\nu}_0)}{\Delta\bar{\nu}^2 + (\bar{\nu} - \bar{\nu}_0)^2} \right] \quad \dots (5)$$

$$= I.p.S \quad \dots (6)$$

where  $S$  is the shape function. The expression for the contribution of the Debye line at zero frequency to the net susceptibility at a frequency  $\bar{\nu}(\text{cm}^{-1})$  with the line width parameter  $\Delta\bar{\nu}_0$  is obtained by putting  $\bar{\nu}_0 = 0$  and taking half the value of  $I.p.$  in the expression (5) above. The expression is:

$$\delta_m' = \frac{I.p}{2} \left[ \frac{2\Delta\bar{\nu}_0^2}{\Delta\bar{\nu}_0^2 + \bar{\nu}^2} \right] \quad \dots (7)$$

Hence the net value of the magnetic susceptibility at a frequency  $\bar{\nu}$  taking into account the contributions of the nonresonant and resonant lines is:

$$\delta_m = \delta'_m + \delta''_m = I.P. \left[ \frac{\Delta\bar{\nu}^2 + \bar{\nu}_0(\bar{\nu} + \bar{\nu}_0)}{\Delta\bar{\nu}^2 + (\bar{\nu} + \bar{\nu}_0)^2} + \frac{\Delta\bar{\nu}^2 - \bar{\nu}(\bar{\nu}_0 - \bar{\nu}_0)}{\Delta\bar{\nu}^2 + (\bar{\nu} - \bar{\nu}_0)^2} + \frac{\Delta\bar{\nu}_0^2}{\Delta\bar{\nu}^2 + \bar{\nu}_0^2} \right] \dots (8)$$

The values of  $I.p.$  have been calculated at different pressures (Maryott and Birnham, 1955) and tabulated in Table I.

TABLE I

Values of intensity factor at different pressures and at  $20^\circ\text{C}$

	Pressure in Atmospheres			
	1	2	25	50
$I.p \times 10^6$	0.59	1.19	14.89	29.77

#### DISPERSION NEAR $2\text{CM}^{-1}$

The dispersion curves have been calculated for the individual lines at  $\frac{1}{2}$  atmospheric pressure where most of the lines are resolved and for the pressure broadened envelope at higher pressures. The value of the line width parameter has been taken to be  $1.94 \text{ Mc/mm Hg}$  and its variation with pressure has been assumed to be linear. Table II gives the various frequencies of transitions (Artman 1953 and Burkhalter *et al.*, 1950) together with their relative intensities. The intensities have been calculated by the following formulae:

$$(I.\Delta\bar{\nu})_- = 2.917 \times 10^{-14} \frac{(\nu_k_-)^2(K+1)(2K-1)}{T^3 K} \exp \left[ -\frac{2.072K(K+1)}{T} \right] \frac{10^{-6}\text{cm}^{-1} \text{ MC}}{\text{mmHg}}$$

$$(I.\bar{\Delta\nu})_+ = 2.917 \times 10^{-14} \frac{(\nu_{k+})^2}{T^3} \frac{K(2K+3)}{K+1} \exp \left[ -\frac{2.072K(K+1)}{T} \right] \cdot \frac{10^{-6} \text{cm}^{-1} \text{Mc}}{\text{mm Hg}}$$

The value of  $(I.\bar{\Delta\nu})$  for the most intense transition  $J = 9$  to  $J = 10$  is  $41.01 \times 10^{-6} \text{ cm}^{-1} \text{ Mc/mm Hg}$ . Fig. 1 shows the complex dispersion pattern calculated at

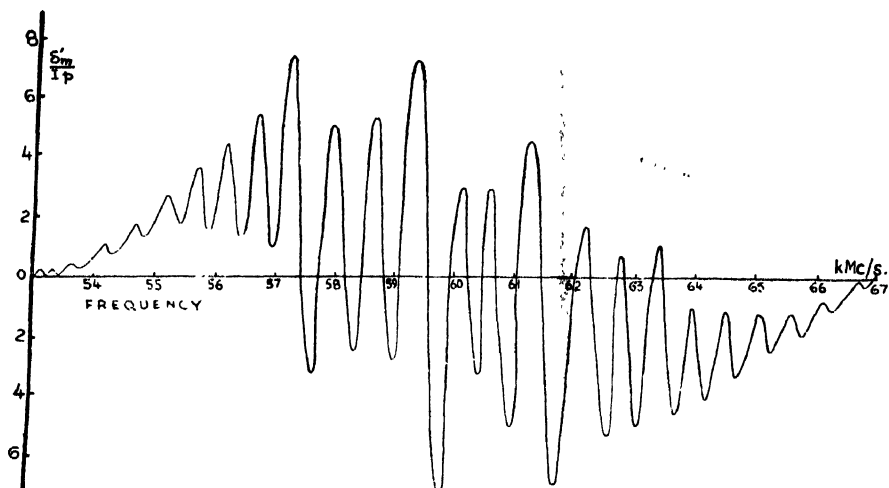


Fig. 1. Dispersion curves of oxygen at .25 atmospheric pressure in the  $2 \text{ cm}^{-1}$  region.

a pressure of  $\frac{1}{4}$  atmosphere for individual lines and then added up for all the lines. The relative intensities of the absorption lines are given in Table II. The lines lose their individuality at higher pressures and hence the curves drawn in Fig. 2 at pressures of 1, 10, 25, 50 atmosphere show single broad dispersion curves due

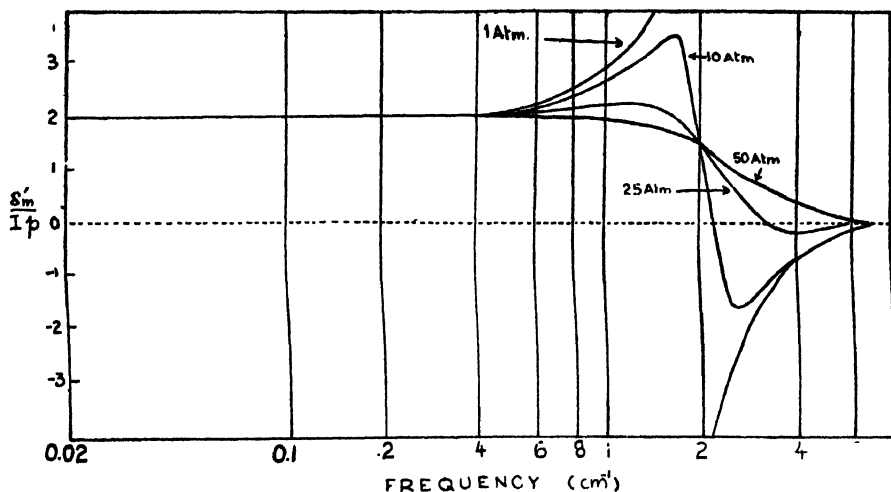


Fig. 2. Dispersion curves of oxygen at 1, 10, 25 and 50 atmospheric pressure in the wide frequency band due to the resonance line at  $2 \text{ cm}^{-1}$ .

to the envelope. It is observed that in case of oxygen low pressure conditions prevail even at one atmosphere pressure because of its small collision diameter ( $\sim 4 \text{ \AA}$ ) as compared to the average distance between the molecules ( $\sim 30 \text{ \AA}$ ).

TABLE II

K	Negative transitions $J = K \rightarrow J = K - 1$		Positive transitions $J = K \rightarrow J = K + 1$	
	Frequency	Intensity	Frequency	Intensity
1	118.750 kMc/s	0.732	56.265 kMc/s	0.205
3	62.486	0.631	58.446	0.560
5	60.306	0.840	59.592	0.823
7	59.163	0.930	60.435	0.972
9	58.324	0.909	61.152	1.000
11	57.612	0.804	61.800	0.926
13	56.969	0.654	62.412	0.796
15	56.363	0.492	62.998	0.616
17	55.784	0.348	63.568	0.447
19	55.221	0.226	64.128	0.356
21	54.673	0.139	64.679	0.194
23	54.130	0.080	65.223	0.116
25	53.592	0.043	65.762	0.065
27	53.066	0.022	66.296	0.034
29	×		66.828	0.017

### DEBYE DISPERSION

Contribution to the magnetic susceptibility of the gas by the diagonal component of the matrix element magnetic dipole moment has been calculated on the basis of expression (7). Since the exact value of  $\bar{\Delta\nu}_0$  is still not known, dispersion curves are plotted in Fig. 3 for the value of  $\bar{\Delta\nu}_0 = 0.02 \text{ cm}^{-1}/\text{atmosphere}$  at pressures of 1, 2, 20 and 50 atmospheres. The dispersion is very sharp at low pressures and as the pressure is increased, it broadens and extends to the higher frequency region.

The net value of the magnetic susceptibility of the gas can be obtained by adding the two component values from the graphs or calculating it from the general



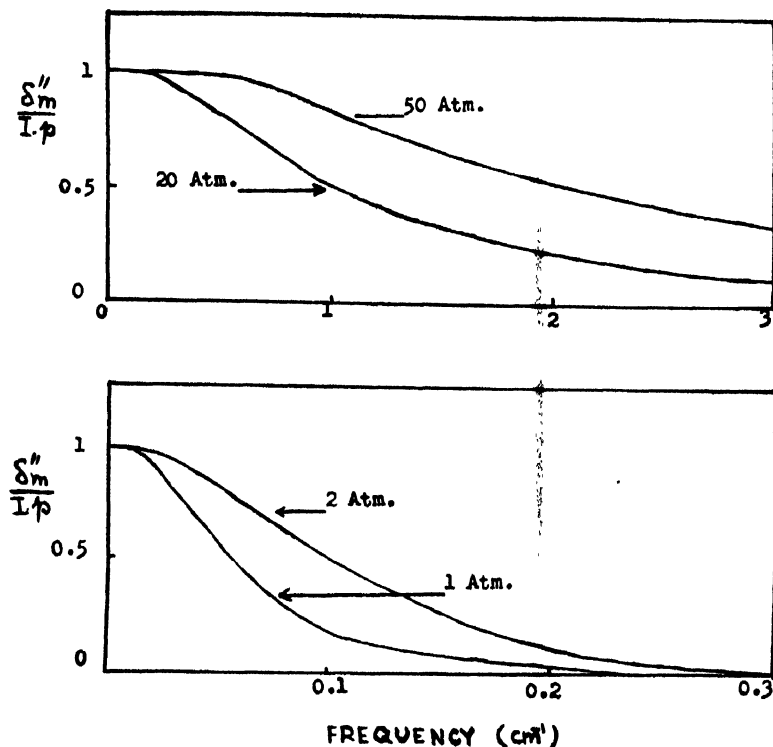


Fig. 3. Dispersion curves of oxygen at 1, 2, 20 and 50 atmospheric pressure in the wide frequency band due to the nonresonant or Debye line at zero frequency.

expression (8). The value of static magnetic susceptibility at one atmospheric pressure and 20°C comes out to be :

$$\begin{aligned}
 (\mu' - 1)_0 &= \delta'_{m0} + \delta'_{n0} \\
 &= 3 I \cdot p = 1.78 \times 10^{-6}.
 \end{aligned}$$

This value compares very well with the value of  $(\mu' - 1)$  as  $1.8 \times 10^{-6}$  quoted by Birnbaum *et al* (1951). More experimental work specially at higher wavelengths is needed in this direction.

#### REFERENCES

- Artman, J. O., 1953 Columbia Rad. Lab. Report, June 1.  
 Birnbaum, G., S. J. Kryder and H. Lyons, 1951, *J. Appl. Phys.*, **22**, 95.  
 J. H. Burkhalter, R. S. Anderson, W. V. Smith and W. Gordy, 1950, *Phys. Rev.* **79**, 651.  
 Maryott, A. A. and Birnbaum, 1955, *G., Phys. Rev.*, **99**, 1886.  
 Prem Swarup, 1956, *Phys. Rev.*, **104**, 89.  
 Townes, C. H. and Schawlow, A. L. 1955, *Microwave Spectroscopy* (McGraw Hill).  
 Van Vleck, J. H., 1947, *Phys. Rev.*, **71**, 413.  
 Van Vleck, J. H. and Weisskopf, V. F., 1945, *Rev. Mod. Phys.*, **17**, 227.

# A MINIMISATION METHOD OF BOOLEAN FUNCTIONS

AMARENDRA MUKHOPADHYAY

INSTITUTE OF RADIO PHYSICS AND ELECTRONICS,

UNIVERSITY OF CALCUTTA

(Received June 10, 1960)

**ABSTRACT.** Algebraic, graphical, chart and numerical methods of minimisation of Boolean Functions have been proposed by several authors (Karnaugh, 1953; McClusky 1956; Shannon, 1938; staff of Harvard computation laboratory, 1951 and Troye, 1959). These methods aim at improving the design of switching circuits which are extensively employed now a days in digital equipments. In the present paper we shall put forward a method of minimisation which has been developed by a combination of the principles underlying the methods of Svoboda and McClusky. In particular, a procedure has been suggested which reduces to a great extent the number of trial-repetitions required to minimise functions which form into a cyclic basic cell chart.

## INTRODUCTION

### (a) *The minimal form*

Functions of Boolean variables, like the variables themselves, express the states of binary quantities. The function can have only two values 1 or 0, corresponding to the presence or absence of a particular state. A convenient way of describing the function is to specify in a table the value of the function for each combination of input conditions, such as shown in Table 1, for a three variable function  $f(x_1, x_2, x_3)$ .

TABLE I

$x_1$	$x_2$	$x_3$	$f$	Minterms	Decimal equivalent values of minterms
0	0	0	1	$x'_1x'_2x'_3$	0
0	0	1	0	$x'_1x'_2x_3$	1
0	1	0	0	$x'_1x_2x'_3$	2
0	1	1	1	$x'_1x_2x_3$	3
1	0	0	1	$x_1x'_2x'_3$	4
1	0	1	0	$x_1x'_2x_3$	5
1	1	0	0	$x_1x_2x'_3$	6
1	1	1	1	$x_1x_2x_3$	7

In canonical form,  $f$  can be expressed as

$$\begin{aligned} f &= x'_1 x'_2 x'_3 + x'_1 x_2 x_3 + x_1 x'_2 x'_3 + x_1 x_2 x_3 \\ &= \Sigma(0, 3, 4, 7) [\text{decimal mode of writing } f] \end{aligned}$$

The expression for  $f$  derived from the truth table, called the canonical expansion of  $f$ , can be written in several reduced forms by applying few theorems of Boolean Algebra. But when the function becomes complex, algebraic manipulation is not very helpful and we resort to special methods.

Of all the alternative expressions for  $f$ , we call one (and sometimes more than one) the "minimal form" which involves a minimum number of total operations. The number of operations equals the sum total of "Boolean product" operations to realise the reduced minterms and the "Boolean sum" operations to realise the expansion. It follows from this definition that a minimum of diode circuit elements will be required for physical realisation of the function expressed in the minimal form.

#### (b) *Neighbours, cells and weight*

The terms of the canonical form of a given  $n$ -variable Boolean function can be depicted by nodes of an  $n$ -dimensional cube. A single variable is depicted by two nodes connected by a line. With two variables ( $x_1, x_2$ ) we require four nodes connected by four lines. When there are  $n$  variables, we take  $(n+1)$  vertical dotted line, and number them 0, 1, 2, ...  $n$  from left. We construct  $n_{e_0}, n_{e_1}, \dots, n_{e_n}$  number of nodes over each of these lines respectively and name the nodes with binary numbers having no '1', one '1', two '1's, and so on up to  $n$  '1's, i.e. having index values  $r = 0, 1, 2, \dots, n$ , over the  $(n+1)$  vertical lines. These are then arranged from top to bottom over any line having increasing decimal equivalent value. Lines are then drawn between nodes which differ in exactly one variable and no line is drawn further. The vertices of the cube represent all possible minterms of the canonical expansion and the cube can be considered to be made up of cells (Urbano and Mueller, 1956).

0-cell or vertex	-a point	$k = 0$
1-cell	-a line	$k = 1$
2-cell	-quadrilateral	$k = 2$
3-cell	-hexahedron	$k = 3$
$k$ -cell		$k = k$

where  $k$  denotes the order of the cells.

The nodes or vertices which are joined to a particular node or vertex, are called the neighbours or adjacent states of the vertex. The total number of

neighbours belonging to the body of the specified Boolean function with reference to a particular vertex is called the weight of the vertex, and this equals to the number of 1-cells incident with the vertex.

To illustrate the above terms let us take the function expressed in canonical form as

$$f(x_5, x_4, x_3, x_2, x_1, x_0) = \Sigma (0, 1, 3, 5, 7, 8, 10, 12, 15, 16, 17, \\ 21, 24, 26, 28, 29, 30, 32, 33, 34, 35, \\ 37, 39, 40, 42, 45, 46, 49, 50, 54, 55, \\ 58, 59, 60, 61, 62, 63) \quad \dots \quad (1)$$

We shall find all the cells incident with each vertex and also the weights of the vertices.

The above is a six-variable function. In Svoboda's method the function is first projected in a modified Veitch diagram. The different cells are found by using six contact grids and the weight of each vertex is found by using six directional grids (Svoboda, 1956 and Choudhury, 1959). Following McClusky (McClusky, 1956) we shall adopt a method in which the ideas of cells and weight can be directly incorporated and which can be easily extended to cover cases involving more than six variables.

To start with Table II is prepared as follows:

The decimal numbers corresponding to the vertices of the given function [Eq. (1)] are entered in column (a) in groups (indicated by separations) having increasing index values viz.,  $r = 0, 1, \dots 6$ .

The combinations entered in column (b) are selected from column (a) taking two numbers having index values  $r$  and  $r+1$  respectively when

$$M_{r+1} - N_r = 2^k \quad \dots \quad (2)$$

where  $k = 0, 1, 2 \dots$  and  $M_{r+1}, N_r$  are numbers belonging to the groups having index values  $r+1$  and  $r$  respectively. The terms in column (b) will then show all possible 1-cells present in the given function. The difference expressed by Eq.(2) is entered within brackets. Thus 1 and 3 form a 1-cell, but 1 and 10 will not form a 1-cell.

The combinations in column (c) are derived from column (b), taking two terms from any two consecutive groups (i.e. on two sides of a separation line) when their first difference [Eq.(2)] tally and the second difference between leading numbers is again positive and equals  $2^k$ , ( $k = 0, 1, 2, \dots$ ), these differences being indicated in brackets. The terms in this column show all possible 2-cells present in the given function. We need only enter cells whose vertices form an increasing sequence of decimal numbers.

Similarly, column (d) has been prepared from column (c) when both the first and second differences tally and the third difference between leading numbers is again  $2^k$ . The term in column (d) shows the only 3-cell present in the function.

Check marks are placed at any stage of combination when cells of a given  $k$ -value combine to form a cell of next higher order. We also check mark the cells which will give rise to alternative modes of formation of any higher order  $k$ -cell. Thus 1-cells 0, 1 (1) and 16, 17 (1) and also 0, 16 (16) and 1, 17 (16) are check marked since they form the 2-cell 0, 1, 16, 17 (1, 16). The unchecked cells are called the basic cells or the prime implicants of the given function.

Column (b) of Table II contains all information about the neighbours and weight of each vertex. The number of times a given vertex combine in this column is equal to its weight and the companions are its neighbours. Thus the vertex 1 has neighbour 0 in the top group and 3, 5, 17, 33 in the group just below the top, and we need not look down the column after the 1-cell 1, 33 (32), because 1 can never occur below this term. Hence weight of 1 is 5. Thus one can quickly compute the weight of each vertex, and find its neighbours, as listed in Table III.

### THE MINIMISATION METHOD

The determination of minimum sum essentially consists of selecting a minimum number of basic cells so that their sum gives the specified output for all combinations of input variables.

TABLE II  
Determination of cells

	(a) ✓	(b) ✓	(c)	(d)
$r = 0$	0 ✓	0, 1 (1) ✓	0, 1, 16, 17 (1, 16)— <i>W</i>	1, 3, 5, 7, 33, 35, 37, 39 (2, 4, 32)— <i>A</i>
	1 ✓	0, 8 (8) ✓	0, 1, 32, 33 (1, 32)— <i>V</i>	
	8 ✓	0, 16 (16) ✓	0, 8, 16, 24 (8, 16)— <i>U</i>	
$r = 1$	16 ✓	0, 32 (32) ✓	0, 8, 32, 40, (8, 32)— <i>T</i>	
	32 ✓	1, 3 (2) ✓	1, 3, 33, 35, (2, 32) ✓	
	3 ✓	1, 5 (4) ✓	1, 3, 5, 7, (2, 4) ✓	
	5 ✓	1, 17 (16) ✓	1, 5, 17, 21 (4, 16)— <i>S</i>	
	10 ✓	1, 33 (32) ✓	1, 5, 33, 37 (4, 32) ✓	
	12 ✓	8, 10 (2) ✓	1, 17, 33, 49 (16, 32)— <i>R</i>	
$r = 2$	17 ✓	8, 12 (4) ✓	8, 10, 24, 26 (2, 16)— <i>Q</i>	
	24 ✓	8, 24 (16) ✓	8, 10, 40, 42 (2, 32)— <i>P</i>	
	33 ✓	8, 40 (32) ✓	8, 12, 24, 28 (4, 16)— <i>O</i>	
	34 ✓	16, 17 (1) ✓	32, 33, 34, 35 (1, 2)— <i>N</i>	
	40 ✓	16, 24 (8) ✓	32, 34, 40, 42 (2, 8)— <i>M</i>	
	7 ✓	32, 33 (1) ✓	3, 7, 35, 39 (4, 32)	
	21 ✓	32, 34 (2) ✓	5, 7, 37, 39 (2, 32)	
	26 ✓	32, 40 (8) ✓	10, 26, 42, 58 (16, 32)— <i>L</i>	

TABLE II---(contd.)

Determination of cells

	(a) ✓	(b) ✓	(c)	(d)
$r = 3$	28 ✓	3,7(4) ✓	24,26,28,30(2,4)— <i>K</i>	
	35 ✓	3,35(32) ✓	33,35,37,39(2,4) ✓	
	37 ✓	5,7(2) ✓	34,42,50,58(8,16)--- <i>J</i>	
	42 ✓	5,21(16) ✓	26,30,58,62(4,32)— <i>I</i>	
	49 ✓	5,37(32) ✓	28,29,60,61(1,32)— <i>H</i>	
	50 ✓	10,26(16) ✓	28,30,60,62(2,32)— <i>G</i>	
	15 ✓	10,42(32) ✓	42,46,58,62(4,16)— <i>F</i>	
	29 ✓	12,28(16) ✓	50,54,58,62(4,8)— <i>E</i>	
	30 ✓	17,21(4) ✓	54,55,62,63(1,8)— <i>D</i>	
	39 ✓	17,49(32) ✓	58,59,62,63(1,4)— <i>C</i>	
$r = 4$	45 ✓	24,26(2) ✓	60,61,62,63(1,2)— <i>B</i>	
	46 ✓	24,28(4) ✓		
	54 ✓	33,35(2) ✓		
	58 ✓	33,37(4) ✓		
	60 ✓	33,49(16) ✓		
	55 ✓	34,35(1) ✓		
$r = 5$	59 ✓	34,42(8) ✓		
	61 ✓	34,50(16) ✓		
	62 ✓	40,42(2) ✓		
$r = 6$	63 ✓	7,15(8)— <i>b</i>		
		7,39(32) ✓		
		21,29(8)— <i>a</i>		
		26,30(4) ✓		
		26,58(32) ✓		
		28,29(1) ✓		
		28,30(2) ✓		
		28,60(32) ✓		
		35,39(4) ✓		
		37,39(2) ✓		
		37,45(8)— <i>Z</i>		
		42,46(4) ✓		
		42,58(16) ✓		
		50,54(4) ✓		
		50,58(8) ✓		
		29,61(32) ✓		
		30,62(32) ✓		
		39,55(16)— <i>Y</i>		
		45,61(16)— <i>X</i>		
		46,62(16) ✓		
		54,55(1) ✓		
		54,62(8) ✓		
		58,59(1) ✓		
		58,62(4) ✓		
		60,61(1) ✓		
		60,62(2) ✓		
		55,63(8) ✓		
		59,63(4) ✓		
		61,63(2) ✓		
		62,63(1) ✓		

TABLE III  
Determination of weight and neighbours

Vertex	Neighbours	Weight
0	1, 8, 16, 32	4
1	0, 3, 5, 17, 33	5
8	0, 10, 12, 24, 40	5
16	0, 24, 17	3
32	0, 33, 34, 40	4
3	1, 7, 35	3
5	1, 7, 21, 37	4
10	8, 26, 42	3
12	8, 28	2
17	1, 16, 21, 49	4
24	8, 16, 26, 28	4
33	1, 32, 35, 37, 49	5
34	32, 35, 42, 50	4
40	8, 32, 42	3
7	3, 5, 15, 39	4
21	5, 17, 29	3
26	10, 24, 30, 58	4
28	12, 24, 29, 30, 60	5
35	3, 33, 34, 39	4
37	5, 33, 39, 45	4
42	10, 34, 40, 46, 58	5
49	17, 33	2
50	34, 54, 58	3
15	7	1
29	21, 28, 61	3
30	26, 28, 62	3
39	7, 35, 37, 55	4
45	37, 61	2
46	42, 62	2
54	50, 55, 62	3
58	26, 42, 50, 59, 62	5
60	28, 61, 62	3
55	39, 54, 63	3
59	58, 63	2
61	29, 45, 60, 63	4
62	30, 46, 54, 58, 60, 63	6
63	55, 59, 61, 62	4

McClusky's method consists essentially of drawing a prime implicant table, selecting the basis rows, then ruling out each row which is covered by another. The first step is now repeated and the procedure continued until all the states are included or a cyclic prime implicant chart results. Then a trial repetition process is followed to obtain the minimal sum.

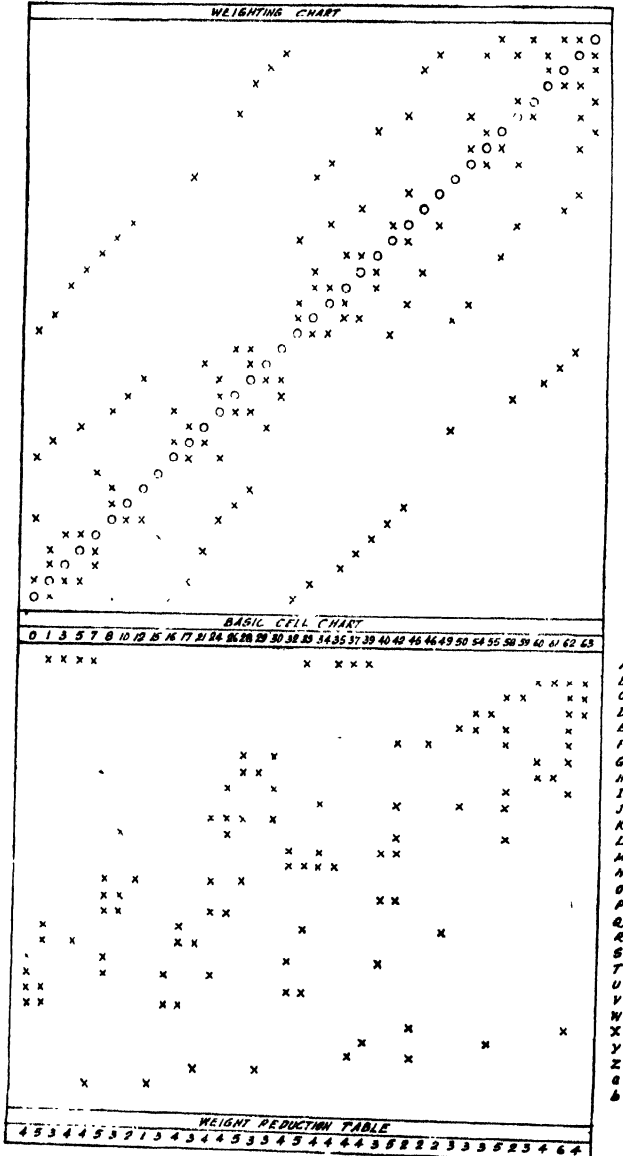


Fig. 1. The basic-cell chart, the weighting chart and the weight reduction table for the function expressed by Eqn. (1).



Svoboda follows a few methodical steps realised by applying the contact grids and directional grids on a modified Veitch diagram. We shall adapt these steps to McClusky's chart, with some obvious advantages. The method may be illustrated by taking the example of minimising the function given in Eq. (1).

A basic cell chart, which is what McClusky calls "the prime implicant table", is first drawn (Fig. 1). The columns carry at their heads the decimal numbers corresponding to all the vertices which are contained in the expression of the function and the horizontal rows correspond to basic cells. The vertices which combine to form a basic cell are cross-marked at the intersections with the horizontal row representing the particular basic cell. Thus the basic cell Z has been formed by combining 1, 3, 5, 7, 33, 35, 37, 39 and crosses in the A row are placed under these columns only and so on for all other rows.

We shall now introduce one new chart and a table. Over the basic cell chart, a weighting chart is placed which depicts all the neighbours of each vertex and hence determines the weight of the latter. This chart is drawn from the data in Table III or directly from column (b) of Table II or, if anybody prefers, with the help of a Karnaugh map. Small circles are entered over each of the vertex of the given function in successive horizontal lines so that the circles are located over a diagonal line. Crosses entered in the horizontal line are the neighbours of the vertex represented by the circle in that horizontal line. Thus, crosses corresponding to 1, 8, 16, 32, are the neighbours of the circle representing the vertex 0. The weighting chart has the interesting property that it is symmetrical about the diagonal line.

Below the basic cell chart, a weight reduction table is formed. In the first row of this table, weights of all vertices computed from the weighting chart are entered under corresponding columns.

We shall now proceed to utilise Svoboda's methodical steps (Svoboda, private communication) to obtain the minimal form.

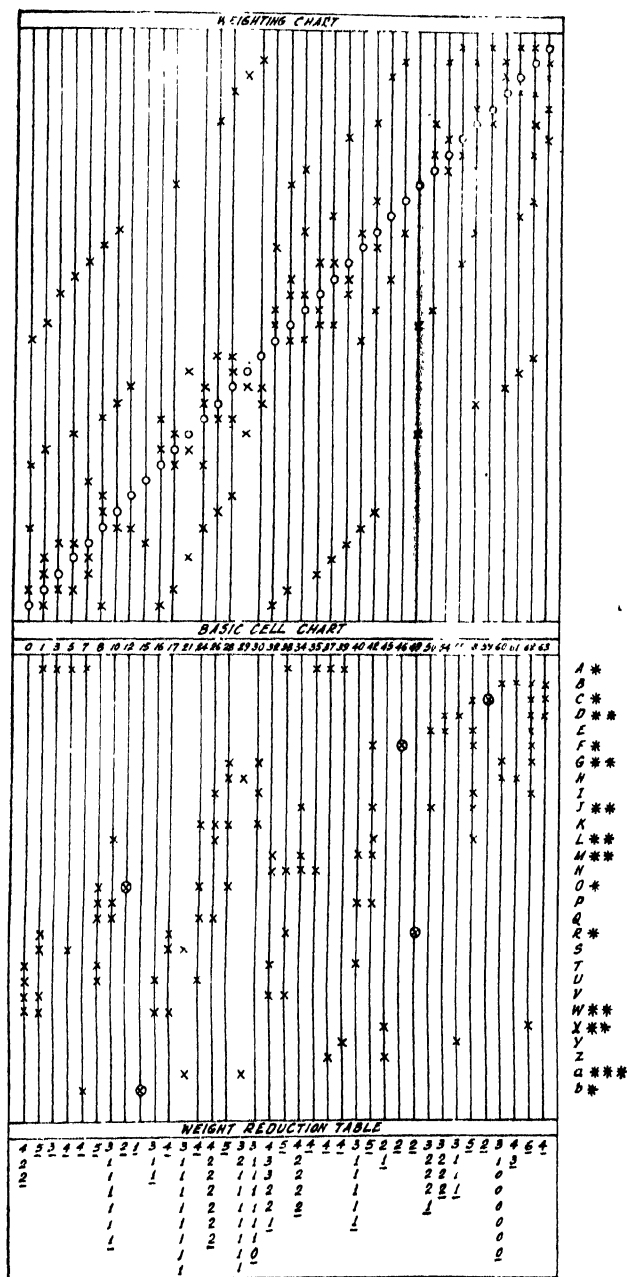
# FIRST STEP

The terms which are essential for inclusion in all possible minimal forms satisfy the theorem:

"Theorem I: The sufficient condition for inclusion of a term  $T$  in (any of) the minimal forms of the function is the incidence of the corresponding  $k$ -cell  $t$  with a vertex  $V$  of weight  $k$ ".

We begin with cells having smallest weight. If the weight of a vertex is zero or one, one always obtains a term satisfying the above condition. In Fig. 3 there is no vertex with weight  $k = 0$ . The vertex 15 has weight  $k = 1$  and there is the 1-cell b(7, 15) in row (b), which therefore is an essential term. Again, the vertices 12, 46, 49, 59 have weights  $k = 2$ , and to each of them is incident one





**Theorem I.** We do not require to look into the vertices of weights  $k = 4, 5, 6$ , since it is evident from Table II, that for the function in question, there is no cell of order 4, 5, or 6.

Thus, by the first methodic step we have selected rows A, C, F, O, R, b, marked by asterisk at the extreme right of the rows (Fig. 2). It is interesting to note that this step is identical with the first step in McClusky's method e.g., finding the columns which contain only one cross and selecting the rows as the basis rows in which these crosses occur.

All the columns in which the essential rows have entries are lined out, because the vertices corresponding to these columns have become bound to the chosen configuration of cells in the first step. The lining out is also extended to the weighting chart so that the free neighbours of the free vertices become apparent (see Fig. 2).

*Definition :* The free weight  $W$  of a vertex  $V_0$  is equal to the number of 1-cells belonging to the body of the Boolean function incident with the vertex  $V_0$  and incident with  $W$  free vertices  $V_1, V_2 \dots V_W$ . The vertices  $V_1, V_2 \dots V_W$  are called free neighbours of the vertex  $V_0$ .

The reduced or the free weights of free vertices are now easily computed by counting the number of unrulcd crosses occurring in the horizontal line for any vertex. Thus for the free vertex 0, we find the number of unrulcd crosses is equal to 2 corresponding to the free neighbours 16 and 32. Hence the reduced weight of the vertex is 2. The weighting chart, therefore, not only enables to compute the reduced weight, but also shows which neighbours of a particular vertex are still free.

The reduced weight of each free vertex is computed and entered in the second row of the weighting table, under corresponding columns of the vertices. Each of the vertices which is bound in the first step is marked in this table by putting a bar under the number representing its weight. The appearance of the charts is shown in Fig. 2.

## SECOND STEP

The second step is to select those terms which might be included in at least one of the minimal forms. For this we utilise the theorem :

**Theorem II :** A sufficient condition for a term  $T_{n+1}$  to be included in at least one of the minimal forms is satisfied when all the following propositions are true :

(1) The partial form  $F_n = T_1 + T_2 + \dots + T_n$  (corresponding to the body of all bound vertices built from cells  $t_1, t_2 \dots t_n$ ) has been included in one of the minimal forms.

(2) There is a  $K$ -cell  $t_{n+1}$  incident with a free vertex  $V_0$ , with all free neighbours  $V_1, V_2 \dots V_W$ , with free vertices  $V_{W+1}, V_{W+2}, \dots V_{W+p}$  and with any number of bound vertices ( $W \leq K$  being the free weight of the vertex  $V_0$ ).

- (3) There is no  $k$ -cell incident with the  $V_0$  and with another free vertex not belonging to the set  $V_0, V_1 \dots V_{W+p}$ .
- (4) All  $k$ -cells incident with  $V_0$  have  $k \leq K$ .
- (5) The term  $T_{n+1}$  corresponds to the  $K$ -cell  $t_{n+1}$

In Fig. 4, the free vertex 45 has free weight  $W = 1$ . It will be seen that there is a  $K$ -cell  $X(45, 61)$  satisfying the sufficient conditions of Theorem II. Columns 45 and 61 are lined out and the lining out is extended to the weighting chart.

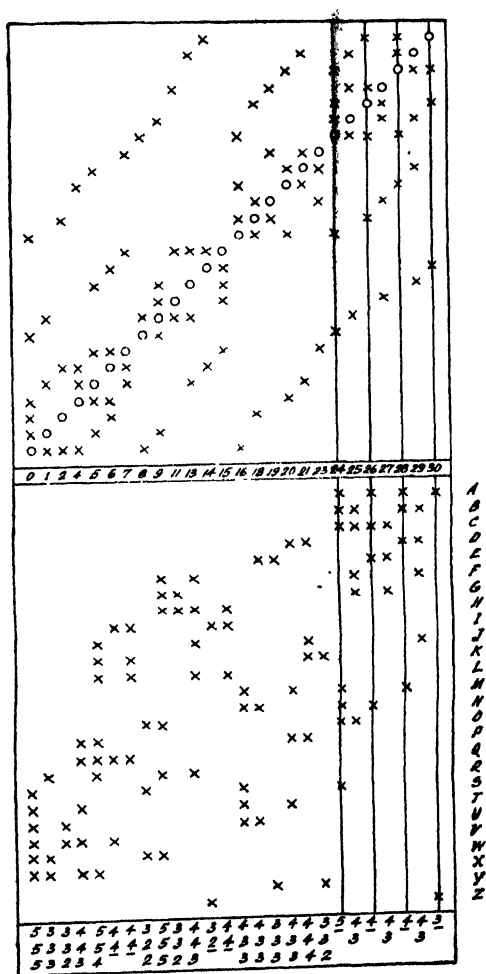


Fig. 4. Selection of cell A in the problem of minimising the function expressed in Eq. (iv).

Now, due to ruling out 61, weights of 60 and 29 are reduced further by unity. The weights for other free vertices remain unchanged. The free-weights are now written in the third row of the weighting table (Fig. 3).

The vertex 60 has free weight  $W = 0$ , but no cell incident on it (e.g., B, G, H) satisfies the sufficient condition of Theorem II, because with B, the vertex 30 of  $G$  or vertex 29 of  $H$  are not covered. Similar arguments apply to cells G or H. From the vertices having free weight  $W = 1$ , are incident 2-cells  $U$  and  $W$  with 16; both of these take all the free neighbours—here 0 only—of 16. Also  $K = 2 > W = 1$ ; all  $k$ -cells have  $k = K$ , so that we can take either. But for vertex 10, cell  $L$  takes its only free neighbour 26, but there is a cell  $P$  incident with 10 containing the vertex 40 which is not included in cell  $L$ ; hence  $L$  cannot be included. The vertex 21 has  $W = 1$ . The cell 'a' incident with 21 takes its only neighbour 29, its  $K = 1 = W$ , but there is a  $k$ -cell  $S$  having  $k = 2 > K$ ; thus, it cannot be included. We can check similarly why cells incident with 29, 30, 40 for which  $W = 1$ , do not satisfy the conditions of Theorem II. But cell  $D$  incident with 55 having free weight  $W = 1$ , can be included.

Let us take  $W$ . The reduced weights of free vertices are shown in the fourth row of the weighting table.

Now, vertex 60 of  $W = 0$ , cannot still be included. With vertices 10, 21, 29, 30, 40, of weight  $W = 1$ , there is no cell incident satisfying conditions of Theorem II. With vertex 55 of weight  $W = 1$  is incident cell  $D$  which takes 55's only neighbour 54 and for this all  $k < K$ ; so row  $D$  is selected. The vertices 54, 55 are bound thereby. The weights of free vertices are computed and written in the fifth row of the weighting table. Another cell  $Y$  incident with 55 cannot be included. In the same way row  $J$  incident with 50 is selected and the free weights of the free vertices are reduced and entered in the sixth row of the weighting table. Next, row  $M$  incident with 32 is selected. The resulting reduced weights of the free vertices are shown in the seventh row of the weighting table. Now, two cells  $L$  and  $Q$  incident with 10, satisfy sufficient conditions for inclusion. We take  $L$  and reduce the weights of the free vertices. Note that when vertex 40 was unbound,  $L$  could not be included as an acceptable cell incident with 10). Next, incident with vertex 30 of  $W = 0$ , three cells, names,  $G, I, K$  satisfy sufficient conditions of inclusion. Let us take  $G$ , since it also bounds the free vertex 60 of free weight  $W = 0$ . The cells selected at the second step are indicated by two asterisks.

The form of the chart at this stage is shown in Fig. 3. Two vertices, 21 and 29 are still free, and Theorem II is not applicable to them.

### THIRD STEP

When both theorems I and II cannot be applied any further, the general procedure will be to start with a vertex having smallest free weight and pick out the minimal form by trying all possible cells covering the neighbours of the vertex, and completing the minimal form for each trial, by a repetition of the second methodic step. In case, the second step made after a trial does not include all

the free vertices, a second trial is to be made, repeating a third step followed by another repetition of a second step. From all the trials, we call the one minimal which introduces minimum number of operations.

In the example that we have chosen, this step is trivial. The vertices 21 and 29 are selected by cell 'a' marked by three asteriks and there is no other alternative.

Thus one of the minimal forms of the Boolean Function given by Eq. (i) is

$$\begin{aligned} f &= A + C + F + O + R + b && \text{(first step)} \\ &+ X + W + D + J + M + L + C && \text{(second step)} \\ &+ a && \text{(third step)} \quad \dots \text{ (iii)} \end{aligned}$$

To write the algebraic equivalent of a basic cell, for example, of the cell *F* given by 42, 46, 58, 62(4, 16) we write the leading number 42 in binary form, eliminate variable  $x_k$  whenever a difference  $2^k$  appears in the bracket, and for the remaining digits '1' stands for an unprimed variable and '0' for a primed variable.

$2^k$	$k$	$x_5$	$x_4$	$x_3$	$x_2$	$x_1$	$x_0$	$F$
4, 16	2, 4	1	$\phi$	1	$\phi$	1	0	$= 42 \quad x_5 x_3 x_1 x'_0$

and so on for the other cells.

We can also obtain alternative minimal forms by interchanging cells without increasing the number of operations. Thus, we have seen that interchange is possible between *W* and *U* or *L* and *Q*, which will produce three more minimal forms. We also note that if *L*, *M* and *D* are not eliminated, we could interchange *J* with *E* producing a fourth minimal form and so on.

#### MODIFIED THIRD STEP AND CYCLIC BASIC CELL CHART

The third step of trial-repetition in both Svoboda's and McClusky's method is not very smooth. In fact when the cyclic basic cell chart (\*) is considerably complex, there is no way out to break through the structure in McClusky's method. In Svoboda's method, however, there is one clue: start with vertices of smallest weights. At this point a modification might be introduced which will reduce the number of trial repetitions to a great extent. The modification is as follows:

(a) Start always with a vertex having smallest weight.

(b) Select the cell incident with the vertex which includes all the neighbours of the vertex. In case there are more than one such cells, selection of any one of them will suffice. But, if cells are incident with the chosen vertex which include not only the neighbours but other non-neighbour free vertices, select that row which includes the maximum number of non-neighbour free vertices. If this

\*A basic cell chart is here said to be cyclic when with none of the vertices is incident a cell satisfying the conditions of both Theorem I and II.

number be the same for more than one cell, selection of any one of them will suffice.

(c) If a cell incident with a chosen vertex does not include all neighbours, select that cell which covers the maximum number of neighbours, and if there are more than one such cell, selection of any one of them will suffice. But, if there are cells incident with the vertex which not only includes the same maximum number of neighbours, but also some other non-neighbour free vertices, select that cell which includes the maximum number of non-neighbour free vertices. If this latter number be the same for more than one cell, selection of any one of the mwill suffice.

After each selection of a cell in (b) or (c), reduce the weights of the free vertices and repeat the procedure until all the vertices are bound.

To illustrate the above procedure we choose a problem which can not be readily solved by McClusky's trial repetition method. McClusky gave an approximate solution of this problem by his method of selecting consistent-row set (McClusky, 1956).

The problem is to obtain the minimum sum of

$$\begin{aligned} f(x_3, x_2, x_1, x_0) = & (0, 1, 2, 4, 5, 6, 7, 8, 9, 11, \\ & 13, 14, 15, 16, 18, 19, 20, 21, \\ & 23, 24, 25, 26, 27, 28, 29, 30) \end{aligned} \quad \dots \quad (iv)$$

The basic-cell chart, the weighting chart, and the weight reduction table are shown in Fig. 4. This is a cyclic basic cell chart. Incident with the vertex 30 of weight  $W = 3$ , there are two cells  $A$  and  $Z$ ; neither of them covers all the neighbours of 30 viz., 14, 26, 28 so that criterion (b) is not applicable. Since  $A$  takes two neighbours and also a non-neighbour vertex 24, while  $Z$  only one. We select  $A$  [criterion (c)]. Columns heading 24, 26, 28, 30 are lined out, lining out extended to the weighting charts, reduced weights of free vertices are written in the second row of the weighting table (See Fig. 4). Now, the vertices 8 and 14 have free weight  $W = 2$  and to both of them criterion (b) is applicable. The cell  $I$  incident with 14 takes two neighbours of 14 viz., 6, 15 and one non-neighbour free vertex 7. Also, cell  $W$  incident with vertex 8 takes the two neighbours of 8-0, 9 and one non-neighbour free vertex 1. Hence any one of the cells will do. Let us take  $I$ . The bound columns are lined out. Weights of the free vertices are reduced and entered in the third row of the weighting table. Now, vertices 2, 8, 11 have free weights  $W = 2$ . We can take either  $U$  or  $W$  or  $G$  at this stage, since all of them cover the free neighbours of 2, 8, 11 respectively and each has one non-neighbour free vertex, viz., 16, 1, 27 respectively. It is to be noted that vertex 23 also has free weight  $W = 2$ , but there is no cell incident covering all the free neighbours. Hence it is not considered. Let us take  $G$  and reduce the free weights.

The form of the charts after selection of  $A$ ,  $I$  and  $G$  is shown in Fig. 5. Now, the vertex 8 has minimum free weight  $W = 1$ . We can select either  $W$  or  $S$



[criterion (b)]. Let us take  $W$  and reduce weights of free vertices. Selection of  $U$  is now unique [criterion (b)]. Weights of free vertices are reduced and shown

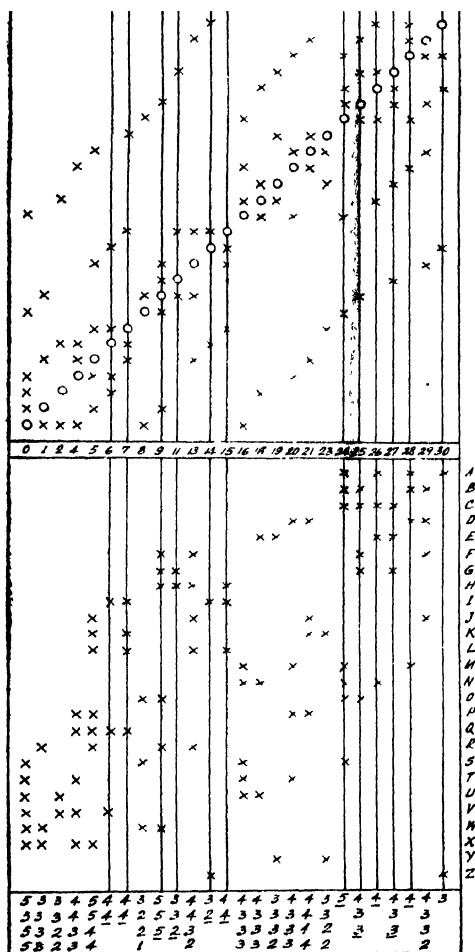


Fig. 5. The form of the charts after selection of cells  $A, I, G$ .

in the sixth row of the weighting table. Selection of  $Y$  is then unique. Free weights are reduced and shown in the seventh row. Then vertices 4, 13, 20, 29 have weights  $W = 2$ . Both 13 and 29 are covered by  $J$  and this cell besides providing for the neighbours, also include one non-neighbour free vertex. The cell  $P$  incident with 20, also satisfies similar conditions; let us, however, take  $J$ . This reduces free weights of 4 and 20 to  $W = 1$ . The condition of the charts is now shown in Fig. 6. We can include the vertices 4 and 20 at a time either by  $T$  or  $P$ . Let us take  $T$ . The minimal form, therefore, is

$$f = A + I + G + W + U + Y + J + T \quad \dots \quad (v)$$

There are situations when all the alternative minimal forms can be obtained directly from one minimal form by interchange of variables or by priming variables or by both. For example, let us take the four variable function

$$f(x_3, x_2, x_1, x_0) = (0, 1, 3, 5, 8, 10, 11, 13, 15) \quad \dots \quad \text{(vii)}$$

The basic-cell chart, weighting chart and weight reduction table (for two trials) are shown in Fig. 7. If we start with vertex 0 and select cell *A* applying criterion (c) we shall obtain the minimum sum as

$$f_1 = A + F + G + E + \overset{\circ}{I} \quad \text{(viii)}$$

The sequence of operation is evident from weighting Table I. If, instead of *A*, we start with cell *B*, we shall obtain the solution (weighting Table II)

$$f_2 = B + H + C + G + \overset{\circ}{I} \quad \text{(ix)}$$

Now,  $f_2$  can be directly obtained from  $f_1$  by priming  $x_1$  and  $x_3$  and interchanging, since the above operation will leave the function unchanged; vertices 0, 1 are changed with vertices 10, 11 respectively so that cells *A*, *E*, *F* are changed to *H*, *B*, *C* respectively. This property of the function is called group invariance.

### CONCLUSION

A method of minimisation of Boolean Functions in the form of a minimum sum has been presented in this paper by applying the methodical steps of Svoboda on McClusky's chart with the help of a weighting chart and a weight reduction table. The merit of this method is that it can be conveniently extended to cover cases involving more than six variables whereas the application of Svoboda's method to such cases becomes considerably inconvenient. Furthermore, in this method the basic cells incident with any vertex are easily obtained by looking along the column representing the vertex, whereas in Svoboda's method they will have to be searched out by several trials involving tossing and turning of the grids having different combinations.

A modification has been suggested on the third step of trial-repetition, which is particularly useful for minimising functions which form into cyclic basic cell charts.

The introduction of weighting chart has greatly systemetised the advantages of the methods of both Svoboda and McClusky.

### ACKNOWLEDGMENT

The author wishes to express his indebtedness to Professor J. N. Bhar, D.Sc., F.N.I., for his keen interest in the work, and to Dr. A. K. Choudhury, M.Sc., D.Phil., for guidance and helpful discussions.

REFERENCES

- Caldwell, S. H., 1958, *Switching Circuits and Logical Design*, John Wiley, New York.
- Choudhury, A. K., 1959, *Journal of Inst. of Telecom. Engineers*, 5, June.
- Karnaugh, M., 1953, *Trans. A.I.E.E.*, 72, Part I, Nov.
- Keister, W., Ritchie, A. E., Washburn, S., 1951, *The Design of Switching Circuits*. D. Van Nostrand Co. Inc., New York.
- McClusky, E. J. (Jr.), 1956, *Bell System Tech. Jour.*, 35, 1417-1444.
- Phister, Montgomery, Mr., 1958, *Logical Design of Digital Computers*. John Wiley & Sons, Inc.,
- Shannon, C. E., 1938, *Trans. A.I.E.E.*, 57, 713-723.
- Svoboda, A., "Some Applications of Contact Grids" (Private Communication).
- Svoboda, A., 1956, N.T.F-4, *Nachrichtentechnische Fachberichte, Beihefte der NTZ*, Publ. Fr. Vieweg & Sohn, Braunschweig "Graphical-mechanical aids for the synthesis of relay circuits".
- Staff of Harvard Computation Laboratory, 1951, *Synthesis of Electronic Computing and Control Circuits*. Harvard University Press.
- Troye, N. C. de., 1959, *Philips Research Reports*, 14,
- Urbano, R. H. and Mueller, R. K., 1956, *I.R.E. Trans. on Electronic Computers* EC-5, Sept.



# VARIOUS APPROXIMATIONS FOR THE ISOTOPIC THERMAL DIFFUSION FACTOR. I. APPLICATION TO HELIUM ISOTOPES

S. C. SAXENA AND P. A. PARDESHI

CHEMISTRY DIVISION, ATOMIC ENERGY ESTABLISHMENT TROMBAY, BOMBAY, INDIA

(Received, September 8, 1960)

**ABSTRACT.** Various formulae for the isotopic thermal diffusion factor have been reviewed and a new formula has been derived. Numerical calculations have been performed for the particular case of  $\text{He}^3$ - $\text{He}^4$  in a region where quantum effects are negligible. These calculations establish the relative adequacy of a comparatively simpler formula advanced by us and will be useful to interpret the recent experimental results of Saxena, Kelley and Watson on the thermal diffusion factor as a function of temperature.

## 1. INTRODUCTION

Knowledge of the thermal diffusion factor for helium isotopes is important, for thermal diffusion has been used by McInteer, Aldrich and Nier (1948) and Schuette, Zucker and Watson (1950) to enrich  $\text{He}^3$  despite its extremely low abundance ( $1.3 \times 10^{-4}\%$ ) in natural helium and still lower abundance for well helium. Measurements of the isotopic thermal diffusion factor,  $\alpha_T$ , as a function of temperature are also important to investigate the intermolecular forces. Moran and Watson (1958) measured the thermal diffusion factor for  $\text{He}^3$ - $\text{He}^4$  in the temperature range 233°K to 571°K by using an elegant apparatus "Trennschaukel" introduced by Clusius and Huber (1955). Recently Saxena, Kelley and Watson (1960) have extended these measurements to still lower temperatures. These measurements show a much steeper temperature dependence for  $\alpha_T$  than given by the existing theoretical expressions. Approximate quantum mechanical calculations of  $\alpha_T$  by Saxena (1960) reveal that the quantum corrections are negligible even at the lowest temperature (233°K). Thermal diffusion factor like other transport properties, emerges from the theory as the ratio of infinite determinants, Chapman-Cowling (1953). There are two alternative procedures developed separately by Chapman and Cowling (1953) and by Kihara (1949) to expand these infinite determinants into infinite convergent series. The use of varying number of terms of these series lead to the various approximations on the two schemes. As Moran and Watson (1958) compared their experimental results only with an approximate formula, valid more rigorously for a mixture of heavy isotopes, it would be interesting to explore the possibility of this anomaly

in the use of an inadequate theoretical expression. The purpose of the present paper is to evaluate  $\alpha_T$  for  $\text{He}^3\text{-He}^4$  according to the expressions derived on the two approximation schemes. This will establish the relative usefulness and limitations of the various formulae. A new formula has been derived on the Kihara approximation scheme, taking into consideration terms containing upto the second power of the reduced mass.

## 2. GENERAL FORMULAE FOR THE ISOTOPIC THERMAL DIFFUSION FACTOR

The Chapman-Enskog kinetic theory of gases expresses the  $m$ -th Chapman-Cowling approximation for  $\alpha_T$  as follows:

$$[\alpha_T]_m = \frac{5}{2} [X_1 \dot{X}_2 A_{00}^{(m)}]^{-1} \left[ X_1 A_{01}^{(m)} \left( \frac{M_1 + M_2}{2M_1} \right)^{\frac{1}{2}} + X_2 A_{0-1}^{(m)} \left( \frac{M_1 + M_2}{2M_2} \right)^{\frac{1}{2}} \right]. \quad (1)$$

Here  $X_1$  and  $X_2$  are the mole fractions of the two components of molecular weights  $M_1$  and  $M_2$  respectively. The quantity  $A^{(m)}$  represents a determinant of  $(2m+1)$  order, the general term of which is  $a_{ij}$  where  $i$  and  $j$  range from  $-m$  to  $+m$  including zero. The minor of  $A^{(m)}$  obtained by deleting the row and column containing  $a_{ij}$ , is denoted by the symbol  $A_{ij}^{(m)}$ . To the first approximation, Eq.(1) can be written into the following convenient form:

$$[\alpha_T]_1 = \frac{(6C^* - 5)(X_1 S_1 - X_2 S_2)}{X_1^2 Q_1 + X_2^2 Q_2 + X_1 X_2 Q_{12}}, \quad \dots \quad (2)$$

where

$$S_1 = \left[ \frac{M_1}{M_2} \left( \frac{2M_2}{M_1 + M_2} \right)^{\frac{1}{2}} A^* - \frac{4M_1 M_2 A^*}{(M_1 + M_2)^2} - \frac{15M_2(M_2 - M_1)}{2(M_1 + M_2)^2} \right],$$

$$Q_1 = \left[ \frac{2}{M_2(M_1 + M_2)} \left( \frac{2M_2}{M_1 + M_2} \right)^{\frac{1}{2}} A^* \left\{ \left( 5 - \frac{6}{5} B^* \right) M_1^2 + 3M_2^2 + \frac{8}{5} M_1 M_2 A^* \right\} \right],$$

and

$$Q_{12} = \left[ 15 \left( \frac{M_1 - M_2}{M_1 + M_2} \right)^2 \left( 5 - \frac{6}{5} B^* \right) + \frac{4M_1 M_2 A^*}{(M_1 + M_2)^2} \left( 11 - \frac{12}{5} B^* \right) + \frac{8}{5} \left( \frac{M_1 + M_2}{M_1 M_2} \right)^{\frac{1}{2}} A^{*2} \right].$$

The expressions for  $S_2$  and  $Q_2$  are obtained from those of  $S_1$  and  $Q_1$  by an interchange of the subscripts for the molecular masses. Here the functions  $\Omega^{(b,n)*}$  are the reduced Chapman-Cowling collision integrals and the functions  $A^*$ ,  $B^*$  and  $C^*$  are ratios of  $\Omega^{(b,n)*}$  and have been tabulated by Hirschfelder, Curtiss and Bird (1954) as a function of the reduced temperature. Second and higher

approximations are conveniently left in the determinant form of Eq. (1) for computational purposes.

For the case of heavy isotopes where the reduced mass,  $\frac{M_1 - M_2}{M_1 + M_2}$ , is small, Eq. (1) can be expanded in the powers of the reduced mass. Retaining terms only up to the first power of the reduced mass, one obtains;

$$[\alpha_T]_m = [\alpha_0]_m \left( \frac{M_1 - M_2}{M_1 + M_2} \right), \quad \dots \quad (3)$$

where  $[\alpha_0]_m$  is dimensionless thermal diffusion factor and has been given by Mason (1954, 1957a) for  $m = 1, 2$  and 3. For  $m = 1$ ,  $\alpha_0$  is given by

$$[\alpha_0]_1 = \frac{15(6C^* - 5)(2A^* + 5)}{2A^*(16A^* - 12B^* + 55)} \quad \dots \quad (4)$$

Expressions for  $m$  equal to 2 and 3 are rather lengthy and will not be repeated here.

Eq. (2) transforms into the following form for the case of heavy isotopes when one retains terms up to the second power of the reduced mass,  $M$ , (Chapman, 1941):

$$[\alpha_0]_1' = [\alpha_0]_1 [1 - \gamma M(X_1 - X_2)], \quad \dots \quad (5)$$

where

$$\gamma = \frac{3(5 - A^*)}{2(5 + 2A^*)} - \frac{2(12B^* + 5)}{(16A^* - 12B^* + 55)}.$$

It is interesting to note that  $[\alpha_0]_1'$  is now dependent on the relative proportions of the two isotopes unlike Eq. (4).

Kihara (1949) developed an alternative scheme to expand these infinite determinants into convergent infinite series. This procedure is mathematically less straightforward than that of Chapman-Cowling but it has a more physical basis and gives simpler expressions at least in the earlier approximations. Recently, Mason (1957a) has elaborated and extended this procedure and has given the expression upto the second approximation for the thermal diffusion factor. The general formula for the  $m$ -th approximation to the thermal diffusion factor on Kihara scheme remains the same as given by Eq. (1) except that now  $a_{ij}$  have different meaning. The first approximation  $[\alpha_T]_1$  is again given by Eq. (2) except that the  $Q$ 's are now defined as follows:

$$Q_1' = \left[ \frac{2}{M_2(M_1 + M_2)} \left( \frac{2M_2}{M_1 + M_2} \right)^{\frac{1}{2}} A^* \left\{ M_1^2 + 3M_2^2 + \frac{8}{5} M_1 M_2 A^* \right\} \right],$$

and

$$Q_{12}' = \left[ 15 \left( \frac{M_1 - M_2}{M_1 + M_2} \right)^2 + \frac{32 M_1 M_2 A^*}{(M_1 + M_2)^2} + \frac{8}{5} \frac{M_1 + M_2}{(M_1 M_2)^{\frac{1}{2}}} A^{*2} \right] \quad \dots (6)$$

Using the extended Kihara scheme, Mason (1957a) gave the following formula for the second approximation to  $\alpha_T$ :

$$[\alpha'_T]_2 = [\alpha_T]_1 (1 + K'_1) + K'_2, \quad \dots (7)$$

where

$$K'_1 = h_3 h_5 + h_4 h_{-6} + h_{-3} h_{-5} + h_{-4} h_6, \quad \dots (8)$$

and

$$\begin{aligned} K'_2 = & \frac{5}{2\bar{X}_1} \left( \frac{M_1 + M_2}{2M_2} \right)^{\frac{1}{2}} (h_{-1} h_{-5} + h_1 h_6 - h_2 h_4 + h_{-2} h_3) \\ & - \frac{5}{2\bar{X}_2} \left( \frac{M_1 + M_2}{2M_1} \right)^{\frac{1}{2}} (h_1 h_5 + h_{-1} h_{-6} - h_{-2} h_{-4} + h_2 h_{-3}). \quad \dots (9) \end{aligned}$$

In Eq. (7),  $[\alpha_T]_1$  is given by Eq. (2) and the various  $h_K$  are similar to those given by Mason (1957a) except that the subscripts characterising the molecular species are all the same.

For the case heavy isotopes,  $\alpha'_T$  can again be put in the form of Eq. (3), where  $[\alpha'_0]_1$  is now given by the following simpler form:

$$[\alpha'_0]_1 = \frac{15(6C^* - 5)}{16A^*} \quad \dots (10)$$

The second approximation  $[\alpha'_0]_2$  can be written in the following form:

$$[\alpha'_0]_2 = [\alpha'_0]_1 (1 + K'_0). \quad \dots (11)$$

Here  $[\alpha'_0]_1$  is given by the Eq. (4) and  $K'_0$  is a correction factor given by Mason (1957a).

Using Kihara's scheme for approximating transport coefficients, we have worked out the following first approximation to the thermal diffusion factor for a mixture of heavy isotopes in which terms containing upto the second power of the reduced mass have been retained:

$$[\alpha'_0]_1' = [\alpha'_0]_1 \left\{ 1 - \frac{(5 - 3A^*)}{2(2A^* + 5)} M(X_1 - X_2) \right\}. \quad \dots (12)$$

This formula is slightly simpler than the one given by Eq. (5) and as shown in the next section, is very useful for the accurate evaluation of  $\alpha_T$  of isotopic mixtures



where  $M$  is not quite small. Such isotopic mixtures are the mixtures of helium and hydrogen isotopes.

### 3. CALCULATION OF THE THERMAL DIFFUSION [FACTOR FOR HELIUM

Detailed calculations for the thermal diffusion factor of helium have been performed on both the approximation schemes, according to the various formulae discussed in the previous section. The results of this calculation are tabulated in Table I and refer to the following  $L-J(12-6)$  law for intermolecular force:

$$E(r) = 4\epsilon \left[ \left( \frac{\sigma}{r} \right)^{12} - \left( \frac{\sigma}{r} \right)^6 \right]. \quad (13)$$

Here  $E(r)$  is the potential energy of the two molecules at a separation distance  $r$  and  $\sigma$  is the molecular separation for which the interaction energy is zero.  $\epsilon$  is the value of the maximum negative potential energy. The various collision integrals required for these calculations are tabulated by Hirschfelder, Curtiss and Bird (1954).<sup>\*</sup> In those calculations of Table I where the system has been treated as a binary mixture of  $\text{He}^3$  and  $\text{He}^4$ , we have chosen arbitrarily the concentration of  $\text{He}^3$  as 5%, a value close to the one used in the work of Moran and Watson (1958). Further, these calculations were performed on a desk calculator and have been subjected to only spot-checking.

TABLE I

Calculated values of the isotopic thermal diffusion factor for Helium

Chapman-Cowling approximation scheme					Kihara approximation scheme				
$T^*$	$[\alpha_T]_1^{mix}$	$[\alpha_T]_1^{iso}$	$[\alpha_T']_1^{iso}$	$[\alpha_T]_2^{mix}$	$[\alpha_T']_1^{mix}$	$[\alpha_T']_1^{iso}$	$[\alpha_T']_1^{iso}$	$[\alpha_T]_2^{mix}$	$[\alpha_T']_2^{iso}$
5	0.0671	0.0695	0.0677	0.0690	0.0702	0.0718	0.0707	0.0694	0.0716
7	0.0724	0.0751	0.0732	0.0747	0.0742	0.0759	0.0747	0.0755	0.0779
9	0.0744	0.0788	0.0753	0.0760	0.0779	0.0797	0.0785	0.0778	0.0803
20	0.0767	0.0794	0.0774	0.0803	0.0802	0.0820	0.0808	0.0809	0.0832
40	0.0768	0.0794	0.0774	0.0801	0.0802	0.0820	0.0808	0.0808	0.0832
60	0.0764	0.0791	0.0771	0.0799	0.0799	0.0816	0.0805	0.0804	0.0827
80	0.0763	0.0789	0.0769	0.0796	0.0797	0.0814	0.0803	0.0805	0.0826
100	0.0761	0.0787	0.0767	0.0794	0.0795	0.0812	0.0800	0.0800	0.0829
200	0.757	0.0781	0.0762	0.0784	0.0790	0.0806	0.0795	0.0797	—

<sup>\*</sup>It may be pointed out that there is a misprint in the value of the collision integ at  $\Omega(1,1)^*$  for  $T^* = 100$ . It should read as 0.5170 instead 0.5130.

In columns 2, 3, 4 and 5 of Table I are recorded the values of the different approximations to  $\alpha_T$  as a function of the reduced temperature ( $T^* = kT/\epsilon$ ) according to Chapman-Cowling scheme; while the columns 6, 7, 8, 9 and 10 report the results on Kihara scheme. Values of  $\alpha_T$  listed in columns 2 and 3 of Table I have been obtained according to the Eqs. (2) and (4) respectively. The two sets of values differ appreciably and reveal the fact that for Helium, terms involving only first power of the reduced mass are not enough; a result previously pointed out by Winter (1950). It is, therefore, interesting to consider terms involving still higher powers of  $M$ . Chapman (1941) derived an expression, Eq. (5), which takes into account the terms upto the second power of  $M$ . Calculated values according to this formula are given in column 4 of Table I. It will be seen that these values are appreciably different ( $\approx 2.4\%$ ) from  $[\alpha_T]_1^{iso}$  but are in good agreement with the  $[\alpha_T]_1^{mix}$  values ( $\approx 0.9\%$ ). Values of  $[\alpha_T]_2$  computed according to Eq. (1) with  $m = 2$  are shown in column 5. These values are approximately 4% higher than the  $[\alpha_T]_1^{mix}$  values, establishing thereby that the convergence of the series is fast enough and the error involved, because of the neglect of the third and higher approximations, is small. This inference is very welcoming in view of the fact that the higher approximations will involve evaluation of seven and higher order determinants and can be safely avoided till we considerably improve the precision and accuracy of the measurements. It is also very interesting to note that  $[\alpha_T]_1'^{iso}$  values are in better agreement with the  $[\alpha_T]_2^{mix}$  values than the  $[\alpha_T]_1^{mix}$  values. The authors therefore feel that the simple formula for  $\alpha_T$  as given by Eq. (5) is preferable to the complicated form of Eq. (2) and still more complicated form as given by Eq. (1).

Results obtained using similar approximations, but on Kihara scheme are listed in columns 6, 7, 8 and 9, and are seen to follow the same qualitative trend. In column 10 are tabulated for comparison the results obtained from a formula which considers terms upto the second approximation but retains only the first power of reduced mass, Saxena and Mason (1958). These values of  $[\alpha_T]_2'^{iso}$  are systematically higher than the  $[\alpha_T]_2^{mix}$  values. As the convergence for the Kihara approximation scheme is still faster than that of Chapman-Cowling, we are of the opinion that the neglect of the second power of the reduced mass is much more serious. A critical examination of all the values obtained on Kihara approximation scheme again leads to the same conclusion that the values obtained by using the simpler formula, Eq. (12), which considers terms upto the second power of reduced mass, is preferable to the rest of all, both for accuracy and simplicity.

A critical examination of the various approximations for  $\alpha_T$  on the two approximation schemes for realistic intermolecular potentials and for a few mathematically simple systems, was done by Mason (1957a and 1957b). Mason (1957b) considered three types of mixtures viz. (1) Lorentzian, (2) Quasi-Lorentzian and (3) Heavy isotopic mixtures. Unfortunately our system is not identical to any of these

but resembles to (3) in as much as all the interactions are identical but the two masses differ considerably. Our numerical calculations of Table I reveal that Kihara approximation scheme is preferable to Chapman-Cowling and is in conformity with the conclusions of Mason (1957b) for mixtures of heavy isotopes.

#### 4. CONCLUSIONS

Our numerical calculations for  $\alpha_T$  of helium isotopes establish that Kihara approximation procedure is better than that of Chapman and Cowling. With  $\text{He}^3$  present in trace, a simple formula derived, treating the mixture of  $\text{He}^3$  and  $\text{He}^4$  as a heavy isotopic mixture but retaining terms upto the second power of the reduced mass, will yield results within the range of experimental error. This formula is also preferable in view of comparative simplicity and accuracy.

#### ACKNOWLEDGMENT

The authors are thankful to Dr. J. Shankar for his kind interest and making available to us all the facilities.

#### REFERENCES

- Chapman, S., 1941, *Proc. Roy. Soc.*, **A177**, 38.  
 Chapman, S. and Cowling, T. G., 1953, *The Mathematical Theory of Non-Uniform gases*, Cambridge University Press, England.  
 Clusius, K. and Huber, M., 1955, *Z. Naturforsch.*, **10A**, 230.  
 Hirschfelder, J. O., Curtiss, C. F., and Bird, R. B., 1954, *The Molecular Theory of Gases and Liquids*, John Wiley & Sons, Inc., New York.  
 Kihara, T., 1949, *Imperfect Gases*, originally published in Japanese (Asakusa Book Store, Tokyo) and translated into English by the U.S. office of Air Research, Wright-Patterson Air Force Base, Chap. 6; see also 1953, *Revs. Modern Phys.*, **25**, 831.  
 Mason, E. A., 1954, *J. Chem. Phys.*, **22**, 169.  
 Mason, E. A., 1957a, *J. Chem. Phys.*, **27**, 75.  
 Mason, E. A., 1957b, *J. Chem. Phys.*, **27**, 782.  
 McInteer, B. B., Aldrich, L. T., and Nier, A. O., 1948, *Phys. Rev.*, **74**, 946.  
 Moran, T. L., and Watson, W. W., 1958, *Phys. Rev.*, **109**, 1184.  
 Saxena, S. C., 1960, unpublished calculations.  
 Saxena, S. C., Kelley, T. G. and Watson, W. W., 1960, In course of publication.  
 Saxena, S. C., and Mason, E. A., 1958, *J. Chem. Phys.*, **28**, 623.  
 Schuette, O. F., Zucker, A. and Watson, W. W., 1950, *Rev. Sci. Instr.*, **21**, 1016.  
 Winter, E. R. S., 1950, *Trans Faraday Soc.*, **46**, 81.

# X-RAY THERMAL DIFFUSE SCATTERING IN AZELAIC AND PIMELIC ACIDS\*

R. L. BANERJEE, M. L. CANUT AND J. L. AMOROS

Sección de Termodinámica Cristalina

DEPARTAMENTO DE CRISTALOGRAFIA. C.S.I.C. MADRID

(Received, November 9, 1960)

## Plate II

**ABSTRACT.** Thermal diffuse scattering of azelaic and pimelic acids is studied by X-ray diffraction methods and compared with the observed diffuse scattering in other dicarboxylic acids. The interpretation of such diffuse scattering is done both by considering the propagation of thermal elastic waves accordingly with the crystal structure and by using the difference Fourier transform approach which gives account of the extended continuous regions of diffuse scattering. Also, the dynamic symmetry of the crystals is studied as deduced from the consideration of the observed diffuse scattering.

The study of X-ray thermal diffuse scattering is interesting because it gives the unique insight of the dynamics of the crystal. The treatment of this problem is complicated and the thermal wave theory is perhaps the best approach to the question in simple (ionic) crystals. In molecular crystals, however, where there is evidently a far complicated atomic pattern, the problem can be reduced greatly by considering the fact that the molecules can be treated as rigid bodies and therefore most of its dynamical picture is given by the movement of big structural units, the molecules. A long term programme of research was developed in the Departamento de Cristalografía, Madrid, with the aim of elucidating the status of the molecular crystals. Many types of such crystals were studied (hexamine Canut and Amorós, 1958), pentaerythritol (Alonso *et al.*, 1958), naphthalene (Acha *et al.*, 1958), anthracene (Annaka and Amorós, 1960, etc.) and a general theory was given to explain the continuous thermal diffuse scattering discovered in such crystals (Amorós *et al.*, 1960). It is therefore of interest to check the theory in another group of molecular crystals for which no previous computations were made. The group of molecular substances chosen is that of the dicarboxylic acids with odd number of carbon atoms.

The interest of the present research lies in the fact that the dicarboxylic acids with even number of carbon atoms have already been studied (Canut and

---

\*This research was in part supported by the Directorate of Solid-State Sciences, Air Force Office of Scientific Research, through the European Office of Air Research and Development Command, under Contract AF 61(052)—193.

Amorós, 1957) and therefore a direct comparison of the two groups can easily be done and thereby a general picture of the lattice dynamics of long-chain compounds can be drawn.

#### ANTECEDENTS

The structure of pimelic acid  $\text{COOH}-(\text{CH}_2)_6-\text{COOH}$  has been determined by MacGillavry and his coworkers (1948). The crystal belongs to the monoclinic system and space group  $I\ 2/a$  and contains four molecules per unit cell.

The unit cell dimensions are :

$$a = 9.84 \text{ \AA}, \quad b = 4.89 \text{ \AA}, \quad c = 22.43 \text{ \AA} \quad \text{and} \quad \beta = 130^\circ 46'$$

The crystal structure of azelaic acid  $\text{COOH}-(\text{CH}_2)_7-\text{COOH}$  has not been determined as yet. According to Caspari (1928) the crystal belongs to the monoclinic system and contains four molecules per unit cell.

The unit cell dimensions are :

$$a = 9.72 \text{ \AA}, \quad b = 4.83 \text{ \AA}, \quad c = 27.14 \text{ \AA} \quad \text{and} \quad \beta = 129^\circ 30'$$

The space group of azelaic acid has not been determined, but a careful observation of the distribution of the diffuse scattering of azelaic acid studied in the present work reveals that the distribution of the diffuse maxima obeys the same extinction condition as those of pimelic acid, i.e.,  $h+k+l = \text{even}$ . Therefore, the space group of azelaic acid should be the same as that of pimelic acid, i.e.,  $I\ 2/a$ , and the crystal structures of the two acids should also be the same, except for the difference in length of the molecules.

While obtaining azelaic acid crystals at room temperature from a slightly warm acetone solution, we happened to obtain azelaic acid crystals of another modification stable at room temperature. Much earlier Caspari (1929) obtained a high temperature modification of azelaic acid by slowly cooling down a hot solution of the acid.

Later, Dupré La Tour (1935) obtained this modification by slowly cooling down the azelaic acid melt.

The lattice constants of the modification that we have obtained along with those of the modification obtained by Caspari are given below:

	$a$	$b$	$c$	$\beta$
Azelaic acid (II)	5.69 Å	9.57 Å	27.78 Å	136°39'
$\alpha$ -azelaic acid (9)	5.61 Å	9.58 Å	25.35 Å	136°10'

#### EXPERIMENTAL METHOD

Single crystals were obtained from an acetone solution. The crystal used in the experiment had the dimensions of about  $1.5 \times 1.0 \times 1.0 \text{ mm}^3$ . It was

mounted with its [010] axis vertical and considering its monoclinic symmetry. Laue photographs were taken at each  $5^\circ$  of a zone of  $180^\circ$ . Ilford industrial G films, filtered Cu  $K\alpha$  radiation at 40KV., 20mA, and a Unicam camera with cylindrical film holder was used. The exposure time was 2 hours. In order to register the thermal diffuse scattering on the reciprocal lattice level [010], the reciprocal co-ordinates  $\xi$  and  $\eta$  were measured for each diffuse spot with the help of the Wernicke Chart after subtracting the size of the corresponding Laue spot to correct for the crystal size and the divergence of the x-ray beam effects. We plotted the diffuse reflections on each reciprocal lattice level by using transparent paper and Martin's Chart (1956). This method saves much time in the tedious task of passing the photographic record of the diffuse scattering to the diffraction space (i.e. the reciprocal space). The crystal, x-ray beam orientation becomes unequivocally fixed when the diffuse scattering domains of each level of the reciprocal lattice are compared with the corresponding reciprocal lattice net, due to the fact that the thermal diffuse scattering maxima are always to be on the reciprocal lattice points.

#### Diffuse scattering domains in [010] of acetic acid

Laue patterns of dicarboxylic acids show two types of diffuse spots:

- Streaks, characteristic of the molecules in chains, extended between the reciprocal lattice points when plotted in it.
- Independent, round and definite spots, some of them very strong, giving a diffuse cloud around non-forbidden reciprocal lattice points.

With the [010] mounting of the crystals, the streaks always appear in the photograph setting the equator at right angles and extending across the higher levels (Fig. 1, Plate II).

#### [010] level :

The diffuse domains of this level are shown in the Fig. 2. The strongest round diffuse spot is associated with the reciprocal lattice point 200. The planes corresponding to this point contain the layers of the chains. Other round spots appear at the reciprocal lattice points with  $h = 2n$  and  $l = 2n$ , that is, at the non-forbidden ones. The most prominent of them being those associated with 200, 402, 602, 406, 4010, 4022, 6012, 6010, lattice points. Continuous diffuse scattering domains appear in the rows of the reciprocal lattice points having  $k = \text{const} = \text{even}$ .

The strongest continuous domains are extended along the rows with

$$l = 10, 16, 20, 22, 23$$

#### [010] level :

The round diffuse spots of this level (Fig. 3) follow the extinction condition

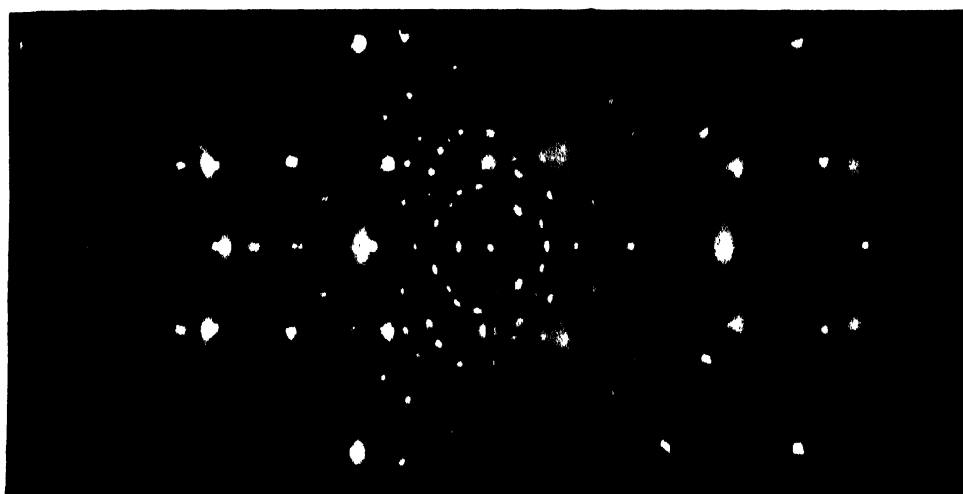


Fig. 1. Laue photograph. Azelaic acid. Vertical axis  $[010]$ .





The streaks of this level unlike those of the zero level, do not appear in the very well defined continuous zones of  $l = \text{const.}$

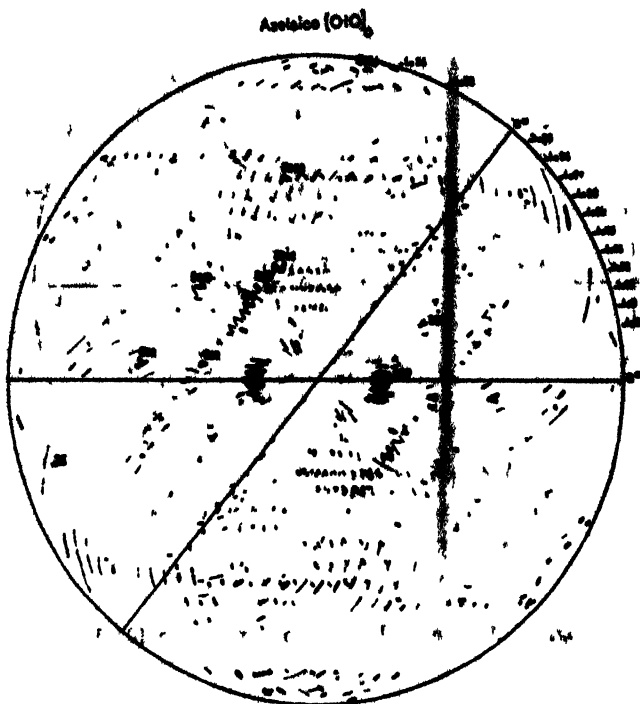


Fig. 2. Azelaic acid. Diffuse domains in  $[010]_c$ .

The strongest diffuse spots are associated with the following reciprocal lattice points:  $110$ ,  $21\bar{1}$ ,  $011$ ,  $310$ ,  $11\bar{2}$ ,  $11\bar{1}\bar{0}$ ,  $11\bar{2}$ ,  $21\bar{2}\bar{1}$ .

$[010]_c$  level:

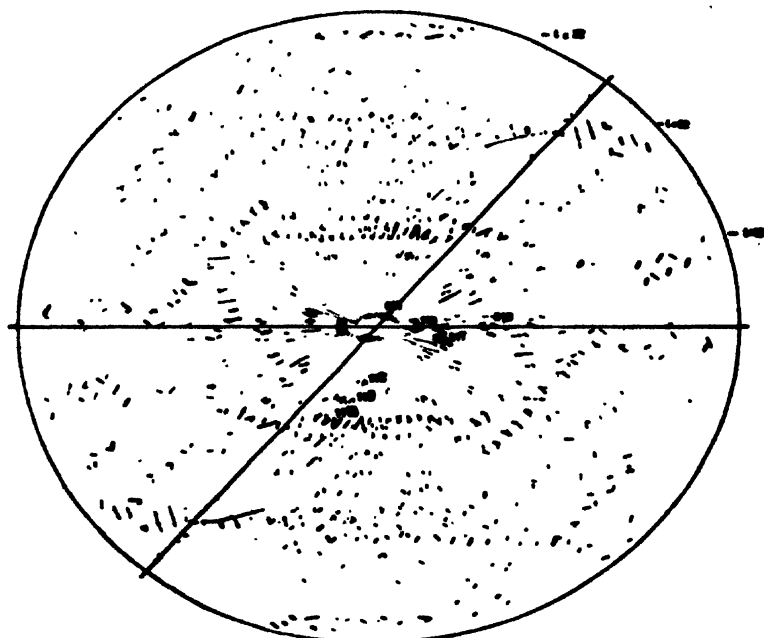
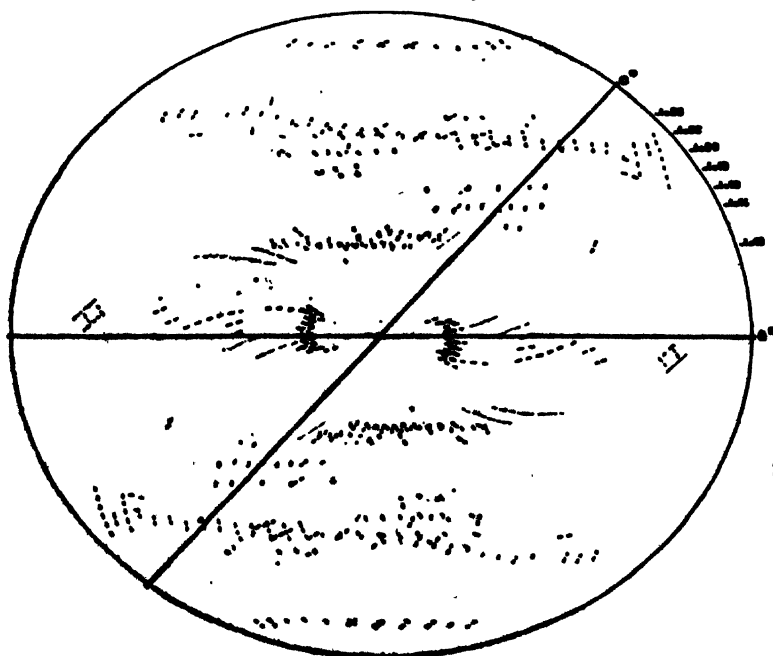
The plotting of the diffuse reflections in this inter-layer (Fig. 4) was done only for those which extend across the zero and the first levels.

Moderately strong continuous domains of diffuse scattering appear in this level extended along the rows of the reciprocal lattice points having  $l = 10, 22, 32$ .

Apart from this there appears a strong diffuse domain at  $2\frac{1}{2}0$  which is the section of the very strong round diffuse spot  $200$  of the zero level.

### THREE DIMENSIONAL ANALYSIS OF THE DIFFUSE SCATTERING

From the analysis of the domains of the continuous diffuse scattering, it is clear that these domains, which appear along the rows of reciprocal lattice points with  $l = \text{const.}$ , that is, perpendicular to the chain direction ( $c$  axis), in all the levels  $[010]_c$ ,  $[010]_c$ , and  $[010]_c$ , are actually sheets perpendicular to  $c$  axis of the crystal

Azelaic [010]<sub>1</sub>Fig. 3. Azelaic acid. Diffuse domains in  $[010]_1$ . $[010]_2$ Fig. 4. Azelaic acid. Diffuse domains in  $[010]_2$ .

in three dimensions. The sheets passing through the reciprocal lattice planes with  $l = 10, 22$  and  $32$  are the most prominent ones. These sheets are confined within a zone of  $90^\circ$  about the chain direction extending  $45^\circ$  on either side of it.

#### COMPARISON BETWEEN THERMAL DIFFUSE SCATTERING OF AZELAIC AND PIMELIC ACID

The morphology of the thermal diffuse scattering of pimelic acid has previously been studied by Canut and Amorós (1957). Fig. 5 shows the diffuse scattering domains of pimelic acid in the  $[010]_0$  level.

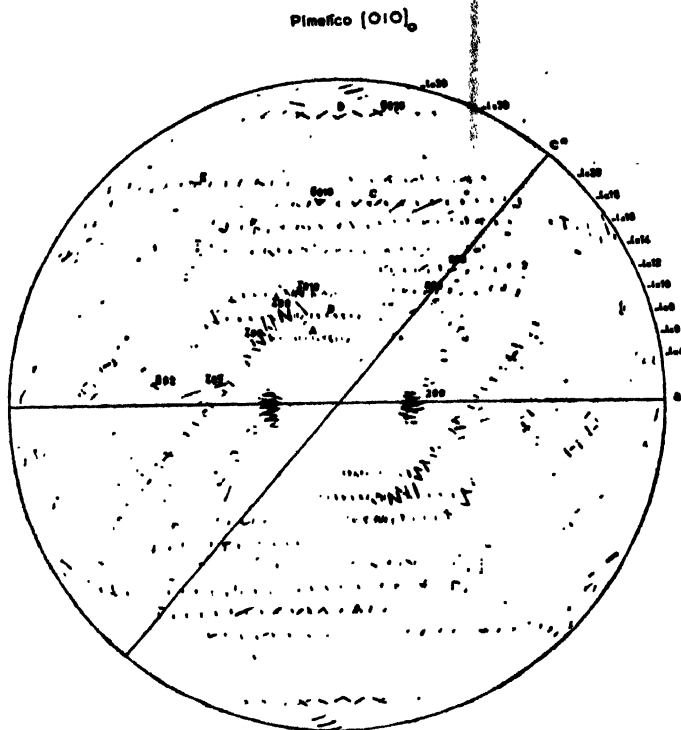


Fig. 5. Pimelic acid. Diffuse domains in  $[010]_0$ .

Comparison of the diffuse scattering domains of azelaic acid in  $[010]_0$  level (Fig. 2) with that of pimelic acid (Fig. 5) reveals the fact these two acids, belonging to the odd series of dicarboxylic acids, give extremely similar diffuse scattering patterns. The only difference is that whereas in pimelic acid the strongest continuous diffuse scattering domains appear extended along the reciprocal lattice planes having  $l = \text{const} = 6, 8, 10$ , etc., those of azelaic acid appear in the planes having  $l = \text{const} = 10, 18, 20, 22$  and  $32$ .

But this is only an apparent difference. In fact the spatial distribution of these domains is the same in both the cases. The differences in the values of  $l$  are due to the fact that the lattice constants of the two acids are different.

### INTERPRETATION

The interpretation of the diffuse scattering of pimelic and azelaic acids will be done together in order to have a correlated idea about the dynamics of the odd-dicarboxylic acids, and to be able to relate the results of this series with those of the even-series already studied in this laboratory.

### PROPAGATION OF WAVES

It is well known that thermal waves in the crystals affect the form and extension of the diffuse scattering domains in the reciprocal space. This has been shown by Lonsdale (1948) and others.

The theory of crystal dynamics shows that the diffuse scattering domains always extend in the reciprocal space in the direction of the propagation of the waves, either longitudinal or transverse.

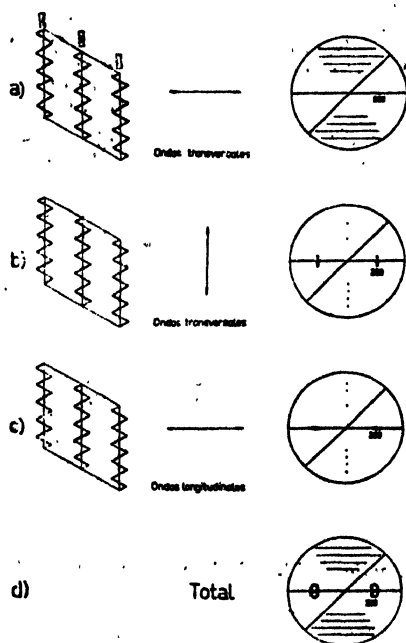


Fig. 6. Scheme of the effect of wave propagation in reciprocal space of a chain-like crystal.  
 a) Transverse waves travelling at right angles to the chains.  
 b) Transverse waves travelling along the chains.  
 c) Longitudinal waves travelling at right angles to the chains.  
 d) Total effect.

Fig. 6 (Amorós and Canut, 1958) shows the effects of different types of wave on the distribution of diffuse scattering in the reciprocal lattice. Thus

Fig. 6 (a) shows the effect of the transverse waves propagating perpendicular to the chain direction which affect the relative chain-chain positions but not those of the atoms within the chains, in the distribution of diffuse scattering in the reciprocal lattice level  $[010]_0$ . Figs. 6 (b) and 6 (c) show the effects of transverse waves which propagate parallel to the chains affecting the relative positions of the atoms in the chains, and longitudinal waves which propagate perpendicular to the chains affecting the chain-chain interspace, respectively in the same reciprocal lattice level. Fig. 6 (d) shows the combined effect of the three types of waves mentioned above, on the form of the diffuse scattering domains in the said reciprocal lattice level.

The effect of the longitudinal waves in the direction of the chain has not been observed in either cases of the dicarboxylic acids studied.

In the dicarboxylic acids the molecular chains are parallel to  $[001]$  axis of the crystal therefore, the streaks that we have observed in the Laue photographs and are represented by the diffuse domains extended at right angles to the chain direction in the reciprocal lattice, are due to the waves of the first kind, i.e., the transverse vibrations of the chains propagating in the direction perpendicular to them. This we suppose to be the most important movement in these acids. As this kind of movement does not affect the relative positions of the atoms within the chain it is not easily detectable by normal structural method.

The second and the third kind of waves mentioned above determine the form of the diffuse domain around the reciprocal lattice point 200. This is the second feature of these crystals and is explicable with the help of the Figs. 6(b) and 6(c).

#### EXTENDED CONTINUOUS DOMAINS OF DIFFUSE SCATTERING

As we have stated above, the effect of the transverse wave propagating perpendicular to the chain direction on the shape of the diffuse scattering domains is to make them elongated along the direction perpendicular to that of the chain. Fig. 6(a) schematically represents this effect. While this figure explains the presence of the continuous domains of diffuse scattering extended along the rows of reciprocal lattice points having  $l = \text{constant}$ , it does not say anything about the extent of the elongation of these domains. On the other hand, the presence of continuous diffuse scattering regions has been observed in the cases of hexamine, anthracene, pentaerythritol, naphthalene, etc, studied in this laboratory; where the presence of the kind of transverse wave represented by fig. 6(a) might not be very important.

Moreover this kind of diffuse scattering is more clearly observed in a zone of  $90^\circ$  about the chain direction extending  $45^\circ$  on either side of it and these diffuse domains extend even across the forbidden reciprocal lattice points.

Therefore in order to explain this kind of diffuse scattering we have undertaken the "difference Fourier transform" (DFT) approach (Amorós *et al*; 1980) which assumes the presence of independent molecular vibrations in the crystal. The theory of this approach is given in the following paragraph.

#### DIFFERENCE FOURIER TRANSFORM

The Fourier transform of a molecule "at rest" is given by

$$G_R = \sum_{n=1}^N f_n \exp (2\pi i \bar{r}_n \cdot \bar{S}), \quad \dots (1)$$

where  $f_n$  is the atomic scattering factor without temperature correction. The effect of a harmonic movement in the molecule is the correction of the atomic scattering factor by the well known Debye factor,

$$f \exp (-M). \quad \dots (2)$$

The Fourier transform of a molecule under thermal agitation is given by

$$G_T = \sum_{n=1}^N f_n \exp (-M) \exp (2\pi i \bar{r}_n \cdot \bar{S}). \quad \dots (3)$$

Since the molecular Fourier transform is the scattered radiation of the molecule, the difference

$$G_R - G_T \quad \dots (4)$$

corresponds to the modification of the scattering space by the thermal motion of the molecule.

Thermal diffuse scattering is due to the x-ray diffraction of crystals under thermal agitation. Therefore relation (4) can be a direct clue to the interpretation of such diffuse scattering. In order to compare directly the observed values of the thermal diffuse scattering (intensities) with the molecular-transform functions, we must multiply  $G$  by its complex conjugate  $G^*$ .

A general way to compute molecular Fourier transforms is to use

$$G = \sum f_n \exp 2\pi i (hx_n + ky_n + lz_n) \quad \dots (5)$$

where  $h, k, l$  can be fractional numbers. The expression (5) corresponds to the molecular structure factor at the point  $(hkl)$  of reciprocal space. In the case of a unit cell with four molecules, the x-ray scattered intensity of the four independent molecules (neglecting phase relationship) will be given by

$$\sum I_j^2 = \sum (A_j^2 + B_j^2) \quad \dots (6)$$

corresponding to the molecules at rest. When subject to thermal motion, the intensity of the four independent molecules will be given by

$$I_{mot} = \sum_1^4 (A_j^2 + B_j^2) 1 - \exp \left( -2B \frac{\sin^2 \theta}{\lambda^2} \right) \quad \dots \quad (7)$$

and the effect of the independent motion of the 4 molecules will be given by

$$DFT = I_{rest} - I_{mot} = \sum_1^4 (A_j^2 + B_j^2) \left\{ 1 - \exp \left( -2B \frac{\sin^2 \theta}{\lambda^2} \right) \right\} \quad \dots \quad (8)$$

Expression (8) is just the difference in scattered intensities of the four molecules at rest and at motion. This expression gives in a direct way the effect, in diffraction space of the independent molecular motion in crystals. It has, for simplicity, been named the "difference Fourier transform" (*DFT*) of the molecules.

#### COMPUTATION OF THE MOLECULAR FOURIER TRANSFORMS OF PIMELIC ACID

For the computation of the molecular transform of pimelic acid we have utilised the atomic co-ordinates given by Mac-Gillavry and others (1948).

Scattering amplitudes for the individual molecules are calculated and hence we have got the difference of the intensities of scattering ( $I_{rest} - I_{mot}$ ) by the individual molecules at rest and on vibration, by multiplying the squares of the scattering amplitudes by a factor  $1 - \exp (-2B \sin^2 \theta / \lambda^2)$ , where  $B$  is the temperature factor. In our case of pimelic acid, owing to the unavailability of the value of  $B$ , we have used  $B = 2 \text{ \AA}^2$ . This value of  $B$  has been found to be that for succinic acid in the direction of the carbon chain. But as we are making the calculation of a limited zone of the reciprocal lattice about the direction of the chain, where the effect of the independent movement is more important, we have adopted this value of  $B$  (i.e.  $B = 2$ ) as an approximate one for pimelic acid.

Because of the two-fold axis of symmetry of the molecules, scattering amplitude corresponding to  $h = 2n$  (where  $n$  is any integer), comprises of only  $A$  and those corresponding to  $h = 2n+1$ , of only  $B$ , where

$$A = \sum_n f_n \cos 2\pi(hx + hy + lz)$$

and

$$B = \sum_n f_n \sin 2\pi(hx + ky + lz)$$

Now, we have to calculate the  $\Sigma(I_{rest} - I_{mot})$  i.e., the *DFT* for all the four molecules of the unit cell.

But due to the symmetry of the crystal we have the following relations among the A's and B's of the different molecules of the cell:

$$\begin{aligned}
 B_1 &= B_2 = B_3 = B_4 = 0 && \text{when } h = 2n \\
 A_1 &= A_2 = A_3 = A_4 = 0 && \text{when } h = 2n+1 \\
 A_1 &= A_3 && \text{when } h = 2n \text{ and } l = 2n \\
 A_1 &= -A_3 && \text{when } h = 2n \text{ and } l = 2n+1 \\
 A_1 &= A_4 && \text{when } h = 2n \text{ and } l = 2n \\
 A_1 &= -A_4 && \text{when } h = 2n \text{ and } l = 2n+1 \\
 B_1 &= B_3 && \text{when } h = 2n+1 \text{ and } l = 2n \\
 B_1 &= -B_3 && \text{when } h = 2n+1 \text{ and } l = 2n+1 \\
 B_1 &= B_4 && \text{when } h = 2n+1 \text{ and } l = 2n \\
 B_1 &= -B_4 && \text{when } h = 2n+1 \text{ and } l = 2n+1
 \end{aligned}
 \tag{R}$$

Thus we see that the absolute values of A's and B's for a particular reflection are the same for all the four molecules of the unit cell.

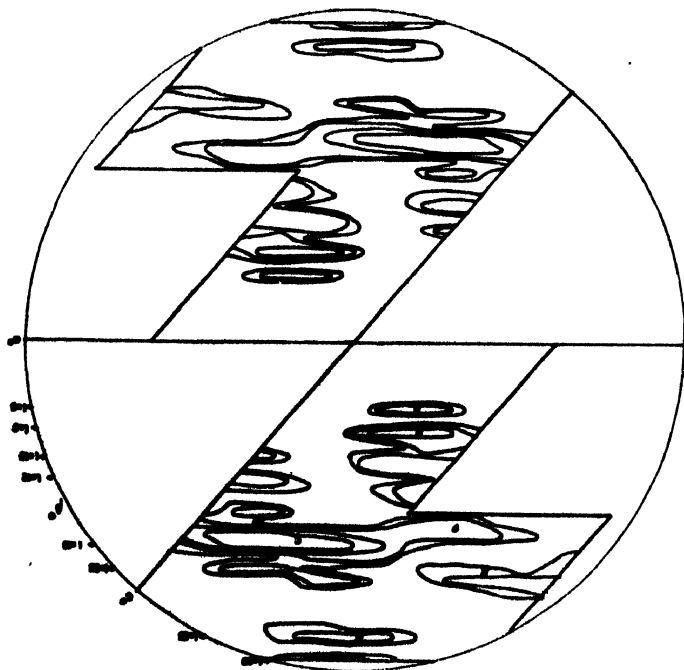


**Fig. 7.** Pimelic acid. Theoretical isodiffusion lines computed with DFT in the region where the effect of independent motion can be considered.



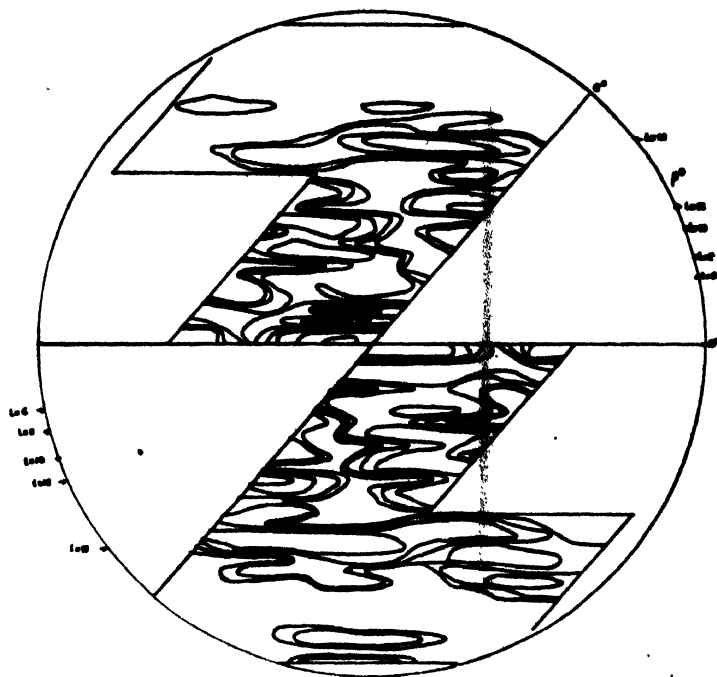


Fig. 8. Pimelic acid.  $[010]_0$ .

Upper part: Molecular  $FT_{rest}$ . Lower part: Molecular  $FT_{mot}$ .

Now by definition,

$$DFT = \sum_1^j (I_{rest} - I_{mot})_j \quad \text{where } j = 1, 2, 3, 4$$

$$= \sum_1^j (A_j^2 + B_j^2) \{1 - \exp(-2B \sin^2 \theta / \lambda^2)\}$$

where  $j$  is the number of molecule of the unit cell.

So, in our case, applying the relations (8), we get

$$DFT = \sum_1^4 (I_{rest} - I_{mot})_j$$

$$= 4A_1^2 \{1 - \exp(-2B \sin^2 \theta / \lambda^2)\} \quad \text{for } h = 2n$$

and

$$= 4B_1^2 \{1 - \exp(-2B \sin^2 \theta / \lambda^2)\} \quad \text{for } h = 2n+1$$

The difference of intensity ( $I_{rest} - I_{mot}$ ) thus calculated have then been plotted on the reciprocal lattice net and the lines of equal ( $I_{rest} - I_{mot}$ ) values of 20, 35, 70 and 140 have been drawn.

Figs. 5 and 7 are the experimental diffuse scattering pattern and the corresponding DFT map, respectively. The strong continuous diffuse scattering domains

A, B, C and D as also the comparatively weaker ones E and F in Fig. 5 are represented by strong A, B, C, D, and weak E and F of Fig. 7.

The agreement between the experimental and theoretical patterns (Figs. 5 and 7) amply justifies the validity of the DFT approach of interpreting the observed distribution of the extended continuous diffuse scattering and their origin. Fig. 8 shows the molecular Fourier transform maps of the molecules at rest and on motion. Comparison of the Fig. 8 with Fig. 7 shows the superiority of the DFT approach over that of molecular Fourier transform as expected theoretically.

### THERMAL MOTION AND CRYSTAL SYMMETRY

We have observed in our present work as also in the previous work in this laboratory that the streaks which appear in the Laue photographs do not always follow the space group extinctions; in the sense that they extend even across the forbidden points of the reciprocal lattice.

This we explain to be due to the fact that the space group symmetry at some instantaneous positions of the molecules of the crystal undergoing thermal vibration (dynamic space group) is different from that of the crystal considered at rest (static space group) (Amorós and Canut, 1960).

Normal methods of structure analysis determine only the static space group. This procedure cannot detect the existence of the dynamic space group because of the fact that the instantaneous change of symmetry due to thermal motion does not change the positions of the Bragg reflections which depend only on the average central positions of the atoms. The thermal motion has got no effect on the Bragg reflections other than diminishing their intensities. Thus, this change of symmetry due to thermal vibrations cannot be detected by normal Fourier methods of Structure analysis.

Fig. 9 shows one complete unit cell containing the molecules in their respective positions and another containing the elements of symmetry corresponding to the space group  $I2/a$  of the azelaic acid crystal.

The antiphase vibration represented by the arrow (1) is that due to a transverse wave propagating along the normal to the chain direction. Due to this kind of vibration of the glide plane  $a$ , the two fold axes in the centres of the molecules and the centres of symmetry within the hydrogen bonds vanish, giving the space group  $P2_{1/n}$  to the crystal at some instantaneous state of the molecules undergoing vibrations.

The symmetry elements that vanish as a result of the vibration represented by the arrow (1) in the Fig. 9 also vanish as a result of that represented by the arrow (3). Therefore, the space group (dynamic) due to the latter kind of vibration is also  $P2_{1/n}$ .

The arrow (2) represents the antiphase libration of the chains about the axes along their direction. The screw axes lying in between the chains vanish at some instantaneous state of the molecules undergoing libration giving the space group (dynamic)  $P_{2/n}$  to the crystal.

The systematic extinctions in  $[010]_0$  levelowing to  $n$  are the same as those for  $I$  and, therefore, the extinction condition  $h+l = \text{even}$ , in the  $[010]_0$  level is maintained.

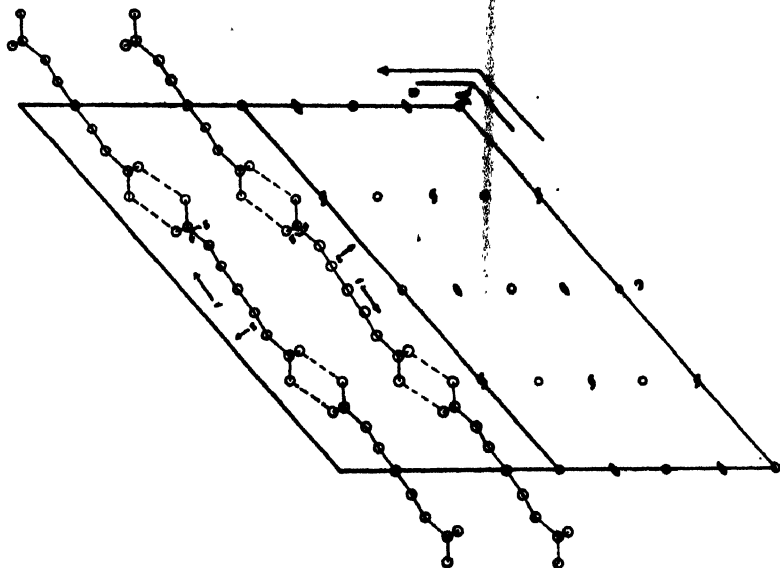


Fig. 9. Pimelic acid. Projection of the structure on (010).

#### COMPARISON BETWEEN THERMAL DIFFUSE SCATTERING OF THE DICARBOXYLIC ACIDS OF EVEN AND ODD SERIES

The difference between the distributions of the diffuse scattering zones in the reciprocal lattice of the acids belonging to the two series is not very great. The general features of these distributions are essentially the same. In the case of the acids belonging to the even series the extended continuous zones of diffuse scattering appear as well defined, even by spaced sheets perpendicular to the chain direction in the reciprocal space. The spacing of these sheets is reciprocal to  $2.5\text{\AA}$ . This distance  $2.5\text{\AA}$  corresponds to the zig-zag distance of the carbon atoms of the molecular chain and the length of the hydrogen bond binding the molecules of the same chain. That means the periodicity in the distribution of the continuous diffuse zones along the direction of the chain in the reciprocal space shows a well marked reciprocal relation to that of the chains. This reciprocal relation

is also clearly exhibited by the DFT maps of the acids of the even series (Amorós and Canut, 1958).

But it is less clearly exhibited by the distribution of the continuous diffuse zones and their DFT representations of the acids of the odd series. A probable reason of the observed difference between the distributions of the continuous diffuse zones of the acids belonging to the two series is that in the case of the even series acids the chains are well defined but those in the case of the odd series are distorted. In the case of even series the carbon atoms of a chain are coplanar and the long axes of the molecules in the same chain are colinear whereas in the case of odd series neither the carbon atoms are coplanar nor the molecular axes are colinear.

#### REFERENCES

- Acha A., Canut M. L. and Amoros, J. L., 1958, *Bol. R. Soc. Esp. Hist. Nat.*, (G) **56**, 405.  
Alonso, P., Canut, M. L. and Amoros, J. L., 1958, *Bol. R. Soc. Esp. Hist. Nat.*, **56**, 379.  
Annaka, S. and Amoros, J. L., *Z. Kristallog.*, (In press).  
Amoros, J. L. and Canut, M. L., 1958, *Bol. R. Soc. Esp. Hist. Nat.*, (G) **56**, 25.  
Amoros, J. L. and Canut, M. L., 1958, *Bol. R. Soc. Esp. Hist. Nat.* (G) **56**, 305.  
Amoros, J. L., Canut, M. L. and Acha, A., 1960, *Z. Kristallog*, **114**, 39.  
Amoros, J. L. and Canut, M. L., 1960, *Bol. R. Cos. Esp. Hist. Nat.*, (G) **57**,  
Canut, M. L. and Amoros, J. L., 1957, *P. Dep. Crist. Min.*, **3**, 15.  
Canut, M. L. and Amoros, J. L., 1957, *P. Dep. Christ. Min.*, **3**, 27.  
Canut, M. L. and Amoros, J. L., 1958, *Bul. R. Soc. Esp. Hist. Nat.*, (G) **56**, 323.  
Caspari, W. A., 1928, *J. Chem. Soc. London*, **30**, 3235.  
Caspari, W. A., 1929, *J. Chem. Soc. London*, **30**, 2709.  
Dupre la Tour F., 1935, *Compt. Rendus*, 479.  
Lonsdale, K., 1948, *Crystals and X-rays*, London, Bell, Sons.  
Mac Gillavry, C. H., Hoodchagen G. and Sixma, F. L. J., 1948, *Rec. trav. Chem. Pays. Bas.*,  
**67**, 869.  
Martin, W. G., 1956, *J. Appl. Phys.* **27**, 514.

# INVESTIGATIONS INTO THE LOW ENERGY GAMMA RAY BACKGROUND AND ITS VARIATIONS

BIJON ROY, PROBIR K. SANDELL AND AJOY K. CHOUDHURY

DEPARTMENT OF EXPERIMENTAL MEDICAL SCIENCES,  
INSTITUTE OF POST-GRADUATE MEDICAL EDUCATION & RESEARCH, CALCUTTA

(Received, July 7, 1960)

**ABSTRACT.** The gamma-ray background of Calcutta as determined by scintillation spectrometry using a NaI (thallium activated) crystal consists of two broad energy bands being contributed by the radioactive substances present in the soil, air and building materials and identified as those from the radium and thorium family. The background so determined indicates that there are two possible regions of low level counting which is achieved by choosing an optimum channel level and channel width. The variation in intensity of the background is restricted mostly to lower energy region of the background spectrum and is under further investigation.

## INTRODUCTION

In low level counting using scintillation counters the background count is always a limiting factor. On the other hand in certain low level counting, as in bio-medical tracer technique different authorities, (Johnston, 1955; Anderson and Libby, 1957) Medical Research Council (Report 1956) have stressed the need of low doses of radioactive tracers in diagnostic and investigative works. Possibly it is safe to use a dose which is of the order of the natural background in its activity. Furthermore, in *in vivo* measurements during bio-medical tracer works, an effective shielding against the background is often not possible. Thus, in all the above cases an attempt at low level scintillation counting must essentially be preceded by a survey of the nature of the background at the particular place. This means the determining of the energy distribution in the background spectrum, the position of its main peaks, if any, and their relative intensities. As the gamma-emitters usually used in low level counting as in bio-medical work, like I (131), Fe (55), Cr (51), Au (198) etc., have characteristic energies below 700 KeV it is of interest to analyse spectrometrically the region below this.

Recently, many excellent review works on low level counting have been published (Hayes, Anderson and Langham, 1955; Anderson and Hayes, 1956). But hardly any attempt has been made in this country towards a spectrometric study of the background of the place before undertaking such studies. In this laboratory, this spectrometric work has been carried on for the last one year. In the following paper it is desired to report the results of the one-year investigation

on the subject, the variations observed and the possible importance of the results obtained in low-level counting, for instance, in bio-medical tracer technique.

#### METHODS AND MATERIALS

The studies on the radioactive background of Calcutta were carried out with the help of RIDL Scientillation Spectrometer consisting of a Scaler model no. 16D, B-152; Ratemeter/Electronic Sweep Meter type 114-B, serial B-79; and Scintillation counter No. 43A with interchangeable NaI (thallium activated) crystal of  $\frac{1}{2}$ " thickness. The gamma energy distribution was determined under the following conditions: crystal used = NaI  $\frac{1}{2}$ " thick; counter voltage = 700 volts; period of sweep =  $\frac{1}{4}$  hour; ratemeter scale multiplying factor = 0.5; channel width = 2.0; percentage standard deviation = 10%. A full automatic sweep (without any attenuation) was taken in every case in differential position from 100-0 channel volts, the reset level heliopot being kept at '0'. The graphic record was made with the help of a Honeywell Brown Electronik Recorder automatically.

At the above setting of the instrument, graphic records of the background spectrum was taken throughout the whole year. At the same time, keeping the same instrument settings, scans of I (131) and Cr (51) spectrum were made and their peaks, 364 KeV and 330 KeV respectively were used to calibrate the background spectrum so obtained.

In order to eliminate possible influence of circuit oscillations in the discriminator or elsewhere, and also of photomultiplier noise on the background spectrum, the crystal of the counter was removed from the top of photomultiplier tube and the rest of the counter (consisting of photomultiplier tube, cathode follower, etc.) was wrapped light-tight completely in black paper and a full scan from 100-0 channel level volts was taken keeping the settings of the spectrometer as before.

To study the effect of shielding of the counter on the background spectrum, the counter was inserted in a lead castle with walls  $1\frac{1}{4}$ " thick and a full scan from 100-0 channel level volts was made under same instrumental settings. Observations were also made on the variation in background spectra with the changes in atmospheric conditions. Thus an attempt was made to note the variation of intensity below 75 KeV at different times of the day at two hours interval.

After calibration, the energies corresponding to the different peaks in the average spectra obtained were found to tally with those of radium and thorium emanations. To examine this fully the spectra of the important naturally occurring isotopes, viz., Ra (226) in the form of needle and Th (230) as crystal sample were recorded in the same graph containing the background spectrum under same instrumental settings. An attempt was made to trace the sources contributing to the background and the following materials were analysed: (1)

sand from Mogra, (usually used for the building materials here), (2) the silt from the banks of the Ganges, (3) soil samples from the northern and southern parts of the city and (4) the soil from around the building housing the spectrometer. To examine these, a lead chamber having 1 cu. ft. (approximately) of internal volume was constructed with walls 3" thick. A background tracing with only the counter inside was taken initially and then each of the above samples was packed in the space with the counter placed in the middle. Care was taken to preserve the relative geometry of the counter with respect to the surroundings the same in every case.

## RESULTS

The background spectrum consists of two broad energy bands. One such graph is given in Fig. 1. The whole energy spectrum extends from 50 to 275 KeV (Table I). On removing the crystal, a graph was obtained as shown in Fig. 2. This therefore gives the contribution due to circuit oscillations and photomultiplier noise. Comparing Figs. 1 and 2 one can easily recognise the resultant background intensities in this low energy region. Shielding of the counter with lead  $1\frac{1}{2}$ " thick cuts off completely the broader higher energy band and attenuates the lower energy region to about  $\frac{1}{3}$  of its unshielded value (Fig. 3). From Fig. 4, where the Ra (226) and Th (230) graphs are superposed on the background, one finds that the energy peaks corresponding to values round about 230—270 KeV and 105—120 KeV could be associated with the gamma-rays of Ra (226) and Th (230). These elements have been traced in the sand of the building materials and the soil of the city (Figs. 5-9; Table II). From these figures the relative contributions of the sand or of the soil may be clearly seen. Scanning for whole day at two hours intervals showed a variation in the intensity under 55 KeV. The maximum increase of the intensity in this region occurred round about afternoon. Attempts have also been made to indicate this variation together with that of atmospheric temperature and humidity as obtained from the Meteorological office, Alipore.

TABLE I

Results of the gamma ray spectrometric analysis of the background of Calcutta

	Energy range in KeV	Peak values in KeV	Maximum intensity range	Natural radio- active isotope with same energy range
Higher energy band	275-105	275, 245, 230, 185, 175, 170, 160, 135, 125, 105.	160-135	Radium and Thorium family

TABLE II

Samples	Gamma ray energy range in KeV	Maximum intensity range in KeV
1. Sand (from Mogra)	215-50	130-125
2. Soil (from the Ganges)	170-50	145-125
3. Soil (from Lake area)	265-50	140-125
4. Soil (from Science College compound)	175-50	140-130
5. Soil (from S.S.K.M. Hospital compound)	220-50	135-126

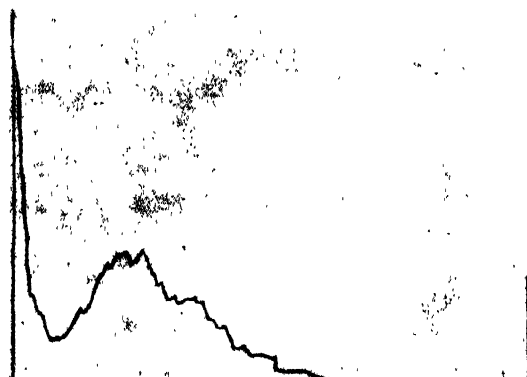


Fig. 1. Shows the radiation background of Calcutta. The scanning was done with the help of RIDL scintillation spectrometer from right to left. The energy of the gamma rays extends from 275-50 KeV.

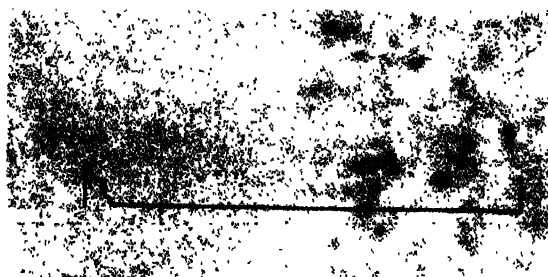


Fig. 2. Shows the contribution due to circuit oscillation and photomultiplier noise. This was taken with the crystal (NaI—thallium activated) removed.



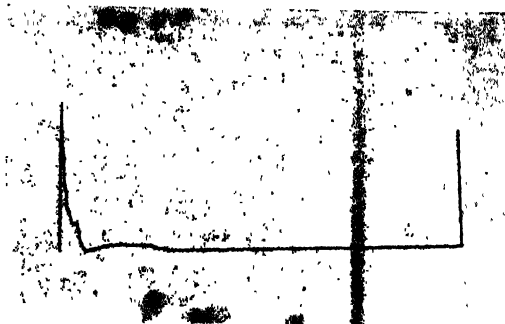


Fig. 3. Indicates the effect of shielding the probe with lead,  $1\frac{1}{2}$ " thick. It shows the complete cutting off of the broader higher energy band and attenuation of the lower energy region to about  $\frac{1}{3}$  of its unshielded value.

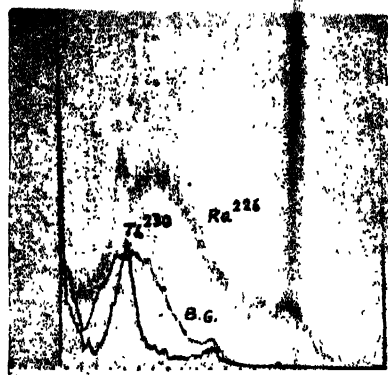


Fig. 4. Shows the superimposition of the tracings due to Ra (226) and Th (230) on the background tracing. Note that the energy peaks of the background could be associated with the gamma rays of radium and thorium family.



Fig. 5. Shows the gamma ray contribution of soil, collected from lake area (South Calcutta), to the background of the place. The gamma ray energy range due to this extends from 265-50 KeV.

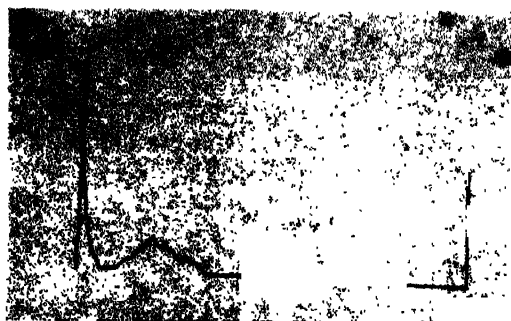


Fig. 6. Shows the gamma ray contribution of soil, collected from Science College (Calcutta) compound, to the background of the place. The gamma ray energy range due to this extends from 175–50 KeV.



Fig. 7. Shows the gamma ray contribution of sand, collected from Mogra, to the background of the place. The gamma ray energy range due to this extends from 215–50 KeV.

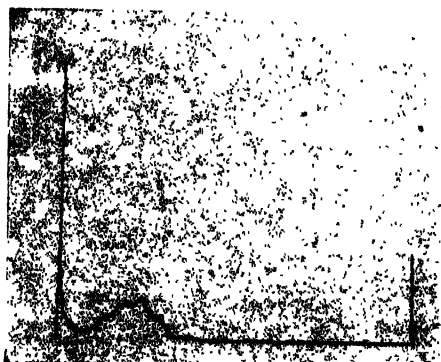


Fig. 8. Shows the gamma ray contribution of soil, collected from the Ganges, to the background of the place. The gamma ray energy range due to this extends from 170–50 KeV.

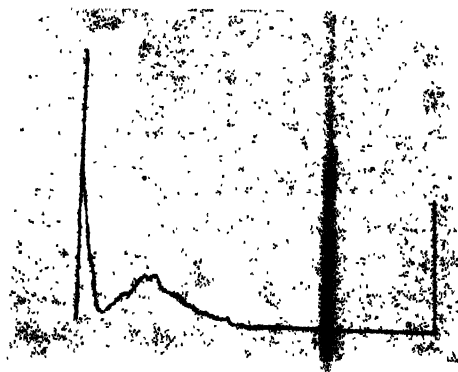


Fig. 9. Shows the gamma ray contribution of soil collected from the S.S.K.M Hospital compound, to the background of the place. The gamma ray energy range due to this extends from 220-50 KeV.

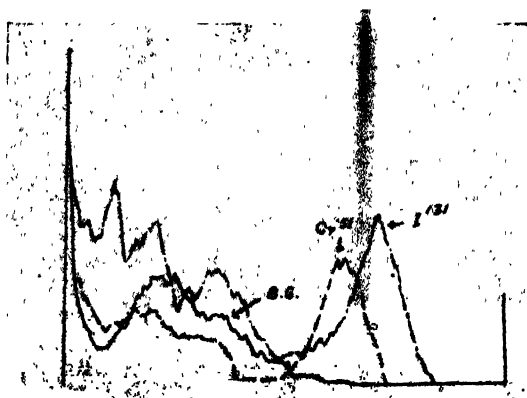


Fig. 10. Shows the superimposition of the three gamma ray spectra due to the background (—), radio-iodine (I-131, -.-) and radio-chromium (Cr-51, — — —). It shows that 50% of the count due to the two isotopes for a particular sample lie above the highest energy limits of the background.

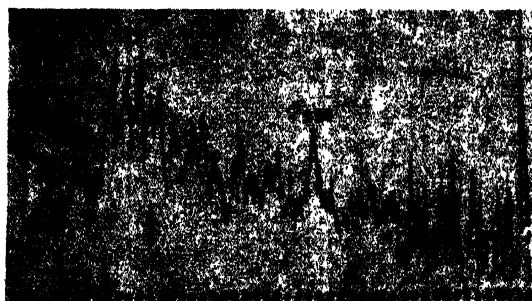


Fig. 11. Shows the background scan carried out at Eindhoven, Holland, with the help of Philips Scintillation Spectrometer. Note the important peaks round about 90 and 220 KeV with possible peaks at 50 and 28 KeV.

Scanning with samples of I (131) and Cr (51) showed that nearly 50% of the counts resulting from particular sample were above the highest energy limits of the background (Fig. 10). This, more or less, was experienced with the other isotopes mentioned above except Fe (55) in which case the radiations were found to be concentrated in the region 90–105 KeV.

A similar background scan was carried out at Eindhoven, Holland, by one of the authors with the help of Philips scintillation spectrometer. The graph thus obtained has important peaks round about 90 and 220 KeV with possible peaks at 28 and 50 KeV, and is similar to the ones obtained here. The intensity of the energy round about 80 to 90 KeV was greatest. The energies in the spectrum would correspond to those found in the members of the uranium and radium family (Fig. 11).

### DISCUSSION

The background of Calcutta consists of 2 broad energy bands being contributed by the radioactive substances present in the soil, air and the building materials. The radioactive elements present are those of the Radium and Thorium family.

From the background spectra obtained it is evident that most of the background counts are concentrated in 2 regions—the first between 260 to 135 KeV after which on both sides the counts fall off rapidly and the second region is found to be below 65 KeV. Therefore, in low level counting as with the isotopes for bio-medical tracer work it is necessary only to adjust the channel level of the pulse-height analyser in such a way as to eliminate these regions. The background counts automatically will then fall off without going into the problem of shielding. The best procedure would be to set the channel level potentiometer to a value which corresponds to energies higher than 270 KeV and then expanding the channel window to include the characteristic peak of the isotope being used within the channel window which lies above 275 KeV. The window width preferably should be greater than  $2W$  where 'W' is the recorded half width of the photo-peak of the isotope used. In the case of Fe (55) the window should be adjusted near about the trough found between the higher and lower energy bands, i.e., between 65 and 105 KeV. Hence there are 2 regions of low level counting—one above 270 KeV and the other in trough between the higher and lower energy band, i.e. between 60–105 KeV. Thyroid uptake measurements with low doses using the above procedure yielded more reproducible results.

The effect of shielding on the 2 energy bands of the background may at first sight seem to be anomalous as because the lower energy region is expected to be cut off more easily than the higher energy rays on shielding. Possibly, low energy secondary radiations produced by cosmic rays in the material of the shield is responsible for this.

The reason for the variation in the intensity of the low energy region as obtained during certain period of the day cannot be explained satisfactorily right now without further investigation. According to Wait (1937) there is some fluctuation in the gamma-ray content of the atmosphere with a maximum at about noon. This is in agreement with our observation. Further, others (Wilkening, 1952) have reported the variation in the radon and thoron content of the atmosphere with the time of the day. The present investigation points out that this variation in background is restricted mostly to low energy region of the background spectrum. This is a subject matter of further investigation.

#### ACKNOWLEDGMENT

Grateful thanks are due to Prof. S. D. Chatterjee, D. Sc., F. N. I. and Prof. S. N. Bose, F.R.S., for their helpful discussion and constant encouragement. Authors also like to acknowledge indebtedness Major General A. K. Gupta, Director, Institute of Post-graduate Medical Education and Research, for kindly permitting them to carry on the work and also for the facilities obtained.

#### REFERENCES

- Anderson, E. C. and Hayes, F. N., 1955, *Ann. Rev. Nuclear Sc.*, **6**, 303.  
Anderson, E. C. and Libby, W. F., 1957, *Adv. Biol. Med. Phys.*, **5**, 385.  
Blifford, I. H., Friedman, H., Lockhart, L. B. and Baus, R. A., 1956, *J. Atmospheric and Terrest. Phys.*, **9**, 1.  
Hayes, F. N., Anderson, E. C. and Langham, W. H., 1955, *Proc. Intern. Conf. Peaceful uses of Atomic energy.*, **14**, 182.  
Johnston, W. H., 1955, *Peaceful uses of Atomic Energy International Conf.*, **14**, 149-54.  
Wait, 1937, *Terrestrial Magnetism & Atmospheric Electricity.*, **42**, 1.  
Wilkening, M. H., 1952, *Nucleonics.*, **10**, 6, 36.

# DETERMINATION OF UNLIKE INTERACTIONS FROM BINARY VISCOSITY

I. B. SRIVASTAVA

INDIAN ASSOCIATION FOR THE CULTIVATION OF SCIENCE, CALCUTTA-32

(Received, December 22, 1960)

**ABSTRACT.** Experimental viscosity data for the binary gaseous mixtures He-A, Ne-A and  $H_2-C_3H_8$  have been utilised for determining the potential parameters for unlike pairs on the L-J (12-6) model. Three different methods have been employed, the first method being applicable only to mixtures exhibiting a maxima with respect to variations in the composition. The other two methods can be used for all gas pairs for which accurate viscosity data are available in a wide temperature range. The parameters thus obtained are tabulated along with those from other sources.

## 1. INTRODUCTION

Intermolecular potentials between like molecules have been determined with sufficient accuracy by the use of equilibrium and transport properties. For calculating transport properties of pure gases, the force constants used are those determined mainly from viscosity data. There is, however, considerable uncertainty in the values of the force parameters for unlike molecules as determined from the experimental data of inter-diffusion and thermal diffusion, the properties utilised by many workers. This is due to the non-availability of accurate data over a large temperature range and in the case of thermal diffusion there is the additional complication that the higher approximation terms are not negligible. So for the theoretical calculations of the transport properties of mixtures, the force constants for unlike pairs are calculated by the help of some semi-empirical combination rules which are not rigorously true. It is therefore important to be able to derive the unlike interaction parameters by other methods. Recently, Hirschfelder, Taylor and Kihara (1960) have pointed out that the accurate measurements of viscosity of gaseous mixtures as a function of both temperature and concentration can provide a good method of determining the unlike intermolecular forces.

In the present work three different methods have been developed for the determination of the unlike force parameters, provided accurate experimental data are available.

## 2. THEORY AND FORMULAE

On the basis of the Chapman-Enskog theory, the transport properties have been expressed in terms of a set of reduced collision integrals  $\Omega^{(L)*}$  which depend

on the law of molecular interaction and are tabulated by Hirschfelder, Curtiss and Bird (1954) for different potential forms. The Lennard-Jones (12:6) potential is given by the relation

$$\phi(r) = 4\epsilon \left[ \left( \frac{\sigma}{r} \right)^{12} - \left( \frac{\sigma}{r} \right)^6 \right] \quad (1)$$

where  $\phi(r)$  is the potential energy between two molecules separated by a distance  $r$ ,  $\sigma$  is the value of  $r$  at  $\phi(r) = 0$  and  $\epsilon$  is the depth of the potential well.

The viscosity of a binary gas mixture  $\eta_{mix}$  to the first approximation, is given by

$$[\eta_{mix}]_1 = \frac{1 + Z_\eta}{X_\eta + Y_\eta} \quad (2)$$

with

$$X_\eta = \frac{x_1^2}{\eta_1} + \frac{2x_1x_2}{\eta_{12}} + \frac{x_2^2}{\eta_2}$$

$$Y_\eta = \frac{3}{5} A_{12}^* \left\{ \frac{x_1^2}{\eta_1} \left( \frac{M_1}{M_2} \right) + \frac{2x_1x_2}{\eta_{12}} \left( \frac{M_1 + M_2}{4M_1M_2} \right) \cdot \left( \frac{\eta_{12}^2}{\eta_1\eta_2} \right) + \frac{x_2^2}{\eta_2} \left( \frac{M_2}{M_1} \right) \right\}$$

$$Z_\eta = \frac{3}{5} A_{12}^* \left\{ x_1^2 \cdot \left( \frac{M_1}{M_2} \right) + 2x_1x_2 \left[ \left( \frac{M_1 + M_2}{4M_1M_2} \right) \left( \frac{\eta_{12}}{\eta_1} + \frac{\eta_{12}}{\eta_2} \right) - 1 \right] + x_2^2 \left( \frac{M_2}{M_1} \right) \right\}$$

$x_1, x_2$  are the mole fractions,  $\eta_1, \eta_2$  the viscosities and  $M_1, M_2$  are the molecular weights of components 1 and 2 respectively.  $\eta_{12}$  is the viscosity of a hypothetical gas given by

$$\eta_{12} \times 10^7 = 266.93 \cdot \frac{\sqrt{2M_1M_2T}/(M_1 + M_2)}{\sigma_{12}^2 \Omega_{12}^{(2,2)*}(T_{12}^*)} \quad (3)$$

### 3. DETERMINATION OF THE POTENTIAL PARAMETERS

(a) Hirschfelder, *et al.* (1960) have obtained the relation for the maximum or minimum of the viscosity of binary gas mixtures, by differentiating Eq. (2) with respect to  $x_1$  and equating  $(d\eta_{mix}/dx_1)$  to zero. The relation for the maximum or minimum viscosity may be written in the form

$$\frac{(\eta_{mix})_{max}}{(\eta_1\eta_2)^{1/2}} = \frac{\beta_c(\beta + \beta^{-1}) - 2\beta_c}{\beta_c^2 - 1}$$

$$\text{where} \quad \beta = (\eta_1/\eta_2)^{1/2} \quad \dots \quad (4)$$

$$\text{and} \quad \beta_c = K(2R)^{-1}(1-\alpha+f) \quad \dots \quad (5)$$

$$\text{with} \quad R = (M_1 + M_2)^{1/2}/(4M_1M_2)^{1/4}$$

$$K = \frac{\sigma_1\sigma_2\sqrt{\Omega_{11}^{(2,2)*}(T^*)\cdot\Omega_{22}^{(2,2)*}(T^*)}}{\sigma_{12}^2\Omega_{12}^{(2,2)*}(T_{12}^*)} \quad \dots \quad (6)$$

$$\alpha = 3/5 A_{12}^* \text{ and } f^2 = (1-\alpha)^2 + 4\alpha R^4$$

Here for getting maximum in the viscosity  $\beta$  must lie between  $\beta_c$  and  $\beta_c^{-1}$ .

The maximum value of experimental viscosity is obtained from the graph of  $\eta_{mix}$  against  $x_1$  for each temperature. This is substituted in Eq. (4) along with the experimental values of  $\eta_1$  and  $\eta_2$  and the equation solved for  $\beta_c$ . Let the values of  $\beta_c$  at two temperatures  $T_1, T_2$  be  $(\beta_c)_1, (\beta_c)_2$ . Then using the subscripts 1 and 2 to denote the quantities at temperatures  $T_1$  and  $T_2$  we get from eqns. (5) and (6)

$$(\beta_c)_1/(\beta_c)_2 = \left( \frac{K_1}{K_2} \cdot \frac{(1-\alpha_1+f_1)}{(1-\alpha_2+f_2)} \right) \quad (7)$$

$$\text{and} \quad K_1/K_2 = \left( \frac{\Omega_{12}^{(2,2)*}(T_2^*)}{\Omega_{12}^{(2,2)*}(T_1^*)} \right) \cdot \left( \frac{\Omega_{11}^{(2,2)*}(T_1^*)}{\Omega_{11}^{(2,2)*}(T_2^*)} \frac{\Omega_{22}^{(2,2)*}(T_1^*)}{\Omega_{22}^{(2,2)*}(T_2^*)} \right) \quad (8)$$

With the help of the Eqns. (7) and (8) and the tabulations of Hirschfelder *et al.* (1954), for the collision integrals and  $A_{12}^*$ , the ratio  $(\beta_c)_1/(\beta_c)_2$  is calculated for a number of arbitrarily chosen values of  $\epsilon_{12}/k$  and a graph drawn for  $(\beta_c)_1/(\beta_c)_2$  versus  $\epsilon_{12}/k$ . The desired value of  $\epsilon_{12}/k$  for the gas pair is then read from the graph corresponding to the value of  $(\beta_c)_1/(\beta_c)_2$  determined from Eq. (4). The value of  $\sigma_{12}$  can be calculated easily with the help of Eqns. (5) and (6) by using this value of  $\epsilon_{12}/k$ .

In the present work the force parameters for He-A and H<sub>2</sub>-C<sub>3</sub>H<sub>8</sub> interaction have been calculated by this method. For He-A, the recent data of Rietveld, *et al.* (1953) at temperatures 291.1°K, 229.5°K and 192.5°K could be successfully combined to give three sets of  $\epsilon_{12}/k$  and  $\sigma_{12}$  values, the mean of which is recorded in Table I. Only one set of force constants of H<sub>2</sub>-C<sub>3</sub>H<sub>8</sub> could be obtained as the data at only two temperatures 500°K and 550°K taken from Trautz and Kurz (1931) could be used successfully.

This method can give accurate and consistent values for force constants, provided accurate experimental data are available even at two temperatures but it is applicable to only those binary gas mixtures which show maxima or minima in viscosity at some concentration.



(b) *Method of Intersection :*

The graphical methods of intersection and Lennard-Jones translation discussed in detail by Srivastava and Srivastava (1959) can be successfully used for obtaining the unlike force parameters on the L-J (12 : 6) potential from the data on viscosity of gas mixtures. For this purpose Eq. (2) is solved for  $\eta_{12}$  giving

$$\eta_{12} = \frac{-b \pm \sqrt{b^2 - 4ac}}{2a} \quad \dots (9)$$

where  $a = \frac{6}{5} A_{12}^* \cdot \left( \frac{x_1 x_2}{\eta_1 \eta_2} \right) \left( \frac{(M_1 + M_2)^2}{4M_1 M_2} \right) \cdot (\eta_{mix} - \eta_1 - \eta_2)$

$$b = \frac{3}{5} A_{12}^* \left[ 2x_1 x_2 + x_1^2 \cdot \left( \frac{M_1}{M_2} \right) \cdot \left( \frac{\eta_{mix}}{\eta_1} \right) + x_2^2 \cdot \left( \frac{M_2}{M_1} \right) \left( \frac{\eta_{mix}}{\eta_2} \right) - x_1^2 \cdot \left( \frac{M_1}{M_2} \right) - x_2^2 \cdot \left( \frac{M_2}{M_1} \right) \right] + \eta_{mix} \left( \frac{x_1^2}{\eta_1} + \frac{x_2^2}{\eta_2} \right) - 1$$

and

$$c = 2x_1 x_2 \eta_{mix}$$

Now by substituting the experimental values of  $\eta_1$ ,  $\eta_2$  and  $\eta_{mix}$  at any temperature,  $\eta_{12}$  is obtained in terms of  $A_{12}^*$  which is a temperature dependent function and whose values are tabulated by Hirschfelder, *et al.* (1954). Then  $\eta_{12}$  is calculated for one temperature by substituting the value of  $A_{12}^*$  corresponding to any arbitrarily chosen value of  $\epsilon_{12}/k$  and by using this  $\eta_{12}$  value the corresponding  $\sigma_{12}$  value can be obtained from Eq. (3). In this way a set of  $\epsilon_{12}/k$  and  $\sigma_{12}$  values are calculated at one temperature. The same process is repeated for getting sets of values of  $\epsilon_{12}/k$  and  $\sigma_{12}$  at other temperatures. Graphs are then plotted for  $\epsilon_{12}/k$  against  $\sigma_{12}$  at each temperature. The intersection point gives the required values of  $\epsilon_{12}/k$  and  $\sigma_{12}$  for the gas pair.

This method has been utilised to determine the force parameters for the gas pairs He-A and Ne-A. There is usually some uncertainty in exactly locating the intersection point when the experimental data are not very accurate. In view of the extensive data on mixture viscosities, however, this method can serve as a useful supplement to other methods for determining unlike force parameters.

(c) *Translation Method :*

If experimental data are available in a large range of temperature, the translation method can be applied with the following device. From table,  $A_{12}^*$  is found to vary very slowly with  $T^*$  and can therefore be taken to be constant over a very small range of  $T^*$ , say, for a change of about 3%. It is thus possible

to calculate  $A^*_{12}$  at any temperature with sufficient accuracy by using the value of  $\epsilon_{12}/k$  obtained from the combination rule, as the true value of  $\epsilon_{12}/k$  is not likely to differ from the combination rule values by more than about 3%. Knowing  $A^*_{12}$  in this manner,  $\eta_{12}$  can be determined from Eq. (9) by utilising the experimental values of  $\eta_{mix}$ ,  $\eta_1$  and  $\eta_2$ . Thus knowing  $\eta_{12}$  at different temperatures and using Eq. (3), the Lennard-Jones translation method can be applied for getting  $\epsilon_{12}/k$  and  $\sigma_{12}$ . In case this value of  $\epsilon_{12}/k$  is much different from the value previously selected from the combination rule, the process can be repeated by using this refined value of  $\epsilon_{12}/k$ .

This method is used here for determining the force parameters for the gas pairs He-A and Ne-A.

#### 4. RESULTS

The force parameters determined by these methods are given in Table I along with those determined from other sources.

TABLE I  
Unlike Force Parameters on the L-J (12 : 6) model

Gas Pair	Force Parameters	Present work			Previous work			Ref. for data
		From maximum viscosity	Inter-section method	Translation method	Comb. rules	From inter-diffusion	From Thermal diffusion	
He-A	$\epsilon_{12}/k^\circ\text{K}$	36.97	36.97	36.9	35.6	33.8 <sup>a</sup>	37.91 <sup>b</sup>	A
	$\sigma_{12}\text{\AA}$	2.96	2.985	3.028	2.997	2.99	3.025	
Ne-A	$\epsilon_{12}/k^\circ\text{K}$	..	69.0	66.37	66.6	64.5 <sup>c</sup>	67.6 <sup>b</sup>	B
	$\sigma_{12}\text{\AA}$	..	2.943	2.932	3.104	3.098	3.079	
H <sub>2</sub> -C <sub>3</sub> H <sub>8</sub>	$\epsilon_{12}/k^\circ\text{K}$	103.8	..	..	98.25	..	..	C
	$\sigma_{12}\text{\AA}$	4.019	..	..	3.988	..	..	

(A) Rietveld and Itterboek (1953).

(B) Trautz and Binkels (1930).

(C) Trautz and Kurz (1931)

(a) Srivastava and Srivastava (1959)

(b) Saxena (1955)

(c) Srivastava (1959).

#### 5. DISCUSSION

It will be seen from the table that the three methods employed here give quite consistent values of the unlike force parameters which agree well with the values obtained from the combination rules. This shows clearly that the viscosity data on mixtures of gases can be employed to give quite reliable values for the unlike interaction parameters. Unfortunately the large amount of exist-

ing data on mixture viscosities had never been directly utilised so far for calculating the unlike force parameters. The present investigations show that this is quite feasible and desirable.

The values of the unlike parameters obtained by others using thermal diffusion data show good agreement with the present determinations, but those obtained from inter-diffusion data exhibit noticeable discrepancies. It is worth nothing that in the evaluation of the unlike force parameters from inter-diffusion data, the force parameters for like interactions were not utilised, while all the other methods cited here depend upon the accuracy of the force parameters for pure components also.

#### ACKNOWLEDGMENTS

The author is grateful to Prof. B. N. Srivastava, D.Sc., F.N.I., for suggesting the problem and many helpful discussions throughout the progress of this work.

#### REFERENCES

- Hirschfelder, J. O., Curtiss, C. F. and Bird, R. B., 1954. *Molecular Theory of Gases and Liquids*, John Wiley and Sons, Inc., New York.
- Hirschfelder, J. O., Taylor, M. H. and Kilbara, T., 1960, Report, WIS-OOR-29.
- Rietveld, A. O., Van Itterbeek, A. and Van Der Berg, G. J., 1953, *Physica*, **19**, 517.
- Saxena, S. C., 1955, *Ind. Jour. Phys.*, **29**, 131.
- Srivastava, B. N. and Srivastava, K. P., 1959, *J. Chem. Phys.*, **30**, 984.
- Srivastava, K. P., 1959, *Physica*, **25**, 571.
- Trautz, M., and Binkels, H. E., 1930, *Ann. Physik*, **5**, 561.
- Trautz, M. and Kurz, F., 1931, *Ann. Physik*, **9**, 981.

# A LOW PRESSURE EXPANSION CLOUD CHAMBER

M. RAMA RAO

SAHA INSTITUTE OF NUCLEAR PHYSICS, CALCUTTA-9

(Received, December 17, 1960)

**ABSTRACT.** A pressure defined expansion cloud chamber has been constructed and operated satisfactorily up to total pressures of 5 cm of Hg. The best track conditions for different total pressures as a function of the expansion ratio have been determined and discussed using ethyl, *n*-butyl and iso-amyl alcohols as condensant vapour and argon as permanent gas. Photographs of  $Po^{210}$ - $\alpha$  tracks taken at 5 cm. of Hg with iso-amyl alcohol and argon mixture are presented.

## 1. INTRODUCTION

A low pressure cloud chamber finds special applications in the study of uranium fission and of other low energy interactions of heavy charged particles with matter. Where the ranges of the observed track lengths in a gas at atmospheric pressure in such interactions are so short that the track lengths are not measurable, advantage of the fact that lowering of pressure of the gas-vapour mixture in the active volume of the chamber "magnifies" the ranges of the particles has been utilised to get greater details of the interaction. Thus, Joliot (1934) has operated a low pressure cloud chamber in order to study the mechanism by which heavy ions, resulting from radioactive decay, lose their energy. R. G. Mills (1953) has used a mechanical expansion mechanism to actuate a low pressure cloud chamber and operated at pressures of 4.5 cm in the investigation of the stopping power of He and water vapour.

Operation of a cloud chamber at low pressures involves additional difficulties which are not in common with cloud chambers generally used over a wide range of pressures. Lowering of the initial pressure is achieved by reducing the partial pressure of the permanent gas. The gamma coefficient of the vapour-gas mixture becomes smaller and in order to obtain the necessary supersaturation for condensation of the vapour on ions higher expansion ratios are needed. At the same time lowering of the partial pressures of the permanent gas restricts the uniform diffusion of the condensing vapour on growing drops. This effect becomes important in the low pressure region as the vapour-gas mixture has a low heat capacity. The low heat capacity and the large temperature variations involved for obtaining the necessary supersaturation result in an intensive and fast heat exchange between the filling mixture and the chamber walls leading

to the lowering of the supersaturation and a consequent shortening of the sensitive time. For this reason a fast expansion mechanism is of extreme importance in the operation of a low pressure cloud chamber.

The higher expansion ratios needed to work the cloud chamber at low pressures as mentioned earlier introduces the undesirable effects of turbulence motion of the gas molecules within the chamber, thereby resulting in the distortions of the tracks. This situation can be avoided by a suitable choice of the gas-vapour mixture such that good quality of tracks can be obtained for a given pressure with a relatively smaller and conveniently reproducible expansion ratio. Further the choice of the gas-vapour mixture has a vital role to play with reference to the particular mode of operation in which we are interested. In all randomly operated cloud chambers operating at low as well as high pressures, water vapour or some form of alcohol is used as a condensant vapour, together with a non-condensable gas like air or argon. Since the cloud chamber is intended to be triggered by an internal counter controlled mechanism such that the desired events can be selected and photographed by suitably running an open counter in the proportional region (Hodson *et al.*, 1950), a selective choice of the gas-vapour mixture has to be made so as to make a compromise between obtaining good tracks and at the same time operating the counter within for the same gas-vapour filling. In counter operation the production of gas multiplication depends on the electrons remaining freely mobile and electron attachment must be avoided. For this reason oxygen and water vapour have been excluded and our choice has been narrowed down to the study of several alcohols as condensants and argon as the non-condensable gas.

This paper describes the constructional details of a pressure defined expansion cloud chamber. Results of an investigation on the adequate choice of the gas-vapour mixture for obtaining best track conditions at different initial total pressures in relation to the expansion ratios are also presented.

## 2. CONSTRUCTIONAL DETAILS OF THE CHAMBER

The cloud chamber constructed is a pressure defined expansion chamber of the rubber diaphragm type and the assembly of the different components of the apparatus is shown in Fig. 1.

The front chamber which constitutes the active volume of the chamber is made of a perspex cylinder 10 inches i.d. and 2 inches in height, the wall thickness being  $1/4$  inch. A circular glass plate  $1/2$  inch thick covering the top of the perspex cylinder forms the window of the main chamber which faces the camera mounted vertically upwards for taking stereoscopic pictures. A thin rubber diaphragm  $1/32$  inch thick isolates the main chamber volume from a pan-shaped back chamber made of copper. The back chamber is separated from the vacuum ballast having a volume approx. 10 litres by means of an expan-



any major dismantling of the components of the apparatus, by means of a mutually coupled gear system as shown in Fig. 1. The perforated disc at the top is similar to the one at the bottom and is covered with a screen wire mesh which is faced with a black velvet cloth to form a uniform photographic background. The drill holes in the top plate together with the wire mesh and the pores in the velvet will define the stream lines of motion of the gas and reduce the turbulence of the gas molecules when the rubber diaphragm is being pulled down so that the tracks are free from distortion.

The underside of the glass plate is coated with a ring of Aquadag to make the surface electrically conductive. A sweep field of +45 volts is applied between this coating and the base of the chamber, which serves to remove the background ions produced by the tracks during the preceding expansion. For illumination of the tracks, two Mazda flash tubes, F.A.2 rated at 500 Joules are used. Two banks of condensers each 64  $\mu F$  normally charged to 2000 volts are discharged through the flash tubes by a spark coil. The spark coil is triggered by discharging a small condenser through the primary of the coil. Cylindrical lenses are used to collimate the light from the flashing units, into a parallel fan-shaped beam limited in height by diaphragms in order to avoid direct light reaching the top and the bottom of the chamber.

### 3. AUTOMATIC PRESSURE CONTROL DEVICE

The equipment shown at the right hand top of Fig. 1 is an automatic device for setting back the pressure in the back chamber to the same desired level after every expansion. The mechanism can be understood as follows: As soon as the magnet valve opens, expansion of the chamber takes place and there is a lowering of the back chamber pressure owing to its communication with the ballast which is maintained at a sufficiently low pressure. A little later the magnet current is short circuited by closing a relay included in the electronic sequence arrangement (not shown here) which returns the valve to its normal position and thus isolating the back chamber from the vacuum ballast. Simultaneously, the pressure difference in the back chamber is communicated to a mercury manometer *M*, through an auxiliary connection, taken from the bottom of the chamber. There are a number of contact points of tungsten fused into the right hand limb of the manometer at regular intervals and by changing the point of contact; the pressure in the back chamber can be cut off at discrete levels. In the present position of the mercury level as indicated in the manometer representing the state of affairs immediately after expansion, the relay coil  $C_1$  is energised and the relay is pulled down, thus interrupting the current in the coil  $C_2$  of the air admittance valve. This valve is the Edwards magnetic air admittance valve 1/16 inch bore, maintained closed magnetically against a spring which opens the valve to atmosphere when the current is switched off.

Thus, when the current in the magnet coil is switched off air is admitted through the valve into the back chamber and simultaneously the mercury level in the manometer is pushed down to a level just below the variable contact point. At this stage the relay coil  $C_1$  is de-energised and the current path for the air admittance valve is restored thus closing the magnet valve and preventing any further admittance of air.

In practice, however, after running for several days a thin conducting coating is formed on the inner glass walls of the mercury manometer owing to impurities in the mercury so that the spacing between the several variable contact points is electrically bridged up and the purpose of discretely cutting off the pressures is not achieved. This is avoided by cleaning the tungsten contacts and also rinsing the manometer with dilute Hydrofluoric acid and also filtering the mercury at intervals.

#### 4. RESULTS AND DISCUSSION

The main chamber was completely evacuated initially and simultaneously the back chamber was also evacuated to prevent implosion of the rubber diaphragm. 5 c.c. of dehydrated alcohol was injected into the main chamber and the desired total pressure in the working chamber has been set up by introducing argon whose flow is regulated by a needle valve. The total pressures in the main chamber are recorded by means of a mercury manometer, connected to

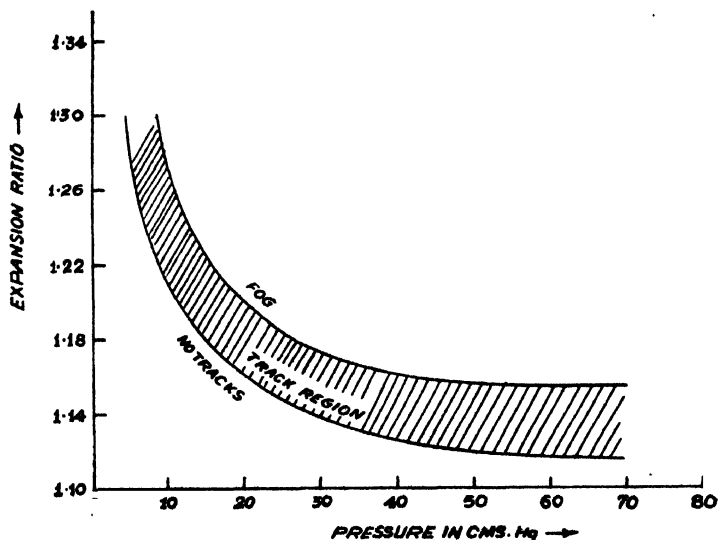


Fig. 2. A typical curve showing the variation of expansion ratio with initial total pressures for any alcohol showing the ion and cloud limits. This particular curve is that for iso-amyl alcohol.

the main chamber, not shown in Fig. 1. The expansion ratio, defined as the ratio of the initial to the final pressures, has been adjusted by defining the position of the stopping plate. The best track conditions were visually and photo-



graphically determined for different initial total pressures, each time the desired total pressure being built up by leaking in argon into the working chamber.

Fig. 2 presents the variation of expansion ratio with total pressures obtained for iso-amyl alcohol and argon.

The shaded area represents the region of track formation. The best track conditions, however, lie close to the lower boundary of this region. As we go towards the interior of this region and away, the tracks are masked with a background fog and the quality of tracks deteriorates. Observations have been carried out with different alcohols with a view to choose a suitable gas-vapour mixture for operating the chamber at very low pressures with conveniently reproducible expansion ratios. The results of investigation obtained with ethyl, *n*-butyl, iso-amyl alcohols are shown in Fig. 3 and in each of these curves only the best track conditions are presented.

In the above series of experiments  $\text{Po}^{210}$  tracks were visually observed and photographed at different pressures. The source in the form of a foil prepared in the laboratory from used random needles is mounted on a perspex base and supported inside the chamber from the wall of the perspex cylinder.

The interpretation of the general trend of the curves can be better understood from the following considerations.

The supersaturation produced as a result of expansion is given as (Das Gupta and Ghosh, 1946)

$$S = \frac{p_1}{p_2} (1 + \epsilon)^\gamma \quad \dots (1)$$

Where  $(1 + \epsilon)$  is the expansion ratio  $p_1, p_2$  are the saturation pressures at the initial and final temperatures.

$\gamma$  = ratio of specific heats of the complex gaseous mixture in the chamber. If  $p_g$  and  $p_v$  be the partial pressures of the gas and vapour with the corresponding  $\gamma'_g, \gamma'_v$  and  $\gamma_v, \gamma$  for the composite mixture is given by the formula due to Richarz (1906) as

$$\frac{1}{\gamma - 1} = \frac{1}{\gamma'_g - 1} \cdot \frac{p_g}{P} + \frac{1}{\gamma'_v - 1} \cdot \frac{p_v}{P} \quad (2)$$

where  $P$  is the total pressure equal to  $(p_g + p_v)$ .

It is seen from equation 2 that when the total pressure  $P$  is decreased by diminishing the gas pressure  $p_g$ ,  $p_v/P$  increases while  $p_g/P$  remains practically the same for  $p_g \gg p_v$  as a result the value of  $\gamma$  decreases. For a given expansion ratio the fall of temperature is therefore less and the supersaturation produced smaller. Thus, one needs a higher expansion ratio to attain the same degree of supersaturation. The curves plotted in Fig. 3 for the best rack conditions with different alcohol vapours show a functional dependence of the expansion ratio on the total initial pressures,

It is further observed by an intercomparison of the curves drawn for different alcohols that there is a finite dependence of the expansion ratio on the molecular weights of the alcohols involved. The heavier the alcohol, smaller is the expansion ratio needed to bring about the same degree of supersaturation for a

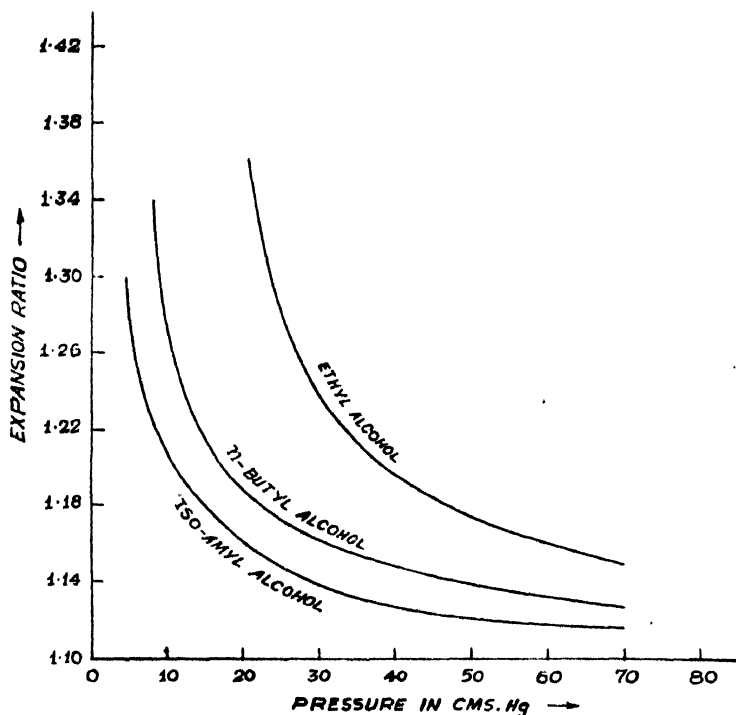


Fig. 3. Variation of expansion ratio with initial total pressures for best track conditions with different alcohols.

given pressure. Flood (1934) found that the value of supersaturation at the ion limit or cloud limit depends strongly upon the type of vapour used in the chamber. Thus, iso-amyl alcohol with a molecular weight 88.15 requires a much smaller expansion ratio than *n*-butyl alcohol whose molecular weight is 74.12.

It was shown by Powell (1928) that when the partial pressures of a condensable vapour becomes a large fraction of the whole pressure, many factors operate which restrict the growth of supersaturation. The supersaturation reached is much smaller than that deduced from adiabatic expansion. The effect is attributed to the evaporation of hot vapours from the free liquid surface in the chamber. Joliot (1934) has shown that the working expansion ratio increases from 1.305 at atmospheric pressure to about 2 when only saturated water vapour remains. It is thus apparent that the operation of a conventional cloud chamber with pure alcohols is a matter of considerable difficulty and the permanent gas plays an important role in its operation.

In the present set of observations it is seen that by using heavier alcohol, the initial total working pressure can be pushed down to lower pressures than with the lighter alcohols. In case of iso-amyl alcohol it is as low as 5 cm. This is perhaps on account of the fact that for a given total pressure, the vapour pressure contributed by the heavier alcohol is in a smaller proportion to the total pressure than for the lighter alcohols with the result that the permanent gas which is in considerable quantity plays its role for proper condensation at conveniently reproducible expansion ratios.



Fig. 4. A typical photograph of  $Po^{210} - \alpha$  tracks at 5 cm of Hg using iso-amyl alcohol and argon.

Fig. 4 shows a typical photograph of  $Po^{210} - \alpha$  tracks obtained at 5 cm of Hg using iso-amyl alcohol and argon as the filling mixture and the tracks can be seen stretched to lengths extending over the entire diameter of the chamber. Thus, the advantages of such magnified track lengths can be appreciated when one has to work with fission fragments or such other reaction products with low energy which have ranges of only few millimeters at atmospheric pressures.

#### ACKNOWLEDGMENTS

The author is indebted to Prof. B. D. Nag Chaudhuri, Director, Saha Institute of Nuclear Physics, for suggesting the problem and continued guidance through the progress of the work. Grateful thanks are due to Prof. D. N. Kundu for his helpful suggestions and discussions. In the earlier stages Mr. A. P. Patro was associated with the work, to whom thanks are also due.

## REFERENCES

- Das Gupta, N. N. and Ghosh, S. K., 1946, *Rev. Mod. Phys.*, **18**, 225.  
Flood, C. H., 1934, *Z. Phys. Chem.*, **170**, 294.  
Hodson, A. L., Loria, A. and Ryder, N. V., 1950, *Phil. Mag.*, **41**, 826.  
Joliot, F., 1934, *J. Phys. Radium*, **5**, 216.  
Mills, R. G., 1953, *Rev. Sci. Instr.*, **24**, 1041.  
Powell, C. F., 1928, *Proc. Roy. Soc., A*, **119**, 553.  
Richarz, F., 1906, *Ann. d. Physik*, **19**, 639.

# Letters to the Editor

The Board of Editors will not hold itself responsible for opinions expressed in the letters published in this section. The notes containing reports of new work communicated for this section should not contain many figures and should not exceed 500 words in length. The contributions must reach the Assistant Editor not later than the 15th of the second month preceding that of the issue in which the letter is to appear. No proof will be sent to the authors.

1

## EQUIVALENT PRESSURE CONCEPT IN CROSSED ELECTRIC AND MAGNETIC FIELD IN ELECTRODELESS DISCHARGE

S. N. SEN AND A. K. GHOSH

DEPARTMENT OF PHYSICS, JADAVPUR UNIVERSITY, CALCUTTA-32

(Received December 29, 1960)

Wehrli (1922) calculated the effect of a magnetic field on the breakdown condition of a gas by assuming that  $\lambda$ , the mean free path of the electron, is constant for all the electrons and under the action of the magnetic field the electrons will describe a cycloidal path and the mean free path  $\lambda$  will change to  $\lambda'$  such that

(1)

Where  $H$  is the magnetic field in Gauss,  $e$  and  $m$  are the charge and mass of the electron and  $E$  is the breakdown voltage per centimetre length of the discharge tube. Hence the effect of magnetic field is equivalent to an increase of pressure  $P$  to  $P_e$  such that

$$P_e = \frac{P}{\left[1 + \frac{eH^2\lambda}{8Em}\right]} \quad \dots \quad (2)$$

Blevin and Haydon (1958) arrived at a new expression for equivalent pressure by calculating the electron mass energy and drift velocity in a magnetic field and  $P_e$  in their case is given by

$$P_e = P \sqrt{1 + \frac{CH^2}{P^2}} \quad (3)$$

where

$$C = \left( \frac{e}{m} \cdot \frac{L}{u} \right)^2$$

$L$  is the mean free path of the electron in the gas at a pressure of 1 m.m. and  $u$  is the velocity of the electron. It can be seen from equation (3) that

$$P_e = P \sqrt{1 + \frac{e^2}{m^2} \cdot \frac{L^2}{u^2} \cdot \frac{H^2}{P^2}}$$

and if it can assumed that  $\frac{1}{2}mu^2 = eEd$  where  $d$  is the length of the discharge tube then

$$\frac{P_e}{P} = \sqrt{1 + \frac{1}{2} \cdot \frac{e}{m} \cdot \frac{L^2 H^2}{P^2 E d}} \quad (\text{Blevin and Haydon's formula})$$

and from Eqn. (2)

$$\frac{P_e}{P} = \left[ \frac{1}{8PEm} \right] \quad (\text{Wehrli's formula}) \quad \dots (4)$$

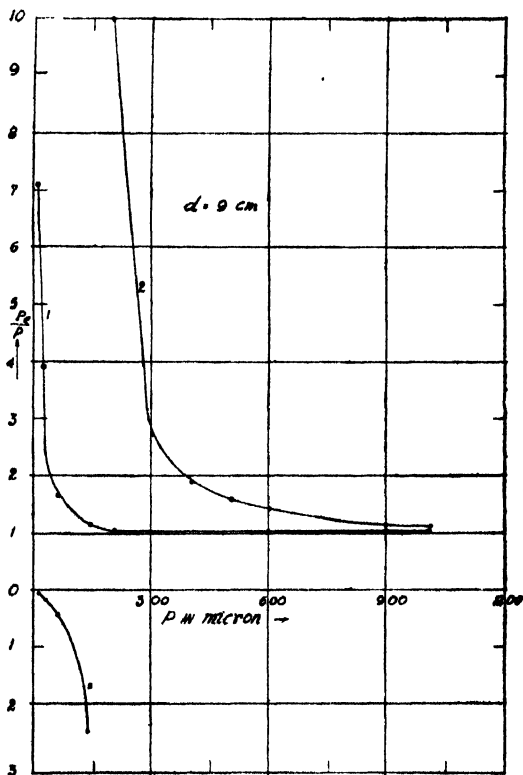


Fig. 1

We have recently measured the breakdown potential in air in crossed electric and magnetic field within the pressure range  $1 \times 10^{-3}$  to 1 mm of Hg, the discharge being excited by means of a 10 KV transformer. The magnetic field has been varied from 50 Gauss to 2000 Gauss and three discharge tubes of length

9 cm, 22.5 cm. and 26.5 cm. have been used. From the measured breakdown potential data, the values of  $P_e/P$  have been calculated using both the expressions in Eqn. (4) where the magnetic field has been taken as 100 Gauss and in Figs. (1) and (2),  $P_e/P$  has been plotted against the corresponding pressure. From the curves it appears that the relative change of pressure as obtained from Blevin and Haydon's formula is large when the pressure is very small, that is below  $60\mu$  of Hg. and then drops suddenly and becomes insignificant above  $200\mu$ . On the other hand, Wehrli's formula predicts negative values of equivalent pressure at low pressure which is anomalous. At about  $20\mu$  of Hg,  $P_e/P$  becomes very large in the case of Wehrli's formula and then drops suddenly and both the curves become asymptotic to the straight line  $P_e/P = 1$  at higher pressures. Values of  $P_e/P$  calculated for higher magnetic fields also give similar nature of the curve. If calculations for the equivalent pressure be made using Wehrli's formula for

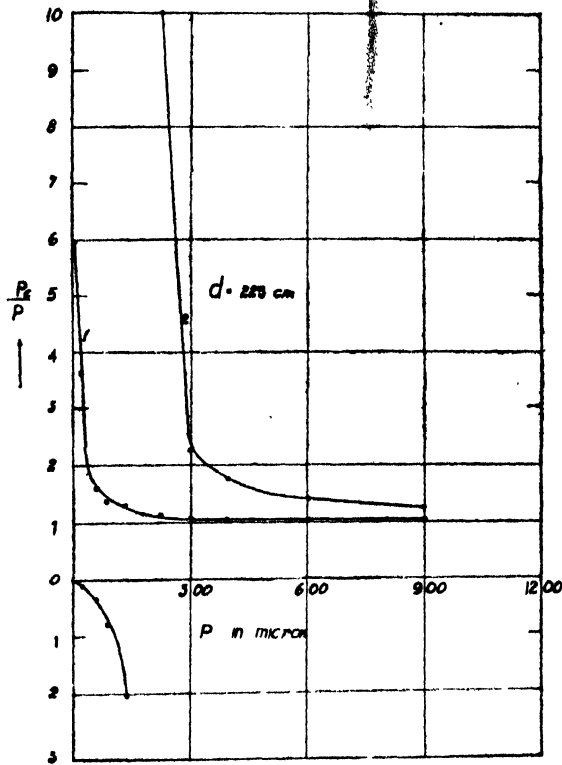


Fig. 2

Fig. 2

small values of magnetic field of the order of 15 to 30 Gauss then it predicts positive values of  $P_e$  at low pressure. Thus at low pressure, Wehrli's formula becomes valid only if the magnetic field is small. It can be seen from Fig. 1, that both the curves almost provide the same value of  $P_e/P$  above  $900\mu$  of Hg.

and above  $200\mu$  the change of  $P_0/P$  is insignificant. But in our experiment it has been noted that the effect of magnetic field on breakdown potential is dominant at higher pressure also. Thus it can be concluded that both the above expressions for  $P_0$  are of limited applicability and the concept of equivalent pressure alone cannot explain all the observed results. So far the variation of  $\gamma$ , Townsend's second coefficient in a magnetic field, has been neglected, but we have recently deduced an expression for variation of  $\gamma$  with  $(E/P)$  (Sen and Ghosh 1961) and it is hoped that the incorporation of variation of  $\gamma$  with  $H$  along with equivalent pressure concept will explain the observed changes better.

#### ACKNOWLEDGMENT

The present work forms of a programme on scheme on "Electrical discharge through gases and vapours and its investigation by microwave probe and optical method" and the authors are indebted to Council of Scientific and Industrial Research for financing the project. One of the authors (A.K.G.) is grateful for the award of a junior scholarship.

#### REFERENCES

- Blevin, H. A. and Hayden, S. C., 1958, *Aust. J. Phys.*, **11**, 18.  
Sen, S. N. and Ghosh, A. K., 1961, *Proc. Ind. Sci. Cong.*, 48th Session.  
Wehrli, M., 1922, *Ann. d. Phys.*, **4**, 69.



# A NOTE ON THE PROBLEM OF INTRODUCING SPHERICALITY CORRECTION TO CONSERVATIVE SCATTERING STELLAR ATMOSPHERE MODEL

K. K. SEN

LECTURER IN PHYSICS, UNIVERSITY OF MALAYA, SINGAPORE

(Received, March 21, 1960)

**ABSTRACT.** The relative magnitude of the correction to be applied for the curvature in the study of the radiative transfer problem in the conservative scattering stellar atmosphere has been calculated. Wick-Chandrasekhar method of solution for the integro-differential equation of transfer has been employed in the first approximation. The results are shown in a tabular as well as graphical form.

The problem of transfer of radiation in the case of extended atmospheres of stars in which the curvatures of the layers of atmospheres has significant effect on the transfer problem, has been considered by Kosirev (1934) and Chandrasekhar (1934). On the other hand, it is quite well known in the theory of radiative transfer that for most stars such as the sun, the atmosphere can be considered to be plane parallel. In a recent paper, Barbier (1956) discussed the problem for near solar case and established that it is not necessary to consider the atmosphere as spherically symmetrical. The purpose of the present note is to examine the magnitude of correction involved in passing from plane parallel to the spherically symmetrical case for different values of optical thickness of the stellar atmosphere in the conservative scattering case.

In the present case, the atmosphere chosen is thin, finite and conservative scattering. The equation of transfer appropriate to the problem of spherically symmetric atmosphere is given by (Radiative Transfer—Chandrasekhar, p. 364)

$$\mu \frac{\partial I(r, \mu)}{\partial r} + \frac{p - \mu^2}{r} \frac{\partial I(r, \mu)}{\partial \mu} = -k\rho I(r, \mu) + \frac{1}{2}k\rho \int_{-1}^{+1} I(r, \mu') d\mu' \quad \dots (1)$$

and appropriate equation for the plane case is given by

$$\mu \frac{dI}{dr}(r, \mu) = -k\rho I(r, \mu) + \frac{1}{2}k\rho \int_{-1}^{+1} I(r, \mu') d\mu' \quad \dots (2)$$

Here  $I(r, \mu)$  is the specific intensity of radiation at a distance  $r$  from the centre of the star in a direction  $\mu$  where  $\mu = \cos \nu$ ,  $\nu$  being the angle between the direction of the ray and the outward drawn normal to the atmosphere. Both of

these equations are solved by the method of Wick-Chandrasekhar in the first approximation. Thus Eq. (1) is transformed into the following group of equations (Radiative Transfer—Chandrasekhar, p. 366) :

$$\left. \begin{aligned} \frac{d}{dr} \Sigma a_i \mu_i I_i + \frac{2}{r} \Sigma a_i \mu_i I_i &= 0 \\ \frac{d}{dr} \Sigma a_i \mu_i^2 I_i + \frac{1}{r} \Sigma a_i (3\mu_i^2 - 1) I_i &= -k\rho \Sigma a_i \mu_i I_i \end{aligned} \right\} \dots (3)$$

And for the plane parallel case, the Eq. (2) can be written out formally by dropping out the second term on the right hand side of (1) and that in the Eq. (129) of Radiative Transfer, p. 366.

$$\left. \begin{aligned} \frac{d}{dr} \Sigma a_i \mu_i I_i &= 0 \\ \frac{d}{dr} \Sigma a_i \mu_i^2 I_i &= -k\rho \Sigma a_i \mu_i I_i \end{aligned} \right\} \dots (4)$$

In the case of the first approximation  $a_{+1} = a_{-1} = 1$  and  $\mu_{+1} = \frac{1}{\sqrt{3}} = -\mu_{-1}$ .

The boundary conditions under which the equation is to be solved are the following :

(1) At the inner boundary of the atmosphere denoted by  $r = r_0$ , the outward intensity  $I_{+1}$  is very strong in comparison with  $I_{-1}$ , the inward intensity.

(2) At the outer boundary of the atmosphere denoted by  $r = R$ , there is no incident radiation from outside ( $I_{-1}$  is zero).

The solution of the first of Eqs. (3) yields

$$\frac{1}{2} F = \Sigma a_i \mu_i I_i = \frac{1}{2} \cdot \frac{F_0}{r^2}, \text{ where } F_0 \text{ is a constant.}$$

Hence 
$$I_{+1} - I_{-1} = \frac{\sqrt{3}}{2} \cdot \frac{F_0}{r^2} \quad (5)$$

The second of Eq. (3) solves as

$$\begin{aligned} \frac{1}{3} \frac{d}{dr} (I_{+1} + I_{-1}) &= -\frac{k\rho}{\sqrt{3}} (I_{+1} - I_{-1}) = \frac{k\rho}{2} \cdot \frac{F_0}{r^2} \\ (I_{+1} + I_{-1}) &= \frac{3}{2} F_0 \int_r^\infty \frac{k\rho dr}{r^2} + A \end{aligned} \quad (6)$$

where  $A$  is a constant, and this can be determined by the boundary condition (1)

$$A = \frac{\sqrt{3}}{2} \cdot \frac{F_0}{r_0^2} - \frac{3}{2} F_0 \int_{r_0}^R \frac{k \rho dr}{r^2} \quad \dots (7)$$

$$\therefore I_{+1} + I_{-1} = \frac{\sqrt{3}}{2} \cdot \frac{F_0}{r_0^2} - \frac{3}{2} F_0 \int_{r_0}^R \frac{k \rho dr}{r^2} + \frac{3}{2} F_0 \int_r^R \frac{k \rho dr}{r^2} \quad \dots (8)$$

At  $r = R$ , the outer boundary of the atmosphere

$$(I_{+1})_{r=R} = \frac{\sqrt{3}}{2} \frac{F_0}{r_0^2} - \frac{3}{2} F_0 \int_{r_0}^R \frac{k \rho dr}{r^2} \quad \dots (9)$$

In the plane case, we can proceed in the similar way. The solution of the first of the Eq. (4)

$$\sum a_i \mu_i I_i = \frac{1}{2} F = \frac{1}{2} \frac{F_0}{r_0^2} \quad \dots (10)$$

where  $F_0$  and  $r_0$  have the same meaning as before. The flux is constant in the plane parallel case

$$I_{+1} - I_{-1} = \frac{\sqrt{3}}{2} \frac{F_0}{r_0^2} \quad (11)$$

The second of Eqs. (4) yields

$$I_{+1} + I_{-1} = \frac{3}{2} \frac{F_0}{r_0^2} \int_r^R k \rho dr + B \quad (12)$$

Using the boundary condition (1)

$$B = \frac{\sqrt{3}}{2} \frac{F_0}{r_0^2} - \frac{3}{2} \frac{F_0}{r_0^2} \int_{r_0}^R k \rho dr \quad (13)$$

$$I_{+1} + I_{-1} = \frac{\sqrt{3}}{2} \frac{F_0}{r_0^2} - \frac{3}{2} \frac{F_0}{r_0^2} \int_{r_0}^R k \rho dr + \frac{3}{2} \int_r^R k \rho dr \quad (14)$$

Then from the boundary condition (2), the incident radiation from outside at the outer boundary of the atmosphere may be taken to be zero

$$(I_{+1})_{r=R} = \frac{\sqrt{3}}{2} \frac{F_0}{r_0^2} - \frac{3}{2} \frac{F_0}{r_0^2} \int_{r_0}^R k \rho dr \quad \dots (15)$$

In the astrophysical context,  $k\rho$  is generally taken to vary as an inverse power of  $r$  (greater than unity)

$$\therefore k\rho = Cr^{-n}, \text{ where } C \text{ is a constant} \quad \dots (16)$$

The optical thickness  $\tau$ , measured from  $r = R$  inwards is given by

$$\int_r^R k\rho dr = \frac{C}{n-1} \left[ \frac{1}{r^{n-1}} - \frac{1}{R^{n-1}} \right] \quad \dots (17)$$

$$\therefore \tau_1 = \frac{C}{n-1} \left[ \frac{1}{r_0^{n-1}} - \frac{1}{R^{n-1}} \right] \quad \dots (18)$$

i.e.,  $\tau = \tau_1$  denotes the photospheric surface at  $r = r_0$ . When  $n = 2$ , the emergent intensity  $(I_{+1})_R$  for the spherical and the plane case is given by the two Eqns. (19) and (20).

For the spherical case

$$\frac{(I_{+1})_{\tau=0}}{\sqrt{\frac{3}{2}} F_0/r_0^2} = (1 - \sqrt{3}\tau_1) + \frac{\tau_1}{\sqrt{3}} \left[ 2 - \frac{r_0}{R} - \frac{r_0^2}{R^2} \right] \quad \dots (19)$$

and for the plane case

$$\frac{(I_{+1})_{\tau=0}}{\sqrt{\frac{3}{2}} F_0/r_0^2} = (1 - \sqrt{3}\tau_1) \quad \dots (20)$$

$$\therefore \frac{(I_{+1})_{\tau=0} \text{ (spherical)}}{(I_{+1})_{\tau=0} \text{ (plane)}} = 1 + \left[ \frac{\tau_1}{\sqrt{3}(1 - \sqrt{3}\tau_1)} \left( 2 - \frac{r_0}{R} - \frac{r_0^2}{R^2} \right) \right] \quad \dots (21)$$

The term within box bracket is obviously the term which arise from the curvature of the atmosphere and can be called sphericity correction in the present approximation for  $n = 2$ . The value of correction for different values of optical thickness  $\tau_1$  corresponding to several values  $\frac{R-r_0}{r_0}$  are shown below in Table I.

The results are shown in Fig. 1.

In the similar way, it can be shown that for  $n = 3$ , the equation corresponding to (21) turns out to be

$$\frac{(I_{+1})_{\tau=0} \text{ (spherical)}}{(I_{+1})_{\tau=0} \text{ (plane)}} = 1 + \left[ \frac{\sqrt{3}\tau_1}{2(1 - \sqrt{3}\tau_1)} \left( 1 - \frac{r_0^2}{R^2} \right) \right] \quad \dots (22)$$

The values of the correction terms within box bracket in the present approximation for  $n = 3$  are noted below for different values of  $\tau_1$  and  $R-r_0$  in Table II.

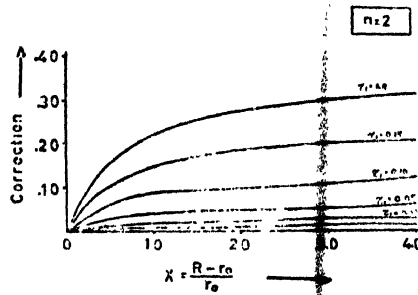


Fig. 1

TABLE I

$\tau_1 \cdot \frac{R-r_0}{r_0}$	0.25	0.50	1.00	2.00	4.00
0	0	0	0	0	0
0.01	0.003	0.003	0.007	0.009	0.010
0.025	0.008	0.013	0.019	0.023	0.026
0.050	0.018	0.028	0.037	0.047	0.056
0.10	0.039	0.062	0.087	0.098	0.123
0.15	0.066	0.104	0.146	0.182	0.206
0.20	0.099	0.157	0.221	0.275	0.311

TABLE II

$\tau_1 \cdot \frac{R-r_0}{r_0}$	0.25	0.50	1.00	2.00	4.00
0	0	0	0	0	0
0.01	0.003	0.004	0.006	0.008	0.008
0.025	0.008	0.011	0.017	0.020	0.021
0.05	0.017	0.025	0.033	0.040	0.046
0.10	0.038	0.055	0.078	0.084	0.101
0.15	0.064	0.093	0.131	0.156	0.168
0.20	0.095	0.140	0.199	0.236	0.254

The results are shown in Fig. 2.

From the graphs it is clear that there is no common region of applicability for the equation of transfer in the plane-parallel and the spherically symmetric

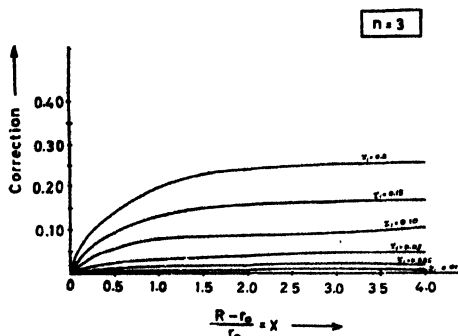


Fig. 2

case. As is physically expected, for any particular  $\tau_1$ , the smaller value of  $\frac{R-r_0}{r_0}$ , the smaller will be the magnitude of the correction term; and for any value of  $\frac{R-r_0}{r_0}$ , the smaller the value of  $\tau_1$ , the less significant will be the correction term.

In conclusion, the author takes pleasure in recording his gratitude to Prof. N. R. Sen for the benefit of discussion at the initial stage of the preparation of the paper and to Monsieur Spite of Laboratoire d'Astronomie, Lille, France for some active suggestions.

#### REFERENCES

- Chandrasekhar, S., 1934. *Monthly Notices Roy. Astro. Soc. London.*, **94**, 444-457.  
 Chandrasekhar, S., *Radiative Transfer*, p. 23, 364-370.  
 Kosirev, N. A., 1934. *Monthly Notices Roy. Astro. Soc. London.*, **94**, 430-443.  
 Barbier, 1956. *Annales d'Astrophysique*, **19**, 4.

# THEORY OF INDIRECT EXCHANGE INTERACTION IN SPINEL-LIKE SYSTEMS\*

K. P. SINHA

NATIONAL CHEMICAL LABORATORY, POONA-8

(Received, September 1, 1960)

**ABSTRACT.** A theoretical study of the indirect exchange interaction for the spin coupling in spinel type magnetic compounds is made on the basis of a mechanism suggested by us recently. Detailed calculations are carried out for the elementary, four-centre (A-O-B<sub>2</sub>; A and B represent the cations and O denotes the anion) and five-electron system. This furnishes the appropriate model for describing both A-B and B-B types of interactions.

The relative energies of the ferromagnetic (Quartet  $Q$ ) and the two ferrimagnetic (Doublets  $D_1$  and  $D_2$ ) states are assessed for the above model. It is shown that, within the framework of the present mechanism, the ferrimagnetic state  $D_1$ , which represents antiparallel spins in A-B and parallel in B-B, is the most stable state. This is in agreement with the observed situation.

## 1. INTRODUCTION

Some recent papers (Anderson, 1959; Koide, Sinha and Tanabe, 1959) on superexchange interaction have led to a reappraisal of the types of mechanisms responsible for the spin coupling of magnetic ions in certain magnetic compounds (see also Kanamori, 1959; Keffer and Oguchi, 1959). It seems that of the various mechanisms proposed some are only apparently distinct and others embrace complementary features of the physical situation. However, it remains to establish as to which of these play the dominant role.

One of these mechanisms, which is analogous to spin-polarization around a nucleus that leads to nuclear indirect exchange was recently suggested by us (Koide, Sinha and Tanabe, 1959). It constitutes an important spin dependent effect and the contributions due to this mechanism needs to be fully assessed for each type of crystal structure while discussing the magnetic properties of such compounds. The previous paper, in addition to dealing with the general formulation of the mechanism in terms of semi-localized orbitals for the anion electrons, furnishes a quantitative calculation for the collinear three centre and four electron system applicable to magnetic compounds having rock salt or perovskite type structures. In another paper (Sinha and Koide, 1960), we have given a theoretical study of this interaction by choosing an elementary unit

\* Contribution No. 415 from the National Chemical Laboratory, Poona 8.

which is appropriate for zinc-blends type structures. In the present paper we give an analysis of the indirect exchange interactions in spinel-like systems, using, as in our previous papers, the Heitler-London method with the inclusion of the correlation effect which involves spin dependent transitions of the anion electrons.

## 2. THEORETICAL MODEL

It is appropriate to discuss briefly the relevant features of spinel structure before coming to the model chosen for calculation (for a fuller description of the structure see Gorter, 1954). The ideal spinel structure can be described as a cubic close packed lattice of anions (e.g.,  $O^{2-}$ ) with metal ions partly filling the tetrahedral (half of the 16 A sites) and the octahedral (half of the 32 B sites) interstices. There are eight molecules in the cubic unit cell, the molecular formula being  $AB_2O_4$ . The immediate environment of each metal ion is thus cubic. The oxide ion, however, has four nearest neighbour metal ions of which three are at octahedral (B) sites and the fourth is in a tetrahedral (A) site. The three octahedral cations are situated at a distance  $R_o$  along three mutually perpendicular directions from the oxide ion. The tetrahedral cation is in the  $\langle 111 \rangle$  direction at a distance  $R_t$  and away from the octant which contains the three octahedral cations. The immediate symmetry around the oxide ion i.e., of the unit  $A-O-B_3$  is described by the point group  $C_{3v}$ ; the next nearest neighbours of this oxide ion are twelve oxide ions of the face centred cubic lattice.

According to Neel's (1948) phenomenological theory for ferromagnetic spinels, there are three types of negative interactions, namely A-A, B-B and A-B, the relative strengths of which determine the ultimate coupling; assuming, of course, the presence of one kind of magnetic ion (e.g.,  $Fe^{3+}$ ) only. If the AB interaction is much stronger than A-A and B-B interactions, the spin ordering  $\vec{A} [\vec{B}_2]$  is favoured. This constitutes the fundamental assumption of the two sub-lattice model of Neel. However, when either of A-A and B-B interaction is comparable with A-B interaction, further generalizations as envisaged by Yafet and Kittel (1952) by dividing A into two sub-lattices  $A_1$  and  $A_2$  and B into four sub-lattices  $B_1$ ,  $B_2$ ,  $B_3$  and  $B_4$ , have to be considered. These considerations lead to certain triangular arrangements of the spin vectors associated with the sub-lattices.

The strengths of these interactions would depend on the nature and mechanism of the fundamental types of indirect exchange interactions involving the anion lattice as well as the cation-anion-cation angles and cation-cation and cation-anion distances. Aside from qualitative discussions (Wollan, 1960), no non-empirical analysis of such indirect exchange interactions in spinel-like systems has been made. In what follows, we consider a detailed calculation for one of the mechanisms suggested before, on the basis of an appropriate model chosen.



In view of the large A-A distance and unfavourable angles, we shall disregard the study of the A-A interaction. As is supported by experimental results this interaction, in any way, is too feeble. The problem then is to select a model which includes the effect of both A-B and B-B interactions. Although we shall always keep the unit A-O-B<sub>3</sub> (with  $C_{3v}$  symmetry) in mind, we choose a still smaller unit, namely, A-O-B<sub>2</sub>, which furnishes the appropriate model for describing both types of interactions. At times, while considering the symmetry of orbitals involved in the study, we shall refer to the complete unit having  $C_{3v}$  symmetry. If the O<sup>2-</sup> ion in the unit A-O-B<sub>2</sub> was in the plane of A-B<sub>2</sub>, the symmetry of A-O-B<sub>2</sub> would have been taken as  $C_{2v}$ . Since, O<sup>2-</sup> is slightly below this plane, this symmetry is lost. However, we shall make use of some symmetry planes even for this unit in order to classify the orbitals and to study the nature of wavefunctions. The geometry of the unit is shown in Fig. 1.

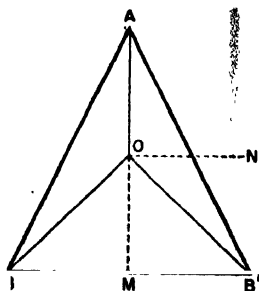


Fig. 1

### 3. THE WAVE FUNCTIONS OF THE CATION ELECTRONS

We consider one representative electron each from the three magnetic ions i.e., one at the tetrahedral, site A, and the other two at the octahedral sites B and B<sup>1</sup>. Each electron is assumed to be coupled strongly by intraatomic spin dependent interaction while moving in the field of their respective ion cores. Only one type of magnetic ions are considered for simplicity with  $d^5$  electronic configuration and in  ${}^6S_{5/2}$  state e.g., Fe<sup>3+</sup>.

We denote the orbital functions of the electrons of the two octahedral cations by  $u_1$  and  $u_2$  and that of the tetrahedral cation by  $v$ . In the choice of the explicit forms of these orbitals, we shall be guided by their degree of overlap with the anion orbitals, and the splitting of the  $d$  orbitals in the crystal field. It is well known that in the cubic field due to octahedrally situated six surrounding ions the  $3d$  level of the magnetic ion splits up into lower triplets ( $t_{2g}$ ) and the upper doublets ( $e_g$ ), the triplets being  $d_{xy}$ ,  $d_{yz}$  and  $d_{zx}$  and the two doublets being  $d_{x^2-y^2}$  and  $d_{z^2}$ . When the cations are tetrahedrally surrounded by the anions, the situation is reversed and the triplets are higher than the doublets.

If the three cartesian axes are taken to be the lines joining the anion to the three octahedral cations, then the obvious choice for  $u_1$  and  $u_2$  would be one of the  $e_g$  orbitals, in particular, the  $d$ -function having axial symmetry with respect to the bonds BO and B'O (see Fig. 1). For  $v$  one can take the appropriate  $t_{2g}$  orbital. Any other choice of axes (e.g., AO as the  $z$  axis and  $x$  parallel to BB' and passing through O) would not make any difference in the calculations presented below in that the orbitals can be re-expressed by suitable transformations. Thus we assume the following behaviour of  $u_1$ ,  $u_2$  and  $v$  under reflection in the plane  $AM$  normal to the figure (Fig. 1).

$$u_1 \longleftrightarrow u_2 \quad \text{and} \quad R_{AM}v = v$$

where  $R_{AM}$  denotes the corresponding operation. Switching over to the condition  $R_{AM}v = -v$  would not bring about any difference in the physical arguments involved in the calculations.

Including the spin functions, we shall have eight Slater determinants for the three cation electron system. We shall choose such linear combinations of these which are eigenstates of the  $S^2$  operator. We have one quartet and two doublet states. These are given below :

$$|^4\Phi_{od}(M_s = \frac{3}{2})>_c = [u_1u_2v] \quad \dots \quad (3.1)$$

$$|^2\Phi_{od}(\frac{1}{2})>_c = \{[u_1\bar{u}_2v] + [\bar{u}_1u_2v] - 2[u_1u_2\bar{v}]\} / \sqrt{6} \quad \dots \quad (3.2)$$

$$|^2\Phi_{ev}(\frac{1}{2})>_c = \{[u_1\bar{u}_2v] - [\bar{u}_1u_2v]\} / \sqrt{2} \quad \dots \quad (3.3)$$

Here the bracket notation represents the usual Slater determinant multiplied by  $(N!)^{-1}$  (in this case  $(3!)^{-1}$ ). The orbitals without bar include up spin and with bar down spin functions of the electrons in them. The suffix  $c$  outside the kets refers it with respect to cation electrons and the suffixes  $od$  or  $ev$  denote that the states are odd or even under the operation  $R_{AM}$ .

The classification of the states with respect to the symmetry operation  $R_{AM}$  has the following advantage. The quartet  $|^4\Phi_{od}>_c$ , of course, would represent the ferromagnetic state. The ferrimagnetic state  $|^2\Phi_{od}>_c$  represents the situation where the spins in A and B are antiparallel, while that of BB are parallel. In effect, this would represent a dominant negative A-B interaction. The state  $|^2\Phi_{ev}>_c$ , however, represents the reverse situation with antiparallel spins of BB and parallel spins of AB. This represents the case with stronger B-B interaction. The picture remains incomplete unless the effect of anion electrons is included.

#### 4. THE WAVE FUNCTIONS OF THE ANION ELECTRONS

Unlike our previous papers, where for anion electrons semilocalized orbitals are used, we shall follow a perturbation procedure right through in the present

formulation. We consider two anion electrons which play the dominant role in our mechanism. The appropriate  $2p$  orbitals of the anion (e.g.,  $O^{2-}$ ) are no longer degenerate in the crystal field for the unit  $A-O-B_3$  with  $C_{3v}$  symmetry. For the choice of axes along the three octahedral cations, the crystal field  $VC_{3v}$  gives rise to one non-degenerate orbital,

$$p_1(A_1) = \frac{1}{\sqrt{3}}(p_x + p_y + p_z) \quad \dots \quad (4.1)$$

belonging to  $A_1$  representation of  $C_{3v}$  group and two degenerate orbitals, belonging to  $E$  representations i.e.,

$$\left. \begin{aligned} p_2(E) &= \frac{1}{\sqrt{2}}(p_x - p_y) \\ p_3(E) &= \frac{1}{\sqrt{6}}(2p_z - p_x - p_y) \end{aligned} \right\} \quad \dots \quad (4.2)$$

If, on the other hand, AO is taken as the  $z$  axis and ON as the  $x$  axis, it can be easily shown that  $p_z$  belongs to  $A_1$  representation and its energy differs from the doubly degenerate orbitals  $p_x$  and  $p_y$  belonging to  $E$  representation. It is seen for both cases that the orbital belonging to  $A_1$  representation has a larger overlap with the orbitals of the cation electrons.

We represent the zeroth order ground state for the anion system by considering the representative two electrons with coupled spins in the orbital belonging to  $A_1$  representation. We denote this symbolically by  $\phi$ . It may be added that for the restricted unit  $A-O-B_2$  we shall replace  $p_1(A_1)$  by

$$p_1 = (p_z + p_x)/\sqrt{2} \quad (4.3)$$

with OB as  $z$  axis and OB' as  $x$  in that the effect of  $p_y$  would be negligible. Thus our  $\phi$  would represent  $p_1$  as given by (4.3) or  $p_z$  depending on the choice of axes. In effecting the actual transformation the vector-like nature of the  $p$  orbitals should be taken into account.

The wave functions of the two anion electrons in the zeroth order ground state is expressed as

$$|{}^1\chi^{(0)}_{av} >_a = [\phi\phi] \quad (4.4)$$

which is even under  $R_{AM}$ .

We defer the specific choice of excited orbitals until later sections and consider their effect in terms of some symmetry properties. It would suffice to consider the configurational interactions in terms of transitions to two types of orbitals, one even under  $R_{AM}$  and the other odd. They are respectively denoted by  $\gamma$  and  $\eta$ .

We have the following triplet states for the two anion electrons under consideration.

$$|^3\chi_{ev}>_a : \left\{ \begin{array}{l} [\phi\gamma] \\ \{[\phi\bar{\gamma}] + [\bar{\phi}\gamma]\} / \sqrt{2} \\ [\bar{\phi}\bar{\gamma}] \end{array} \right\} \quad \dots (4.5)$$

$$|^3\chi_{od}>_a : \left\{ \begin{array}{l} [\phi\eta] \\ \{[\phi\bar{\eta}] + [\bar{\phi}\eta]\} / \sqrt{2} \\ [\bar{\phi}\bar{\eta}] \end{array} \right\} \quad \dots (4.6)$$

Singlet states for the two anion electrons involving  $\gamma$  or  $\eta$  will have much higher energy than those described above and accordingly we omit them.

## 5. THE WAVE FUNCTIONS OF THE TOTAL SYSTEM

We first consider the zeroth order ground states of the total five electron and four centre system. The lowest state of the two anion electrons is  $|^1\chi_{ev}>_a$  (cf. Eq. (4.4)) and hence the lowest ferromagnetic and two ferrimagnetic states are given by the products of (4.4) with (3.1), (3.2) and (3.3) respectively.

*Ground states :*

$$|^4\bar{\psi}_{od}^{(1)}> = ({}^4\bar{\Phi}_{od}^{(1)})_c ({}^1\chi_{ev}^{(0)})_a > = [u_1 u_2 v \phi \bar{\phi}] \quad \dots (5.1)$$

$$\begin{aligned} |{}^2\bar{\psi}_{od}^{(1)}> &= |({}^2\bar{\Phi}_{od}^{(1)})_c ({}^1\chi_{ev}^{(0)})_a > \\ &= \{[u_1 \bar{u}_2 v \phi \bar{\phi}] + [\bar{u}_1 u_2 v \phi \bar{\phi}] - 2[u_1 u_2 \bar{v} \phi \bar{\phi}]\} / \sqrt{6} \quad \dots (5.2) \end{aligned}$$

$$\begin{aligned} |{}^2\bar{\psi}_{ev}^{(1)}> &= |({}^2\bar{\Phi}_{ev}^{(1)})_c ({}^1\chi_{ev}^{(0)})_a > \\ &= \{[u_1 \bar{u}_2 v \phi \bar{\phi}] - [\bar{u}_1 u_2 v \phi \bar{\phi}]\} / \sqrt{2} \quad \dots (5.3) \end{aligned}$$

A large number of excited states for the total system is possible. These are the products of the cation states (3.1), (3.2) and (3.3) and the excited triplet states of the anion, namely, (4.5) and (4.6). We shall write down only those states which have the appropriate symmetry corresponding to the respective zeroth order ferromagnetic and ferrimagnetic states. Others with different symmetry are of no consequence in that they do not interact with the corresponding ground states described by (5.1) to (5.3). The excited states involving transitions to  $\gamma$  and  $\eta$  type orbitals are given below :

## Excited States

*Quartets*

$$\begin{aligned} |{}^4\bar{\psi}_{od}^{\gamma_1}(\frac{1}{2})> &= \sqrt{\frac{2}{5}} |({}^4\bar{\Phi}_{od}^{(1)})_c ({}^3\chi_{ev}^{(1)})_a > - \sqrt{\frac{2}{5}} |({}^4\bar{\Phi}_{od}^{(1)})_c ({}^3\chi_{ev}^{(0)})_a > \\ &= \{2[(\bar{u}_1 u_2 v \phi \gamma) + [u_1 \bar{u}_2 v \phi \gamma] + [u_1 u_2 \bar{v} \phi \gamma]] \\ &\quad - 3[(u_1 \bar{u}_2 v \phi \bar{\gamma}) + [\bar{u}_1 u_2 v \phi \bar{\gamma}]]\} / \sqrt{30} \quad \dots (5.4) \end{aligned}$$

$$\begin{aligned}
 |^4\bar{\psi}_{od} \gamma^2(\frac{3}{2})\rangle &= |(^2\bar{\Phi}_{od}^{(1)})_o(^3\chi_{ov}^{(1)})_a\rangle \\
 &= \{2[u_1u_2\bar{v}\phi\gamma] - [u_1\bar{u}_2v\phi\gamma] - [\bar{u}_1u_2v\phi\gamma]\} / \sqrt{6} \quad \dots (5.5)
 \end{aligned}$$

Doublets

$$\begin{aligned}
 |^2\bar{\psi}_{od} \gamma^1(\frac{1}{2})\rangle &= \sqrt{\frac{6}{15}} |(^2\bar{\Phi}_{od}^{(1)})_o(^3\chi_{ov}^{(0)})_a\rangle - \sqrt{\frac{4}{15}} |(^2\bar{\Phi}_{od}^{(-1)})_o(^3\chi_{ov}^{(1)})_a\rangle \\
 &= \{([u_1\bar{u}_2v\phi\bar{\gamma}] + [u_1\bar{u}_2v\bar{\phi}\gamma] + [\bar{u}_1u_2v\phi\bar{\gamma}] + [\bar{u}_1u_2v\bar{\phi}\gamma] \\
 &\quad - 2[u_1u_2\bar{v}\phi\bar{\gamma}] - 2[u_1u_2\bar{v}\bar{\phi}\gamma]) \\
 &\quad + (2[u_1\bar{u}_2\bar{v}\phi\gamma] + 2[\bar{u}_1u_2\bar{v}\phi\gamma] - 4[\bar{u}_1\bar{u}_2v\phi\gamma])\} / \sqrt{36} \quad \dots (5.6)
 \end{aligned}$$

$$\begin{aligned}
 |^2\bar{\psi}_{od} \gamma^2(\frac{1}{2})\rangle &= \sqrt{\frac{2}{3}} |(^4\bar{\Phi}_{od}^{(1)})_o(^3\chi_{ov}^{(-1)})_a\rangle - \sqrt{\frac{2}{3}} |(^4\bar{\Phi}_{od}^{(1)})_o(^3\chi_{ov}^{(0)})_a\rangle \\
 &\quad + \sqrt{\frac{2}{3}} |(^4\bar{\Phi}_{od}^{(-1)})_o(^3\chi_{ov}^{(1)})_a\rangle \\
 &= \{3[u_1u_2v\bar{\phi}\gamma] - ([\bar{u}_2u_2v\phi\bar{\gamma}] + [\bar{u}_1u_2v\bar{\phi}\gamma] + [u_1\bar{u}_2v\phi\bar{\gamma}] \\
 &\quad + [u_1\bar{u}_2v\bar{\phi}\gamma] + [u_1u_2\bar{v}\phi\bar{\gamma}] + [u_1u_2\bar{v}\bar{\phi}\gamma] \\
 &\quad + ([\bar{u}_1\bar{u}_2v\phi\gamma] + [\bar{u}_1u_2\bar{v}\phi\gamma] + [u_1\bar{u}_2\bar{v}\phi\gamma])\} / \sqrt{18} \quad \dots (5.7)
 \end{aligned}$$

$$\begin{aligned}
 |^2\bar{\psi}_{ov} \gamma^1(\frac{1}{2})\rangle &= \sqrt{\frac{2}{3}} |(^2\bar{\Phi}_{ov}^{(1)})_o(^3\chi_{ov}^{(0)})_a\rangle - \frac{2}{\sqrt{6}} |(^2\bar{\Phi}_{ov}^{(-1)})_o(^3\chi_{ov}^{(1)})_a\rangle \\
 &= \{[u_1\bar{u}_2v\phi\bar{\gamma}] + [u_1\bar{u}_2v\bar{\phi}\gamma] - [\bar{u}_1u_2v\phi\bar{\gamma}] - [\bar{u}_1u_2v\bar{\phi}\gamma] \\
 &\quad - 2[u_1\bar{u}_2\bar{v}\phi\gamma] + 2[\bar{u}_1u_2\bar{v}\phi\gamma]\} / \sqrt{12} \quad \dots (5.8)
 \end{aligned}$$

Excited states involving transition to  $\eta$  type orbital.

Quartets :

$$\begin{aligned}
 |^4\psi_{od} \eta^1(\frac{3}{2})\rangle &= |(^2\Phi_{ov}^{(1)})_o(^3\chi_{od}^{(1)})_a\rangle \\
 &= \{[u_1\bar{u}_2v\phi\eta] - [\bar{u}_1u_2v\phi\eta]\} / \sqrt{12} \quad \dots (5.9)
 \end{aligned}$$

Doublets :

$$|^2\bar{\psi}_{od} \eta^1(\frac{1}{2})\rangle = \sqrt{\frac{2}{3}} |(^2\Phi_{ov}^{(1)})_o(^3\chi_{od}^{(0)})_a\rangle - \frac{2}{\sqrt{6}} |(^2\Phi_{ov}^{(-1)})_o(^3\chi_{od}^{(1)})_a\rangle \quad (5.10)$$

The explicit form for (5.10) is the same as (5.8) except that the orbital  $\gamma$  is replaced by  $\eta$ .

$$|^2\bar{\psi}_{ov} \eta^1(\frac{1}{2})\rangle = \sqrt{\frac{2}{15}} |(^2\Phi_{od}^{(1)})_o(^3\chi_{od}^{(0)})_a\rangle - \sqrt{\frac{4}{15}} |(^2\Phi_{od}^{(-1)})_o(^3\chi_{od}^{(1)})_a\rangle \quad \dots (5.11)$$

$$\begin{aligned}
 |^3\tilde{\Psi}_{od}{}^{\gamma_2}(\frac{1}{2})\rangle &= \sqrt{\frac{2}{5}}|^4\Phi_{od}(\frac{1}{2})_o(^3\chi_{od}{}^{(-1)})_a\rangle - \sqrt{\frac{3}{5}}|^4\Phi_{od}(\frac{1}{2})_o(^3\chi_{od}{}^{(0)})_a\rangle \\
 &+ \sqrt{\frac{1}{5}}|^4\Phi_{od}(-\frac{1}{2})_o(^3\chi_{od}{}^{(1)})_a\rangle \quad \dots \quad (5.12)
 \end{aligned}$$

The explicit forms of (5.11) and (5.12) are respectively obtained by putting the orbital  $\eta$  in place of  $\gamma$  in (5.6) and (5.7).

## 6. EVALUATION OF THE ENERGY MATRIX

The Hamiltonian (in atomic units  $e = \hbar = m = 1$ ) is

$$H = -\frac{1}{2}\sum_i \nabla_i^2 + \sum_i V(r_i) + \sum_{i,j} \frac{1}{r_{ij}} \quad \dots \quad (6.1)$$

where  $V(r_i)$  is the potential acting on the  $i$ th electron due to the four nuclei and all other electrons except the five under consideration. The energy matrix of the Hamiltonian within the manifold described in the previous section is given below :

### Diagonal elements

Ground states :

$$\langle ^4\tilde{\Psi}_{od} | H | ^4\tilde{\Psi}_{od} \rangle = [Q_0 - J(u_1 u_2) - 2J(u_1 v) - 2J(u_1 \phi) - J(v\phi)] \quad \dots \quad (6.2)$$

$$\langle ^2\tilde{\Psi}_{od} | H | ^2\tilde{\Psi}_{od} \rangle = [Q_0 - J(u_1 u_2) + J(u_1 v) - 2J(u_1 \phi) - J(v\phi)] \quad \dots \quad (6.3)$$

$$\langle ^2\tilde{\Psi}_{ov} | H | ^2\tilde{\Psi}_{ov} \rangle = [Q_0 + J(u_1 u_2) - J(u_1 v) - 2J(u_1 \phi) - J(v\phi)] \quad \dots \quad (6.4)$$

Excited states involving transition to  $\gamma$  type orbital.

Quartets :

$$\begin{aligned}
 \langle ^4\tilde{\Psi}_{od}{}^{\gamma_1} | H | ^4\tilde{\Psi}_{od}{}^{\gamma_1} \rangle &= [Q_\gamma - J(u_1 u_2) - 2J(u_1 v) - J(\phi\gamma) \\
 &- \frac{1}{2}\{J(u_1 \phi) + J(u_1 \gamma)\} - \frac{1}{2}\{J(v\phi) + J(v\gamma)\}] \quad \dots \quad (6.5)
 \end{aligned}$$

$$\begin{aligned}
 \langle ^2\tilde{\Psi}_{od}{}^{\gamma_2} | H | ^2\tilde{\Psi}_{od}{}^{\gamma_2} \rangle &= [Q_\gamma - J(u_1 u_2) + J(u_1 v) - J(\phi\gamma) \\
 &- \frac{1}{2}\{J(u_1 \phi) + J(u_1 \gamma)\} - \frac{1}{2}\{J(v\phi) + J(v\gamma)\}] \quad \dots \quad (6.6)
 \end{aligned}$$

Doublets :

$$\begin{aligned}
 \langle ^2\tilde{\Psi}_{od}{}^{\gamma_1} | H | ^2\tilde{\Psi}_{od}{}^{\gamma_1} \rangle &= [Q_\gamma - J(u_1 u_2) + J(u_1 v) - J(\phi\gamma) \\
 &+ \frac{1}{2}\{J(u_1 \phi) + J(u_1 \gamma)\} - \frac{1}{2}\{J(v\phi) + J(v\gamma)\}] \quad \dots \quad (6.7)
 \end{aligned}$$

$$\begin{aligned}
 \langle ^2\tilde{\Psi}_{od}{}^{\gamma_2} | H | ^2\tilde{\Psi}_{od}{}^{\gamma_2} \rangle &= [Q_\gamma - J(u_1 u_2) - 2J(u_1 v) - J(\phi\gamma) \\
 &+ \frac{1}{2}\{2J(u_1 \phi) + 2J(u_1 \gamma) + J(v\phi) + J(v\gamma)\}] \quad \dots \quad (6.8)
 \end{aligned}$$

$$\begin{aligned} \langle {}^2\bar{\Psi}_{\sigma\sigma} \gamma_1 | H | {}^2\bar{\Psi}_{\sigma\sigma} \gamma_1 \rangle &= [Q_\gamma + J(u_1 u_2) - J(u_1 v) - J(\phi \gamma) \\ &\quad - J(u_1 \phi) - J(u_1 \gamma) + \frac{1}{2}\{J(v\phi) + J(v\gamma)\}] \end{aligned} \quad (6.9)$$

For transition to  $\eta$  type orbital.

*Quartet :*

$$\begin{aligned} \langle {}^4\bar{\Psi}_{\sigma\sigma} \eta_1 | H | {}^4\bar{\Psi}_{\sigma\sigma} \eta_1 \rangle &= [Q_\eta + J(u_1 u_2) - J(u_1 v) - J(u_1 \phi) - J(u_1 \eta) \\ &\quad - J(v\phi) - J(v\eta) - J(\phi \eta)] \end{aligned} \quad (6.10)$$

*Doublets :*

$$\langle {}^2\bar{\Psi}_{\sigma\sigma} \eta_1 | H | {}^2\bar{\Psi}_{\sigma\sigma} \eta_1 \rangle = \text{as in (6.9) with } \gamma \text{ replaced by } \eta. \quad (6.11)$$

$$\langle {}^2\bar{\Psi}_{\sigma\sigma} \eta_1 | H | {}^2\bar{\Psi}_{\sigma\sigma} \eta_1 \rangle = \text{as in (6.7) with } \gamma \text{ replaced by } \eta. \quad (6.12)$$

$$\langle {}^2\bar{\Psi}_{\sigma\sigma} \eta_2 | H | {}^2\bar{\Psi}_{\sigma\sigma} \eta_2 \rangle = \text{as in (6.8) with } \gamma \text{ replaced by } \eta. \quad (6.13)$$

The symbols occurring in the right hand side of Eqns. (6.2) to (6.13) stand for the following :

$$\begin{aligned} Q_0 &= \{2\epsilon_u + \epsilon_v + 2\epsilon_\phi + K(u_1 u_2) + 2K(u_1 v) + 4K(u_1 \phi) \\ &\quad + 2K(v\phi) + K(\phi\phi)\} \end{aligned} \quad (6.14)$$

$$\begin{aligned} Q_a &= \{2\epsilon_u + \epsilon_v + \epsilon_\phi + \epsilon_a + K(u_1 u_2) + 2K(u_1 v) + 2K(u_1 \phi) \\ &\quad + 2K(u_1 a) + K(v\phi) + K(va) + K(\phi a)\} \end{aligned} \quad (6.15)$$

$$\left. \begin{aligned} K(ab) &\equiv \langle ab | g_{12} | ab \rangle, \text{ the coulomb integral} \\ J(ab) &\equiv \langle ab | g_{12} | ba \rangle, \text{ the exchange integral} \end{aligned} \right\} \quad (6.16)$$

[see also (6.24) ]

$$\text{and } \epsilon_a \equiv \langle a | -\frac{1}{2}\nabla^2 + V | a \rangle \text{ the one electron term.} \quad (6.17)$$

In writing down the final expressions we have made use of the conditions  $u_1 \leftrightarrow u_2$  under  $R_{AM}$ . It is to be noted that the diagonal matrix elements (6.2) to (6.4) for the zeroth order ground states are degenerate if we neglect the relatively feeble direct exchange integrals such as  $J(u_1 u_2)$  and  $J(u_1 v)$ . It is essential, therefore, to study the interaction of these states with the corresponding excited states in order to determine the effective coupling on the basis of the present mechanism. The off-diagonal matrix elements will be described now.

### Off-diagonal elements

(i) Involving transition to  $\gamma$ .

$$\begin{aligned} \langle {}^4\bar{\psi}_{od} | H | {}^4\bar{\psi}_{od} \gamma^1 \rangle &= -\sqrt{\frac{5}{6}} \{ \langle u_1 \gamma | g_{12} | \phi u_1 \rangle + \langle u_2 \gamma | g_{12} | \phi u_2 \rangle \\ &\quad + \langle v \gamma | g_{12} | \phi v \rangle \} \quad \dots \quad (6.18) \end{aligned}$$

$$\begin{aligned} \langle {}^4\bar{\psi}_{od} | H | {}^4\bar{\psi}_{od} \gamma^2 \rangle &= -\sqrt{\frac{1}{6}} \{ \langle u_1 \gamma | g_{12} | \phi u_1 \rangle + \langle u_2 \gamma | g_{12} | \phi u_2 \rangle \\ &\quad - 2 \langle v \gamma | g_{12} | \phi v \rangle \} \quad \dots \quad (6.19) \end{aligned}$$

$$\begin{aligned} \langle {}^2\bar{\psi}_{od} | H | {}^2\bar{\psi}_{od} \gamma^1 \rangle &= -\sqrt{\frac{1}{6}} \{ 2 \langle u_1 \gamma | g_{12} | \phi u_1 \rangle + 2 \langle u_2 \gamma | g_{12} | \phi u_2 \rangle \\ &\quad - \langle v \gamma | g_{12} | \phi v \rangle \} \quad \dots \quad (6.20) \end{aligned}$$

$$\begin{aligned} \langle {}^2\bar{\psi}_{od} | H | {}^2\bar{\psi}_{od} \gamma^2 \rangle &= -\sqrt{\frac{2}{6}} \{ \langle u_1 \gamma | g_{12} | \phi u_1 \rangle + \langle u_2 \gamma | g_{12} | \phi u_2 \rangle \\ &\quad - 2 \langle v \gamma | g_{12} | \phi v \rangle \} \quad \dots \quad (6.21) \end{aligned}$$

$$\langle {}^2\bar{\psi}_{ev} | H | {}^2\bar{\psi}_{ev} \gamma^1 \rangle = \frac{3}{\sqrt{6}} \langle v \gamma | g_{12} | \phi v \rangle \quad \dots \quad (6.22)$$

(ii) For interactions with excited states involving transition to  $\eta$  like orbital, we have one composite expression for the off-diagonal elements, i.e.,

$$\begin{aligned} \langle {}^4\bar{\psi}_{od} | H | {}^4\bar{\psi}_{od} \eta^1 \rangle &= \langle {}^2\bar{\psi}_{od} | H | {}^2\bar{\psi}_{od} \eta^1 \rangle = \langle {}^2\bar{\psi}_{ev} | H | {}^2\bar{\psi}_{ev} \eta^1 \rangle \\ (6.23) \quad &= \frac{1}{\sqrt{2}} \langle {}^2\bar{\psi}_{ev} | H | {}^2\bar{\psi}_{ev} \eta^2 \rangle = \frac{1}{\sqrt{2}} \{ \langle u_1 \eta | g_{12} | \phi u_1 \rangle \\ &\quad - \langle u_2 \eta | g_{12} | \phi u_2 \rangle \} \quad \dots \quad (6.23) \end{aligned}$$

The notations like  $\langle ab | g_{12} | cd \rangle$  in the diagonal and off-diagonal elements represents the integral

$$\int \int a^*(\mathbf{r}_1) b^*(\mathbf{r}_2) \frac{1}{r_{12}} c(\mathbf{r}_1) d(\mathbf{r}_2) d\mathbf{r}_1 d\mathbf{r}_2 \quad \dots \quad (6.24)$$

6. STUDY OF INTERACTION BY PERTURBATION.

### 7. STUDY OF INTERACTION BY PERTURBATION. PROCEDURE

If we examine the diagonal matrix elements of the excited states i.e., Eqns. (6.5) to (6.13) it is seen that the term like  $Q(a)$  (explicitly given by (6.15)) is common to all the expressions for transition to 'a' type orbital. Since this contains terms such as the one electron and the coulomb integrals  $K(ab)$ , it is by far the dominant



term as compared to those involving the exchange integrals  $J(ab)$ , which are relatively very negligible. We can thus safely use the approximation.

$${}^4E_a \simeq {}^2E_a = E_a' \quad \dots (7.1)$$

where  $E'$  represents the mean energy of the excited states involving 'a' orbital. Further, we use the notation

$$E_a = E_a' - E_0 \quad \dots (7.2)$$

where

$${}^4E_0 = {}^2E_0 = E_0$$

i.e., the degenerate energy of the zeroth order ground quartet and doublet states.

As shown in our previous papers (Koide, Sinha and Tanabe, 1959; Sinha and Koide, 1960), the spin dependent energy depressions of the various lower states, within the framework of the present formalism, appears in the second order term of the perturbation treatment. This is expressed as

$$\begin{aligned} \delta E_n &= \sum_n \langle 0 | H | n \rangle \langle n | H | 0 \rangle / (E_n - E_0) \\ &\approx (E_a)^{-1} \sum_n \langle 0 | H | n \rangle \langle n | H | 0 \rangle \end{aligned} \quad \dots (7.3)$$

using (7.1) and (7.2).

It is expedient to consider certain symmetry situations before giving the explicit expressions for the energy depressions of the various quartet and doublet states based on (7.3).

Under the operation  $R_{AM}$  we take, as pointed before,  $u_1 \longleftrightarrow u_2$ ; the behaviour of  $v$  either as even or odd function, would not affect the hybrid exchange integrals  $\langle vb | g_{12} | cv \rangle$  occurring in the off-diagonal elements. Further, under the operation  $R_{ON}$  i.e., reflection on the plane  $ON$  normal to the Fig. 1.,  $\phi$  is expected to behave as  $R_{ON}\phi = -\phi$  because  $\phi$  is either a  $p_z$  orbital or a combination of  $p$  orbitals by (4.3) depending on the choice of axes. As noted before, for  $\eta$  we take  $R_{AM}\eta = -\eta$ . In the case of  $\gamma$ , we consider two possibilities.

$$(a) \quad R_{AM}\gamma = \gamma \text{ (always)}$$

$$(b) \quad i) \quad R_{QN}\gamma = \gamma \quad \text{or} \quad ii) \quad R_{ON}\gamma = -\gamma.$$

We shall consider the energy depressions of the states with the condition  $R_{ON}\gamma = \gamma$ ; then we have only to show that the lowest available excited orbital of  $\gamma$  type has this symmetry.

We now consider the explicit expression for the energy depressions of the zeroth order ground states (5.1), (5.2) and (5.3) due to the second order perturba-

tion terms as contained in (7.3), under various conditions. The respective depressions will be symbolically denoted by  $\delta Q$ ,  $\delta D_1$  and  $\delta D_2$ . These are dealt with casewise.

*Case I.* (Perturbation by excited states involving transition to  $\gamma$  type orbital).

It is convenient to introduce the following abbreviations

$$\langle u_1\gamma | g_{12} | \phi u_1 \rangle \equiv u_1 J_{\gamma\phi} ; \langle v\gamma | g_{12} | \phi v \rangle \equiv v J_{\gamma\phi} \text{ etc.} \quad \dots (7.4)$$

We also note that  $u_2 J_{\gamma\phi} = u_1 J_{\gamma\phi}$  because of the symmetry  $u_1 \longleftrightarrow u_2$  under  $R_{AM}$  and that  $R_{ON} v J_{\gamma\phi} = -v J_{\gamma\phi}$ . Thus making use of these conditions in the appropriate off-diagonal elements, the depressions of the various states are expressed below :

$$\delta Q : \left\{ \frac{5}{8} |(2u_1 J_{\gamma\phi} - v J_{\gamma\phi})|^2 + \frac{1}{8} |(2u_1 J_{\gamma\phi} + 2v J_{\gamma\phi})|^2 \right\} / E_\gamma \quad \dots (7.5)$$

$$\delta D_1 : \left\{ \frac{1}{8} |(4u_1 J_{\gamma\phi} + v J_{\gamma\phi})|^2 + \frac{2}{8} |(2u_1 J_{\gamma\phi} + 2v J_{\gamma\phi})|^2 \right\} / E_\gamma \quad \dots (7.6)$$

$$\delta D_2 : \frac{1}{8} \{9 |v J_{\lambda\phi}|^2\} / E_\gamma \quad \dots (7.7)$$

It follows, therefore, that

$$\delta Q - \delta D_1 = 6 |u_1 J_{\gamma\phi}| |v J_{\gamma\phi}| / E_\gamma \quad \dots (7.8)$$

$$\delta Q - \delta D_2 = \{-4 |u_1 J_{\gamma\phi}|^2 + 2 |u_1 J_{\gamma\phi}| |v J_{\gamma\phi}|\} / E_\gamma \quad \dots (7.9)$$

$$\delta D_2 - \delta D_1 = \{4 |u_1 J_{\gamma\phi}|^2 + 4 |u_1 J_{\gamma\phi}| |v J_{\gamma\phi}|\} / E_\gamma \quad \dots (7.10)$$

It is easily seen from the above equations that the depression of the  $D_1$  is maximum and it is the lowest of the three states for transition to the  $\gamma$  type orbital.  $D_2$  will probably lie above  $Q$ .

*Case II.* (Involving transition to  $\eta$  type orbital). Noting,  $R_{AM} u_1 J_{\eta\phi} = -u_1 J_{\eta\phi}$ , the depressions of the various states are :

$$\delta Q : 2 |u_1 J_{\eta\phi}|^2 / E_\eta \quad \dots (7.11)$$

$$\delta D_1 : 2 |u_1 J_{\eta\phi}|^2 / E_\eta \quad \dots (7.12)$$

$$\delta D_2 : \{2 |u_1 J_{\eta\phi}|^2 + 4 |u_1 J_{\eta\phi}|^2\} / E_\eta \quad \dots (7.13)$$

$$\text{Hence} \quad \delta Q - \delta D_1 = 0 \quad \dots (7.14)$$

$$\text{and} \quad \delta Q - \delta D_2 = 4 |u_1 J_{\eta\phi}|^2 / E_\eta \quad \dots (7.15)$$

In this case,  $D_2$  is the lowest state and  $Q$  and  $D_1$  lie above and are degenerate. Of the two cases discussed above the fact as to which will dominate would depend on the magnitude of  $E_\gamma$  and  $E_\eta$  as well as the hybrid exchange integrals  ${}^a J_{\phi\phi}$  involved. However, it is more appropriate to discuss the case when they are of the same magnitude.

*Case III.* (The energies of  $\gamma$  and  $\eta$  are equal. We can use the approximation  $E_\gamma = E_\eta = E$ .) Then we have

$$\delta Q - \delta D_1 = 6 |u_1 J_{\gamma\eta}| |^v J_{\gamma\eta}| / E \quad \dots (7.16)$$

$$\begin{aligned} \delta Q - \delta D_2 &= \{4 |u_1 J_{\eta\eta}|^2 - 4 |u_1 J_{\gamma\eta}|^2 + 2 |u_1 J_{\gamma\eta}| |^v J_{\gamma\eta}| \} / E \\ &\approx 2 |u_1 J_{\gamma\eta}| |^v J_{\gamma\eta}| / E \quad \dots (7.17) \end{aligned}$$

$$\begin{aligned} \delta D_2 - \delta D_1 &= \{4 |u_1 J_{\gamma\eta}|^2 - 4 |u_1 J_{\eta\eta}|^2 + 4 |u_1 J_{\gamma\eta}| |^v J_{\gamma\eta}| \} / E \\ &\approx 4 |u_1 J_{\gamma\eta}| |^v J_{\gamma\eta}| / E \quad \dots (7.18) \end{aligned}$$

assuming that

$$|u_1 J_{\gamma\eta}| \approx |^v J_{\gamma\eta}|.$$

If this was the case, then  $D_1$  would be the lowest state,  $D_2$  and  $Q$  representing the higher states in respective orders. It may be mentioned again that the ferrimagnetic state  $D_1$ , represents the situation where negative A-B coupling dominates over B-B;  $D_2$  represents the reverse situation. The above analysis shows that the ferro-magnetic state  $Q$  is least likely, in agreement with observed cases.

We shall, however, proceed further and investigate deeper into the specific nature of the excited orbitals  $\gamma$  and  $\eta$  available in actual crystals of magnetic spinels and the like systems. After assessing the relative energies of the available excited orbitals, and the magnitude of the hybrid exchange integrals ( $^a J_{be}$ ), a semi-quantitative discussion of the effective coupling in these systems will be given and compared with results.

## 8. APPLICATION TO THE REAL SYSTEMS

In order to have a semiquantitative discussion of the model and ideas developed in the preceding sections as related to spinel-like systems, we shall select a typical representative. Simple examples are  $\text{Mn}[\text{Fe}_2]\text{O}_4$  or  $\gamma\text{-Fe}_2\text{O}_3$ , in which all the cations have  $d^5$  configuration and can be assumed to exist in  $^6S_{5/2}$  state.

The first problem is the identification of  $\gamma$  and  $\eta$  type excited orbitals among the lowest available orbitals in the actual crystals. We classify these and ascertain their relative energies with respect to the full unit—A-O-B<sub>3</sub>—having  $C_{3v}$  symmetry. In discussing the excited orbitals permissible for this point symmetry group, we shall be guided, as before, (Koide, Sinha and Tanabe, 1959), by two models. First we consider the "excitation model" which involves the transition of an electron to the lowest excited orbitals of the anion under the influence of the crystal field of the appropriate symmetry. Second is the charge "transfer model" and describes transitions to such linear combinations of the empty cation orbitals which form base functions of the irreducible representations of the point symmetry group. The lowest lying among these are, of course,

most effective in the transition process (virtual in the present case) being considered here. It may be added that from group theoretical point of view both models represent the same orbitals expressed in slightly different ways of approximations. They should better be termed as localized crystal orbitals.

The excited orbitals of  $O^{2-}$  that may be considered on the basis of the "excitation model" are  $3s$ ,  $3p$  and  $3d$ . In order to have a rough estimate of the relative energy scale for these, we consider the effect of the four cations in the unit  $A-O-B_3$  (point symmetry  $C_{3v}$ ) treated as point charges, as well as the twelve oxygen ion neighbours (treated not as point charges but ions with a distribution of charge).

The calculation is carried out by the usual method of crystal field theory (Bethe, 1929; Moffit and Ballhausen, 1956) where the potential is expanded in a series of spherical harmonics, the presence or absence of the terms being governed by the point symmetry group and certain group theoretical ideas. The matrix elements of the potential, thus expressed, were calculated by using the equivalent operator method (Bleaney and Stevens, 1953). The splittings of the orbital levels are proportional to  $\langle r^2 \rangle / R^2$ ,  $\langle r^4 \rangle / R^4$  etc., depending on whether the orbital is  $p$ -type or  $d$ -type. Here ' $r$ ' is the orbital radius and  $R$  is the distance of the neighbour in question.

A knowledge of the radial part of the respective wave-functions is needed; however, it is very hard to determine this non-empirically. One can, at best, make a plausible approximation. From the work on excitons for certain systems (Knox and Inchauspe, 1959), it is known that, in the excitation model (Dexter, 1951; 1957) the majority of the charge is confined within the equivalent sphere with its centre at the anion and the surface extending upto the cation centres. Keeping this fact in mind we choose the radial part of the wave-function by the following tentative method.

For example for the  $3d$  orbital, we assume that the maximum of the wave-function lies midway between the anion and the cation i.e., for the present case approximately at 2 a.u. distance from the oxygen centre.

In view of the approximations used, it would serve no purpose to give here the details of the calculation. We only enumerate the rough results. Thus, with AO as the  $z$  axis and ON as the  $x$  axis, we get the following energy sequence :

$$3d_{z^2} < 3d_{xz} = 3d_{yz} \leq 3p_z < 3s < 3p_x = 3p_y < 3d(x^2-y^2) = 3d_{xy}$$

The energy of the  $3d_{z^2}$  is lowered by about 6 e.v. with respect to the continuum. It would therefore lie below the conduction band. However, one cannot place too much reliance on the above figure. The important thing is the derived energy sequence and that on the excitation model, a proper choice for  $\gamma$  would be  $3d_{z^2}$  orbital and for  $\eta$   $3d_{xz}$ . (A different choice of axes will not alter the essen-

tial features; the orbitals will then be the appropriate linear combinations which preserve the symmetry and the sequence). It may be noted, in passing, that  $3d_{z^2}$  as  $\gamma$  and  $3d_{xz}$  as  $\eta$  satisfy the requisite requirements taken into account in section 7.

We now turn to the charge transfer model in which  $\gamma$  or  $\eta$  are to be constituted out of a linear combination of empty cation orbitals. For the cations considered, we take the  $4s$  or orbital or an  $sp$  hybrid of the  $4s$  and  $4p$  orbitals of the respective action having maximum charge density pointing towards the anion and having axial symmetry. We denote them (for the unit A-O-B<sub>3</sub>) by  $\sigma_t$ ,  $\sigma_1$ ,  $\sigma_2$  and  $\sigma_3$  respectively. They form base functions of a reducible representation of dimension 4 for the  $C_{3v}$  group. This can be decomposed into the various irreducible representations (for the group theoretical nomenclatures see Landau and Lifshitz, 1958). Thus :

$$\chi\{\Gamma(R)\} = 2\chi(A_1) + \chi(E) \quad \dots \quad (8.1)$$

Accordingly, we have the following combinations :

$$\left. \begin{aligned} \psi_1(A_1) &= \{a_t\sigma_t + a(\sigma_1 + \sigma_2 + \sigma_3)\}/(\text{Normalization}) \\ \psi_2(A_1) &= \{a_t\sigma_t - a(\sigma_1 + \sigma_2 + \sigma_3)\}/(\text{Normalization}) \end{aligned} \right\} \quad \dots \quad (8.2)$$

$$\left. \begin{aligned} \psi_3(E) &= (\sigma_1 - \sigma_2)/\sqrt{2} \\ \psi_4(E) &= (\sigma_1 + \sigma_2 - 2\sigma_3)/\sqrt{6} \end{aligned} \right\} \quad \dots \quad (8.3)$$

Among these some are of no physical interest for the unit A-O-B<sub>2</sub> (Cf. Fig. 1) and we consider only three in the following approximate forms.

$$\psi_a = [\sigma_t + (\sigma_1 + \sigma_2)]/\sqrt{3} \quad (8.4)$$

$$\psi_b = [\sigma_t - (\sigma_1 + \sigma_2)]/\sqrt{3} \quad (8.5)$$

$$\psi_c = [\sigma_1 - \sigma_2]/\sqrt{2} \quad (8.6)$$

Now  $\psi_c$  is orthogonal to  $\phi$ ; however,  $\psi_a$  and  $\psi_b$  are not orthogonal to it. It can be easily seen that the overlap integral of  $\psi_b$  with  $\phi$  is much higher than that of  $\psi_a$  with  $\phi$ . Thus, the energy of  $\psi_b$  is pushed higher up due to mixing with  $\phi$  and the hybrid exchange integral involving it would also be negligible. We can, therefore, safely disregard the effect of  $\psi_b$ . Finally, we select  $\psi_a$  and  $\psi_c$  for  $\gamma$  and  $\eta$  respectively. Since the non-orthogonality of  $\psi_a$  with  $\phi$  is negligible, the orbital energies of  $\psi_a$  and  $\psi_c$  are expected to be nearly equal. Further, the hybrid exchange integrals involving  $\psi_a$  and  $\psi_c$  will not differ much. This situation leads to the case III dealt with in the Section 7.

It may be emphasised that it is difficult to determine as to which of the two models described above furnish the lowest lying excited orbitals. Since

group-theoretically they are so akin, we shall adopt that model for a semi-quantitative estimate which appeals to our chemical intuition. Accordingly, we choose the charge transfer model and identify  $\gamma$  with  $\psi_a$  and  $\eta$  with  $\psi_b$ .

The arguments of case III, Section 7 shows that the doublet state  $D_1$ , which represents the state with antiparallel spins in A-B and parallel in B-B lies lowest.  $D_2$ , representing the reverse situation, lies between the quartet  $Q$  and  $D_1$ . If we consider the energy level in such a manner that  $Q$  represents the zero level, then (7.16) gives the position of  $D_1$ . In the following we give the estimate for the difference  $Q-D_1$  in terms of  $\psi_a$  and  $\psi_b$  i.e., equations (8.4) and (8.6). Thus we have

$$Q-D_1 = 6\{ | \langle u_1 \psi_a | g_{12} | \phi u_1 \rangle | | \langle v \psi_b | g_{12} | \phi v \rangle | \} / E$$

$$\approx 2\{ | \langle u_1 \sigma_1 | g_{12} | \phi u_1 \rangle | | \langle v \sigma_1 | g_{12} | \phi v \rangle | \} / E \quad \dots (8.7)$$

Further, we use  $p_1$  for  $\phi$ , namely  $p_1 = \frac{1}{\sqrt{2}}(p_z + p_x)$ . The hybrid exchange

integrals of the type  $\langle u_1 \sigma | g_{12} | p_z u_1 \rangle$  have been evaluated in the previous paper (Koide, Sinha and Tanabe, 1959) for similar cations and anions. These are of the order of 0.01 a.u. or 0.27 e.v. for the separations involved in spinels. For determining  $E \sim (E_a - E_o)$ , the ionization potential and electron affinity data for the cation and anions were respectively used. The order is of about 1 a.u. However, for the present purpose, we shall use the range 0.5 to 1.5, a.u., Using these values the difference  $\Delta E \equiv Q-D_1$  is set out in Table 1.

TABLE I

$E$ a.u.	$\Delta E$	
	a.u.	$^{\circ}\text{K}$
0.5	$4 \times 10^{-4}$	125
1.0	$2 \times 10^{-4}$	62.5
1.5	$1.33 \times 10^{-4}$	42

A reasonable estimate for  $(Q-D_1)$  pertaining to the systems such as  $\text{Mn Fe}_2\text{O}_4$  would be around  $50^{\circ}\text{K}$ . The above is for a single representative electron from each cation. No attempt is made to relate this difference with the Curie temperature of the ferrites.

## 9. DISCUSSION

The purpose of the analysis presented in the foregoing sections has been to explore the nature of indirect exchange interaction for ferrosinels on the basis of the mechanism proposed. The stability of the ferromagnetic and the

two ferrimagnetic states have been studied. It emerges from these considerations that the ferrimagnetic state, symbolized, by  $D_1$  is most stable. In contrast, the ferromagnetic state is least stable. This conclusion is in agreement with Neel's assumption and also the observed situation in most ferrosinels where the negative A-B interaction is the most dominant effect (Gorter, 1954).

It may be pointed, however, that the state symbolised by  $D_2$  (i.e., where B-B are antiparallel and A-B parallel), may become important under certain conditions. If the situation as discussed in Case III of Section 7, prevails,  $D_2$  is more stable compared to the ferromagnetic state  $Q$ . However, to ascertain as to when it dominates over  $D_1$  also, a precise knowledge of the excited orbitals is needed. It seems probable that  $D_2$  may become most stable when the cation at the tetrahedral site is in a low spin state as compared to both the cations at the octahedral sites.

This paper does not assess the importance of this mechanism as compared to others. The greatest difficulty for all mechanisms lies in getting an accurate idea of the wave functions of electrons in crystals. Non-empirical calculations are obviously formidable. It is hoped that experiments may eventually resolve some of these difficulties.

#### 10. ACKNOWLEDGEMENTS

The author is grateful to Dr. S. Koide of Japan for a critical perusal of the paper and to Dr. A. B. Biswas for his interest in this work.

#### REFERENCES

- Anderson, P. W., 1959, *Phys. Rev.*, **115**, 2.  
 Bethe, H., 1929, *Ann., Physik.*, **3**, 133.  
 Bleaney, B. and Stevens, K. W. H., 1953, *Repts. Progr. Phys.*, **16**, 108.  
 Dexter, D. L., 1951, *Phys. Rev.*, **83**, 435.  
 Dexter, D. L., 1957, *Phys. Rev.*, **108**, 707.  
 Gorter, E. W., 1954, *Philips Research Report*, **9**, 295, 321, 403.  
 Kanamori, J., 1959, *J. Phys. Chem. Solids*, **10**, 87.  
 Keffer, F. and Oguchi, T., 1959, *Phys. Rev.*, **115**, 1428.  
 Knox, R. S. and Inchaupse, N., 1959, *Phys. Rev.*, **116**, 1093.  
 Koide, S., Sinha, K. P. and Tanabe, Y., 1959, *Progr. Theor. Phys.*, **22**, 647.  
 Landau, L. D. and Lifshitz, E. M., 1958, *Quantum Mechanics*, Pergamon Press, London.  
 Moffit, W. E. and Ballhausen, C. J., 1956, *Ann. Rev. Phys. Chem.*, **7**, 107.  
 Neel, L., 1948, *Ann. Phys. Paris*, **3**, 137.  
 Sinha, K. P. and Koide, S., 1960, *Sci. Pap. Coll. Gen. Education, Unversity of Tokyo*, **10**, 195.  
 Wollan, E. O., 1960, *Phys. Rev.*, **117**, 387.  
 Yafet, Y. and Kittel, C., 1952 *Rev.*, **87**, 290.

# A NOTE ON THE CROSS-SECTION OF THE LUMINOUS DISCHARGE CHANNEL IN A GLOW DISCHARGE

KUMARI D. V. NAGAMANI\* AND V. T. CHIPLONKAR

INSTITUTE OF SCIENCE, BOMBAY

(Received, September 17, 1960)

**ABSTRACT.** The variation in the cross-section  $x$  and the H.W.R. of a luminous discharge channel has been studied for different points in the cathode dark space of a glow discharge in hydrogen and air. Results show that,

- (1) the cross-section  $x$  reaches a minimum value at some distance  $Z$  in front of the cathode,
- (2) the value of the minimum cross-section as well as its location in the cathode dark space is a function of the pressure,
- (3) both the H.W.R. and  $x$  decrease with decreasing pressure for the range 400-252 microns to 100-150 microns. For lower pressures the variation of the two parameters is opposite in character.

## INTRODUCTION

In a previous paper (Chiplonkar *et al.*, 1957) it had been shown that significant changes occur, with decrease in pressure, in the cross section as well as the radial intensity distribution of the luminous discharge channel of a glow discharge in air, mostly in the abnormal regime of the discharge. Similar changes were observed when observations were made on the channel at different points in the cathode dark space. At low pressures, when these changes are most pronounced, it was shown that the channel starts with a large cross-section, with a radial distribution of the flat maximum type (observed by Chaudhri and Baqui, 1952) and shows a progressive decrease in the cross-section as it proceeds towards the cathode. At the same time the radial distribution changes into an approximately Gaussian form (Chiplonkar, 1940 and 1947; Kamke 1950). These changes are to be expected and are in general agreement with the theory of Kamke. An important observation made by us that there is an increase in the cross-section of the channel in the immediate vicinity of the cathode, suggested a more detailed investigation of this interesting aspect of the problem which it is the object of the present paper to report.

## 2. EXPERIMENTAL RESULTS

The variation in the radial intensity distribution in the discharge channel was studied as before<sup>1</sup> (Chiplonkar, *et al.*, 1957) at various distances in the

---

\* Working at present at the Indian Institute of Science, Bangalore.



cathode dark space, extending the observation in some cases to points in the negative glow for discharge in air (voltages 0.68–9.80 kV, pressure 252–52 microns, current = 1.0 mA) and hydrogen (Voltages 0.20–9.83 kV, pressures 400–40 microns, current = 1.0 mA). For the above conditions electrical oscillations were not present in the discharge tube.

Following the procedure used previously, the experimental results are discussed with the help of the following parameters.

$x$  = width of the axial region of the channel over which the intensity is constant

$Z$  = distance of the channel from the cathode

$d$  = D.S.L. = length of the cathode dark space

H.W.R. = half width radius for the total radial distribution as measured directly from the microphotometer curves.

A few typical individual observations are given in Tables I–III and Fig. 1, while the final results are presented in Table IV.

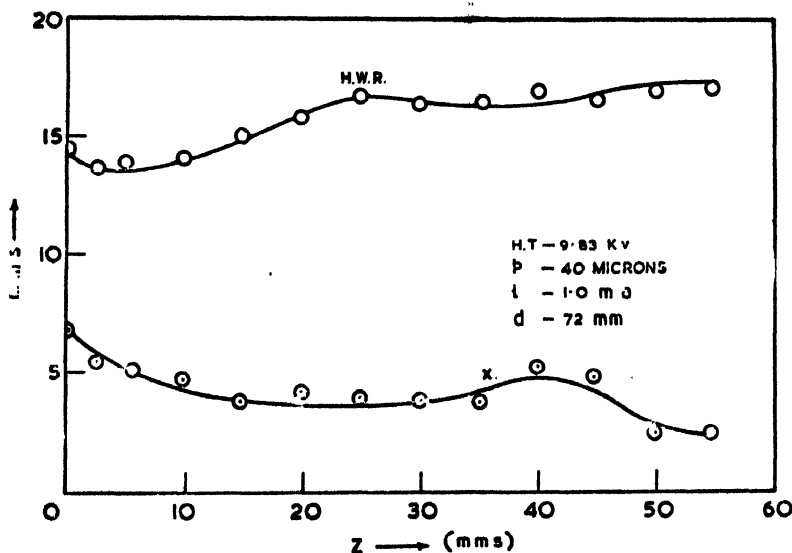


Fig. 1. Variation in the value of  $x$  and H.W.R. with  $Z$  for discharge in hydrogen.

### 3. DISCUSSION

The value of  $x$  and the half width radius (H.W.R.) can be taken as an adequate measure of the localisation of the discharge channel. An increase in the localisation being equivalent to a decrease in both the cross-section parameter  $x$  and the H.W.R. for the distribution. It will be noticed that in the case of all the observations reported here, the cross-section  $x$  of the discharge channel attains a minimum value for some point in front of the cathode. The variation of  $x_0$ , the value of the cross section at the cathode, and of the minimum value

TABLE I  
Discharge in air

$H-T = 6.14 \text{ KV,}$	$i = 1.0 \text{ mA}$	$p = 53 \text{ microns}$	$d = 50 \text{ mm}$
$Z(\text{mm})$	$x(\text{mm})$	$H.W.R.(\text{mm})$	
0.0	07.4	16.9	
3.0	05.2	14.1	
8.0	05.1	13.9	
15.0	04.6	14.0	
25.0	04.3	14.6	
30.0	04.1	16.5	
35.0	04.8	16.9	
40.0	04.7	16.8	
45.0	04.7	16.5	
50.0	05.5	17.0*	

TABLE II  
Discharge in hydrogen

$H-T = 0.84 \text{ KV,}$	$i = 1.0 \text{ mA}$	$p = 155 \text{ microns}$	$d = 22 \text{ mm}$
$Z(\text{mm})$	$x(\text{mm})$	$H.W.R.(\text{mm})$	
0.0	14.0	9.2	
3.0	13.9	14.2	
6.0	13.0	11.1	
9.0	12.0	12.0	
12.0	12.4	16.9	
15.0	12.6	16.8	
18.0	13.2	11.4	
21.0	15.1	13.4	
23.0	17.6	17.0*	

TABLE IV

Discharge in air		At cathode $Z=0$		At D.S.L. $Z=d$		$x_{min}$		Position of $x_{min}$ (mm.)		Minimum value of H.W.R.(mm.)		Position of H.W.R. min. (mm.)	
HT(KV)	$p$ (microns)	$d$ (mm)	$x_0$ (mm)	(H.W.R.) (mm)	$x_d$ (mm)	(H.W.R.) (mm)	$x_{min}$ of $x$ (mm)	$x_{min}$	$x_{min}$	$x_{min}$	$x_{min}$	$x_{min}$	$x_{min}$
0.68	205	10	26.2	16.4	~	27	16.4	20.0	6.0	15.9		3.0	
1.18	100	18	15.8	10.7	~	12	17.0	9.6	14.0	10.6		3.0	
1.96	73	30	13.8	—	—	15.6	17.0	12.0	15.0	12.6		15.0	
3.94	58	42	11.0	12.8	~	10	17.0	7.6	20.0	12.8		0.0	
6.14	53	50	7.4	16.9	—	5.5	17.0	4.1	30.0	13.9		8.0	
9.89	52	54	9.8	15.0	—	—	—	3.9	15.0	15.0		0.0	
Discharge in hydrogen													
0.20	400	10	27.1	15.4	—	17.0	17.0	15.3	6.0	15.4		0.0	
0.84	155	22	14.0	9.2	—	17.6	17.0	12.0	9.0	9.2		0.0	
2.03	81	40	10.1	12.8	—	12.0	17.0	5.7	25.0	11.4		3.0	
4.14	57	54	4.6	8.8	—	4.1	—	2.1	25.0-30.0	6.8		30.0	
7.28	45	65	7.6	17.0	—	—	—	4.1	30.0	12.8		20.0	
9.83	40	72	7.2	14.6	—	—	—	3.9	15.0	13.6		3.0	

TABLE III  
Discharge in hydrogen

<i>H.T.</i> = 4.14 KV <i>i</i> = 1.0 mA <i>p</i> = 57 microns <i>d</i> = 54 mm.		
<i>Z</i> (mm)	<i>x</i> (mm)	<i>H.W.R.</i> (mm)
0.0	4.6	8.8
3.0	4.0	9.3
6.0	3.9	10.5
10.0	3.6	10.8
15.0	3.5	9.4
20.0	2.7	7.6
25.0	2.1	7.3
30.0	2.1	6.8
35.0	2.5	7.5
40.0	2.7	—
45.0	3.2	—
50.0	3.1	—
55.0	4.1	—

\* Radius of the discharge tube  $\sim 17.0$  mm.

of  $x$  with pressure in the case of the two cases, shown in Fig. 2, are observed to be quite similar. Both of them show a minimum value for values of  $p \sim 50$  microns. That there is a significant change in the state of the discharge at this pressure is indicated by Fig. 3 which shows the variation in the location of the minimum, with the pressure in the discharge tube. In the high pressure region

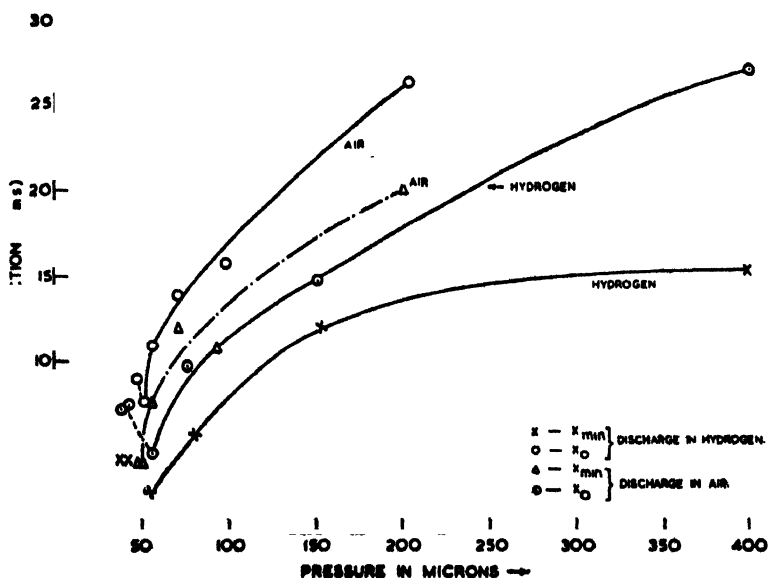


Fig. 2. Variation in the cross-section of discharge channel with pressure for discharge in air and hydrogen.

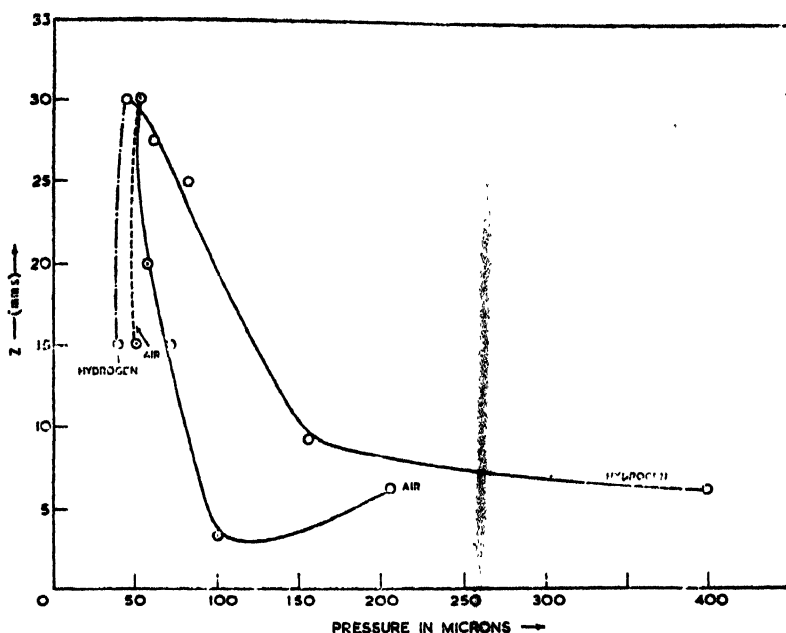


Fig. 3. Variation in the position of  $x_{min}$  with pressure for discharge in air and hydrogen.

(400–250 microns to 50 microns) the position of the minimum moves away from the cathode as the pressure is reduced. Its distance from the cathode reaches a maximum value at about this pressure; there are definite indications that it shows a sharp movement towards the cathode for pressures lower than this value.

The gradual constriction of the discharge channel from its origin at the beginning of the cathode dark space towards the cathode, could be explained in terms of the processes visualised in Kamke's theory (Kamke 1950). The increase in the cross-section in the neighbourhood of the cathode and its peculiar dependence on the pressure described above, however, may be taken to indicate the occurrence of a new process (like the photoelectric emission from the cathode) which is independent of the radial distribution of the positive ions coming towards the cathode. The positive ions and/or the fast neutral particles that enter this region have high velocities and therefore are not expected to be sensitive to changes in the nature and the distribution of the space-charge in this region; for although there is a net positive space-charge in the region of the cathode dark space, it is likely that the space-charge becomes electronic in the immediate vicinity of the cathode.

The variation of the H.W.R. with the pressure under the same conditions is shown in Fig. 4. The observations reveal that for the range of pressures (400–250 to 100–150 microns) there is a decrease of the H.W.R. with decreasing

pressure, a variation which is similar to the one observed for the  $x$  values for these pressures. The variation in the lower pressure range is, however, very peculiar; after reaching a minimum value for  $p \sim 100$ –150 microns the H.W.R.

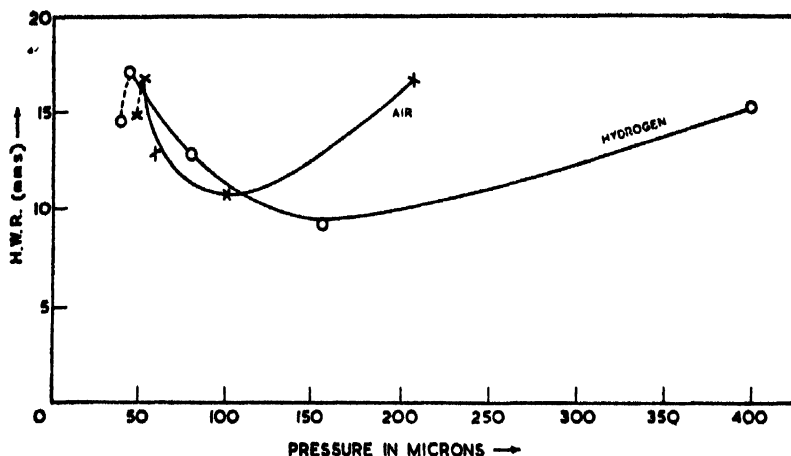


Fig. 4. Variation in the value of H.W.R. (at  $Z = 0$ ) with pressure for discharge in air and hydrogen.

rises to a maximum for  $p \sim 50$  microns (the same pressure for which  $x$  attains its minimum value) after which there are indications of a sharp fall. The physical significance of this observation does not seem to be clear at this stage.

#### REFERENCES

- Chiplonkar, V. T., Mangaly, J. and Kum. Nagamani, D. V., 1957, *Proc. Ind. Acad. Sci.*, **46**, 272.  
 Chaudhri, R. M. and Baqui, M. A., 1952, *Proc. Phys. Soc. (Lond.)*, **65B**, 324.  
 Chiplonkar, V. T., 1940, *Proc. Ind. Acad. Sci.* **12**, 440; 1947, **25**, 453.  
 Kamke, D., 1950, *Zeits. f. Physik*, **128**, 212.

# LIGHT SCATTERING IN CELLULOSE ACETATE SOLUTIONS\*

N. K. SUBRAMANIAN

DEPARTMENT OF PHYSICS, INDIAN INSTITUTE OF SCIENCE, BANGALORE 12

AND

S. R. SIVARAJAN

AHMEDABAD TEXTILE INDUSTRY'S RESEARCH ASSOCIATION, AHMEDABAD

(Received, December 20, 1960)

**ABSTRACT.** A detailed investigation of the light scattered by solutions of blank and dyed samples of cellulose acetate in acetone has been carried out. The method developed by Horn *et al.* has been employed for the estimation of molecular length  $L$  of the cellulose acetate molecules from the observed depolarisation factor  $\rho_v$  and the angular distribution of intensity. In a solution of dyed samples the dye molecules cause a shielding between the dyed molecules, thus producing a decrease in intermolecular interaction. Dyeing in general causes a straightening of the wave-like form of the cellulose acetate molecules thus producing an increase in molecular length. In this respect surface dyeing is less effective than either the interior dyeing or full penetration. The dispersion of depolarisation  $\rho_v$  and dissymmetry  $Z$  of the scattered light from these samples have also been discussed from considerations of intermolecular and intramolecular interactions.

## INTRODUCTION

Light scattering studies on solutions of cellulose acetate in acetone were carried out for the first time by Doty and Kaufman (1945). A more extensive study on cellulose acetate was made by Stein and Doty (1946). They determined the particle size, shape and molecular weight of cellulose acetate in acetone and established that the smaller molecules were fully extended in solution i.e., the molecules were more or less rod-like, but the larger ones were built up in the form of gentle waves.

The present work on the scattering of light in cellulose acetate solutions was undertaken in order to study the effect of dyeing on cellulose acetate. Here the cellulose acetate molecules will be assumed to be rod-like after Stein and Doty (1946) because the theory of light scattering has been thoroughly dealt with for rod-shaped particles.

\* Communicated by Prof. R. S. Krishnan.

## 2. PREPARATION OF SAMPLES

The cellulose acetate used here is a secondary cellulose acetate staple fibre soluble in acetone and only about 2.5 groups on an average are acetylated. For practical purposes this has been taken as blank cellulose acetate fibre.

The dyed samples of cellulose acetate were prepared in the following manner. The samples were deposited by double decomposition technique for  $\text{PbCrO}_4$ ,  $\text{PbI}_2$  and Ag. The washed and boiled fibres were immersed in saturated lead acetate solution for a few hours, the excess liquid was squeezed out and then the fibre was immersed for a few hours in 5%  $\text{K}_2\text{Cr}_2\text{O}_7$  for getting  $\text{PbCrO}_4$  deposits.  $\text{fibre} + \text{PbAc} \rightleftharpoons \text{PbAc} + \text{fibre} + \text{K}_2\text{Cr}_2\text{O}_7 \rightleftharpoons \text{PbCrO}_4$  on fibre KAc etc. The fibre was immersed in polyiodide solution for  $\text{PbI}_2$  deposits. For Ag deposits, the fibres were immersed in  $\text{AgNO}_3$  solution for a few hours and the excess  $\text{AgNO}_3$  solution was squeezed out. The fibres were then immersed in boiling 3% glucose solution, whereby reduction of Ag was completed. Fibres were all finally thoroughly washed, soaped and boiled in water, dried and combed out to remove loosely adhering particles.

Three types of dyeing were employed.

(a) *Fully penetrated*: This was accomplished by prolonged soaking of the fibres (1 week) in each of the solutions used.

(b) *Interior dyed*: These samples were obtained by stripping of from the fibre surface the deposits formed there using dilute acid for 15-25 seconds.

(c) *Surface dyed*: These were obtained by immersion in each of the solutions used for 15-30 minutes.

The dye deposits in the surface dyed samples are in the grooves of the surface only. Interior dyed fibres contain deposits only in the channels inside the fibre, while the fully penetrated dyed fibres are interior and surface dyed.

The eleven samples obtained are the following :—

- 1 Blank cellulose acetate
- 2  $\text{PbCrO}_4$  on cellulose acetate (fully penetrated)
- 3     "                 "                 " (surface dyed)
- 4     "                 "                 " (interior dyed)
- 5  $\text{PbI}_2$                  "                 " (fully penetrated)
- 6     "                 "                 " (surface dyed)
- 7     "                 "                 " (interior dyed)
- 8 Ag                   "                 " (fully penetrated)  
  dev with  $\text{H}_2\text{O}_2$
- 9     "                 "                 " (surface dyed)
- 10 Ag                   "                 " (fully penetrated)  
  dev with glucose
- 11    "                 "                 " (surface dyed)



10 mgs of each sample was carefully weighed and dissolved in 100 ml of double distilled analar acetone. This was taken as the parent solution. Its concentration was obviously 0.01 gm/ml. The lower concentrations of the samples were then prepared by diluting the parent solution adding known volumes of the solvent. In this manner for each sample, four different solutions with concentrations (0.01, 0.005, 0.0025 and 0.00125 gm/100 cc) were prepared.

These samples were prepared at the chemical laboratories of ATIRA and the physical measurements were carried out at the Physics Department of the Indian Institute of Science.

### 3. EXPERIMENTAL DETAILS

The measurements of the intensity of scattering were carried out with a photoelectric photometer constructed here. The optical arrangement is of the conventional type. A RCA 931-A photomultiplier tube served as a detector. A cathode follower amplifier was used to amplify the current from the PM. A balanced arrangement was employed to minimise the drift voltages. The amplified output was read on a microammeter or on a sensitive galvanometer when more accuracy was required. The readings obtained with this instrument were found to be quite reliable. This was checked by comparison with a Brice-Phoenix instrument.

Provision was made for interposing polaroids in the incident and scattered sides for getting vertically and horizontally polarised components. The sensitivities of the photomultiplier set up for vertically and horizontally polarised light were measured and the differences were found to be usually less than two per cent. Necessary corrections were made in the readings taken with the instrument while working with cellulose acetate solution.

The sample to be studied was kept in a cylindrical glass vessel which was provided with flattened openings for entrance and exit of the incident beam. Measurements of the angular distribution of the intensities of the three components  $V_v$ ,  $V_h$  and  $H_h$  of the scattered light were carried out for the following values of the scattering angle  $\theta$ ; 45°, 55°, 65°, 75°, 90°, 105°, 115° and 125° from the forward direction. For each sample the angular distribution of the intensity of scattered light were measured for three different wavelengths, namely, 4358 Å, 5461 Å, 5790 Å and for four different concentrations. All the readings were converted to the same arbitrary unit. These values were corrected for effective volume by multiplying them by the corresponding value of  $\sin \theta$ .

### 4. RESULTS

Table I gives the corrected values of intensity of scattering for various angles for the three components for one typical case, namely,  $\text{PbCrO}_4$  on cellulose acetate (interior dyed) of concentration 0.005 gm/100 cc at 5461 Å.

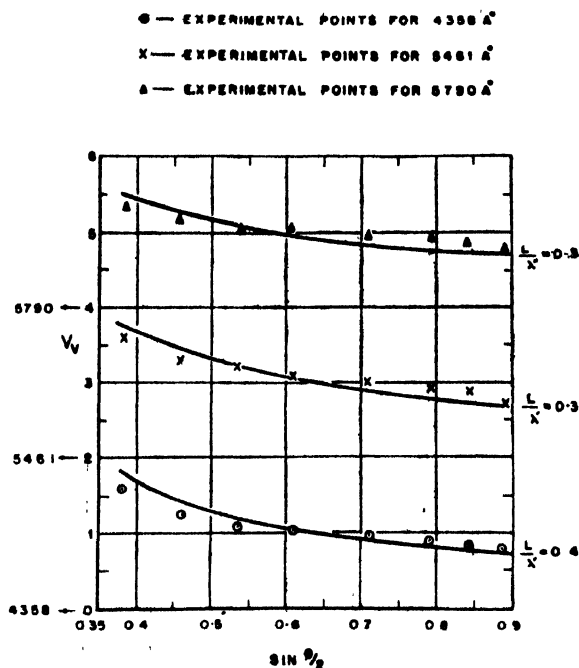


TABLE II  
Particle length

No.	Samples	Length A.U.
1.	Blank cellulose acetate	560
2.	PbCrO <sub>4</sub> (F. Penetrated)	430
3.	PbCrO <sub>4</sub> (S. Dyed)	960
4.	PbCrO <sub>4</sub> (I. Dyed)	1280
5.	PbI <sub>2</sub> (F. Penetrated)	980
6.	PbI <sub>2</sub> (S. Dyed)	640
7.	PbI <sub>2</sub> (I. Dyed)	1040
8.	Ag (F. Penetrated) dev. H <sub>2</sub> O <sub>2</sub>	1165
9.	Ag (S. Dyed)	900
10.	Ag (F. Penetrated) dev. glucose	1200
11.	Ag (S. Dyed)	1160

taking the total intensity of the components i.e.,  $(V_v + 2V_h + H_h)$  for each angle. Typical results obtained with eleven samples for one concentration, namely 0.005 gm/100 cc., are given in Table III.

TABLE III

Depolarisation $\rho_v\%$					dissymmetry $Z$			
Samples No.	Dimensions AU	4358Å	5461Å	5790Å	4358Å	5461Å	5790Å	Total intensity at 90° for 5461Å zero concn.
1	560	9.8	5.5	7.0	4.08	5.17	3.59	190
2	430	6.5	6.1	6.4	3.90	4.94	3.45	90
3	960	25.0	21.6	24.4	2.54	3.18	2.35	155
4	1280	24.0	19.0	24.0	1.83	2.42	1.60	180
5	980	33.3	30.6	26.4	1.86	2.46	1.80	185
6	640	8.7	9.5	8.5	2.80	3.69	2.80	120
7	1040	25.0	23.0	27.0	2.69	3.01	2.43	130
8	1165	29.0	30.3	29.0	2.15	2.80	2.09	150
9	900	11.6	9.3	11.2	2.69	3.37	2.56	130
10	1200	28.9	27.3	26.0	1.93	2.76	1.95	190
11	1160	34.7	28.7	31.2	2.13	2.90	2.08	170

## 5. DISCUSSION

It is well known that the dissymmetry of scattering arises from interferences due to interaction of waves scattered by different parts of the molecule (intramolecular) and also due to the interaction between the waves originating from different molecules (intermolecular).

The dependence of dissymmetry on concentration assuming the hard sphere model has been given in an approximate form by Oster (1949) and Doty *et al.* (1951). This can be written as  $Z = Z_0 \left( 1 - \frac{Kc}{\lambda^2} \right)$  where  $Z_0$  is the dissymmetry at zero concentration. This equation can be extended to the case of rods.

From the above equation it is evident that the presence of intermolecular effect is to increase the dissymmetry with wavelength and is proportional to  $\left( 1 - \frac{K}{\lambda^2} \right)$  Mommaerts (1951, 1957), Oster (1948, 1949). The presence of intramolecular effect is to decrease the dissymmetry as the wavelength increases and is proportional to  $1/\lambda$  (Horn, *et al.*, 1951). At finite concentration these two effects will contribute to the total dissymmetry and hence the dispersion of dissymmetry may not be linear. This has been observed experimentally.

It is seen from the figure of dissymmetry against  $L/\lambda'$  for various values of  $\delta$  (Horn 1955) that for one value of  $Z$ ,  $\delta$  increases as  $L/\lambda'$  increases, i.e.,  $\delta$  in-

creases as  $\lambda$  decreases at infinite dilution. But  $\rho_v = 3\delta^2/5 + 4\delta^3$ . Therefore  $\rho_v$  increases as  $\lambda$  decreases. From the same figure we also note that for any one value of  $L/\lambda'$  dissymmetry increases as  $\rho_v$  decreases. Thus the variation of depolarisation factor  $\rho_v$  with wavelength is opposite to the variation with wavelength of dissymmetry.

In Table II are given the estimated values of the molecular length of eleven cellulose acetate samples. It is seen that the lengths of the dyed samples are in general greater than that of blank cellulose acetate sample. This increase in length of the dyed samples can be explained as a straightening of wavelike form of cellulose acetate chain as the dye penetrates into its pores. The lengths of the cellulose acetate molecules in fully penetrated sample and interior dyed sample are nearly the same but greater than that in surface dyed samples. In the case of sample 2, vide Table II, the micellar length comes out to be smaller than the corresponding values of the other samples. The depolarisation factor  $\rho_v$  is also the lowest for this sample. In the process of preparing the fully penetrated dyed sample, the micelles appear to have broken into smaller sizes.

#### ACKNOWLEDGMENTS

The authors wish to express their sincere thanks to Professor R. S. Krishnan for guidance and encouragement. Thanks are also due to Dr. P. S. Narayanan and Mr. S. Subramanian for valuable discussions.

#### REFERENCES

- Doty *et al.*, 1951, *Adv. Prot. Chem.*, **6**, 37.
- Doty, P. and Kaufman, H. S., 1945, *J. Phys. Chem.*, **49**, 583.
- Horn, P., Thesis, Strasbourg, 1955.
- Horn, *et al.*, 1951, *J. Chim. Phys.*, **48**, 530.
- Mommaerts, W. F. H. M., 1951, *J. Biol. Chem.*, **188**, 553.
- Mommaerts, *et al.*, 1957, *J. Biol. Chem.*, **224**, 277 .
- Oster, G., 1948, *Chem. Rev.*, **43**, 309.
- Oster, G., 1949, *Rec. Trav. Pays. Bas.*, **68**, 1123.
- Stein, R. S. and Doty, P., 1946, *J. Am. Chem. Soc.*, **68**, 159.

# A COMPARATIVE STUDY OF SINGLET $\rightarrow$ TRIPLET ABSORPTION IN SOME HALOGENATED TOLUENES IN THE VAPOUR AND LIQUID STATES\*

J. K. ROY

OPTICS DEPARTMENT, INDIAN ASSOCIATION FOR THE  
CULTIVATION OF SCIENCE, CALCUTTA-32.

(Received, January 25, 1961)

**ABSTRACT.** The absorption spectra in the near ultraviolet region due to singlet  $\rightarrow$  triplet transition in the vapours of *o*-chlorotoluene, *p*-chlorotoluene, *m*-bromotoluene and *p*-bromotoluene at 24°C have been investigated using a path length of 18.9 metres at the respective saturation vapour pressures and these spectra have been compared with those for the equivalent path lengths of the liquids. It has been observed that the absorption due to singlet  $\rightarrow$  triplet transition is of continuous nature and the long wavelength limit of maximum absorption in the liquid state is found to be at about 29000 cm<sup>-1</sup> for all the compounds, but in the case of the vapours the limit is shifted towards higher frequencies, the shift being smaller for the *para* compounds than for the *ortho* or *meta* compounds. It has been concluded that singlet  $\rightarrow$  triplet transition is enhanced by the influence of heavy atoms of the surrounding molecules in the liquid state.

## INTRODUCTION

Kasha (1952) reported that the very weak singlet  $\rightarrow$  triplet absorption bands of  $\alpha$ -chloronaphthalene is strengthened considerably in solution in ethyliodide, and he attributed this to an intermolecular spin-orbit perturbation due to the heavy iodine atom (Z-effect). Later, McClure *et al.* (1954) also observed the Z-effect in singlet  $\rightarrow$  triplet absorption bands of halogen substituted benzenes and naphthalenes and put forward a simple theory to explain it. The dependence of intensity of continuous absorption due to singlet  $\rightarrow$  triplet transition on the atomic number of the substituent atoms in the case of some halogenated toluenes in the liquid state was also studied by Roy (1960).

It was first shown by Evans (1956) that the discrete absorption bands around 3300 Å observed by previous workers in the spectra due to long absorption path of liquid benzene disappear when the dissolved atmospheric oxygen is removed from the liquid. He next studied (Evans, 1957a) the absorption spectra of solutions of benzene, fluorobenzene, diphenyl, styrene and fluorene in chloroform

\*Communicated by Professor S. C. Sirkar.

saturated with oxygen gas at high pressures and observed some discrete bands due to singlet→triplet absorption in most of the cases. He further observed that in the case of solution of  $\alpha$ -bromonaphthalene there was only continuous absorption in the region 4000 Å—5000 Å, but when the solution was saturated with oxygen gas at a pressure of 76 atmospheres sharp bands appeared in this region without appreciable rise in the absorption coefficient. On the other hand, he observed that when a 0.0M solution of naphthalene in chloroform was saturated with oxygen gas at different pressures up to 100 atmospheres, the absorption coefficient increased proportionately with the increase in the pressure of the gas.

Robertson and Reynolds (1958) carried out an interesting experiment to prove the correctness of the theory of probability of singlet→triplet transition put forward by McClure (1949, 1952) and by Mizushima and Koide (1952). Kasha (1952) had suggested that the probability of singlet→triplet transition is enhanced when the molecules are surrounded by heavy atoms owing to the perturbation of the spin-orbital coupling by the heavy atoms. Since the spin-orbital coupling operator depends on the inverse third power of the distance between the  $\pi$ -electron and the heavy atom, Kasha (1952) suggested that hydrostatic pressure would increase the perturbation. Robertson and Reynolds (1958) subjected a mixture of  $\alpha$ -chloronaphthalene and ethyl iodide to pressures ranging from 1 to 3644 atmospheres and observed that there was a two-fold increase in the singlet→triplet absorption with the increase of pressure mentioned above. In the case of pure  $\alpha$ -chloronaphthalene, however, the singlet→triplet absorption was much weaker and no such pressure effect was observed.

The perturbation of the spin-orbital coupling by the magnetic field of surrounding paramagnetic molecules in the gaseous state was first observed by Evans (1957b). He introduced in the absorption cell containing vapours of either benzene or fluorobenzene at a pressure of 70 mm of Hg oxygen gas at pressures up to 130 atmospheres and observed intense absorption bands in the region 3000 Å—3400 Å. The influence of neighbouring molecules of the same kind on such singlet→triplet absorption was, however, not known and it was recently investigated by Sirkar and Roy (1960) using long absorbing paths of the vapour. It was observed by them that benzene vapour at a pressure of 120 mm and with path length 18.90 metres shows only very feeble continuous absorption in the region 3000 Å—3400 Å and an equivalent path length of liquid benzene shows very slightly stronger absorption in this region. In the case of *o*-bromotoluene vapour with similar path length, however, the continuous absorption in the region 3400 Å—3600 Å was observed to be much stronger and it increased considerably when an equivalent path length of the liquid was used. These results show that the spin-orbital coupling of the  $\pi$ -electron is perturbed by heavy atoms in surrounding molecules of the same kind. In order to find out whether such a general conclusion can be drawn from these results, the investigations have been extended

to a few other substituted benzene compounds and the results have been discussed in the present paper.

## EXPERIMENTAL

The substances selected for studying the absorption spectra due to singlet→triplet transition in the present investigation are, orthochlorotoluene, parachlorotoluene, matabromotoluene and parabromotoluene. Chemically pure samples of *o*-chlorotoluene and *p*-chlorotoluene obtained from British Drug House, England, *p*-bromotoluene obtained from Fisher Scientific Company, U.S.A. and *m*-bromotoluene from City Chemical Corporation, New York, U.S.A. were distilled several times under reduced pressure before being used in the investigation.

The experimental arrangement was the same as that employed in an earlier investigation (Sirkar and Roy, 1960). The absorption spectra of the substances in the vapour state were photographed first by filling up the absorption cell, 18.90 metres long, with the vapours of the compounds at the saturation pressures at about 24°C. The pressure was measured carefully with a differential manometer and the short empty cell for the liquid was also placed in the path of light in order to take into account the loss of incident light during its passage through this empty cell. The pressure was found to be about 55 mm for the bromotoluenes and about 50mm for the chlorotoluenes. After photographing the absorption spectrum of the vapour of each of the compounds the long vapour cell was evacuated and the short cell of length 7 mm for the bromo compounds and 6.5 mm for the chloro-compounds was filled with the distilled liquid and the absorption spectrum of the liquid was photographed on the same film with the same time of exposure and under identical conditions. In order to test the genuineness of the absorption observed in case of the substances in the vapour state with a path length of 18.90 metres, the absorption spectra were also studied for shorter path lengths. Using a path length of 9.45 metres, the absorption spectrum of *p*-bromotoluene in the vapour state was, therefore, photographed and compared with the spectrum for a path length of 3.5 mm of the liquid. A Hilger medium quartz spectrograph and Agfa Isopan films were used to photograph the spectra. The time of exposure was about 10 hours in every case. Iron arc spectrum was photographed in each spectrogram as comparison. Microphotometric records of the spectrograms were obtained with a self-recording microphotometer supplied by Kipp and Zonen. The wavelengths in the continuous absorption spectra were measured by drawing a sharp line on the film in the position of a known iron line in the adjacent iron arc spectrum and comparing the microphotometric records of the iron arc and absorption spectra.

## RESULTS AND DISCUSSION

The microphotometric records of the absorption spectra due to pure metabromotoluene and parabromotoluene in the liquid and vapour states are repro-

duced in Figs. 1(a)—1(d), respectively, and the absorption spectra due to pure orthochlorotoluene and parachlorotoluene in the liquid and vapour states are reproduced in Figs. 2(a)—2(d), respectively. Figs. 3(b) and 3(a) show the spectra due to path lengths of 9.45 metres of *p*-bromotoluene in the vapour state and 3.5 mm of the liquid respectively. The reference line in the records has the wavelength  $4051\text{ \AA}$ .

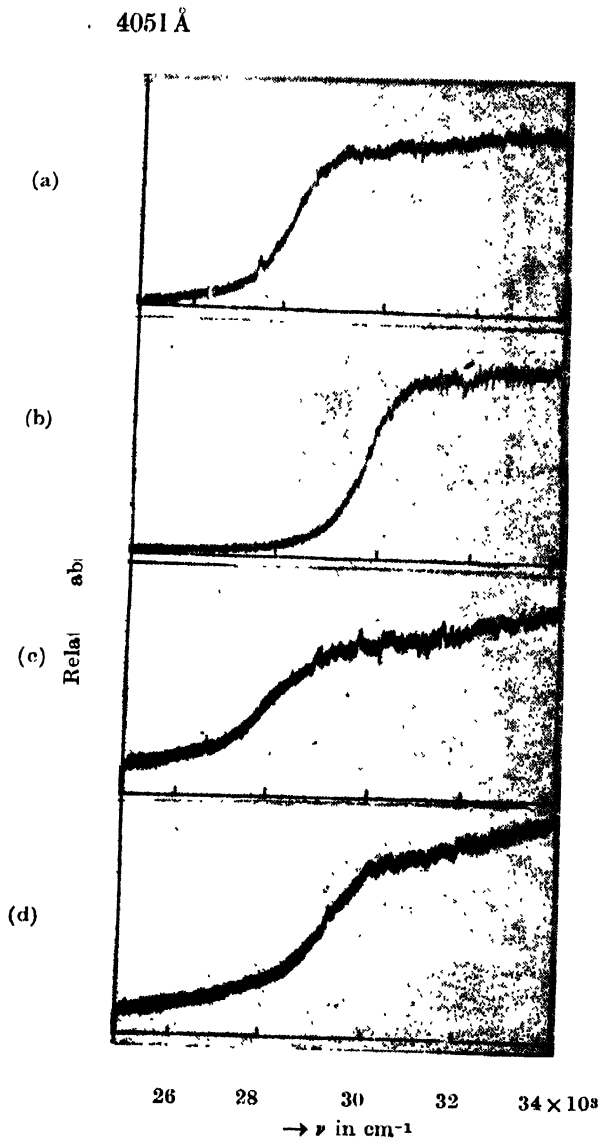


Fig. 1. (a) *m*-Bromotoluene (liquid);  
 (b) " (vapour)  
 (c) *p*-Bromotoluene (liquid)  
 (d) " (vapour)



The microphotometric records of the absorption spectra reproduced in Figs. 1 and 2 show that in the cases of all the four compounds the absorption spectrum due to the liquid is displaced towards red with respect to that due to the vapour phase. This shift is however, different for the different compounds.

4051 Å

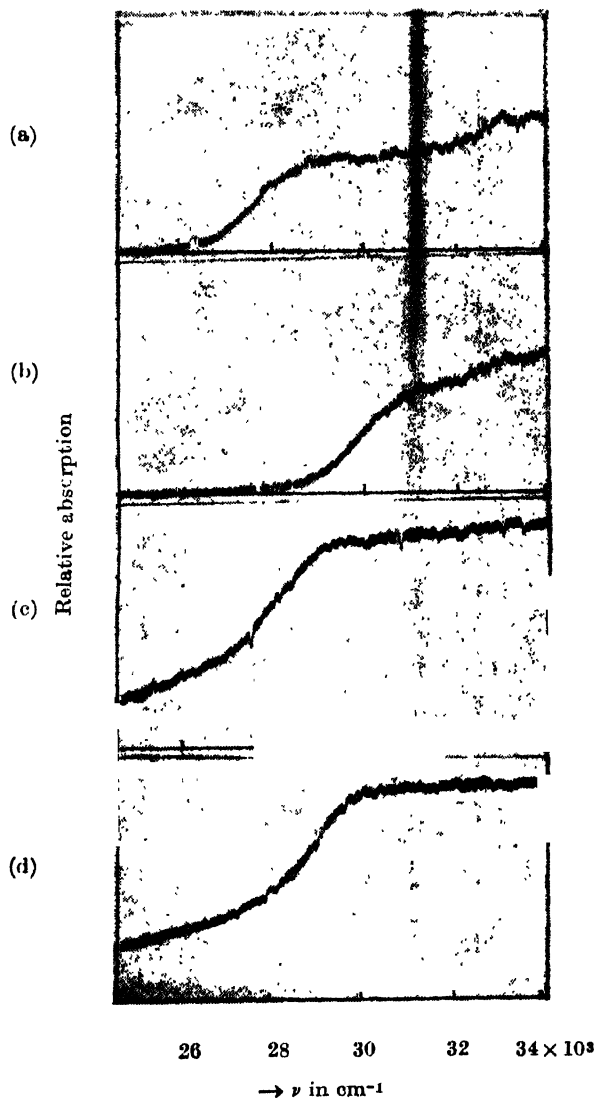


Fig. 2. (a) *o*-Chlorotoluene (liquid)  
 (b) " (vapour)  
 (c) *p*-Chlorotoluene (liquid)  
 (d) " (vapour)

A comparison of the curves in Fig. 1 shows that the spectrum due to the parachlorotoluene in the vapour state is shifted towards red by about  $1000\text{ cm}^{-1}$  with respect to that due to the ortho compound in the vapour state. Similarly, Fig. 2, shows that the spectrum due to *p*-bromotoluene in the vapour state is shifted towards red by about  $500\text{ cm}^{-1}$  with respect to that due to the meta compound. When the vapours are liquefied there is further shift of the spectrum towards red, but although in the case of *o*-chlorotoluene the position of maximum absorption on the long wavelength side shifts from  $31000\text{ cm}^{-1}$  to  $29000\text{ cm}^{-1}$  with the liquefaction of the vapour, such shift is from  $29600\text{ cm}^{-1}$  to  $29000\text{ cm}^{-1}$  in the case of *p*-chlorotoluene. In the case of *p*-bromotoluene, on the other hand, such shift is from  $30000\text{ cm}^{-1}$  to  $29000\text{ cm}^{-1}$  and in the case of *m*-bromotoluene the shift is a little more, being from  $30500\text{ cm}^{-1}$  to  $29000\text{ cm}^{-1}$ . As the 0,0 band due to singlet→singlet transition occurs in the neighbourhood of  $36000\text{ cm}^{-1}$  (Roy, 1956) in all these cases, the absorption in the region of  $30000\text{ cm}^{-1}$  cannot

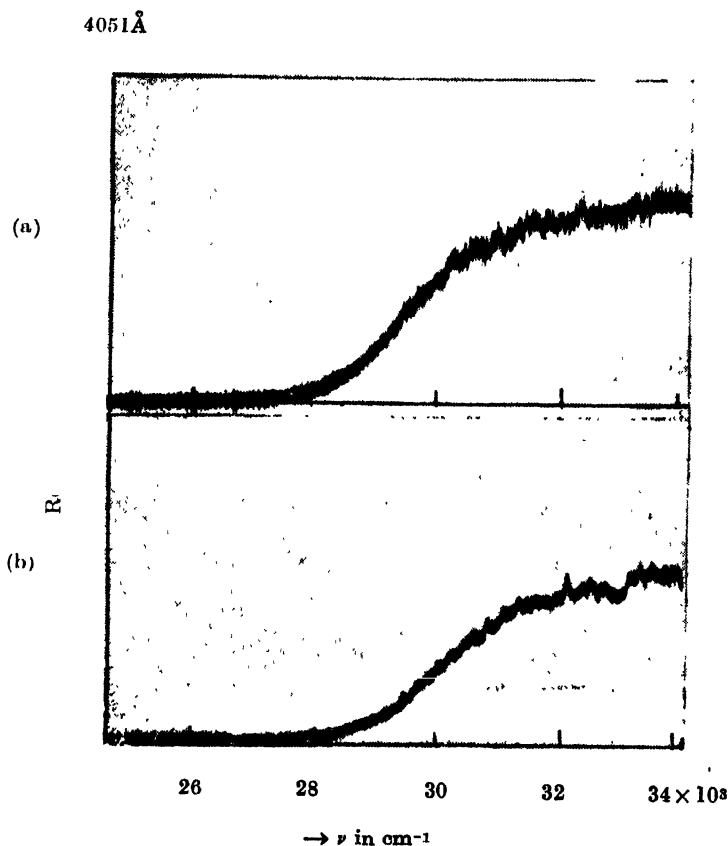


Fig. 3. (a) *p*-Bromotoluene (liquid)  
(b) (vapour)

be due to an extension of the singlet→singlet absorption towards longer wavelengths, and therefore, it is due to singlet→triplet transition. A comparison of Fig. 1(d) with Fig. 3(b), further shows that when the path length of the vapour is halved, the absorption in the region from 30000  $\text{cm}^{-1}$  to 31000  $\text{cm}^{-1}$  diminishes considerably. This shows the genuineness of the absorption due to the longer path of the vapour.

It is evident from the above results that probability of such transition is enhanced much more in the case of ortho or meta halogen substituted toluenes than in the case of the para compounds, when the vapours are liquefied. It is to be pointed out further, that the wavelength limit of maximum absorption in the liquid state is almost at the same position (about 29000  $\text{cm}^{-1}$ ) in all the four cases. It is evident from these results that the enhancement of singlet→triplet absorption with the liquefaction of the vapour is due to the influence of the substituent halogen atoms in the surrounding molecules in the liquid state, because in the case of benzene such enhancement is extremely small (Sirkar and Roy, 1960). The difference observed in the case of the para compound and that in the case of ortho or meta compound can be explained on the hypothesis that as in the case of the para compound the halogen atom is far away from the  $\text{CH}_3$  group it acts as a better shield against the interaction between the  $\pi$ -electrons of the ring and the halogen atom of the neighbouring molecule than in the case of the ortho or meta compound. In the ortho compound, the  $\pi$ -electrons in consecutive four carbon atoms being exposed to the influence of the halogen atom in the neighbouring molecule, there may be greater chance of the perturbation of the spin-orbital coupling than in the case of the para compound.

It can be seen from the curves in Figs. 1 and 2 that the absorption spectrum due to singlet→triplet transition is of continuous nature. As mentioned earlier, some previous workers observed discrete bands due to singlet→triplet transition induced by the influence of paramagnetic molecules on the  $\pi$ -electrons. It is highly probable that some preferentially orientated magnetic field due to the paramagnetic molecules produces such quantised new levels of the  $\pi$ -electrons while in the field of surrounding heavy atoms, such field has only random orientation giving rise to very broad perturbed levels.

#### ACKNOWLEDGMENT

The author is highly indebted to Professor S. C. Sirkar, D.Sc., F.N.I., for kindly suggesting the problem and for guidance throughout the progress of the work.

#### REFERENCES

- Evans, D.F., 1956, *Nature*, **178**, 534.  
Evans, D.F., 1957a, *J. Chem. Soc.*, 1351.

- Evans, D.F., 1957b, *J. Chem. Soc.*, 3885.  
Kasha, M., 1952, *J. Chem. Phys.*, **20**, 71.  
McClure, D.S., 1949, *J. Chem. Phys.*, **17**, 665.  
McClure, D.S., 1952, *J. Chem. Phys.*, **20**, 682.  
McClure, D.S., Blake, N. W. and Hanst, P. L., 1954, *J. Chem. Phys.*, **22**, 255.  
Mizushima, M. and Koide, S., 1952, *J. Chem. Phys.*, **20**, 765.  
Robertson, W. W. and Reynolds, R. E., 1958, *J. Chem. Phys.*, **29**, 138.  
Roy, J. K., 1960, *Ind. J. Phys.*, **34**, 331.  
Roy, S.B., 1956, *Ind. J. Phys.*, **30**, 276, 590.  
Sirkar, S. C. and Roy, J. K., 1960, *Ind. J. Phys.*, **34**, 581.

# INFRARED SPECTRA OF *O*-BROMOPHENOL IN THE LIQUID STATE AND IN SOLUTIONS IN DIFFERENT SOLVENTS\*

S. B. BANERJEE AND A. K. CHAKRABORTY

OPTICS DEPARTMENT, INDIAN ASSOCIATION FOR THE CULTIVATION OF  
SCIENCE, CALCUTTA-32

(Received, January 25, 1961)

**ABSTRACT.** The infrared spectra of *o*-bromophenol in the liquid state and in solutions in carbon tetrachloride, cyclohexane and chloroform in the 3200-3700  $\text{cm}^{-1}$  region have been studied with a Perkin-Elmer Model 21 spectrophotometer. As regards the OH band, the pure liquid exhibits a broad absorption band at about 3460  $\text{cm}^{-1}$  while sharp peaks at 3522, 3522 and 3490  $\text{cm}^{-1}$  are exhibited by 3% solutions of the compound in carbon tetrachloride, cyclohexane and chloroform respectively. In the case of 12% solutions in carbon tetrachloride and cyclohexane, sharp peaks at 3474 and 3484  $\text{cm}^{-1}$  are observed. In each of these two cases there is also an inflexion at about 3540  $\text{cm}^{-1}$ .

It has been concluded that in the liquid state most of the molecules are present as dimers as suggested by Pauling and in the case of the dilute solutions the majority of the molecules are single. It has been pointed out that an idea of relative abundance of associated molecules and single molecules can be found from a comparison of the areas of the absorption peaks due to these two types of molecules present in concentrated solutions.

## INTRODUCTION

In explaining the infrared spectrum of *o*-chlorophenol, Pauling (1945) pointed out that the liquid may contain double molecules formed through O-H...O intermolecular bond, while the OH group and chlorine atom of the same molecule may be linked in the *cis*-position. In a recent investigation on the infrared spectra of dilute solutions of *o*-chlorophenol in carbon tetrachloride and cyclohexane (Sirkar *et al.*, 1958) it was observed that the intermolecular hydrogen bond in associated molecules breaks up in dilute solutions. Davies (1940) studied the infrared spectrum of *o*-bromophenol in dilute solutions in carbon tetrachloride and observed a band at 3520  $\text{cm}^{-1}$  and a weaker one at 3595  $\text{cm}^{-1}$ , which were assigned by him to the O-H frequencies in the case of the OH group respectively in *cis*- and *trans*-position with respect to the bromine atom in the same molecule. Similar investigations in the first harmonic region were also reported by Wulf *et al.* (1936). They, however, did not report any data for the pure liquid. In the

\*Communicated by Professor S. C. Sirkar.

present work it was, therefore, intended to study the nature of hydrogen bonding in *o*-bromophenol in the liquid state and the influence of environment on the population of such associated molecules, and the infrared spectra of *o*-bromophenol in the liquid state and in solutions of different concentrations in carbon tetrachloride, cyclohexane and chloroform, have been studied. The results have been discussed in the present paper.

## EXPERIMENTAL

Chemically pure *o*-bromophenol purchased from E. Merck was fractionated and the proper fraction was collected and redistilled under reduced pressure. Carbon tetrachloride, cyclohexane and chloroform used as solvents were also of chemically pure quality and were also distilled under reduced pressure before use.

The infrared spectra were recorded with a double beam Perkin-Elmer Model 21 spectrophotometer with rocksalt optics. The slit was adjusted at 927. The instrument was placed in an airconditioned room maintained at a temperature of 26°C.

The strengths of solutions used were 3% and 12% for solution in carbon tetrachloride and cyclohexane and 3% for solution in chloroform. The thickness of the cell was 0.1 mm in the case of dilute solutions and 0.025 mm in the case of the concentrated solutions. The spectrum of the pure liquid was recorded using a thin film of the liquid pressed between two rocksalt plates. In studying the spectra of the solutions, the bands of the solvents were eliminated by using an equivalent compensation cell containing the solvents in the reference beam.

## RESULTS AND DISCUSSION

The absorption curves due to *o*-bromophenol and its solutions in carbon tetrachloride, cyclohexane and chloroform are reproduced in Figs. 1 and 2. In the case of the pure liquid broad absorption extending from  $3550\text{ cm}^{-1}$  to  $3200\text{ cm}^{-1}$  is observed which suggests that the absorption curve is produced by superposition of more than one broad bands. The maximum of absorption is at about  $3460\text{ cm}^{-1}$  which is broadened towards lower frequencies with a gradual fall in intensity. In 3% solution in carbon tetrachloride and cyclohexane, however, the intense broad band at  $3460\text{ cm}^{-1}$  is totally absent and only a sharp peak at  $3522\text{ cm}^{-1}$  is observed. Davies (1940) observed a band at  $3520\text{ cm}^{-1}$  and a very much weaker band at  $3595\text{ cm}^{-1}$  in the spectrum of .09M solution of *o*-bromophenol in carbon tetrachloride. He attributed the first band to the O-H vibration in the OH group in the *cis*-position with respect to bromine atom and the second one to the O-H group in the *trans*-position. On comparing these results, it appears that the intense broad peak at  $3460\text{ cm}^{-1}$  in the pure liquid may represent the O-H vibration in the dimeric molecules present in the liquid, the

hydrogen atom of the OH group of a molecule being attached to the oxygen atom in a neighbouring molecule (Pauling, 1945).

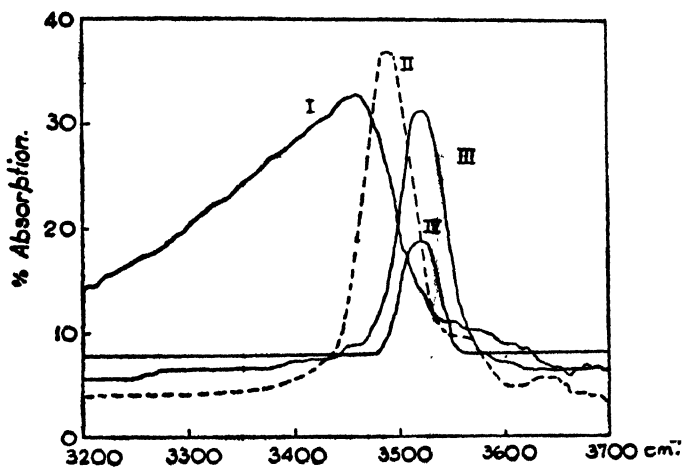


Fig. 1. Infrared absorption spectra of *o*-bromophenol  
 Curve I. Pure liquid  
 Curve II. 3% solution in chloroform  
 Curve III. 3% solution in carbon tetrachloride  
 Curve IV. 3% " " cyclohexane

When the molecules are dispersed in 3% solutions in carbon tetrachloride and cyclohexane, the intermolecular O-H...O bond is broken and the observed frequency at  $3522\text{ cm}^{-1}$  represents the O-H stretching oscillation in the OH group in the single molecule. As pointed out in a previous paper (Sirkar *et al.*, 1958) this frequency may not belong to *cis*-configuration. The peak due to solution in  $\text{CCl}_4$  is, however, much larger than that due to the solution in cyclohexane. This shows the influence of the environment on the strength of absorption. The weak OH stretching band assigned to *trans*-molecules reported by Davies has, however, not been observed in the present investigation. In 3% solution of *o*-bromophenol in the polar solvent chloroform, the OH vibrational frequency is only at  $3490\text{ cm}^{-1}$ , which may indicate an influence of the field of the polar solvent molecules on this frequency of the dispersed molecules of *o*-bromophenol.

When the concentration of *o*-bromophenol in carbon tetrachloride and cyclohexane is increased to 12%, sharp peaks at  $3474$  and  $3484\text{ cm}^{-1}$  respectively are observed. In this case the strength of absorption is also relatively higher than at  $3522\text{ cm}^{-1}$  in the case of the 3% solution with equivalent path length. This peak is accompanied in each case by a weak inflexion at about  $3540\text{ cm}^{-1}$ . Thus the concentrated solutions in both the solvents seem to contain large number of dimeric molecules and a few single molecules and the two frequencies due to

each of these 12% solutions probably represent OH stretching oscillations in intermolecular OH...O bonded group and in the OH group in the *trans*-position in the single molecule as pointed out by Sirkar *et al.* (1958).

It is interesting to note that the results discussed above give definite indication of the predominance of dimeric molecules in the pure liquid state of

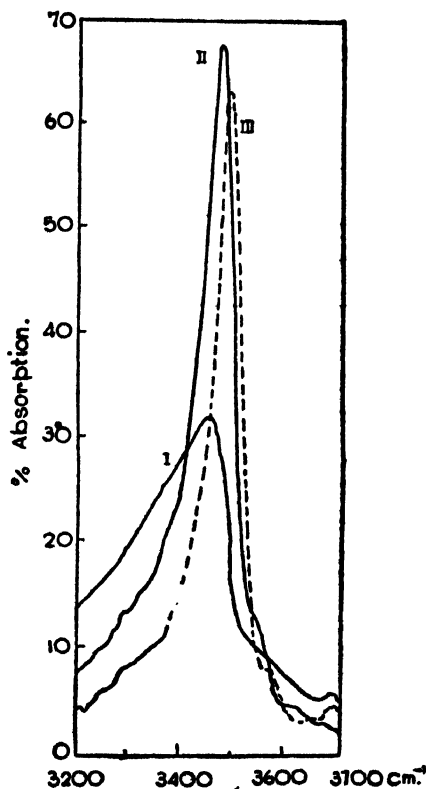


Fig. 2. Infrared absorption spectra of *o*-bromophenol

Curve I. Pure liquid

Curve II. 12% solution in carbon tetrachloride

Curve III. 12% solution in cyclohexane

*o*-bromophenol and also give an idea about the relative abundance of dimeric molecules over the *trans*-type single molecules in the case of solutions of concentration above 10%. In fact, a quantitative estimation of the relative population of O-H...O bonded double molecules with OH group in *cis*-configuration with respect to that of the single molecules can be made from the ratio of the areas of the peaks at  $3474\text{ cm}^{-1}$  and  $3540\text{ cm}^{-1}$  respectively observed in the case of concentrated solutions if the change in the strength of absorption per molecule with the change from the *trans* to the *cis* position of the OH group is first determined.



ACKNOWLEDGMENT

The authors are grateful to Professor S. C. Sirkar, D.Sc., F.N.I., for his kind interest in the work.

REFERENCES

- Davies, M. M., 1940, *Trans. Faraday. Soc.*, **36**, 333.  
Pauling, L., 1945, *The Nature of the Chemical Bond*, p. 324.  
Sirkar, S.C., Deb, A. R. and Banerjee, S.B., 1958, *Ind. J. Phys.*, **32**, 345.  
Wulf, O.R., Liddel, U. and Hendricks, S. B., 1936, *J. Am. Chem. Soc.*, **58**, 2287.,

# ON THE ABSORPTION OF 3.18-CM MICROWAVES IN SOME ALIPHATIC ALCOHOLS AND THEIR SOLUTIONS\*

T. J. BHATTACHARYYA

OPTICS DEPARTMENT, INDIAN ASSOCIATION FOR THE CULTIVATION OF  
SCIENCE, CALCUTTA-32

(Received, January 30, 1961)

**ABSTRACT.** The dependence on temperature of absorption of microwaves of wave-length 3.18 cm in *n*-propyl, *n*-butyl, isopropyl-, isobutyl-, *n*-octyl- and *n*-heptyl alcohol and in their solutions in CCl<sub>4</sub> and heptane at different concentrations have been studied by simple optical method.

It is observed that in the case of lower alcohols absorption increases with the increase of temperature without showing any definite maximum in the curve, while the higher alcohols and the solutions of all the six alcohols show absorption maxima at temperatures depending on their viscosities.

From a comparison of different results it has been concluded that most of the molecules in the lower alcohols in the pure state are in the form of dimers which break up in the solutions into single molecules. In the case of higher alcohols the molecules being large, some of the molecules do not form such dimers and remain as single molecules.

Applying Debye's theory the radius of the rotor has been calculated, and the value has been found to be near about 1.96 Å in all the cases. The rotor has been identified with the OH group.

## INTRODUCTION

The anomalous dielectric dispersion in alcohols in the region of radio-waves of wave-lengths ranging from decimetre to metre region was studied by Mizushima (1927). He found that some aliphatic alcohols show absorption in the metre region and the region of such anomalous dispersion shifts towards longer wave-lengths as the length of the molecule increases. With a particular frequency he observed (Mizushima, 1929) that the temperature at which the maximum absorption occurs becomes higher for higher alcohols. He concluded that the theory proposed by Debye (1913) correlating time of relaxation with the dielectric constant at any frequency was verified by these results and that the whole molecule was the rotor in these cases. Later, Ghosh (1954, 1955) studied the absorption of 3.18cm microwaves in some aromatic liquids with the molecules having OH group as a

\*Communicated by Prof. S. C. Sirkar

substituent and by varying the temperature of the liquids he observed maximum absorption at a particular temperature in each case. From the values of the time of relaxation and the viscosity of the liquids at those temperatures he calculated the radius of the rotor and found it to be of the order of 1.5 Å. He concluded that the rotor was the OH group and not the whole molecule in these cases.

Recently, Imanov and Abbasov (1957) used microwaves of wave-lengths ranging from 10 cm to 180 cm to measure the dielectric loss in several normal and iso-alcohols in this region. They observed maximum loss at particular wave-lengths in the region from 18 cm to 60 cms in five alcohols, but no such maxima were observed in methyl and ethyl alcohol in the whole wave-length range 12 cm—180 cm. They did not identify the rotor in the above cases.

It would be interesting, however, to find out whether in these pure aliphatic alcohols in the liquid state the OH group has any freedom of rotation and whether the influence of solvents affects such freedom. With this object in view the absorption of 3.18 cm microwaves in a few aliphatic alcohols in the liquid state and also in solution in suitable solvents has been investigated.

## EXPERIMENTAL

The experimental arrangements and procedure adopted in the present investigations were the same as those used previously (Bhattacharyya 1958). The liquids used were *n*-propyl-, *n*-butyl-, isopropyl-, isobutyl-, *n*-heptyl-, and *n*-octyl alcohol. In order to make the alcohols free from water the lower alcohols were mixed with dehydrated magnesium sulphate and were kept in this condition for two days. After filtration they were treated with fresh quick-lime and subjected to fractional distillation. The two higher alcohols were distilled in vacuum after proper dehydration. The absorption was studied in the pure liquids as well as in their solutions of different concentrations in  $\text{CCl}_4$  and heptane in the range of temperature from 28°C to 140°C. The graphs showing the relation between temperature and the attenuation coefficients of different liquids were drawn. The values of static dielectric constant, refractive indices and coefficients of viscosity for the pure liquids were obtained from the standard tables. These data for the solutions were determined experimentally. With the help of Debye's theory and using these data, the radius of rotor was calculated in each case.

## RESULTS AND DISCUSSIONS

Fig. 1 shows the temperature-dependence of the attenuation coefficients of pure alcohols. The lower alcohols like *n*-butyl-, *n*-propyl-, isobutyl- and isopropyl alcohol do not show any absorption maxima. The absorption in these cases increases rapidly with the increase of the temperature. Similar results were also obtained in the case of pure ethylene chlorhydrin (Bhattacharyya, 1959). The higher alcohols, however, show definite absorption maxima. Octyl alcohol

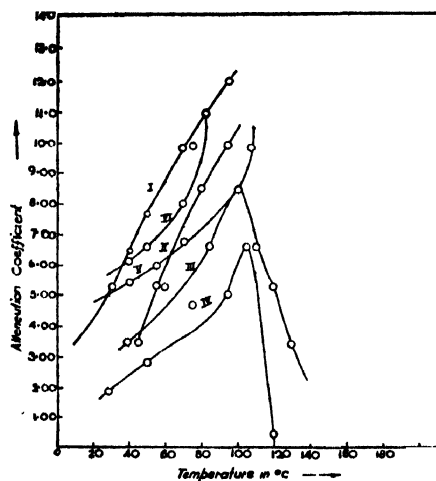


Fig. 1. Temperature dependence of the attenuation coefficient for pure alcohols

- I—*n*-Propyl alcohol.  
 II—*n*-Butyl alcohol.  
 III—*n*-Heptyl alcohol.  
 IV—*n*-Octyl alcohol.  
 V—iso-Butyl alcohol.  
 VI—iso-Propyl alcohol.

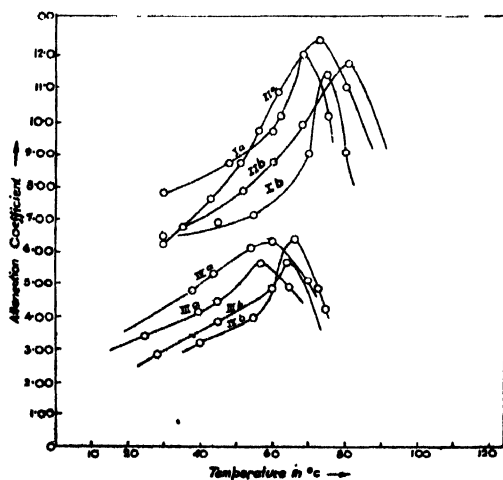


Fig. 2. Temperature dependence of the attenuation coefficient of the solutions of *n*-alcohols in  $\text{CCl}_4$ .

- Ia—20% solution of heptyl alcohol in  $\text{CCl}_4$ .  
 Ib—30% " " " " "  
 IIa—20% solution of octyl alcohol in  $\text{CCl}_4$ .  
 IIb—30% " " " " "  
 IIIa—30% solution of propyl alcohol in  $\text{CCl}_4$ .  
 IIIb—50% solution of butyl alcohol in  $\text{CCl}_4$ .

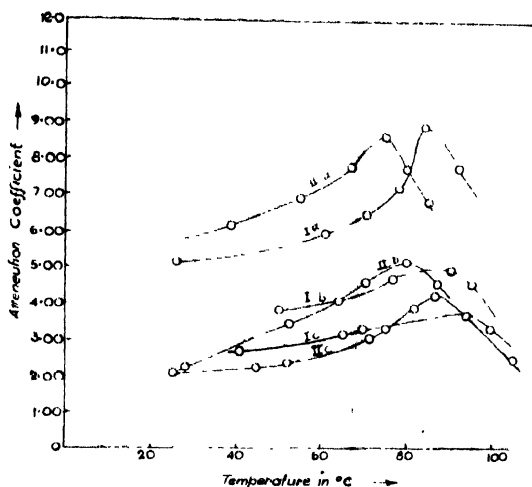


Fig. 3. Temperature dependence of the attenuation coefficient of the solution of iso-alcohols in  $\text{CCl}_4$ .

Ia—30% solution of isopropyl alcohol in  $\text{CCl}_4$ .

Ib—50% " " " " " "

IIa—30% solutions of isobutyl alcohol in  $\text{CCl}_4$ .

IIb—50% " " " " " "

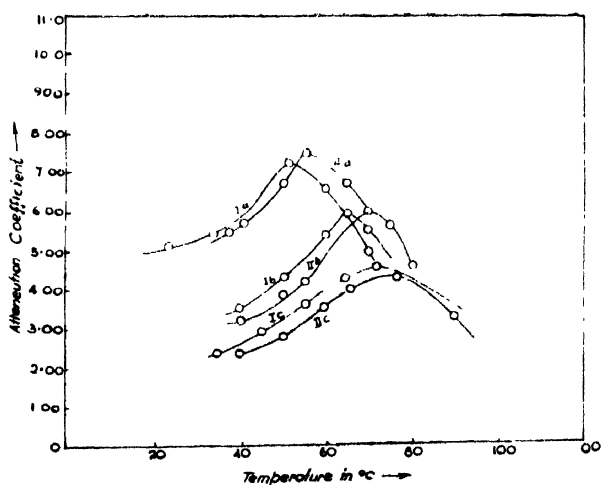


Fig. 4a. Temperature dependence of the attenuation coefficient of the solutions of lower alcohols in heptane.

Ia—30% solutions of *n*-propyl alcohol in heptane.

Ib—50% " " " " " "

Ic—70% " " " " " "

IIa—30% solutions of *n*-butyl alcohol in heptane.

IIb—50% " " " " " "

IIc—70% " " " " " "

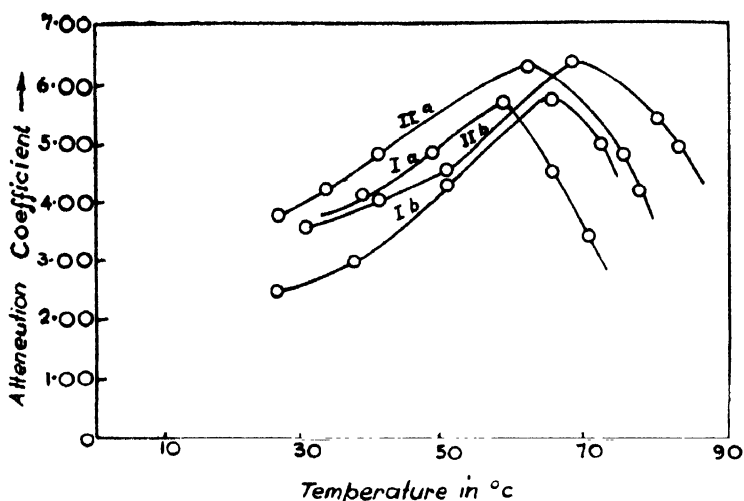


Fig. 4b. Temperature dependence of the attenuation coefficient of the solutions of higher alcohols in heptane.

Ia—30% solutions of octyl alcohol in heptane.

Ib—50% " " " " " "

Ic—70% " " " " " "

IIa—30% solutions of heptyl alcohol in heptane.

IIb—50% " " " " " "

Iic—70% " " " " " "

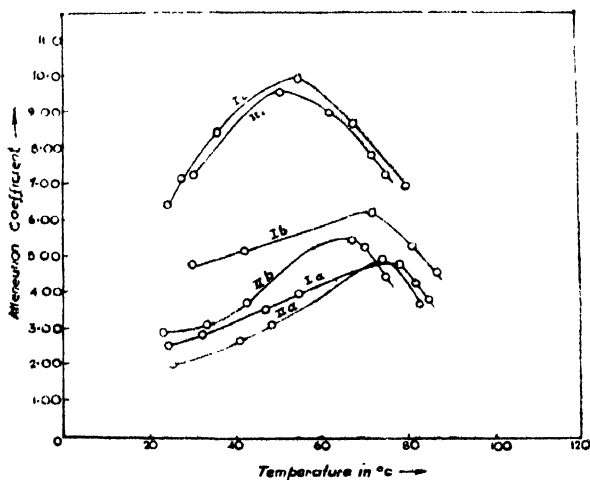


Fig. 5. Temperature dependence of the attenuation coefficient of the solutions of iso-alcohol in heptane.

Ia—70% solution of isobutyl alcohols in heptane.

Ib—50% " " " " " "

Ic—30% " " " " " "

IIa—70% solution of isopropyl alcohol in heptane.

IIb—50% " " " " " "

Iic—30% solution of isopropyl alcohol in heptane.

shows the maximum at 105°C while heptyl alcohol shows it at 100°C. The absence of any absorption maxima in the case of lower alcohols cannot be explained on the assumption that these occur at higher temperatures i.e. at temperatures higher than 100°C, because heptyl and octyl alcohols which have higher viscosity show their respective maxima near about 100°C. When the lower alcohols are dissolved in the solvents, carbon tetrachloride and heptane we get absorption maxima at certain temperatures as shown in Figs. 2, 3, 4 and 5. This difference in the behaviour of the pure liquids and solutions may be explained on the assumption that in the pure liquid most of the molecules are in the form of dimers formed by weak linkage through the H-O—H-O bond and as the dimers break up with the rise of temperature contribution to absorption from new single molecules increases gradually without attaining a constant value. In the case of the higher alcohols, however, the molecules being long, some of the molecules do not form dimers and exist as single molecules. As the viscosity attains the proper value with the rise of temperature of the liquid a maximum absorption is exhibited by these molecules in these cases.

An attempt was made to calculate the radius of the rotor from Debye's theory in the cases in which maximum absorption has been observed. The data required for this purpose as well as the values of  $\tau$ , the time of relaxation and  $a$ , the radius of the rotor are given in Table I. It is interesting to note that the values of  $a$ , the radius of the rotor, is almost the same in all these cases, the mean value being about 1.96 Å. Evidently, the rotor is not the whole molecule in any of the liquids and the solutions and the common group present in the molecules being the OH group, the rotor may be identified with this group. In previous investigations the radius of the rotor for the OH group in aromatic compounds was calculated and it was found to be of the order of 1.5 Å (Ghosh, 1955a, 1954), but no such data for aliphatic alcohols are available. It cannot be expected that radius of the OH group as the rotor in the case of aliphatic compounds should be the same as that for the aromatic compounds, as the radius of such rotor is expected to be dependent on the bond angle and other factors. Ghosh (1955a) observed in *o*-methoxy phenol, a typical aromatic compound, the radius of the OH rotor to be 1.7 Å which is slightly larger than the value observed in the case of *p*-chlorophenol, *p*-chlorocresol etc., So, the rotor in the present case can be identified with OH group of the alcohol molecules.

The comparison of the curves for the pure liquids with those for their solutions thus leads to the conclusion that in the lower alcohols in the pure state most of the molecules are in the state of loosely coupled dimers and in the solutions these dimers break up into single molecules. Application of Debye's method in these cases gives consistent results and also furnishes much information about the state of association of the molecules in the liquids.

TABLE I

Substance	Concentration	$\epsilon$	$\sqrt{\epsilon_0}$	Temperature	100%	$\tau \times 10^{11}$ sec	$a \times 10^8$ cm.
Propyl alcohol	30%	6.57	1.44	57°C	0.6886	1.42	1.95
+ CCl <sub>4</sub>	50%	8.60	1.44	64°C	0.7317	1.32	1.83
Butyl alcohol	30%	4.66	1.44	60°C	0.6910	1.55	2.00
+ CCl <sub>4</sub>	50%	6.30	1.42	66°C	0.7531	1.45	1.93
Isopropyl alcohol	30%	7.54	1.43	58°C	0.6913	1.38	1.94
+ CCl <sub>4</sub>	50%	11.1	1.42	65°C	0.6035	1.22	1.96
Isobutyl alcohol	30%	4.93	1.44	62°C	0.7333	1.53	1.97
+ CCl <sub>4</sub>	50%	5.75	1.43	68°C	0.7197	1.48	1.97
Heptyl alcohol	30%	3.80	1.45	75°C	0.8402	1.61	1.94
+ CCl <sub>4</sub>	20%	3.28	1.45	68°C	0.7957	1.64	1.97
Octyl alcohol	30%	3.56	1.45	81°C	0.8572	1.62	1.92
+ CCl <sub>4</sub>	20%	3.12	1.45	73°C	0.8024	1.65	1.98
Heptyl-alcohol	Pure	4.20	1.43	100°C	0.8000	1.58	2.01
Octyl alcohol	Pure	3.40	1.43	105°C	0.8800	1.63	1.97
Propyl alcohol	70%	10.97	1.39	72°C	0.6028	1.22	1.97
+ heptane	50%	9.50	1.39	65°C	0.6001	1.28	1.99
	30%	8.68	1.39	51°C	0.6031	1.32	1.98
Butyl alcohol	70%	9.50	1.39	76°C	0.6446	1.28	1.97
+ heptane	50%	8.85	1.39	70°C	0.6206	1.31	1.99
	30%	8.20	1.39	55°C	0.6200	1.34	1.98
Isopropyl alcohol	70%	14.54	1.39	74°C	0.6021	1.10	1.91
+ heptane	50%	10.90	1.39	68°C	0.5962	1.22	1.97
	25%	8.95	1.39	50°C	0.5785	1.31	2.00
	70%	10.57	1.39	78°C	0.6387	1.24	1.96
Isobutyl alcohol	50%	9.65	1.39	72°C	0.6204	1.28	1.98
+ heptane	25%	8.25	1.39	55°C	0.6194	1.34	1.98
Heptyl alcohol	75%	4.45	1.43	87°C	0.8999	1.56	1.90
+ heptane	50%	3.82	1.41	80°C	0.8762	1.61	1.92
	30%	3.42	1.40	75°C	0.8222	1.63	1.96
Octyl alcohol	75%	3.95	1.43	95°C	0.8704	1.60	1.95
+ heptane	50%	3.45	1.41	90°C	0.8418	1.63	1.98
	30%	3.12	1.40	84°C	0.8303	1.65	1.98



ACKNOWLEDGMENT

The author is indebted to Professor S. C. Sirkar, D.Sc., F.N.I., for his constant guidance throughout the progress of the work.

REFERENCES

- Bhattacharyya, T. J., 1958, *Ind. J. Phys.* **32**, 573.  
Bhattacharyya, T. J., 1959 *Ind. J. Phys.* **33**, 498.  
Debye, P. 1913, *Verh. Deut. Phys.* **15**, 770.  
Ghosh, D. K., 1954, *Ind. J. Phys.* **28**, 191.  
Ghosh, D. K., 1955, *Ind. J. Phys.* **29**, 581.  
Imanov, L. M. and Abbasov Ya, 1957. *Doklady Akad Nauk Azerbaidzhan S.S.R.* **13**, 475-80.  
Mizushima, S., 1927, *Sc. Papers Inst. Phys. Chem. Research.*, (Tokyo) **5**, 201.  
Mizushima, S., 1929, *Sc. Papers Inst. Phys. Chem. Research.*, (Tokyo) **9**, 292.

# Statement about ownership and other particulars about "INDIAN JOURNAL OF PHYSICS"

## FORM IV

- |                                   |     |     |   |
|-----------------------------------|-----|-----|---|
| 1. Place of Publication           | ... | ... | 2 and 3 Lady Willingdon Road,<br>Calcutta-32. |
| 2. Periodicity of its publication | ... | ... | Monthly                                       |
| 3. Printer's Name                 | ... | ... | Kalipada Mukherjee                            |
| Nationality                       | ... | ... | Indian,                                       |
| Address                           | ... | ... | 204/1, B. T. Road, Alambazar,<br>Calcutta-35. |
| 4. Publisher's Name               | ... | ... | Samarendra Nath Sen                           |
| Nationality                       | ... | ... | Indian,                                       |
| Address                           | ... | ... | 2 and 3 Lady Willingdon Road,<br>Calcutta-32. |
- 
- |                   |    |   |     |  |
|-------------------|----|---|-----|--|
| 5. Editors' Names | 1. | Prof. S. C. Sirkar (Secy.,<br>Board of Editors)   | 6.  | Prof. S. N. Bose,  |
| Nationality       |    | Indian,   |     | Indian,  |
| Address           |    | Indian Association for<br>the Cultivation of Science,<br>Jadavpur, Calcutta-32.   |     | President,<br>I.A.C.S.,<br>Calcutta-32.  |
|                   | 2. | Prof. K. Banerjee,  | 7.  | Prof. S. K. Mitra,   |
|                   |    | Indian,<br>Director,<br>I. A. C. S.,<br>Jadavpur,<br>Calcutta-32.   |     | Indian,<br>Institute of Radio<br>Physics & Electronics,<br>92, Upper Circular<br>Road, Calcutta-9.       |
|                   | 3. | Prof. D. M. Bose,   | 8.  | Prof. D. S. Kothari,   |
|                   |    | Indian,<br>Bose Institute,<br>93/1 Upper Circular Rd,<br>Calcutta-9.  |     | Prof. of Physics, Delhi<br>University, Delhi-8.  |
|                   | 4. | Prof. S. R. Khastgir,<br>Palit Prof. of Physics,<br>Saha Institute of Radio<br>Physics,<br>92, Upper Circular Rd.,<br>Calcutta-9. | 9.  | Prof. K. R. Rao,   |
|                   |    |   |     | Indian,<br>Principal & Hd. of the<br>Dept. of Physics,<br>Andhra University,<br>Waltair.                 |
|                   | 5. | Prof. P. S. Gill,   | 10. | Dr. D. B. Sinha,   |
|                   |    | Indian,<br>Prof. of Physics,<br>Muslim University,<br>Aligarh.  |     | Dept. of Applied<br>Physics, University<br>College of Science,<br>92, Upper Circular Rd.,<br>Calcutta-9. |
|                   |    |   |     |  |
|                   |    |   |     | 11. Prof. B. N. Srivastava,  |
|                   |    |   |     | Indian,<br>I. A. C. S.,<br>Jadavpur, Calcutta-32.  |
- 
6. Name and address of the proprietor...Indian Association for the Cultivation  
of Science, Jadavpur, Calcutta-32.

I, Samarendra Nath Sen, hereby declare that the particulars given above  
are true to the best of my knowledge and belief.

Date 16-3-61

(Sd) Samarendra Nath Sen,  
*Signature of Publisher*



# SCATTERING OF ELECTRON BY THOMAS-FERMI POTENTIAL

S. C. MUKHERJEE

DEPARTMENT OF THEORETICAL PHYSICS, INDIAN ASSOCIATION FOR THE CULTIVATION OF SCIENCE, JADAVPUR, CALCUTTA-32

(Received, February 18, 1961)

**ABSTRACT.** In this paper the elastic scattering cross-section of electrons by the Thomas-Fermi potential as represented by the analytical forms due to Gombas and Tietz has been calculated by the Born approximation method. Our results are in fair agreement with those calculated with the exact numerical form of Thomas-Fermi potential. Further comparison shows that the Gombas-Tietz form is as good as those of Rozental and Buchdahl.

## INTRODUCTION

The scattering of electron by a heavy atom is a many body problem, the electron to be scattered is influenced by the positively charged nucleus and the negatively charged electrons surrounding the nucleus. It is difficult to calculate accurately the electrical potential due to such an atom. Of the two available methods, the self-consistent field method of Hartree and Fock is more accurate than the statistical one of Thomas and Fermi. The difficulty of calculation by Hartree's method increases with the complexity of the atom, whereas the more complex the atom is the more valid is the calculation for the Thomas-Fermi potential, because the electrons of the complex atom are treated as a statistical ensemble. The form of the Thomas-Fermi potential is taken to be

$$V(r) = - \frac{Ze^2}{r} \phi(r)$$

where  $\phi$  is the Thomas-Fermi function for the free neutral atom and is the solution of

$$\frac{\partial^2 \phi}{\partial x^2} = \frac{\phi^{3/2}}{x^4}$$

where  $x = r/\mu$ ;  $\mu = \frac{0.88534}{Z^{1/3}} a_0$ ,  $a_0$  being the first Bohr radius and  $Z$  is the atomic number. The above equation does not admit of an exact solution which is available only in the form of a numerical table; however, various approximations in analytical forms have been suggested by several authors like Sommerfeld (1932), Rozental (1935), Gombas (1949), March (1950), Kerner (1951), Tietz

(1955, 1956), Brinkman (1954), Umeda (1955), Buchdahl (1956) and Latter (1955). It is not possible to calculate analytically the scattering cross section with the forms of Sommerfeld, March, Umeda and Latter. The form of Kerner is not quite suitable. Majewasky and Tietz (1957) have calculated scattering cross section in the Born approximation with the forms of Brinkman, Buchdahl and Rozental. The form of Gombas (1949) is valid only in a region near the nucleus and that of Tietz (1954) holds good outside this region. We propose to calculate the scattering cross section with the Gombas-Tietz form. We are led to this choice of the potential, because Tsang (1959) taking the form of Gombas has got good agreement of binding energies of electrons with those obtained by using the Thomas-Fermi potential and by Hartree's method. In this paper we have calculated by the Born approximation method the elastic scattering cross section of electrons by a central potential which is of the form of Gombas between the range  $0 \leq x \leq 1$  and of Tietz for  $x \geq 1$ . We have compared our findings obtained by such a potential with the results of Mott and Massey (1949) obtained with Thomas-Fermi potential and that of Tietz and Majewasky (1957) calculated with the potentials of Rozental (1935) and Buchdahl (1956).

For electrons having 50 KeV energy scattered by Krypton ( $Z=36$ ) the differential cross section decreases with increasing angle upto  $70^\circ$ ; thereafter it fluctuates with two maxima at  $80^\circ$  and  $110^\circ$ . Unfortunately there is no experimental data to compare with our theoretical findings.

#### CALCULATION

The amplitude of scattering by a central potential  $V(r)$ , according to the Born approximation, is given by

$$f(\theta) = -\frac{8\pi^2m}{h^2} \int_0^\infty \frac{\sin kr}{kr} V(r)r^2dr \quad \dots (1)$$

where  $\theta$  is the scattering angle,

$$K = k \cdot n_0 - n = \frac{4\pi \sin \theta/2}{\lambda} ; \lambda = \frac{2\pi}{k} = \frac{h}{mv}$$

$n_0$  being the unit vector along the  $Z$ -axis,  $n$  is a unit vector along the direction of  $r$ .

In the case of scattering of electrons by an atom we choose the potential as

$$\begin{aligned} V(r) &= V_G \quad \text{valid for } 0 \leq x \leq 1 \\ &= V_T \quad \text{valid for } x \geq 1 \end{aligned} \quad \dots (2)$$

where  $V_G$  has the form as given by Gombas,

$$V_G = - \frac{Ze^2}{x\mu} \{0.878 - 0.546x + 0.415(x-0.5)^2\}$$

where  $x = \frac{r}{\mu}$ ;  $\mu = \frac{0.88534}{Z^{1/3}} a_0$ , and  $a_0$  being the first Bohr radius for hydrogen and  $Z$  is the atomic number, and the form of  $V_T$  is due to Tietz,

$$V_T = - \frac{Ze^2}{x\mu} \left\{ \frac{a^2}{(x+a)^2} \right\}$$

where  $a = 1.86$ , the values of  $x$  and  $\mu$  are the same as in  $V_G$ . Substituting the form of (2) in Eq. (1), we get

$$f(\theta) = - \frac{8\pi^2 m \mu^3}{\hbar^2 p} \left\{ \int_0^1 \sin px V_G x dx + \int_1^\infty \sin px V_T x dx \right\}$$

where

$$p = 2\mu k \sin \theta/2 = K\mu$$

$$K = 2k \sin \theta/2.$$

$$\begin{aligned} \therefore \frac{f(\theta)}{Z^{1/3}} &= \frac{83.07 \times 10^{-10}}{p} \left[ \sin p \left( -\frac{0.131}{p^2} \right) + \cos p \left( \frac{0.830}{p^3} - \frac{0.435}{p} \right) \right. \\ &+ \frac{0.981}{p} - \frac{0.830}{p^3} + a^2 \left\{ \frac{\sin p}{1+a} - p \left( \cos pa \operatorname{Ci}\{p(1+a)\} + \sin pa \operatorname{Si}\{p(1+a)\} \right. \right. \\ &\quad \left. \left. - \sin pa \frac{\pi}{2} \right) \right\} \left. \right] \end{aligned}$$

where

$$\operatorname{Si}(x) = \int_0^x \frac{\sin t}{t} dt ; \operatorname{Ci}(x) = - \int_x^\infty \frac{\cos t}{t} dt$$

For the sake of comparison we give also the results of Tietz and Majewasky (1957) who have calculated the same with the potential forms of Rozental and Buchdahl.

The Rozental form is as follows :

$$\phi(x) = \sum_{i=1}^3 C_i e^{-a_i x}$$

where  $C_i$  and  $a_i$  are constants and their values are  $c_1 = 0.255$ ,  $c_2 = 0.581$ ,  $c_3 = 0.164$ ,  $a_1 = 0.246$ ,  $a_2 = 0.947$ ,  $a_3 = 4.356$ .

The Buchdahl form is as follows :

$$\phi(x) = [(1+Ax)(1+Bx)(1+Cx)]^{-1}$$

where  $A = 0.9288$ ,  $B = 0.1536$ ,  $C = 0.05727$ .

TABLE I

Comparison of our results for  $|f(\theta)|^2$  with the numerical results of Mott and Massey and results of Rozental and Buchdahl

$p=2\mu K \sin \theta/2$	$ f(\theta) ^2 Z^{-2/3}$ in units of $10^{-18} \text{cm}^2$			
	Mott & Massey	Rozental	Buchdahl	Present author
0.1	1460	1525	1257	1296
0.2	678	654	690	642
1.0	18.7	17.1	21.2	20.79
2.0	2.52	2.49	2.45	2.74
5.0	0.089	0.096	0.091	0.094
6.0	0.047	0.048	0.046	0.051
8.0	0.016	0.016	0.017	0.016
10.0	0.0064	0.0063	0.0065	0.0057

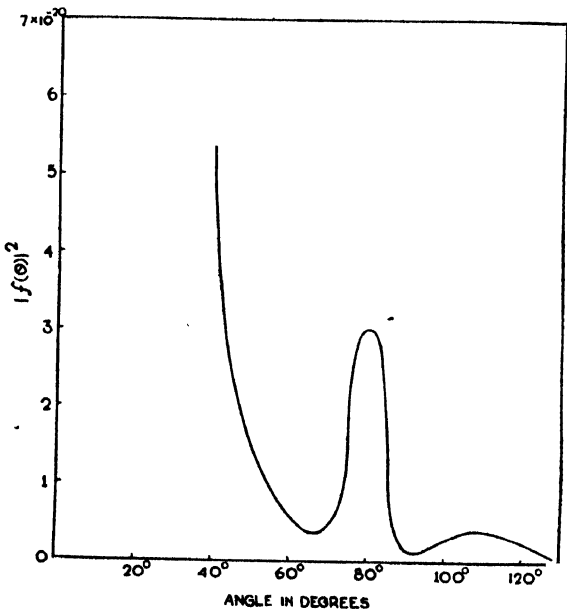


Fig. 1. Angular distribution of electrons at 40 KeV scattered by krypton ( $z=36$ )

## DISCUSSION

From the table of comparison it appears that our result of differential scattering cross section calculated with the Gombas-Tietz form agrees pretty well with the results of Mott and Massey. Our results are as good as those calculated with the forms of Rozental and Buchdahl.

From the calculation it is found that when  $p$  is large the contribution to the scattering from the Gombas potential is much larger than that from the Tietz potential whereas when  $p$  is small the reverse is the case. This finding is in conformity with the physical picture; the larger the value of  $p$  is, greater is the number of particles coming under the influence of Gombas part of the potential.

For 50 KeV electrons scattered by Krypton ( $Z = 36$ ) the differential cross section decreases with increasing angle till  $70^\circ$ , after which there are small rise and fall of the values giving two maxima which are analogous to diffraction phenomenon.

## ACKNOWLEDGMENT

The author is grateful to Prof. D. Basu for suggesting the problem and for his constant guidance throughout the progress of this work.

7

## REFERENCES

- Brinkman, H. C., 1954, *Physica* **20**, 44.
- Buchdahl, H. A., 1956, *Ann. Physik* **17**, 238.
- Gombas, P., 1949, *Die Statistische Theorie des Atoms und ihre Anwendungen* (Springer-Verlag).
- Korner, E. H., 1951, *Phys. Rev.*, **83**, 71.
- Latter, R., 1955, *Phys. Rev.* **99**, 510.
- March, N. H., 1950, *Proc. Cambridge Phil. Soc.* **46**, 356.
- Mott, N. F., & Massey, H. S. W., *The Theory of Atomic Collisions* (Oxford University Press, New York, 1949, Second Edition, Ch. IX).
- Rozental, S., 1935, *Z. Physik*, **98**, 742.
- Sommerfeld, A., 1932, *Z. Physik*, **78**, 283.
- Tietz, T., 1955, *J. Chem. Phys.* **23**, 1167.
- Tietz, T., 1956, *Nuovo Cimento* **4**, 1192 (1956).
- Tietz, T. & Majewasky, M., 1957, *Phys. Rev.* **108**, 193.
- Tsang, T., 1959, *Physica*, **25**, 1241.
- Umeda, K., 1955, *J. Phys. Soc. Japan*, **10**, 749.

# A SIMPLE STUDY OF THE NUCLEAR SELF-CONSISTENT FIELD PROBLEM\*

N. V. V. J. SWAMY

DEPARTMENT OF PHYSICS, KARNATAK UNIVERSITY, DHARWAR

(Received, October 10, 1960)

**ABSTRACT.** Assuming a nucleon-nucleus potential and a phenomenological nucleon density distribution, a Hartree type self-consistent field calculation has been carried out for  $O^{16}$ . Three cycles have indicated that the nucleus collapses in each cycle if only a pure central attraction of the Yukawa type is assumed to exist between the nucleons. Introduction of a repulsive core, other than the usual hard sphere type, has led to the conclusion that angular momentum dependent potentials have to be used in order to obtain convergence in successive cycles and adequate binding energy of the nucleus. An estimate has been made of the correlation length of the resulting non-local potential, as also of the effective mass as a function of position.

There can be no question that the many-body approach of Brueckner and Bethe (1955, 1956) is the correct one for studying the nuclear self-consistent field problem. However it has been noticed that the application of this method to finite nuclei bristles with outstanding computational difficulties. It is the purpose of this paper to point out that when a Hartree type self-consistent field calculation has been carried out based on a single-particle approach, the qualitative results so obtained did not differ in physical content very much from those of the many body theory.

The earlier effort in this direction has been that of Talman (1956) who had chosen a two-body interaction of the Yukawa type between all pairs of nucleons

$$\vec{t}(\vec{r}_1, \vec{r}_2) = g^2 \frac{e^{-p|\vec{r}_1 - \vec{r}_2|}}{|\vec{r}_1 - \vec{r}_2|} \quad \dots \quad (1)$$

$g$  being the coupling constant or strength of the two-body force and  $p^{-1}$  the range of the force. Using a uniform nucleon density distribution

$$\begin{aligned} \vec{\rho}(r) = \rho(r) &= \frac{3\Lambda}{4\pi a^3} & r < a \\ &= 0 & r > a \end{aligned} \quad \dots \quad (2)$$

---

\*Work supported by the United States Atomic Energy Commission. This work was performed when the author was at the Florida State University, Tallahassee, Florida. A summary of the results reported herein was included in a lecture given by the author at the First Summer School in Theoretical Physics held at Mussoorie during May-June 1959.



the nucleon-nucleus potential was computed in accordance with

$$V(\vec{r}_1) = \int d\vec{r}_2 \rho(\vec{r}_2) V(\vec{r}_1, \vec{r}_2) \quad \dots \quad (3)$$

With this potential Talman has solved the Schrodinger equation numerically and from the wave functions thus obtained a new density distribution was computed which in turn gave a potential in accordance with Eq. (3) above. Proceeding in this manner he found that, at the end of one complete cycle of calculation, the nucleus collapsed and the total energy of a system of 150 nucleons was low, yielding a binding energy per particle of about .94 MeV.

It is not sufficient if self-consistency is achieved between a nuclear potential and any density, but the density should be in agreement with experiment. The Levy (1953) potentials for instance show saturation but not at true density. The uniform density used by Talman is rather unrealistic from a phenomenological point of view. We have, therefore, attempted to ascertain the results of successive cycles in a self-consistent field calculation using phenomenological densities given by Green (1956), which have the virtue of close agreement with the Stanford charge distributions. The density distribution obtained by Green of nucleons moving in a square well with an exponentially diffuse boundary, involves Bessel functions of exponential functions. Therefore, in their original form, the wave functions are too complicated to handle. Choosing a closed-shell light nucleus of  $O^{16}$ , the nodeless  $s$  and  $p$  radial wave functions have been approximated (Swamy 1958) by Slater type functions :

$$\begin{aligned} R_{1s} &= 1.764r^{1.429}e^{-1.318r} \\ R_{1p} &= 1.122r^{3.195}e^{-1.737r} \end{aligned} \quad \dots \quad (4)$$

For simplicity in an initial effort, Coulomb, exchange and tensor forces were neglected. Assuming a purely direct and central interaction between any two nucleons, of the form given in Eq. (1), the zero stage potential was calculated by means of Eq. (3) where in the integrand the approximate phenomenological density was used. The multiplying constant in Eq. (1) has been chosen such that the nucleon-nucleus potential 'strength' matches that of the square well with exponentially diffuse boundary. The two-body force range was chosen, as an experiment, to be 1.144 fermis.

As in the Hartree method, the potential felt by any one particle is obtained by subtracting its own contribution from the total nuclear potential. The second phase of the self-consistent field treatment is to secure a new nucleon density by solving the Schrodinger equation for each single particle state with the potential thus obtained. All the particles in the nucleus chosen being in their ground states, a variational method has been used to solve the Schrodinger equation approximately. This method has the advantage of being speedier than

a numerical solution of the differential equation and is fairly reasonable for forming a qualitative estimate of the trend of affairs as we go through successive cycles. In the detail of the variational calculation a scale factor multiplying the radial coordinate has been used as the variational parameter (Hartree, 1955). The trial function used was

$$\phi_e = \sqrt{\lambda} R_{1e}(\lambda r) \quad (5)$$

the variational parameter being  $\lambda$ . With the help of the wave functions thus obtained the expectation values of the potential and kinetic energy operators have also been calculated in order to know the total binding energy of the nucleus. Further going back to Eq. (3) a second stage potential has been computed and the cycle was set going once again. The results of three full cycles of such calculations have been that

- (a) the nucleus shrinks in each cycle, though not too rapidly and the potential becomes more diffuse in each cycle;
- (b) the energy eigenvalue of a single particle state increases in each cycle, though perhaps slightly;
- (c) the total energy of the system is positive in sign and becomes increasingly positive in each cycle thus giving no binding at all.

These results are shown in Table I. With a view to ascertaining the sensitiveness of the rate of collapse to the two body force range, a different two body force range has been chosen and the calculations repeated. Table II shows that this sensitiveness is considerable.

TABLE I

Results of two successive cycles showing shrinkage of nucleus

	Zero stage	End of I cycle	End of II cycle
Mean square radius of potential in fermi (Bruecner <i>et al.</i> , 1955)	15.305	14.944	14.469
Expectation of kinetic energy operator for $s$ state $\langle T_s \rangle$ in MeV	11.726	12.772	13.793
-do- for $p$ state $\langle T_p \rangle$	18.239	19.522	20.939
Expectation of potential energy operator for $s$ state $\langle V \rangle_s$ in MeV	-35.367	-37.865	-40.966
-do- for $p$ state $\langle V \rangle_p$	-28.099	-30.163	-32.601
Energy eigen value of $s$ state in MeV $W_s$	-23.641	-25.093	-27.173
-do- for $p$ state $W_p$	-9.860	-10.641	-11.662
Total binding energy in MeV	+26.444	+28.648	+28.908

TABLE II

Two body force range in fermi	Mean square radius of potential in fermi (Brueckner <i>et al.</i> , 1958)
1.143	15.305 Zero stage 14.944 End of I Cycle 14.462 End of II Cycle
0.500	8.943 Zero Stage 6.418 End of I Cycle 5.585 End of II Cycle

With a purely attractive two body interaction, therefore, it has not been possible to achieve stability and convergence in successive cycles of the self-consistent field calculation. Now it has been fairly well known that exchange plus a repulsive core ensures saturation. A repulsive term was therefore introduced into the two body interaction as the next logical step in the study. The repulsive cores that exist in the literature consist of hard sphere interactions at a distance of 4 or 5 fermis between two nucleons. Introduction of such a

core in  $G(r_1, r_2)$  would make the integral in Eq. (3) singular, unless some cut-off device is introduced. As an alternative, however, a form of interaction is assumed which would give a very large repulsion at short distances and becomes infinite only when the two nucleons collide. A Green's function of the following form containing an integrable singularity will ensure this behaviour :

$$G(r_1, r_2) = -g_A^2 \frac{e^{-p_A |\vec{r}_1 - \vec{r}_2|}}{|\vec{r}_1 - \vec{r}_2|} + g_R^2 \frac{e^{-p_R |\vec{r}_1 - \vec{r}_2|}}{|\vec{r}_1 - \vec{r}_2|} \dots \quad (6)$$

Here the subscripts  $A$  and  $R$  stand for attraction and repulsion respectively. It is interesting to note that such a Green's function does arise out of a non-linear meson theory (Green, 1949). The effect of introducing such a repulsion has been studied in two ways—(a) the coupling constant of the repulsive term  $g_R$  is varied keeping other things constant, (b) keeping the coupling constant fixed, the range of repulsion  $p_R^{-1}$  is varied. In both cases the attractive force range is 1.144 fermis and the attractive coupling constant 35.543 MeV. The zero stage values of  $\langle r^2 \rangle$  of the  $s$  and  $p$  orbitals are respectively 5.780 and 8.084 fermi (Brueckner *et al.*, 1955). The results are shown in Table III. It can be seen from this that either there is no convergence in successive cycles (nucleus collapsing in each cycle) or where there is an approach to convergence, the total binding energy becomes much too small. It has thus not been possible to choose one set of four parameters  $g_A$ ,  $p_A^{-1}$ ,  $g_R$ ,  $p_R^{-1}$  in order to meet the dual requirements

of stability and convergence in successive cycles as well as obtaining the experimental total binding energy of the nucleus. On the other hand, an approach which has proved to be a successful way out of this difficulty is that of choosing different coupling constants for the two angular momentum states viz.,  $s$  and  $p$  states. The following set of parameters have been effective in indicating convergence in successive cycles, as well as yielding a total binding energy of 124.34 MeV.

$$\begin{array}{llllll}
 s \text{ state} & g_A^2 = 2177.5e^2 & g_R^2 = 8912.9e^2 & p_A^{-1} = 1.414 & p_R^{-1} = .143 \\
 & & & \text{fermis} & \text{fermis} \\
 p \text{ state} & g_A^2 = 2177.5e^2 & g_R^2 = 9333.1e^2 & p_A^{-1} = 1.414 & p_R^{-1} = .143 \\
 & & & \text{fermis} & \text{fermis}
 \end{array}$$

$e = \text{charge of an electron}$

TABLE III  
Effect of repulsive term in the two body interaction

$g_R^2$ in MeV	35.543	35.543	35.543	7.109	25.543	71.087
$P_R^{-1}$ in fermi	0.500	0.667	1.000	0.500	0.500	0.500
$s$ state						
$\langle r^2 \rangle$ in fermi (Brueckner, <i>et al.</i> , 1955)	4.007	4.381	4.822	3.742	4.007	4.147
$W_s$ in MeV	-49.300	-42.866	-28.903	-57.460	-49.300	-39.310
$\langle T_s \rangle$ in MeV	14.366	13.143	11.395	15.395	14.366	13.889
$\langle V \rangle_s$ in MeV	-63.666	-56.009	-40.838	-72.855	-63.666	-53.197
Contribution to total binding per particle in MeV	-17.467	-14.862	-8.404	-21.032	-17.467	-12.711
$p$ state						
$\langle r^2 \rangle$ in fermi	5.681	6.603	7.429	4.922	5.681	6.141
$W_p$ in MeV	-32.526	-26.856	-14.654	-41.059	-32.526	-23.241
$\langle T_p \rangle$ in MeV	25.065	21.573	19.184	28.961	25.065	23.206
$\langle V \rangle_p$ in MeV	-57.590	-48.429	-32.838	-70.025	-57.590	-46.452
Contribution to total binding per particle in MeV	-3.731	-2.641	+2.265	-6.047	-3.731	-0.200

The parameters of the attractive term are taken from Gammel (1957). It is clear, of course, that because of the rather crude method used in solving the Schrodinger equation the numerical figures arrived at constitute no more than

an indication of the trend of affairs leading to the important conclusion that the nucleon-nucleus potential turns out to be angular momentum dependent or momentum dependent in general.

Momentum dependent potentials can, in coordinate space, be represented by a non-local potential i.e., a potential matrix (Bethe, 1956). The Schrodinger equation for the relative motion of a nucleon in this potential is

$$\frac{\hbar^2}{2M} \Delta^2 \vec{\psi}_e(\vec{r}) + E_e \vec{\psi}_e(\vec{r}) = \int (\vec{r}^1 | V | \vec{r}) \vec{\psi}_e(\vec{r}^1) d\vec{r}^1 \quad \dots (7)$$

Comparing this with the following equation which is satisfied by the potentials discussed above

$$\frac{\hbar^2}{2M} \Delta^2 \vec{\psi}_e(\vec{r}) + E_e \vec{\psi}_e(\vec{r}) = V_e \vec{\psi}_e(\vec{r}) \quad \dots (8)$$

we readily get the relation

$$V_e(\vec{r}) \vec{\psi}_e(\vec{r}) = \int (\vec{r}^1 | V | \vec{r}) \vec{\psi}_e(\vec{r}^1) d\vec{r}^1 \quad \dots (9)$$

Following Frahn and Lemmer (1957) we have assumed that

$$(\vec{r}^1 | V | \vec{r}) = \frac{V \left( \frac{|\vec{r} + \vec{r}^1|}{2} \right) e^{-\frac{(\vec{r} - \vec{r}^1)^2}{a_e^2}}}{\pi^{3/2} a_e^3} \quad \dots (10)$$

where  $a_e$  is a 'non-locality parameter' or 'correlation length'. This correlation length has been estimated to be 1.1 fermis. In the effective mass approximation, the equation of motion of a particle in a momentum dependent potential well is replaced by one describing the motion in a static well, but having a variable mass which now becomes function of position. In this case the kinetic energy operators have to operate on the mass and, in order to meet the requirement of Hermiticity and relativistic invariance, have to be properly symmetrized. Frahn and Lemmer (1957) have shown that the appropriate Schrodinger equation is

$$-\frac{\hbar^2}{8} \left[ \Delta^2 \frac{1}{M(r)} + \Delta \frac{2}{M(r)} \Delta + \frac{1}{M(r)} \Delta^2 \right] \vec{\psi}(\vec{r}) + V(r) \vec{\psi}(\vec{r}) = E \vec{\psi}(\vec{r}) \quad \dots (11)$$

where the effective mass  $M(r)$  is related to the actual mass  $M$  through the local potential  $V(r)$  by

$$M(r) = \frac{M}{1 - a_e^2 M V(r)} \quad (12)$$

Using Eqns. (6), (3), (9), (10) and the radial part of Eq. (11) the equivalent  $V(r)$  and hence  $M(r)$  in Eq. (12) have been calculated. The latter is shown in Fig. 1.

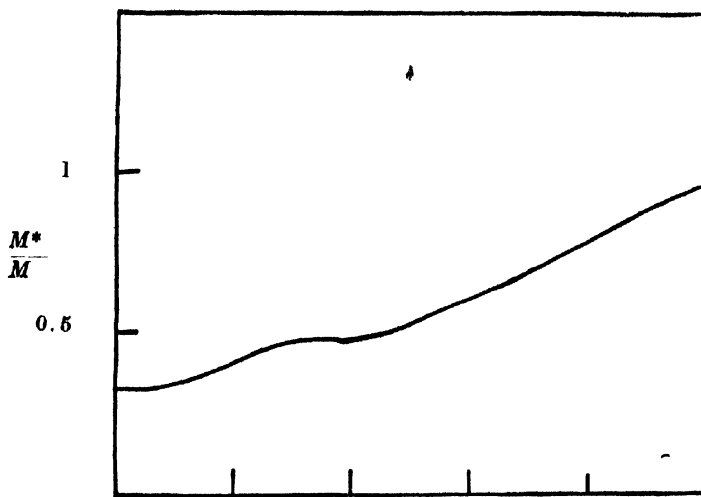


Fig. 1. Spatial variation of effective mass.  $M$  is the true nucleon mass.

In conclusion we have to state that, while the calculations do not have the certainty of accuracy because of the approximations used, the results arrived at through a simple single-particle approach do agree with the more fundamentally thorough many-particle approach.

It is a pleasure to acknowledge the interest and constant guidance received from Dr. Alex E. S. Green during the course of this work. The financial assistance of the U.S. Atomic Energy Commission is gratefully acknowledged.

#### REFERENCES

- Bethe, H. A., 1956, *Phys. Rev.*, **103**, 1353.  
 Brueckner, K. A. and Levinson, C. A., 1955, *Phys. Rev.*, **97**, 1344.  
 Frahn, W. E., and Lemmer, R. H., 1957, *Nuovo Cimento*, **5**, 1564.  
 Gammel, J. L., Christian, R. S., and Thaler, R. M., 1957, *Phys. Rev.*, **105**, 311.  
 Green, A. E. S., 1948, *Phys. Rev.*, **73**, 26.  
 Green, A. E. S., Lee, K., and Berkoley, R., 1956, *Phys. Rev.*, **104**, 1625.  
 Hartree, D. R., Douglas, A. S. and Runciman, W. A., 1955, *Proc. Cam. Phil. Soc.*, **51**, 486.  
 Levy, M. M., 1953, *Phys. Rev.*, **88**, 575.  
 Swamy, N. V. V. J., Ph.D. Thesis (unpublished), 1958.  
 Talman, J. D., 1956, *Phys. Rev.*, **102**, 455.

# POTENTIAL CONSTANTS AND CALCULATED THERMODYNAMIC PROPERTIES OF NITRYL FLUORIDE AND NITRYL CHLORIDE

P. G. PURANIK AND E. V. RAO

DEPARTMENT OF PHYSICS, UNIVERSITY COLLEGE OF SCIENCE,  
OSMANIA UNIVERSITY, HYDERABAD 7. (A.P.)

(Received, January 7, 1961)

**ABSTRACT.** Using a most general quadratic potential energy expression the molecule  $\text{NO}_2\text{R}$ , where R is either F or Cl, is subjected to normal coordinate treatment. Two sets of thirteen force constants for each molecule have been proposed, and the fundamental frequencies have been calculated with the help of Wilson's F-G matrix method. The calculated and the observed values of the frequencies closely agree. Thermodynamic properties for the fluoride and the chloride have been calculated for temperatures in the range of 100-1000 °K.

## I. INTRODUCTION

The infrared and Raman spectra of nitryl fluoride are reported by Rolfe and Woodward (1956) and that of nitryl chloride have been studied by Ryason and Wilson (1954). The latter authors have assigned the frequencies of the chloride molecule. Assuming the valence force potential function Hariharan (1958) has used the observed values of the frequencies and calculated the force constants by using Wilson's F-G matrix method and assigned the fundamental frequencies of both the molecules. His assignments differ from those of Ryason and Wilson so far as frequencies 651 and 411  $\text{cm}^{-1}$  are concerned. Ryason and Wilson have assigned 651  $\text{cm}^{-1}$  to class  $A_1$  and 411  $\text{cm}^{-1}$  to class  $B_2$ , whereas Hariharan has reversed the assignments. Hariharan has neglected most of the interaction force constants and his value for  $f_a$  in the case of nitryl fluoride is negative which cannot be justified.

With a view to checking the earlier assignments the authors, using a most general quadratic potential energy expression, and assuming a planar configuration for the molecules and the point group  $C_{2v}$ , have carried out normal coordinate treatment, according to Wilson's F-G matrix method.

## II. NORMAL COORDINATE TREATMENT

The planar configuration of  $\text{NO}_2\text{R}$  where R can be either F or Cl has a symmetry of  $C_{2v}$  point group ( $3A_1$ ,  $2B_2$ ,  $B_2$ ). The symbols used for the equilibrium values of bond distances and interbond angles are shown in Fig. 1.

The examples of possible types of potential constants arising out of various types of interactions are given below.

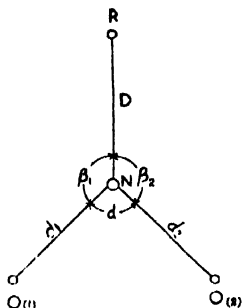


Fig. 1.

$f_d$  = N-O stretching constant.

$f_\alpha$  =  $\angle$ O-N-O bending constant.

$f_{\beta^\beta}$  =  $\angle$ R-N-O(1) and  $\angle$ R-N-O(2) angle angle interaction constant.

$f_d^d$  = N-O(1) and N-O(2) bond bond interaction constant.

$f_d^{\beta}$  = N-O(1) and  $\angle$ R-N-O(2) bond angle interaction constant.

The most general quadratic expression for potential energy is

$$2V = f_D(\Delta D)^2 + f_d\{(\Delta d_1)^2 + (\Delta d_2)^2\} + d^2 f_\alpha(\Delta \alpha)^2 + d^2 f_{\beta\beta}\{(\Delta \beta_1)^2 + (\Delta \beta_2)^2\} + 2f_d^d \Delta d_1 \Delta d_2 + \\ + 2f_D^d \Delta D(\Delta d_1 + \Delta d_2) + 2df_D^\alpha \Delta D \Delta \alpha + 2df_d^\beta \Delta d(\Delta \beta_1 + \Delta \beta_2) + 2df_d^\alpha(\Delta d_1 + \Delta d_2)\Delta \alpha \\ + 2d^2 f_\alpha^\beta \Delta \alpha(\Delta \beta_1 + \Delta \beta_2) + 2d^2 f_{\beta\beta}^\beta \Delta \beta_1 \Delta \beta_2 + 2df_D^\beta \Delta D(\Delta \beta_1 + \Delta \beta_2).$$

The symmetry coordinates for  $A_1$  type of vibrations are :

$$R_1 = \Delta D.$$

$$R_2 = 1/\sqrt{2}(\Delta d_1 + \Delta d_2).$$

$$R_3 = 1/\sqrt{6}(2\Delta \alpha - \Delta \beta_1 - \Delta \beta_2).$$

$$R_4 = 1/\sqrt{3}(\Delta \alpha + \Delta \beta_1 + \Delta \beta_2) = 0 \quad (\text{Redundant}).$$

For  $B_1$  type :-

$$R_5 = 1/\sqrt{2}(\Delta d_1 - \Delta d_2).$$

$$R_6 = 1/\sqrt{2}(\Delta \beta_1 - \Delta \beta_2).$$

For type  $B_2$  (Out of plane)

$$R_7 = d\Delta \gamma.$$

The symmetry coordinates are normalized and orthogonal. From the potential energy matrix i.e. 'f' matrix and the matrix formed by the coefficients



contained in the symmetry coordinated the following 'F' matrix elements are obtained.

The 'F' matrix elements are

For type  $A_1$

$$F_{11} = f_D$$

$$F_{12} = \sqrt{2}f_D^d.$$

$$F_{13} = \sqrt{(2/3)}d(f_D^a - f_D^b).$$

$$F_{22} = f_d + f_d^d.$$

$$F_{23} = 1/\sqrt{3}d(2f_d^a - f_d^b - f_d'^b).$$

$$F_{33} = 1/3d^2(2f_a + f_b + f_b^b - 4f_a^b).$$

For the type  $B_1$ .

$$F_{11} = f_d - f_d^d.$$

$$F_{12} = d(f_d^b - f_d'^b).$$

$$F_{22} = d^2(f_b - f_b^b).$$

For the type  $B_2$ .

$$F_{11} = f_\gamma.$$

Elements of G matrices\* obtained with the help of Decius Tables (1948) are as follows.

For the type  $A_1$ .

$$G_{11} = \mu_N + \mu_R.$$

$$G_{12} = \sqrt{2}\mu_N \cos \beta.$$

$$G_{13} = \sqrt{(2/3)}a\mu_N \left\{ \sin \beta - \frac{2 \cos \beta}{\sin \alpha} (1 - \cos \alpha) \right\}$$

$$G_{22} = \mu_0 + \mu_N(1 + \cos \alpha)$$

$$G_{23} = \mu_N/\sqrt{3} \left[ \frac{1}{\sin \beta} (a - b \cos \beta) \cos \beta + (b - a \cos \beta)(1 + \cos \alpha) - 2a \sin \alpha \right]$$

$$G_{33} = 1/3[4a^2\{\mu_0 + \mu_N(1 - \cos \alpha)\} + b^2\mu_R + a^2\mu_0 + \mu_N(a^2 + b^2 - 2ab \cos \beta) + b^2\mu_R y + \mu_N\{(b - 2a \cos \beta)by\} + a^2\{\sin^2 \beta(1 - \bar{y}^2) + y \cos \alpha\} - 4\mu_0 a^2 x - 4\{(a - a \cos \alpha - b \cos \beta)ax + (\sin \alpha \sin \beta(1 - \bar{x}^2) + x \cos \beta)ab\}\mu_N].$$

For type  $B_1$ .

$$G_{11} = \mu_0 + \mu_N(1 - \cos \alpha).$$

$$G_{12} = -(\mu_N/\sin \beta)(b - a \cos \beta)(1 - \cos \alpha).$$

$$G_{22} = (\mu_R/\sin^2 \beta)b^2(1 - \cos \alpha) + \mu_0 a^2 + (\mu_N/\sin^2 \beta)(b - a \cos \beta)^2(1 - \cos \alpha).$$

For type  $B_2$ .

$$G_{11} = (1/2)\mu_0 \cos^2 \beta + \mu_N \frac{(D-d \cos^2 \beta)}{D^2 \cos^2 \beta} + \mu_R d^2/D^2.$$

In the above expressions

$$a = 1/d, \text{ and } b = 1/D$$

$$x = (\cos \beta - \cos \alpha \cos \beta)/\sin \alpha \sin \beta.$$

$$y = (\cos \alpha - \cos^2 \beta)/\sin^2 \beta.$$

For calculating the  $g$  matrix elements the values of bond distances, bond-bond angles and the masses of different atoms are taken from Table I (1958).

TABLE I

Bond distances, interbond angles, masses of different atoms, and moments of inertia of nitril fluoride and nitril chloride

	Bond distances		Mass of the atom.	
	F-NO <sub>2</sub>	Cl-NO		
N-O (d)	1.22 Å	1.16 Å	$m_O = 16.00$ (a.w.u.)	
N-R (D)	1.50 Å	1.98 Å	$m_N = 14.008$ (a.w.u.)	
			$m_{O1} = 35.457$ (a.w.u.)	
			$m_F = 19.000$ (a.w.u.)	
	Interbond angles		Moments Of Inertia.	
<O-N-O ( $\alpha$ )	150°	130°	$I_x^F = 40.7369$ , $I_y^F = 41.436$ , $I_z^F = 85.173$ .	
<R-N-O ( $\beta$ )	105°	115°	$I_x^{C1} = 110.212$ , $I_y^{C1} = 35.367$ , $I_z^{C1} = 145.579$	

Note:—The symmetry number for this form is 2.

The moments of inertia are given in units of (a.w.u.Å<sup>2</sup>).

In the first calculations the force constants derived by Hariharan were used in toto and interaction constants which he has ignored, were proposed by the authors, keeping in view the proper order of the magnitude of such force constants. After a few modifications the observed frequencies were reproduced by calculations with an error within one per cent. The force constants finally proposed by the authors are given in Table II. The six corresponding force constants derived by Hariharan are given for comparison.

The observed and the calculated values of the in-plane fundamental vibrational frequencies of both the molecules are given in Table III. The agreement between the observed and the calculated values is a check on the probable accuracy of the force constants proposed.

### III. THERMODYNAMIC PROPERTIES

The heat capacity  $C_p^\circ$ , heat content  $(H_0 - E_0^\circ)/T$  free energy  $-(F_0 - E_0^\circ)/T$  and entropy  $S^\circ$  at constant pressure for both the molecules with a rigid rotator and harmonic oscillator approximation for the ideal gaseous state at one atmos-

pheric pressure were calculated for twelve temperatures in 100–1000°K range. The results are given in Tables IV and V.

TABLE II  
Potential constants for nitril fluoride and nitril chloride

Pot. Constants	Nitril fluoride		Nitril chloride	
	Authors	Hariharan	Authors	Hariharan
$f_d$	12.3	10.88	10.25	9.48
$f_D$	3.3	3.51	4.19	4.19
$f_d^d$	2.7	2.04	0.95	0.52
$f_D^d$	1.5	—	1.0	1.41
$f_\beta$	1.10	1.13	0.59	0.62
$f_\beta^d$	0.48	—	0.30	—
$f_\alpha^d$	0.40	—	0.25	—
$f_D^\beta$	0.30	—	0.20	—
$f_\alpha$	0.15	-0.13	0.35	0.36
$f_d'\beta$	0.12	—	0.10	—
$f_D^\alpha$	0.10	—	0.06	—
$f_{\alpha\beta}$	0.06	—	0.02	—
$f_{\beta\beta}$	0.05	—	0.03	—

Note :—Bond constants and bond-bond interactions constants are given in md/A, bond-angle interaction constants in md/rad, and angle constants and angle-angle interaction constants are given in mdA/rad<sup>2</sup>.

TABLE III  
Observed and calculated values of the fundamental frequencies of nitril fluoride and nitril chloride

Type	Nitril fluoride		Nitril Chloride	
	Observed	Calculated	Observed	calculated
$A_1(\nu_1)$	1312	1312	1293	1296
$A_1(\nu_2)$	822	828	794	798
$A_1(\nu_3)$	460	459	411	404
$B_1(\nu_4)$	1793	1791	1685	1683
$B_1(\nu_5)$	570	567	367	360

TABLE IV

Heat capacity, heat content, free energy and entropy for nitril fluoride

Temp. (K)	$C_p^0$	$(H_0-E_0^0)/T$	$-(F_0-E_0^0)/T$	$S^0$
100	8.11	7.97	43.90	51.87
200	9.86	8.42	49.52	57.95
273	11.42	9.02	52.23	61.25
293	11.82	9.19	52.87	62.07
303	12.02	9.29	53.11	62.40
400	13.64	10.15	55.88	66.03
500	14.90	10.98	58.23	69.22
600	15.88	11.72	60.30	72.02
700	16.62	12.36	62.15	74.51
800	17.19	12.93	63.83	76.76
900	17.64	13.43	65.39	78.82
1000	17.98	13.87	66.83	80.70

TABLE V

Heat capacity, heat content, free energy and entropy for nitril chloride

Temp (K)	$C_p^0$	$(H_0-E_0^0)/T$	$-(F_0-E_0^0)/T$	$S^0$
100	8.44	8.04	45.88	53.91
200	10.74	8.80	51.65	60.45
273	12.26	9.53	54.50	64.03
293	12.62	9.73	55.17	65.09
303	12.84	9.85	55.44	65.29
400	14.25	10.73	58.35	69.08
500	15.41	11.56	60.84	72.40
600	16.29	12.27	63.01	75.28
700	16.97	12.91	64.96	77.87
800	17.48	13.44	66.71	80.15
900	17.88	13.91	68.31	82.22
1000	18.20	14.33	69.80	84.13

## IV. REFERENCES

- Decius, J. C., 1948, *J. Chem. Phys.* **16**, 1025.  
 Hariharan, T. A. 1958, *Proc. Ind. Acad. Sci.* **48**, 49.  
 Rolfe, Dodd and Woodward, L. A. 1956, *Trans. Farad. Soc.* **52**, 145.  
 Ryason, Raymond and Wilson, Kent, 1954, *J. Chem. Phys.* **22**, 2000.

# A STUDY OF DEVELOPMENT DEFECTS AND TRACK STRUCTURES IN NUCLEAR EMULSIONS USING AMIDOL DEVELOPERS

O. N. KAUL

SAHA INSTITUTE OF NUCLEAR PHYSICS, CALCUTTA.

(Received, December 30, 1960)

**ABSTRACT.** Development defects in nuclear emulsions, and also the dependence of track and grain structures on the various development parameters have been investigated.

Modified formulae have been suggested for the removal of microscopic fog, coloration defects, and also for the background eradication.

The procedures of investigation followed during the course of this work, differ from the ones adopted by others like Fatzer, Yagoda, Barschall, and Liebermann; and the results, although identical in most of the cases, differ slightly in certain respects as reported.

Some work has been reported on the elimination of development defects by various workers, e.g., Yagoda, (1948), Liebermann and Barschall (1943) and others. The present aim of the author has been to make a comprehensive study of all development defects introduced by Amidol developers to compare the methods suggested by various workers for their elimination and also to suggest modified formulae suitable for work in this laboratory.

Besides this, a critical study of the track and grain structures pertaining to their dependence on various development parameters (temperature, time, and sodium sulphite concentration) has been made by methods somewhat different (from those adopted by Fatzer (1959)).

Ilford C<sub>2</sub> nuclear emulsions of 100, 200 and 400 micron thickness were used and the problem studied under the following heads :

- (1) Elimination of the development defects introduced by Amidol developers.
- (2) Dependence of track and grain structures on the hot stage temperature,, hot stage time and sodium sulphite concentration.
- (3) Removal of microscopic fog from the plates.
- (4) Background eradication in nuclear emulsion by the accelerated fading of the latent images.

(1) *Elimination of the development defects introduced by the use of Amidol developers :*

Decrease in the development temperature gives rise to development defects, which are evidenced by a total or partial destruction of the developed image and also a coloration, extending to a considerable depth in the emulsion.

By a series of trials carried out by the author, it was found necessary to increase the ratio sodium sulphite/Amidol for the development temperatures from 18°C to 24°C.

It is an accepted fact that a decrease in the development temperature minimizes distortion in nuclear emulsions. Monothermal development suggested by Yagoda (1955) and Marguin (1957) in which temperature variations are replaced by P. H. variations, was avoided because of its complexity of operation. To avoid distortion, the development was, therefore, carried out at lower than usual temperatures which in turn gave rise to coloration defect, besides an irregularity in development.

To obviate this difficulty, four types of developers as indicated below were tried by the author.

TABLE I  
Developer compositions : (in gms/lit. of the solution)

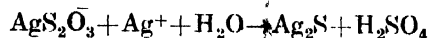
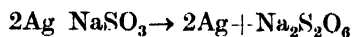
gms/lit. potassium bromide (KBr)	1.2	1.2	1.2	1.2
gms/lit. sodium sulphite (Na <sub>2</sub> SO <sub>3</sub> )	11	10	17	20
gms/lit. Amidol	4.0	2.8	2.8	2.8
gms/lit. boric acid (H <sub>3</sub> BO <sub>3</sub> )	30	20	20	20
Ratio of sodium sulphite : Amidol	2.75	3.57	6.07	7.14

By a comparative study of these formulae it was found that to develop reliably at low temperatures, it was necessary to increase the ratio sodium sulphite/Amidol to minimize the coloration. In certain cases of low sodium sulphite concentration, it was observed that the emulsion showed zones of good development, whereas the rest of the plate became useless. Further, in such cases the images were found to show a blue or red transparency. The development was carried out at temperatures higher and lower than 18°C and the coloration was found to be more predominant at lower temperatures, as well as to be a function of development time.

Results, almost resembling those indicated above, were reported by Birge (1954) and others. In some cases the images were completely destroyed,

but one thing is clear that this image destruction has nothing to do with the corrosion which sets in during prolonged fixation, and is more or less a surface phenomenon. In the present case, the disappearance of the image begins deep down in the emulsion.

These phenomena as already reported by James and Vonselow (1953) are due to the displacement of the adsorption equilibria of organic compounds and sodium sulphite, on silver halide grains. The following equation as suggested by Chateau (1956) can explain the phenomenon



All the three sets of plates of 100, 200 and 400 micron thickness were tried, and it was found that all the three sets showed the coloration defect; but the thicker ones are less coloured than their thinner counterparts.

In conclusion, it was found necessary to choose a sodium sulphite to Amidol ratio which is 75% greater than the ratio adopted in Brussels or Chicago developers. Further, the following processing conditions used by the author were found to give best results :

TABLE II

Emulsion thickness (microns)	Water pre-soak		Developer pre-soak		Development time	Stop bath 1% CH <sub>3</sub> COOH	
	Temp. T°C	Time Hrs.	Temp. T°C	Time Hrs.		Temp. T°C	Time Hrs.
100	4	0.4	4	0.4	Variable	4°C	0.4
200	4	1.0	4	1.0	Variable	4°C	1.0
400	4	2.6	4	2.6	Variable	4°C	2.6

(Microns)	Fixation (40% hypo)		Washing		Glycerinization One percent	
	Temp. T°C	Time Hrs.	Temp. T°C	Time Hrs.	Temp. T°C	Time Hrs.
100	18	3.5	8	4.0	6	0.5
200	18	8.0	8	10.0	6	1.0
400	18	24.0	8	28.0	6	2.0

Fog was removed by rubbing immediately after the stop bath treatment.

2) *Dependence of track and grain structures on the hot stage temperature, hot stage time and sodium sulphite concentration :*

In this connection various parameters, viz., diameter of the track grains, volumetric grain density, total gap length, mean gap length and blob density

were studied by the author, in the case of Ilford C<sub>x</sub> 200 micron plates, some work has already been reported by Fatzer (1959) in this connection. Sodium sulphite/Amidol ratios and temperatures different from those used by Fatzer have been used. Results, although identical with those reported by Fatzer, differ in the peak values of the curves as reported :

a) Diameter of the track grains :

Mean grain diameters were plotted against the development time, for two temperatures and two sodium sulphite concentrations. The results obtained are plotted in Figs. 1 and 2.

Mean diameter of the track grains was found to increase rapidly with the time, in the region of under-development. It, however, attained a constancy in value for longer development periods (Figs. 1 and 2).

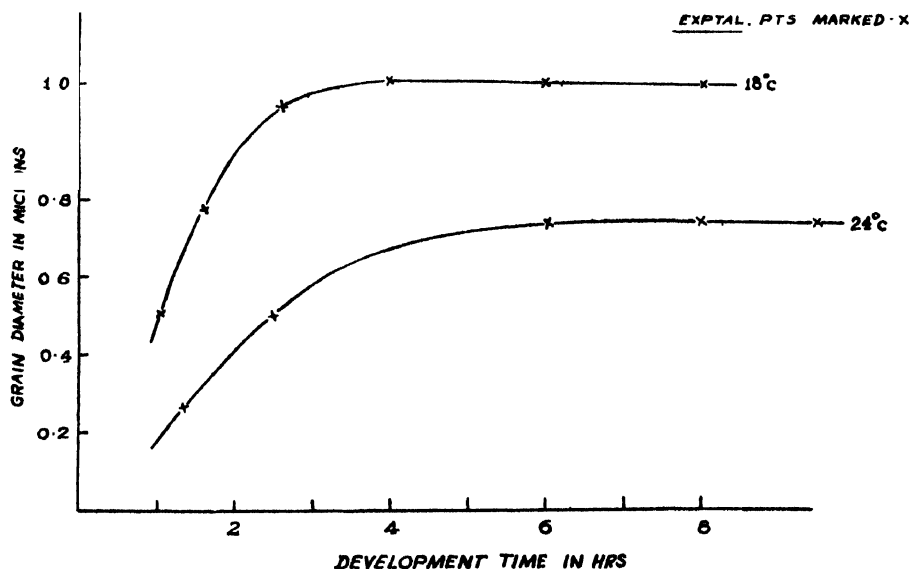


Fig. 1. Grain diameters plotted against development time for two different temperatures.

$$(\phi) \frac{\text{Sod. sulphite}}{\text{Amidol}} = 10$$

Further, it was observed that an increase in the sodium sulphite concentration and development temperatures causes a decrease in the grain diameters.

b) Volumetric grain density :

Volumetric grain density was found to increase with an increase in the hot stage time and the sodium sulphite concentration. The observations are plotted in Fig. 3.



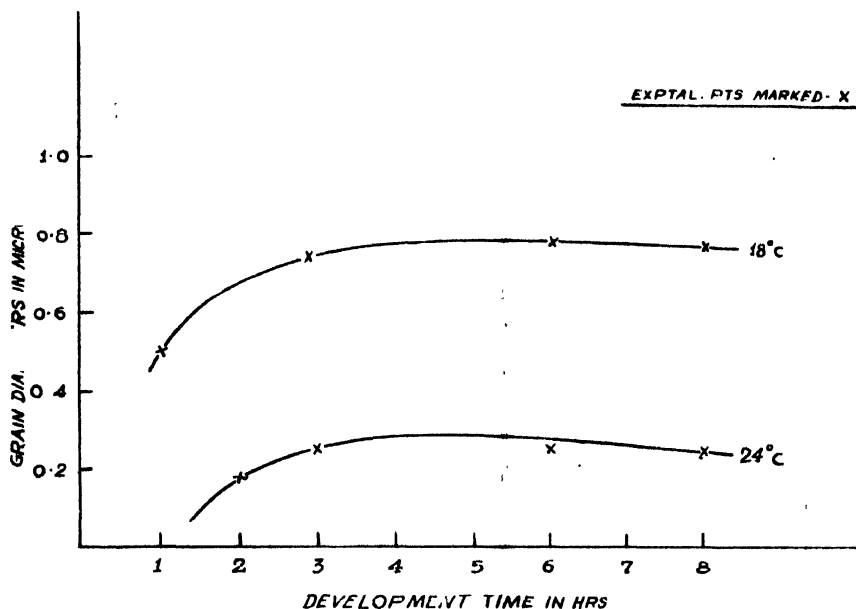


Fig. 2. Grain diameters plotted against the development time at two different temperatures.

( $\phi$ )  $\frac{\text{Sod. sulphite}}{\text{Amidol}} = 15$

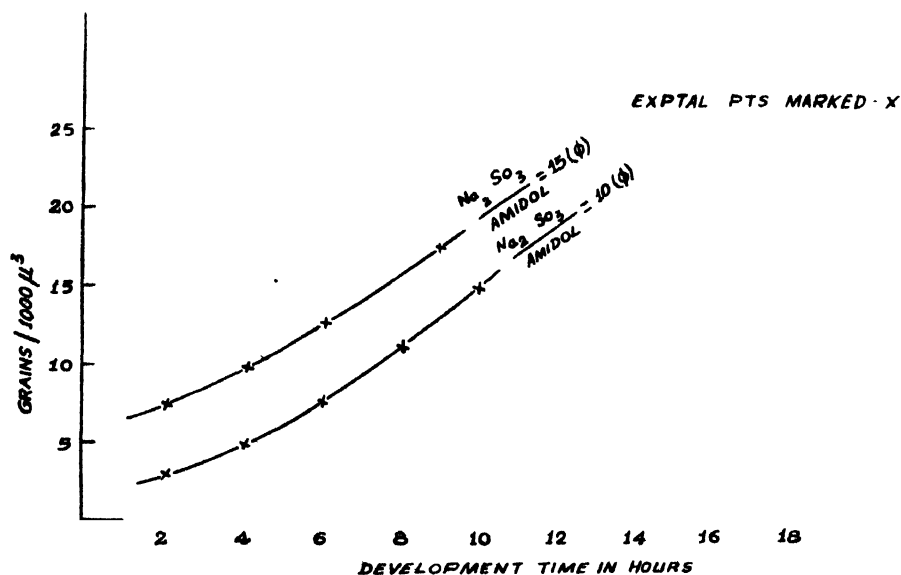


Fig. 3. Volumetric grain density plotted against hot stage time at two  $\text{Na}_2\text{SO}_3$  concentrations.

1) *Total gap length :*

In the region of under-development total gap length was found to decrease with an increase in the development time. At longer development periods, the total gap length becomes constant. At normal developments, however, the total gap length decreases with increasing temperature and is independent of sodium sulphite concentration. (Fig. 4).

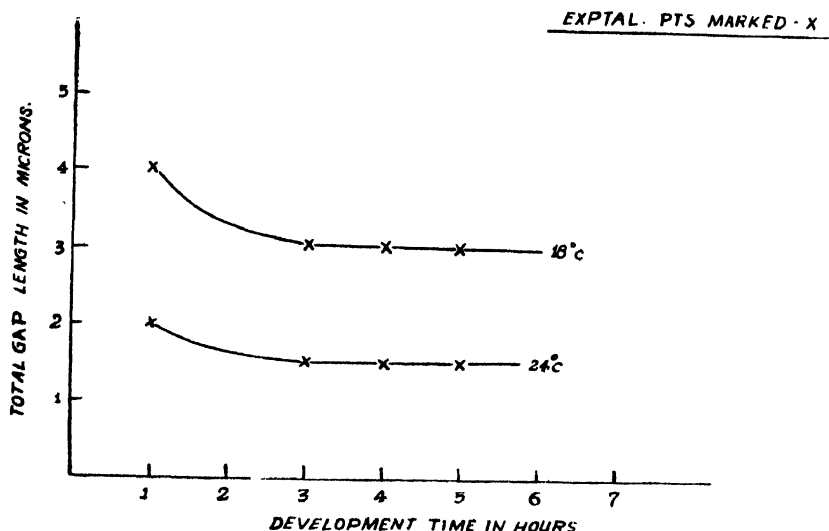


Fig. 4. Total gap length plotted against development time in hours.

2) *Mean gap length :*

The following points were observed in connection with the mean gap length, which was calculated by dividing the total gap length by the number of blobs.

1) M.G.L. is independent of the duration of hot stage time, excepting in the case of under-development.

2) M.G.L. decrease with an increase in temperature.

3) It does not vary with a change in sodium sulphite concentration.

5) *Variation of blob density.*

Blob density was calculated by dividing the number of blobs by the total length of the tracks. It was observed that the blob density increases in the region of under-development. Rise in temperature was found to cause a considerable rise in the blob density and after a certain value of development time, the blob density attained constancy in value. These observations are incorporated in Fig. 6.

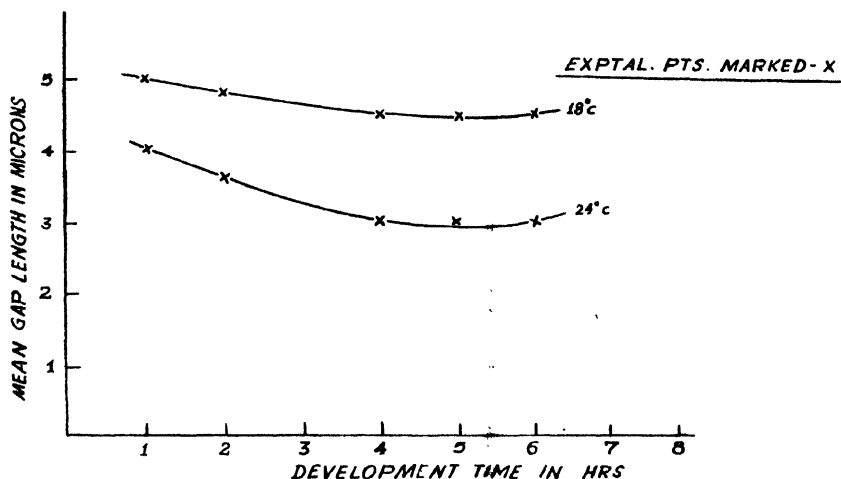


Fig. 5. Mean gap length plotted against the development time at two different temperatures.

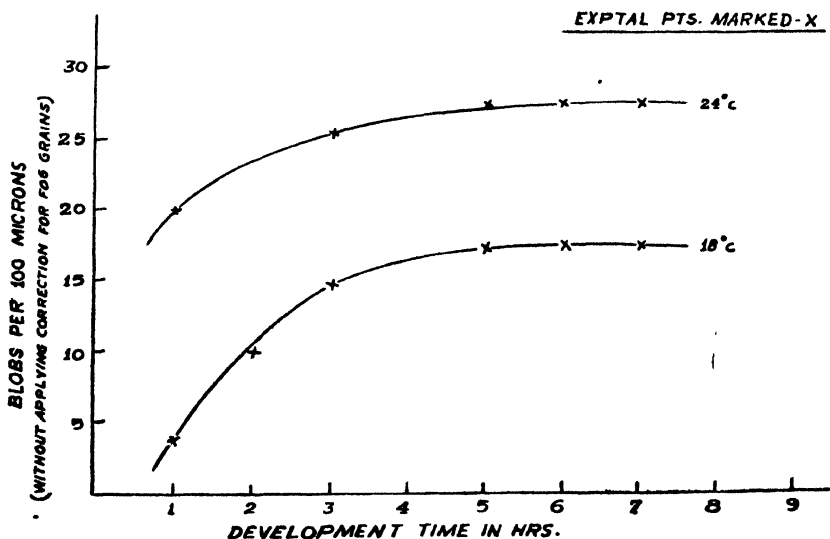


Fig. 6. Blob density plotted against development time in hrs.

### (3) Removal of microscopic fog from the plates :

Background of developable but unexposed grains of silver bromide, manifesting itself in the form of microscopic fog, is a great handicap in the emulsion work. The idea underlying removal of fog is to develop an unexposed plate to reduce all the developable silver bromide grains, to free silver, which is then removed by reduction. Photographic reducers consist of oxidising agents which

oxidise free silver to a suitable salt, which in turn causes a reduction in the opacity of the image.

Well known formulae using potassium permanganate and potassium bichromate were used in this laboratory. Potassium permanganate formula was found to give better results, and also it was observed that potassium bichromate formula does not cause complete reduction and the grains thus reduced partially are again developable.

Out of the formulae suggested by various workers, the following formula modified by the author was found to give best results, without affecting silver bromide in the emulsion.

Sol. 1—Potassium permanganate— 3 gms water to make  
1000 cc

Sol. 2—Sulphuric acid— 8 cc water to make  
1000 cc.

*Procedure :*

The plate was first developed in the Eastman developer *D-11* for a time greater than the usual, so as to be sure about the development of undesirable grains. The plate was then washed and immersed for about 40 minutes in a freshly prepared mixture of equal volumes of solutions 1 and 2. This procedure was tried for plates of various thicknesses. Following timings were found necessary:

Plate thickness (microns)	100	200	400
Time in minutes	30	40	55

Thus longer time was needed for the clearance of thick plates, as compared to their thinner counterparts. In order to remove the brown stain produced by potassium permanganate, the plate was again washed and placed for 15 minutes in a 10% solution of sodium bisulphite. This procedure was found best for the removal of the background fog.

4) *Background eradication in nuclear emulsion*

The background is partly due to the accumulated latent images of  $\alpha$  tracks and stars produced by traces of Ra and Th, normally present as impurities in the emulsion and partly due to the cosmic ray background.

It was found that storage for several hours in humid atmosphere goes a long way in accelerating the fading of latent images due to the background. The emulsions thus treated were then dessicated for 1 to 2 hrs. over calcium chloride.

Further, the effect of both the temperature and humidity on fading was investigated so as to find out their effect on the eradication of the background tracks.

*Effect of temperature on fading :*

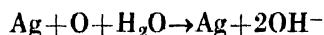
The variation of the fading rate with the storage temperature may be determined from a consideration of the effect of temperature on the velocity of a gas solid chemical reaction, such as is assumed to occur during fading between certain constituents of the atmosphere and the silver development centres of the exposed emulsion. This gives a form of the Arrhenius relation with  $-dN/dt$ , the rate of disappearance of the development centres, as the equation

$$\frac{dN}{dt} = Ce^{K/T}$$

where  $C$  and  $K$  are constants and  $T$  the absolute storage temperature. The equation shows that the fading produced under otherwise fixed conditions will be an exponential function of the reciprocal of the absolute temperature, a result confirmed by Farragi (1949). This shows the effect of storage temperature on the background eradication and it is found that the experimental findings are in accord with the theory.

*Effect of humidity on fading:*

According to Albouy and Farragi (1949) fading is a result of the oxidation of the development specks by the atmospheric oxygen in the presence of water, the reaction as proposed by Albouy and Farragi proceeds as



It is evident that the presence of an excess of  $\text{OH}^-$  ions i.e. PH value above 7, will act to inhibit the reaction, while the more acid conditions accelerate it. Thus, an increase in the humidity causes a decrease in the fading rate.

The following graph showing the effect of both temperature and humidity on the background eradication is in accord with the theory.

Theoretical investigations due to Beiser (1951) also lead to the following equation for the fading coefficient

$$\frac{D_0 - D}{D_0} = 1 - \text{Exp.}(-Ct)$$

where  $D_0$  = grain density produced upon immediate development

$D$  = grain density after a time  $t$

$C$  = constant depending upon the size of Ag specks

The fading coefficient plotted as a function of  $t$ , for various values of  $C$ , is in agreement with the experimental curves.

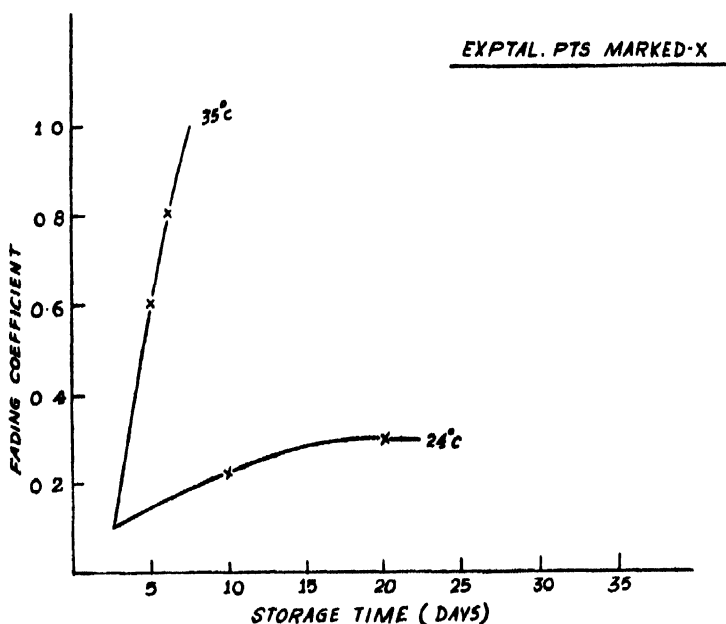


Fig. 7. The variation of the fading coefficient with the time of storage at various temperatures.

#### ACKNOWLEDGMENTS

The author expresses his deep sense of gratitude to Prof. B. D. Nag Chaudhuri, under whose direction and guidance this work has been carried out. The author is also thankful to Mr. S. K. Mukherjee for providing the laboratory facilities ; and to Messrs. Naresh Sen and Barin Chatterjee for their valuable assistance.

#### REFERENCES

- Albouy, G. and Farragi, H., 1949, *J. Phys. Et. Radium*.  
 Beiser, A., 1951 *Phys. Rev.*, **81**, 153.  
 Birge, 1954, *Bull. Uni. Cal. Rad. Lab.*, September 8, 2690.  
 Chateau, H., 1956, *Sci. Ind. Phot.*, **27**, 81.  
 Fatzer, G. D., 1959, *Rev. Sci. Inst.*, **30**, 22.  
 James, H. and Vogu, 1952, *Sci. Ind. Phot.*, **23**, 144.  
 James T. H. and Vanselow, Collig., *Revue Optique Paris*, **122**, Emul. Phot.  
 Liebermann, L. N. and Barschall, H. H., 1943, *Rev. Sci. Inst.*, **14**, No. 4.  
 Marguin, G., 1957, *Sci. Ind. Phot.*, **28**, 321.  
 Yagoda, H., 1948, *Phys. Rev.*, **73**, 634.  
 Yagoda, H., 1955, *Rev. Sci. Inst.*, **26**, 263.

# INTERPENETRATION OF TWO IONIZED GAS CLOUDS

J. N. TANDON\*

DEPARTMENT OF PHYSICS, UNIVERSITY OF DELHI, DELHI-8

(Received, October 26, 1960)

**ABSTRACT.** Collisions of two ionized gas clouds have been considered and it is shown that the counter streaming will, in general, be unstable and the double stream will form small clouds of space charge at the expense of streaming energy of the clouds. These small clouds are responsible for the geomagnetic storms and for the generation of radio noise from colliding galaxies.

## INTRODUCTION

Collision of two fully ionized gas clouds is of considerable importance in explaining the geomagnetic storms and the generation of radio noise from the colliding galaxies. It is found that the counter streaming of gas cloud will in general be unstable except for the case when the density of one of the streams is extremely low as compared to that of the other. The double stream will form small clouds of space charge at the expense of the streaming energy of the clouds. These small clouds may be able to reach the earth and diffuse through the geomagnetic field producing geomagnetic storm. These space charge clouds, because of their stray electric fields, may be responsible for the generation of radio noise from the colliding galaxies.

## COUNTERSTREAMING OF IONIZED GAS CLOUDS

Suppose that a completely ionized neutral gas cloud of initial uniform density  $N_{o1}$  electrons and  $N_{o1}$  protons per  $\text{cm}^3$  moving with initial uniform velocity  $\mathbf{V}_{o1}$ . Let a similar stream with density  $N_{o2}$  electrons and  $N_{o2}$  protons per  $\text{cm}^3$  be moving with velocity  $-\mathbf{V}_{o2}$ . We shall further assume that the temperature and velocity of each stream be such that the thermal motion among the particles and the collisions by coulomb interaction may be ignored.

Let us consider that these two gas clouds impinge upon one another. After the counterstreaming we shall assume the deviation in the densities and velocities from the initial uniform streaming to be of the first order only and are regarded as functions of position and time. We shall use the subscripts 1 and 2 to refer to the two streams and subscripts  $e$  and  $p$  to denote the electrons and protons respectively. Thus we let their densities and velocities be

\* Senior Fellow of University Grants Commission, India.

$$N_{e1} = N_{o1} + n_{e1}; \quad N_{p1} = N_{o1} + n_{p1} \quad \dots \quad (1)$$

$$N_{e2} = N_{o2} + n_{e2}; \quad N_{p2} = N_{o2} + n_{p2} \quad \dots \quad (2)$$

$$\mathbf{V}_{e1} = \mathbf{V}_{o1} + \mathbf{v}_{e1}; \quad \mathbf{V}_{p1} = \mathbf{V}_{o1} + \mathbf{v}_{p1} \quad \dots \quad (3)$$

$$\mathbf{V}_{e2} = -\mathbf{V}_{o2} + \mathbf{v}_{e2}; \quad \mathbf{V}_{p2} = -\mathbf{V}_{o2} + \mathbf{v}_{p2} \quad \dots \quad (4)$$

Then if the electric field is  $E$ , we have the Poisson equation

$$\text{div } E = 4\pi e(n_{e1} - n_{p1} + n_{e2} - n_{p2}) \quad \dots \quad (5)$$

The equations of motion are

$$\left[ \frac{\partial}{\partial t} + (\mathbf{V}_{e1} \cdot \text{grad}) \right] \mathbf{V}_{e1} = -\frac{e}{m} \mathbf{E} \quad \dots \quad (6)$$

$$\left[ \frac{\partial}{\partial t} + (\mathbf{V}_{p1} \cdot \text{grad}) \right] \mathbf{V}_{p1} = -\frac{e}{M} \mathbf{E} \quad \dots \quad (7)$$

$$\left[ \frac{\partial}{\partial t} + (\mathbf{V}_{e2} \cdot \text{grad}) \right] \mathbf{V}_{e2} = -\frac{e}{m} \mathbf{E} \quad \dots \quad (8)$$

$$\left[ \frac{\partial}{\partial t} + (\mathbf{V}_{p2} \cdot \text{grad}) \right] \mathbf{V}_{p2} = -\frac{e}{M} \mathbf{E} \quad \dots \quad (9)$$

and the equations of continuity are

$$\left[ \frac{\partial}{\partial t} + (\mathbf{V}_{e1} \cdot \text{grad}) \right] N_{e1} + N_{e1} \text{div } \mathbf{V}_{e1} = 0 \quad \dots \quad (10)$$

$$\left[ \frac{\partial}{\partial t} + (\mathbf{V}_{p1} \cdot \text{grad}) \right] N_{p1} + N_{p1} \text{div } \mathbf{V}_{p1} = 0 \quad \dots \quad (11)$$

$$\left[ \frac{\partial}{\partial t} + (\mathbf{V}_{e2} \cdot \text{grad}) \right] N_{e2} + N_{e2} \text{div } \mathbf{V}_{e2} = 0 \quad \dots \quad (12)$$

$$\left[ \frac{\partial}{\partial t} + (\mathbf{V}_{p2} \cdot \text{grad}) \right] N_{p2} + N_{p2} \text{div } \mathbf{V}_{p2} = 0 \quad \dots \quad (13)$$

Here  $e$  and  $m$  are the electronic charge and mass respectively and  $-e$  and  $M$  are the respective quantities for the protons. Combining equations of the motion (Eqns. (6) to (9)) and equations of continuity (Eqns. (10) to (12)) and using Eqns (1) to (5) we get after some simplification

$$\left[ \frac{\partial}{\partial t} + (\mathbf{V}_{o1} \cdot \text{grad}) \right]^2 n_{e1} = -\omega_{e1}^2 (n_{e1} - n_{p1} + n_{e2} - n_{p2}) \quad \dots \quad (14)$$

$$\left[ \frac{\partial}{\partial t} + (\mathbf{V}_{o1} \cdot \text{grad}) \right]^2 n_{p1} = \omega_{p1}^2 (n_{e1} - n_{p1} + n_{e2} - n_{p2}) \quad \dots \quad (15)$$



$$\left[ \frac{\partial}{\partial t} - (\mathbf{V}_{o2} \cdot \text{grad}) \right]^2 n_{e2} = -\omega_{e2}^2 (n_{e1} - n_{p1} + n_{e2} - n_{p2}) \quad \dots (16)$$

$$\left[ \frac{\partial}{\partial t} - (\mathbf{V}_{o2} \cdot \text{grad}) \right]^2 n_{p2} = \omega_{p2}^2 (n_{e1} - n_{p1} + n_{e2} - n_{p2}) \quad \dots (17)$$

Here  $\omega$ 's represent the electron or proton plasma frequencies in the two streams, viz,

$$\omega_e^2 = \frac{4\pi N_o e^2}{m} \quad \text{and} \quad \omega_p^2 = \frac{4\pi N_o e^2}{M} \quad \dots (18)$$

Subtracting Eq. (15) from equation (14) and Eq. (17) from Eq. (16) and putting

$$a_1 = n_{e1} - n_{p1} \quad \text{and} \quad a_2 = n_{e2} - n_{p2} \quad \dots (19)$$

$$\omega_1^2 = \omega_{e1}^2 + \omega_{p1}^2 \quad \text{and} \quad \omega_2^2 = \omega_{e2}^2 + \omega_{p2}^2 \quad \dots (20)$$

We find

$$\left[ \frac{\partial}{\partial t} + (\mathbf{V}_{o1} \cdot \text{grad}) \right]^2 a_1 = -\omega_1^2 (a_1 + a_2) \quad \dots (21)$$

$$\left[ \frac{\partial}{\partial t} - (\mathbf{V}_{o2} \cdot \text{grad}) \right]^2 a_2 = -\omega_2^2 (a_1 + a_2) \quad \dots (22)$$

The solutions involving  $a$ 's can be represented as

$$a = a_o \exp i(\sigma t + \overset{\rightarrow}{\kappa} \cdot \mathbf{r}) \quad \dots (23)$$

here  $\mathbf{r}$  is the space vector.

In the solution of the above type, with a given real  $\overset{\rightarrow}{\kappa}$ , the counterstreaming will be unstable for which  $\sigma$  is a complex quantity. In this case the amplitude of the corresponding oscillations can grow indefinitely. The minimum value of wave number  $\kappa_{min}$  for which this is possible gives the maximum value of the wave length  $\lambda_{max}$  at which there is instability. The double stream will then be unstable for complex value of  $\sigma$  and will form small clouds of space charge with maximum length  $\lambda_{max}$  at the expense of the streaming energy of the beam.

To determine the dispersion relation between  $\sigma$  and  $\kappa$  we substitute equation (23) into Eqns. (21) and (22) and after rearrangement we get

$$[\{\sigma + (\mathbf{V}_{o1} \cdot \overset{\rightarrow}{\kappa})\} - \omega_1^2] a_{o1} = \omega_1^2 a_{o2} \quad \dots (24)$$

and

$$[\{\sigma - (\mathbf{V}_{o2} \cdot \overset{\rightarrow}{\kappa})\} - \omega_2^2] a_{o2} = \omega_2^2 a_{o1} \quad \dots (25)$$

Elimination of  $a_{o1}$  and  $a_{o2}$  from Eqns. (24) and (25) gives the relations between  $\sigma$  and  $\kappa$ , viz.,

$$\begin{aligned} & \{\sigma + (\mathbf{V}_{o1} \cdot \vec{\kappa})\}^2 \{\sigma - (\mathbf{V}_{o2} \cdot \vec{\kappa})\}^2 - \omega_1^2 \{\sigma - (\mathbf{V}_{o2} \cdot \vec{\kappa})\}^2 \\ & - \omega_2^2 \{\sigma + (\mathbf{V}_{o1} \cdot \vec{\kappa})\}^2 = 0 \end{aligned} \quad \dots (26)$$

#### DISPERSION RELATIONS

To study the nature of  $\sigma$  for all real values of  $\kappa$  we substitute

$$\left. \begin{aligned} \mathbf{V}_{o1} + \mathbf{V}_{o2} &= 2U \\ \mathbf{V}_{o1} - \mathbf{V}_{o2} &= 2V \end{aligned} \right\} \quad (27)$$

$$p = \omega + \mathbf{V} \cdot \vec{\kappa} \quad \dots (28)$$

and

$$\Omega = \mathbf{U} \cdot \vec{\kappa} \quad \dots (29)$$

in dispersion relation (26) and obtain

$$\{p^2 - \Omega^2\}^2 - (\omega_1^2 + \omega_2^2)(p^2 + \Omega^2) + 2(\omega_1^2 - \omega_2^2)p\Omega = 0 \quad \dots (30)$$

Further, let us put

$$N_{o2} = bN_{o1} \quad \dots (31)$$

Thus we have

$$\begin{aligned} \omega_2^2 &= b\omega_1^2 \\ &= b\omega^2 \text{ (say)} \end{aligned} \quad \dots (32)$$

and Eq. (30) reduces to

$$(p^2 - \Omega^2)^2 - (1 + b)\omega^2(p^2 + \Omega^2) + 2(1 - b)\omega^2p\Omega = 0 \quad \dots (33)$$

This is the most general relation and difficult to solve exactly. We shall therefore study Eq. (33) for some specific cases of astrophysical interest.

Case (i)  $b \approx 1$ . Let us first consider that the streams have initially the same densities. Thus for  $b = 1$  and Eq. (33) reduces to

$$(p^2 - \Omega^2)^2 - 2\omega^2(p^2 + \Omega^2) = 0$$

$$\text{or} \quad p^4 - 2p^2(\Omega^2 + \omega^2) + \Omega^2(\Omega^2 - 2\omega^2) = 0 \quad \dots (34)$$

It can readily be shown that for all real values of  $\vec{\kappa}$  and for

$$\Omega^2 > 2\omega^2 \quad \dots (35)$$

$p^2$  is always real and positive. However, there exists a real and negative value for  $p^2$  provided

$$\Omega^2 < 2\omega^2 \quad \dots (36)$$

Let this value of  $p^2$  be  $-q^2$ . Thus we have

$$\sigma = -\mathbf{V} \cdot \vec{\kappa} + iq \quad \dots (37)$$

and hence for such a value of  $\sigma$  it is evident that the oscillations will go on building up with the time and will therefore make the whole system unstable.

The minimum value of  $\vec{\kappa}$ ,  $\kappa_{min}$  for such system may be evaluated from

$$\vec{\kappa}_{min} \cdot \mathbf{U} = \sqrt{\frac{8\pi N_o e^2 (\bar{m} + M)}{mM}} \quad \dots (38)$$

and

$$\lambda_{max} = \frac{2\pi}{\kappa_{min}} \quad \dots (39)$$

Kahn (1957) has discussed a particular case in which the two streams of equal density are moving in opposite direction having equal velocity  $U$  along the  $x$ -axis. For this case we obtain

$$\lambda_{max} = \sqrt{\frac{\pi m M}{2 N_o e^2 (m + M)}} \quad \dots (40)$$

Our results are somewhat different from those of Kahn (1957) because of his assuming only the electrons interactions. The protons were assumed to provide a uniform background of positive charge because of their heavier mass, which in our opinion may not be a valid assumption.

Let us further assume that one of the streams is stationary, say  $\mathbf{V}_{oz} = 0$ . This gives

$$\mathbf{U} = \mathbf{V} \quad (41)$$

and hence the stream will again be unstable and the maximum stable length will be given by equation (39) in conjunction with equation (38).

Case (ii)  $b \approx 0$ . Let us assume that a gas cloud is impinging into vacuum. Thus for  $b \approx 0$  we get from Eq. (33) after simplification

$$(p^2 - \Omega^2)^2 - \omega^2(p - \Omega)^2 = 0 \quad \dots (42)$$

It is evident from Eq. (42) that  $p$  and hence  $\sigma$  is always real for all real values of  $\kappa$ . Therefore the stream will plunge into vacuum without having any instability.

When  $b \gg 1$  the situation is similar to that discussed for case (ii). For  $0 \leq b \leq 1$  the problem cannot be solved explicitly. The above discussion and the inspection of Eq. (33) reveals that the beam will in general be unstable except for  $b \approx 0$  and for  $b \gg 1$ .

#### DISCUSSION OF RESULTS

It has been shown above that two penetrating streams will, in general, be unstable even when one of the streams is at rest. This is of great significance in regard to the magnetic storm theory, where the solar ion streams emanating from the disturbed solar regions produce geomagnetic storms on reaching the earth. These solar-ion streams while penetrating the solar atmosphere will become unstable and will form small clouds of space charge moving towards the earth. These clouds on entering the geomagnetic field may diffuse into the earth's magnetic field and a belt of trapped particles may be produced within the geomagnetic field, which may be responsible for the main phase of the geomagnetic storm. Kahn (1957) has alternatively suggested that the counter-streaming will be stopped because of this instability. Such an effect would prevent the passage of solar-ion stream through the solar atmosphere and interplanetary matter. Thus, in our opinion, such an interpretation of instability may not be probable.

This instability and the formation of small clouds of space charge may also explain the generation of radio noise from the colliding galaxies e.g. Cygnus A, NGC 5128 and NGC 1275. These space charge clouds will produce the stray electric fields and the charged particles moving under the influence of this field may be responsible for the radio emission.

#### REFERENCE

Kahn, F. D., 1957, *J. Fluid Mech.*, **2**, 601.

## GROWTH OF HYDROMAGNETIC SHOCK WAVES

I. J. SINGH

OIL AND NATURAL GAS COMMISSION, DEHRADUN, INDIA

AND

K. P. CHOPRA

ENGINEERING CENTER, UNIVERSITY OF SOUTHERN CALIFORNIA

LOS ANGELES, CALIFORNIA, U.S.A.\*

(Received, September 21, 1960)

**ABSTRACT.** In this technical note we consider the influence of a transverse magnetic field on the formation of a shock wave in an electrically conducting fluid. We conclude that the presence of a transverse magnetic field is conducive to the growth of compression waves and the decay of the expansion waves.

It is well known that the ordinary hydrodynamic compression shock wave involves an increase in entropy and that the rarefaction shock wave decays immediately into a continuous expansion wave. This is so because in a compression wave, the waves nearer the source tend to overtake those further from it with the result that the wave profile becomes more and more steep until the pressure gradients become infinite. In this way a compression shock is formed which grows in strength as the process continues. In a rarefaction shock, on the other hand, the waves nearer the shock lag more and more behind those in front of it, the wave profile flattens till the pressure gradients vanish and ultimately no discontinuity effects are observed. In fact if a rarefaction shock is established, even momentarily, it would decay immediately into a continuous expansion wave. We will consider, in this note, the influence of a transverse magnetic field on the formation of a shock wave in an electrically conducting fluid. It will be seen that the presence of a transverse magnetic field is conducive to the formation of a shock wave.

For the sake of simplicity we will consider a plane one-dimensional shock wave propagating in a fluid of infinite electrical conductivity and specific volume  $\tau$  with an external magnetic field  $H$  oriented in a direction normal to the direction in which the shock propagates. We define the quantities  $p^*$  and  $c^*$  according to Hoffmann *et al.*, 1950.

$$p^* = p + \frac{H^2}{8\pi}, \quad \text{and} \quad c^* = (c^2 + v_{AL}^2)^{1/2} \quad \dots \quad (1)$$

---

\*Present Address: Aerodynamics Laboratory, Polytechnic Institute of Brooklyn  
Brooklyn, N. Y., U. S. A.

These quantities take account of the contributions of the hydromagnetic interaction to the pressure  $p$  and the velocity of sound  $c$  through the magnetic pressure  $(H^2/8\pi)$  and the Alfvén speed  $v_{ALF} = H(\tau/4\pi)^{1/2}$ . We will call  $p^*$  and  $c^*$  the total pressure and the modified velocity of sound respectively.

Let us now suppose that the properties of the fluid at two adjacent points differ in magnitude by  $d\tau$ ,  $dH$ ,  $dv$ ,  $dp^*$  and  $dc^*$  where  $v$  denotes the gas speed. We also assume that the respective parts of the wave passing through these points differ in speed of propagation by  $dv_w$ . For the sake of simplicity, let us further assume that the gradients of temperature and velocity are small so that the dissipative effects of viscosity and heat conduction are negligible. Therefore each elementary part of the wave travels with the local speed of sound with respect to the fluid. The velocity of propagation  $v_w$  of this part of the wave with reference to a fixed coordinate system is

$$V_w = v + c^* \quad \dots (2)$$

and the velocity of propagation of an adjacent part of the wave is

$$v_w + dv_w = v + dv + c^* + dc^* \quad \dots (3)$$

so that

$$\frac{dV_w}{dp^*} = \frac{dv}{dp^*} + \frac{dc^*}{dp^*} \quad \dots (4)$$

Let us assume that the entire fluid was initially at rest with uniform pressure and temperature, and that each particle of the fluid undergoes isentropic changes. Therefore, the increments in pressure and density between adjacent particles obey the relation

$$c^{*2} = -\tau^2 \frac{dp^*}{d\tau} \quad \dots (5)$$

which yields on differentiation

$$2c^* \frac{dc^*}{dp^*} = -\frac{d\tau}{dp^*} \frac{d}{d\tau} \left( \tau^2 \frac{dp^*}{d\tau} \right) \quad \dots (6)$$

Again it can be shown from the equations of constant mass flux and constant momentum flux that

$$\frac{dv}{dp^*} = \frac{\tau}{c^*} \quad \dots (7)$$

On carrying out the substitutions from (6) and (7) in (4) we finally obtain

$$\frac{dV_{\omega}}{dp^*} = - \frac{\tau}{2c^*} \frac{(d^2p^*/d\tau^2)}{(dp^*/d\tau)} \quad \dots \quad (8)$$

Now if  $(dV_{\omega}/dp^*)$  is positive, the high pressure parts of the wave overtake the low pressure parts and a wave of compression steepens as it progresses. Similarly a wave of rarefaction becomes less steep. On the other hand if  $(dV_{\omega}/dp^*)$  is negative, a wave of compression becomes less steep and a wave of rarefaction steepens into a compression shock.

A fluid is said to be thermodynamically stable if it does not collapse or expand catastrophically. For a fluid to be thermodynamically stable,  $dV_{\omega}/dp^*$  must be positive. It follows from (8) that the sign of  $dV_{\omega}/dp^*$  depends on the sign of

$$\frac{d^2p^*}{d\tau^2} - \frac{d^2p}{d\tau^2} + \frac{3H^2}{4\pi\tau^2} \quad \dots \quad (9)$$

From the considerations outlined above, we immediately arrive at the following conclusions :

(i) Compression waves steepen and rarefaction waves flatten when

$$\tau^2 \frac{d^2p}{d\tau^2} + \frac{3H^2}{4\pi} > 0 \quad \dots \quad (10)$$

This happens when

either (a)  $d^2p/d\tau^2$  is positive

or (b)  $d^2p/d\tau^2$  is negative, and

$$\left| \frac{d^2p}{d\tau^2} \right| < \frac{3H^2}{4\pi\tau^2}$$

Therefore, a flattening wave of compression will begin to steepen as soon as a magnetic field of suitable strength is switched on.

(ii) Compression waves flatten and rarefaction waves steepen when

$$\tau^2 \frac{d^2p}{d\tau^2} + \frac{3H^2}{4\pi} < 0 \quad (11)$$

This happens when  $(d^2p/d\tau^2)$  is essentially notgative and

$$\frac{d^2p}{d\tau^2} > \frac{3H^2}{4\pi\tau^2} \quad \dots \quad (12)$$

Hence it may be concluded that the magnetic field enhances the steepening of a compression wave and flattening of a rarefaction wave. Hence the presence of a transverse magnetic field is conducive to the growth of compression waves and the decay of the expansion waves.

#### REFERENCES

Hoffmann, F. de and Teller, E., 1950. *Phys. Rev.*, **80**, 692.



# ELECTRONIC SPECTRA OF *m*-CHLOROPHENOL AND *o*-BROMOANISOLE IN DIFFERENT STATES\*

T. N. MISRA AND S. B. BANERJEE

OPTICS DEPARTMENT, INDIAN ASSOCIATION FOR THE CULTIVATION OF SCIENCE, CALCUTTA-32

(Received, February 25, 1961)

**ABSTRACT.** The ultraviolet absorption spectra of *m*-chlorophenol and *o*-bromoanisole in the vapour, liquid and solid states have been studied. In the vapour phase, *m*-chlorophenol yields about fifty sharp bands with the 0,0 band at  $35761\text{ cm}^{-1}$ . The observed frequencies are 151, 190 and  $235\text{ cm}^{-1}$  in the ground state and 120, 180, 225, 362, 503, 612, 737, 858, 959, 1029 and  $1086\text{ cm}^{-1}$  in the excited state. In the spectrum of the liquid, the bands are broad and the 0,0 band is displaced by about  $260\text{ cm}^{-1}$  towards red with respect to its position in the vapour phase. When the liquid is frozen and cooled to  $-180^{\circ}\text{C}$ , no further change in the spectrum is observed.

In the spectrum of *o*-bromoanisole in the vapour state the 0,0 band is at  $35615\text{ cm}^{-1}$  and the observed excited state frequencies are 221, 358, 517, 632, 685, 744, 955, 1031 and  $1233\text{ cm}^{-1}$ . The bands observed in the spectrum of the liquid are broad and the 0,0 band is shifted by about  $390\text{ cm}^{-1}$  towards longer wavelengths from its position in the spectrum of the vapour. With solidification of the liquid and cooling to  $-180^{\circ}\text{C}$ , no appreciable change is observed in the spectrum.

## INTRODUCTION

The ultraviolet absorption spectra of a large number of disubstituted benzene compounds in different states have been investigated in this laboratory to study the influence of intermolecular forces on the position and structure of absorption bands in the liquid and solid states. The present work is an extension of such investigations to the case of *m*-chlorophenol and *o*-bromoanisole.

It appeared that the ultraviolet absorption spectra of these compounds in any state had not been studied by any previous worker. The absorption spectra of the compounds in the vapour, liquid and solid states have, therefore, been analysed and the changes in the spectra observed with the change of state and temperature have been discussed in the present paper.

## EXPERIMENTAL

The experimental set-up was the same as that described in an earlier paper (Banerjee, 1956). Chemically pure *m*-chlorophenol and *o*-bromoanisole obtained from Fisher Scientific Co., U.S.A., were used after fractional and

\* Communicated by Professor S. C. Sirkar.

repeated vacuum distillation. For studying the absorption spectrum in the vapour state, cells of length 50 cm and 20 cm respectively and provided with quartz windows and a bulb attached to a side tube for containing the liquid, were used. In order to obtain suitable pressure of the absorbing vapour, the temperature of the liquid was varied from  $-20^{\circ}\text{C}$  to  $32^{\circ}\text{C}$  by immersing the container in suitable low temperature baths while the absorption tube was kept at the room temperature (about  $32^{\circ}\text{C}$ ).

Thin films of the substances of thickness of the order of a few microns were required to produce bands in the liquid and solid states. The spectrograms were taken on Agfa Isopan films with a Hilger E I spectrograph giving a dispersion of about 3 Å per mm. in the 2600 Å region. Microphotometric records were taken with a Kipp and Zonen type Moll microphotometer and the absorption spectra were calibrated with the help of microphotometric records of iron arc spectrum photographed on each spectrogram as explained in a previous paper (Banerjee, 1956).

## RESULTS AND DISCUSSION

The microphotometric records of the absorption spectra of *m*-chlorophenol and *o*-bromoanisole are reproduced in Figs. 1, 2, 3 and 4. The wave numbers of the bands with their approximate visual intensities and probable assignments are given in Tables I, II, III and IV.

The near ultraviolet absorption system in the case of the molecules of both the compounds, belonging to  $C_s$  point group, is due to an allowed  $A'-A'$  transition, with the transition moment lying in the plane of the molecule. Accordingly, the spectrum in each case consists of a number of intense bands with a strong 0, 0 band. The results obtained for the two compounds are discussed separately in the following paragraphs.

### *m*-Chlorophenol

About fifty sharp bands have been recorded in the spectrum due to *m*-chlorophenol in the vapour state. The most intense band at  $35761\text{ cm}^{-1}$  on the long wavelength side of the spectrum which persists at low pressure of the absorbing vapour has been taken as the 0, 0 band. The other bands may then be explained in terms of frequencies 151, 190 and  $235\text{ cm}^{-1}$  in the ground state and 120, 180, 225, 362, 503, 569, 612, 737, 858, 959, 1029 and  $1086\text{ cm}^{-1}$  in the excited state. The Raman spectrum of the substance was studied by Kohlrausch and Pongratz (1935) who reported the frequency shifts, 193(3), 241(2b), 409(3), 527(1), 684(3), 769(0), 890(1), 995(6), 1066(3), 1088( $\frac{1}{2}$ ), 1157(0), 1253(2b), 1304(0), 1583(3b) and  $3070(0)\text{ cm}^{-1}$ , the intensities being given in the parentheses. It can be seen that the frequencies observed in the present investigation can be correlated with the

TABLE I

Ultraviolet absorption bands of *m*-chlorophenol in the vapour state

Wave No. (cm <sup>-1</sup> ) and Intensity	Assignment	Wave No. (cm <sup>-1</sup> ) and Intensity	Assignment
35526 (m)	0-235	36988 (vw)	0+1227 0+2×612
35572 (w)	0-190	37071 (w)	0+959+362
35610 (w)	0-151	37212 (vw)	0+858+612 0+959+503
35678 (m)	0-83	37232 (vw)	0+2×737
35710 (m)	0-235+180	37316 (w)	0+1555 0+959+612 0+1029+503
35761 (s)	0,0	37386 (m)	0+1625
35793 (w)	0+180-151	37470 (m)	0+2×858 0+959+737
35834 (m)	0+225-151	37568 (m)	0+959+858
35881 (s)	0+120	37604 (m)	0+1086+737 0+3×612
35941 (m)	0+180	37670 (s)	0+2×959
35986 (m)	0+225	37700 (vw)	0+1086+858
36123 (w)	0+362	37736 (vw)	0+959+1029
36264 (w)	0+503	37810 (vw)	0+959+1086 0+2×1029
36330 (w)	0+569	37856 (w)	0+1029+1086
36373 (m)	0+612	37949 (m)	0+2×1086
36498 (m)	0+737	37982 (m)	0+3×737
36619 (m)	0+858	38033 (m)	0+2×959+362
36653 (m)	0+858+180-151	38346 (m)	0+3×858
36672 (w)	0+858+225-151 0+959-235+180	38420 (s)	0+2×959+737
36720 (s)	0+959	38526 (w)	0+2×959+858
36753 (w)	0+959+180-151	38643 (s)	0+3×959
36790 (m)	0+1029		
36847 (s)	0+1086		

TABLE II

Ultraviolet absorption spectra of *m*-chlorophenol in the liquid and solid states

Liquid at 32°C		Solid at -180°C	
Wave No. (cm <sup>-1</sup> ) and Intensity	Assignment	Wave No. (cm <sup>-1</sup> ) and Intensity	Assignment
35508 (sbb)	0,0	35564 (sb)	0,0
36447 (sbb)	0 + 939	36485 (sb)	0 + 921
37398 (wb)	0 + 2 × 939	37414 (wbb)	0 + 2 × 921

ground state frequencies observed by Kohlrausch and Pongratz. The upper state frequencies 180 and 225 cm<sup>-1</sup> correspond probably to the Raman frequencies 193 and 241 cm<sup>-1</sup>; the observed ground state frequencies 190 and 235 cm<sup>-1</sup> are also in good agreement with the Raman data. The frequency 120 cm<sup>-1</sup> may be

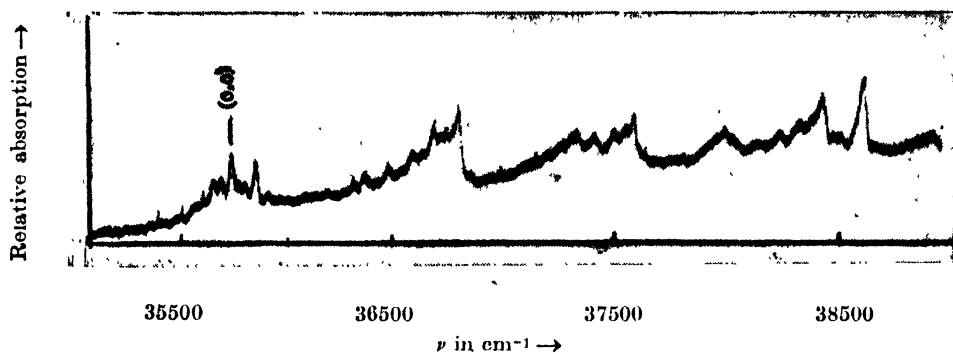


Fig. 1. Microphotometric record of the ultraviolet absorption spectrum of *m*-chlorophenol in the vapour state.

the excited state value of the observed ground state frequency 151 cm<sup>-1</sup>. Though Kohlrausch *et al.* did not report any Raman shift of this magnitude, we are probably justified in taking 151 cm<sup>-1</sup> as a fundamental frequency, because such low frequency fundamentals are usually observed in the ultraviolet absorption spectra of phenol compounds (Swamy, 1953; Ramasastry, 1951). This frequency probably represents an out of plane deformation vibration. The other excited state frequencies 362, 503, 612, 737, 858, 959 and 1029 cm<sup>-1</sup> can be correlated with the ground state frequencies 409, 527, 684, 769, 890, 995 and 1066 cm<sup>-1</sup> respectively, observed in Raman effect. The strong band at 36847 cm<sup>-1</sup> may be analysed as 0 + 1086 cm<sup>-1</sup>, there being two weak ground state frequencies 1088 and 1157 cm<sup>-1</sup> reported by Kohlrausch *et al.* Similarly, the weak band at 36988 and 37316 cm<sup>-1</sup> may be assigned as 0 + 1227 and 0 + 1555 cm<sup>-1</sup> respectively,

since there are two Raman lines at 1253 and 1583  $\text{cm}^{-1}$ , but these two bands can also be alternatively assigned as combination frequencies as shown in Table I. The band at 35710  $\text{cm}^{-1}$ , on the longer wavelength side of the 0, 0 band at a distance of 51  $\text{cm}^{-1}$  and those at 35793 and 35834  $\text{cm}^{-1}$  with shifts of 32 and 73  $\text{cm}^{-1}$  from the 0, 0 band on the short wavelength side may be explained as  $v' \rightarrow v$  transitions as shown in Table I.

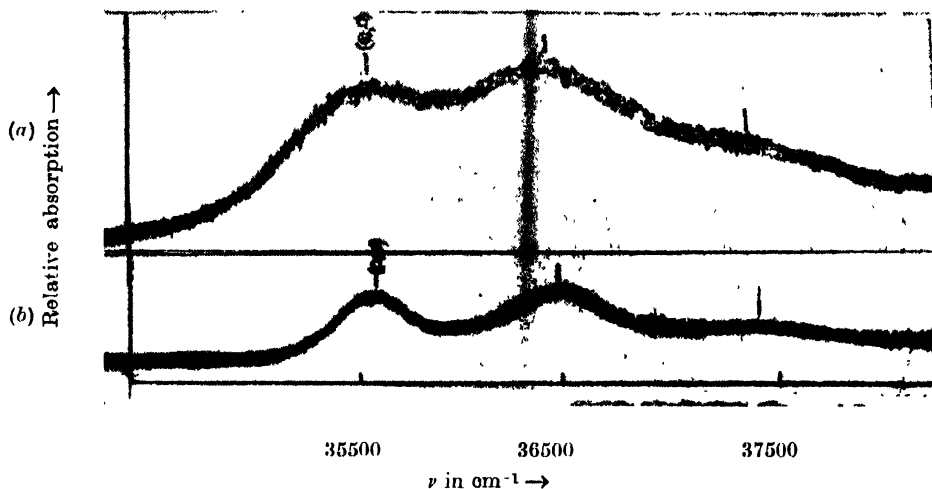


Fig. 2. Microphotometric records of the ultraviolet absorption spectra of *m*-chlorophenol. (a) Liquid at 32°C. (b) Solid at  $-180^{\circ}\text{C}$ .

In the spectrum of the liquid there are three broad bands with centres approximately at 35508, 36447 and 37398  $\text{cm}^{-1}$ , the centre of the first band being taken as the position of the 0, 0 band. Thus it is seen that the liquefaction of the vapour results in a shift of about 260  $\text{cm}^{-1}$  towards red of the 0, 0 band. The three bands due to the liquid show a constant separation of about 939  $\text{cm}^{-1}$ . Comparing this with the frequencies observed in the spectrum of the vapour, it appears that this smaller value may be due to uncertainty in the location of the 0, 0 band exactly in the case of the liquid. The shift of the 0, 0 band may be due to association of the molecules through the O—H group.

When the liquid is frozen and cooled to  $-180^{\circ}\text{C}$  there is no appreciable change in the position of the 0, 0 band. The bands are a little sharper but still quite broad. This large width of the bands may be produced by the interaction of the permanent dipoles in the neighbouring molecules with the transition moment of the excited molecule. It is well known that large splittings are observed in some cases of substituted toluenes and dichlorobenzenes (Swamy, 1952, 1953; Sen, 1957). In the present case such splitting may be small and the large width of the individual bands may be responsible for the overlapping of the components and producing only a single broad band in place of its resolved components.

*o*-Bromoanisole

The absorption spectrum of *o*-bromoanisole in the vapour state consists of about 17 prominent bands. The strongest band on the long wavelength side at  $35615\text{ cm}^{-1}$ , which persists at  $-20^\circ\text{C}$ , has been taken as the 0, 0 band. The other bands have been interpreted on the basis of the fundamental frequencies  $221, 358, 517, 632, 685, 744, 955, 1031$  and  $1233\text{ cm}^{-1}$  in the upper state and their combinations, and frequencies  $189\text{ cm}^{-1}$  and  $233\text{ cm}^{-1}$  in the ground state. The acid frequencies  $517, 632, 685, 744, 955, 1031$  and  $1233\text{ cm}^{-1}$  evidently correspond to the ground state frequencies  $544, 659, 743, 792, 1023, 1122$  and  $1237\text{ cm}^{-1}$  observed in the infrared (Lecomte, 1938). No infrared data are available for frequencies lower

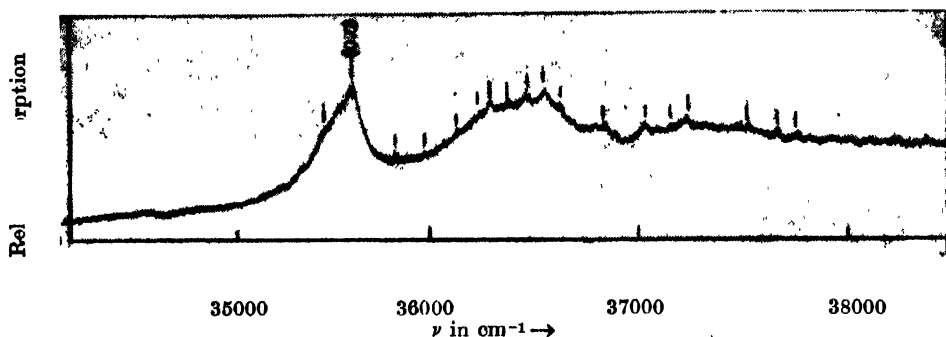


Fig. 3. Microphotometric record of the ultraviolet absorption spectrum of *o*-bromoanisole in the vapour state.

than  $500\text{ cm}^{-1}$  and the Raman spectrum had not been studied by any previous worker, but the assignment of the frequencies  $221$  and  $358\text{ cm}^{-1}$  to fundamental modes is probably justified. The frequency  $358\text{ cm}^{-1}$  represents in all probability in the excited state one of the components of the  $e_g^+$  mode ( $606\text{ cm}^{-1}$  in the ground state) of the benzene molecule which splits up into two totally symmetric components in the  $C_2$  point group. Further, similar band has also been observed in the case of other substituted anisoles (Suryanarayana and Rao, 1956). The frequency  $221\text{ cm}^{-1}$  may be correlated to the observed ground state frequency  $233\text{ cm}^{-1}$ , which again may represent an out of plane bending mode usually observed in the spectrum of disubstituted benzenes.

In the spectrum of the liquid only four broad bands are observed. Taking  $35225\text{ cm}^{-1}$  as the position of the 0, 0 band, the other bands are separated from the 0, 0 band by  $221, 961\text{ cm}^{-1}$  and the first harmonic of  $961\text{ cm}^{-1}$ . Thus it is seen that with the liquefaction of the vapour, the 0, 0 band is shifted by about  $390\text{ cm}^{-1}$  towards red.

When the liquid is solidified and cooled to  $-180^\circ\text{C}$ , no further resolution of the bands into components is observed. Taking  $35139\text{ cm}^{-1}$  as the position of the 0, 0 band of the system, it is seen that the band system is further shifted towards longer wavelengths by about  $86\text{ cm}^{-1}$  with the solidification of the liquid. The other bands of the solid represent excited state frequency  $970\text{ cm}^{-1}$ .

TABLE III

Ultraviolet absorption bands of *o*-bromoanisole in the vapour state

Wave No. ( $\text{cm}^{-1}$ ) and Intensity	Assignment
35382 (w)	0 - 233
35438 (w)	0 - 189
35615 (vs)	0,0
35836 (w)	0 + 221
35973 (w)	0 + 358
36132 (mw)	0 + 517
36247 (mw)	0 + 632
36300 (s)	0 + 685
36359 (mw)	0 + 744
36468 (ms)	0 + 632 + 221
36570 (ms)	0 + 955
36646 (w)	0 + 1031
36848 (w)	0 + 1233
37039 (m)	0 + 685 + 744
37192 (w)	0 + 955 + 632
37246 (m)	0 + 955 + 685
37520 (m)	0 + 2 $\times$ 955
37620 (w)	0 + 2 $\times$ 685 + 632

TABLE IV

Ultraviolet absorption bands of *o*-bromoanisole in the liquid and solid states

Liquid at 32°C		Solid at -180°C	
Wave No. ( $\text{cm}^{-1}$ ) and Intensity	Assignment	Wave No. ( $\text{cm}^{-1}$ ) and Intensity	Assignment
35225 (s)	0,0	35139 (s)	0,0
35496 (w)	0 + 221		
36186 (s)	0 + 961	36109 (s)	0 + 970
37136 (s)	0 + 2 $\times$ 961	37081 (s)	0 + 2 $\times$ 970

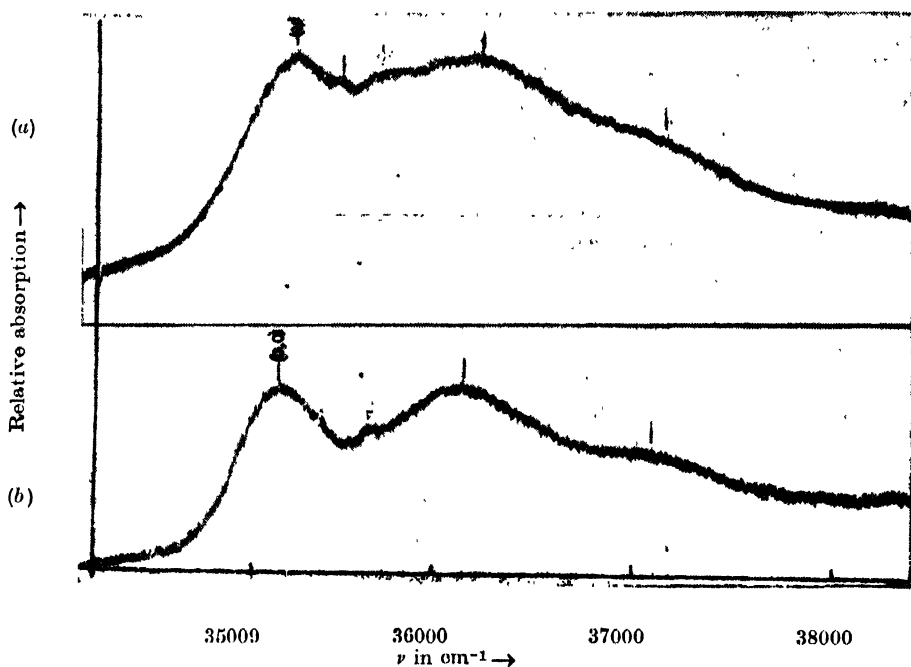


Fig. 4. Microphotometric records of the ultraviolet absorption spectra of *o*-bromoanisole. (a) Liquid at 32°C, (b) Solid at -180°C.

The disappearance of the other bands is due to broadening and consequent overlapping of the bands of the vapour, in the states of aggregation.

The bands are broad in the case of the liquid and the solid states. In the former case, both  $\nu \rightarrow \nu$  transition and fluctuating intermolecular field may be responsible for the large width. Since both these causes disappear in the solid state, the persistence of the large width of the bands in this case may be due to unresolved components into which each band may have been split up by the interaction of the transition moment and permanent dipole of the surrounding molecules in the lattice.

#### ACKNOWLEDGMENT

The authors are grateful to Professor S. C. Sirkar, D.Sc., F.N.I., for his kind interest in the work and for valuable suggestions.

#### REFERENCES

- Banerjee, S. B., 1956, *Ind. J. Phys.*, **30**, 106.
- Kohlrausch, K. W. F. and Pongratz, A., 1935, *Monatsch. f. Chemie*, **65**, 199.
- Lecomte, P. J., 1938, *J. de. Physique et Radium*, **9**, 13.
- Ramasastri, C., 1951, *Proc. Nat. Inst. Sc. (Ind.)*, **17**, 349.
- Sen, S. K., 1957, *Ind. J. Phys.*, **31**, 99.
- Suryanarayana, V. and Rao, V. R., 1956, *Ind. J. Phys.*, **30**, 117.
- Swamy, H. N., 1952, *Ind. J. Phys.*, **26**, 445.
- " " - 1953, *Ind. J. Phys.*, **27**, 119.



## BOOK REVIEW

**MODERN GEOMETRICAL OPTICS**—By Max Herzberger\*. Pp 504+xii.  
Interscience Publishers, New York, London, 1958. Price \$ 15.00

This book gives purely mathematical theories of image formation by optical systems. By representing the laws of reflection and refraction by an equation in which the vector product of two vectors in the object space is equated to a corresponding product in the image space, the problem of ray tracing has been reduced to that of solving equations involving vectors.

The book is divided into ten Parts, each part consisting of several Chapters. Part I of the book deals with the tracing of rays through optical systems and this can be done with the help of numerous formulae involving vectors and the necessary calculations can be made with the help of electronic computers. The terms 'diapoint' and 'diamagnification' have been introduced in this part and the properties of these points have been utilised in the succeeding parts. Part II deals with Gaussian Optics and its applications to different systems including thick lenses.

The general laws governing the passage of manifold of rays through optical systems have been discussed in Part III. As before, the vector equations have been given for these laws and the basic formulae of Hamilton and Lagrange have been discussed in this part. The formation of images by concentric systems has been discussed in Part IV and the vector formulae for the formation of images by rotation-symmetric systems including the discussions on image-error theory and limitations of optical image formation have been given in Part V.

The approximation theory of image formation in normal systems has been given in the different chapters of Part VI and the third and fifth-order image-error theories have been discussed in Part VII. In Chapter 31 of this Part formulae for the calculation of the characteristic functions for a combined system with the help of those for the parts of the systems have been derived.

Part VIII deals with interpolation theory of the optical image. The author himself has suggested an alternative method of solving the problem of image formation by complicated optical systems. In place of the actual ray tracing, help of some interpolation formulae is taken in this method. The analysis of spot diagrams is discussed in Chapter 33 in this Part.

Geometrical optics in inhomogeneous media is discussed in Part IX. Part X comprising four chapters, gives appendices dealing with 1) Vector analysis,

\*The unusual delay in the publication of this review due to oversight is very much regretted. Editor.

2) Miscellaneous mathematical tools, 3) Numerical examples and 4) Historical remarks. A Bibliography is also given at the end.

The author himself has made remarkable contributions in this field and he has stated in the Preface that this book is the result of more than fourteen years' continuous labour. The tremendous amount of calculations required for the derivation of the numerous formulae and for their verification will show the amount of labour involved in the preparation of this volume which is a great treasure to opticians engaged in the design of high-precision optical systems. The book is especially useful to those workers in the field who have facilities for using electronic computers. It is also useful to post-graduate students interested in applied optics. The get-up is excellent.

*S. C. S.*

# EFFECT OF WORLD-WIDE CHANGES OF ISOTROPIC COSMIC RAY INTENSITY ON THE DAILY VARIATION OF COSMIC RAYS

R. P. KANE

PHYSICAL RESEARCH LABORATORY, AHMEDABAD

(Received, February 14, 1961)

**ABSTRACT.** Various methods of evaluating the 12 bi-hourly values required for a study of the daily variation of cosmic ray intensity are discussed. Estimates are obtained of the distortions produced in the genuine daily variation due to slope, curvature and short-term effects of the world-wide fluctuations in isotropic cosmic ray intensity. A method for correcting for such effects is suggested and examined critically.

## I. INTRODUCTION

The daily variation of cosmic ray intensity is a very important tool for the study of anisotropy of cosmic rays. Daily variation is usually studied by examining the form of the daily curve as a whole or by resolving the same into its Fourier components. It can be studied for individual days, if the statistical accuracy of the data is good enough, or for averages over groups of days. For data having large statistical errors on individual days, histograms of harmonic components obtained for individual days could still lead to useful conclusions.

However, while studying the daily variation of cosmic ray intensity, allowances are to be made for the effects due to world-wide changes of the isotropic cosmic ray intensity as these are likely to distort the true form of a genuine local-time daily variation. Whereas the possibility of such distortions is recognised by workers in this field, some of the recently published results seem to indicate that the extent of these distortions is not fully appreciated. The purpose of the present communication is to estimate the magnitude of such distortions under various conditions and for various aspects of study of the daily variation.

## II. METHODS OF STUDY OF DAILY VARIATION

The basic requirement for a study of the daily variation is the evaluation of hourly or bi-hourly percent deviations from mean. Since most of the workers use bi-hourly deviations, we will henceforth consider only these. Percent bi-hourly deviations are usually obtained by the following methods :—

**Method A :** Evaluating the arithmetic mean of 12 successive bi-hourly values and expressing each bi-hourly value as percent deviation from this mean.

**Method B :** Applying correction for the linear gradients of cosmic ray intensity by subtracting the 0 hour value of one day from the 0 hour value of the next day. The difference so obtained is expressed as percentage of the day's mean. If this percentage value is designated as  $d$ , one subtracts the factor  $\left(n \frac{-6.5}{12}\right) \times d$  from the  $n$ th bi-hourly deviation obtained by method A above.

**Method C :** Applying correction for the linear gradients by evaluating moving averages of 12 successive bi-hourly values and subtracting these from the original bi-hourly values. Since a mean of 12 successive values has an hour of centering not coincident with any bi-hourly value but lying half-way between two bi-hourly values, two alternatives are usually adopted :

- (i) Moving averages of 12 bi-hourly values are further subjected to moving averages over 2 consecutive values so that the new means so obtained have centering coincident with the original bi-hourly intervals.
- (ii) Moving averages are calculated for 13 successive bi-hourly values instead of 12 successive values so that the centering is the same as for original bi-hourly values.

In principle, procedure (ii) is less rigorous; because moving averages over 13 consecutive bi-hourly values leave some residual daily variation in the means. In practice, both methods give almost similar results.

Fig. 1 is an illustration of the three methods and the daily variations obtained by using them for a sample bi-hourly data for the neutron monitor at Sulphur Mountain for September 21—25, 1957, when the cosmic ray intensity undergoes a depression of about 10% in 2 days and then recovers to almost its original values in the next 2 days. The dotted line at the top (Curve X) is the plot of original bi-hourly values while the full curve Y superimposed on it is the plot of moving averages over 12 consecutive bi-hourly values. Curves A, B, C show the daily variations obtained by methods A, B and C respectively.

The following characteristics will be noticed from Fig. 1 :

- (a) The daily variation obtained by method A is not corrected for linear gradients of the cosmic ray intensity and hence bi-hourly percent deviations for the 1st day (September 22, 1957) are positive for the first half of the day and negative for the latter half, creating a false impression of an early morning maximum of the daily variation. For the second

day, the daily variation is characterised by a minimum which is coincident with the point of inflection in the general trend of intensity change. On the third day, the pattern is reverse to that of first day, creating a false impression of afternoon maximum.

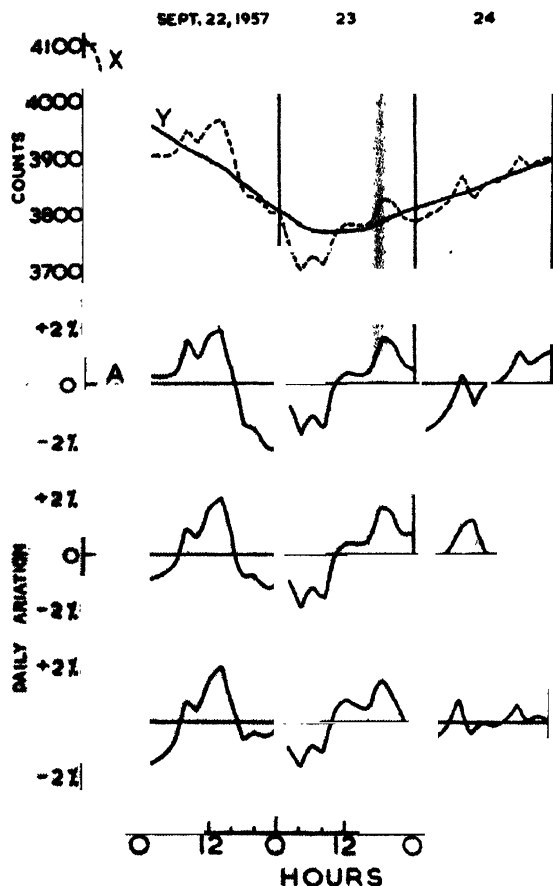


Fig. 1. Bi-hourly values and daily variation for neutron intensity at Sulphur Mountain for September 21-25, 1957.

- (b) The daily variation obtained by method B is comparatively free from effects due to gradients on the 1st and 3rd day. However, for the 2nd day, the correction factor has been almost zero as the cosmic ray intensity has gone down and recovered again and the 0 hour values at the beginning of the second and third day are almost the same. Hence the daily variation on the second day is the same as the daily variation for second day obtained by method A.

- (c) The daily variation obtained by method C is less affected by effects due to gradients as compared to the daily variations obtained by methods A and B.

### III. COMPARISON OF METHODS A AND C FOR THE STUDY OF VARIOUS ASPECTS OF DAILY VARIATION

As seen in the previous section, the daily variation obtained by method A is subject to distortions due to gradients in cosmic ray intensity. If method B is employed, these effects are reduced to some extent but not fully, because the gradient is evaluated only from two bi-hourly values. In method C, the gradient is estimated at every bi-hourly interval by averaging 12 consecutive bi-hourly values around the bi-hourly interval under consideration. Method C is, therefore, superior to methods A and B. Since methods A and C are at the two extremes and method B has intermediate characteristics, we will consider only methods A and C and estimate the order of magnitude of distortions involved when linear gradients are neglected in various types of analysis.

#### (1) *Study of daily variation averaged over a group of days*

The effect of the gradients is to introduce extra contributions in the bi-hourly percent deviations. Larger the gradients, larger will be the distortions. However, gradients are both positive and negative. Hence for averages over a group of days, it is expected that effects due to gradient of opposite signs will cancel each other to some extent. The cancellation will be more effective for larger groups of days. Fig. 2 shows the average daily variation curves for the neutron monitor at Climax obtained by methods A and C for a 20-day interval and a 6-month interval. It will be seen that whereas for the 20-day interval the peak-to-peak amplitudes are 1.5% and 1.3% for methods A and C respectively, the amplitudes are almost equal for the 6-monthly period. It should be noted that the amplitudes obtained by method A need not necessarily be larger. Distortions due to gradients will enhance or reduce the amplitudes depending upon whether the phase of the extra contribution is similar or opposite to the phase of the genuine variation.

#### (2) *Study of the frequency distributions of the amplitudes and time of maxima of the diurnal and the semi-diurnal components of the daily variation.*

A useful way of studying the daily variation is by resolving the 12 bi-hourly percent deviations into Fourier (harmonic) components for every day and studying the frequency distributions of the amplitudes and time of maxima. However, such frequency distributions will suffer distortions if the general level of cosmic ray intensity is increasing

or decreasing with constant gradients. The effects of linear gradientst can be estimated by subjecting to harmonic analysis idealised bi-hourly deviations giving straight line plots. Table I below gives such estimates for the amplitudes and time of maxima of the 1st and 2nd harmonics for positive and negative linear gradients of 1.0% over 24 hours.

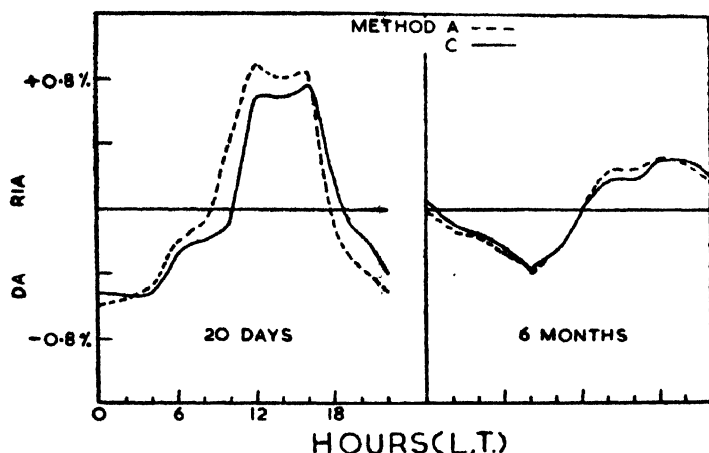


Fig. 2. Average daily variation for neutron intensity at Climax for a 20-day and a 6-month period.

TABLE I

	Amplitude $r_1$	Time of max. $\phi_1$	Amplitude $r_2$	Time of max. $\phi_2$
Linear increase of 1.0%/24 hours.	0.32%	$\pi \pm 75^\circ$	0.17%	$\pi \pm 60^\circ$
Linear decrease of 1.0%/24 hours.	0.32%	$75^\circ$	0.17%	$60^\circ$

In practice, these vectors will be superimposed upon the genuine diurnal and semi-diurnal vectors.

To see how these distortions occur in actual data, the bi-hourly values of neutron intensity at Climax were treated by methods A and C and harmonically analysed for individual days for a 12 month period. Fig. 3 shows the frequency distributions for the amplitudes ( $r_1$  and  $r_2$ ) and the time of maxima ( $\phi_1$  and  $\phi_2$ ) of the first and second harmonics respectively obtained by methods A and C. It will be noted that the amplitudes of the first harmonic extend to larger values in method A. Also the frequency distribution of the time of maximum  $\phi_1$  of the first harmonic has a larger spread in method A.

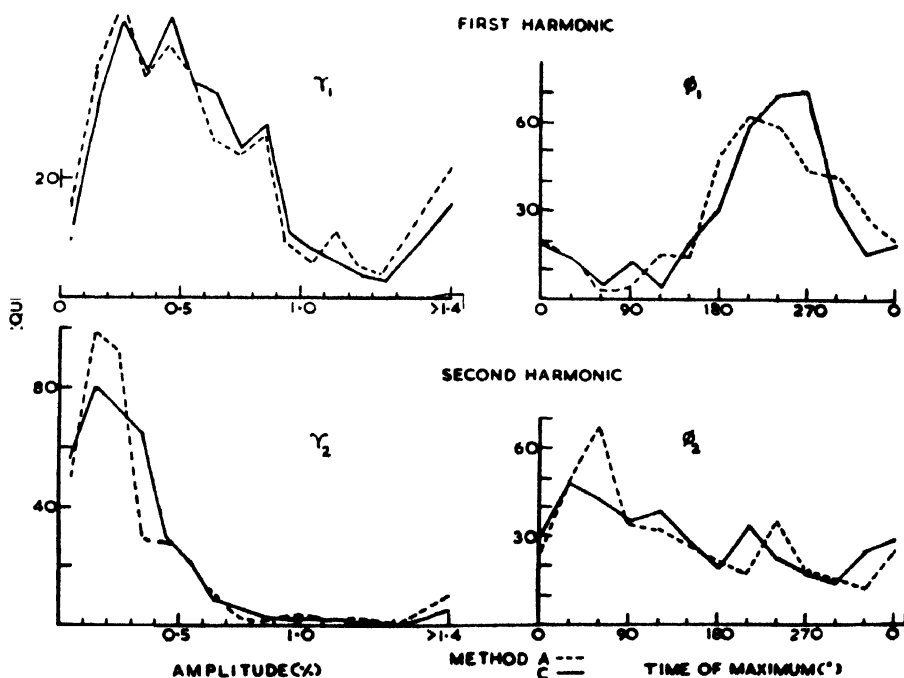


Fig. 3. Frequency distributions for the amplitudes ( $r_1$  and  $r_2$ ) and times of maxima ( $\phi_1$  and  $\phi_2$ ) for the first and second harmonics for Climax neutrons.

(3) *Relationship between daily variation and daily mean intensity.*

For studying a relationship of this type, it is obvious that method A is not suitable; because the daily variation is already distorted by gradients in daily mean intensity to the extent indicated in Table I.

(4) *Solar and Terrestrial relationships of daily variation*

It is well known that the daily mean intensity of cosmic rays is related to geomagnetic disturbances as well as some solar phenomena. If, therefore, the daily variation of cosmic rays is studied by method A, all such relationships will affect the characteristics of the daily variation also. Therefore, for this type of analysis, method A is not suitable.

(5) *Study of individual bi-hourly deviations*

As can be seen from Fig. 1, the individual bi-hourly deviations obtained by method A can be greatly distorted by the general trend in the daily mean intensity. Hence, method A is not suitable for this type of study.

It may be concluded, therefore, that except for periods when the fluctuations in the daily mean intensity are small compared to the expected amplitudes of



daily variations or except when daily variations averaged over long periods are under consideration, the use of method A is undesirable for a study of the daily variation, as it is distorted by what may be termed as "Slope effects". Method B is better than method A but has its limitations as already referred to above. Method C is more rigorous and has a smaller Poisson standard error and hence is preferable to methods A and B for most purposes.

#### IV. A CRITICAL APPRAISAL OF METHOD C

It was shown in the previous section that amongst the three methods for obtaining the bi-hourly percent deviations from mean, method C is the best. However, it is necessary to examine whether method C is completely free from effects due to gradients.

The bi-hourly cosmic ray intensity  $I'(t)$  observed at  $U.T.(t)$  may be expressed as

$$\begin{aligned} I'(t) &= I(t) + f(T, t) \\ &= I(t) + \sum_n r_n \sin \{n(t + \psi) + \phi_n\} \end{aligned} \quad \dots (1)$$

where  $I(t)$  is the isotropic level of world-wide cosmic ray intensity and  $f(T, t)$  is the daily variation, which can be resolved into Fourier components. Since all harmonics of periodicities of 24 hours or fractions thereof, reduce to zero when averages over 24 hours are taken, averages of  $I'(t)$  over 12 successive bi-hourly values will be equal to similar averages of  $I(t)$ . In method C, it is assumed that such averages of  $I'(t)$  values for 12 successive bi-hourly intervals are good estimates of the instantaneous values of  $I(t)$  for the middle of the interval. Such an assumption is valid only when  $I(t)$  changes occur with constant gradients. If the gradients (i.e. slopes) change, distortions will be produced which will be roughly proportional to the second derivative  $d^2I/dt^2$  of the ( $I$  vs.  $t$ ) plot. It is obvious, therefore, that method C will give incorrect results during periods when the gradients  $dI/dt$  undergo large changes.

The distortions produced due to changes in gradients can be broadly classified into 2 types:

- (i) Long-term changes of world-wide cosmic ray intensity with time constant exceeding 24 hours. These will produce distortions which will be termed as "Curvature effects".
- (ii) Short-term (hours-to-hour) fluctuations of a world-wide nature in the cosmic ray intensity. These will be termed as "Short-term effects".

The contribution of "Curvature effects" to the daily variation can be estimated if the pattern of the intensity change is known. Consider, for example, the patterns A and B shown in Fig. 4, which represent linear gradient changing signs abruptly. In Fig. 4, pattern A corresponds to a constant gradient of

+0.1%/hr. for 18 successive bi-hourly values, followed by a sudden change to a constant gradient of -0.1%/hr. for the next 18 bi-hourly values. This pattern corresponds to a change of about 2.4% per day which is not uncommon for cosmic ray neutron intensity at high latitudes. Pattern B corresponds to a form exactly opposite to pattern A.

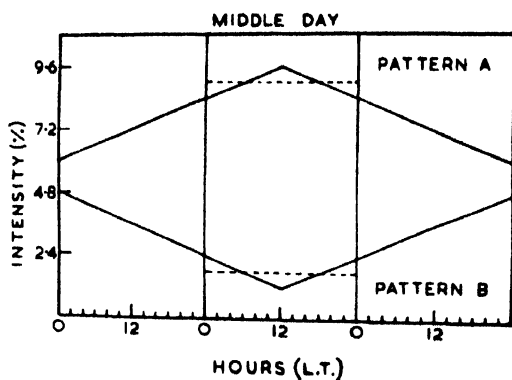


Fig. 4. Sample patterns of sudden changes in the linear gradients of cosmic ray intensity.

If the point of inflection is assumed to coincide with 12 noon (L.T) for the middle day and the data are treated by method C and the bi-hourly percent deviations harmonically analysed, the amplitudes and time of maxima of the first and second harmonics for the middle day are as given in Table II.

TABLE II

	1st harmonic		2nd harmonic	
	Amp.	Time of max.	Amp.	Time of max.
Pattern A	0.24%	180°	0.08%	0°
Pattern B	0.24%	0°	0.08%	0°

It will be seen that amplitudes of the order of 1/4% can arise due to "Curvature effects" on individual days, if the day includes the inflection point. For other days, as also for averages over groups of days, the contribution due to "Curvature effects" will be negligible.

As regards the contribution of "Short-term effects" to daily variation, it is difficult to investigate patterns as there are innumerable ways in which individual bi-hourly values can be affected by world-wide short-term fluctuations of isotropic cosmic ray intensity. From the data from a single station it is impossible to estimate the contribution of such changes to individual bi-hourly values.

# V. AN EFFECTIVE METHOD OF ESTIMATING THE WORLD-WIDE SHORT-TERM CHANGES OF COSMIC RAY INTENSITY

As seen in previous section, data from a single station are inadequate to separate out the genuine daily variation of cosmic ray intensity from its experimentally obtained form distorted by possible "Short-term and Curvature effects". For long-term averages, such effects are expected to even out, but for averages over only a few days, there is a possibility of distortions. Unfortunately, it is not possible to estimate their magnitude from the data of a single station.

A little consideration shows, however, that there is a possibility of such an estimate if data from more than one station are utilised. This is already pointed out by Sekido *et al.* (1952). Referring back to Eq. (1), let us assume that cosmic ray data are available for a number of stations which are at the same geomagnetic latitude and are at equally spaced longitudes all round the globe. Then, the cosmic ray intensity  $I'_K(t)$  at the  $k$ -th station at time ( $t$ ) would be given by

$$I'_K(t) = I(t) + \sum_n r_n \sin \{n(t + \psi_k) + \phi_n\} \quad \dots (2)$$

where  $r_n$  and  $\phi_n$  represent the amplitude and phase of the  $n$ th harmonic for a station of longitude zero ( $\psi_0 = 0$ ) and  $\psi_k$  is the longitude of the  $k$ th station. If values of  $\psi_k$  for successive stations differ by a constant quantity  $360/m$ , where  $m$  is the number of stations, then

$$\psi_k = (k-1) \frac{360}{m} \quad \dots (3)$$

and

$$\sum_{k=1}^m r_n \sin \left[ n \left\{ t + \frac{360(k-1)}{m} \right\} + \phi_n \right] = 0 \quad \dots (4)$$

for  $n \neq \beta m$ , where  $\beta$  is a positive integer,

provided that the amplitudes  $r_n$  and phases  $\phi_n$  remain constant for more than 24 hours. Thus, if we concentrate our attention only on the first harmonic ( $n = 1$ ), even two stations ( $m = 2$ ) separated by  $360/m = 180^\circ$  will ensure that Eq. (4) is satisfied. To eliminate the second harmonic also ( $n = 2$ ), we will need 3 stations,  $120^\circ$  apart in longitude. If data from 3 such stations are available, then the average of the percent cosmic ray values at the 3 places for the same universal time ( $t$ ) will be devoid of the first or second harmonic of genuine daily variation.

It is obvious, therefore, that if the world-wide bi-hourly percent mean intensity obtained by adding the percent values at the same U.T. of 3 stations at roughly the same geomagnetic latitude and spaced  $120^\circ$  apart in geographic longitude

is subjected to an analysis of daily variation by method C, one would get an idea of the characteristics of the *apparent* daily variation introduced due to short-term and curvature effects of the world-wide isotropic intensity changes. With this view, data obtained during I.G.Y. were examined to select out suitable groups of stations. A study of the geographical distribution of neutron monitor stations shows that there is a preponderance of stations in the European and American longitudes but a marked scarcity in the Far East. The following factors have also to be kept in mind :

- (a) The stations should be at roughly the same geomagnetic latitude to ensure similar cut-off energies.
- (b) They should have similar energy responses related to the altitude.
- (c) They should have been corrected for barometric effect by the same pressure coefficients (say,  $0.72 \pm 0.02\%/mb.$  Hg.).
- (d) Data for each of them should be fairly continuous for about 12 months to give a large number of common days.
- (e) The counting rate at each station should be fairly high (bi-hourly standard error about  $0.5\%$ ).
- (f) They should be  $120 \pm 10^\circ$  apart in geographic longitude.

It was found that the following stations could be utilised for analysis:

- (1) Lincoln or Climax in Americas.
- (2) Gottingen or Weissenau and some others in Europe.
- (3) Yakutsk in the Far East.

From the point of view of spacing in geographical longitude, Climax, Gottingen and Yakutsk is a very convenient group. Since Climax is a high altitude station, Lincoln, Gottingen and Yakutsk is perhaps a more appropriate choice. Table III gives the details about the geographical locations and energy responses etc. for the 4 stations.

TABLE III

Station	Geomag. latitude	Geographical longitude	Altitude (meters)	Cut-off energy (BeV)	Mean Fonger energy response (BeV)
Climax	48°	106°W	3400	3.0	9.7
Lincoln	51°	97°W	350	2.6	12.1
Gottingen	52°	10°E	273	2.4	12.1
Yakutsk	51°	129°E	105	2.2	12.1

The bi-hourly values for Climax, Lincoln, Gottingen and Yakutsk were obtained from the Japanese publication "Cosmic Ray Intensity during the

I.G.Y.—No. 1-2". Values for the same bi-hourly (G.M.T.) intervals were added to yield bi-hourly values of  $W$  and  $W'$  series defined as follows :—

$$W = \frac{1}{3} (\text{Climax} + \text{Gottingen} + \text{Yakutsk})$$

$$W' = \frac{1}{3} (\text{Lincoln} + \text{Gottingen} + \text{Yakutsk})$$

If the pattern of daily variation remains constant for more than 24 hours, the bi-hourly values of  $W$  or  $W'$  would be devoid of the 1st, 2nd, 4th and 5th harmonics. The 3rd and 6th harmonics will be retained.

The bi-hourly values of  $W$  and  $W'$  were treated by method C and the percent bi-hourly deviations obtained for the 12 successive bi-hourly intervals centered at 01, 03...23hr. G.M.T. were considered as a U.T. apparent daily variation\* which would give a measure of the distortion involved on any particular date. Except for the fact that the 3rd and 6th harmonics are still retained in  $W$  or  $W'$  and that some discrepancies would creep in, if the genuine daily variation is of a transient type (this is discussed further in Sec. VII), the characteristics of the daily variation exhibited by  $W$  or  $W'$  would give an estimate of the "Curvature and Short-term effects" that vitiate the genuine daily variation. In the next section, results obtained for the 12 month period July 1957–June 1958 are described.

## VI. CHARACTERISTICS OF THE APPARENT DAILY VARIATION DUE TO "CURVATURE AND SHORT-TERM EFFECTS"

### (1) *Variance of daily variation :*

A useful criterion for studying the magnitude of daily variation is the variance which we define as

$$V = \sum_x (\delta I_x)^2$$

where  $(\delta I_x)$  is the percent deviation from the day's mean for the bi-hour  $x$ .  $V$  is a gross measure of the daily variation on any particular day without any reference to the phase of the daily variation, and apart from the contribution due to random statistical fluctuations, is a good measure of the average disturbance.

Variances have been calculated for the world-wide isotropic neutron intensities  $W$  and  $W'$  as also for the neutron intensities at Climax, Gottingen, Lincoln and Yakutsk. The frequency distributions of  $V$  for the period July 1957 to June 1958 are shown in Fig. 5. It will be seen that the variance of the apparent daily variation of  $W$  or  $W'$  is not negligible and there is an indication that a portion of the daily varia-

\* Recently, Parsons (year?) has attempted to estimate the U.T. contribution to the monthly average daily variation curves for the experimental data of several high latitude neutron monitor stations.

tion observed on individual days is attributable to curvature and short-term effects.

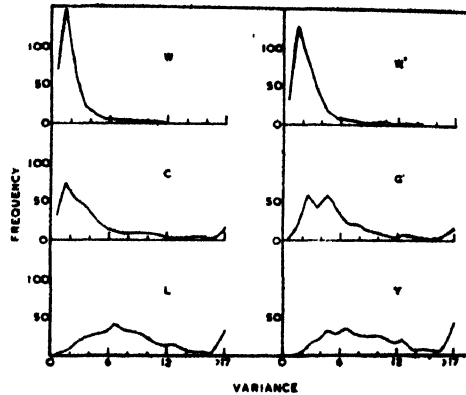


Fig. 5. Frequency distributions of variances for  $W, W',$  Climax ( $C$ ), Lincoln ( $L$ ), Gottingen ( $G$ ) and Yakutsk ( $Y$ ).

(2) *Amplitudes and times of maxima of daily variation :*

A convenient way of studying the daily variation vector is to resolve the 12 bi-hourly values into the first and second harmonics by the usual methods of Fourier analysis. This can be done either for individual days or for averages over a number of days. It would be interesting to see how much of the daily variation on individual days is contributed by short-term and curvature effects. To study this, the percentage bi-hourly deviations for the intensity  $W$  and  $W'$ , treated by method C, were harmonically analysed for every day for which full data were available during July 1957 to June 1958. Fig. 6 shows the frequency distributions for  $r_1, r_2, \phi_1$  and  $\phi_2$  i.e., the amplitudes and times of maxima of the first and second harmonics. For comparison, similar distributions for neutron intensity at Climax, Lincoln, Gottingen and Yakutsk for the same period, are shown. It will be noticed that the amplitudes  $r_1$  and  $r_2$  for  $W$  and  $W'$  are not negligible compared to those for Climax, etc. This confirms our earlier conclusion drawn from the variance distribution that the daily variation on individual days is partly due to short-term and curvature effects as depicted by  $W$  and  $W'$ . It must be emphasised here that these apparent amplitudes cannot be attributed to random statistical fluctuations. From the known bi-hourly counting rates at the various stations, the Poisson standard errors of the amplitudes on individual days can be calculated. The  $2\sigma$  levels are indicated in Fig. 6 by vertical dotted lines in the  $r_1, r_2$  frequency distributions. It will also be observed that the distribution of the times of maxima for  $W$  and  $W'$  shows, as expected, no preference for any particular hours,

while for Climax, etc., directions near local noon are favoured most for the first harmonic.

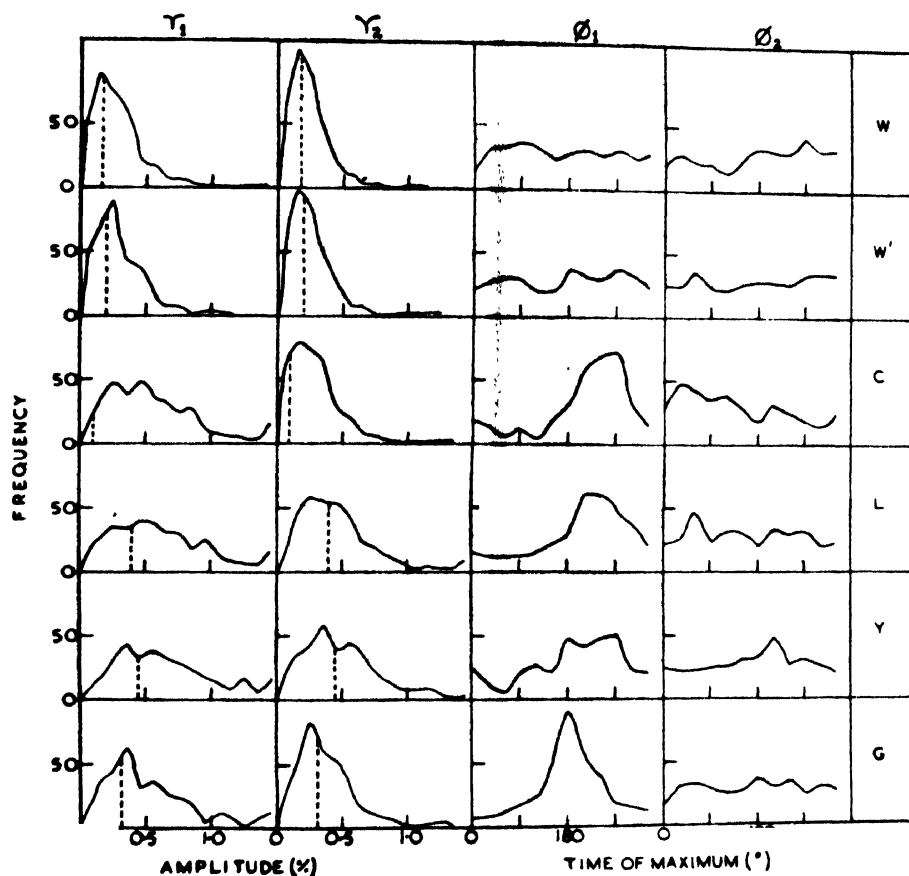


Fig. 6. Frequency distributions for the amplitudes ( $r_1$ ,  $r_2$ ) and times of maxima ( $\phi_1$ ,  $\phi_2$ ) of the first and second harmonics for  $W$ ,  $W'$ , Climax, Lincoln, Göttingen and Yakutsk. Vertical dotted lines in  $r_1$ ,  $r_2$  distributions are  $2\sigma$  limits.

### (3) Monthly mean daily variation :

It will be interesting to estimate the contribution of the apparent daily variation when averages over groups of days are considered. Table IV gives the amplitudes and the times of maxima of the 1st and 2nd harmonics of the monthly average daily variations for  $W$ ,  $W'$  and Climax for July 1957 to June 1958. It will be seen that the monthly averages for  $W$  and  $W'$  are not negligible. The amplitudes for  $W$  and  $W'$  are about  $\frac{1}{3}$ rd of those for Climax for individual months but less than  $\frac{1}{5}$ th for the yearly averages. It is clear, therefore, that the apparent daily variation depicted by  $W$  and  $W'$  progressively reduces in amplitude

TABLE IV

Month	W			W'			Climax					
	$r_1(\%)$	$\phi_1$	$r_2(\%)$	$\phi_2$	$r_1(\%)$	$\phi_1$	$r_2(\%)$	$\phi_2$	$r_1(\%)$	$\phi_1$	$r_2(\%)$	$\phi_2$
July, 1957	0.12	$\pi + 65^\circ$	0.06	$\pi + 34^\circ$	0.13	$\pi + 94^\circ$	0.08	$\pi - 7^\circ$	0.36	$\pi + 57^\circ$	0.13	$30^\circ$
August	0.14	$\pi - 21^\circ$	0.09	$\pi + 32^\circ$	0.16	$\pi + 47^\circ$	0.05	$\pi - 53^\circ$	0.49	$\pi - 54^\circ$	0.08	$68^\circ$
September	0.04	$135^\circ$	0.08	$\pi + 50^\circ$	0.03	$\pi + 45^\circ$	0.06	$\pi + 59^\circ$	0.57	$\pi + 32^\circ$	0.13	$103^\circ$
October	0.02	$90^\circ$	0.05	$\pi + 53^\circ$	0.02	$27^\circ$	0.06	$\pi + 45^\circ$	0.37	$\pi + 54^\circ$	0.03	$135^\circ$
November	0.07	$27^\circ$	0.08	$\pi + 90^\circ$	0.05	$-11^\circ$	0.08	$\pi - 67^\circ$	0.42	$\pi + 43^\circ$	0.12	$96^\circ$
December	0.12	$95^\circ$	0.02	$\pi - 27^\circ$	0.09	$117^\circ$	0.02	$\pi - 90^\circ$	0.09	$\pi + 20^\circ$	0.07	$21^\circ$
January, 1958	0.03	$\pi + 71^\circ$	0.03	$\pi - 18^\circ$	0.09	$144^\circ$	0.04	$56^\circ$	0.34	$\pi - 73^\circ$	0.06	$15^\circ$
February	0.15	$53^\circ$	0.05	$\pi + 37^\circ$	0.06	$-9^\circ$	0.07	$-34^\circ$	0.48	$-34^\circ$	0.13	$156^\circ$
March	0.06	$\pi - 9^\circ$	0.04	$\pi + 27^\circ$	0.09	$\pi + 32^\circ$	0.02	$\pi - 63^\circ$	0.23	$\pi + 76^\circ$	0.07	$-7^\circ$
April	0.04	$-27^\circ$	0.07	$-63^\circ$	0.05	$-53^\circ$	0.05	$-79^\circ$	0.34	$\pi + 72^\circ$	0.05	$130^\circ$
May	0.03	$109^\circ$	0.05	$-53^\circ$	0.06	$\pi - 9^\circ$	0.04	$-56^\circ$	0.29	$\pi + 91^\circ$	0.06	$139^\circ$
June	0.12	$104^\circ$	0.05	$-90^\circ$	0.10	$151^\circ$	0.03	$-45^\circ$	0.49	$-56^\circ$	0.09	$86^\circ$
Yearly average	0.03	$108^\circ$	0.04	$\pi + 63^\circ$	0.03	$\pi - 18^\circ$	0.03	$\pi - 90^\circ$	0.32	$\pi + 69^\circ$	0.06	$83^\circ$



when averages over large periods (about an year) are obtained. For smaller periods, considerable distortions can occur.

- (4) *Contribution of the apparent daily variation to averages over groups of days selected on physical criteria :*

For studying solar and geomagnetic relationships of the daily variation, the usual procedure is to select groups of days according to certain criteria and evaluate the average daily variations. For example, one could compare average daily variations on magnetically disturbed and quiet days. One could attempt to find correlated changes between daily variation and daily mean intensity and so on. Several workers have reported results of these types in the past.

It must be noted, however, that in some of these criteria the days selected are such that they are associated with large gradients and curvatures of cosmic ray intensity. For these, the apparent daily variation due to curvature and short-term effects is expected to be large. A preliminary analysis conducted by us for groups of days selected on the usual geomagnetic criteria has indicated that many of the characteristics reported for daily variation for days conforming to such criteria are shown to some extent by the apparent daily variation also. This does not exclude the possibility that such characteristics will be depicted by genuine daily variation. It needs to be confirmed, however, that such characteristics are still shown when the observed daily variation is corrected for effects due to the apparent daily variation.

It must be pointed out here that the estimates of the apparent daily variation due to short-term and curvature effects as given above are only for middle latitude, neutron monitor intensities. The effects are roughly proportional to the range of fluctuations of cosmic ray intensity. Since the daily mean intensities of neutron component and meson component at equator show fluctuations about  $\frac{1}{2}$  and  $\frac{1}{3}$  to  $\frac{1}{4}$  respectively of the mean intensity fluctuations of neutron intensity at middle latitudes, it would seem that the distortions due to apparent daily variation would be lesser in the above proportions for equatorial neutrons and mesons. This will certainly be true for curvature effects which are of periodicities greater than 24 hours. For short-term fluctuations, it requires to be checked whether hour-to-hour changes of world-wide isotropic intensities have also the same latitude dependence as fluctuations of daily mean intensity.

#### VII. METHOD OF STUDYING THE GENUINE DAILY VARIATION OF COSMIC RAY INTENSITY

It is clear from the above discussion that the daily variation of cosmic ray intensity can be in error when studied for short periods from the data of only one

station. The results will be distorted due to the presence of an apparent daily variation due to world-wide fluctuations of isotropic intensity. The magnitude of the latter can be estimated by combining data from three or more stations at roughly the same geomagnetic latitude and equally spaced in geographical longitudes. On the other hand, to eliminate the contribution of the apparent daily variation and to study the genuine daily variation of cosmic ray intensity, it would be necessary to subtract the world-wide intensity fluctuations from the original data of any one station. To give a specific example, we have, in the present communication, combined the data from the stations Climax, Gottingen and Yakutsk for similar bi-hourly intervals (U.T.) to obtain the series  $W$ . One could now subtract the bi-hourly values of  $W$  from the bi-hourly values of Climax, Gottingen or Yakutsk for the same U.T. and obtain series of bi-hourly values which, when considered according to the local time of the particular station, would give the basic 12 bi-hourly values for study of the daily variation. To improve the statistics, one could superimpose the local time bi-hourly values of the three stations. On the other hand, since the daily variation may be of a transient nature, one may prefer to study the data obtained for the three stations individually and observe the 8 hourly changes in the nature of the daily variation. Such an analysis may prove very fruitful for studying the influence of S.C. storms as well as solar flares which are comparatively of short duration.

It is necessary, however, to discuss at this stage the merits and demerits of this method for all aspects of the study of daily variation. The necessity of adopting the present method arises from the existence of short-term and long-term world-wide changes in the mean level of isotropic cosmic ray intensity. Also, its success depends upon its ability to eliminate these changes without eliminating a genuine daily variation. This is achieved if the genuine daily variation is of a constant pattern. In practice, however, one is likely to encounter complex patterns of daily variation. It is necessary to study in detail the various types of effects that one may observe in daily data. Since the basic data are averaged over a bi-hourly interval, we will consider bi-hourly percent deviations as our basic unit. Samples of various cases are illustrated in Fig. 7, where  $C$ ,  $G$  and  $Y$  represent bi-hourly values at Climax, Gottingen and Yakutsk respectively, for the same U.T. indicated on abscissa, and  $W$  represents the average given by

$$W = \frac{1}{3} (C + G + Y)$$

- (i) Climax, Gottingen and Yakutsk all show a positive (or negative) bi-hourly deviation of the same magnitude at a particular bi-hourly interval. Then  $W$  will also show a similar deviation at the same hour. This is illustrated in Fig. 7(i) and is a true world-wide effect with magnitudes remaining the same for  $C$ ,  $G$ ,  $Y$ , as also for  $W$ .

- (ii) Climax shows a bi-hourly deviation at a particular hour U.T. and Gottingen and Yakutsk show the same deviation but 8 and 16 hours

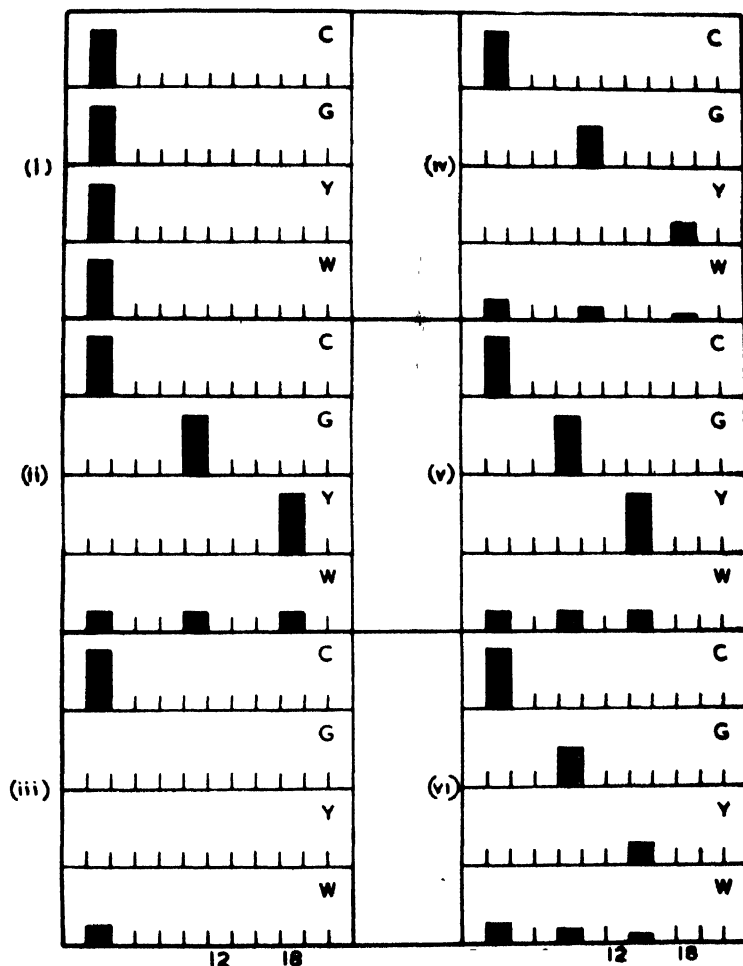


Fig. 7. Sample patterns of bi-hourly deviations for Climax (C), Gottingen (G), Yakutsk (Y) and their average (W).

later respectively. This is a genuine L.T. daily variation effect. It is illustrated in Fig. 7 (ii) and its effect on W will be to produce three humps 8 hours apart and 1/3rd in size. If harmonically analysed, the W curve for such a day will show an absence of 1st, 2nd, 4th and 5th harmonic. The 3rd and 6th harmonics will be present.

- (iii) Climax shows a bi-hourly deviation at a particular hour U.T. but Gottingen and Yakutsk do not show any effect at this hour or 8 and 16 hours later. This is an impact zone type effect where Climax was in a location suitable for observing the effect but Gottingen and

Yakutsk were not. This is illustrated in Fig. 7 (iii) and produces a deviation in  $W$  of magnitude about 1/3rd of that at Climax. This could as well occur at Gottingen or Yakutsk and in each case,  $W$  curve will be biased towards that station.

It should also be noted that for individual bi-hourly values, such an impact zone effect cannot be distinguished from high positive or negative deviations occurring at different stations at certain hours due to instrumental troubles unless data from stations in about the same geographical region and altitude are available for comparison.

- (iv) Climax shows a bi-hourly deviation at a particular hour U.T. and Gottingen and Yakutsk show reduced or negligible amplitudes 8 and 16 hours later. This is a genuine daily variation, the amplitude of which is changing rapidly, during the course of a few hours [Fig. 7 (iv)]. In this case, the various harmonics will not cancel out in the average curve  $W$ . In fact,  $W$  will show roughly the same type of variation as in (iii) above.
- (v) Climax shows a bi-hourly deviation at a particular hour U.T. and Gottingen and Yakutsk show the same amplitudes but not 8 and 16 hours later, but somewhat earlier [Fig. 7(v)]. This is a case where a genuine daily variation is constant in amplitude but has a *changing phase*. Here again, the daily variation will not cancel out in  $W$  but will leave a residual variation of about 1/3rd amplitude. In extreme cases where phase shifts are very large, the effect in  $W$  could be comparable in magnitude to that at Climax or Gottingen or Yakutsk.
- (vi) One could imagine cases where both the amplitudes and phases change rapidly in the course of a few hours as in Fig. 7(vi). Here again the maximum amplitude in  $W$  would be lesser than the maximum disturbance among the three stations.

If now an attempt is made to study the genuine daily variation by subtracting  $W$  curve from the  $C$ ,  $G$  and  $Y$  curves and considering  $(C-W)$ ,  $(G-W)$  and  $(Y-W)$  as representative of the *genuine* daily variations for Climax, Gottingen and Yakutsk respectively, the following will happen :

- (i) The genuine daily variation so obtained will be completely free from any distortion effects due to *world-wide* changes of cosmic ray intensity. This will be true for individual bi-hourly values and hence for all the harmonics of a daily variation.
- (ii) If the daily variation is constant in amplitude and phase for more than 24 hours, this method will give correct results for the 1st, 2nd, 4th and 5th harmonics. The 3rd and 6th harmonics will, however, be missing. For individual bi-hourly deviations, this method will show such deviations reduced to about 2/3rd of their original values.

- (iii) If the genuine daily variation is of a rapidly changing pattern, the effect of the present method will be again to reduce the amplitudes to about 2/3rd of their original values. This will roughly be true for bi-hourly deviations as also for the various harmonics. In the case of the latter, distortions in phases would also be expected.
- (iv) All abnormalities like impact zone effects or bi-hourly deviations due to faulty data will be reduced to about 2/3rd of their original values.

Therefore, while taking a decision as to whether one should study daily variation of cosmic ray intensity by the present method or by the usual method C adopted for individual stations, one has to choose between two alternatives viz., to eliminate world-wide short-time fluctuations of cosmic ray intensity but in this process to reduce the amplitudes of the rapidly changing portion of daily variation to about 2/3rd of its original amplitude or, to retain fully all genuine daily variation but allow distortions due to world-wide short term fluctuations of isotropic intensity. Such a decision would largely depend upon the relative magnitudes of the genuine daily variation and the apparent daily variation produced by short-term world-wide fluctuations. It would be worthwhile getting an estimate as to how often world-wide short term fluctuations occur in a given data. For this purpose the data for  $W$  as described in the present paper were considered as follows:

Since the Poisson bi-hourly standard errors of Climax, Gottingen, Yakutsk and  $W$  are 0.12%, 0.41%, 0.56% and 0.24% respectively, amplitudes of about 0.3% and 0.5% or more, are significant on a  $2\sigma$  level (95% surety) for Climax and  $W$  respectively, but not for Gottingen and Yakutsk. However, since the standard error of *Gottingen plus Yakutsk* is about 0.69%, a value of 1.4% or more for this *sum* would be significant on a  $2\sigma$  level. Hence, days were selected on which at least one bi-hourly deviation for  $W$  exceeded 0.5% numerically. Such days were termed as disturbed days. Now,  $W$  is related to Climax, Gottingen and Yakutsk as

$$W = \frac{1}{3}(C + G + Y).$$

Therefore, it was further examined whether a particular large bi-hourly deviation of  $W$  was largely due to  $C$  (Climax) or due to Gottingen and/or Yakutsk or due to all the three. The following categories were obtained :

Category (a): ( $W$ due to world-wide isotropic change.)	For positive $W$ values, (i) $W \geq +0.6\%$ (ii) $C \geq +0.3\%$ (iii) $(3W - C) > +1.4\%$	For negative $W$ values, (i) $W \leq -0.6\%$ (ii) $C \leq -0.3\%$ (iii) $(3W - C) < -1.4\%$
Category (b): ( $W$ attributable to Climax only)	For positive $W$ values, (i) $W \geq +0.6\%$ (ii) $C \geq +0.3\%$ (iii) $(3W - C) < +1.4\%$	For positive $W$ values, (i) $W \leq -0.6\%$ (ii) $C \leq -0.3\%$ (iii) $(3W - C) > -1.4\%$
Category (c): ( $W$ due to Gottingen and/or Yakutsk only)	For positive $W$ values, (i) $W \geq +0.6\%$ (ii) $C < +0.3\%$	For negative $W$ values, (i) $W \leq -0.6\%$ (ii) $C > -0.3\%$

On actually separating out the experimental data by the above criteria, the following statistics were obtained:

Total No. of days for which data were available	...	...	318
Total No. of days on which not a single bi-hourly for <i>W</i> exceeded 0.5% numerically (Quiet days)	...	...	61
No. of disturbed days	...	...	257
No. of days of Category (a) ( <i>W</i> world-wide)	...	...	121
No. of days of Category (b) ( <i>W</i> Climax-dominated)	...	...	94
No. of days of Category (c) ( <i>W</i> dominated by Gottingen or Yakutsk)	...	...	178

It is obvious, however, that many days are common to the three categories (a), (b) and (c). A further breakdown was therefore attempted and yielded the following results:

Total No. of disturbed days.	...	...	...	...	257
Category A :	Days on which one or more bi-hourly deviations of <i>W</i> were due to all the three stations (exclusive world-wide effect)	...	...	...	39
Category B :	Days on which one or more bi-hourly deviations of <i>W</i> could be attributed to Climax <i>exclusively</i> ...	...	...	...	28
Category C :	Days on which one or more bi-hourly deviation of <i>W</i> could be attributed <i>exclusively</i> to Gottingen and/or Yakutsk.	...	...	...	80
Category D :	Days on which some bi-hourly deviations were due to Climax and some due to world-wide effect. (a)+(b) category.	...	...	...	12
Category E :	Days on which some bi-hourly deviations were due to Climax and some due to Gottingen and/or Yakutsk. (b)+(c) category.	...	...	...	28
Category F :	Days on which some bi-hourly deviations were due to world-wide effect and some due to Gottingen and/or Yakutsk. (a)+(c) category.	...	...	...	44
Category G :	Days on which some bi-hourly deviotions were due to Climax, some due to world-wide effect and some due to Gottingen and/or Yakutsk. (a)+(b)+(c) category.	...	...	...	26
Total (A + .....G)					257

It seems, therefore, that almost all types of variations are present in the data in various degrees. Thus, categories B, C and E are solely due to fluctuations at Climax, or Gottingen or Yakutsk. Due to lack of statistical accuracy, it is impossible to judge which of these are due to genuine daily variation of constant pattern and which are due to genuine daily variation of rapidly changing pattern. Also, all impact zone effects as well as abnormal fluctuations due to faulty data

would be included here! Category A represents days *exclusively* of the world-wide type while categories D, F and G are of a world-wide as well as individual type, category G having the utmost disturbance.

The effect of each one of these categories on the results of daily variation studied by the present method is already discussed above. It would be interesting to see what is the contribution of these to the amplitudes of the first harmonic of daily variation of  $W$ . Since frequency distribution for a few days would not be very meaningful nor are the categories completely unambiguous, the various categories referred to above were grouped as follows:

Group 1...Category B, C, E ... Days 136

Group 2...Category A, D, F, G ... Days 121

Fig. 8 shows the frequency distribution of  $r_1$ , the first harmonic of the daily variation of  $W$  for the two groups. It will be seen that the amplitudes of Group 1 which contains effects on  $W$  of L.T. variations at all the three stations as also impact zone and faulty data effects, are confined to lower magnitudes than the amplitudes of Group 2 which represents world-wide fluctuations.

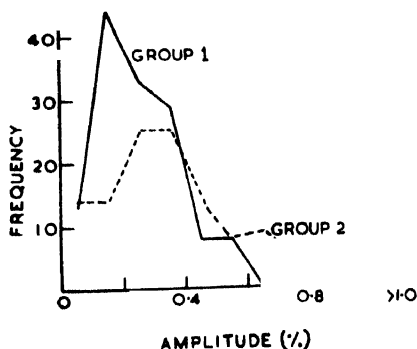


Fig. 8. Frequency distribution of the amplitude of first harmonic ( $r_1$ ) of  $W$  for Groups 1 and 2.

It would seem, therefore, that on almost half the number of disturbed days (121 in 257), the large values of  $W$  are either fully or partly due to world-wide effects which can produce apparent amplitudes as large as 0.5% for the first harmonic of daily variation. It would hardly be necessary to emphasise the necessity of correcting for this effect by subtracting  $W$  from the individual stations. On the other hand, such a procedure would reduce the amplitudes of the changing type of daily variation for 218 days (Categories B, C, D, E, F, G) to about 2/3rd of their original values. For many of these days, the amplitudes will be due to instrumental faults, because as shown in an earlier publication (Kane, 1960), many of the I.G.Y. neutron monitor stations have discrepancies of the order of 1—2% in their bi-hourly values. Also, there will be no reduction in amplitude or

distortions of phase for the 1st, 2nd, 5th and 6th harmonics if the genuine daily variation has not changed its pattern radically during the course of a day. The reduction will be only for genuine daily variation patterns which change rapidly within a few hours. Due to statistical uncertainties, it is impossible to estimate the number of days on which only such patterns existed.

The choice is, therefore, between allowing apparent daily variations of amplitudes as high as 0.5% to distort the genuine daily variation or to eliminate the apparent variation and in this process, reduce the amplitudes of genuine daily variations of rapidly changing patterns to about 2/3rd their original value. The present author feels that the latter would be the lesser evil. The reduction effect given by  $\left(1 - \frac{1}{m}\right)$  when  $m$  = Number of stations could be greatly minimised if data from more than three stations equally spaced in geographic longitude and confined to roughly the same geomagnetic latitude were available for analysis. Unfortunately, in the grid of I.G.Y. neutron monitor stations, it is difficult to pick out even groups of three equally spaced stations. The best one can do is to concentrate on groups like Climax (or Lincoln), Gottingen, Yakutsk and to study the daily variation after subtracting from each one of these the corresponding  $W$  curve. Work in this direction is in progress.

### VIII. CONCLUSION

The results of the present analysis may be summarised as follows :

- (1) Except for studying averages over very long periods (about an year), it is necessary to apply corrections for the slope, curvature and short term effects due to world-wide fluctuations of mean cosmic ray intensity.
- (2) The slope effects can be effectively corrected for by assuming linear changes as done in method B or method C. The curvature effects are difficult to correct but are fortunately of a small magnitude ( $\sim 0.2\%$ ). The short-term world-wide effects are the most important ones, on occasions, as large as 0.5% for neutrons at middle latitudes, and cannot be corrected for unless data from stations in the same geomagnetic latitude belt and equally spaced in geographic longitude are available.
- (3) For studying only the first harmonic of daily variation, two stations  $180^\circ$  apart are adequate. If, however, higher harmonics are to be considered, the number of stations should be at least three. In view of the several complicated patterns of daily variation which are known to exist, the larger the number of stations, the better. Unfortunately, the present distribution of neutron monitor stations in the world is not quite adequate for this purpose. Attention is drawn of active workers



in this field to the gaps in the longitudinal distribution of cosmic ray recording instruments.

- (4) An analysis of data from Climax, Gottingen and Yakutsk indicates that the curve  $W$  obtained as an average of these three, exhibits an apparent daily variation having some characteristics similar to those reported as belonging to the genuine daily variation of cosmic ray intensity. It seems necessary to correct for the apparent daily variation produced due to world-wide fluctuations of isotropic cosmic ray intensity.
- (5) The magnitude of the distortions is directly proportional to the fluctuations of isotropic intensity. Fluctuations of daily mean intensity are roughly in the proportion 1:2 for equatorial and high latitude neutron intensities. Therefore, distortions due to slope and curvature effects would be about half at equatorial stations. For meson intensity the effects would be still less. It is not known, however, whether the short-term (hour-to-hour) fluctuations have the same latitude dependence as the daily mean intensities. This needs further scrutiny.

#### ACKNOWLEDGMENTS

The author is grateful to Prof. V. A. Sarabhai for helpful discussions. Thanks are due to Miss Kundabala and others for computational assistance and to the Atomic Energy Commission of India for financial assistance.

#### REFERENCES

- Kano, R. P., 1960, *Proc. Ind. Acad. Sc.*, **52A**, 69.  
Sekido, Y., Yoshida, S. and Kamiya, Y., 1952, *Rep. Ionos. Res. Japan*, **6**, 195.  
Parsons, N. R., "Phase changes in the daily variation of the cosmic ray nucleonic component" (under publication).

# $F^{19}$ NUCLEAR MAGNETIC RESONANCE IN POLYCRYSTALLINE $MgF_2$

S. K. GHOSH, J. LAHIRI AND S. K. SINHA

SAHA INSTITUTE OF NUCLEAR PHYSICS, CALCUTTA

(Received, February 21, 1961)

**ABSTRACT.** Fluorine ( $F^{19}$ ) nuclear magnetic resonance line shape has been recorded in polycrystalline  $MgF_2$ . The second moment of the recorded line-shape has been compared with that computed from the known lattice structure of  $MgF_2$  crystal as given by X-ray diffraction studies. The agreement is satisfactory.

## 1. INTRODUCTION

The nuclear magnetic resonance (N.M.R.) lines in solid substances are generally broad, and very often show fine structures (Pake, 1948; Gutowsky *et al.*, 1949). Though the prominent fine-structures observed in single crystals are considerably obliterated in polycrystalline samples, the line-shape study in polycrystalline samples can yield significant informations regarding the lattice structures of the crystals concerned (Andrew, 1955).

In general, the energy levels available to a system of nuclear spins placed in a steady external magnetic field  $H_0$ , are sharp when there is no mutual interactions between the nuclear spins. In such cases the absorption lines observed in the usual N.M.R. experiments are also sharp. When the mutual interactions are present, the discrete energy levels described above are spread almost into a continuum, and the populations of these energy levels are mainly determined by the spatial configuration of the nuclear spins in the system. As a result the absorption lines become broad, and their shapes reflect the above spatial arrangement. Thus, in principle, one can test a suggested spatial arrangement of nuclear spins (for example, the lattice structure of a crystal) by computing the expected line-shape with known forms of the mutual interactions between the spins, and comparing it with the observed line-shape in N.M.R. experiments. It is, however, seen (Broer, 1943) that even if only the magnetic dipole interactions between the nuclear spins are considered, the rigorous derivation of the complete line-shape becomes prohibitively complicated when the effective number of the interacting spins is large. In such general cases (distinct from the systems containing strongly interacting pairs) the first and the second moments of the line shape function can be computed easily (Van Vleck, 1948; Pake *et al.*, 1948) and can be compared with that obtained from the experimentally recorded line shape. This method of second moment has been shown (McCall and Hamming, 1959)

to be capable of leading one to establish the correct lattice structure in a single crystal, where one has to start from a plausible structure and change the lattice parameters in a systematic way to fit the observed second moments recorded with different crystal orientations with respect to the external magnetic field.

However, in powdered crystals such studies are obviously not possible. Here the expression for the second moment is to be suitably averaged over all orientations of the crystals with respect to the external magnetic field, and one observes only this averaged second moment. This again can be computed on the basis of a suggested crystal structure and compared with the observed value. Such comparison is quite an efficient method of checking that suggested lattice structure, especially when only the magnetic dipole interaction is predominant.

The present report describes the study of F<sup>19</sup> resonance in MgF<sub>2</sub> powder by the steady N.M.R. method, and a comparison of the second moment thus observed with the value computed from the lattice structure of MgF<sub>2</sub> crystals as given by X-ray diffraction. The agreement is fairly good. In Section II, the results obtained for MgF<sub>2</sub> powder are presented and discussed.

## II. F<sup>19</sup> N.M.R. LINE SHAPE IN MgF<sub>2</sub> POWDER

The steady line shape was recorded in a Varian NMR Spectrometer (V4200B) with the Varian electromagnet system (V2100A). A G-10 recorder was used to record the derivative of the F<sup>19</sup> absorption signal. The precision field scanning dial was calibrated by observing the rotation of the dial required to bring back a proton signal (from H<sub>2</sub>O) when the *rf* was shifted by a known amount. This change in *rf* was measured by a beat method with the help of a standard frequency generator (HP200D) in conjunction with a harmonic generator.

The sample was polycrystalline MgF<sub>2</sub> (B.D.H. analar grade), sealed in a Pyrex glass tube.

The F<sup>19</sup> signal was observed at two different settings of the spectrometer. In both of them the *rf* amplitude, the sweep amplitude and the field scanning rate were kept low enough to avoid extra broadening and distortion of the line. In one set (*rf* ~ 6.6 Mc/sec), the values of the above quantities were ~20 m. gauss, ~0.5 gauss, and ~6 m. gauss/sec. respectively; and in the other (*rf* ~ 10.7 Mc/sec), they were ~30 m. gauss, ~0.5 gauss and ~11 m. gauss/sec. respectively. Fig. 1 shows one of these recorded derivative curves.

Experiments were carried out at room temperature (80°F).

The second moment,  $\langle \Delta H^2 \rangle_{av}$  has been calculated directly from the derivative curves by using the formula

$$\langle \Delta H^2 \rangle_{av} = \frac{1}{3} \left[ \int_{-\infty}^{+\infty} (\Delta H)^3 \frac{dg(\Delta H)}{d(\Delta H)} d(\Delta H) \right] / \left[ \int_{-\infty}^{+\infty} (\Delta H) \frac{dg(\Delta H)}{d(\Delta H)} d(\Delta H) \right] \quad (1)$$

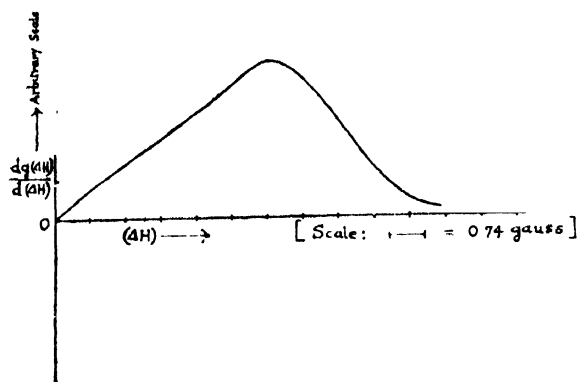


Fig. 1. Derivative of  $F^{19}$  N.M.R. absorption signal from  $MgF_2$  powder.

where  $\Delta H = H^* - H$ ,  $H^*$  being the resonance value of the magnetic field, corresponding to the centre of the line, and  $g(\Delta H)$  is the amplitude of the absorption signal. The average value from nine independently recorded derivative curves (made symmetric by graphical method) has been considered. This value together with the value computed from the lattice structure as given by X-ray diffraction studies (Baur, 1956) is shown in Table I. The X-ray diffraction method shows that a unit cell in  $MgF_2$  crystal can be drawn as shown in Fig (2), with the following values for the lattice parameters :

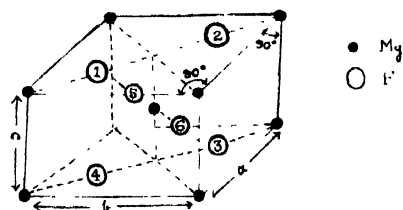


Fig. 2. Unit cell of  $MgF_2$  crystal (X-ray diffraction).

$$a = b = 4.625 \pm 0.002 \text{ \AA}$$

$$c = 3.052 \pm 0.03 \text{ \AA}$$

and the distances of the fluorine atoms from the central magnesium atom are

$$Mg-F(N) = 1.997 \pm 0.005 \text{ \AA}, \text{ for } N = 1, 2, 3, 4$$

$$\text{and } Mg-F(N) = 1.982 \pm 0.007 \text{ \AA}, \text{ for } N = 5, 6$$

$a$ ,  $b$ , and  $c$  are perpendicular to each other.

For computation of the second moment from the above lattice structure the following formula (Van Vleck, 1948) has been used,

$$\langle \Delta H^2 \rangle_{av} = 316.9148(1/m) \sum_{j=1}^{m} \sum_{k=1}^N r_{jk}^2 + 6.960(1/m) \sum_{k=1}^m \sum_{f=1}^N r_{kf}^2 \dots \quad (2)$$

Here 'm' is the number of fluorine atoms in the group that repeats itself throughout the crystal, and N is the total number of fluorine atoms in the sample.  $r(\text{\AA})$  is the radial distance between two nuclei, and 'j', 'k' refer to fluorine nuclei whereas 'f' refers to magnesium nuclei. As is seen from the relation (2), only the magnetic dipole interaction between the nuclear spins has been considered, and the lattice has been assumed rigid. The "exchange interaction" (Bloembergen and Rowland, 1955) between Mg<sup>25</sup> and F<sup>19</sup> has not been considered since its contribution to the second moment is expected to be very small. The second term in Eq. (2) has also not been computed since the natural abundance of Mg<sup>25</sup> is only 10.05% and its magnetic moment is also small compared to that of F<sup>19</sup>. In computing second moment from Eq.(2), only the nearest neighbours at distances less than 10 $\text{\AA}$  have been taken into account. The neighbours further apart will add only a negligibly small contribution.

TABLE I

Second moment  $\langle \Delta H^2 \rangle_{av}$  of F<sup>19</sup> resonance line from MgF<sub>2</sub> powder

	$\langle \Delta H^2 \rangle_{av}$ in gauss <sup>2</sup>
Computed from given lattice structure	8.54
From the recorded N.M.R. line shape	8.5 $\pm$ 0.5

As seen in Table I, the agreement between the observed and the computed second moments is quite satisfactory.

#### ACKNOWLEDGMENT

The authors are thankful to Professor A. K. Saha for kindly going through the manuscript, and for his interest in the work. They are also thankful to Mrs. T. Roy for many of her critical comments.

#### REFERENCES

- Andrew, E. R., 1955, "Nuclear Magnetic Resonance", Chapter 6. The University Press, Cambridge.
- Baur, W. H., 1956, *Acta Cryst.*, **9**, 515.
- Bloembergen, N. and Rowland, T. J., 1955, *Phys. Rev.*, **97**, 1679.
- Broer, L. J. F., 1943, *Physica*, **10**, 801.
- Gutowsky, H. S., Kistiakowsky, G. B., Pake, G. E. and Purcell, E. M., 1949, *J. Chem. Phys.*, **17**, 972.
- McCall, D. W. and Hamming, R. W., 1959, *Acta Cryst.*, **12**, 81.
- Pake, G. E., 1948, *J. Chem. Phys.*, **16**, 327.
- Pake, G. E. and Purcell, E. M., 1948, *Phys. Rev.*, **74**, 1184.
- Van Vleck, J. H., 1948, *Phys. Rev.*, **74**, 1168.

# DECAY OF IONIZATION BELOW THE F-LAYER AT NIGHT

P. BANDYOPADHYAY AND S. K. CHATTERJEE

INSTITUTE OF RADIOPHYSICS AND ELECTRONICS, CALCUTTA UNIVERSITY

(Received, January 31, 1961)

**ABSTRACT.** Titheridge's (1959 *b*) experimental results of variation of the total amount of ionization below the night-time *F*-layer have been re-examined. It has been shown that it is not possible, on the basis of the above results, to discriminate between Titheridge's constant  $\alpha$ -model and Mitra's (1957*a, b*) time dependent  $\alpha$ -model. On other physical grounds, however, it is concluded that while Titheridge's model will possibly hold in the upper part of the region studied, Mitra's model will be valid near the bottom.

## 1. INTRODUCTION

Ionization in the different ionospheric layers below the *F*-region decays rapidly after sunset and as the plasma frequency  $f_N$  of the ionization goes below  $f_{lim}$ , the low-frequency limit of the ionosonde—usually 1.0 mc/s—the ionization can no longer be 'seen' in the ionogram. A residual ionization, however, then persists at these levels throughout the night. Recently, Titheridge (1959*a*) has developed a method of estimating the total amount of this low-lying ionization extending downwards from the bottom of the *F*-layer (where  $f_N$  equals 1.0 mc/s) upto *D*-region heights. He has studied by this method its nocturnal variation over Slough and Watheroo in different seasons and at different epochs of the sunspot cycle. The observed variation of the ionization has been interpreted by Titheridge (1959*b*) to mean that throughout the above height range (200-100 km, roughly) the recombination coefficient remains constant with time around an average value of  $1.9 \times 10^{-8}$  cm<sup>3</sup>/sec.

This conclusion of Titheridge, as applied to the lowermost levels of the above height range, is in contradiction with the recombination coefficient model as suggested by Mitra (1957*a, b*). In the model of Mitra the night-time recombination coefficient,  $\alpha$ , at these heights does not remain constant but decreases with time from about  $3 \times 10^{-8}$  cm<sup>3</sup>/sec. at sunset to  $3 \times 10^{-9}$  cm<sup>3</sup>/sec. at midnight.

It is the purpose of this note to re-examine Titheridge's results on the basis of a possible time variation of the night-time recombination coefficient as in Mitra's model and assumed valid for the whole of the height range in question. It will be shown that the variation of the total amount of the low-lying ionization is insensitive to the  $\alpha$ -model used. Consequently, it is not possible, on the basis of Titheridge's results, to discriminate between his 'constant'  $\alpha$ -model and

Mitra's 'time dependent'  $\alpha$ -model or to find an upper height limit to the range of validity of the latter model. On other physical grounds, however, it can be shown that while Titheridge's model will probably hold for the upper part of the height range in question, Mitra's model will be valid near the bottom.

## 2. INTERPRETATION OF RESULTS

For  $\alpha$  constant in time, the nocturnal variation of the total amount of the low-lying ionization is given by

$$\frac{n(t)}{n(0)} = \frac{1}{1 + \alpha N_0 t} \quad \dots (1)$$

where  $n(t)$  is the value of the total ionization at any time  $t$  and  $n(0)$  the value of the same at sunset ( $t = 0$ ) and  $\alpha N_0$  is assumed constant with height.

Curves marked  $T_1$ ,  $T_2$ , and  $T_3$  in Fig. 1 show this variation for three possible values of  $\alpha N_0$  chosen by Titheridge, namely  $0.5 \times 10^{-3} \text{ sec}^{-1}$ ,  $1.0 \times 10^{-3} \text{ sec}^{-1}$  and  $2.0 \times 10^{-3} \text{ sec}^{-1}$ . His conclusion about constancy of  $\alpha$  with time from sunset to midnight is based on the fact that the different sets of his experimental points

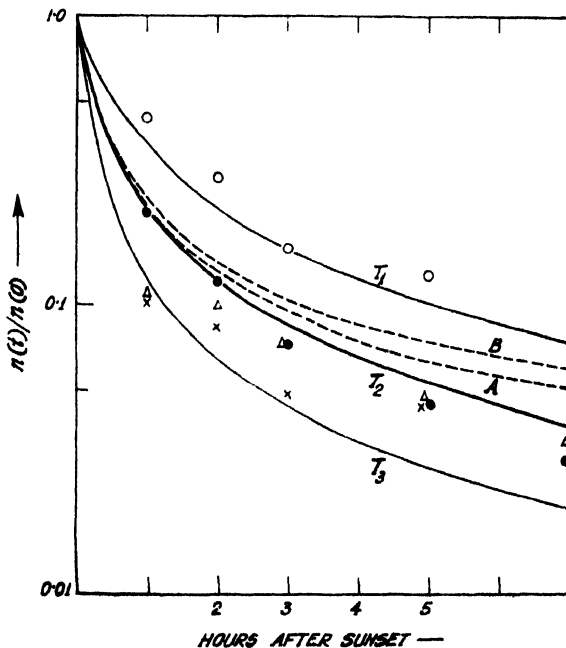


Fig. 1. Relative amount of ionization below night-time F-layer. Solid lines show the variation after Titheridge for three different values of  $\alpha N_0$  when  $\alpha$  is independent of time. Broken lines show the variation for the same initial value of  $\alpha N_0$  as the curve marked  $T_2$  but with  $\alpha$  dependent on time. Open circles, filled circles, triangles, and crosses indicate different sets of experimental values obtained by Titheridge.

(circles, triangles and crosses in Fig. 1) for these hours follow theoretical curves of the above type fairly closely.

When, however,  $\alpha$  is time dependent, we may proceed to calculate the variation of the total amount of the low-lying ionization as follows :

We may put, following Mitra (1954)

$$\alpha = \alpha_0 e^{-pt}$$

or since  $p$  is small

$$\alpha = \alpha_0 - mt \quad \dots (2)$$

where  $\alpha_0$  is the value of  $\alpha$  at sunset.

Integration of the continuity equation,

$$\frac{\partial N}{\partial t} = -\alpha N^2 \quad \dots (3)$$

with  $\alpha$  as given by (2) yields

$$N = \frac{N_0}{1 + \left( \alpha_0 \frac{N_0}{2} \right) N_0 t} \quad \dots (4)$$

where  $N_0$  is the value of  $N$  at sunset. The total amount of the low-lying ionization at any time  $t$  is then given by

$$n(t) = \int_0^{h_1} N dh = \int_0^{h_1} \frac{N_0}{1 + \alpha_0 \frac{N_0}{2} N_0 t - \frac{1}{2} m N_0 t^2} \quad \dots (5)$$

where, as mentioned already,  $h_1$  is the height at which  $f_N = 1.0$  mc/s.

Integration of (5) requires an advance knowledge of the sunset electron density distribution  $N_0$ . First we use a simplified model (broken line curve of Fig. 2) in which in the height range of our interest (200 km-100 km roughly)  $N_0$  is constant. This may be taken as the idealization of an actual profile (full line) given in Fig. 2. Assuming after Titheridge that  $\alpha_0 N_0$  has no height variation

$$\frac{n(t)}{n(0)} = 1 + \alpha_0 N_0 t - \frac{1}{2} m N_0 t^2 \quad (6)$$

The decay of the total ionization represented by Eq. (6) is shown in Fig. 1 (curve marked  $\Lambda$ ).

The value of  $m$  used is  $4.9 \times 10^{-15}$  cm<sup>3</sup>/sec<sup>2</sup>. It is taken from Mitra's (1957a) experimental model based on the critical frequency data of the night-time E-layer at Watheroo.  $\alpha_0 N_0$  is chosen as  $1.0 \times 10^{-3}$ /sec. to correspond to one of Titheridge's curves (marked T2) in Fig. 1. Since Titheridge's average value of  $\alpha_0$  is  $1.9 \times 10^{-8}$  cm<sup>3</sup>/sec. the above choice of  $\alpha_0 N_0$  yields  $N_0$  as  $5.3 \times 10^4$ /cm<sup>3</sup>.



A comparison of the curve marked T2 with that marked A in Fig. 1 shows that for the first few hours after sunset the difference between the two modes of decay—one with 'constant  $\alpha$ ' and the other with 'time dependent  $\alpha$ '—does not become appreciable.

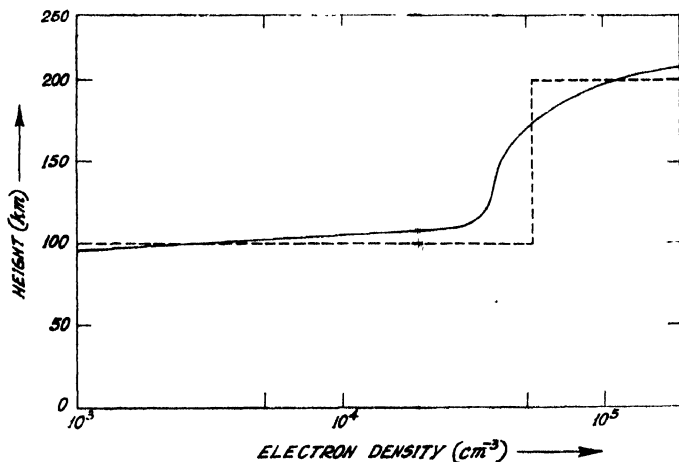


Fig. 2. Electron density distribution at sunset. Broken line curve is the idealization of an actual distribution shown by full line.

Instead of using the idealized profile of Fig. 2 we may take the actual distribution of ionization shown in the same figure. This distribution has been given by Titheridge for Watheroo at 5 minutes before sunset. Taking this to be the sunset distribution we have calculated, using Eq. (4), the ionization profiles at Watheroo for successive hours after sunset. The variation of  $\frac{n(t)}{n(0)}$ , as obtained by numerical integration of these profiles for heights below 200 km, is shown in Fig. 1 (curve marked B). The close agreement between this curve and those marked T2 and A is again noticeable.

Fig. 1 shows that the difference between the modes of decay represented by the curves marked T2, A and B, becomes appreciable only when observations are continued for sufficiently long hours. One may expect, therefore, that data for the later hours may be useful in distinguishing between them. At such hours, however, the situation becomes complicated by the preponderance of another factor, so far neglected, namely, the effect of vertical drift of ionization.

In the preceding calculations we have used Mitra's time-dependent  $\alpha$ -model for the whole of the height range from the bottom of the *F*-layer down to *E*-region heights. But that is just to show the insensitiveness of Titheridge's results to the recombination coefficient model chosen. On physical grounds, however, the time dependent  $\alpha$ -model of Mitra cannot be used much beyond *E*-region heights. Its essential feature, namely, the time-dependence of  $\alpha$ , is due to the

slow emergence of metallic ions of the type  $X^+$  which have a very low value of the recombination coefficient ( $\sim 10^{-12}$  cm<sup>3</sup>/sec). These ions are, most probably, meteoric in origin. Although their distribution with height is not precisely known, it is believed that their concentration will not be appreciable much above 120 or 130 km. In the absence of these ions  $X^+$  in the higher regions, which extend up to the bottom of the  $F$ -layer, electron annihilation at night will take place, as in day-time, through dissociative recombination of the positive molecular ion  $O_2^+$ . For this case, therefore, we may use Mitra's (1959) day-time model, namely,

$$\alpha = \frac{2 \times 10^{-10} n(O_2)}{2 \times 10^{-11} n(O_2) + 1 \times 10^{-8} N}$$

where  $n(O_2)$  is the concentration of neutral oxygen molecules and  $N$  is the electron density.

At first sight, it may appear that here too,  $\alpha$  will be time-dependent because it includes electron-density  $N$ , which is variable. Actually, however, this is not so. The electron density of the low-lying ionization is always small. Hence the term involving  $N$  in the denominator of the above expression for  $\alpha$  will remain negligible compared to the neutral particle density term upto considerable heights. Even at 200 km, near the bottom of the  $F$ -layer, and with  $N$  as  $5 \times 10^4$ /cm<sup>3</sup>, a typical value, the particle density term is more than five times greater than the electron density term. Consequently,  $\alpha$  in this region will be sensibly constant with time.

Finally, therefore, it seems probable that while the recombination coefficient has a substantial night-time variation at  $E$ -region heights up to the level where meteoric contribution to ionization has an appreciable value, in the region above and extending up to the bottom of the  $F$ -layer the coefficient is practically independent of time.

#### ACKNOWLEDGMENTS

The work forms part of the programme of the Radio Research Committee of the Council of Scientific and Industrial Research. We are indebted to Professor J. N. Bhar for advice and to Dr. A. P. Mitra for helpful discussions.

#### REFERENCES

- Mitra, A. P., 1954, Scientific Report No. 68, Ionosphere Research Laboratory, Pennsylvania State University.
- Mitra, A. P., 1957a, *J. Atmosph. Terr. Phys.*, **10**, 140.
- Mitra, A. P., 1957b, *J. Atmosph. Terr. Phys.*, **10**, 153.
- Mitra, A. P., 1959, *J. Geophys. Res.*, **64**, 733.
- Titheridge, J. E., 1959a, *J. Atmosph. Terr. Phys.*, **17**, 110.
- Titheridge, J. E., 1959b, *J. Atmosph. Terr. Phys.*, **17**, 126.

# TRANSMISSION CHARACTERISTICS OF PULSE-SLOPE-MODULATED SIGNALS THROUGH BAND-LIMITED SYSTEMS

J. DAS

INDIAN INSTITUTE OF TECHNOLOGY, Kharagpur

(Received, October 31, 1960)

**ABSTRACT.** Distortion, crosstalk and noise characteristics of P.S.M. have been determined. Maximum harmonic distortion is about 2 per cent for slow cut-off rate of the medium and about 5% for sharp-cut-off filters. Slicers introduce more distortion and non-linearity in modulation. Crosstalk ratios are better than those in P.A.M. for slow cut-off rate and improvement in crosstalk may be affected by simultaneous introduction of h.f. and l.f. cut-offs. Output S/N ratios show considerable threshold effect and are approximately proportional to the square root of the video bandwidth.

## I. INTRODUCTION

The important parameters of a pulse are its amplitude, duration, phase, frequency and slope of the leading and trailing edges. In P.A.M., P.L.M., P.P.M. and P.F.M. systems, the slope is preferably maintained constant at a very high value, whereas in Pulse-slope-modulation (Das, 1954), the slope is varied in accordance with the modulating signal, keeping other parameters constant. The modulating signal is recovered by differentiation and 'Box-car' demodulation

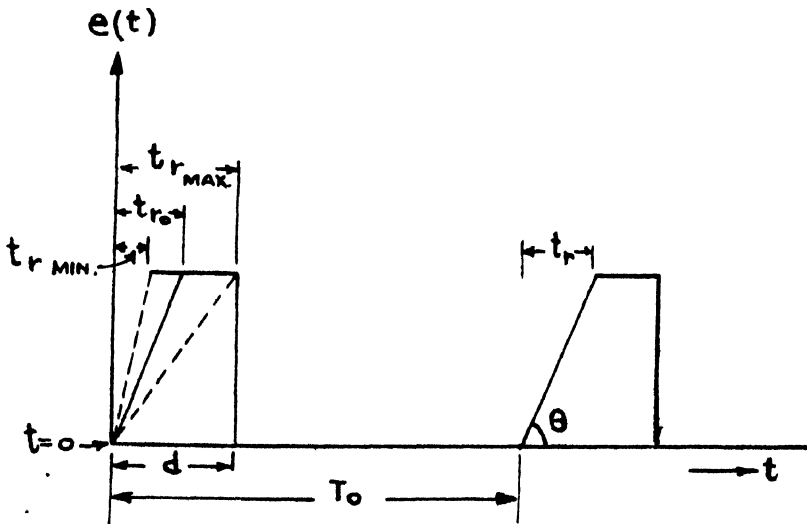


Fig. 1(a). P. S. M. signal. Ch. I.

of the slope-modulated pulses. The frequency spectrum (Das, 1955) of the P.S.M. signal is given by Fig. 1(a) & 1(b):

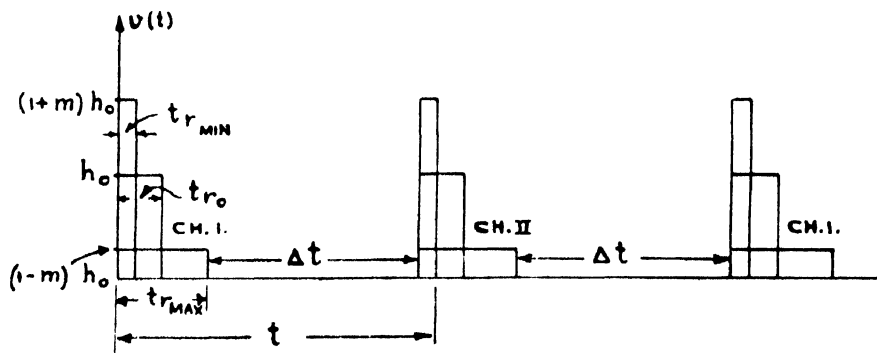


Fig. 1(b) Differentiated signal. Ch. I and Ch. II.

$$F(t) = \frac{Ad}{T_0} - \frac{At_r_o}{2T_0(1+m \sin \phi)} + \frac{2A}{T_0} \sum_{n=1}^{\infty} \frac{\sin \omega n(d-t)}{\omega n} \\ + \frac{2A}{T_0} \sum_{n=1}^{\infty} \frac{(1+m \sin \phi)}{t_r_o \omega^2 n^2} \left[ \cos \omega n \left\{ t - \frac{t_r_o}{(1+m \sin \phi)} \right\} - \cos \omega n t \right] \dots \quad (1)$$

where,

$t_{r_o}$  = mean risetime

$m$  = modulation index =  $\frac{t_{r_{max}} - t_{r_{min}}}{t_{r_{max}} + t_{r_{min}}}$

$\omega = \frac{2\pi}{T_0}$

$E \sin \phi$  = modulating voltage.

The differentiated signal consists of a pulse train containing both amplitude modulation and inverse width modulation, as is seen from

$$F'(t) = \frac{2A}{T_0} \sum_{n=1}^{\infty} -\cos \omega n(t-d) \\ + \frac{2A}{T_0} \sum_{n=1}^{\infty} \frac{(1+m \sin \phi)}{t_r_o \omega n} \left[ \sin \omega n \left\{ \frac{t_r_o}{(1+m \sin \phi)} - t \right\} + \sin \omega n t \right] \dots \quad (2)$$

The inverse width modulation is however cancelled by the use of the 'Box-car' demodulator and the audio output is due only to the amplitude modulation of the differentiated pulses.

Usefulness of a transmission system is determined by the effects of non-ideal circuits and limited bandwidth on its various characteristics—specially audio distortion, crosstalk and noise. These have been discussed here for a P.S.M. system. Since the slope distortion due to limited bandwidth occurs before the 'Box-car' circuit, the effect of both amplitude modulation and inverse width modulation has to be considered for the purpose of determining harmonic distortion and crosstalk. We can generally assume that the system is linear and passive up to the differentiator and on this basis, calculate the theoretical harmonic distortion and crosstalk in the system. For determining the effect of noise, the slope variation only due to noise pulses is calculated for different bandwidths.

The experimental set-up used for the determination of various characteristics had the following specifications (Fig. 2) :

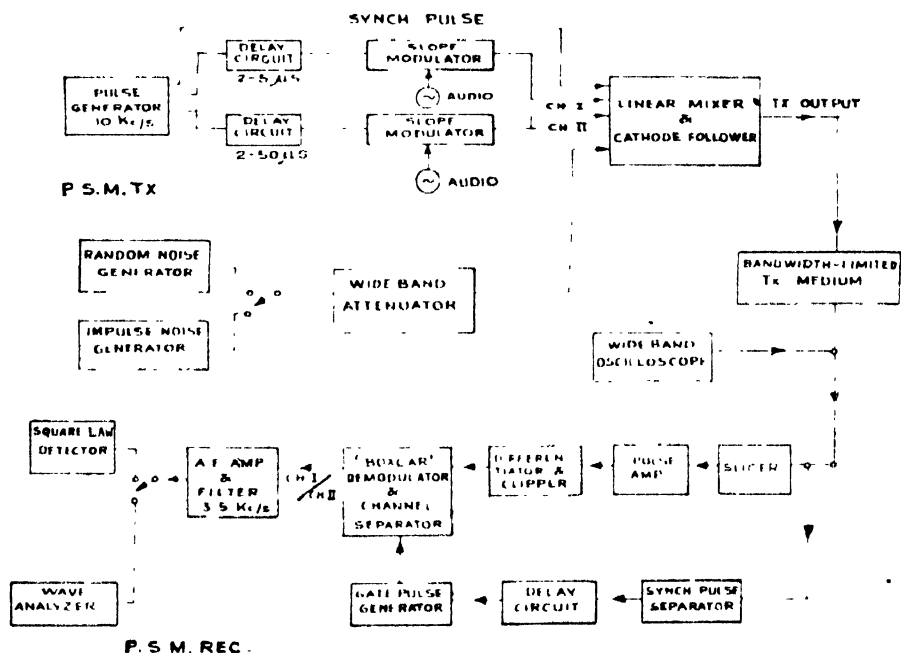


Fig. 2. Experimental set-up—P.S.M. Transmitter and Receiver.

$$\text{P.R.F.} = 10\text{Kc/s.} = 1/T_0$$

$$\text{Pulse duration } d = 2-15 \mu \text{ sec.}$$

$$\text{Mean risetime } t_{r_0} = 1-5 \mu \text{ sec.}$$

$$\text{Delay between Ch. I and Ch. II} = 2-50 \mu \text{ sec.}$$

$$\text{System bandwidth} = 1 \text{ Mc/s.}$$

Audio frequency passband = 0 to 3.5 Kc/s

A.F. modulating frequency = 1 Kc/s.

The modulation was linear for an audio volume range of 40 db. The total harmonic distortion in the received audio output was 2.0% with the peak detector and 0.8% with the 'Box-car' demodulator for a modulation range of 35 db. The inherent crosstalk and noise in the system was approximately 65 db below the signal level.

## II. DISTORTION

Harmonic distortion occurs due to non-ideal differentiators, high frequency cut-off, low frequency cut-off and due to the use of slicers for elimination of noise. An ideal differentiator gives an output amplitude equal to  $\tau_1/t_r$ , where  $\tau_1$  is a constant. But with a simple  $RC$  differentiator, the amplitude of the differentiated pulses is given by

$$V(t) = \frac{\tau_1}{t_r} [1 - \exp(-t/\tau_1)] - \frac{\tau_1}{t_r} \left[ 1 - \exp\left\{-\frac{(t-t_r)}{\tau_1}\right\} \right] \cdot U(t-t_r) \quad \dots (3)$$

where  $U(t-t_r)$  = Unit step function starting at  $t = t_r$ , and  $\tau_1 = RC$  of the differentiator.

It is thus seen that the output signal does not reach its peak value immediately and with large  $\tau_1$ , the peak value will not be reached at all for small values of  $t_r$ . Due to the associated inverse width modulation, the sharper pulses, corresponding to the peaks of the modulating voltage, will be more attenuated than the wider pulses and the resulting audio output will have its peaks flattened. The use of a peak detector then will give rise to pronounced second harmonic distortion. However, with a 'Box-car' pulse-lengthener circuit, the narrow gate pulse is arranged to occur at  $t \leq t_{r_{min}}$  and the amplitude of the output pulses becomes proportional to  $(1/t_r)$ . With gate pulses narrower than the differentiated pulses, the harmonic distortion is very small even for large values of  $\tau_1$ , as shown in Fig. 3. The experimental total distortion for the peak detector, also shown in Fig. 3, agrees sufficiently with the theoretical values calculated from Eq. (3).

A transmission medium with 6db/octave high frequency cut-off rate, simulated by a simple  $RC$ -lowpass filter, gives a differentiated output:

$$V(t) = \frac{\tau_1}{t_r} \left[ 1 - \exp\left(-\frac{t}{\tau_2}\right) \right] - \frac{\tau_1}{t_r} \left[ 1 - \exp\left\{-\frac{(t-t_r)}{\tau_2}\right\} \right] \cdot U(t-t_r) \quad (4)$$

where

$\tau_1$  = differentiation constant;  $\tau_2 = RC$  of the lowpass filter.

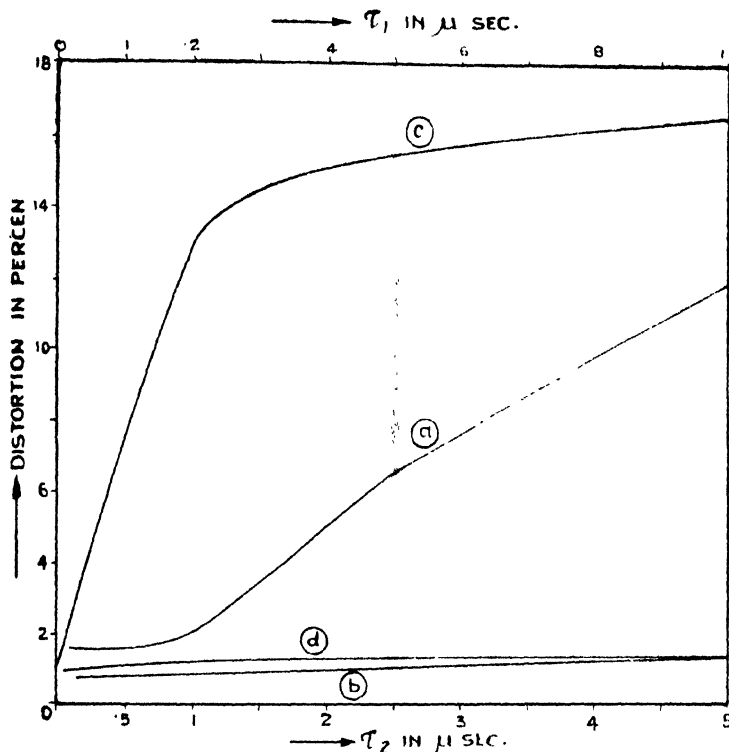


Fig. 3. Experimental total distortion with R-C differentiators and lowpass filters.

$d = 10\mu\text{sec}$ ,  $t_{r0} = 1.8\mu\text{sec}$ ,  $m = 0.82$ , Input level  $-3\text{db}$ .

- (a) For R-C differentiator having different  $\tau_1$  using Peak detector.
- (b) " " " " " " " " 'Box-car' circuit.
- (c) For R-C l.p. filter having different  $\tau_2$  using Peak detector.
- (d) " " " " " " " " 'Box-car' circuit.

As in the case of Eq. (3), the peak amplitude reached by the pulses of different widths will not be proportional to  $\tau_1/t_r$  and with a peak detector, there will be considerable second harmonic distortion. But with a 'Box-car' circuit, arranged to gate at  $t \leq t_{min}$ , the distortion is very much minimised, as is seen in Fig. 3.

With transmission media, having sharp high frequency cut-off, the pulse response is oscillatory and considerable distortion occurs with a peak detector. With the 'Box-car' demodulator circuit, the gate pulse is arranged to occur before the oscillation starts; even then, the amplitude of the output pulses is not strictly proportional to  $\tau_1/t_r$  and there is some distortion in the audio output. The experimental results, as shown in Fig. 4, have been obtained with a variable cut-off electronic filter having 18 db/oct. and 36 db/oct. slopes.

The effect of low frequency cut-off, having sharp as well as slow rate of cut-off, is rather small. Theoretically, the peak amplitude of the differentiated pulses

occurs at  $t = 0$ , and the audio output is distortionless. But with higher cut-off frequency, there is a trailing-edge overshoot (Bhattacharyya, 1953) with distorted

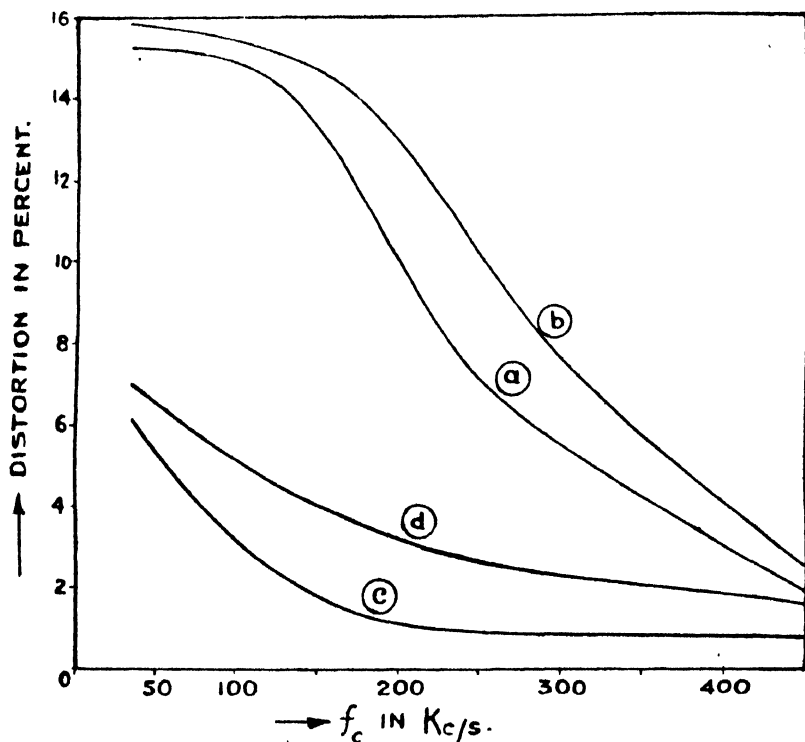


Fig. 4. Experimental total distortion with lowpass electronic filter.

$d = 10\mu\text{sec}$ ,  $tr_0 = 1.8\mu\text{sec}$ ,  $m = 0.82$ ; Input level  $= -3\text{db}$ .

(a) With  $18\text{db/oct}$  cut-off using peak detector.

(b) With  $36\text{db/oct}$  .. .. .

(c) With  $18\text{db/oct}$  .. .. 'Box-car' circuit.

(d) With  $36\text{db/oct}$  .. .. .

modulation on it. With a peak-detector, this gives rise to certain distortion in the audio output, whereas, the 'Box-car' circuit nullifies the effect of the trailing-edge modulation and the output has very little distortion—approximately 1% only for all practical bandwidths.

A slicing circuit introduces some more non-linearity in modulation and harmonic distortion in the audio output. From noise considerations, the slicing level is generally maintained at half the height of the received pulses. Due to slicing, the differentiated pulses are time-displaced and even after 'Box-car' demodulation, some amount of distorted pulse-length-modulation occurs. However, on further analysis, it is found that the overall distortion due to this P.L.M. is always less than 2%.



The distortion caused by the lowpass band-limited system in the sliced output is rather serious. For pulses with small  $t_r$ , the half level is reached much after  $t_r$  and the corresponding slope is less than that attained by the unsliced distorted pulses. This makes it necessary to lower the slicing level such that the slicing time  $t_s \leq t_{rmin}$ . Fig. 5 shows the nature of the distortion obtained at optimum slicing levels corresponding to the different values of  $\tau_2$  and  $f_c$ . For highpass filters, the slicer circuits do not contribute to any further distortion, as has been verified experimentally.

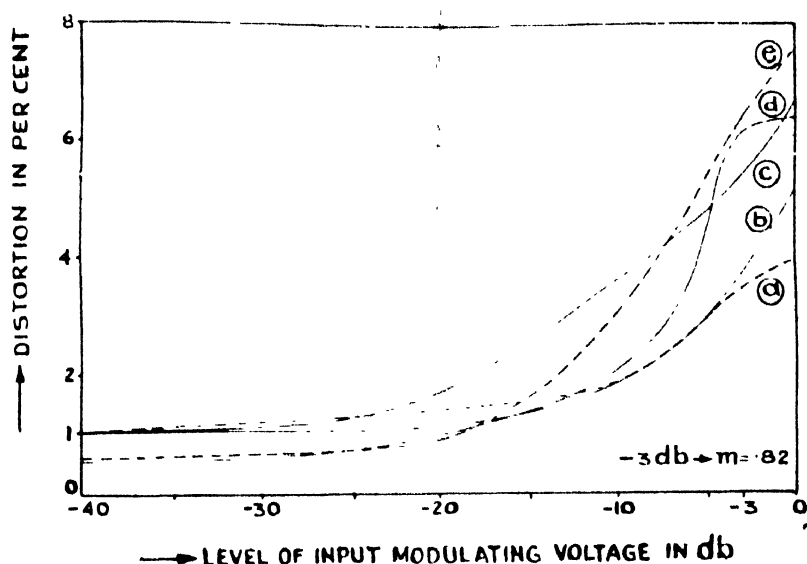


Fig. 5. Experimental total distortion with sliced inputs using 'Box-car' circuit for lowpass filters having different  $\tau_2$  and  $f_c$ .

$d = 10\mu S$ ,  $t_{r0} = 1.8\mu S$ , Input level =  $-3db$  for  $m = 0.82$ .

- (a) With R-C L.p. filter ( $6db/oct$ );  $\tau_2 = 0.5\mu sec$ ;  $h_g = 0.5h_0$ .
- (b) With " " " " "  $\tau_2 = 1\mu sec$ ;  $h_g = 0.36h_0$ .
- (c) With " " " " "  $\tau_2 = 3\mu sec$ ;  $h_g = 0.15h_0$ .
- (d) With electronic l.p. filter,  $f_c = 200$  Kc/s;  
 $18db/oct$  slope;  $h_g = 0.6h_0$ .
- (e) With electronic l.p. filter;  $f_c = 200$  Kc/s;  
 $36db/oct$  slope;  $h_g = 0.6h_0$ .

### III. CROSSTALK

Due to limited bandwidth, amplitude and phase distortion occur to the transmitted pulses and there is normally a carry-over of energy from one pulse to the following pulses. The crosstalk thus developed, may be caused either by high frequency cut-off or by low frequency cut-off. For high frequency cut-off

with 6 db/oct. slope, simulated by an  $R-C$  lowpass filter, the peak-to-peak carry-over voltage is found to be

$$V_0(t) = h_0 \exp\left(-\frac{t}{\tau_2}\right) \left[ (1+m) \left\{ \exp\left(\frac{t_{rmin}}{\tau_2}\right) - 1 \right\} - (1-m) \left\{ \exp\left(\frac{t_{rmax}}{\tau_2}\right) - 1 \right\} \right] \quad \dots (5)$$

where  $h_0$  = mean height of the differentiated pulses.

$\tau_2$  =  $RC$  of the lowpass filter.

The crosstalk ratio is then given by

$$\text{C.T. ratio} = \frac{2m \cdot \exp(t/\tau_2) \cdot \left[ 1 - \exp\left(-\frac{t_{rmin}}{\tau_2}\right) \right]}{\left[ (1+m) \left\{ \exp\left(\frac{t_{rmin}}{\tau_2}\right) - 1 \right\} - (1-m) \left\{ \exp\left(\frac{t_{rmax}}{\tau_2}\right) - 1 \right\} \right]} \quad (6)$$

Since for high frequency cut-off,  $V_0(t)$  decreases rapidly with time, it is only necessary to consider the carry-over voltage from the channel pulse previous to the signal pulse. The numerical evaluation of Eq.(5) shows that  $V_0(t)$  is of opposite phase to that of the signal voltage. The experimental values of crosstalk ratios, with  $d = 10 \mu$  sec,  $t_{r0} = 1.82 \mu$  sec and  $m = 0.82$ , are shown in Fig. 6 for various values of  $\tau_2$  and the channel separation  $\Delta t$ . These results agree closely with values obtained from Eq.(6).

For low frequency cut-off with 6 db/oct. slope, the crosstalk ratio for the carry-over voltage from the single previous channel ( $\tau_3$  small) is given by :

$$\text{C.T. ratio} = \frac{2m \cdot \exp\left(\frac{t - t_{rmin}}{\tau_3}\right)}{\left[ (1+m) \left\{ 1 - \exp\left(-\frac{t_{rmin}}{\tau_3}\right) \right\} - (1-m) \left\{ 1 - \exp\left(-\frac{t_{rmax}}{\tau_3}\right) \right\} \right]}$$

where  $\tau_3 = RC$  of the highpass filter.

The carry-over voltage in this case is found to be of the same phase as that of the signal voltage. The experimental results with small values of  $\tau_3$  are also shown in Fig. 6 and they agree sufficiently with the results of Eq. (7).

As the coupling and decoupling circuits of pulse amplifiers are generally made large, the carry-over voltages from other previous channels have also to be considered to determine the net crosstalk ratio. With certain simplifying assumptions, it is found that the crosstalk ratio now is given by

$$\text{C.T. ratio} = \frac{2m\omega_m\tau_3T_0}{[(1-m)t_{rmax} - (1+m)t_{rmin}]} \quad (8)$$

where  $\omega_m =$  modulating angular frequency  $\ll 1/T_0$ ; and  $T_0 \ll \tau_3$ . This result is similar to that obtained in case of P.A.M. (Flood, 1951). The carry-over voltage now is of opposite phase to that of the signal voltage.

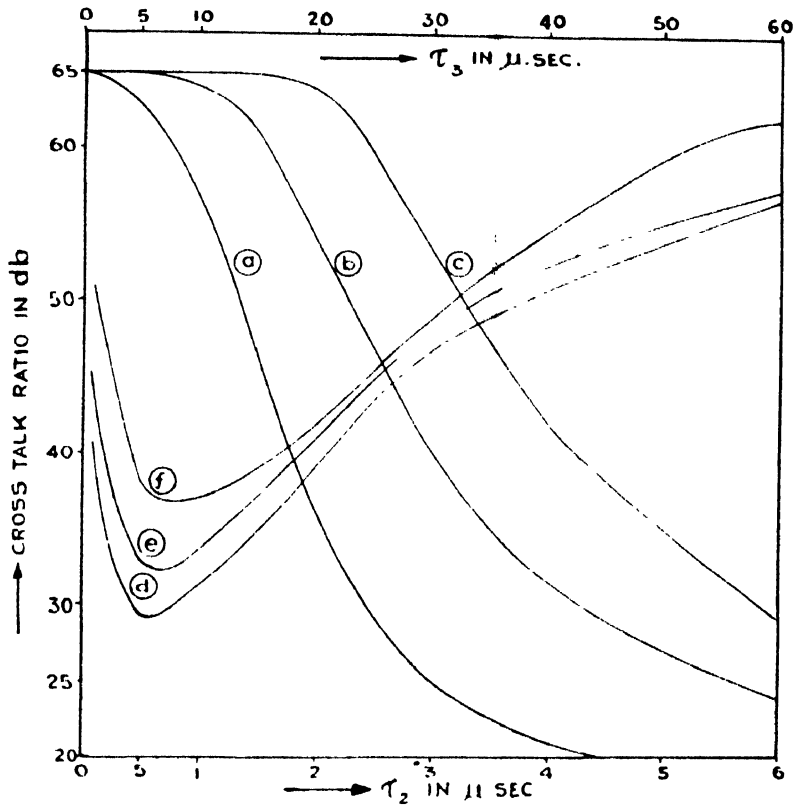


Fig. 6. Experimental crosstalk ratios with R-C filters for various  $\tau_2$ ,  $\tau_3$  and channel separation  $\Delta t$ .

$d = 10 \mu S$ ,  $tr_0 = 1.8 \mu S$ ,  $m = -0.82$ , Input level  $= -3db$ .

(a) For R-C l.p. filter ( $\tau_2$ ) (6db/oct),  $\Delta t = 5 \mu sec$ .

(b) " " " " ,  $\Delta t = 10 \mu sec$ .

(c) " " " " ,  $\Delta t = 15 \mu sec$ .

(d) For R-C h.p. filter ( $\tau_3$ ) (6db/oct),  $\Delta t = 5 \mu sec$ .

(e) " " " " ,  $\Delta t = 10 \mu sec$ .

(f) " " " " ,  $\Delta t = 15 \mu sec$ .

Since with reference to the phase of the signal voltage, the carry-over voltage due to h.f. cut-off is of opposite phase and that due to l.f. cut-off with small

values of  $\tau_3$  is of same phase, it is possible to minimise crosstalk by using simultaneous h.f. and l.f. cut-offs. The crosstalk ratio is now found to be

C.T. ratio

$$= \frac{2m \left[ \exp \left( -\frac{t_{r_{min}}}{\tau_3} \right) - \exp \left( -\frac{t_{r_{min}}}{\tau_2} \right) \right]}{\left\{ (1+m) \left[ \exp \left( -\frac{t}{\tau_3} \right) \left\{ 1 - \exp \left( \frac{t_{r_{min}}}{\tau_3} \right) \right\} - \exp \left( -\frac{t}{\tau_2} \right) \left\{ 1 - \exp \left( \frac{t_{r_{min}}}{\tau_2} \right) \right\} \right] \right.} \\ \left. - (1-m) \left[ \exp \left( -\frac{t}{\tau_3} \right) \left\{ 1 - \exp \left( \frac{t_{r_{max}}}{\tau_3} \right) \right\} - \exp \left( -\frac{t}{\tau_2} \right) \left\{ 1 - \exp \left( \frac{t_{r_{max}}}{\tau_2} \right) \right\} \right] \right\} \dots \quad (9)$$

The C.T. ratio will be maximum for certain relative values of  $\tau_2$  and  $\tau_3$ . It is also possible to forecast the relative values of matching  $\tau_2$  and  $\tau_3$  for a certain channel separation  $\Delta t$ , as is given by

$$\Delta t = \left[ \frac{\tau_2 \tau_3}{\tau_3 - \tau_2} \cdot \ln \left( \frac{D-C}{A-B} \right) \right] - [t_{r_{max}} + t_{r_{min}}] \quad (10)$$

$$\text{where, } A = \frac{(1+m)}{\tau_3} \left[ \exp \left( \frac{t_{r_{min}}}{\tau_3} \right) - 1 \right]$$

$$B = \frac{(1-m)}{\tau_3} \left[ \exp \left( \frac{t_{r_{max}}}{\tau_3} \right) - 1 \right]$$

$$C = \frac{(1+m)}{\tau_2} \left[ 1 - \exp \left( \frac{t_{r_{min}}}{\tau_2} \right) \right]$$

$$D = \frac{(1-m)}{\tau_2} \left[ 1 - \exp \left( \frac{t_{r_{max}}}{\tau_2} \right) \right]$$

Experimental results with simultaneous h.f. and l.f. cut-offs are shown in Fig. 7 and they agree closely with the results of Eq.(9) and of Eq. (10).

The pulse response with sharp cut-off filters is oscillatory (Guillemin, 1935) and the peak-to-peak carry-over voltage, for uniform transmission upto  $\omega_c$ , is given by

$$C_0(t) = \frac{h_0}{\pi} \{ 2m \cdot Si(\omega_c t') + (1+m) \cdot Si[\omega_c(t' - t_{r_{min}})] \\ + (1-m) \cdot Si[\omega_c(t' - t_{r_{max}})] \} \dots \quad (11)$$

where,  $t' = t - t_d = (\Delta t + t_{r_{max}} + t_{r_{min}})$ ;

$-t_d \omega$  = phase shift within the pass band;

$$t_d \cong \pi / \omega_c$$

The crosstalk ratio is now  $|4mh_0f_c \cdot t_{r_{min}}/C_0(t)|$ . The oscillatory nature of the C.T. ratio is shown in the experimental results of Fig. 8, obtained with an electronic filter.

In case of highpass sharp cut-off filters, the crosstalk ratio is given by

$$\text{C.T. ratio} = \frac{2m\pi}{\{(1+m) \cdot \text{Si}[\omega_c(t'-t_{r_{min}})] - (1-m) \cdot \text{Si}[\omega_c(t'-t_{r_{max}})] - 2m \cdot \text{Si}(\omega_c t')\}} \quad \dots (12)$$

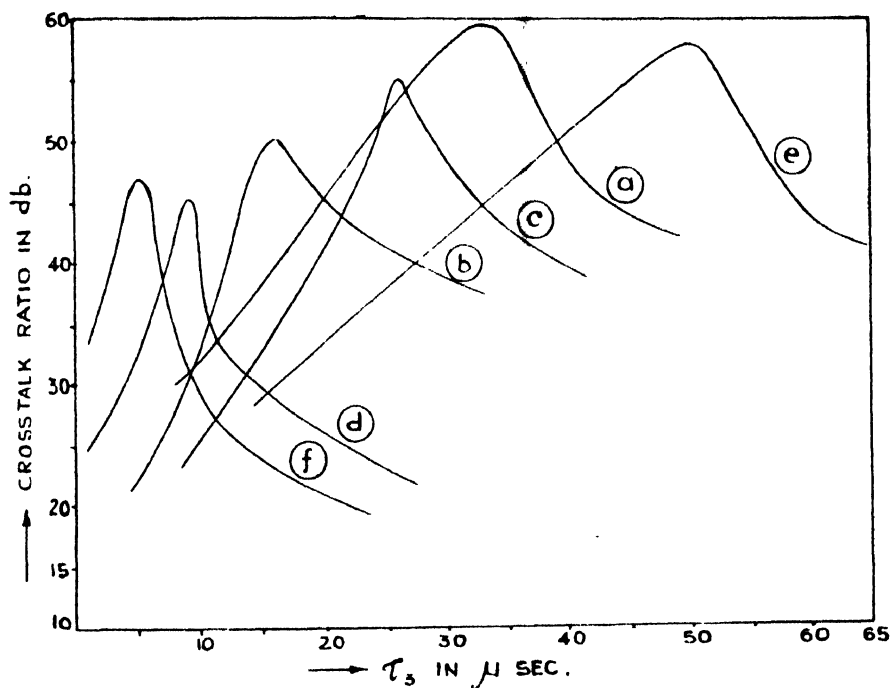


Fig. 7. Experimental crosstalk ratios due to combined H.F. and L.F. cut-off.  
 $\tau_2$  = R-C of l.p. filter;  $\tau_3$  = R-C of h.p. filter;  $d = 10 \mu\text{S}$ ,  $m = 0.82$ .  
 (a)  $\Delta t = 5 \mu\text{S}$ ;  $\tau_2 = 1 \mu\text{S}$  (d)  $\Delta t = 10 \mu\text{S}$ ;  $\tau_2 = 6 \mu\text{S}$   
 (b)  $\Delta t = 5 \mu\text{S}$ ;  $\tau_2 = 2 \mu\text{S}$  (e)  $\Delta t = 15 \mu\text{S}$ ;  $\tau_2 = 3 \mu\text{S}$   
 (c)  $\Delta t = 10 \mu\text{S}$ ;  $\tau_2 = 3 \mu\text{S}$  (f)  $\Delta t = 15 \mu\text{S}$ ;  $\tau_2 = 8 \mu\text{S}$

Here the oscillations start only after the cut-off frequency becomes comparable with the pulse repetition frequency. Since the carry-over voltage due to both highpass and lowpass filters are oscillatory, it is possible to minimise crosstalk by simultaneous use of h.f. and l.f. cut-offs. In Fig. 8, certain minima on the C.T. ratio-curve could be improved to the points  $X_1'$ ,  $X_2'$ , ... etc. by the use of highpass filters having suitable cut-off frequencies. The values of the cut-off frequencies  $f_{c_2}$  for the highpass filters are indicated on the same figure.

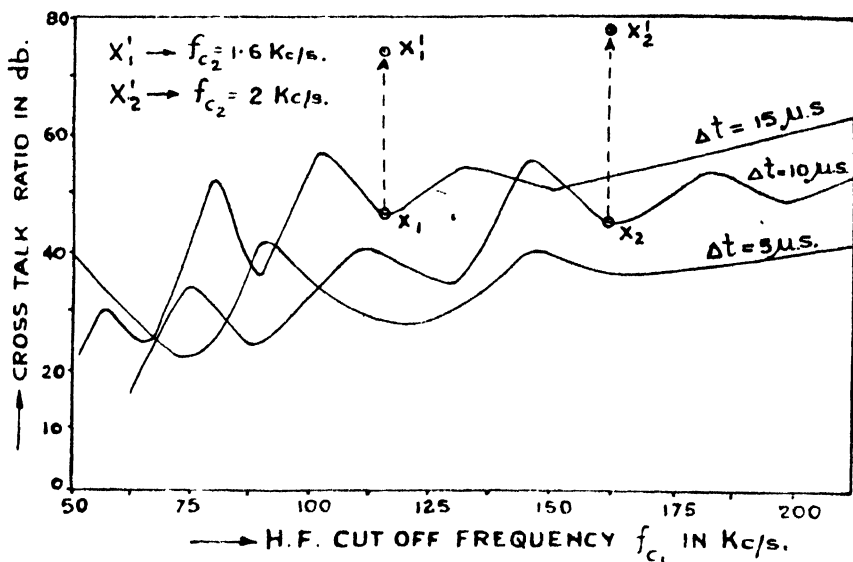


Fig. 8. Experimental crosstalk ratios due to electronic lowpass filter having 18db/oct. slope.

$d = 10\mu s$ ;  $m = 0.82$ ;  $f_{c1}$  = cut-off frequency of l.p. filter.

$f_{c2}$  = cut-off frequency of h.p. filter.

$X'_1$  = Improved C.T. ratio with simultaneous use of l.p. and h.p. filters,

$f_{c2} = 1.6 \text{ Kc/s.}$

$X'_2$  = Improved C.T. ratio with simultaneous use of l.p. and h.p. filters,

$f_{c2} = 2 \text{ Kc/s.}$

When the slicer circuit is used, the slopes contain whatever carry-over voltages already present and the only difference is in the time of differentiation. Due to slicing, the differentiated pulses correspond to the slopes at a time later than  $t = 0$ , but the effective crosstalk ratios are not affected.

#### IV. NOISE

In case of random noise, the effective noise modulation with sharp cut-off media has been shown to be (Das, 1956)

$$(\Delta \tan \theta_N)_{\text{eff.}} = 0.1148 f_o \times N(\text{peak}) \quad \dots (13)$$

where,

$$\Delta \tan \theta_N = (\tan \theta_N - \tan \theta_{(\text{mean})})$$

$N(\text{peak})$  = peak amplitude of noise pulses

$f_o$  = cut-off frequency.

The total audio noise power accepted by the a.f. amplifier is then proportional to

$$(\Delta \tan \theta_N)^2_{\text{eff}} \cdot F_a \propto \left[ \frac{tr_o^2}{T_0^2} + \left( \frac{2}{\pi^2} \right) \cdot \sum_{n=1}^{T_0 f_c} \frac{1}{n^2} \cdot \sin^2 \left( \frac{\pi n t r_o}{T_0} \right) \right] \dots \quad (14)$$

Numerical evaluation of Eq.(14), with  $tr_o = 1 \mu \text{ sec}$ ,  $d = 10 \mu \text{ sec}$ ,  $m = 0.9$ ,  $f_c = 1 \text{ Mc/s}$  and  $F_a = \text{audio passband} = 0 \text{ to } 3.5 \text{ Kc/s}$ , shows that

$$\frac{\text{R.M.S. audio signal}}{\text{Effective audio noise}} \text{ (in the output)} = \frac{A}{(1.414 T_0)} \cdot \frac{m A}{0.0956 (\Delta \tan \theta_N)_{\text{eff}}} \propto \left( \frac{f_c}{F_a} \right)^{\frac{1}{2}} \dots \quad (15)$$

$$= 10.9 \cdot \frac{A}{N_{(\text{peak})}}$$

This gives an output signal-to-noise ratio in db equal to  $\left[ 20.74 + 20 \log \frac{A}{N_{(\text{peak})}} \right]$ .

For the extreme value of  $\frac{A}{N_{(\text{peak})}}$  equal to 2, the output signal-to-noise ratio is 26.74 db. After this threshold point, the improvement in the output  $S/N$  ratio in db is constant, but approximately varies as  $(f_c/F_a)^{\frac{1}{2}}$ . The theoretical and experimental results agree favourably as is shown in Fig. 9. The results of the impulse-noise tests show a further improvement in the output  $S/N$  ratios.

With transmission media having slower rate of cut-off, the equivalent bandwidth (Cherry, 1949) is determined and the above method is used for calculating the output  $S/N$  ratio. For simple  $R-C$  lowpass filters, the equivalent cut-off frequency  $f_o$  is  $1/4\tau$ , and the minimum risetime is  $2\tau$ . To obtain a bandwidth of 1Mc/s, the time constant  $\tau$  has to be  $0.25 \mu \text{ sec}$  only.

## V. DISCUSSION

Distortion in the P.S.M system has been very much minimized by using 'Box-car' pulse-lengthener circuit. The average distortion does not exceed 2% for media with 6 db/oct. cut-off rate. But for sharp cut-off media, the distortion is up to 5% with larger modulation index. Distortion due to l.f. cut-off is less for all cases. Linearity of modulation and distortion characteristics are poorer when the slicer circuit is used. For higher level of modulation, the percentage distortion exceeds 5% at optimum slicing levels. But in case of P.L.M., Kretzmer (1947)

has shown that even with large video bandwidths and ideal filters and amplifiers, the audio distortion is of the order of 4%. Levy (1949) has reported a P.P.M. system, where the overall distortion in audio characteristics was of the order of 5%. With bandwidth restriction, the distortion increases in P.L.M. and with  $\tau_2 = 2 \mu \text{ sec}$ , the total distortion is found to be approximately 8% for similar pulse-width and repetition frequency.

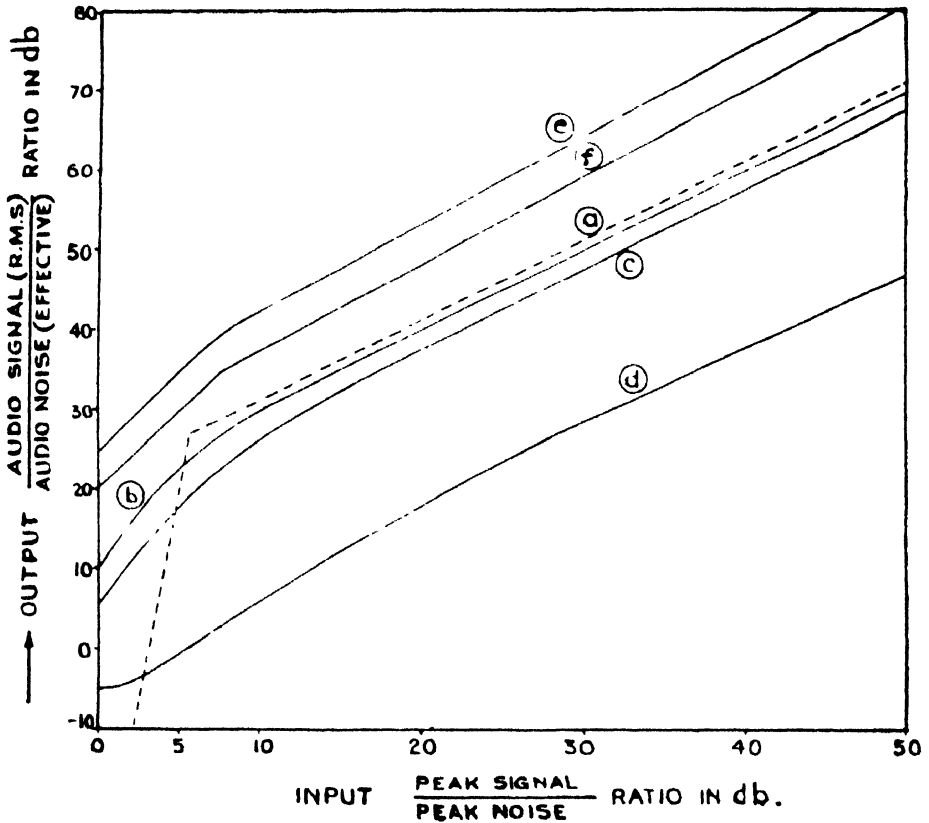


Fig. 9. Improvements in signal-to-noise ratio with sharp cut-off filters using slicers.

$d = 10 \mu \text{S}$ ,  $F_a = 3.5 \text{ Kc/s}$ , P.R.F. = 10 Kc/s.

- (a) Theoretical S/N ratio with random noise,  $f_c = 1 \text{ Mc/s}$ ,  $t_{ro} = 1 \mu \text{ sec}$ .
- (b) Experimental " " " " " " " "
- (c) " " " " " "  $f_c = 0.5 \text{ Mc/s}$ ;  $t_{ro} = 1.82 \mu \text{S}$ .
- (d) " " " " " " without slicer,  $f_c = 1 \text{ Mc/s}$ .
- (e) Experimental S/N ratio with impulse noise,  $f_c = 1 \text{ Mc/s}$ ;  $t_{ro} = 1 \mu \text{S}$ , impulse width =  $1 \mu \text{S}$ , P.R.F. of impulses = 500 c/s.
- (f) Experimental S/N ratio with impulse noise,  $f_c = 1 \text{ Mc/s}$ ;  $t_{ro} = 1 \mu \text{S}$ , impulse width =  $1 \mu \text{S}$ ; P.R.F. of impulses = 5 Kc/s.



The other advantage of the P.S.M. system is in its better crosstalk characteristics. For a P.A.M. system with same pulse duration, the crosstalk ratio with  $R$ - $C$  lowpass filters is given as  $\left( 8.686 \times \frac{t}{\tau_2} \frac{d}{\tau_2} \right) db$ . In case of P.L.M. and P.P.M. (Delorainc, 1944) there is an approximate improvement factor of  $\left( \frac{2t_m}{t_r} \right)$ , where  $t_m$  is the time displacement due to modulation. From above, the improvement in P.S.M. crosstalk ratios are 10 to 17  $db$  over those of P.A.M. and with a similar P.T.M. system, the crosstalk ratios would be at least equal.

In case of  $R$ - $C$  highpass filters, Flood (1951) has shown that the crosstalk ratio in P.A.M. is  $\left( \frac{\omega_m T_0 \tau_3}{d} \right)$  for large  $\tau_3$  and small  $\omega_m$ . Comparing with Eq. (8), the improvement in the P.S.M. crosstalk ratio with reference to P.A.M. is given by

$$\frac{\text{C.T. ratio in P.S.M.}}{\text{C.T. ratio in P.A.M.}} = \frac{2md}{\{(1-m)t_{r_{\max}} - (1+m)t_{r_{\min}}\}} = 44.3 \text{ db.} \quad \dots (16)$$

for  $d = 2 \mu \text{ sec}$ ;  $t_{r_{\max}} = 10 \mu \text{ sec}$ ;  $t_{r_{\min}} = 1 \mu \text{ sec}$ ;  $m = 0.82$ .

Even with the improvements obtained in P.P.M. and P.L.M. (Flood, 1952) the P.S.M. crosstalk ratios would be better.

In Fig. 9, it is seen that above 10  $db$  input  $S/N$  ratio, the experimental values are only 1.4  $db$  below the theoretical values and there is an apparent threshold point at 7  $db$  input  $S/N$  ratio for 1 Mc/s bandwidth. In a P.L.M. system with same maximum pulse duration and bandwidth, the improvement (Das, 1955) in the output  $S/N$  ratio is approximately 33  $db$  over the input  $S/N$  ratio, whereas in P.S.M., the improvement is only about 21  $db$ . However, the P.S.M. noise characteristics are definitely superior to those of P.A.M. and F.M. systems.

As an example of the overall performance of P.S.M., with filter-like transmission media, it is seen from Fig. 8, that the crosstalk ratio could be improved to about 80  $db$  with  $f_{c1} = 160 \text{ Kc/s}$  and  $f_{c2} = 2 \text{ Kc/s}$ , and the corresponding distortion from Fig. 4 is only  $1.5\% \pm 1\%$  for the highpass filter to be used in tandem. The improvement in the output  $S/N$  ratio is now only 16.5  $db$ . If, then, the input  $S/N$  ratio is about 25  $db$ , the total noise plus distortion in the output of the system will be about 3% only. This is a considerable advantage of the P.S.M. system.

Fourier expansion of the trapezoidal pulses shows that the useful modulated harmonic amplitudes vary as  $1/n^2$ , whereas for rectangular pulses the harmonic amplitudes vary as  $1/n$ ,  $n$  being the order of the harmonic of the p.r.f. The P.S.M. signal which consists of trapezoidal pulses will then require a lesser nominal bandwidth for transmission. As the noise characteristics of P.S.M. are slightly

inferior but the crosstalk and distortion characteristics are generally superior to those of P.T.M. systems for smaller bandwidths, P.S.M. will be more useful in low-noise bandwidth-limited systems like partially compensated cables and lines, electronic exchanges and others. If the noise level is low, the slicing level will be low and there will be very little audio distortion in the output.

#### ACKNOWLEDGMENT

The author records his thanks to Prof. H. Rakshit, D.Sc., F.N.I., for, his kind interest in the work.

#### REFERENCES

- Bhattacharyya, B. K., 1953, *Ind. J. Phys.*, **27**, 269.  
Cherry, C., 1949, "Pulses and transients in communication circuits", Chapman and Hall.  
Das, J., 1954, *Ind. J. Phys.*, **28**, 449.  
Das, J., 1955, *Electronic Engg.*, **27**, 482.  
Das, J., 1955, *Electronic Engg.*, **27**, 406.  
Das, J., 1956, *Electronic Engg.*, **28**, 16.  
Deloraine, E. M. and Labin, E., 1944, *Elec. Communication*, **22**, 91.  
Flood, J. E., 1951, *Proc. Inst. of Elec. Engineers*, **98**, Part III, 279.  
Flood, J. E., 1952, *Proc. Inst. Elec. Engineers*, **99**, Part IV, 64.  
Guillemin, E. A., 1935, "Communication Networks" Vol. 2, John Wiley & Sons.  
Kretzmer, E. R., 1947, *Proc. I.R.E.*, **35**, 1230.  
Levy, M. M., 1949, *J. Brit. Instn. Radio Engineers*, **9**, 386.

# SPACE GROUPS OF CRYSTALS OF $\alpha$ -, $\beta$ - AND $\gamma$ -PICOLINE AT $-180^{\circ}\text{C}$

S. G. BISWAS

OPTICS DEPARTMENT,

INDIAN ASSOCIATION FOR THE CULTIVATION OF SCIENCE, CALCUTTA-32

(Received, March 28, 1961)

## Plate III

**ABSTRACT.** The dimensions of the unit cell, number of molecules per unit cell and the space groups of crystals of  $\alpha$ -,  $\beta$ - and  $\gamma$ -picoline at  $-180^{\circ}\text{C}$  have been determined by studying the Debye-Scherrer patterns of the crystals. All the crystals are found to have the monoclinic lattice. The space group assigned to the  $\alpha$ -picoline crystal is  $P2_1/m$  with  $a = 9.97$ ,  $b = 10.91$ ,  $c = 10.90 \text{ \AA}$ ,  $\beta = 111^{\circ}54'$ , that of  $\beta$ -picoline is  $P2_1/m$  with  $a = 6.95$ ,  $b = 11.87$ ,  $c = 7.05 \text{ \AA}$ ,  $\beta = 94^{\circ}12'$  and that of the  $\gamma$ -picoline crystal is  $P2_1/c$  with  $a = 7.21$ ,  $b = 7.69$ ,  $c = 10.20 \text{ \AA}$ ,  $\beta = 110^{\circ}42'$ .

## INTRODUCTION

In continuation of the previous work on the analysis of the Debye-Scherrer patterns of crystals of toluene (Biswas and Sirkar, 1957), pyridine (Biswas, 1958), chlorobenzene and bromobenzene (Biswas, 1958), 1, 3, 5-trichlorobenzene (Biswas, 1957) and ortho-, meta- and paraxylene (Biswas, 1960), the present investigation was undertaken to study the Debye-Scherrer patterns of  $\alpha$ -,  $\beta$ - and  $\gamma$ -picoline at  $-180^{\circ}\text{C}$  and to find out the dimensions of the unit cell, number and molecules per unit cell and the space group to which the crystals belong.

## EXPERIMENTAL

The Debye-Scherrer patterns of crystals of  $\alpha$ -,  $\beta$ - and  $\gamma$ -picoline at  $-180^{\circ}\text{C}$  were photographed with a low temperature camera used previously (Biswas, 1958). The radius of the camera was derived from the Debye-Scherrer pattern of Al powder and it was found to be 4.50 cm. A Seifert X-ray tube running at 32 KV and 26 mA was used to photograph the patterns. An exposure of three and half hours using Cu K $\alpha$  radiation was sufficient to record the patterns with appropriate density.

## RESULTS AND DISCUSSION

In determining the dimensions of the unit cells of the crystals of these isomers Ito's method (Ito, 1950) was applied and all the crystals were found to belong to the monoclinic system. The crystals could not be assigned to any lattice of

symmetry higher than that of the monoclinic system. Lipson's method (Lipson, 1949) was also tried, but significant constant differences in the values of  $\sin^2\theta$  were not observed.

*$\alpha$ -Picoline* : The Debye-Scherrer pattern due to crystals of  $\alpha$ -picoline at  $-180^\circ\text{C}$  is reproduced in Fig. 1, Plate III. The values of  $Q$  ( $1/d_{hkl}^2$ ), where  $d_{hkl}$  is the spacing of the direct lattice calculated from the Debye-Scherrer rings are tabulated in column 1, Table I. The dimensions of the unit cell of the reciprocal lattice which are found to explain all the observed  $Q$ -values satisfactorily are :

$$\begin{array}{ll} a^* = 0.0916 & \alpha^* = 59^\circ 42' \\ b^* = 0.0988 & \beta^* = 90^\circ \\ c^* = 0.1161 & \gamma^* = 90^\circ \end{array}$$

The values of  $Q$  observed from the photograph and those calculated with the dimensions of the unit cell given above, the intensities and the proposed indices for the reciprocal lattice are also given in Table I. The dimensions of the unit cell of the direct lattice corresponding to the reciprocal lattice are :

$$\begin{array}{ll} a = 9.97 \text{ \AA} & \\ b = 10.92 \text{ \AA} & \beta = 120^\circ 18' \\ c = 11.70 \text{ \AA} & \end{array}$$

The above cell was reduced further (Buerger, 1958) and the dimensions of the reduced cell are :

$$\begin{array}{ll} a = 9.97 \text{ \AA} & \\ b = 10.92 \text{ \AA} & \beta = 111^\circ 54' \\ c = 10.90 \text{ \AA} & \end{array}$$

The indices referred to this reduced direct lattice are given in the last column of Table I.

On examining the powder pattern, it was noticed that there was some indication of the preferential orientation of the crystallites with a particular axis orientated around the vertical axis of the specimen. The primitive translation along the preferred axis is found to be about 10.94 Å. This value agrees with the length either of the  $b$ -edge or of the  $c$ -edge of the reduced unit cell. The positions of the diffraction maxima on the different layer lines, however, indicate that the preferred axis is the  $b$ -axis. The layer lines in which the different maxima due to reflections from planes of different indices are actually present are given in Table II. The positions of the maxima in the different layer lines thus confirm the correctness of the indices assigned to the corresponding reflecting planes.

To determine the number of molecules per unit cell the density of the substance at  $-180^\circ\text{C}$  was determined by the method described earlier (Biswas and

TABLE I

Indexing of the powder pattern of  $\alpha$ -picoline crystals

$Q$ (observed)	$Q$ (calculated)	$h'k'l'$ (reciprocal lattice)	$hkl$ (reduced direct lattice)
0.0293 (m)	0.0293	021	101
0.0335 (m)	0.0336	200	020
0.0345 (m)	0.0348	011	201
0.0378 (w)	0.0377	121	111
0.0388 (w)	0.0390	020	200
0.0420 (m)	0.0416	202	102
0.0435 (s)	0.0434	210	120
	0.0433	111	211
0.0475 (m)	0.0476	120	002
	0.0471	201	210
			121
0.0542 (s)	0.0540	002	202
0.0665 (m)	0.0665	031	201
0.0680 (s)	0.0685	211	221
0.0755 (s)	0.0759	021	030
	0.0756	300	301
0.0808 (w)	0.0802	222	022
	0.0806	132	112
0.0880 (m)	0.0876	202	031
		030	300
			222
0.0956 (m)	0.0962	130	310
	0.0954	112	
0.1046 (w)	0.1048	113	131
0.1162 (w)	0.1162	312	132
0.1172 (w)	0.1172	042	202
			222
0.1251 (w)	0.1247	122	123
0.1350 (vw)	0.1344	400	040
			401
0.1390 (vw)	0.1391	043	103
	0.1394	022	402
0.1628 (w)	0.1633	330	330
	0.1622	024	410
0.1732 (m)	0.1634	420	240
	0.1730	222	123
0.1890 (w)	0.1886	240	420
	0.1884	402	004
0.2086 (w)	0.2090	312	702
			502
0.2302 (w)	0.2301	023	430
0.2551 (m)	0.2559	403	205
0.3025 (w)	0.3024	600	060
0.3230 (w)	0.3226	151	151

TABLE II

Layer line	Indices for the maxima present
Zero layer line	101
	201
	200
	102
	002
	202
	201
First layer line	111
	211
	210
	012
Second layer line	020
	120
	121
	221

Sirkar, 1957) and was found to be  $1.134 \text{ gm cm}^{-3}$ . With this value of the density and the dimensions the unit cell given above the number of molecules per unit cell was found to be 8.08. Thus the unit cell contains eight molecules.

It can be easily seen from Table I that there is no restriction regarding reflection from different planes. There is, however, no space group with eight equivalent points not showing any restriction of reflection. The space group  $C_{2h}^{12} - P2/m$  does not show any restriction but it has only four equivalent positions with an asymmetric molecule at each position. It is evident, therefore, that there are two molecules forming an asymmetric unit at each equivalent position in the crystals of  $\alpha$ -picoline and the space group is  $C_{2h}^{12}$ .

**$\beta$ -Picoline:** The Debye-Scherrer pattern due to crystals of  $\beta$ -picoline at  $-180^\circ\text{C}$  is reproduced in Fig. 2, Plate III. The values of  $Q$  observed from the photograph are given in column 1, Table III.

In this case the dimensions of the unit cell of the reciprocal lattice which could explain all the  $Q$ -values satisfactorily are :

$$a^* = 0.1533$$

$$\alpha^* = 90^\circ$$

$$b^* = 0.2614$$

$$\beta^* = 90^\circ$$

$$c^* = 0.0843$$

$$\gamma^* = 85^\circ 48'$$

The dimensions of the unit cell of the direct lattice with  $b$ -axis as the unique axis corresponding to those of the reciprocal lattice are :

$$a = 6.95 \text{ \AA}$$

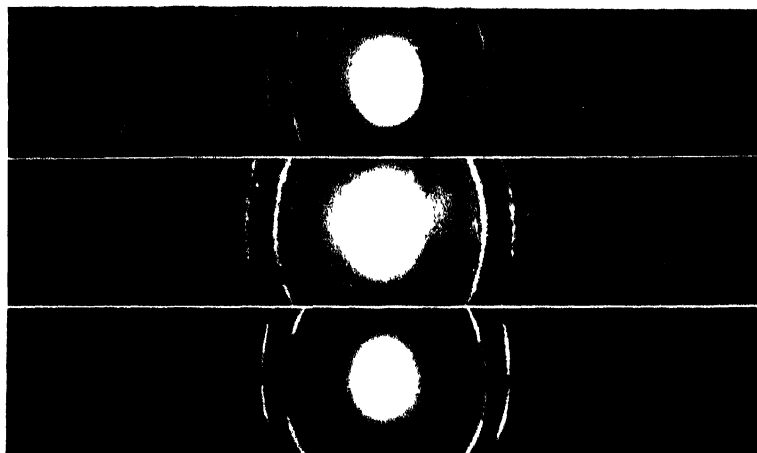
$$b = 7.05 \text{ \AA}$$

$$c = 11.87 \text{ \AA}$$

Fig. 1.

Fig. 2.

Fig. 3.



Debye-Scherrer patterns

Fig. 1.  $\alpha$ -picoline at  $-180^{\circ}\text{C}$ Fig. 2.  $\beta$ -picoline at  $-180^{\circ}\text{C}$ Fig. 3.  $\gamma$ -picoline at  $-180^{\circ}\text{C}$





# Space Groups of crystals of $\alpha$ -, $\beta$ - and $\gamma$ -Picoline at $-180^{\circ}\text{C}$ 265

It can be easily seen that the above cell cannot be reduced further. So the dimensions of the unit cell of the  $\beta$ -picoline crystal are as given above. The indices of the planes referred to the direct lattice are given in the last column of Table III.

TABLE III  
Indexing of powder pattern of  $\beta$ -picoline crystals

$Q$ (observed)	$Q$ (calculated)	$h'k'l'$ (reciprocal lattice)	$hkl$ (final direct lattice)
0.0380 (w)	0.0380	110	101
0.0440 (w)	0.0440	110	101
0.0450 (w)	0.0449	111	111
0.0495 (s)	0.0493	012	120
0.0510 (vs)	0.0509	111	111
0.0660 (vw)	0.0665	112	121
0.0724 (m)	0.0725	112	121
0.0810 (vs)	0.0808	200	002
0.0830 (vs)	0.0832	020	200
0.1020 (s)	0.1018	113	131
0.1140 (s)	0.1140	004	040
0.1338 (m)	0.1342	104	041
0.1595 (w)	0.1592	213	132
0.1705 (w)	0.1710	213	132
0.1815 (vw)	0.1818	300	003
0.1875 (vw)	0.1872	030	300
0.2060 (w)	0.2055	131	311
0.2185 (m)	0.2187	131	311
0.2515 (w)	0.2512	033	330
0.2565 (vw)	0.2560	006	060
0.2900 (m)	0.2900	224	242
0.3015 (w)	0.3012	034	340

The density of the substance at  $-180^{\circ}\text{C}$  was found to be  $1.098 \text{ gm cm}^{-3}$ . The number of molecules per unit cell calculated with this density is found to be 4.01. Thus the unit cell contains 4 molecules. It can be easily seen from Table III that the conditions limiting possible reflections are :

$hkl$  : no condition

$hol$  : no condition

$oko$  :  $k = 2n$

So, the probable space group which can be assigned to the crystal is  $C_{2h}^{2k}-P2_1/m$ .

$\gamma$ -Picoline : The Debye-Scherrer pattern due to crystals of  $\gamma$ -picoline at  $-180^{\circ}\text{C}$  is reproduced in Fig. 3, Plate III. The  $Q$ -values observed from the photograph are given in column 1, Table IV.

The dimensions of the unit cell of the reciprocal lattice which could account for all the  $Q$ -values observed in this case are :

$$a^* = 0.1049$$

$$\alpha^* = 90^{\circ}$$

$$b^* = 0.1300$$

$$\beta^* = 69^{\circ}18'$$

$$c^* = 0.1483$$

$$\gamma^* = 90^{\circ}$$

The dimensions of the unit cell of the direct lattice corresponding to those of the reciprocal lattice after  $a$  and  $c$  axes being interchanged are :

$$\begin{aligned} a &= 7.21 \text{ \AA} \\ b &= 7.69 \text{ \AA} \\ c &= 10.20 \text{ \AA} \end{aligned} \quad \beta = 110^\circ 42'$$

It can be easily seen that the above cell cannot be reduced further. So, the dimensions of the unit cell of the  $\gamma$ -picoline crystal are as given above. The indices referred to this direct lattice are given in the last column of Table IV.

TABLE IV  
Indexing of the powder pattern of  $\gamma$ -picoline crystals

$Q$ (observed)	$Q$ (calculated)	$h'k'l'$ (reciprocal lattice)	$hkl$ (final direct lattice)
0.0450 (vs)	0.0448	200	002
		201	102
0.0678 (vs)	0.0676	020	020
0.0880 (s)	0.0880	002	200
0.0888 (m)	0.0888	202	202
		201	102
0.1124 (m)	0.1124	220	022
		221	122
0.1376 (vw)	0.1381	112	211
0.1560 (s)	0.1566	022	220
	0.1564	221	122
		321	123
		222	222
0.1768 (w)	0.1768	202	202
		203	302
0.1792 (vs)	0.1792	400	004
		402	204
0.2230 (m)	0.2234	321	123
0.2456 (w)	0.2452	222	222
		401	104
		403	304
0.2466 (s)	0.2468	420	024
0.2702 (m)	0.2704	040	040
0.2922 (w)	0.2924	041	140
		141	141
0.3142 (s)	0.3146	141	141
0.3588 (vw)	0.3590	602	206
	0.3584	042	420
0.3802 (vw)	0.3805	523	325
0.4500 (m)	0.4496	440	044
0.4705 (vw)	0.4708	620	026
0.4915 (w)	0.4912	604	406
0.5432 (w)	0.5437	152	251
0.6080 (w)	0.6084	060	060
0.6228 (vw)	0.6222	044	440
	0.6234	602	206
0.7120 (m)	0.7120	523	325
0.7245 (m)	0.7241	414	414

The density of the substance at  $-180^{\circ}\text{C}$  was found to be  $1.163\text{ gm cm}^{-3}$ . The number of molecules per unit cell calculated with this density is found to be 4.03. Thus the unit cell contains four molecules.

Table IV shows that the reflections from the planes (010), (030) and (050) are absent because the  $Q$  values for these planes are 0.0169, 0.1521 and 0.4225 respectively and these do not agree with any of the observed values. Hence it is concluded that ( $oko$ ) reflection are absent when  $k$  is odd.

The calculated values of  $Q_{hol}$  with  $l$  odd together with those observed in the neighbourhood of some of these values are given in Table V.

TABLE V

$Q_{hol}$	Computed	Nearest value observed	Difference
$Q_{101}$	0.0222		
$Q_{101}$	0.0442	0.0450 (002)	0.0008
$Q_{201}$	0.0772		
$Q_{103}$	0.0898	0.0888 (202)	-0.0010
$Q_{201}$	0.1212		
$Q_{203}$	0.1228		
$Q_{103}$	0.1558	0.1560	0.0002
$Q_{301}$	0.1762	0.1768	0.0006
$Q_{301}$	0.2422		
$Q_{203}$	0.2548		

The difference between  $Q_{002}$  and  $Q_{101}$  and that between  $Q_{103}$  and  $Q_{203}$  are beyond experimental error which is less than 0.0005. Hence (101) and (103) reflections are most probably absent. Reflections from the (103) planes may, however, be superposed on that from (220) and the (301) reflection may lie very close to (202) reflection, but since the other ( $hol$ ) reflections with  $l$  odd are definitely absent it is concluded that all such reflections are absent.

Table IV then shows the following conditions limiting possible reflections :

$hkl$  : no condition

$hol$  :  $l = 2n$

$oko$  :  $k = 2n$

So, the probable space group of the crystal is  $C^{15}_{2h} - P2_1/c$ .

Finally, it has to be pointed out that in all the cases mentioned above assignment of alternative unit cell dimensions leads to serious difficulties, because either some of the intense reflections cannot be accounted for or the number of molecules per unit cell differs considerably from whole numbers. On the other hand, with cell dimensions given above these difficulties disappear completely.

## ACKNOWLEDGMENT

The author is indebted to Professor S. C. Sirkar, D.Sc., F.N.I., for his kind interest and guidance during the progress of this work. The author is also indebted to the Council of Scientific and Industrial Research for financing the scheme under which this work was done.

## REFERENCES

- Biswas, S. G. and Sirkar, S. C., 1957, *Ind. J. Phys.*, **31**, 141.  
Biswas, S. G., 1958, *Ind. J. Phys.*, **32**, 13.  
Biswas, S. G., 1958, *Acta Cryst.*, **11**, 882.  
Biswas, S. G., 1959, *Ind. J. Phys.*, **33**, 371.  
Biswas, S. G., 1960, *Ind. J. Phys.*, **34**, 263.  
Buerger, M. J., 1957, *Zeits. f. Krist.*, **109**, 42.  
Ito, T., 1950, X-ray studies on polymorphism, (Maruzen Co. Ltd., Tokyo p. 210-214.)  
Lipson, H., 1949, *Acta. Cryst.*, **2**, 49.

## BOOK REVIEWS

**ORGANIC ELECTRONIC SPECTRAL DATA.** Vol. I, 1946-52—By Mortimer J. Kamlet, Editor. Pp. 1208. Interscience Publishers, New York, London, 1960. Price \$ 28.50. Vol. II. 1953-55—By Herbert E. Ungnade, Editor. Pp. 919. Interscience Publishers, New York, London, 1960. Price \$ 17.50.

These two volumes give the wavelengths of absorption maxima and the values of  $\log(\epsilon)$  in the ultraviolet and visible regions for organic compounds reported by various workers during the years 1946-52 and 1953-55 respectively. It is stated in the preface that the data were taken from 60 chemical and allied journals. The data are given in four columns, the first of which contains the chemical formula and the name of the compound. The solvent or the state in which the spectra have been studied is given in column 2 and the wavelengths of absorption maxima and the values of  $\log(\epsilon)$  at the maxima are given in column 3. The last column gives the reference in which the journal is represented by a number and the paper by another number. The details of the corresponding references are given at the end of each volume. The references are arranged according to the alphabetical order of the names of the journals.

Such data are immensely helpful not only to chemists engaged in research in synthesis or analysis of organic chemicals but also to many physicists who are interested in the electronic spectra of such compounds. To research workers the value of the data depend on the degree of their completeness. The Board of Editors secured contributions from 51 specialists from different countries, and therefore, it has been possible to compile the data from a large number of journals in different languages which are ordinarily not available to many research workers. As stated above, 60 journals in Chemistry and allied subjects have been consulted to compile the data, and evidently, journals in physics have been scrupulously avoided. It is difficult to understand why the Board of Editors assumed that data on electronic spectra of organic compounds cannot be published in journals in physics. In fact, such an assumption only results in omission of certain data which might be useful to research workers. As for instance, it might be pointed out that during the years 1949-1955 a few papers dealing with ultraviolet absorption spectra of some organic compounds were published in this journal and some of these papers have been mentioned by Wolf in Solid State Physics, Vol. 9, but these data have not been taken notice of in the volumes under review.

Nevertheless, the publication of the volumes will enable a large number of research workers all over the world to save their valuable time in procuring the

data and will thus hasten the progress of research in chemistry and some branches of physics. It is stated in the Introduction of Vol. II that the next three volumes are in preparation. It is fervently hoped that the above remarks regarding omission of certain data will be taken notice of by the Board of Editors before the next three volumes are published.

The get-up of the volumes is excellent and in view of the fact that the co-operation of a large number of specialists has been required to publish the volumes the prices are considered to be quite moderate.

*S. C. S.*

# THERMODYNAMIC PROPERTIES OF FLUID FLOW ACROSS A MAGNETIC FIELD

I. J. SINGH

OIL AND NATURAL GAS COMMISSION, DEHRADUN, INDIA

AND

K. P. CHOPRA\*

ENGINEERING CENTRE, UNIVERSITY OF SOUTHERN CALIFORNIA, LOS ANGELES,  
CALIFORNIA

(Received August 31, 1960)

**ABSTRACT.** This paper deals with the study of the various thermodynamic quantities like internal energy, enthalpy, entropy, etc., involved in the investigation of the flow of a conducting fluid in the presence of a uniform transverse magnetic field. The analogues of Rayleigh and Fanno lines readily follow from the basic equations. It is shown that the internal energy and enthalpy of an electrically conducting fluid obeying perfect gas depends, in the presence of a transverse magnetic field, on its density and the strength of the magnetic field. The entropy and the specific heat at constant volume do not seem to be affected by the presence of the magnetic field. The behaviour of the specific heat at constant pressure depends on which of the gas pressure and the total pressure is kept constant. A transverse magnetic field reduces the specific heat at constant gas pressure and the corresponding adiabatic constant by a factor proportional to the ratio of the magnetic pressure to the gas pressure. However, if the total pressure is kept constant, the magnetic field has no effect on the specific heat. Lastly, the effect of the magnetic field on the velocity of sound is discussed. In the limiting cases of weak and strong magnetic fields, the velocity of sound reduces to the ordinary sonic speed and the Alfvén speed respectively.

## I. INTRODUCTION

The hydrodynamical motion of an electrically conducting fluid in the presence of a transverse magnetic field gives rise to induced electric currents which interact with the magnetic field to produce mechanical forces thereby affecting the fluid flow. Therefore, it is necessary to take account of this hydromagnetic interaction, and hence, the terms involving magnetic field appear in the equations governing the fluid flow (Alfvén, 1950; and Hoffmann and Teller, 1950). The investigation of the compressible fluid flow in the presence of a transverse magnetic field was initiated by Hoffmann and Teller (1950) who described the relativistic and nonrelativistic propagation of plane hydromagnetic shock waves in a medium of infinite electrical conductivity.

\* Present Address: Polytechnic Institute of Brooklyn, New York, U.S.A.

In order to take account of the contribution of the magnetic field to the pressure and internal energy of the fluid, we define total pressure  $p^x$  and total internal energy  $E^x$  as

$$p^x = p + \frac{H^2}{8\pi} \quad \dots$$

and

$$E^x = E + \frac{H^2}{8\pi\rho} \quad \dots \quad (2)$$

The unstarred quantities  $p$  and  $E$  refer to the gas pressure and internal energy in the absence of the magnetic field  $H$ . These quantities are connected by the relation

$$E = \frac{1}{\gamma-1} \frac{p}{\rho} \quad \dots \quad (3)$$

In terms of the total pressure  $p$ , the total internal energy  $E^x$  is given by

$$E^x = \frac{1}{\gamma-1} \left( \frac{p^x}{\rho} \right) + \frac{\gamma-2}{\gamma-1} \left( \frac{H^2}{8\pi\rho} \right) \quad \dots \quad (4)$$

where  $\gamma$  is the ratio of the specific heat at constant pressure to the specific heat at constant volume.

Similarly, the total enthalpy  $h^x$  may be defined as

$$h^x = E^x + \frac{p^x}{\rho} = h + \frac{H^2}{4\pi\rho} \quad \dots \quad (5)$$

where  $h$  is the enthalpy in the absence of the magnetic field.

In terms of the Alfvén speed

$$V_{\text{AU}} = \left( \frac{H^2}{4\pi\rho} \right)^{\frac{1}{2}} \quad \dots \quad (6)$$

the expression for total enthalpy  $h^x$  becomes

$$h^x = h + V_{\text{AU}}^2 \quad \dots \quad (7)$$

From the equations obtained for the limiting case of infinitesimal disturbances in the Hoffmann-Teller paper (1950), we may write the equations governing the thermodynamics of hydromagnetic fluid flow as the following:

The equation of continuity or constant mass flux

$$\rho v = \text{constant} = M \quad \dots \quad (8)$$



the equation of constant momentum flux

$$\rho v^2 + p^x = \bar{p}^x \quad (9)$$

and the equations

$$\frac{1}{2}v^2 + h^x = \bar{h}^x \quad \dots \quad (10)$$

and

$$Hv = \text{constant} \quad \dots \quad (11)$$

where  $\bar{p}^x$  and  $\bar{h}^x$  are the stagnation values of total pressure and total enthalpy. Eq. (10) is analogous to the first law of thermodynamics, while the Eq. (11) describes the relation of magnetic field strength and gas velocity  $v$ . From Eqs. (8) and (11) it follows that

$$\frac{H}{\rho} = \text{constant} = \alpha \quad (12)$$

In other words, the changes in magnetic field strength and density are such that the strength of the magnetic field is always proportional to density.

## II. RAYLEIGH AND FANNO LINES

The elimination of  $v$  between Eqs. (8) and (9) yields

$$p^x + \frac{M^2}{\rho} = p + \frac{H^2}{8\pi} + \frac{M^2}{\rho} = \bar{p}^x \quad (13)$$

which is the analogue of the Rayleigh line in ordinary gasdynamics.

Similarly, the elimination of  $v$  between (8) and (10) gives

$$h^x + \frac{1}{2} \left( \frac{M}{\rho} \right)^2 = h + \frac{H^2}{4\pi\rho} + \frac{1}{2} \left( \frac{M}{\rho} \right)^2 = \bar{h}^x \quad \dots \quad (14)$$

which is analogous to the customary Fanno line.

On expressing  $H$  in terms of  $\rho$  with the help of Eq. (12), these equations reduce to

$$p + \frac{\alpha^2}{8\pi} \rho^2 + \frac{M^2}{\rho} = \bar{p}^x \quad \dots \quad (15)$$

and

$$h + \frac{\alpha^2}{4\pi} \rho + \frac{1}{2} \left( \frac{M}{\rho} \right)^2 = \bar{h}^x \quad \dots \quad (16)$$

The constant  $\alpha$  is determined from the initial value of the magnetic field and gas density when the gas is at rest.

### III. CHANGE IN INTERNAL ENERGY

From Eq. (2) we have for the change in internal energy

$$dE^x = d \left( E + \frac{H^2}{8\pi\rho} \right)$$

which, with the help of Eq. (12), reduces to

$$dE^x = dE + \frac{H^2}{8\pi\rho^2} d\rho \quad \dots \quad (17)$$

For a gas satisfying the perfect gas law

$$p = RT\rho \quad \dots \quad (18)$$

with  $R$  and  $T$  as the universal gas constant and absolute temperature, the change in internal energy is given by

$$\left( \frac{\partial E^x}{\partial \rho} \right)_T = \left( \frac{\partial E}{\partial \rho} \right)_T + \frac{H^2}{8\pi\rho^2} = \frac{1}{2} \left( \frac{V_{Ay}^2}{\rho} \right) \quad \dots \quad (19)$$

where  $V_{Ay}$  is the Alfvén speed. In the limit of zero magnetic field

$$\left( \frac{\partial E^x}{\partial \rho} \right)_T \rightarrow \left( \frac{\partial E}{\partial \rho} \right)_T = 0$$

Hence, the internal energy of a perfect gas of infinite electrical conductivity in the presence of a transverse magnetic field depends—unlike in the thermodynamics of ordinary fluid flow—on its density.

### IV. CHANGE IN ENTHALPY

Similarly, on combining Eqs. (5) and (12), we have for the change in enthalpy

$$dh^x = \left( h + \frac{H^2}{4\pi\rho} \right)$$

$$dh + d \frac{H^2}{4\pi\rho^2} d\rho \quad \dots \quad (20)$$

For a gas obeying Eq. (18), the last equation yields

$$\left( \frac{\partial h^x}{\partial \rho} \right)_T = \frac{H^2}{4\pi\rho^3} = \frac{V^2 \Delta \mu}{\rho} \quad \dots \quad (21)$$

and for  $H \rightarrow 0$ .

$$\left( \frac{\partial h^x}{\partial \rho} \right)_T \rightarrow \left( \frac{\partial h^*}{\partial \rho} \right)_T = 0$$

Therefore, it may be concluded that, like internal energy, the enthalpy also depends on the density of a conducting fluid in the presence of a transverse magnetic field.

## V. CHANGE IN ENTROPY

Here it will be shown that the terms involving magnetic field do not appear in the expression for the change in entropy (Sen, 1956)

$$ds^x = \frac{dQ^x}{T} = \frac{1}{T} \left[ dE^x + p^x d \left( \frac{1}{\rho} \right) \right] \quad (22)$$

because, on substitution for  $p^x$  and  $dE^x$  from Eqs. (1) and (17), we have

$$\begin{aligned} ds^x &= \frac{1}{T} \left[ dE + \frac{H^2}{8\pi\rho^2} d\rho + p d \left( \frac{1}{\rho} \right) - \frac{H^2}{8\pi\rho^2} d\rho \right] \\ &= \frac{1}{T} \left[ dE + p d \left( \frac{1}{\rho} \right) \right] = \frac{dQ}{T} \\ &= ds \end{aligned} \quad (23)$$

## VI. SPECIFIC HEATS OF GAS

The specific heat of the fluid at constant volume is given by

$$C_{vol}^x = \left( \frac{\partial E^x}{\partial T} \right)_{vol.} = \left( \frac{\partial E}{\partial T} \right)_{vol.} = C_{vol.} \quad (24)$$

Therefore, the specific heat at constant volume is not affected by the magnetic field.

The influence of a transverse magnetic field on the specific heat at constant pressure depends, however, on which of the gas pressure  $p$  or the total pressure  $p^x$  is kept constant. If the gas pressure  $p$  is kept constant, then

$$C_p^x = \left( \frac{\partial h^x}{\partial T} \right)_p = C_p + \frac{H^2}{4\pi p^2} \left( \frac{\partial \rho}{\partial T} \right)_p \quad \dots \quad (25)$$

which, for a perfect gas, becomes

$$C_p^x = C_p - 2R \left( \frac{H^2}{8\pi\rho} \right)$$

$$\text{or } C_p^x - C_p = -2R \frac{\text{Magnetic pressure}}{\text{Gas pressure}} \quad \dots (26)$$

Hence, the presence of a transverse uniform magnetic field reduces, in this case, the specific heat at constant gas pressure by an amount proportional to the ratio of the magnetic pressure and the gas pressure.

In the second case, when the total pressure  $p^x$  is kept constant, we similarly have

$$\begin{aligned} C_{p^x}^x &= \left( \frac{\partial h^x}{\partial T} \right)_{p^x} = \left[ \frac{\partial}{\partial T} \left\{ E + \frac{p^x}{\rho} + \frac{H^2}{8\pi\rho} \right\} \right]_{p^x} \\ &= C_{vol.} + p^x \frac{\partial}{\partial T} \left( \frac{1}{\rho} \right)_{p^x} + \frac{H^2}{8\pi\rho^2} \left( \frac{\partial \rho}{\partial T} \right) \quad \dots (27) \\ &= C_{vol.} + p^x \frac{\partial}{\partial T} \left( \frac{1}{\rho} \right) \end{aligned}$$

[by virtue of Eq. (12)]

$$= C_p$$

In this case, the terms involving magnetic field do not appear in the expression for the specific heat which has the same value as in the nonmagnetic case. Similarly, the adiabatic constant of the gas is influenced by the transverse magnetic field if the gas pressure is maintained constant.

## VII. LOCAL VELOCITY OF SOUND

The new velocity of sound  $C^x$  is analogically defined with the help of Eqs. (1) and (12), as

$$C^x = (C^2 + V_A^2)^{\frac{1}{2}} \quad (28)$$

where  $C$  is the velocity of sound in the absence of the magnetic field. In the case of magnetic field, the new velocity of sound in a conducting fluid is increased, the increment being proportional to the ratio of the magnetic pressure and the gas

pressure. However, if the magnetic field exceeds the gas pressure considerably, the new velocity of sound approaches the Alfvén speed. The coincidence with the Alfvén speed is purely accidental. Although the sound waves appear to have precisely the same velocity as that of Alfvén waves, they are longitudinal in character whereas the Alfvén waves are transverse in nature. Similarly, the Mach number, in the case of very strong magnetic fields, is defined by the ratio of the flow speed and the Alfvén speed.

#### REFERENCES

- Alfvén, H., 1950. *Cosmical Electrodynamics*, Oxford University Press.  
Hoffmann, F. de and Teller, E., 1950, *Phys. Rev.*, **80**, 692.  
Sen, H. K., 1956, *Phys. Rev.*, **102**, 5.

# SCATTERING OF ELECTRONS BY A SCREENED COULOMB FIELD IN HIGHER BORN APPROXIMATION

T. K. MITRA

DEPARTMENT OF THEORETICAL PHYSICS,

INDIAN ASSOCIATION FOR THE CULTIVATION OF SCIENCE, JADAVPUR, CALCUTTA-32

(Received March 28, 1961)

**ABSTRACT.** The relativistic scattering of electrons by heavy atoms has been studied by taking the Rozental approximation of the Thomas-Fermi potential. The differential cross section of scattering has been calculated in the Born approximation up to second order in the expansion of  $\frac{Ze^2}{\hbar v}$ . The numerical results of the scattering of electrons of energy 150 KeV at an angle  $90^\circ$  have been given for the elements, argon, krypton, xenon and mercury.

## INTRODUCTION

We propose to study the scattering of the fast electrons by heavy atoms. For high energy scattering the potential of the atom is usually taken as that due to the nuclear charge alone, the screening effects of the atomic electrons being neglected. It is, however, worth while to investigate the effects of screening due to the atomic electrons on electron scattering. The Hartree-Fock method which takes good account of the screening in the potential function is suitable only for light atoms, considering the practical difficulties involved. For heavy atoms the treatment of the screened potential by the statistical method of Thomas-Fermi is more practicable. Unfortunately there is no analytic expression for the Thomas-Fermi potential. Various approximate representations of the Thomas-Fermi potential are cited in the literature (Majewsky and Tietz, 1957). Among them the Rozental form which is a combination of three potentials of Yukawa type with different weight factors, is suitable for analytic treatment in higher Born approximations. With this potential the differential cross section for electron scattering up to second order has been calculated. Numerical results are given for the elements argon ( $Z = 18$ ), krypton ( $Z = 36$ ), xenon ( $Z = 54$ ) and mercury ( $Z = 80$ ) at 150 KeV incident electron energy. These are compared with the corresponding numerical results for the Coulomb potential without screening. The differential scattering cross section are expressed as the ratio of  $d\sigma$  to  $d\sigma_R$  where  $d\sigma_R$  is the well-known Rutherford scattering cross section.

# RESULTS AND DISCUSSION

Taking relativistic units  $\hbar = c = m = 1$ , the Dirac equation can be written as

$$[E - i(\alpha \cdot \nabla) + \beta]\psi = -Ze^2 V\psi$$

$$V = \frac{1}{r}\phi(r) = \frac{1}{\mu x} [0.255e^{-.246x} + 0.581e^{-.947x} + 0.164e^{-4.356x}]$$

where

$$x = \frac{r}{\mu}, \quad \mu = \frac{1}{4} \left( \frac{9\pi^2}{2Z} \right)^{1/3} a_0, \quad a_0 = \text{First Bohr radius}$$

Following Vachaspati (1954), the expression for the scattering cross section in Born approximation up to second order can be written as

$$d\sigma = d\sigma_1 + d\sigma_2$$

$$\text{where} \quad d\sigma_1 = 4(Z\alpha)^2 |a_1|^2 k^2 \cos^2 \theta / 2 \left( 1 + \frac{1}{k^2} \sec^2 \theta / 2 \right)$$

$$d\sigma_2 = 16(Z\alpha)^3 a_1 E k^2 \cos^2 \theta / 2 \left[ (a_{3r} + \frac{1}{2} a_{2r}) + \frac{1}{k^2} a_{2r} \sec^2 \theta / 2 \right]$$

$$a_1 = \frac{1}{4\pi} (\mathbf{k}_1 | V | \mathbf{k}_0), \quad \mathbf{k}_0 = \text{initial momentum}, \quad \mathbf{k}_1 = \text{final momentum}$$

$$|\mathbf{k}_0| = |\mathbf{k}_1| = k$$

$$a_{2r} = \frac{1}{4\pi(2\pi)^3} P \int \frac{(\mathbf{k}_1 | V | \mathbf{k}')(\mathbf{k}' | V | \mathbf{k}_0)}{k'^2 - k^2} d^3 k'$$

$$= \frac{4\pi}{(2\pi)^3} \sum_{i < j=1}^3 \frac{\alpha_i \alpha_j}{k^3} M_3(\lambda_i, \lambda_j) + \frac{4\pi}{(2\pi)^3} \sum_{i=1}^3 \frac{\alpha_i^2}{k^3} M_3(\lambda_i, \lambda_i)$$

$$a_{3r} = \frac{1}{4\pi(2\pi)^3(n, P)} P \int \frac{(\mathbf{k}_1 | V | \mathbf{k}')(n \cdot \mathbf{k}')(\mathbf{k}' | V | \mathbf{k}_0)}{k'^2 - k^2} d^3 k'$$

$$= \frac{4\pi}{(2\pi)^3 P^2} \sum_{i < j=1}^3 \left\{ \frac{4k^2 + \lambda_i^2 + \lambda_j^2}{k^3} M_3(\lambda_i, \lambda_j) + \frac{2}{k} M_2(\lambda_i, \lambda_j) - I_i - I_j \right\} \alpha_i \alpha_j$$

$$+ \frac{4\pi}{(2\pi)^3 P^2} \sum_{i=1}^3 \left\{ \frac{2k^2 + \lambda_i^2}{k^3} M_3(\lambda_i, \lambda_i) + \frac{1}{k} M_2(\lambda_i, \lambda_i) - I_i \right\} \alpha_i^2$$

$M_2$  and  $M_3$  are given by Lewis (1956) and quoted in the Appendix.

$$\alpha_1, \alpha_2, \alpha_3 = 0.255, 0.581, 0.164; \quad \lambda_1, \lambda_2, \lambda_3 = 0.246, 0.947, 4.356.$$

The Rutherford scattering cross section is  $d\sigma_R = \frac{(Ze^2)^2}{4} \frac{1-\beta^2}{\beta^4 \sin^4 \theta/2}$ . The value of  $k$  for 150 KeV incident electron energy is 0.820534 and the ratios  $d\sigma_1/d\sigma_R$  and  $d\sigma_2/d\sigma_R$  are given by

$$\frac{d\sigma_1}{d\sigma_R} = \frac{2k^4(k^2+2)}{(k^2+1)} |a_1|^2$$

$$\frac{d\sigma_2}{d\sigma_R} = 8Ze^2a_1E \frac{k^6}{k^2+1} \left[ a_{3r} + \left( 0.5 + \frac{2}{k^2} \right) a_{2r} \right]$$

TABLE I

Z	$d\sigma_1/d\sigma_R$		$d\sigma_2/d\sigma_R$		$d\sigma/d\sigma_R$	
	Coulomb	Rozental	Coulomb	Rozental	Coulomb	Rozental
18	0.798815	0.796772	0.054211	0.061621	0.853026	0.858393
36	0.798815	0.795642	0.108422	0.127284	0.907237	0.922926
54	0.798815	0.794643	0.162634	0.194867	0.961449	0.989510
80	0.798815	0.793438	0.240939	0.294507	1.039754	1.087945

In Table I, the value of  $\frac{d\sigma_1}{d\sigma_R}$  i.e., the ratio of the first order relativistic scattering cross section calculated with the Rozental potential and the Coulomb potential, to the Rutherford cross section (non-relativistic Coulomb scattering cross section) are given at 150 KeV incident electron energy for different values of the atomic number  $Z$ . Correspondingly, the ratio  $\frac{d\sigma_2}{d\sigma_R}$ , shows the contribution of the second order term only in the scattering cross section and finally there is a column for  $d\sigma/d\sigma_R$  which is equal to  $\frac{d\sigma_1 + d\sigma_2}{d\sigma_R}$ . It is found that  $d\sigma_1/d\sigma_R$  for the Rozental potential is slightly less (e.g. about 0.5% less for  $Z = 54$ ) than the corresponding ratio for Coulomb potential; the difference between the two ratios increases as  $Z$  increases. This is quite in agreement with the expectation that the screening should decrease the scattering cross section, though the very small difference between the two ratios indicates that the effect of screening is not appreciable at this energy. It is interesting to note, however, that the ratio for the Rozental potential is considerably larger than the corresponding ratio for the Coulomb potential (e.g. about 20% larger for  $Z = 54$ ). We can obtain  $d\sigma_2$  for the Coulomb potential from the Rozental potential, after putting  $\lambda_i = 0$ ,  $i = 1, 2, 3$  and  $\alpha_i = \alpha_i = 0$ ,  $\alpha_k = 1$ , then  $a_{3r}$  reduce to zero in this limit, and  $a_{2r}$  gives a non-zero value which correctly reduces  $d\sigma_2$  for the Rozental case to the corresponding



expression for the Coulomb case. In the Rozental case, however, the contribution to the cross section from the terms associated with  $a_{2r}$  is not negligible; in fact it is found to be about twenty per cent of the contributions due to the other terms.

## APPENDIX

In our calculations we have utilised the following expressions given by Lewis (1956):

$$Re M_2(\mu, \nu) = Re\{k \int d^3k' [(K_1^2 + \mu^2)(K_2^2 + \nu^2)]^{-1}\} = \frac{2\pi^2 k}{K} \arctan \left[ \frac{K}{\mu + \nu} \right]$$

$$Re M_3(\mu, \nu) = Re\{k^3 \int d^3k' [(k'^2 - k^2 - i\epsilon)(K_1^2 + \mu^2)(K_2^2 + \nu^2)]^{-1}\} \\ = \pi^2 k^3 [k^2(K^2 + \mu^2 + \nu^2)^2 - \rho^2 \mu^2 \nu^2]^{-\frac{1}{2}}$$

$$\left\{ \arctan \left[ \frac{k[K^2 + (\mu + \nu)^2] + [k^2(K^2 + \mu^2 + \nu^2)^2 - \rho^2 \mu^2 \nu^2]^{-\frac{1}{2}}}{\mu\nu(\mu + \nu)} \right] \right. \\ \left. - \arctan \left[ \frac{k[K^2 + (\mu + \nu)^2] - [k^2(K^2 + \mu^2 + \nu^2)^2 - \rho^2 \mu^2 \nu^2]^{-\frac{1}{2}}}{\mu\nu(\mu + \nu)} \right] \right\}$$

$$Re M_3(\mu, \mu) = 2\pi^2 k^3 \{[k^2 K^2 + 4k^2 \mu^2 + \mu^4]^{-\frac{1}{2}}/K\} \times \\ \arctan \{K\mu[k^2 K^2 + 4k^2 \mu^2 + \mu^4]^{-\frac{1}{2}}\}$$

$$Re I_i = Re\{ \int d^3k' [(K_1^2 + \lambda_i^2)(k'^2 - k^2 - i\epsilon)]^{-1} \} = \frac{\pi^2}{k} \arctan \frac{2k}{\lambda_i} \text{ with.}$$

$$\mathbf{K} = \mathbf{k}_i - \mathbf{k}_f = \mathbf{k}_0 - \mathbf{k}_1; \mathbf{P} = \mathbf{k}_0 + \mathbf{k}_1; \mathbf{K}_1 = \mathbf{k}_0 - \mathbf{k}'; \mathbf{K}_2 = \mathbf{k}' - \mathbf{k}_1.$$

## ACKNOWLEDGMENT

The author is indebted to Prof. D. Basu, Ph.D., for suggesting the problem and for his constant guidance.

## REFERENCES

- Majewsky and Tietz, 1957, *Phys. Rev.*, **108**, 103.  
 Vachaspati, 1954, *Phys. Rev.*, **93**, 502.  
 Lewis, R. R., 1956, *Phys. Rev.*, **102**, 537.

# FLUORESCENCE SPECTRA OF SOME URANYL SALTS

K. V. NARASIMHAM

DEPARTMENT OF APPLIED PHYSICS

MADRAS INSTITUTE OF TECHNOLOGY, CHROMEPET, MADRAS

(Received October 10, 1960)

Plate IV (A and B) Plate V (A and B)

**ABSTRACT.** The fluorescence spectra of uranyl acetate, nitrate, sulphate, fluoride I, chloride, potassium uranyl sulphate and ammonium uranyl sulphate have been reinvestigated at room and liquid air temperatures and new analyses have been proposed for each spectrum on the basis of a single electronic allowed transition.

## INTRODUCTION

The fluorescence spectra of uranyl compounds are studied in detail by many workers since the first investigations were made by Becquerel (1872) and Becquerel and Onnes (1909). In our earlier paper (Rao and Narasimham, 1956), a comprehensive review of the available literature on the spectroscopic properties of the uranyl salts was given. It was shown that the earlier analyses of Freymann (1946) and Pant (1945, 1950) were open to question in several respects. The most satisfactory analysis of the compounds has been proposed by Dieke and Duncan (1949) but they gave analysis for the spectra of only two salts—caesium uranyl nitrate and caesium uranyl chloride. Therefore investigations are again carried out on uranyl acetate ( $2\text{H}_2\text{O}$ ), nitrate ( $6\text{H}_2\text{O}$ ), sulphate ( $3\text{H}_2\text{O}$ ), chloride ( $1\text{H}_2\text{O}$ ), fluoride I ( $\text{XH}_2\text{O}$ ), potassium sulphate ( $2\text{H}_2\text{O}$ ) and ammonium sulphate ( $2\text{H}_2\text{O}$ ) at room and liquid air temperatures and new analyses have been proposed for the fluorescence bands of each compound on the basis of a single electronic transition with one upper state and one lower state. In the case of ammonium uranyl sulphate, the analysis of the fluorescence bands has been proposed for the first time.

## EXPERIMENTAL

The experimental set-up for fluorescence consists of a brass rod with a circular slot of 5 cm. depth in the middle in which a small glass tube containing the investigating salt in fine powder form is placed tightly. The brass rod has three small holes bored at the middle of the slot (2.5 cm. from the top) two in one line to allow the incident light on the substance from two mercury arcs on opposite sides and the third perpendicular to the line joining the above two. This allows the fluorescence from the substance into the spectrograph.

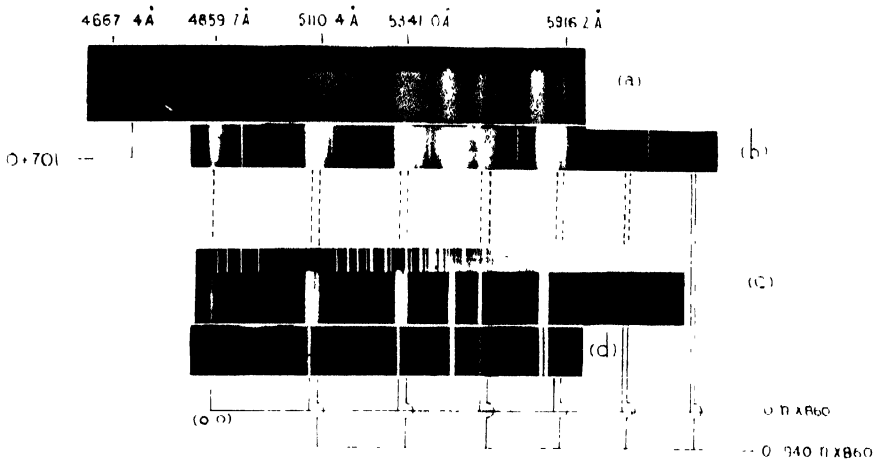


Fig. 1. Fluorescence spectra of uranyl acetate

- (a) At room temperature.
- (b) At liquid air temperature ( exposure 1 hour ).
- (c) At liquid air temperature ( exposure 20 minutes ).
- (d) At liquid air temperature ( exposure 5 minutes ).

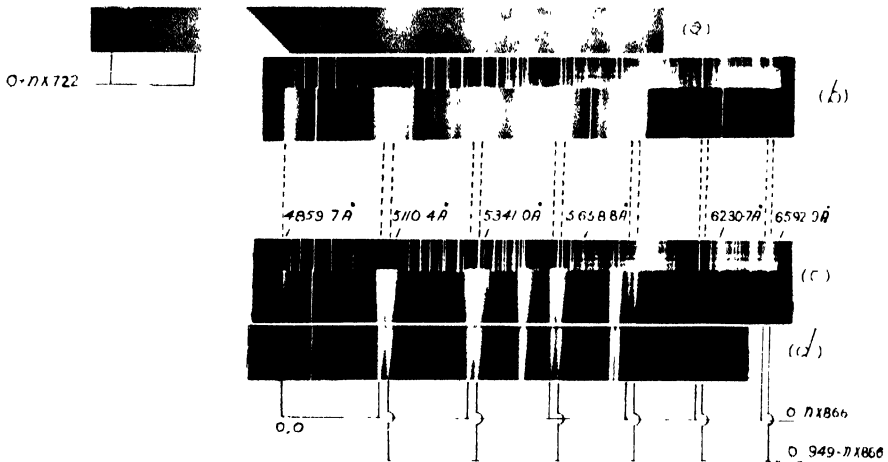


Fig. 2. Fluorescence spectra of uranyl nitrate

- (a) At room temperature.
- (b) At liquid air temperature ( exposure 1 hour ).
- (c) At liquid air temperature ( exposure 20 minutes ).
- (d) At liquid air temperature ( exposure 5 minutes ).

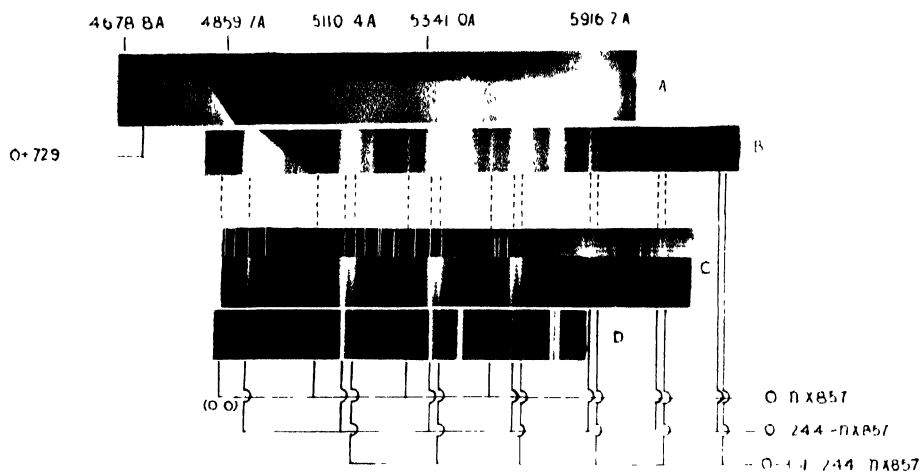


Fig. 3. Fluorescence spectra of uranyl sulphate

- (a) At room temperature.
- (b) At liquid air temperature ( exposure 1 hour ).
- (c) At liquid air temperature ( exposure 20 minutes ).
- (d) At liquid air temperature ( exposure 5 minutes ).

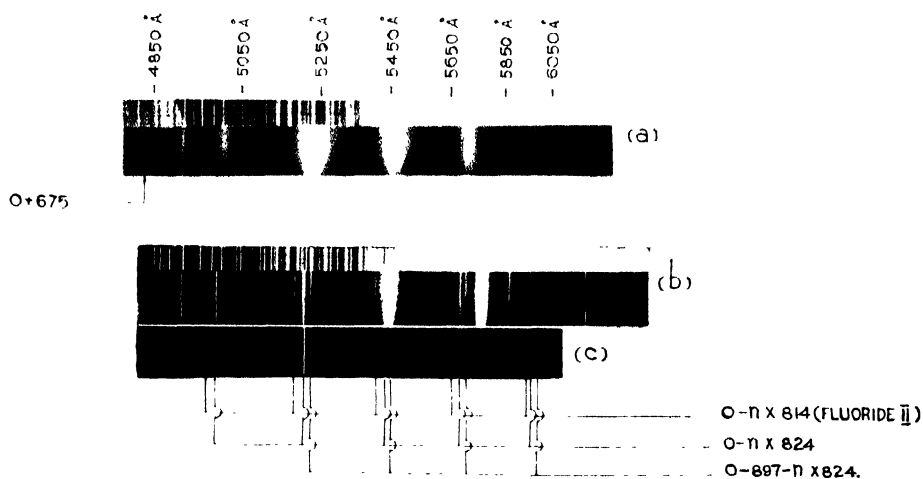


Fig. 4. Fluorescence spectra of uranyl fluoride I

- (a) At room temperature.
- (b) At liquid air temperature ( long exposure ).
- (c) At liquid air temperature ( short exposure ).

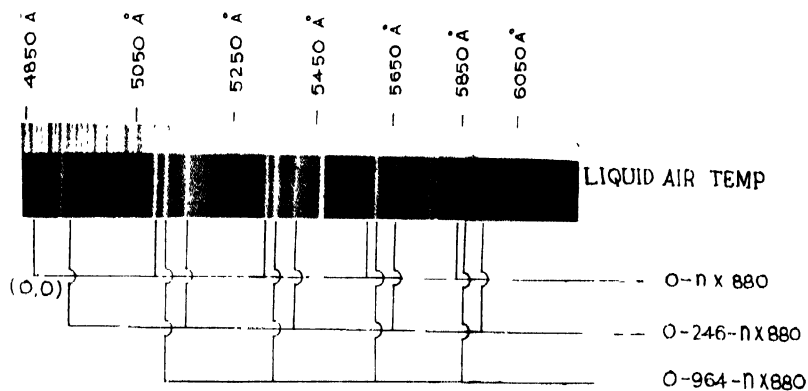


Fig. 5. Fluorescence spectrum of uranyl chloride

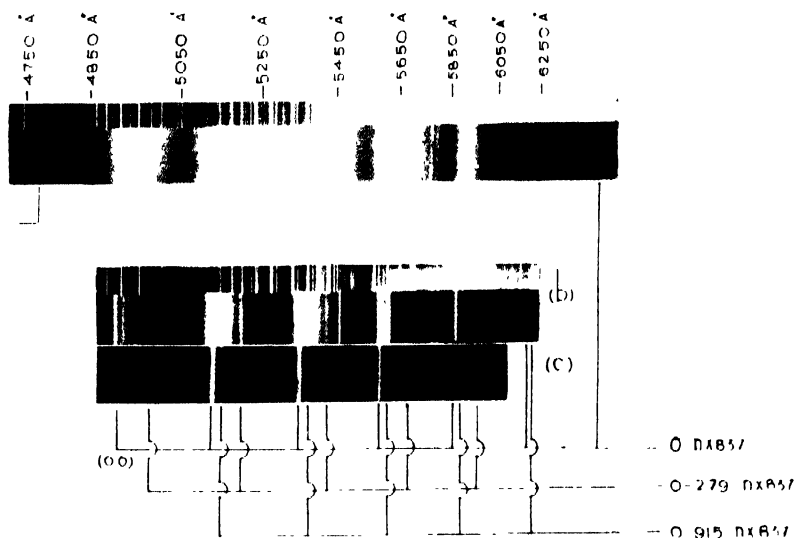


Fig. 6. Fluorescence spectra of potassium uranyl sulphate

- (a) At room temperature.
- (b) At liquid air temperature ( long exposure ).
- (c) At liquid air temperature ( short exposure ).

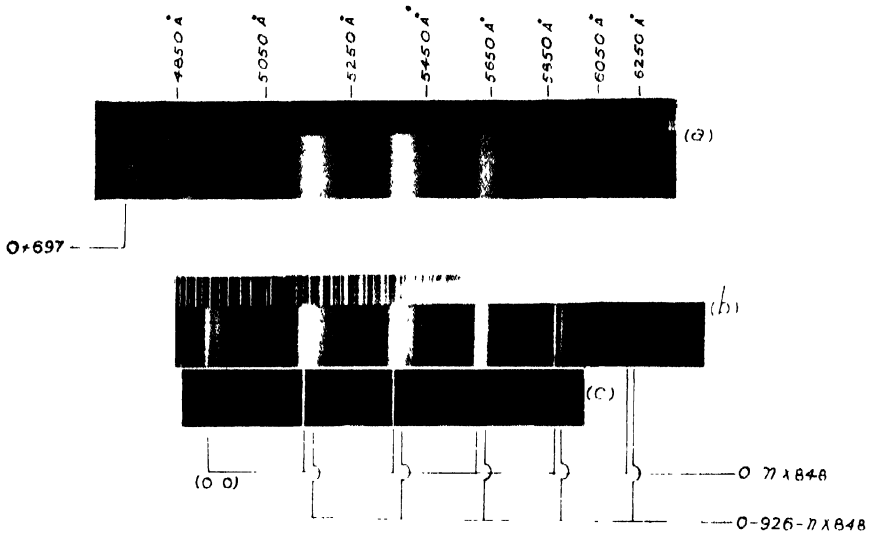


Fig. 7. Fluorescence spectra of ammonium uranyl sulphate

- (a) At room temperature.
- (b) At liquid air temperature ( long exposure )
- (c) At liquid air temperature ( short exposure ).

A special type of quartz Dewar flask (supplied by Thermal Syndicate Ltd.) is used as the container for the liquid air to study the fluorescence spectra at liquid air temperature. The Dewar flask has three fused plane windows on each wall. The holes in the brass rod could be aligned parallel to these windows. The brass rod is suspended by means of a wire into the liquid air contained in the Dewar flask. The specimen under investigation was found to acquire a temperature of  $-177^{\circ}\text{C}$ . The spectrum is photographed on a Fuess spectrograph (dispersion of  $33 \text{ \AA/mm}$  at  $45000 \text{ \AA}$ ) using Ilford HP3 panchromatic plates.

With this set-up, exposures are given ranging from a few minutes to one hour. A very intense picture with even the weakest bands can be obtained in one hour exposure while five minute's exposure is sufficient for bringing out the principal bands of the spectrum.

The fluorescence spectra are taken at liquid air and room temperatures. In all cases, mercury arcs are used as sources of exciting radiations and glass filters having a low transmission value from the blue green to higher wavelengths are used to eliminate the mercury lines in the fluorescence region. The bands are measured against standard iron arc lines. The accuracy of measurements for the sharp bands is  $2 \text{ cm}^{-1}$ ,  $5 \text{ cm}^{-1}$  for moderate diffuse bands and  $15 \text{ cm}^{-1}$  for very diffuse bands. The intensities given are visual estimates from the spectrograms in the 1 to 10 scale and the following abbreviations are adopted for the description of the bands.

vsh—very sharp      d—diffuse  
sh—sharp      vd—very diffuse  
msh—medium sharp

## RESULTS AND DISCUSSION

The fluorescence spectra of the uranyl acetate, nitrate, sulphate, chloride fluoride I, potassium sulphate and ammonium sulphate at liquid air and room temperatures with different exposure times are reproduced in Figs. 1 to 7, Plates IV and V. At room temperature, new bands which are diffuse, are recorded in the region of absorption corresponding to the upper state fundamental of the symmetric stretching frequency of the uranyl ion. At liquid air temperature a few additional bands extending the previous data, are also recorded in the case of uranyl acetate, nitrate and sulphate.

The bands, in general, form into about seven or eight groups separated by about  $860 \text{ cm}^{-1}$  corresponding to the symmetric stretching frequency of the  $\text{UO}_2$  in the ground state. In all the spectra except that of fluoride I, we find the strong doublet pattern of bands repeating at regular intervals with the long wavelength member of each pair weaker than the shorter wavelength component. In the case of fluoride I a strong triplet pattern of bands repeats at regular intervals. In between the groups, a number of weaker bands are observed.

*Earlier analyses :*

Pant (1945) studied the fluorescence spectra of uranyl acetate, sulphate, chloride, fluoride I, fluoride II and potassium uranyl sulphate and analysed the bands of each spectrum on the basis of two electronic transitions with two close lying ground states and a common upper state. Freymann and co-workers (1946, 1947) published another analysis of the fluorescence bands of uranyl acetate, nitrate, chloride and fluoride II. They interpreted the bands on the basis of a forbidden transition with a very weak or totally absent band as (0,0) (Pant's  $A_0$  band). The defects of both these two types of analyses have been discussed at length in our earlier paper (Rao and Narasimham, 1956).

*Present analysis*

The fluorescence bands of each substance have been analysed on the basis of a single electronic allowed transition (Table I to VII). The important features in the analysis of each compound are given below.

*Uranyl acetate*

The (0,0) band in the fluorescence spectrum of the acetate is fixed at  $20587\text{ cm}^{-1}$ . The reasons for this choice are

- (i) This band is strong both in fluorescence and absorption.
- (ii) In fluorescence, this is the first strong band on the short wavelength side.
- (iii) At room temperature, a fluorescence band is obtained at  $21288\text{ cm}^{-1}$ , with a shift of  $701\text{ cm}^{-1}$  from this band alone and the frequency corresponds to the upper state fundamental of the symmetric stretching vibration of the uranyl ion, recorded in absorption.
- (iv) In absorption experiments, two pairs of emission bands have been recorded on the long wavelength side of the (0,0) band agreeing with the first two strong pairs of fluorescence bands. These emission bands could be interpreted as  $0\cdot n \times 860$  and  $0\cdot 940\cdot n \times 860$  with the (0,0) band at  $20587\text{ cm}^{-1}$  (Narasimham and Rao, 1960).

Out of the 57 bands in acetate, about 46 bands could be interpreted on the basis of four fundamentals in the ground state  $860$  (U—O symmetric stretching),  $940$  (U—O asymmetric stretching),  $222$  (O—U—O symmetric bending) and  $36\text{ cm}^{-1}$  (crystal lattice vibration) and three frequencies in the upper state  $701$ ,  $210$  and  $33\text{ cm}^{-1}$  (see Table I). The band at  $19968\text{ cm}^{-1}$  is taken as due to the fundamental  $599$  characteristic of the acetate radical. This suggestion is only a possibility adopted from Dieke's (1949) observation that, in acetates, a fundamental of about  $600\text{ cm}^{-1}$  is generally observed.

*Uranyl nitrate*

For the same reasons as in acetate, the strong band at  $20582\text{ cm}^{-1}$  has been



chosen as the (0,0) band. Out of a total 60 bands, 51 bands could be interpreted on the basis of four fundamentals in the ground state  $866\text{ cm}^{-1}$  (U—O symmetric stretching),  $949\text{ cm}^{-1}$  (U—O asymmetric stretching)  $222\text{ cm}^{-1}$  (symmetric bending) and  $31\text{ cm}^{-1}$  (crystal lattice frequency) and three fundamentals in the upper state  $722\text{ cm}^{-1}$  (corresponding to  $860\text{ cm}^{-1}$  in the ground state),  $210$  and  $33\text{ cm}^{-1}$  (Table II). The band at  $20028\text{ cm}^{-1}$  is interpreted as due to a fundamental  $554\text{ cm}^{-1}$ . Two more such bands are observed in the next groups. A possible suggestion is that this may be a fundamental of the nitrate radical.

### Uranyl sulphate

The fixing up of the (0, 0) band in the sulphate spectrum is a problem of special interest. At liquid air temperature the first prominent band in fluorescence is at  $20316\text{ cm}^{-1}$ .

TABLE I  
Fluorescence bands of uranyl acetate

Wave-number of the band $\text{cm}^{-1}$	Intensity	Shift from (0,0) band ( $\Delta\nu$ )	Assignment		
			Present author	Freymann (1947)	Pant (1945)
(1)	(2)	(3)	(4)	(5)	(6)
21288**	2 vd	+ 701	0 + 701 = 701		
20739*?	1 d	+ 152		(0,0)	$A_0$
20620*	1 msh	+ 33	0 + 33 = 33		
20587*	8 sh		(0,0)	0 + 720 - 860	$B_0$
20551	3 msh	- 36	0 - 36 = 36		
20463	2 sh	- 124			
20426	3 sh	- 161		0 + $2 \times 720 - 2 \times 860$	$D_0$
20365	2 sh	- 222	0 - 222 = 222	0 + 720 - 860 - 210	$B_0 - 235$
20270	2 sh	- 317		0 + 720 - 930 - 210	$A_0 - 2 \times 235$
20146	3 sh	- 441	0 - $2 \times 222 = 444$	0 + 720 - 860 - $2 \times 210$	$B_0 - 2 \times 235$
20112	2 sh	- 475	0 - 36 - $2 \times 222 = 480$		
20059	1 sh	- 528			
19988	1 sh	- 599	0 - 599 = 599		
19874	2 sh	- 713	0 + 210 - 940 = 730	0 - 860	$A_0 - 855$
19808	1 msh	- 778			
19763	2 msh	- 824	0 + 33 - 860 = 827		
19727***	10 sh	- 860	0 - 860 = 860	0 + 720 - $2 \times 860$	$B_0 - 855$
19683	3 d	- 904	0 - 36 - 860 = 896		
19647***	6 sh	- 940	0 - 940 = 940	0 + 720 - 860 - 930	$A_0 - 855 - 235$
19618	2 d	- 969	0 - 36 - 940 = 976		
19556	3 sh	- 1031		0 + 720 - $2 \times 930$ or 0 + $2 \times 720 - 3 \times 860$	$D_0 - 855$
19509	3 sh	- 1078	0 - 222 - 860 = 1082	0 + 720 - $2 \times 860 - 210$	$B_0 - 855 - 235$
19461	3 sh	- 1126	0 - 36 - 222 - 860 = 1118		
19411	3 sh	- 1176		0 + 720 - 860 - 930 - 210	$A_0 - 855 - 2 \times 235$
19366	1 d	- 1221			$B_0 - 855 - 2 \times 235$

TABLE I (Contd.)

Wave-number of the band $\text{cm}^{-1}$	Intensity	Shift from (0,0) band ( $\Delta F$ )	Assignment		
			Present author	Freymann (1947)	Pant (1945)
(1)	(2)	(3)	(4)	(5)	(6)
19312]	2 d	-1275]	$0 - 2 \times 222 - 860 = 1304$		
19255]	2 d	-1332]			
19168	1 msh	-1419			
19107	2 msh	-1480			
19020	2 sh	-1567	$0 \mid 210 - 940 - 860 = 1590$	$0 - 2 \times 860$	$A_0 - 2 \times 855$
18898	1 d	-1689	$0 \mid 33 - 2 \times 860 = 1687$		
18866***	10 sh	-1721	$0 - 2 \times 860 = 1720$	$0 + 720 - 3 \times 860$	$B_0 - 2 \times 855$
18789***	8 sh	-1798	$0 - 940 - 860 = 1800$	$0 \mid 720 - 2 \times 860 - 930$	$A_0 - 2 \times 855 - 235$
18746	2 msh	-1841	$0 - 36 - 940 - 860 = 1836$		
18705	2 sh	-1882		$0 + 720 - 860 - 2 \times 930$ or $0 \mid 2 \times 720 - 2 \times 860$	$D_0 - 2 \times 855$
18664	2 sh	-1923	$0 - 222 - 2 \times 860 = 1942$	$0 + 720 - 3 \times 860$	
18608	2 sh	-1979			$B_0 - 2 \times 855 - 235$
18552	2 sh	-2035		$0 \mid 720 - 2 \times 860 - 930 - 210$	$A_0 - 2 \times 855 - 2 \times 235$
18412	1 d	-2175	$0 - 2 \times 222 - 2 \times 860 = 2104$		
18153	1 msh	-2434	$0 \mid 210 - 940 - 2 \times 860 = 2450$	$0 - 3 \times 860$	$A_0 - 3 \times 855$
18009	8 sh	-2578	$0 - 3 \times 860 = 2580$	$0 \mid 720 - 4 \times 860$	$B_0 - 3 \times 855$
17982	2 msh	-2605	$0 - 36 - 3 \times 860 = 2616$		
17926	6 sh	-2661	$0 - 940 - 2 \times 860 = 2660$		$A_0 - 3 \times 855 - 235$
17895	1 d	-2692	$0 - 36 - 940 - 2 \times 860 = 2696$		
17802	2 d	-2785			
17771	1 msh	-2816	$0 - 222 - 3 \times 860 = 2802$		$B_0 - 3 \times 855 - 235$
17678	1 d	-2909		$0 + 720 - 3 \times 860 - 930 - 210$	$A_0 - 3 \times 855 - 2 \times 235$
17147	6 sh	-3440	$0 - 4 \times 860 = 3440$	$0 + 720 - 5 \times 860$	
17072	4 sh	-3515	$0 - 940 - 3 \times 860 = 3520$	$0 + 720 - 4 \times 860 - 930$	
17053	1 msh	-3534	$0 - 36 - 940 - 3 \times 860 = 3556$		
17005	2 d	-3582			
16482	1 d	-4105			
16303	1 d	-4284			
16273	3 sh	-4314	$0 - 5 \times 860 = 4300$	$0 + 720 - 6 \times 860$	
16205	2 sh	-4382	$0 - 940 - 4 \times 860 = 4380$	$0 + 720 - 5 \times 860 - 930$	
16091	1 msh	-4496	$0 - 222 - 5 \times 860 = 4522$		
15439	2 sh	-5148	$0 - 6 \times 860 = 5160$		
15392	2 sh	-5195	$0 - 940 - 5 \times 860 = 5240$		

\* These bands are recorded in absorption also.

\*\* This band is obtained at room temperature.

\*\*\* These bands are obtained in absorption as emission bands.

TABLE II  
Fluorescence bands of uranyl nitrate

Wave number of the band $\text{cm}^{-1}$	Intensity	Shift from (0,0) band	Assignment	
			Present author	Freyman (1947)
(1)	(2)	(3)	(4)	(5)
22001**	1 vd	+ 1419	$0 + 2 \times 722 = 1444$	
21304**	2 vd	+ 722	$0 + 722 = 722$	
20618*	1 d	+ 36	$0 + 36 = 36$	
20582*	8 sh		(0,0)	$0 + 720 - 860$
20551	3 msh	— 31	$0 - 31 = 31$	
20523	1 d	— 59	$0 - 2 \times 31 = 62$	
20440	3 msh	— 142		
20392	2 sh	— 190	$0 + 36 - 222 = 186$	$0 + 720 - 860 - 230$
20360	2 sh	— 222	$0 - 222 = 222$	
20114	2 msh	— 468	$0 - 2 \times 222 = 444$	
20028	1 msh	— 554	$0 - 554 = 554$	
19924	3 sh	— 658	$0 + 210 - 866 = 656$	$0 + 720 - 860 - 3 \times 230$
19887	3 sh	— 695	$0 - 31 + 210 - 866 = 687$	
19823	2 d	— 759	$0 + 210 - 949 = 739$	$0 - 930$
19762	2 d	— 820	$0 + 36 - 866 = 830$	
19716***	10 sh	— 866	$0 - 866 = 866$	$0 + 720 - 2 \times 860$
19683	3 d	— 899	$0 - 31 - 866 = 897$	
19633***	6 sh	— 949	$0 - 949 = 949$	$0 + 720 - 860 - 930$ or $0 - 860 - 230$
19588	2 d	— 994	$0 - 31 - 949 = 980$	
19545	2 msh	— 1037		$0 + 720 - 2 \times 860 - 930$ or $0 - 930 - 230$
19505	3 sh	— 1077	$0 - 222 - 866 = 1088$	
19455	3 sh	— 1127	$0 - 31 - 222 - 866 = 1119$	$0 + 720 - 860 - 930 - 230$
19316	2 d	— 1266	$0 - 2 \times 222 - 866 = 1310$	$0 + 720 - 2 \times 860 - 2 \times 230$
19225	2 d	— 1357		$0 + 720 - 860 - 930 - 2 \times 230$
19160	1 d	— 1422	$0 - 554 - 866 = 1420$	
19057	3 msh	— 1525	$0 + 210 - 2 \times 866 = 1522$	$0 + 720 - 2 \times 860 - 3 \times 230$
18965	2 msh	— 1617	$0 + 210 - 949 - 866 = 1605$	$0 - 860 - 930$
18854***	8 sh	— 1728	$0 - 2 \times 866 = 1732$	$0 + 720 - 3 \times 860$
18827	2 d	— 1755	$0 - 31 - 2 \times 866 = 1763$	
18777***	8 sh	— 1805	$0 - 949 - 866 = 1815$	$0 + 720 - 2 \times 860 - 930$ or $0 - 2 \times 860 - 230$
18738	2 d	— 1844	$0 - 31 - 949 - 866 = 1846$	
18688	2 msh	— 1894		$0 + 720 - 3 \times 860 - 230$ or $0 - 860 - 930 - 230$
18635	2 sh	— 1947	$0 - 222 - 2 \times 866 = 1954$	$0 + 720 - 2 \times 860 - 930 - 230$
18593	2 msh	— 1989	$0 - 31 - 222 - 2 \times 866 = 1984$	
18562	1 msh	— 2020		
18530	1 msh	— 2052		
18494	1 d	— 2088		$0 + 720 - 3 \times 860 - 2 \times 230$
18412	2 d	— 2170	$0 - 2 \times 222 - 2 \times 866 = 2176$	
18185	1 d	— 2397	$0 + 210 - 3 \times 866 = 2388$	
18105	1 d	— 2477		$0 - 2 \times 860 - 930$

TABLE II (contd)

Wave number of the band $\text{cm}^{-1}$	Intensity	Shift from (0,0) band	Assignment	
			Present author	Freyman (1947)
(1)	(2)	(3)	(4)	(5)
17984	6 sh	-2598	0-3 $\times$ 866 = 2598	0   720-4 $\times$ 860
17916	6 sh	-2666	0-949-2 $\times$ 866 = 2681	0   720-3 $\times$ 860-930 or 0-3 $\times$ 860-230
17803	2 d	2779		
17770	2 msh	-2812	0-222-3 $\times$ 866 = 2820	0   720-3 $\times$ 860-930-230
17726	2 msh	-2856	0-31-222-3 $\times$ 866 = 2850	
17501	2 d	-3081	0-2 $\times$ 222-3 $\times$ 866 = 3042	0   720-3 $\times$ 860-930 -2 $\times$ 230
17458	1 d	-3124	0-554-3 $\times$ 866 = 3152	
17199	1 d	-3383	0-210-949-3 $\times$ 866 = 3337	
17137	4 sh	-3445	0-4 $\times$ 866 = 3464	0   720-5 $\times$ 860
17042	4 sh	-3540	0-949-3 $\times$ 866 = 3547	0   720-4 $\times$ 860-930 or 0-4 $\times$ 720-230
17011	2 msh	-3571	0-31-949-3 $\times$ 866 = 3578	0   720-5 $\times$ 860-230 or 0-3 $\times$ 860-930-230
16898	2 msh	-3684	0-222-4 $\times$ 866 = 3686	0   720-4 $\times$ 860-930-230
16629	2 d	-3953	0-2 $\times$ 222-4 $\times$ 866 = 3908	0   720-860-930-2 $\times$ 230
16267	3 sh	-4315	0-5 $\times$ 866 = 4330	0   720-6 $\times$ 860
16193	3 sh	-4389	0-949-4 $\times$ 866 = 4413	0   720-5 $\times$ 860-930 or 0-5 $\times$ 860-230
16045	2 msh	-4537	0-222-5 $\times$ 866 = 4552	
15900	1 d	-4682		
15780	1 d	-4802	0-2 $\times$ 222-5 $\times$ 866 = 4774	
15438	2 msh	-5144	0-6 $\times$ 866 = 5196	0   720-7 $\times$ 860
15362	2 d	-5220	0-949-5 $\times$ 866 = 5279	0-6 $\times$ 869-230

\* These bands are recorded in absorption also.

\*\* These bands are observed at room temperature.

\*\*\* These bands are recorded in absorption as emission bands.

However, at the same temperature but with longer exposures, a less prominent band develops at  $20560 \text{ cm}^{-1}$ . The frequency shift between these two is  $244 \text{ cm}^{-1}$ . The values for these bands in absorption are  $20317$  and  $20561 \text{ cm}^{-1}$  respectively. But the band at  $20561 \text{ cm}^{-1}$  is much stronger than that at  $20317 \text{ cm}^{-1}$ . It is possible to understand this intensity variation if we assume the (0, 0) band to be at  $20560 \text{ cm}^{-1}$  and interpret the  $20316 \text{ cm}^{-1}$  as  $0-244$  ( $\nu_2$  bending frequency). In the fluorescence spectra of many organic molecules the (0, 0) band is extremely weak compared with some of the fundamentals due to the phenomenon of self-absorption. A similar process may be considered as responsible for the weakness of this (0, 0) band in fluorescence ( $20560 \text{ cm}^{-1}$ ).

The analysis of the sulphate spectrum (Table III) presents some unique features. The actual fundamentals are  $857$ ,  $931$ ,  $244$  and  $25 \text{ cm}^{-1}$  in the ground state of the uranyl ion and  $729$ ,  $242$  and  $32 \text{ cm}^{-1}$  in the upper state. In the

acetate and nitrate spectra, the frequency  $222\text{ cm}^{-1}$  represented by a weak band whereas in the sulphate, this frequency  $244\text{ cm}^{-1}$  has a high intensity. All strong bands of the spectrum could be interpreted only in terms of combination with this fundamental. It is clear that this fundamental  $244$  plays an important role in the fluorescence spectrum. Another fundamental  $962\text{ cm}^{-1}$  is assigned as a possible sulphate ion frequency.

Sevchenko and Stepanov (1949) studied the infra red absorption of the sulphate and observed frequencies forbidden for a linear model of the uranyl ion. Therefore, they concluded that the uranyl ion is bent in sulphate. The fact that the bending frequency  $244\text{ cm}^{-1}$  is very strong in the fluorescence spectrum of the sulphate is a further justification for the idea that the uranyl ion is bent in sulphate.

TABLE III  
Fluorescence bands of uranyl sulphate

Wave number of the band $\text{cm}^{-1}$	Intensity	Shift from (0,0) band $\text{cm}^{-1}$ obs. value	Assignment
(1)	(2)	(3)	(4)
21289**	2 vd	— 729	0 + 729 = 729
21066**	1 vd	+ 506	
20560*	1 sh		(0,0)
20442*	1 sh	— 118	
20379*	2 sh	— 181	0 + 2 × 32 - 244 - 180
20348*	2 sh	— 212	0 + 32 - 244 - 212
20316*	7 vsh	— 244	0 - 244 - 244
20291	3 vsh	— 269	0 - 25 - 244 - 269
20262	2 sh	— 298	0 - 2 - 25 - 244 - 294
20228	1 sh	— 332	
20177	3 sh.	— 383	
20149	3 sh	— 411	
20124	1 sh	436	
20095	1 msh	— 465	0 + 32 - 2 × 244 - 456
20065***	3 sh	— 495	0 - 2 × 244 - 488
20040	2 msh	— 520	0 - 25 - 2 × 244 - 513
19987	1 msh	— 573	0 + 32 + 242 - 857 - 583
19949	2 sh	— 611	0 + 242 - 257 - 615
19929	1 msh	— 631	0 - 25 + 242 - 857 = 640
19890	2 msh	— 670	
19864	1 msh	— 696	
19810	2 sh	— 750	0 - 3 × 244 = 732
19776	1 msh	— 784	
19703***	6 vsh	— 857	0 - 857 = 857
19629	2 sh	— 931	0 - 931 = 931
19598	1 msh	— 962	0 - 962 = 962
19560	1 msh	— 1000	
19521	3 msh	— 1039	0 + 2 × 32 - 244 - 857 = 1037
19498	4 msh	— 1062	0 + 32 - 244 - 857 = 1069
19464***	10 vsh	— 1096	0 - 244 - 857 = 1101

TABLE III (contd.)

Wave number of the band cm <sup>-1</sup>	Intensity	Shift from (0,0) band cm <sup>-1</sup> obs. value	Assignment
(1)	(2)	(3)	(4)
19430	2 sh	- 1130	0-25-244-857=1126
19392	1 sh	-1168	0-2×25-931-244=1151
19372***	6 vsh	- 1188	0-931-244=1175
19337	1 msh	- 1223	
19316	2 sh	-1244	
19259	1 msh	- 1301	
19216	2 sh	-1344	0-2×244-857=1345
19195	2 msh	- 1365	0-25-2×244-857=1370
19111	1 msh	-1449	0+242-2×857=1472
19009	2 msh	-1551	0-3×244-857=1589
18910	1 msh	-1650	
18858	6 sh	-1702	0-2×857=1714
18787	1 msh	-1773	0-962-857=1819
18609***	10 vsh	-1951	0-244-2×857=1958
18574	2 sh	-1986	0-25-244-2×857=1983
18528***	8 vsh	-2032	0-931-244-857=2032
18465	2 msh	-2095	
18337	2 msh	-2223	0+2×244-2×857=2202
18243	2 msh	-2317	0+242-3×857=2329
18207	2 msh	-2353	
17992	4 vsh	- 2567	0-3×857=2571
17924	1 d	-2636	0-962-3×857=2676
17759	8 vsh	-2801	0-244-3×857=2815
17671	6 vsh	-2889	0-931-244-2×857=2889
17576	2 msh	-2984	
17490	1 d	-3070	0-2×244-3×857=3059
17186	1 d	-3374	
17141	2 sh	-3419	0-4×857=3428
17024	1 sh	-3536	0-962-3×857=3533
16896	6 vsh	-3664	0-244-4×857=3672
16806	6 vsh	-3754	0-931-244-3×857=3746
16720	2 sh	-3840	
16613	1 msh	-3947	0-2×244-4×857=3916
16535	1 msh	-4025	0+242-5×857=4041
16378	1 d	-4182	
16171	1 msh	-4389	0-962-4×857=4390
16119	1 msh	-4441	
16061	2 sh	-4499	0-244-5×857=4529
15980	2 sh	-4580	0-931-244-4×857=4603
15908	1 msh	-4652	
15210?	1 d	-5350	0-244-6×857=5386
15136?	1 d	-5424	0-931-244-5×857=5460

\* These bands are recorded in absorption also.

\*\* These bands are obtained at room temperature.

\*\*\* These bands are recorded in absorption as emission bands.

Uranyl fluoride—I :

Out of the three fluorides i.e., anhydrous fluoride and two hydrated varieties called by Pant (1945) as fluoride I and fluoride II, fluoride I is the only compound which has shown fluorescence. The triplet pattern of bands observed in the fluorescence spectrum of fluoride I immediately makes us suspect whether this spectrum is entirely due to fluoride I or possibly due to any other fluoride that may exist as an impurity in fluoride I. On a comparison of the two bands at 20012 and 20092  $\text{cm}^{-1}$  with those two observed in absorption of fluoride I and fluoride II, it was noted that the band at 20092  $\text{cm}^{-1}$  in fluorescence can be attributed to fluoride II while the stronger band at 20012  $\text{cm}^{-1}$  can be attributed to fluoride I. If we take these two as the (0, 0) bands for the two fluorides, all the bands could be explained on the basis of two series: Series I consisting of the comparatively weaker bands made out of the short-wavelength components of the triplet structure to be attributed to fluoride II and series II consisting of the central strong bands and the long wave length components of the triplet structures making the usual doublet patterns obtained in all other fluorescence spectra and interpreted on the same lines. This classification is indicated in fig. 4, Plate IV (B) and Table IV.

The shift between the two (0, 0) bands of the two fluorides is 80  $\text{cm}^{-1}$ . The values of the symmetric stretching fundamental ( $\nu_1$ ) in fluoride I and fluoride II are respectively 824 and 814  $\text{cm}^{-1}$  while the value of the asymmetric stretching frequency ( $\nu_3$ ) in fluoride I is 891  $\text{cm}^{-1}$ . The  $\nu_3$  frequency of fluoride II may have about 70  $\text{cm}^{-1}$  shift from the  $\nu_1$  and it makes its  $\nu_3$  fundamental and its combinations with the  $\nu_1$  fall on the  $\nu_1$  fundamental and its overtones of fluoride I. This might account for the singlet structure of the bands attributed to fluoride II.

TABLE IV  
Fluorescence bands of uranyl fluoride I and II

Wave-number of the band $\text{cm}^{-1}$	Intensity	Shift from (0,0) F. I	Shift from (0,0) F. II	Assignment		Pant. (1945)
				Present author Fluoride I	Fluoride II	
(1)	(2)	(3)	(4)	(5)	(6)	(7)
20687*	1 vd	+ 675	+ 595	0 + 675 = 675		
20092**	4 vsh	+ 80			(0,0)	B <sub>0</sub>
20070**	1 msh	+ 58	— 22			
20012**	7 vsh		— 80	(0,0)		A <sub>0</sub> —176
19980	1 msh	— 32	— 112	0—32=32		D <sub>0</sub>
19918	1 msh	— 94	— 174			B <sub>0</sub> —176
19894	2 msh	— 118	— 198		0—198=198	
19812	1 msh	— 200	— 280	0—200=200		D <sub>0</sub> —176
19591	2 msh	— 421	— 501	0—2×200=400		B <sub>0</sub> —3×176
19489	1 msh	— 523	— 603			

TABLE IV—(contd).

Wave-number of the band $\text{cm}^{-1}$	Inten-sity	Shift from (0,0) F. I	Shift from (0,0) F. II	Assignment		Pant (1945)
				Present author Fluoride I	Fluoride II	
(1)	(2)	(3)	(4)	(5)	(6)	(7)
19453	1 msh	— 559	— 639			
19278***	6 vsh	— 734	— 814		0—814=814	B <sub>0</sub> —819
19188***	10 vsh	— 824	— 904	0—824=824		A <sub>0</sub> —827—176
19121***	7 vsh	— 891	— 971	0—891=891		B <sub>0</sub> —819—176
19085	1 msh	— 927	— 1007		0—198—814 =1012	
18911	2 sh	— 1101	— 1181	0—200—891=1091		A <sub>0</sub> —827—2×176
18810	3 sh	— 1202	— 1282	0—2×200—824 =1224		A <sub>0</sub> —827—3×176
18763	2 msh	— 1249	— 1329			
18726	1 msh	— 1286	— 1366			B <sub>0</sub> —819—3×176
18639	3 sh	— 1373	— 1453			
18574	1 msh	— 1438	— 1518	0—3×200—824 =1424		
18542	1 d	— 1470	— 1550			
18502	1 d	— 1510	— 1590			A <sub>0</sub> —2×827
18463***	5 vsh	— 1549	— 1629		0—2×814 =1628	B <sub>0</sub> —2×819
18405	2 sh	— 1607	— 1687			D <sub>0</sub> —2×795
18363***	8 sh	— 1649	— 1729	0—2×824=1648		A <sub>0</sub> —2×827—176
18295***	6 sh	— 1717	— 1797	0—891—824=1715		B <sub>0</sub> —2×819—176
18154	1 msh	— 1858	— 1938	0—200—2×824 =1848		B <sub>0</sub> —2×795—176
18125	1 msh	— 1887	— 1967			
18082	1 sh	— 1930	— 2010	0—200—891—824 =1915		B <sub>0</sub> —2×819 —2×176
18026	2 sh	— 1986	— 2066			
17934	1 d	— 2078	— 2158	0—2×200—2×824 =2048		B <sub>0</sub> —3×819 —2×176
17657	3 sh	— 2355	— 2435		0—3×814 =2442	B <sub>0</sub> —3×819
17595	2 sh	— 2417	— 2497			B <sub>0</sub> —3×795
17542	6 sh	— 2470	— 2550	0—3×824=2472		A <sub>0</sub> —3×827—176
17480	4 sh	— 2532	— 2612	0—891—2×824 =2539		B <sub>0</sub> —3×819—176
17191	2 d	— 2821	— 2901			
17031	2 sh	— 2981	— 3061			
16838	2 msh	— 3174	— 3254		0—4×814=3256	
16777	2 msh	— 3235	— 3315			
16704	4 sh	— 3308	— 3388	0—4×824=3296		
16653	3 sh	— 3359	— 3439	0—891—3×824 =3363		
15913	1 msh	— 4099	— 4179	0—5×824=4120		
15855	1 msh	— 4157	— 4237	0—891—4×824 =4187		

\* This band is recorded at room temperature.

\*\* These bands are obtained in absorption also.

\*\* These bands are obtained as emission bands in absorption experiments.



The other fundamentals obtained in the fluorescence spectrum of fluoride I are the bending frequency of  $200\text{ cm}^{-1}$  ( $\nu_2$ ), the crystal lattice frequency of  $32\text{ cm}^{-1}$  in the ground state and  $675\text{ cm}^{-1}$  of the  $\nu_1$  frequency in the upper state.

TABLE V  
Fluorescence bands of uranyl chloride

Wave-number of the band $\text{cm}^{-1}$	Intensity	Shift from (0,0) band	Assignment		
			Present author	Freyman (1947)	Pant (1945)
(1)	(2)	(3)	(4)	(5)	(6)
20547*	1 msh	+ 26	0 + 26	0 + 720 - 875	$B_0$
20521*	5 sh		(0,0)		
20443*	2 msh	- 78		0 + 720 - 930 or	$A_0 - 246$
20275	3 sh	- 246	0 - 246 - 246	0 - 230	
20213	2 d	- 308		0 + 720 - 875 - 230	$B_0 - 246$
20144	1 d	- 377		0 + 720 - 930 - 230	
19641	10 sh	- 880	0 - 880 - 880		$A_0 - 2 \times 246$
19557	10 sh	- 964	0 - 964 = 964	0 + 720 - 2 \times 875	$B_0 - 876$
19391	5 sh	- 1130	0 - 964 - 880 = 1126	0 + 720 - 875 - 930 or	$A_0 - 876 - 246$
19327	2 d	- 1194	0 - 246 - 880 = 1126	0 - 875 - 230	
19248	1 d	- 1273	0 - 246 - 964 = 1210	0 + 720 - 2 \times 875 - 230	$B_0 - 876 - 246$
18762	8 sh	- 1759	0 - 2 \times 880 - 1760	or 0 - 930 - 230	
18681	10 sh	- 1840	0 - 964 - 880 = 1844	0 + 720 - 3 \times 875	
18515	5 sh	- 2006	0 - 246 - 2 \times 880 = 2006	0 + 720 - 2 \times 875 - 930 or	
18452	1 d	- 2069	0 - 246 - 964 - 880 = 2090	0 - 2 \times 875 - 230	
18370	1 d	- 2151		0 + 720 - 3 \times 875 - 230 or	
17884	4 sh	- 2637	0 - 3 \times 880 = 2640	0 - 875 - 930 - 230	
17806	8 sh	- 2715	0 - 964 - 2 \times 880 = 2724	0 + 720 - 4 \times 875	
17636	4 msh	- 2885	0 - 246 - 3 \times 880 = 2886	0 + 720 - 4 \times 875 - 230	
17551	1 d	- 2970	0 - 246 - 964 - 2 \times 880	0 - 2 \times 875 - 930 - 230	
16989	2 sh	- 3532	= 2970 0 - 4 \times 880 = 3520	0 + 720 - 5 \times 875	
16920	4 sh	- 3601	0 - 964 - 3 \times 880 = 3604		
16755	1 d	- 3766	0 - 246 - 4 \times 880 = 3766	0 + 720 + 4 \times 875 - 930 or	
				0 - 4 \times 875 - 230	
				0 + 720 - 5 \times 875 - 230 or	
				0 - 3 \times 875 - 930 - 230	

These bands are obtained in absorption also.

TABLE VI  
Fluorescence bands potassium uranyl sulphate

Wave-number of the band $\text{cm}^{-1}$	Intensity	Shift from (0,0) band	Assignment	
			Present author	Pant (1945)
(1)	(2)	(3)	(4)	(5)
21035**	1 vd	+ 662	$0 + 662 = 662$	
20476*	1 d	+ 103	$0 + 3 \times 30 = 90$	$A_o$
20431*	2 sh	+ 58	$0 + 2 \times 30 = 60$	
20373*	10 vsh	(0,0)	(0,0)	$B_o$
20329*	2 sh	- 44	$0 - 44 = 44$	
20302*	4 sh	- 71	$0 - 2 \times 44 = 88$	$A_o - 172$
20263	2 sh	- 110		$D_o$
20241*	3 sh	- 132		
20211	3 sh	- 162		
20179	2 msh	- 194	$0 - 194 = 194$	$B_o - 172$
20148	1 msh	226		
20094	6 sh	279	$0 - 279 = 279$	$A_o - 2 \times 172$
20046	2 sh	327	$0 - 44 - 279 = 323$	$B_o - 2 \times 172$
19956	2 sh	417	$0 - 417 = 417$	$A_o - 3 \times 172$
19895	1 msh	478		$D_o - 2 \times 172$
19850	1 msh	523		
19824	1 msh	549	$0 - 2 \times 279 = 558$	
19776	1 msh	597	$0 - 597 = 597$	$A_o - 4 \times 172$
19706	1 sh	667		$B_o - 4 \times 172$
19636	2 d	737	$0 + 3 \times 30 - 837 = 747$	$A_o - 833$
19601	3 msh	772	$0 + 2 \times 30 - 837 = 777$	
19566	5 msh	807	$0 + 30 - 837 = 807$	
19536***	10 vsh	837	$0 - 837 = 837$	$B_o - 833$
19458***	7 vsh	915	$0 - 915 = 915$	$A_o - 833 - 172$
19109	3 sh	964	$0 - 44 - 915 = 959$	
19372	5 vsh	1001	$0 - 1001 = 1001$	$B_o - 833 - 172$
19346	2 d	- 1027	$0 - 194 - 837 = 1031$	
19314	2 d	- 1059		
19260	7 sh	- 1113	$0 - 279 - 837 = 1116$	$A_o - 833 - 2 \times 172$
19219	2 msh	- 1144	$0 - 44 - 279 - 837 = 1160$	$B_o - 833 - 2 \times 172$
19155	1 d	- 1218		
19104	3 msh	- 1269	$0 - 417 - 837 = 1254$	$A_o - 833 - 3 \times 172$
19063	2 msh	- 1310		$B_o - 833 - 2 \times 172$
18936	2 msh	- 1437	$0 - 597 - 837 = 1434$	$A_o - 833 - 4 \times 172$
18872	2 msh	- 1501		$B_o - 833 - 4 \times 172$
18804	1 d	- 1509		
18765	2 d	- 1608	$0 + 2 \times 30 - 2 \times 837 = 1614$	
18732	5 msh	- 1641	$0 + 30 - 2 \times 837 = 1644$	
18703***	10 vsh	- 1670	$0 - 2 \times 837 = 1674$	
18626***	6 vsh	- 1747	$0 - 915 - 837 = 1752$	
18587	1 d	- 1786	$0 - 44 - 915 - 837 = 1796$	
18536	5 sh	- 1837	$0 - 1001 - 837 = 1838$	
18483	1 d	- 1890	$0 - 194 - 2 \times 837 = 1868$	
18431	4 sh	- 1942	$0 - 279 - 2 \times 837 = 1953$	
18376	3 sh	- 1997	$0 - 44 - 279 - 2 \times 837 = 1997$	

TABLE VI (contd.)

Wave-number of the band $\text{cm}^{-1}$	Intensity	Shift from (0,0) band $\text{cm}^{-1}$	Assignment	
			Present author	Pant (1945)
(1)	(2)	(3)	(4)	(5)
18299	2 d	-2074	$0-417-2 \times 837=2091$	
18097	1 msh	-2276	$0-795-2 \times 837=2271$	
18032	1 msh	-2341		
17903	3 d	-2470	$0+30-3 \times 837=2481$	
17875	8 sh	-2498	$0-3 \times 837=2511$	
17797	5 sh	-2576	$0-915-2 \times 837=2589$	
17744	1 d	-2629	$0-44-915-2 \times 837=2633$	
17706	3 sh	-2667	$0-1001-2 \times 837=2675$	
17646	1 d	-2727	$0-194-3 \times 837=2705$	
17592	2 msh	-2781	$0-279-3 \times 837=2790$	
17541	2 msh	-2832	$0-44-279-3 \times 837=2834$	
17461	1 msh	-2912	$0-417-3 \times 837=2928$	
17357	1 d	-3016		
17184	1 d	-3189		
17143	1 d	-3230		
17055	2 msh	-3318	$0+30-4 \times 837=3318$	
17024	5 sh	-3349	$0-4 \times 837=3348$	
16951	3 sh	-3422	$0-915-3 \times 837=3426$	
16851	2 sh	-3522	$0-1001-3 \times 837=3512$	
16774	1 msh	-3599	$0-279-4 \times 837=3627$	
16706	1 msh	-3667	$0-44-279-4 \times 837=3671$	
16583	1 msh	-3790	$0-417-4 \times 837=3675$	
16482	1 d	-3891		
16202	2 sh	-4171	$0-5 \times 837=4185$	
16134	1 sh	-4239	$0-915-4 \times 837=4263$	
15326**	1 vd	-5047	$0-6 \times 837=5022$	

\* These bands are also obtained in absorption.

\*\* These bands are recorded at room temperature only.

\*\*\* These bands are obtained as emission bands in absorption experiments.

### Uranyl chloride

The first strong band in fluorescence is at  $20521 \text{ cm}^{-1}$  which is also strong in absorption (value  $20530 \text{ cm}^{-1}$ ). Therefore, this band is chosen as the (0, 0) band. The other bands could be interpreted on the basis of three fundamentals in the ground state  $880 \text{ cm}^{-1}$  (symmetric stretching),  $964 \text{ cm}^{-1}$  (asymmetric stretch-

ing) and  $246\text{ cm}^{-1}$  (symmetric bending) and one fundamental in the upper state  $26\text{ cm}^{-1}$  (crystal lattice frequency) (Table V). It is seen that the 880 fundamental and its overtones are weaker in intensity than 964 fundamental and its combinations with 880 fundamental fig. 5, Plate V (A) which shows violation of selection rules due to the crystalline fields.

#### *Potassium uranyl sulphate*

The first strong band at  $20373\text{ cm}^{-1}$  is chosen as the (0, 0) band for reasons similar to those in acetate. Most of the other bands could be explained on the basis of five fundamentals in the ground state  $837\text{ cm}^{-1}$  (symmetric stretching),  $915\text{ cm}^{-1}$  (asymmetric stretching),  $194$  and  $279\text{ cm}^{-1}$  (symmetric bending) and  $44\text{ cm}^{-1}$  (crystal lattice frequency) and two fundamentals in the upper state  $662\text{ cm}^{-1}$  (symmetric stretching) and  $30\text{ cm}^{-1}$  (crystal lattice frequency) (Table (VI). Among the two fundamentals belonging to the bending vibration,  $194\text{ cm}^{-1}$  corresponds to the in-plane bending frequency and  $279\text{ cm}^{-1}$  corresponds to the out-of-plane bending frequency of the uranyl ion. These two frequencies arise due to the removal of degeneracy in the linear  $\text{O}-\text{U}-\text{O}$  ion which becomes slightly bent in the crystalline fields. The out-of-plane bending fundamental is stronger than the in-plane bending fundamental. As in sulphate, in the case of potassium uranyl sulphate also, the bands analysed as  $0-279-n \times 837$  appear with moderately strong intensity which shows the importance of the bending frequency. This may be taken as an indication that the uranyl ion is slightly more bent than in acetate, nitrate, etc. Sevchenko and Stepanov (1949) who studied the infra red absorption of this substance have come to the conclusion that the ion is slightly bent as some bands forbidden for a linear model of the uranyl ion are present in the spectrum.

Three possible fundamentals  $417$ ,  $597$ , and  $1001\text{ cm}^{-1}$  of the sulphate ion have been used in the analysis to explain some of the weak bands. These frequency values agree well with the Raman values given for the sulphate ion in sulphuric acid (Hibben, 1939).

#### *Ammonium uranyl sulphate*

The first strong band at  $20348\text{ cm}^{-1}$  has been chosen as the (0, 0) band for the same reasons as in acetate etc. About 45 bands have been analysed on the basis of the five fundamentals in the ground state  $848\text{ cm}^{-1}$  (symmetric stretching),  $926$  (asymmetric stretching),  $207\text{ cm}^{-1}$  (in-plane bending) frequency,  $273\text{ cm}^{-1}$  (out-of-plane bending frequency) and  $29\text{ cm}^{-1}$  (crystal lattice frequency) and two fundamentals in the upper state  $697$  and  $24\text{ cm}^{-1}$  (Table VII). As in the case of potassium uranyl sulphate, the two frequencies  $207$  and  $273\text{ cm}^{-1}$  arise due to the removal of degeneracy in the linear  $\text{O}-\text{U}-\text{O}$  ion, which becomes slightly bent in the crystal line fields. Three possible fundamentals  $473$ ,  $626$ , and  $1195\text{ cm}^{-1}$

TABLE VII

Fluorescence bands of ammonium uranyl sulphate

Wave-number of the band $\text{cm}^{-1}$	Intensity	Shift from (0,0) band $\text{cm}^{-1}$	Assignment
(1)	(2)	(3)	(4)
21045*	1 vd	+ 697	$0 + 697 = 697$
20410**	1 d	+ 62	$0 + 2 \times 24 = 48$
20372	3 d	+ 24	$0 + 24 = 24$
20348**	7 sh		(0,0)
20319	4 d	— 29	$0 - 29 = 29$
20248	4 d	— 100	
20171	1 d	— 177	$0 + 24 - 207 = 183$
20141	2 msh	— 207	$0 - 207 = 207$
20075	3 sh	— 273	$0 - 273 = 273$
19995	1 msh	— 353	
19931	1 msh	— 417	$0 - 2 \times 207 = 414$
19875	2 sh	— 473	$0 - 473 = 473$
19722	1 sh	— 626	$0 - 626 = 626$
19695	1 d	— 653	$0 - 29 - 626 = 655$
19563	2 d	— 785	$0 + 2 \times 24 - 484 = 800$
19529	4 d	— 819	$0 + 24 - 848 = 824$
19500***	10 sh	— 848	$0 - 848 = 848$
19422***	8 sh	— 926	$0 - 926 = 926$
19311	4 d	— 1037	$0 - 207 - 848 = 1055$
19225	4 d	— 1123	$0 - 278 - 848 = 1121$
19153	2 msh	— 1195	$0 - 1195 = 1195$
19092	1 msh	— 1256	$0 - 2 \times 207 - 848 = 1262$
19031	3 sh	— 1317	$0 - 473 - 848 = 1321$
18967	1 msh	— 1381	
18878	2 sh	— 1470	$0 - 626 - 848 = 1474$
18718	1 d	— 1630	$0 + 2 \times 24 - 848 = 1648$
18687	2 d	— 1661	$0 + 24 - 2 \times 848 = 1672$
18666***	10 sh	— 1682	$0 - 2 \times 848 = 1696$
18583***	8 sh	— 1765	$0 - 926 - 848 = 1774$
18468	4 d	— 1880	$0 - 207 - 2 \times 848 = 1903$
18378	4 d	— 1970	$0 - 273 - 2 \times 848 = 1969$
18307	1 d	— 2041	$0 - 1195 - 848 = 2043$
18187	2 sh	— 2162	$0 - 473 - 2 \times 848 = 2169$
18120	1 msh	— 2228	
18036	2 sh	— 2312	$0 - 626 - 2 \times 848 = 2322$
17842	1 d	— 2506	
17830	8 sh	— 2518	$0 - 3 \times 848 = 2544$
17750	6 sh	— 2598	$0 - 926 - 2 \times 848 = 2622$
17642	3 d	— 2706	$0 - 207 - 3 \times 848 = 2751$
17537	3 d	— 2811	$0 - 273 - 3 \times 848 = 2817$
17556	2 msh	— 2891	$0 - 1195 - 2 \times 848 = 2891$
17378	1 msh	— 2970	$0 - 2 \times 207 - 3 \times 848 = 2958$
17361	1 d	— 2987	$0 - 473 - 3 \times 848 = 3017$
17192	1 d	— 3156	$0 - 726 - 3 \times 848 = 3170$

TABLE VII (*contd.*)

Wave-number of the band $\text{cm}^{-1}$	Intensity	Shift from (0,0) band $\text{cm}^{-1}$	Assignment
(1)	(2)	(3)	(4)
16959	6 sh	-3389	$0-4 \times 848 = 3392$
16878	4 sh	-3470	$0-926-3 \times 848 = 3470$
16791	2 sh	-3557	$0-207-4 \times 848 = 3599$
16686	1 msh	-3662	$0-273-4 \times 848 = 3655$
16147	2 sh	-4201	$0-5 \times 848 = 4240$
16073	2 sh	-4275	$0-926-4 \times 848 = 4318$
16016	1 d	-4332	

\* This band is recorded at room temperature only.

\*\* These bands are obtained in absorption also.

\*\*\* These bands are obtained as emission bands in absorption experiments.

of the sulphate ion are also identified and used in the analysis to explain some weak bands in between the groups. These frequency values are found to agree well with the Raman values given for the sulphate ion in sulphuric acid (Hibben, 1939).

#### ACKNOWLEDGMENTS

This work has been carried out in the Spectroscopy Laboratory of Andhra University, Waltair. The author's thanks are due to Dr. V. Ramakrishna Rao, for his inspiring guidance and to Prof. K. Rangadhama Rao, for his interest in the work. The author is also thankful to Prof. R. K. Asundi for some helpful suggestions in the course of investigation.

#### REFERENCES

- Bacquerel, E., 1872, *Compt. Rend.*, **75**, 296.  
 Becquerel, E. and Onnes, 1909, *Leiden Communications*, 110.  
 Dieke, G. K. and Duncan, A. B. F., 1949, *Spectroscopic Properties of Uranium Compounds* (Mcgraw Hill Publication).  
 Freymann, M., Guilmar, T. and Freymann, R., 1946, *Compt. Rend.*, **223**, 573.  
 Freymann, M., 1947, *Compt. Rend.*, **225**, 529.  
 Hibben, J. H., 1939, *The Raman Effect and its Chemical Applications* (Reinhold Publications Corporation, New York).  
 Narasimham, K. V. and Ramakrishna Rao, V., 1960, *J. Sci. Industr. Res.*, **19B**, 285.  
 Pant, D. D., 1945, *Proc. Ind. Acad. Sci.*, **22A**, 95.  
 „, 1945, *Proc. Ind. Acad. Sci.*, **22A**, 110.  
 „, 1950, *Proc. Ind. Acad. Sci.*, **31A**, 35.  
 Ramakrishna Rao, V. and Narasimhan, K. V., 1956, *Ind. J. Phys.*, **30**, 334.  
 Sevchenko, A. N. and Stopanov, B. I., 1949, *Zuhr. Exptl. Teoret Fiz.*, **19**, 1113.

# A GENERAL TREATMENT OF PENETRATION FACTOR IN ALPHA-DECAY

S. K. DUTTA

DEPARTMENT OF THEORETICAL PHYSICS,

INDIAN ASSOCIATION FOR THE CULTIVATION OF SCIENCE, JADAVPUR, CALCUTTA-32

(Received March 29, 1961)

**ABSTRACT.** A general treatment of the calculation of the penetration probability of alpha-particles through a potential barrier of Woods-Saxon diffuse type nuclear potential along with the Coulomb potential has been given according to the one-body model for arbitrary values of the angular momentum of the emitted alpha-particles. In the region where practically only the Coulomb potential is present the rigorous solution of Schrödinger equation has been taken from that of Abramowitz. Near the nuclear boundary where both the potentials operate, the Schrödinger equation has been solved by an ingenious method due to Lanczos.

## INTRODUCTION

Uptil now, the calculation of the penetration factor in alpha-decay has mostly been based on the WKB method. But it does not seem justified to put much reliance on the results derived by this method without proper investigation specially when the validity of that method has been doubted at times (Blatt and Weisskopf, 1954). So this problem has been tried by a method due to Lanczos (1938). In doing so, the one-body model was followed and for the nuclear potential use was made of the Woods-Saxon diffuse potential which drops exponentially beyond the nuclear surface, besides that the Coulomb potential is present throughout the region. In the region where the Coulomb field predominates the Schrödinger equation has been solved by the Riccati-I method as treated by Abramowitz (1949) (c.f. Froberg, 1955). The Schrödinger equation in the neighbourhood of the nuclear boundary has been solved by the method of Lanczos (1938).

In a previous publication by Dutta, Mitra and Sil (1960), hereafter referred to as I, a calculation of the penetration factor in the process of alpha-decay following one body model has been given for the case of  $l = 0$ , where the potential field was the same as in this case. In I, for the sake of simplification the Coulomb potential was taken to be constant near the nuclear surface. In the present paper that simplification has been dispensed with and the equation takes into account any arbitrary values of  $l$ . Consequently the method of solution for this general case has been different from that of I.

In the method given in I, the differential equation was equated instead of to zero, to an error term proportional to the Tshebysheff's polynomial of a given order. As a result a finite power series solution was obtained, the coefficients of which were easily calculated with the help of a set of recursion relations. In that case the error term vanished at the zero points of the Tshebysheff's polynomial and the error involved in the solution was at the most 1 in  $10^8$ .

In the present case, the differential equation contains the Woods-Saxon exponential term, the Coulomb  $\frac{1}{r}$  term and the centrifugal  $\frac{l(l+1)}{r^2}$  term and the method of solution, though different from that in I, has also been given by Lanczos (1938). The approximate solution of such a general differential equation which can not be equated to any polynomial, is obtained in the form of a finite power series solution. The coefficients of the power series are evaluated by demanding the vanishing of the differential equation at the zero points of the Tshebysheff's polynomial and thus by solving a set of simultaneous linear equations.

The method given here is a generalisation of the method given in I, to include the cases of differential equation with non-rational coefficients; for the differential equation with rational coefficients this method yields exactly the same coefficients obtained by the method given in I.

The penetration factor has been calculated from the value of the wave function at the point near the nuclear boundary where the potential energy is equal to the kinetic energy of the emitted alpha-particle.

On comparing our results with those obtained by the WKB method it appears that both the sets agree well with each other.

#### MATHEMATICAL FORMULATION

The equation for  $u$ , which is  $r$  times the wave function of the radial part of the Schrödinger equation can be written as

$$\frac{d^2u}{dr^2} + \frac{2m}{\hbar^2} \left[ E - U(r) - V(r) \right] u = 0, \quad \dots (1)$$

where 
$$U(r) = \frac{2(Z-2)e^2}{r} + \frac{\hbar^2}{2m} \cdot \frac{l(l+1)}{r^2}$$

and 
$$V(r) = \frac{-V_0}{1 + e^{(r-R)/a}}.$$

For convenience of calculation, we neglect  $V(r)$  beyond the point  $r_1$  where the nuclear potential drops to  $\frac{-V_0}{100}$ .



To solve Eq. (1) the space is divided into two regions  $r_2 \leq r \leq r_1$  and  $r > r_1$ ,  $r_2$  being the point where the potential energy is equal to the kinetic energy of the emitted  $\alpha$ -particle. In the latter region only the Coulomb potential is of any value.

To solve Eq. (1) in the region  $r_2 \leq r \leq r_1$  Eq. (1) is rewritten by changing the independent variable to  $x = r/a$ , as follows :

$$\frac{d^2 u}{dx^2} + \left[ \frac{\lambda^2}{1 + \beta e^x} - f(x) - K^2 \right] u = 0, \quad \dots (2)$$

where  $\lambda^2 = \frac{2ma^2}{\hbar^2} V_0$ ,  $\beta = e^{-R/a}$ ,  $K^2 = \frac{2ma^2}{\hbar^2} \{U(ax_1) - E\}$

and  $f(x) = \frac{2ma^2}{\hbar^2} [U(ax) - U(ax_1)]$ .

$U(ax)$  and  $U(ax_1)$  being the values of  $U(r)$  and  $U(r_1)$  respectively on changing the independent variable.

Let us suppose the solution to be of the form,

$$u \sim e^{\mp Kx} \cdot F_{\mp}$$

Thus the Eq. (2) becomes

$$-\frac{d^2 F_{\mp}}{dx^2} \mp 2K \frac{dF_{\mp}}{dx} + \left\{ \frac{\lambda^2}{1 + \beta e^x} - f(x) \right\} F_{\mp} = 0 \quad \dots (3)$$

Again, substituting  $z = e^{-x}$  and putting  $\frac{z + \beta}{z} f(x) = \phi(z)$ , the Eq. (3) becomes

$$z(z + \beta) \frac{d^2 F_{\mp}}{dz^2} + (z + \beta)(1 \pm 2K) \frac{dF_{\mp}}{dz} + \{\lambda^2 - \phi(z)\} F_{\mp} = 0 \quad \dots (4)$$

For later calculations the independent variable occurring as the argument of the Tshebysheff's polynomial has to be normalised such that it varies from zero to one; so we make the transformation

$$p = \frac{z - z_1}{z_2 - z_1}$$

Thus we get from Eq. (4)

$$(p + \mu)(p + \nu) \frac{d^2 F_{\mp}}{dp^2} + \delta(p + \nu) \frac{dF_{\mp}}{dp} + \{\lambda^2 - \chi(p)\} F_{\mp} = 0, \quad \dots (5)$$

where  $\mu = \frac{z_1}{z_2 - z_1}$ ,  $\nu = \frac{z_1 + \beta}{z_2 - z_1}$ ,  $\delta = 1 \pm 2k$ ,  $\chi(p) = \phi(z)$ .

For  $F$ , a certain polynomial of  $n$  th order in  $p$  has been assumed which satisfy the above differential equation at the zeros of the Tshebysheff's polynomial of order  $n$ .

Let  $F = \sum_{i=0}^n a_i p^i$ , where  $a_0 = 1$ .

and  $p_1, p_2, \dots, p_n$  are the roots of the equation

$$T_n(p) = 0,$$

where  $T_n(p)$  is the Tshebysheff's polynomial of order  $n$ . Then on substitution of the polynomial  $\sum_{i=0}^n a_i p^i$  for  $F$  in the Eq. (5) we have a set of  $n$  simultaneous equations :

$$(p_i + \mu)(p_i + \nu) \left( \frac{d^2 F}{dp^2} \right)_{p_i} + \delta(p_i + \nu) \left( \frac{dF}{dp} \right)_{p_i} + \{\lambda^2 - \chi(p_i)\} F = 0, \quad \dots \quad (6)$$

which may be written after rearrangement as

$$a_1 f_1(p_i) + a_2 f_2(p_i) + a_3 f_3(p_i) + \dots + a_n f_n(p_i) = g(p_i),$$

$f_r$ 's and  $g$  are known functions of  $p$  and are given by

$$f_r(p_i) = r(r-1)p_i^{r-2}(p_i + \mu)(p_i + \nu) + r p_i^{r-1} \delta(p_i + \nu) + p_i^r \{\lambda^2 - \chi(p_i)\}$$

and

$$g(p_i) = -\{\lambda^2 - \chi(p_i)\}.$$

This set of  $n$  simultaneous linear equations can be written as

$$\begin{pmatrix} f_{11} & f_{21} & f_{31} & \dots & f_{n1} \\ f_{12} & f_{22} & f_{32} & \dots & f_{n2} \\ . & . & . & . & . \\ . & . & . & . & . \\ . & . & . & . & . \\ f_{1n} & f_{2n} & f_{3n} & \dots & f_{nn} \end{pmatrix} \begin{pmatrix} a_1 \\ a_2 \\ . \\ . \\ . \\ a_n \end{pmatrix} = \begin{pmatrix} g_1 \\ g_2 \\ . \\ . \\ . \\ g_n \end{pmatrix}$$

where  $f_{jk} = f_j(p_k)$  and  $g_k = g(p_k)$ .

From the above the values of the coefficients of the power series are determined. Therefore the solution of the differential equation is known except for an arbitrary

constant multiplier. The two values of  $\delta$  give two solutions  $F_+(p)$  and  $F_-(p)$  corresponding to negative and positive value of  $\delta$ . Therefore, the solution near the surface of the nucleus ( $r_2 < r < r_1$ ) is

$$u = Ae^{-kx} F_-(p) + Be^{+Kx} F_+(p). \quad \dots (7)$$

Now, in the region ( $r > r_1$ ) only Coulomb potential is effective and the Schrödinger equation takes the form

$$\frac{d^2u}{d\rho^2} + \left\{ 1 - \frac{2\eta}{\rho} - \frac{l(l+1)}{\rho^2} \right\} u = 0, \quad \dots (8)$$

where  $\rho = \alpha \cdot r = \sqrt{\frac{2mE}{\hbar^2}} \cdot r, \quad 2\eta = \frac{2m}{\hbar^2} \cdot \frac{2(Z-2)e^2}{\alpha}.$

The Eq. (8) has two solutions:  $F_l(\eta, \rho)$  regular at the origin and  $G_l(\eta, \rho)$  irregular at the origin, and are defined by their asymptotic behaviour :

$$F_l(\eta, \rho) \sim \sin \theta_l,$$

$$G_l(\eta, \rho) \sim \cos \theta_l,$$

when

$$\rho \rightarrow \infty.$$

where  $\theta_l = \rho - \eta \log 2\rho - \frac{l}{2}\pi + \sigma_l$  and  $\sigma_l = \arg \Gamma(i\eta + l + 1).$

The boundary condition that at infinity the alpha-particle should behave as a free out-going particle is satisfied by the linear combination  $G_l + iF_l$ , which represents a pure out-going wave.

When  $l$  is an integer,  $F_{l+1}$  (or  $G_{l+1}$ ) can be computed with the help of a set of recurrence relations given by Powell (1947) provided  $F_l$  (or  $G_l$ ) and its first derivative  $F'_l$  (or  $G'_l$ ) are known. If  $y_l$  stands for either  $F_l(\eta, \rho)$  or  $G_l(\eta, \rho)$  the recurrence relations satisfied by it are :

$$(l+1) \frac{dy_l}{d\rho} = \left[ \frac{(l+1)^2}{\rho} + \eta \right] y_l - [(l+1)^2 + \eta^2] y_{l+1}, \quad \dots (9)$$

$$l[(l+1)^2 + \eta^2] y_{l+1} = (2l+1) \left[ \eta + \frac{l(l+1)}{\rho} \right] y_l - (l+1)[l^2 + \eta^2] y_{l-1}, \quad (10)$$

$$l \frac{dy_l}{d\rho} = (l^2 + \eta^2) y_{l-1} - \left( \frac{l^2}{\rho} + \eta \right) y_l, \quad (11)$$

If the values of  $F_0$  (or  $G_0$ ) and  $F'_0$  (or  $G'_0$ ) are known by the application of Eq. (9)  $F_1$  (or  $G_1$ ) can be computed and subsequently by the application of Eq. (10) the values of  $F_l$  (or  $G_l$ ) for higher values of  $l$  can be obtained. The values of  $F'_l$  (or  $G'_l$ ) are computed with the help of Eq. (11).

Now  $F_0$  and  $G_0$  have different representations in the different ranges defined by the values of  $\rho$  and  $\eta$ . In the range where  $\rho < 2\eta$ , which is the case here,

the representations of  $F_0$  and  $G_0$  are given by Abramowitz, based on Riccati's method as quoted by C. G. Froberg (1955).

$$F_0 = \frac{1}{2} e^{\Phi(t, \eta)} \quad G_0 = e^{\tilde{\Psi}(t, \eta)}, \quad \text{where } t = \frac{\rho}{2\eta}.$$

$$\Phi(t, \eta) = 2\eta g_0 + g_1 + (2\eta)^{-1} g_2 + (2\eta)^{-2} g_3 + \dots$$

$$\tilde{\Psi}(t, \eta) = -2\eta g_0 + g_1 - (2\eta)^{-1} g_2 + (2\eta)^{-2} g_3 - \dots$$

where  $g_0, g_1, g_2 \dots$  etc are given functions of  $t$ .

The values of the constants  $A$  and  $B$  in Eq. (7) are found with the help of the continuity condition of  $u$  and  $du/dr$  at the point  $r = r_1$ . The values of  $F_l$  and  $dF_l/dr$  are found to be negligible in comparison with that of  $G_l$  and  $dG_l/dr$  at that point. Next, the value of  $u$  at  $r = r_2$  is calculated from the Eq. (7), from which the penetration factor is determined by following the definition of Blatt and Weisskopf (1954).

$$P = \frac{1}{|u(r_2)|^2}.$$

$u(r_2)$  is given by the following expression :

$$u(r_2) = A e^{-K^{x_2}} F_1(1) + B e^{+K^{x_2}} F_1(1)$$

since at  $r = r_2$ ,  $p = 1$ .

We may write the disintegration constant as

$$\lambda = N.P,$$

where  $N$  is the number of times the  $\alpha$ -particle hits the barrier wall. If the  $\alpha$ -particle moves with a velocity  $v$  within the crater of the nucleus of radius  $R$ , then  $N = v/2R$ . We determine  $v$  from the condition that the motion of the  $\alpha$ -particle within the nucleus of radius  $R$  is such that the associated waves form nodes at  $r = R$ .

If  $x_{l,k}$  is the  $(k+1)$ th root ( $kR = 0$ , being the first root) of the equation  $J_{l+\frac{1}{2}}(kR) = 0$ ,

$$\text{then} \quad N = \frac{h}{4mR^2} \cdot \frac{x_{l,k}}{\pi}.$$

Now the half-life can be calculated from the expression

$$T = \frac{\log_e 2}{\lambda}.$$

where

$$\lambda = \frac{h \cdot P}{4mR^2} \cdot \frac{x_{l,k}}{\pi}$$

TABLE I

Ele- ment	A mass no.	Z charge no.	R in fermi nuclear radius	m in gm. the reduced mass of the $\alpha$ - particle	$l$	$r_2$ in fermi where $P.E.$ $=K.E.$ of the screening $\alpha$ - particle	E in Mev. the $\alpha$ - particle	$F_{-}(1)$	$F_{+}(1)$	P calculated by WKB method	T in sec. Expt. value of half-life	
Rn	218	86	9.3749	$6.5223 \times 10^{-24}$	0	9.5726	7.162	+ .78267	-1.2319	$3.555 \times 10^{-19}$	$4.67 \times 10^{-19}$	$.6747 \times 10^{-2}$
					2	9.5230	6.564	- .76893	-1.9406	$1.220 \times 10^{-21}$	$1.62 \times 10^{-21}$	$107.16 \times 10^{-2}$
Th	230	90	9.5231	$6.5286 \times 10^{-24}$	0	9.5538	4.718	+ .72373	-4.54306	$4.937 \times 10^{-33}$	$6.61 \times 10^{-33}$	$.5019 \times 10^{12}$
					3	9.50198	4.404	- .71005	-6.32904	$.7447 \times 10^{-35}$	$1.04 \times 10^{-35}$	$149.456 \times 10^{12}$
Pu	238	94	9.6190	$6.5325 \times 10^{-24}$	0	9.64396	5.535	+ .725805	-4.7645	$7.543 \times 10^{-30}$	$9.30 \times 10^{-30}$	$.335 \times 10^9$
					4	9.5777	5.394	+ .711196	-7.13057	$1.911 \times 10^{-31}$	$2.45 \times 10^{-31}$	$4.994 \times 10^9$

TABLE II

Ele- ment	A	Z	l	E in Mev.	m in gm.	Value of P by the method of calculation		P by WKB method	Value of T calculated from that of P obtained by using the method		Expt. value of T in sec.
						As given in I	As given in this paper		given in I in sec.	given in this paper in sec.	
Po	214	84	0	7.714	$6.52 \times 10^{-24}$	1.237 $> 10^{-16}$	1.179 $\times 10^{-16}$	1.58 $\times 10^{-16}$	.177 $\times 10^{-4}$	.2012 $\times 10^{-4}$	1.636 $\times 10^{-4}$

## RESULTS

The numerical calculations have been done for the following elements, for different values of  $l$ , to show the applicability of the method. The values of parameters are the same as used by Igo and Thaler (1957).

$$R = 1.35A^{1/3} + 1.3 \text{ fermi, } a = 0.5 \text{ fermi, } V_0 = 45 \text{ Mev.}$$

In our calculation we have taken  $n = 4$  and  $k = 1$ . Results are shown in Table I.

The values of half-life as calculated here are lower than the experimental values of the same for the case  $l = 0$  only, whereas for  $l = 2, 3$ , or  $4$  they are all greater than the experimental values. The values of the penetration factor calculated by the method given here appear to be consistently lower than that calculated by the WKB method for all values of  $l$ . The values of  $P$  by WKB method and the experimental value of half-life and that of  $E$  are taken from the table given by Rassmussen (1959) in his paper on the penetration probability of alpha-particles.

It may be worth while to compare the results for the case  $l = 0$  as obtained here with that of the previous method where the Coulomb potential near the nuclear boundary was taken to be of constant value. In our present case, as expected, the value of  $P$  is slightly lower than that obtained by the previous method. The differences in the figures given in Table II indicate the measure of error involved in the approximation about the Coulomb potential in the previous method.

In the paper I, due to some numerical slip in the value of  $a$  parameter, the penetration factor of  $^{214}\text{Po}_{84}$  for  $l = 0$  was found to be  $.059 \times 10^{-16}$  which should, instead, be  $1.3373 \times 10^{-16}$ .

## ACKNOWLEDGMENTS

The author is indebted to Prof. D. Basu, Ph. D., for suggesting the problem and helpful guidance throughout the progress of the work and he also wishes to thank Dr. N. C. Sil for many valuable discussions.

## REFERENCES

- Abramowitz, M., 1949, *Quart. Appl. Math.*, **7**, 75.  
 Blatt and Weisskopf, 1954, *Theoretical Nuclear Physics*, p. 332 & 362, John Wiley & Sons, N.Y.  
 Dutta, Mitra and Sil, 1960, *Ind. J. Phys.*, **34**, 205.  
 Froberg, C. E., 1955, *Rev. Mod. Phys.*, **27**, 405.  
 Igo, G. and Thaler, R. M., 1957, *Phys. Rev.*, **106**, 126.  
 Lanczos, C., 1938, *Jour. Math. Phys.*, **17**, 123.  
 Powell, J. L., 1947, *Phys. Rev.*, **72**, 626.  
 Rassmussen, J. O., 1959, *Phys. Rev.*, **113**, 1593.

# INTENSITY MEASUREMENTS IN MOLECULAR BANDS

N. R. TAWDE, B. G. JYOTI AND M. I. SAVADATTI

DEPARTMENT OF PHYSICS, KARNATAK UNIVERSITY, DHARWAR

(Received March 14, 1961)

**ABSTRACT.** Peak and integrated intensities of  $N_2$  II positive bands have been measured. The peak values have been corrected according to the procedure of Floyd and King. The data have been obtained with a view to assess the reliability of peak intensity measurements and also the correction due to Floyd and King.

Intensity of a band to be accurate has to be obtained by summing over the intensities of the rotational lines that form the band. Phillips (1957) tried to use this principle for the  $C_2$  (Swan) system excited in a furnace of known temperature. Since the lines were badly blended he calculated band profiles by combining the profiles of individual rotational lines. He concludes that the results so obtained may be quite uncertain for weak bands. However, a rigorous application of the method is too laborious and many times it is not practicable or even possible. So simpler, but reliable, methods of estimating intensity are to be thought of. The method—known as integrated intensity method—of measuring intensities with a low dispersion spectrograph by integrating over the entire intensity contour of the bands is the one which gives intensity values nearest to the true intensity of a band. The requirements for the results to be reliable are (i) the band structure should not be resolved and (ii) there should be no overlapping from the neighbouring bands. The first requirement can be easily met by a proper choice of the spectrograph, but the second requirement is too rarely satisfied, because in almost all actual band systems there is an overlapping from neighbouring bands. When the overlapping is present, the band profiles are judiciously extrapolated and the effect of overlapping separated. But such a procedure is purely subjective and the results might be in great error for weaker bands overlapped by strong bands.

In case of overlapping, the intensity at the head of the band may be taken to represent band intensity (peak intensity method) or a known fraction of band intensity near head may be used to derive band intensity (fractional band intensity method, Robinson and Nicholls, 1958).

Ornstein and Brinkman (1931) were the earliest to use the peak intensity of CN bands to represent band intensity and concluded that the rotational energy distribution varies from band to band and hence the method is not valid. Tawde and Patankar (1943) have shown for  $N_2$  second positive system that the ratio of

the band head intensity to integrated intensity is not a constant, while Young (1954) has shown experimentally for the same system that the mean deviation for this ratio is only 6.2%.

Floyd and King (1955) have developed a method of obtaining total band intensity from the band head intensity, by assigning a representative rotational quantum number for the band head ( $J_h$ ) and also taking into account the number of lines forming the head ( $\Delta J$ ). This method finds immediate application to singlet systems or for those systems which can be approximated to singlet systems. A difficulty in applying the method is that the temperature of the source (emitting the band system) which enters into the equation is, in general, not precisely known. For many sources true temperatures are not easily available or estimable. So the method might not find rigorous application to all the band systems. However, a fairly satisfactory intensity value may be obtained, if we can assume some reasonable temperature or approximate the term containing temperature to a constant. This can be done provided the rotational quantum number at the band head has a small range of variation in the bands considered.

Robinson and Nicholls (1958) have developed a fractional band intensity method which correlates the sum of intensities of a few rotational lines at and near the head with the band intensity. This method also suffers from lack of knowledge of temperature which has therefore to be assumed.

A possible error in peak intensity and fractional band intensity measurements is the effect of self-absorption on the intensity at the peak. This effect becomes appreciable when the intensity of the blended rotational lines reaches a significant fraction of the intensity of a black body at the same temperature and wavelength. In that case one will have to consider the manner of blending of rotational lines at the band head.

Robinson and Nicholls (1958) have developed a rotational line intensity method, where the intensities of rotational lines are plotted against the energy of upper levels of transition. The intercept on this graph can be used to obtain band intensity. The method is satisfactory provided rotational thermodynamic equilibrium exists in the source.

Intensities of  $\text{NO}(\beta)$  and  $\text{O}_2$  (II negative) systems were measured by these methods by the above authors and the results were found to compare satisfactorily with the integrated intensity values. But it may be noted here that the integrated intensity values are subject to the error due to overlapping by the neighbouring bands.

In order to judge the merits and demerits of any method for intensity measurements, it is necessary to possess integrated intensity values on bands which have no appreciable overlapping. So it was decided to measure the intensities of bands  $\text{N}_2$  (II positive) system with a view to ascertain the reliability of peak intensities and peak intensities corrected according to the method of Floyd



and King (1955). The reason for selecting only these two is that such values are easily available and an evaluation of their reliability is naturally much useful. The bands (1-6), (2-7), (3-8), (1-5), (2-6) and (3-7) have almost negligible overlapping from neighbouring bands and hence they have been particularly chosen for this study. The intensities have been measured photographically using an a.c. discharge through air as a source of  $N_2$  (11 positive) bands. The measurements have been repeated with two spectrographs to ascertain the effect of varying dispersion on the intensity measurements and also as a general check on the measurements.

TABLE I  
Intensity measurements— $N_2$  II P. (small quartz spectrograph)

Transition	$*I_p$	$*I_{pc}$	$*I$	$I_p/I$	Devn. from mean	$I_{pc}/I$	Devn. from mean
1-6	25.36	26.92	30.61	0.83	0.09	0.88	0.07
2-7	32.64	34.93	38.13	0.86	0.06	0.92	0.03
3-8	28.69	31.19	32.89	0.87	0.05	0.95	0.00
1-5	93.94	92.11	95.34	0.99	0.07	0.97	0.02
2-6	100.00	100.00	100.00	1.00	0.08	1.00	0.05
3-7	65.01	65.72	66.24	0.98	0.06	0.99	0.04
				Mean 0.92		Mean 0.95	
				Mean % devn. : 7.5		Mean % devn. : 4.2	

TABLE II  
Intensity measurements— $N_2$  II P. (medium quartz spectrograph)

Transition	$*I_p$	$*I_{pc}$	$*I$	$I_p/I$	Devn. from mean	$I_{pc}/I$	Devn. from mean
1-6	20.43	21.39	19.09	1.07	0.07	1.12	0.09
2-7	23.27	24.65	22.53	1.03	0.03	1.09	0.05
3-8	21.16	22.78	21.89	0.97	0.03	1.04	0.00
1-5	99.98	98.14	98.16	1.02	0.02	1.00	0.04
2-6	100.00	100.00	100.00	1.00	0.00	1.00	0.04
3-7	70.20	71.58	74.83	0.94	0.06	0.96	0.08
				Mean 1		Mean 1.04	
				Mean % devn. : 5		Mean % devn. : 5	

\*  $I_p$  Peak intensity,

$I$ , Integrated intensity, and

$I_{pc}$ , Peak intensity corrected according to Floyd and King (see Appendix).

The results are collected in Tables I and II. It is observed that the percentage mean deviation is not more than 7% in the case of uncorrected peaks and not more than 5% in the case of corrected peaks. Considering the fact that photographic photometry has errors of these magnitude, we feel that the peak values compare fairly well with integrated values; and corrected peak values, in general, give a better comparison with integrated values. In connection with corrected values, it may be noted that the exponential term containing the rotational temperature has been approximated to a constant. However, if a temperature, say 300°C, is assumed for the discharge, the change in value of intensities is  $\sim 2\%$  and hence the approximation of the term might be justified.

#### APPENDIX

$$I_{pc} - I_p \left[ J_h \Delta J \right]^{-1} \exp \left[ \frac{B_v' J_h (J_h - 1)}{kT} \right]$$

where  $J_h$  the rotational quantum number at band head, is expressed as

$$J_h = \frac{B_{v'} + B_{v''}}{2(B_{v'} - B_{v''})}$$

and  $\Delta J$  the number of lines forming band head is given by

$$= \frac{\text{Const}}{\lambda_h} \left[ \frac{d\lambda}{ds} (B_{v'} - B_{v''}) \right]^{\frac{1}{2}}$$

where  $\lambda_h$  — wavelength at band head.

The symbols in the above have their usual meaning (Herzberg, 1950).

#### ACKNOWLEDGMENT

One of the authors (B.G.J.) acknowledges his gratitude to the Ministry of Scientific Research and Cultural Affairs, Government of India, for the award of a Senior Research Training Scholarship which enabled him to participate in this particular piece of work in the general programme in hand.

#### REFERENCES

- Floyd, A. L. and King, R. B., 1955, *J. Opt. Soc. Am.*, **45**, 249.  
 Herzberg, G., 1950, 'Molecular Spectra and Molecular Structure', Vol. I, D. Van Nostrand, New York.  
 Ornstein, L. S. and Brinkmann, H., 1931, *Proc. Roy. Acad. Amsterdam*, **34**, 33.  
 Phillips, J. G., 1957, *Ap. J.*, **125**, 153.  
 Robinson, D. and Nicholls, R. W., 1958, Scientific Rep. No. 3, Contract AF 19 (604)-1718.  
 Tawde, N. R. and Patankar, V. S., 1943, *Proc. Phys. Soc.*, **55**, 396.  
 Young, B. G., 1954, M.Sc. Thesis, Univ. of Western Ontario.

## ON THE SUPERHEAT OF LIQUIDS

D. B. SINHA AND A. K. JALALUDDIN

DEPARTMENT OF APPLIED PHYSICS, CALCUTTA UNIVERSITY

(Received March 11, 1961)

**ABSTRACT.** A new method for measuring maximum superheat temperatures of liquids has been devised. A thin-walled degassed pyrex glass bulb, set vibration free and dipped in liquid, was heated by a coil immersed in mercury filling the bulb. This heating surface was chosen because it introduced minimum heterogeneity at the liquid-solid interface. The temperature of the liquid bulk was kept close to the boiling point using a paraffin oil bath. The temperature of the heater surface was increased in regular steps and the temperature at which the boundary film of the liquid exploded with vigorous ebullition was taken as the maximum superheat temperature of the liquid. Results obtained with carbon tetrachloride, chloroform, acetone, benzene, methyl alcohol, carbon disulphide, diethyl ether, *n*-pentane and ethyl bromide have been compared with the values obtained by Kenrick, Gilbert and Wismer (1924) as well as with those deduced from Van der Waals equation. The agreement is fair.

The set-up seems to offer a practical method for studying the effect of varying the nature of the interface on the superheat of liquids.

## INTRODUCTION

The study of superheat of liquids is important for investigating the theoretical basis of homogeneous nucleation and also from the standpoint of defining the heterogeneity in a two-phase heating system. The latter has received a great impetus in recent years with the introduction of the bubble chamber as a means of detecting charged particles.

Many different methods have been used to investigate the maximum degree of superheat attainable in liquids at atmospheric pressure. Wismer *et al.* (1924) adopted the method of superheating liquids in capillaries, Briggs (1951, 1955) carried out his tests using a centrifuge, while Harvey *et al.* (1947) used the pressure pulse method; in both the latter cases the liquids tended to cavitate under negative pressure. The work of Wakeshima and Takata (1958) in this field is more recent. In their device droplets of liquids were introduced into a vertical column of an immiscible liquid possessing a steady temperature gradient in order to find at which temperature-level the liquid drop exploded during its ascent.

These methods have the common purpose of reaching the theoretical maximum superheat temperature. They are hardly applicable to constant flow or steady transfer systems in which a thin layer in contact with the heater surface becomes strongly heated whilst the bulk of the liquid remains at a temperature near the boiling point.

The principle of the present work is based on a model of practical heat transfer systems. Here a thin-walled pyrex glass bulb filled with mercury is chosen as the heating surface. The bulb is degassed and dipped into the liquid to be studied. The mercury in the bulb is heated electrically by a coil and the temperature of the liquid bulk is kept very close to its boiling point by regulating its temperature with the help of a jacketting paraffin oil bath. In the steady heat flow condition the temperature of the stagnant film of the liquid in contact with the outer surface of the glass bulb naturally attains a steady high value ; just beyond it the temperature falls sharply. As the heat input of the coil is increased in steps and sufficient time is allowed for the system to acquire steady-state for each step, the boundary liquid film becomes increasingly superheated in the successive steps until it ruptures with explosion, giving rise to vigorous ebullition from innumerable centres on the bulb surface simultaneously. The highest steady state surface temperature of the bulb is taken to be the maximum superheat temperature of the liquid and this is calculated from the steady temperature of the mercury after correcting for the temperature drop across the glass wall of the bulb.

The results obtained with different organic liquids agree fairly well with

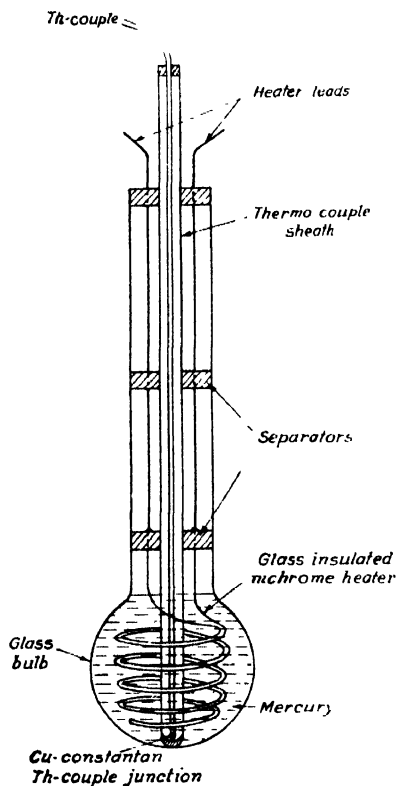


**Fig. 1.** Glass-bulb heater assembly.

those of Wismer *et al.* (1924) and also with the theoretical values calculated from Temperley's (1947) adaptation of the Van der Waals equation.

#### EXPERIMENTAL APPARATUS

The experimental set-up consists of (1) glass bulb heater assembly, (2) degassing flask, and (3) the temperature regulating bath.

1. A schematic diagram of the glass bulb heater assembly is given in Fig. 1. A pyrex brand glass tube of 0.76 cm. bore and 30 cm. in length was taken and a spherical bulb of 2.1 cm. diameter with a fairly uniform wall thickness of 0.05 cm. was blown at one end. The bulb was filled with mercury. A glass insulated nichrome wire (33 swg) heater coil was immersed in the mercury. In positioning the coil care was taken to ensure that it did not touch the inner surface of the glass bulb. The electrical input to the heating coil was taken from 220 volts D.C. mains and it was closely regulated and controlled by a bank of rheostats so that the temperature of the mercury could be increased very slowly. Temperature of the mercury was measured by a copper-constantan thermocouple, contained in a thin-walled glass sheath, the reference junction being at the ice point. The thermocouple was calibrated after insertion in the glass bulb. The thermocouple voltage was measured by a Diesselhorst Potentiometer.

2. The provisions for degassing the bulb is shown in Fig. 2.

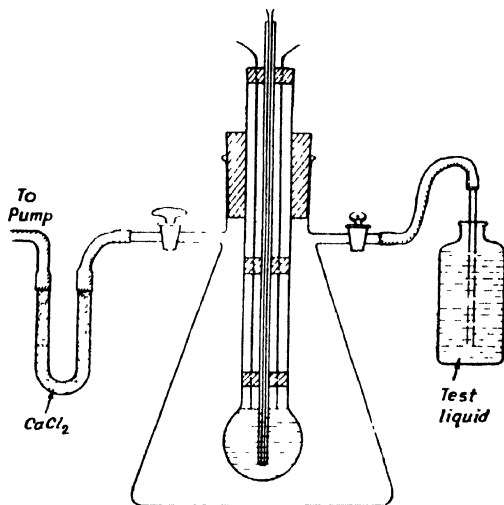


Fig. 2. Degassing arrangement.

3. To prevent bulk superheating as well as subcooled boiling of the test liquid a temperature regulating device was necessary. About half a litre of the test liquid was contained in a glass cylinder which was immersed in a bath of paraffin oil (Fig. 3). The temperature of the test liquid was kept within narrow

limits near the boiling point by regulating the temperature of the paraffin oil bath. Mercury-in-glass thermometers graduated to  $0.1^{\circ}\text{C}$  were used to indicate temperature.

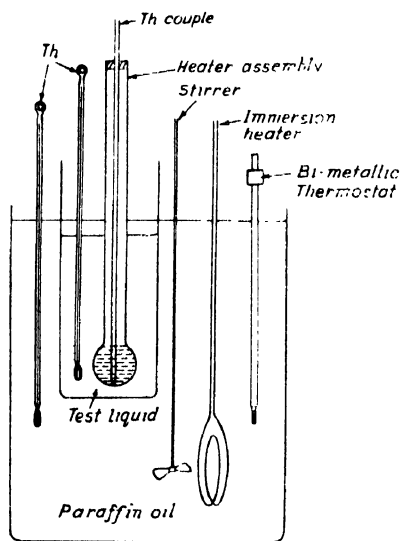


Fig. 3. Bath arrangement.

#### EXPERIMENTAL PROCEDURE

The heater bulb, annealed at  $400^{\circ}\text{C}$  over a period of 48 hours, was thoroughly washed with conc. sulphuric acid saturated with potassium dichromate and was then rinsed several times with water. The bulb thus cleaned was introduced into the degassing flask through a rubber cork fitting closely into its mouth. The flask was gradually evacuated to a pressure of about  $10^{-3}$  mm. of mercury, and the mercury in the heater bulb was simultaneously heated to  $200^{\circ}\text{C}$ . The process was continued for an hour; the connection to the pump was then closed and the test liquid was drawn into the flask while the bulb was still hot so that the bulb surface could be covered with a thin layer of the test liquid before transferring it to the test bath. The flask was then brought close to the test bath and the heater assembly quickly transferred to it.

The liquid in the test bath (about 500 ml) was boiled off to two-thirds of the initial volume. The heater was then switched off and the sample was allowed to reach quiescence. After an interval of 16 to 20 hours the heater was again switched on and was adjusted to a series of gradually ascending step values (successive steps not differing by more than  $2^{\circ}\text{C}$ ). The temperature of the bulk liquid was kept at the reference value, within a limit of  $0.05^{\circ}\text{C}$ ., for each value of the heat input by suitably adjusting the bath temperature. For any given heat input the heater bulb attained steady state within a minute. To ensure that

steady state readings were taken, about 5 minutes were allowed to elapse at each step before measurements were noted. Finally, a temperature was reached such that a slight increase in the heat input made the liquid film explode with an appreciable popping sound. It was noted that the loudness of the explosion increased significantly with the degree of superheat. The nucleation centres were innumerable and were found to be evenly distributed on the bulb surface. Within a few seconds of explosions the temperature of the mercury in the bulb suddenly dropped through 20°–25°C and attained a steady lower value within a minute. Liquids with larger superheat values showed a larger temperature drop at this stage. During any set of experiment the liquid did not fall in level by more than a centimetre. The test bath beaker and the heater assembly were held in massive stands resting on compressed felt slabs to keep them free from vibration. The steady state temperature gradient from mercury to the liquid bulk is shown in Fig. 4.

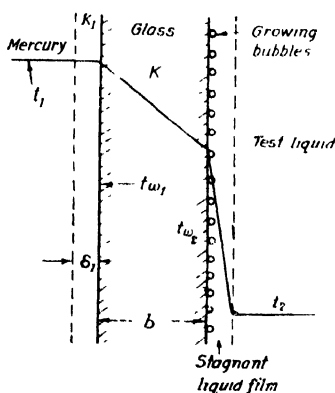


Fig. 4. Drop of temperature from mercury to test liquid.

#### CALCULATION OF MAXIMUM SUPERHEAT TEMPERATURE

At the steady state, assuming that heat is transferred across the stagnant mercury film wholly by conduction,

$$t_1 - t_{\omega_1} = \frac{\delta_1}{AK_1} Q \quad \dots (1)$$

$$t_{\omega_1} - t_{\omega_2} = \frac{b}{AK} Q \quad \dots (2)$$

where  $t_1$  = bulk temperature of mercury,  $t_{\omega_1}$  = inner wall temperature of the glass bulb,  $t_{\omega_2}$  = outer wall temperature of the glass bulb,  $K_1$  = conductivity of mercury,  $K$  = conductivity of laboratory pyrex glass,  $A$  = mean surface area of the glass bulb,  $b$  = mean wall thickness of the glass bulb,  $\delta_1$  = thickness of

the stagnant mercury film,  $Q$  = heat input at any steady state. Adding Eqs. (1) and (2), we have

$$t_1 - t_{\omega_2} = \frac{Q}{A} \left( \frac{\delta_1}{K_1} + \frac{b}{K} \right) \quad \dots(3)$$

But,  $\delta_1 \ll b$  and  $K_1 \gg K$  and  $\delta_1/K_1 \ll b/K$ . So Eq. (3) reduces to

$$t_{\omega_2} = t_1 - \frac{Qb}{AK} \quad \dots (4)$$

The value of  $t_{\omega_2}$  at the highest steady state is noted as the maximum superheat temperature of a liquid.

### RESULTS

More than twenty repeat tests were made with fresh samples for each of nine different organic liquids (carbon tetrachloride, chloroform, acetone, benzene, methyl alcohol, carbon disulphide, di-ethyl ether, *n*-pentane and ethyl bromide) allowing different intervals of standing between runs in order to achieve reproducibility of results. Reproducible values of the maximum superheat within the range of 5°C was attained when the boiled sample was allowed to stand overnight and the heat input to the bulb increased slowly. Any sudden fluctuation of the mercury temperature, even through 0.5°C., or a slight vibration of the support of the bulb assembly, was found sufficient to initiate nucleation at high liquid superheat.

The maximum superheat temperatures and the temperature drops (Eq. 4) are shown in Table I.

TABLE I

Liquid	Boiling point °C	Mercury temperature °C	Temperature drop $\left( \frac{Qb}{AK} \right)$ °C	Maximum superheat temperature °C	Bulk temperature of the liquid °C	Superheat °C
Carbon tetrachloride	76.7	142	7	135	76.0	58
Chloroform	61.0	161	12	149	60.4	88
Acetone	56.5	188	23	165	56.5	108.5
Benzene	80.1	211	20	191	80.5	111
Methyl alcohol	64.0	211	29	182	65.0	118
Carbon disulphide	46.3	166	9	157	48.6	111
Di-ethyl ether	34.5	177	25	152	34.0	117.5
<i>n</i> -Pentane	36.1	142	10	132	35.2	96
Ethyl bromide	38.4	162	13	149	38.0	111



The values of  $A$  and  $b$  for the glass bulb used were measured optically. The conduction heat loss along the heater leads and the stem of the glass heater and the part of the  $I^2R$  wattage not absorbed by the mercury medium, added together, amounts to about 5% of the total heat input and so the value of  $Q$  taken was reduced by that amount. As regards the conductivity of glass, the standard value for laboratory brand of pyrex, type 475/636 as quoted by Jakob (6) (corrected for the mean temperature) has been taken.

## DISCUSSION

The possible sources of error in our calculation of superheat might lie in the (1) measurement of the surface area of the glass bulb and its wall thickness and (2) estimation of the magnitude of the heat losses. It is estimated, however, that the error in superheat temperature due to uncertainties in these quantities would not exceed 3°C. at its maximum value.

The general agreement of the experimental values of superheat in the present case with those of Wismer *et al.* and the graph resulting from theoretical values

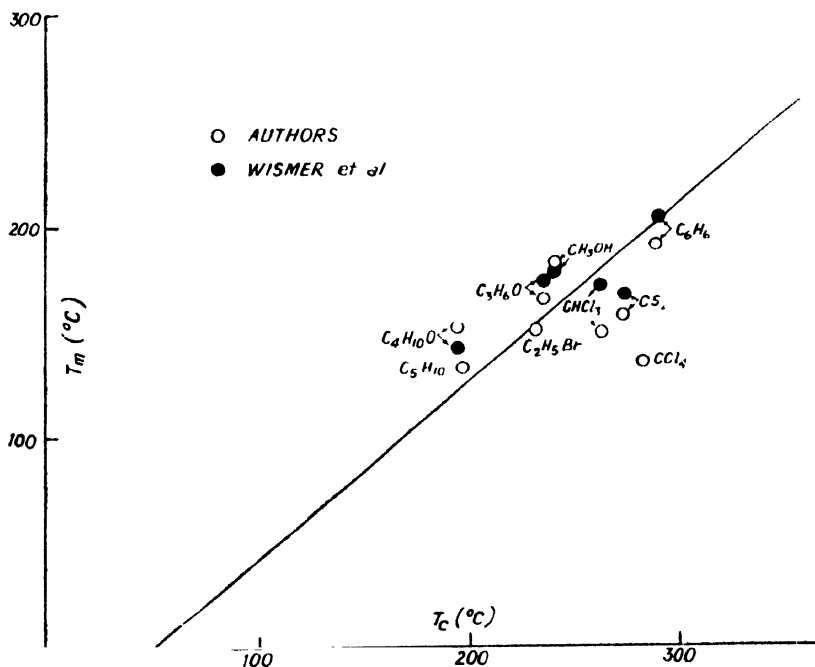


Fig. 5. Maximum superheat of liquids—comparison of results of the authors, and Wismer *et al.*, and deductions from Van der Waals equation.

$T_m$  = Limiting temperature for existence of a liquid phase at atmospheric pressure  
 $T_c$  = Critical temperature.

Straight line  $\frac{T_m}{T_c}$ , deduced from Van der Waals equation.

is given in Fig. 5. Exact agreement can not be expected since the Van der Waals equation on which the theoretical curve is based is at best approximate only.

The fairly high values of superheat of the liquids obtained by the present method lend support to the contention that cavitation of the liquid film at the glass surface was initiated in the absence of gas nuclei at the interface. The divergence of the maximum superheat temperatures of different liquids from the theoretical curve seems to be due to their relative deviations from Van der Waals equation.

#### REMARKS

1. Since the liquid boundary film is superheated, the measurement of the superheat temperatures is not influenced in the present method by the presence of chemically inert notes in it.

2. Since cavitation takes place at the glass-liquid interface, the method offers special advantage for studying the effect of any variation of the nature of the interface on the superheat of liquids.

#### ACKNOWLEDGMENT

The authors like to thank Prof. G. G. Haselden of the Leeds University and Prof. J. W. Westwater of the Illinois University for helpful criticism of the work.

#### REFERENCES

- Wismer, K. L., 1922, *J. Phys. Chem.*, **26**, 301.  
Kenrick, F. B., Gilbert, C. S. and Wismer, K. L., 1924, *Ibid.*, **28**, 1297.  
Briggs, L. J., 1951, *J. Chem. Phys.*, **19**, 970.  
Briggs, L. J., 1955, *J. Appl. Phys.*, **26**, 1001.  
Harvey, E. N., McElroy, D. M. and Whiteley, H., 1947, *J. Appl. Phys.*, **18**, 162.  
Wakeshima, H. and Takata, K., 1958, *J. Phys. Soc., Japan*, **13**, 1398.  
Temperley, H. N. V., 1947, *Proc. Phys. Soc. (London)*, **49**, 203.  
Jakob, Max, "Heat Transfer", Vol. 1, Wiley (1955).

# Letters to the Editor

*The Board of Editors will not hold itself responsible for opinions expressed in the letters published in this section. The notes containing reports of new work communicated for this section should not contain many figures and should not exceed 500 words in length. The contributions must reach the Assistant Editor not later than the 15th of the second month preceding that of the issue in which the letter is to appear. No proof will be sent to the author*

## 2

### A NEW METHOD FOR MEASURING ABSOLUTE MAGNETIC SUSCEPTIBILITIES

P. K. GHOSH

DEPT. OF MAGNETISM, I.A.C.S. JADAVPUR, CALCUTTA-32.

(Received, March 17, 1961)

A coil carrying an electric current possesses a magnetic moment. If introduced in a magnetic field with its moment parallel to the field-direction, it will behave as a magnetic body. So, in a Curie-balance type set-up, if we place the sample inside the coil, then by adjusting the current, we can make the moment of the coil equal and opposite to the moment induced in the sample and the system will experience no translatory force.

The working formula can be shown to be

$$\chi = \left( \frac{i - i_c}{i_s - i_c} - \chi_s \right) \cdot \frac{m_s}{m} + \frac{K_a}{\rho}$$

where

$\chi$  = mass-susceptibility of the sample

$\rho$  = density of the sample

$m$  = mass of the sample.

$\chi_s$ ,  $\rho_s$  and  $m_s$  are the respective values for a standard substance.

$K_a$  = volume susceptibility of air

$i$  = current necessary to balance the force on the sample

$i_s$  = same with the standard substance

$i_c$  = current necessary to balance the force on the coil alone.

It is better to have a calibration curve by working with a number of different samples of known susceptibilities.

The advantages of the method over the older method are :

- (a) remote control eliminates manual rotation of torsion head, thus reducing the effects of vibration, etc.
- (b) since the balancing force is applied directly on the sample itself, no torsion on the suspension fibre is required and the system remains perfectly undisturbed.
- (c) electric currents can be very accurately measured.
- (d) the balance chamber can easily be made vacuum-proof and can be kept dry.

The method has been tried experimentally and the instrument was found to work satisfactorily. Details will be published later.

My thanks are due to Professor A. Bose for his kind interest in the work.

### 3

## INTERMOLECULAR POTENTIALS OF $H_2$ AND $D_2$

I. B. SRIVASTAVA AND A. K. BARUA\*

INDIAN ASSOCIATION FOR THE CULTIVATION OF SCIENCE, CALCUTTA-32

(Received April 12, 1961)

The importance of the quantum effects for  $H_2$  and  $D_2$  at low temperatures makes the determination of their potential energy functions very interesting. Further, it is likely to show whether their potential energy functions are the same, as it should be for two isotopes, provided their non-spherical nature may be neglected. Although it is known that there should be some difference in the inter-molecular potentials of  $H_2$  and  $D_2$  due to the difference in their zero-point energies, it was so long thought that this effect can be neglected (Mason and Rice, 1954). Moreover the earlier experimental data were not accurate enough to test this conclusively. Very recently Michels *et al.* (1960a) have determined the second and third virial coefficients of  $H_2$  and  $D_2$  by using a precise method (Michels *et al.* 1960b) utilising their compressibility data (Michels, *et al.* 1959) between the temperature range from  $-175^\circ\text{C}$  to  $150^\circ\text{C}$ . They have observed that the force constants for  $H_2$  and  $D_2$  determined previously on the L-J (12 : 6) model cannot represent the virial data satisfactorily. Hence they have redetermined the force

---

\* Present Address: Metcalf Chemical Laboratory, Brown University, Providence, R.I., U.S.A.

constants for  $\text{H}_2$  and  $\text{D}_2$  and have found them to differ from each other by more than what can be ascribed to be experimental errors. They have also considered the non-spherical nature of the potential energy functions to represent the virial data.

It was therefore considered desirable to have a more detailed investigation of the intermolecular potentials of  $\text{H}_2$  and  $\text{D}_2$  to test whether the results obtained by Michels *et al.* (1960a) are true for other potentials as well. We have thus fitted the second virial coefficient,  $B(T)$ , data of Michels *et al.* (1960a) to the exp-six model by taking into consideration the quantum effects. The results obtained are shown in Table I. In Table II the experimental and the calculated values of  $B(T)$  are shown. For the sake of comparison the values calculated on the exp-six model from the force constants determined by Mason and Rice (1954), and those calculated by Michels *et al.* (1960a), are also shown.

It may be seen from the Tables I and II that the results obtained on the exp-six model confirm the finding of Michels *et al.* (1960a) that the force fields of  $\text{H}_2$  and  $\text{D}_2$  are not exactly the same. However, the agreement with the experimental data calculated on the exp-six model from the force constants determined by us is very good over the entire temperature range and hence further consideration of the non-spherical nature of the potentials may not be necessary.

TABLE I

Force parameters for  $\text{H}_2$  and  $\text{D}_2$  on the exp-six model

Substance	Present work			Mason and Rice (1954)		
	$\alpha$	$\epsilon/k$ °K	$r_m$ Å	$\alpha$	$\epsilon/k$ °K	$r_m$ Å
$\text{H}_2$	14.0	38.02	3.339	14.0	37.3	3.337
$\text{D}_2$	14.0	37.33	3.334	Assumed to be the same as those of $\text{H}_2$		

It is to be noted that Michels *et al.* (1960a) could not find agreement in the whole temperature range with their force constants on L—J (12 : 6) potential model, within the experimental accuracy. Thus it appears that the exp-six potential model is an improvement over the L—J (12 : 6) model which has been already pointed out by Mason and Rice (1954).

Further work, by taking into consideration the third virial coefficient and the quantum corrections to the transport coefficients, is in progress.

The authors are grateful to Prof. B. N. Srivastava, D. Sc., F.N.I., for his valuable discussions.

TABLE II

Second virial coefficient for H<sub>2</sub> and D<sub>2</sub> in cm<sup>3</sup> mole<sup>-1</sup>

$T^{\circ}\text{K}$	Hydrogen				Deuterium		
	Calculated			Expt.	Calculated		Expt.
	Exp-6 present work	Exp-6 Mason & Rice	$L-J(12-6)$ Michel <i>et al.</i>		Exp-6 present work	$L-J(12-6)$ Michel <i>et al.</i>	
98	-3.14		-3.16	-3.06	-4.48	-4.35	-4.59
103	-1.69		1.76	-1.69	-2.93	-2.84	-3.03
113	+0.62		0.68	0.67	-0.38	-0.30	-0.38
123	2.79	3.34	2.71	2.63	1.78	1.78	1.79
138	5.18		5.10	5.01	4.38	4.29	4.38
153	7.05		6.95	6.89	6.26	6.19	6.36
173	9.01	9.27	8.82	8.84	8.25	8.20	8.37
198	10.66		10.60	10.65	10.22	10.07	10.20
223	12.06	12.24	11.93	11.98	11.52	11.45	11.53
248	12.99		12.95	12.97	12.54	12.51	12.53
273	13.73	13.93	13.75	13.76	13.31	13.34	13.30
298	14.36	14.51	14.40	14.38	13.98	14.00	13.90
323	14.86	14.97	14.92	14.87	14.46	14.53	14.38
348	15.22	15.34	15.34	15.27	14.87	14.97	14.76
373	15.59	15.63	15.69	15.60	15.27	15.33	15.07
398	15.86	15.88	15.97	15.86	15.41	15.63	15.33
423	16.05	16.07	16.21	16.08	15.62	15.87	15.54

## REFERENCES

- Mason, E. A. and Rice, W. E., 1954, *J. Chem. Phys.*, **22**, 522.  
 Michels, A., De Graaff, W., Wassenaar, T., Lovelt, J. M. II. and Lauwerson, P., 1959, *Physica*, **25**, 25.  
 Michels, A., De Graaff, W., and Ten Seldam, C. A., 1960a, *Physica*, **26**, 393.  
 Michels, A., Abels, J. C., Ten Seldam, C. A. and De Graaff, W., 1960b, *Physica*, **26**, 381.

## BOOK REVIEW

INTRODUCTION TO PHYSICAL CHEMISTRY, VOL. III. by S. N. Mukherjee  
Art Union, Calcutta. 832 pages, ix. 1960(?) Price Rs. 25/-.

The third volume of Introduction to Physical Chemistry by Prof. S. N. Mukherjee, is intended for the post-graduate students of Indian universities. It is an advanced treatise divided into eleven chapters dealing with kinetic theory of gases, chemical thermodynamics, quantum theory and quantum mechanics, statistical mechanics and structure of molecules. In a book like this where a variety of topics has to be treated it is probably not easy to maintain a balance in the matter of emphasis given to one topic or the other. However, this volume is to be read along with its companion volumes, particularly volume II. Together with the preparatory chapter on electromagnetism more than two-fifths of the book are devoted to quantum theory and quantum mechanics. But the section on the theory of electrolytes has been very meagrely treated without reference to its recent developments. The same remark applies to the theory of reaction rates. It is gratifying that most of the topics have been presented clearly without sacrificing rigour and accuracy. The author's long experience as a teacher of physical chemistry has naturally helped him to keep the conceptual difficulties of students in mind.

The book is not, however, free from drawbacks. Some of them the reviewer would like to point out here hoping that they may be given consideration while preparing a future edition of it.

The chapters on electromagnetism and on relativistic mechanics, particularly the former, could be reduced in size to the necessary minimum. Quite a number of topics in the chapters on chemical thermodynamics, structure of molecules, and even in the most exhaustively treated chapters on quantum theory and quantum mechanics have been dealt with too briefly. The author has given on several occasions alternative derivations of certain formulae. Some of them are no doubt instructive but become too discursive in an advanced treatise like this. What the author could have done was to prepare suitable problems at the end of each chapter based on these alternative deductions. In fact, this is a valid complaint of the reviewer that the author has not thought it necessary to incorporate a large number of problems including numerical ones as he did in earlier volumes of this treatise. In this way some portions of the book could go in the form of problems thus reducing its bulk to a reasonable size. Again in some of the deductions the number of steps written could easily be curtailed. Similar types of deductions have also been unnecessarily repeated. Portions of the book

dealing with mathematical operations proper, viz., algebra of operators, polynomials, etc., could have gone as appendices.

As written, the book has emphasised more fully on the theoretical aspects, derivation of equations, etc., but the experimental side could have been developed a little further.

A number of authors have been mentioned by name and their work has also been described, but there is hardly any reference, except in a few cases, to books or journals where the work referred to may be read in greater detail and in original.

Printing mistakes abound but except in a few instances none of them are particularly harmful.

Although the number of lines written in connection with the drawbacks have exceeded those written in its appreciation the reviewer must admit that he has enjoyed reading some of the chapters, and it is hoped that the teachers and students alike will find the book useful to them.

S. K. M.



# MICROWAVE ANALOGUE FOR X-RAY DIFFRACTION PART II. SIZE OF THE SCATTERERS

G. S. SANYAL AND G. B. MITRA

INDIAN INSTITUTE OF TECHNOLOGY, KHARAGPUR

(Received March 8, 1961)

**ABSTRACT.** The variation with the azimuthal angle of scattering of amplitude of electromagnetic waves scattered by conducting spheres of sizes (a) comparable and (b) negligible with respect to the wave-length has been studied. A workable theoretical expression has been obtained and evaluated by carrying out numerical computations. The theoretical expressions to be computed contain high order Hankel functions, Legendre polynomials and their derivatives numerical values of which are not given in ordinarily available tables. These values have been calculated and used in the numerical computations. The resultant curves show that the conducting sphere with  $2\pi a/\lambda = 2$ , where 'a' is the radius of the sphere and  $\lambda$  the wavelength of the e.m. waves is the nearest approximation to several atoms as far as scattering behaviour towards X-rays is concerned.

## I. INTRODUCTION

Recently, Allen (1955) and Mitra and Sanyal (1960) have studied the scattering of electromagnetic waves in the microwave region by three dimensional arrays of metallic scatterers. While Allen (1955) worked with metallic discs as scatterers, Mitra and Sanyal (1960) used small cylinders for the purpose. Such scatterers, however, can hardly be used to build a true analogue in the microwave region for the diffraction of X-rays by crystals. The scatterers which are meant to simulate the atoms in the crystal lattices lack the spherical or near spherical symmetry possessed by atoms. Moreover, the variation of amplitude of electromagnetic waves scattered by these scatterers with the azimuthal angle of scattering should be similar to the atomic scattering factor graphs to make the analogue serve any useful purpose. It appears obvious that a solid sphere of dielectric or conducting material and of a proper size should serve the purpose, more or less, adequately. Hence, it has been decided to investigate theoretically the scattering patterns of conducting spheres to find out the proper size whose scattering pattern will approximate to the atomic scattering factor graphs. Since ionic radii of atoms are of the order of X-ray wavelengths, it has been intuitively felt that the proper size of the diffracting sphere would probably be comparable to the wavelength used. The case of vanishing sphere-size has also been studied to investigate the effect of diminishing the sphere-size.

Although the problem of diffraction of electromagnetic waves by spheres and spheroids has been studied by various authors [Mic. (1908), Blumer (1925, 1926a,

1926b and 1926c)] investigations of the type envisaged by us have not been carried out so far. Hence it has been decided to plot the graphs of the amplitude of microwaves scattered by spheres against the azimuthal angle of scattering for conducting spheres of sizes given by  $\rho = 6$ ,  $\rho = 2$  and  $\rho \rightarrow 0$  where  $\rho = 2\pi a/\lambda$ , 'a' being the radius of the sphere and  $\lambda$  the wavelength used. Only conducting spheres have been considered to render the already formidable numerical computations somewhat less complicated.

## II. THEORETICAL CONSIDERATIONS

Let a plane electromagnetic wave, propagating in free-space along the  $z$ -axis and polarised linearly along the  $x$ -axis, be incident on a *perfectly conducting sphere* of radius 'a' located at the origin of a spherical co-ordinate system  $r, \theta, \phi$  as shown in Fig. 1. The scattering process will be such that the resultant electromagnetic field satisfies the boundary conditions on the surface of the sphere and also reduces to a plane wave at a large distance  $r$ . The expressions for the scattered electromagnetic fields have been given by Stratton (1941). Thus for an incident plane electromagnetic wave expressed as

$$\vec{E}_i = \hat{i}_x E_0 \exp i(\beta z - \omega t)$$

$$H_i = \hat{i}_y (E_0 / \sqrt{\mu_0/\epsilon_0}) \exp i(\beta z - \omega t),$$

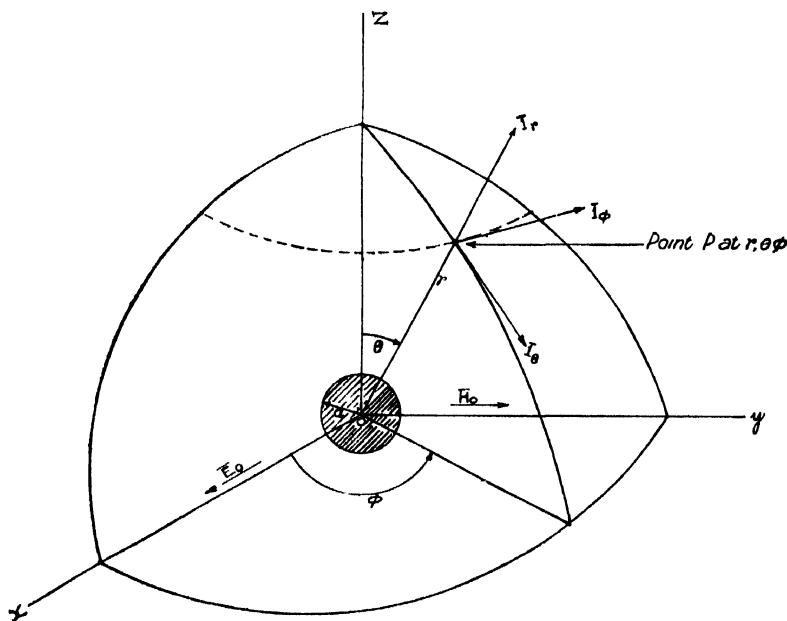


Fig. 1. Conducting sphere of radius 'a' located at the origin of a spherical coordinate system.  $\hat{i}_r, \hat{i}_\theta, \hat{i}_\phi$  are mutually orthogonal unit vectors at the point P.

the scattered electric field vector at any point  $P(r, \theta, \phi)$  outside the sphere is

$$E_S = E_0 \exp(-i\omega t) \sum_{n=1}^{\infty} i^n \frac{2n+1}{n(n+1)} [a_n^S \bar{m}_{01n} - i b_n^S n_{e1n}] \dots \quad (1)$$

where,  $E_0$  is the amplitude of the incident electric field

$\beta$ , the phase constant of the plane wave in free-space  $= \omega \sqrt{\mu_0 \epsilon_0} = 2\pi/\lambda_0$ ,  
 $\lambda_0$  being the free-space wavelength

$\mu_0$ , the permeability of free-space  $= 1.257 \times 10^{-6}$  H/metre

$\epsilon_0$ , the permittivity of free-space  $= 8.854 \times 10^{-12}$  F/metre

$\omega = 2\pi f$ ,  $f$  being the frequency of the incident wave

$m_{01n}$ , an odd vector function

$$= \bar{I}_\theta \left[ \frac{1}{\sin \theta} h^{(1)}_n(\beta r) P^n_{1n}(\cos \theta) \cos \phi \right]$$

$$= \bar{I}_\phi \left[ h^{(1)}_n(\beta r) \frac{\partial P^n_{1n}(\cos \theta)}{\partial \theta} \sin \phi \right]$$

$n_{e1n}$  an even vector function

$$= \bar{I}_r \left[ \frac{n(n+1)}{\beta r} h^{(1)}_n(\beta r) P^n_{1n}(\cos \theta) \cos \phi \right]$$

$$+ \bar{I}_\theta \left[ \frac{1}{\beta r} \frac{\partial \{ \beta r h^{(1)}_n(\beta r) \}}{\partial (\beta r)} \frac{\partial P^n_{1n}(\cos \theta)}{\partial \theta} \cos \phi \right]$$

$$= \bar{I}_\phi \left[ \frac{1}{\beta r \sin \theta} \frac{\partial \{ \beta r h^{(1)}_n(\beta r) \}}{\partial (\beta r)} P^n_{1n}(\cos \theta) \sin \phi \right]$$

$$a_n^S = -j_n(\rho)/h^{(1)}_n(\rho)$$

$$b_n^S = - \left[ \frac{d}{d\rho} \{ \rho j_n(\rho) \} \right] / \left[ \frac{d}{d\rho} \{ \rho h^{(1)}_n(\rho) \} \right]$$

$$j_n(\rho) = \sqrt{(\pi/2\rho)} J_{n+\frac{1}{2}}(\rho)$$

$$h^{(1)}_n(\rho) = \sqrt{(\pi/2\rho)} H^{(1)}_{n+\frac{1}{2}}(\rho)$$

$$\rho = 2\pi a/\lambda$$

$J_{n+\frac{1}{2}}$  and  $H_{n+\frac{1}{2}}^{(1)}$  are respectively Bessel and first kind Hankel functions each of order  $n+\frac{1}{2}$

$P_n^1(\cos \theta)$  is an associated Legendre polynomial.

The theoretical scattering pattern at a very large distance away from the conducting sphere may now be calculated from Eq.(1). The form given by Morse and Feshbach (1953) requires to be further simplified for direct computation and will not be used in this article. It is enough for our purpose to consider the variation of the electric field vector alone, since at a large distance the scattered field reduces to a uniform plane wave. The simplified asymptotic form of Eq. (1) valid at a large distance i.e.  $\beta r \gg 1$  and  $r \gg a$  may be arrived at by noting that

$$\lim_{\beta r \gg 1} h_n^{(1)}(\beta r) \rightarrow \frac{1}{\beta r} (-i)^{n+1} \exp(i\beta r)$$

$$\lim_{\beta r \gg 1} \frac{1}{\beta r} \frac{d\{\beta r h_n^{(1)}(\beta r)\}}{d(\beta r)} \rightarrow \frac{1}{\beta r} (-i)^n \exp(i\beta r).$$

Substitution of the limiting values of the above two expressions in Eq.(1) yields the components of the scattered electric field vector at a large distance as

$$E_{Sr} \rightarrow 0$$

$$E_{S\theta} = - \frac{iE_0 \cos \phi}{\beta r} \exp - i(\beta r - \omega t)$$

$$\sum_{n=1}^{\infty} \frac{2n+1}{n(n+1)} \left[ a_n^s \frac{P_n^1(\cos \theta)}{\sin \theta} + b_n^s \frac{dP_n^1(\cos \theta)}{d\theta} \right]$$

$$E_{S\phi} = \frac{iE_0 \sin \phi}{\beta r} \exp - i(\beta r - \omega t)$$

$$\sum_{n=1}^{\infty} \frac{2n+1}{n(n+1)} \left[ a_n^s \frac{dP_n^1(\cos \theta)}{d\theta} + b_n^s \frac{P_n^1(\cos \theta)}{\sin \theta} \right] \quad \dots \quad (2)$$

The rate of convergence of the above expressions for the  $\theta$  and  $\phi$  components of the scattered field depends largely upon the convergence of  $a_n^s$  and  $b_n^s$  for successively increasing values of  $n$ . For values of  $\rho$  large compared to unity, both the terms inside the square brackets of Eq.(2) converge very slowly and the

summation has to be carried out over a large value of  $n$ . In the special case when  $\rho$  is finite but very much less than unity,  $a_n^s$  and  $b_n^s$  can be expanded in powers of  $\rho$  giving to the first order of approximation

$$\begin{aligned} b_n^s &\simeq -\frac{2}{3} i \rho^3 & \text{for } n=1 \\ &\simeq 0 & \text{for } n > 1 \\ a_n^s &\simeq \frac{1}{3} i \rho^3 & \text{for } n=1 \\ &\simeq 0 & \text{for } n > 1 \end{aligned}$$

Substitution of these values of  $a_n^s$  and  $b_n^s$  in Eq. (2) yields the scattered fields in the far zone due to a finite but very small conducting sphere as

$$\begin{aligned} E_{s\theta} &= \frac{1}{2} \frac{E_0 \cos \phi}{\beta r} \rho^3 (1 - 2 \cos \theta) \exp i(\beta r - \omega t) \\ &\quad - \frac{2\pi^2 E_0 \cos \phi}{\lambda^2 r} a^3 (1 - 2 \cos \theta) \exp i(\beta r - \omega t) \\ E_{s\phi} &= \frac{1}{2} \frac{E_0 \sin \phi}{\beta r} \rho^3 (2 - \cos \theta) \exp i(\beta r - \omega t) \\ &\quad - \frac{2\pi^2 E_0 \sin \phi}{\lambda^2 r} a^3 (2 - \cos \theta) \exp i(\beta r - \omega t) \end{aligned} \quad (3)$$

### III. NUMERICAL COMPUTATION

To study the nature of the variation of the scattered field with the polar angle  $\theta$ , the summation in Eq. (2) has to be performed over a sufficiently large value of  $n$ . In this article  $n$  has been so chosen that the numerical result may be correct to, at least, the third decimal place. Numerical computation for only  $E_{s\phi}$  and that too for three values of  $\rho$ , (i)  $\rho \ll 1$  i.e.,  $a \ll \lambda$ , (ii)  $\rho = 2$  i.e.,  $a = \lambda/\pi$  and (iii)  $\rho = 6$  i.e.,  $a \simeq \lambda$  has been carried out, since these results are significant enough to indicate the general nature of variation of the scattered fields with  $\theta$  and also to show the effect of the radius of the sphere on the scattering pattern. The first case e.g.  $\rho \ll 1$  has been calculated using Eq. (3) and the other two cases by using Eq. (2).

Calculation of the coefficients  $a_n^s$  and  $b_n^s$  in Eq. (2) requires tables of  $j_n$  and  $h_n^{(1)}$  functions and their derivatives. Since these tables are not available the coefficients were obtained as follows :

$$a_n^s = -\frac{j_n(\rho)}{h_n^{(1)}(\rho)} \quad \frac{J_{n+1}(\rho)}{H_{n+1}^{(1)}(\rho)}$$

$$b_n s = - \left[ \frac{d}{d\rho} \{ \rho j_n(\rho) \} \right] / \left[ \frac{d}{d\rho} \{ \rho h_n^{(1)}(\rho) \} \right]$$

$$= - \frac{J_{n+1}(\rho) + \rho [J_{(n-1)+\frac{1}{2}}(\rho) - J_{(n+1)+\frac{1}{2}}(\rho)]}{H_{n+\frac{1}{2}}^{(1)}(\rho) + \rho [H_{(n-1)+\frac{1}{2}}^{(1)}(\rho) - H_{(n+1)+\frac{1}{2}}^{(1)}(\rho)]}$$

The Hankel function  $H_\nu^{(1)}$  itself was computed from the formula

$$H_\nu^{(1)}(x) = [J_{-\nu}(x) - J_\nu(x) \exp(-\nu\pi i)] / [i \sin \nu\pi]$$

and the tables for  $J_\nu$  and  $J_{-\nu}$  as given by Watson (1922).

Again the numerical computation of Eq.(2) requires the use of the tables of  $P_n^1(\cos \theta)$  and its derivate for different values of  $n$ . Since these tables also are not available for large  $n$ , their values were computed and tabulated for the value of the order  $n$  up to 10 by using the recurrence relations :

$$P_{n+1}^1(\cos \theta) = [(2n+1) \cos \theta P_n^1(\cos \theta) - (n+1)P_{n-1}^1(\cos \theta)]/n$$

$$d/d\theta [P_n^1(\cos \theta)] = [nP_{n+1}^1(\cos \theta) - (n+1) \cos \theta P_n^1(\cos \theta)]/\sin \theta$$

from the lower order polynomials given by Jahnke and Emde (1943).

Eq.(2) can now be evaluated term by term for successively increasing values of  $n$  and the summation obtained.

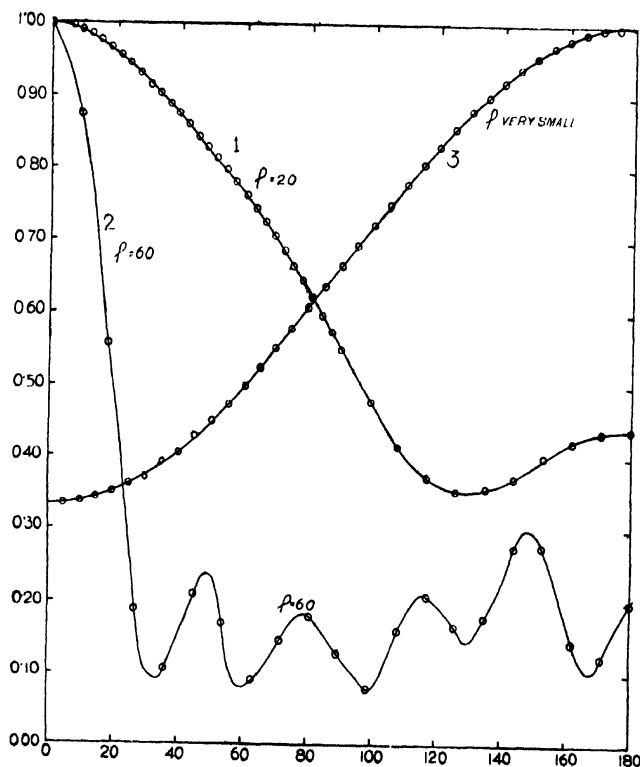


Fig. 2. Scattering patterns of conducting spheres of several sizes (Curve 1,  $\rho = 2.0$ , Curve 2,  $\rho = 6.0$  and Curve 3,  $\rho$  very small).

## IV. DISCUSSIONS

The theoretical scattering patterns for conducting spheres as computed for the three cases mentioned before are plotted graphically in Fig. 2. Since for each case the relative variation of the scattered field amplitude is of interest, the maximum value of the amplitude has been taken to be equal to 1.00. The scattering patterns show that for the cases when the radius of the sphere is comparable to  $\lambda$  the amplitude gradually decreases with the scattering angle  $\theta$ . For  $\rho = 6$ , the curve rapidly decreases from a maximum at  $\theta = 0^\circ$  to a minimum at  $\theta \simeq 35^\circ$  after which the curve becomes oscillating. For  $\rho = 2$ , the amplitude falls from a maximum at  $\theta = 0^\circ$  almost exponentially till  $\theta = 135^\circ$  when there is a tendency to rise rather slowly. The curve for  $\rho \rightarrow 0$  shows that the scattered amplitude gradually increases with  $\theta$ . Thus, the sphere with  $\rho = 2$  is found to behave, of the three cases considered, in a way nearest to that of atoms as far as the scattering curve is concerned. Fig. 3 shows the variations of amplitude of

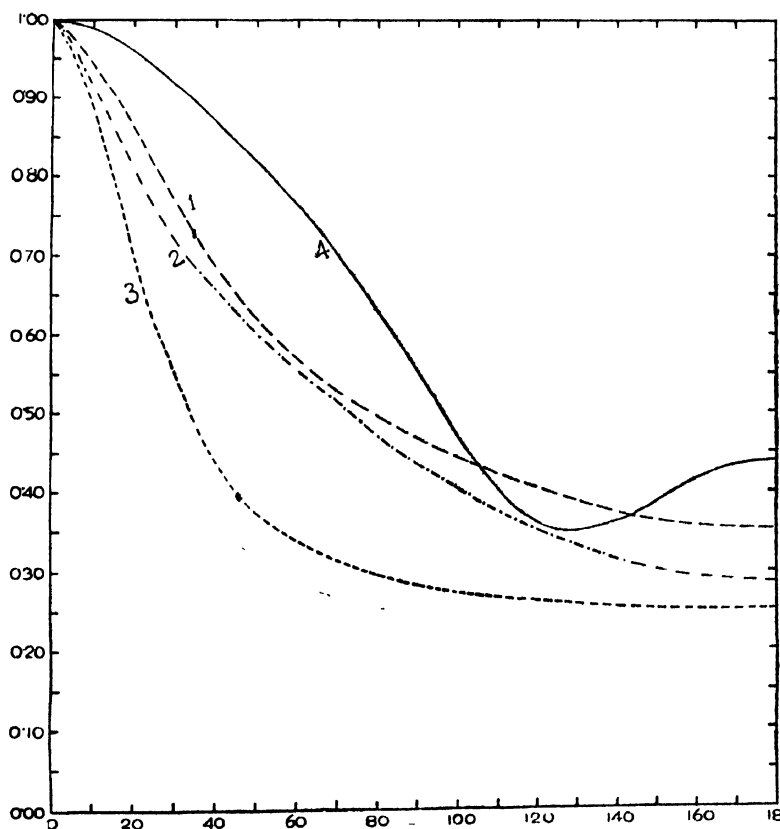


Fig. 3. Variation of the amplitude of X-rays scattered by atoms of copper, aluminium and carbon. Curve 1—copper, Curve 2—aluminium, Curve 3—carbon, Curve 4—scattering pattern of conducting sphere for  $\rho = 2.0$ .

X-rays scattered by atoms of copper, aluminium and carbon (James and Brindley, 1931) and for c.m. waves for a conducting sphere with  $\rho = 2$ . It is observed that the nature of all these curves agree to a large extent. Perhaps better agreement can be achieved with values of  $\rho$  which are near to but not exactly equal to 2 or perhaps spheres with different dielectric constants will give better agreement. These cases have not been investigated by us as yet. However, we may safely conclude that with conducting spheres,  $\rho$  must have a value very nearly equal to 2 so that the atoms are adequately simulated as far as scattering behaviour is concerned.

## REFERENCES

- Allen, R. A., 1955, *Am. J. Phys.*, **23**, 297  
Blumer, H., 1925, *Z. Physik*, **32**, 119  
Blumer, H., 1926a, *Z. Physik*, **38**, 304  
Blumer, H., 1926b, *Z. Physik*, **38**, 920  
Blumer, H., 1926c, *Z. Physik*, **39**, 195  
Jahnke, E. and Emde, F., 1943, *Tables of Functions*, Dover Publications, New York.  
James, B. W., and Brindley, G. W., 1931, *Phil. Mag.*, **12**, 81.  
Mie, G., 1908, *Ann. Physik*, **25**, 377.  
Mitra, G. B. and Sanyal, G. S., 1960, *Ind. J. Phys.*, **34**, 103.  
Morse, P. M. and Feshbach, H., 1953, *Methods of Theoretical Physics*, Mc-Graw Hill, 1882.  
Stratton, J. A., 1941, *Electromagnetic Theory*, Mc-Graw Hill, 564.  
Watson, G. H., 1922, *A Treatise on the Theory of Bessel Functions*, Cambridge University Press.



# POTENTIAL FUNCTION OF HELIUM-LIKE ATOMS AND ELECTRON SCATTERING BY THE BORN APPROXIMATION

S. C. MUKHERJEE

DEPARTMENT OF THEORETICAL PHYSICS  
INDIAN ASSOCIATION FOR THE CULTIVATION OF SCIENCE,  
JADAVPUR, CALCUTTA-32

(Received March 30, 1961)

**ABSTRACT.** In this paper the potential function of helium-like atoms has been derived by using the wave function of Hartree and Ingman (1933) and the scattering cross section of electron by the helium-like atoms has been calculated by the method of Born approximation. The theoretical results at low angular range are found to be in excellent agreement with the experimental findings of Hughes, McMullen and Webb (1932).

## INTRODUCTION

In calculating the energy eigen values of helium-like atoms by the variational methods the trial wave function has often been chosen as a product of two functions i.e.  $f(r_1) \cdot f(r_2)$ , where  $r_1$  and  $r_2$  are the position vectors of the two electrons with respect to the nucleus as origin (c.f. Huzinaga, 1960). This type of wave function makes the calculation simple, however, from physical grounds we would expect some dependence of the wave function on  $r_{12}$  the mutual distance between the two electrons. Therefore the simple wave function  $f(r_1)f(r_2)$  may be modified by a multiplication of a function  $\chi(r_{12})$  which depends on the distance between the electrons. This function  $\chi(r_{12})$  is called the correlation function. Several authors like Hylleraas (1929), Hartree and Ingman (1933), and Roothaan (1960) have suggested this type of improved approximation of analytical wave function for helium like atoms.

In the present paper we propose to evaluate the nature of the potential functional function and to calculate the cross section of elastic scattering of electron by helium-like atom in the ground state by taking a wave function as suggested by Hartree and Ingman (1933). They have taken both the electrons in the  $K$  shell and they argue that the correlation function should approach a constant value for  $r_{12} \rightarrow \infty$ , expressing the separability of the wave function when the electrons are far apart and the decrease to a finite though smaller value for  $r_{12} \rightarrow 0$ . The success of such a wave function can also be judged by the improvement in the value of the eigen-energy. The upper limit for the ground state energy of the helium atom obtained by Hartree and Ingman

using the above wave function is  $-2.89e^2/a_0$ ,  $a_0$  being the Bohr radius, the experimental value being  $-2.904e^2/a_0$ , whereas Hylleraas, using a wave function without  $\chi(r_{12})$ , has obtained  $-2.847e^2/a_0$  as the value for the same.

In the first part of this paper the function due to Hartree and Ingman has been normalized and the potential function has been evaluated by using the above mentioned wave function. In the second part the differential scattering cross section of electron has been calculated by the Born approximation method neglecting the exchange effect. At 500 eV (the range of energy where the Born approximation method is fairly valid) the differential cross section of scattering of electron by helium atom agrees very well at small angles with the experimental findings of Hughes, McMillen and Webb (1932), but for large angles our theoretical results deviate slightly from the experimental ones. By comparing our results at 700 eV with those of Sachl (1958) who has calculated the same problem in higher Born approximation we find that in the angular range  $60^\circ$  to  $135^\circ$ , our expression gives better agreement with experimental findings than that of Sachl (1958). No data below  $60^\circ$  angle has been given by Sachl.

#### METHODS OF CALCULATION

The wave function  $\psi$  due to Hartree and Ingman is

$$\psi \sim e^{-\xi(r_1+r_2)}(1 - Ce^{-\eta r_{12}})$$

where  $\xi = 1.8395$ ,  $C = 0.88784$ ,  $\eta = 0.047827$ ,

and the distances are represented in Bohr unit.

The wave function is normalized as shown in Appendix 1.

The potential function is calculated by the formula (vide Mott and Massey, 1949).

$$V(r) = -e^2 \int \left( \frac{Z}{r} - \sum_{n=1,2} \frac{1}{|\mathbf{r} - \mathbf{r}_n|} \right) |\psi(\mathbf{r}_1, \mathbf{r}_2)|^2 d\mathbf{r}_1 d\mathbf{r}_2, \quad \dots (1)$$

where  $Z$  is the atomic number and  $\psi$  is the wave function.

Thus

$$V(r) = -\frac{Ze^2}{r} + \frac{2e^2}{N^2} \{I(2\xi, 0) - 2CI(2\xi, \eta) + C^2I(2\xi, 2\eta)\} \quad \dots (2)$$

where  $N$  is the normalization factor (vide Appendix 1) and

$$I(\mu, \eta) = \int \frac{e^{-\mu(r_1+r_2)-\eta r_{12}}}{|\mathbf{r} - \mathbf{r}_1|} d^3\mathbf{r}_1 d^3\mathbf{r}_2.$$

From the identity

$$\frac{e^{-\lambda r}}{r} = \frac{1}{2\pi^2} \int \frac{e^{\pm i\mathbf{p} \cdot \mathbf{r}}}{p^2 + \lambda^2} d^3\mathbf{p}$$

we get

$$I(\mu, \eta) = \frac{\mu^2 \eta}{2\pi^3} \int \frac{e^{-i\mathbf{p} \cdot \mathbf{r}_1 + i\mathbf{q} \cdot \mathbf{r}_2 + i\mathbf{s} \cdot (\mathbf{r}_1 - \mathbf{r}_2) - i\mathbf{k} \cdot (\mathbf{r} - \mathbf{r}_1)}}{(p^2 + \mu^2)^2 (q^2 + \mu^2)^2 (\delta^2 + k^2)} d^3 \mathbf{r}_1 d^3 \mathbf{r}_2 d^3 \mathbf{p} d^3 \mathbf{q} d^3 \mathbf{s} d^3 \mathbf{k}$$

Applying the properties of  $\delta$ -function

$$\int_{-\infty}^{\infty} e^{i(\mathbf{p} - \mathbf{k}) \cdot \mathbf{x}} d^3 \mathbf{x} = (2\pi)^3 \delta(\mathbf{p} - \mathbf{k})$$

we get

$$\therefore I(\mu, \eta) = \frac{\mu^2 \eta}{\pi^2} \int e^{-i\mathbf{k} \cdot \mathbf{r}} d^3 \mathbf{k} \cdot f(k^2)$$

where

$$f(k^2) = \int \frac{d^3 \mathbf{s}}{\{(s+k)^2 + \mu^2\}^2 \{s^2 + \mu^2\}^2 \{s^2 + \eta^2\}^2 \cdot k^2}$$

$$\begin{aligned} \text{i.e. } I(\mu, \eta) = \frac{\mu^2 \eta}{r} 2^6 \pi \int \frac{1}{ik} e^{ikr} \left[ \frac{1}{(\mu^2 - \eta^2)^2} \left\{ \frac{\mu + \eta}{\eta(k^2 + \delta^2)(k^2 + \lambda^2)} - \frac{4\mu(\mu + \eta)}{(k^2 + \delta^2)^2(k^2 + \lambda^2)} \right. \right. \\ \left. \left. + \frac{2}{(k^2 + 4\mu^2)^2} \right\} - \frac{2}{(\mu^2 - \eta^2)^3} \left\{ \frac{1}{(k^2 + \delta^2)} - \frac{1}{(k^2 + 4\mu^2)} \right\} \right] dk \end{aligned}$$

where

$$\mu + \eta = \delta; \quad \mu - \eta = \lambda$$

After evaluation of the integral we have

$$\begin{aligned} I(\mu, \eta) = \frac{2^6 \mu \eta \pi^2}{r(\mu^2 - \eta^2)^2} \left\{ \frac{\mu + \eta}{\eta(\delta^2 - \lambda^2)} \left[ \frac{1}{\lambda^2} - \frac{e^{-\lambda r}}{\lambda^2} - \frac{1}{\delta^2} + \frac{e^{-\delta r}}{\delta^2} \right] \right. \\ \left. - 4\mu(\mu + \eta) \left[ \frac{1}{\delta^4 \lambda^2} - \frac{e^{-\lambda r}}{\lambda^2(\delta^2 - \lambda^2)^2} + \frac{e^{-\delta r}}{\delta^2(\delta^2 - \lambda^2)^2} + \frac{e^{-\delta r}}{\delta^4(\delta^2 - \lambda^2)} + \frac{e^{-\delta r}}{2\delta^2(\delta^2 - \lambda^2)} \right] \right. \\ \left. + \frac{1}{8\mu^3} \left[ \frac{1}{\mu} - \frac{e^{-2\mu r}}{\mu} - e^{-2\mu r} r \right] - \frac{2}{\delta^2(\mu^2 - \eta^2)} \{1 - e^{-\delta r}\} + \frac{[1 - e^{-2\mu r}]}{2\mu^2(\mu^2 - \eta^2)} \right\} \end{aligned}$$

The scattering amplitude, by the Born approximation method is given by

$$f(\theta) = \frac{1}{4\pi} \frac{2m}{\hbar^2} \int V(r) e^{i\mathbf{k} \cdot \mathbf{r}} d^3 \mathbf{r} \quad \dots \quad (3)$$

where  $V(r)$  is the potential and  $\mathbf{k} = \frac{2mv}{\hbar} (\mathbf{n}_0 - \mathbf{n})$ ,  $\mathbf{n}_0$  and  $\mathbf{n}$  are the unit vectors

along the incident and scattered directions respectively. Substituting in Eq. (3) the value of  $I(r)$  from Eq. (1) we have,

$$f(\theta) = \frac{e^2}{4\pi} \frac{2m}{\hbar} \left[ - \int \frac{Z}{r} e^{i\mathbf{k}\cdot\mathbf{r}} d^3\mathbf{r} + \frac{2}{N^2} \{I(2\xi, 0) - 2CI(2\xi, \eta) + C^2I(2\xi, 2\eta)\} \right] \quad (4)$$

$$\text{where} \quad I(\mu, \nu) = \int e^{-\mu(\mathbf{r}_1 + \mathbf{r}_2) - \nu\mathbf{r}_{12}} \frac{i\mathbf{k}\cdot\mathbf{r}}{|\mathbf{r} - \mathbf{r}_n|} d^3\mathbf{r}_1 d^3\mathbf{r}_2 d^3\mathbf{r}$$

with  $n = 1, 2$

After integration (vide Appendix 2), we obtain

$$I(\mu, \nu) = \frac{2^8 \pi^3 \mu \nu}{k^2} \left[ \frac{1}{(\mu^2 - \nu^2)^2} \left\{ \frac{\lambda/\nu + 2}{(k^2 + \delta^2)(k^2 + \lambda^2)} - \frac{4\mu\delta}{(k^2 + \delta^2)^2(k^2 + \lambda^2)} \right. \right. \\ \left. \left. - \frac{2}{(k^2 + 4\mu^2)^2} \right\} - \frac{2}{(\mu^2 - \nu^2)^3} \left\{ \frac{1}{k^2 + \delta^2} - \frac{1}{k^2 + 4\mu^2} \right\} \right]$$

where  $\mu + \nu = \delta, \quad \mu - \nu = \lambda$

TABLE I

Comparison of the differential scattering cross section of electron of energy 500 eV scattered by helium atom

Differential cross section in units of $10^{-20}\text{cm}^2$		
Angle in degrees	Experimental value	Theoretical results (present author)
9.5	1195.0	1190.4
12.0	1047.0	1037.16
22.0	467.0	475.64
27.0	284.5	287.01
47.0	60.8	69.8
67.0	15.88	20.04
87.0	6.14	9.23

TABLE II

Comparison of the differential scattering cross section of electron of energy 700eV scattered by helium atom

Angle in degrees	Differential cross section in units of $10^{-20}$ cm <sup>2</sup>		
	Experimental value	Theoretical results Suchl	Theoretical results (present author)
60	15	24	15.75
90	5	8.6	4.04
120	3.5	5.2	1.864
135	3.4	1.8	1.405

## DISCUSSION

From the calculation it is observed that the screening effect is more prominent for small angles of scattering whereas for large angles it becomes negligible. This is because when the scattering angle is large the particle moves very near the nucleus, where the screening effect due to the surrounding electrons is negligible.

The better agreement of our theoretical calculations with experiment for small angles of scattering is due to the fact that in these cases the particle passes far from the nucleus, where the potential is very weak on account of the screening effect and as such, the perturbation calculations are quite valid.

## ACKNOWLEDGMENT

The author is greatly indebted to Prof. D. Basu for suggesting the problem and for his helpful guidance throughout the progress of the work. Thanks are also due to Dr. N. C. Sil for valuable discussion.

## APPENDIX I

In the present case the wave function is

$$\psi = \frac{1}{N} e^{-\xi(r_1 + r_2)} (1 - C'e - \eta r_{12}),$$

the normalization factor  $N$  is evaluated from the requirement

$$\int \psi \psi^* d\tau = 1.$$

Thus,

$$N^2 = I''(2\xi, 0) - 2CI''(2\xi, \eta) + C^2I''(2\xi, 2\eta)$$

$$\begin{aligned} \text{where} \quad I''(\mu, \lambda) &= \int e^{-\mu(r_1+r_2)} e^{-\lambda r_{12}} d^3r_1 d^3r_2 \\ &= 2\pi^2 \int_0^\infty ds \int_0^s du \int_0^u dt e^{-\mu s} e^{-\lambda u} u(s^2-t^2) \end{aligned}$$

$$\text{where} \quad s = r_1 + r_2, \quad t = -r_1 + r_2, \quad u = r_{12} \quad (\text{vide Hylleraas, 1929})$$

$$\begin{aligned} &= 2\pi^2 \int_0^\infty ds \int_0^s du e^{-\mu s} e^{-\lambda u} \left( s^2 u^2 - \frac{u^4}{3} \right) \\ &= 2\pi^2 \int_0^\infty ds e^{-\mu s} (s^2 I_2 - \frac{1}{3} I_4) \end{aligned}$$

$$\text{where} \quad I_n = \int_0^s e^{-\lambda u} u^n du = \left( -\frac{\partial}{\partial \lambda} \right)^n I_0; \quad I_0 = \int_0^s e^{-\lambda u} du = \left[ \frac{e^{-\lambda u}}{-\lambda} \right]_0^s$$

$$\begin{aligned} \therefore I''(\mu, \lambda) &= \left[ \int_0^\infty e^{-\mu s} s^2 \frac{2}{\lambda^3} ds - \int_0^\infty \frac{1}{3} e^{-\mu s} \frac{24}{\lambda^5} ds \right. \\ &\quad \left. - \int_0^\infty e^{-(\lambda+\mu)s} \left\{ \frac{2}{\lambda^3} s^2 + \frac{2}{\lambda^2} s^3 + \frac{1}{\lambda} s^4 \right\} ds \right. \\ &\quad \left. + \frac{1}{3} \int_0^\infty e^{-(\lambda+\mu)s} \left\{ \frac{24}{\lambda^5} + \frac{24}{\lambda^4} s + \frac{12}{\lambda^3} s^2 + \frac{4}{\lambda^2} s^3 + \frac{1}{\lambda} s^4 \right\} ds \right] \end{aligned}$$

$$\text{i.e.,} \quad I''(\mu, \lambda) = \frac{8\pi^2}{\mu^3(\lambda+\mu)^5} \{ \lambda^2 + 5\lambda\mu + 8\mu^2 \}$$

$$\text{Since} \quad \int_0^\infty e^{-\nu s} s^n ds = \frac{n!}{\nu^{n+1}}$$

## APPENDIX 2

The value of  $I'(\mu, \nu)$  we get as

$$I'(\mu, \nu) = \iiint e^{\frac{-\mu(r_1+r_2) - \nu r_{12} + i\mathbf{k}\cdot\mathbf{r}}{|\mathbf{r}-\mathbf{r}_1|}} d^3r_1 d^3r_2 d^3r_3$$

$$= \frac{\mu^2 \nu}{(\pi^2)^3 2\pi^2} \int \int \int \frac{e^{-i\mathbf{p} \cdot \mathbf{q}(\mathbf{r}-\mathbf{r}_1)}}{p^2} d^3\mathbf{p} \int \frac{e^{i\mathbf{q} \cdot \mathbf{r}}}{(q^2+\mu^2)^2} d^3\mathbf{q} \int \frac{e^{i\mathbf{t} \cdot \mathbf{r}_2}}{(t^2+\mu^2)^2} d^3\mathbf{t} \\ \int \frac{e^{i\mathbf{s} \cdot (\mathbf{r}_1-\mathbf{r}_2)}}{(s^2+\nu^2)^2} d^3\mathbf{s} \int e^{i\mathbf{k} \cdot \mathbf{r}} d^3\mathbf{r} d^3\mathbf{r}_1 d^3\mathbf{r}_2$$

Since

$$\frac{e^{-\lambda r}}{r} = \frac{1}{2\pi^2} \int_{-\infty}^{\infty} \frac{e^{i\mathbf{p} \cdot \mathbf{r}}}{p^2 + \lambda^2} d^3\mathbf{p}$$

and

$$e^{-\lambda r} = \int_{-\infty}^{\infty} \frac{e^{i\mathbf{p} \cdot \mathbf{r}} d^3\mathbf{p}}{(p^2 + \lambda^2)^2}$$

$$\therefore I'(\mu, \nu) = \frac{\mu^2 \nu (2\pi)^9}{2\pi^8} \int \frac{\delta(\mathbf{k}-\mathbf{p})\delta(\mathbf{p}+\mathbf{q}+\mathbf{s})\delta(\mathbf{t}-\mathbf{s})d^3\mathbf{p} d^3\mathbf{q} d^3\mathbf{t} d^3\mathbf{s}}{p^2(q^2+\mu^2)^2(t^2+\mu^2)^2(s^2+\nu^2)^2} \\ = \frac{2^8 \mu^2 \nu \pi}{k^2} \int \frac{d^3\mathbf{s}}{(|\mathbf{k}+\mathbf{s}|^2+\mu^2)^2(s^2+\mu^2)^2(s^2+\nu^2)^2} \\ = \frac{2^8 \pi^2 \mu^2 \nu}{k^3} \int \frac{\mathbf{s} d\mathbf{s}}{(s^2+\mu^2)^2(s^2+\nu^2)^2\{(s-k)^2+\mu^2\}}$$

Applying the following identity,

$$\left[ (p^2+\mu^2)(p^2+\nu^2) \right]^{-2} = \frac{1}{(\mu^2-\nu^2)^2} \left[ \frac{1}{(p^2+\nu^2)^2} + \frac{1}{(p^2+\mu^2)^2} \right] \\ - \frac{2}{(\mu^2-\nu^2)^3} \left[ \frac{1}{(p^2+\nu^2)} - \frac{1}{(p^2+\mu^2)} \right]$$

$$\therefore I'(\mu, \nu) = \frac{2^8 \pi^2 \mu \nu}{k^2} \left[ \frac{1}{(\mu^2-\nu^2)^2} \left\{ \frac{1}{(k^2+\delta^2)(k^2+\lambda^2)} \left\{ \frac{\mu-\nu}{\nu} + 2 \right\} - \frac{4\mu(\mu+\nu)}{(k^2+\delta^2)^2(k^2+\lambda^2)} \right. \right. \\ \left. \left. + \frac{2}{(k^2+4\mu^2)^2} \right\} - \frac{2}{(\mu^2-\nu^2)^3} \left\{ \frac{1}{k^2+\delta^2} - \frac{1}{k^2+4\mu^2} \right\} \right]$$

where

$$\mu+\nu = \delta \quad \text{and} \quad \mu-\nu = \lambda$$

## REFERENCES

- Hartree D. R., and Ingman, 1933, *Mem. Proc. Manchester. Lit & Phil Soc.* **77**, 79.  
Hughes, A. L., McMillen, J. H. and Webb, G. M. 1932, *Phys. Rev.* **58**, 154.  
Huzinaga, S., 1960, *Prog. Theo. Phys.*, **23**, 562.  
Hylleraas, E. A., 1929, *Z. Physik.*, **54**, 347.  
Mott, N. F. & Massey, H. S. W. 1949, *Theory of Atomic Collision*, Oxford University Press, New York. (2nd Edition).  
Roothan, C. C. J., 1960, *Rev. Mod. Phys.*, **32**, 178, 194.  
Sachl, V., 1958, *Phys. Rev.*, **110**, 891.



# DETERMINATION OF PHOTOELASTIC CONSTANTS IN THE PRESENCE OF TILT OF THE AXES

K. V. KRISHNA RAO

PHYSICS DEPARTMENT, OSMANIA UNIVERSITY, HYDERABAD-7

(Received January 2, 1961)

**ABSTRACT.** This paper describes a direct method of determining the differential stress-optical constants, when the axes of polarisation in a stressed crystal do not coincide with the principal directions of stress. The method is verified by studies on barium nitrate and strontium nitrate crystals.

## INTRODUCTION

With the application of the group-theoretical methods by Bhagavantam (1942) to derive the number of non-vanishing photoelastic constants for different classes of crystals and the discovery of several errors in the schemes given earlier by Pockels (1889), interest in the photoelastic effect in crystals was revived and an intensive study of the subject was undertaken by Bhagavantam and collaborators in recent years (Nye, 1957; Krishnan, 1958). During the course of these studies, it was found (Bhagavantam and Krishna Rao, 1953a) that, for some orientations of cubic crystals, the principal axes of polarisation of the stressed crystal do not coincide with the principal directions of stress. This phenomenon has been referred to as the tilt of the axes. When there is tilt of the axes, if the usual experimental method for determining the differential stress-optical constants, is employed, one should first find the positions of the axes of polarisation of the stressed crystal and adjust the Babinet compensator, such that its principal directions coincide with the axes of polarisation of the stressed crystal. On the other hand, if the principal directions of the compensator are kept vertical and horizontal, as usual, and the crystal is stressed vertically, it has been found that the shift of the Babinet fringe is not proportional to the applied stress and the fringe vibrates about the initial position, as the stress is gradually increased. It will now be shown that, from a knowledge of the stress required to bring back the Babinet fringe to its initial position, the stress-optical constant can be evaluated directly, without necessitating the determination of the tilt of the axes.

## THEORY

Let  $OX_1, OY_1$  (Fig. 1) be the principal directions of polarisation of the stressed crystal in the  $XY$  plane (normal to the direction of observation),  $OX_2, OY_2$  the

principal directions of the compensator and OP the direction of vibration of the incident plane polarised beam of light of amplitude  $a$ . Let  $\alpha$  and  $\beta$  be angles  $X_1OP$  and  $X_1OX_2$  respectively.

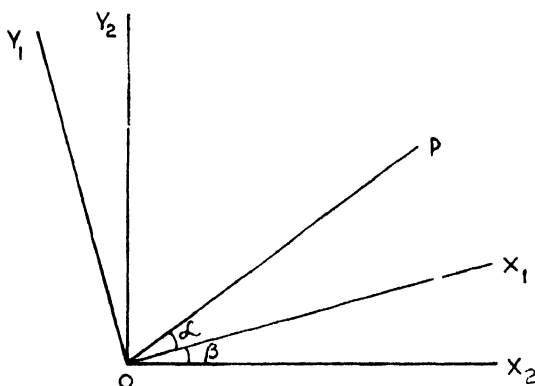


Fig. 1. Showing the principal directions of the stressed crystal ( $OX_1$ ,  $OY_1$ ), the principal directions of the compensator ( $OX_2$ ,  $OY_2$ ) and the direction of vibration (OP) of the incident light.

On entering the stressed crystal, the incident beam will be resolved into two components, one of amplitude  $a \cos \alpha$  and direction of vibration  $OX_1$  and the other of amplitude  $a \sin \alpha$  and direction of vibration  $OY_1$ . These components will have a phase difference, say  $\delta$ , when they leave the crystal. When the beam enters the compensator, each of the above-mentioned two components will split further into two components with their vibration directions along  $OX_2$  and  $OY_2$ . The amplitude of the component, with the vibration direction along  $OX_2$ , is the resultant of the two components of amplitudes  $a \cos \alpha \cos \beta$  and  $-a \sin \alpha \sin \beta$  and phase difference  $\delta$ . Similarly, the amplitude of the component with vibration direction along  $OY_2$  is the resultant of two components of amplitudes  $a \sin \alpha \cos \beta$  and  $a \cos \alpha \sin \beta$  and phase difference  $\delta$ . The amplitude  $A$  of the component with the vibration direction along  $OX_2$  is given by

$$A^2 = a^2 \{ \cos^2(\alpha - \beta) - \frac{1}{2} \sin 2\alpha \sin 2\beta (1 + \cos \delta) \}. \quad (1)$$

The phase of this vibration  $\Delta_1$  is given by

$$\tan \Delta_1 = \frac{\sin \alpha \sin \beta \sin \delta}{\cos \alpha \cos \beta - \sin \alpha \sin \beta \cos \delta} \quad \dots \quad (2)$$

Similarly, the amplitude  $B$  of the component whose vibration direction is along  $OY_2$  is given by

$$B^2 = a^2 \{ \sin^2(\alpha + \beta) - \frac{1}{2} \sin 2\alpha \sin 2\beta (1 - \cos \delta) \} \quad (3)$$

and its phase  $\Delta_2$  is given by

$$\tan \Delta_2 = \frac{\sin \alpha \cos \beta \sin \delta}{\cos \alpha \sin \beta + \sin \alpha \cos \beta \cos \delta} \quad (4)$$

From Eqs. (2) and (4), we get

$$\tan (\Delta_2 - \Delta_1) = \frac{\sin 2\alpha \sin \delta}{\sin 2(\alpha + \beta) - 2 \cos 2\beta \sin 2\alpha \sin^2 \delta / 2} \quad (5)$$

The fringe shift in the compensator gives  $(\Delta_2 - \Delta_1)$  which would obviously be equal to  $\delta$  when the tilt of the axes  $\beta$  is zero. Eq. (5) shows that, as  $\delta$  is increased,  $(\Delta_2 - \Delta_1)$  first increases, reaches a maximum and then reduces to zero when  $\delta = \pi$ . On a further increase of  $\delta$ ,  $\Delta_2 - \Delta_1$  changes sign, reaches a maximum and again reduces to zero when  $\delta = 2\pi$ . Thus the Babinet fringe completes one oscillation as the phase difference  $\delta$  increases from zero to  $2\pi$ . The variation of  $\Delta_2 - \Delta_1$  with  $\delta$ , evaluated for values of  $\alpha$  and  $(\alpha + \beta)$ ,  $30^\circ$  and  $45^\circ$  respectively, using Eq. (5), is shown in Fig. 2. It is clear that the stress  $P$ , required for one complete

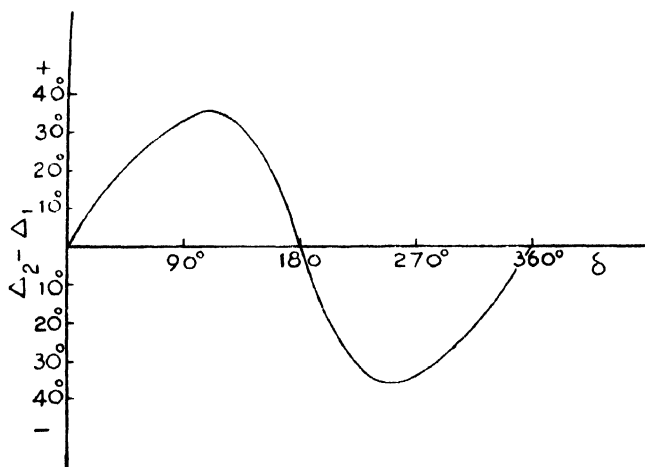


Fig. 2. Variation of  $(\Delta_2 - \Delta_1)$  with  $\delta$ .

oscillation of the Babinet fringe, gives the stress required for a path difference  $\lambda$  (wavelength of the light used) between the two components with their vibration directions along the principal directions of the stressed crystal. Hence the differential stress-optical coefficient  $C'$  is given by

$$C' = \frac{2\lambda}{n^3 P t},$$

where  $t$  is the thickness of the crystal parallel to the direction of observation and  $n$  the refractive index of the crystal in the unstressed state.

## EXPERIMENTAL

To verify the foregoing method, crystal prisms of barium nitrate and strontium nitrate, with faces parallel to  $(111)$ ,  $(01\bar{1})$  and  $(\bar{2}11)$  planes, have been studied applying the stress, by a lever arrangement, along  $[\bar{2}11]$  and making the observations along  $[01\bar{1}]$  employing the usual arrangement (Fig. 3) for determining the differential stress-optical constants. The stress-optical constant  $U$  for this ori-

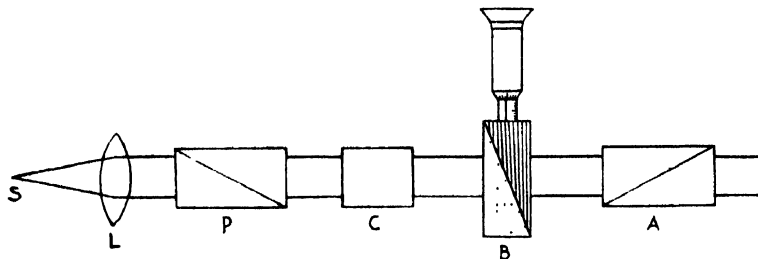


Fig. 3. Experimental set-up for determining differential stress-optical constants.

- S—Source of light
- L—Condensing lens
- P—Polarising Nicol
- C—Crystal
- B—Babinet compensator
- A—Analysing Nicol

entation of  $T_h$  ( $m_3$ ) class of crystals, to which these two substances belong, is related to the stress-optical coefficients  $q_{11}$ ,  $q_{12}$ ,  $q_{13}$  and  $q_{44}$  by (Bhagavantam, 1953) :

$$U = \frac{1}{3} \sqrt{\frac{1}{4} (A + 5q_{44})^2 + 2(A - q_{44})^2} \quad \dots (7)$$

where,  $A = \frac{1}{2} (2q_{11} - q_{12} - q_{13})$ .

In the case of barium nitrate, the load required for one oscillation of the Babinet fringe is found to be 2380 grams, the mechanical advantage of the lever arrangement being 3.992. The length of the prism parallel to  $[111]$  direction, which enters the calculations, is 0.330 cm. With these values, taking  $n$  as 1.570 (Landolt and Bornstein, 1931), the stress-optical constant is evaluated, using Eq (6). The value obtained,  $10.8 \times 10^{-13} \text{ cm}^2 \text{ dyne}^{-1}$ , is found to be in agreement with 10.2, evaluated using Eq. (7), taking the values of  $A$  and  $q_{44}$  (Bhagavantam and Krishna Rao, 1953b) as 20.60 and 1.69 respectively.

For strontium nitrate, the load for one oscillation of the Babinet fringe is 3300 grams. The length of the prism parallel to  $[111]$  is 0.264 cm. The stress-optical constant, evaluated using Eq. (6), taking  $n$  as 1.567 (Landolt and Bornstein, 1931) is found to be 6.3, in close agreement with 6.27, evaluated using Eq (7),

taking  $A$  and  $q_{44}$  ((Bhagavantam and Krishna Rao, 1954) as 13.61 and 1.38 respectively.

#### REFERENCES

- Bhagavantam, S., 1942, *Proc. Ind. Acad. Sci.*, **A16**, 359.  
Bhagavantam, S., 1953, *Proc. Ind. Acad. Sci.*, **A37**, 585.  
Bhagavantam, S., and Krishna Rao, K. V., 1953a, *Proc. Ind. Acad. Sci.*, **A37**, 589.  
Bhagavantam, S., and Krishna Rao, K. V., 1953b, *Acta Cryst.*, **6**, 799.  
Bhagavantam, S., and Krishna Rao, K. V., 1954, *Curr. Sci.*, **23**, 257.  
Krishnan, R. S., 1958, *Progress in Crystal Physics*, Madras.  
Landolt, H. H. and Bornstein, R., 1931, *Physikalische Chemische Tabellen*.  
Nye, J. F., 1957, *Physical Properties of Crystals*, Oxford: Clarendon Press.  
Pockels, F., 1889, *Ann. der. Phys.*, **37**, 144.

## STUDY OF ULTRASONIC VELOCITY IN LIQUIDS

P. R. K. L. PADMINI AND B. RAMACHANDRA RAO

ULTRASONIC LABORATORY, PHYSICS DEPARTMENT, ANDHRA UNIVERSITY,  
WALTAIR*(Received January 11, 1961)*

**ABSTRACT.** Ultrasonic velocity measurements are carried out in a number of new organic liquids, low melting point organic solids in the molten state and corrosive inorganic liquids. The important constants adiabatic compressibility,  $\beta_{ad}$ ,  $\gamma$ ,  $C_v$ , Van der Waals' "b" and molecular radii are computed. A method different from that of Schaaffs was followed in computing the value of "b" for atoms and linkages and the values for some atoms and linkages are obtained. It is found that the contribution of semipolar bond to Van der Waals' "b" is negative.

## INTRODUCTION

Extensive studies of ultrasonic velocity in liquids and their interpretation in the light of molecular structure have been made by several investigators like Parthasarathy (1935, 1936, 1937), Schaaffs (1945, 1950, 1951), Baccaredda and Giacomini (1945, 1946, 1947, 1949, 1950), Lagemann (1948, 1953, 1957), Rao and others (1940, 1941). An important advance has been made when Rao (1941) has discovered  $R$  the molar sound velocity, a temperature independent constant and it is characteristic of the atoms and linkages in a molecule. Schaaffs (1957) has shown that the measurement of ultrasonic velocity enables the computation of certain thermodynamic constants such as  $\beta_{ad}$  and  $C_v$  and the molecular constants as Van der Waals' "b" and molecular radii. It has already been established by many workers that Van der Waals' "b" is an additive function of the atoms and linkages as some other physical properties like parachor "P" critical volume "V<sub>c</sub>" etc. Schaaffs (1950) has given values of  $b$  for various elementary groups and atoms with different linkages. He tested the validity of this additive law in some compounds and obtained a good agreement between the calculated and experimental values of "b" as well as ultrasonic velocity "V".

In the present investigation the authors presented the ultrasonic velocity data and the various thermodynamic constants for many new liquids. An attempt is made to compute the value of Van der Waals' "b" for atoms and various linkages by following a method different from that of Schaaffs and it is tested in many common organic liquids for which the ultrasonic velocity data are available.

## RESULTS

The ultrasonic velocity data along with the various constants calculated for the liquids studied are presented in Table I. The ultrasonic velocities for the

TABLE I

Compound	Temp °C	Velocity m/s V	$\beta_{ad}$ X 10 cm <sup>2</sup> / dyne	Ratio of speci- fic heat	$C_p$	$r \times 10^8$ cm	$r$ from
Diethylamine	23.5	1103	118.00	1.149	1.8870	2.142	2.133 (27.5°C)
Isopropylamine	20.0	1089	123.50	—	—	1.994	1.998 (27.5°C)
Dimethyl sulphate	31.0	1223	50.74	—	—	2.075	2.018 (27.0°C)
Diethyl sulphate	31.2	1199	59.17	—	—	2.310	2.320
Sulphur chloride	26.0	1173	43.57	2.187	0.4211	1.956	2.272 (20.8°C)
Thionyl chloride	30.6	1023	58.86	2.197	0.4610	1.894	2.061 (10.0°C)
Sulphuryl chloride	30.6	925	70.50	1.877	0.5194	1.961	2.041 (20.0°C)
Triethyl phosphate	30.6	1226	62.59	—	—	2.513	2.811 (27.5°C)
Triphenyl phosphate	58.0	1385	43.33	—	—	2.961	3.239 (55.0°C)
Azoxy benzene	29.9	1532	36.43	—	—	2.530	2.922 (27.5°C)
Azo benzene	67.7	1355	52.29	1.299	1.0620	2.538	—
Vinyl acetate	25.7	1122	85.88	—	—	1.783	1.809 (27.0°C)
Methyl methacrylate	29.7	1179	76.58	—	—	2.140	2.186
Ethyl methacrylate	25.0	1180	78.57	—	—	2.258	2.309
Naphthalene	89.6	1183	73.07	1.317	0.3045	2.294	2.403 (99.0°C)
Diphenyl	74.8	1361	54.69	—	—	2.466	2.746 (78.0°C)
Phenyl salicylate	69.8	1336	48.34	1.232	1.3280	2.592	2.885 (48.0°C)
Maleic anhydride	86.2	1433	35.91	—	—	1.893	—
Phenol	64.6	1396	49.49	1.237	1.8920	2.354	2.220 (45.0°C)
<i>p</i> -dichloro benzene	67.7	1118	64.83	1.487	0.8390	2.227	2.437 (56.0°C)
Antimony trichloride	100.0	88.8	38.59	—	—	1.997	—
Sodium acetate	90.0	1701	27.10	—	—	—	—

**TABLE II**  
Temperature 20°C

Compound	Formula	Experi- men- tal value of "b"	Computed value of "b"
Nonane	$C_9H_{20}$	164.60	161.70
Ethyl alcohol	$C_2H_5OH$	52.46	52.08
Propyl alcohol	$C_3H_7OH$	64.62	67.51
Pentachloro ethane	$C_2H_5Cl_5$	127.20	122.00
Tetrachloro ethane	$C_2H_2Cl_4$	99.65	106.20
Carbon tetrachloride	$CCl_4$	90.63	90.79
Amyl bromide	$C_5H_{11}Br$	116.10	108.20
Bromoform	$CHBr_3$	83.03	84.08
Tetrabromo ethane	$C_2H_2Br_4$	111.90	118.50
Propyl iodide	$C_3H_7I$	91.52	88.77
Ethyl iodide	$C_2H_5I$	75.08	73.34
Chloro benzene	$C_6H_5Cl$	96.23	95.67
Orthochloro toluene	$C_6H_5CH_2Cl$	122.80	111.10
Toluene	$C_6H_5CH_3$	100.30	95.38

**Table III**

Values of Van der Waals' 'b' for some atoms and linkages

$$C = 3.23$$

$$H = 6.11$$

$$N = 16.14$$

$$Cl = 21.89 \quad (\cdot\cdot) \text{ in } (C=O) = 12.55$$

$$Br = 24.95 \quad (=) \text{ i } (C=C) = 24.05$$

$$I = 36.38 \quad (=) = 8.11$$

$$S = 17.50 \quad \text{Benzene ring} = 23.90$$

$$P = 15.95$$

$$Sb = 12.71$$

$$O = 9.02$$



TABLE IV  
Temperature 20° C

Compound	Velocity (m/sec) V	Density (gm/cc)	Experi- mental value of " $\mu$ "	Computed value of " $\mu$ "
* Diethylamine	1150	0.7071	96.16	96.16
Isopropylamine	1089	0.6836	79.69	81.73
* Dimethyl sulphate	1255	1.333	89.82	89.82
Diethyl sulphate	1244	1.188	123.30	121.38
* Sulphur chloride	1198	1.622	78.79	78.79
Thionyl chloride	1148	1.839	60.94	65.59
Sulphuryl chloride	940	1.673	75.48	75.91
Ethyl phosphate	1219	1.074	152.40	158.90
Triphenyl phosphate	1510	1.236	184.90	269.30
Azo benzene	1494	1.083	161.70	203.90
Azoxy benzene	1558	1.180	161.90	208.90
Vinyl acetate.	1152	0.9315	96.36	104.16
Methyl methacrylate	1220	0.949	99.19	119.59
Ethyl methacrylate	1201.5	0.919	117.00	134.80
Naphthalene.	1392	1.030	118.50	132.80
Diphenyl	1534	1.035	149.00	147.60
Phenyl salicylate	1489	1.196	172.50	190.40
Phenol	1528	1.079	82.77	88.90
<i>p</i> -dichloro benzene	1252	1.292	108.10	110.50
* Antimony trichloride.	1128	2.780	78.38	78.38
* Phosphorus trichloride	995	1.580	81.62	81.62

\*These liquids have been taken for standardization.

organic liquids and the low melting point organic solids are measured by the fixed path variable frequency interferometer. The corrosive liquids are studied with a special type of all glass cell using pulse techniques. The glass cell is made by fusing two parallel ground glass plates to the two ends of a cylindrical tube. The length of the cell is about 4.5 cms. The crystals are attached to the two sides of the cell. The liquids used are of E. Merck samples. The densities are determined by a specific gravity bottle. The physical constants, specific heat and thermal expansion required in computing the constants  $C_V$ ,  $\gamma$  are taken from

International Critical Tables. As the measurements reported in Table I are made at different temperatures, the ultrasonic velocities in all the different substances are reduced to the same temperature of 20°C to facilitate comparison by using the known temperature variation data obtained by the authors. The results thus obtained are presented in Table IV along with Van der Waals' "b" and density.

It may be noticed that there are some low melting point solids in which the ultrasonic velocity is measured in the liquid state at temperature above the melting point. The values of ultrasonic velocity given for these substances extrapolated to 20°C represent hypothetical values which these substances would have had if they exist in liquid state at 20°C.

#### DISCUSSION

The velocity data represented in Table IV follows well the rules proposed by Parthasarathy (1935, 1936, 1937) and Schaaffs (1948). After a detailed study of the ultrasonic velocity data available in the liquid state the authors also arrived at the general conclusion that in the homologous or progressive series of organic molecules the ultrasonic velocity varies in the same sense as the density, i.e., increasing with increase in density or decreasing with decrease in density progressively for higher members. The compressibility variation is exactly opposite. Exceptions to this rule are found in the series involving either a halogen atom or a lighter group (COOH, CH<sub>3</sub>, etc).

Examining the velocity data in the light of the rules proposed by Parthasarathy (1937), Schaaffs (1950) and by the authors it is seen that the velocity is higher and the compressibility is lower in diethylamine than that in isopropylamine which has less chain length. Ultrasonic velocities in the monomers, methyl methacrylate and ethyl methacrylate also show a decrease for the higher member along with a decrease in density and this feature is also similar and in agreement with the general rule. The compounds ethyl sulphate and methyl sulphate also follow the same rule, though the acid radical is inorganic.

The interesting result which the authors obtained from a study of the sulphur compounds, SOCl<sub>2</sub>, SO<sub>2</sub>Cl<sub>2</sub> is that the presence of a semipolar double bond reduces the ultrasonic velocity. This is confirmed when we remember the fact that the contribution of semipolar double bond to molar sound velocity is negative. The high velocities of malic anhydride and phenol may be attributed to the presence of hydroxyl groups which enhance the velocity according to Parthasarathy (1937). Comparison of measurements for the two phosphates involves an aliphatic and an aromatic compound. The triphenyl phosphate has a high molecular weight and higher density than triethyl phosphate. Besides it has the contribution of three benzene rings whose presence always increases the velocity; on both these considerations the ultrasonic velocity in triphenyl phosphate is higher than that in triethyl phosphate. A study of the structures of the two compounds azobenzene

and azoxybenzene reveals that the azoxybenzene contains one additional oxygen atom besides a semipolar bond. It is known that the effect of addition of an atom or an increase of molecular weight is generally to increase the velocity while the semipolar bond has the effect of decreasing the velocity. As the ultrasonic velocity increases for the latter accompanied by an increase of density it appears that the increase of velocity due to addition of oxygen atom is greater than the negative effect of the semipolar bond. Again the parallel increase of density and velocity and the decrease of compressibility for the higher member is in accordance with the general rule of velocity variation with density given by the author.

Comparing the velocities of naphthalene, diphenyl and phenyl salicylate, the diphenyl is a longer molecule with high molecular weight and density than naphthalene and this again leads to further increase in velocity and decrease in compressibility. Phenyl salicylate shows a departure from this behaviour and it has not been possible to explain this variation.

Phenol and paradichlorobenzene are substitution compounds of benzene and it will be appropriate to compare the velocities of the three substances at 20°C. The velocity of phenol is greater than that in benzene due to the presence of the hydroxyl group and the velocity of *p*-dichlorobenzene is less than that in benzene due to the presence of two chlorine atoms.

It is well known that the ratio of specific heats generally lies between 1 and 1.5 for all the organic liquids. In the present investigation the range of the values computed for some liquids which lie between 1.237 and 1.482 is the agreement with the general range of variation expected for organic liquids. In the case of the few inorganic liquids, the  $\gamma$  values are quite high being greater than 1.8. The  $C_p$  and  $\gamma$  values for some of the liquids investigated are obtained for the first time and are reported in Table I. Schaaffs (1951) has shown that Van der Waals' "b", and the molecular radii  $r$  of any molecule can be calculated from the relations,

$$b = \frac{M}{\rho} \left[ 1 - \frac{RT}{MV^2} \left\{ \sqrt{1 - \frac{MV^2}{3RT}} - 1 \right\} \right]$$

$$r = 3\sqrt{\frac{3b}{16\pi N}}$$

where  $M$  = Molecular weight

$\rho$  = density

$T$  = Temperature in degrees absolute

$V$  = Velocity of sound

$R$  = Gas constant

$b$  -- Van der Waals'  $b$

$N$  -- Avogadro number

$r$  can also be calculated from the refractive index measurements by using the relation.

$$r = 3\sqrt{\frac{3}{4\pi N} \frac{\mu^2 - 1}{\mu^2 + 2} \frac{M}{\rho}}$$

where  $\mu$  -- refractive index

The  $r$  values calculated by both these methods for most of the liquids investigated are presented in Table I. It will be seen that these values obtained by both these methods are in good agreement with each other. Although there are significant deviations in the case of the inorganic compounds like sulphur chloride, thionyl chloride and triphenyl phosphate, and also in azoxy benzene this discrepancy may be attributed partly to structural influences and partly to the impurity of chemicals.

From a study of the ultrasonic velocities in homologous series of organic liquids at 20°C Schaaffs has deduced the  $b$  values for some of the common elements having certain common linkages as for instance,  $-\text{H}->\text{C}< >\text{C}=\text{O}=(\text{O})$ , etc. He has also calculated  $b$  values for certain organic groups which commonly occur in organic liquids. He has given different values for these groups depending on whether they are linked to aliphatic series or aromatic series. As  $b$  is found to be additive in nature, Schaaffs (1948) has calculated the  $b$  values for several organic liquids using the data for groups and atoms thus obtained, and compared these with the values calculated from ultrasonic velocities and found them to be in good agreement.

The authors have attempted an investigation on similar lines following however, a different procedure for the computation of Van der Waals'  $b$ . While Schaaffs has considered " $b$ " values for atoms and atomic groups, the authors have considered the contribution as due to atoms and linkages like double, triple, and semipolar double bonds. The values thus obtained for various atoms linkages and ring structures using the data available in literature for some common organic liquids are given in the Table III. To check up the accuracy in the estimation of  $b$  values obtained for atoms and linkages, the  $b$  values for some other organic liquids are calculated from the ultrasonic velocity data and are compared with the computed values. This data is presented in Table III. Considering the fact that " $b$ " is constitutive in nature to a certain extent and that the value of  $b$  for the same atom linked with different atoms has generally slightly different values, the agreement may be taken as quite satisfactory. Such of those differences which are significant may be attributed to the constitutive influences.

Using the " $b$ " values for atoms, the  $b$  value for semipolar double bond is deduced from the calculated  $b$  value from ultrasonic velocities of the five liquids,

ethyl phosphate, methyl and ethyl sulphate, thionyl and sulphuryl chlorides, leaving the two liquids azoxy benzene and triphenyl phosphate. The interesting result was that the contribution of Van der Waals'  $b$  to semipolar linkage is negative and small. The negative value for  $b$  indicates that there is effectively a contraction in the volume of the molecule. This result is analogous to the negative value of parachor reported by Sugden (1930) and of molar sound velocity obtained by us. Since the structural formulae of azoxy benzene and triphenyl phosphate are quite large involving benzene ring and double bonds, the values of  $b$  estimated for them are not accurate. Perhaps that may be the reason why the contribution for semipolar bond in the two liquids turned up as positive.

Comparing the experimental values of  $b$  with the computed ones for the liquids investigated here, the agreement may be considered as gratifying for most of the liquids except naphthalene, phenyl salicylate, triphenyl phosphate, azo and azoxy benzenes. The large deviations observed in these liquids are due to constitutive effects which sometimes alter the values of the individual atomic contributions widely.

Since Schaaffs (1950) has attributed " $b$ " values for groups instead of linkages it has limited application in computing the  $b$  value for a new liquid. According to his method the values for a large number of groups are to be known in order to compute the value of  $b$  for any new liquid, since there are so many possible combinations of atoms with various linkages, occurring normally in all the organic liquids. The author's method has wide application in the computation of " $b$ " values for liquids but some times the computed values show large deviations from the experimental results due to constitutive influences.

#### REFERENCES

- Baccaredda, M. and Gaicemini, A., 1945, *Ricerca Scientifica*, **15**, 161.  
Baccaredda, M. and Gaicemini, A., 1946, *Ricerca Scientifica*, **16**, 611, 662.  
Baccaredda, M. and Gaicemini, A., 1947, *Ricerca Scientifica*, **17**, 1108.  
Baccaredda, M. and Gaicemini, A., 1949, *Ricerca Scientifica*, **19**, 358.  
Baccaredda, M. and Gaicemini, A., 1950 *Ricerca Scientifica*, **20**, 133.  
Lagemann, R. T., 1948, *J. Chem. Phys.*, **16**, 247.  
Lagemann, R. T., 1953, *J. Chem. Phys.*, **21**, 819.  
Lagemann, R. T., 1948, *J. Am. Chem. Soc.*, **70**, 2994, 2996.  
Lagemann, R. T., 1957, *J. Am. Chem. Soc.*, **79**, 3213, 5891.  
Lagemann, R. T. and Dunbar, W. S., 1949, *J. Phys. Chem.*, **49**, 428.  
Parthasarathy, S., 1935, *Proc. Ind. Acad. Sci.*, **2**, 497.  
Parthasarathy, S., 1936, *Proc. Ind. Acad. Sci.*, **3**, 285, 518.  
Parthasarathy, S., 1937, *Proc. Ind. Acad. Sci.*, **4**, 59, 213.  
Rao, M. R., 1940, *Ind. J. Phys.*, **14**, 109.  
Rao, M. R., 1941, *J. Chem. Phys.*, **9**, 682.  
Schaaffs, W., 1948, *Zeits. Natur. for sch.*, **13A**, 396.  
Schaaffs, W., 1950, *Zeits. Phys. Chem.*, **195**, 136.  
Schaaffs, W., 1951, *Zeits. Phys. Chem.*, **196**, 397, 413.  
Sugden, S., 1930, *Parachor and Valency*.

# GAS PROPERTIES AT HIGH TEMPERATURES ON THE EXPONENTIAL MODEL

P. K. CHAKRABORTI

INDIAN ASSOCIATION FOR THE CULTIVATION OF SCIENCE, JADAVPUR, CALCUTTA-32

(Received March 15, 1961)

**ABSTRACT.** High temperature viscosity data have been utilised to obtain the potential parameters for the exponential model for He, A, N<sub>2</sub>, O<sub>2</sub> and CO<sub>2</sub>. These parameters can reproduce the experimental viscosity data at high temperatures more satisfactorily than the parameters determined from scattering experiments. The combination rules proposed for the exponential model have been tested in relation to the high temperature inter-diffusion coefficient and the results so obtained are discussed.

## I N T R O D U C T I O N

The knowledge of the gas properties at high temperatures is of great importance particularly in connection with high speed gas dynamics, combustion, detonation etc. In the experimental determination of the required gas properties at very high temperatures, many difficulties are to be surmounted and even then the results are liable to large errors. Further, the graphical extrapolation of the low temperature data is likely to give unsatisfactory results at high temperatures. More satisfactory values for the transport coefficients can, however, be obtained by calculating the intermolecular potential from high temperature properties and utilising the equations of the kinetic theory to calculate the required transport property.

At high temperatures small intermolecular separations are predominant (Hirschfelder *et al.*, 1954). Above the Boyle point the attractive part of the intermolecular potential becomes less important than the repulsive part. Hence in the consideration of the high temperature gas properties we may neglect the attractive part of the potential and assume only the repulsive part (Cottrell, 1956). At low and intermediate temperatures the intermolecular potential is believed to be represented reasonably well by the various molecular models (e.g. Lennard-Jones 12 : 6, exp-6, etc.), but their applicability to gases at high temperatures is open to question (1958a, 1958b).

Amdur and his co-workers (1954-57) have tried to fit their molecular scattering data to a potential of the form

$$\phi(r) = \frac{A}{r^8} \quad \dots \quad (1)$$

where  $A$  and  $s$  are constants and  $r$  is the intermolecular separation. Subsequently Amdur and Mason (1958a) have calculated a large number of gas properties at high temperatures from the low and intermediate temperature data and have suggested that a potential of the form

$$\phi(r) = A e^{-\frac{r}{\rho}} \quad \dots (2)$$

may be able to reproduce the experimental data over a wide range of temperatures than the inverse power model. They have obtained the constants  $A$  and  $\rho$  for several substances from the scattering experiments, but could not test the accuracy of the values by comparison with experimental transport property data, as the collision integrals on the exp-model were not available. Quite recently Monchick (1959) has evaluated the various collision integrals on the exp-model; therefore evaluation of the potential parameters from transport data is also possible. Walker and Westenberg (1960) have utilised these collision integrals to determine the unlike potential parameters from their experimental diffusion data for the gas pairs  $\text{CO}_2\text{--O}_2$ ,  $\text{CH}_4\text{--O}_2$ ,  $\text{H}_2\text{O--O}_2$  and  $\text{CO--O}_2$  and obtained some interesting results. In the present paper we have determined the potential parameters for the exponential model from the data on high temperature viscosity of pure components. These have been compared with the values available from other sources.

#### CALCULATION OF POTENTIAL PARAMETERS FROM HIGH TEMPERATURE VISCOSITY

Large amount of experimental data in the temperature range where Eq. (2) is applicable exists for viscosity (1930, 1945, 1958, 1959). It was, however, found that the constants  $A$  and  $\rho$  given by Amdur and Mason (1958) fail to reproduce these data satisfactorily. Hence it was felt desirable to obtain the constants  $A$  and  $\rho$  on the exponential model directly from the viscosity data at high temperatures. These constants are likely to reproduce the transport properties better than those determined from the scattering data. The viscosity data for He, Ar,  $\text{N}_2$ ,  $\text{O}_2$  and  $\text{CO}_2$  in the temperature range 800°K–1500°K were utilised for this purpose.

On the Chapman-Enskog theory the viscosity coefficient  $\eta$  is given to the first approximation as (Hirschfelder *et al.*, 1954).

$$[\eta]_1 \times 10^7 = 266.93 \sqrt{T} \times M / \sigma^2 \Omega^{(2,2)*} \text{ g/cm-sec.} \quad \dots (3)$$

where  $T$  is the absolute temperature,  $M$  the molecular weight of the substance  $\Omega^{(2,2)*}$  are the collision integrals,  $\sigma$  is some arbitrary length parameter which is defined by  $\phi(r)$  and is given by (Monchick, 1959).

$$\sigma^2 \Omega^{(l,s)*} = 8\pi^2 I_{(l,s)}(\alpha) / (s+1)! [1 - \frac{1}{2}\{1 + (-1)^l\} / (1+l)] \quad \dots (4)$$

where  $l, s$  are integral numbers,  $I(\alpha)_{(l,s)}$  are in the form of integrals depending upon  $\alpha$ , and  $\alpha$  is related to  $A$  in Eq. (2) by (Monchick, 1959).

$$\alpha = \ln(A/kT) \quad \dots \quad (5)$$

Values of the integrals  $I(\alpha)_{(l,s)}$  are tabulated (Monchick, 1959) as function of  $\alpha$ .

Comparing Eq. (3) and (4) we get ( $l = s = 2$ , for  $\eta$ )

$$11 \times 10^7 = 133.46 \sqrt{T.M/\alpha^2 \rho^2 I(\alpha)_{(2,2)}} \quad (6)$$

In Eq. (6)  $\rho$  is temperature independent and  $\alpha^2 I(\alpha)_{(2,2)}$  is temperature dependent. Let  $\eta_1$  and  $\eta_2$  be the viscosities at temperatures  $T_1$  and  $T_2$  respectively. Then

$$[\eta_2/\eta_1] = (T_2/T_1)^2 (\alpha_1/\alpha_2)^2 [I(\alpha)_{(2,2)}]_2 / [I(\alpha)_{(2,2)}]_1 \quad (7)$$

where  $[I(\alpha)_{(2,2)}]_1$  and  $[I(\alpha)_{(2,2)}]_2$  represent the collision integrals corresponding to  $\alpha_1$  and  $\alpha_2$  respectively. Hence by knowing the quantities  $\eta_1$  and  $\eta_2$  experimentally, values of  $A$  can be so adjusted that the right hand side of Eq. (7) becomes equal to  $[\eta_2/\eta_1]_{\text{expt}}$ . For a particular substance different experimental values of the ratio  $[\eta_2/\eta_1]$  were taken and  $A$  values were found in each case. The geometric mean of the  $A$  values so obtained was taken as the true values of the constants for the substance. Once  $A$  is obtained the value of  $\rho$  can be found from Eq. (6). The arithmetic mean of all  $\rho$  values thus obtained was taken as the true value for the substance. The values of the constants thus obtained are given in Table I. For the sake of comparison the values of the constants obtained by Amdur and Mason (1958) from scattering experiments are also given in the Table I.

TABLE I

Values of the constants  $A$  and  $\rho$  on the exp-model

Substance	From Viscosity			From Scattering		
	$A \times 10^8$ ergs.	$\rho$ in Å	Range of rigid sphere diameter $r_0$ in Å	$A \times 10^8$ ergs.	$\rho$ in Å	Range of rigid sphere diameter $r_0$ in Å
H <sub>2</sub>	0.0615	0.225	1.946–1.984	0.0618	0.220	1.3–2.3
A	5.125	0.244	3.106–3.214	5.174	0.224	2.2–3.4
N <sub>2</sub>	1.053	0.295	3.292–3.383	2.163	2.063	2.4–3.6
O <sub>2</sub>	1.086	0.275	3.082–3.222	--	—	
CO <sub>2</sub>	1.149	0.328	3.654–3.843	--	--	

The potential parameters determined from viscosity and scattering data are not quite consistent.



TABLE II

Substance	T°K	$\eta \times 10^7$ g cm.sec. expt.	$\eta \times 10^7$ g/cm. sec. calculated with force constants from	
			Viscosity	Scattering
He	800	3840 <sup>T</sup>	3873	4042
	850	4000 <sup>a</sup>	4049	4226
	900	4154 <sup>a</sup>	4222	4407
	950	4304 <sup>a</sup>	4394	4584
	1000	4455 <sup>T</sup>	4587	4764
A	800	4621 <sup>r</sup>	4677	5412
	900	4960 <sup>a</sup>	4961	5870
	1000	5302 <sup>r</sup>	5282	6263
	1100	5636 <sup>a</sup>	5626	6649
	1200	5947 <sup>r</sup>	5948	7044
	1300	6256 <sup>a</sup>	6272	7437
	1400	6532 <sup>a</sup>	6601	7802
	1500	6778 <sup>r</sup>	6900	8196
N <sub>2</sub>	800	3493 <sup>r</sup>	3379	3764
	972.5	3916 <sup>r</sup>	3856	4287
	1000	4011 <sup>c</sup>	3929	4367
	1020.7	4017 <sup>c</sup>	3986	4430
	1068.8	4119 <sup>c</sup>	4108	4563
	1120.2	4216 <sup>c</sup>	4240	4710
	1166	4374 <sup>c</sup>	4359	4838
	1220.5	4461 <sup>c</sup>	4499	4984
	1273.2	4582 <sup>r</sup>	4629	5134
	1500	5050 <sup>c</sup>	5174	5728
O <sub>2</sub>	800	4115 <sup>a</sup>	4131	
	1000	4720 <sup>a</sup>	4806	
	1130	5230 <sup>c</sup>	5240	
	1166	5382 <sup>c</sup>	5342	
	1203	5480 <sup>c</sup>	5459	
	1278	5677 <sup>c</sup>	5685	
	1292	5715 <sup>c</sup>	5728	
CO <sub>2</sub>	800	3391 <sup>r</sup>	3375	
	900	3676 <sup>a</sup>	3657	
	1000	3935 <sup>r</sup>	3925	
	1100	4200 <sup>a</sup>	4188	
	1200	4453 <sup>r</sup>	4442	
	1300	4688 <sup>a</sup>	4736	
	1400	4912 <sup>a</sup>	4933	
	1500	5139 <sup>r</sup>	5169	

<sup>T</sup> Trautz, M. and Zink, R. (1930).<sup>r</sup> Vasilescu, V. (1945).<sup>c</sup> Raw, C. J. G. and Ellis, C. P. (1958).<sup>e</sup> Raw, C. J. G. and Ellis, C. P., (1959).<sup>a</sup> Values obtained from the interpolation of available high temperature viscosity data.

## COMPARISON WITH EXPERIMENT

(a) *Viscosity*

An obvious test of the success of any molecular model is its ability to reproduce various experimental data with the same set of constants. In Table II, the experimental and the calculated values of the viscosity coefficients of He, A, O<sub>2</sub>, N<sub>2</sub> and CO<sub>2</sub> at high temperatures are given. The calculated values on the exp-model from the force-constants obtained by Amdur and Mason (1958) from scattering data are also given. It can be seen from Table II that the experimental viscosity data are reproduced much better on the exponential model with the force constants determined in the present work than with those determined from scattering data. This is due to the fact that the rigid sphere diameter range of validity of the two sets of parameters are different. Parameters from scattering data are expected to be more appropriate at still higher temperatures.

(b) *Inter-diffusion coefficient*

The binary diffusion coefficient may be written to the first approximation as (Hirschfelder *et al.*, 1954)

$$[D_{12}]_1 = 0.002628 \sqrt{T^3(M_1 + M_2)/2M_1M_2/p\sigma_{12}^2\Omega_{12}^{(1,1)}} \quad (8)$$

where  $p$  is the pressure in atmospheres,  $M_1$  and  $M_2$  are the molecular weights of the species 1 and 2 respectively. Using the values of  $\sigma_{12}^2\Omega_{12}^{(1,1)*}$  as determined with the help of Eq. (4), the expression (8) for the diffusion coefficient on the exp-model becomes,

$$[D_{12}]_1 = 0.002628 \sqrt{T^3(M_1 + M_2)/2M_1M_2/4p\alpha_{12}^2\rho_{12}^2I_{(1,1)}(\alpha_{12})} \quad (9)$$

The constants  $A_{12}$  and  $\rho_{12}$  for the pair 1-2 may be approximated by the use of the combination rules given by Amdur and Mason (1958)

$$1/\rho_{12} = 1/2(1/\rho_1 + 1/\rho_2) \quad (10)$$

$$A_{12} = (A_1 \times A_2)^{1/2} \quad (11)$$

and  $\alpha_{12}$  is defined as before

$$\alpha_{12} = \ln(A_{12}/kT) \quad (12)$$

The values of the integrals  $I_{(1,1)}(\alpha_{12})$  as functions of  $\alpha_{12}$  have been tabulated by Monchick (1959).

Recently Walker and Westenberg (1958, 1959 and 1960) have measured the inter-diffusion coefficients at high temperatures for a number of gas pairs by the "point source technique." By using the combination rules, Eqs. (10) and (11), the inter-diffusion coefficients for the systems He-A, He-N<sub>2</sub>, CO<sub>2</sub>-N<sub>2</sub> and CO<sub>2</sub>-O<sub>2</sub> have been calculated by us with the force constants determined from viscosity.

The results of these calculations together with the experimental values are given in Table III. Examination of the results in Table III shows that the agreement between the calculated and the experimental values of the diffusion coefficients is very poor for systems involving  $\text{CO}_2$ . This discrepancy in the case of  $\text{CO}_2$  can be attributed to the fact that the  $\text{CO}_2$  molecule is a much poorer approximation to spherical elastic particle than the other simple molecules and the simple combining rules valid for central force fields are not as appropriate. This has also been observed by Walker and Westenberg. Further, Mason *et al.* (1960) have pointed out that the effect of excitation or charge exchange will be important in case of high temperature diffusion and thermal diffusion in particular. Besides, multiplicity of the different interaction energy curves governing collisions should also be taken into account.

TABLE III

Calculated and experimental values of binary diffusion coefficients for system He-A, He- $\text{N}_2$ ,  $\text{CO}_2$ - $\text{N}_2$  and  $\text{CO}_2$ - $\text{O}_2$

System	T°K	$D_{12}$ cm <sup>2</sup> /sec. expt.	$D_{12}$ cm <sup>2</sup> /sec. cal- culated with force constants from viscosity
He-A	700	3.500	3.062
	800	4.355	3.852
	900	5.338	4.692
	1000	6.1905	6.067
	1100	7.207	7.131
He- $\text{N}_2$	700	3.000	3.074
	800	3.828	3.864
	900	4.686	4.747
	1000	5.614	5.676
	1100	6.572	6.674
$\text{CO}_2$ - $\text{N}_2$	700	0.8095	0.6232
	800	1.022	0.7794
	900	1.251	0.9506
	1000	1.486	1.134
	1100	1.724	1.345
	1200	1.937	1.544
$\text{CO}_2$ - $\text{O}_2$	700	0.7696	0.6469
	800	0.9759	0.8102
	900	1.197	0.9872
	1000	1.440	1.180
	1100	1.679	1.387

The small amount of discrepancy observed in the calculated and the experimental values of the diffusion coefficients for He-A at the lower temperature can be explained by assuming that the diffusion corresponds to more penetrating collisions than other transport properties at the same temperature (Hirschfelder and Eliason, 1957) and therefore the parameters from scattering data are expected to give better agreement.

## ACKNOWLEDGMENTS

The author wishes to express his thanks to Prof. B. N. Srivastava, D.Sc., F.N.I., for his valuable guidance. Thanks are also due to Dr. A. K. Barua for suggesting the problem and valuable discussions throughout the progress of the work.

## REFERENCES

- Amdur, I. and Ross, J., 1958, *Combustion and Flame*, **2**, 412.  
Amdur, I. and Harkness, A. L., 1954, *J. Chem. Phys.*, **22**, 664.  
Amdur, I. and Mason, E. A., 1954, *J. Chem. Phys.*, **23**, 415.  
Amdur, I. and Mason, E. A., 1954, *J. Chem. Phys.*, **22**, 670.  
Amdur, I. and Mason, E. A., 1955, *J. Chem. Phys.*, **23**, 2268.  
Amdur, I. and Mason, E. A., 1956, *J. Chem. Phys.*, **25**, 624.  
Amdur, I., Mason, E. A. and Jordhan, 1957, *J. Chem. Phys.*, **27**, 527.  
Amdur, I. and Mason, E. A., 1958, *Phys. Fluids*, **1**, 370.  
Cottrell, T. L., 1956, *Disc. Faraday. Soc.*, **22**, 10.  
Hirschfelder, Curtiss and Bird, 1954, *Molecular Theory of Gases Liquids*, (John Wiley & Sons, Inc., N.Y.)  
Hirschfelder, J. O. and Eliason, E. A., 1957, *Ann. N.Y. Acad. Sci.*, **67**, 451.  
Monchick, L., 1959, *Phys. Fluids*, **2**, 695.  
Mason, E. A., Vanderslice, J. T. and Yos, J. M., 1960, *Phys. Fluids*, **2**, 686.  
Raw, C. J. G. and Ellis, C. P., 1958, *J. Chem. Phys.*, **28**, 1198.  
Raw, C. J. G. and Ellis, C. P., 1959, *J. Chem. Phys.*, **30**, 574.  
Trautz, M. and Zink, R., 1930, *Ann. Physik*, **7**, 427.  
Vasilescu, V., 1945, *Ann. Physique*, **20**, 292.  
Walker, R. E. and Westenberg, A. A., 1958, *Chem. Phys.*, **29**, 1147.  
Walker, R. E. and Westenberg, A. A., 1959, *J. Chem. Phys.*, **31**, 519.  
Walker, R. E. and Westenberg, A. A., 1960, *J. Chem. Phys.*, **32**, 436.

# AN INTERNAL COUNTER CONTROLLED LOW PRESSURE CLOUD CHAMBER

M. RAMA RAO

SAHA INSTITUTE OF NUCLEAR PHYSICS, CALCUTTA

(Received February 15, 1961)

**ABSTRACT.** A low pressure internal counter controlled cloud chamber operating at a pressure of 8 cm of Hg is described. The details of the electronic circuitry for running the chamber automatically are also presented.

## I. INTRODUCTION

During the early stages of work with cloud chambers, the instrument has been operated in a random fashion. In the study of rare events as in cosmic rays and other infrequent nuclear processes, the chances that an ionizing event passes through the chamber right at the instant a random expansion is initiated being very uncertain, one has to take a prohibitively large number of photographs to get any useful information, for most of the photographs will go blank. A random mode of operation, therefore, suffers from the drawback that an investigation undertaken along such lines is very uneconomical from the point of view of the large film consumed and the long time involved. Such a situation was answered for the first time by Blackett and Occhialini (1933) who, while conducting experiments on cosmic rays, evolved a new technique in which the release mechanism of the expansion cloud chamber is actuated only in the event of an ionizing particle traversing through the chamber. The technique is well known. An array of Geiger counters is placed external to the cloud chamber at the top and bottom and when the charged particle under consideration traverses through all the three constituents of the assembly, the electronic counter circuits give rise to a triggering pulse within a few microseconds of the travel of the chamber by the desired ionizing particle which releases the expansion mechanism and puts a series of other electronic controls into operation thus making it possible to have the tracks automatically photographed. The vast improvement in efficiency achieved by working the cloud chamber in conjunction with Geiger counters has made this arrangement a standard practice with all present day cloud chambers which are known as counter controlled cloud chamber".

But in the investigations of low energy particles produced within the chamber, the control arrangement with the aid of external counters would be of little avail, since the particles with their short ranges are absorbed within the walls of the

chamber itself, thereby preventing the particles from reaching the counters placed outside. Under such circumstances, it would, therefore, be an appropriate choice to place the counter inside the chamber itself. Bridge *et al.* (1948) and Leighton *et al.* (1949) have tried to work with thin-walled ion chambers and Geiger counters in the sensitive volume of the chamber. But even with the conventional counters placed inside the cloud chamber, the particle could still get absorbed by the cathode of the counter which normally is a hollow thin copper cylinder sealed within a glass envelope. This difficulty was overcome by Hodson and Loria (1950) who first succeeded in controlling a cloud chamber by using an "open counter" in which the cathode consisted of a cylindrical arrangement of thin rods or wires, instead of the usual metal tube. Thus by using wire electrodes which defined the cathode configuration of the counter inside the chamber, it was possible to make the counter volume a part of the sensitive region of the chamber and there was no material except the filling gas itself to retard the motion of the low energy particles. They operated the cloud chamber and consequently the counter at a pressure of 1.5 atmospheres and the filling mixture used was argon saturated with ethyl alcohol vapour.

In the present work, the technique of internal counter controlled operation has been extended to very low pressures. This paper includes details of the electronic sequence circuitry for running the cloud chamber automatically, together with some preliminary results testing the working of the instrument.

## II. EXPERIMENTAL ARRANGEMENT

When an ionizing event takes place within the cloud chamber, the gas inside is ionized and the electron component of the ionized gas is collected by the central wire of the proportional counter operated within the chamber at a positive high potential. The electronic counter circuits thus give rise to a triggering voltage pulse and this pulse is used to set off a sequence of events so as to make a photographic record of the tracks of the charged particles automatically.

Fig. 1 presents the block diagram of the electronic timing circuit for the expansion chamber. The events take the following sequence :

1. The counter pulses are passed through a preamplifier and then suitably amplified by means of a high gain amplifier.
2. The pulses are admitted into a discriminator circuit where pulses due to the desired events can be discriminated.
3. The discriminated pulse is employed to run a high voltage quenching circuit which removes the high voltage on the counter before the positive ions along the path of the incident particle have had time to move any appreciable distance and the track is therefore visible and undistorted even within the sensitive volume of the counter.

4. The same pulse after discrimination is utilised to open the expansion valve which goes to complete the expansion of the cloud chamber.

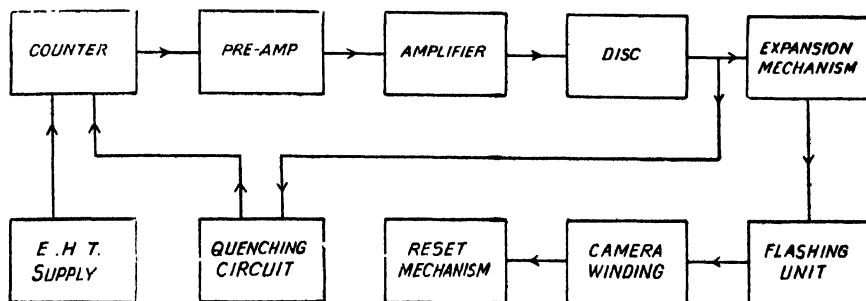


Fig. 1. Block diagram for automatic operation of the cloud chamber.

5. The flashing units are fired after a suitable delay to illuminate the tracks of droplets formed and the camera catches the photograph of the event.
6. The camera automatically winds up providing fresh film for a subsequent event.
7. The pressure in the back chamber, thereby expansion ratio, in the meantime, is automatically adjusted and the chamber kept ready for another expansion.

### III. CONSTRUCTIONAL DETAILS OF THE COUNTER

The counter is mounted across the middle of the cloud chamber, the details of which have been published elsewhere (Rama Rao, 1961). The counter is 20 cms in length and 3.0 cms in diameter. The cathode assembly of the counter is defined by four rods 1 mm in diameter supported at the ends by copper rings. The anode is a 3 mil tungsten wire stretched axially with respect to the cylinder defined by the cathode assembly. The cathode supporting rings are fitted with perspex discs. To one end of the anode wire a glass bead is fused and held against a small hole at the centre of the perspex disc. The other end of the wire is taken through the centre of the perspex disc facing the previous one and is fused into a brass screw and the wire is kept straight by applying suitable tension and tightening the nut against the perspex disc. Proper care is taken to prevent any twisting of the wire while fixing up. A connecting lead is soldered to the screw and brought out through a narrow drill hole in the wall of the perspex chamber. The chamber is made leak tight at this point by applying transparent glyptal. The whole counter assembly is mounted on two rigid supports made of copper that take the form of brackets bent in the form of a right angle and screwed on firmly to the metallic flange of the chamber. Thus the cathode of the counter is kept at the ground potential by grounding the

metallic casing of the cloud chamber. The details of mounting the counter within the chamber are shown in Figs. 2 and 2a.

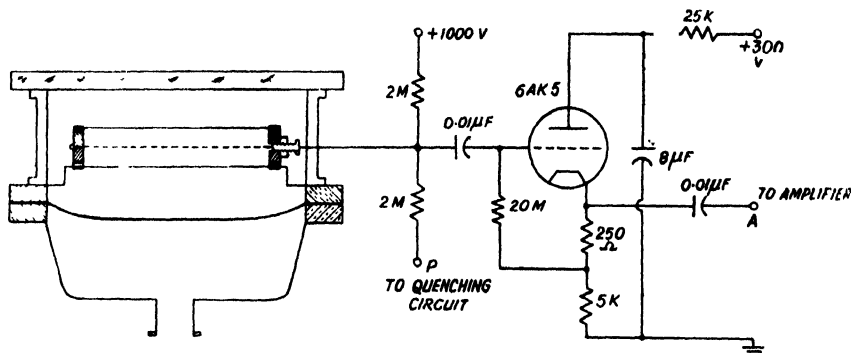


Fig. 2. Counter mounting within the chamber and cathode follower pre-amplifier.

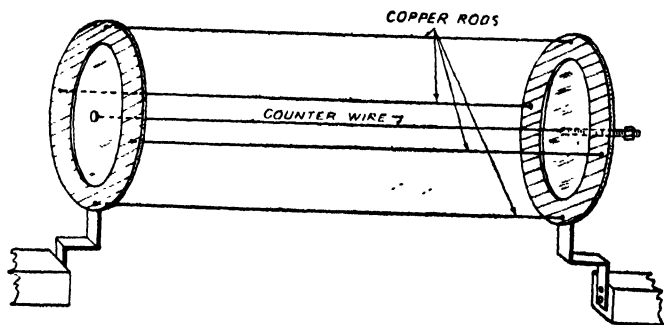


Fig. 2a. Perspective view of the counter.

#### IV. CHOICE OF GAS-VAPOUR FILLING

In the present set-up, the proportional counter which is incorporated within the cloud chamber is not isolated from the chamber volume by glass envelope whatsoever, but forms a part of the sensitive region of the chamber itself. Such being the case, the choice of the gas-vapour mixture filling the chamber comes up as a major consideration. The same gas-vapour composition must play the dual role of a satisfactory cloud chamber filling mixture for obtaining good tracks and at the same time a satisfactory filling for operating the counter in the proportional region.

When an ionizing particle moves through the gas of the counter, it gives rise to a number of electrons and an equal number of positive ions along its track. The electrons created by the primary ionizing particle can be drawn towards the anode which is maintained at a positive potential. If the attractive voltage acting on the electrons is suitably adjusted, the electrons can be drawn into the near vicinity of the wire and there they enter a region in which the field strength



rapidly increases in magnitude. Thus in traversing through a short distance, the electrons originally produced along the track now acquire between collisions with atoms and molecules sufficient kinetic energy to result in further multiplication of ions due to secondaries which remain proportional to the initial ionization as long as the counter is operated in the proportional region. It can thus be seen that such gas multiplication is possible only when the electrons remain freely mobile and the gas-vapour composition does not exhibit appreciable electron affinity. For this reason, oxygen and water vapour both of which have great affinity for electron attachment had to be excluded from the chamber filling. A filling of commercial argon (99.8% purity, oxygen-free) and isoamyl alcohol has been found to be a satisfactory mixture for operating the chamber in the region of 5 cms of Hg. Detailed investigations on the choice of gas-vapour composition had been undertaken and the results were communicated in an earlier paper (Rama Rao, 1961). The same composition is now found to go well with the counter operating in the proportional region.

#### V. INTERNAL COUNTER OPERATION FOR EXPANDING THE CLOUD CHAMBER

The anode of the counter is operated at a positive high potential while the cathode rods are earthed. When an ionizing particle passes through the cloud chamber and therefore the counter, the gas inside is ionized leaving positive ions and electrons. Since pure argon has been used as the permanent gas in the cloud chamber, there is very little tendency for the electrons to attach themselves to the gas molecules to form negative ions. Thus all the electrons are now accelerated towards the central anode wire of the counter and get collected there. The negative pulse collected by the wire is amplified by a high gain linear amplifier and is utilised in bringing about the expansion of the cloud chamber.

The collection of electrons by the counter is completed within an interval of a few microseconds. It is known that the mobility of electrons is much higher than that of the heavier ions. This leads to the advantage that if the voltage pulse due to the electron collection triggers the expansion of the cloud chamber, the slow positive ions, which have not had time to diffuse to any appreciable extent, would act as condensation nuclei for the vapour and enable to obtain a photograph of the tracks that are responsible for triggering the chamber.

The present counter with its dimensions mentioned earlier has a suitable proportional region over the range 850-1000 volts when operated at pressures of 8 cms of Hg. With this set of operating conditions it has been found possible to reproduce the pulse sizes in the counter over a period of 2 to 3 days. Thereafter, the pulse size diminished steadily owing to change in the composition of the gas-vapour mixture as a result of slow diffusion of air into the chamber through the rubber gaskets and also due to release of oxygen and moisture from the walls



put pulses of approximately 80 volts amplitude are taken from the plate of the second tube of the discriminator and are used to drive the voltage quenching circuit and the sequence circuit.

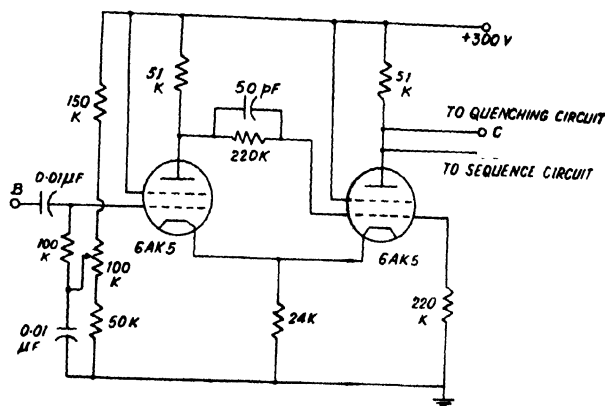


Fig. 4. Discriminator circuit.

#### b) High voltage quenching circuit

It is necessary to remove the high voltage on the proportional counter as soon after the collection of the electron component of the ionization event as possible so that the positive ions have had little time to disperse in the gas medium under the action of the strong electric field in the vicinity of the counter, which other-wise would result in broadening and distortion of the tracks. A portion of the track is also lost in the sensitive volume of the counter. The lowering of voltage on the counter much below the operating point is achieved by using a quenching circuit in the voltage supply of the proportional counter.

The operation of the voltage quenching circuit is explained with reference to Fig. 5 and Fig. 2. The discriminator pulse is taken to point C of the voltage

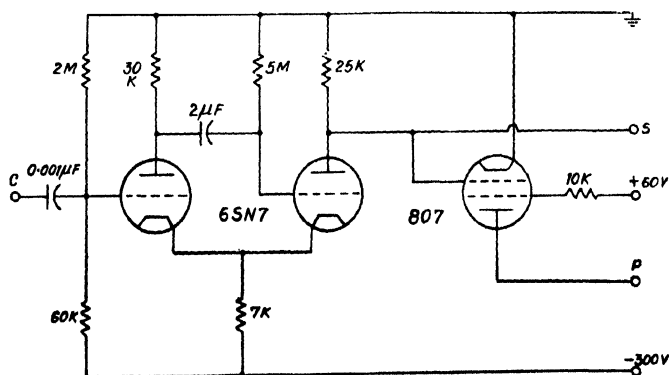


Fig. 5. High voltage quenching circuit

quenching circuit which is composed of a cathode coupled multivibrator circuit and a 'voltage quenching tube'. Type 6SN7 tube is used for the multivibrator part of the circuit and type 807 is the quenching tube. The plate point of 807 is tied to the anode of the counter through a  $2M\Omega$  resistor. The plate point of the conducting half of 6SN7 is connected to the grid of 807 tube so that the grid of 807 is maintained at a high negative potential with respect to the cathode and the tube does not draw any current. Therefore, at the start the full voltage applied on the counter also resides on the plate of 807. Now when the multivibrator circuit is triggered by the incoming pulse, the conducting section of 6SN7 tube becomes non-conducting and the grid of 807 is raised to zero potential. The 807 tube now conducts and there is a voltage drop across the plate load of 807 which is experienced by the counter anode. The voltage on the counter is thus lowered from a positive high voltage to a few volts in a very short interval of time and the voltage on the counter remains lowered until the multivibrator recovers to its normal state, determined by the CR value of the circuit which is of the order of a few seconds. By suitably adjusting this delay, the voltage on the counter has been kept lowered until the cloud chamber expansion is completed and photographs of tracks have been obtained.

(c) *Sequence control circuit*

The sequence circuit (Fig. 6) includes the chamber expansion device and other auxiliary time sequence control circuits for the flashing of lamps, winding the camera, and resetting the chamber after every cycle of operation.

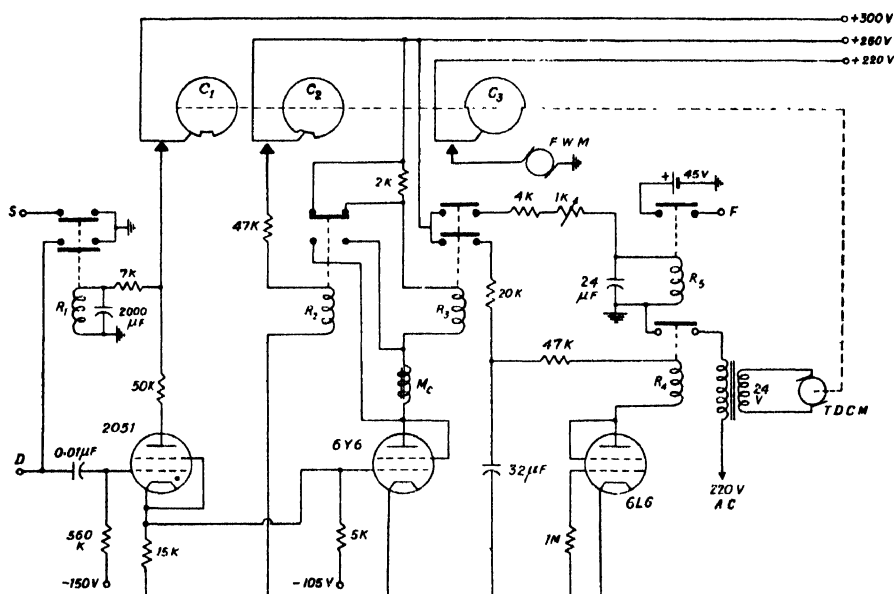


Fig. 6. Timing sequence circuit.

The magnet coil  $M_c$  of the high vacuum magnetic valve which brings about the expansion of the chamber is included in the plate circuit of 6Y6 tube. The magnet is of the type that normally remains closed under gravity. The grid bias on 6Y6 tube is initially maintained sufficiently negative such that the tube does not conduct and hence the magnet is not energized. The grid of 6Y6 tube is tied to the cathode point of the thyatron tube 2051. When the voltage pulse from the discriminator is fed to the grid of 2051, the tube fires and the voltage developed across the cathode resistor of 2051 raises the grid potential of 6Y6 to zero volt and makes 6Y6 conducting. The plate draws current and the magnet coil is energized, thus opening the magnet valve so as to expand the chamber.

$R_3$  is a relay operating in series with the magnet coil. Normally the relay is in the off-position and is energized along with the magnet coil of the main expansion magnet. With the help of relay  $R_3$ , two circuits are operated with suitable delays introduced in their paths. The circuit operated from one set of contact points is intended for running flashing units and the one from the other set drives a time delay cam motor (T.D.C.M.).

The action of T.D.C.M. can be understood as follows : When the relay  $R_3$  is energized, H.T. is supplied to the plate of 6L6 thus making it conducting. The relay  $R_4$  which is in the plate circuit is now energized and the primary circuit of the transformer which is connected across the contact points of this relay is completed. A 24 volt motor is operated from the secondary of the transformer and the speed of the motor is cut down by suitable reduction gear system. Cams  $C_1, C_2, C_3$  are mounted axially on the shaft of the motor. The cams are made of small circular perspex discs. Shallow slots of varying widths are cut on the periphery of these discs. Three contact switches are mounted on an insulated base plate close to the discs such that the switches sweep out the periphery of the perspex discs as the motor shaft carrying these discs begins to rotate. When one of the prongs of the switches falls into the slot, the contact breaks and the corresponding circuit operated by this particular switch is disconnected. Thus the elevated portions on the three cams determine the time scale for which a particular circuit is held in operation. A magnified picture of the time delay cams is presented in Fig. 7.

When once the thyatron is fired and the sequence circuit is put into operation, the cam begins to rotate until the switch on cam  $C_1$  interrupts the plate voltage of the thyatron tube. The time for a complete revolution is set at 3 minutes and this gives the operation cycle of the cloud chamber. It can thus be seen that the magnet coil of the expansion magnet also remains energized for the whole time the thyatron is in the conducting state. But we wish to return the magnet valve to its normal condition as soon after photography of the ionizing event as possible so as to isolate the back chamber from the vacuum ballast and raise the pressure in the back chamber to the present value by admitting air through an

auxiliary air admittance valve, details of which have been described in an earlier paper (Rama Rao, 1961). The magnet valve is returned to its normal position

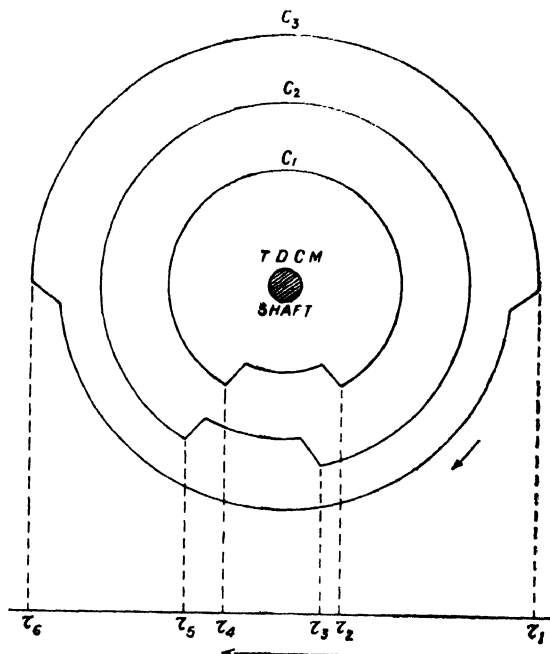


Fig. 7. Magnified diagram of the time delay cams.

by short circuiting the magnet coil. This is done with the help of relay  $R_2$  which operates through the contact switch mounted on Cam  $C_2$ . The slot on cam  $C_2$  is slightly displaced with respect to the one on cam  $C_1$  so that as the cam rotates the switch on cam  $C_2$  comes into operation a little while after the expansion is complete. As soon as the relay  $R_2$  is pulled down, the magnet coil is short circuited thus shutting the valve and a  $2K$  resistance appears in series with the relay coil  $R_3$  keeping the total plate load of 6Y6 unaltered. The magnet coil is thus short circuited for the complete cycle, as long as the contact switch on  $C_2$  is closed which is released only after the contact switch on  $C_1$  is opened.

#### d) *Flashing circuit*

The tracks of ionizing particles are photographed under strong illumination which lasts momentarily. The illumination is provided by two Mazda flashing lamps F.A.2 with a rating of 2500 VDC and 500 joules dissipation. The circuit for operating these tubes is showing in Fig. 8.

Along with the expansion of the magnet, the relay  $R_3$  is energized and through one set of contact points of the relay  $R_3$  voltage is applied to the relay  $R_5$  which is energized after a delay determined by the CR value in the circuit. Closing of the relay contacts gives rise to a positive pulse from a battery of 45 volts which is

fed to the point F to trigger a cathode coupled multivibrator (Fig. 8). The negative rectangular pulse taken from the plate of the first half of 6SN7 tube is dif-

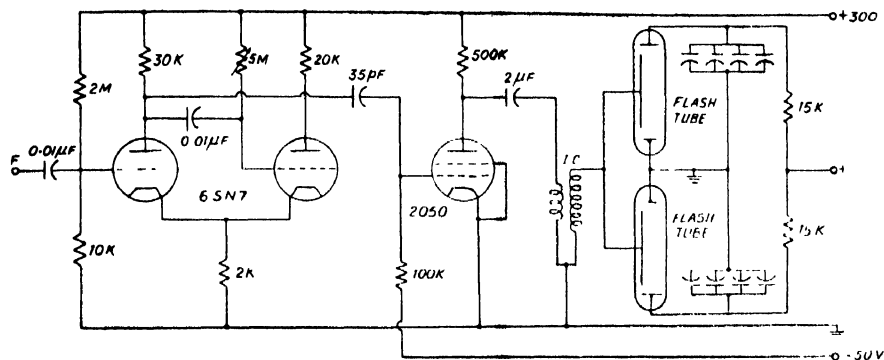


Fig. 8. Flashing unit.

ferentiated by the 35pf and 100KΩ net work. The positive spike of the differentiated pulse is utilized to fire the thyatron tube 2050. The triggering action of 2050 can be delayed with respect to the input pulse at F by 5 MΩ potentiometer. When the switching action of the thyatron takes place, a 2μf condenser which is previously charged to 300V is now discharged producing a current surge in the primary of the Ignition coil (I.C.). The high voltage pulse developed across the secondary which is of the order of several KV is applied to the trigger electrode of the flash tubes. Two banks of condensers, each 64μf, connected across the flash lamps and charged to 1500 volts D.C., get discharged through the tubes owing to the breakdown of the gap between the electrodes as a result of the sudden rise in the electric field and thus an intense burst of light is obtained.

### e) *Photography and film winding*

The camera for taking stereoscopic pictures is mounted vertically above the cloud chamber. The camera is of the open shutter type and hence the cloud chamber had to be operated in a dark room.

After the event has been photographed, the film is wound up and set ready for the next photograph. This is done by a slow motion motor (F.W.M.) which is kept in motion by the operation of the contact switch on cam C<sub>3</sub>. The time for which the motor is running to wind up the exposed portion of the film is determined by the length of the slot on the cam C<sub>3</sub>.

### f) *Reset mechanism*

When once the thyatron of the sequence circuit is fired and the sequence circuit put into operation, the grid loses its control on the performance of 2051 tube and the tube remains conducting and consequently the associated circuits on, until the switch on cam C<sub>1</sub> interrupts the plate voltage on 2051. As the cam

rotates after a complete cycle of operations of the sequence when the slotted portion faces the switch on  $C_1$ , the voltage on 2051 is removed, rendering it non-conducting and thus the rest of the circuit is thrown out of action. The circuit has to be set ready for a subsequent operation by restoring the voltage on the plate of 2051. This is achieved as follows :

As soon as the switch contact on cam  $C_1$  is broken, 2051 is extinguished and hence 6Y6 becomes non-conducting, de-energising the relay  $R_3$ . Though the plate supply for 6L6 tube which it gets through the relay contacts of  $R_3$  is cut off, the charge accumulated by the  $32\mu\text{f}$  condenser supplies the voltage for the relay coil  $R_5$  and holds it in the on-position and consequently the T.D.C. motor running. This continued operation of the motor for a little while after the main source of supply voltage is cut off overshoots the slotted portion of the cam  $C_1$  so that the contact of the switch on  $C_1$  is re-established and occupies the position indicated in (Fig. 6). The plate voltage on 2051 is thus restored and the tube is ready for triggering on the arrival of a fresh pulse at the grid of the tube.

g) *Spurious operation of the chamber*

It was occasionally detected in a few blank operations that at the time of establishing the switch contact on cam  $C_1$  after a complete cycle of operations, due to faulty contact, a spark at the contact point was a source of disturbance which after having been picked up and amplified is fed to the grid of 2051, thus driving the circuit and giving a fake expansion without a real pulse from the counter being fed.

This was avoided by cleaning the contacts regularly and also by ensuing smooth contacts by adjusting the gap between the contact points. Additional precaution was taken to ground the grid of 2051 during the time the switch contact was being established. This can be understood by referring to the operation of relay  $R_1$  in (Fig. 6). When the contact switch is in the slotted portion of cam  $C_1$ , the relay  $R_1$  is disengaged and the input to the grid of 2051 is grounded through a pair of contact points of relay  $R_1$ . When the contact switch on cam  $C_1$  is being pulled out of the slot and voltage on plate of 2051 restored, the relay  $R_1$  is energized but slowly owing to the high value of the capacitor,  $2000\mu\text{f}$ , thus the grounding of the input to 2051 is released only after firm contact of the  $C_1$  cam-switch is established.

For the time the grid of 2051 is grounded, the grid of 807 tube is also kept at ground potential by connecting the grid of 807 at the contact point S of relay  $R_1$ . This brings about the removal of voltage on the counter once again thereby avoiding the production of fresh ionization by discharges in the counter.

## VII. RESULTS AND DISCUSSION

A preliminary testing of the set-up has been made by initiating the expansion of the cloud chamber using  $\alpha$ -pulses picked up by the counter. Fig. 9 shows a photograph of  $\alpha$ -tracks obtained at 8 cm of Hg.



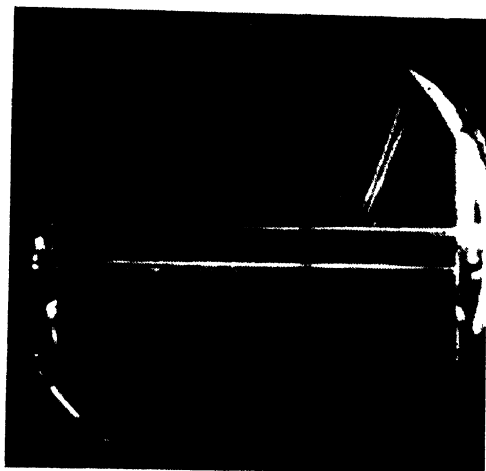


Fig. 9. Photograph of  $\alpha$ -tracks obtained at 8 cms of Hg using argon and iso amyl alcohol as filling mixture

It may be mentioned here that the quality of tracks mainly depends upon the diffusion of ions. The width of the track is a function of the speed of expansion which is defined as the time elapsed between the moment the particle passes through the counter and the achievement of the expansion of the chamber. The time taken by the magnet to open fully is the predominant factor for obtaining sharp tracks as the delays introduced in the electronic circuit being of negligible order. The magnetic valve used in the present experiment is a high speed expansion valve and a rough estimate shows that it is of the order 5 m.sec.

#### ACKNOWLEDGMENTS

The author is indebted to Prof. B. D. Nag Chaudhuri, Director of the Institute, for his constant guidance and encouragement. The author is grateful to Prof. D. N. Kundu for his keen interest and valuable discussions.

#### REFERENCES

- Blackett, P. M. S. and Occhialini, G. P. S., 1933, *Proc. Roy. Soc.*, **139**, 699.  
Bridge, H. S., Hazen, W. E., Rossi, B. and Williams, R. W., 1948, *Phys. Rev.*, **74**, 1083.  
Elmore, W. C. and Sands, M., *Electronics* (McGraw-Hill Book Company, Inc., New York, 1949), National Nuclear Energy Series, V-1.  
Hodson, A. L., Loria, A. and Ryder, N. V., 1950, *Phil. Mag.*, **41**, 826.  
Leighton, R. B., Anderson, C. D. and Sheroff, A., 1949 *Phys. Rev.*, **75**, 1432.  
Rama Rao, M., 1961, *Ind. J. Phys.*, **35**, 92.

# Letters to the Editor

*The Board of Editors will not hold itself responsible for opinions expressed in the letters published in this section. The notes containing reports of new work communicated for this section should not contain many figures and should not exceed 500 words in length. The contributions must reach the Assistant Editor not later than the 15th of the second month preceding that of the issue in which the letter is to appear. No proof will be sent to the authors.*

## 4

### THE CRYSTAL STRUCTURE OF BENZALAZINE

U. C. SINHA

PHYSICS DEPARTMENT, ALLAHABAD UNIVERSITY,  
ALLAHABAD, INDIA

(Received April 22, 1961)

In an earlier communication (Sinha, 1959), the space group of benzalazine along with other crystallographic data has already been published. However, the axial lengths were redetermined from high angle Bragg reflections in Weissenberg photographs by the method of Lipson and Farquhar (1946), after necessary correction for film-shrinkage error, etc. The revised values of the axial parameters thus obtained are

$$\left. \begin{array}{l} a_0 = 13.09 \text{ \AA} \\ b_0 = 11.76 \text{ \AA} \\ c_0 = 7.62 \text{ \AA} \end{array} \right\} \alpha = \beta = \gamma = 90^\circ,$$

the space-group being  $D^{12}_{2n}$ -Pben, containing four molecules per unit cell. This space-group containing a centre of symmetry has eight equivalent points in the unit cell. The structural formula of the molecule of benzalazine is  $\text{C}_6\text{H}_5 \cdot \text{CH} : \text{N} : \text{N} : \text{CH} \cdot \text{C}_6\text{H}_5$ . It shows that the molecule has a centre of symmetry. This indicates that the centre of the N—N bond must lie at the centre of symmetry which has been chosen to be the origin of the coordinates.

The relative intensities of the reflections  $hko$ ,  $hol$  and  $okl$  were measured by photographic method, absolute values were obtained by comparing these with the known absolute values of  $F_{hkl}$  of aluminium and hence the structure factors were obtained.

The intensity of (002) diffuse reflection suggested that the orientation of the benzene ring of the molecule would be near about (001) plane. In addition, by a consideration of the high intensity ( $hko$ ) reflections of higher indices using the method adopted by Robertson and White (1945) for coronane, the approximate co-ordinates ( $x, y$ ) were obtained after giving a few trials. Using these trial coordinates, the phases of the structure factors were calculated for computing the electron density projection  $\rho(x, y, 0)$  along  $[001]$  with the observed values of the structure factors  $F(hko)$ . The preliminary structure thus obtained was refined by three successive  $[001]$  axis Fourier projections to give the more and more accurate values of  $x$  and  $y$  co-ordinates. Trial  $z$ -coordinates were worked out from the standard bond lengths of the molecule in order to calculate the phases of ( $hol$ ) reflections. The  $z$ -coordinates were finally determined from the second electron density projection  $\rho(x, 0, z)$  obtained with the observed values of  $F(hol)$ . The co-ordinates of the benzalazine molecule are given in Table I.

TABLE I

Atoms	X in Å	Y in Å	Z in Å
N	0.69 <sub>1</sub>	0.12 <sub>7</sub>	1.07
C <sub>1</sub>	1.23 <sub>9</sub>	1.00 <sub>3</sub>	-0.32 <sub>6</sub>
C <sub>2</sub>	2.68 <sub>3</sub>	1.26 <sub>4</sub>	0.16 <sub>5</sub>
C <sub>3</sub>	3.27 <sub>2</sub>	2.40 <sub>6</sub>	-0.66
C <sub>4</sub>	4.60 <sub>3</sub>	2.66 <sub>5</sub>	0.50 <sub>8</sub>
C <sub>5</sub>	5.40	1.76 <sub>1</sub>	1.04 <sub>6</sub>
C <sub>6</sub>	4.84 <sub>3</sub>	0.62 <sub>7</sub>	1.063 <sub>5</sub>
C <sub>7</sub>	3.49 <sub>5</sub>	0.36 <sub>5</sub>	-1.04 <sub>9</sub>

The reliability index factor

$$R = \frac{\sum (|F_o| - |F_c|)}{\sum |F_o|}$$

came out to be 0.20 for  $F(hko)$  reflections and 0.24 for  $F(hol)$  reflections. In the calculation of the structure factors, the atomic scattering factors for carbon and nitrogen (McWeeny, 1951) have been used after imposing an isotropic B-factor of  $3.00 \times 10^{-16}$ .

The structure of benzalazine is being further refined by the method of difference synthesis and other standard methods and the detailed results will be published in near future.

The author wishes to express his gratitude to Prof. K. Banerjee, Director, Indian Association for the Cultivation of Science, Jadavpur, Calcutta, for his kind interest throughout the progress of this work and to Dr. S. C. Chakravarty for his valuable advice and help and to the Government of India, Ministry of Education, for financial assistance.

## R E F E R E N C E S

- Lipson, H and Farquhar, M. C. M., 1946, *Proc. Phys. Soc.*, **58**, 200.  
McWeeny, R., 1951, *Acta Cryst.*, **4**, 513.  
Robertson, J. M. and White, J. C., 1945, *J. Chem. Soc.*, p.607.  
Sinha, U. C., 1959, *Bull Nat. Inst. Sci. India*, No. **14**, 107.

# WING OF THE RAYLEIGH LINE RECORDED WITH A SELF-RECORDING GRATING SPECTROPHOTOMETER

S. C. SIRKAR, S. B. ROY AND D. K. GHOSH

OPTICS DEPARTMENT,

INDIAN ASSOCIATION FOR THE CULTIVATION OF SCIENCE, CALCUTTA-32

(Received March 29, 1961)

**ABSTRACT.** A self-recording spectrophotometer has been constructed using a Bausch and Lomb plane grating with Ebert mounting, a thirteen-dynode photomultiplier, a D.C. amplifier and a Honeywell-Brown pen recorder. The resolution is found to be much higher than that given by the commercial recording spectrophotometers in which prisms are used as the dispersing system.

The wing of the Rayleigh line due to benzene at different temperatures and that due to liquid oxygen have been studied with this instrument. Benzene at 5°C shows two broad maxima in the wing which disappear when the liquid is heated to 75°C. Liquid oxygen shows a feeble wing with inflections about 38, 49 and 60  $\text{cm}^{-1}$  away from the Rayleigh line. These results have been discussed.

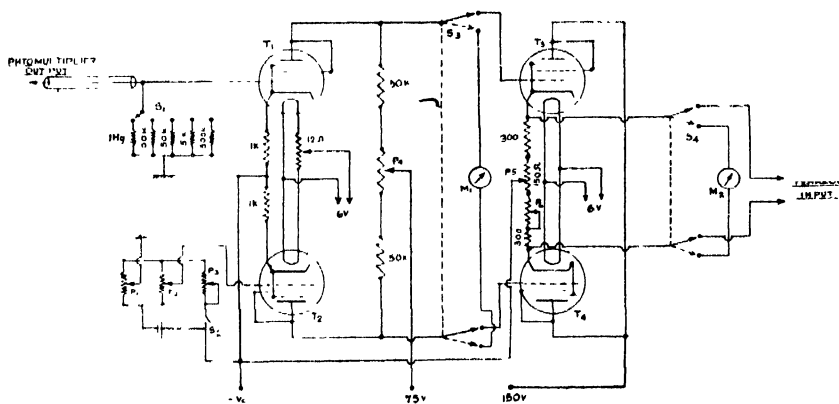
## INTRODUCTION

The use of plane grating with Ebert mounting (Ebert, 1889) as the dispersing system in a recording monochromator was discussed recently by Fastie (1952) who constructed such a monochromator with a resolving power of about 91000 in the first order. Besides the high resolving power the monochromator has also high light gathering power. In this respect such a monochromator is better than most of the commercial recording spectrophotometers in which prisms are used as the dispersing system. A recording spectrophotometer with high resolving power has another advantage which is not possessed by spectrographs having high resolving power. For studying the relative intensity of a weak satellite or a feeble wing close to an intense line the photographic method is quite unsuitable, because the exposure necessary to record the weak satellite makes the stronger line overexposed and scattering in the grains of the emulsion makes the width of the line much larger than its actual width produced by the dispersing system. Therefore, the photographic method is unsuitable for the study of distribution of intensity in the wing of the Rayleigh line. As the true distribution of intensity in the wing might throw some light on the structure of the liquid a programme was undertaken to study it with the help of a self-recording grating spectrophotometer and an attempt was made to construct a spectrophotometer similar to the monochromator constructed by Fastie (1952). The performance of such a spectrophotometer constructed in the laboratory and also some preliminary

## DESCRIPTION OF THE SPECTROPHOTOMETER

A 6256 photomultiplier tube supplied by E.M.I. Research Laboratories of England is used as the detector. The tube is mounted coaxially in a horizontal brass cylinder surrounded by a spiral of copper tubing through which alcohol cooled by liquid oxygen can be circulated to cool the photomultiplier tube. The window of the brass cylinder is provided with an annular electric heater to prevent condensation of moisture on the window of the photomultiplier tube. The maximum voltage applied to each dynode is about 155 V. A voltage stabiliser purchased from Hungary and capable of supplying 3000 volts is used to supply the voltages to the dynodes. The electron current from the anode can flow

### DC AMPLIFIER CIRCUIT DIAGRAM



through any one of the resistances of values 10K, 40K, 100K and 1 Megohm depending on the sensitivity required.

The output voltage of the photomultiplier tube is amplified by a D.C. amplifier designed on the principles of the circuit used by Chien and Bender (1947). The circuit had, however, to be modified in order to make it suitable for use with a Honeywell and Brown pen recorder. It was found initially that when the potential-drop across a high resistance was used to drive the pen recorder the pen became sluggish during its return sweep, broadening thereby the base of the peak due to any spectral line. So, the output of the balanced-bridge D.C. amplifier was fed to two cathode followers in balanced condition to reduce the effective resistance. The circuit diagram is given in Fig. 1. A photograph of the whole assembly is reproduced in Fig. 2.

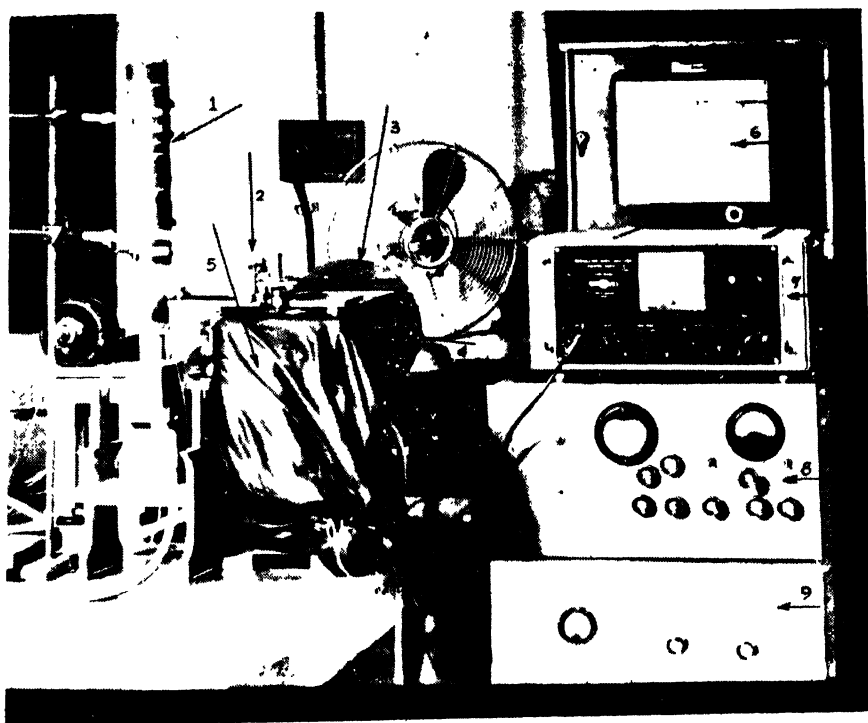


Fig. 2. Photograph of the recording spectrophotometer 1—Unsilvered Dewar flask of Pyrex glass, 2—gear system for turning the grating, 3—Schlieren concave mirror, 4—All-metal body of the spectrograph, 5—Photomultiplier mount covered with black cloth, 6—Pen recorder, 7—High voltage stabilizer, 8—D. C. amplifier, 9—Stabilizer for D. C. amplifier.

#### EXPERIMENTAL

In order to study the wing of the Rayleigh line due to benzene a horizontal Raman tube of diameter about 25 mm provided with a jacket was used. Ice-cold water was first circulated through the jacket and the temperature of the

liquid was thereby brought down to 5°C. After recording the wing accompanying the Rayleigh line 4047Å of Hg, the liquid was heated to 75°C by circulating hot water through the jacket and the wing in the same region was again recorded. Several records were taken for each of the temperatures to verify the genuineness of the curves.

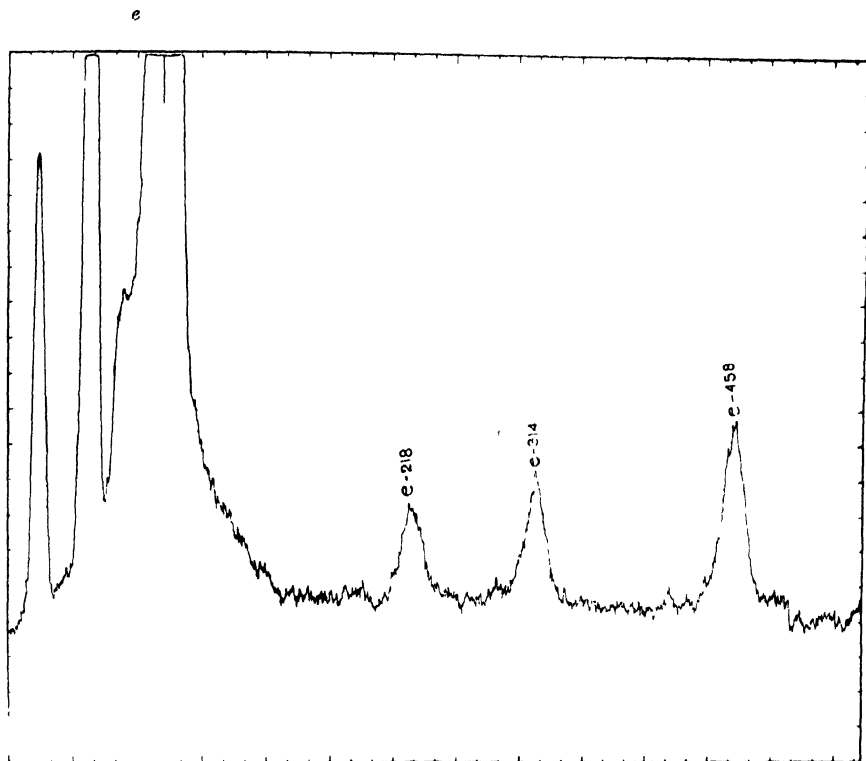
A special Dewar vessel of Pyrex glass was made for studying the wing due to liquid oxygen. Two plane parallel Pyrex discs were fused parallel to each other in a horizontal position in the two walls at the bottom of the Dewar vessel. A Pyrex glass tube with blackened tail and closed at the lower end was placed inside the Dewar vessel with its tapered and blackened tail at the top. The Dewar vessel was then filled up with liquid oxygen filtered with filter paper. The liquid filled the inner tube by entering into it through a hole in its wall. The scattered light coming out through the bottom of the Dewar vessel was reflected by a right-angled prism and focussed with a long-focus lens on the entrance slit of the spectrophotometer. Finally, the record of the spectrum of the mercury lines reflected by gray paper was taken to compare the width of the peaks with those due to the scattered light.

#### RESULTS AND DISCUSSION

The records of the Raman spectra due to  $\text{CCl}_4$  and  $\text{CHCl}_3$  are reproduced in Figs. 3(a) and 3(b). The spectra of light scattered by benzene at 5°C and 75°C are reproduced in Figs. 4 and 5 respectively and Fig. 6 shows the spectrum due to liquid oxygen. The record of the spectrum of incident light is also reproduced in Fig. 7 for comparison.

It is evident from Fig. 4 that the wing due to benzene at 5°C shows two broad maxima at about 44  $\text{cm}^{-1}$  and 73  $\text{cm}^{-1}$  respectively with a continuous background between them and the curve due to benzene at 75°C given in Fig. 4 shows that there is only one inflexion at about 49  $\text{cm}^{-1}$  and that the curve extends up to a shorter distance. Crystals of benzene at -10°C show three lines at 44, 60 and 100  $\text{cm}^{-1}$  respectively (Sirkar and Ray, 1950) and the frequency-shifts increase to 48, 60 and 116  $\text{cm}^{-1}$  respectively when the temperature of the crystals is lowered to -100°C. The broad maxima at 44  $\text{cm}^{-1}$  and 73  $\text{cm}^{-1}$  in the wing due to the benzene at 5°C may therefore correspond respectively to the lines 60 and 100  $\text{cm}^{-1}$  due to the crystals at -10°C, the frequency-shifts diminishing with the rise of temperature from -10°C to 5°C and with the change of state. The band corresponding to the line 48  $\text{cm}^{-1}$  of the crystal may have merged with the strong half-width of the Rayleigh line which extends up to about 38  $\text{cm}^{-1}$  from the centre of the line in this case. All these facts show that these bands are not produced by the rotation of the molecules in the liquid state but they originate most probably from vibrations in groups of molecules which are formed in the liquid at 5°C and break up when the temperature is raised to 75°C. The

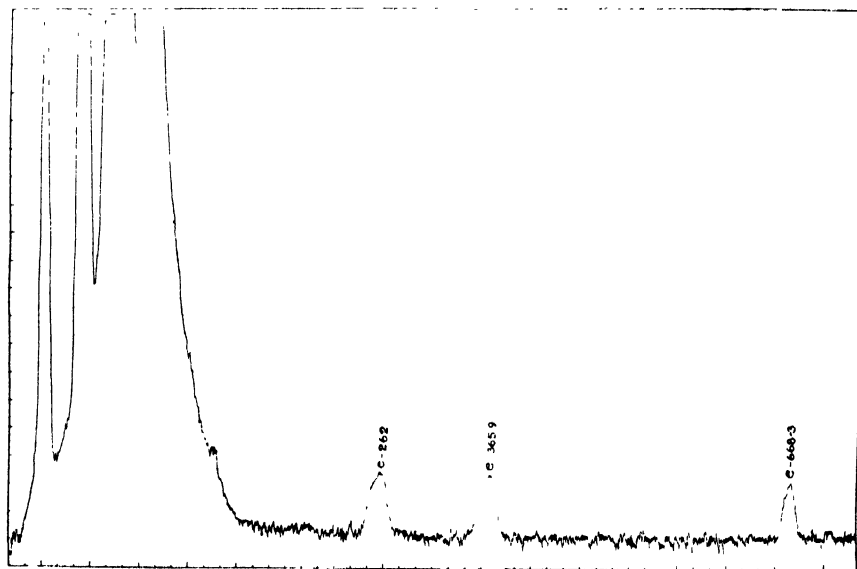


Fig. 3(a). Raman spectrum of  $\text{CCl}_4$ .

sharp lines observed in spectra of the crystals are therefore produced by such vibrations in groups of molecules, the intermolecular bond being slightly stronger in the case of the crystals. These results confirm the observations made by Kastha (1958) who studied the distribution of intensity in the wing of the Rayleigh line due to a few organic liquids at different temperatures and found evidence of formation of groups of molecules giving rise to continuous wing at temperatures a few degrees above the melting points of the substances.

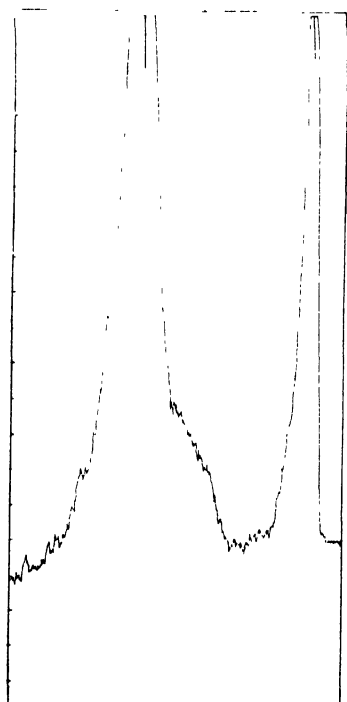
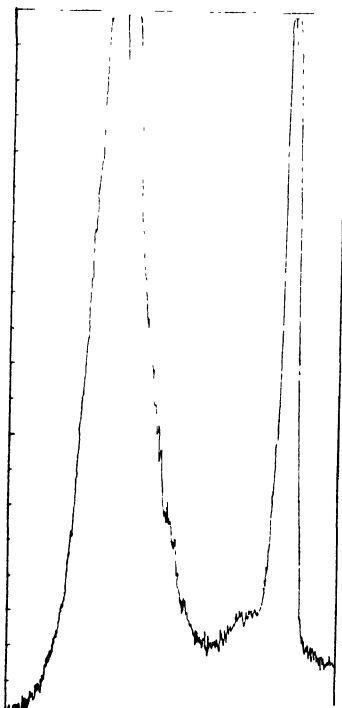
A comparison of the curve due to the 4046 Å line of Hg scattered by liquid oxygen reproduced in Fig. 6 with that due to the incident line shown in Fig. 7 indicates that the scattered line is much broader than the incident line probably due to the existence of a strong wing close to the Rayleigh line. The peak is unsymmetrical due to sluggishness of the pen during return sweep. It is further observed that on the Stokes sides of the 4046 Å line the wing extends up to about  $100\text{ cm}^{-1}$  from the centre of the Rayleigh line and there are inflexions at distances of about  $38\text{ cm}^{-1}$ ,  $49\text{ cm}^{-1}$  and  $60\text{ cm}^{-1}$ , the intensity falling off rapidly after each inflexion. It would be interesting to compare these results with those due to the gas. Unfortunately, the spectrum due to the gas at a temperature just above  $-180^\circ\text{C}$  has not been investigated by any

Hg e

Fig. 3(b). Raman spectrum of  $\text{CHCl}_3$ .

Hg k

Hg k

Fig. 4. 'Wing' due to benzene at  $5^\circ\text{C}$ .Fig. 5. 'Wing' due to benzene at  $75^\circ\text{C}$ .

previous worker. Theoretical values of the relative intensities of the rotational lines of  $O_2$  at  $-120^\circ C$  are given in Table I.

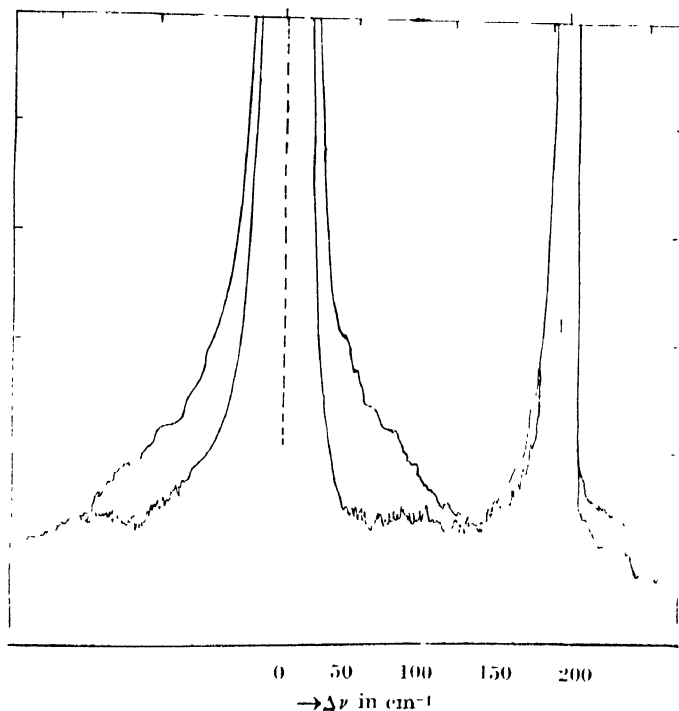


Fig. 6. Rotational wing due to liquid oxygen.

TABLE I

Initial value of $J$	$\Delta\nu$ in $cm^{-1}$	Relative intensity in arbitrary units
1	14.26	0.153
3	25.88	0.226
5	37.36	0.221
7	48.88	0.160
9	60.20	0.092
11	71.80	0.042

It can be seen from Table I that the second and third rotational Raman lines of  $O_2$  are expected to be almost of the same intensity and the strongest lines in the rotational spectrum. The fourth line at about  $49\text{ cm}^{-1}$  would be much weaker than either of these two lines and the fifth line should be less than half as intense as the second or the third line. The inflexions at  $38\text{ cm}^{-1}$ ,

49  $\text{cm}^{-1}$  and 60  $\text{cm}^{-1}$  observed in the spectrum of liquid oxygen at  $-180^\circ\text{C}$  agree closely with the rotational lines of  $\text{O}_2$  at  $180^\circ\text{C}$  both in respect of positions and relative intensities. The appearance of broad inflexions in place of sharp peaks shows that the intermolecular collision in the liquid broadens the lines.

The region from the edge of the Rayleigh line upto about 14  $\text{cm}^{-1}$  would be free from any scattered intensity theoretically, but Fig. 6 shows an intense scattering in this region extending upto about 35  $\text{cm}^{-1}$  and masking the two rotational maxima at about 14.26  $\text{cm}^{-1}$  and 25.88  $\text{cm}^{-1}$ . This broadening is not due to any difference in the intensities of the Rayleigh line and the inner incident line reproduced in Fig. 6, because the width of the line 4077 Å is the same in both the cases. It has to be concluded, therefore, that probably some of the  $\text{O}_2$  molecules form  $\text{O}_4$  molecules with loose coupling between them so that the vibration and rotation of such dimeric molecules produce a strong wing extending upto about 35  $\text{cm}^{-1}$  from the centre of the Rayleigh line.

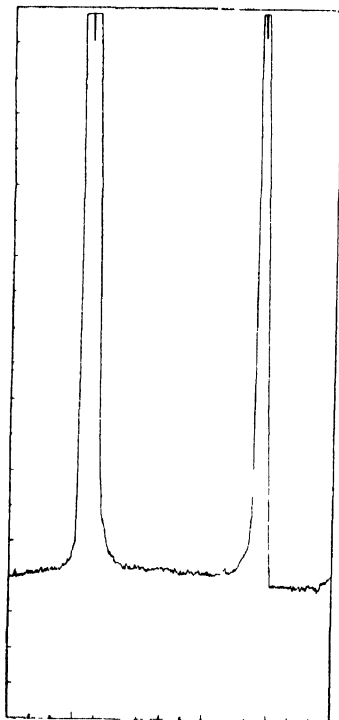


Fig. 7. Record of incident Hg lines.

The wing of the Rayleigh line due to liquid oxygen was studied previously by several workers by using prism spectrographs and photographic method. Saha (1940) first observed a continuous wing with a maximum at a distance of 50  $\text{cm}^{-1}$  from the centre of the Rayleigh line. Later, Crawford *et al.* (1952) reported that they failed to detect any maximum in the continuous wing due to

liquid oxygen. Kastha repeated the investigation in 1954 and by carefully superposing the microphotometric record of the incident mercury line  $4047\text{ \AA}$  on that of the line scattered by liquid oxygen, found a maximum at  $40\text{ cm}^{-1}$  from the Rayleigh line in the continuous wing due to liquid oxygen. The distances of the maximum found by Kastha (1954) is almost the same as that of the first inflexion observed in the present investigation, but the larger intensity upto  $35\text{ cm}^{-1}$  from the edge of the Rayleigh line could not be detected by Kastha (1954). The photographic method is thus inferior to the photoelectric method for such an investigation when in the latter case a grating with high resolving power is used, so that the wing is clearly separated from the Rayleigh line.

## ACKNOWLEDGMENT

The authors' thanks are due to Dr. A. R. Deb who rendered some help in the initial stages of the construction of the spectrophotometer and to the staff of the workshop of the Association who made some parts of the spectrophotometer and assembled the different parts to make the complete instrument.

## REFERENCES

- Chen, Jen-Yuan and Bender, Paul, 1947, *J. Chem. Phys.*, **15**, 376.  
Crawford, M. F., Welsh, H. L. and Harrold, J. H., 1952, *Canad. J. Phys.*, **30**, 81.  
Ebert, H., 1889, *Weid. Ann.*, **38**, 489.  
Fastie, W. G., 1952, *J. Opt. Soc. America*, **52**, 641.  
Kastha, G. S., 1954, *Ind. J. Phys.*, **28**, 329.  
Kastha, G. S., 1958, *Ind. J. Phys.*, **32**, 473.  
Saha, B., 1940, *Ind. J. Phys.*, **14**, 123.  
Sirkar, S. C. and Ray, A. K., 1950, *Ind. J. Phys.*, **24**, 189.  
Trumphy, B., 1933, *Z. f. Phys.*, **84**, 282.

# STRUCTURE OF THE SPECTRUM OF DOUBLY IONISED BROMINE

Y. BHUPALA RAO

OIL AND NATURAL GAS COMMISSION, DEHRA DUN

(Received November 17, 1960)

Plate VI and Plate VII (A and B)

**ABSTRACT.** The earlier analysis of the spectrum of Br III is revised and extended. A large number of levels belonging to the various configurations are newly identified, leading to the classification of more than 200 lines, which bring the total of classified lines to about 230. The doublets are correctly identified and are confirmed by the intercombinations with the quartets. The third ionisation potential of bromine given in the earlier analysis is verified to be correct.

## INTRODUCTION

The first important investigation on the spectrum of doubly ionised bromine is by Bloch and Bloch (1927) who have given a fairly extensive list of the lines of Br III in the region 6600-2200Å using a source of electrodeless discharge. Lacroute (1935) has extended the list with measurements in the vacuum ultra-violet region on a 1-metre normal incidence vacuum grating spectrograph using a source of electrodeless discharge similar to the one employed by Bloch and Bloch.

Rao and Krishna Murty (1937) are the first to make a beginning towards the correct analysis of the structure of the spectrum. They have rejected the analysis given by Deb (1930) and successfully identified the deepest and fundamental quarters of the  $4p^3$ ,  $5s$ ,  $5p$  and  $6s$  configurations and calculated the ionisation potential from the two members of the  $ns\ ^4P$  series. They have given a tentative list of some levels belonging to  $4d$  and  $5d$  configurations basing the assignments on the magnitude of the levels but without specific designation as that would be uncertain in the absence of other evidence.

They have also given a tentative identification of some of the doublets of  $4p^3$ ,  $5s$  and  $5p$  configurations, independent of the quarters. The identifications are based, as stated by them, mainly on the detection of several pairs in the region below 1000Å having the characteristic interval  $1664\text{ cm}^{-1}$  which is of the order of the predicted interval  $4p^3\ ^2P_{1/2}^0 - 4p^3\ ^2P_{1/2}^0$ . From these pairs the doublet groups  $4p^3\ ^2D^0$ ,  $^2P^0 - 5s\ ^2P$ ,  $5s'\ ^2D$  are built up although some of the combinations are absent. By extrapolation into the shorter wavelength region some of the  $5p$  doublet levels have been located. It is also remarked that some of the levels assigned to the  $4d$  and  $5d$  configurations might in fact be doublet levels. Pending

further investigation the publication of intercombinations was withheld. In a later communication Rao (1944) has reported the identification of a few intercombinations and has given the interval  $4p^3\ ^4S_{11}^0 - 4p^3\ ^2D_{11}^0$  as  $15042\text{ cm}^{-1}$ .

Moore (1952) has collected in the book "Atomic Energy Levels, Vol. II" all the energy levels given in the paper of Rao and Krishna Murty (1937) arranging them in the ascending order of magnitude with  $4p^3\ ^4S_{11}$  as zero. She has added the correction  $15042\text{ cm}^{-1}$  (Rao, 1944) to all the doublets starting with  $4p^3\ ^2D_{11}^0$  as zero.

Still there remain quite a large number of lines unclassified, and the analysis is very far from complete and needs confirmation. In pursuance of the analysis obtained of the spectrum of Br II (Bhupala Rao, 1958), a revision of the analysis of the spectrum of Br III has been undertaken. The extensive experimental work on the spectrum done in connection with Br II has served for the purpose of this analysis also. The investigation has shown that while the quartet levels are confirmed, the doublets and intercombinations given by Rao and Krishna Murty (1937) and Rao (1944 and unpublished work) need revision except the level  $4p^3\ ^2D_{21}^0$ . A large number of new levels are also identified and intercombinations are definitely established leading to the classification of more than 200 additional lines bringing the total of classified lines to about 230.

#### EXPERIMENTAL

The sources of radiation and other details about excitation and recording of the spectrum are given in the paper on Br II (Bhupala Rao, 1958).

As already mentioned in the paper on Br II (Bhupala Rao, 1958) in addition to the data obtained from the experimental work at the Andhra University by the author, a large number of photographs were also kindly made available to the author by Prof. K. R. Rao and were of very great help. These pictures extending from 1085 to 480A were taken at Upsala with a Grazing Incidence Spectrograph long ago and well preserved. The dispersion was about  $3.2\text{A/mm}$  near 950A. The sources consisted of a vacuum spark between electrodes tipped with Rb Br and Cs Br. Full details regarding the pictures are given by Rao and Badami (1931) in the paper on Se IV.

The lines of Br III are distinguished from the lines of Br II in the infra-red, visible and near ultraviolet regions by the criterion that a complete or partial suppression of the second and higher spark lines occurs when a suitable inductance is placed in the condensed discharge circuit while the intensity of the first spark lines either remains unaltered or increases. Several of the Br III lines are hazy and have large intense wings on the long wavelength side in the condensed discharge, which make their measurement difficult. The lines of Br. IV are comparatively sharp and are completely suppressed when the inductance is included in the circuit. Since some of the Br III lines also are completely suppressed on

including the inductance the behaviour of the lines in rectified discharge also is taken into consideration for distinguishing the lines of Br III from the lines of Br IV. In the rectified discharge, under suitable conditions, some of the Br IV lines appear with more intensity than in the condensed discharge. Though these criteria give fairly good results they are not entirely critical and cannot be depended upon to give absolutely correct results, because for a given ion lines from higher energy states behave in much the same way as those from next ion. In the vacuum ultraviolet region where lines from lower energy states occur, several lines of Br III appear in the inductance picture also with comparable intensity and it is difficult to distinguish them from the Br II lines. In this region a few higher stage spark lines also seem to be present in the inductance picture. An intensive examination of the entire spectrum and a line by line scrutiny has become necessary for the ultimate assignment.

All the lines of Br III classified in this investigation are given in Table II with their intensities in condensed discharge, wavelengths, wavenumbers and classifications. As in the case of Br II, in this paper also the wavelengths below 2000Å are values in vacuum.

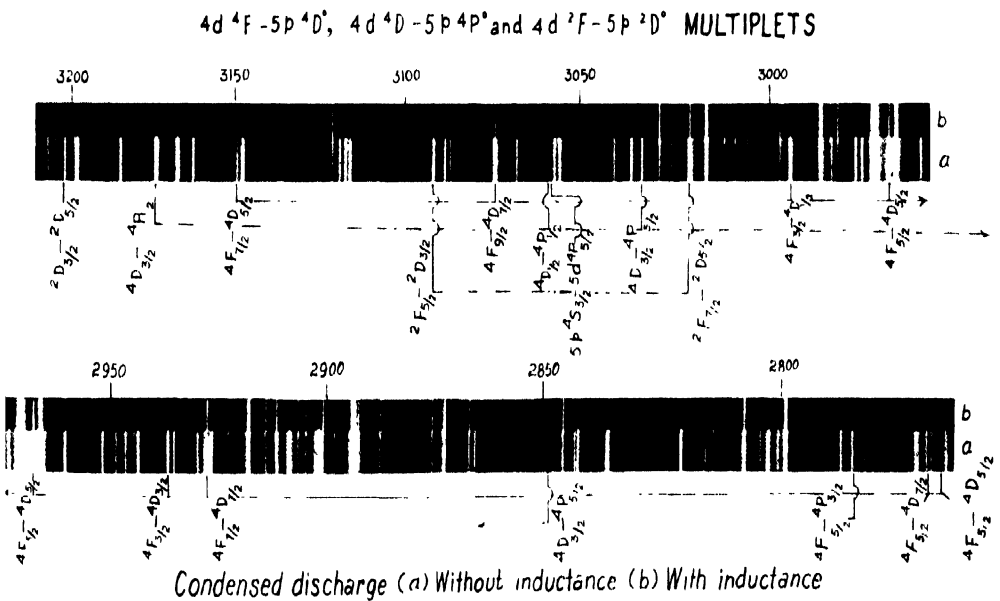
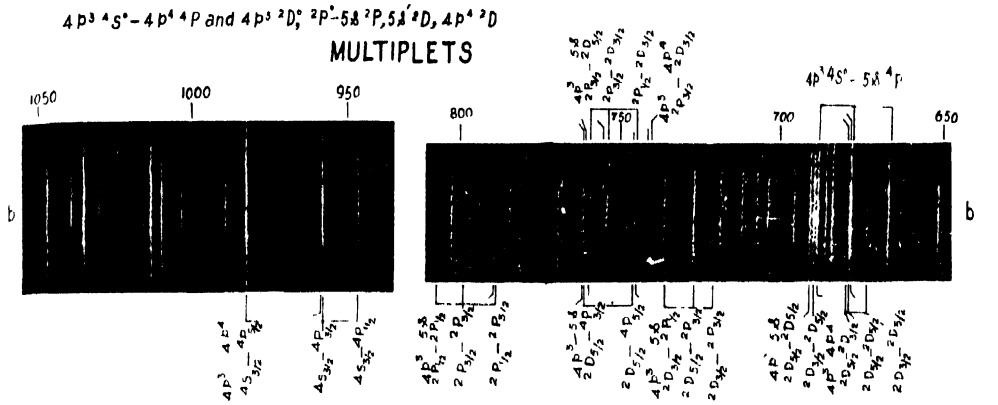
#### ANALYSIS

Br III is isoelectronic with As I, Se II, and Kr IV which have been respectively investigated by Meggers, Shenstone and Moore (1950), by Krishna Murty and Rao (1935) and Martin (1935) and by Boyce (1935) and Rao and Krishna Murty (1939). The structures of As I and Se II are almost completely known but the analysis of Kr IV is sketchy and far from complete.

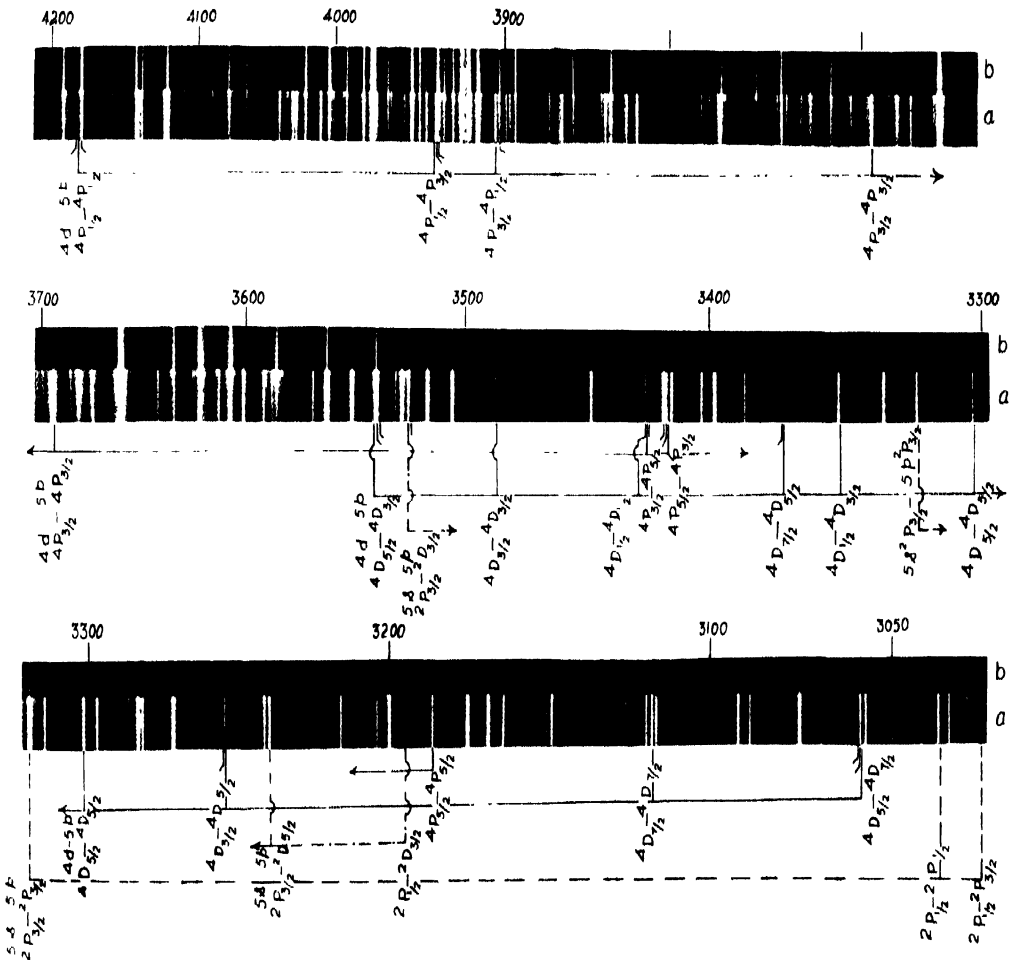
The predicted terms of Br III are given in Table I. Terms identified completely or partially are underlined. Those identified in the earlier investigations are marked with an asterisk also. All the newly identified levels are already given in the preliminary note (Bhupala Rao, 1956) in the ascending order of magnitude based on  $4p^3\ ^4S^0_{11}$  as zero. Following the notation adopted by Moore (1952) levels arising from the  $^1D$  and  $^1S$  states of the Br IV ion are distinguished by affixing a single prime and a double prime respectively to the running electron.

The analysis presented in this paper shows that there is a considerable overlapping of the terms of the same configuration and also of the terms of different configurations. The term intervals are as large as and sometimes even larger than the separations between the neighbouring terms showing very great departure from L-S coupling. The ratios of the intervals of the individual terms also show large deviations from the values predicted on the basis of L-S coupling. Unlike in Br II the combinations between even and odd levels are not profuse and it makes the analysis very difficult. Particularly, the combinations between the doublets of even and odd configurations are only a few. Some of the doublets give more combinations with the quartets than with the doublets, the intercombinations being thus relatively more intense.









Condensed discharge ( a ) Without inductance ( b ) With inductance

5p-5d MULTIPLETS

A careful examination of the plates has confirmed the previous identification of the quartets of  $4p^3$ ,  $5s$ ,  $5p$  and  $6s$  configurations. The intensity and behaviour of the lines are in conformity with the classifications. Examination of the doublets previously suggested is then taken up. A series of trials have been made to enlarge the scheme of classification assuming Rao and Krishna Murthy's identification of doublets as correct. All the attempts have proved to be unsuccessful. It is presumed that it is the failure to make correct assignment of the doublets and the intercombinations with the quartets that might have led to difficulty in extending the analysis further by Rao and Krishna Murty themselves. Therefore an independent and fresh approach to the identification of doublets is made with the aid of the irregular doublet law. The application of the irregular doublet law in the manner done by Bowen and Millikan and used by Rao (1927) in the analysis of the Sn III spectrum for transitions where the principal quantum number changes, is employed. By comparing with the values in As I and Se II using the irregular doublet law, the positions for the  $4p^3 \ ^2D_{3/2}^0 - 5s \ ^2P_{1/2}$ ,  $4p^3 \ ^2D_{1/2}^0 - 5s \ ^2P_{1/2}$ ,  $4p^3 \ ^2P_{1/2}^0 - 5s \ ^2P_{1/2}$  and  $4p^3 \ ^2P_{1/2}^0 - 5s \ ^2P_{1/2}$  combinations in Br III are calculated to be 136387, 133843, 123902 and 121705  $\text{cm}^{-1}$  respectively. With the help of these calculated values and the predicted intervals for the  $4p^3 \ ^2D^0$ ,  $^2P^0$  and  $5s \ ^2p$  terms the identifications of the doublets are made. With the assignments of Rao and Krishna Murty no intercombinations between the  $5s \ ^2P$  levels and the  $5p$  quarters could be observed. With the present choice the intercombination lines are observed in the calculated positions. Also, the intensities of the lines confirm the present assignments. From these it has been possible to establish the  $4p^3 \ ^2D^0, ^2P^0, 4p^4 \ ^2D, 5s \ ^2P$  and  $5s' \ ^2D$  terms. The identification of the  $5s' \ ^2D$  and  $4p^4 \ ^2D$  terms proved to be more difficult because of the intensity anomalies in their combinations and their proximity to each other. Starting with the doublets of the  $5s$  configuration and by a comparison of the position of  $np^2 (n+1)s \ ^2P_{1/2} - np^2(n+1)p \ ^2P_{1/2}^0$  combinations in the spectra isoelectronic with F III, Cl III and Br III the  $5p \ ^2P_{1/2}^0, ^2D_{3/2}^0$  levels are located at 105581.0 and 107331.0 respectively. Proceeding from these with the help of the estimated intervals of the  $5p$  doublets the  $5p \ ^2D^0, ^2P^0$  and  $^2S^0$  terms are identified completely. This also proved somewhat difficult because of the poor development of the multiplets. The  $5p$  doublets combine only with a few of the terms of the even configurations. Attempts to identify the  $5p'$  doublet levels with the help of the  $5s' \ ^2D$  interval have been unsuccessful. The transitions between the doublets of  $4p^3$  and  $5s$ ,  $4p^4$  configurations are shown in Plate VI and the combinations between the doublets of  $5s$  and  $5p$  configurations in Plate VIIA.

From a study of the position of the  $4p^3 \ ^4S^0 - 4p^4 \ ^4P$  multiplet and the intervals of the  $4p^4 \ ^4P$  term in spectra isoelectronic with F III, Cl III and Br III this multiplet in Br III is estimated to be in the region 100,000—110,000  $\text{cm}^{-1}$  with  $^4P_1 - ^4P_{1/2}$  and  $^4P_{1/2} - ^4P_{3/2}$  intervals of the order of —1260 and —2650 respectively. After a close scrutiny of the plates for three lines in that region with the estimated

intervals, the lines 105380, 104129 and 101532  $\text{cm}^{-1}$  are classified as the combinations respectively of  $4p^4 \text{}^4P_{1,1,2,1}$  levels with  $4p^3 \text{}^4S_{1,1}^0$ . Their intervals -1251 and -2597 agree well with the predicted values. These classifications are confirmed by the large number of combinations between the resulting levels and the  $5p$  quartet terms. The  $4p^3 \text{}^4S^0-4p^4 \text{}^4P$  multiplet is shown in Plate VI.

Rao and Krishna Murty (1937) have assigned nine levels to the  $4d$  configuration on consideration of their magnitude. But they have stated that some of them might actually be doublet levels. Attempts to identify the  $4d$  levels starting with the  $5p \text{}^4D^0$  and  $\text{}^4P^0$  intervals have resulted in the identification of the  $4p^4 \text{}^2P$  term, all the  $4d$  quartets, the  $4d \text{}^2F$  term, the  $4d \text{}^2D_{1,1}$ ,  $\text{}^2P_{1,1}$  levels and three other levels designated 1, 2 and 3. Of the nine given by Rao and Krishna Murty, only the five levels 2, 3, 5, 6 and 9 are found to be real, and of these the level 2 is identified as  $4p^4 \text{}^2P_{1,1}$ . The  $4p^4 \text{}^2P$  term does not combine with any of the  $4p^3$  levels.

The  $4d \text{}^4F$ ,  $\text{}^4D$  terms combine well with the  $5p \text{}^4D^0$  term, but seldom with  $5p \text{}^4P^0$  term. In the case of the  $4d \text{}^4P$  term, the  $4d \text{}^4P-5p \text{}^4P^0$  multiplet and  $4d \text{}^4P_{1,1}-5p \text{}^4D_{1,1}^0$ ,  $4d \text{}^4P_{1,1}-5p \text{}^4S_{1,1}^0$  and  $4d \text{}^4P_{1,1}-5p \text{}^2P_{1,1}^0$  combinations alone could be located. Except for two lines the  $4d$  levels do not give any combinations with the  $5p \text{}^2P^0$  and  $\text{}^2S^0$  terms. Even with the  $5p \text{}^2D^0$  term the combinations are only a few. The  $4d \text{}^4P$  term is inverted while the other terms are regular. But none of these is in conformity with L-S coupling. The  $4d \text{}^4F-5p \text{}^4D^0$ ,  $4d \text{}^4D-5p \text{}^4D^0$  and  $4d \text{}^4P-5p \text{}^4P^0$  multiplets are shown in Plates VI and VIIA.

The  $5d$  quartet terms also are arrived at with the help of the intervals of the  $5p$  quartets. Only two, 11 and 13, of the seven levels 10 to 16 assigned by Rao and Krishna Murty to the  $5d$  configuration, could be confirmed. The  $5d$  terms exhibit combining characteristics similar to the  $4d$  terms and their combinations with the odd levels are not profuse. Here too the term intervals are not regular and show large deviations from L-S coupling. The  $5d \text{}^4P$  term also is inverted. This inversion of the  $nd \text{}^4P$  term is a feature present in the spectra of F III and Cl III also.

The diagonal lines of the  $5p \text{}^4D^0-5d \text{}^4F$  multiplet are diminishing in intensity with increasing J values. From this trend in the variation of intensity the combination  $5p \text{}^4D_{3,1}^0-5d \text{}^4F_{4,1}$  is expected to be very weak, and since this is the only combination the  $5d \text{}^4F_{4,1}$  level gives with the  $5p$  levels, it is not found possible to fix this line. Consequently the  $5d \text{}^4F_{4,1}$  level is not identified. The  $5p \text{}^4D^0-5d \text{}^4F$ ,  $5p \text{}^4D^0-5d \text{}^4D$  and  $5p \text{}^4P^0-5d \text{}^4P$  multiplets are marked on Plate VII B.

The doublets of the  $5d$  and  $6s$  configurations are all expected to be of the same order of magnitude and it is not possible to distinguish between the levels of the two configurations. So, all these levels are designated arbitrarily by numerals 4 to 22.

TABLE I  
Terms of Br III

Configuration			Terms			
4s <sup>2</sup>	4p <sup>3</sup>		4S <sup>o</sup> *	2D <sup>o</sup>	2P <sup>o</sup>	
4s	4p <sup>4</sup>		4P	2P	2D	2S
Basic terms of Br IV			3P	1D		1S
4s <sup>2</sup>	4p <sup>2</sup>					
4s <sup>2</sup>	4p <sup>2</sup>	5s	1P*	2P	2D	2S
4s <sup>2</sup>	4p <sup>2</sup>	4d	1F	1D	1P	2(1 2F 3D 2F 2S
			2F	2D	2P	2D
4s <sup>2</sup>	4p <sup>2</sup>	5p	1D <sup>o</sup> *	1P <sup>o</sup> *	4S <sup>o</sup> *	2F <sup>o</sup> 2D <sup>o</sup> 2P <sup>o</sup>
			2D <sup>o</sup>	2P <sup>o</sup>	2S <sup>o</sup>	2P <sup>o</sup>
4s <sup>2</sup>	4p <sup>2</sup>	6s	1P*	2P	2D	2S
4s <sup>2</sup>	4p <sup>2</sup>	5d	1F	1D	1P	2(1 2F 2D 2P 4S
			2F	2D	2P	2D
4s <sup>2</sup>	4p <sup>2</sup>	6p	1D <sup>o</sup>	1P <sup>o</sup>	4S <sup>o</sup>	2F <sup>o</sup> 2D <sup>o</sup> 2P <sup>o</sup>
			2D <sup>o</sup>	2P <sup>o</sup>	2S <sup>o</sup>	2P <sup>o</sup>

\* . . . . . Identified in previous investigations.

TABLE II  
Newly classified lines of Br III

Intensity	$\lambda(\text{air})$	$\nu(\text{vac})$	Classification	Remarks
0bh	7696.1	12990	5d 4F <sub>3/2</sub> - 23 <sup>o</sup>	
2	7673.1	13029	4p <sup>4</sup> 2D <sub>11</sub> - 5p 4P <sup>o</sup> <sub>1</sub>	
2	7192.8	13899	6s 4P <sub>21</sub> - 23 <sup>o</sup>	
00b	6899.8	14489	4p <sup>4</sup> 2D <sub>11</sub> - 5p 4P <sup>o</sup> <sub>12</sub>	Br II line
1	6459.21	15477.5	5s' 2D <sub>11</sub> - 5p 4P <sup>o</sup> <sub>1</sub>	
1hb	5947.90	16808.0	6s 4P <sub>11</sub> - 23 <sup>o</sup>	
1	5764.09	17344.0	5d 4P <sub>11</sub> - 24 <sup>o</sup>	
1	5693.40	17559.3	11 - 24 <sup>o</sup>	
2	5446.80	18354.3	4p <sup>4</sup> 2D <sub>21</sub> - 5p 2D <sup>o</sup> <sub>14</sub>	
0	5440.38	18376.0	4p <sup>4</sup> 2D <sub>11</sub> - 5p 4S <sup>o</sup> <sub>11</sub>	Br II line

TABLE II (contd.)

Intensity	$\lambda(\text{air})$	$\nu(\text{vac})$	Classification	Remarks
00	5245.25	19059.6 5s'	$2D_{1\frac{1}{2}} - 5p$ $4P^0_{2\frac{1}{2}}$	
3	5175.87	19315.1 4d	$2P_{1\frac{1}{2}} - 5p$ $4D^0_{\frac{1}{2}}$	
1	5146.32	19426.0 6s	$4P_{1\frac{1}{2}} - 240$	
0	4896.67	20416.4 5p	$2P^0_{1\frac{1}{2}} - 6$	
1	4803.14	20813.9 5s'	$2D_{1\frac{1}{2}} - 5p$ $2S^0_{\frac{1}{2}}$	
00	4661.58	21446.0 5p	$4S^0_{1\frac{1}{2}} - 5$	
3	4556.49	21940.6 5s'	$2D_{2\frac{1}{2}} - 5p$ $2D^0_{1\frac{1}{2}}$	
4	4519.74	22119.0 4d	$4P_{1\frac{1}{2}} - 5p$ $4D^0_{\frac{1}{2}}$	
3	4393.51	22754.5 5s'	$2D_{1\frac{1}{2}} - 5p$ $2P^0_{1\frac{1}{2}}$	
3	4383.91	22804.3 4d	$2P_{1\frac{1}{2}} - 5p$ $4P^0_{\frac{1}{2}}$	
1	4319.49	23144.4 5p	$4S^0_{1\frac{1}{2}} - 7$	
0	4316.15	23162.3 4d	$2D_{1\frac{1}{2}} - 5p$ $4P^0_{\frac{1}{2}}$	
1hb	4219.15	23694.8	$3 - 5p$ $4P^0_{\frac{1}{2}}$	
1h	4190.82	23855.0	$2 - 5p$ $4D^0_{\frac{1}{2}}$	
1	4181.73	23906.8 4d	$4P_{\frac{1}{2}} - 5p$ $4P^0_{\frac{1}{2}}$	
00yb	4166.58	23993.8 5p	$4P^0_{2\frac{1}{2}} - 6$	
3	4120.34	24263.0 4d	$2P_{1\frac{1}{2}} - 5p$ $4P^0_{1\frac{1}{2}}$	
2H	4116.70	24284.5 5s	$2P_{1\frac{1}{2}} - 5p$ $4P^0_{1\frac{1}{2}}$	
		4d	$2F_{3\frac{1}{2}} - 5p$ $4D^0_{2\frac{1}{2}}$	
3hb	4086.63	24463.2 5s'	$2D_{2\frac{1}{2}} - 5p$ $2D^0_{2\frac{1}{2}}$	Br II line
00b	4078.36	24512.8	$2 - 5p$ $4D^0_{1\frac{1}{2}}$	
011b	4059.99	24623.7 4d	$2D_{1\frac{1}{2}} - 5p$ $4P^0_{1\frac{1}{2}}$	
0	3977.83	25131.3 5p	$4P^0_{1\frac{1}{2}} - 4$	
0b	3974.34	25154.3	$3 - 5p$ $4P^0_{1\frac{1}{2}}$	
0	3963.18	25225.2 5p	$4S^0_{1\frac{1}{2}} - 8$	
0	3946.00	25335.0 5p	$4P^0_{1\frac{1}{2}} - 5$	
00	3941.13	25366.3 4d	$4P_{\frac{1}{2}} - 5p$ $4P^0_{1\frac{1}{2}}$	
4	3903.95	25607.9 4d	$4P_{1\frac{1}{2}} - 5p$ $4P^0_{\frac{1}{2}}$	
0b	3880.25	25764.3 5s	$2P_{\frac{1}{2}} - 5p$ $4P^0_{\frac{1}{2}}$	
2hb	3838.34	26045.6 4d	$2F_{2\frac{1}{2}} - 5p$ $4D^0_{2\frac{1}{2}}$	
2	3788.67	26387.0 4d	$2P_{1\frac{1}{2}} - 5p$ $4P^0_{2\frac{1}{2}}$	



TABLE II (contd.)

Intensity	$\lambda(\text{air})$	$\nu(\text{vac})$	Classification	Remarks
2	3785.77	26407.2 5s	$2P_{1/2} - 5p$ $4P^o_{2/2}$	
0h	3760.72	26583.1	$2 - 5p$ $4D^o_{2/2}$	
00	3744.57	26697.1 4d	$2F_{3/2} - 5p$ $4D^o_{3/2}$	Br II line
1	3731.07	26794.4 5p	$4P^o_{1/2} - 5$	
2h	3724.75	26839.8 5p	$4D^o_{3/2} - 7$	
2b	3704.01	26990.1 5p	$4P^o_{2/2} - 8$	
5	3693.53	27066.7 4d	$4P_{1/2} - 5p$ $4P^o_{1/2}$	
00	3672.22	27223.8 5s	$2P_{1/2} - 5p$ $4P^o_{1/2}$	Br II line
0	3655.12	27351.1 5p	$4D^o_{2/2} - 4$	
3	3612.33	27675.1	$1 - 5p$ $4D^o_{1/2}$	
6	3551.08	28152.4 4d	$2P_{1/2} - 5p$ $4S^o_{1/2}$	
00	3543.29	28214.3 4d	$4D_{2/2} - 5p$ $4D^o_{1/2}$	
2	3531.54	28308.2 5p	$4P^o_{1/2} - 9$	
4	3528.86	28329.7 4d	$2P_{1/2} - 5p$ $2D^o_{1/2}$	?
2	3527.98	28336.8 5p	$4D^o_{2/2} - 6$	Br II line
3	3526.07	28352.1 5s	$2P_{1/2} - 5p$ $2D^o_{3/2}$	
0	3512.97	28457.8 4d	$2F_{2/2} - 5p$ $4D^o_{3/2}$	
6	3506.47	28510.6 4d	$2D_{1/2} - 5p$ $4S^o_{1/2}$	
2	3487.63	28664.6 4d	$4D_{1/2} - 5p$ $4D^o_{1/2}$	
2	3433.96	29112.6 5p	$4P^o_{1/2} - 8$	
3vb	3425.29	29186.3 4d	$4D_{1/2} - 5p$ $4D^o_{1/2}$	
1	3424.89	29189.7 4d	$4P_{1/2} - 5p$ $4P^o_{2/2}$	
5	3417.61	29251.9 5p	$4D^o_{2/2} - 7$	
2h	3417.23	29255.1 4d	$4P_{1/2} - 5p$ $4S^o_{1/2}$	Br II line
2b	3416.39	29262.3 4d	$4P_{2/2} - 5p$ $4P^o_{1/2}$	
3	3397.88	29421.7 5p	$4D^o_{1/2} - 4$	Br II line
2	3370.94	29656.8 4d	$4D_{3/2} - 5p$ $4D^o_{2/2}$	
5	3349.75	29844.4 4d	$4D_{1/2} - 5p$ $4D^o_{1/2}$	
6	3321.08	30102.1 5s	$2P_{1/2} - 5p$ $2P^o_{1/2}$	
5	3301.21	30283.2 4d	$4D_{2/2} - 5p$ $2D^o_{2/2}$	
00b	3287.71	30407.6 5p	$4D^o_{1/2} - 6$	

TABLE II (*contd.*)

Intensity	$\lambda(\text{air})$	$\nu(\text{vac})$	Classification	Remarks
2b	3285.21	30430.7	5p $4P_{01} - 9$	
1b	3277.15	30505.6	1-5p $4P_{01}$	
5	3270.07	30571.6	5p $4P_{01} - 8$	
3	3252.74	30734.5	4d $4D_{11} - 5p$	$4D_{02}$
5	3237.98	30874.6	5s $2P_{11} - 5p$	$2D_{02}$
4	3214.59	31099.2	5s $2P_{11} - 5p$	$2S_{01}$
4	3202.90	31212.7	4d $2D_{11} - 5p$	$2D_{02}$
0	3194.85	31291.4	5s $2P_{11} - 5p$	$2D_{01}$
4	3185.21	31386.1	4d $4P_{21} - 5p$	$4P_{02}$
5	3174.15	31495.4	4d $4D_{11} - 5p$	$4P_{01}$
4	3149.36	31743.3	4d $4F_{31} - 5p$	$4D_{02}$
0bh	3134.75	31891.3	5p $4P_{01} - 9$	
0bh	3133.04	31908.7	5p $2P_{11} - 5d$	$4P_{11}$
00h	3127.41	31966.1	1-5p $4P_{01}$	
7	3117.29	32069.9	4d $4D_{31} - 5p$	$4D_{03}$
7	3091.94	32332.8	4d $2F_{21} - 5p$	$2D_{01}$
10	3074.42	32517.0	4d $4F_{11} - 5p$	$4D_{03}$
111	3059.60	32674.5	4d $4D_{11} - 5p$	$4P_{01}$ Br II line
2hb	3058.49	32686.4	5p $4S_{01} - 5d$	$4P_{21}$
5	3057.57	32696.2	4d $4D_{21} - 5p$	$4D_{03}$
2h	3042.08	32862.7	5p $4S_{01} - 11$	?
00	3040.04	32884.8	4d $4P_{11} - 5p$	$2P_{01}$
7	3036.45	32923.6	5s $2P_{11} - 5p$	$2P_{01}$
6	3033.63	32954.2	4d $4D_{11} - 5p$	$4P_{01}$
4	3025.63	33041.4	5s $2P_{11} - 5p$	$2P_{01}$
0	3022.17	33079.2	5p $4S_{01} - 5d$	$4P_{11}$
10	3020.76	33094.6	4d $2F_{31} - 5p$	$2D_{02}$
8	2994.04	33390.0	4d $4F_{11} - 5p$	$4D_{01}$
7	2969.00	33671.6	4d $4F_{21} - 5p$	$4D_{02}$
0hb	2952.88	33855.4	5p $4P_{01} - 5d$	$4F_{21}$

TABLE II (contd.)

Intensity	$\lambda(\text{air})$	$\nu(\text{vac})$	Classification	Remarks
3vhh	2946.26	33931.4	5p $^1P^0_{11} - 5d$	$^1F_{11}$
6	2936.22	34047.5	4d $^4F_{11} - 5p$	$^1D^0_{11}$
2	2932.68	34088.6	1 - 5p	$^1P^0_{21}$
8	2926.96	34155.2	4d $^4F_{31} - 5p$	$^4D^0_{31}$
4	2901.89	34450.2	5p $^1P^0_{21} - 5d$	$^4P_{21}$
4	2901.00	34460.8	5s $^4P_{21} - 5p$	$^2D^0_{21}$
1h	2869.11	34843.8	5p $^4P^0_{21} - 5d$	$^4P_{11}$
00b	2852.83	35042.6	5p $^4P^0_{31} - 5d$	$^4D_{11}$
2h	2849.91	35078.5	4d $^1D_{11} - 5p$	$^4P^0_{21}$
2h	2843.79	35154.0	5p $^1S^0_{11} - 13$	
0h	2837.56	35231.2	4p <sup>1</sup> $^2P_{11} - 5p$	$^1D^0_{11}$
6	2804.16	35650.8	4p <sup>4</sup> $^2P_{11} - 5p$	$^1D^0_{11}$
3	2793.97	35780.8	5p $^1P^0_{11} - 5d$	$^1D_{11}$
6b	2785.28	35892.5	4d $^1F_{21} - 5p$	$^1P^0_{11}$
3b	2784.21	35906.3	5p $^1S^0_{11} - 14$	
3	2781.09	35946.5	5p $^1D^0_{31} - 5d$	$^4D_{21}$
8H	2772.62	36056.4	5p $^4P^0_{11} - 10$	
6	2770.50	36083.9	4d $^4F_{21} - 5p$	$^1D^0_{31}$
2	2767.89	36118.0	4d $^4F_{11} - 5p$	$^1D^0_{21}$
?	2766.26	36139.2	5p $^4P^0_{11} - 5d$	$^1D_{21}$
0h	2765.93	36143.6	5p $^1P^0_{21} - 12$	
3	2753.35	36308.7	4p <sup>1</sup> $^2P_{11} - 5p$	$^1D^0_{11}$
4H	2752.06	36325.7	5p $^4P^0_{21} - 5d$	$^1D_{11}$
3H	2747.18	36390.2	4d $^4D_{21} - 5p$	$^1S^0_{11}$
2H	2742.36	36454.2	5p $^2P^0_{11} - 17$	
7H	2735.83	36541.2	5p $^1D^0_{21} - 5d$	$^1D_{11}$
00	2733.43	36573.3	5p $^4P^0_{11} - 5d$	$^1P_{21}$
			4d $^1D_{21} - 5p$	$^2D^0_{11}$
1h	2731.35	36601.1	5s $^4P_{11} - 5p$	$^4S^0_{11}$
1	2720.15	36751.8	5p $^4P^0_{11} - 11$	

TABLE II (contd.)

Intensity	$\lambda(\text{air})$	$\nu(\text{vac})$	Classification	Remarks
3h	2719.39	36762.1	5p $4D^0_{1\frac{1}{2}} - 5d$	$4F_{1\frac{1}{2}}$
00	2715.37	36816.5	5p $4D^0_{2\frac{1}{2}} - 10$	
1	2710.83	36878.2	4d $4F_{1\frac{1}{2}} - 5p$	$4P^0_{\frac{1}{2}}$
4	2704.28	36967.5	5p $4P^0_{1\frac{1}{2}} - 5d$	$4P_{1\frac{1}{2}}$
7h	2671.53	37420.6	5p $4D^0_{\frac{1}{2}} - 5d$	$4F_{1\frac{1}{2}}$
2	2649.82	37727.2	5p $P^0_{1\frac{1}{2}} - 5d$	$4P_{\frac{1}{2}}$
0	2645.19	37793.2	5p $4P^0_{1\frac{1}{2}} - 6s$	$4P_{2\frac{1}{2}}$
7h	2639.60	37873.3	5p $4D^0_{1\frac{1}{2}} - 5d$	$4D_{\frac{1}{2}}$
4	2632.88	37969.9	5p $2D^0_{2\frac{1}{2}} - 21$	
7h	2629.23	38022.6	4d $4D_{\frac{1}{2}} - 5p$	$4S^0_{1\frac{1}{2}}$
10H	2626.52	38061.9	4p <sup>4</sup> $2P_{\frac{1}{2}} - 5p$	$4P^0_{\frac{1}{2}}$
3	2617.08	38199.9	5p $4D^0_{2\frac{1}{2}} - 5d$	$4F_{2\frac{1}{2}}$
7h	2616.26	38211.1	5p $4P^0_{\frac{1}{2}} - 11$	
10H	2613.13	38256.9	5p $4D^0_{3\frac{1}{2}} - 5d$	$4D_{3\frac{1}{2}}$
7H	2608.15	38329.9	$4S^0_{1\frac{1}{2}} - 18$	
9H	2606.20	38358.6	5p $4D^0_{2\frac{1}{2}} - 5d$	$4D_{2\frac{1}{2}}$
3h	2601.58	38426.7	5p $4P^0_{\frac{1}{2}} - 5d$	$4P_{1\frac{1}{2}}$
1H	2597.69	38484.3	5p $2P^0_{1\frac{1}{2}} - 20$	
8h	2595.98	38509.7	5p $4D^0_{3\frac{1}{2}} - 5d$	$4F_{3\frac{1}{2}}$
6H	2594.48	38531.9	5p $4D^0_{\frac{1}{2}} - 5d$	$4D_{\frac{1}{2}}$
10	2589.14	38611.3	5p $4D^0_{1\frac{1}{2}} - 5d$	$4D_{1\frac{1}{2}}$
8h	2584.99	38673.3	5p $4P^0_{2\frac{1}{2}} - 15$	
6H	2573.17	38850.9	5p $4D^0_{3\frac{1}{2}} - 13$	
7H	2570.83	38886.3	5p $4D^0_{1\frac{1}{2}} - 10$	
2h	2565.22	38971.3	5p $4D^0_{2\frac{1}{2}} - 11$	
1	2554.21	39139.3	4p <sup>4</sup> $2P_{1\frac{1}{2}} - 5p$	$4P^0_{\frac{1}{2}}$
7h	2551.09	39187.1	5p $4P^0_{\frac{1}{2}} - 5d$	$4P_{\frac{1}{2}}$
			5p $4D^0_{2\frac{1}{2}} - 5d$	$4P_{1\frac{1}{2}}$
7	2529.49	39251.8	4p <sup>4</sup> $2P_{\frac{1}{2}} - 5p$	$4P^0_{1\frac{1}{2}}$
1h	2527.92	39546.3	5p $4D^0_{\frac{1}{2}} - 10$	

TABLE II (contd.)

Intensity	$\lambda(\text{air})$	$\nu(\text{vac})$	Classification	Remarks
1h	2524.43	39601.0	5p $4D^o_{3\frac{1}{2}} - 14$	
00	2513.08	39779.8	4d $4P^o_{2\frac{1}{2}} - 5p$	$4S^o_{1\frac{1}{2}}$
5	2497.43	40029.1	5p $4P^o_{2\frac{1}{2}} - 17$	
6	2482.60	40268.2	5p $4D^o_{1\frac{1}{2}} - 5d$	$4P^o_{2\frac{1}{2}}$
3h	2469.17	40487.2	5p $4D^o_{2\frac{1}{2}} - 12$	
6	2462.39	40598.7	4p <sup>4</sup> $2P^o_{1\frac{1}{2}} - 5P$	$4P^o_{1\frac{1}{2}}$
1bh	2450.44	40796.6	5p $4P^o_{1\frac{1}{2}} - 15$	
3h	2443.01	40920.7	5p $4D^o_{2\frac{1}{2}} - 5d$	$4P^o_{3\frac{1}{2}}$
4h	2435.76	41042.5	5p $4D^o_{1\frac{1}{2}} - 11$	
0h	2423.08	41257.3	5p $4D^o_{1\frac{1}{2}} - 5d$	$4P^o_{1\frac{1}{2}}$
1h	2422.71	41263.6	5p $4D^o_{2\frac{1}{2}} - 13$	
4b	2397.31	41700.7	5p $4D^o_{1\frac{1}{2}} - 11$	
1	2396.07	41722.3	5p $4P^o_{1\frac{1}{2}} - 16$	
3	2379.48	42013.2	5p $4D^o_{2\frac{1}{2}} - 14$	
4	2378.73	42026.4	5p $4D^o_{3\frac{1}{2}} - 18$	
00	2375.50	42083.5	5p $4D^o_{1\frac{1}{2}} - 6s$	$4P^o_{2\frac{1}{2}}$
3	2371.63	42152.2	5p $4P^o_{1\frac{1}{2}} - 17$	
0	2365.79	42256.3	5p $4P^o_{1\frac{1}{2}} - 15$	
0	2349.06	42557.2	5p $4D^o_{1\frac{1}{2}} - 12$	
4	2339.95	42722.8	4p <sup>4</sup> $2P^o_{1\frac{1}{2}} - 5p$	$4P^o_{2\frac{1}{2}}$
2	2326.41	42971.5	5p $4S^o_{1\frac{1}{2}} - 22$	
0	2323.96	43016.8	5p $4D^o_{2\frac{1}{2}} - 15$	
6	2313.29	43215.2	5p $4D^o_{1\frac{1}{2}} - 12$	
0	2299.66	43471.3	5p $4D^o_{3\frac{1}{2}} - 19$	
8vbh	2293.44	43589.2	4p <sup>4</sup> $2P^o_{1\frac{1}{2}} - 5p$	$2D^o_{1\frac{1}{2}}$
4	2292.27	43611.4	5p $4P^o_{1\frac{1}{2}} - 17$	
1bh	2289.49	43664.4	5p $4P^o_{1\frac{1}{2}} - 19$	
0	2274.94	43943.6	5p $4D^o_{2\frac{1}{2}} - 16$	
4	2270.02	44038.8	4d $4P^o_{1\frac{1}{2}} - 5p$	$2P^o_{1\frac{1}{2}}$
1	2256.52	44302.3	5p $4P^o_{1\frac{1}{2}} - 20$	

TABLE II (contd.)

Intensity	$\lambda(\text{air})$	$\nu(\text{vac})$	Classification	Remarks
0	2249.63	44437.9	5p $4D^0_{2\frac{1}{2}} - 18$	
1	2243.43	44560.7	5p $4P^0_{1\frac{1}{2}} - 21$	
00	2234.59	44737.0	5p $4P^0_{2\frac{1}{2}} - 22$	
00	2210.63	45221.8	4p <sup>3</sup> $2P_{\frac{1}{2}} - 5p$ $2P^0_{\frac{1}{2}}$	
2	2184.55	45761.7	5p $4P^0_{\frac{1}{2}} - 20$	
3	2178.74	45883.7	5p $4D^0_{2\frac{1}{2}} - 19$	
2	2172.62	46012.9	5p $4D^0_{1\frac{1}{2}} - 16$	
0	2172.30	46019.7	5p $4P^0_{\frac{1}{2}} - 21$	
?	2153.68	46418.2	4p <sup>4</sup> $2P_{1\frac{1}{2}} - 5p$ $2P^0_{1\frac{1}{2}}$	
?	2152.52	46442.5	5p $4D^0_{1\frac{1}{2}} - 17$	
4	2133.35	46859.8	5p $4P^0_{1\frac{1}{2}} - 22$	
3	2118.51 (vac)	47188.0	4p <sup>4</sup> $2P_{1\frac{1}{2}} - 5p$ $2D^0_{2\frac{1}{2}}$	
2	1475.1	67790	4p <sup>4</sup> $4P_{\frac{1}{2}} - 5p$ $4D^0_{\frac{1}{2}}$	
00	1434.7	69703	4p <sup>4</sup> $4P_{1\frac{1}{2}} - 5p$ $4D^0_{1\frac{1}{2}}$	
5	1402.9	71283	4p <sup>4</sup> $4P_{\frac{1}{2}} - 5p$ $4P^0_{\frac{1}{2}}$	
1	1393.0	71789	4p <sup>4</sup> $4P_{1\frac{1}{2}} - 5p$ $4D^0_{2\frac{1}{2}}$	
2	1383.1	72303	4p <sup>4</sup> $4P_{2\frac{1}{2}} - 5p$ $4D^0_{1\frac{1}{2}}$	
2	1351.4	73996	4p <sup>4</sup> $4P_{1\frac{1}{2}} - 5p$ $4P^0_{1\frac{1}{2}}$	
1	1344.6	74374	4p <sup>4</sup> $4P_{2\frac{1}{2}} - 5p$ $4D^0_{2\frac{1}{2}}$	
5	1313.5	76135	4p <sup>4</sup> $4P_{1\frac{1}{2}} - 5p$ $4P^0_{2\frac{1}{2}}$	
1	1305.6	76591	4p <sup>4</sup> $4P_{2\frac{1}{2}} - 5p$ $4P^0_{1\frac{1}{2}}$	
0	1304.9	76632	4p <sup>4</sup> $4P_{\frac{1}{2}} - 5p$ $4S^0_{1\frac{1}{2}}$	Oxygen I
0	1303.7	76708	4p <sup>3</sup> $2P^0_{1\frac{1}{2}} - 4p^4$ $4P_{\frac{1}{2}}$	
3	1302.2	76794	4p <sup>4</sup> $4P_{2\frac{1}{2}} - 5p$ $4D^0_{3\frac{1}{2}}$	Oxygen I
1	1297.5	77074	4p <sup>3</sup> $2P^0_{\frac{1}{2}} - 4p^4$ $4P_{1\frac{1}{2}}$	
0	1283.7	77903	4p <sup>4</sup> $4P_{1\frac{1}{2}} - 5p$ $4S^0_{1\frac{1}{2}}$	
00	1272.8	78567	4p <sup>4</sup> $4P_{\frac{1}{2}} - 5p$ $2P^0_{1\frac{1}{2}}$	
2	1270.3	78724	4p <sup>4</sup> $4P_{2\frac{1}{2}} - 5p$ $4P^0_{2\frac{1}{2}}$	
3	1242.2	80500	4p <sup>4</sup> $4P_{2\frac{1}{2}} - 5p$ $4S^0_{1\frac{1}{2}}$	
9	984.9	101532	4p <sup>3</sup> $4S^0_{1\frac{1}{2}} - 4p^4$ $4P_{2\frac{1}{2}}$	

TABLE II (contd.)

Intensity	$\lambda(\text{vac})$	$\nu(\text{vac})$	Classification	Remarks
8	960.4	104129	$4p^3 \ 4S^0_{1\frac{1}{2}} - 4p^4 \ 4P_{1\frac{1}{2}}$	
7	949.0	105380	$4p^3 \ 4S^0_{1\frac{1}{2}} - 4p^4 \ 4P_{\frac{1}{2}}$	
2	807.4	123856	$4p^3 \ 2P^0_{\frac{1}{2}} - 5s \ 2P_{\frac{1}{2}}$	
0	805.7	124116	$4p^3 \ 2P^0_{1\frac{1}{2}} - 4d \ 4P_{\frac{1}{2}}$	
5	798.8	125186	$4p^3 \ 2P^0_{1\frac{1}{2}} - 5s \ 2P_{1\frac{1}{2}}$	
0	794.1	125926	$4p^3 \ 2P^0_{\frac{1}{2}} - 3$	
00	788.7	126794	$4p^3 \ 2P^0_{\frac{1}{2}} - 5s \ 2P_{1\frac{1}{2}}$	Br II
00	773.2	129339	$4p^3 \ 2D^0_{2\frac{1}{2}} - 4d \ 4D_{2\frac{1}{2}}$	
3	768.8	130075	$4p^3 \ 2D^0_{1\frac{1}{2}} - 4d \ 4D_{1\frac{1}{2}}$	
1	761.3	131361	$4p^3 \ 2D^0_{2\frac{1}{2}} - 5s \ 4P_{1\frac{1}{2}}$	
2	759.9	131596	$4p^3 \ 2P^0_{1\frac{1}{2}} - 5s' \ 2D_{2\frac{1}{2}}$	
3	754.5	132535	$4p^3 \ 2P^0_{1\frac{1}{2}} - 5s' \ 2D_{1\frac{1}{2}}$	
1	746.6	133948	$4p^3 \ 2D^0_{2\frac{1}{2}} - 5s \ 4P_{2\frac{1}{2}}$	
2	745.5	134142	$4p^3 \ 2P^0_{\frac{1}{2}} - 5s' \ 2D_{1\frac{1}{2}}$	
2	740.8	134984	$4p^3 \ 2P^0_{1\frac{1}{2}} - 4p^4 \ 2D_{1\frac{1}{2}}$	
00	739.9	135150	$4p^3 \ 2D^0_{1\frac{1}{2}} - 5s \ 4P_{2\frac{1}{2}}$	
6	736.4	135801	$4p^3 \ 2D^0_{1\frac{1}{2}} - 5s \ 2P_{2\frac{1}{2}}$	
00	731.7	136674	$4p^3 \ 2D^0_{2\frac{1}{2}} - 3$	
6	727.0	137546	$4p^3 \ 2D^0_{2\frac{1}{2}} - 5s \ 2P_{1\frac{1}{2}}$	
00	720.8	138742	$4p^3 \ 2D^0_{1\frac{1}{2}} - 5s \ 2P_{1\frac{1}{2}}$	
8	690.2	144890	$4p^3 \ 2D^0_{2\frac{1}{2}} - 5s' \ 2D_{1\frac{1}{2}}$	
3	688.9	145153	$4p^3 \ 2D^0_{1\frac{1}{2}} - 5s' \ 2D_{2\frac{1}{2}}$	
1	678.7	147351	$4p^3 \ 2D^0_{2\frac{1}{2}} - 4p^4 \ 2D_{1\frac{1}{2}}$	
6	677.8	147545	$4p^3 \ 2D^0_{2\frac{1}{2}} - 4p^4 \ 2D_{2\frac{1}{2}}$	
0	672.3	148741	$4p^3 \ 2D^0_{1\frac{1}{2}} - 4p^4 \ 2D_{2\frac{1}{2}}$	
6	620.4	161199	$4p^3 \ 4S^0_{1\frac{1}{2}} - 5s' \ 2D_{1\frac{1}{2}}$	
9	611.1	163650	$4p^3 \ 4S^0_{1\frac{1}{2}} - 4p^4 \ 2D_{1\frac{1}{2}}$	

Attempts to locate the 6p levels with the help of the 6s  $^4P$  intervals have led to the identification of the two levels  $23^{\circ}$  and  $24^{\circ}$ .

Using the Rydberg formula the absolute value of  $5s \ ^4P_{2\frac{1}{2}}$  is obtained by Rao and Krishna Murty as  $139269.0 \text{ cm}^{-1}$  from the two members of the  $ns \ ^4P$  series.

This gives the limit  $289529 \text{ cm}^{-1}$  corresponding to a third ionisation potential of 35.89 volts. The calculation is verified and found correct. This is, therefore, adopted as the limit.

#### ACKNOWLEDGMENTS

The author is indebted to Prof. K. R. Rao for guidance throughout the progress of this work, which was done during the author's stay at the Andhra University, Waltair. He is thankful to Dr. K. Sreerama Murty and Dr. S. Paddi Reddy for their kind and constant help.

#### REFERENCES

- Bhupala Rao, Y., 1956, *Ind. J. Phys.*, **30**, 371.  
 Bhupala Rao, Y., 1958, *Ind. J. Phys.*, **32**, 497.  
 Bloch, L. and Bloch, E., 1927, *Ann. de. Phys.*, **7**, 205.  
 Boyce, J. C., 1935, *Phys. Rev.*, **47**, 718.  
 Deb, S. C., 1930, *Proc. Roy. Soc. London.*, **A127**, 197.  
 Krishna Murty, S. G. and Rao, K. R., 1935, *Proc. Roy. Soc. London.*, **A149**, 56.  
 Lueroite, P., 1935, *Ann. de. Phys.*, **3**, 3.  
 Martin, D. C., 1935, *Phys. Rev.*, **48**, 938.  
 Meggers, W. F., Shenstone, A. G. and Moore, C. E., 1950, *Bur. Std. Jour., of Research* **45**, 346.  
 Moore, C. E., 1952, *Atomic Energy Levels*, Vol. II.  
 Rao, A. B., and Krishna Murty, S. G., 1939, *Proc. Phys. Soc.*, **51**, 772.  
 Rao, K. R., 1927, *Proc. Phys. Soc.*, **39**, 161.  
 Rao, K. R., 1944, *Curr. Sci.*, **13**, 72.  
 Rao, K. R., and Krishna Murty, S. G., 1937, *Proc. Roy. Soc. London.*, **A161**, 38.  
 Rao, K. R., and Badami, J. S., 1931, *Proc. Roy. Soc., London.*, **A131**, 154.



# TOPOTACTIC TRANSFORMATIONS IN IRON OXIDES AND OXYHYDROXIDES\*

D. R. DASGUPTA\*\*

INDIAN ASSOCIATION FOR THE CULTIVATION OF SCIENCE,

JADAVPUR, CALCUTTA-32

(Received March 26, 1961)

## Plate VIII (A and B)

**ABSTRACT.** This paper records an investigation of the structures and chemical relations of iron oxides, hydroxides and oxyhydroxides. In the course of the work structural relations were also found between them which exemplified the new concept of topotaxy or change of composition of crystals occurring without any large discontinuity of structures. Starting with  $\text{Fe}(\text{OH})_2$  whose structure is built up of hexagonal close-packed hydroxyl layers, it is seen that when it decomposes into  $\text{FeO}$  there is an oriented relationship between the two phases. The  $[001]$  of  $\text{Fe}(\text{OH})_2$  becomes the  $[111]$  of cubic  $\text{FeO}$  and  $[110]$  of the former becomes  $[110]$  of the latter. Again, when  $\text{Fe}(\text{OH})_2$  is oxidised by strong  $\text{H}_2\text{O}_2$  or  $(\text{NH}_4)_2\text{S}_2\text{O}_8$  solution to  $\delta\text{-FeO.OH}$ , the arrangement of the close-packed layers changes from  $\text{AeB}$  to  $\text{A}_{1/2}\text{cB}_{1/2}\text{A}$ , the directions of the axes remaining the same. As it was not possible to get any single crystals of green rusts, direct evidences about the oriented relationship between them and their transformation products could not be found. But the proposed structure for the green rusts definitely speaks in favour of the oriented relationships. The transformations of  $\gamma\text{-FeO.OH}$  to  $\gamma\text{-Fe}_2\text{O}_3$  and then to  $\alpha\text{-Fe}_2\text{O}_3$  have been studied in great detail. It was found that the  $[100]$ ,  $[010]$  and  $[001]$  axes of  $\gamma\text{-FeO.OH}$  become  $[001]$ ,  $[110]$  and  $[1\bar{1}0]$  of  $\gamma\text{-Fe}_2\text{O}_3$  after transformation. In the second transition from  $\gamma\text{-Fe}_2\text{O}_3$  to  $\alpha\text{-Fe}_2\text{O}_3$ , crystals of the latter grow with their  $[001]$  axes parallel to  $[111]$  of  $\gamma\text{-Fe}_2\text{O}_3$  and their  $[110]$  directions being parallel to  $[110]$  of  $\gamma\text{-Fe}_2\text{O}_3$ . The same sort of oriented relationship as in between  $\gamma\text{-Fe}_2\text{O}_3$  and  $\alpha\text{-Fe}_2\text{O}_3$  was found in the transformation of  $\text{Fe}_3\text{O}_4$  to  $\alpha\text{-Fe}_2\text{O}_3$ . Several forms of  $\gamma\text{-Fe}_2\text{O}_3$  prepared by various methods have also been studied by X-rays. The transformation of rhombohedral  $\text{FeCO}_3$  to cubic  $\text{FeO}$  and  $\text{Fe}_3\text{O}_4$  has also been found to have oriented relationship. The similarity of the structures of  $\text{FeCO}_3$  and  $\text{FeO}$  suggested that the triad axis of  $\text{FeCO}_3$  would be parallel to one of the triad axes of  $\text{FeO}$  and that the three diad axes of both phases were interchanged,  $\text{FeO}$  and  $\text{Fe}_3\text{O}_4$  having parallel orientation to each other. The transformation of  $\beta\text{-FeO.OH}$  to  $\alpha\text{-Fe}_2\text{O}_3$  could not be explained in terms of oriented relationship. From the similarity of the powder patterns and also the comparison of intensities of the diffraction lines, it is thought that  $\beta\text{-FeO.OH}$  has a structure similar to Hollandite mineral ( $\alpha\text{-MnO}_2$ ).

## INTRODUCTION

Up to the present time physico-chemical studies have shown the existence of three forms of iron oxyhydroxides referred to as  $\alpha$ ,  $\beta$  and  $\gamma\text{-Fe}_2\text{O}_3$ ,  $\text{H}_2\text{O}$  or  $\text{FeO.OH}$ .

\*This work was submitted as a part of the thesis for the Ph.D. degree of the University of London.

\*\*At present Senior Mineralogist, Geological Survey of India, 29, Chowringhee, Cal-16.

Of the anhydrous oxides of iron,  $\alpha$ -Fe<sub>2</sub>O<sub>3</sub>,  $\gamma$ -Fe<sub>2</sub>O<sub>3</sub> and Fe<sub>3</sub>O<sub>4</sub> can be obtained by dehydrating some of the oxyhydroxides (FeO.OH), by direct precipitation or by oxidation of Fe(OH)<sub>2</sub> with different types of oxidising agents. The remaining anhydrous oxide, FeO, may be obtained by decomposing Fe(OH)<sub>2</sub> or some organic ferrous salts in vacuo or in an inert atmosphere. Most of these hydrous and anhydrous oxides of iron can be found as natural minerals. Together with the study of various physical and chemical properties of these compounds, a number of methods have been found for preparing them synthetically. Welo and Baudisch (1925, 1933, 1935) reviewed all the work done on the iron oxides and oxyhydroxides up to that time and tried to draw up a general relationship between the different iron compounds. However, they themselves expressed doubts about the existence of some members in the iron oxide-oxyhydroxide system and also about the modes of transformation between the compounds. Although various methods of preparing the different oxides and oxyhydroxides and also how one can be obtained from the other are known, the structural inter-relationships among these compounds are quite unknown.

The structures of most of the oxides and oxyhydroxides of iron are built up of close-packed oxy/hydroxyl layers. It seems possible that when one form of iron oxides or oxyhydroxides transforms into another, the change may be effected simply by removing or adding close-packed oxy/hydroxyl layers from or to the original structures. Thus one might expect to find an oriented relationship between the original and transformed products. Such a relationship, which is not limited to any particular type of crystal, was observed by Goldsztanb (1931, 1935) in the transformation of  $\alpha$ -FeO.OH to  $\alpha$ -Fe<sub>2</sub>O<sub>3</sub>. This sort of relationship occurs frequently in metals and also in inorganic compounds. A striking example of this oriented relationship can be found in the case of cubic and hexagonal metallic cobalt crystals. There the basal hexagonal face becomes one of the {111} faces of the face-centred cubic form. Similarly, in the transformation between  $\alpha$  and  $\gamma$ -iron, the {110} faces of the body-centred form becomes the close-packed {111} faces of the face-centred cubic form. All these changes mean that the main determining elements of the lattice do not change and the other elements only move from one symmetrical position to another in substantially the same cell. The minimum disturbances caused when the hydroxyl ions are removed as water molecules also suggest that the evidence of oriented relationship among the oxides and oxyhydroxides of iron may be found.

The best method of studying these oriented transformations is to make X-ray investigations on single crystals of different compounds before and after the transformation and also during it, if possible. If an oriented relationship exists, the diffraction photographs taken both before and after the transformation will show some common directions. When single crystals are not available, the powder diffraction method can provide indirect evidence. Sometimes, accord-

ing to the nature of transformation, a multiplicity of the reflections may correspond to a single direction from the original crystal. In this case, the similarities between the structure of the two phases may throw some light on any possible inter-relationship.

This sort of inter-relationship can be explained in terms of topotaxy, a term proposed by Gorter to denote the transformation from one crystalline phase to another, where there are definite oriented relationships between the axes of the original and transformed crystals. In general, the topotactic change consists of two parts, geometrical and chemical. The geometrical part classifies the way in which one lattice can be transformed into another while retaining the original network of the structure. The chemical part, on the other hand, accounts for the possibility of replacing one kind of atom by another and also the increase or lowering the total number of atoms per unit of lattice. True topotactic changes involve more than internal rearrangements of atoms along with the substitution, removal or addition of atoms to the original structure. In general, topotactic changes involving the loss or gain of atoms will leave the main symmetry directions of the crystals unchanged. But it also seems possible that an asymmetrical crystals may, by the loss of its atoms, transform into a form of higher symmetry. Further topotactic changes may occur on the newly formed crystals.

Thus with the aim of establishing what structural relationships exist between the different phases, most of iron oxides and oxyhydroxides and their transformations from one to the other have been studied in great detail. The results of the investigations are given in the next section.

#### EXPERIMENTAL RESULTS

##### (a) *Ferrous hydroxide* ( $\text{Fe}(\text{OH})_2$ )

Thesn ow-white precipitate of  $\text{Fe}(\text{OH})_2$  which is obtained when an alkali is added to a ferrous salt solution, turns greenish as soon as it comes in contact with air. To show the true colour of  $\text{Fe}(\text{OH})_2$  precipitate, it is necessary to boil both the alkali and salt solution before mixing in order to eliminate the dissolved oxygen and the precipitation must be carried out in an inert atmosphere. Natta and Casazza (1928) from the powder diffraction photograph determined the structure of  $\text{Fe}(\text{OH})_2$ . They found it to be hexagonal with one formula unit in the unit cell of axial parameters  $a = 3.24 \text{ \AA}$  and  $c = 4.47 \text{ \AA}$ . The structure is built of two hexagonal close-packed  $\text{OH}'$  layers having Fe in the octahedral position in between them. The atomic coordinates are one Fe at (0,0,0) and two OH at  $\pm(2/3, 1/3, Z)$  with  $Z = 0.26$ . It is to be noted here that the  $\text{OH}'$  layer has  $\text{Fe}^{++}$  on one side of it, whereas on the other side it is bound to another  $\text{OH}'$  layer by hydroxyl bonds.

Though it is thought that  $\text{Fe}(\text{OH})_2$  is very unstable at ordinary temperature and in contact with air, recent work by Shipko and Douglas (1956) had shown

that pure  $\text{Fe}(\text{OH})_2$ , in contact with a solution of potassium chloride or excess of hydroxyl ion with complete exclusion of oxygen, was stable for a period of six months. Moreover, Gayer and Woontter (1957) reported from their chemical analysis that the green precipitate, observed at the initial stage of the oxidation of white  $\text{Fe}(\text{OH})_2$ , no traces of ferric ions were found. Our (1960) work also showed that even when 20% of  $\text{Fe}^{++}$  ion in  $\text{Fe}(\text{OH})_2$  was oxidised to  $\text{Fe}^{+++}$ , there was no change in the structure of  $\text{Fe}(\text{OH})_2$ .

When the white precipitate of  $\text{Fe}(\text{OH})_2$  is washed with oxygen free water and then heated to dryness it decomposes to  $\text{FeO}$ , some  $\text{Fe}_3\text{O}_4$  also being formed at the same time. Recently, Goodman (1958) has shown from electron microscope and electron diffraction study of single crystal of  $\text{Mg}(\text{OH})_2$  that on dehydration of  $\text{Mg}(\text{OH})_2$  to  $\text{MgO}$  there is an oriented relationship between the two phases: the  $[001]$  of the hexagonal  $\text{Mg}(\text{OH})_2$  crystal transforms into  $[111]$  of the cubic  $\text{MgO}$  and the  $[110]$  of  $\text{Mg}(\text{OH})_2$  becomes  $[110]$  of  $\text{MgO}$ . As  $\text{Fe}(\text{OH})_2$  is very unstable, it was not possible to study the oriented relationship between  $\text{Fe}(\text{OH})_2$  and  $\text{FeO}$  using single crystal. From the fact that both  $\text{Mg}(\text{OH})_2$  and  $\text{Fe}(\text{OH})_2$  have the same structure ( $\text{CdI}_2$  type) and also from the similarity between the  $\text{MgO}$  and  $\text{FeO}$  structure ( $\text{NaCl}$  type), it seems reasonable to think that in the transformation of  $\text{Fe}(\text{OH})_2 \rightarrow \text{FeO}$ , the same type of oriented relationship occurs. Fig. 1 shows how two hydroxyl layers in  $\text{Fe}(\text{OH})_2$  could combine together to form a single

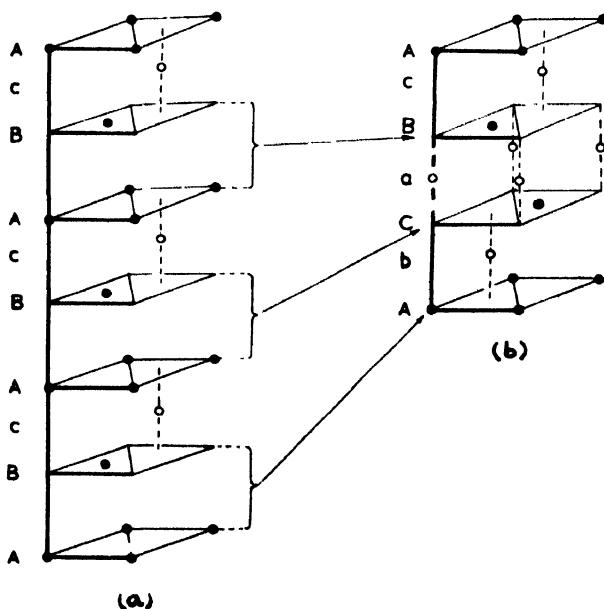


Fig. 1 Transformation of  $\text{Fe}(\text{OH})_2 \rightarrow \text{FeO}$ .

- (a) The arrangement of hydroxyl layers along  $[001]$  of  $\text{Fe}(\text{OH})_2$   
 (b) The arrangement of oxygen layers along  $[111]$  of  $\text{FeO}$ .

layer of oxygen in FeO. The oriented relationship which occurs between FeO and Fe<sub>3</sub>O<sub>4</sub> has been discussed later on.

(b) *Delta ferric oxyhydroxide* ( $\delta$ -FeO.OH)

Fe(OH)<sub>2</sub> in alkaline solution, when oxidised by air or oxygen, transforms into  $\alpha$ -FeO.OH. The possibility of oriented relationship between Fe(OH)<sub>2</sub> and  $\alpha$ -FeO.OH has been reported by Francombe and Rookshy (1959).

Glemser and Gwinner (1939) reported that Fe(OH)<sub>2</sub>, when oxidised by H<sub>2</sub>O<sub>2</sub> or (NH<sub>4</sub>)<sub>2</sub>S<sub>2</sub>O<sub>8</sub> in excess, transformed into a ferromagnetic compound, which they called  $\delta$ -Fe<sub>2</sub>O<sub>3</sub>. The X-ray photograph of this  $\delta$ -Fe<sub>2</sub>O<sub>3</sub> was interpreted by them in terms of a hexagonal cell with axial parameters  $a = 5.09 \text{ \AA}$  and  $c = 4.41 \text{ \AA}$ . This particular compound was studied by us in great detail and found not to be an anhydrous oxide of iron but an oxyhydroxide (FeO.OH). Moreover, the X-ray diffraction photograph was indexed in terms of a smaller hexagonal cell with  $a = 2.941 \pm 0.005 \text{ \AA}$  and  $c = 4.49 \pm 0.01 \text{ \AA}$  (Bernal, Dasgupta and Mackay, 1959).

Though stable at room temperature,  $\delta$ -FeO.OH could not be obtained in the form of a single crystal. Hydrothermal treatment was attempted but it was found that when powdered  $\delta$ -FeO.OH was heated in a bomb at 100°C, it was converted into  $\alpha$ -Fe<sub>2</sub>O<sub>3</sub>. From the similarity of the powder pattern and axial parameters of  $\delta$ -FeO.OH and Fe(OH)<sub>2</sub> and also from the fact that the pattern of  $\delta$ -FeO.OH could be obtained from that of  $\alpha$ -Fe<sub>2</sub>O<sub>3</sub> by choosing lines with  $l$  indices divisible by 3, it seems reasonable that the structure of  $\delta$ -FeO.OH is intermediate between those of Fe(OH)<sub>2</sub> and  $\alpha$ -Fe<sub>2</sub>O<sub>3</sub>. It should be pointed out here that in Fe(OH)<sub>2</sub>, OH layers have Fe on one side of it, whereas on the other side they are connected to another OH layer by hydroxyl bonds. But in  $\alpha$ -Fe<sub>2</sub>O<sub>3</sub>, the hexagonal close-packed oxygen layers have Fe, in the octahedral sites, on both the sides. The striking feature of the powder pattern of  $\delta$ -FeO.OH is the very weak (often absent) (001) reflection. This suggests that iron must be in the octahedral position on both sides of the close packed O'/OH' layers. The density of  $\delta$ -FeO.OH allows only one formula unit in the unit cell. The number of iron in the unit cell is thus one. To satisfy the condition for the 001 reflection, half of this iron should occupy the octahedral position on side of the closepacked layer, the other half being placed at the octahedral side on the other side of the layer. Fig. 2. shows the probable structure of  $\delta$ -FeOH compared to that of Fe(OH)<sub>2</sub>.

Feitknecht (1943) observed a similar type of structure for Cd(OH)F, where Cd<sup>++</sup> ions are distributed equally between two octahedral sites between two hexagonal close-packed layers of mixed OH' and F' ions. However, in the case of  $\delta$ -FeO.OH a better agreement between the observed and calculated intensities was found when 78% of the total iron was placed equally at the two octahedral sites (0,0,0; 0, 0,  $\frac{1}{2}$ ) and the remaining part of iron in the four tetrahedral positions at  $\pm(1/3, 2/3, 1/8)$  and  $\pm(2/3, 1/3, 3/8)$ .

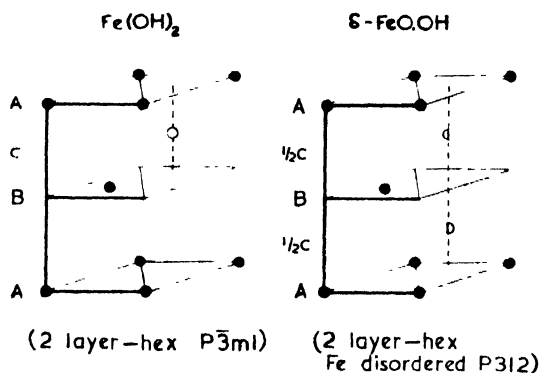


Fig. 2 Comparison of  $\text{Fe(OH)}_2$  and  $\delta\text{-FeO.OH}$  structure, the layers being shown along [001] axes.

(c) *The basic ferrous complexes*

When alkali insufficient to allow the complete precipitation of  $\text{Fe(OH)}_2$  is added to ferrous salt solution a series of unstable complexes of ferrous salts are formed. Keller (1948) reported three basic chlorides obtained by partial precipitation from  $\text{FeCl}_2$  with various concentrations of alkali. The basic complexes and their transformation on oxidation or dehydration have been studied by (1959). Of these complexes two are from  $\text{FeCl}_2$  solution and the other from  $\text{FeSO}_4$  solutions, are of great importance as they, on oxidation transform into  $\gamma\text{-FeO.OH}$ . These two complexes have been referred as green rust I and II respectively. The green rust I was found to belong to the hexagonal crystal system but the axial parameters varies for different preparations as follows :

- (i)  $a = 3.198 \pm 0.005 \text{ \AA}$ ,  $c = 24.21 \pm 0.01 \text{ \AA}$  from  $\text{FeCl}_2$
- (ii)  $a = 3.23 \pm 0.01 \text{ \AA}$ ,  $c = 22.50 \pm 0.01 \text{ \AA}$  from  $\text{FeSO}_4$
- (iii)  $a = 3.18 \pm 0.01 \text{ \AA}$ ,  $c = 22.80 \pm 0.01 \text{ \AA}$  from  $\text{FeBr}_2$ .

During oxidation green rust I, prepared from  $\text{FeSO}_4$  solution, passed through another phase before being finally converted into  $\gamma\text{-FeO.OH}$ . This phase, termed as green rust II, also belongs to hexagonal crystal system with  $a = 3.17 \pm 0.01 \text{ \AA}$  and  $c = 10.90 \pm 0.01 \text{ \AA}$ .

Due to the instability of the green rusts it was not possible to make a complete study of their structures. However, from the dimensions of their axial lengths and the nature of the layer structures of almost all the oxides and hydroxides of iron some speculations can be made as to their structures in terms of the packing of equal spheres, if the following assumptions are made.

- (i) Hexagonal layers of anions ( $\text{O}^{2-}$  or  $\text{OH}^-$ ) are stacked so that regular tetrahedra fill the space. The layer distance is thus  $0.817a$  where  $a$  is the diameter of the anion.

(ii) There will be empty tetrahedral and octahedral sites available for cations. There is no great distortion of the structure in filling these and the consideration is restricted only to the octahedral holes.

(iii) The sharing of faces by co-ordination octahedra (or tetrahedra) round the cation is rejected (Pauling's rule).

(iv) The compounds are all stoichiometric. There are then only the following number of possibilities of stacking, where A, B, C denote the anions at  $(0, 0, Z)$ ;  $(1/3, 2/3, Z)$  and  $a, b, c$  denote the anions with the same co-ordinates.

(a) 2 layers: Composition  $\text{AO}_2$ ; sequence of layers  $\text{AcB}-\text{A}$  ( $c = 1.633a$  hexagonal)

(b) 3 layers: (i) composition  $\text{AO}$ ; sequence of layers  $\text{AcBaCbA}$  (cubic  $a = 1.414a$ ), (ii) composition  $\text{A}_2\text{O}_3$ ; sequence of layers,  $\text{AcBbC}-\text{A}$  ( $c = 2.45a$  hexagonal), (iii) composition  $\text{AO}_3$ ; sequence of layers  $\text{AcB}-\text{C}-\text{A}$  ( $c = 2.45a$  hexagonal).

(c) 4 layers: composition  $\text{A}_2\text{O}_4$ ; sequence of layers  $\text{AcB}-\text{AbC}-\text{A}$  or  $\text{A}-\text{BcAbC}-\text{A}$  ( $c = 3.27a$  hexagonal).

(d) 6 layers: composition  $\text{AO}_2$ ; sequence of layers  $\text{AcB}-\text{cbA}-\text{BaC}-\text{A}$ . ( $c = 4.90a$ , rhombohedral).

(e) 9 layers: composition  $\text{A}_2\text{O}_3$ ; sequence of layers  $\text{AcBaC}-\text{BaCbA}-\text{CbAcB}-\text{A}$  (rhombohedral); composition  $\text{AO}_3$ ; sequence of layers  $\text{AcB}-\text{C}-\text{BaC}-\text{BaC}-\text{A}-\text{CbA}-\text{A}$  or  $\text{A}-\text{B}-\text{CbA}-\text{C}-\text{AbC}-\text{BcA}$  ( $c = 7.35a$ , rhombohedral).

From the above considerations, it appears that as a first approximation the green rust I has the 9-layers rhombohedral structure ( $c/a = 7.2$  observed) and green rust II has a 4-layers structure ( $c/a = 3.4$  observed). Fig. 3 shows the possible structures of green rust I and II based on these assumptions.

(d)  $\alpha$  and  $\gamma$ -Ferric oxyhydroxides ( $\alpha$  and  $\gamma$ - $\text{FeO.OH}$ )

These two oxyhydroxides of iron occur as natural mineral Goethite and Lepidiscite respectively. Synthetically, Goethite ( $\alpha$ - $\text{FeO.OH}$ ) can be prepared by oxidising the green rusts. There are also other methods of preparation of these two oxyhydroxides synthetically.

$\alpha$ - $\text{FeO.OH}$  transforms into  $\alpha$ - $\text{Fe}_2\text{O}_3$  on dehydration. Goldsztaub (1931), while studying the transformation of single crystals of  $\alpha$ - $\text{FeO.OH}$  into  $\alpha$ - $\text{Fe}_2\text{O}_3$ , found an oriented relationship between them. He showed that the  $[100]$ ,  $[010]$  and  $[001]$  axes of the orthorhombic cell of  $\alpha$ - $\text{FeO.OH}$  transformed into  $[111]$ ,  $[110]$  and  $[112]$  axes respectively of the rhombohedral cell of  $\alpha$ - $\text{Fe}_2\text{O}_3$ .

$\gamma$ - $\text{FeO.OH}$ , on the other hand, transforms into  $\gamma$ - $\text{Fe}_2\text{O}_3$  on dehydration and then to  $\alpha$ - $\text{Fe}_2\text{O}_3$  on further heating. The transformation of  $\gamma$ - $\text{FeO.OH} \rightarrow \gamma$ - $\text{Fe}_2\text{O}_3 \rightarrow \alpha$ - $\text{Fe}_2\text{O}_3$  was studied by us (Bernal, Dasgupta and Mackay, 1957) using single

crystals of  $\gamma\text{-FeO.OH}$ . It was found that  $\gamma\text{-Fe}_2\text{O}_3$  crystals are formed with their [001], [110] and [110] axes parallel to [100] [010] and [001] axes respectively of

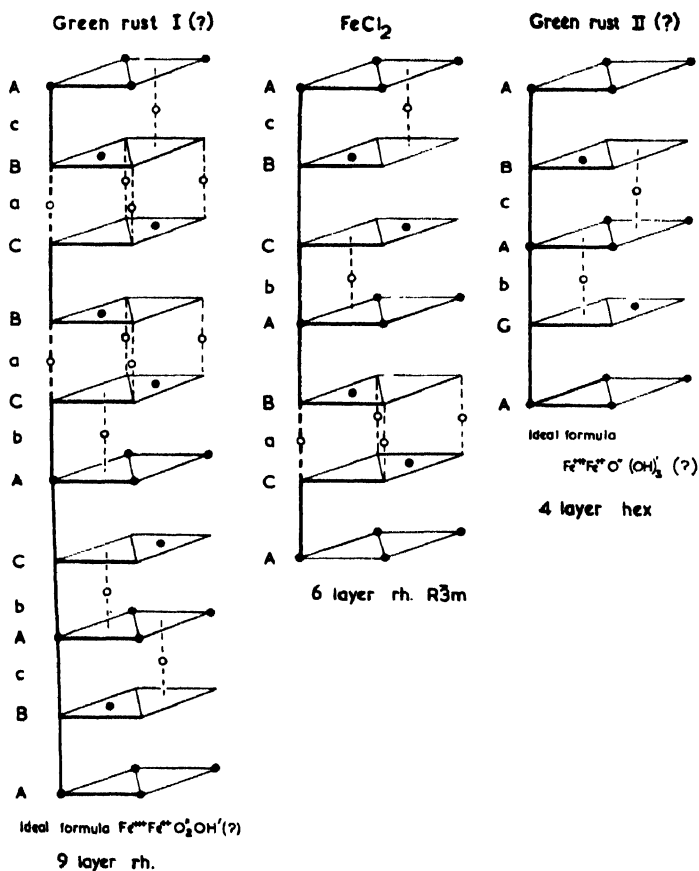


Fig. 3 Proposed structures of green rust I & II.

$\gamma\text{-FeO.OH}$ . That the [100] of  $\gamma\text{-FeO.OH}$  is parallel to one of the cubic axes [001] of  $\gamma\text{-Fe}_2\text{O}_3$  could be seen from the X-ray photograph (Plate VIIIA, Fig. 4(a)(b)). In the second transition from  $\gamma\text{-Fe}_2\text{O}_3$  to  $\alpha\text{-Fe}_2\text{O}_3$ , crystals of the latter grow with their [001] axes parallel to [111] direction of  $\alpha\text{-Fe}_2\text{O}_3$  and their [110] directions being parallel to the [110] directions of  $\alpha\text{-Fe}_2\text{O}_3$  Fig. 6.

The mechanism of the transformation can be explained as follows. Fig. 7 shows the similarity between  $\gamma\text{-FeO.OH}$  and  $\gamma\text{-Fe}_2\text{O}_3$  (spinel type) structures. The transition would require the removal of half of the hydroxyl group together with the hydrogen in the adjoining hydroxyl sheet, as water molecules. This is followed closing up of the (010) layers from  $12.57\text{\AA}$  to  $8.85\text{\AA}$ , that is, by 30% or  $1.86\text{\AA}$  per layer in the [010] direction of  $\gamma\text{-FeO.OH}$ . There is also a shift of half an



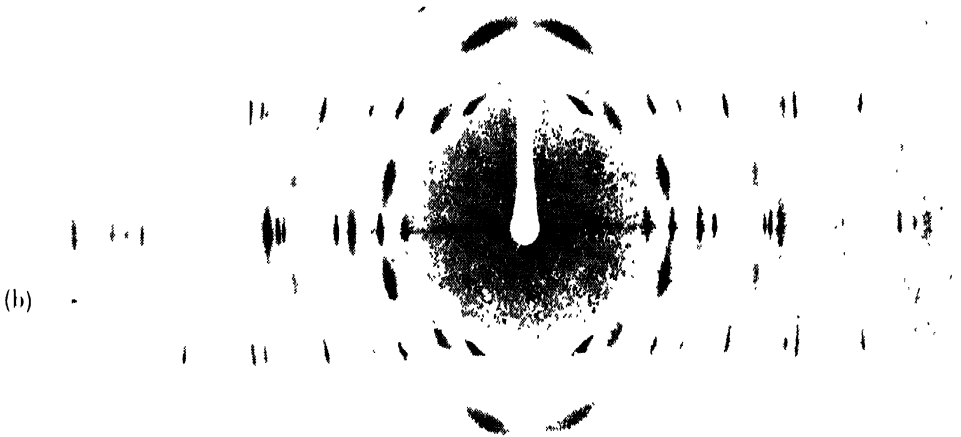
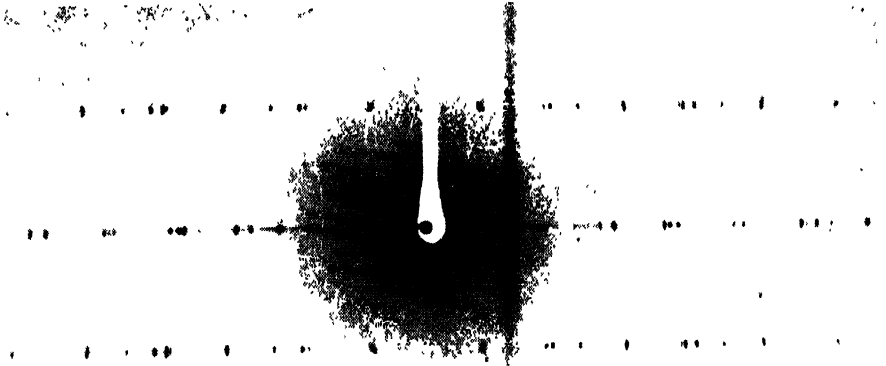


Fig. 4(a) Single crystal X-ray rotation photograph of  $\gamma\text{-FeO}$  taken along  $[100]$ .

Fig. 4(b) Rotation photograph of a single crystal of  $\gamma\text{-FeO.OH}$  heated at  $250^\circ\text{C}$  for 3 hrs, showing the transformation  $\gamma\text{-FeO.OH} \rightarrow \gamma\text{-Fe}_2\text{O}_3$ . The sharp spots correspond to unchanged  $\gamma\text{-FeO.OH}$  and the diffuse spots to  $\gamma\text{-Fe}_2\text{O}_3$ . The photograph was taken along the  $[100]$  axis of  $\gamma\text{-FeO.OH}$  and that corresponds to  $[001]$  axis of  $\gamma\text{-Fe}_2\text{O}_3$ .

(c)

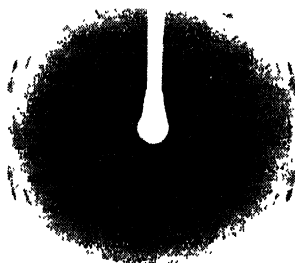


Fig. 4(c) Rotation photograph of single crystal of  $\gamma\text{-Fe}_2\text{O}_3$  heated to  $250^\circ\text{C}$  for 24 hrs showing the transformation of  $\gamma\text{-Fe}_2\text{O}_3 \rightarrow \alpha\text{-Fe}_2\text{O}_3$ . The sharp spots are due to  $\alpha\text{-Fe}_2\text{O}_3$  and the diffuse spots are due to  $\gamma\text{-Fe}_2\text{O}_3$ .



Fig. 5. Single crystal X-ray rotation photograph of  $\text{Fe}_3\text{O}_4$  heated to  $600^\circ\text{C}$  for 26 hrs. taken along  $[100]$  of  $\text{Fe}_3\text{O}_4$ . The sharp spots are due to  $\text{Fe}_3\text{O}_4$ , while the weaker spots are due to  $\gamma\text{-Fe}_2\text{O}_3$ .

oxygen ion width (1.94 Å) in the [100] direction. The resulting strain due to the shift may explain the disorder in the  $\gamma\text{-Fe}_2\text{O}_3$  crystal (diffuseness of the spots). From the fact that the  $\alpha\text{-Fe}_2\text{O}_3$  crystals are oriented with respect to those of  $\gamma\text{-Fe}_2\text{O}_3$  and not to those of  $\gamma\text{-FeO.OH}$ , it seems reasonable to think that the formation of  $\alpha\text{-Fe}_2\text{O}_3$  is subsequent to that of  $\gamma\text{-Fe}_2\text{O}_3$ . This transformation does not involve any loss or gain of material but only a restacking of close-packed oxygen atoms (cubic to hexagonal) on the {111} faces of  $\gamma\text{-Fe}_2\text{O}_3$  (Fig. 6).

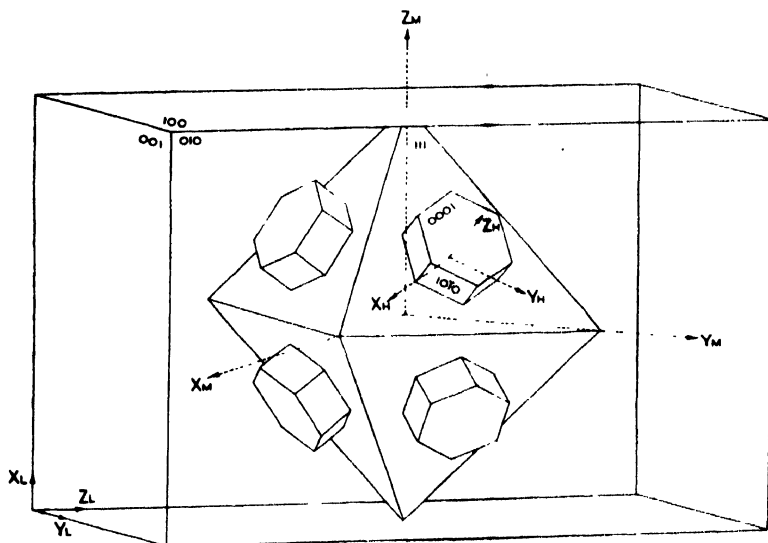


Fig. 6 Epitaxial relationship in the transformation  $\gamma\text{-FeO.OH} \rightarrow \gamma\text{-Fe}_2\text{O}_3 \rightarrow \alpha\text{-Fe}_2\text{O}_3$ .  
Lepidocrocite                      Magnetite                      Haematite

(c) *Magnetite* ( $\text{Fe}_3\text{O}_4$ ) and *Magnetite* ( $\gamma\text{-Fe}_2\text{O}_3$ )

The most important ferrite, Magnetite ( $\text{Fe}_3\text{O}_4$ ), which may be written as  $\text{FeO.Fe}_2\text{O}_3$ , is the only certain oxide intermediate between ferrous and ferric oxides. Magnetite was known from very early ages to be one of the few ferromagnetic compounds as natural mineral. Magnetite which is cubic (face-centred) transforms into  $\gamma\text{-Fe}_2\text{O}_3$  (cubic) on oxidation.  $\gamma\text{-Fe}_2\text{O}_3$ , on further heating, transforms into  $\alpha\text{-Fe}_2\text{O}_3$  (hexagonal). The transition of  $\text{Fe}_3\text{O}_4 \rightarrow \gamma\text{-Fe}_2\text{O}_3 \rightarrow \alpha\text{-Fe}_2\text{O}_3$  brought up by heating magnetite in air has been studied by several workers. It was found that synthetic magnetite transformed more easily into  $\gamma\text{-Fe}_2\text{O}_3$  than the natural magnetite. While oxidising synthetic magnetite, it was found that there are four forms of  $\gamma\text{-Fe}_2\text{O}_3$ . Three of them belong to the cubic system, while the other belong to the tetragonal system (Bernal, Dasgupta and Mackay, 1959; Van Oosterhout and Rooymans, 1958). The oxidation of  $\text{Fe}_3\text{O}_4$  on heating has received considerable attention largely because of the difference in the behaviour of the natural and synthetic  $\text{Fe}_3\text{O}_4$ . Experimental

works of Schmidt and Vermaas (1955), Lepp (1957) and of many others showed that synthetic  $\text{Fe}_3\text{O}_4$  oxidised first to  $\gamma\text{-Fe}_2\text{O}_3$  and then to  $\alpha\text{-Fe}_2\text{O}_3$ , whereas natural  $\text{Fe}_3\text{O}_4$  oxidised only to  $\alpha\text{-Fe}_2\text{O}_3$  usually at a high temperature. Our X-ray study on the natural single crystal of  $\text{Fe}_3\text{O}_4$  also confirmed this observation, Plate VIIIB, Fig. 5. The early workers found, on oxidation of  $\text{Fe}_3\text{O}_4$  to  $\gamma\text{-Fe}_2\text{O}_3$ , that some extra lines appeared in the X-ray photographs, the general pattern remaining the same. It was found that those extra lines could be accounted for if  $\gamma\text{-Fe}_2\text{O}_3$  had a primitive cell ( $\text{Fe}_3\text{O}_4$  is face-centred cubic) of the approximate dimensions of  $\text{Fe}_3\text{O}_4$ . In recent years, various workers have expressed doubts about the structure of  $\gamma\text{-Fe}_2\text{O}_3$ , which was proposed by Thewlis (1931). Hagg (1953) from his X-ray diffraction study of  $\gamma\text{-Fe}_2\text{O}_3$  concluded that the changes in the intensities of the diffraction lines and also in the density of  $\gamma\text{-Fe}_2\text{O}_3$ , from those of  $\text{Fe}_3\text{O}_4$ , were produced by the vacant sites in the iron atom lattice in the spinel phase rather than by the addition of oxygen. The suggested structure for  $\gamma\text{-Fe}_2\text{O}_3$  was a defect spinel with cation vacancies in an oxygen ion frame work. Hence, when  $\text{Fe}_3\text{O}_4$  is written as  $\text{Fe}_8^{++}\text{Fe}_{16}^{+++}\text{O}_{32}^{--}$ ,  $\gamma\text{-Fe}_2\text{O}_3$  can be written as  $\text{Fe}^{++1+}_{21.33}\square_{2.67}\text{O}_{32}^{--}$  where  $\square_{2.67}$  denotes cation vacancies. Verwey (1935) also suggested a similar structure where the vacancies were preferentially located at the octahedral sites

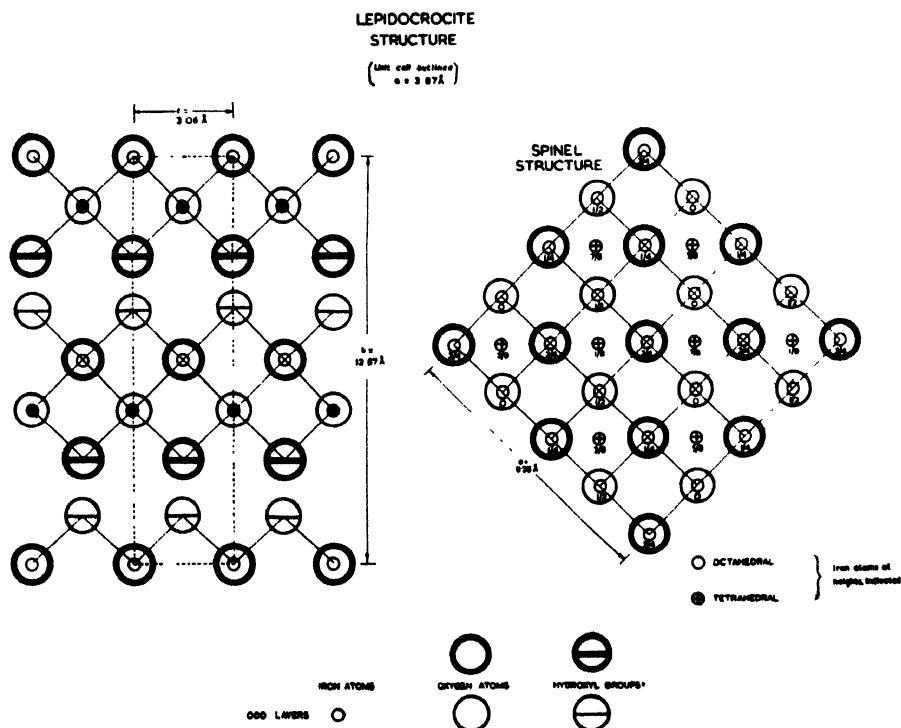


Fig. 7 Similarity of the  $\gamma\text{-FeO.OH}$  and  $\gamma\text{-Fe}_2\text{O}_3$  (spinel) structures.

for Fe. This was supported by Henry and Boehm (1955) from their measurements of magnetic moment and also by Ferguson and Hass (1958) from their neutron diffraction study of  $\gamma\text{-Fe}_2\text{O}_3$ .

Since 1935, it has been generally accepted that  $\gamma\text{-Fe}_2\text{O}_3$  is cubic with  $10\frac{2}{3}$  molecules of  $\gamma\text{-Fe}_2\text{O}_3$  in the unit cell. Van Oosterhout and Rooyman (1958) have shown that in  $\gamma\text{-Fe}_2\text{O}_3$ , prepared by decomposing ferrous oxalate dihydrate in an atmosphere of steam and nitrogen followed by an oxidation at  $250^\circ\text{C}$ , some extralines appeared in the x-ray photographs. It has been possible for them to assign indices to all these extra lines using a tetragonal cell having  $c = 3a$  with  $a$  same as that of the cubic cell. The new cell provides 32 molecules of  $\gamma\text{-Fe}_2\text{O}_3$  instead of  $10\frac{2}{3}$  in the cubic cell. It is seen that the structure of  $\gamma\text{-Fe}_2\text{O}_3$  can be obtained from that of  $\text{Fe}_3\text{O}_4$ , when there is deficiency of Fe atoms in the octahedral sites of  $\text{Fe}_3\text{O}_4$  structure. The relationship between  $\text{Fe}_3\text{O}_4$  (or  $\gamma\text{-Fe}_2\text{O}_3$ )

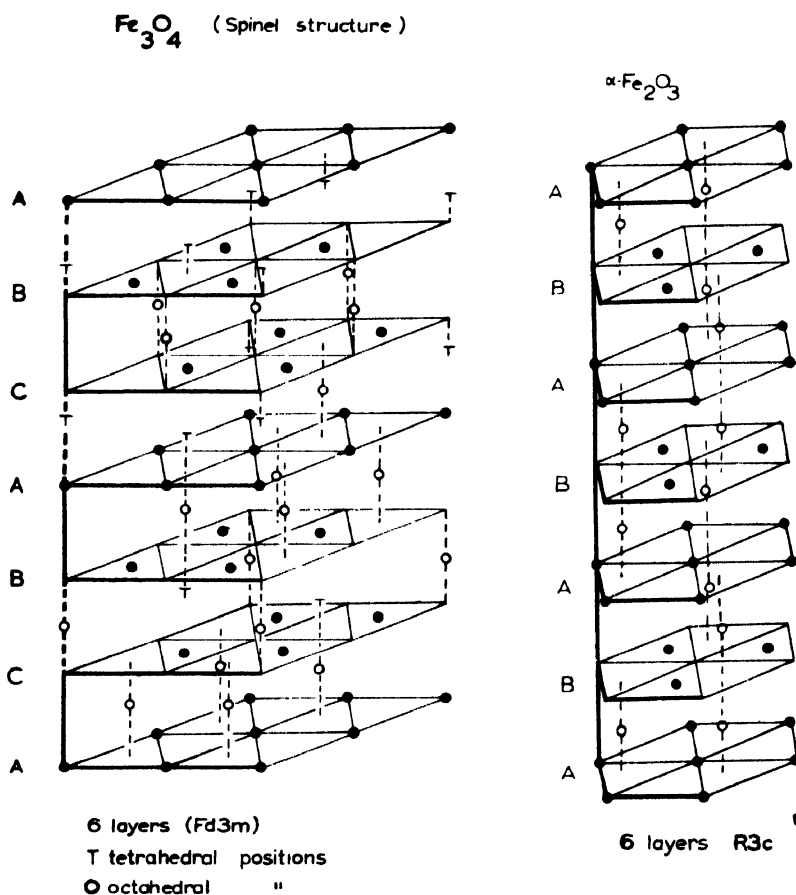


Fig. 8. Structural relationship between  $\text{Fe}_3\text{O}_4$  and  $\alpha\text{-Fe}_2\text{O}_3$  along their [111] and [001] axes respectively.

and  $\alpha$ - $\text{Fe}_2\text{O}_3$  structures has already been explained earlier and is shown diagrammatically in Fig. 8.

(f) *Siderite or  $\text{FeCO}_3$ .*

Though  $\text{FeCO}_3$  does not fall in the iron oxide and oxyhydroxide series, yet it has been included in the present paper as it decomposes into  $\text{FeO}$  and  $\text{Fe}_3\text{O}_4$  when heated at high temperature.

Single crystal of  $\text{FeCO}_3$  was heated in a sealed tube to  $550^\circ\text{C}$ . At that temperature it was not magnetic but on cooling it becomes highly magnetic. Though this magnetism was accompanied by a change of colour, the crystal retained its original sharp edged rhombohedral form. The faces of the crystal appeared to be very rough when viewed with a high power microscope. An X-ray photograph taken with the heated crystal rotating along the apparent  $[110]$  axis shows it to be transformed into  $\text{FeO}$  and  $\text{Fe}_3\text{O}_4$ , both of them having an oriented relationship with the original crystal. From the measurement of the X-ray photograph, it was seen that there was no unchanged  $\text{FeCO}_3$  or  $\text{Fe}$ . The indices of the spots along the zero layer line shows that the cubic phases ( $\text{FeO}$  and  $\text{Fe}_3\text{O}_4$ ) are oriented parallel to each other. The diad axis of the  $\text{FeCO}_3$  crystal becomes one of the diad axes of  $\text{FeO}$  and  $\text{Fe}_3\text{O}_4$ . The oriented relationship between  $\text{FeO}$  and  $\text{Fe}_3\text{O}_4$  can be easily understood from the similarity of their structures. (Fig. 9).

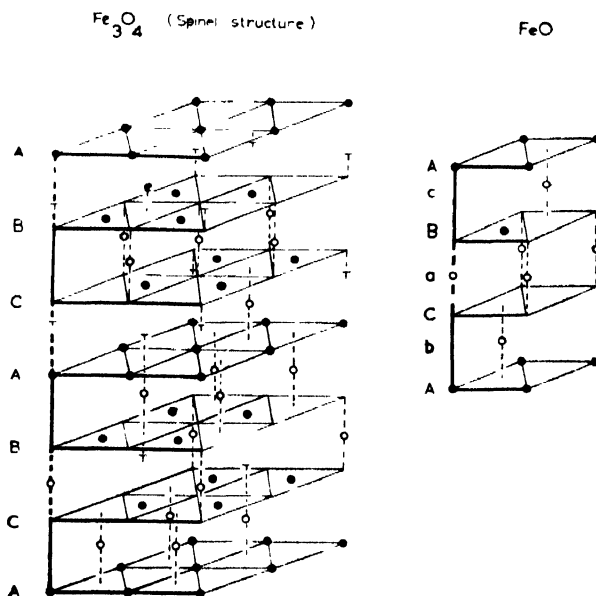


Fig. 9. Similarities between  $\text{FeO}$  and  $\text{Fe}_3\text{O}_4$  structures showing the close-packed oxygen layers along the  $[111]$  directions.

The structure of  $\text{FeCO}_3$  (rhombohedral), which is shown in Fig. 10, is not very different from those of  $\text{NaCl}$  or  $\text{FeO}$ . The  $\text{FeO}$  lattice compressed along  $[111]$

axis would flatten out to become rhombohedral and make room for disc-shaped  $\text{CO}_3$  ions in place of spherical O ions. So, it appears that  $\text{FeO}$  must derive from  $\text{FeCO}_3$  simply by expulsion of  $\text{CO}_2$  and change of angles between the sheet of atoms from  $72^\circ$  to  $90^\circ$ . The similarity also suggests that the triad axis of  $\text{FeCO}_3$  will be parallel to one of the triad axes of the cubic crystal and that the three diad axes of both phases are interchanged. It is most remarkable that in spite of the loss of more than half of the oxygen atoms from the structure, the orientation is still preserved.

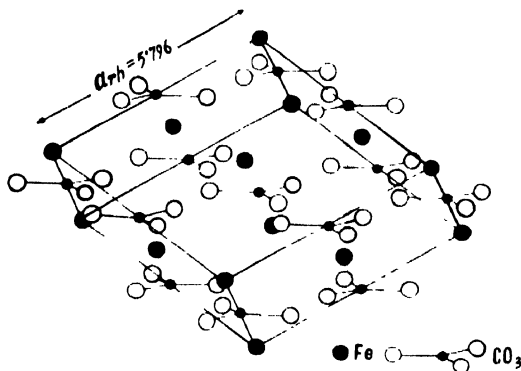


Fig. 10. structure of  $\text{FeCO}_3$ .

(g)  *$\beta$ -Ferric oxyhydroxide ( $\beta\text{-FeO.OH}$ )*

Weiser and Milligan (1935) reported this oxyhydroxide of iron. They found that when  $\text{FeCl}_3$  was hydrolysed at  $95^\circ\text{C}$  for 6 hrs. the resultant brown precipitate was quite different from any of the existing oxides or oxyhydroxides of iron. From their dehydration isobar study, they concluded that it was a monohydrate of iron oxide ( $\text{Fe}_2\text{O}_3$ ,  $\text{H}_2\text{O}$  or  $\text{FeO.OH}$ ). In the present study it was found that not only  $\text{FeCl}_3$ , but  $\text{FeF}_3$  and also any other ferric salts in presence of  $\text{Cl}^-$  or  $\text{F}^-$  ions gave  $\beta\text{-FeO.OH}$  on hydrolysis. Kratky and Nowotny (1938) tried to index all the lines of the powder diffraction pattern of  $\beta\text{-FeO.OH}$  in terms of an orthorhombic cell with  $a = 10.46\text{ \AA}$ ,  $b = 10.24\text{ \AA}$  and  $c = 2.34\text{ \AA}$ . During the present investigation, it was found that all the lines in the powder photograph could be indexed in terms of a tetragonal cell with  $a = 10.48 \pm 0.01\text{ \AA}$  and  $c = 3.023 \pm 0.005\text{ \AA}$ . It will be worthwhile to mention here that no close pairs, such as (200, 020), (400, 040) were observed which could distinguish  $\beta\text{-FeO.OH}$ , as belonging to the orthorhombic crystal class.

As it was not possible to obtain any single crystals of  $\beta\text{-FeO.OH}$ , no detailed structure analysis could be carried out. Recently, Bystrom and Brystrom (1950) have determined the structure of the mineral hollandite and the related manganese oxide minerals.  $\alpha\text{-MnO}_2$  is tetragonal with  $a = 9.8\text{ \AA}$  and  $c = 2.86\text{ \AA}$  and Hollandite has a pseudotetragonal cell with  $a = 9.96 \pm 0.05\text{ \AA}$  and  $c = 2.86 \pm 0.01\text{ \AA}$ . The systematic absences in the case of hollandite are

the reflections with  $h+k+l \neq 2n$ . From the similarity of the powder pattern, axial lengths and the conditions for reflection (for  $\beta$ -FeO.OH,  $h+k+l \neq 2n$ ), it seems that the two structures are similar. Fig. 11 shows the structure of Hollandite projected on (001). It can be seen that the metal ions are at the centre of the  $\text{MO}_6$  octahedra and there are open channels parallel to  $c$  axis. In the case of Hollandite,  $\text{Ba}^{++}$  ions (its diameter being greater than the length of  $c$  axis) are distributed along these channels statistically. From the fact that the percentages of  $\text{Cl}^-$  or  $\text{F}^-$  ions, which are essential for the formation of  $\beta$ -FeO.OH, are not constant in  $\beta$ -FeO.OH, it is highly probable that in case of  $\beta$ -FeO.OH, also  $\text{Cl}^-$  or  $\text{F}^-$  ions enter the structure but are not present stoichiometrically. It appears that the  $\text{Fe}^{+++}$  ions, in the case of  $\beta$ -FeO.OH, should be at the centre of  $\text{Fe}(\text{O}, \text{OH})_6$  octahedra whereas the  $\text{Cl}^-$  or  $\text{F}^-$  ions are distributed statistically along the channel parallel to the  $c$  axis.

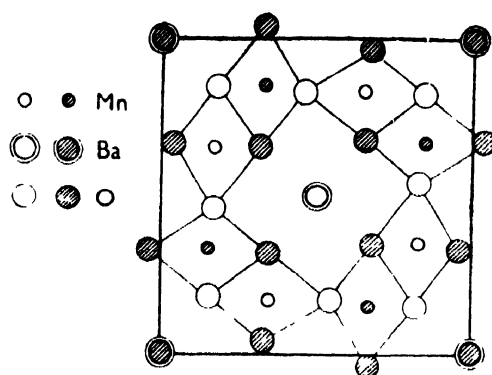


Fig. 11. Structure of Hollandite, open circles denote ions at  $Z = 0$  and the filled circles at  $Z = \frac{1}{2}$ .

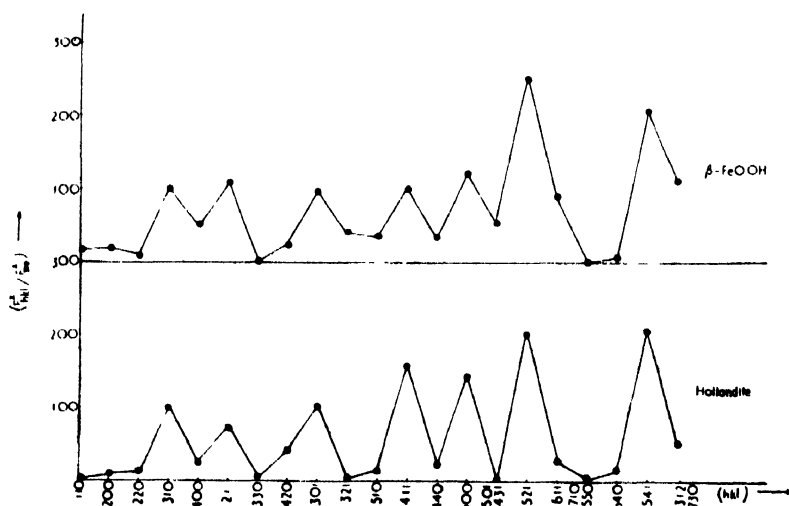


Fig. 12. Comparison of  $F^2_{hk}/F^2_{31}$  values for Hollandite and  $\beta$ -FeO.OH.



The diameter of the  $\text{Cl}^-$  ion (3.62 Å) is greater than the  $c$  dimension of  $\beta\text{-FeO}$ . OH ( $3.023 \pm 0.005$  Å). This also suggests that Cl cannot be present in the structure stoichiometrically. The reason that  $\beta\text{-FeO.OH}$  could not be prepared from any ferric salt containing Br<sup>-</sup> ions can be explained by the fact that the diameter of  $\text{Br}^-$  ion (3.90 Å) is too big for being placed along the  $c$  axis of  $\beta\text{-FeO.OH}$ . Moreover, the similarity between the curves for  $F_{hkl}^2/F_{310}^2$  ratio of Hollandite (calculated) and  $\beta\text{-FeO.OH}$  (observed), as shown in Fig. 12, also suggests a similarity between the two structures.

#### DISCUSSION

From the present study of iron oxides and hydroxides it seems quite evident that there are two definite series. The starting point of one series is the white  $\text{Fe(OH)}_2$  and the basic ferrous salts, prepared by adding insufficient alkali, give rise to the other series. Most of the oxides and oxyhydroxides are the result of oxidation or dehydration of  $\text{Fe(OH)}_2$ .  $\gamma\text{-FeO.OH}$ , which could not be prepared from  $\text{Fe(OH)}_2$  in any way, definitely belongs to the other series.

The formations and transformations of almost all the oxides and oxyhydroxides of iron can now be well represented by the Fig. 13. It is quite certain that all of them except  $\beta\text{-FeO.OH}$  are built up of close-packed oxygen layers and the nature of packing depends upon the structures of the individual phases. Fig. 13 shows the different form of transformations from one phase to another. As has been described in earlier chapters, the nature of all these transformations suggest that they take place, not by the complete breakdown of the structures of the origin phases but by simple shifting and re-stacking the different layers in the original structures. These observations naturally support the idea that whenever the steric conditions permit, solid state transformation, even if a large amount of the material is lost from the system, can proceed by a minimum rearrangement of the structures of the single crystals, involving little more than the mechanisms of dislocation glides, such as producing stacking faults and twinning.

The most interesting feature of the different members of the iron oxides and hydroxides groups is that most of them are built up of hexagonal close-packed or cubic close-packed layers of oxygen and hydroxyl ions. The sequences of the layers may be represented by ABABAB... or ABCABCABC... respectively. In some cases, some slight variations in the stacking of layers other than the conventional ones are possible.

$\text{Fe(OH)}_2$  is built up of hexagonal close-packed layers, the sequence of the layers being  $\text{AcB-AcB}$ , where the capital letters denote the positions of the anions and the small letters denote the position of the cation. When it changes into  $\delta\text{-FeO.OH}$ , on oxidation by strong oxidant, there is no substantial change in the arrangement of layers. As it can be seen from the proposed structure for  $\delta\text{-}$

$\text{FeO} \cdot \text{OH}$ , the arrangement of layers is the same as that of  $\text{Fe}(\text{OH})_2$ . The difference in the two structures is that in  $\delta\text{-FeO} \cdot \text{OH}$  the one H ion must leave the lattice and

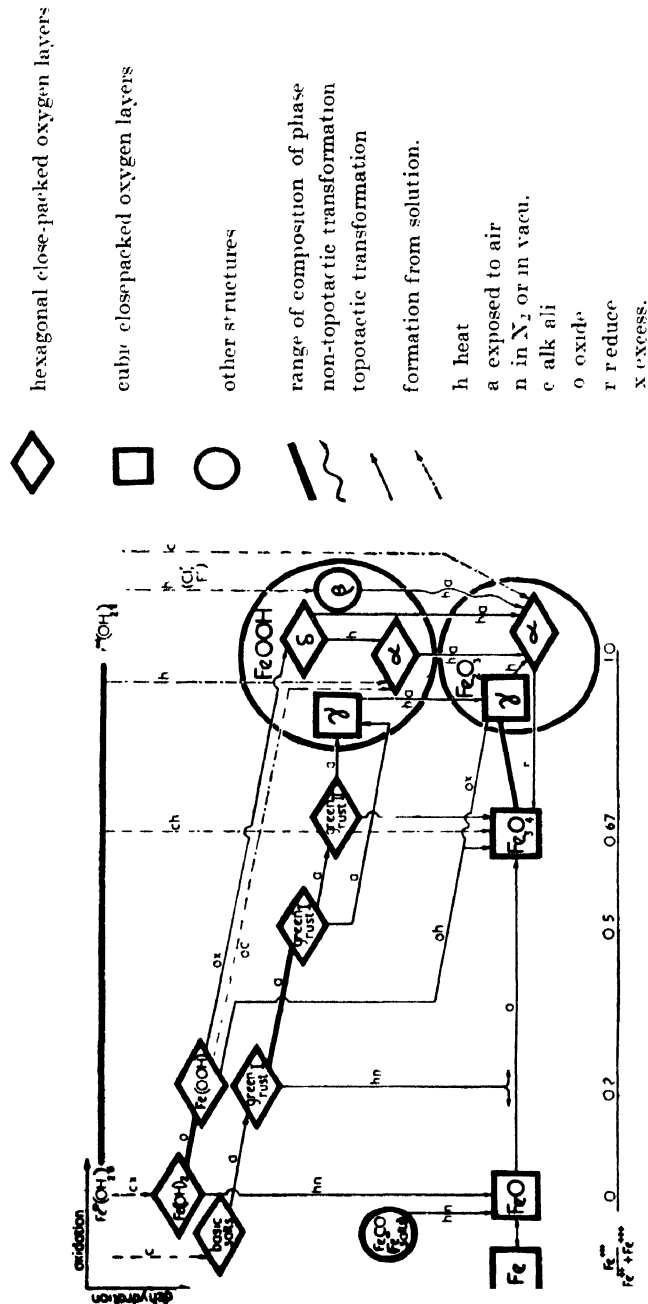


Fig. 13. Structural transformation in the iron oxide/hydroxide system.

the iron ion is divided into two parts so that the two octahedral positions between the oxygen and hydroxyl layers may be occupied. Thus, from the sequence AcB-AcB in  $\text{Fe(OH)}_2$  it changes into  $A\frac{1}{2}cB\frac{1}{2}cA\dots$  in  $\delta\text{-FeO.OH}$ . Again, in the transformation of  $\text{Fe(OH)}_2 \rightarrow \text{FeO}$ , it can be seen that the two hydroxyl layers in the former give up hydrogen in the form of water and form a single layer of oxygen in FeO. Here the hexagonal close-packed layers in  $\text{Fe(OH)}_2$  transform into cubic close-packed layers in FeO, the original [001] axis of  $\text{Fe(OH)}_2$  becoming the [111] axis of FeO. The transformation of  $\text{FeO} \rightarrow \text{Fe}_3\text{O}_4$  can also be explained in terms of topotaxy. The addition of extra oxygen to FeO does not make any substantial change in the original structure so far as the stacking of the oxygen layers except changing the axial lengths (the axial lengths of  $\text{Fe}_3\text{O}_4$  are nearly double those of FeO). The directions of the principal axes remain the same after transformation into  $\text{Fe}_3\text{O}_4$ . Though all the transformations such as  $\text{Fe(OH)}_2 \rightarrow \delta\text{-FeO.OH}$ ,  $\text{Fe(OH)}_2 \rightarrow \text{FeO}$  and  $\text{FeO} \rightarrow \text{Fe}_3\text{O}_4$  can be explained in terms of topotaxy, it is not yet known how  $\text{Fe(OH)}_2$  can convert directly into  $\text{Fe}_3\text{O}_4$  on oxidation. If FeO were found in between  $\text{Fe(OH)}_2$  and  $\text{Fe}_3\text{O}_4$ , then it would have been possible to describe the whole transformation as topotactic.

That two topotactic transformations can take place one after another was clearly illustrated by the transformation of a single crystal of Lepidocrocite ( $\gamma\text{-FeO.OH}$ ) into Maghemite ( $\gamma\text{-Fe}_2\text{O}_3$ ) and then into Hematite ( $\alpha\text{-Fe}_2\text{O}_3$ ). Lepidocrocite is built up of nearly cubic close-packed oxygen-hydroxyl layers, but their cubic faces are arranged at approximately  $45^\circ$  to the *c*-axis. When it is heated, one of the two adjoining hydroxyl layers is removed as water, converting the two layers into a single layer of oxygen only. The whole arrangement of the atoms then corresponds to a spinel structure (maghemite) having an oriented relationship with the original structure. When this transformed crystal is heated further, further change takes place. On the (111) faces of the freshly prepared Maghemite (transformed from  $\gamma\text{-FeO.OH}$ ) the Hematite crystals grow up beautifully. Here, the [111] axis of the Maghemite becomes the [001] axis of the hematite crystals. The sequence of the oxygen layers is ABCABC in  $\gamma\text{-Fe}_2\text{O}_3$ , and ABABAB in  $\alpha\text{-Fe}_2\text{O}_3$ , maghemite being cubic and hematite rhombohedral. There is also another interesting point to note in this transformation. In the X-ray photographs, the spots due to Maghemite are diffuse, whereas the spots due to Hematite are fairly sharp. The diffuseness of the maghemite spots indicates the change from an asymmetrical arrangement of the oxy-hydroxyl layers in  $\gamma\text{-FeO.OH}$  to a more symmetrical arrangement of oxygen layers in  $\gamma\text{-Fe}_2\text{O}_3$ . The more exact fit between Maghemite and Hematite, which permits easy recrystallisation, accounts for the sharpness of the Hematite spots. The Maghemite-Hematite transformation is very close to that which occurs in the Magnetite-Ilmenite transformation found in natural minerals. Here the original titaniferrous Magnetite breaks down into Ilmenite ( $\text{FeTiO}_3$ ), the structure of which is similar to that of Hematite ( $\alpha\text{-Fe}_2\text{O}_3$ ).

As in the former transformation, here also the *c*-axis of Ilmenite becomes parallel to the [111] axis of Magnetite.

Some irregular arrangements of the oxy-hydroxyl layers other than the conventional ones, can be seen in the green rust I and II. In green rust I the arrangement of the layers is AB'CBC'ACA'B, whereas in II it is like A'BACA'BAC. Both these green rusts contain blocks of cubic and hexagonal close-packed layers. The cubic and hexagonal portions are ABC and BCB respectively in green rust I and BAC and ABA respectively in green rust II. Though the transformation of these two green rusts into  $\mu$ - $\gamma$ -FeO.OH or to FeO could not be demonstrated using single crystals, it appears that both the transformations are topotactic. Indirect evidence that the change is topotactic is provided by the fact that the green rusts I and II always give rise to cubic close-packed oxides or hydroxides. It can be seen that by suppressing one layer in three of the green rust I and one layer in every four in green rust II, as shown by the dashed letters, both the rusts transform into cubic close-packed structures, with the stacking of layers as ACBACB...and BACBAC... in green rust I and II respectively, whereas the direct oxidation of the hexagonal close-packed Fe(OH)<sub>2</sub> leads to two hexagonal close-packed oxyhydroxides, depending upon the nature and rate of oxidation.

A topotactic change involving the loss of atoms at one state and a gain of atoms at the next stage is also clearly illustrated in the transformation of  $\text{FeCO}_3 \rightarrow \text{FeO} \rightarrow \text{Fe}_3\text{O}_4$ . In the first stage CO<sub>2</sub> leaves the original structure; in the second stage oxygen enters into the lattice. This removal and the addition of atoms did not prevent a topotactic transformation.

It is now clear that most of the reactions shown in Fig. 13 can be expected to take place with oriented relationships between the original and the transformed phases. The exception is  $\beta$ -FeO.OH  $\rightarrow$   $\alpha$ -Fe<sub>2</sub>O<sub>3</sub>. There is no similarity between the structures of  $\beta$ -FeO.OH and  $\alpha$ -Fe<sub>2</sub>O<sub>3</sub>; on dehydration, the structure of  $\beta$ -FeO.OH breaks down completely and renucleation is needed for the transformation process.

#### ACKNOWLEDGMENTS

The work reported in this paper was a part of a research on the structures and properties of substances of geomagnetic interest carried out (in Birkbeck College Research Laboratory, London) under the guidance of Prof. J. D. Bernal, M.A., F.R.S., to whom the author is very much indebted. He is very grateful to his colleague Dr. A. L. Macky for his valuable suggestions and criticism during the progress of the work. Thanks are also due to Prof. K. Banerjee, D.Sc., F.N.I., who had kindly gone through the manuscript of this paper and given valuable suggestions.

# REFERENCES

- Bernal, J. D., Dasgupta, D. R., and Mackay, A. L., 1957, *Nature*, **180**, 645.
- Bernal, J. D., Dasgupta, D. R. and Mackay, A. L., 1959, *Clay Min. Bull.*, **4**, 15.
- Bystrom, A. and Bystrom, A. M., 1950, *Acta Cryst.*, **3**, 146.
- Dasgupta, D. R., 1955, *Proc. Nat. Inst. Sci. Ind.*, **21A** 338.
- Dasgupta, D. R., and Mackay, A. L., 1959, *Jour. Phys. Soc. Japan*, **14**, 932.
- Feitknecht, W. and Bucher, H., 1943, *Helv. Chim. Acta.*, **26**, 2177.
- Ferguson, G. A. and Hass, M., 1958, *Phys. Rev.*, **112**, 1130.
- Glemser, O. and Gwinner, E., 1939, *Z. Anorg. Chem.*, **240**, 163.
- Goldsztaub, S., 1931, *Compt. Rend.*, **193**, 533.
- Goodman, J. F., 1958, *Proc. Roy. Soc.*, **A247**, 345.
- Goldsztaub, S., 1935, *Bull. Soc. Franc. Min.*, **58**, 6.
- Hagg, G., 1953, *Z. Krist.*, **B29**, 95.
- Henry, W. E. and Boehm, M. J., 1956, *Phys. Rev.*, **101**, 1253.
- Keller, G., Thesis, 1948, Bern University.
- Kratky, O. and Nowotny, H., 1938, *Zeit. Krist.*, **A100**, 356.
- Leop, H., 1957, *Amer. Min.*, **42**, 679.
- Natta, G. and Casazza, A., 1928, *Gazz. Chim. ital.*, **58**, 344.
- Schmidt, E. R. and Vermaas, F. H. S., 1955, *Amer. Min.*, **40**, 422.
- Thewlis, J., 1931, *Phil. Mag.*, **12**, 1089.
- Von Ossterhout, G. W. and Rooymans, C. J. M., 1958, *Nature*, **181**, 44.
- Welo, L. A. and Baudisch, O., 1933, *Naturwissenschaften*, **21**, 659.
- Welo, L. A. and Baudisch, O., 1925, *Phil. Mag.*, **50**, 399.
- Weiser, H. B. and Milligan, W. O., 1935, *J. Phys. Chem.*, **39**, 25.
- Weiser, H. B. and Milligan, W. O., 1935, *J. Amer. Chem. Soc.*, **57**, 238.

# ON THE ELECTRONIC SPECTRA OF 2-AMINOPYRIDINE AND 3-AMINOPYRIDINE IN DIFFERENT STATES AND IN SOLUTIONS\*

T. N. MISRA

OPTICS DEPARTMENT,

INDIAN ASSOCIATION FOR THE CULTIVATION OF SCIENCE,

CALCUTTA-32

(Received June 22, 1961)

## Plate IX

**ABSTRACT.** The ultraviolet absorption spectra of 2-amino- and 3-aminopyridine in different states and also of their solutions in alcohol and *n*-hexane have been photographed and analysed. In the vapour phase, both the substances exhibit two systems of discrete bands due to  $n \rightarrow \pi^*$  transition and  $\pi \rightarrow \pi^*$  transition respectively. In the case of 2-aminopyridine in the liquid state and in solution, the system due to  $\pi \rightarrow \pi^*$  transition shifts towards longer wavelengths so that the bands due to the  $n \rightarrow \pi^*$  transition are not observed due to superposition of the two systems on each other. In the case of the solid state at the room temperature and also at  $-180^\circ\text{C}$ , the spectrum seems to consist of two parts just separated from each other, the first part being the  $\pi \rightarrow \pi^*$  system, which is shifted towards red by  $3740\text{ cm}^{-1}$  and the second part is exactly in the same region in which the bands due to  $n \rightarrow \pi^*$  transition in the vapour appear. In the case of 3-aminopyridine, the bands due to  $n \rightarrow \pi^*$  transition is observed in the spectrum due to its solution in *n*-hexane, but no conclusion could be drawn regarding the presence or absence of  $n \rightarrow \pi^*$  transition in the cases of solution in alcohol and pure liquid and also in the case of the solid at the room temperature and at  $-180^\circ\text{C}$  owing to the superposition of the two systems.

It has been pointed out that the large shifts observed with the liquefaction of the vapour may be due to strong association of the molecules in the liquid state. There is also an increase in the width of the region of absorption with solidification of 3-aminopyridine and this has been attributed to the influence of neighbouring polar molecules in the crystal on the transition moment.

## INTRODUCTION

It was first pointed out by Stephenson (1954) that near ultraviolet absorption spectrum of 3-bromopyridine in solution in iso-octane consists of two systems of bands due to  $n \rightarrow \pi^*$  and  $\pi \rightarrow \pi^*$  transitions, while in the case of 2-bromopyridine either in the solution or in the vapour state the former system is absent. It was also observed recently by the present author (Misra, 1960) that the spectrum of 3-bromopyridine in the vapour state consists of two systems of bands arising out

---

\*Communicated by Professor S. C. Sirkar

of  $n \rightarrow \pi^*$  and  $\pi \rightarrow \pi^*$  transitions and in the spectrum of 2-bromopyridine in the vapour state the  $n \rightarrow \pi^*$  transition is absent. As pointed out by Stephenson (1954), this is due to the inductive influence of the halogen atom on the  $sp^2$  electron of the adjacent nitrogen atom. It was observed further (Misra, 1960) that in the case of 3-bromopyridine in the liquid state and in the solid state at  $-180^\circ\text{C}$ , the  $n \rightarrow \pi^*$  transition is absent and this was explained to be due to formation of associated groups through the non-bonding electron of the nitrogen atom and the hydrogen atom of the neighbouring molecules. The  $n \rightarrow \pi^*$  transition was also found to be absent in the spectra due to solutions in alcohol because of formation of hydrogen bond through the  $sp^2$  electron of the nitrogen atom of the pyridine ring and the OH group of the alcohol molecule. Similar conclusions were also drawn in the cases of pyridine and other substituted pyridines by Stephenson (1954), Banerjee (1956, 1957) and Roy (1958).

The ultraviolet absorption spectra of 2-amino and 3-aminopyridine in the vapour state did not appear to have been studied by any earlier worker and therefore, the influence of the  $\text{NH}_2$  group on such  $n \rightarrow \pi^*$  transition was not known. The present investigation was undertaken to analyse the absorption spectra of these two substances in the vapour state and also to study the influence of substitution of  $\text{NH}_2$  group in place of the Br atom in the 2- and 3-position of the pyridine ring on the absorption spectra.

The absorption spectra of these two compounds in the liquid state, in the solid state at the room temperature and at  $-180^\circ\text{C}$  and in solutions in different solvents have also been investigated in order to study the influence of different environments on the two transitions mentioned above.

## EXPERIMENTAL

Chemically pure samples of 2-aminopyridine and 3-aminopyridine supplied by Fluka, Switzerland were fractionated and the proper fractions were distilled under reduced pressure just before use. Cells of length 50 cm, 25 cm and 10 cm were used to study the spectra due to the vapours. The absorption cell was filled up with the vapour at saturation vapour pressures at different temperatures. Two separate electrical heaters, one for the absorption cell and the other for the bulb containing the liquid and attached to the absorption cell, were used to control the temperature. The bulb containing the liquid was always kept at a temperature about  $10^\circ\text{C}$  lower than that at any part of the absorption cell.

To produce low pressures in the vapour in the absorption tube, the reservoir containing the liquid was immersed in suitable low temperature baths while the tube was left at the room temperature.

With an absorption cell of length 25 cm, the bulb containing the compound was kept at  $35^\circ\text{C}$  to record both the  $n \rightarrow \pi^*$  and  $\pi \rightarrow \pi^*$  system of 2-aminopyridine.

A 50 cm long absorption cell with the reservoir at 60°C was needed to record the bands due to the  $n \rightarrow \pi^*$  and  $\pi \rightarrow \pi^*$  transitions in 3-aminopyridine. The temperature of the bulb was raised to 70°C to record the  $n \rightarrow \pi^*$  system distinctly.

Very thin films of thickness of the order of a few microns of the substances were required to produce the absorption bands in the solid state. To study the spectra in the liquid state, the thin films of the substances enclosed between two quartz plates were placed in a heating chamber which was kept at temperatures about 5°C above the respective melting points of the substances.

The solvents used to study the absorption spectra of the substances in the solutions were ethyl alcohol and *n*-hexane. The solvents were found to produce no absorption bands in the region under consideration. A brass cell of thickness 1 cm provided with quartz window was used for the solutions and the strength of the solution for each compound was about .01% by weight.

Spectrograms were taken on Agfa Isopan films backed by a metal sheet with a Hilger E 1 spectrograph giving a dispersion of the order of 3Å per mm in the region of 2600Å. Iron arc spectrum was photographed on each spectrogram as a comparison.

Microphotometric records were taken with a Kipp and Zonen self-recording microphotometer. The absorption spectra were calibrated with the help of microphotometric records of the iron lines using the method described in an earlier paper (Sirkar and Misra, 1959). As the infrared absorption spectra of these substances had not been studied thoroughly by previous workers, the infrared absorption spectra of solution of 2-aminopyridine in  $\text{CCl}_4$  and that of 3-aminopyridine in chloroform were recorded with a Perkin Elmer Model 21 spectrophotometer using rocksalt optics in order to find out the ground state vibrational frequencies and these were utilised to check the excited state frequencies obtained from the ultraviolet absorption spectra.

## RESULTS AND DISCUSSIONS

### *2-Aminopyridine*

Microphotometric records of the absorption spectra of 2-aminopyridine in different states and in solution in different solvents are reproduced in Figs. 1–3, and the spectrum of the substance in the vapour phase is reproduced in Plate IX, Fig. 4(a). The wave numbers of the bands in  $\text{cm}^{-1}$  with their approximate strengths and probable assignments are given in Tables I–III.

#### (a) *Spectrum of the vapour phase :*

It can be seen from Fig. 1 that the absorption spectrum of 2-aminopyridine in the vapour phase shows two distinct systems of bands. One of these two systems (Transition I) consisting of sharp, narrow line-like bands starts from



about 32700  $\text{cm}^{-1}$  and extends to the region of the other system which consists of broad bands resembling those due to other substituted benzenes. The former system has been attributed to the  $n \rightarrow \pi^*$  transition after Kasha (1950) and the latter to the  $\pi \rightarrow \pi^*$  transition. The analysis of the bands of these two systems is discussed separately in the following sections.

**TABLE I**

Ultraviolet absorption bands of 2-aminopyridine in the vapour phase

Transition I		Transition II	
Wave number ( $\text{cm}^{-1}$ ) and strength	Assignment	Wave number ( $\text{cm}^{-1}$ ) and strength	Assignment
32885 (w)	0 — 564	34324 (s)	0,0
32999 (w)	0 — 455	34618 (w)	0 + 294
33070 (w)	0 — 379	34796 (s)	0 — 472
33157 (w)	0 — 292	34987 (m)	0 + 663
33223 (w)	0 — 226	35259 (s)	0 + 926
33364 (m)	0 + 210 — 292	35559 (s)	0 + 1235
33449 (vs)	0,0	35765 (s)	0 + 1441
33519 (w)	0 + 525 — 455	36025 (w)	0 + 1235 + 472
33660 (w)	0 + 210	36177 (ms)	0 + 2 + 926
33705 (m)	0 + 256	36572 (m)	0 + 2 + 663 + 926
33789 (s)	0 + 340	36896 (w)	0 + 2 + 663 + 1235
33879 (m)	0 + 430	37098 (m)	0 + 3 + 926
33974 (vs)	0 + 525		
34044 (m)	0 + 2 + 340 — 85		
34125 (w)	0 + 2 + 340 0 + 256 + 430		
34260 (w)	0 + 811		
34316 (w)	0 + 340 + 525 0 + 2 + 430		
34332 (w)	0 + 210 + 676		
34437 (vw)	0 + 988		
34496 (m)	0 + 2 + 525		
34857 (w)	0 + 1408 0 + 2 + 515 + 340		
34942 (w)	0 + 2 + 340 + 811		

(i)  $n \rightarrow \pi^*$  Transitions (Transition I)

The sharp band at  $33449 \text{ cm}^{-1}$  which persists with undiminished intensity even at the low pressure of the absorbing vapour has been taken as the 0, 0 band of this system. Most of the remaining strong bands represent transitions involving excited state vibration frequencies 210, 256, 340, 525, 811, 988 and  $1408 \text{ cm}^{-1}$  and also ground state frequencies 226, 292, 379, 455 and  $564 \text{ cm}^{-1}$  as shown in

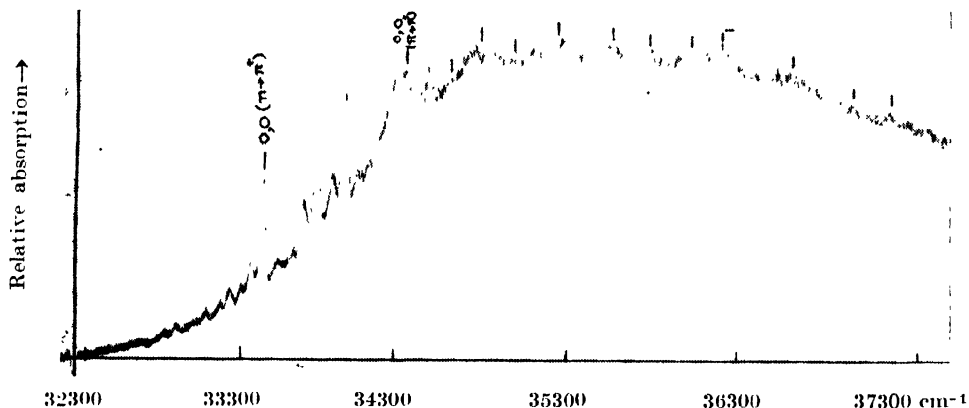


Fig. 1. Microphotometric record of the ultraviolet absorption spectrum of 2-aminopyridine in the vapour phase.

Table I. The bands of wave numbers higher than  $34125 \text{ cm}^{-1}$  are superposed on those due to  $\pi \rightarrow \pi^*$  transition and this makes their accurate measurement somewhat uncertain. The band of medium strength at  $33364 \text{ cm}^{-1}$  is probably not due to a  $v \rightarrow 0$  transition as no corresponding  $0 \rightarrow v$  transition with greater strength could be detected. It was, therefore, assigned to a  $v \rightarrow v'$  transition as shown in Table I. The weak band at a distance of  $70 \text{ cm}^{-1}$  from the 0, 0 band on the high energy side is also similarly assigned as a  $v \rightarrow v'$  transition.

(ii)  $\pi \rightarrow \pi^*$  Transition (Transition II)

The band system in the region  $34300 \text{ cm}^{-1}$  to  $37200 \text{ cm}^{-1}$  consisting of broad bands which are distinctly different from the sharp narrow bands due to the Transition I has been attributed to the  $\pi \rightarrow \pi^*$  transition from their resemblance with the bands in the substituted benzene compounds.

It was difficult to find out the exact position of the 0, 0 band of this system because of the superposition of some bands due to  $n \rightarrow \pi^*$  transition on these bands. However, the centre of the strongest broad band on the long wavelength side of of this system is at  $34324 \text{ cm}^{-1}$  and this has been taken as the position of the 0, 0 band. The other bands could then be assigned as progressions and combinations of excited state frequencies 294, 472, 663, 926, 1235 and  $1441 \text{ cm}^{-1}$ .

The infrared absorption spectrum above  $990 \text{ cm}^{-1}$  of this compound was earlier studied by Katritzky and Hands (1958) who reported the frequencies 991(ms)

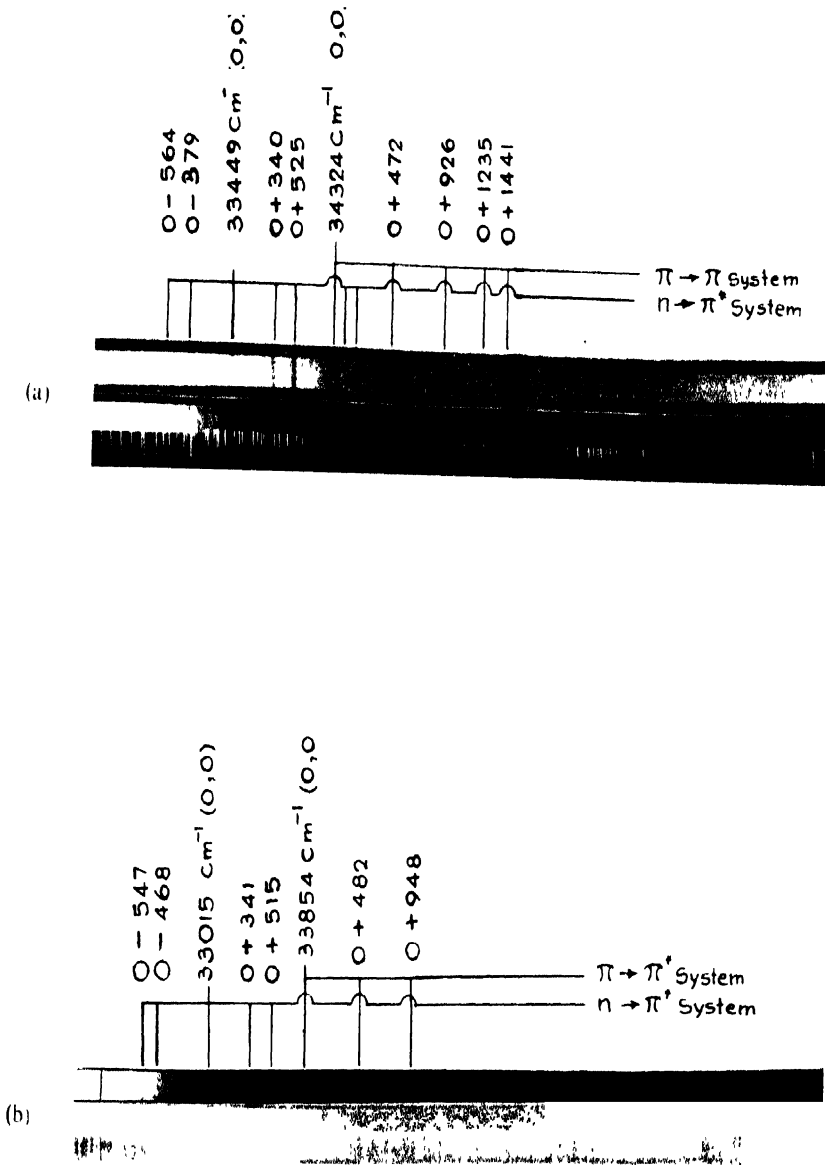


Fig. 4. Ultraviolet absorption spectra of aminopyridines in the vapour phase

(a) 2- Aminopyridine vapour.

(b) 3- Aminopyridine vapour.



TABLE II

 Ultraviolet absorption bands of 2-aminopyridine ( $\pi \rightarrow \pi^*$  systems)

.01% solution in alcohol at 32°C		.01% solution in <i>n</i> -hexane at 32°C	
Wave number (cm <sup>-1</sup> ) and strength	Assignment	Wave number (cm <sup>-1</sup> ) and strength	Assignment
Broad absorption band extending from 32414 cm <sup>-1</sup> to 36000 cm <sup>-1</sup> without any discrete structure		32885 (s)	0,0
		33363 (m)	0 + 478
		33830 (m)	0 + 945
		34317 (m)	0 + 1432
		34782 (m)	0 + 2 × 945
		35755 (m)	0 + 2 × 1432

1038 (m), 1148 (s), 1270 (ms), 1317 (s), 1441 (s), 1483 (vs), 1574 (s) and 1602 (vs), being the strengths of the bands are given in parentheses. The infrared spectrum of solution of 2-aminopyridine in CCl<sub>4</sub> was reinvestigated down to 600 cm<sup>-1</sup> and besides the above frequencies a band at 710 cm<sup>-1</sup> was observed.

The excited state frequencies 663cm<sup>-1</sup>, 926 cm<sup>-1</sup> and 1235 cm<sup>-1</sup> evidently correspond respectively to the ground state frequencies 710 cm<sup>-1</sup>, 991 cm<sup>-1</sup> and 1270 cm<sup>-1</sup> observed in the infrared spectra. Two ground state frequencies 1441 cm<sup>-1</sup> and 1483 cm<sup>-1</sup> have been reported by Katritzky and Hands (1958) and it may be noted that the band assigned to the excited state frequency 1441 cm<sup>-1</sup> in the present investigation is quite broad and it may comprise two unresolved bands.

(b) Influence of intermolecular field on the spectra

(i) Spectra of the solutions

In the spectrum of solution of 2-aminopyridine in *n*-hexane (Fig. 2) a band system consisting of broad absorption bands is observed in the region 32500 cm<sup>-1</sup>

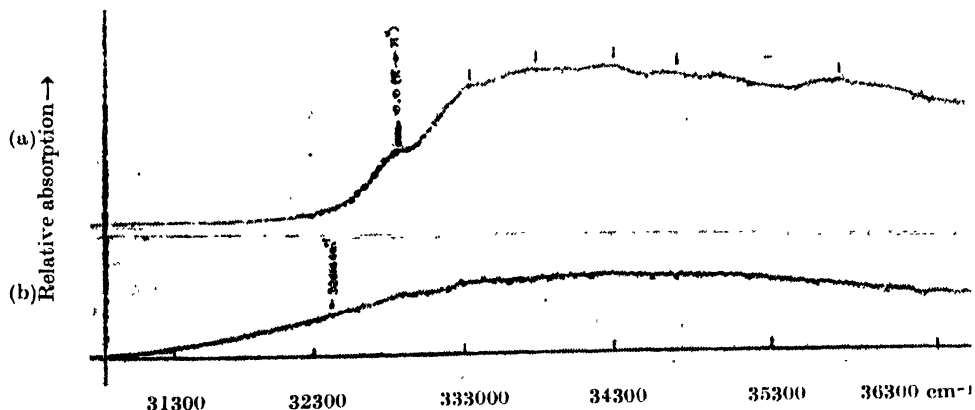


Fig. 2. Microphotometric records of the ultraviolet absorption spectra of solutions of 2-amino pyridine.

(a) .01% solution in *n*-hexane.

(b) .01% solution in ethyl alcohol.

to  $36000\text{ cm}^{-1}$ . From the structure of this band system, it appears that this system corresponds to the  $\pi \rightarrow \pi^*$  transition in the vapour phase. Taking the first strong band at  $32885\text{ cm}^{-1}$  as the 0,0 band of this system, the other bands can be analysed in terms of the excited state frequencies  $478\text{ cm}^{-1}$ ,  $945\text{ cm}^{-1}$  and  $1432\text{ cm}^{-1}$  and their harmonics. Thus in the case of *n*-hexane solution this band system is shifted towards red by  $1461\text{ cm}^{-1}$ . As the 0,0 band in the  $n \rightarrow \pi^*$  system due to the vapour is at  $33449\text{ cm}^{-1}$  and the 0,0 band of the  $\pi \rightarrow \pi^*$  transition in solution of hexane is at  $32885\text{ cm}^{-1}$  it is quite probable that the former system is masked by the strong system due to  $\pi \rightarrow \pi^*$  transition.

In the spectrum of .01% solution of 2-aminopyridine in ethyl alcohol (Fig. 2) only one very broad band due to  $\pi \rightarrow \pi^*$  transition is in the region  $32000\text{ cm}^{-1}$  to  $36000\text{ cm}^{-1}$ . If the 0,0 band is assumed to be at about  $32414\text{ cm}^{-1}$ , which is the long wavelength edge of the broad band the band system seems to be shifted towards red by about  $1910\text{ cm}^{-1}$  from its position in the case of the vapour.

The appearance of the band system due to the solution in alcohol is different from that of the system due to the *n*-hexane solution and it is similar to that of the pure liquid. The shift of the system is also much larger than that observed in the case of the solution in hexane. These results probably indicate the formation of associated groups of 2-aminopyridine molecules with neighbouring alcohol molecules due to hydrogen bond-formation as suggested by Stephenson (1954) and Roy (1958) in the cases of other pyridine compounds.

(ii) *Spectra due to the substances in the liquid and solid states*

In the spectrum of 2-aminopyridine in the liquid state at  $70^\circ\text{C}$  a broad absorption band without any discrete structure is observed in the region from  $32368$

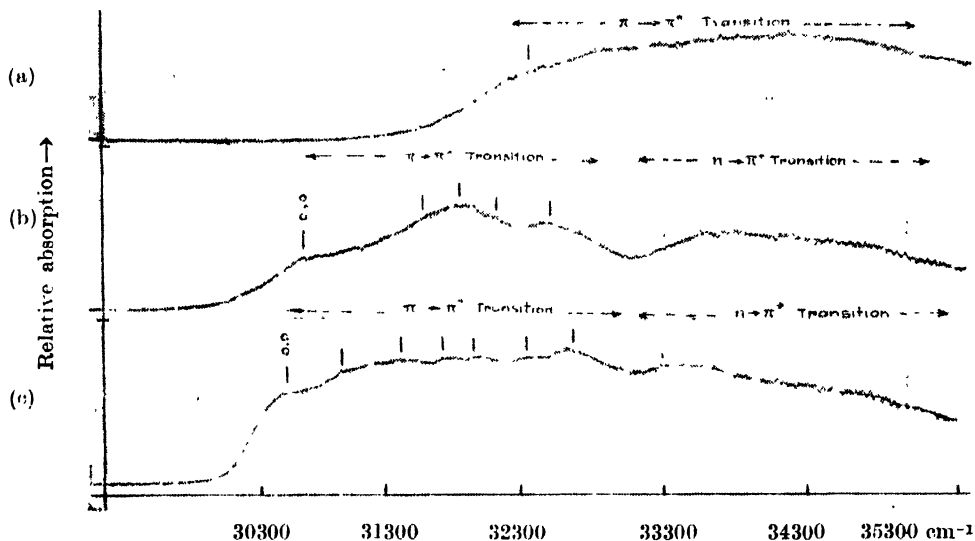


Fig. 3. Microphotometric records of the ultraviolet absorption spectra of 2-aminopyridine.  
(a) Liquid at  $70^\circ\text{C}$ . (b) Solid at  $33^\circ\text{C}$ . (c) Solid at  $-180^\circ\text{C}$ .

$\text{cm}^{-1}$  to  $35421 \text{ cm}^{-1}$ . This absorption appears to be due to the  $\pi \rightarrow \pi^*$  transition. If we assume that the 0, 0 band of this transition lies near about the hump at  $32368 \text{ cm}^{-1}$  on the long wavelength edge of the system, the 0, 0 band seems to be displaced towards red by about  $2440 \text{ cm}^{-1}$  on liquefaction of the vapour.

This shift of the band system and the absence of discrete structure of the system may be due to formation of associated groups among neighbouring molecules. On comparing these results with those for the solution in alcohol it is found that the nature of association in the two cases is different, because the shift of the band system is much larger in the case of the pure liquid than in the solution in alcohol.

TABLE III

Ultraviolet absorption bands of 2-aminopyridine in the liquid and solid states

System	Liquid at 70°C		Solid at 32°C		Solid at 180°C	
	Wave number ( $\text{cm}^{-1}$ ) and strength	Assignment	Wave number ( $\text{cm}^{-1}$ ) and strength	Assignment	Wave number ( $\text{cm}^{-1}$ ) and strength	Assignment
Transition II	Broad absorption extending from $32368 \text{ cm}^{-1}$ to $35421 \text{ cm}^{-1}$		30684 (m)	0, 0	30497 (s)	0, 0
			31611 (m)	0 927	30968 (m)	0 471
			31929 (s)	0 1245	31430 (m)	0 933
			32134 (m)	0 1450	31746 (m)	0 1249
			32535 (m)	0 2 927	31964 (m)	0 1467
					31357 (m)	0 2 x 933
Transition I	Not observed		Broad band in the region $33300 \text{ cm}^{-1}$ — $35000 \text{ cm}^{-1}$		32680 (ms)	0 933 + 1249
					Broad band in the region $33300 \text{ cm}^{-1}$ — $35000 \text{ cm}^{-1}$	

When the liquid is solidified at room temperature discrete band structure is observed, but the spectrum seems to be somewhat different from that due to the vapour phase. Not only the band system due to the solid is shifted towards red but also the individual bands are much broader so that they are not resolved clearly. This may be due to small splitting caused by the influence of the neighbouring polar molecules in the crystal on the transition moment. Taking the 0, 0 band to be at  $30684 \text{ cm}^{-1}$  the excited state frequencies  $927 \text{ cm}^{-1}$ ,  $1245 \text{ cm}^{-1}$  and  $1450 \text{ cm}^{-1}$  may be attributed to the other bands. It also appears that the spectrum consists of two parts, the second part starting from about  $33200 \text{ cm}^{-1}$  and extending upto about  $35000 \text{ cm}^{-1}$ . As the 0, 0 band of the  $n \rightarrow \pi^*$  system of the vapour is at  $33449 \text{ cm}^{-1}$  probably this second portion of the spectrum due to the substance in the solid state is produced by the  $n \rightarrow \pi^*$  transition. The bands due to  $n \rightarrow \pi^*$  transition are too broad to be resolved from each other probably

because of the same reason as indicated above. Thus it appears that in this case the  $n \rightarrow \pi^*$  transition persists in the solid state. In the spectrum due to the liquid also, this second part seems to be superposed on the first part but the shift of the first part being smaller than that in the case of the solid the two parts are not separated from each other.

When the solid is cooled to  $-180^\circ\text{C}$ , the bands are found to remain broad and the absorption becomes stronger. The strong band at  $30497\text{ cm}^{-1}$  has been taken as the 0,0 band and the upper state fundamentals  $471$ ,  $933$ ,  $1249$  and  $1467\text{ cm}^{-1}$  have been observed, as shown in Table III. The second part due to  $n \rightarrow \pi^*$  transition seems to persist at  $-180^\circ\text{C}$  in the same position as at the room temperature.

As the  $n \rightarrow \pi^*$  transition seems to persist in this solid state also, it seems that the nitrogen atom of the ring does not take part in weak bond-formation. It is quite probable that the  $\text{NH}_2$  group is responsible for hydrogen bond-formation with the neighbouring molecules and in that case the effect is expected to be similar to that of the substitution of a hydrogen atom of the ring and consequently a shift of the band system towards red is expected. In the case of the solid at the room temperature the shift is about  $3740\text{ cm}^{-1}$  from its position in the case of the vapour, while with further cooling to  $-180^\circ\text{C}$ , the 0,0 band experiences a further shift of  $187\text{ cm}^{-1}$  towards red. The large shift of the 0,0 band on solidification of the liquid and very small shift with further cooling and also the small splitting to which the broadening of the bands were attributed may be due to the influence of intermolecular field in the crystal on the electronic energy levels of the molecule.

### 3-Aminopyridine

Microphotometric records of the absorption spectra of 3-aminopyridine in different states and in solutions in different solvents are reproduced in Figs. 5-7 and the spectrum of the substance in the vapour phase is reproduced in Plate IX, Fig. 4(b). Wave numbers of the bands in  $\text{cm}^{-1}$ , their approximate strengths and their probable assignments are given in Table IV-VI.

#### (a) Spectrum due to the vapour phase

The absorption spectrum of 3-aminopyridine in the vapour phase shows two distinct systems of bands as shown in Fig. 5. In the case of the vapour at the saturation pressure at  $60^\circ\text{C}$  and with a path length of  $50\text{ cm}$  a system consisting of sharp, narrow bands appears on the long wavelength side of another system consisting of broad bands. As in the case of 2-aminopyridine, the former system has been attributed to the  $n \rightarrow \pi^*$  transition and the latter to the  $\pi \rightarrow \pi^*$  transition.



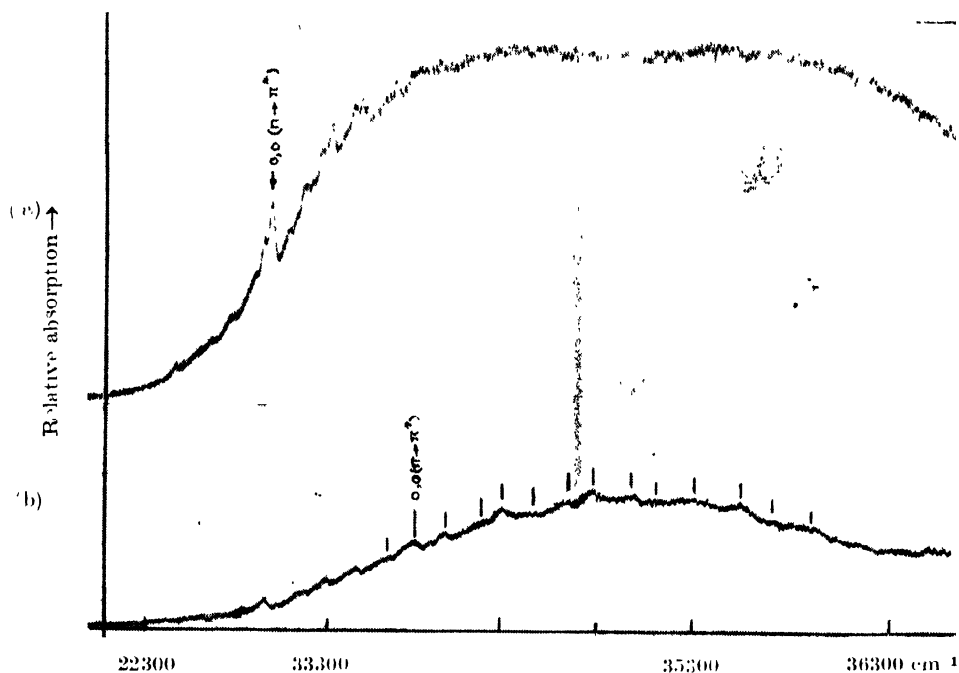


Fig. 5. Microphotometric records of the ultraviolet absorption spectra of 3-aminopyridine in the vapour phase.

(a)  $n \rightarrow \pi^*$  transition. (b)  $\pi \rightarrow \pi^*$  transition.

TABLE IV

Ultraviolet absorption bands of 3-aminopyridine in the vapour phase

Transition I		Transition II	
Wave number (cm <sup>-1</sup> ) and strength	Assignment	Wave number (cm <sup>-1</sup> ) and strength	Assignment
32462 (w)	0 547	33690 (m)	0 164
32547 (w)	0 — 468	33854 (s)	0,0
32691 (w)	0 — 324	34004 (ms)	0 150
32777 (m)	0 — 238	34208 (m)	0 ± 354
32891 (w)	0 — 124	34336 (s)	0 ± 482
32961 (w)	0 ± 181 — 238	34494 (w)	0 ± 640
33015 (vs)	0,0	34712 (m)	0 ± 858
33119 (m)	0 ± 104	34802 (s)	0 ± 948
33196 (m)	0 ± 181	35009 (m)	0 ± 1160
			0 ± 2 × 150 ± 858
33301 (m)	0 ± 270	35128 (m)	0 ± 1274
			0 ± 2 × 640
33356 (s)	0 ± 341	35353 (m)	0 1499
			0 ± 858 ± 640
33520 (m)	0 ± 515	35579 (w)	0 ± 2 × 858
		35754 (w)	0 ± 2 × 948
		35918 (w)	0 ± 150 ± 2 × 948

(i)  $n \rightarrow \pi^*$  transition (Transition I)

The bands due to  $n \rightarrow \pi^*$  transition in 3-aminopyridine lie in the region  $32300 \text{ cm}^{-1}$  to  $33800 \text{ cm}^{-1}$ . The sharp and strong band at  $33015 \text{ cm}^{-1}$  has been taken as the 0, 0 band of the system the other bands have been analysed in terms of upper state fundamentals 104, 181, 270, 341 and  $515 \text{ cm}^{-1}$  and their combinations. The corresponding ground state vibrational wave numbers as obtained from  $v \rightarrow 0$  transitions are probably 124, 238, 324, 468 and  $547 \text{ cm}^{-1}$ .

It may be noted for comparison that the excited state variational wave numbers  $131 \text{ cm}^{-1}$ ,  $158 \text{ cm}^{-1}$ ,  $264 \text{ cm}^{-1}$ ,  $499 \text{ cm}^{-1}$ ,  $545 \text{ cm}^{-1}$  and  $580 \text{ cm}^{-1}$  were reported by Rush and Spomer (1952) in the case of  $n \rightarrow \pi^*$  transition in 3-methylpyridine and in the case of 3-bromopyridine the corresponding wave numbers were found to be  $230 \text{ cm}^{-1}$ ,  $279 \text{ cm}^{-1}$ ,  $349 \text{ cm}^{-1}$  and  $579 \text{ cm}^{-1}$  (Misra, 1960).

The band at  $32961 \text{ cm}^{-1}$  on the longer wavelength side of the 0, 0 band has been assigned as a  $v \rightarrow v'$  transition. The assignments of the bands on the high energy side of the system is somewhat uncertain due to overlapping of the bands due to  $n \rightarrow \pi^*$  transition with those due to  $\pi \rightarrow \pi^*$  transition.

(ii)  $\pi \rightarrow \pi^*$  transitions (Transition II)

The band system due to  $\pi \rightarrow \pi^*$  transition in 3-aminopyridine in the vapour phase lies in the region from  $33600 \text{ cm}^{-1}$  to  $36500 \text{ cm}^{-1}$ . As in the case of 2-aminopyridine there is some uncertainty in locating exactly the 0, 0 band of this system due to the overlapping of the two transitions in this region, as stated in the previous section. However, the strong band on the long wavelength side of this system at  $33854 \text{ cm}^{-1}$  wherefrom the broad absorption system seems to start at higher pressure of the absorbing vapour is taken tentatively as the 0, 0 band. Most of the remaining bands represent transitions involving excited state vibrational frequencies 150, 354, 482, 640, 858, 948, 1160, 1274 and  $1499 \text{ cm}^{-1}$  as shown in Table IV. Moreover, a ground state frequency  $164 \text{ cm}^{-1}$  is observed as  $v \rightarrow 0$  transition. In order to find out the ground state vibrational frequencies, the infrared absorption spectrum of 3-aminopyridine in chloroform solution was studied with a Perkin Elmer Model 21 spectrophotometer with NaCl optics. The wave numbers of some of the observed infrared bands are 690 (m), 790 (m), 885 (m), 1013(s), 1042(s), 1090 (w), 1220 (w), 1255 (m), 1285 (s), 1438 (vs), 1485 (s), 1580 (vs)  $\text{cm}^{-1}$ , the strength of absorption being given in the parentheses. The infrared frequencies  $690 \text{ cm}^{-1}$  and  $885 \text{ cm}^{-1}$  may correspond to the excited state frequencies  $640 \text{ cm}^{-1}$  and  $858 \text{ cm}^{-1}$  observed in the ultraviolet absorption spectrum. There are two medium strong infrared absorption bands of ground state frequencies  $1013 \text{ cm}^{-1}$  and  $1042 \text{ cm}^{-1}$  but only one excited state frequency  $948 \text{ cm}^{-1}$  is observed in the ultraviolet absorption spectrum. The bands at a distance of  $1160 \text{ cm}^{-1}$ ,  $1274 \text{ cm}^{-1}$  and  $1499 \text{ cm}^{-1}$  from the 0, 0 band shown as combinations, may also be fundamentals as there are strong bands with vibrational frequencies  $1220 \text{ cm}^{-1}$ ,  $1285 \text{ cm}^{-1}$  and  $1580 \text{ cm}^{-1}$  in the infrared spectrum.

## (b) Influence of intermolecular field on the spectra

## (i) Spectra due to the solutions

In the spectrum of 3-aminopyridine in *n*-hexane solution broad absorption bands corresponding to those due to the  $\pi \rightarrow \pi^*$  transition in the vapour phase

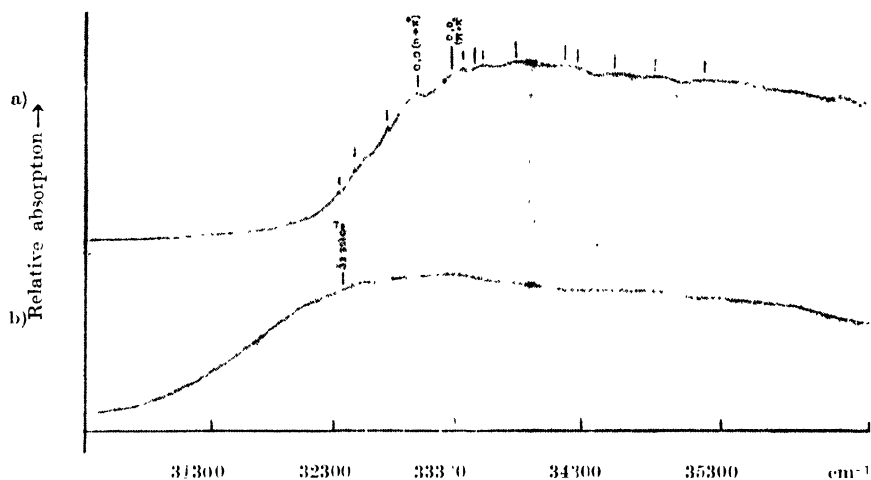


Fig. 6. Microphotometric record of the ultraviolet absorption spectra of solutions of 3-aminopyridine.

(a) 0.01% solution in *n*-hexane. (b) 0.01% solution in ethyl alcohol.

TABLE V

Ultraviolet absorption bands of 3-aminopyridine in solution

System	Solution in alcohol at 32°C		Solution in <i>n</i> -hexane at 32°C	
	Wave number (cm <sup>-1</sup> ) and strength	Assignment	Wave number (cm <sup>-1</sup> ) and strength	Assignment
Transition II	Broad absorption band extending from 31437 cm <sup>-1</sup> to 35857 cm <sup>-1</sup>		33301 (s)	0,0
			33461 (m)	0 + 160
			33779 (m)	0 + 478
			34154 (m)	0 + 853
			34248 (m)	0 + 947
			34473 (m)	0 + 1173
			34784 (m)	0 + 1483
			35200 (m)	0 + 2 × 947
Transition I	Absent		32472 (w)	0 — 543
			32776 (w)	0 — 239
			33015 (s)	0,0
			33357 (w)	0 + 342
			33524 (m)	0 + 509

are observed. Assuming the broad band at  $33301\text{ cm}^{-1}$  as the 0, 0 band of the system, the other bands can be explained in terms of excited state frequencies  $160, 478, 853, 947, 1173, 1483\text{ cm}^{-1}$  and their combinations as shown in Table V. These upper state fundamentals agree fairly well with those observed in the spectrum due to the vapour.

In addition to the above broad bands a few sharp weak bands are also observed in the spectrum of 3-aminopyridine in *n*-hexane solution at  $33015, 32776$  and  $32468\text{ cm}^{-1}$ . There are also two weak bands at  $33357\text{ cm}^{-1}$  and  $33520\text{ cm}^{-1}$ . The positions of these bands are found to be identical with those of bands of  $n \rightarrow \pi^*$  system due to the vapour phase and therefore the  $n \rightarrow \pi^*$  system persists in the solution in *n*-hexane. So, the  $n \rightarrow \pi^*$  transition is not affected appreciably by the solvent molecules.

In alcohol solution, however, no banded structure is observed and only a very broad absorption band extending from  $31437\text{ cm}^{-1}$  to  $35857\text{ cm}^{-1}$  is observed. As in the case of 2-amino isomer, this absorption seems to correspond to the  $\pi \rightarrow \pi^*$  transition. The absorption increases rapidly and becomes large at  $32321\text{ cm}^{-1}$ . So, the system seems to be shifted by about  $1500\text{ cm}^{-1}$  towards red from its position in the spectrum due to the vapour. The position of the system due to the  $n \rightarrow \pi^*$  transition is almost at the maximum of the broad band. So it is not possible to come to any conclusion regarding the appearance or otherwise of this system in case of the solution in alcohol.

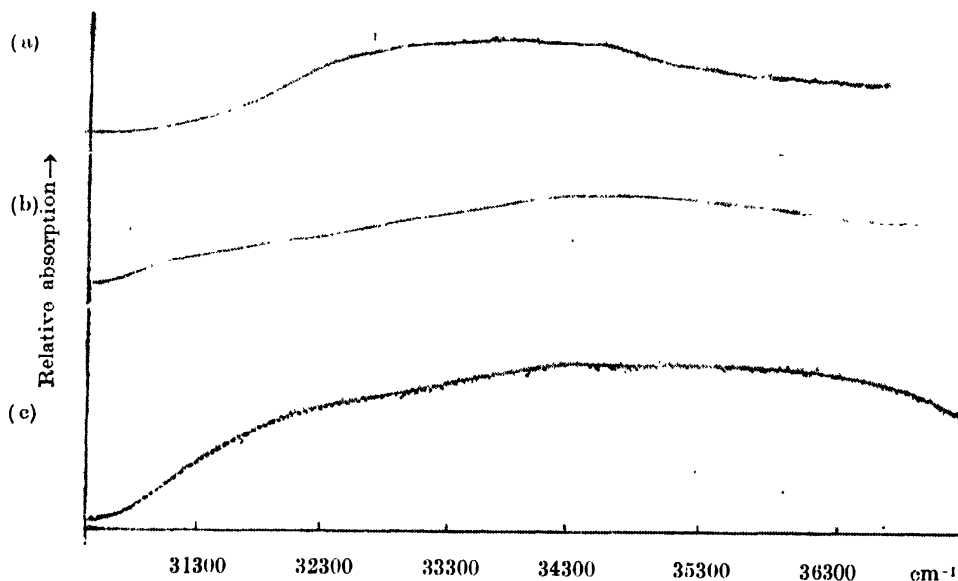


Fig. 7. Microphotometric records of the ultraviolet absorption spectra of 3-aminopyridine

(a) Liquid at  $70^{\circ}\text{C}$ .

(b) Solid at  $32^{\circ}\text{C}$ .

(c) Solid at  $-180^{\circ}\text{C}$ .

(ii) *Spectra in the liquid and solid states*

In the liquid state 3-aminopyridine shows only a very broad absorption band without any discrete structure in the region  $31650\text{ cm}^{-1}$  to  $35450\text{ cm}^{-1}$  as shown in Fig. 7. The appearance is similar to that due to the solution in alcohol. In this case also nothing can be said about the presence or absence of the system due to the  $n \rightarrow \pi^*$  transition.

TABLE VI  
Ultraviolet absorption bands of 3-aminopyridine in the liquid and solid states

Liquid at $70^\circ\text{C}$	Solid at $32^\circ\text{C}$	Solid at $-180^\circ\text{C}$
Broad absorption band extending from $31650\text{ cm}^{-1}$ to $35450\text{ cm}^{-1}$	Broad absorption band extending from $30760\text{ cm}^{-1}$ to $36780\text{ cm}^{-1}$	Broad absorption band extending from $30760\text{ cm}^{-1}$ to $36780\text{ cm}^{-1}$

When the substance is solidified at the room temperature no discrete structure of the band system is observed but the region of absorption becomes extended on both sides. When the substance is further cooled to  $-180^\circ\text{C}$ , no further appreciable change in the spectrum takes place. It is interesting, however, that in this case the width of the region of absorption is about  $6000\text{ cm}^{-1}$ . This is double the breadth of the  $\pi \rightarrow \pi^*$  system due to the vapour phase. This increase in the width of the region may be due to the large unresolved splitting of the system caused by the intermolecular field in the crystal lattice.

ACKNOWLEDGMENT

The author is indebted to Professor S. C. Sirkar, D.Sc., F.N.I., for his kind interest and guidance in the work. Thanks are also due to Dr. S. B. Banerjee for many helpful discussions.

REFERENCES

- Banerjee, S. B., 1956, *Ind. J. Phys.*, **30**, 480.  
 Banerjee, S. B., 1957, *Ind. J. Phys.*, **31**, 11.  
 Kashua, M., 1950, Discussion of the Faraday Society No. **9**, 14.  
 Katritzky, A. R., and Hands, A. R., 1958, *J. Chem. Soc.*, Part II, p. 2202.  
 Misra, T. N., 1960, *Ind. J. Phys.*, **34**, 381.  
 Roy, S. B., 1958, *Ind. J. Phys.*, **32**, 323.  
 Rush, J. H. and Sponer, H., 1952, *J. Chem. Phys.*, **20**, 1847.  
 Sirkar, S. C. and Misra, T. N., 1959, *Ind. J. Phys.*, **33**, 45.  
 Stephenson, H. P., 1954, *J. Chem. Phys.*, **22**, 1077.

# Letters to the Editor

*The Board of Editors will not hold itself responsible for opinions expressed in the letters published in this section. The notes containing reports of new work communicated for this section should not contain many figures and should not exceed 500 words in length. The contributions must reach the Assistant Editor not later than the 15th of the second month preceding that of the issue in which the letter is to appear. No proof will be sent to the authors.*

## 5

### ON THE EVALUATION OF THE COEFFICIENTS OF THERMAL EXPANSION OF CRYSTALS FROM X-RAY DATA

V. T. DESHPANDE AND V. M. MUDHOLKER

DEPARTMENT OF PHYSICS, UNIVERSITY COLLEGE OF SCIENCE,  
OSMANIA UNIVERSITY, HYDERABAD-7.

(Received December 6, 1960)

The purpose of this note is to call attention to some small but vital differences obtained in the methods used in processing X-ray data for the evaluation of the coefficients of thermal expansion. In view of the increased importance of this property of crystalline solids in relation to their structural imperfections, it has become necessary to know, not merely the average values of the coefficient of expansion but also the temperature dependence of the instantaneous values. It is essential, therefore, that the methods used in processing the X-ray data be chosen in a way so as to bring out the correct form of this temperature variation. It is, of course, assumed that the data on cell dimensions are obtained with the highest possible accuracy, taking care to correct all errors, systematic or random.

An important step in this processing is the determination of the derivative  $(da/dt)$  at different temperatures. This, with the help of the definition,  $\alpha = (1/a_0)(da/dt)$ , gives the values of the zero coefficient of expansion at those temperatures. Different methods are in use for the evaluation of this derivative. One of these, used by Wilson (1941), is to obtain the mean value of the derivative over small intervals of temperature by subtracting the experimental values of 'a' and dividing these by the corresponding temperature differences. A variation of this procedure, employed by some workers (Owen and Richards, 1936 and Deshpande and Mudholker, 1960) consists in obtaining the mean values of the derivative from a carefully drawn graph between 'a' and 't'. The values of 'a' are then evaluated for every temperature at which the derivative is found. Least squares treatment of the  $\alpha$ -t data, thus obtained, then gives the temperature

dependence of ' $\alpha$ '. This dependence may or may not be linear, a fact which comes out readily from the  $\alpha$ - $t$  plot. If the relation is non-linear it is usually expressed in the form given in Eq. (1).

$$\alpha = \alpha_0 + \beta t + \gamma t^2 \quad \dots (1)$$

In another method (Stokes and Wilson, 1941 ; Kempter and Elliot, 1959 ; Pathak and Pandya, 1960 and Pathak and Pandya, 1960a) the lattice constant is first expressed as quadratic function of temperature, by the usual method of least squares, giving an expression, as in Eq. (2).

$$a = a_0 + bt + ct^2 \quad \dots (2)$$

Differentiation of Eq. (2) with respect to temperature, then, gives the coefficient of expansion as a linear function of temperature as shown in Eq. (3)

$$\alpha = \alpha_0 + \beta t \quad \dots (3)$$

This procedure appears to be more rigorous than the first one, but has a serious limitation in as much as the temperature dependence of ' $a$ ' comes out necessarily to be linear. This may or may not be its real form. Wilson (1941) has found that this method does not give the best possible representation of the derivative ( $da/dt$ ), and Stokes and Wilson (1941) have pointed out that in principle, the quadratic function is not satisfactory.

There is thus a fundamental difference between the two methods outlined above. While the first method brings out the non-linear character of the  $\alpha$ - $t$  relation, the second one suppresses it. This limitation in the second method can be removed if a cubic function in ' $t$ ' is used instead of Eq. (2). Owen and Williams (1954) have given such an expression for the lattice constant of silver. Similar procedure has also been used by Dheer and Surange (1958) in their macroscopic study on lead. However, this procedure is rarely followed, perhaps because of the larger amount of computational work involved in it.

As a sample case, we have processed the X-ray data on sodium chlorate (Deshpande and Mudholker 1960) by all these method. The results are shown in Fig. 1. Curves I and II represent the results of the first two methods respectively and curve III is obtained by the use of the cubic expression. It is clear from the that there is a close agreement between the curves I and III. Curve II not only suppresses the non-linear variation of ' $\alpha$ ' with ' $t$ ' but, in this particular case, there are significant differences in the values of ' $\alpha$ ' at some temperatures. For other substances the values of ' $\alpha$ ' given by the three methods may agree with each other, within certain limits, but the possible non-linear nature of  $\alpha$ - $t$  curve can not be brought by the second method. The amount of calculations involved in the third method makes it rather lengthy and hence, the first method seems

to offer a practicable procedure for obtaining dependable results on the temperature variation of the coefficient of thermal expansion.

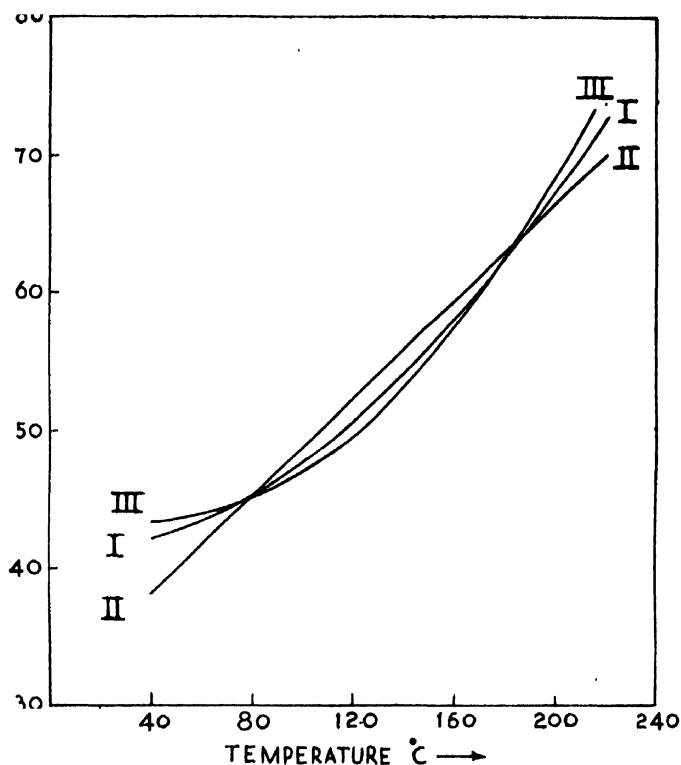


Fig. 1. ' $\alpha$ ' vs ' $T$ ' plots for sodium chlorate as obtained by the three methods of processing X-ray data.

One of the authors, (V.M.M.) is grateful to the Council of Scientific and Industrial Research for the award of a Junior Research Fellowship.

#### REFERENCES

- Deshpande, V. T. and Mudholker, V. M., 1960, *Acta Cryst.*, **13**, 482.  
 Dheer, P. N. and Surange, S. L., 1958, *Low Temperature Physics and Chemistry*, p. 592, Edited by Dillinger, The University of Wisconsin Press.  
 Kempter, C. P. and Elliot, R. O., 1959, *J. Chem. Phys.*, **30**, 1524.  
 Owen, E. O. and Richards, T. Ll., 1936, *Phil. Mag.*, **22**, 304.  
 Owen, E. O. and Williams, G. L., 1954, *J. Sci. Instr.*, **31**, 49.  
 Pathak, P. D. and Pandya, N. V., 1960, *Current Science*, **29**, 14.  
 Pathak, P. D. and Pandya, N. V., 1960 a, *Ind. J. Phys.*, **34**, 416.  
 Stokes, A. R. and Wilson, A. J. C., 1941, *Proc. Phys. Soc.*, **53**, 658.  
 Wilson, A. J. C., 1941, *Proc. Phys. Soc.*, **53**, 235.



# LIGHT ABSORPTION IN PARAMAGNETIC IONS IN STATE OF SOLUTION. PART III. $\text{Cr}^{3+}$ ION

A. MOOKHERJI AND N. S. CHHONKAR

PHYSICS LABORATORIES, AGRA COLLEGE, AGRA.

(Received March 27, 1961)

**ABSTRACT.** Light absorption in  $\text{Cr}^{3+}$  ion salts is studied by a Hilger's "UVISPEK" spectrophotometer in the range 3900 Å to 10,000 Å and the results are discussed in the light of crystalline electric field theory.

It is observed that the overall cubic splitting is much larger in  $\text{Cr}^{3+}$  salts compared to  $\text{Cu}^{2+}$ ,  $\text{Ni}^{2+}$  and  $\text{Co}^{2+}$  ion salts. The co-valency factor  $f^2$  as deduced from the lowering of the term separation arises from  $\sigma$ - and  $\pi$ -orbital overlap in  $\text{Cr}^{3+}$  ion salts.

The average magnetic moment and g-values evaluated with the help of the optical data agree very well with those observed experimentally.

The effect of the long range fields on the water cluster was found to depend on the value of  $f^2$ , since this is dependent on stabilizing energy, which is measured by  $f^2$ -values. It was observed that this effect was most pronounced in  $\text{Co}^{2+}$  ion ( $f^2 = 0.95$ ) and the least pronounced in  $\text{Cr}^{3+}$  ion ( $f^2 = 0.75$ ).

## INTRODUCTION

In the second part of this paper (Mookherji and Chhonkar, 1960), which we shall refer as Part II hereafter, a systematic optical investigation of the consequences of the crystalline electric field on the optical and magnetic behaviour of  $\text{Ni}^{2+}$  ion in about twenty salts in aqueous solution has been reported. A number of interesting results that have been obtained are:

a) The energy of separation of the mean centre of the absorption bands is almost wholly determined by the cubic part of the crystal field and that the anisotropic part has little influence on this.

b) There is weak covalent bonding in  $\text{Ni}^{2+}$  ion arising from the partial overlap with  $\sigma$ - and  $\pi$ -orbitals of the surrounding atoms, which lowers the term separation from the free ion value.  $\pi$ -orbital overlap is negligible in the ordinary salts of  $\text{Ni}^{2+}$  ion.

c) The measured finer splitting of the bands due to the tetragonal part of the field gave excellent agreement with the magnetic anisotropy values obtained from the susceptibility measurements.

d) The contribution of the distant atoms to the anisotropy of the water cluster about the  $\text{Ni}^{++}$  ion was found to be pronounced in certain salts; while in others they were not so pronounced.

The ground state of the free  $\text{Cr}^{+++}$  ion is an  $F$ -state ( $3d^3\ ^4F$ ) like  $\text{Ni}^{++}$  ion ( $3d^8\ ^3F$ ) but with a spin moment  $3/2$  instead of  $1$  as in  $\text{Ni}^{++}$  ion. Just like octahedrally coordinated  $\text{Ni}^{++}$  ions  $\Gamma_2$  orbital singlet level lies lowest in the Stark pattern for  $\text{Cr}^{+++}$  ion with similar coordination. But two facts, that the spin-orbit coupling in  $\text{Cr}^{+++}$  ion is  $+87\text{ cm}^{-1}$  (Laporte, 1928) as against  $-328\text{ cm}^{-1}$  in  $\text{Ni}^{++}$  ion and that  $\text{Cr}^{+++}$  ion with 3 electrons as against 8 in  $\text{Ni}^{++}$  ion has Kramers spin degeneracy, make the situation for  $\text{Cr}^{+++}$  ion somewhat different. Moreover, due to larger charge on  $\text{Cr}^{+++}$  ion the electrons of oxygens of the water cluster about  $\text{Cr}^{+++}$  ion will have a greater tendency to move into the central ion orbitals in order to stabilize its potential energy and hence both  $\sigma$ - and  $\pi$ -orbital overlap may be present in  $\text{Cr}^{+++}$  ions (Owen, 1955). This stabilization may tend to reduce the secondary distortions of the octahedral cluster and hence the splitting by the tetragonal part of the field will be very small. The small positive value of  $\lambda$  together with the small tetragonal splitting will make the magnetic anisotropy for  $\text{Cr}^{+++}$  ion much smaller compared to the anisotropy of the  $\text{Ni}^{++}$  ion and the magnetic moment will tend to have almost the spin-only value. Moreover, spin-orbit contribution from the upper cubic levels will be smaller compared to  $\text{Ni}^{++}$  ions and hence the effect of the distant atoms may be expected to be less pronounced in  $\text{Cr}^{+++}$  ion salts. It is, however, to be remembered that owing to the lowest state in Stark pattern being an orbital singlet, Jahn-Teller distortion should be almost absent and practically the entire anisotropy should arise from the induced distortion of the octahedron by the effect of the long range atoms.

It would, therefore, be interesting to study the optical absorption spectra of a number of chromic salts and view them in the light of the findings of magnetic susceptibility and other measurements.

#### EXPERIMENTAL

The measurements were carried out by Hilger's "UVISPEK" spectrophotometer and the same procedure as in Part I of this paper (Mookherji and Chhonkar, 1959) was adopted. The chemicals used were of 'Merck's gravimetric reagent quality. Triple distilled water was used for making solutions.

The measurements were centred round  $27^\circ\text{C}$ , but no observable change in the position of the absorption bands was noted for small room temperature variations.

#### RESULTS

The results of measurements are collected in Table I. The locations of the absorption bands for various salts of solution are given both in wavelengths and

in wave numbers. In order to get prominent absorption peaks for the salts studied we had to use dilute solutions. Progressive dilution from that concentration at which prominent absorption peaks are obtained does not change the positions of the absorption peaks.

TABLE I

Salts	Concentrations %	Maximum absorption			
		Wave length in Å		Wave numbers (cm <sup>-1</sup> )	
		I	II	I	II
Cr <sub>2</sub> (SO <sub>4</sub> ) <sub>3</sub>	0.5	5880	4225	17,010	23,670
Cr <sub>2</sub> (SO <sub>4</sub> ) <sub>3</sub> ·K <sub>2</sub> SO <sub>4</sub>	1.0	5790	4095	17,270	24,420
CrCl <sub>3</sub>	1.0	5810	4115	17,210	24,300
Cr(NO <sub>3</sub> ) <sub>3</sub>	1.0	5775	4085	17,310	24,480
Cr(C <sub>2</sub> H <sub>3</sub> O <sub>2</sub> ) <sub>3</sub>	0.3	5670	4110	17,640	24,330

The variation of absorption in different salt solutions are shown graphically in Figs. 1 to 2.

# DISCUSSION

## a) *The absorption spectra*

In all the five chromic salts studied by us the absorption spectra consist of two maxima, one at about 17,300 cm<sup>-1</sup> and the other at about 24,300 cm<sup>-1</sup>. We shall designate them as I and II respectively. The maximum which lies in the ultra violet region near 38,000 cm<sup>-1</sup> (Owen, 1955) will be known as III.

The spin-orbit coupling constant  $\lambda = +87$  cm<sup>-1</sup> is only one fourth of that of nickel salts and hence the splitting due to the tetragonal field will be very small compared to the Ni<sup>++</sup> ion. This is also what is observed experimentally (Krishnan, Mookherji and Bose, 1939) and hence optically we should expect only three main transitions, two being in the visible region and the other one in the ultra violet region.

The maxima I and II may be identified as arising due to the transitions between the Stark levels ( $\Gamma_2 - \Gamma_5$ ) and ( $\Gamma_2 - \Gamma_4$ ) respectively. In our later discussions these transitions will be represented as  $\Delta E_b$  and  $\Delta E_c$  respectively (Fig. 3).

## b) *Crystal field and energy levels*

The ground state of free Cr<sup>+++</sup> ion is 3d<sup>3</sup> <sup>4</sup>F and the term of the same multiplicity (<sup>4</sup>p) lies 13,770 cm<sup>-1</sup> above it (Moore, 1952). The type of the complex ions that we shall be dealing in this paper has the Cr<sup>+++</sup> ion at the centre of a

compressed octahedron of water molecules i.e. four dipoles  $\mu$  at  $(\pm a, 0, 0)$  and  $(0, \pm a, 0)$  and two dipoles  $\mu'$  at  $(0, 0, +b)$ . Then the electric field potential at  $(x, y, z)$  near the  $\text{Cr}^{+++}$  ion at  $(0, 0, 0)$  is of the form as given by Eq. (1) of Part II.

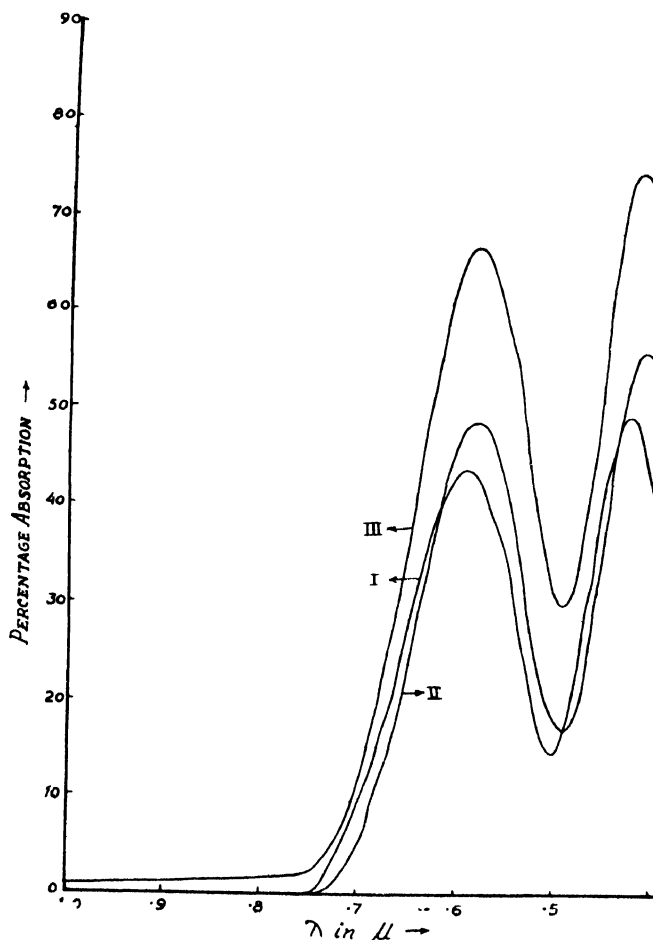


Fig. 1. Absorption curves (aqueous solution) of

- (I) 0.5%  $\text{Cr}_2(\text{SO}_4)_3$
- (II) 1.0%  $\text{Cr}_2(\text{SO}_4)_3 \cdot \text{K}_2\text{SO}_4$
- (III) 1.0%  $\text{CrCl}_3$

The crystal field conforming to a potential as given by Eq.(1) of Part II splits the ground state  $^4\text{F}$  into a number of levels whose approximate energies, according to Owen (1955) are shown in Fig. 3 and also given by Eq. (2) of Part II.

The measured magnetic anisotropy for  $\text{Cr}^{+++}$  ion in crystals is very small (Krishnan *et al.*, 1939), and tetragonal separation in state of solution will be

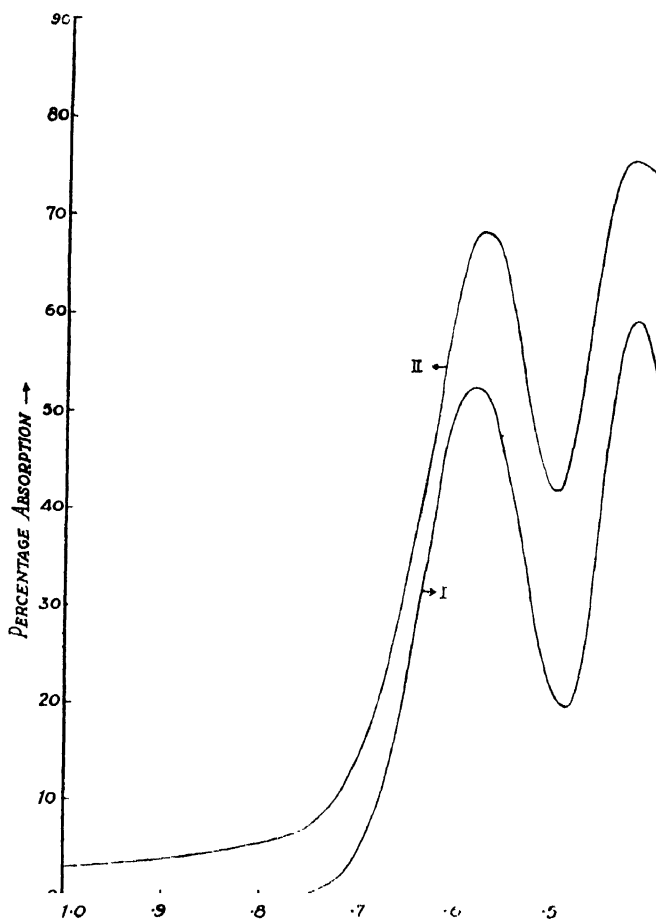


Fig. 2. Absorption curves (aqueous solution) of

(I) 1.0%  $\text{Cr}(\text{NO}_3)_3$

(II) 0.3%  $\text{Cr}(\text{C}_2\text{H}_3\text{O}_2)_3$

correspondingly less and hence neglecting  $T_4$  and  $T_2$  terms in Eq. (2) of Part II we have

$$\frac{6}{7} K - X = \Delta E_c$$

and

$$\frac{10}{21} K = \Delta E_b$$

We have observed both  $\Delta E_c$  and  $\Delta E_b$  experimentally (Table I) and hence  $K$  and  $X$  can be approximately evaluated. These are given in Table II.

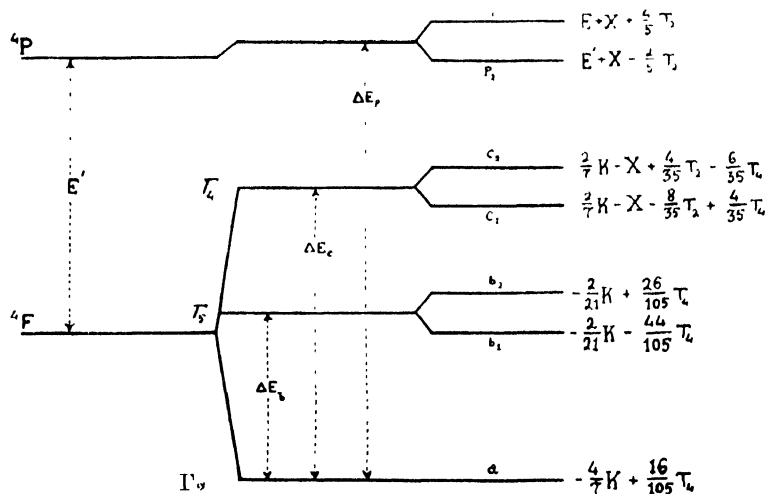
Fig. 3 Stark splitting of the ground state of  $\text{Cr}^{+++}$  ion.

TABLE II

Salts	K $\text{cm}^{-1}$	X $\text{cm}^{-1}$	$E'$ $\text{cm}^{-1}$	f2
$\text{Cr}_2(\text{SO}_4)_3$	35,720	6950	9870	0.717
$\text{Cr}_2(\text{SO}_4)_3 \cdot \text{K}_2\text{SO}_4$	36,267	6666	10950	0.795
$\text{CrCl}_3$	36,140	6680	10650	0.773
$\text{Cr}(\text{NO}_3)_3$	36,350	6680	10030	0.730
$\text{Cr}(\text{C}_2\text{H}_3\text{O}_2)_3$	37,045	7420	9810	0.712

These  $K$ -values indicate that in state of solution all the six members of the cluster about the  $\text{Cr}^{+++}$  ion may be the same in all the salts except the last in Table II studied by us.

It would be interesting to compare the magnitudes of  $K$ -values of  $\text{Cu}^{++}$  and  $\text{Ni}^{++}$  ions with those of  $\text{Cr}^{+++}$  ion. We find that in ordinary ionic salts of  $\text{Cu}^{++}$  ion (Part I, 1959) and of  $\text{Ni}^{++}$  ion (Part II) the magnitudes of  $K$  are about  $25,000 \text{ cm}^{-1}$  and  $17,700 \text{ cm}^{-1}$  respectively, while in ordinary chromic salts its value is approximately  $36,300 \text{ cm}^{-1}$ . Hence the overall separations  $(10/21 K)$  in  $\text{Cu}^{++}$  ion and  $(6/7K)$  in  $\text{Ni}^{++}$  ion and  $\text{Cr}^{+++}$  ion are  $12,400 \text{ cm}^{-1}$ ,  $15,200 \text{ cm}^{-1}$  and  $24,400 \text{ cm}^{-1}$  respectively and hence it is highest in  $\text{Cr}^{+++}$  ion salts.

#### c) Evaluation of the term separation ( $E'$ )

For  $\text{Cr}^{+++}$  ion where  $^4F$ -term lies lowest, the term separation  $E'$  in crystals which is an important spectroscopic constant, can be evaluated from the expression (1) as given below (Owen, 1955):

$$X = - \left( \frac{E' + \frac{2}{7} K}{\alpha} \right) + \left[ \left( \frac{E' + \frac{2}{7} K}{\alpha} + K \right)^2 \right]^{1/2} \quad (1)$$

where symbols have their usual meanings.

Now utilising our calculated  $K$ - and  $X$ -values (Table II) we have evaluated  $E'$ -values from Eq. (1). These are given in Table II. It is seen that there is a lowering of the term separation for  $\text{Cr}^{+++}$  ions in crystals from the free ion value  $E = 13,770 \text{ cm}^{-1}$ . Following Owen (1955) this lowering may be attributed to the covalency factor  $f^2$ , where  $f^2 = f_\sigma^2 \cdot f_\pi^2$ , arising from partial overlap of the 3d-orbitals with  $\sigma$ - and  $\pi$ -orbitals of the surrounding atoms. Accordingly,

$$\frac{E'}{E} = f^2 \quad \dots (2)$$

From Eq. (2) one can calculate  $f^2$  which are given in Table II.

Primarily this covalency factor should not be different for all the salts in which  $\text{Cr}^{+++}$  ion is similarly coordinated with six water molecules, but there might be an appreciable change in the overlap between  $\text{Cr}^{+++}$  ion and oxygen and hence in the covalency factor from salt to salt arising from the effect of distant atoms. In state of solution distant atom effect will be negligible and hence covalency factor should not vary appreciably from salt to salt with similar coordination. Bose and Mitra (1952) in their masterly survey of the comparative influence of short and long range fields on the magnetic behaviour of salts of iron group of elements came to the conclusion that long range field effect in  $\text{Cr}^{+++}$  ion salts will be less pronounced than  $\text{Ni}^{++}$  ion salts.

It is seen that these  $f^2$ -values are considerably smaller than those of  $\text{Cu}^{++}$  (0.85) and  $\text{Ni}^{++}$  (0.9) ions. This demands a stronger bonding in  $\text{Cr}^{+++}$  ion, which is to be attributed to the larger charge on it. As a result of this larger charge the electrons on the oxygen have got a tendency to move into the central chromic ion in order to even out the charge distribution. Under such state of affairs we are no longer justified to take  $\pi$ -bonding as weak and hence  $f^2$  in them will consist of both  $f_\sigma^2$  and  $f_\pi^2$ . Moreover, if  $\sigma$ -bonding is strong there may be some amount of  $\pi$ -bonding which will decrease the hyperfine structure in hydrated complexes of  $\text{Cr}^{+++}$  ions as actually observed by Bowers (1952) and Baker and Bleaney (1952).

From the above discussion it seems that in  $[\text{Cr}(\text{H}_2\text{O})_6]^{+++}$  complexes  $f_\pi^2$  will tend to a value  $\sim 0.9$  and  $f_\sigma^2$  to a value  $\sim 0.85$ , making  $f^2 = f_\sigma^2 \cdot f_\pi^2 = 0.76$  as actually observed (Table II).

#### d) Calculation of magnetic moment values :

The expression for the mean magnetic moment for  $\text{Cr}^{+++}$  ion will be almost similar to that for  $\text{Ni}^{++}$  ion excepting that the spin-only value will be 15 instead of 8, and will be given by the Eq. (9) of Part II and hence the mean magnetic moment is given by

$$\mu^2 = 15[1 + (8\lambda - 3kT) \cdot \alpha'] \quad \dots (3)$$

where 
$$\alpha' = f^2 \cdot \alpha = - \frac{f^2}{\Delta E_b} = -2.1 \frac{f^2}{K}$$

It is interesting to note that the last two terms in the expression (3) which represent the deviation of the effective magnetic moment from its spin-only value are of opposite sign. The comparative strengths of the two terms at 300°K will be

$$8\lambda = 696 \text{ cm}^{-1}$$

and

$$3kT = 630 \text{ cm}^{-1}$$

The difference in them is only  $\sim 66 \text{ cm}^{-1}$  which when multiplied by  $\alpha'$  having a negative value will bring down the spin-only value by about 0.004. Hence the relative contribution from these two terms is very very small as is shown below :

$$\mu^2 = 15(1 - 0.04 + 0.037)$$

It is therefore clear that in chromium salts there will be very small deviation ( $\approx 0.4\%$ ) from the spin-only value.

Now utilising our calculated values of  $K, f^2$  and the Eq. (3) we have evaluated  $\mu$ -values for  $\text{Cr}^{+++}$  ion in state of solution for different salts. These are given in Table III. For comparison we have included solution values in the Table. It is seen that the two values (optical and magnetic) agree well within the experimental errors.

These values of the mean magnetic moment for  $\text{Cr}^{+++}$  ion salts have almost the spin-only value (3.87) as has already been shown above.

TABLE III

Salts	$\mu$ -Values		g-Values	
	Optical (soln.)	Magnetic (soln.)	Optical	Crystal
$\text{Cr}_2(\text{SO}_4)_3$	3.867	3.850*2	1.970	1.980*
$\text{Cr}_2(\text{SO}_4)_3 \cdot \text{K}_2\text{SO}_4$	3.866	3.778*3	1.968	1.980*
$\text{CrCl}_3$	3.867	3.850*2	1.989	1.990**
$\text{Cr}(\text{NO}_3)_3$	3.867	3.745**	1.968	2.260***
$\text{Cr}(\text{C}_2\text{H}_3\text{O}_2)_3$	3.868	3.756*1	1.972	—

\*Ting and Williams, 1951.

\*\*Kozyrev, Salikhov and Shamonin, 1952.

\*\*\*Lancaster and Gordy, 1951.

\*1 Mookherji, T. (Unpublished)

\*2 Cabrera, Marquina, 1922.

\*3 Welo, 1929.

\*4 Fahlenbrach, 1932.

} For complete reference consult Selwood's, *Magnetochemistry*.



e) Calculation of  $g$ -values :

The spectroscopic splitting factor  $g$  for  $\text{Cr}^{+++}$  ion according to Owen (1955) is given by

$$g = 2 - \frac{12\lambda}{\Delta E_b} f^2 = 2 - \frac{25.2\lambda}{K} f^2 \quad \dots (4)$$

Substituting the values of  $K$  and  $f^2$  from Table II,  $g$ -values could be calculated which are given in Table III. In the absence of any experimental  $g$ -values in state of solution for  $\text{Cr}^{+++}$  ion we have included crystal  $g$ -values in the table for comparison. It is seen that  $g$ -values in state of solution and in crystal do not vary appreciably.

From our optical measurements we observe that  $f^2$ -values in  $\text{Cr}^{+++}$ ,  $\text{Cu}^{++}$ ,  $\text{Ni}^{++}$  and  $\text{Co}^{++}$  ions are  $\sim 0.75$ ,  $\sim 0.85$ ,  $\sim 0.9$  and  $\sim 0.95$  respectively (Mookherji and Chhonkar, 1959, 1960).  $f^2$ -Values give the covalent character of the ions; so the covalent character will go on decreasing as we go from  $\text{Cr}^{+++}$  to  $\text{Co}^{++}$  ions. Further, more covalent the ion is, the more stable will be the water cluster surrounding it. As a result, the stabilizing energy in case of  $\text{Cr}^{+++}$  ion will be larger compared to others and that this will tend to minimise the secondary distortions of the octahedral cluster. We have already seen that these secondary distortions will be produced by the effect of the distant atoms alone and that too will be minimised by the high stability of the water cluster. That this effect is very small is also supported by magnetic anisotropy measurements (Krishnan *et al*, 1939). It is therefore, clear from the above discussion that the distant atom effect in  $\text{Cr}^{+++}$  ion will not be pronounced; whereas this should be most pronounced in  $\text{Co}^{++}$  ion, less in  $\text{Ni}^{++}$  and almost negligible in  $\text{Cu}^{++}$  ions.

#### ACKNOWLEDGMENTS

The work was carried out at the Physics Laboratories of Agra College, Agra,. We wish to express our sincere thanks to University Grants Commission whose generous grants enabled us to carry out this piece of work.

Our sincere thanks are also due to Professor A. Bose, D.Sc., F.N.I. for his helpful criticisms and concrete suggestions.

#### REFERENCES

- Bowers, K. D. 1952, *Proc. Phys. Soc.*, **65**, 860.  
 Baker J. M. and Bleaney, B. 1952, *Proc. Phys. Soc.*, **65**, 952.  
 Bose, A. and Mitra, S. K. 1952, *Ind. J. Phys.*, **26**, 543.  
 Kozyrev, B. M. Salikhov, S. G. and Shamonin Yu. Ya. 1952, *J. Exp. Theor. Phys.* **22**, 56.  
 Krishnan, K. S., Mookherji, A. and Bose, A. 1939, *Phil. Trans., Roy Soc.* **239A**, 125.  
 Lancaster, F. W. and Gordy, W., 1951, *J. Chem. Phys.*, **19**, 1181.  
 Laporte, O. 1928, *Z. Phys.* **47**, 761.  
 Mookherji, A. and Chhonkar, N. S. 1959, *Ind. J. Phys.* **33**, 74.  
 Mookherji, A. and Chhonkar, N.S., 1960, *Ind. J. Phys.* **34**, 147, 336, 363.  
 Moore, C.E., 1952, Atomic Energy Levels -*Nat. Bur. Stand. Circ.* 467, Vol. 11.  
 Owen, J. 1955, *Proc. Roy. Soc.*, 227, 183.  
 Ting, Y. and Williams, D., 1951, *Phys. Rev.* **82**, 507.

# ANELASTIC MEASUREMENT OF DIFFUSION IN $\alpha$ -AgCd ALLOYS

M. A. QUADER

DEPARTMENT OF GENERAL PHYSICS & X-RAYS,

INDIAN ASSOCIATION FOR THE CULTIVATION OF SCIENCE, CALCUTTA-32

(Received May 1, 1961)

**ABSTRACT.** Measurements of the internal friction peak are made for three  $\alpha$ -AgCd alloys with 24.3, 29.3 and 33.8 atomic percent Cd and 30.8% Zn  $\alpha$ -brass. The peaks are due to changes in local order with the external stress. The activation energy corresponding to the relaxation process is found to be 39.36, 38.77 and 38.45 K cal/mole for the 24.3, 29.3 and 33.8 at. % Cd alloys respectively. For the grain boundary relaxation effects the activation energy is 39.7 K cal/mole for the 29.3% Cd alloy. The corresponding activation energies for the 30.8% brass are 39.17 and 39.84 K cal/mole.

The measured values of the relaxation time  $\tau$  are used to calculate the diffusion coefficient of the Ag-Cd alloys. The calculated values are in good agreement with the directly measured diffusion coefficients of alloys of corresponding compositions.

## INTRODUCTION

The measurements of anelastic effects caused by stress induced ordering and observed as an internal friction peak in some substitutional alloys present a method of obtaining diffusion coefficient at lower temperatures and in a time of the order of that required by a single atomic jump. The method has been applied extensively to study the diffusion in  $\alpha$ -AgZn (Nowick, 1952) and  $\alpha$ -CuZn (Leclaire, 1951) alloys and to a lesser extent in some other alloys. Both these authors have pointed out the advantages which may be gained by using this method to study small scale atomic movements in cases where conventional diffusion techniques are inapplicable on account of the long times and high temperature required. The principle of the method is briefly as follows: The application of stress to a random solid solution will, in general change the equilibrium configuration to a non-random one. Atomic redistribution must, therefore, follow the application of stress; this redistribution is accompanied by typical anelastic effects, such as, an internal friction peak and an elastic after effect.

This internal friction effect in substitutional solid solutions, first seen by Zener (1943) in 30%  $\alpha$ -brass, has been observed later in many other substitutional alloys. These studies revealed that the magnitude of the effect goes up roughly

as the square of the solute concentration, and the process is an activated one with an activation energy close to that for diffusion in the alloys. On this evidence Zener (1947) interpreted the above effect as being due to a preferential orientation, under applied stress, of the axis of pairs of adjacent solute atoms into a particular crystallographic direction such that the axial strain set up by each pair in the lattice as a result of the different sizes of the solute and solvent atoms, would be partially relieved. Later, Nowick (1952) and Leclaire and Lomer (1954) have postulated more elaborate geometrical schemes for the process. They have, however, retained Zener's idea that the effect arises fundamentally from a microscopic rearrangement of atoms when the material is placed under stress, i.e. stress-induced short range ordering. The latter workers presume that the relaxation arises from lattice dilatation accompanying changes in the degree of order and express the damping of a given alloy in terms of a number of parameters including the short range order parameter,  $\sigma$ . The effect of the degree of order on damping has been verified by Lulay and Wert (1956) in MgCd alloys.

In the present paper an account is given of the investigations of the anelastic effects in  $\alpha$ -AgCd alloys. This was chosen since the diffusion data for it are available through the measurement of tracer diffusion by Manning (1959) and these could be utilized to compare and interpret the results of the anelastic measurements. Internal frictions in 30.8%  $\alpha$ -brass was also measured in order to compare the efficiency of the torsion pendulum constructed by the author.

#### THEORY AND FORMULAE

Nowick (1952) made the assumption that since the essential atomic process involved in a change in order, which is responsible for the relaxation of strain when a stress is applied to the solid, is the replacement, on a number of lattice sites, of one type of atom by another, then the relaxation rate  $1/\tau$  should be simply proportional to  $\Gamma_r$ , the mean rate at which a replacement on a given site occurs. Thus

$$1/\tau = \alpha \Gamma_r \quad \dots (1)$$

$$\text{and} \quad D = \beta a^2 \Gamma_r \quad \dots (2)$$

where  $D$  is the diffusion coefficient of the alloy in the absence of concentration gradients, ' $a$ ' is the lattice parameter and  $\beta$  is a geometrical factor and is  $1/12$  for f.c.c. lattice. The dimensionless proportionality constant  $\alpha$  is of the order of unity. The relaxation time  $\tau$  obeys the Arrhenius type equation

$$\tau = \tau_0 e^{H/RT} \quad \dots (3)$$

where  $H$  is the activation energy,  $R$  the gas constant and  $T$  the absolute temperature.

For the standard linear solids in the sense defined by Zener (1948), strain is not simply proportional to the stress but the two quantities are also connected with their first time derivatives by means of a linear relation which, for a vibrating solid, leads to an expression for the internal friction,  $Q^{-1}$  in terms of the angular frequency of oscillation  $\omega$  and a mean relaxation time  $\tau$ .

$$Q^{-1} = \Delta_M \frac{\omega\tau}{1 + (\omega\tau)^2} \quad \dots \quad (4)$$

where  $\Delta_M$  'the relaxation strength' is a measure of the magnitude of the effect. Eq.(4) gives the well known internal friction peak with maximum value of  $\omega\tau = 1$ . Thus if  $T_m$  is the temperature of maximum damping, we have

$$\tau(T_m) = \frac{1}{\omega} \quad \dots \quad (5)$$

as the basis for the determination of  $\tau$  at one particular temperature  $T_m$  from an internal friction peak.

#### EXPERIMENTAL MEASUREMENT OF INTERNAL FRICTION

The internal friction measurements were carried out in a torsional pendulum which is patterned after Kê(1947) and is shown diagrammatically in Fig. 1. The wire specimen  $S$  is firmly clamped between the upper V-grip  $V$  and the lower pinvice  $p$ . The pinvice is welded to a thick nichrome wire (B and S gauge No. 13) which is a poor conductor of heat but has a much higher rigidity than the test wire at various higher temperatures. A galvanometer mirror  $M$  mounted on the nichrome wire reflects the image of a straight filament on to the photographic recorder two meters away. BB is a torsional bar about 8" inches long carrying at each end a small iron weight. The torsional vibration can be set up by momentarily actuating two small electromagnets placed at a suitable distance from the iron weights and the vibrations are recorded photographically on a rotating drum. The pendulum is heated in an electrically heated tube furnace and the temperature is recorded by a calibrated chromel-alumel thermocouple placed close to the specimen.

$\alpha$ -AgCd alloys with 33.8, 29.3 and 24.3 at. % Cd and  $\alpha$ -brass with 30.8 at. % Zn were prepared by melting appropriate quantities of the spectroscopically pure metals as described earlier (Quader, 1960). The alloys thus prepared were taken in evacuated Pyrex tubes and homogenized at 650°C for two days, then reduced in diameter by rolling and finally drawn down to wire of 1 mm diameter for use in the torsional pendulum. The wires were cut to proper size (7" long), straightened and again sealed in evacuated Pyrex tubes and annealed at 600°C for 6 hours and thereby developed uniform grains with the average grain size of .02 cm.

The AgCd specimen was mounted in the pendulum and annealed there for 15 mins. at about 430°C, and internal friction measurements were obtained during cooling and subsequent heating of the pendulum. The maximum ampli-

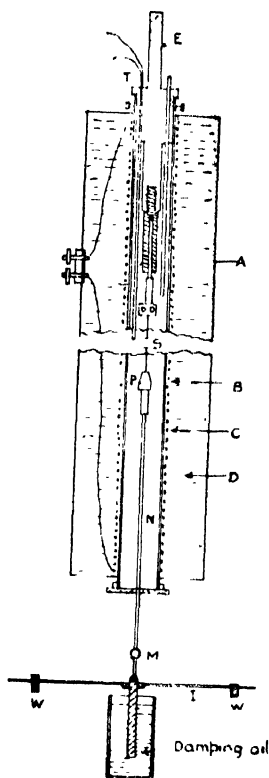


Fig. 1. Torsional pendulum.

tude of oscillation in all the measurements was not allowed to exceed that corresponding to a torsional strain of  $4 \times 10^{-5}$ . For this small strain the decrement was found to be independent of the amplitude. At the ends of the measurements the wires were examined by taking X-ray diffraction photographs to ensure that no appreciable loss of Cd had occurred during measurements. The  $\alpha$ -brass specimen was annealed at 530°C for one hour after mounting in the pendulum and measurements were taken both during cooling and heating of the pendulum.

The internal friction and rigidity were obtained by measuring respectively the logarithmic decrement and the frequency of the free torsional vibration of the pendulum. The measure of internal friction ( $Q^{-1}$ ) herein adopted was the logarithmic decrement divided by  $\pi$ .

## EXPERIMENTAL RESULTS

(a) *AgCd Measurements* :

Typical internal friction curves for the three  $\alpha$ -AgCd alloys, measured at two different frequencies of vibrations, are shown in Fig. 2 and have been plotted as

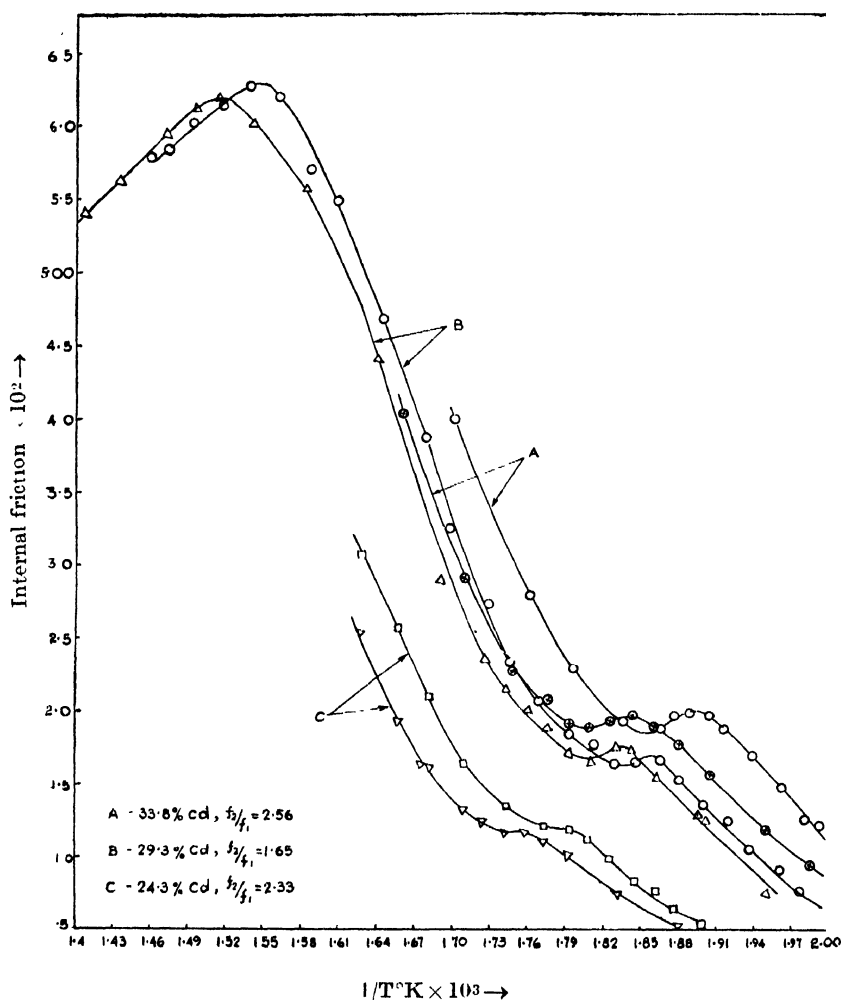


Fig. 2. Internal friction, inverse temperature for  $\alpha$ -Ag-Cd alloys.

a function of reciprocal of the absolute temperature. In these curves a small peak occurs (such as one at  $266^{\circ}\text{C}$  at 0.88 c/s for the 29.3 % alloy) followed by a broader grain boundary peak at a higher temperature. The weak internal friction peak is due to the relaxation effects similar to that observed by Zener (1943) and Kê (1948) in 30%  $\alpha$ -brass and is due to stress induced ordering in the alloy.

From the curves it is evident that the peak height increases with increasing Cd content and varies roughly as the square of the Cd-concentration. Since the grain boundary relaxation greatly affects the height of the order peak, a correct estimation of the relaxation strength which is twice the height of the peak is not possible. However, the location of the peak, which, according to Nowick (1952), is unaffected by the grain size, can be obtained from the graph within  $\pm 1^\circ\text{C}$ . Hence from the frequency and the temperature at the maximum, the corresponding relaxation time can be obtained from Eq.(5). The activation energy  $H$  is obtained from the shift of the maximum with the frequency with the help of the relation.

$$H = R \ln(f_2/f_1) / \left( \frac{1}{T_1} - \frac{1}{T_2} \right) \quad \dots (6)$$

where the two frequencies  $f_1$  and  $f_2$  correspond to the temperatures  $T_1$  and  $T_2$ . The results are given in Table I.

TABLE I  
Activation energy for the Zener and grain boundary relaxations

Alloy system	Composition at. % solute	$H_{\text{order}}$ in K cal/mole	$H_{gb}$ in K cal/mole
Ag-Cd	24.3	39.36	39.1
	29.3	38.77	
	33.8	38.45	
Cu-Zn	30.8	39.17	39.84

The activation energy is found to decrease with increase of cadmium concentration in a linear fashion. Hence, by extrapolating the straight line plot of the activation energy against Cd concentration to 0 % Cd we get  $H_{0\%Cd} = 41.6\text{K}$  cal/mole which is close to the value  $41.7\text{K}$  cal/mole for tracer diffusion of Cd in pure silver (Tomizuka *et al.*, 1954). However, in case of AgZn alloy Nowick got  $H_{0\%Zn} = 40.6\text{K}$  cal which he assumed to correspond to the activation energy of self diffusion of silver.

The internal friction maximum due to grain boundary relaxation was measured only in 29.3% Cd alloy, and the corresponding activation energy  $H_{gb} = 39.17$  K cal/mole was obtained. According to Pearson (1956),  $H_{gb} = 38.00\text{K}$  cal/mole for i.e 32.4% Cd alloy. The mechanism of grain boundary relaxation is not clearly

known, but various observations show that it is probably connected with the movements of dislocation in grain boundary.

(b) *CuZn Measurement :*

The internal friction in 30.8 at % Zn  $\alpha$ -brass was measured at three different frequencies and the results are shown in Fig. 3. The curves are similar to those

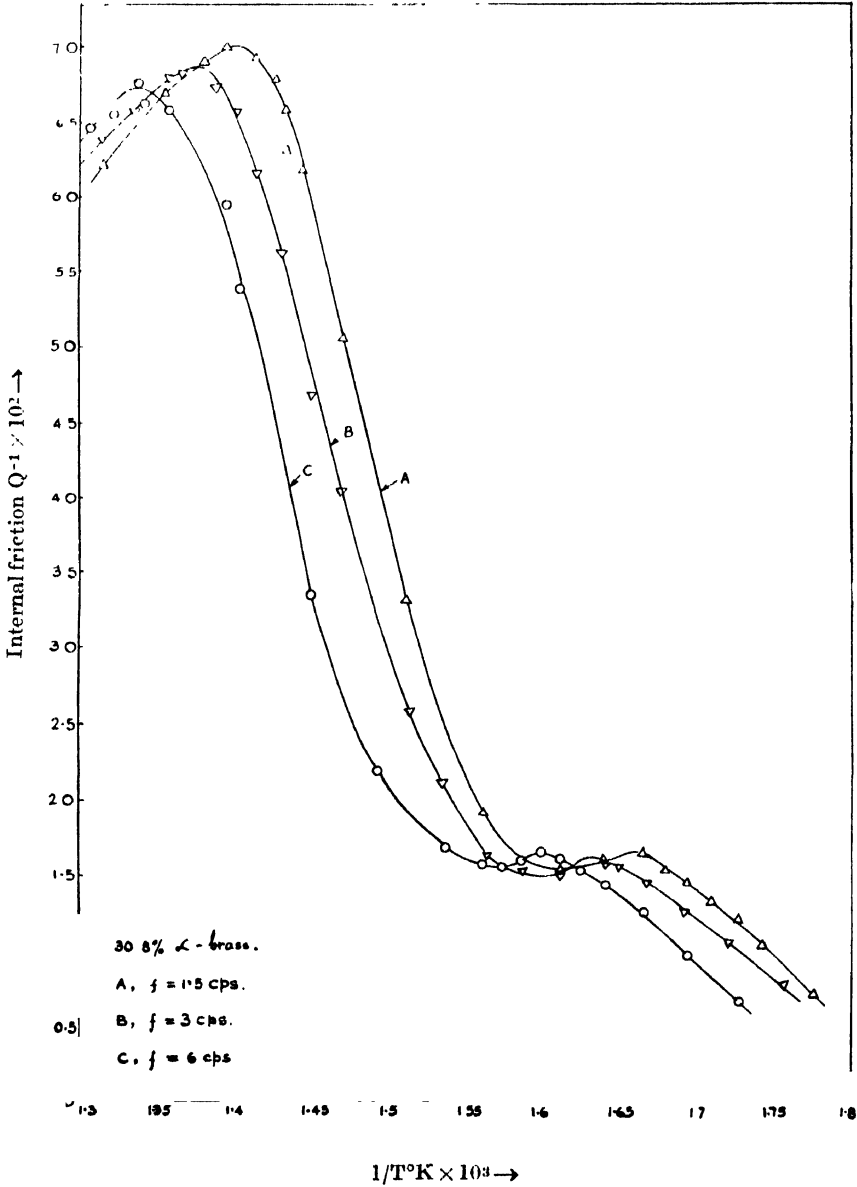


Fig. 3. Internal friction, inverse temperature for 30.8%  $\alpha$ -brass.



obtained by Kê (1948) for polycrystalline 29 at.%  $\alpha$ -brass. The activation energy was calculated from the shift of the peaks and  $H_{order} = 39.17$  Kcal/mole and  $H_{gb} = 39.84$  Kcal/mole are obtained for the Zener and grain boundary relaxations respectively. According to Kê the corresponding values are  $H_{order} = 41.7$  Kcal/mole and  $H_{gb} = 41.00$  Kcal/mole for the 29 at. % brass whereas Leclaire (1954) in a precision measurement with single crystal wire specimen got  $H_{order} = 37.3 \pm 1$  Kcal/mole. The latter workers put forward a new theory of relaxation strength based on the assumption of lattice dilatation accompanying changes in the order and obtained satisfactory agreement between the theoretically calculated and experimentally measured relaxation strength in a series of  $\alpha$ -CuZn alloys.

c) *Measurement of rigidity modulus :*

The frequency of vibration of the pendulum was measured at different temperatures along with the internal friction measurements. Since the rigidity modulus  $G$  of the wire is proportional to the square of the frequency of vibration when the internal friction is small, some additional information may be obtained from a plot of frequency squared against temperature. Such curves for the 29.3% AgCd and 30.8% CuZn alloys are shown in Fig. 4. The curves are similar to

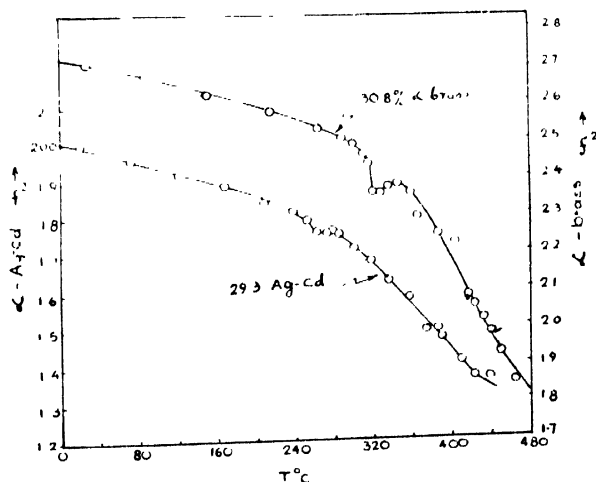


Fig. 4.  $f^2 - T$  for 29.3% AgCd and 30.8% CuZn alloys.

that obtained by Kê (1948) for  $\alpha$ -brass and represent the variation of rigidity with temperature. The deviation of the rigidity from linearity at higher tem-

peratures, say, above 200°C for the 29.3% alloy, is due to the grain boundary relaxation effects. The small dip at 266° corresponds to the internal friction peak due to ordering. Similar is the case with  $\alpha$ -brass when the dip occurs at 328°C corresponding to the order peak.

## DISCUSSION

If the relaxation effects are to be ascribed to the local atomic rearrangement produced under stress, then the relaxation time  $\tau$  should be of the order of the atomic jump rate  $a^2/12D$ , where  $D$  is the diffusion coefficient in the absence of a concentration gradient. That this is so has been shown experimentally by Leclaire (1954) for a no. of alloys where both the diffusion and relaxation data are available. A similar comparison between the relaxation times and the diffusion coefficients is shown in Fig. 5 for the Ag-Cd alloys in which  $\log D$  and  $\log a^2/12\tau$  values are

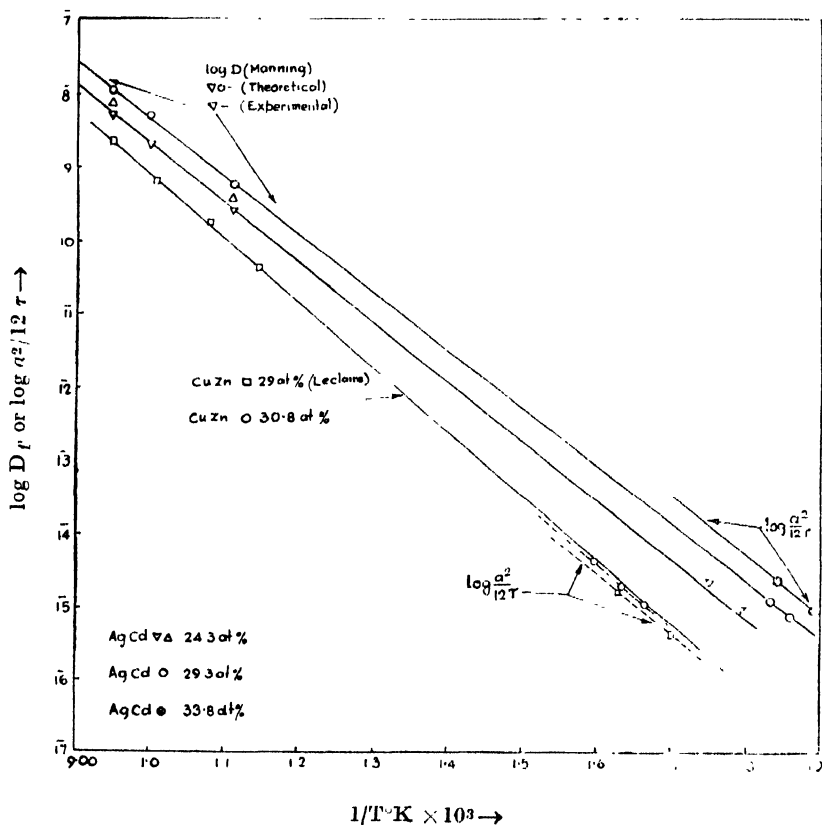


Fig. 5. Comparison of diffusion coefficient and  $a^2/12\tau$  values.

plotted against inverse absolute temperature. The approximate values of chemical diffusion coefficients,  $D_{chem}$  for the 24.3 and 29.3% Cd alloys at three different

temperatures were obtained from Manning's (1959) curves, who measured the tracer diffusion in AgCd alloys up to 27 at. % Cd. He also calculated  $D_{chem}$  from the Darkens' (1948) theoretical relation,

$$D_{chem} = (f_{Ag}D_{Cd} + f_{Cd}D_{Au}) \left( 1 + \frac{d(\ln \gamma_i)}{d(\ln f_i)} \right) \quad \dots (7)$$

using Schoen's tracer diffusion values  $D_i$  and the thermodynamic factor from Herasymenko's (1956) vapour pressure data. The experimental  $D_{chem}$  values are usually higher than the calculated ones, and are, according to Manning, probably somewhat in error at the limiting concentrations. The  $D_{chem}$  values for the 29.3% alloy were, therefore, obtained by extrapolating the theoretical curves only. However, for the 24.3% alloy both the theoretically calculated and experimental values of  $D_{chem}$  were read out directly from his curves. The  $D_{chem}$  values were corrected for the thermodynamic factor, also obtained from Manning, before use for comparison with the anelastic data. The value of  $D$  so obtained are given in Table II. The  $\log a^2/12\tau$  values for all the alloys are recorded in Table III.

TABLE II

Directly measured diffusion coefficients of AgCd alloys as obtained from Manning (1959)

Composition at. % Cd.	$1 + \frac{d(\ln \gamma_i)}{d(\ln f_i)}$	T K	$1/T$ K <sup>-1</sup> $\times 10^3$	$\log D$ calculated from theo- retical curve	$\log D$ calculated from experi- mental curve
24.3	2.5	900	1.111	10.394	10.530
		1000	1.000	9.309	9.309
		1053	0.949	9.716	9.852
29.3	3.0	900	1.111	10.753	
		1000	1.000	9.602	
		1053	0.949	8.025	

For the sake of comparison the  $\log a^2/12\tau$  values for 30.8%  $\alpha$ -brass are also shown in Fig. 5 along with the diffusion and anelastic data for the 29%  $\alpha$ -brass taken from Leclaire (1951). For the 30.8% brass the  $\log a^2/12\tau$  values are higher than those of 29% brass and are, as expected, giving a higher value for the diffusion coefficient.

TABLE III

Diffusion coefficient calculated from anelastic measurements

Alloy system	Composition at. % solute	T °K	1/T °K $\times 10^3$	$\log a^2/12\tau$
Ag-Cd	24.3	558	1.793	16.965
	—	572	1.750	15.333
	29.3	538.5	1.858	16.858
	—	546	1.832	15.077
	33.8	529	1.891	16.940
	—	543	1.842	15.349
Cu-Zn	30.8	601	1.664	15.038
		612	1.633	15.283
		626	1.597	15.603

It is evident from Fig. 5 that for AgCd alloys the  $\log a^2/12\tau$  values are, within the limits of the experimental error, either slightly above or in the same line with the  $\log D$  values obtained from Manning's theoretical curves. But when the experimental values of  $D_{hem}$  were considered the anelastic data fall below the extrapolated  $\log D$ , and this for the 24.3% alloy is shown in Fig. 5. These results are in agreement with the observations of Laclaire (1954) in other alloys supporting Nowick's conclusion that  $\tau$ , unlike  $D$ , is governed mainly by the diffusion rate of the more slowly moving components. Based on the above assumption Nowick gave an approximate relation for  $\Gamma_\tau$ , the mean rate of replacement

$$\frac{1}{\Gamma_\tau} \approx \frac{a^2}{24} \left( \frac{1}{f_A D_A} + \frac{1}{f_B D_B} \right) \quad \dots \quad (8)$$

connecting  $D_A$  and  $D_B$ , the atom self-diffusion coefficients. Leclaire (1954) in a critical discussion argued that the Eq. (8) should not hold for extreme compositions where the atoms of one type are, for the most part, distributed singly in a matrix of the other. Movements of such isolated atoms, if sufficiently far apart, would not affect the order or give rise to a relaxation of stress or strain and the effects observed would correspond to rearrangements involving groups of two or more solute atoms. The  $\Gamma_\tau$  appropriate to the extreme concentrations will be more nearly the mean  $\Gamma_\tau$  of an intermediate concentration.

Nowick made an estimate of  $\alpha$  (see, Eq. 1) by assuming for  $\tau_0$  an expression similar to that derived by Zener (1948) for the case of  $D_0$  in self-diffusion and comparing with the value of  $\tau_0$  obtained experimentally. Thus he obtained  $\alpha \approx 0.3$  for the AgZn alloys. For the 30%  $\alpha$ -brass Leclaire calculated Eq.(8) in terms of  $D_{zn}$  and  $D_{zn}/D$  and compared the measured ( $\tau$ ) and calculated ( $\alpha\tau$ ) values. In this calculation he used a constant value of 1.26 for  $D_{zn}/D$  for all the temperatures. From the observation he concluded that at least for 30%  $\alpha$ -brass Nowick's relation seems to be valid with  $\alpha$  closely equal to unity.

Nowick's expression was recalculated for the AgCd alloys in terms of  $D$  ( $D = f_A D_B + f_B D_A$ ) and  $D_{Cd}/D_{Ag}$  values of Manning's tracer diffusion measurements. The logarithm of the calculated ( $\alpha\tau$ ) and measured ( $\tau$ ) values are plotted against  $1/T$  in Fig. 6. Reference to the figure shows that the  $\alpha\tau$  and  $\tau$  values do

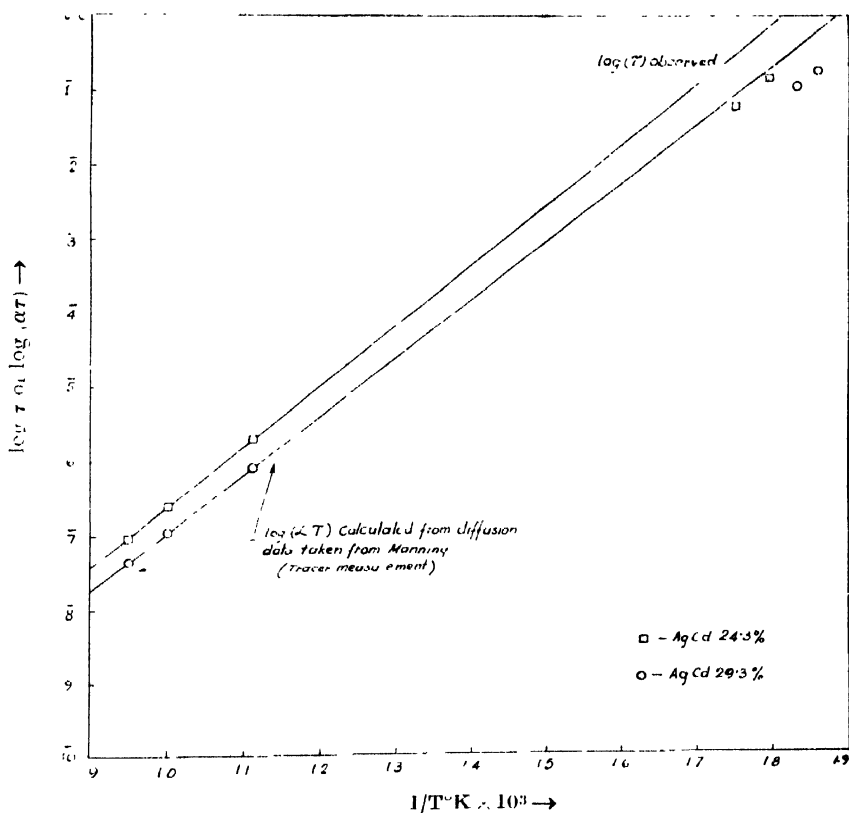


Fig. 6. Comparison of  $\log(\alpha\tau)$  calculated and  $\log(\tau)$  observed for 24.3 and 29.3% AgCd alloys.

not fall on the same line, the former being higher, showing that the  $\alpha$  is greater than unity. To make the calculated  $\tau$  values fall on the same line with the measured ones,  $\alpha$  should be equal to 2.8 and 3.1 respectively for the 29.3 and 24.3% alloys. This result that  $\alpha$  is higher than unity seems unreasonable, since

it means that the relaxation frequency is somewhat more than the rate controlling jump frequency. Thus it would appear that either Nowick's relation does not hold for the AgCd  $\alpha$ -phase alloys or the diffusion data are somewhat in error. Clearly therefore, additional data for  $\tau$  in the case of these alloys are required at temperatures close to those of the diffusion measurements so as to avoid the uncertainties introduced by extrapolation.

#### ACKNOWLEDGMENT

The author is indebted to Prof. B. N. Srivastava, D.Sc., F.N.I., for suggesting the problem and continued guidance through the progress of the work.

#### REFERENCES

- Childs, G. B. and Leclaire, A. D., 1954, *Acta Meta*, **2**, 718.  
Herasymenko, P., 1956, *Acta, Meta.*, **4**, 1.  
Kê, T. S., 1947, *Phys. Rev.*, **71**, 533.  
Kê, T. S., 1948, *J. App. Phys.*, **19**, 285.  
Leclaire, A. D., 1951, *Phil. Mag.*, **42**, 673.  
Leclaire, A. D., and Lomer, W. M., 1954, *Acta Meta*, **2**, 731.  
Lulay, J., and Wert, C., 1956, *Acta Meta*, **4**, 627.  
Manning, J. R., 1959, *Phys. Rev.*, **116**, 69.  
Nowick, A. S., 1952, *Phys. Rev.*, **88**, 925.  
Pearson, S. and Rotherham, L., 1956, *J. Metals, Trans. Sec.*, **8**, 894.  
Quader, M. A., 1960, *Ind. J. Phys.*, **34**, 506.  
Tomizuka, C. T. and Slifkin, L., 1954, *Phys. Rev.*, **96**, 610.  
Zener, C., 1943, *Trans. AIMME*, **152**, 122.  
Zener, C., 1947, *Phys. Rev.*, **71**, 34.

# ON THE PROCESSING OF NUCLEAR EMULSIONS

O. N. KAUL

SAHA INSTITUTE OF NUCLEAR PHYSICS  
CALCUTTA-9.

(Received March 28, 1961)

**ABSTRACT.** The paper gives an account of the comparative study of the various processing formulae used by the author during the course of the emulsion work, using both thick and thin plates. Modified formulae for various processing stages found to give the best results have also been suggested.

The paper also gives the penetration time needed for various developers both in the case of presoaked and non-presoaked emulsions of various thicknesses, and also an account of the study of shrinkage factor in nuclear emulsions.

The author has made a detailed study of the processing technique using Ilford C<sub>2</sub> nuclear emulsions of 100, 200 and 400 micron thickness, and also K<sub>0</sub> and G<sub>5</sub> plates. The details of the investigation are given below under the various heads.

## *Pre-soaking stage*

Before starting with the development, it is necessary to soak the emulsion in water, so that the penetration of the developer may become easier and more rapid. For this, the temperature and time limits suggested by various workers were used, and the following time and temperature limits were found to give the best results :

Emulsion thickness	Time	Temperature
100	0.5 hrs.	2°C
200	0.75 hrs.	4°C
400	1.25 hrs.	6°C

To facilitate penetration, presoaking in distilled water with or without the addition of the wetting agent is frequently made use of. This acts to swell the gelatine, permitting more rapid diffusion of the developer. It, however, does not effect the actual development as with the alkaline developments (Dilworth *et al*, 1948; Mortier and Vermaesen, 1948; Picciotto, 1949). The suitable temperature at which the penetration is to occur has been found to be 4°C. Below this tem-

perature the penetration time was found to be too long, and above it, the rate of developer penetration increases less rapidly than its activity.

### *Development*

Thin emulsions of 100  $\mu\text{m}$  order :

Two degrees of development were found possible for thin emulsions. Moderate development was found useful when grain densities of comparatively dense tracks (e.g. protons and  $\alpha$  tracks of several MeV energy) are to be measured. Since in this case it is essential that the grains be discrete, moderate development is preferred. This has an additional advantage of great reduction in the fog density. Strong development, on the other hand, although accompanied by an increased fog background, permits a full utilization of the emulsion sensitivity, and the heavy ionizing particles appear as solid columns of silver grains. Series of development tests were conducted to determine the development time giving the most preferred combination of background and track densities. The results thus obtained are indicated below :

Thickness	Procedure	Time
100	(moderate development)	10 min,
100	(strong development)	40 min.
		no agitation

### *Thick emulsions of 400 micron order and above*

For thick emulsions, the two developer solution method as suggested by Blau and Defilice (1948) is found to give the best results to secure the even development. The first contains the developing agent without any alkali, permitting the diffusion of the developer into the emulsion without any appreciable amount of actual development occurring. The second bath containing an excess of alkali permits the development to take place.

This method requires that the velocity of the travel of a  $p\text{H}$  change should exceed that of the developer itself;—a condition which is not actually satisfied. Also, up to 400  $\mu\text{m}$  thickness the two bath method eliminates any danger of reticulation.

It has been found by the author that the following modified formulae give the best results in the case of thick emulsions so far as two-bath development is concerned :

#### Sol. A.

Elon	1 gm
Sod. sulphite	20 gms
Hydroquinone	3.5 gms
Pot. bromide	2.0 gms
Distilled water	2 litres



## Sol. B.

Stock Eastman D <sub>19</sub>	...	400 c.c.
Distilled water	...	1600 c.c.
Sod. carbonate	...	12 gms

For 200 micron plates the following single solution development formula was found to give the best results. It is the Brussels formula slightly modified by the author :

Sod. sulphite	...	36 gms.
Pot bromide	...	0.8 gms.
Amidol	..	2.8 gms.
Boric acid	...	12 gms.
Water	...	1 lit.

*Penetrating time needed for various developers*

The penetration time in minutes of presoaked and non-presoaked emulsions was investigated by the author at 18°C.

<i>Developer</i>	<i>Penetration time in min.</i>		
Azol	100 $\mu$ m	200 $\mu$ m	400 $\mu$ m
Presoaked	4.5	16	38
Non-presoaked	6	19	50
D-19			
Presoaked	3.0	8.5	21
Non-presoaked	4.5	10.5	37
Amidol			
Presoaked	1.5	5.0	12
Non-presoaked	3.0	9.0	20
Amidol bisulphite			
Presoaked	2.5	6.0	12
Non-presoaked	2.5	8.0	20

*Processing formulae of thick and thin emulsions :* The following processing formulae were found to be most suitable for 100, 200 and 400  $\mu$ m plates.

Stage	Temperature	Time in min.		
		100 $\mu$ m	200 $\mu$ m	400 $\mu$ m
Presoaking	4°C	30	40	100
	5°C	25	35	90
Penetration of the cold developer	4°C	30	40	100
	5°C	26	36	92
Warm dry development	18°C	25	40	80
	24°C	20	35	70
Dry cooling	18°C to 5°C	5	5	5
Stop bath acetic acid (0.5%)	5°C	30	45	100
,, (1.0%)	5°C	20	35	75
Fixation (clearing time + 50% more)	18°C	3 hrs.	8 hrs.	24 hrs.
Washing	8°C	3 hrs.	8 hrs.	24 hrs.

The following processing formula was found exclusively suitable for thick plates :

Distilled water	1000 c.c.
Sod. sulphite (anhydrous)	12 gms.
Pot. bromide (10% solution)	8 cc
Amidol	3.8 gms.
pH of the developer	7.4

**Fixing bath (pH 5.3)**

Distilled water	1000 cc.
Sod. thiosulphate	400 gms
Sod. bisulphite	10 gms
NH <sub>4</sub> Cl	7 gms

**Clearing solution (pH 4.2)**

Distilled water	500 cc
Ammonium acetate	15 gms
Citric acid	8 gms
Thio-urea	8 gms

Small quantities of sodium bisulphite and ammonium chloride reduce staining and hasten the fixation of the emulsion. But large concentrations of these ingredients lead to distortion. Further, in the fixing solution, one half of the quantity of hypo was replaced at several intervals, thus avoiding salt concentration shoak. For the same reason, washing was also preceded by a gradual dilution of the fixing solution.

*Shrinkage*

The considerable reduction in the thickness of nuclear emulsions after fixing is due to the high concentration of the silver bromide in nuclear emulsions. The ratio of the emulsion thickness before and after fixing were found, and the following results were observed :

Emulsion thickness in $\mu$ m.	
Before processing	After processing
100	96
200	181
400	359

Increase in the shrinkage factor of Ilford C<sub>2</sub> emulsions :

The increase in the shrinkage factor of the emulsions was investigated at 80% relative humidity.

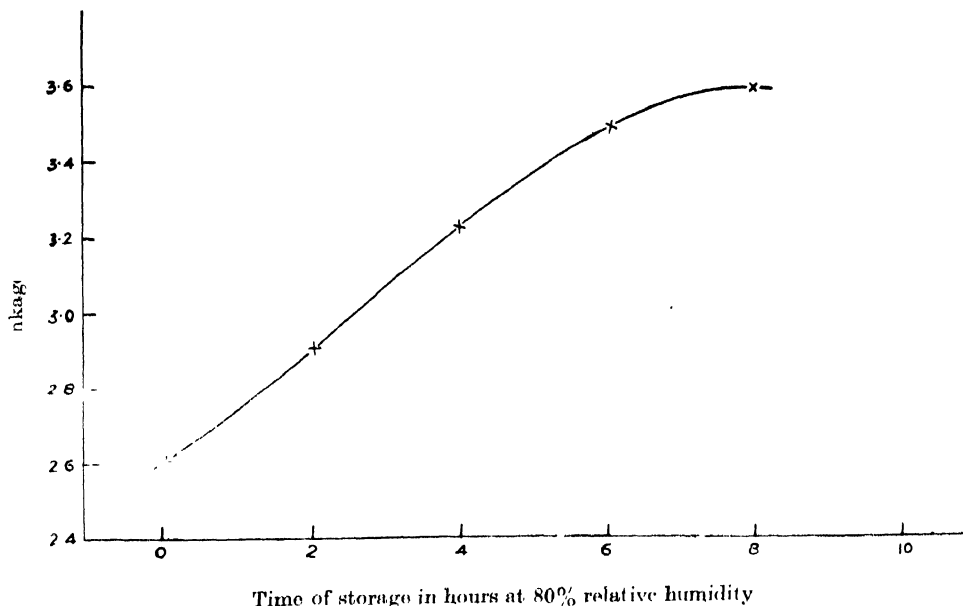


Fig. 1. Shrinkage factor plotted against the time of storage in hours for Ilford C<sub>2</sub> nuclear emulsions.

### *Drying of the emulsion*

Plates of either thicknesses were soaked in glycerine solution and dried gently. Rapid drying was avoided, because it produces a skin at the surface which traps the water lower down. This in turn produces stresses at the soft emulsion which produce severe distortions in the tracks. Blowing over the surface was avoided, because it introduces severe distortions, although the temperature was slightly increased to accelerate the process (Dilworth, 1951). Edges of the plates usually dry first causing surface deformations in the emulsion, which was also minimized as far as possible.

### ACKNOWLEDGMENTS

The author is grateful to Prof. B. D. Nagechaudhuri, Director of the Institute, for his encouragement and guidance.

Thanks are also due to Prof. D. N. Kundu, Head of the Accelerator Division, for providing the laboratory facilities and to Mr. Bhupesh Purkayastha, Head of the Nuclear Chemistry Division, for many helpful discussions.

## REFERENCES

- Blau, M., and De Felice, J. A., 1948, *Phys. Rev.*, **74**, 1198.
- Dilworth, C. C., Occhialini, G. P. S., and Vermaesen L., 1951, "Fundamental Mechanism of Photographic Sensitivity", Butterworth Scientific Publications London, p. 297.
- Dilworth, C. C., Occhialini, G. P. S. and Payne, R. M., 1948, *Nature*, **164**, 102.
- Mortier, M. and Vermaesen, L., 1948, *Centre de Physique Nucleaire de Bruxelles*, Note No. 5.
- Picciotto, E., 1949a, *Compt. rend.* **228**, 173.
- Picciotto, E., 1949b, *Compt. rend.* **228**, 2020.
- Picciotto, E., 1949c, *Compt. rend.*, **229**, 117.

# STUDIES ON BINARY DIFFUSION OF THE GAS PAIRS O<sub>2</sub>-A, O<sub>2</sub>-Xe AND O<sub>2</sub>-He

R. PAUL and J. B. SRIVASTAVA

INDIAN ASSOCIATION FOR THE CULTIVATION OF SCIENCE, CALCUTTA-32

(Received May 18, 1961)

**ABSTRACT.** The mutual diffusion coefficient of oxygen with argon, xenon and helium at  $-30^{\circ}\text{C}$ ,  $0^{\circ}\text{C}$ ,  $30^{\circ}\text{C}$  and  $60^{\circ}\text{C}$  has been determined by the two-bulb technique of Ney and Armistead (1947). Diffusion was allowed to take place through a precision capillary tube connecting the two diffusion bulbs and samples of the gas were analysed at different times with the help of a previously calibrated thermal conductivity analyser.

A least square method was employed to calculate from the experimental  $D_{12}$  values at different temperatures, the unlike interaction parameters on the Lennard-Jones (12 : 6) model. These constants were used to calculate the diffusion coefficients. Further, the thermal conductivity of the mixtures was calculated using experimental values of the mutual diffusion coefficient and other transport properties of pure components and reasonable agreement with the experimental data was obtained.

## INTRODUCTION

Many properties of gaseous mixtures can be fully explained only if the forces between unlike molecules are known. Among the transport properties of gases ordinary diffusion and thermal diffusion offer the best means for the determination of the intermolecular forces. Unfortunately, accurate experimental data suitable for intermolecular force determination are scanty, specially for the polyatomic molecules. A summary of the diffusion data available in the literature has been given by Westenberg (1957), and some recent references are available in an earlier paper by the present authors (Paul and Srivastava, 1961).

It was therefore decided to perform a series of accurate diffusion coefficient measurements of different gaseous mixtures over a fairly wide range of temperature. Several workers (Srivastava and Srivastava, 1959a; Srivastava, 1959; Srivastava and Barua, 1959) have measured binary diffusion of inert gases in the temperature range of  $0^{\circ}\text{C}$  to  $45^{\circ}\text{C}$ , by using the two-bulb diffusion method and have used their data to determine unlike molecular interaction parameters on the L-J (12 : 6) model.

In the present case the same technique has been used for measuring  $D_{12}$  for oxygen with several monatomic gases in the temperature range  $-30^{\circ}\text{C}$  to  $60^{\circ}\text{C}$ .

The experimental data obtained here have been used to determine the force constants for unlike molecular interaction on the L--J (12 : 6) model.

#### DESCRIPTION OF THE APPARATUS

The apparatus consisted of two bulbs made of Pyrex glass, connected by a precision brass capillary. The diffusion can be started by opening a stop-cock, situated between the two bulbs.

For analysing the gas a differential thermal conductivity analyser similar to that employed by Srivastava and Srivastava (1959) was constructed. Two conductivity cells form the two arms of a wheatstone bridge, one of the cells containing a suitable standard gas while the other contains a sample of the gas to be analysed. The other two arms of the wheatstone bridge are two fixed resistances, which together with the conductivity analyser are kept immersed in an oil bath maintained at  $34.2^\circ \pm 0.05^\circ\text{C}$ . Gas samples can be withdrawn through a fine leak from one diffusion bulb to the conductivity analyser. The analyser requires only 0.3 cc. of gas at N.T.P. for analysis and therefore does not disturb the pressure of the gas in the two diffusion bulbs.

The conductivity analyser has to be calibrated for each pair of gases. Mixtures of known compositions are introduced in the analyser cell and the bridge is balanced by introducing a variable resistor adjustable to 0.1 ohm. in parallel to one of the fixed resistors, keeping the bridge current constant. In this way a calibration curve is drawn for each pair giving the composition of the mixture for any value of the parallel resistance.

The diffusion apparatus is kept inside a thermostat which can be maintained at any desired temperature with fluctuations of the order of  $0.05^\circ\text{C}$ . The thermal regulator consists of a low wattage heater and an electronic relay with a proportioning toluene head. For maintaining temperature near  $0^\circ\text{C}$ , the inner chamber of the thermostat containing the diffusion bulbs is cooled by an outer chamber packed with ice. For  $-30^\circ\text{C}$ , alcohol replaces water as bath liquid and liquid oxygen is poured into the outer chamber containing alcohol.

#### THEORY AND FORMULAS

The theory of this method has been considered in detail by Ney and Armistead (1947) where it has been shown that the relaxation time  $1/\alpha$  of the system as defined by the relation

$$(C_1^\infty - C_1^t)/(C_1^\infty - C_1^0) = \exp(-\alpha t) \quad \dots (1)$$

is given by

$$\alpha = \frac{D_p A}{l} \cdot \frac{V_0}{V_1 V_2} \quad \dots (2)$$

where  $C_1^0$ ,  $C_1^t$  and  $C_1^\infty$  are respectively the concentration of the heavier gas initially, at time  $t$  seconds, and after complete mixing.  $V_1$  and  $V_2$  are the volumes of the bulbs in cc. and  $V_0 = V_1 + V_2$ .  $D_p$  is the coefficient of diffusion in  $\text{cm}^2/\text{sec}$  at a pressure of  $p$  cm. of mercury.  $A$  and  $l$  are the effective cross sectional area and effective length of diffusion path respectively.

From Eq. (1) it is evident that a plot of  $\log_{10} (C_1^\infty - C_1^t)$  against  $t$  gives a straight line, its slope being  $-\alpha$ . Knowing  $\alpha$ ,  $D_p$  can be calculated from Eq. (2).  $D_{\text{atm}}$ , the diffusion coefficient at atmospheric pressure is related to  $D_p$  by the Eq.,

$$D_{\text{atm}} = \frac{D_p \cdot p}{76} \quad (3)$$

### EXPERIMENTAL RESULTS

The gases used were supplied by British Oxygen Company, England and were quoted to be spectroscopically pure, except xenon which contained about 1% krypton.

#### *Constants of the diffusion apparatus*

Volume of bulb I	325 cc.
Volume of bulb II	547 cc.
Length of the diffusion capillary	9.058 cm.
Diameter of the diffusion capillary	0.316 cm.

$$C_1^\infty = 0.373.$$

$C_1^\infty$  is calculated from the initial concentration in the two bulbs, which was further checked for some runs by determining the concentration at an interval of seven times the relaxation time.

Table I shows a typical set of observations.

TABLE I  
Observed concentration of He at different times for  $\text{O}_2$ -He at  $-29.5^\circ\text{C}$

Time in minutes	R in ohms	$C_1^t$	$C_1^t - C_1^\infty$	$\log_{10} (C_1^t - C_1^\infty)$
0	....	1.000	0.627	1.7973
15	243.2	0.868	0.495	1.6946
35	234.6	0.746	0.373	1.5717
66	225.6	0.611	0.238	1.3766
96	217.8	0.512	0.139	1.1430

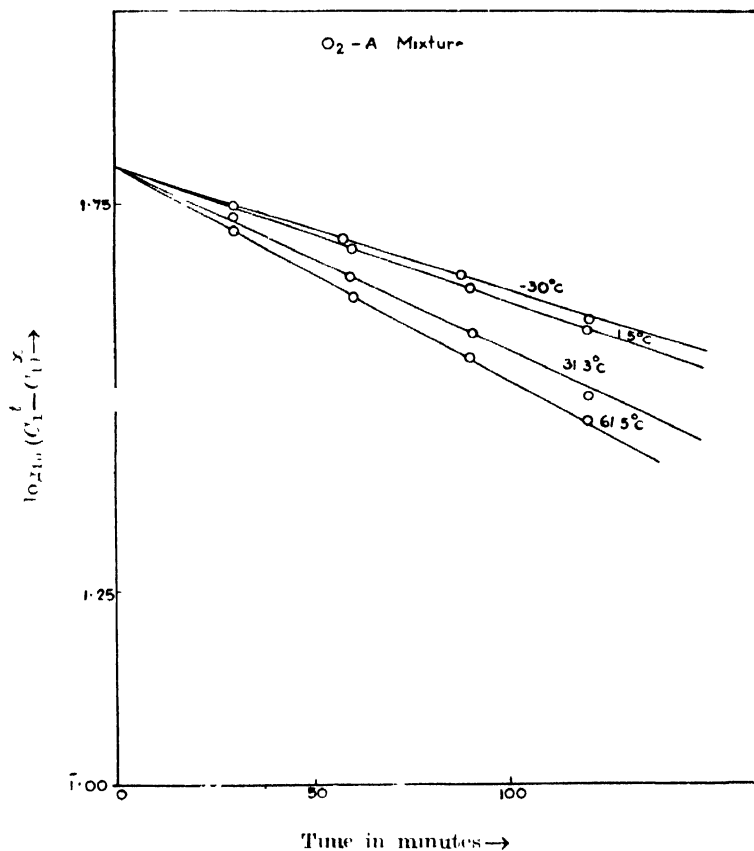


Fig. 1. Plot of  $\log_{10} (C_1^t - C_1^\infty)$  against  $t$ .

Fig. 1 gives the plots of  $\log_{10}(C_1^t - C_1^\infty)$  versus  $t$  for  $O_2$ -A at all temperatures. The values of diffusion coefficients have been given in Table II.

#### DETERMINATION OF POTENTIAL PARAMETERS

The various methods for determining the potential parameters from the measured diffusion coefficients such as (a) the ratio method, (b) translation method of Keesom (1912) and Lennard-Jones (1924), (c) the inter section method of Buckingham (1937) and (d) the combination method using other transport properties in addition, have been fully discussed by Bunde (1955) and Srivastava and Srivastava (1959a), pointing out their advantages and limitations. In the present case the intersection method has been found to be most suitable for the determination of the force constants on the Lennard-Jones (12 : 6) model. As some scatter



TABLE II

Observed values of the diffusion coefficient in cm<sup>2</sup>/sec.

Gas mixture	Temp. °K	Pressure in mm Hg.	$D_p$	$D_{atm}$	Previous work	$D_{12}$ calc. from force constant fitted to diffusion data.
O <sub>2</sub> -Xo	242.2	58.4	1.0929	0.084		0.082
	274.75	58.7	1.2950	0.100		0.104
	303.55	64.1	1.4939	0.126		0.125
	333.6	63.1	1.7944	0.149		0.149
O <sub>2</sub> -A	243.2	61.0	1.6819	0.135		0.135
	274.7	70.3	1.8163	0.168		0.168
	293.2				0.200 <sup>a</sup>	0.189
	304.5	63.7	2.4990	0.202		0.202
	334.0	66.3	2.7398	0.239		0.238
	244.2	63.1	6.4554	0.536		0.533
O <sub>2</sub> -He	274.0	60.9	7.9876	0.640		0.646
	304.4	62.3	9.2872	0.761		0.771
	334.0	63.3	11.1264	0.912		0.901

<sup>a</sup> Boardman and Wild (1937).

was found in the intersection points of the curves, the force constants determined by this method were considered as approximate ones. These approximate values were used to calculate the parameters more accurately by the method of least square fitting (Margenau and Murphy, 1952). The method followed here is analogous to that of Whalley and Schneider (1955) for determining the potential parameters from the second virial coefficients.

Let the approximate values of  $\sigma_{12}$  and  $\epsilon_{12}/k$  be  $(\sigma_{12})_0$  and  $(\epsilon_{12}/k)_0$  then

$$\sigma_{12} = (\sigma_{12})_0 + a, \quad \dots (4)$$

$$\text{and } \epsilon_{12}/k = (\epsilon_{12}/k)_0 + b, \quad \dots (5)$$

where  $a$  and  $b$  are small correction terms. The normal equations for computing the correction terms can be written as

$$\Sigma[(u_i a + v_i b) - F_i] u_i = 0 \quad \dots \quad (6)$$

$$\text{and} \quad \Sigma[(u_i a - v_i b) - F_i] v_i = 0 \quad \dots \quad (7)$$

where

$$F_i = (D_{12})_{\text{expt.}} - (D_{12})_{\text{cal.}}$$

$$u_i = -2(D_{12})_{\text{cal.}}/(\sigma_{12})_0$$

$$v_i = [(D_{12})_{\text{cal.}}\{T^*/(\epsilon_{12}/k)_0 \Omega_{12}^{11}(T^*)\}](\partial \Omega_{12}^{11}(T^*)/\partial T^*)$$

Here  $(D_{12})_{\text{cal.}}$ ,  $F_i$ ,  $u_i$  and  $v_i$  are to be calculated using the values of  $(\epsilon_{12}/k)_0$  and  $(\sigma_{12})_0$ . It was found even in the extreme case of  $\text{O}_2\text{-He}$ , the contribution due to second approximation in the value of  $D_{12}$  amounted to less than 1% and hence  $(D_{12})_{\text{cal.}}$  was evaluated only up to first approximation. The normal equations are then solved for  $a$  and  $b$ . Using these new values of  $\epsilon_{12}/k$  and  $\sigma_{12}$ , the whole process was repeated till the values of  $a$  and  $b$  came vanishingly small. The force constants thus determined are tabulated in Table III together with the values obtained from the usual combination rules. It is easily seen that the two sets of force constants agree within the limits of experimental error, though the combination rule value of  $\sigma_{12}$  is always larger as is expected.

TABLE III

Potential parameters on the (12 : 6) model from the experimental data.

Gas pair	Present work	From combination rule	
		Using force constants from viscosity	Using force constants from second virial coefficients
<hr/>			
<b>O<sub>2</sub>-X<sub>0</sub></b>			
<b>ε<sub>12</sub>/k(°K)</b>	<b>167.5</b>	<b>160.9</b>	<b>164.0</b>
<b>σ<sub>12</sub> (Å)</b>	<b>3.730</b>	<b>3.744</b>	<b>3.818</b>
<b>O<sub>2</sub>-A</b>			
<b>ε<sub>12</sub>/k(°K)</b>	<b>109.4</b>	<b>118.4</b>	<b>120.7</b>
<b>σ<sub>12</sub> (Å)</b>	<b>3.461</b>	<b>3.425</b>	<b>3.499</b>
<b>O<sub>2</sub>-He</b>			
<b>ε<sub>12</sub>/k(°K)</b>	<b>36.35</b>	<b>33.98</b>	<b>34.65</b>
<b>σ<sub>12</sub> (Å)</b>	<b>2.978</b>	<b>3.004</b>	<b>3.078</b>

# COMPARISON WITH EXPERIMENTS

## (a) *Mutual diffusion coefficients*

The values of the potential parameters obtained here have been used to calculate the mutual diffusion coefficient of the different gas pairs on the Lennard-Jones (12 : 6) model and the calculated values are compared with the experimentally observed values in Table II. Other experimental data where available for these gas pairs are recorded in column (7) for the sake of comparison. The good agreement between the measured values and those calculated from our force constants shows that the force constants determined by us are quite reliable and can be used to calculate other transport properties. As pointed out by Walker and Westenberg (1960) the reliability of the force constants could further be tested if high temperature data for those substances were available.

## (b) *Thermal conductivity of mixtures*

The experimental values of  $D_{12}$  together with other experimentally determined properties such as self-diffusion, thermal conductivity and viscosity of the pure gases, were used to calculate the thermal conductivity of mixtures, without assuming any particular form of the interaction potential except a central force. This method has been suggested by Weissman *et al.* (1960) for testing how well a mixture confirms to the basic assumptions of Chapman-Enskog theory or for determining the consistency of the experimental measurements.

Hirschfelder (1957) has obtained the following expression for  $K_{mix}$ , the thermal conductivity of gas mixture, consisting of a diatomic gas denoted by subscript 1 and a monatomic gas denoted by subscript 2.

$$K_{mix} = [K_{mix}]_{mon} + \{K_1 - (K_1)_{mon}\} [1 + (x_2/x_1)(D_{11}/D_{12})]^{-1} \quad \dots \quad (8)$$

where the symbol have their usual meanings and expressions have been given for them on the Chapman-Enskog theory by Hirschfelder, Curtiss and Bird (1954).  $(K_1)_{mon}$  and  $D_{11}$  were calculated by using the experimental values of  $\eta_1$ , the viscosity of the diatomic gas, with the help of the following expressions

$$(K_1)_{mon} = \frac{15}{4} \frac{R}{M} \eta_1 \quad \dots \quad (9)$$

$$D_{11} = 98.42 \frac{A_1^* \eta_1 T}{pM} \quad \dots \quad (10)$$

$A^*$  has been shown by Weissman and Mason (1960) to be nearly independent of either temperature or force law and its contribution to the final result is

negligible. Therefore a rough estimate of  $A^*$  is often adequate. Here we have used the known force constants to find  $A^*_{12}$  from the tables.

$(K_{mix})_{mon}$  involves  $(K_1)_{mon}$ ,  $K_2$ ,  $(K_{12})_{mon}$ ,  $A^*_{12}$  and  $B^*_{12}$ . The value of  $(K_{12})_{mon}$  has been calculated from experimental  $D_{12}$  values using the relation

$$(K_{12})_{mon} = \frac{25}{8} \frac{pD_{12}}{(A^*_{12})T} \quad \dots (11)$$

$A^*_{12}$  has again been found from tables using our force constants, while  $B^*_{12}$  has been obtained with the help of experimental values of  $D_{12}$  and the following expression given by Weissman *et al.* (1960).

$$B^*_{12} = (1/12)[2(\partial \ln D_{12}/\partial \ln T) - 1][9 - 2(\partial \ln D_{12}/\partial \ln T)] \quad \dots (12)$$

Thus  $K_{mix}$  has been calculated with the help of only experimental quantities, and recorded in Tables IV and V together with the observed values. It can be seen that the agreement between the experimental values of thermal conductivity and the values calculated here from other experimental data is within the limits of experimental errors for all the mixtures.

This shows that the diatomic oxygen molecule can be taken to be spherically symmetric for calculating the transport properties.

TABLE IV

Thermal conductivity of  $O_2$ -Xe and  $O_2$ -He at 30°C in cal. cm<sup>-1</sup>. sec<sup>-1</sup> deg<sup>-1</sup>.

Gas pair % of monatomic constituent.	$O_2$ -Xe		$O_2$ -He	
	$K_{expt.} \times 10^5$	$K_{calc} \times 10^5$	$K_{expt} \times 10^5$	$K_{calc} \times 10^5$
100	1.294 <sup>a</sup>	1.294	36.37 <sup>a</sup>	36.37
85	1.684	1.740	27.00	27.26
70	2.223	2.270	20.14	20.65
55	2.804	2.907	15.64	16.06
40	3.564	3.650	12.30	12.58
25	4.301	4.545	9.642	9.850
10	5.500	5.616	7.621	7.670
0	6.442	6.442	6.441	6.441

<sup>a</sup> Srivastava and Barna (1960)

TABLE V

Thermal conductivity of O<sub>2</sub>-A mixture at 38°C in cal. cm<sup>-1</sup> sec<sup>-1</sup>, deg<sup>-1</sup>.

Gas pair % of O <sub>2</sub>	$K_{\text{calc.}} \times 10^5$	$K_{\text{exp.}} \times 10^5$
100	6.461 <sup>b</sup>	6.461
90	6.015	6.228
80	5.655	5.989
70	5.400	5.764
60	5.225	5.554
50	5.055	5.330
40	4.905	5.129
30	4.760	4.164
20	4.615	4.728
10	4.480	4.534
0	4.350	4.350

<sup>b</sup> Srivastava and Srivastava (1959b)

## DISCUSSIONS

In an attempt to determine the interaction parameters between two unlike gas molecules, we have tried to increase the range of our mutual diffusion experiments both in the higher and lower temperature sides. In the present case also no systematic departure from the empirical combination rules for calculating unlike interaction parameters has been observed. This is partly due to the fact that the individual force constants have not been determined with sufficient accuracy.

The discrepancy in the case of O<sub>2</sub>-A interaction seems to be more pronounced. There are practically no other data on mutual diffusion or thermal diffusion of these gas pairs and hence it is difficult to test the accuracy of these results except by seeing how well they reproduce our experimental data.

## ACKNOWLEDGMENT

The authors are grateful to Prof. B. N. Srivastava, D.Sc., F.N.I., for guidance and valuable discussions. One of the authors (R.P.) is thankful to C.S.I.R., New Delhi, for financial assistance.

## REFERENCES

- Boardman, L. E., and Wild, N. E., 1937, *Proc. Roy. Soc.*, **A162**, 511.
- Buckingham, R. A., 1938, *Proc. Roy. Soc. (London)*, **A168**, 264.
- Hirschfelder, J. O., 1957, *Sixth International Symposium of Combination* (Reinhold Publishing Corp., N. Y.), p. 351.
- Hirschfelder, J. O., Curtiss, C. F., and Bird, R. B., 1954, *Molecular Theory of Gases and Liquids* (John Wiley & Sons Inc., N. Y.), Chap 8.
- Keesom, W. H., 1912, *Leiden, Comm. Suppl.*, No. **25**.
- Lennard-Jones, J. E., 1924, *Proc. Roy. Soc. (London)*, **A106**, 463.
- Margenau, H., and Murphy, G. M., 1952, *Mathematics of Physics and Chemistry* (Van Nostrand, N. Y.)
- Noy, E., and Armistead, F. C., 1947, *Phys. Rev.*, **71**, 14.
- Paul, R., and Srivastava, I. B., 1961, *J. Chem. Phys.*, in Press.
- Srivastava, B. N. and Barua, A. K., 1960, *J. Chem. Phys.*, **32**, 427.
- Srivastava, B. N. and Srivastava, K. P., (1959a), *J. Chem. Phys.*, **30**, 984.
- Srivastava, B. N. and Srivastava, R. C., (1959b), *J. Chem. Phys.*, **30**, 1200.
- Srivastava, K. P., 1959, *Physica*, **25**, 571.
- Srivastava, K. P., and Barua, A. K., 1959, *Ind. J. Phys.*, **33**, 229.
- Walker, R. E., and Westenberg, A. A., 1960, *J. Chem. Phys.*, **32**, 426.
- Weissman, S., and Mason E. A., 1960, *Physica*, **26**, 531.
- Weissman, S., Saxena, S. C., and Masor E. A., 1960, *Phys. Fluids*, **3**, 510.
- Westenberg, A. A., 1957, *Combustion and Flame*, **1**, 346.
- Whalley, E., and Schneider, W. G., 1955, *J. Chem. Phys.*, **23**, 1644.

# PERIODIC FADING IN OBLIQUE INCIDENCE SHORT-WAVE TRANSMISSIONS

B. RAMACHANDRA RAO, M. G. SESHAGIRI RAO AND  
D. SATYANARAYANA MURTY

IONOSPHERIC RESEARCH LABORATORIES, PHYSICS DEPARTMENT, ANDHRA UNIVERSITY,

WALTAIR, INDIA

(Received April 19, Resubmitted May 30, 1961)

**ABSTRACT.** This paper deals with the interpretation of periodic fading observed in oblique incidence CW transmissions as due to changes in phase-paths of the interfering waves produced by critical frequency changes in the reflecting layer. Using Booker's equation as modified by Rao and Rao (1958), changes in path lengths and hence the number of interference maxima have been calculated and compared with the experimental results and a good agreement is observed. By comparing the theoretically calculated values with experimentally obtained ones due to the interference of the different modes, the possible modes by which the transmissions from Calcutta and Madras arrive at the receiving station (Waltair), have been determined. By using the number of interference maxima and the critical frequency values at any instant, a method of calculating critical frequency changes in small time intervals has been proposed.

## INTRODUCTION

Continuous wave-signal strength records due to radio-wave transmissions from distant stations usually show both random and periodic fading depending upon the ionospheric conditions. Appleton and Beynon (1947) observed and interpreted periodic fading of magneto-ionic origin. Periodic fading of a different origin was observed in oblique incidence short-wave CW transmissions by Banerjee and Mukherjee (1946) who interpreted this type of fading as due to continuously varying path difference between two interfering waves singly reflected and doubly reflected from a single layer having vertical movement or singly reflected from two different layers when one or both the layers undergo vertical movement. Later, Khastgir and Das (1950a) studied similar type of periodic fading in short-wave transmissions from distant stations and these authors have interpreted the observed fading as due to interference of two or more waves undergoing different Doppler frequency shifts when reflected from one or two ionospheric layers moving vertically. In a later communication, Khastgir and Das (1950b) have shown that these two apparently different interpretations are equivalent to each other.

In the present investigation the authors have attempted a quantitative interpretation of periodic fading observed in short-wave transmissions from

distant A.I.R. stations, on the assumption that there is a continuous phase path change in one or both the ionospherically reflected waves due to ionisation changes.

#### SOME RELEVANT THEORETICAL CONSIDERATIONS

For the purpose of interpreting quantitatively the observed periodic fading, the phase paths of the ordinary waves are calculated by using the approximate formula for phase-path developed by Rao and Rao (1958). The phase-path of an e.m. wave in the ionised medium is given by

$$\int \mu \cdot ds \quad \dots (1)$$

where  $ds$  is an infinitesimal element along the path of the wave and  $\mu$  is the phase refractive index at that particular element. According to the treatment of Booker (1939),  $\mu'$  can be resolved into the vertical component  $\mu_\psi \cos \psi (= q)$  and the horizontal component  $\mu_\psi \sin \psi (= \sin i = s)$ , where  $\psi$  is the angle of refraction at the particular point under consideration and  $\mu_\psi$  is the refractive index at the same point. Similarly,  $ds = dh \cos \psi$ , where  $dh$  is an infinite small element of height 'h' at the same point.

Thus integral (1) can be expressed in terms of  $q$  and  $h$  as

$$\int \frac{q^2 + s^2}{q} \cdot dh \quad \dots (2)$$

For the evaluation of the above integral, a knowledge of the variation of  $q$  with  $h$  is required. Booker (1939, 1949) had deduced for the case of obliquely incident radio waves a quartic equation giving the variation of 'q', with  $x$  for any given values of wave frequency 'f', the earth's magnetic field  $H$ , the angle of incidence  $i$ , and the collisional frequency  $\nu$ . Rao *et al.* (1958) observed that the following empirical relation

$$q^2 = C'^2 \cdot \Delta x \quad \dots (3)$$

gives close agreement with the  $q-x$  curves as obtained by the quartic equation of Booker. The value of  $\Delta$  is determined from the limiting values of  $q$  and  $x$  and is given by  $C'^2/x_r^1$ , where  $C'$  is  $\cos i$  and  $x_r$  is the value of  $x$  at the point of reflection i.e., at  $q = 0$ . If parabolic distribution of ionisation with height is assumed, then  $x$  and  $h$  are related by the well known expression

$$\beta h^2 - \alpha h + x = 0 \quad \dots (4)$$

where

$$\alpha = \frac{2f_0^2}{f^2 h_m}, \text{ and } \beta = \frac{f_0^2}{f^2 h_m^2}$$



where  $f_0$  is the critical frequency of the ordinary ray,  $f$  — operating frequency,  $h_m$  is the semi-thickness of the layer. Using the above relations (3) and (4),  $q$  can be expressed in terms of  $h$  alone and the integral (2) can now be written as

$$\int \frac{(\epsilon^2 \Delta(\beta h^2 - \alpha h) + S^2)}{[\epsilon^2 + \Delta(\beta h^2 - \alpha h)]^{1/2}} \cdot dh \quad \dots (5)$$

As the above expression involves only one variable  $h$ , it can be evaluated between the required limits. Actual integration and simplification gives the final equation for the phase path  $P$  as

$$P = Ch_m + h_m \cdot \frac{f}{f_0} \left[ 2 - \epsilon^2 - \frac{f_0^2}{f^2} \right] \ln \frac{1 + D}{1 - D} \quad \dots (6)$$

where  $D = \frac{f \cdot \cos. i}{f_0}$

Using the above expression, phase paths for the ordinary ray are calculated at two different times knowing the values of critical frequencies at those times. The change in phase path of any interfering mode due to the varying electronic density is thus obtained. By estimating the change in the phase path difference between the two interfering modes, the number of fading maxima expected to occur in that interval of time can be calculated.

## EXPERIMENTAL DETAILS AND RESULTS

Using an Eddystone communication receiver of the model S-504, with a D.C. amplifier and an Esterline-Angus pen recorder, periodic fading in short wave transmissions of 6.085Mc/sec from Madras, and 7.21 Mc/sec from Calcutta at distances of 620 and 730Km respectively from the receiving station (Waltair) has been studied.

The records have been taken during the early afternoon hours from 1230 to 1500 hrs I.S.T. with a view to minimise the contribution to path changes due to the vertical movement of the reflecting layers. The heights and semi-thicknesses assumed for the  $E$ ,  $F_1$  and  $F_2$  layers are 100Km and 20Km, 220Km and 60Km, and 320Km and 140Km respectively. The vertical equivalent frequencies ( $f \cdot \cos. i$ ) for the different layers for the different modes of propagation for both the stations, Madras and Calcutta, are presented in Table I.

Preliminary experimental investigation has been made with transmissions on 6.085Mc/sec from Madras between 1300 and 1400 hrs. I.S.T. The critical frequencies for the  $E$  layer at these times during which records have been taken are 3.4Mc/sec and 3.3Mc/sec and for  $F_1$  layer during those hours are 4.6 and 4.5 Mc/sec respectively. Typical results of calculations made for a record taken on 14.2.55 are given below. From considerations of the  $f \cdot \cos. i$  values given in

TABLE I

Station	Operating frequency $f$	Distance from the receiving station	f. cos. i. values					
			1E	2E	1F <sub>1</sub>	2F <sub>1</sub>	1F <sub>2</sub>	2F <sub>2</sub>
Madras	6.085 Mc/s	620 Km	1.86	3.30	3.52	4.98	4.37	5.51
Calcutta	7.21 Mc/s	730 Km	1.90	3.47	3.72	5.56	4.76	6.26

Table I, 1E, 2E, 1F<sub>1</sub> and 2F<sub>2</sub> modes of propagation are possible. The interference between any two of the above possible four modes gives rise to periodic fading. Actual calculation and a comparison of those results showed that interference between 1E and 2E, and 1E and 1F<sub>1</sub> are only present. The frequency of fading for 1E and 2E interference observed is 16 as against the calculated value of 22. The observed value of frequency of fading for 1E and 1F<sub>1</sub> interference is 2 as against the calculated value of 1.44. The critical frequency data are taken as reported from the Ahmedabad Ionospheric Station because no critical frequency data are available from Madras for the E and F<sub>1</sub> layers. The agreement between the calculated and the observed values of fading frequency may be considered as good in view of the approximate values assumed for the critical frequencies.

Further investigation on these lines has been carried out extensively using transmissions on 7.21 Mc/s from Calcutta station between 1230 and 1330 hrs. I.S.T., in the months of November and December, 1956, and between 1400 and 1500 hrs. I.S.T. during the months of February and March, 1957. The heights and semi-thicknesses of the different layers are assumed as before and the *f. cos. i.* values for single and double hop, reflections for the different layers are as presented in Table I. Comparing the vertical equivalent frequencies for 1E, 1F<sub>1</sub> and 1F<sub>2</sub> modes of propagation with the  $f_0E$ ,  $f_0F_1$  and  $f_0F_2$  values at those hours, it has been found that 1F<sub>1</sub> and 1F<sub>2</sub> modes are not possible, as each mode suffers reflection from the lower layer. Further the 2F<sub>1</sub> mode is not possible as the equivalent frequency for this mode is found to be very close to and sometimes less than  $f_0F_1$ . The 2F<sub>2</sub> mode, though theoretically possible, is likely to suffer very large deviative and non-deviative absorption and hence it is unlikely to be present in significant strength. Thus the single and double hop reflections from E layer will be the predominant modes of propagation for transmissions from Calcutta received at Waltair. The experimental fact that most of the records show simple fading patterns with a single periodicity of large amplitude confirms the assumption that 2F<sub>2</sub> mode is not present in significant strength. Two such typical records of this type are shown in Fig. 2. Complicated patterns indicating superposition of more than one periodicity appeared only occasionally. Phase paths and frequencies of fading have been calculated for the months of November and December using relation (6) and the critical frequency data are taken from the

Ionospheric Research Station, Ahmedabad. The  $f_oE$  values at Ahmedabad are found to be lower than those at Waltair and higher than those at Calcutta by about 0.1 Mc/sec. Hence the Ahmedabad data are taken to represent fairly well the conditions existing at the reflecting point as its latitude is midway between those of Calcutta and Waltair. Taking any two of the three possible

TABLE II

The results of theoretical calculations of interference maxima in fading records and comparison with experimental values—Calcutta -7210Kc/sec.

Date	Beginning time of the record hrs.	Time duration mts.	Critical frequency E layer		No. of interference maxima per minute	
			At 1230 hrs. in Mc/sec.	At 1330 hrs in Mc/sec.	Calculated	Observed
20.11.'56	1258	5	4.00	3.85	9.0	11.4
20.11.'56	1312	5	4.00	3.85	9.0	13.8
21.11.'56	1234	5	3.95	3.80	10.0	12.6
22.11.'56	1243	5	4.00	3.90	6.0	8.4
23.11.'56	1237	6	3.95	3.80	10.0	13.8
26.11.'56	1251	5	3.95	3.75	14.2	13.3
27.11.'56	1238	10	3.95	3.80	9.0	*17.2
30.11.'56	1238	4	4.10	3.90	10.0	*17.5
30.11.'56	1243	5	4.10	3.90	10.0	*16.3
3.12.'56	1252	11	3.95	3.80	10.0	11.8
4.12.'56	1243	10	3.95	3.80	10.0	13.5
11.12.'56	1245	6	3.95	3.80	10.0	11.8
12.12.'56	1243	5	4.00	3.85	9.0	8.6
20.12.'56	1251	10	3.95	3.80	10.0	*16.0

\*Presence of  $E_s$  suspected.

modes of propagation, the difference in the phase paths and hence the frequency of fading per minutes have been calculated. The calculated frequency of fading is about 1C'/mnt. for  $1E$  and  $2F_2$  interference, about 12C'/mnt. for  $1E$  and  $2E$  interference and about 20C'/mnt. for  $2E$  and  $2F_2$  interference. There is fairly wide variation in these values depending upon the critical frequency values of  $E$  and  $F_2$  layer on the particular day of observation. The observed frequency of fading centres round the value 13.00C'/mnt. for most of the days. Thus it is evident that  $1E$  and  $2E$  interference is mainly responsible for the observed periodic fading. The results of the detailed calculations for the indivi-

TABLE III

Results of critical frequency changes in *E* layer deduced from fading records and comparison with those deduced from critical frequency data

Date	Starting time of record hrs. I.S.T.	Observed no. of peaks per minute	Time duration in minutes	$f_oE$ in Mc/s		Reference frequency in Mc/s	Change in $f_oE$ in Kc/s during the time of record.	
				1400 hrs	1500 hrs		Deduced from fading records	From $f_oE$ data
7.2.57	1426	19.0	6	3.8	3.6	3.70	21	20
12.2.57	1421	24.8	4	---	---	---	---	---
16.2.57	1416	12.3	12	3.9	3.7	3.8	36	40
20.2.57	1426	14.4	7	3.9	3.6	3.8	24.5	35
25.2.57	1443	15.4	8	3.8	3.6	3.75	24	26.7
26.2.57	1424	11.1	5	3.8	3.6	3.75	10	16.7
Do	1452	14.6	8	3.8	3.6	3.70	24	26.7
27.2.57	1410	13.0	8	3.9	3.6	3.85	32	40
1.3.57	1419	10.0	6	3.8	3.6	3.80	15	20
Do	1453	10.0	7	3.8	3.6	3.65	17.5	23.3
3.3.57	1404	12.4	5	3.9	3.8	3.90	15	8.3
Do	1412	9.1	10	3.9	3.8	3.80	20	16.7
4.3.57	1430	17.5	8	3.8	3.6	3.70	28	26.7
5.3.57	1444	14.4	8	3.9	3.7	3.75	24	26.7
6.3.57	1450	11.5	10	3.9	3.8	3.80	25	16.7
7.3.57	1445	12.3	8	4.0	3.8	3.90	28	26.7
8.3.57	1411	15.3	6	4.0	3.8	3.95	30	20
Do	1438	13.3	10	4.0	3.8	3.90	40	33.7
9.3.57	1415	21.6	5	3.7	3.6	3.80	25	25

dual days are shown in Table II. An examination of Table II shows that the observed frequency of fading is agreeing fairly well with the theoretically calculated value for  $1E$  and  $2E$  interference for most of the days. In view of the approximation involved in the phase-path formula and lack of critical frequency data from a station close to the point of reflection, the agreement may be considered as reasonably good. However, weak signals by  $2F_2$  mode are received occasionally as evidenced by a secondary periodicity superposed on the common type periodic fading.

A METHOD OF DETERMINING CRITICAL FREQUENCY  
CHANGE FROM THE OBSERVED PERIODIC  
FADING PATTERNS

The above study has suggested to the authors the possibility of making use of such experimentally obtained periodic fading records for the study of minute ionisation changes in the reflecting layer. The rate of change of path difference with time between the two modes suffering reflection from the same layer and interfering to produce fading is dependent upon the ionisation changes in the reflecting layer, provided the layer height remains the same. Thus the observed fading period is related to the critical frequency change.

The path difference between  $1E$  and  $2E$  reflections expressed in terms of operating wavelength is calculated for different values of  $f_o$  of the reflecting layer and a graph is drawn between this path difference and the corresponding

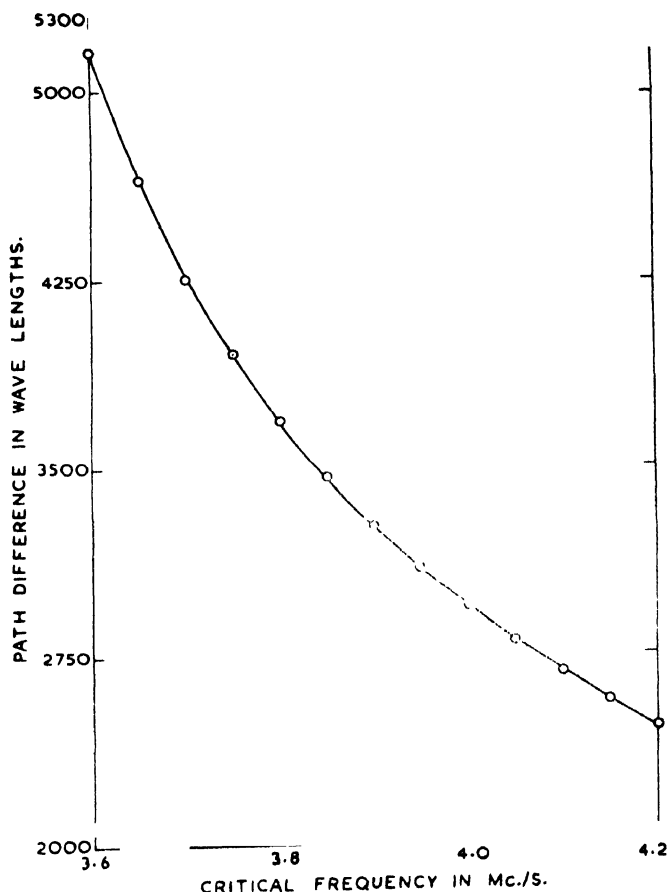


Fig. 1. Critical frequency-path difference curve of  $1E$  and  $2E$ , in Calcutta transmissions on 7210Kc/sec.

$f_0$  values as shown in Fig. 1. If a fading record is taken in a known interval of time and if the critical frequency of the  $E$  layer is known either at the beginning or end of the record, the critical frequency corresponding to each fading at each interval of one cycle can be calculated as well as the critical frequency change for the duration of the record.

This latter method has been used by the authors to evaluate critical frequency changes in short intervals of time from the observed fading periods. The critical frequency change during the short interval of the record is read from Fig. 1, assuming the  $f_0$  value at the beginning of the record. This value is then compared with the expected  $f_0 E$  change in that interval, calculated from hourly values of

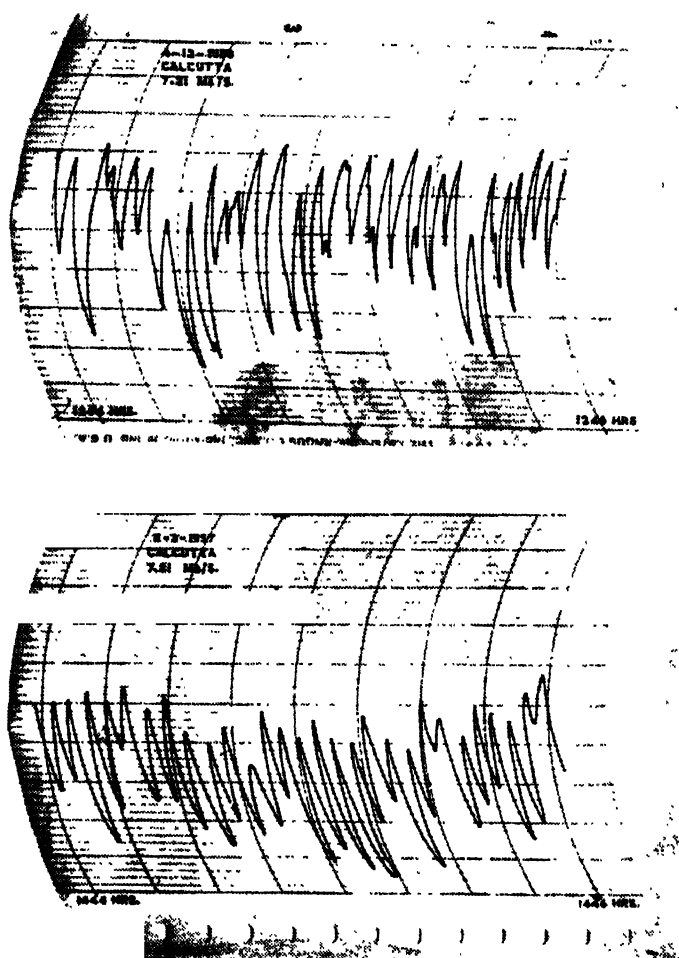


Fig. 2. Periodic fading in Calcutta transmissions on 7210Kc/sec. received at Waltair, due to the interference between 1E and 2E reflections.

$f_0E$  given in Ionospheric Data Bulletin assuming linear variation of  $f_0E$  with time in one hour interval.

A large number of records were taken during February and March, 1957 for Calcutta transmission on 7.21Mc/sec between 1400 and 1500 hrs. I.S.T. and as in the previous months, it is found that 1E and 2E interference is the predominant cause of periodic fading. The contribution to phase path change due to height variation is found to be negligible compared to that due to critical frequency change. The results of the calculation are presented in Table III.

An examination of the above Table III shows that there is good agreement between the theoretically calculated and experimentally observed values. This confirms the correctness of the interpretation of the periodic fading as due to the interference of 1E and 2E reflections. As the change in critical frequency deduced from the graph depends not only upon the frequency of fading, but also upon this reference critical frequency, any inaccuracy in choosing this reference frequency will introduce some error in the calculation of the critical frequency change. One significant fact to be noted is that the day to day fluctuations in the critical frequency values and the magnitudes of their change are regularly observed as a change in the frequency of fading.

The present method of interpretation adopted by the authors has the advantage that the observed fading period is directly related to the critical frequency change of the ionospheric layers and hence it has been possible to estimate particularly the short period critical frequency changes from the fading records. The method has the advantage that the technique is simple.

#### ACKNOWLEDGMENT

One of the authors (D. S. M.) wishes to express his deep gratitude the Council of Scientific and Industrial Research for the financial support rendered during the progress of the work.

#### REFERENCES

- Appleton, E. V. and Beynon, W.J.G., 1947, *Proc. Phys. Soc.* **58**, 59.
- Banerjee, S. S and Mukherjee, G. C., 1946, *Sci & Cult.* **11**, 571.
- Booker, H. G., 1939, *Phil. Tran. Roy. Soc. A.* **237**, 411.
- Booker, H. G., 1949, *J. Geophys. Res.* **54**, 243.
- Khastgir, S. R and Das, P. M., 1950, *Proc. Phys. Soc.*, **63**, 924.
- Khastgir, S. R and Das, P. M., 1950, *Sci & Cult.* **15**, 445-446.
- Rao, B. R. and Rao, M. S., 1958, *J. Atm. Terr. Phys.* **12**, 293-305.

# THE ROLE OF EMPTY ORBITALS IN SUPEREXCHANGE INTERACTION

K. P. SINHA

NATIONAL CHEMICAL LABORATORY, POONA-8, INDIA.

(Received April 3, 1961)

**ABSTRACT.** In the wake of our spin polarization mechanism developed for the indirect exchange interaction in some magnetic systems, certain additional superexchange effects involving empty orbitals are explored. Analysis of the usual 'three-centre and four-electron' system reveals that the delocalization of two electrons, one each from the two magnetic ions, to the lowest available empty orbital for the unit, always stabilizes the singlet state. This type of perturbation thus leads to antiferromagnetic superexchange effect.

An estimate of the relevant interaction term shows that the effect is quite appreciable and strengthens the former mechanism, which also operates through the agency of such empty orbitals. The importance of these two mechanisms, in relation to those emanating from singly occupied orbitals for fundamentally antiferromagnetic compounds is stressed.

## INTRODUCTION

An indirect exchange interaction mechanism involving empty localized crystal orbitals was recently proposed by us (Koide, Sinha and Tanabe, 1959; hereafter referred to as I) which contributes significantly towards the spin coupling in magnetic compounds where the paramagnetic ions are otherwise separated by the intervening diamagnetic ions. According to this mechanism, the spin coupling between the paramagnetic ions is achieved via those perturbations which entail a spin dependent transition of one of the intervening ion electrons to the lowest available empty orbitals for the appropriate unit in the crystal. This treatment developed originally for magnetic compounds having rock salt or perovskite type structure (I), has been extended to those having zinc blende (Sinha and Koide, 1960) and spinel (Sinha, 1961) type structures.

In the present paper, certain additional superexchange effects invoking the interplay of the empty orbitals are envisaged. In this scheme the main interaction term arises due to two electron transitions to the lowest excited orbital, one each from the two paramagnetic ions. It may, however, be remarked that we do not here consider the superexchange effects which involve transitions to singly occupied orbitals. Such mechanisms have been discussed by others (Anderson, 1950, 1959; Keffer and Oguchi, 1959; Nesbet, 1958 and 1960). The moti-



vation behind our present series of papers is to assess the various types of exchange interactions arising through the role of empty excited orbitals hitherto not considered for the magnetic systems of interest.

# FORMULATION OF THE INTERACTION MECHANISM

As in I, we consider a system of two magnetic ions with an intervening non-magnetic ion situated collinearly. This is the usual three centre problem represented by  $M^{2+} - X^{2-} - M^{2+}$ . Since the superexchange effect arising out of the spatial and spin correlation between the electrons of the intervening ion has been studied in detail in the previous paper (I), we shall consider two electrons of the central ion in the singlet state and occupying the same orbital  $\phi_0$  (i.e.  $np\pi$ ), in the present analysis. The  $d$  orbital wave functions of the two electrons one from each magnetic ions are denoted by  $u_1$  and  $u_2$  respectively. These will be used to describe the zeroth order ground states of the four electron system in the appropriate ion-core frame work ( $M^{2+} - X - M^{2+}$ ). In the present formalism, only the excited states involving transitions of the cation electrons to empty excited orbitals are considered. For the symmetrical unit under consideration, the appropriate lowest orbital has even symmetry and is accordingly represented by  $\phi_g$  (I). Including the spin functions with the above spatial orbitals, we can construct the following states which are the eigenfunctions of the  $S^2$  operator for the four electron system :

Ground states :

*Triplet :*

$$|^3\psi_0\rangle = {}^3\{^3(u_1u_2)^1(\phi_0^2)\} = |u_1\phi_0\phi_0u_2| \quad \dots \quad (1)$$

*Singlet :*

$$|^1\psi_0\rangle = {}^1\{^1(u_1u_2)^1(\phi_0^2)\} = \{[u_1\phi_0\bar{\phi}_0\bar{u}_2] - [\bar{u}_1\phi_0\bar{\phi}_0u_2]\} / \sqrt{2} \quad \dots \quad (2)$$

Excited states : (Involving single electron transition to  $\phi_g$ )

*Triplets :*

$$|^3\psi_1\rangle = {}^3\{^3(u_1\phi_g)^1(\phi_0^2)\} = [u_1\phi_0\bar{\phi}_0\phi_g] \quad \dots \quad (3)$$

$$|^3\psi_2\rangle = {}^3\{^3(\phi_gu_2)^1(\phi_0^2)\} = |\phi_g\phi_0\bar{\phi}_0u_2| \quad \dots \quad (4)$$

*Singlets :*

$$|^1\psi_1\rangle = {}^1\{^1(u_1\phi_g)^1(\phi_0^2)\} = \{[u_1\phi_0\bar{\phi}_0\bar{\phi}_g] - [\bar{u}_1\phi_0\bar{\phi}_0\phi_g]\} / \sqrt{2} \quad \dots \quad (5)$$

$$|^1\psi_2\rangle = {}^1\{^1(\phi_gu_2)^1(\phi_0^2)\} = \{[\phi_g\phi_0\bar{\phi}_0\bar{u}_2] - [\bar{\phi}_g\phi_0\bar{\phi}_0u_2]\} / \sqrt{2} \quad \dots \quad (6)$$

Excited state involving two electron transitions to  $\phi_g$ :

*Singlet :*

$$|^1\psi_3\rangle = {}^1\{^1(\phi_g^2)^1(\phi_0^2)\} = [\phi_g\phi_0\bar{\phi}_0\bar{\phi}_g] \quad \dots \quad (7)$$

(As before, the square bracket notation denotes the Slater determinants multiplied by the appropriate normalizing factor; we indicate the down spin function by putting a bar over the orbital and up spin function without a bar)

The Hamiltonian (in atomic units) is taken as (I)

$$H = \sum_i H_i + \sum_{i < j} \frac{1}{r_{ij}} \quad \dots \quad (8)$$

where  $H_i$  is the one electron operator which contains, in addition to the kinetic energy operator, the potential acting on the  $i$ th electron due to the three nuclei and other electrons except the four under consideration. There is no point in writing the explicit forms of all the matrix elements of the Hamiltonian within the manifold described above. We consider those which are relevant to the present discussion. The orbitals  $\phi_g$  and  $\phi_0$  are orthogonal from symmetry consideration; however, to simplify the calculations the non-orthogonality of others will be neglected. The effect of this for  $u_1$ ,  $u_2$  and  $\phi_g$  can be included, if the choice of  $\phi_g$  warrants it.

In the absence of the feeble direct exchange interaction between the magnetic ions, the diagonal matrix elements of the triplet and singlet ground states are degenerate,

$$\langle {}^3\psi_0 | H | {}^3\psi_0 \rangle = \langle {}^1\psi_0 | H | {}^1\psi_0 \rangle = E_0 \quad (9)$$

The excited state of interest to us in the present scheme is

$$\langle {}^1\psi_3 | H | {}^1\psi_3 \rangle = E_m \quad (10)$$

Actually, we shall need the explicit form of the difference of Eqs. (10) and (9) i.e.,

$$\Delta E = E_m - E_0$$

$$\begin{aligned} \approx \{ [2\epsilon(\phi_g) - \epsilon(u_1) - \epsilon(u_2)] + [4K(\phi_g\phi_0) - 2K(u_1\phi_0) - 2K(u_2\phi_0)] \\ + [J(u_1\phi_0) + J(u_2\phi_0) - 2J(\phi_g\phi_0)] + [K(\phi_g\phi_g) - K(u_1u_2)] \} \end{aligned} \quad (11)$$

where  $\epsilon(a)$ ,  $K(ab)$  and  $J(ab)$  denote the one electron, coulomb and exchange integrals respectively. A study of the diagonal terms  $\langle {}^3\psi_1 | H | {}^3\psi_1 \rangle$ ,  $\langle {}^1\psi_1 | H | {}^1\psi_1 \rangle$  etc. and the off diagonal terms  $\langle {}^3\psi_0 | H | {}^3\psi_1 \rangle$  and  $\langle {}^1\psi_0 | H | {}^1\psi_1 \rangle$  reveals that interactions involving single cation electron transition for both singlet and triplet states have common dominant terms. Such terms would not, therefore, lead to any appreciable singlet triplet splitting up to second order of perturbation theory. Hence, we do not give any detailed considerations for interaction involving single electron transition.

The important of diagonal element is thus :

$$\langle {}^1\psi_0 | H | {}^1\psi_3 \rangle = \sqrt{2} \langle u_1\phi_g | g_{12} | u_2\phi_g \rangle \quad \dots \quad (12)$$

where

$$\langle ab | g_{12} | cd \rangle = \int a^*(\mathbf{r}_1) b(\mathbf{r}_1) 1/r_{12} c^*(\mathbf{r}_2) d(\mathbf{r}_2) d\mathbf{r}_1 d\mathbf{r}_2.$$

This would give rise to a lowering of the singlet ground state only, the depression according to second order perturbation being given by :

$$\begin{aligned} \delta E &= | \langle {}^1\psi_0 | H | {}^1\psi_3 \rangle |^2 / (E_m - E_0) \\ &= 2 | \langle u_1\phi_g | g_{12} | u_2\phi_g \rangle |^2 / (E_m - E_0) \quad \dots \quad (13) \end{aligned}$$

For further clarification of the results obtained, we shall consider the derivation of the exchange interaction term by the Dirac spin operator method as modified by Serber (1934). The ground state orbitals for the four electron systems are  $(u_1u_2)$  and  $(\phi_0^2)$ ; for the excited states we have  $(\phi_g^2)$  and  $(\phi_0^2)$ . In both the ground and excited states the two electrons occupying  $\phi_0$  are in singlet states with  $S$  value zero. Let the spin operators associated with the two electrons of the magnetic ions be  $\vec{S}_1$  and  $\vec{S}_2$  respectively. Then for the ground state the vectors sum is denoted by  $\vec{S}_1 + \vec{S}_2 = \vec{S}$ . In the excited configuration these two occupy the same orbital  $\phi_g$  and hence they must be in the singlet state. Accordingly, the effect of the second order perturbation on the zeroth order ground state can be expressed by an effective Hamiltonian defined by :

$$\langle S | H_{eff} | S' \rangle = \Sigma \langle S | H_m | 0 \rangle \langle 0 | H_m | S' \rangle / \Delta E \quad \dots \quad (14)$$

where  $\Delta E$  is the energy difference between the ground triplet or singlet states and the excited states which corresponds to  $\vec{S}_1 + \vec{S}_2 = 0$ .  $H_m$  is the spin dependent Hamiltonian which is of the following form in the present case

$$H_m = \text{constant term} - \sqrt{2} {}^oJ_{12} P_{12} \quad \dots \quad (15)$$

with  ${}^oJ_{12}$  standing for  $\langle u_1\phi_g | g_{12} | u_2\phi_g \rangle$  and  $P_{12}$  is the Dirac identity  $P_{12} = (1/2)(1 + 4\vec{S}_1 \cdot \vec{S}_2)$ . The factor  $\sqrt{2}$  in Eq. (15) is used as the necessary correction in going from non equivalent  $(u_1u_2)$  to equivalent  $(\phi_g\phi_g)$  orbitals. In fact, it has been shown by Anderson (1950) that the transition matrix element must be multiplied by  $\sqrt{2}$  for each pair of identical orbitals in either configuration which do not also appear in the other configuration. We introduce a projection operator which annihilates all states with parallel spin for 1 and 2 i.e.  $O_p = (1/4)(1 - 4\vec{S}_1 \cdot \vec{S}_2) = O_p^2$ .

Thus we can write :

$$\langle S | H_m | 0 \rangle = \langle S | H_m O_p | S' \rangle$$

It follows then,

$$H_{eff} = (H_m O_p H_m) / \Delta E = (2^g J_{12}^2) [P_{12} O_p P_{12}] / \Delta E \quad \dots (16)$$

Using the properties of spin operators, it is a trivial matter to prove that  $P_{12} O_p P_{12} = O_p = (1/4)(1 - 4\vec{S}_1 \cdot \vec{S}_2)$ . Eq. (16), therefore, reduces to

$$H_{eff} = (2^g J_{12}^2) [(1/4)(1 - 4\vec{S}_1 \cdot \vec{S}_2)] / \Delta E \quad \dots (17)$$

It can be easily seen that the effect of this operator for the triplet state (where  $\vec{S}_1 \cdot \vec{S}_2 = 1/4$ ) is identically zero. However, it reduces the energy of the singlet state ( $\vec{S}_1 \cdot \vec{S}_2 = -3/4$ ) by

$$\delta E = (2^g J_{12}^2) / \Delta E \quad \dots (18)$$

which is the same expression as Eq (13). Thus the superexchange effect due to the present scheme always favours the antiferro-magnetic coupling of the spin of magnetic ions.

#### DISCUSSION AND ESTIMATES

In this section, the relationship of the scheme envisaged here with the previous mechanism (I) will be discussed. We shall also consider certain semi-quantitative features based on an identification of the orbital  $\phi_g$ .

For a straightforward comparison, it is better to write the previous result for the orbitals considered in this paper i.e.  $u_1, u_2, \phi_0, \phi_g$ . (In I, we had treated the two anion electrons by the method of semi-localized orbitals). Thus for the symmetrical case  $u_1 \longleftrightarrow u_2$ , the second order perturbation term, which involves a spin dependent transition of one of the anion electrons to  $\phi_g$ , gives the effective interaction terms as

$$H_{eff} = (2u_1 J_{g0}^2) (\frac{1}{2} - 2\vec{S}_1 \cdot \vec{S}_2) / \Delta E' \quad (19)$$

where  $u_1 J_{g0} = \langle u_1 \phi_g | g_{12} | u_1 \phi_0 \rangle$  and  $\Delta E'$  is the energy denominator involved in this case (I). According to this, the stabilization of the singlet state is thrice as much as that of the triplet. The total lowering of the singlet state relative to the triplet state owing to both the effects is then given by

$$2 | \langle u_1 \phi_g | g_{12} | u_2 \phi_g \rangle |^2 / \Delta E + 4 | \langle u_1 \phi_g | g_{12} | u_1 \phi_0 \rangle |^2 / \Delta E' \quad \dots (20)$$

A reasonable estimate of Eq. (18) i.e., the first term of Eq. (20), would of course, depend on the choice of  $\phi_g$  which is in conformity with the physical situation existing in magnetic crystals. In I, we have given a quantitative estimate for  $\text{MnO}$ ; it is easier for comparison if we choose the same system for the present purpose.

However, the choice of a  $3d_{5/2}$  on the oxide ion centre would not be appropriate for  $\phi_g$  in that it would involve an excessive accumulation of charge at the intervening ion. Furthermore, its nonorthogonality with  $u_1$  and  $u_2$  may not be negligible. The greatest difficulty lies in having an unambiguous knowledge about the energy of this orbital. While the role of this type of empty orbital may be of significance in the spin-polarization mechanism involving anion electrons (I), it seems more appropriate for the present purpose to consider orbitals constituted out of a linear combination of available cation orbitals. As in I, we take the  $\sigma$ -type hybridised orbitals from each cation namely  $\chi_1$  and  $\chi_2$ . In the present mechanism, the importance of the ground state anion odd orbital  $\phi_0$  enters in virtue of its mixing with the odd combination  $\chi_1 - \chi_2$  and pushing its energy further up. Here again, the appropriate lowest orbital available to us is the even orbital.

$$\phi_g^e = (\chi_1 + \chi_2)/\sqrt{2} \quad (21)$$

Fortunately, the estimate in the previous paper is also based on the above orbital. In the following, we make a rough estimate with the same choice of  $\phi_g$ . Neglecting the overlap of functions, when their suffixes are different, and using real function, we have

$$u_1(1)\phi_g(1)|g_{12}|u_2(2)\phi_g(2) \approx \frac{1}{2} < u_1(1)\chi_1(1)|g_{12}|u_2(2)\chi_2(2) \quad (22)$$

Following the method described in the Appendix of I, we replace the factors  $u_1\chi_1$  and  $u_2\chi_2$  by two uniformly charged spheres of radius 1 a.u. each with density  $(\rho_0\rho_V)^{1/2}$  situated at the appropriate distances deduced from the observed inter atomic distance. This method of calculation yields  $< u_1\phi_g^e|g_{12}|u_2\phi_g^e > \approx 0.006$  a.u. Although this approximation is likely to underestimate the integral, it furnishes a rough guidance. We shall, however place reliance in the value 0.01 a.u. i.e. around 0.25 eV with confidence. This is of the same order of magnitude as the integral  $< u_1\phi_g^e|g_{12}|u_1\phi_0 >$  occurring in the numerator of the second term of Eq. (20).

The relevant energy denominator  $\Delta E$ , expressed in terms of  $\phi_g^e = (\chi_1 + \chi_2)/\sqrt{2}$  to orders of coulomb integral, is

$$\begin{aligned} \Delta E \approx \{ & [c(\chi_1) - c(u_1)] + [\epsilon(\chi_2) - \epsilon(u_2)] + [\frac{1}{2}K(\chi_1\chi_1) + \frac{1}{2}K(\chi_1\chi_2) - K(u_1u_2)] \\ & + 2[K(\chi_1\phi_0) - K(u_1\phi_0)] + 2[K(\chi_2\phi_0) - K(u_2\phi_0)] \} \end{aligned} \quad (23)$$

Making use of the integrals evaluated in the previous papers (I; and Sinha and Koide, 1960), the following order of magnitude assessment is possible.

$$\begin{aligned} [\frac{1}{2}K(\chi_1\chi_1) + \frac{1}{2}K(\chi_1\chi_2) - K(u_1u_2)] & \approx 0.2 \text{ a.u.} \\ [K(\chi_1\phi_0) - K(u_1\phi_0)] & \approx 0.1 \text{ a.u. etc.} \end{aligned}$$

The main difficulty remains about the assessment of one electron terms such as  $[\epsilon(\chi_1) - \epsilon(u_1)]$ . If, however, it is taken that the  $3d$  shell for the magnetic atoms in

crystals is extended upto  $4s$  and  $4p$  orbitals when hybrid orbitals are formed (Goodenough 1955), then the difference between  $\epsilon(\chi_1)$  and  $\epsilon(u_1)$  etc. will be extremely small. On the basis of this, one would arrive at a lower limit of  $\Delta E$  at about 0.5 to 0.6 a.u. (i.e. around 15 eV). In case it is underestimated, we shall take an upper limit, by including the energy difference between the configurations  $d^4S(^6D)$  and  $d^5(^6S)$ . From the calculations of Tanabe and Sugano (1954), for  $3d$  electrons in complexes, this is ascertained to be about 12 eV. i.e. around 0.5 a.u. We shall therefore choose a range for  $\Delta E$  from 0.5 a.u. to 2 a.u.

The denominator  $\Delta E'$  for the spin-polarisation effect i.e. second term of Eq. (20) was estimated to be of the order of 1 a.u. (See I). It is thus concluded that the term due to the present mechanism i.e.  $2|<u_1\phi_g|g_{12}|u_2\phi_g>|^2/\Delta E$  is at best (with  $\Delta E \approx 0.5$  a.u.) of the same order of magnitude and at worst (with  $\Delta E \approx 2.0$  a.u.) 25% of the term due to the previous mechanism  $4|<u_1\phi_g|g_{12}|u_1\phi_0>|^2/\Delta E'$ . In either limit, it leads to an appreciable contribution towards antiferromagnetic superexchange interaction. In fact, both the mechanisms, the previous (I) and the present, favour anti-ferro-magnetic coupling reinforcing each other effectively. The role of the empty orbital such as  $\phi_g$  involves juxtaposition of the interactions effect owing to the delocalization of the two magnetic ion electrons and their spread in this orbital, as well as the correlation effects wherein an anion electron makes a spin dependent transition to  $\phi_g$ . One can describe the physical situation further by stating that the interactions are such that the cation electrons have some probability in the vicinity of the anion and the anion electrons at the cation centres through the empty orbitals.

The importance of superexchange effects involving singly occupied orbitals such as  $u_1$  and  $u_2$  is, of course, also admitted. The contributions due to the correlation effects arising out of the transitions of the two anion electrons to  $u_1$  and  $u_2$  (Nesbet 1958, 1960) and the delocalisation effect involving virtual migration of an electron from one magnetic ion to another (Anderson, 1959), seems to be, at best, of the same order of magnitude as the terms in Eq. (20).

Since all mechanisms are acting in the same direction, the actual transition temperatures observed in such antiferro-magnetic systems are related to the sum of these interactions i.e. arising through singly occupied as well as empty orbitals. An attempt to derive the integrals so as to fit with the transition temperature as done by some authors amounts to overemphasising their mechanism.

We, therefore, conclude with the remark that the role of empty orbitals is of considerable importance in superexchange interaction effects and proper cognisance ought to be taken for these while studying the spin coupling in such magnetic systems.

#### ACKNOWLEDGMENT

The author is grateful to Dr. A. B. Biswas for his interest in this work,

REFERENCES

- Anderson, P. W., 1950, *Phys. Rev.* **79**, 350.  
Anderson, P. W., 1959, *Phys. Rev.*, **115**, 2.  
Goodenough, J. B., 1955, *Phys. Rev.* **100**, 107.  
Keffer, F., and Oguchi, T., 1959, *Phys. Rev.* **115**, 1428.  
Koide, S., Sinha, K. P., and Tanabe Y., 1959, *Prog. Theo. Phys.*, **22**, 647.  
Nesbet, R. K., 1958, *Ann. Phys.* **4**, 87.  
Nesbet, R. K., 1960 *Phys. Rev.* **119**, 658.  
Serber, R., 1934, *Phys. Rev.* **45**, 461.  
Sinha, K. P. and Koide, S., 1960, *Sci. Pap. Coll. Gen. Ed. University of Tokyo*, **10**, 195.  
Sinha K. P., 1961, *Ind. J. Phys.*, **35**, 111.  
Tanabe Y., and Sugano S., 1954, *J. Phys. Soc. (Japan)* **9**, 766.





# APPLICATION OF THE UREY-BRADLEY AND THE ORBITAL VALENCY FORCE FIELDS TO SOME TETRAHEDRAL IONS

T. A. HARIHARAN

DEPARTMENT OF PHYSICS, REGIONAL ENGINEERING COLLEGE,  
SURATHKAL, MYSORE STATE

(Received June 30, 1961)

**ABSTRACT.** In the case of the tetrahedral ions  $\text{CrO}_4^{2-}$ ,  $\text{MoO}_4^{2-}$ ,  $\text{GaBr}_4^-$ ,  $\text{InBr}_4^-$  and  $\text{TlBr}_4^-$  the force constants have been calculated using the Urey-Bradley type of potential function and the orbital valency force field. The appropriate potential function for each case is discussed.

## INTRODUCTION

Among the various types of potential functions used for studying the problem of molecular vibrations the valence force function is more extensively adopted than the others. Instead of a simple valence force function containing only quadratic terms, the one which takes into account the various interaction terms is found to be more satisfactory. However, a proper choice of these interaction terms or their adequate physical interpretation is not quite simple. A modification of the valence force function has been brought about by Urey and Bradley (1931) by introducing repulsion terms between non-bonded atoms of the type  $a/R^n$  where 'a' and 'n' are constants and  $R$  the distance between the atoms. A systematic investigation by Heath and Linnet (1948) on a number of tetrahedral halides of the group IV elements revealed that in a majority of cases  $n$  comes out to be nearly 4.5. This value was not acceptable for two reasons : (a) for the value  $n = 4.5$  the stretching of the bonds would be more than what has been actually observed, (b) the Lennard-Jones (1924) relation  $V = a/R^{12} - b/R^6$ , for the inert gas atoms are more reasonable because the bonded halogen atoms resemble electronically the inert gas atoms. According to the Lennard-Jones function,  $n$  can be taken as 12 after neglecting the second term which corresponds to attraction and is small compared to the first term. The potential function consists of four constants, namely, the stretching constant  $K_1$ , the bending constant  $K_2$ ,  $A \left( = \frac{1}{2} \frac{d^2 V}{dR^2} \right)$  and  $B \left( = -\frac{1}{R} \frac{dV}{dR} \right)$  where  $V$  is the function mentioned above. The relation between  $A$  and  $B/R$  becomes fixed for any particular value of  $n$ , i.e.,  $A: B/R = n+1: 2$ .

Another modification of the simple valence force field is what is known as the orbital valency force field first introduced by Heath and Linnet (1948). The

main feature of this function is that it makes use of the same constant for both the in plane and out of plane vibrations in the case of planar molecules and it differs from the simple valency force field only in its treatment of angular vibrations. According to Pauling's (1931) idea of directed valency the orbitals of an atom are set at definite angles to each other and the most stable bond between two atoms, say  $P$  and  $Q$ , is formed when one of the bond forming orbital of  $P$  overlaps to a maximum extent the bond forming orbitals of  $Q$ . Whenever there is a displacement from the maximum overlap during molecular vibrations restoring forces will be called into play and these can be assumed to be proportional to the displacements (which are of course small) if the vibrations are simple harmonic.

There are two ways by which the overlap of the bond forming orbitals can be increased during the vibrations. In the case of tetrahedral molecules or ions with which we are concerned here the orbitals of the central atom might be rotated as a whole in such a way as to improve the overlap. On the other hand, the orbitals of the central atom might change their hybridisation ratios by changing the angles at which they are set with each other so as to follow the movements of the outer atoms. This idea has been called orbital following.

The orbital valency force field without taking into account the idea of orbital following also consists of four constants  $K_1$ ,  $K_\alpha'$  (instead of  $K_\alpha$  as in the simple valency force field),  $A$  and  $B/R$ . Heath and Linnet (1948) have observed that for the ions  $\text{ClO}_4^-$ ,  $\text{SO}_4^{2-}$ ,  $\text{SeO}_4^{2-}$  and  $\text{PO}_4^{3-}$  the orbital valency force field is quite satisfactory. Such a force field is assumed in the present investigation to evaluate the force constants of the ions  $\text{CrO}_4^{2-}$ ,  $\text{MoO}_4^{2-}$ ,  $\text{GaBr}_4^-$ ,  $\text{InBr}_4^-$  and  $\text{TlBr}_4^-$ .

#### THE POTENTIAL ENERGY FUNCTION

The potential energy function for tetrahedral molecules  $XY_4$  can be written in the form

$$U = \sum_i f(r_i) + \sum_{i,j} F(R_{ij}) + \sum_{i,j} \frac{1}{2} K_\alpha (\Delta\alpha_{ij})^2 \quad \dots (1)$$

the first term arising due to change in the  $X-Y_i$  distance ( $r_i$ ), the second term due to changes in the  $Y_i-Y_j$  distance ( $R_{ij}$ ), and the last term due to changes in the angles  $Y_iXY_j(\alpha_{ij})$ . For small values of these variations the functions  $f(r_i)$  and  $F(R_{ij})$  can be expanded in powers of  $r_i$  and  $R_{ij}$  which denote the changes in  $r_i$  and  $R_{ij}$  from their equilibrium values  $r_i^0$  and  $R_{ij}^0$ . Retaining powers only up to the second we have

$$\begin{aligned} U = & \sum_i f(r_i^0) + \sum_i f'(r_i^0) \Delta r_i + \sum_i \frac{1}{2} f''(r_i^0) \Delta r_i^2 \\ & + \sum_{i,j} F(R_{ij}^0) + \sum_{i,j} F'(R_{ij}^0) \Delta R_{ij} + \sum_{i,j} \frac{1}{2} F''(R_{ij}^0) \Delta R_{ij}^2 + \sum_{i,j} \frac{1}{2} K_\alpha (\Delta\alpha_{ij})^2 \quad \dots (2) \end{aligned}$$

Taking into consideration the above type of potential function the equations for the frequencies can be written as

I For the simple valency force field :

$$\text{Type } A_1 \quad \lambda_1 = \mu_y(K_1 + 8A) \quad \dots \quad (3)$$

Type  $T_2$

$$\begin{aligned} \lambda_2 + \lambda_3 = (\mu_y + \frac{4}{3}\mu_x) \left( K_1 + \frac{8}{3}A - \frac{4}{3}\frac{B}{R} \right) + (\mu_y + \frac{8}{3}\mu_x) \left( 2K_\alpha + \frac{4}{3}A + \frac{16}{3}\frac{B}{R} \right) \\ - \frac{8}{3}\mu_x \left( \frac{8}{3}A - \frac{4}{3}\frac{B}{R} \right) \quad \dots \quad (4) \end{aligned}$$

$$\begin{aligned} \lambda_2\lambda_3 = (\mu_y^2 + 4\mu_x\mu_y) \left[ \left( K_1 + \frac{8}{3}A - \frac{4}{3}\frac{B}{R} \right) \right. \\ \left. \left( 2K_\alpha + \frac{4}{3}A + \frac{16}{3}\frac{B}{R} \right) - \frac{1}{2} \left( \frac{8}{3}A - \frac{4}{3}\frac{B}{R} \right)^2 \right] \quad \dots \quad (5) \end{aligned}$$

$$\text{Type } E. \quad \lambda_4 = \mu_y \left( 3K_\alpha + 2A + \frac{B}{R} \right) \quad \dots \quad (6)$$

II For orbital valency force field :

$$\text{Type } A_1 \quad \lambda_1 = \mu_y(K_1 + 8A) \quad \dots \quad (7)$$

Type  $T_2$

$$\begin{aligned} \lambda_2 + \lambda_3 = (\mu_y + \frac{4}{3}\mu_x) \left( K_1 + \frac{8}{3}A - \frac{4}{3}\frac{B}{R} \right) \\ + (\mu_y + \frac{8}{3}\mu_x) \left( K'_\alpha + \frac{4}{3}A + \frac{16}{3}\frac{B}{R} \right) \\ - \frac{8}{3}\mu_x \left( \frac{8}{3}A - \frac{4}{3}\frac{B}{R} \right) \quad \dots \quad (8) \end{aligned}$$

$$\begin{aligned} \lambda_2\lambda_3 = (\mu_y^2 + 4\mu_y\mu_x) \left[ \left( K_1 + \frac{8}{3}A - \frac{4}{3}\frac{B}{R} \right) \right. \\ \left. \left( K'_\alpha + \frac{4}{3}A + \frac{16}{3}\frac{B}{R} \right) - \frac{1}{2} \left( \frac{8}{3}A - \frac{4}{3}\frac{B}{R} \right)^2 \right] \quad \dots \quad (9) \end{aligned}$$

$$\text{Type } E \quad \lambda_4 = \mu_y(K'_\alpha + 2A + \frac{B}{R}) \quad \dots \quad (10)$$

$\mu_x$  and  $\mu_y$  denote the reciprocal of the masses of the atoms  $X$  and  $Y$  respectively and  $\lambda_i = 4\pi^2 c^2 \nu_i^2$ . If the interaction function between non-bonded-atoms is assumed as  $V = a/R^n$

$$\text{then} \quad \frac{B}{R^0} = \frac{na}{(R^0)^{n+2}} \quad \text{and} \quad A = \frac{n(n+1)a}{2(R^0)^{n+2}}$$

so that

$$\frac{A}{(B/R^3)} = \frac{n+1}{2}$$

#### EVALUATION OF THE CONSTANTS

The values of  $K_a$  and  $K_a'$  can be obtained in terms of  $A$  from the equation for the doubly degenerate frequency  $\lambda_4$ . These can be then substituted in the first equation for the triply degenerate vibrations  $T_2$  which will give an equation in  $K_1$  and  $A$  which can be solved simultaneously with the equation for the totally symmetric class  $A_1$ . By substituting the values of the force constants in the second equation for  $T_2$ , the calculated and observed values of  $\lambda_2\lambda_3$  can be compared.

#### RESULTS

The fundamental frequencies of the ions are taken from the published results on their Raman spectra and they are given in Table I. In Table II to V the values of the force constants for the six ions have been given while Table VI contains the observed and calculated values of  $\lambda_2\lambda_3$ . All the force constants are given in  $10^5$  dynes/cm.

TABLE I  
Frequencies in  $\text{cm}^{-1}$

Ion	$\nu_1(A_1)$	$\nu_2(T_2)$	$\nu_3(T_2)$	$\nu_4(E)$	Reference
$\text{CrO}_4^{=}$	858	510	875	485	Landolt Bornsteins's Tables, 1953
$\text{MnO}_4^-$	940	365	895	220	
$\text{GaBr}_4^-$	210	102	278	71	Woodward and Nord, (1955)
$\text{InBr}_4^-$	197	79	239	55	Woodward and Bill, (1955)
$\text{TlBr}_4^-$	190	64	209	51	Relfe, Sheppard and Woodward (1954)

TABLE II  
S.V.F.F.  $n = 4.5$

Ion	$K_1$	$A$	$B/R$	$K_a$
$\text{CrO}_4^{=}$	4.209	0.3416	0.1242	0.4703
$\text{MoO}_4^{=}$	5.503	0.3536	0.1286	0.0634
$\text{GaBr}_4^-$	1.269	0.101	0.0367	-0.0004
$\text{InBr}_4^-$	1.307	0.0654	0.0237	-0.004
$\text{TlBr}_4^-$	1.26	0.055	0.02	-0.0024

TABLE III

S.V.F.F.  $n = 12$ 

Ion	$K_1$	$\Lambda$	B/R	$K_\alpha$
$\text{CrO}_4^{=}$	4.466	0.3095	0.0476	0.517
$\text{MoO}_4^{=}$	5.73	0.3252	0.05	0.1085
$\text{GaBr}_4^{=}$	1.054	0.1276	0.0197	-0.0126
$\text{InBr}_4^{=}$	1.365	0.058	0.009	0.0058
$\text{TlBr}_4^{=}$	1.303	0.0495	0.0076	0.0053

TABLE IV

O.V.F.F.  $n = 4.5$ 

Ion	$K_1$	$\Lambda$	B/R	$K_\alpha'$
$\text{CrO}_4^{=}$	3.50	0.43	0.1564	1.201
$\text{MoO}_4^{=}$	5.408	0.3654	0.1328	0.1623
$\text{GaBr}_4^{=}$	1.269	0.1009	0.0367	-0.0011
$\text{InBr}_4^{=}$	1.313	0.0646	0.0235	-0.012
$\text{TlBr}_4^{=}$	1.263	0.0545	0.0198	-0.0063

TABLE V

O.V.F.F.  $n = 12$ .

Ion	$K_1$	$\Lambda$	B/R	$K_\alpha'$
$\text{CrO}_4^{=}$	3.741	0.4	0.0615	1.3568
$\text{MnO}_4^{=}$	5.581	0.3438	0.0529	0.2856
$\text{GaBr}_4^{=}$	1.345	0.0915	0.014	0.0404
$\text{InBr}_4^{=}$	1.357	0.059	0.009	0.0153
$\text{TlBr}_4^{=}$	1.296	0.0504	0.0078	0.0139

TABLE VI

Ion	$\frac{\lambda_2 \lambda_3}{\mu_y^2 + 4\mu_x \mu_y}$		$\frac{\lambda_2 \lambda_3}{\mu_y^2 + 4\mu_x \mu_y}$ calculated		O.V.F.F.	
	observed	S.V.F.F. $n = 4.5$	$n = 12$	$n = 4.5$	$n = 12$	
$\text{CrO}_4^{=}$	$7.936 \times 10^{10}$	$8.691 \times 10^{10}$	$8.105 \times 10^{10}$	$9.754 \times 10^{10}$	$9.41 \times 10^{10}$	
$\text{MoO}_4^{=}$	$5.692 \times 10^{10}$	$6.146 \times 10^{10}$	$5.017 \times 10^{10}$	$6.461 \times 10^{10}$	$5.557 \times 10^{10}$	
$\text{GaBr}_4^{=}$	$3.195 \times 10^9$	$3.573 \times 10^9$	$2.391 \times 10^9$	$3.755 \times 10^9$	$3.033 \times 10^9$	
$\text{InBr}_4^{=}$	$2.085 \times 10^9$	$2.1948 \times 10^9$	$1.693 \times 10^9$	$2.117 \times 10^9$	$1.763 \times 10^9$	
$\text{TlBr}_4^{=}$	$1.545 \times 10^9$	$1.792 \times 10^9$	$1.379 \times 10^9$	$1.761 \times 10^9$	$1.444 \times 10^9$	

It can be seen from Table VI that in the case of  $\text{MoO}_4$ ,  $\text{GaBr}_4$  and  $\text{TlBr}_4$  the orbital valency force field with  $n = 12$  is more satisfactory than the others while for  $\text{InBr}_4$  the same field with  $n = 4.5$  instead of 12 suits better. For the chromate ion the simple valency force field with  $n = 12$  yields better results than the others. This simple valency force field with  $n = 4.5$  is least satisfactory for all the ions. In the case of the ions  $\text{ClO}_4^-$ ,  $\text{SO}_4^{2-}$ ,  $\text{SeO}_4^{2-}$  and  $\text{PO}_4^{3-}$ , Heath and Linnet (1948) have observed that the orbital valency force field holds better. The difference between observed and calculated values of  $\lambda_2\lambda_3$  can be further reduced by introducing modifications such as orbital following.

## REFERENCES

- Heath, D.F. and Linnet, J. W., 1948, *Trans Farad. Soc.* **44**, 561.  
Heath, D. F. and Linnet J. W., 1948, *Trans Farad. Soc.* **44**, 873.  
Heath, D. F. and Linnet, J. W., 1948, *Trans Farad. Soc.* **44**, 884.  
Lennard Jones, J. E., 1924, *Proc. Roy. Soc.* **106A**, 463.  
Pauling, L., 1931, *J. Am. Chem. Soc.* **53**, 1367.  
Rolfe, J. A. Sheppard D. E. and Woodward, L.A., 1954, *Trans Farad. Soc.* **50**, 1275.  
Urey, H.C. and Bradley, C. A., 1931, *Phys. Rev.* **38**, 1969.  
Woodward, L. A. and Bill, P. T., 1955, *J. Chem. Soc.*, 1699.  
Woodward, L. A. and Nord, A. A., 1955, *J. Chem. Soc.* 2655.

# X-RAY STUDY OF A DEHYDRATED PHASE OF COPPER AMMONIUM SULPHATE HEXAHYDRATE

GOURI BHOWMIK

MAGNETISM DEPARTMENT, I. A. C. S., CALCUTTA-32

(Received June 9, 1961)

## Plate X

**ABSTRACT.** The cell-dimensions of  $\text{Cu}[(\text{NH}_4\text{SO}_4)_2 \cdot 6\text{H}_2\text{O}]$  (monoclinic, space-group  $P2_1/a$ ) as determined from rotation photograph are found to be  $a = 9.27\text{\AA}$ ,  $b = 12.50\text{\AA}$ ,  $c = 6.33\text{\AA}$   $\beta = 106^\circ 5'$ , with 2 molecules per unit cell. The results have been utilised to index the powder pattern of the substance. Analysis of the powder pattern by Lij son's method of the first stage dehydration product,  $\text{Cu}[\text{NH}_4(\text{SO}_4)]_2 \cdot 2\text{H}_2\text{O}$  formed at  $65^\circ\text{C}$  shows that the product has orthorhombic structure, the cell dimensions being  $a = 14.84\text{\AA}$ ,  $b = 12.52\text{\AA}$ ,  $c = 10.69\text{\AA}$ . The probable space groups are  $\text{Pmn } 2_1$  and  $\text{Pnmm}$  with 8 molecules per unit cell.

## INTRODUCTION

Magnetic measurements of the single crystals of a large number of Tutton salts (general formula  $\text{M}(\text{R X Y}_4)_2 \cdot 6\text{H}_2\text{O}$  where  $\text{M} = \text{Mg, Zn, Cd, Cu, Ni, Co, Fe, etc.}$   $\text{R} = \text{K, Rb, Cs, NH}_4$ ,  $\text{XY}_4 = \text{SO}_4, \text{SeO}_4$  or  $\text{BeF}_4$ ) showed (Bose *et al.* 1957 and 58) that they lose their magnetic anisotropies in the range  $338^\circ - 393^\circ\text{K}$  the exact temperature depending upon the particular salt. This is evidently due to changes in crystal structure accompanying loss of water of crystallisation which causes the single crystals to become polycrystalline. Since the crystalline magnetic properties are intimately connected with the structure it would be interesting to study these changes in structure in order to elucidate the changes in the magnetic properties. As a typical case, the thermal dehydration of  $\text{Cu}[(\text{NH}_4)\text{SO}_4]_2 \cdot 6\text{H}_2\text{O}$  was undertaken and the corresponding changes in crystal structure investigated.

## 2. X-RAY MEASUREMENTS ON $\text{Cu}[(\text{NH}_4\text{SO}_4)_2 \cdot 6\text{H}_2\text{O}]$

X-ray data on single crystals of  $\text{Cu}[(\text{NH}_4)\text{SO}_4]_2 \cdot 6\text{H}_2\text{O}$  is lacking, though one of the isomorphous salts  $\text{Mg}[(\text{NH}_4)\text{SO}_4]_2 \cdot 6\text{H}_2\text{O}$  has been studied using trial and error method by Hofmann (1931). By analogy with the latter it follows that  $\text{Cu}[(\text{NH}_4)\text{SO}_4]_2 \cdot 6\text{H}_2\text{O}$  is also monoclinic having 2 molecules in the unit cell and belongs to

the space-group  $P2_1/a$ . We have determined the dimensions of the unit cell from rotation photographs about the three crystallographic axes. They are

$$a = 9.27 \text{ \AA}$$

$$b = 12.50 \text{ \AA}$$

$$c = 6.33 \text{ \AA}$$

$$\beta = 106^\circ 5'.$$

The monoclinic angle  $\beta$  is found from the zero layer-line of the rotation photograph about  $b$ -axis.

A powder diffraction pattern has also been taken at room-temperature and the spacings indexed with the help of the above values of cell dimensions.

TABLE 1

dÅ	Intensity	1/d <sup>2</sup> observed	1/d <sup>2</sup> calculated	Indices
7.193	vw	0.0193	0.0190	110
6.105	ms	0.0268	0.0270	001
5.456	ms	0.0336	0.0334	011
5.129	w	0.0380	0.0384	120
4.418	w	0.0502	0.0504	200
4.188	vs	0.0570	0.0568	210
3.759	vs	0.0708	0.0702	130
3.620	w	0.0763	0.0758	220
3.386	ms	0.0872	0.0870	131
3.061	s	0.1067	0.1066	112
2.486	s	0.1235	0.1239	212
2.715	w	0.1357	0.1353	321
2.556	m	0.1531	0.1528	240
2.441	s	0.1678	0.1673	331
2.229	ms	0.2013	0.2017	400
2.176	w	0.2112	0.2104	042]
			0.2104	250]
2.144	w	0.2175	0.2170	251
2.097	ms	0.2274	0.2273	420
2.031	w	0.2424	0.2431	003
1.963	w	0.2595	0.2593	430
1.922	ms	0.2707	0.2712	313
1.858	w	0.2897	0.2897	233]
			0.2893	312]
1.816	w	0.3032	0.3040	440
1.768	w	0.3200	0.3206	510
1.736	w	0.3318	0.3312	351
1.701	w	0.3456	0.3454	043



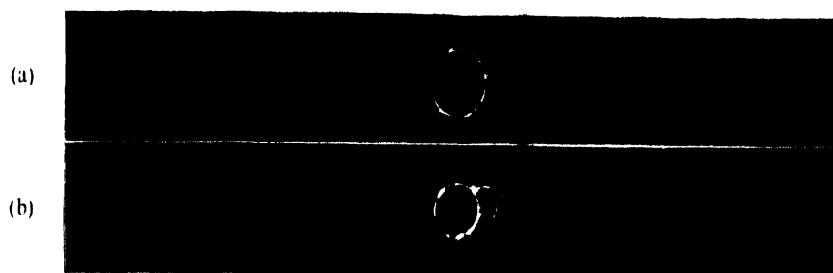


Fig. 1. Debye-Scherrer patterns

- (a) Copper ammonium sulphate hexahydrate  $\text{Cu} [ (\text{NH}_4 ) \text{SO}_4 ]_2 \cdot 6\text{H}_2\text{O}$
- (b) Copper ammonium sulphate dihydrate  $\text{Cu} [ (\text{NH}_4 ) \text{SO}_4 ]_2 \cdot 2\text{H}_2\text{O}$



The conditions of reflection satisfied are :

$hkl$  : no condition

$h0l$  :  $h = 2n$ .

There is no powder-line with  $0k0$  reflection. But rotation photographs show that for  $0k0$ ,  $k = 2n$  spots are present. Hence the space-group is  $P2_1/a$  which supports the earlier assumptions.

#### STUDIES ON THE DEHYDRATION PRODUCT

Next powdered sample of  $\text{Cu}[(\text{NH}_4)\text{SO}_4]_2 \cdot 6\text{H}_2\text{O}$  of weighed quantity is heated automatically controlled thermostatic oven and the loss of weight at different temperatures is determined. At  $338^\circ\text{K}$  it shows an abrupt loss of weight which corresponds to 4 molecules of water. When the temperature is brought down the sample soon regains its original weight. It indicates that  $\text{Cu}[(\text{NH}_4)\text{SO}_4]_2 \cdot 6\text{H}_2\text{O}$  undergoes a reversible transformation to a dihydrate at  $65^\circ\text{C}$ . This is also evident from the X-ray powder pictures.

It is interesting to study the structure of the dehydrated product. Since the dehydrated powder absorbs moisture rather quickly, instead of packing the dehydrated powder in capillary tubes in the usual way, the capillary tube is first packed with finely powdered  $\text{Cu}[(\text{NH}_4)\text{SO}_4]_2 \cdot 6\text{H}_2\text{O}$ , now the fine tube packed and open at both ends is heated in the oven at a constant temperature somewhat above  $65^\circ\text{C}$  for 24 hours when it attains constant weight.

The capillary tube is now quickly sealed at both ends so that the treated sample does not come in contact with moisture from the atmosphere. The sample is mounted in a camera of 57.3 mm radius and X-ray powder photograph is taken with  $\text{CuK}_\alpha$  radiation from a Raymax 60 Diffraction unit running at 50KV and 10 mA. The powder pattern thus obtained is entirely different from that for  $\text{Cu}[(\text{NH}_4)\text{SO}_4]_2 \cdot 6\text{H}_2\text{O}$ . Besides, the spacings measured for the powder-line has no spacing common with the known spacings of either of  $(\text{NH}_4)_2\text{SO}_4$  or  $\text{CuSO}_4$  (anhydrous) or  $\text{CuSO}_4 \cdot \text{H}_2\text{O}$ . This shows that the dehydrated product is a new double salt having a unique crystal structure. If the dehydrated powder is cooled to room-temperature in contact with atmosphere and photograph taken, the original powder pattern of  $\text{Cu}[(\text{NH}_4)\text{SO}_4]_2 \cdot 6\text{H}_2\text{O}$  is obtained. The powder photograph is the only source of information regarding the structure of the new compound since, in spite of many attempts the substance could not be obtained as single crystals from aqueous medium. Hence attempt has been made to index the powder-photograph taking the substance to have the molecular formula  $\text{Cu}[(\text{NH}_4)\text{SO}_4]_2 \cdot 2\text{H}_2\text{O}$ .

First attempts were made to index the powder lines in terms of cubic, tetragonal and hexagonal system. Since the data do not fit with either of these systems Lipson's method (Lipson, 1949) was applied to find if the crystal belongs to the

orthorhombic system. For orthorhombic system,  $\sin^2 \theta$  values obtained from each pair of Debye-Scherrer ring can be written as

$$\sin^2 \theta_{hkl} = \frac{\lambda^2}{4a^2} h^2 + \frac{\lambda^2}{4b^2} k^2 + \frac{\lambda^2}{4c^2} l^2$$

$$= Ah^2 + Bk^2 + Cl^2 \quad \text{where} \quad A = \frac{\lambda^2}{4a^2} \quad B = \frac{\lambda^2}{4b^2} \quad C = \frac{\lambda^2}{4c^2}$$

TABLE II

dÅ	Intensity	$\sin^2 \theta$ observed	$\sin^2 \theta$ calculated	Indices
12.199	w	0.0039	0.0038	010
8.023	s	0.0092	0.0090	011
6.193	s	0.0155	0.0152	020
5.771	w	0.0178	0.0179	120
5.345	s	0.0209	0.0208	002
4.551	w	0.0287	0.0282	310
4.331	vs	0.0317	0.0312	221
4.312	vs	0.0319	0.0316	202
3.952	ms	0.0381	0.0387	122
3.785	ms	0.0415	0.0421	131
3.642	w	0.0448	0.0447	321
3.508	w	0.0483	0.0484	401
			0.0488	312
3.364	vw	0.0525	0.0522	411
3.268	vs	0.0557	0.0550	032
3.226	vs	0.0571	0.0577	132
3.150	m	0.0599	0.0603	311
3.064	vs	0.0631	0.0635	140
3.033	vs	0.0646	0.0640	402
			0.0647	132
2.960	w	0.0679	0.0678	412
2.885	w	0.0714	0.0713	510
2.447	ms	0.0788	0.0792	422
			0.0793	332
2.657	ms	0.0842	0.0843	142
2.614	w	0.0904	0.0898	114
2.495	w	0.0955	0.0950	050
2.450	s	0.0990	0.0984	024
2.298	w	0.1126	0.1124	610
2.139	s	0.1299	0.1302	414
2.081	s	0.1373	0.1368	060
			0.1365	115
1.983		0.1511	0.1508	443
1.922		0.1609	0.1611	360
1.762	ms	0.1915	0.1010	016
1.730	ms	0.1986	0.1983	741
1.521	w	0.2571	0.2575	107
1.497	w	0.2653	0.2661	715

The values of  $\sin^2 \theta_{hkl}$  known as  $q$ -values observed from the pattern are listed in Table II. With the above values of  $\sin^2 \theta$ , the difference diagram is drawn according to Lipson's method. The diagram shows frequently-occurring values

from which the values of the constants  $A, B, C$  are determined in the following way.

If we choose the first three values of  $\Delta q$  from the Lipson's chart i.e., 0.0028, 0.0038, 0.0052, we find that (1) the 4 fold and 9 fold multiples of  $A$  i.e., .0110, .0250 are present, (2) the 4 fold, 9 fold, 16 fold multiples of  $B$  i.e., 0.0152, 0.0340, 0.061 are frequently occurring, (3) the 9 fold, 16 fold and 25 fold multiples of  $C$  i.e., 0.046, 0.083 and 0.1300 are also present in the chart.

There are no other value of  $\Delta q$  in the Lipson's chart which has so many multiples present. So these are the most probable values of constants  $A, B, C$ . With these values of  $A, B, C$  all the values of  $\sin^2 \theta_{hkl}$  in Table II can be successfully indexed. For better adjustment  $A$  is taken as 0.0027 and the agreement between the observed and calculated values is highly satisfactory, the discrepancy lying within experimental errors. So it is concluded that the crystal belongs to the orthorhombic system, with the dimensions of the unit cell as calculated from  $A, B, C$

$$a = 14.84 \text{ \AA}$$

$$b = 12.52 \text{ \AA}$$

$$c = 10.69 \text{ \AA}$$

Measurement of the density of the dihydrate is very difficult since it always tends to be converted into the hexahydrate when exposed to atmosphere. The hexahydrate powder is taken in a specially designed pyknometer and treated in the furnace at  $70^\circ\text{C}$  for about 24 hours so that the dihydrate is obtained. The pyknometer is cooled in a dessicator and weighed. Since the substance is highly soluble in water its density is measured with respect to paraffin oil of known density. Repeated measurements show that the density of the dihydrate is 2.04 gm/c.c.

With this value of density and the dimensions of the unit cell given above, the number of molecules per unit comes out as  $7.50 \approx 8$ . The agreement is satisfactory in view of the fact that due to the extreme instability of the dihydrate, at room temperature, sufficient accuracy cannot be obtained in the determination of the density. This integral value also supports the choice of the unit cell of the crystal.

The conditions limiting possible reflections indicated by Table II are

$hko$  : no condition

$okl$  : no condition

$hol$  :  $h+l = 2n$

$hko$  : no condition

$hoo$  :  $h = 2n$ .

$oko$  : no condition

$ool$  :  $l = 2n$ ,

The conditions agree with both the space groups  $P_{mn}2_1$  and  $P_{mmm}$ . Since the substance has not yet been obtained in the single crystal form it is not possible to ascertain the space-group uniquely from single crystal photograph.

#### 4. DISCUSSIONS

It is interesting to note that the orientation of the crystalline principal magnetic axes in the (010) plane of the crystal of  $\text{Cu}[(\text{NH}_4\text{SO}_4)]_2 \cdot 6\text{H}_2\text{O}$  changes by about  $19^\circ$  in the range  $90^\circ\text{K}$  to  $338^\circ\text{K}$  slowly at first and then rapidly as the transition temperature of  $338^\circ\text{K}$  is approached. Correspondingly the relative orientation between the approximate tetragonal axes of the two equivalent  $\text{Cu}^{2+} \cdot 6\text{H}_2\text{O}$  octahedra equally inclined to the  $b$ -axis of the unit cell, change by about  $10^\circ$  (Bose *et al.*, 1957). This indicates that even before the transition temperature is reached a rapid rearrangement of the constituents of the unit cell is taking place, owing to increased thermal motions, tending to make the four water molecules of coordination redundant for the stable equilibrium of the lattice at the transition point, which becomes apparent by the fact that as soon as this temperature is reached these water molecules are thrown out of the lattice and the constituents of the unit cell assume the new symmetry of the orthorhombic class for the dihydrate. The manner of reorientation by rotation of the  $\text{Cu}^{2+} \cdot 6\text{H}_2\text{O}$  groups about the  $b$ -axis previous to transition and the X-ray finding that the  $b$ -axial lengths of the hexahydrate and dihydrate are equal seem to indicate that there is a correspondence between the  $b$ -axes of the monoclinic and the orthorhombic varieties. Also the transition from monoclinism to orthorhombicity is attained at the transition temperature by a continuous approach of the  $a$  and  $c$  axes of the monoclinic cell towards orthogonality.

More X-ray data on the structure of the salt before and after transition would verify the predictions and attempts are being made to obtain these.

#### ACKNOWLEDGMENT

The author expresses her sincere thanks to Prof. A. Bose, D.Sc., F.N.I. for his kind interest and constant guidance and to Mr S. Ray, M.Sc. for many helpful discussions during the progress of the work.

#### REFERENCES

- Bose A., Mitra S. C. and Dutta S. K., 1957, *Proc. Roy. Soc. A* **239**, 165.
- Bose A., Mitra S. C. and Dutta S. K. 1958. *Proc. Roy. Soc. A* **248**, 153.
- Hofmann, W. 1931. *Zeits. f. Krist.* **78**, 279.
- Lipson, H., 1949., *Acta. Cryst.*, **2**, 43.

# THE CRYSTALLITE ORIENTATION IN MESTA FIBRE

SUBHRENDU KAR\* AND R. K. BASU

TECHNOLOGICAL RESEARCH LABORATORIES, INDIAN CENTRAL JUTE COMMITTEE,  
REGENT PARK, CALCUTTA.

(Received January 20, 1961)

**ABSTRACT.** The orientations of crystallites in mesta fibres raw, delignified and treated with different concentrations of caustic soda have been studied. The Hermans' orientation factor, the average angle of orientation and angle for 40% intensity for five samples have been determined from intensity distribution curves of the equatorial arcs in the X-ray diffraction photographs. It has been observed that for mesta, the average angle of orientation varies from  $11^\circ$  to  $14^\circ$  and Hermans' orientation factor varies from 0.91 to 0.94.

## INTRODUCTION

Mesta, a substitute fibre for jute, has its crystalline structure similar to that of jute. It has been established that in jute fibres, the crystallites have their 'b' axis nearly parallel to the fibre axis making a small angle. The other axes of the crystallites are randomly oriented. The average angle of orientation is generally measured from the distribution of intensity along the arcs into which the diffraction spots are drawn. These have been measured for cotton, jute, ramie etc. The relation between orientation and physical properties for cotton has been studied by many workers. Sen and Wood (1949) studied the orientations for jute and ramie. They compared Hermans' orientation factor and half maximum intensity angle for jute and ramie. They also observed a difference in orientation factors for different varieties of jute.

The present work was undertaken in order to study the orientation factor for mesta fibre and compare it with established values of cotton, jute and ramie, and also to investigate the variation in orientations in the raw and delignified fibres and fibres treated with different strengths of caustic soda. The Hermans' orientation factor, the average orientation angle and angle for 40% intensities were determined.

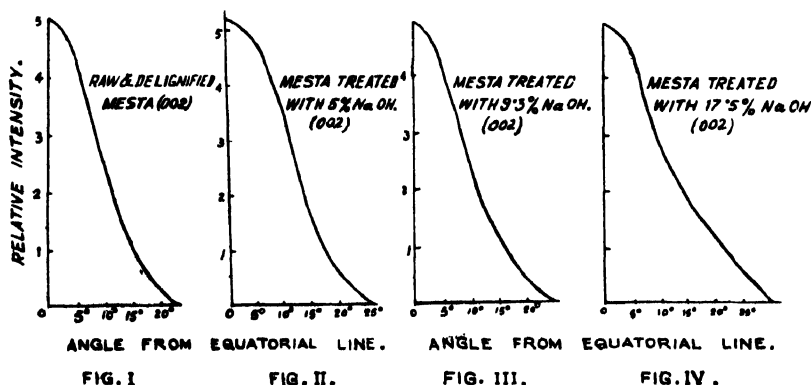
## PROCEDURE

Samples of alkali treated fibres were prepared by treating raw mesta fibre with different strengths of NaOH solution. Delignified samples were prepared in the usual way by the 'Textone' process. X-ray diffraction photographs were taken for all samples with  $CuK_\alpha$  radiation (nickel filtered) from a Hadding type

\*Now at Defence Metallurgical Research Laboratory, Ishapore, West Bengal.

X-ray tube. The camera used was a flat cassette plate camera. Photographs of moderate intensity suitable for microphotometer work were taken.

Following Hermans *et al.* (1939) a series of microphotometer curves of (002) and composite (101) and (10 $\bar{1}$ ) interferences were recorded starting from the equatorial lines of the diffraction photographs and proceeding in radial lines at angular intervals of 2°30'. Densities of the photometer curves were converted into intensities from a density—log intensity curve, drawn experimentally by comparison with the curve of a standard calibration strip having intensities at various points proportional to the distance from zero intensity point. From these, curves were drawn for intensities against angular distances with equatorial lines for the (002)



reflections. The curves are shown in Figs. I-IV. These intensity distribution curves represent the statistical distribution of the paratropic planes of the crystallites of the fibres. Intensity may be designated by  $I = F(\alpha)$  where  $\alpha$  is the angular distance from the equator. According to Hermans the average angle of orientation  $\alpha_m$  is given by

$$\sin^2 \alpha_m = \sin^2 \alpha_1 + \sin^2 \alpha_2$$

$$\overline{\sin^2 \alpha_1} = \frac{\int_0^{\pi/2} F(\alpha_1) \sin^2 \alpha_1 \cos \alpha_1 d\alpha_1}{\int_0^{\pi/2} F \cos \alpha_1 d\alpha_1}$$

and

$$\sin^2 \alpha_2 = \frac{\int_0^{\pi/2} F(\alpha_2) \sin^2 \alpha_2 \cos \alpha_2 d\alpha_2}{\int_0^{\pi/2} F \cos \alpha_2 d\alpha_2}$$

and the Hermans' orientation factor

$$f_z = 1 - \frac{3}{2} \sin^2 \alpha_m$$

In the case of raw fibres, it has been found that  $F(\alpha_1) = F(\alpha_2)$ ; hence only  $F(\alpha)$  for (002) is shown in the curves. (Only for the case of fibres treated with



17.5% NaOH both the (002) and (101) (Fig. 5) reflections were taken into consideration for calculating  $\alpha_m$  and  $f_x$ ). Empirical intensity curves were drawn

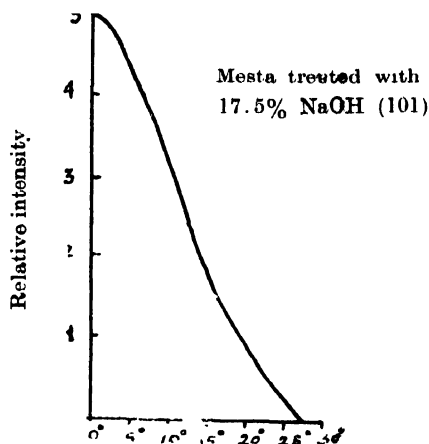


Fig. V. Angle from equatorial line.

by plotting the values of  $I \sin^2 \alpha \cos \alpha$  and  $I \cos \alpha$  against angular distances and the usual method of graphical integration of both curves were done. The ratio of integrals were then found out. From these,  $\overline{\sin^2 \alpha_m}$  were determined and from them  $\alpha_m$  and  $f_x$  were evaluated. Values of angles at 40% intensity were also determined from the intensity distribution curves.

#### RESULTS AND DISCUSSION

In Table I are given the values of  $f_x$ ,  $\alpha_m$  and angle at 40% intensity in the intensity distribution curves for (002) reflections. The results obtained show that the average angle of orientation  $\alpha_m$  and  $f_x$  do not change substantially till

TABLE I

Showing the average angle of orientation, 40% intensity angle and Hermans' orientation factor

Sample	Average angle of orientation	40% intensity angle	Hermans' orientation factor
Raw mesta	11.6°	11.0°	0.940
Delignified mesta	11.6°	11.0°	0.940
Raw mesta treated with 5% NaOH	10.5°	10.8°	0.950
Raw mesta treated with 9.3% NaOH	12°	11.0°	0.935
Raw mesta treated with 17.5% NaOH	14.86° (002) 14.14° (101)	15.0° (002) 14.0° (101)	0.900] 0.910] 0.905

treatment with 9.3% NaOH, but for samples treated with 17.5% NaOH, the values obtained differ considerably from the former ones.

The average angle of orientation  $\alpha_m$  and orientation factor  $f_x$  for raw mesta are found to be  $\alpha_m = 11.60$  and  $f_x = 0.94$ , whereas the average angle for jute fibres varies from  $8^\circ$  to  $9^\circ$  approximately and  $f_x$  varies from 0.96 to 0.97 as determined by Sen and Chowdhury (1957). In the case of ramie these are given by  $7^\circ 36'$  and 0.973 (Hermans).

#### ACKNOWLEDGMENTS

The authors are deeply grateful to Dr. R. K. Sen for his generous advice and helpful suggestions during the progress of this work and for his constant encouragement. They are also indebted to Dr. P. B. Sarkar, Director of the Institute for his keen interest in the work.

#### REFERENCES

- Hermans, P. H., Kratky, O., and Platzek, P., 1939, *Kolloid Zeit.*, **86**, 245.
- Hermans, P. H., 1946, "Contribution to the Physics of Cellulose Fibres", Amsterdam.
- Sen, M. K. and Woods, H. J., 1949, *Proc. Leeds Phil. Soc.*, **5** (II,) 155.
- Sen, R. K. and Choudhury, S. K., 1957, *Textile Research Journal* **27**, 193.

# THE DIELECTRIC PROPERTIES OF ROSIN-MALEIC ANHYDRIDE RESIN

A. K. SEN AND G. N. BHATTACHARYA

DEPARTMENT OF APPLIED PHYSICS,  
CALCUTTA UNIVERSITY.

(Received May 19, 1961)

**ABSTRACT.** The dielectric properties of rosin-maleic anhydride resin have been measured over the temperature range of 25°C to 170°C and the frequency range of 1 Kc/s to 500 Kc/s. Within this range of temperature and frequency it behaves as a polar resin in the anomalous dispersion range. Its dielectric constant vs temperature curve shows however a peculiar behaviour at high temperatures. At about 150°C dielectric constant values attain a maximum after gradually rising with temperature in the normal way of polar resins. But above this temperature a sudden and steep rise in the permittivity is observed. An attempt has been made to explain this peculiarity on the basis of its estimated rotor dimension and infrared absorption spectrogram.

## INTRODUCTION

Rosin plays an important part in the production of several semi-synthetic resins. It is widely used as a modifier in the production of so-called modified synthetic resins, such as rosin modified phenol formaldehyde resins or alkyds. Another type of synthetic resin derived from rosin is the rosin-maleic anhydride adduct formed by the method of Diels-Alder reaction known as the "diene synthesis". This method of synthesis involves a "diene" system i.e. a system having conjugated double bonds reacting with a component having an ethylenic linkage flanked by carbonyl or carboxyl groups in such a manner that the "diene" system opens up and the terminal carbons become affixed at the double bond of the ethylenic linkage.

The chemical structure of rosin or abietic acid shows that it possesses a conjugated system of double bonds and consequently it reacts with maleic anhydride giving an addition compound. In fact, this diene synthesis confirms the presence of the conjugated double bonds in the structure of the abietic acid molecule. It should be noted that this compound is the partial anhydride of a tribasic acid and hence its acid value must be reduced and this is usually done by esterification with any polyhydric alcohol like glycerol, mannitol, pentaerythritol etc.

Now X-ray studies on the rosin maleic-anhydride resins and ester gum by Beal and co-workers (1932) have revealed that they show precisely the same

rings which are associated with raw rosin. Esterification with glycerol or reacting it with maleic anhydride does not change its inherent character.

Because of the large size of the esterified rosin-maleic anhydride molecule, its rotation as a whole, when placed in the rapidly alternating electric field, is unlikely. Obviously, if dielectric loss occurs due to orientation it may only be due to contributions from side groups attached to the main molecule. Although rosin has been found to be present in this resin as a constituent unit, its freedom of rotation has been severely restricted by a pair of carbon-carbon bonds with the maleic anhydride on the one hand and by its linkage with the pentaerythritol molecule through the esterification of its carboxyl group on the other.

From a previous study of the dielectric properties of rosin it has been observed by the authors (Sen and Bhattacharya, 1958b) as well as by Kitchin and Muller (1928) that the dimension of its rotating unit is about  $4.6\text{\AA}$  which is in close agreement with the actual dimension of the abietic acid molecule calculated on the basis of its accepted chemical structure. This agreement led the authors to the obvious conclusion that the rotation of the entire abietic acid molecule was responsible for its dielectric behaviour. But a similar study in the case of ester gum (Sen and Bhattacharya, 1958a) or copal ester (Sen and Bhattacharya, 1960) revealed a different story. In both the cases the dimensions obtained for the rotating units were exactly the same as that of a hydroxyl group. The presence of hydroxyl groups in these resins was also confirmed from their infra-red absorption spectrograms. These evidences tend to suggest that instead of the whole molecule the hydroxyl groups in these resins are probably the rotating units. Hence it is inferred that when molecules of abietic acid (rosin) or copalic acid (copal) combine (e.g., by esterification with glycerol) to form larger molecules, their rotation as a whole is restricted and only the rotation of smaller groups can occur in the investigated range of frequency. In this context it is therefore of interest to study the dielectric properties of rosin-maleic anhydride adduct in relation to those of rosin and obtain the dimension of its rotating units.

#### EXPERIMENTAL

The same experimental procedure as was followed in the case of other resins and the details of which appeared elsewhere (Sen and Bhattacharya, 1958a, 1958b) has been employed. The sample used in this investigation was a pentaerythritol ester of the rosin-maleic anhydride adduct manufactured by the Imperial Chemical Industries Ltd., London, and sold under the trade name of Bedesol—74.

The results of measurements of dielectric constant  $\epsilon'$ , dielectric loss  $\epsilon''$  and power factor  $\tan \delta$  at different temperatures and frequencies are shown graphically in Figs. 1, 2 and 3. Quite contrary to our expectation, these graphs give clear evidence of the typical polar nature of this resin. The loss factor-temperature and the power factor-temperature curves shown in Figs. 2 and 3, are the usual absorption curves of a polar material. These curves begin to rise at a compara-

tively higher temperature viz, about 100°C for almost all the frequencies except that of 1 Kc/s. The loss peaks are also more or less of the same heights.

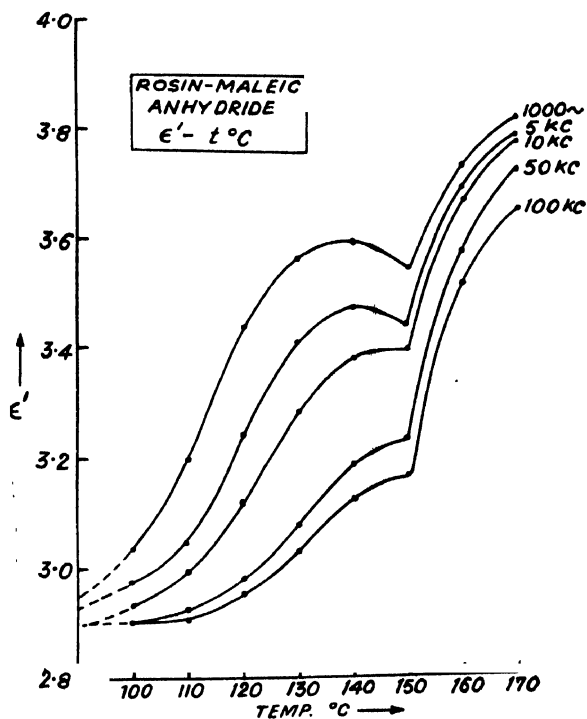


Fig. 1

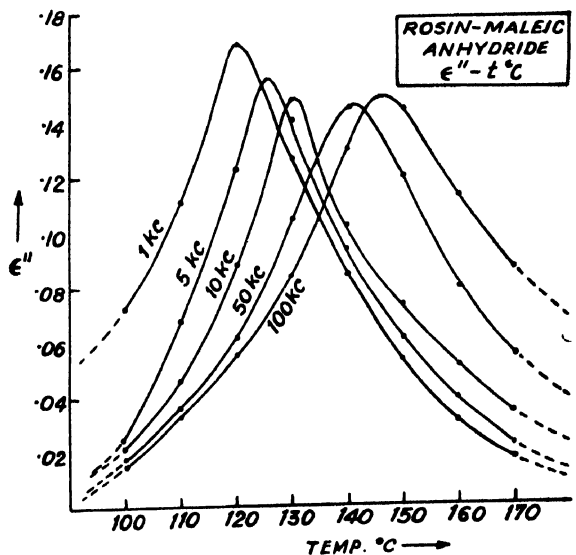


Fig. 2

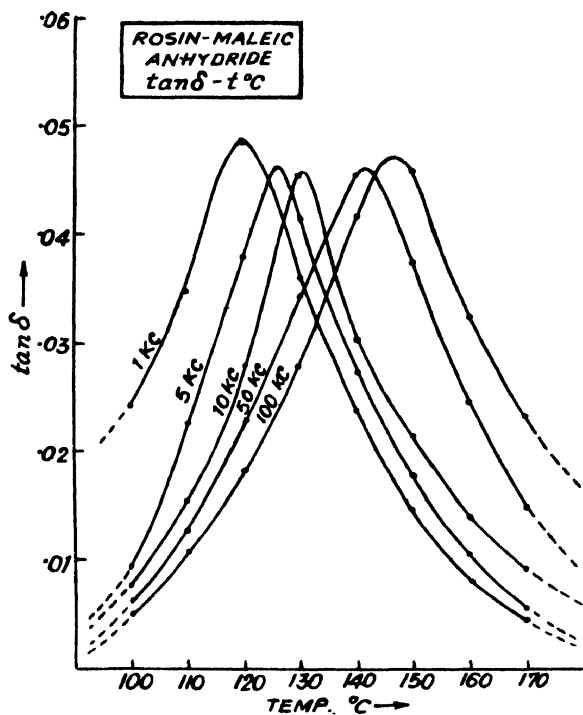


Fig. 3

But the dielectric constant-temperature graphs show a peculiar behaviour. It may be noticed from Fig. 1 that the permittivity for all the frequencies begins to rise from about 100°C in the usual way and attains a maximum at temperatures between 130°C to 150°C. But peculiarly enough, after 150°C it is found to make

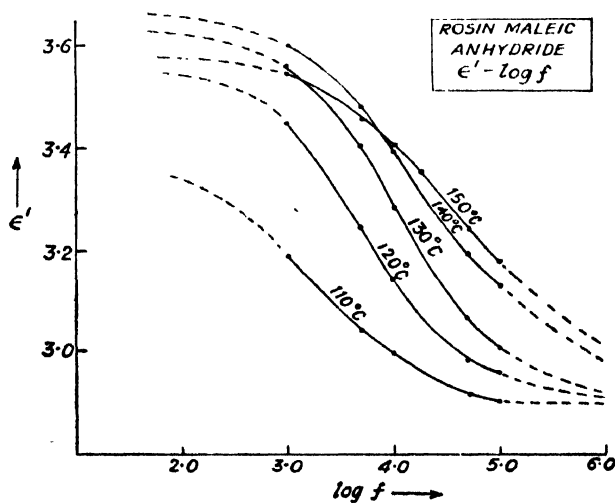


Fig. 4

a sudden and steep rise again. Measurements were carried out up to  $170^{\circ}\text{C}$  only as it was apprehended that the resin might polymerize after that temperature. This peculiar behaviour can only be explained on the supposition that at temperatures higher than  $150^{\circ}\text{C}$  the resin becomes unstable and more and more dipoles are somehow set free which now increase the orientation polarization and make the permittivity to rise. Hence an estimation of the size of the rotating unit is considered interesting in this case.

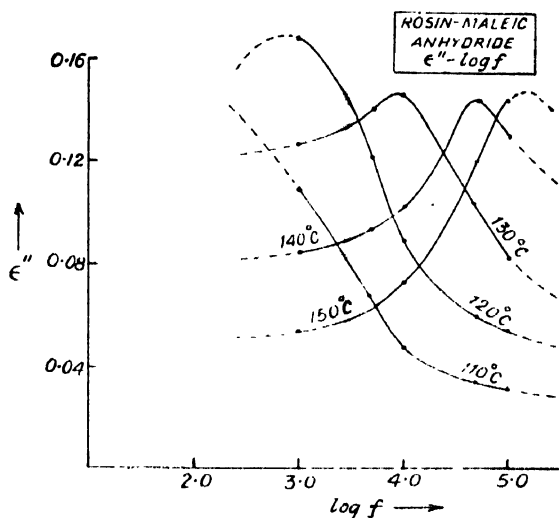


Fig. 5

The radius of the rotating unit was estimated from the calculated relaxation time at the temperature of loss maximum corresponding to a particular frequency and the melt viscosity at that temperature. The melt viscosity of this resin at

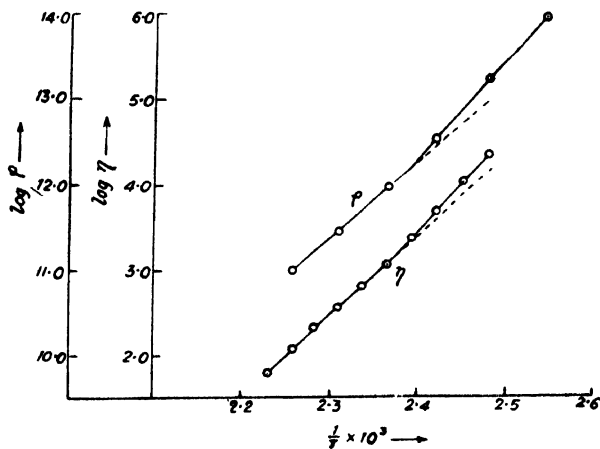


Fig. 6

different temperatures was measured by the same method as reported earlier (Sen and Bhattacharya, 1957) and the results are shown in Table I. Fig. 6 shows the logarithm of viscosity plotted against the reciprocal of absolute temperature and the graph is a straight line. For the sake of comparison the logarithm of resistivity is also plotted against the reciprocal of absolute temperature using the same scale. The conductivity and resistivity data appear in Table II. Once again the slopes of both these graphs are found to be the same. Upto the temperature of 170°C, however, none of these graphs shows any abnormality to indicate any likely polymerization within this temperature region.

TABLE I  
Viscosity-temperature data

Temperature		$\frac{1}{T} \times 10^3$	Viscosity $\eta$ in poise	log $\eta$
t°C	T°K			
130	403	2.481	22,970	4.3612
135	408	2.451	11,000	4.0414
140	413	2.421	4,900	3.6902
145	418	2.392	2,340	3.3692
150	423	2.364	1,200	3.0792
155	428	2.336	635	2.8028
160	433	2.309	355	2.5502
165	438	2.283	210	2.3222
170	443	2.257	120	2.0792
175	448	2.232	60	1.7782

TABLE II  
D.C. conductivity or resistivity-temperature data

Temperature		$\frac{1}{T} \times 10^3$	Conductivity $K$ in mho cm <sup>-1</sup> .	Resistivity $\rho$ in ohm cm.	log $\rho$
t°C	T°K				
120	393	2.545	$0.1042 \times 10^{-13}$	$9.596 \times 10^{13}$	13.9821
130	403	2.481	$0.5970 \times 10^{-13}$	$1.675 \times 10^{13}$	13.2240
140	413	2.421	$0.2935 \times 10^{-12}$	$3.407 \times 10^{12}$	12.5324
150	423	2.364	$0.1067 \times 10^{-11}$	$9.369 \times 10^{11}$	11.9717
160	433	2.309	$0.3339 \times 10^{-11}$	$2.894 \times 10^{11}$	11.4614
170	443	2.257	$0.1036 \times 10^{-10}$	$9.654 \times 10^{10}$	10.9847



The results of calculation of the radius of the rotating units are shown in Table III.

TABLE III  
Calculated relaxation time and radius of the rotator

Frequency in kc/s	Loss maximum temperature $t_m$ in $^{\circ}\text{C}$	Relaxation time $\tau$ in sec.	$\log \eta$ at $t_m$	Radius of the rotator in $\text{\AA}$
5	126	$2.80 \times 10^{-5}$	4.60 (extrapolated)	1.45
10	131	$1.39 \times 10^{-5}$	4.30	1.45
50	142	$2.76 \times 10^{-6}$	3.60	1.46
100	147	$1.39 \times 10^{-6}$	3.27	1.51

From these results we find again that the same value of the dimension of the hydroxyl group is obtained here for the radius of the rotator in this resin. We should examine therefore if there is any possibility for this resin of containing hydroxyl groups as probable rotating units. As in the production of this resin pentaerythritol is employed it is not unlikely for some of the four hydroxyl groups of the pentaerythritol molecule to remain unesterified in the same way as some hydroxyl groups of glycerol were found to remain unesterified in ester gum (Sen and Bhattacharya, 1958a) and copal ester (Sen and Bhattacharya, 1960). Moreover this possibility may also provide an explanation for the observed phenomenon of abnormal rise in permittivity above  $150^{\circ}\text{C}$ . For some of these hydroxyl groups may form hydrogen bonds amongst themselves at ordinary temperatures and these may be disturbed only at temperatures above  $150^{\circ}\text{C}$ . Consequently

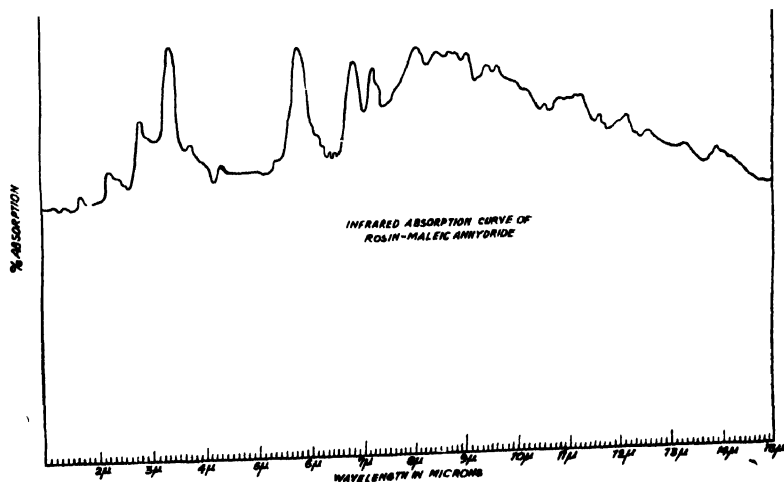


Fig. 7

upto 150°C only the free hydroxyl groups can contribute towards polarisation there being no contribution from the bonded hydroxyl groups. But at temperatures above 150°C these hydrogen bonds may break and the released hydroxyl groups may contribute further towards polarization thereby increasing the dielectric constant. Or, in the alternative there may be condensation-polymerisation above 150°C and the released water vapour may contribute towards increased dielectric constant.

The infrared absorption spectra of this resin was obtained in the manner indicated previously (Sen and Bhattacharya, 1960) and the spectrogram shown in Fig. 7. In this figure no absorption peak occurs at the wave length region of  $2.93\mu$  corresponding to the bonded hydroxyl group but the peak due to the free hydroxyl group occurs at about  $2.78\mu$ . The second explanation for increased values of dielectric constant above 150°C seems therefore reasonable. The free hydroxyl groups may be the unesterified hydroxyl groups of the pentaerythritol molecule as stated earlier. As chances of rotation of the entire resin molecule are remote, only side groups attached to the main molecule or segments of it are capable of orientation. Therefore hydroxyl groups attached to the molecule seem to be the probable rotating units.

#### REFERENCES

- Beal, Anderson and Long, 1932, *Ind. Eng. Chem.*, **24**, 1068.  
Kitchin, D. W. and Muller, H., 1928, *Phfs. Rev.*, **32**, 979.  
Sen, A. K. and Bhattacharya, G. N., 1957, *7. Assoc. App. Physicists*, **4**, 72.  
Sen, A. K. and G. N., 1958a, *Ind. J. Phys.*, **32**, 49.  
Sen, A. K. and Bhattacharya, G. N., 1958b, *Ind. J. Phys.*, **32**, 49.  
Sen, A. K. and Bhattacharya, G. N., 1960, *Ind. J. Phys.*, **34**, 461.

## VIBRATIONAL SPECTRA OF THIOGLYCOLLIC ACID

P. G. PURANIK, K. VENKATA RAMIAH AND VIJAY KUMAR

DEPARTMENT OF PHYSICS, UNIVERSITY COLLEGE OF SCIENCE  
OSMANIA UNIVERSITY, HYDERABAD 7*(Received May 30, 1961)*

**ABSTRACT.** The infrared and Raman spectra of thioglycollic acid and its solutions in different solvents have been recorded and the assignments of some of the frequencies have been proposed.

## INTRODUCTION

The Raman spectrum of thioglycollic acid has been earlier reported by Thatte and Ganesan (1933), but these authors have not recorded any line in the region of  $2500\text{ cm}^{-1}$  corresponding to S-H stretching vibrations. Hibben (1936) while discussing the Raman spectra of thioacids, interpreted the absence of a line in the region of  $2500\text{ cm}^{-1}$  in these compounds, as due to the absence of S-H group. There appears to be no mention in literature regarding the studies of infrared spectrum of thioglycollic acid. The authors have studied the infrared and Raman spectra of the acid and in various solvents in order (a) to assign the various vibrational frequencies of the monomer and associated molecules and (b) to study the effects of the solvents on the frequencies of the O-H, S-H and C = O stretching absorption bands.

## EXPERIMENTAL

A Perkin-Elmer Model 21 Infrared Spectrophotometer with NaCl optics was used to obtain the infrared spectra. The infrared spectrum of the pure liquid was obtained by pressing a drop of the liquid between two NaCl plates, along with an NaCl plate of equivalent thickness inserted into the reference beam. The spectra in solutions were obtained with a pair of matching cells of 0.1 and 1 mm thickness.

The Raman spectra were obtained by using a Fuess glass spectrograph having a dispersion of  $19\text{ cm}^{-1}$  in the  $\lambda 4358$  region along with a Hilger Raman source unit.  $\lambda 4358$  was the exciting radiation.

Thioglycollic acid (*E. Merck*) was distilled under reduced pressure and the fraction collected at  $123^\circ\text{C}$  and 29 mm pressure was used for the investigation. The fact that this acid forms an aqueous mixture of constant boiling point has been noted and absolutely anhydrous acid was used in the investigations.

## RESULTS

The Raman and infrared frequencies of thioglycollic acid as recorded by the authors are given in Table I. The Raman spectrum reported by Thatte and Ganesan is given for comparison. The microphotometric trace of the Raman spectrum is given in Fig. 1. The infrared spectrum of thioglycollic acid has broad absorption band in the  $3\mu$  region, but this band could be resolved into three peaks in solutions of chloroform and carbon tetrachloride. The Raman spectrum of thioglycollic acid has a sharp and intense line in the region of  $2500\text{ cm}^{-1}$  while the corresponding infrared band is weak. The authors could record a number of Raman lines which have not been reported earlier (Thatte and Ganesan, 1933).

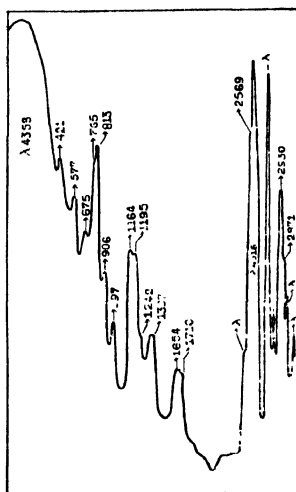


Fig. 1. Microphotometric trace of the Raman spectrum of thioglycollic acid.

## DISCUSSION

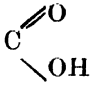
*Assignments :*

The infrared spectrum of thioglycollic acid has a broad absorption band extending from  $3125\text{ cm}^{-1}$  to  $2900\text{ cm}^{-1}$ , but in solutions of chloroform it could be resolved into three distinct peaks at  $3495$ ,  $3125$  and  $2900\text{ cm}^{-1}$ . With increasing dilution, the intensity of the band at  $3125\text{ cm}^{-1}$  becomes less and at  $0.02$  molar concentrations, this band becomes very feeble while the one at  $3495\text{ cm}^{-1}$  is prominent. A characteristic feature of carboxylic acids is their dimeric manifestation, with the result that the intermolecular associations break up progressively with increasing dilution of these substances in chloroform or carbon tetrachloride. Therefore the authors assign the band at  $3495\text{ cm}^{-1}$  to the free O-H stretching vibrations of the monomers and the one at  $3125\text{ cm}^{-1}$  to the same mode of vibrations of the associated molecules. The Raman line which is assigned

to the bonded O-H stretch, has a banded structure extending from 2926 to 2971  $\text{cm}^{-1}$ . A sharp intense Raman line appears at 2930  $\text{cm}^{-1}$  superposed on the hydroxyl band. The band at 2900  $\text{cm}^{-1}$  in the infrared or the one at 2930  $\text{cm}^{-1}$  in the Raman spectrum is assigned to C-H stretching vibrations.

The C = O stretching absorption of thioglycollic acid has two peaks at 1717 and 1730  $\text{cm}^{-1}$ , the former being a weak shoulder. The carbonyl frequency in the Raman spectrum appears as a band at 1654  $\text{cm}^{-1}$  along with a sharp, faint line at 1710  $\text{cm}^{-1}$ . These results indicate that the thioglycollic acid is not a completely associated liquid. With increasing dilution of the acid in chloroform, the peak at 1730  $\text{cm}^{-1}$  becomes more prominent in the infrared spectrum and the band at 1717  $\text{cm}^{-1}$  becomes a shoulder. At a molar concentration of 0.02 in solution of chloroform, only the band at 1730  $\text{cm}^{-1}$  could be recorded. Therefore the infrared frequency at 1717  $\text{cm}^{-1}$  or the Raman line at 1654  $\text{cm}^{-1}$  is assigned to the C = O stretching of the associated molecules and the frequency at 1730  $\text{cm}^{-1}$  in the infrared or the one at 1710  $\text{cm}^{-1}$  in Raman spectrum to the same mode of vibrations of the monomers. The large differences in the infrared and Raman frequencies of the C — O stretch of the thioglycollic acid are in agreement with similar results obtained by Davies and Sutherland (1938) in their investigations of carboxylic acids.

The lines at 1298 and 1397  $\text{cm}^{-1}$  in the Raman and the corresponding frequencies at 1286 and 1412  $\text{cm}^{-1}$  in the infrared can be assigned to C-O stretch

and  deformation. Such assignments have been made by Hadzi and Sheppard (1953) in case of carboxylic acids and by Puranik (1955) in case of esters.

The Raman spectrum of thioglycollic acid has a sharp and intense line at 2569  $\text{cm}^{-1}$  and the corresponding frequency in the infrared is a weak absorption at 2565  $\text{cm}^{-1}$ . The authors assign this band to S-H stretching vibrations. The frequency remains unchanged even in dilute solutions of chloroform. This invariance of the frequency indicates that S-H linkage is a free linkage in thioglycollic acid. The intermolecular associations in this compounds, may therefore be concluded, as of O-H.....O = C type.

The S-H in-plane deformation frequency has been identified by Sheppard (1949) with a Raman line at 832  $\text{cm}^{-1}$  and therefore the Raman line at 813  $\text{cm}^{-1}$  in the thioglycollic acid may be assigned to this mode of vibration. The C-SH stretch is known to appear in the region of 600-700  $\text{cm}^{-1}$  as a strong line in The Raman spectrum (Sheppard, 1950) and therefore a fairly intense Raman line at 675  $\text{cm}^{-1}$  may be assigned to C—SH stretching vibrations.

The 220  $\text{cm}^{-1}$  in the Raman spectrum corresponds to the symmetrical vibrations of the two acid molecules of the dimer through the stretching of the hydrogen bond.

**TABLE I**  
**Raman and infrared frequencies of thioglycollic acid**  
**(in  $\text{cm}^{-1}$ )**

Raman		Infrared
Present authors	Thatto and Ganosan	Present authors
220 (0)	—	—
421 (2)	433 (1d)	—
—	511 (1)	—
577 (2)	580 (1)	—
675 (3)	686 (0)	—
765 (4)	—	755 (w)
813 (6)	818 (4)	—
906 (4)	914 (2)	897 (w)
997 (4)	1004 (0)	990 (vw)
1164 (5)	—	1149 (m)
1195 (3)	—	1199 (m)
1242 (3)	—	—
1298 (0)	—	1286 (s)
1397 (3)	1409 (2d)	1412 (s)
—	1563 (1d)	—
1654 (3d)	—	1717 (s)
1710 (1)	1707 (1d)	1730 (sh)
—	—	2336 (w)
2459 (2)	—	—
2569 (8)	—	2565 (w)
2678 (2)	—	2680 (sh)
2930 (9)	2950 (1d)	—
2926 to 2971	—	2930 to 3125

TABLE II

O—H, S—H and C = O stretching frequencies of thioglycollic acid in different solvents

Solvents	O—H stretch	S—H stretch	C—O stretch
Liquid	2930 to 3125	— 2565	— 1717 1730
Carbon tetrachloride	3510	2575	1718 1731
Chloroform	3500	2565	1717 1730
Acetonitrile	3450	2565	1742
Dioxane	3450	2535	1745
Pyridine	3225	2440	1717 (sh) 1730
$\alpha$ -picoline	—	2440	1709 1724
$\beta$ -picoline	—	2440	1717 1730

### Solvent effect.

The infrared spectrum of thioglycollic acid has been recorded in various solvents and the OH, SH and C = O stretching frequencies in those solvents are given in Table II and the traces are given in Figs. 2 and 3.

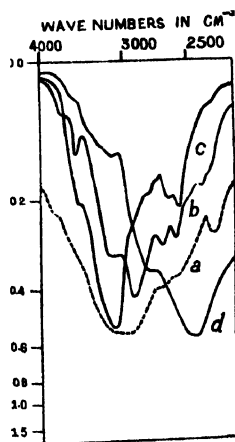


Fig. 2. The O—H, and S—H stretching frequencies in (a) pure liquid (b) chloroform (c) dioxane and (d) pyridine.

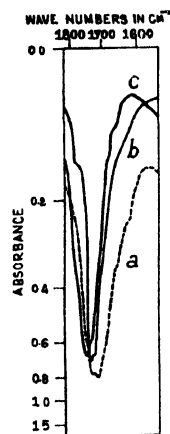


Fig. 3. The C=O stretching frequencies in (a) pure liquid (b) chloroform and (c) dioxane.

The absorption band at  $3495\text{ cm}^{-1}$  in chloroform or at  $3510\text{ cm}^{-1}$  in carbon tetrachloride, which is assigned to the O—H stretch of the monomers, does not appear in the donor solvents. Instead it appears at  $3450\text{ cm}^{-1}$  in dioxane and acetonitrile and at  $3225\text{ cm}^{-1}$  in solutions of pyridine. At these concentrations the carbonyl frequency is at  $1743\text{ cm}^{-1}$  in both dioxane and acetonitrile. In pyridine it is at  $1730\text{ cm}^{-1}$  with a weak shoulder at  $1717\text{ cm}^{-1}$ . Similar results are obtained in solutions of picolines.

The appearance of a single C—O absorption in the donor solvents corresponding to the monomer frequency is an indication that the intermolecular associations have broken up considerably in these solvents. Then the simultaneous reduction in the O—H stretching frequency compared to the monomer frequency in solutions of chloroform or carbon tetrachloride is due to the hydrogen bond formation between the donor groups of the solvent and the O—H group of the monomers of the acid by the OH...N and OH...O bonds. The shift in the O—H stretching frequency is maximum in solutions of pyridine.

The S—H stretching frequency, which has the same value in pure liquid and in dilute solutions of chloroform, decreases to the extent of  $125\text{ cm}^{-1}$  in solutions of pyridine and picolines and becomes broad. In solutions of dioxane this band shifts only to the extent of only  $25\text{ cm}^{-1}$ . The large shifts in S—H stretching frequency in solutions of pyridine and picolines, may be concluded as due to the associations by way of S—H...N bonding.

#### ACKNOWLEDGMENT

One of the authors (V. K.) expresses his sincere thanks to C.S.I.R. Government of India for the award of a Fellowship.

#### REFERENCES

- Davies, M. M., and Sutherland, G. B. B. M., 1938, *J. Chem. Phys.* **6**, 755.  
Hibben, J. H., 1936, *Chem. Rev.* **18**, 92.  
Hadzi, D and Sheppard, N, 1953, *Proc. Roy. Soc.* **216A**, 247.  
Puranik, P. G., 1955, *Proc. Ind. Acad. Sci.* **42**, 326.  
Sheppard, N., 1949, *Trans. Farad. Soc.*, **45**, 693.  
Sheppard, N, 1950, *Trans. Farad. Soc.*, **46**, 429.  
Thatte V.N. and Ganesan, A.S., 1933, *Phil. Mag.* **15**, 51.



# STUDIES ON BINARY DIFFUSION OF THE GAS PAIRS N<sub>2</sub>-A, N<sub>2</sub>-Xe AND N<sub>2</sub>-He

R. PAUL AND I. B. SRIVASTAVA

INDIAN ASSOCIATION FOR THE CULTIVATION OF SCIENCE, CALCUTTA-32

(Received June 22, 1961)

**ABSTRACT.** The mutual diffusion coefficient of N<sub>2</sub>-He, N<sub>2</sub>-Xe and N<sub>2</sub>-A gas pairs over the temperature interval  $-30^{\circ}\text{C}$  to  $60^{\circ}\text{C}$  has been determined by allowing the diffusion to take place between two bulbs through a precision capillary tube. Samples of the gas, withdrawn from one of the bulbs at different times, were analysed by using a previously calibrated thermal conductivity analyser. These experimental data have been utilised for calculating the unlike potential parameters on the Lennard-Jones 12 : 6 model. The parameters have been used to calculate  $D_{12}$  and are found to reproduce the experimental data satisfactorily. Further, the thermal conductivity of the mixtures is calculated using only the experimental values of  $D_{12}$  and other transport properties of pure gases and reasonable agreement with the experimental data is obtained.

## INTRODUCTION

The coefficient of mutual diffusion,  $D_{12}$  is the most suitable transport property for studying unlike molecular interactions, because, to the first approximation, it depends only on the force field of the unlike molecules. But the experimental data suitable for inter-molecular force determination are scanty, specially for the poly-atomic molecules. Therefore, mutual diffusion data for various pairs of gases are most desirable. With this end in view a series of accurate diffusion coefficient measurements of different gaseous mixtures have been done in this laboratory over a fairly wide range of temperature. Several workers (Srivastava and Srivastava, 1959a, Srivastava, 1959, Srivastava and Barua, 1959) have measured the binary diffusion of inert gases in the temperature range  $0^{\circ}\text{C}$ - $45^{\circ}\text{C}$  by using the two-bulb diffusion method and have used their data to determine the unlike interaction parameters on the Lennard-Jones (12 : 6) model. The same technique was further used by Paul and Srivastava (1961a, 1961b) for measuring  $D_{12}$  of binary mixtures containing a diatomic gas, in the temperature range  $-30^{\circ}\text{C}$  to  $60^{\circ}\text{C}$ . In the present work, the mutual diffusion coefficients of N<sub>2</sub> with He, A and Xe have been measured in the above temperature range and the experimental data are used for determining the force constants for unlike interaction on the Lennard-Jones (12 : 6) model.

## APPARATUS AND THEORY

The two-bulb technique of Ney and Armistead (1947) was employed for measuring the diffusion coefficients. The details of the apparatus, experimental

procedure and the theory have been discussed fully by Paul and Srivastava (1961a).

### EXPERIMENTAL RESULTS

The gases used were supplied by British Oxygen Company, England and were quoted to be spectroscopically pure, except xenon which contained about 1% krypton.

#### *Constants of the diffusion apparatus :*

Volume of bulb I	325 cc.
Volume of bulb II	547 cc.
Length of the diffusion capillary	9.058 cm.
Diameter of the diffusion capillary	0.316 cm.

$$C_1^{\infty} = 0.373,$$

$C_1^{\infty}$  is calculated from the initial concentration in the two bulbs, which was further checked for some runs by determining the concentration at an interval of seven times the relaxation time.

TABLE I

Observed concentration of He at different times for N<sub>2</sub>-He at -30°C

Time in minutes	R in ohms	$C_1 t$	$C_1 t - C_1^{\infty}$	$\log_{10}(C_1 t - C_1^{\infty})$
0	—	1.000	0.627	1.7973
35	235.8	0.770	0.397	1.5988
51	229.4	0.691	0.318	1.5024
71	222.8	0.616	0.243	1.3856
91	217.1	0.559	0.186	1.2695

Fig. 1 gives the calibration curve for the three gas pairs and Fig. 2 shows the plots of  $\log_{10}(C_1 t - C_1^{\infty})$  versus  $t$  for N<sub>2</sub>-He at all temperatures.

Table II gives the experimental values of diffusion coefficients for different pairs as determined by the present authors, together with the values obtained by other workers, wherever available, and also the calculated values of  $D_{12}$ , using the force constants obtained by the authors.

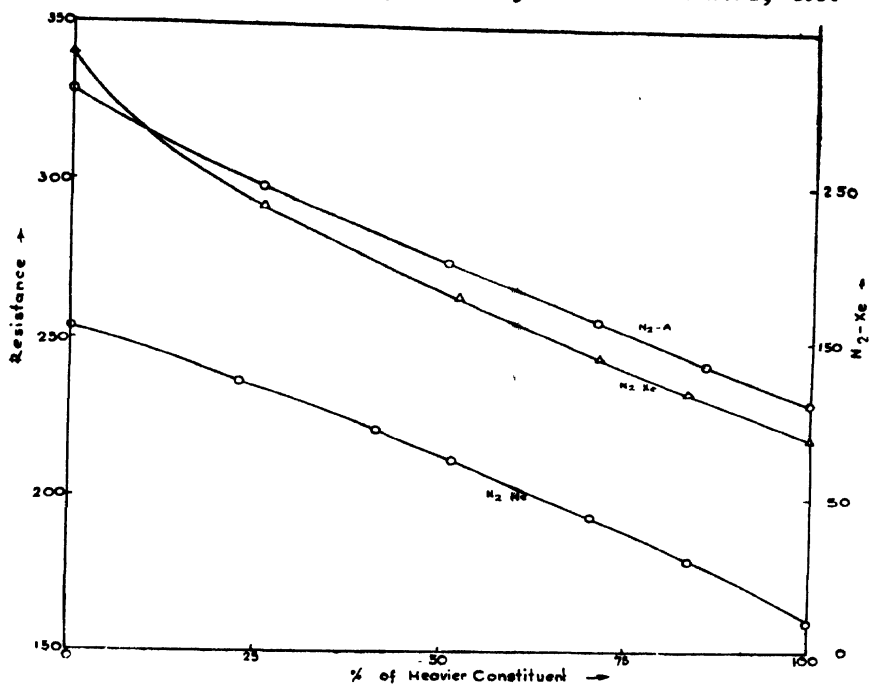


Fig. 1. Calibration curves.

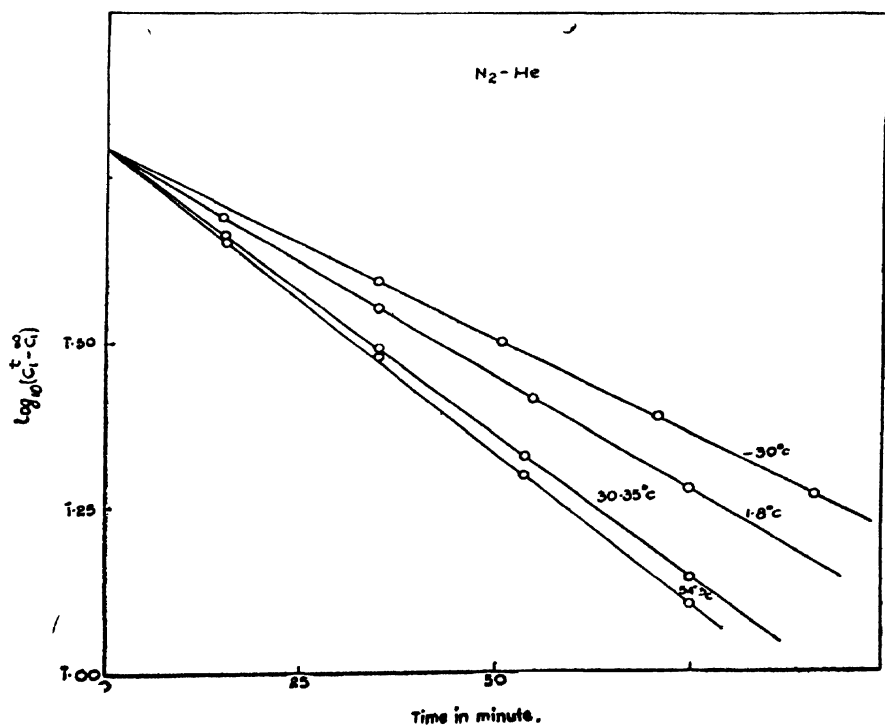


Fig. 2. Plot of  $\log (C_1^t - C_1^\infty)$  versus 't' for  $N_2-He$ .

TABLE II

Observed values of the diffusion coefficient in  $\text{cm}^2/\text{sec}$ 

Gas mixtures	Temp. °K	Pressure in mm. Hg.	$D_p$	$D_{\text{atm.}}$	Previous <sup>a</sup> work	$D_{12}$ calc. from force constants fitted to diffusion data
N <sub>2</sub> - He	243.2	62.0	5.847	0.477		0.484
	275.0	64.5	7.022	0.596		0.597
	298.16	—	—	—	0.7068	0.6797
	303.55	62.1	8.799	0.719	—	0.704
	328.16	—	—	—	0.8212	0.8011
	332.5	65.5	9.410	0.811	—	0.819
	358.16	—	—	—	0.9410	0.9232
N <sub>2</sub> - A	244.2	64.7	1.583	0.1348		0.1363
	274.6	62.2	2.063	0.1689		0.1685
	303.55	64.5	2.355	0.1999		0.2018
	334.7	68.3	2.707	0.2433		0.2399
N <sub>2</sub> - Xe	242.2	63.2	1.027	0.0854		0.0854
	274.6	64.4	1.262	0.1070		0.1078
	303.45	70.0	1.413	0.1301		0.1299
	334.2	60.3	1.952	0.1549		0.1551

<sup>a</sup> Rumpel, W.F. (1955)

## DETERMINATION OF POTENTIAL PARAMETERS

The various methods for determining the potential parameters from the measured  $D_{12}$  values have been fully discussed by Bunde (1955) and Srivastava and Srivastava (1959a), pointing out their advantages and limitations. In the present work, the intersection method of Buckingham (1937) has been used for the determination of the force constants on the Lennard-Jones (12:6) model. As some scatter was found in the intersection points of the curves, the force constants obtained by this method were considered as approximate ones. These approximate values were used to calculate the parameters more accurately by the method of least square fitting. The least square method followed here has been discussed in detail by Paul and Srivastava (1961b).

The force constants determined are tabulated in Table III, together with the values obtained from the combination rules. It is clearly seen that the two sets of force constants agree within the limits of experimental error.

TABLE III

Potential parameters on the Lennard-Jones (12 : 6) model from the experimental data

Gas pair	Present work	From combination rules
$\text{N}_2\text{--He}$		
$\epsilon_{12}/k$ ( $^{\circ}\text{K}$ )	35.44	30.58
$\sigma_{12}$ ( $\text{\AA}$ )	3.129	3.129
$\text{N}_2\text{--Ar}$		
$\epsilon_{12}/k$ ( $^{\circ}\text{K}$ )	107.03	106.5
$\sigma_{12}$ ( $\text{\AA}$ )	3.530	3.549
$\text{N}_2\text{--Xe}$		
$\epsilon_{12}/k$ ( $^{\circ}\text{K}$ )	147.4	144.8
$\sigma_{12}$ ( $\text{\AA}$ )	3.846	3.868

## COMPARISON WITH EXPERIMENTS

(a) *Mutual diffusion coefficient*

The force constants obtained in the present work have been used to calculate the diffusion coefficients, which have been tabulated in Table II. The agreement obtained is excellent. Further, in case of  $\text{N}_2\text{--He}$  where data of other workers (Rumpel, 1955; Walker and Westernberg, 1958) are available upto  $1100^{\circ}\text{K}$ , the diffusion coefficients calculated from our force constants have been compared

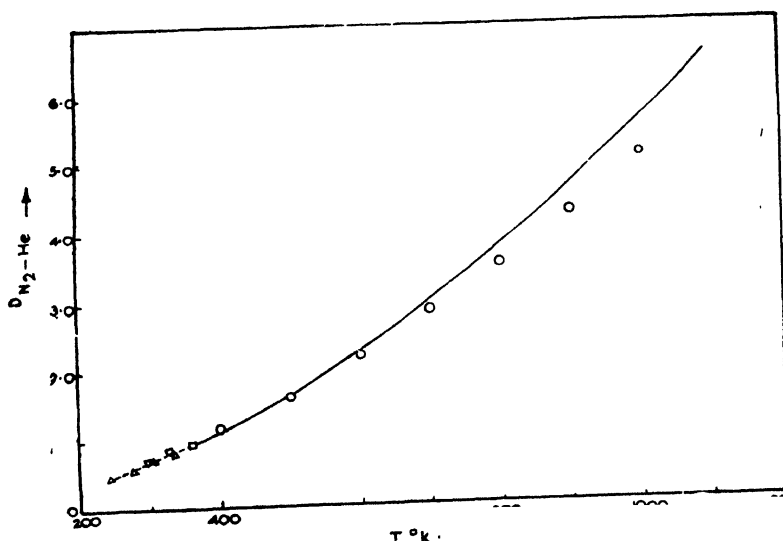


Fig. 3. Temperature variation of the diffusion coefficient of  $\text{N}_2\text{--He}$  system.

— Interpolated from Walker and Westernberg (1958)  
 $\Delta$  Present work.  $\square$  Data taken from Rumpel (1955).  
 $\circ$  Calculated values using force constants obtained in the present paper.

graphically with experimental values in Fig. 3. It will be seen from the figure that up to 700°K, the force constants obtained here reproduce experimental values tolerably well. At higher temperatures there are significant deviations, but the force constants determined from the data in the temperature range 250°K to 350°K are not expected to hold good above 700°K.

(b) *Thermal conductivity of mixtures*

The full procedure for the determination of the thermal conductivity of mixtures from the experimental values of the mutual diffusion coefficient and other transport properties of pure component has been given previously (Paul and Srivastava, 1961a).

Fig. 4 presents the experimental values of the thermal conductivity of the mixtures with those calculated by the above method. The agreement is excellent for all the three mixtures. The experimental values of thermal conductivity are taken from Srivastava and Srivastava (1959b) for  $N_2$ -A and from Barua (1959) for  $N_2$ -He and  $N_2$ -Xe.

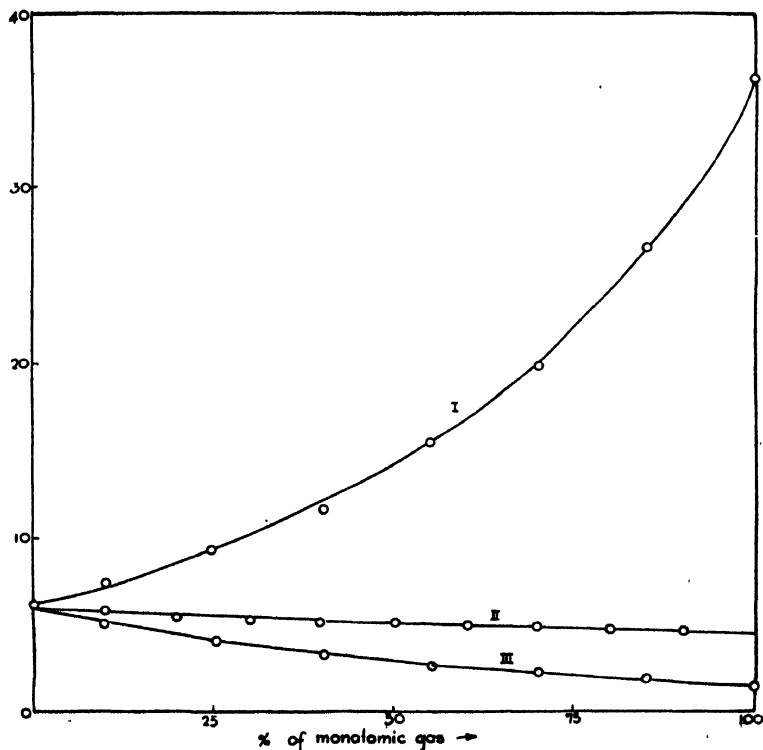


Fig. 4. Comparison of experimental and calculated values of thermal conductivity.  
I.  $E_2$ -He at 30°C, II.  $N_2$ -A at 38°C, and III.  $N_2$ -Xe at 30°C.

#### DISCUSSIONS

As the force constants for the pure components are not known very accurately, it is not possible to test the combination rules critically. However, like previous cases, in the present work also, no systematic departure from the combination rule could be observed.

It will be of considerable interest to see how well our force constants reproduce the transport properties other than diffusion and thermal conductivity, but unfortunately, no such data are available at present.

#### ACKNOWLEDGMENT

The authors are grateful to Prof. B. N. Srivastava, D.Sc., F.N.I., for guidance and valuable discussions. One of the authors (R.P.) is thankful to Council of Scientific and Industrial Research, New Delhi, for financial assistance.

#### REFERENCES

- Barua, A. K., 1959, *Physica*, **25**, 1275.  
Buckingham, R. A., 1938, *Proc. Roy. Soc. (Lond.)*, **A 168**, 264.  
Bunde, R. E., 1955, Univ. of Wisconsin, CM-850  
Noy, E and Armistead, F. C., 1947, *Phys. Rev.*, **71**, 14.  
Paul, R., and Srivastava, I. B., 1961a, *J. Chem. Phys.* In press.  
Paul, R., and Srivastava, I. B., 1961b, *Ind. J. Phys.*, In press.  
Rumpel, W. F., 1955, Univ. of Wisconsin, CM-851.  
Srivastava, B. N. and Srivastava, K. P., 1959a, *J. Chem. Phys.*, **30**, 984.  
Srivastava, B. N. and Srivastava, R. C., 1959b, *J. Chem. Phys.*, **30**, 1200.  
Srivastava, K. P., 1959, *Physica*, **25**, 571.  
Srivastava, K. P., and Barua, A. K., 1959, *Ind. J. Phys.*, **33**, 229.  
Walker, R. E., and Westenberg, A. A., 1958, *J. Chem. Phys.*, **29**, 1147.

# ELECTRON MICROSCOPE STUDIES ON THE COTTON CELLULOSE

D. K. SAHA

(BIOPHYSICS DIVISION,

SAHA INSTITUTE OF NUCLEAR PHYSICS, CALCUTTA-9)

(Received June 30, 1961)

**ABSTRACT** Hydrolysis of cotton cellulose in strong mineral acid shows a disintegrating fibrillar structure under electron microscope. The broken up fibrils and particles have almost the same lateral dimension and there is an indication of layer lattice structure of cellulose. No definite minimum of the length of the particles could be observed.

## INTRODUCTION

Morphological study of cotton cellulose by some workers (Balls and Hancock, 1922) under light microscope shows dislocated striations. Dislocation of striations were also noted in most of the bast fibres prominently in flax (Muhlethaler, 1949). The transverse section shows cell structure in both the varieties (Hock *et al.*, 1940). The molecular structure has been studied by X-ray and the unit cell has been defined (Hessler *et al.*, 1948). The state of orientation and purity of fibre, so far as  $\alpha$ -cellulose content in fibre is concerned, has also been studied (Berkley *et al.*, 1938, 1949).

From the usual X-ray diagram and also from small angle scattering, the average length of cellulose crystallites of Rennie was found to vary between 500 Å and 600 Å (Heyn, 1950). But the exact shape and locations of these crystallites in the fibre could not be ascertained for want of proper technique.

It will be observed that the size of crystallites as suggested from X-ray studies is within the range which could be advantageously studied under electron microscope. The early attempts to study the structure of cellulose with electron microscope by Ruska and others (1940) did not succeed. Subsequently, attempts by replica technique by Astbury and Preston (1948) indicated the fibrillar structure, while Freywisling (1948) using mechanical grinding reported fibrillar structure of varying width and length. Subsequently Ranbi and Ribi (1949 and 1951) and also Mukherjee and Woods (1953) tried acid hydrolysis for the disintegration of fibres. They were successful in breaking the fibrils into discrete particles, believed to be the crystallites of cellulose. The present work contains an account of the electron microscopic studies on Indian cotton cellulose using the acid hydrolysis technique developed by Mukherjee and Woods (1953).



## EXPERIMENTAL PROCEDURE

In this work a sample of raw Indian cotton was dewaxed by soxhlate extraction with Carbon tetra-chloride and after drying, it was further purified by boiling in dilute (2%) sodium hydroxide solution for 4 hours. The purified fibre was next treated in sulphuric acid solution of strength 920 grammes per litre at 32°C. The fibres disintegrated into small fragments and dispersed in the acid. In an attempt to wash this material by distilled water in a centrifuge, the fibres dispersed still further in a colloidal solution at a pH round about 4. The colloidal solution obtained by peptisation at each washing in the centrifuge was collected. This acidic colloidal solution was then dialysed in cellophen bags in distilled water at room temperature. Four to five days had to be allowed in the process of dialysis to raise the pH of the solution to about 5.5. Because the pH of distilled water itself against which the solution was dialysed was 5.8. The dialysed solution was further diluted with distilled water in order to obtain a concentration suitable for electron microscope. The specimen for an electron microscope was obtained by putting a small drop of solution on a collodion coated microscope grid and evaporating the water to leave the cellulose behind. The specimen was next shadowed with chromium and subsequently examined under electron microscope. The microscope used was Siemens' Elmiskop I at 60kV.

TABLE I

Obs. nos.	Width of individual particles on the micrograph (cm)	Actual width of individual particles (cm) $\div$ 17000
1	$1.96 \times 10^{-2}$	$115.3 \times 10^{-8}$
2	2.91	171.2
3	1.97	115.9
4	2.89	170.0
5	1.79	105.3
6	2.13	125.3
7	2.06	121.2
8	1.82	107.1
9	2.83	166.5
10	1.81	106.5
Mean width = $130.4 \pm 8.70 \text{ \AA}$ .		

## DISCUSSION

The electron micrograph (Fig. 1) shows a distinct fibrillar structure with a definite indication of breakdown into elongated discrete particles as could be

seen in the field of observation. It is also observed on the micrograph that the fibrils and the particles have more or less the same lateral dimension. In other

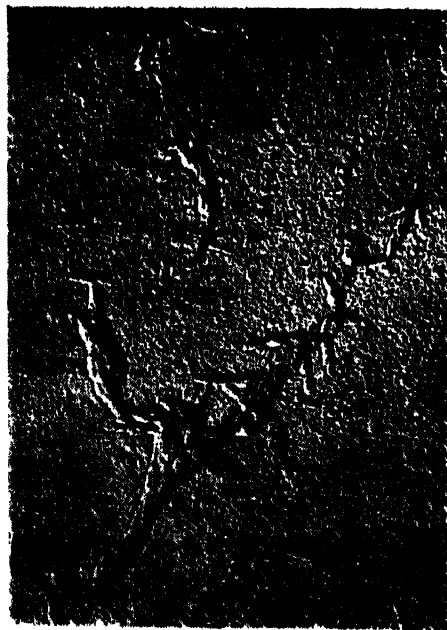


Fig 1.

words the structure as revealed under microscope shows a disintegrating fibrillar structure breaking into particles. On closer observation of the aggregates, there is an indication that they are rather in flat layers which probably are in conformity with the idea of layer lattice, associated with structure of cellulose. No definite minimum of the length of the particle could be observed. But they were found to vary from  $500\text{\AA}$  to  $2500\text{\AA}$  and above. Nevertheless the width of the particles was found to vary within a narrow range, when measured. The average width of the particle was found to be about  $130.4 \pm 8.70\text{\AA}$ .

It is expected that under favourable conditions, by using different time, concentration and temperature of acid it may be possible to study the individual units (fibrils) which is the basis of building mechanism of the structure. This work is being further pursued to see if similar results can be obtained in case of bast fibres and to study the difference, if any, between the bast fibres and comparatively more pure varieties of fibres like cotton and also amongst the bast fibres themselves.

#### ACKNOWLEDGMENT

The author wishes to thank Professor N. N. Das Gupta and Shri M. L. De of the Saha Institute of Nuclear Physics and Dr. S. M. Mukherjee, Principal,

College of Textile Technology, Serampore, for their invaluable assistance in this work.

#### REFERENCES

- Astbury, W. T., Preston, R. D., Nicolai, E., Reed, R. and Millard, A., 1948, *Nature*, **162**, 665.
- Balls, W. L. and Hancock, H. A., 1922, *Proc. Roy. Soc.*, **B 93**, 426.
- Berkley, E. E. and Woodyard, O. C., 1938, *Ind. Eng. Chem.*, **10**, 451.
- Berkley, E. E. and Woodyard, O. C., 1948, *U. S. D. A. Tech. Bull. NO. 949*.
- Freyweissling, A., Muhlethaler, K. and Wyckoff, R. W. C., 1948, *Experimenta*, **4**, 476.
- Hessler, L. E., Marion, E., Simson, and Berkley, E. E., 1948, *Text Res. Jour.*, **18**, 670.
- Heyn, A. J. N., 1950, *Amer. Chem. Soc.*, **72**, 2264.
- Hock, C. W., Ramsey, R. C. and Harris, M., 1940, *J. Res. Nat. Bur. Stand.*, 26.
- Muhlethaler, K., 1949, *Biochem. Biophys. Acta.*, **3**, 15.
- Mukherjee, S. M. and Woods, H. J., 1953, *Biochem. Biophys. Acta*, **10**, 409.
- Ranbi, B. G. and Bibi, E., 1949, *Acta Chem. Scand.*, **3**, 649.
- Ranbi, B. G. and Ribí, E., 1951, *Trans. Farad. Soc. Symp.*, No. 11, 158.
- Ruska, H. and Kretschmer, M., 1940, *Kolloid Z.*, **93**, 163.



# INFLUENCE OF ENVIRONMENT ON THE RAMAN AND INFRARED SPECTRA OF QUINOLINE AND TETRALIN\*

KRISHNA KUMAR DEB

OPTICS DEPARTMENT,

INDIAN ASSOCIATION FOR THE CULTIVATION OF SCIENCE,

CALCUTTA-32

(Received August 14, 1961)

## Plate XI

**ABSTRACT.** The Raman spectra of quinoline and tetralin in the liquid state and in the solid state at  $-180^{\circ}\text{C}$  and also the infrared spectra of the liquids and their solutions in some aliphatic solvents have been investigated and an attempt has been made to assign the prominent Raman and infrared frequencies of quinoline to some of the vibrational modes of the molecule.

In the solid state at  $-180^{\circ}\text{C}$  quinoline exhibits a moderately strong new Raman line  $49\text{ cm}^{-1}$ . On the other hand, tetralin at  $-180^{\circ}\text{C}$  shows two new low-frequency Raman lines of shifts  $61$  and  $92\text{ cm}^{-1}$  respectively under similar conditions. It is found that some of the lines due to intramolecular modes of vibration of both the compounds undergo changes with the solidification of the liquids. The results have been compared with those due to benzene and naphthalene and it has been suggested that the changes mentioned above and the appearance of the new low-frequency Raman lines may be due to intermolecular coupling in the crystal at the low temperature.

## INTRODUCTION

It was observed by Sirkar and Ray (1960) that the crystals of benzene at  $-100^{\circ}\text{C}$  show only three Raman lines in the low-frequency region and the number of these lines increases to five when the temperature is lowered to  $-180^{\circ}\text{C}$ . In the case of pyridine at  $-180^{\circ}\text{C}$ , however, only four such lines were observed by Kastha (1956). The increase in the number of low-frequency lines with lowering of temperature of the crystals was also observed in the Raman spectra of many substituted benzene compounds such as *p*-xylene (Biswas, 1954a), *p*-bromotoluene (Biswas, 1954b) and *m*-dichlorobenzene (Biswas, 1955). It has also been pointed out by Biswas (1957) that the number of the low-frequency lines does not depend on the shape and size of the molecule, but it depends on the nature of the substituents. In the case of naphthalene at  $-180^{\circ}\text{C}$  six such lines have been observed (Ray, 1960). It would be interesting to compare the spectrum of naphthalene

---

\*Communicated by Professor S. C. Sirkar.

with that of quinoline, because the shapes and sizes of the two molecules are similar. Tetraline is another molecule in which one of the two rings of naphthalene has been altered by substitution. The object of the present investigation was to study the Raman spectra of quinoline and tetraline in different states in order to find out the change in the Raman spectra which might take place with change of state and also the number of low-frequency Raman lines in each case.

The infrared spectra of the two substances in the liquid state and also in solution in different solvents have also been studied in order to find out the influence of environment on the spectra.

#### EXPERIMENTAL

The liquids, quinoline and tetralin supplied by the British Drug House, England, were of chemically pure quality. They were further purified by repeated distillation under reduced pressure before each exposure. The arrangements used to record the Raman spectra of the two compounds in the liquid state and in the solid state at  $-180^{\circ}\text{C}$  were the same as those used by Biswas (1954). An iron arc spectrum was superimposed on each spectrogram for comparison. The polarisation of Raman lines of tetralin was studied in the usual way. A Fuess glass spectrograph having a dispersion of  $11\text{\AA}/\text{mm}$  in the  $4047\text{\AA}$  region was used to photograph the spectra on Ilford Zenith plates. The infrared absorption spectra of the two compounds in the liquid state and in solution in  $\text{CS}_2$ ,  $\text{CCl}_4$  and *n*-heptane have been recorded with a Perkin Elmer Model 21 spectrophotometer with NaCl optics. A compensation cell was used in the reference beam in each case.

#### RESULTS

The spectrograms are reproduced in Figs. 1, 2, and 3, Plate XI. The observed Raman shifts of the compounds in the liquid state and in the solid state at  $-180^{\circ}\text{C}$  are tabulated in Tables I and III respectively. The Raman shifts for the corresponding liquids reported by previous workers are also included in the tables for comparison. The totally polarised and depolarised lines are indicated by the letters P and D respectively written by the side of each Raman line in Table III.

The infrared spectra of quinoline in the liquid state and its solutions in  $\text{CS}_2$  and in  $\text{CCl}_4$  are reproduced in Figs. 4, 5(a) & (b) and 6, respectively. Also, the infrared spectra of tetralin in the liquid state and of its solutions in  $\text{CS}_2$  and in  $\text{CCl}_4$  are reproduced in Figs. 7, 8 and 9(a) & (b) respectively. The infrared bands of pure quinoline and its solutions in  $\text{CS}_2$  and in  $\text{CCl}_4$  and those of pure tetraline and its solutions in  $\text{CS}_2$  and in  $\text{CCl}_4$  are tabulated in Tables II and IV respectively. The wave numbers of the bands of the pure liquids given in Landolt-Bornstein Tables are also included in the respective tables for comparison.

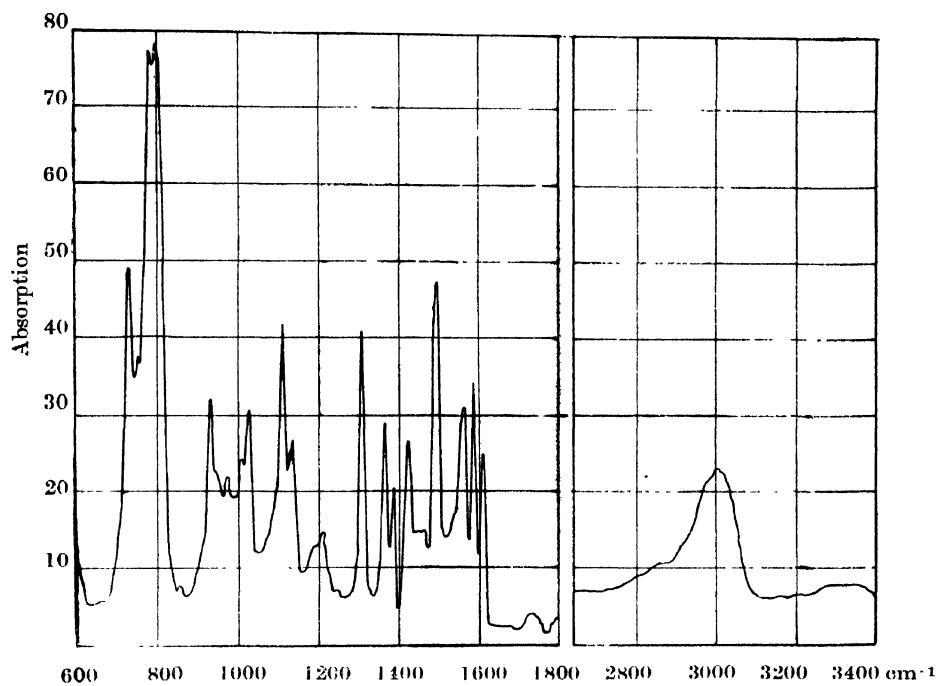
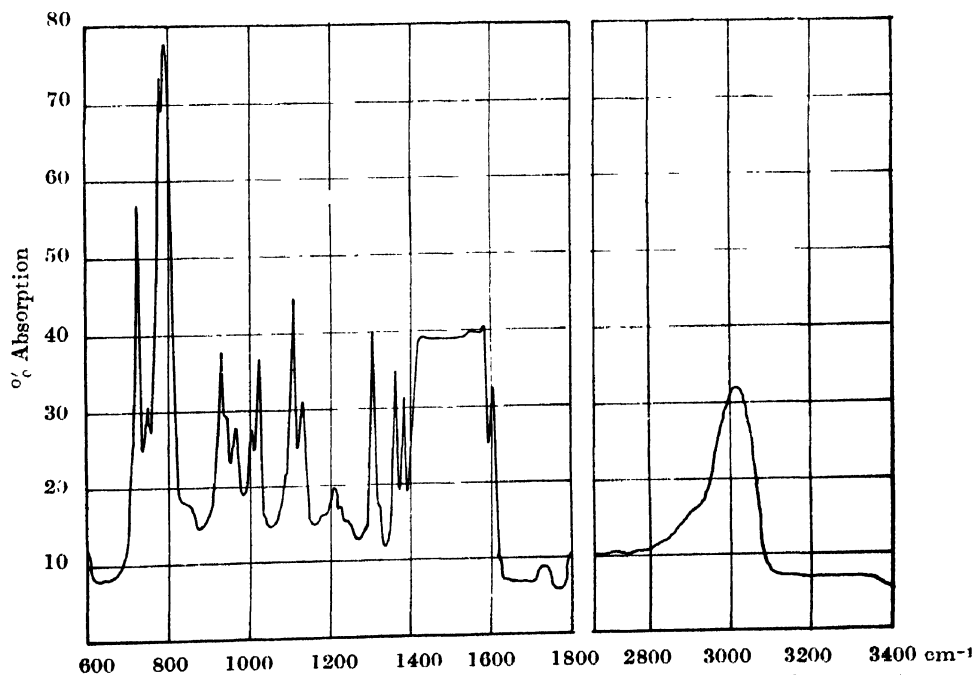


Fig. 4. Infrared spectrum of quinoline (liquid at 26°C).

Fig. 5(a) Infrared spectrum of 5% solution of quinoline in CS<sub>2</sub> (cell .05 mm)

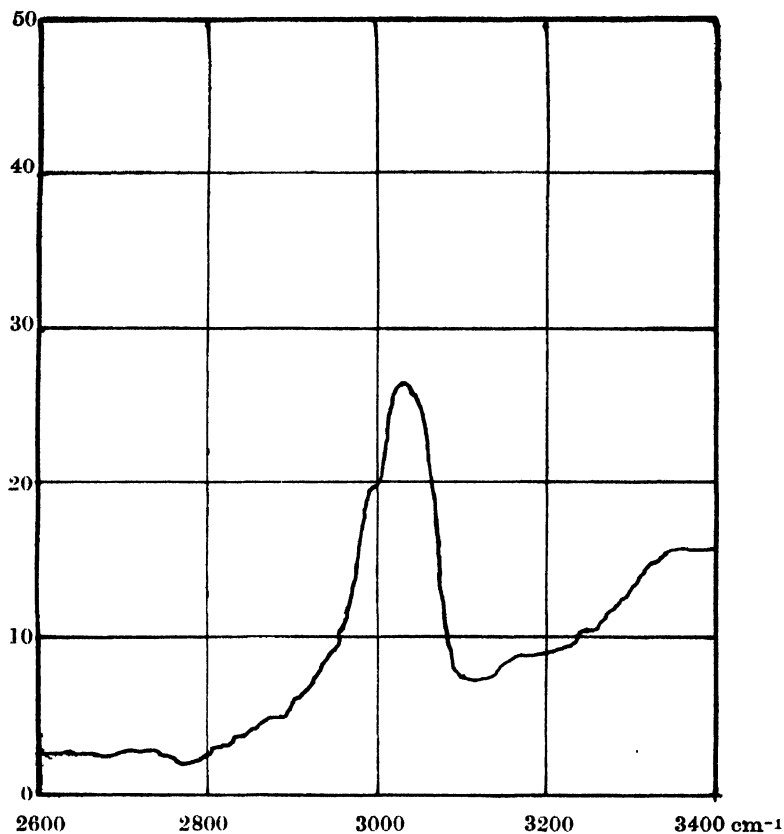


Fig. 5(b). Infrared spectrum of 15% solution of quinoline in CS<sub>2</sub> (cell .05 mm).

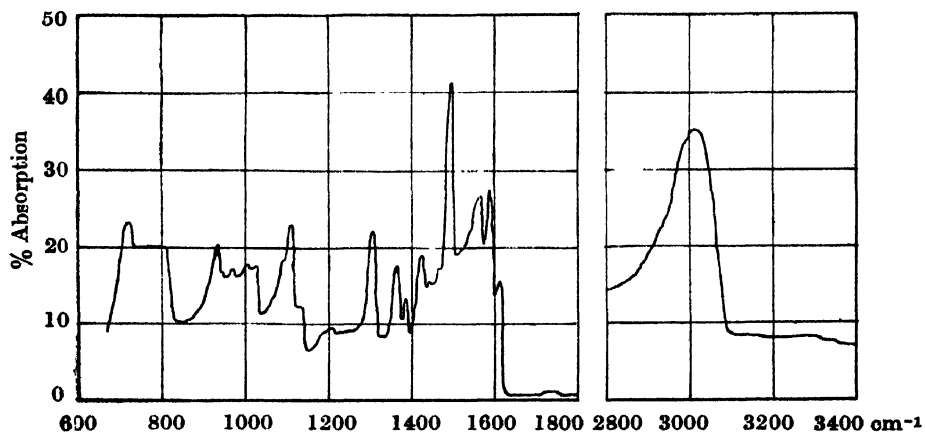


Fig. 6. Infrared spectrum of 5% solution of quinoline in CCl<sub>4</sub>.



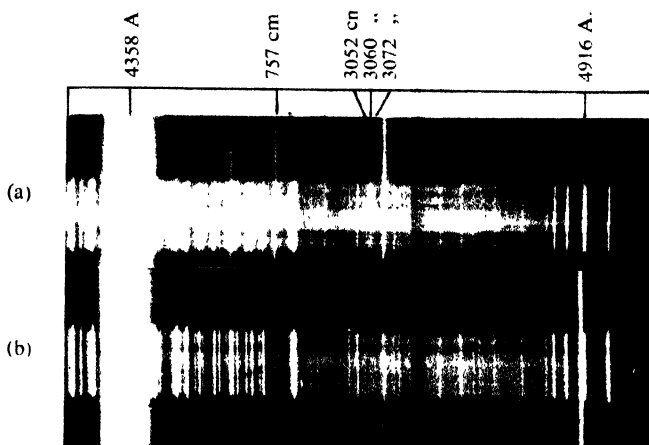
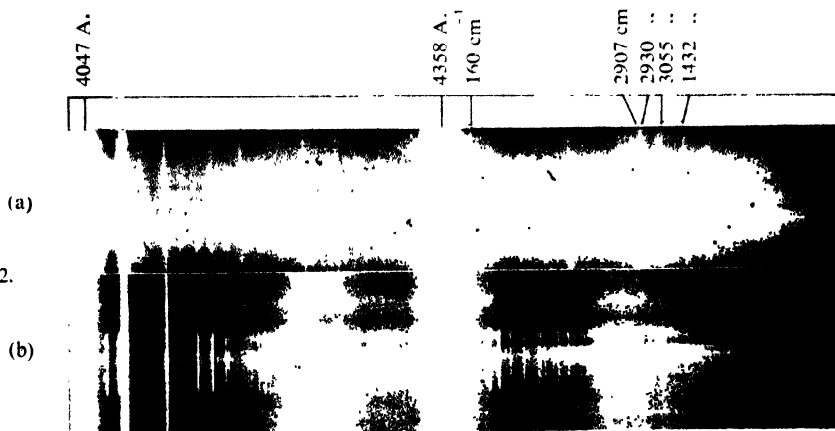


Fig. 2.



**Fig. 3.**

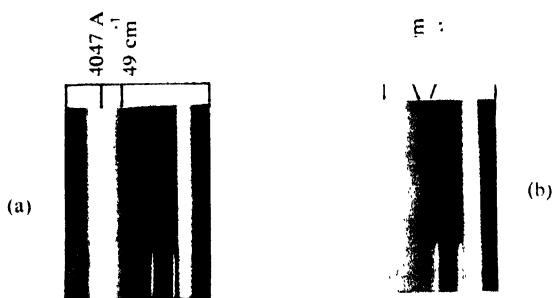
[illegible]

Fig. 2. (a) " " " tetralin, liquid at 30°C  
(b) " " " tetralin, solid at -180°C

Fig. 3. (a) Low frequency band of quinoline at  $-180^{\circ}\text{C}$   
(b) Low frequency Raman lines of tetralin at  $-180^{\circ}\text{C}$



**TABLE I**  
Raman spectra of quinoline— $\Delta\nu$  in  $\text{cm}^{-1}$

Liquid		Solid at $-180^\circ\text{C}$
Landolt-Bornstein Tables (1951)	Present author	Present author
		49 (2b)
	191 (4b)	100 (2b)
388 (1)	386 (4)	384 (0)
518 (5)	519 (8)	516 (6)
701 (0)		
729 (1)		
755 (3)	757 (10)	751 (6)
771 (1)	776 (1)	
949 (1)		
975 (0)	963 (1b)	
1008 (2)	1013 (2)	1014 (0)
1028 (2)	1032 (6)	1030 (3)
1113 (1)	1117 (1)	
1137 (1)	1143 (2)	
1248 (1)		
1337 (0)	1310 (1)	
1367 (6)	1366 (15)	1366 (12)
1388 (2)	1390 (4)	1392 (1)
1428 (3)	1427 (10)	1428 (4)
1460 (1)	1464 (1)	
1491 (1)	1494 (1)	
1568 (4)	1572 (10)	1571 (4)
1589 (1)	1594 (1)	
1615 (0)	1628 (1)	
	2980 (0b)	
3011 (1)	3009 (1b)	
	3052 (4)	
3062 (3b)	3060 (6)	3088 (2Vb)
	3072 (2)	

TABLE II  
Infrared spectra of quinoline— $\nu$  in  $\text{cm}^{-1}$

Pure liquid		5% Solutions (Present author)	
Landolt-Bornstein Tables (1951)	Present author	in $\text{CCl}_4$	in $\text{CS}_2$
	730 ms	720 ms	730 ms
	755 ms		755 w
782 vs	782 vs		780 vs
800 vs	800 vs		798 vs
932 s	932 ms	932 ms	930 ms
950 s	950 vw		945 w
975 ms	975 vw	950 vw	970 w
1005 ms	1010 w	970 w	1010 w
		1005 w	
1030 s	1030 ms	1030 vw	1025 w
1090 vw	1090 vw	1090 vw	1090 vw
1110 vs	1110 s	1110 ms	1110 ms
1135 vs	1135 w	1135 vw	1135 w
1185 vw	1185 vw		
1210 vw	1210 vw	1210 vw	1210 vw
	1230 vw	1235 w	
1310 s	1310 s	1310 ms	
	1365 ms	1365 ms	1365 ms
1370 ms (b)	1390 w	1390 vw	1390 w
1427 s	1427 ms	1430 ms	1430 ms
1450 w	1450 vw	1445 vw	
1465 w	1465 vw	1465 vw	
1495 vs	1495 s	1498 s	
1540 vw	1540 vw	1542 w	
1565 ms	1565 ms	1560 ms	
1590 ms	1588 ms	1590 ms	
1615 ms	1610 ms	1610 w	
	1718 vw	1718 vw	1730 w
	1835 vw	1835 vw	1830 vw
	1860 vw	1860 vw	1870 vw
	1900 w	1820 w	1890 w
	1918 w		1920 w
	1950 w	1950 w	1950 w
	2230 vw		
	2270 vw		2290 w
	2310 w	2305 w	
	2340 vw		
		2415 vw	
	2840 vw		
	2900 vw		
*2890 w			
*2930 w			
*2950 ms			
	2980 s		
*3002 ms	3000 s	2995 ms	2995 ms
*3040 s	3025 s	3025 s (b)	3025 s (b)
*3080 s			

\*Bands observed in solution in  $\text{CCl}_4$

TABLE III  
Raman spectra of tetralin— $\Delta\nu$  in  $\text{cm}^{-1}$

Liquid		Solid at $-180^\circ\text{C}$	
Landolt-Bornstein Table (1951)	Present author	Present author	
		61 (2)	
		92 (8)	
113 (5)	107 (4) D	107 (2)	
163 (6b)	161 (8b) D	137 (2)	
265 (4)	262 (4) P	158 (4)	
311 (1)		265 (1)	
435 (6)	433 (6) P	432 (2)	
457 (4)	458 (1) D	456 (0)	
511 (4)	508 (4) P		
584 (6)	578 (6) P	578 (3)	
725 (8)	722 (12) P	721 (10)	
768 (1)			
805 (3)	804 (2)	804 (0)	
816 (4b)	819 (2) D	819 (2)	
866 (3)	869 (0) D		
905 (2)	915 (1) P		
983 (1)			
1037 (10)	1039 (12) P	1040 (8)	
1067 (4)	1064 (1b) D	1064 (0)	
1116 (1)			
1159 (6)	1162 (4) D	1163 (2)	
1202 (8)	1205 (8) P	1206 (6)	
1237 (3)	1236 (2) D	1236 (0)	
1284 (3)	1280 (8) D	1281 (6)	
1343 (4)	1337 (4b) P		
1381 (1)	1381 (1b) P		
1433 (6)	1432 (6) D	1427 (5)	
1449 (3)	1452 (2)		
1581 (4)	1576 (2) D	1576 (0)	
1603 (6)	1603 (8) D	1603 (6)	
2836 (5)	2832 (6) P	2832 (3)	
2864 (6)	2855 (3) P	2858 (2)	
	2878 (3)	2878 (2)	
2906 (5)	2907 (4)	2923 (4)	
2923 (4)			
2939 (6b)	2930 (10) P	2932 (1)	
		2953 (2)	
3023 (3)	3025 (5b)	3025 (2)	
	3055 (5b) P		
3045 (7)		3064 (3)	

TABLE IV  
Luminescence spectra in the solid state at  $-180^\circ\text{C}$ — $\nu$  in  $\text{cm}^{-1}$

Centres of the bands	Intensity	Separation between the two strong bands and two weak bands	
23690	strong	}	1651
23583	weak		
22039	strong		
21933	weak		
			1650

TABLE V  
Infrared spectra of tetralin,  $\nu$  in  $\text{cm}^{-1}$

Pure liquid		5% Solutions Present author		Solutions Landolt- Bornstein Table (1951)
Lambert and Le Comte (1938) & Wall and McMillan (1940)	Present author	in $\text{CCl}_4$	in $\text{CS}_2$	in $\text{CS}_2$
				580 s 620 ms 650 ms 670 ms 700 ms 740 s 780 s 805 s
740 s	735 vs 780 w 800 ms 810 w	730 ms   810 vw	735 vs 775 w 800 ms 810 w	
960 w	860 vw		855 w	855 w
905 w	895 w 940 ms 980 vw 1000 vw 1030 w 1060 w 1105 xw 1130 vw 1155 vw	890 w 938 w 980 vw 1000 vw 1030 w 1060 w 1105 vw	890 vw 940 ms 980 vw 1000 vw 1025 w 1060 w 1100 w 1130 w 1150 w	890 ms    975 ms  1025 ms 1055 ms 1102 s 1125 ms
1111 w	1240 w 1280 ms 1330 w 1350 w 1430 ms	1238 w 1280 w  1350 vw 1430 s	1240 w 1280 ms 1330 w 1350 w 1425 s	1255 ms    1435 s
1429 w	1445 s	1450 s		
1448 s	1470 ms 1490 s 1575 vw 1598 vw 1630 vw 1640 vw	1475 vs 1490 s 1575 vw	1470 vw 1490 vw 1570 w	
	1660 vw 1680 vw 1760 w 1800 w 1910 w 1940 w 2835 s 2890 s	1660 vw 1675 vw 1750 vw 1800 w 1902 w 1935 vw	1658 vw 1675 vw  1800 w 1905 vw 1930 vw 2835 ms 2890 s	
2898 s	2900 s	2900 s	2900 s	
2975 ms	2985 ms	2985 ms	2985 ms	
3021 ms	3040 ms	3040 w	3040 w	
3058 w	3060 w	3060 w	3060 w	

## DISCUSSION OF RESULTS

*Quinoline**(a) Comparison with previous work*

Table I shows that almost all the Raman frequencies given in the Tables by Landolt and Bornstein agree with those observed in the present investigation excepting the fact that the lines  $191\text{ cm}^{-1}$ ,  $2980\text{ cm}^{-1}$  were not reported by the previous workers and the feeble lines  $701$ ,  $729$ ,  $1248$  and  $1337\text{ cm}^{-1}$  have not been observed in the present investigation. Of these the line  $1248\text{ cm}^{-1}$  excited by  $4047\text{ Å}$  line coincides with the antistokes line  $519\text{ cm}^{-1}$  excited by the  $4358\text{ Å}$  line. There is no indication of the other faint lines mentioned above in the spectrogram obtained in the present investigation. On the other hand, the broad lines  $191\text{ cm}^{-1}$  and  $2980\text{ cm}^{-1}$  are clearly visible on the spectrogram.

*(b) Assignment of some of the Raman lines*

The quinoline molecule is similar to the naphthalene molecule, the only difference being the absence of the centre of symmetry in the former molecule. The assignment of the vibrational frequencies of quinoline to the different fundamental modes was made earlier by Ichishima (1950). More recently, several attempts have been made to assign the frequencies of the naphthalene molecules. Lippincott and O'Reilly (1955) made such assignment by comparing the Raman and infrared frequencies of naphthalene and naphthalene *d*-8. The vibration frequencies of naphthalene have been calculated by Scully and Whiffen (1960) and those of planar vibrations of the molecule have been calculated by Freeman and Ross (1960). A comparison of the infrared and Raman spectra of quinoline with those of naphthalene may be helpful in arriving at the correct assignment of the frequencies of both the molecules, and therefore, an attempt is made here to compare these results.

Two of the nine  $A_g$  fundamentals of the naphthalene molecule given by Lippincott and O'Reilly (1955) do not agree with the corresponding frequencies given by Scully and Whiffen. These are  $1240\text{ cm}^{-1}$  and  $878\text{ cm}^{-1}$ . These fundamentals should appear as strong Raman lines and their frequencies for quinoline are expected to be very near to those of the naphthalene molecule. Table I shows that quinoline produces intense Raman lines corresponding to fundamental frequencies  $519$ ,  $557$ ,  $1032$ ,  $1366$ ,  $1427$ ,  $1572$  and  $3060\text{ cm}^{-1}$ . These agree fairly well with the corresponding frequencies of *g*-class vibrations of the naphthalene molecule given by Scully and Whiffen (1960). As regards the remaining two frequencies of naphthalene of this class, they have given them as  $3025\text{ cm}^{-1}$  and  $1144\text{ cm}^{-1}$ , while Freeman and Ross (1960) have given them as  $3004\text{ cm}^{-1}$  and  $1144\text{ cm}^{-1}$ . In the case of quinoline there is a weak line of Raman shift  $3009\text{ cm}^{-1}$  and another line at  $1143\text{ cm}^{-1}$ , but there is no line of Raman shift  $3025\text{ cm}^{-1}$ . Hence the assignment of the  $A_g$ -class fundamentals of naphthalene made by Freeman and

Ross seems to be corroborated by the appearance of corresponding frequencies of A-class vibration in the Raman spectrum of quinoline. Some of the assignments made by Lippincott and O'Reilly therefore do not seem to be correct.

As the quinoline molecule has no centre of symmetry some of the modes which are antisymmetric to the centre of symmetry in the case of naphthalene and are forbidden in the Raman effect may appear as weak lines in the case of quinoline. The line  $3072\text{ cm}^{-1}$  seems to be such a line. The infrared bands  $1588\text{ cm}^{-1}$  and  $1365\text{ cm}^{-1}$  of medium strength may correspond to the modes  $1595\text{ cm}^{-1}$  and  $1387\text{ cm}^{-1}$  of naphthalene. The strong band  $1310\text{ cm}^{-1}$  is due to a vibration which is of *u*-class in naphthalene, because the mode appears also as a weak Raman line. This may correspond to a mode  $B_{1u}$  of frequency  $1265\text{ cm}^{-1}$  given by Scully and Whiffen. There are two weak Raman lines of shifts  $1628\text{ cm}^{-1}$  and  $1594\text{ cm}^{-1}$ . There are no corresponding strong bands in the infrared. Hence these two lines are due probably to the modes corresponding to two  $B_{1g}$  modes of naphthalene numbered 16 and 17 by Lippincott and O'Reilly (1955).

Thus in the quinoline molecule some of the vibrations of the ring have frequencies very slightly different from those of the naphthalene molecule. This difference is evidently due to the presence of the C-N bond in place of a C-C bond in the ring.

#### (c) *Changes in the Raman spectra of solidification*

It is observed from Table I and Figs. 1(a) & (b) and 3(a) that quinoline in the solid state at  $-180^{\circ}\text{C}$  does not exhibit numerous sharp low-frequency Raman lines unlike naphthalene (Sirkar and Ray, 1950) in the crystalline state. It produces only a moderately strong band with a Raman shift of  $49\text{ cm}^{-1}$  on the Stokes side of the  $4047\text{ \AA}$  line. It was observed earlier (Kastha, 1956) that pyridine in the solid state at  $-180^{\circ}\text{C}$  produces four new low-frequency Raman lines, while benzene produces five such lines under similar conditions.

In the solid state at  $-180^{\circ}\text{C}$  the Raman lines  $3052$ ,  $3060$  and  $3072\text{ cm}^{-1}$  coalesce to form a single broad line with its centre shifted to  $3088\text{ cm}^{-1}$ . Also the Raman line  $757\text{ cm}^{-1}$  corresponding to A-class vibration of quinoline shows a small shift towards the shorter wavelength region under similar conditions. All these changes suggest the formation of intermolecular linkage formed through hydrogen atoms of the neighbouring molecules in the solid state at  $-180^{\circ}\text{C}$ .

#### (d) *Infrared spectra of solutions compared to the spectrum due to the pure liquid*

It can be seen from Table II that some bands given by previous authors appear to differ in intensity and position from those observed in the present investigation. The single broad band  $1370\text{ cm}^{-1}$  given in Landolt-Bornstein Tables appears as a doublet at  $1365$  and  $1390\text{ cm}^{-1}$  in the present investigation. It is observed from Figs. 4; 5(a) & (b) and 6 that the band  $755\text{ cm}^{-1}$  becomes weak in the spectrum due to the dilute solution of quinoline in  $\text{CS}_2$ . Moreover, the first



component of the triplet  $2980\text{ cm}^{-1}$ ,  $3000\text{ cm}^{-1}$  and  $3030\text{ cm}^{-1}$  due to pure quinoline seems to be weakened very much in 5% solutions in  $\text{CS}_2$  and  $\text{CCl}_4$  and it again appears weakly in 15% solution in  $\text{CS}_2$ . This shows that quinoline molecules in the liquid state are probably strongly associated and the  $2980\text{ cm}^{-1}$  band may be due to such associated molecules. The association thus breaks up in the dilute solution. The  $757\text{ cm}^{-1}$  band corresponds to the Raman line of the same vibrational frequency, but the mode being of A-Class, it is forbidden in the infrared in the case of naphthalene. It appears weakly in the case of solution of quinoline in  $\text{CS}_2$  probably because in this case the centre of symmetry is disturbed by the presence of the nitrogen atom in the ring. The fact that the strength of the band increases in the pure liquid clearly shows that the centre of symmetry is perturbed to a greater extent and this also may be due to intermolecular coupling in the pure liquid mentioned above.

It can be seen from Table II that there is no strong infrared band due to C-H vibration of frequency greater than  $3025\text{ cm}^{-1}$ , although naphthalene shows a strong band at  $3072\text{ cm}^{-1}$ . The band at  $3025\text{ cm}^{-1}$  is to be assigned to a mode corresponding to a mode of  $u$ -class of naphthalene. It may correspond to the second  $B_{2u}$  mode listed by Scully and Whiffen (1960). The strong bands  $782\text{ cm}^{-1}$  and  $800\text{ cm}^{-1}$  may be assigned to modes corresponding respectively to mode No. 7 of  $B_{1u}$  class and No. 7 of  $B_{2u}$  class given by Freeman and Ross (1960).

### *Tetralin*

#### *(a) Comparison with previous work*

It is observed from Table III that the doublet  $2923$  and  $2939\text{ cm}^{-1}$  reported by previous workers are not resolved in the present investigation and only one broad line  $2930\text{ cm}^{-1}$  has been observed. An extra line  $2878\text{ cm}^{-1}$  is also present in the spectrogram obtained in the present investigation. Regarding the other Raman lines the agreement is good excepting the lines  $768$  and  $982\text{ cm}^{-1}$  which are not present in the spectrogram.

#### *(b) Changes in the Raman spectra on solidification*

It can be seen from Table III and Fig. (3b, 2a and 2b) that tetralin in the solid state at  $-180^\circ\text{C}$  produces two new low-frequency Raman lines of shifts  $67\text{ cm}^{-1}$  and  $92\text{ cm}^{-1}$  respectively. Of these the line  $92\text{ cm}^{-1}$  is stronger than the former one. It was previously observed (Sirkar and Ray, 1950) that naphthalene in the crystalline state produces six such lines under similar conditions. Similar comparison of the spectra due to benzene and cyclohexane shows that benzene produces five low frequency Raman lines (Sirkar and Ray, 1950) while cyclohexane does not produce any low frequency Raman line (Sirkar and Gupta, 1937). It thus appears that the presence of the six unsaturated  $\pi$ -electrons is necessary for the production of the low frequency lines in the case of compound

containing carbon rings. Tetralin may be regarded as a modified molecule of naphthalene with a cyclohexane ring attached to a benzene ring. Hence the diminution in the number of low frequency Raman lines in the case of the solidified tetralin at  $-180^{\circ}\text{C}$  may be attributed to the diminution in the number of benzene rings in the molecule.

(c) *Other changes in the Raman spectra*

It can be seen from Table III that the Raman line  $161\text{ cm}^{-1}$  which probably corresponds to a  $B_{3u}$  mode in naphthalene (Scully and Whiffen, 1961) is split up into two lines  $137\text{ cm}^{-1}$  and  $168\text{ cm}^{-1}$  respectively when the compound is solidified and cooled to  $-180^{\circ}\text{C}$ . The Raman line  $1432\text{ cm}^{-1}$  which is due to C-H bending mode also shows a small shift towards the shorter wavelength region in the solid state at  $-180^{\circ}\text{C}$ . The line  $2907\text{ cm}^{-1}$  shifts to  $2923\text{ cm}^{-1}$  and the line  $2930\text{ cm}^{-1}$  which is due probably to aromatic C-H stretching mode is split up into two components at  $2932$  and  $2963\text{ cm}^{-1}$  with the solidification of the liquid. Further, the line  $3055\text{ cm}^{-1}$  shifts to  $3064\text{ cm}^{-1}$  at the low temperature. On the other hand, the lines  $2832$ ,  $2855$  and  $2878\text{ cm}^{-1}$  remain unchanged at the low temperature. This shows that the C-H stretching vibrations in the  $\text{CH}_2$  group remain unaffected while these due to C-H group in the ring undergo changes with solidification.

These changes suggest that probably some weak intermolecular coupling is formed in the frozen state of the substance at  $-180^{\circ}\text{C}$  and the low-frequency lines may also be attributed to such coupling.

(d) *Luminescence spectra*

It can be seen from Figs. 3a and 3b that tetralin in the liquid state exhibits strong continuous luminescence, which with lowering of temperature at  $-180^{\circ}\text{C}$ , appears as four discrete bands with centres at about  $21933$ ,  $22039$ ,  $23583$  and  $23690\text{ cm}^{-1}$  respectively as shown in Table IV. In the case of quinoline, no such bands have been observed in the solid state at  $-180^{\circ}\text{C}$ . The separations of the two strong bands and two weak bands are  $1651$  and  $1650\text{ cm}^{-1}$  respectively. This difference may correspond to the wave number  $1680\text{ cm}^{-1}$  assigned to a  $B_{3u}$  mode of naphthalene (Lippincott and O'Reilly, 1955). Probably, this type of vibration makes the triplet $\rightarrow$ singlet electronic transition partially allowed, so that the emission of the fluorescence bands takes place in the solid state at  $-180^{\circ}\text{C}$ .

(e) *Infrared spectrum of solutions compared with the spectrum due to pure liquid*

Table V shows that the infrared bands due to pure tetraline reported by previous workers agree closely with those observed in the present investigation. It can also be seen from Table V that some of the infrared bands of solution of the liquid in  $\text{CS}_2$  observed by previous workers differ in intensity and position from those observed in the present work. Instead of the medium strong band  $1255\text{ cm}^{-1}$  reported in Landolt-Bornstein Tables (1951), two weak bands  $1240\text{ cm}^{-1}$

and  $1280\text{ cm}^{-1}$  have been observed in the present work. Also the relative strengths of the absorption bands  $855$  and  $890\text{ cm}^{-1}$  reported in the Table seem to be reversed.

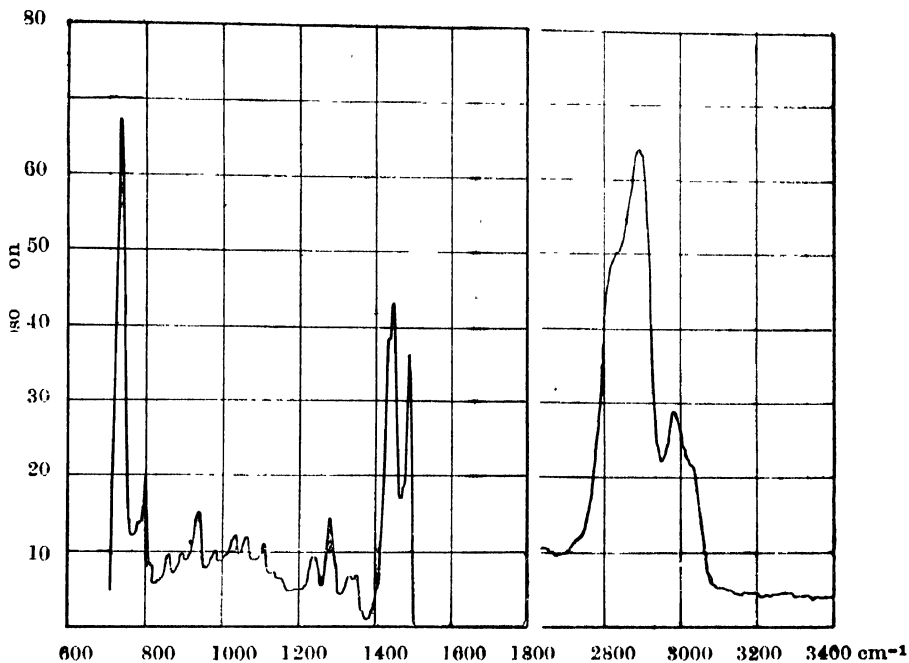


Fig. 7. Infrared spectrum of tetralin (liquid at  $27^{\circ}\text{C}.$ )

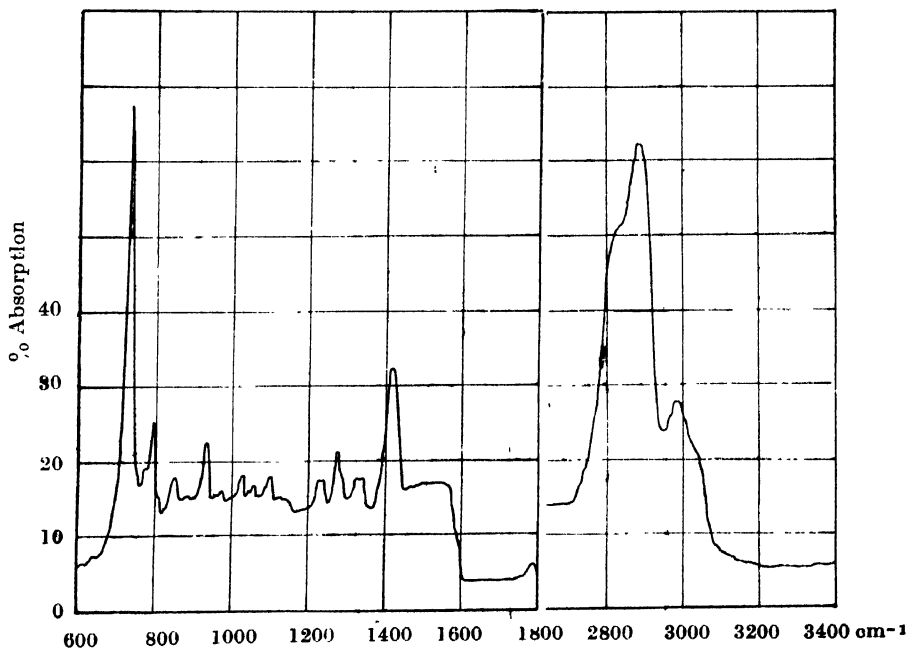
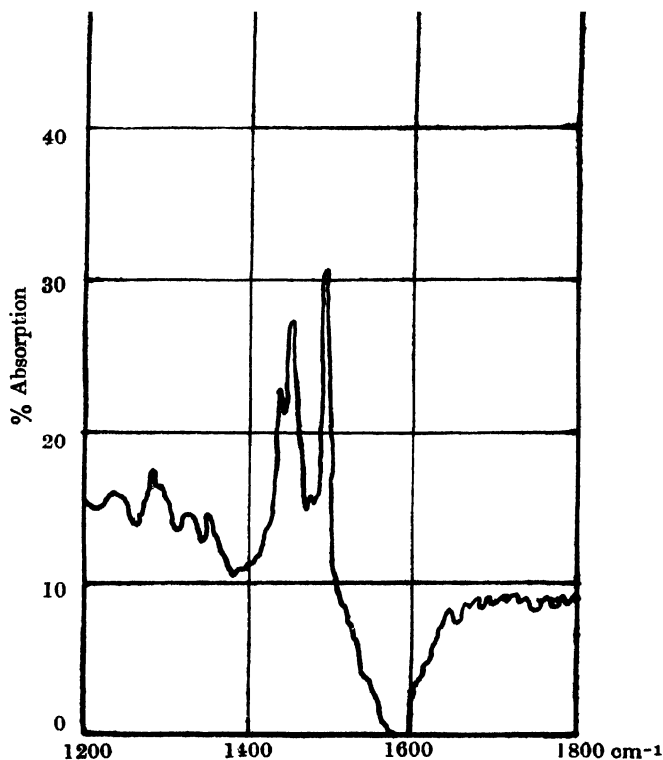
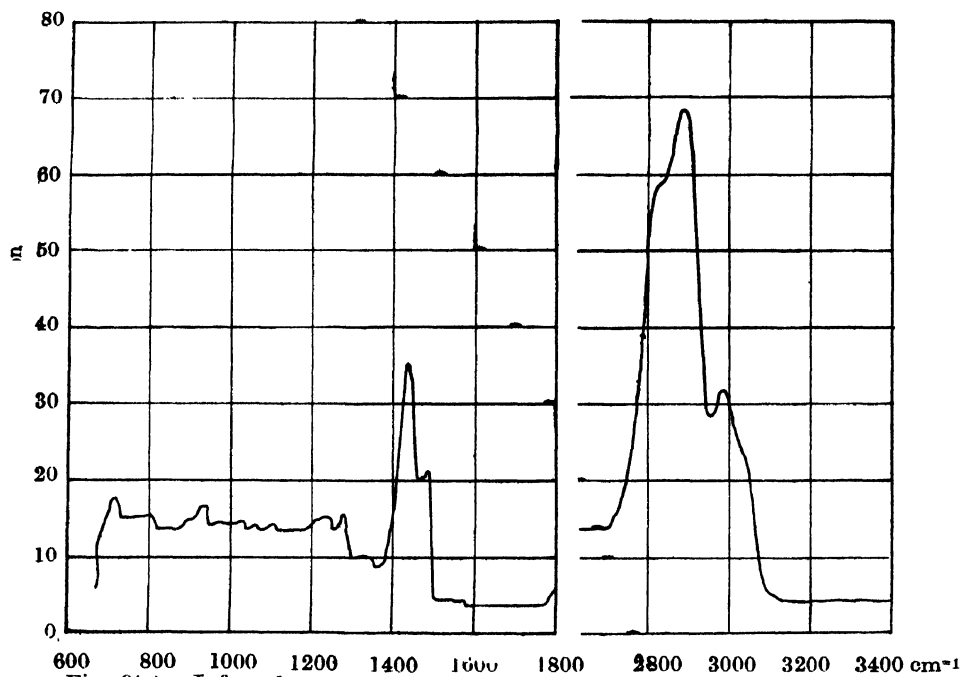


Fig. 8. Infrared spectrum of 5% solution of tetralin in  $\text{CS}_2$  (cell .05 mm.)



It is observed from Figs. 7 and 9(a) & (b) that the relative strengths of the bands  $1490\text{ cm}^{-1}$  and  $1445\text{ cm}^{-1}$  corresponding to C-H bending modes change considerably when the substance is dissolved in  $\text{CCl}_4$ , the band  $1490\text{ cm}^{-1}$  being stronger than the band  $1445\text{ cm}^{-1}$  in the spectrum due to the solution while it is weaker in the spectrum due to the pure liquid. Also the bands  $2835$  and  $2985\text{ cm}^{-1}$ , which correspond respectively to the hydrogen stretching modes in  $\text{CH}_2$  and C-H groups slightly increase in strength when the substance is dissolved in  $\text{CCl}_4$ . No such change is observed in the case of solution in  $\text{CS}_2$ . So, it appears that the chlorine atoms of the solvent have some influence on the absorption due to C-H valance oscillations.

#### ACKNOWLEDGMENT

The author wishes to acknowledge his grateful indebtedness to Prof. S. C. Sirkar, D.Sc., F.N.I., for his kind help and inspiring guidance in carrying out this work. Thanks are also due to Dr. M. Mazumdar for kind co-operation in recording infrared spectra.

#### REFERENCES

- Biswas, D. C., 1954a, *Ind. J. Phys.*, **28**, 303.  
 Biswas, D. C., 1954b, *Ind. J. Phys.*, **28**, 403.  
 Biswas, D. C., 1955, *Ind. J. Phys.*, **29**, 179.  
 Biswas, D. C., 1957, D. Sc. thesis submitted, Calcutta University.  
 Fraeman, D. E., and Ross, I. G., 1960, *Spectrochimica Acta*, **16**, 1303.  
 Ichishima, I., 1950, *J. Chem. Soc. (Japan)*, **71**, 443.  
 Kastha, G. S., 1956, *Ind. J. Phys.* **30**, 519.  
 Landolt-Bornstein, 1951, *Zahlenwerte und Funktionen*, 1 Band Atom- und Molekular Physik Teil (2) p 402, 459, 506 and 546.  
 Lambert, P. and La Comte J., 1932, *Ann Physique (X)* **18**, 329.  
 Lippincott, E. R. and O'Reilly, E. J., 1955, *J. Chem. Phys.*, **23**, 238.  
 Ray, A. K., 1950, *Ind. J. Phys.*, **24**, 549.  
 Sirkar, S. C. and Gupta, J. 1937, *Ind. J. Phys.* **11**, 55.  
 Sirkar, S. C. and Ray, A. K., 1950, *Ind. J. Phys.*, **24**, 189.  
 Scully, D. B. Whiffen, D. H. 1960, *Spectrochimica Acta* **16**, 1409.  
 Wall, F. T. and McMillan, U. 1940, *J. Am. Chem. Soc.*, **62**, 2225.

# ON THE CALCULATION OF LOW-ENERGY NEUTRON SCATTERING BY A COMPLEX POTENTIAL

ARUNDHATI GHOSH AND S. K. DUTTA

DEPARTMENT OF THEORETICAL PHYSICS,  
INDIAN ASSOCIATION FOR THE CULTIVATION OF SCIENCE  
JADAVPUR, CALCUTTA-32

(Received July 20, 1961)

**ABSTRACT.** The scattering of low-energy neutrons by a potential  $V(r) = -(V + iW)$   $[1 + e(r-R)/a]^{-1}$  is calculated by applying a method of Lanczos (1938) for solving the Schrödinger equation. The neutron strength function  $\bar{\Gamma}_n^0/D$  which is the ratio of the average value of neutron width to level spacing is obtained from the scattering amplitude. That this analytic method of solution is fairly exact is borne out by the fact that our results agree closely with the finding of Feshbach, Porter and Weisskopf (1954) who have solved numerically the differential equation with the same potential.

## INTRODUCTION

A number of investigations (Feshbach *et al.*, 1954; Feshbach, 1958) have been made in interpreting the interaction of slow neutrons with a nucleus taking the nuclear potential to be complex. The resonance structure of neutron strength function has been first discussed by Feshbach, Porter and Weisskopf (1954) and they calculated the strength function with a complex square well potential. Later on Feshbach (1958) have solved numerically the Schrödinger equation with the Woods-Saxon potential and the results so obtained have nearly the same general pattern as those of the complex square well. The agreement with experimental findings is fair, Feshbach obtained for the value of  $\bar{\Gamma}_n^0/D$  at  $A = 155$ , one maximum whereas the experimental results indicate two small peaks.

The object of the present paper is to solve analytically the Schrödinger equation with the Woods-Saxon potential for the case of positive energy states, the method employed here is due to Lanczos (1938) which we have already applied to solve the bound state problem (1960). Previously Lawson (1956) has obtained a solution of this problem in the form of infinite series the terms of which converge very badly, as such the solution of Lawson is not so useful in its application to physical problems. In our case if we take the solution up to eighth term the error in the differential equation is of the order of 1 in  $10^6$ . Our results agree well with similar ones of Feshbach (1958).

In the theory of Feshbach, Porter and Weisskopf (1954) it is shown that for

very low energy neutrons the scattering amplitude averaged over resonances is given by

$$\bar{\eta}_0 = e^{-2iKR'}(1 - \pi\bar{\Gamma}_n/D) \quad \dots \quad (1)$$

This gives  $\bar{\Gamma}_n/D$  which is the ratio of the average value of neutron width to level spacing and  $R'/R$  where  $R'$  has the dimension of length and is a slowly varying function of energy. The magnitude of  $R'$  is of the order of nuclear dimension and it plays the role of scattering length;  $K$  is  $\left(\frac{2M}{\hbar^2} E\right)^{\frac{1}{2}}$ . The average total cross section (Feshbach *et al.*, 1954) is

$$\begin{aligned} \sigma_t^{(0)} &= \frac{\pi}{K^2} \{ |1 - \bar{\eta}_0|^2 + |1 - \bar{\eta}_0|^2 \} \\ &= 4\pi R'^2 + \frac{2\pi^2}{K^2} \bar{\Gamma}_n/D \quad \dots \quad (2) \end{aligned}$$

#### MATHEMATICAL FORMULATION AND RESULTS

The interaction potential between the neutron and the nucleus is taken as

$$V(r) = -(V + iW)[1 + e^{(r-R)/a}]^{-1}$$

where  $R$  is a measure of the nuclear size and  $a$  is the diffusivity parameter. The Schrödinger equation for  $l = 0$ , scattering with the above potential may be written as

$$\frac{d^2u}{dx^2} + \frac{\lambda^2}{1 + \beta e^x} u + K'^2 u = 0 \quad \dots \quad (3)$$

where  $x = r/a$ ;  $K'^2 = \frac{ZM}{\hbar^2} E a^2$ ;  $\lambda^2 = \frac{2M}{\hbar^2} (V + iW)a^2$ ;  $\beta = e^{-R/a} = e^{-x_0}$

The wave function  $u = r\psi$  satisfies the necessary boundary conditions for scattering at  $x=0$  and  $x \rightarrow \infty$ .

In the region  $R \leq r < \infty$  we may write the solution as

$$u^0(x) = e^{-iK'x} F_- + \bar{\eta}_0 e^{iK'x} F_+ \quad \dots \quad (4)$$

where  $\bar{\eta}_0$  is the scattering amplitude averaged over neutron resonance energies.

We now make a transformation of the independent variable from  $x$  to  $p = e^{-(x-x_0)}$  such that the new independent variable varies from 0 to 1. Then  $F_{\pm}$  satisfies the differential equation

$$\begin{aligned} D_{\pm}(F_{\pm}) &= 0, \\ D_{\pm}(F_{\pm}) &\equiv p(p+1) \frac{d^2 F_{\pm}}{dp^2} + (p+1)(1 \mp 2iK') \frac{dF_{\pm}}{dp} + \lambda^2 F_{\pm} \end{aligned}$$

Applying the suggestion of Lanczos (1938) we now modify the differential equation by equating it to an error term proportional to Tshebysheff's polynomial  $T_n(p)$  instead of to zero.

$$D_{\pm}(F_{\pm}) = \tau_{\pm} T_n(p) \quad \dots (5)$$

$$\text{Let } T_n(p) = B_0 + B_1 p + B_2 p^2 + \dots + B_n p^n \quad \dots (6)$$

Now we put the finite series

$$\overline{F}_{\pm} = a_0 + a_1 p + a_2 p^2 + \dots + a_n p^n \quad \dots (7)$$

in the differential Eq. (5) and comparing the coefficients of the same power of  $p$  on both sides of the equation we get the recursion formulae

$$\begin{aligned} \tau_{\pm} B_r &= a_r \pm [\lambda^2 + r(r \mp 2iK')] + a_{r+1} \pm [(r+1)(r+1 \mp 2iK')], \\ \tau_{\pm} B_n &= a_n \pm [\lambda^2 + n^2 \mp 2iK'n] \end{aligned} \quad \dots (8)$$

These relations will determine the coefficients  $a_r$  of the approximate solutions and the factor  $\tau_{\pm}$  which estimates the error of the approximation in terms of  $a_0$ .

In the region  $0 < r \leq R$  we write the solution as

$$u^i(x) = e^{i\gamma x} f_+ - e^{-i\gamma x} f_- \quad \dots (9)$$

where

$$\gamma = \sqrt{\lambda^2 + K'^2};$$

We make a transformation of the independent variable from  $x$  to  $q = (e^x - 1)/(e^{x_0} - 1)$  such that the new independent variable varies from 0 to 1. Then  $f_{\pm}$  satisfies the differential Eq.

$$q(q+1) \frac{d^2 f_{\pm}}{dq^2} + (q+1)(1 \pm 2i\gamma) \frac{df_{\pm}}{dq} - \lambda^2 f_{\pm} = 0 \quad \dots (10)$$

(neglecting terms involving  $\beta \approx 10^{-6}$ ) we take

$$f_{\pm} = b_0 + b_1 q + b_2 q^2 + \dots + b_n q^n \quad \dots (11)$$

and get as before the recursion formulae to determine  $b_r$  and  $\tau'_{\pm}$  which estimates the error in terms of  $b_0$ .

$$\begin{aligned} \tau'_{\pm} B_r &= b_r \pm [-\lambda^2 + r(r \pm 2i\gamma)] + b_{r+1} \pm [(r+1)(r+1 \pm 2i\gamma)] \\ \tau'_{\pm} B_n &= b_n \pm [-\lambda^2 + n(n \pm 2i\gamma)] \end{aligned} \quad \dots (12)$$

From the continuity of the solution  $u$  and its derivative we obtain

$$\overline{\eta}_0 = e^{-2iK'x_0} \left[ \frac{[(AG - CE)e^{2i\gamma x_0} + (CF - AH)]}{(BG - DE)e^{2i\gamma x_0} + (DF - BH)} \right] \quad \dots (13)$$



where

$$A = \sum_{r=0}^n a_r^- \quad B = \sum_{r=0}^n a_r^+$$

$$C = -iK'A - \sum_{r=1}^n r a_r^-$$

$$D = iK'B - \sum_{r=1}^n r a_r^+$$

$$E = \sum_{r=0}^n b_r^+; \quad F = \sum_{r=0}^n b_r^-$$

$$G = i\gamma E + \sum_{r=1}^n r b_r^+; \quad H = -i\gamma F + \sum_{r=1}^n r b_r^-;$$

From equations (1) and (13) we obtain the expression for  $\bar{\Gamma}_n/D$  and  $R'/R$  which are calculated with the following values of the parameters  $V_0 = 52 \text{ MeV}$ ;  $W = 3.12 \text{ MeV}$ ;  $R = (1.15A^{1/3} + 0.4)10^{-13} \text{ cm}$ ,  $a = 0.57 \times 10^{-13} \text{ cm}$ . The parameters are the same as taken by Feshbach *et al.* (1958) who obtained the neutron strength function by numerically solving the Schrödinger equation with the same potential. The curves of  $\bar{\Gamma}_n^0/D$  (normalised to 1 ev) and  $R'/R$  are plotted against mass number

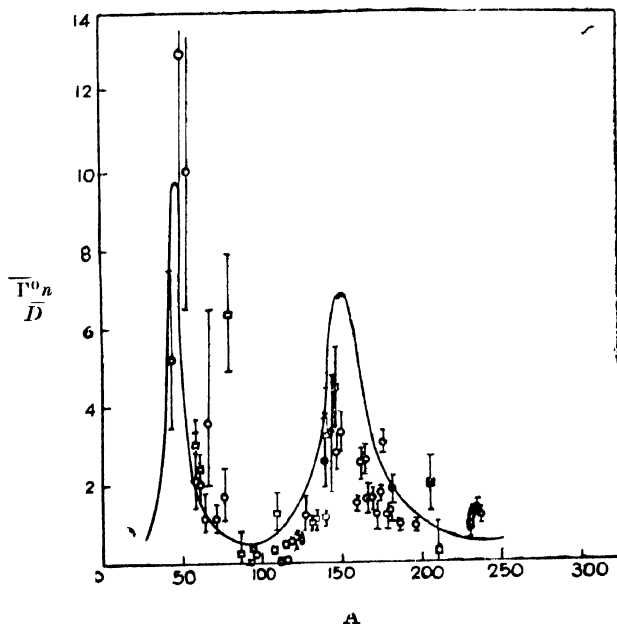


Fig. 1. Ratio  $\bar{\Gamma}_n^0/D$  of neutron width to level spacing. Here  $\bar{\Gamma}_n^0/D$  is normalized to 1 ev.

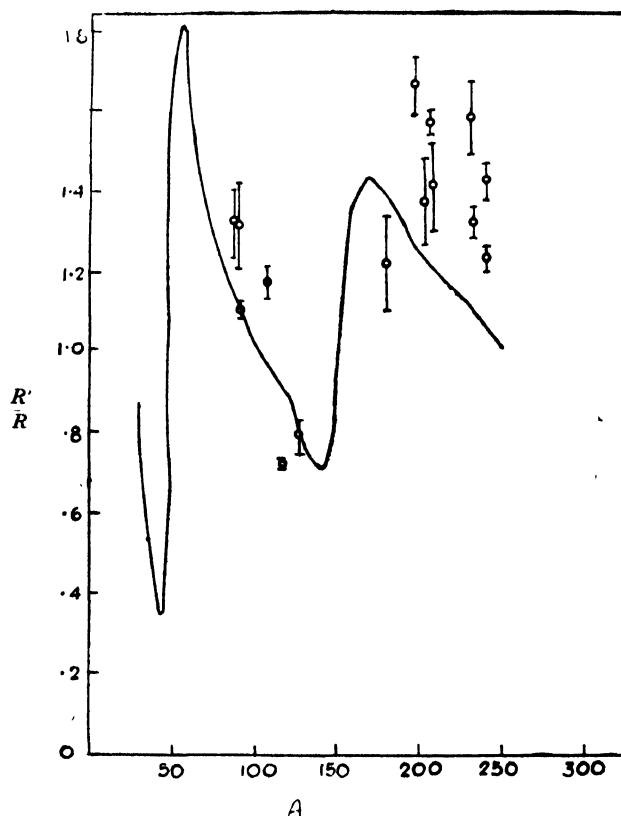


Fig. 2. Ratio of potential scattering length  $R'$  to nuclear radius  $R$ .

in Fig. 1 and Fig. 2 and compared with the experimental results. In the experiment the minimum in  $\Gamma_n^0/D$  between the two resonances is deeper than the theory predicts and the peak at  $A = 155$  is much broader, lower and irregular than that of the calculated curve. A better fit of  $\bar{\Gamma}_n^0/D$  at  $A = 155$  has been obtained by Margolis *et al.* (1957) who has replaced the spherical square well by a spheroidal square well with the idea that the nuclei in this region are not spherically symmetrical. Similarly, in the  $R'/R$  curve closer agreement with the experimental results may be obtained for nuclei with  $A = 200$  if the deformation of these nuclei is taken into account. In our curve of  $\bar{\Gamma}_n^0/D$  the two maxima occur at  $A = 48$  and  $155$  whereas in the calculation of Feshbach (1958) they occur at  $A = 55$  and  $155$ . Except for this shift of the peak point the two curves agree closely. The value of  $R'/R$  at about  $A = 43$  is minimum in both the cases, but our value is numerically higher than that of Feshbach (1958); in all other regions the agreement between the two is good. Unfortunately there is no experimental result in the region  $A = 43$  to indicate which one is superior to the other. In Fig. 3 we present for different elements the average total cross section (sum of elastic scattering and nuclear reactions) of neutrons of energy 500 eV in the unit of  $\pi R^2$ .

The series solution given here has the advantage that the number of terms to be taken in the polynomial is determined by the degree of accuracy one desires in

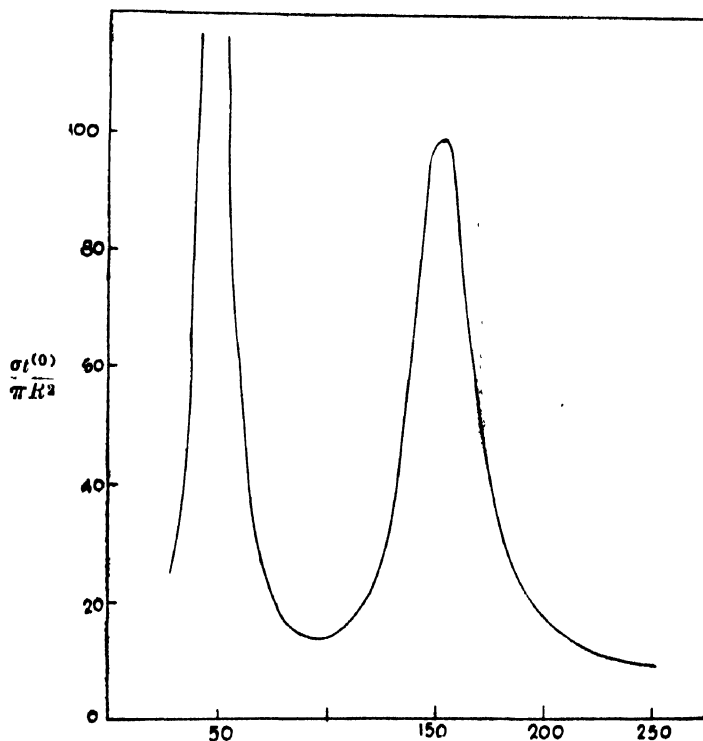


Fig. 3. Calculated total cross section of neutrons as a function of mass number.

the differential equation. For an accuracy of 1 in  $10^6$  in the differential equation it is sufficient to take a polynomial of the order of 8 whereas it is necessary to take several times this number of terms to achieve the same accuracy in Lawson's (1956) series.

We wish to thank Professor D. Basu for his many helpful comments and to Dr. N. C. Sil for taking kind interest in the problem.

#### REFERENCES

- Feshbach, H., Porter, C. and Weisskopf, V. F., 1954, *Phys. Rev.*, **96**, 448.  
 Feshbach, H., 1958, *Annual Rev. of Nuclear Science*, **8**, 22.  
 Ghosh, A. and Sil, N. C., 1960, *Nuclear Phys.*, **17**, 264.  
 Lanczos, C., 1938 *Journal of Mathematics & Phys.*, **17**, 123.  
 Lawson, R. D., 1956, *Phys. Rev.*, **101**, 311.  
 Margolis, B., and Troubetzkoy, E.S., 1957, *Phys. Rev.*, **106**, 105.

# THE SPECTRUM OF $\text{CoCl}$ IN THE PHOTOGRAPHIC INFRARED AND THE VISIBLE

S. V. KRISHNA RAO AND P. TIRUVENGANNA RAO

PHYSICS DEPARTMENT, ANDHRA UNIVERSITY, WALTAIR.

(Received July 13, 1961)

## Plate XII A & B

**ABSTRACT.** The spectrum of  $\text{CoCl}$  has been examined in the photographic infrared and the visible using both low and high dispersion. Several new brief systems have been observed in the visible region  $\lambda$  4600— $\lambda$  5100 Å, and in the photographic infrared region  $\lambda$  6850— $\lambda$  7950 Å. Vibrational constants of the various systems have been derived from the analyses. The new systems, designated in this paper as F, G, H, I are observed to consist of single headed bands while the remaining systems J, K, L,  $\text{N}_1$ ,  $\text{N}_2$  and O are observed to be double headed. It is suggested that the two systems  $\text{N}_1$  and  $\text{N}_2$  in the photographic infrared might belong to two components of a  $^3\Pi$ — $^3\Sigma$  transition.

## INTRODUCTION

The band spectrum of cobalt chloride has been investigated by several earlier workers, Mesnage (1935), More (1938), and Krishnamurty (1952). On the basis of high dispersion spectrograms, taken in the second order of a 21 ft. concave grating spectrograph, More (1938) gave vibrational analyses of three systems designated by him as 1, 2 and 3 in the region ( $\lambda$  4200— $\lambda$  4750 Å). The bands in each of the three systems are single-headed and degraded to longer wavelengths. Recently, Krishnamurty has identified two more systems, designated as 4 and 5 in the same spectral region. These consist also of bands degraded to longer wavelengths. In addition, Krishnamurty proposed the vibrational analyses of six groups of line-like bands slightly degraded to red in the region ( $\lambda$  5350— $\lambda$  6000 Å). on the basis of a  $^5\Pi$ — $^5\Sigma$  transition. His analysis was however based on measurements of plates taken under low dispersion, (25—30 Å/mm).

In a previous paper (Rao *et al.*, 1961) we have reported the results of a study of the spectrum of  $\text{NiCl}$  in the photographic infrared under high dispersion. In continuation of this work we have examined the spectrum of  $\text{CoCl}$  in the photographic infrared and the visible, both under low and high dispersion. This work has disclosed the existence of a number of new band systems of  $\text{CoCl}$  in the photographic infrared region ( $\lambda$  6850— $\lambda$  7950 Å), and in the visible region ( $\lambda$  4600— $\lambda$  5100 Å). The structure and analyses of these new band systems are discussed in this paper.

## EXPERIMENTAL

The spectra were excited both in a heavy current discharge from a 2000 volt d.c. generator and in a high frequency discharge from a 100 watt oscillator

using an anhydrous B.D.H. sample of  $\text{CoCl}_2$ . The spectra were photographed under low dispersion on a Hilger three prism glass Littrow instrument ( $17 \text{ \AA/mm}$ ), and also in the first and second orders of a 21 ft. concave grating spectrograph (dispersion  $2.5 \text{ \AA/mm}$  and  $1.25 \text{ \AA/mm}$ ) using appropriate filters. Exposures of two to five hours duration were found necessary for obtaining the spectra on the grating, using Kodak I.N. plates and Agfa Isopan plates. Second order iron arc lines were used as standards for measurements of all grating plates.

#### RESULTS AND ANALYSIS

All the five band systems observed and analysed by More (1938) and Krishnamurty, (1952) in the spectral region ( $\lambda 4200\text{--}\lambda 4750 \text{ \AA}$ ) were photographed in the present work both under low and high dispersion. In the order of increasing wavelength, systems 3, 2, 4, 5 and 1 are designated as A, B, C, D, E respectively. The bands in each of the systems appear single headed and arise from a transition in which  $\Delta \Lambda = 0$  in Hund's case 'a' or  $\Delta \Omega = 0$  in Hund's case 'c'.

The six groups of line like bands (designated as *M* in this paper) observed and analysed by Krishnamurty in the region ( $\lambda 5350\text{--}\lambda 6000 \text{ \AA}$ ) were too weak to be photographed under high dispersion and therefore they are not considered in the present work. In the spectrum of  $\text{CoCl}$  excited in a high frequency discharge from a 100 Watt oscillator we have observed a number of new band systems in the region ( $\lambda 4600\text{--}\lambda 5100 \text{ \AA}$ ). According to our analyses, based on a close scrutiny of both low and high dispersion spectrograms, the bands of  $\text{CoCl}$  in this region were classified as belonging to seven separate brief systems. Each of these systems is characterised by a strong  $\Delta v = 0$  sequence with weaker  $\Delta v = -1$  or  $+1$  sequence. In the order of increasing wavelength these were designated as *F*, *G*, *H*, *I*, *J*, *K* and *L* systems respectively. The bands in each of the systems *F*, *G*, *H* and *I* are single headed, degraded to red and interpreted as the *R* heads. The bands in *J*, *K* and *L* systems are double headed and interpreted as the *R* and *Q* heads. The data and classifications of these bands are given in Table I. Low dispersion spectrograms of these seven systems are shown in strips (a and b) in Plate XII A, Fig. 1. Grating spectrograms of the prominent bands of the strong  $\Delta v = 0$  sequence in different systems are shown in strips (a, b and c) in Plate XII B, Fig. 2. In the bands of the weaker  $\Delta v = \pm 1$  sequences only the heads of the more abundant  $\text{Co}^{35}\text{Cl}$  species could be identified.

In the spectrum of  $\text{CoCl}$  excited in a heavy current discharge from a 2000 volt D.C. generator we have observed two new systems of bands in the photographic infrared region ( $\lambda 6850\text{--}\lambda 7960 \text{ \AA}$ ). The observed spectrum in the region ( $\lambda 6850\text{--}\lambda 7200 \text{ \AA}$ ) taken under low dispersion can be seen from strip (c) in Plate XII A, Fig. 1, to consist of four characteristic groups of bands. Of these, two stronger groups beginning at  $\lambda = 7117.0 \text{ \AA}$  and  $\lambda 7171.2 \text{ \AA}$  are identified as the two  $\Delta v = 0$  sequences of two components of a  $^3\Pi\text{--}^3\Sigma$  transition. The weaker groups beginning at  $\lambda = 6892.8 \text{ \AA}$  and  $\lambda = 6941.2$  are identified as two  $\Delta v =$

$\pm 1$  sequences respectively. The double headed nature of the bands of this system designated as  $N(N_1$  and  $N_2)$  can be seen clearly from grating spectrograms shown in strip (d) in Plate XII B, Fig. 2. The data and classification of the bands are given in Table II.

TABLE I  
Band heads of CoCl in the region ( $\lambda 4600$ — $\lambda 5100 \text{ \AA}$ )

Wavonumber	Int.	Classification	Wavenumber	Int.	Classification
system—J <sup>a</sup>			system—J		
21640.4	8	0,0	20358.4	7	1,0 R
21639.0	8	1,1	20356.4	5	1,0 Q
21230.5	5	0,1	20339.4	6	2,1 R
21228.2	5	1,2	20337.7	6	2,1 Q
21225.2	5	2,3	19950.9	9	0,0 R
system—G			19945.8	9	0,0 Q
21335.1	8	0,0	19927.5	8	1,1 R
21320.0	8	1,1	19925.1	8	1,1 Q
21306.0	8	2,2	system—K		
20933.1*	5	0,1	20279.6	5	1,0 R
20923.4*	5	1,2	20277.5	4	1,0 Q
20914.2*	5	2,3	20263.1	5	2,1 R
system—H			20260.3	5	2,1 Q
21263.9	10	0,0	19869.7	10	0,0 R
21257.1	7	1,1	19868.1	10	0,0 Q
21247.2	6	2,2	19851.9	8	1,1 R
20847.9*	3	0,1	19849.9	8	1,1 Q
20842.0*	4	1,2	system—L		
20832.7*	4	2,3	19829.5	9	0,0 R
20825.8*	4	3,4	19826.3	9	0,0 Q
system—I			19804.3	9	1,1 R
21372.5*	3	1,0	19801.2	9	1,1 Q
21365.2*	3	2,1	19781.2	7	2,2 R
21357.9*	3	3,2	19779.2	7	2,2 Q
20969.1*	7	0,0	*Measured on low dispersion plates only.		
20963.4*	5	1,1			

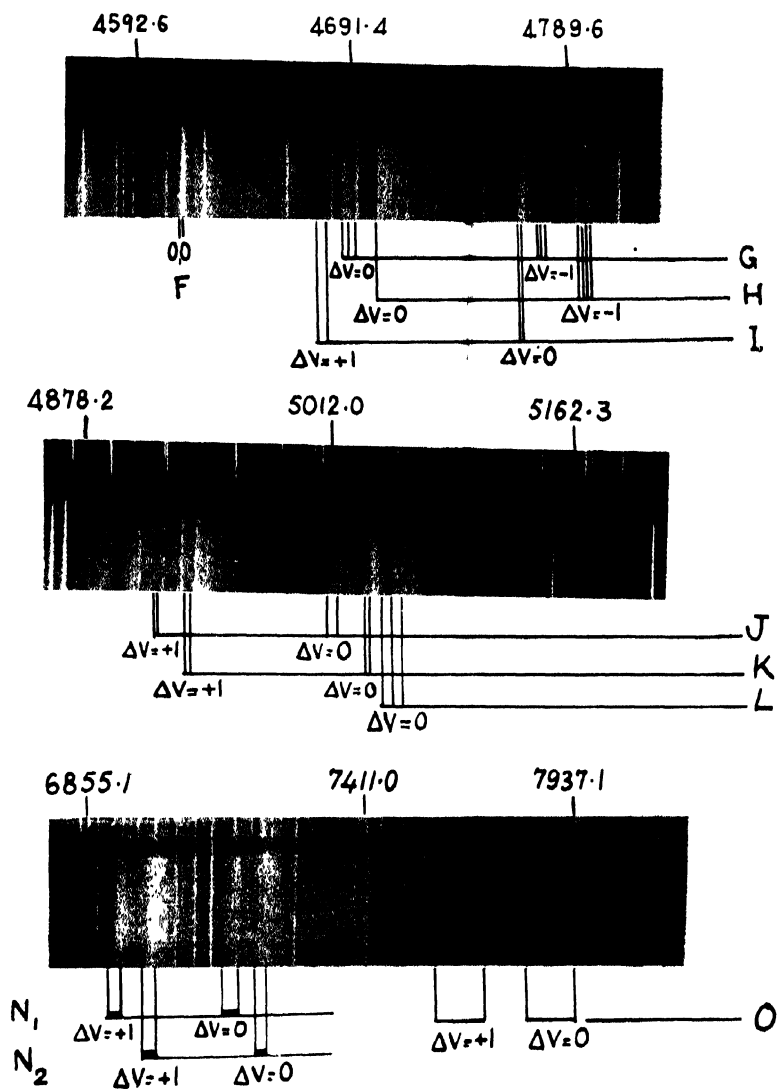


Fig. 1. New band systems of  $\text{CoCl}$  in the photographic infrared and the visible (low dispersion spectrograms).

a — systems F, G, H and I.

b — systems J, K and L.

c — systems  $N_1$ ,  $N_2$  and O.

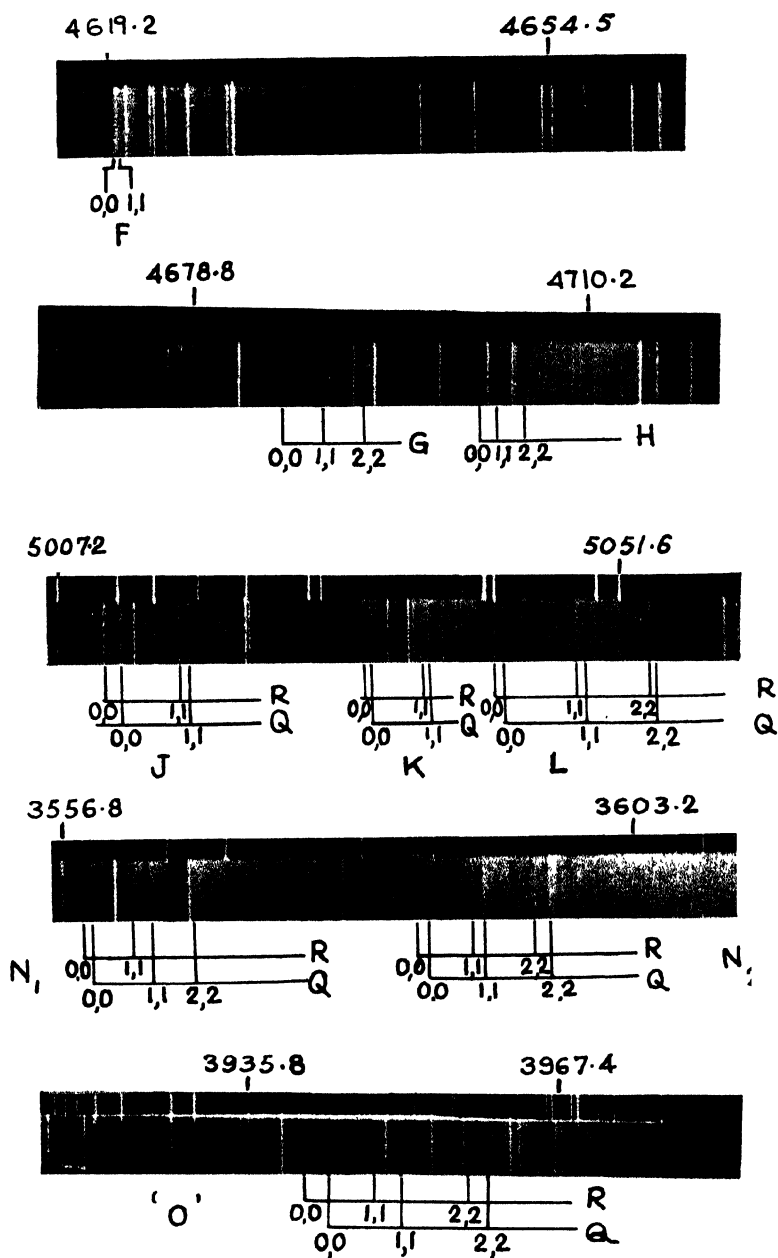


Fig. 2. New band systems of  $\text{CoCl}$  in the photographic infrared and the visible (21 ft. grating spectrograms).

- a —  $\Delta V=0$  sequence of system F.
- b —  $\Delta V=0$  sequence of systems G, H.
- c —  $\Delta V=0$  sequence of systems J, K and L.
- d —  $\Delta V=0$  sequence of systems  $N_1$  and  $N_2$ .
- e —  $\Delta V=0$  sequence of system O.



In the region ( $\lambda 7600$ -- $\lambda 7950 \text{ \AA}$ ) a weaker system (designated as 0) shown in strips (c) in Plate XII A, Fig. 1 and (e) in Plate XII B, Fig. 2, has been observed. The strong group beginning at  $\lambda = 7882.4 \text{ \AA}$  is identified as the  $\Delta v = 0$  sequence and the weaker group beginning at  $\lambda = 7612.2 \text{ \AA}$  as  $\Delta v = +1$  sequence. In the  $\Delta v = 0$  sequence the *R* and *Q* heads are identified while in the weaker  $\Delta v = +1$  sequence only *R* heads have been identified. The data and classifications of the bands are given in Table II. Table III summarizes the vibrational constants of the different band systems of CoCl.

TABLE II  
Band heads of CoCl in the region ( $\lambda 6850$ — $\lambda 7950 \text{ \AA}$ )

Wavenumber	Int.	Classification	Wavenumber	Int.	Classification
system—N <sub>1</sub>			system—O		
14503.9	4	1,0 R	13159.1	4	1,0 R
14501.4	4	1,0 Q	13130.8	5	2,1 R
14483.3	4	2,1 R	13098.8	5	3,2 R
14480.4	5	2,1 Q	12683.0	7	0,0 R
14461.5	6	3,2 R	12674.6	6	0,0 Q
14459.0	6	3,2 Q	12658.6	8	1,1 R
14047.0	3	0,0 R	12650.6	7	1,1 Q
14044.2	3	0,0 Q	12628.2	8	2,2 R
14031.2	5	1,1 R	12621.8	8	2,2 Q
14026.1	5	1,1 Q	*Superposed by atomic line.		
14012.4*	1	2,2 Q			
system—N <sub>2</sub>					
14402.8	4	1,0 Q			
14380.4	5	2,1 Q			
14389.7	5	3,2 Q			
13940.8	4	0,0 R			
13937.7	4	0,0 Q			
13924.1	5	1,1 R			
13920.3	7	1,1 Q			
13904.0	6	2,2 R			
13899.7	10	2,2 Q			

TABLE III

Summary of the vibrational constants of CoCl

System	Wave number of the (0,0) band	$\omega_e'$	$x_e'\omega_e'$	$\omega_e''$	$x_e''\omega_e''$
A	22966.2	420.0	1.66	421.8	1.34
B	22402.7	416.6	0.82	419.4	0.28
C	22182.5	401.0	—	416.2	—
D	22072.3	410.2	—	416.4	—
E	22014.8	420.0	1.14	421.2	0.74
F	21640.4	408.0	—	409.0	—0.45
G	21335.1	391.2	2.15	407.1	2.55
H	21263.9	413.2	2.00	416.8	0.38
I	20969.1	405.0	0.80	409.0	—
J	19945.8	408.6	—1.00	431.0	—
K	19868.1	408.4	—0.50	428.0	—
L	19826.3	—	—	—	—
M	17484.1	412.3	—	416.0	—
N <sub>1</sub>	14044.2	462.5	2.65	482.6	3.65
N <sub>2</sub>	13937.7	467.6	1.25	484.3	0.90
O	12683.0	478.8	1.38	498.4	—1.05

## DISCUSSION

From the magnitude of the vibrational constants of the upper and lower states, More (1938) has suggested that systems A, B and E might belong to a triplet-triplet transition, with intervals of 390 and 562  $\text{cm}^{-1}$ . After the identification of two more systems C and D, Krishnamurty considers that systems E, D and C with separations of 55 and 110  $\text{cm}^{-1}$  may better be represented as belonging to an electronic triplet, while A and B may be identified as two component systems of a triplet  $\rightarrow$  triplet transition. According to us, each of the brief systems A to I consisting of single headed bands arises from a transition with  $\Delta \Lambda = 0$  in Hund's case (a). However in view of the large multiplet splittings known in the ground and low excited states of  $\text{Co}_1$ , it is possible that they are all separate systems with  $\Delta \Omega = 0$  corresponding to Hund's case (c). This view is supported by the fact that Heimer, (1937) from a detailed rotational analysis of CoH bands, has previously identified the  $A \rightarrow X$  transition in CoH as  $\Omega = 4 \rightarrow \Omega = 4$  with  $\Delta \Omega = 0$ , corresponding to Hund's case (c).

The characteristic appearance of the  $N_1$  and  $N_2$  systems observed in the photographic infrared region ( $\lambda 6850\text{--}\lambda 7200\text{\AA}$ ) shown in strip (d) in Plate XII B, Fig. 2, would suggest that they may arise from two components of a  ${}^3\Pi\text{--}{}^3\Sigma$  transition. The magnitude of the vibrational constants of the upper and lower states, the observed double headed nature of the bands, and the close proximity of these two systems lend support to this view. However, both the upper and lower states of this  ${}^3\Pi\text{--}{}^3\Sigma$  transition do not correspond to those observed already in the visible region. They appear to belong to two different excited states of the CoCl molecule. A similar situation is also observed in the band systems of MnF, MnCl and MnBr in the photographic infrared.

#### ACKNOWLEDGMENT

The authors are indebted to Prof. K. R. Rao for his interest in the progress of this work. One of the authors (S.V.K.) acknowledges the financial support from the Council of Scientific and Industrial Research.

#### REFERENCES

- Heimer, A., 1937, *Z. Physik*, **105**, 56.  
Krishnamurty, V. G., 1952, *Ind. J. Phys.*, **28**, 177.  
Krishnamurty, V. G., 1952, Thesis for Doctorate, Andhra Univ., Waltair.  
Mesnage, P., 1935, *C. R., Acad. Sci. Paris*, **200**, 2072.  
Mesnage, P., 1939, *Ann. d. Phys.*, **12**, 5.  
More, K. R., 1938, *Phys. Rev.*, **54**, 122.  
Rao., 1961, *Z. Physik*, (in press)

# ROLE PLAYED BY AMMONIUM SALTS IN THE CLEARING OF NUCLEAR EMULSIONS

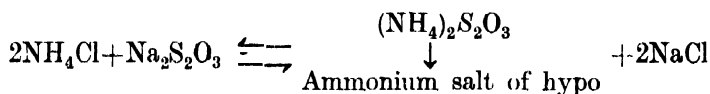
O. N. KAUL

SAHA INSTITUTE OF NUCLEAR PHYSICS, CALCUTTA-9.

(Received March 14, 1961)

**ABSTRACT.** The effect of the addition of various ammonium salts (ammonium chloride, ammonium sulphate, and ammonium acetate) to the usual hypo solution on the clearing time of nuclear emulsions and also their influence on the grain size and the shrinkage factor, have been investigated in view of some contradictory results reported by various authors in recent years. The addition of the ammonium salts has been found to cause a decrease in the clearing time, and then a slight increase after attainment of the optimum concentration. The addition of ammonium salts, however, has been found to have no effect on the grain size or the shrinkage factor of nuclear emulsions. Results obtained have also been explained on the basis of the current theory.

Thick emulsions necessitate longer clearing times, and this prolonged fixation leads to severe distortions in nuclear emulsions. As such, the methods for decreasing the clearing time have been studied by various authors, and it has been found that the addition of ammonium salts to hypo decreases the fixation time considerably, because the ammonium salts of hypo are better complex forming salts with silver halides than the sodium salts of hypo.



Piper worked on this problem, and investigated the change in the clearing time of thin plates with a change in the concentration of ammonium salts. He reported a fall in the clearing time with an increase in the concentration of the ammonium salt, till an optimum concentration is attained, after which, the clearing time has been reported to increase again. Also, according to him the  $\ll \text{Cl} \gg$  ion in ammonium chloride is responsible for eating up the developed grains, near the surface of the emulsion.

Prakash *et al.* (1958) reported a contradiction to the observations made by Piper. According to them, the clearing time decreases up to an optimum concentration of the ammonium salt, after which it remains more or less constant, and does not have an appreciable rise as reported by Piper.

In view of the above contradictions the author found it useful to take up some work in this direction. The observations and the results thus arrived at are reported in this paper.

# EXPERIMENTAL PROCEDURE

The ammonium salts selected were ammonium chloride, ammonium acetate and ammonium sulphate. The first salt was selected, because in addition to ammonium thiosulphate the chlorine ion concentration affects the diffusion rate of the fixer, and therefore, may suppress the reaction and also because it offers a direct verification of the observations made by Piper and those due to Prakash *et al.* Ammonium sulphate and acetate were selected so as to study the effect due of any other two suitable ammonium salts, not tried so far.

For this work Ilford  $K_2$  plates of 100, 200, and 400 microns, and also  $K_0$  and  $G_5$  plates of 200 micron thickness were used, so as to study the effect on the clearing time by a change in the thickness and type of the emulsion. Further, the experiments were conducted in the following stages :

1) Effect of the change in the concentration of ammonium chloride on the clearing time of  $K_2$  Ilford 100 micron plates  $K_2$  and  $G_5$  was studied, using different concentrations of hypo. Plates were directly put in the fixing solution maintained at  $17^\circ\text{C}$ . Care was taken to see that the level of the fixing solution is same in all the three cases. The results are plotted as shown in Fig. 1.

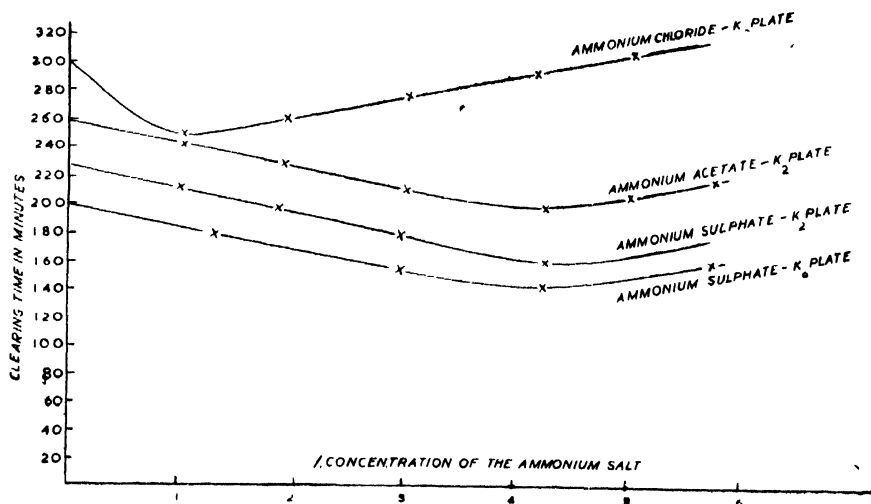


Fig. 1. The percentage concentration of  $\text{NH}_4\text{Cl}$  against the clearing time in minutes for different concentrations of hypo for 100 plates  $K_2$  &  $G_5$  (temperature  $17^\circ\text{C}$ ).

The curves show a fall upto an optimum value of concentration, and then a rise, although the rise is not as pronounced as reported by Piper. Moreover, a shift in the position of optimum concentration was observed with a change in the hypo concentration, as shown in Fig. 1. Change in the type of emulsion, however, has been found to have no effect on the clearing time of the emulsion.

2) Secondly, the change in the clearing time of  $K_2$  and  $K_0$  200 micron plates with a change in the concentration of the three ammonium salts was studied. A

fall, and then a rise has been observed in the case of all the three curves, for ammonium chloride, ammonium sulphate and ammonium acetate. The rise is more pronounced in the case of ammonium chloride than in the case of other two ammonium salts. Results, which have further been found to be independent of the type of emulsion used, are represented in Fig. 2.

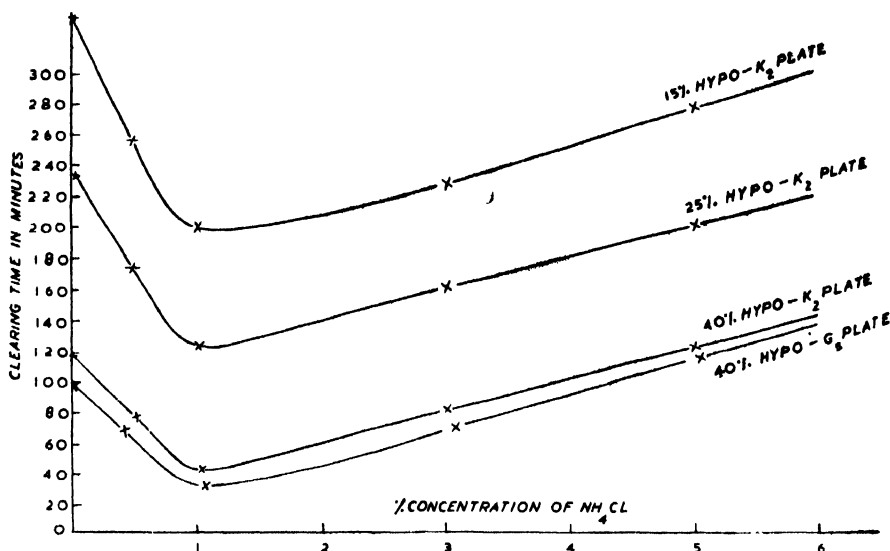


Fig. 2. Percentage concentration of various ammonium salts clearing time in minutes for 200 Ilford K<sub>2</sub> & K<sub>0</sub> plates temperature during clearing 17°C hypo concentration in each solution 40%

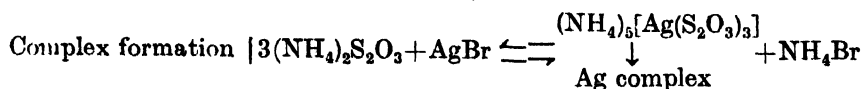
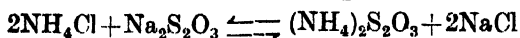
3) Thirdly, the effect of the emulsion thickness over the percentage reduction in the clearing time was investigated in the case of K<sub>2</sub> plates for all the three ammonium salts. The curves were found to have a fall up to 200 microns in all the cases excepting for ammonium chloride where the fall persists beyond 200 microns. These results are plotted as shown in Fig. 3.

#### RESULTS AND DISCUSSION

The results may be discussed in light of the three stages of observations mentioned above.

1. The rise and fall of curves shown in Fig. 1 can be accounted for as follows :

Ammonium salts of hypo being better complex forming salts with silver halides, as compared to sodium salts of hypo, any increase in the concentration of the ammonium salts should decrease the clearing time.



The optimum concentration can be explained on the basis of the reversible nature of the reaction, and so also the shift in the position of the optimum with respect to different hypo concentrations. The rise in the curves may be explained as being due to the fact that higher complexes of ammonium thiosulphate and silver halides are unstable as compared to the higher complexes of sodium thiosulphate, and silver halides. The clearing time, however, is independent of the type of the emulsion as is expected.

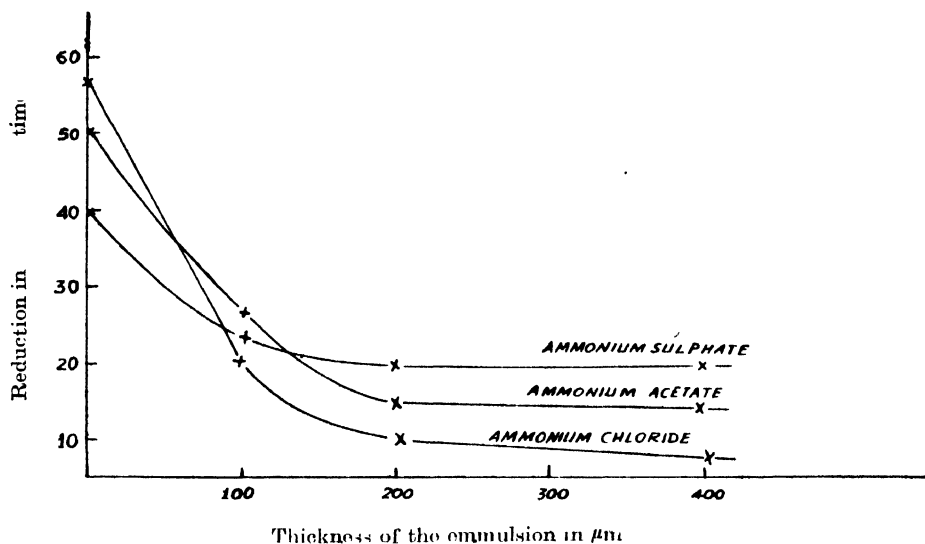


Fig. 3. Emulsion thickness Vs % reduction in the clearing time.

2) A fall, and then a rise in the curves is obtained in case of all the three ammonical salts, as is explained on the basis of the explanations given above. The more pronounced rise observed in the case of ammonium chloride can be explained as being due to the presence of  $\ll \text{Cl} \gg$  ion which effects the rate of diffusion, as chlorine harden the gelatine of the emulsion, thereby increasing the clearing time by effecting the diffusion rate. As this factor is absent in the case of other two ammonium salts, the rise is not as pronounced in their case,

3) The percentage fall goes on decreasing in the case of higher thicknesses for  $\text{NH}_4\text{Cl}$ , whereas for other salts it remains constant after 200 microns. The reason for this is that upto 200 microns the diffusion velocity of the fixing solution decreases with an increase in the thickness, and hence a fall in the curve. In case of ammonium chloride this effect persists beyond 200 microns, because of the contribution of the  $\ll \text{Cl} \gg$  ion, which, however, is not the case with other ammonium salts. Also, the diffusion velocity becomes independent of emulsion thickness beyond  $200\mu\text{m}$ , which explains the flatness of the curves beyond  $200\mu\text{m}$ .

*Effect on the shrinkage factor and the grain size:*

Effect on the grain size was investigated so as to find out whether or not the chlorine eats away the developed grains at the surface as reported by Piper.

For this, the grain size at the top and the bottom of the plate was found in case of pure hypo, and hypo with each of the other ammonium salts. (The optimum concentration being used in each case). The plates of the same type were simultaneously put in the four different baths and the fixing carried out under the same experimental conditions. The observations regarding the shrinkage factor and the grain size are shown in Tables I and II

TABLE I  
Observations regarding the shrinkage factor

Plate thickness in $\mu\text{m}$	Shrinkage factor			
	Pure hypo	Hypo with optimum concentration of $\text{NH}_4\text{Cl}$	$(\text{NH}_4)_2\text{SO}_4$	$\text{NH}_4\text{C}_2\text{O}_4\text{H}_3$
100	2.00	2.16	2.05	2.04
200	2.50	2.60	2.4	2.72
400	2.75	2.50	2.50	2.75

TABLE II  
Observations regarding the grain size

Thickness of the plate in $\mu\text{m}$	Surface of emulsion	Grain size			
		Free hypo	Hypo having optimum concentration of $\text{NH}_4\text{Cl}$	$(\text{NH}_4)_2\text{SO}_4$	$\text{NH}_4\text{C}_2\text{O}_4\text{H}_3$
100	Bottom	0.5	0.75	0.5	0.5
	Top	0.5	0.50	0.5	0.5
200	Bottom	0.75	0.75	0.5	0.75
	Top	0.75	0.75	0.75	0.75
400	Bottom	0.5	0.75	0.5	0.50
	Top	0.75	0.75	0.75	0.50

The study of the shrinkage factor, and the grain size reveals that within the allowed statistics, the shrinkage and the grain size is in no way affected by the addition of the ammonium salts. It also contradicts the hypothesis that chlorine is responsible for eating away the emulsion at the surface. The optimum concentration of the various ammonium salts used by the author are 1.5% for ammonium chloride, 2.5% for ammonium sulphate and 2.5% for ammonium acetate. Relative study of the suitability of these salts as regards the clearing of thick plates :

For thick plates the clearing time depends predominantly upon the diffusion velocity of the fixing solution, as against the thin plates. Consequently then



pH value of the fixing solution becomes an important factor. To make a relative study of the usefulness of these salts as regards the clearing of thick plates, pH values of the various concentrations of these solutions were calculated by the usual formulae, Vogel (1958). The results are shown in Table III:

TABLE III  
Observations regarding clearing time

Conc. of the amm. salt %	.5	1.0	1.5	2.0	2.5	3.0	3.5	4.0
pH-of $(\text{NH}_4)_2 \text{SO}_4$ - (optm. conc.)+ hypo (40%)	5.3	5.6	5.8	6.2	5.7	5.6	5.3	5.0
pH of $\text{NH}_4\text{C}_2\text{O}_4\text{H}_3$ - (optm. conc.)+ hypo (40%)	6.3	6.8	6.9	6.0	7.4	7.8	7.9	8.1
pH-of $\text{NH}_4\text{Cl}$ (optm conc.)+ hypo (40%)	6.1	6.5	6.7	6.8	6.2	5.7	5.4	5.2

The table clearly shows that the pH value of hypo+amm. sulphate and also hypo+amm. chloride solution is well within the acid region, thus ensuring a high diffusion velocity, and the pH value of amm. acetate being in the basic region, it does not have a high diffusion velocity. Therefore, amm. acetate + hypo is not as suitable for clearing as the other two salts. Amm. sulphate, however, has been found to be most suitable for this purpose.

#### ACKNOWLEDGMENTS

The author is grateful to Prof. B. D. Nagchaudhuri, Director of the Institute, for his encouragement and guidance.

Thanks are also due to Prof. D. N. Kundu, head of the *Accelerator Division* for providing the laboratory facilities and to Mr. Bupesh Purkayastha, Head of the *Nuclear Chemistry Division*, for many helpful discussions.

#### REFERENCES

- Piper, "Fundamentals of Photographic Theory", p. 523.  
Prakash, Y., Ahmad, N., and Sharma, A. P., 1958, *Nuovo Cimento* **3**, 717.  
Vogel, A. I., 1958, "A Text Book of Quantitative Inorganic Analysis."

# DIRECTIONAL PROPERTIES OF EXTENSIVE AIR SHOWER ARRAYS

A. BHASKARA RAO AND P. S. GILL

DEPARTMENT OF PHYSICS, MUSLIM UNIVERSITY, ALIGARH

(Received July 12, 1961)

**ABSTRACT.** The simple extensive air shower array proposed by Shen and Singer (1957) for which they claimed about 90% directional efficiency, has been tested by two groups of physicists, McCusker *et al.* (1959) and Layson *et al.* (1960), using it in conjunction with cloud chambers and scintillation counters, respectively. They concluded that the proposed set up has got very poor efficiency in selecting showers in preferred directions. It is pointed out that there are some significant differences between the results of various authors, on this problem and that it is possible to make further improvements in the performance of the device, besides the two methods suggested by McCusker *et al.* (1959).

## INTRODUCTION

Shen and Singer (1957) proposed a simple extensive air shower array consisting of three G. M. counter telescopes, placed at the vertices of a triangle, for which they claimed a directional efficiency of 90%. This arrangement has been tested by McCusker *et al.*, (1959) using a similar unit in conjunction with two cloud chambers. From their experimental results they concluded that there is no great improvement in the angular resolution of the apparatus suggested by Shen and Singer, and it is not of much value in looking for anisotropy in the high energy primary cosmic radiation. Their results indicate that the vertical arrangement leads only to 7% (or at the best 14%) enrichment of showers coming from the near vertical direction. But our results (Bhaskara Rao and Gill, 1960), obtained during the course of an investigation on the influence of geomagnetic field on extensive air showers at Gulmarg, suggest an enrichment value of the order of 55%. With a view to check our Gulmarg data, a similar experiment has been conducted at Aligarh (alt. 680 ft.), again with two telescopes. The experimental results give an enrichment figure of 54% which is very high when compared to that of McCusker *et al.* Moreover, McCusker *et al.*, contented that there is no serious disagreement between their own results and those of Shen and Singer. Even this contention is not justifiable as shown at a latter stage. Further, their results are in disagreement not only with our results, but also with those of Shen and Singer and of Rathgeber (1959). Although the experimental results of Layson *et al.* (1960) agree well with their theoretical calculations, their shower data do not seem to follow the well established  $\cos^2\theta$  law. Finally, whatever might be the actual directional efficiency and usefulness of the shower array proposed by Shen

and Singer, the observed discrepancies are very significant and worth consideration. Further slight improvements can be made in the device.

#### EXPERIMENTAL

The arrangement used consisted of two G.M. counter telescopes of semiangle  $10^\circ$ , with two trays in each. Each tray consisted of four counters connected in parallel. The telescopes could be tilted independently around any axis. All other details of the experiment were exactly the same as mentioned in our paper (Bhaskara Rao and Gill, 1960).

The separation between the telescopes was 40m. Fourfold coincidences were recorded in the East-West and North-South planes, the telescopes being fixed in three positions, vertical,  $45^\circ$  zenith angle and horizontal, in rotation. The position of the telescopes was changed from the E-W plane to N-S plane and vice versa for every twenty days. The data were corrected for pressure and temperature variations using  $\beta = -10\% \text{ cm}^{-1}\text{Hg.}$ , and  $\theta_r = -0.38\%$  per degree C, respectively. Then the average of the shower rates in the two planes was calculated.

#### RESULTS AND DISCUSSION

Here four instances are given, including our own results at Aligarh, to point out the large discrepancies between the results of various authors.

(A) The shower rates corresponding to 40 m separation of the telescopes were given in Table I.

TABLE I  
Coincidence rate vs. zenith angle

Zenith angle 'Z'	Average coincidence rate per hour
$0^\circ$	$4.98 \pm 0.08$
$45^\circ$	$3.69 \pm 0.07$
$90^\circ$	$2.30 \pm 0.06$

$$\text{Percentage enrichment} = \frac{V-H}{V} \times 100\% = 54\%$$

Where  $V$  = Coincidence rate with telescopes in the vertical position,  
 $H$  = Coincidence rate in the horizontal position.

Here it should be remembered that the experimental results of McCusker *et al.*, actually give only 7% enrichment which is very low when compared to our value of 54%.

(B) Some of the experimental results of Rathgeber,

TABLE II

Shower rate in counts per hour

Zenith angle 'Z'	Counters in each telescope.	
	(X) 2 counters	(Y) 3 counters
0°	$1.96 \pm 0.29$	$1.56 \pm 0.27$
90°	$1.25 \pm 0.23$	$0.77 \pm 0.16$

From the columns (X) and (Y), enrichment values can be calculated as 36% and 51% respectively. Evidently, there is large difference between the enrichment values of McCusker *et al.*, and Rathgeber.

(C) Comparison of the experimental results of Shen and Singher and McCusker *et al.*

TABLE III

Experimental determination of zenith angle distribution

Separation between the extreme counters in cms.	Effective zenith angle	Difference of effective zenith angle	Six fold coincidence rate per hour	Percentage difference in the coincidence rate.
Shen and Singer				
(i) 46.2	6.3°	13.2°	0.30±0.020	55%
(ii) 14.8	19.5°		0.46±0.025	
McCusker <i>et al.</i> ,				
(i) 67.0	5.6°	19.2°	0.605±0.039	14%
(ii) 15.0	24.8°		0.692±0.029	

The experimental set up used by McCusker *et al.*, was just similar to that of Shen and Singer. Shen and Singers' results show a difference of 55% in the counting rate for a difference of 13.2° in the effective zenith angle, whereas those of McCusker *et al.*, show only a variation of 14% for 19.2° difference of effective zenith angle. In fact McCusker *et al.*, should have observed a difference larger than 55%. Moreover, McCusker *et al.*, contented that their experimental results are not in serious disagreement with those reported by Shen and Singer. From the above table it is easy to see how they are not justified in their contention.

(D) Experimental results of Layson *et al.*, (1960) :

The directional response of the same set up was also tested by Layson *et al.*, using it in conjunction with the Sydney air shower apparatus. Although they claim that their experimental results are in good agreement with their theoretical calculations, their data do not seem to follow the well known  $\cos^2\theta$  law. The zenithal distribution of showers given by them in the form of histogram, (corres-

ponding to all showers) is compared with the distribution obtained by McCusker *et al.*, with the help of cloud chambers. Even if the directional efficiency of the system were to be low the observed data should have followed the  $\cos^2\theta$  law. Data obtained by McCusker, *et al.*, follows the theoretical distribution well, but the histogram given by Layson *et al.*, is much different from what it ought to be. From Fig. 1(b) it can be seen that the telescopic system records more showers at larger zenith angles (from  $5^\circ$ – $40^\circ$ , at an interval of  $5^\circ$ ) than from the vertical and near vertical i.e.,  $0^\circ$ – $5^\circ$ . In particular the shower rate at  $20^\circ$ – $25^\circ$  is four times the rate at  $0^\circ$ – $5^\circ$ . This discrepancy is of very serious nature, which requires

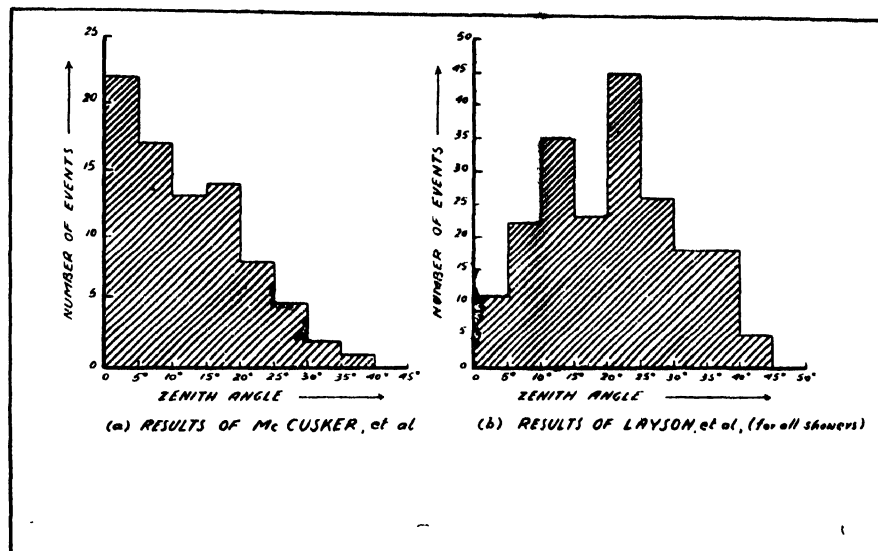


Fig. 1. The frequency of showers of different zenith angles setting off the arrangement.

some explanation. Rossi (1960) attributed the flat distribution of showers observed at Alto (alt. 4100m; shower size  $(10^7 < N < 3 \times 10^7)$  to the fact that the showers are still near their maximum development. But the same arguments cannot hold good in the case of showers recorded at Sydney.

In view of the significant discrepancies in the experimental results of McCusker *et al.*, and other workers, and the irregularities of basic value in the zenithal distribution of showers recorded by Layson *et al.*, one should be cautious in drawing a quantitative conclusion regarding the directional efficiency of the shower array. It is to be emphasized that the directional efficiency of an array decreases at larger zenith angles because of the nonuniformity of the side shower background. McCusker *et al.*, suggested two ways to improve the performance of the device. This can be still improved by using sets of two or more counters connected in parallel, in the telescopes, instead of single counters, at the same time keeping the aperture of the telescopes constant by adjusting the separation between the upper and lower sets suitably. This offers larger sensitive area for shower particles

coming within the defined aperture of the telescopes and helps in reducing the percentage background of side showers from zenith angles, other than the defined aperture, in which we are not interested. This background can also be reduced by increasing the multiplicity of coincidence from six to nine, with a third set of counters in between the upper and lower sets of each telescope. These modifications do not have any significant effect on shower particles falling within the defined angle, but considerably reduce the background.

#### ACKNOWLEDGMENT

One of the authors (A. B. R.) wishes to acknowledge with thanks the valuable discussions he had with Dr. D. E. Page and Dr. B. V. Sreekantan through correspondence. His thanks are also due to the University authorities for the financial help.

#### REFERENCES

- Bhaskara Rao, A. and Gill, P. S., 1960, *Ind. J. Phys.*, **34**, 153.  
Layson, W. M. 1960, *Nucl. Inst. Meth.*, **6**, 179.  
McCusker, C.B.A., 1959, *Phys. Rev.*, **116**, 181.  
Rathgeber, H. D., 1959, *Nature.*, **183**, 386.  
Rossi, B., 1960, *Cosmic Ray Conference, Moscow., Vol. II*, 18-29.  
Shen, K. Y. and Singer, S. F., 1957, *Phys. Rev.*, **106**, 555.

# UNLIKE MOLECULAR INTERACTIONS FOR $\text{CO}_2\text{--N}_2$ AND A FEW OTHER GAS MIXTURES

H. K. SAHOO AND M. N. SHARMA

DEPARTMENT OF PHYSICS  
LUCKNOW UNIVERSITY  
LUCKNOW

(Received August 29, 1961)

**ABSTRACT.** A study of unlike molecular interaction for gas mixtures composed of several slightly non-spherical molecules and also for mixtures having non-spherical and spherical molecules has been done from the observed temperature dependence of second virial coefficient and thermal diffusion factor, assuming a Lennard-Jones (12 : 6) potential energy function. It has been found that this potential energy function which is strictly applicable to spherical molecules can be applied with success to discuss properties of gas mixtures composed of molecules which deviate slightly from spherical symmetry. Further, the values of the potential parameters indicate the inadequacy of simple combining rules for the case of gas mixtures considered here.

## INTRODUCTION

The influence of the law of molecular interaction on properties of gases and gas mixtures is well known and in principle, information about the potential parameters for like and unlike interactions should be obtainable from the experimental determinations of various bulk properties as a function of temperature. Unfortunately, the experimental data for gas mixtures which might lead to a knowledge about the forces between unlike molecules are very meagre. In many cases, the measurements are confined to a single temperature and hence are unsuitable for obtaining any reliable information about intermolecular forces. Thus, generally, for a proper understanding and evaluation of these forces between unlike molecules, use is made of certain empirical combining rules, involving the force parameters of pure components, which have no theoretical justification. Further, these simple combining rules may be valid for central force fields but are certainly not appropriate when we wish to treat molecules like  $\text{CO}_2$ . Thus, it is very useful and desirable to study the unlike molecular interactions from the temperature variation of properties of gas mixtures wherever such data are available.

For discussing and correlating the different properties of gases and gas mixtures, various formulated expressions for the potential energy function are utilized, such as the Lennard-Jones (12:6) and the modified Buckingham (Exp:6) functions. The (Exp:6) function is said to be more realistic and more flexible, but both of

them had practically the same success in predicting the properties of gases and it is difficult to establish the superiority of one potential over the other as has been concluded by Madan (1955), Mason and Rice (1954) and DeRocco and Halford (1958). However, the (12:6) potential energy function is definitely much simpler and easy to handle and has, therefore, been widely used.

Srivastava and Madan (1953) utilized the temperature variation of thermal diffusion factor for the study of the law of molecular interaction for some gas pairs on the (12:6) model. Later, Srivastava and Srivastava (1957, 1959) and Srivastava (1957) used the properties of interdiffusion and thermal diffusion, mostly of rare gas mixtures, for this purpose on the (Exp:6) model. The assumptions in the theory make both the potential energy functions strictly applicable to spherically symmetric molecules, such as those of monatomic gases at moderate pressures. When the molecules of a gas are not spherically symmetric, there are great mathematical difficulties in discussing their properties rigorously and there is no completely adequate analysis of intermolecular forces between asymmetric polyatomic molecules. However, the theory based on the above mentioned potential energy functions has had success in correlating transport phenomena in polyatomic gases and the assumptions may not be a severe limitation as has been discussed by Chapman and Cowling (1952). It is also seen that rather high asymmetry is required before deviations from the force law applicable to spherical molecules become appreciable. Thus, the same law can be taken to describe the properties of molecules which are slightly non-spherical and for all practical purposes, such derivations will be quite adequate. Further, they will also provide a means of extrapolation and interpolation of the existing data into regions of higher or lower temperatures.

In the present paper, we have used the (12.6) model to study the law of molecular interaction involving unlike molecules and have chosen two sets of binary gas mixtures. The one consisting of mixtures of diatomic gases with a common polyatomic gas such as mixtures of  $N_2$ ,  $O_2$  and CO with  $CO_2$  of  $H_2$  with  $BF_3$  and the other consisting of a monatomic gas with diatomic gases and also with a polyatomic gas such as mixtures of A with  $N_2$ ,  $O_2$  and  $CO_2$  and of Kr with  $N_2$ . The latter set is interesting since it involves an interaction between spherical and non-spherical molecules.

Recently, Cottrell *et al.* (1956) determined the second virial coefficients of the mixtures of  $CO_2$  with  $N_2$ ,  $O_2$ , CO and A. Grew *et al.* (1954) have reported the experimental data on thermal diffusion of  $CO_2$ — $N_2$ , A— $N_2$ , Kr— $N_2$  and A— $O_2$  and several other gas mixtures while Raw and Kyle (1956) have reported data on  $H_2$ — $BF_3$  mixtures. We have utilized here both these sets of data for determining the potential parameters. For the gas mixtures chosen, there have been practically no attempts to estimate the potential parameters, in particular, using second virial coefficient and thermal diffusion factor and to correlate the experi-



mental data with the theory based on the Lennard-Jones (12:6) potential. The thermal diffusion of A—N<sub>2</sub> mixture has, however, been used by Srivastava and Srivastava (1957) for an (Exp:6) model and the diffusion data of CO<sub>2</sub>—N<sub>2</sub> and CO<sub>2</sub>—O<sub>2</sub> mixtures by Walker and Westenberg (1958, 1960) for a (12:6) and an (Exp: 6) model but an equilibrium property like the second virial coefficient has not been previously used for this purpose. Although the observed data for second virial coefficient are not too extensive in view of the experimental difficulties and limitations of measurement and also as this is the only data available for gas mixtures at more than one temperature (the other measurements are mostly at a single temperature and hence cannot be used in finding the parameters) it is considered worthwhile to examine these data and make the best possible use of them.

#### THEORY AND FORMULAE

The second virial coefficient  $B_M$ , for a gas mixture is given by the relation

$$B_M = x_1^2 B_{11} + 2x_1 x_2 B_{12} + x_2^2 B_{22} \quad \dots (1)$$

where  $x_1$ ,  $x_2$ ,  $B_{11}$ ,  $B_{22}$  are the mole fractions and second virial coefficients of components 1 and 2 and  $B_{12}$  is the interaction second virial coefficient having a direct relation to the law of unlike molecular interaction through the reduced second virial coefficient  $B^*$  given by Hirschfelder, Curtiss and Bird (1954)

as 
$$B_{12} = b_{12} B_{12}^*(T^*)$$

where 
$$b_{12} = \frac{2\pi}{3} N r_{12}^3 \text{ and } T^* = KT/\epsilon_{12} \quad \dots (2)$$

The parameters  $\epsilon_{12}$  and  $r_{12}$  are the depth of the potential well and the separation distance for zero potential energy for unlike molecular interaction.

The general expression for thermal diffusion factor is quite complicated and moreover, different theoretical expressions are available for this quantity such as those of Chapman and of Kihara. Kihara's expressions are much simpler than the corresponding ones of Chapman and are more accurate as has been observed by Srivastava (1957) and many others and have therefore been used here.  $[\alpha_T]_1$ , Kihara's first approximation formula for thermal diffusion factor may be written in the convenient form

$$[\alpha_T]_1 = (6C^* - 5)g \quad \dots (3)$$

where  $g$  is a complicated expression involving molecular weights, composition and collision integrals for which reference can be made to Srivastava (1957).

The principal contribution towards temperature dependence of thermal diffusion factor comes through the factor  $(6C^* - 5)$  which involves only unlike interactions. The factor  $g$  depends only slightly on temperature. This slight

variation hardly shows any definite trend and is itself liable to uncertainties on account of various errors as has been observed by Srivastava and Madan (1953). Further, even if this variation is considered and is taken account of, as has been done by Srivastava and Srivastava (1957) and Srivastava (1957), the results do not show any appreciable variation, the deviations being well within the limits which result from considerations of the effect of the error in the experimental measurements. Thus  $[\alpha_T]_1$  varying as  $(6C^*-5)$  is quite reasonable for all practical purposes.

#### DETERMINATION OF POTENTIAL PARAMETERS

The methods of determining the potential parameters from the experimental data have been discussed recently by Srivastava and Srivastava (1959), Whalley and Schneider (1955) and Strehlow (1953) and others. They mainly consist of (1) graphical ratio method used successfully by Srivastava and Madan (1953), Madan (1955), (1957), Sharma and Madan (1960) and Bunde (1955); (2) the translational method of Keesom (1912) and Lennard-Jones (1924); (3) the intersection method of Buckingham (1938). The translational method requires data over a large temperature range and unless there are some distinguishable peculiarities in the curve as has been discussed by Srivastava and Srivastava (1957), a multitude of translations is possible and the method fails. The intersection method requires accurate data for only a few temperatures which need not extend over a large temperature interval but the data must be highly accurate, otherwise it is impossible to determine the intersection point. Thus, for most cases, the first method, that is, the graphical ratio method, is quite adequate and suitable for examining and reducing the experimental data appropriately and deducing the potential parameters therefrom. The method is described in detail by Srivastava and Madan (1953), Sharma and Madan (1960) and Madan (1955) and a reference to these can be made.

Usually experimental  $B_{12}$  is obtained from  $B_M$  by using the calculated values of  $B_{11}$  and  $B_{22}$ , utilizing the values of the force parameters obtained from other measurements which is not a very desirable procedure. To determine the parameters between unlike molecules, we have resorted to purely experimental data, that is, to get  $B_{12}$  (experimental), experimentally observed values of  $B_{11}$  and  $B_{22}$  have been utilized. The values of  $\epsilon_{12}/k$  and  $r_{12}$  determined from the temperature dependence of second virial coefficient are reported in Table I, together with the temperature ranges for which they have been calculated. The potential parameters obtained from temperature dependence of thermal diffusion factor are given in Table II(a) & II(b). Using  $\epsilon_{12}/k$ , the value of  $r_{12}$  has been calculated from experimental interdiffusion coefficient wherever such data are available. The potential parameters thus obtained from second virial coefficient and thermal diffusion factor are compared with other determinations including those obtained with the help of the combining rule viz.,  $\epsilon_{12} = (\epsilon_{11}\epsilon_{22})^{1/2}$  and  $r_{12} = \frac{1}{2}(r_{11} + r_{22})$

where  $\epsilon_{11}$ ,  $\epsilon_{22}$  and  $r_{11}$ ,  $r_{22}$  are respectively the depths of the potential wells and the separation distances for zero potential for (1:1) and (2:2) like interactions. These are reported in Tables III and IV.

#### DISCUSSION OF RESULTS

It will be quite interesting to see how far the potential parameters, obtained by us, agree with those derived from other sources and how satisfactorily these parameters can predict another bulk property. The comparison of parameters has been done in Table III and IV from which it can be seen that the parameters obtained by us are different from those derived using combining rules. The values of  $\epsilon_{12}/k$  are higher and those of  $r_{12}$  are lower than the corresponding combining rule values except for  $\text{Kr--N}_2$ . A similar trend was noticed by Barua (1959). This is to be expected as the combining rule for  $r_{12}$  is true only for molecules which behave as rigid spheres.

The system  $\text{CO}_2\text{--N}_2$  is interesting because parameters for this could be determined from both second virial coefficient and the thermal diffusion. The combining rule gives a value 134 for  $\epsilon_{12}/k$  whereas the second virial coefficient gives an indication that this value is  $>>134$  and is about 168. This indication is further confirmed by evaluation of parameters from thermal diffusion factor, which is a more sensitive property and the value obtained is 157.1. This is in agreement with the value obtained by Walker and Westenberg (1958) from the temperature dependence of mutual diffusion. The parameters obtained from equilibrium and non-equilibrium properties are also seen to be different as has also been noticed in general by Hirschfelder *et al.* (1954) and Madan (1955, 1957).

Using the different parameters, we could, for comparison, compute the values of coefficient of interdiffusion, another property for which some data are available for these mixtures. This has been done in Table V. However, in general, the parameters derived from equilibrium properties should not be used for calculation of non-equilibrium properties or vice versa because different properties emphasize the potential energy curves differently and cannot be simply correlated. When we take two similar molecules, for example, two polyatomic molecules, we get a reasonably good agreement, but when we have a mixture of a polyatomic molecule with a simple molecule, the agreement is not satisfactory. The agreement between the theoretical and experimental values is good for  $\text{CO}_2\text{--N}_2$  and  $\text{CO}_2\text{--O}_2$  (rather it is better than that obtained by using parameters from combining rules) but not for  $\text{CO}_2\text{--CO}$  and  $\text{CO}_2\text{--A}$ . In the latter case, for example of  $\text{CO}_2\text{--A}$ , the interaction is between a spherical and a non-spherical molecule. As expected (Srivastava and Srivastava 1959) due to the non-spherical nature of  $\text{CO}_2$  molecule, the potential parameters calculated from second virial coefficient (equilibrium property) do not reproduce the coefficient of mutual diffusion (non-equilibrium property) satisfactorily. In this type of mixture, it seems that the effect of the non-spherical nature of the molecule predominates over that of the spherical

one, even though we can ascribe part of the discrepancy due to possible experimental errors in the measurement of the coefficient of mutual diffusion for this mixture for which there are the data of only one experimenter at a single temperature. This was obtained by Waldmann from a study of diffusion thermo-effect and is subject to much error as has been discussed by Chapman and Cowling (1952). Further, for this mixture, the thermal diffusion factor, a property very sensitive to the force law, increases with decrease of temperature, a peculiar yet unexplained behaviour, and it is not surprising that a good agreement is not obtained in this case.

The case of  $\text{CO}_2$ —CO mixture is different. Here, the interaction is between a symmetrical molecule  $\text{CO}_2$  with an asymmetrical molecule CO, unlike the interactions of  $\text{CO}_2$ — $\text{N}_2$  or  $\text{CO}_2$ — $\text{O}_2$  in which there are symmetrical molecules like  $\text{N}_2$  or  $\text{O}_2$ . Furthermore, the data on second virial coefficient for  $\text{CO}_2$ —CO mixture shows practically no variation with temperature in the range  $30^\circ\text{C}$  to  $60^\circ\text{C}$  and an average curve had to be drawn for the determination of potential parameters which are subject to some uncertainty on this account.

In general, for all the gas mixtures, the non-spherical nature of the molecules does manifest itself and it is not surprising that a single set of parameters fails to give same degree of agreement for two different properties and also over a wide temperature range. For  $\text{CO}_2$ — $\text{N}_2$  mixture, we find good agreement for the coefficient of mutual diffusion, but if the same parameters are used to compute the thermal conductivity, the agreement is not so good as has been reported by Brokaw (1959) and also computed by us and it necessitates the use of a different set of potential parameters for this purpose, even though the discrepancy may also be on account of the complex nature of the phenomenon of thermal conductivity for these molecules.

Unfortunately, for the gas pairs considered here, suitable and extensive data for different properties do not exist and as such, a detailed comparison with experiment is not possible. To arrive at any definite conclusions, it is very desirable to have more experimental data of various properties at different temperatures.

Nevertheless, the analysis is still useful and valid to a good approximation and is definitely of much interest in the absence of sufficient information about the forces between unlike molecules. The evaluation of the potential parameters from the experimental data for the study of forces between unlike slightly non-spherical molecules and the bulk properties of their mixtures, is definitely a better approach than the derivation of these parameters from simple combining rules which are semi-empirical in nature and may be valid only for central force fields.

#### ACKNOWLEDGMENTS

It is a pleasure to thank Dr. M. P. Madan for his guidance and helpful suggestions and Prof. P. N. Sharma for his interest. The work reported here was

supported in part by the Scientific Research Committee, U.P. and the Council of Scientific and Industrial Research, New Delhi. We are also grateful for the award of a Research Assistantship (H.K.S.) by the S.R.C. and a Government of India Research Training Scholarship (M.N.S.)

TABLE I

Values of potential parameters from second virial coefficient

Gas pair	$\text{CO}_2\text{--N}_2$		$\text{CO}_2\text{--A}$		$\text{CO}_2\text{--O}_2$		$\text{CO}_2\text{--CO}$	
Temperature range ( $^{\circ}\text{K}$ )	$\epsilon_{12}/k$ ( $^{\circ}\text{K}$ )	$r_{12}$ ( $\text{\AA}$ )	$\epsilon_{12}/k$ ( $^{\circ}\text{K}$ )	$r_{12}$ ( $\text{\AA}$ )	$\epsilon_{12}/k$ ( $^{\circ}\text{K}$ )	$r_{12}$ ( $\text{\AA}$ )	$\epsilon_{12}/k$ ( $^{\circ}\text{K}$ )	$r_{12}$ ( $\text{\AA}$ )
290–348	166.8	3.560	156.1	3.426	150.3	3.082	179.8	3.272
300–360	169.3	3.516	157.4	3.409	176.5	3.217	179.1	3.281
310–372	170.6	3.492	158.7	3.383	—	—	181.3	3.255
Mean	168.9	3.523	157.4	3.406	163.4	3.449	180.1	3.269

TABLE IIa

Values of potential parameters from thermal diffusion

Gas pair	$\text{CO}_2\text{--N}_2$	$\text{A--N}_2$	$\text{A--O}_2$	$\text{Kr--N}_2$
Temperature range ( $^{\circ}\text{K}$ )	$\epsilon_{12}/k$ ( $^{\circ}\text{K}$ )	$\epsilon_{12}/k$ ( $^{\circ}\text{K}$ )	$\epsilon_{12}/k$ ( $^{\circ}\text{K}$ )	$\epsilon_{12}/k$ ( $^{\circ}\text{K}$ )
125–250	—	—	—	113.8
150–300	—	112.0	121.9	114.5
175–350	—	111.5	115.1	109.4
200–400	—	109.9	119.0	104.2
225–450	—	108.7	122.9	103.7
250–500	176.0	104.2	126.9	105.5
275–550	164.7	—	—	110.5
300–600	154.6	—	—	111.1
325–650	147.7	—	—	115.8
350–700	142.3	—	—	119.0
Mean	157.1	109.2	121.2	110.7
$r_{12}$ ( $\text{\AA}$ )	3.557	3.428	3.309	—

TABLE IIb

$\text{H}_2\text{--BF}_3$		
Temperature range ( $^{\circ}\text{K}$ )	$\epsilon_{12}/k$ ( $^{\circ}\text{K}$ )	Mean $\epsilon_{12}/k$ ( $^{\circ}\text{K}$ )
340–408	104.3	98.9
350–420	98.3	
360–432	94.2	

TABLE III

Comparison of potential parameters obtained from second virial coefficient with those determined from other sources

Gas pair	$\epsilon_{12}/k(^{\circ}K)$			$r_{12}(\text{\AA})$		
	(*)	(a)	(b)	(*)	(a)	(b)
CO <sub>2</sub> -N <sub>2</sub>	168.9	132	134.1	3.523	3.839	4.095
CO <sub>2</sub> -A	157.4	153	150.5	3.406	3.707	3.948
CO <sub>2</sub> -O <sub>2</sub>	163.4	147	149.4	3.449	3.715	3.975
CO <sub>2</sub> -CO	180.1	145	137.6	3.269	3.793	4.125

(\*) Present work

(a) Combining rule, individual parameters from viscosity.

Hirschfelder, Curtiss and Bird (1954).

(b) Combining rule, individual parameters from second virial coefficient.

Cottrell *et al.* (1956)

TABLE IV

Comparison of potential parameters obtained from thermal diffusion with those determined from other sources.

Gas pair	$\epsilon_{12}/k(^{\circ}K)$				$r_{12}(\text{\AA})$			
	(*)	(**)	(a)	(b)	(*)	(**)	(a)	(b)
CO <sub>2</sub> -N <sub>2</sub>	157.1	168.9	157	132	3.557	3.523	3.516	3.839
A-N <sub>2</sub>	109.2	—	—	106	3.428	—	—	3.550
A-O <sub>2</sub>	121.2	—	—	118	3.309	—	—	3.426
Kr-N <sub>2</sub>	110.7	—	—	132				
H <sub>2</sub> -BF <sub>3</sub>	98.9	—	—	80.37				

(\*) From thermal diffusion (present work)

(\*\*) From second virial coefficient (present work)

(a) Walker and Westenberg (1958)

(b) Hirschfelder, Curtiss and Bird (1954). Combining rule and individual parameters from viscosity.

TABLE V  
Comparison of calculated and experimental values of interdiffusion

Gas mixture	Temperature (°K)	(*) $D_{12}$ (cm <sup>2</sup> /Sec)	(a) $D_{12}$ (cm <sup>2</sup> /Sec)	experimental $D_{12}$ cm <sup>2</sup> /Sec. (b)
$\text{CO}_2\text{--N}_2$	273.2	0.141	0.130	0.144
	288.2	0.156	0.143	0.158
	293.2	0.161	0.147	0.160
	298.2	0.166	0.152	0.165(c) 0.167(d) 0.168(e)
$\text{CO}_2\text{--A}$	293.2	0.159	0.136	0.140
$\text{CO}_2\text{--O}_2$	273.2	0.143	0.128	0.139 0.137(f)
	293.2	0.163	0.146	0.160 0.153(f)
$\text{CO}_2\text{--CO}$	273.2	0.163	0.128	0.137

- (\*) Present work, parameters are given in Table I.  
(a) Calculated using combining rules, individual parameters from viscosity. Hirschfelder, Curtiss and Bird (1954).  
(b) Data taken from Hirschfelder, Curtiss and Bird (1954) unless stated otherwise.  
(c) Boyd *et al.* (1951)  
(d) Walker and Westenberg (1958).  
(e) Boardman and Wild (1937)  
(f) Walker and Westenberg (1960)

#### REFERENCES

- Barua, A. K., 1959, *Ind. J. Phys.*, **33**, 221.  
Boardman, L. E. and Wild, N. E., 1937, *Proc. Roy. Soc. (London)*, **A162**, 511.  
Boyd, C.A. 1951, *J. Chem. Phys.*, **19**, 548.  
Brokaw, R. S., 1959, *J. Chem. Phys.*, **31**, 571.  
Buckingham, R. A., 1938, *Proc. Roy. Soc. (London)*, **A 168**, 264.  
Bunde, R. E., 1955, University of Wisconsin, C.M-850, August.  
Chapman, S. and Cowling, T.G., 1952, *The Mathematical Theory of Non-Uniform Gases* (Cambridge University Press, New York)  
Cottrell, T. L., Hamilton, R.A., and Taubinger, R.P., 1956, *Trans. Faraday Soc.*, **52**, 1310.  
De Rocco, A.G., and Halford, J.O., 1958, *J. Chem. Phys.* **28**, 1152.  
Grew, K.E., Johnson, F.A. and Neal, W.E.J., 1954, *Proc. Roy. Soc. (London)* **A 224**, 513.  
Hirschfelder, J.O., Curtiss, C.F., and Bird, R.B., 1954, *Molecular Theory of Gases and Liquids* (John Wiley & Sons, New York).

- Reesom, W.H., 1912, Leiden Comm. Suppl. No. 25.
- Lennard-Jones, J.E., 1924, *Proc. Roy. Soc. (London)*, **A106**, 463.
- Madan, M.P., 1955, *J. Chem. Phys.*, **23**, 763.
- Madan, M.P., 1957, *J. Chem. Phys.*, **27**, 113.
- Mason, E.A. and Rice, W.F., 1954, *J. Chem. Phys.*, **22**, 843.
- Raw, C.J.G., and Kyle, E., 1956, *Trans. Faraday Soc.*, **52**, 1216.
- Sharma, M.N., and Madan, M.P., 1960, *Proc. Nat. Inst. Sci.*, **26A**, 49.
- Srivastava, B.N., and Madan, M.P., 1953, *Proc. Phys. Soc. (London)* **A66**, 277.
- Srivastava, B.N., and Srivastava, K.P., 1957, *Physica*, **23**, 103.
- Srivastava, B.N., and Srivastava, K.P., 1959, *J. Chem. Phys.* **30**, 984.
- Srivastava, K. P., 1957, *J. Chem. Phys.*, **26**, 579.
- Strehlow, R. A., 1953, *J. Chem. Phys.*, **21**, 2101.
- Walker, R. E., and Westenberg, A. A., 1958, *J. Chem. Phys.*, **28**, 1139.
- Walker, R. E., and Westenberg, A. A., 1960, *J. Chem. Phys.*, **32**, 436.
- Whalley, E., and Schneider, W. G., 1955, *J. Chem. Phys.*, **23**, 1644.



# RAMAN AND INFRARED SPECTRA OF 1-FLUORO-2, 4-DINITROBENZENE AND 1-CHLORO-2, 4-DINITROBENZENE\*

K. C. MEDHI

OPTICS DEPARTMENT,

INDIAN ASSOCIATION FOR THE CULTIVATION OF SCIENCE, CALCUTTA-32.

(Received September 2, 1961)

## Plate XIII

**ABSTRACT.** The Raman and infrared spectra of 1-fluoro-2,4-dinitrobenzene and 1-chloro-2,4-dinitrobenzene have been investigated and the observed frequencies have been assigned to different modes of vibration of the ring, by assuming  $C_2$  symmetry for the molecules. Some of the vibrational frequencies due to vibrations within the  $\text{NO}_2$  group have also been identified. It is observed that some of the modes of the skeleton (C-C ring which are forbidden in infrared and *vice versa* in the case of benzene, appear in the spectra and it is concluded that the symmetry of the skeleton ring is disturbed by the substituents.

## INTRODUCTION

The assignment of vibrational frequencies of some trisubstituted benzene compounds was made recently by Deb and Banerjee (1960) by studying the Raman and infrared spectra of the compounds. Such assignment was not made by any previous worker in the case of 1-fluoro-2, 4-dinitrobenzene and 1-chloro-2, 4-dinitrobenzene. In fact, the infrared spectra of these two compounds and the Raman spectra of the fluoro compound were not known. The present investigation was undertaken to study the infrared spectra of these two compounds and the Raman spectrum of 1-fluoro-2, 4-dinitrobenzene and to identify the frequencies of different modes of vibration of the molecules. The fluorine and chlorine substituted compounds have been chosen, because by comparing the spectra it might be possible to get some results which would help accurate assignment of the frequencies.

## EXPERIMENTAL

The compounds supplied by E. Merck were of guaranteed reagent quality. The liquid 1-fluoro-2, 4-dinitrobenzene was distilled under reduced pressure before use while the chloro compound was purified by crystallization from benzene. The infrared spectra were recorded with a Perkin Elmer Model 21 spectrophotometer with rocksalt optics, the resolution dial being set at 927. The absorption

---

\*Communicated by Professor S. C. Sirkar

spectra of very thin films of the substances enclosed between NaCl plates were recorded. In the case of 1-chloro-2,4-dinitrobenzene the molten compound was poured on a hot NaCl plate and a similar hot plate was placed on it so that a thin film of the pure substance was enclosed between the plates. The spectrum of the solidified film was recorded. The Raman spectra of both the compounds were recorded on Ilford Zenith plates using a Fuess Glass Spectrograph of large dispersion. Iron arc spectrum was also photographed on the plate for

TABLE I.

Raman and infrared frequencies of 1-fluoro-2,4-dinitrobenzene

Infrared bands $\nu$ in $\text{cm}^{-1}$ & strength	Raman shift ( $\text{cm}^{-1}$ ) & Intensity	Assignment
	164 (2b)	a'' fundamental
	300 (0)	a' "
	513 (1b)	a' "
630 (w)	634 (3)	
672 (w)		a'' "
706 (s)		a' "
743 (s)	742 (1b)	a'' "
813 (w)	811 (1)	a'' "
840 (vs)	835 (3)	a' "
917 (s)	925 (2)	a'' "
973 (wb)		
1008 (vw)		
1072 (s)	1070 (2)	a' "
1129 (ms)	1129 (1)	a' "
1153 (w)	1151 (5)	a' "
1244 (m)	1241 (2)	a' "
1272 (vs)	1269 (6)	a' "
	1296 (0)	
	1323 (2)	a' "
1347 (vs)	1346 (10)	a' "
1418 (ms)	1415 (3)	a' "
1490 (s)	1490 (2)	a' "
1525 (vs)		a' "
1551 (s)	1546 (6)	a' "
1606 (vs)	1616 (5)	a' "
1805 (w)		743 + 1072
1939 (w)		[706 + 1244 813 + 1129]
2082 (w)		917 + 1153 840 + 1244]
2877 (w)		1272 + 1606 1347 + 1525]
2962 (w)		1551 + 1418
3100 (s)	3102 (2b)	a' fundamental

TABLE II  
Raman and infrared frequencies of 1-chloro-2,4-dinitrobenzene.

Infrared bands $\nu$ in $\text{cm}^{-1}$ & strength	Raman shifts ( $\text{cm}^{-1}$ ) & intensity (Harrand, 1953)	Assignment
	152 (1b)*	a'' fundamental
	205 (0)*	a' "
658 (w)	666 (1)	a'' "
687 (m)		a' "
730 (s)		a' "
745 (m)		a'' "
832 (ms)		a'' "
847 (m)	841 (1)	a' "
900 (s)		a'' "
912 (m)		
980 (vw)		
1040 (s)	1050 (1)	a' "
1080 (vwh)		
1099 (vw)	1109 (1)	a' "
1138 (m)		a' "
1151 (m)	1160 (2)	a' "
1210 (vw)		
1247 (w)	1255 (1)	a' "
1302 (wh)	1301 (2)	a' "
1346 (vs)	1358 (10)	a' "
	1396 (1)	
1421 (mh)		a' "
1459 (m)		a' "
	1472 (0)	
	1494 (0)	
1525 (vs)	1538-50 (1b)	a' "
1550 (s)		
1590 (vs)	1593 (3)	a' "
	1628 ?	
1698 (vw)		658 + 1040
1742 (vwh)		832 + 900
1785 (vw)		745 + 1040
1820 (vwh)		2 $\times$ 900
1967 (w)		832 + 1138
2873 (wh)		1421 + 1459
3053 (w)		1459 + 1590
3100 (s)		a' fundamental

\*Observed in the reinvestigated Raman spectrum by the present author.

comparison. The Hg line 4358 Å was first used to excite the Raman spectra but it was found that in the case of 1-chloro-2, 4-dinitrobenzene the absorption in the neighbourhood of the 4358 Å line was very strong and no line with Raman shift less than  $666\text{ cm}^{-1}$  was observed. Hence the Hg line 5461 Å was used as the exciting line and Agfa Isopan plates were used to photograph the spectra.

## RESULTS AND DISCUSSION

The spectrograms showing Raman lines of 1-fluoro-2, 4-dinitrobenzene and 1-chloro-2, 4-dinitrobenzene are given in Figs. 1 and 2, Plate XIII and the infrared absorption curves are reproduced in Figs. 3(a) & (b) and 4(a) & (b). The

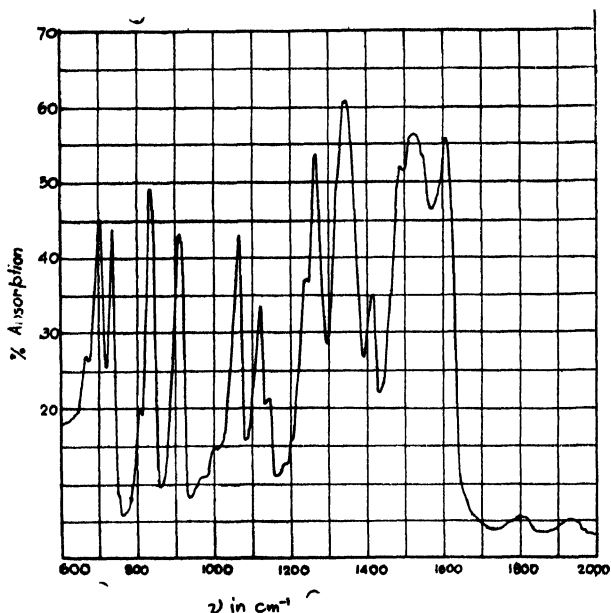


Fig. 3(a). Infrared spectrum of 1-fluoro-2,4 dinitrobenzene (liquid at 26°C)

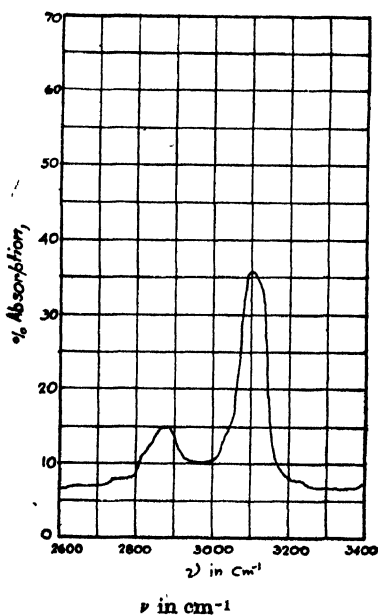


Fig. 3(b). Infrared spectrum of 1-fluoro-2,4 dinitrobenzene (liquid at 26°C)



Fig. 1. Raman spectrum of 1-fluoro-2,4-dinitrobenzene (liquid at 30°C).

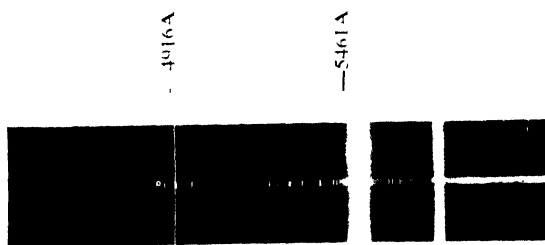


Fig. 2. Raman spectrum of 1-chloro-2,4-dinitrobenzene (solid at 30°C).



Raman shifts of the two substances and the infrared frequencies are given in Tables I and II respectively. The Raman frequencies of 1-chloro-2, 4-dinitrobenzene reported by Harrand (1953) have also been included in Table II. Tentative assignments of the lines are given in the third column of Tables I and II. The numbering of the modes of the vibrations has been made following that for the benzene ring made by Pitzer and Scott (1943).

The molecules of both the compounds belong to  $C_s$  point group, if the  $\text{NO}_2$  group lies in the plane of the molecule. There are four modes of types  $a_{1g}$ ,  $b_{1u}$ ,  $e_g^+$  and  $e_u^-$  in the benzene molecule giving rise to  $a'$  type C—H valence oscillations in these two molecules. The infrared frequency  $3100\text{ cm}^{-1}$  observed in the case of both the compounds represent such  $a'$ -type C—H vibrational frequency and they may be identified with  $e_u^-$  mode in benzene (Mode No. 20) in which the two diametrically opposite C—H vibrate in opposite phases against the ring, the other substituents remaining almost stationary.

In the spectrum of 1-fluoro, 2, 4-dinitrobenzene a characteristic frequency  $1272\text{ cm}^{-1}$  is observed while in the spectrum of 1-chloro-2, 4-dinitrobenzene there is a characteristic frequency  $730\text{ cm}^{-1}$ . These two frequencies approximate to C—F and C—Cl vibrational frequencies respectively and they are to be assigned to  $a'$ -type mode arising from  $e_u^-$  type C—H stretching mode in benzene discussed above.

The degenerate  $e_g^+$  mode of C—C vibration of frequency  $1596\text{ cm}^{-1}$  (No. 8A, B) in benzene will split up into two components with reduction of symmetry to  $C_s$ , one of the components being slightly reduced in frequency and the other remaining almost unaffected. These two components have been identified with the strong infrared bands  $1606$  and  $1551\text{ cm}^{-1}$  of 1-fluoro-2, 4-dinitrobenzene and  $1590$  and  $1550\text{ cm}^{-1}$  of 1-chloro-2, 4-dinitrobenzene. The  $e_u^-$  mode (No. 19A, B) in benzene similarly becomes  $a'$ -type vibration giving rise to the frequencies  $1490$  and  $1418\text{ cm}^{-1}$  of 1-fluoro-2, 4-dinitrobenzene and  $1459$  and  $1421\text{ cm}^{-1}$  of 1-chloro-2, 4-dinitrobenzene. These assignments are in agreement with those proposed for other 1, 2, 4-trisubstituted benzenes (Plyler *et al.*, 1957, Deb and Banerjee, 1960). These lines appear strongly in the Raman effect owing to the lack of centre of symmetry. The Raman frequency  $513\text{ cm}^{-1}$  of 1-fluoro-2, 4-dinitrobenzene might be a component of the  $e_g^+$  vibration of benzene (No. 6A, B), which splits up into two frequencies with lowering of symmetry, the other component having a still lower frequency may be identified with the Raman line  $300\text{ cm}^{-1}$ . This mode may give the Raman line  $205\text{ cm}^{-1}$  in the 1-chloro compound, the other component being too weak to be recorded.

The  $a'$ -components of in-plane CH bending modes of the two molecules may be derived from similar modes  $a_{2g}$  (No. 3),  $b_{2u}$  (No. 15),  $e_g^+$  (No. 9) and  $e_u^-$  (No. 18) of benzene. Superposition of modes  $a_{2g}$  and  $e_g^+$  of benzene may give rise to the mode of frequency  $1244\text{ cm}^{-1}$  and  $1247\text{ cm}^{-1}$  in the fluoro and chloro com-

pound respectively. Similar superposition of modes  $e^-_u$  and  $e^+_g$ , may give rise to the frequencies 1153 and 1151  $\text{cm}^{-1}$  in the two compounds. The frequencies 1129 and 1138  $\text{cm}^{-1}$  of the two respective compounds may be similarly produced by the interaction of  $b_{2u}$  and  $e^-_u$  modes of benzene. The observed frequencies 706

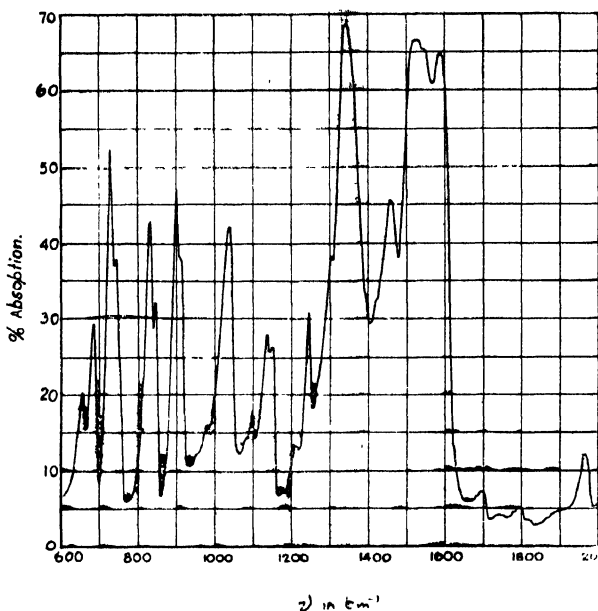


Fig. 4(a). Infrared spectrum of 1-chloro-2,4-dinitrobenzene (solid at 28°C).

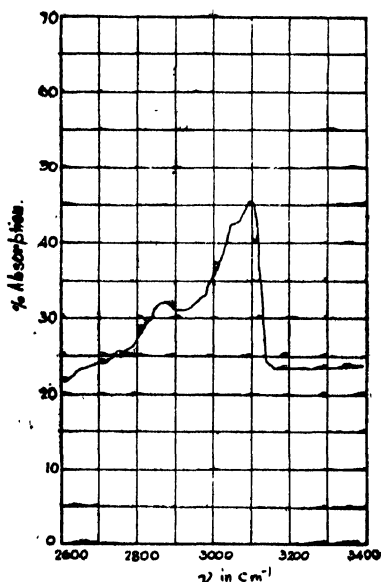


Fig. 4(b). Infrared spectrum of 1-chloro-2,4-dinitrobenzene (solid at 26°C).



and  $1072\text{ cm}^{-1}$  in the case of the fluoro compound and  $687$  and  $1040\text{ cm}^{-1}$  in the case of the chloro compound may represent components of the modes  $e^-_g$  and  $e^+_g$ .

The four out-of-plane CH bending modes of benzene ( $e^-_g$ ,  $a_{2u}$ ,  $e^+_u$  and  $b_{2g}$ ) give such bending modes of type  $a''$  in the case of these molecules assumed to belong to  $C_s$  point group. Superposition of modes  $b_{2g}$  (No. 5) and  $e^-_g$  (No. 10B) may give rise to a mode in which only the two diametrically opposite C—H bonds undergo out of plane bending. This frequency may be  $917\text{ cm}^{-1}$  which appears both in Raman and infrared spectra of 1-fluoro-2, 4-dinitrobenzene ( $900\text{ cm}^{-1}$  in 1-chloro-2, 4-dinitrobenzene). The modes No. 10A and 17A of types  $e^-_g$  and  $e^-_u$  of benzene may similarly interact to produce frequencies  $813$  and  $832\text{ cm}^{-1}$  observed in the spectra of the two compounds.

Norman Jones and Sandorfy (1956) discussed the occurrence of a C—H bending vibrational frequency at about  $745\text{ cm}^{-1}$  in the case of 1, 2, 4-trisubstituted benzenes which is, according to them, known to be active only in Raman effect, but it should be noted that in the present work a strong frequency at  $743\text{ cm}^{-1}$  in the case of 1-fluoro-2, 4-dinitrobenzene and a similar frequency at  $745\text{ cm}^{-1}$  in the case of 1-chloro-2, 4-dinitrobenzene have been observed in the infrared. This can be obtained from superposition of the modes  $e^+_u$  (No 17A) and  $a_{2u}$  (No. 11).

The frequencies  $672$  and  $658\text{ cm}^{-1}$  observed in 1-fluoro-2, 4-dinitrobenzene and 1-chloro-2, 4-dinitrobenzene respectively represent out-of-plane carbon bending vibration corresponding to the  $b_{2g}$  mode in benzene (No.4) which is expected to remain unaltered with substitution. The Raman frequency at  $164\text{ cm}^{-1}$  observed in the case of the fluoro compound and  $152\text{ cm}^{-1}$  in the case of the chloro compound may represent another such out-of-plane bending mode derived from  $e^+_u$  mode in benzene (No.16).

In the case of 1-fluoro-2, 4-dinitrobenzene and 1-chloro-2, 4-dinitrobenzene, frequencies at  $840$  and  $847\text{ cm}^{-1}$  respectively have been observed. Similar frequencies were also observed in the spectra of 2, 4- and 3, 4-dichlorotoluene and 1, 2, 4-trichlorobenzene (Deb and Banerjee, 1960). As suggested in a previous paper (Deb and Banerjee, 1960) these frequencies may originate from superposition of  $a_{1g}$  and  $b_{1u}$  modes (No. 1 and 12) in benzene. The frequencies  $1323\text{ cm}^{-1}$  of 1-fluoro-2, 4-dinitrobenzene and  $1302\text{ cm}^{-1}$  of 1-chloro-2, 4-dinitrobenzene may be a component of the  $e^+_g$  mode of benzene.

Besides these molecular frequencies, the spectra of both the compounds should contain frequencies due to vibration in the  $\text{NO}_2$  groups. The results for fluoronitro- and chloronitrobenzenes obtained by previous workers have been tabulated in Landolt-Börnstein's Tables (1951). On comparing these results the frequencies  $1525$  and  $1347\text{ cm}^{-1}$  of 1-fluoro-2, 4-dinitrobenzene and  $1525$  and  $1346\text{ cm}^{-1}$  of 1-chloro-2, 4-dinitrobenzene can be readily identified with asymmetric and symmetric stretching vibration in  $\text{NO}_2$  groups.

## ACKNOWLEDGMENT

The author is indebted to Professor S. C. Sirkar, D.Sc., F.N.I. for his kind interest and guidance and to Dr. S. B. Banerjee for valuable advice and help during the progress of the work.

## REFERENCES

- Deb, K. K. and Banerjee, S. B., 1960, *Ind. J. Phys.*, **34**, 554.  
Harrand, M., 1953, *Ann. d. Physik.*, **8**, 126.  
Landolt-Börnstein, 1951, *Zahlenwerte und Funktionen*, 1 Band, 2 Teil.  
Norman Jones, R. and Sandorfy, C., 1956, *Chemical Applications of Spectroscopy* (Interscience Publishers Inc., New York)  
Pitzer, K. S., and Scott, D. W., 1943, *J. Am. Chem. Soc.*, **65**, 803.  
Pyler, E. K., Harry, C., Allen Jr. and Tidwell E. D., 1957, *J. Res. Nat. Bureau of Standards*, **58**, 255.

# Letters to the Editor

*The Board of Editors will not hold itself responsible for opinions expressed in the letters published in this section. The notes containing reports of new work communicated for this section should not contain many figures and should not exceed 500 words in length. The contributions must reach the Assistant Editor not later than the 15th of the second month preceding that of the issue in which the letter is to appear. No proof will be sent to the authors.*

6

## PERIODICITY IN NUCLEAR BINDING ENERGY AND CORRELATION BETWEEN THE ISOTOPES OF DIFFERENT NUCLEI

A. K. DUTTA

PALIT PROFESSOR OF PHYSICS, UNIVERSITY COLLEGE OF SCIENCE,  
CALCUTTA-9.

(Received August 31, 1961)

The binding energy of the nuclei is measured by the difference between the observed masses of the nuclei and the sum of the masses of the constituent nucleons. To explain the variation of the binding energy  $E$  for different nuclei, Bethe and Weiszäcker have proposed the following relation

$$E = -a_1A + a_2A^{2/3} + a_3 \frac{Z^2}{A^{1/3}} + a_4 \frac{(N-Z)^2}{4A}$$

where  $A$  is the atomic number,  $N$  and  $Z$  are the numbers of neutrons and protons and  $a_1$ ,  $a_2$ ,  $a_3$  and  $a_4$  are constants to be fixed by actual comparisons. The formula above, though broadly successful, is not adequate to explain precise mass data closely. Various efforts (Green, 1958 and Seeger, 1961) have been made to improve upon the Bethe-Weiszäcker relation by including pairing correction distinguishing nuclei composed of different combination of even and odd number of protons and neutrons, effects of shell structure and nuclear deformation and so on; however, the agreement of these improved formulae with observed data is not satisfactory. In view of this unsatisfactory situation, it is considered worthwhile to emphasize the deviations of the Bethe-Weiszäcker relation from the latest mass data of as many stable nuclei as are available and to see whether the deviations indicate any regular and systematic pattern.

Here we have plotted for different nuclei  $\Delta M$ , the deviation of the experimentally observed binding energy (in MeV) from the Bethe-Weiszäcker relation

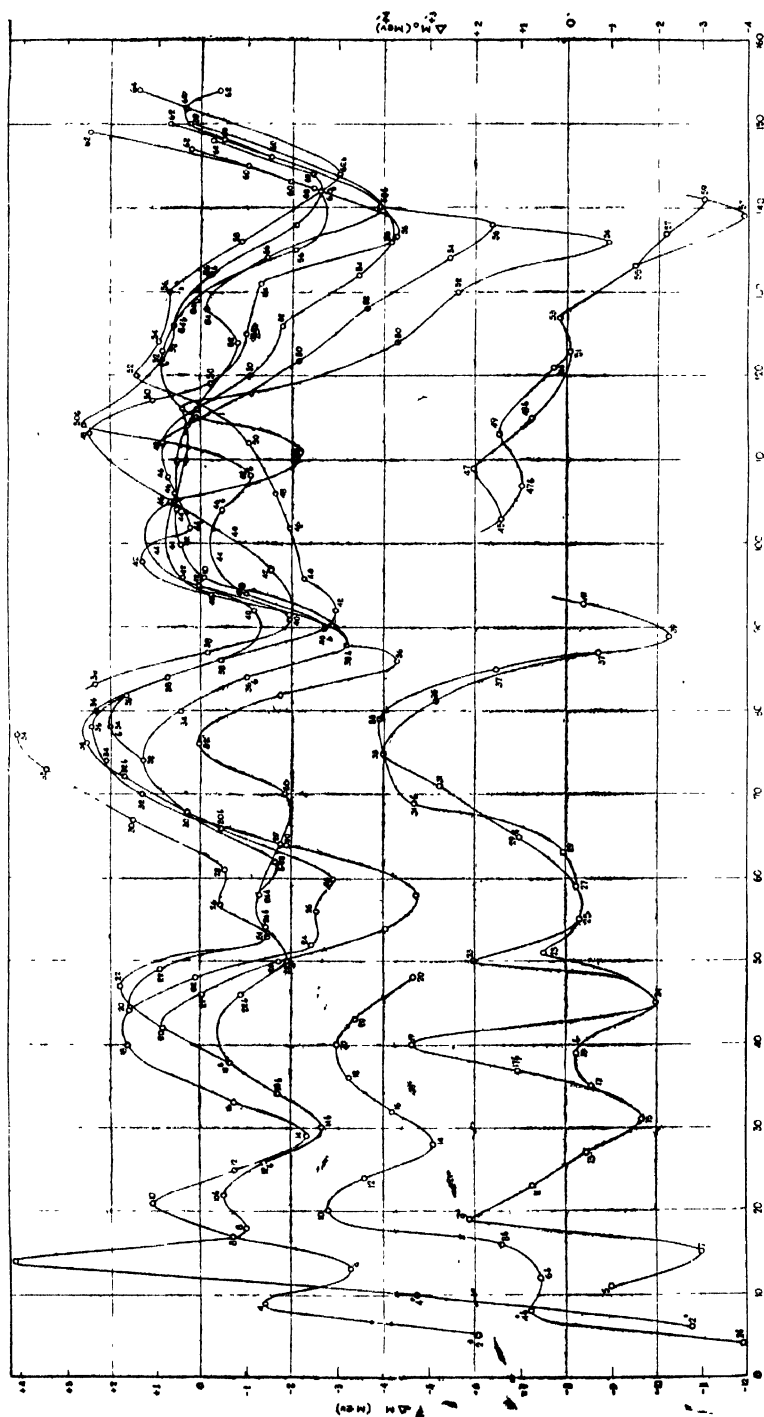


Fig. 1-  $\Delta M$ -A curves for even and odd charge stable nuclei with scales on the left and right sides respectively. Few unstable nuclei are marked with asterisk. The charges are indicated at the points. Most strongly bound nuclei are denoted by 'b' in addition.

with the values of the four constants as given by Green (1954). The experimental data have been taken from the work of Duckworth (1958) up to atomic number  $Z = 62$  for which range the nuclear masses of all the stable isotopes are given except for  $Z = 44$ . For the selection of the points through which to draw a certain curve, we have divided the nuclei into two sets, one with odd values of  $Z$  and the other with even values of  $Z$ . The set of even values of  $Z$  is further subdivided into categories depending upon the excess number of neutrons over protons, whether it is none, one, two, three and etc. When the minimum excess of neutrons changes from one stable element to the next one, the curve is drawn connecting the two minimum excess isotopes even though the excess of neutrons is not the same along the curve. Further when the total number of stable isotopes varies from one element to the next, there is branching or merging of curves depending upon whether the number of isotopes increases or decreases at that point; in the case of ambiguity mostly, near the region of branching or merging the points are so chosen that the curve connecting them follows a regular smooth course.

The curves drawn in accordance with the principles stated above show regular undulating character with a smooth run, the maxima and minima of all the different courses fall at near about the same region of mass number.

From the above curves it is possible by way of interpolation to predict the values of masses of the isotopes of  $Z = 44$  which are not tabulated by Duckworth. The element  $Z = 44$  has seven stable isotopes with mass number  $A = 96, 98, 99, 100, 101, 102$  and  $104$ ; Duckworth has given the masses of the isotopes with  $A = 96, 102$  and  $104$ . By the method of interpolation of curves we have calculated the possible masses of the remaining isotopes. After the completion of this work it has come to our notice that Everling (1960) has supplied the masses of  $A = 98$  and  $99$  as well as of  $A = 96, 102$  and  $104$ , and the agreement of our extrapolated results with Everling's for  $A = 98$  and  $99$  is as good as that of Everling's results with Duckworth's for  $96, 102$  and  $104$ .

#### REFERENCES

- Duckworth, H.E., 1958, *Mass Spectroscopy*, Appendix (Cambridge University Press).  
Everling, F., Konig, L.A., Mathauch, J.H.E., and Wapstra, A.H., 1960, *Nuclear Physics*, **18**, 529.  
Green, A.E.S., 1954, *Phys. Rev.*, **95**, 1006.  
Green, A.F.S., 1958, *Rev. Mod. Phys.*, **30**, 569.  
Seeger, P.A., 1961, *Nuclear Physics*, **25**, 1.

# ON THE APPLICABILITY OF DEBYE'S THEORY IN THE DETERMINATION OF THE TIME OF RELAXATION IN THE CASE OF PURE LIQUIDS

DILIP KUMAR GHOSH

OPTICS DEPARTMENT,

INDIAN ASSOCIATION FOR THE CULTIVATION OF SCIENCE,

CALCUTTA -32.

(Received August 24, 1961)

It is well known that in the case of polar liquids the dipole moment of polar molecules cannot be determined from the polarization of the pure liquid by applying Debye's expression. The object of the present note is to point out that there is some justification in applying Debye's equation for the polarization at high-frequency oscillating field for the determination of the value of  $\tau$ , the time of relaxation even in the case of pure liquids.

In the case of dilute solutions Whiffen and Thompson (1946) have taken the condition for maximum absorption as that for the maximum value of  $\epsilon''$  and the latter occurs when,

$$\omega_{max} \tau_0 = 1 \quad \dots (1)$$

This is justified in the case of dilute solution, because  $\epsilon'$  may be assumed to be independent of frequency,  $\epsilon'$  and  $\epsilon''$  being the real and imaginary parts respectively of the complex dielectric constant  $\epsilon^*$ . It is to be noted, however, that this condition for maximum absorption deduced by previous workers for solution is the condition for the occurrence of maximum value of  $\epsilon''$  and not of  $\tan\delta$ , and therefore, it is not applicable to pure liquids. If we want to find out the condition for maximum value of  $\tan\delta$  in the case of pure liquids we find that  $\tan\delta$  will be maximum when,

$$\omega \tau_0 = \sqrt{\frac{\epsilon_1}{\epsilon_0}} \quad \dots (2)$$

where  $\epsilon_1$  is the dielectric constant for static field and  $\epsilon_0$  that for a field of infinite frequency.

Hence, the condition  $\omega_{max} \tau_0 = 1$  cannot be applied in cases of pure liquids, because in such cases  $\epsilon_1/\epsilon_0$  is much greater than unity and according to Eq. (2)  $\omega \tau_0$  is greater than unity.

On the other hand, according to Debye's equation, the condition for maximum absorption is given by

$$\nu_{max} \tau = \frac{\epsilon_0 + 2}{\epsilon_1 + 2} \cdot \sqrt{\frac{\epsilon_1}{\epsilon_0}} \quad \dots \quad (3)$$

Taking a typical case of benzyl chloride for which  $\epsilon_0 \approx n^2 = 2.4$  and  $\epsilon_1$  is about 8, we get from Eq. (3),  $\tau = 0.792/\omega_{max}$ , but from Eq. (1) we get  $\tau_0 = \frac{1}{\omega_{max}}$

$$\therefore \frac{\tau}{\tau_0} = 0.792$$

So, the value of  $\tau$  deduced from Debye's equation is about 20% smaller than that deduced from Eq. (1). Since the radius of the rotor is proportional to  $\tau^{1/3}$  this difference will not affect the radius of the rotor by more than 7%. This explains why in the case of liquids with molecules having the OH group as a substituent the radius of the rotor deduced from Debye's equation (Ghosh, 1945a, b, 1955a, b, c) was found to be appropriate for the OH group.

#### REFERENCES

- Ghosh, D. K., 1954 a, *Ind. J. Phys.*, **33**, 191.  
 Ghosh, D. K., 1954 b, *Ind. J. Phys.*, **33**, 485.  
 Ghosh, D. K., 1955 a, *Ind. J. Phys.*, **29**, 161.  
 Ghosh, D. K., 1955 b, *Ind. J. Phys.*, **29**, 450.  
 Ghosh, D. K., 1955 c, *Ind. J. Phys.*, **29**, 581.  
 Whiffen, D. H. and Thompson, H. W., 1946, *Trans. Farad. Soc.*, **42A**, 114.

# COHESIVE ENERGIES AND OTHER PROPERTIES OF IONIC CRYSTALS

M. N. SHARMA AND M. P. MADAN

PHYSICS DEPARTMENT,  
LUCKNOW UNIVERSITY,  
LUCKNOW.

(Received June 7, 1961)

Many properties of gases and liquids have been calculated and explained in terms of a commonly used interaction energy function, such as Lennard-Jones (12:6) potential. In an ionic crystal, the charge distribution on each ion has approximately spherical symmetry and they interact according to central force law. Thus, it seems reasonable to assume that ions of an ionic crystal are of the same electronic structure as an inert gas, possess overlap energy (and Van der Waals energy), following a law with the same interionic distance variation as for two inert gas atoms. It is therefore, possible to describe a number of properties of ionic crystals on a common basis with the help of Lennard-Jones (12:6) potential in conjunction with the term for Coulomb energy. This, thus, affords a unified approach for evaluating and interpreting the properties of ionic crystals as well as the knowledge about the interaction forces and it is reasonable to assume that such an analysis will achieve considerable success.

The energy per cell in an ionic crystal may be represented as

$$\phi(r) = \left( -\frac{\alpha e^2}{r} + \frac{B}{r^{12}} - \frac{C}{r^6} + \epsilon_0 \right) \quad \dots \quad (1)$$

where  $\alpha$  is Madelung's constant,  $e$  is the electronic charge,  $r$  is the interionic distance,  $B$  is the repulsive parameter which is calculable,  $C$  is the Van der Waals constant and  $\epsilon_0$  is zero point vibrational energy.

In Eq. (1) we have not considered the dipole-quadrupole Van der Waals term and effect of overlap potentials other than the nearest neighbours because they do not alter the estimates of various properties appreciably.

Finding the first and second derivatives of Eq. (1) and equating it with the well known expressions involving compressibility, molar volume and temperature (Huggins, 1937) expressions for the parameters  $B$  and  $C$  can be derived and their values obtained with the help of the experimental data for various observable properties. Alternatively,  $B$  can be obtained in the above manner and  $C$  can be used directly from the optical data of Huggins and Mayer (1933).



TABLE I

Crystal	Cohesive energy in K Cal/mole				Compressibility in $10^{-12}\text{cm}^2/\text{dyne}$			Coefficient of thermal expansion $\times 10^6$		
	Experi- mental	Calcu- lated (present work)	Calcu- lated (Powder)	Calcu- lated (Cubiccio- tti) <sup>a</sup>	Calcu- lated (Huggins <sup>b</sup> )	Experimental <sup>a</sup>	Calcu- lated (present work)	Experi- mental	Calcu- lated (present work)	Calcu- lated (Born model) <sup>b</sup>
CsF	—	182.4	176.9	179.2	175.7	4.25	3.97	—	—	—
CsCl	157.8	156.8	157.3	153.9	153.1	5.95	5.53	56.0	55.27	56.18
CsBr	152.3	151.6	153.5	151.1	149.6	7.96	6.39	—	—	—
CsI	145.4	142.9	147.7	143.6	142.5	8.57	7.44	—	—	—
	(141.5) <sup>b</sup>									
RbCl	163.6	167.0	165.7	164.3	162.0	6.65	5.45	36.0	31.52	41.05
RbBr	158.0	162.6	160.6	157.6	156.1	7.94	6.60	38.0	42.61	41.90
RbI	149.7	150.1	153.5	149.1	148.0	9.57	8.57	—	—	—
KBr	161.2	165.5	166.3	162.7	161.3	6.70	5.45	40.0	37.44	43.08
KI	152.8	155.1	158.8	153.4	152.4	8.54	7.13	—	—	—
NaI	166.3	166.8	170.8	165.9	164.3	7.07	4.68	48.3	47.99	42.87

(H) Huggins (1937)

(a) Cubicciotti (1959)

(b) Kumar (1960)

pressions can be derived for various crystal properties and the values of the  $B$  and  $C$  can be used to compute them. Following this scheme we calculated the values of the cohesive energy, compressibility and the coefficient of linear expansion for a few representative alkali halide crystals (reported in Table I,) and compared them with the experimental values and also with other determinations. The results based on the Lennard-Jones (12:6) potential are quite consistent with other determinations. The discrepancies with the experimental data become more pronounced as we proceed towards lighter alkali halides but the agreement is quite satisfactory for heavier compounds. Details and also computations for other metal halide crystals heavier than alkali halides will be published later.

#### ACKNOWLEDGMENT

It is a pleasure to thank Professor P. N. Sharma for his interest in this problem. One of us (M.N.S) expresses his appreciation of a Govt. of India Research Training Scholarship awarded to him.

#### REFERENCES

- Cubicecotti, D., 1959, *J. Chem. Phys.*, **31**, 1646.  
Fowler, R.H., 1955, 'Statistical Mechanics' (Oxford University Press).  
Huggins, M.L., 1937, *J. Chem. Phys.*, **5**, 143.  
Huggins, M.L., and Mayor, J.E., 1933, *J. Chem. Phys.*, **1**, 643.  
Kumar, S., 1959, *Proc. Nat. Inst. Sci. India*, **25**, 364.

EMISSION BAND SPECTRUM OF  $\text{SeO}_2$  MOLECULE

P. B. V. HARANATH,\* AND V. SIVARAMAMURTY

PHYSICS DEPARTMENT, ANDHRA UNIVERSITY, WALTAIR

(Received January 20, 1961)

## Plate XIV

**ABSTRACT.** The emission spectrum of pure  $\text{SeO}_2$  vapour as excited in a high frequency discharge from an oscillator and in an uncondensed discharge from a transformer, is found to reveal a number of characteristic bands in the region  $\lambda$  4700 to  $\lambda$  2750. These bands are diffuse and are attributed to the emitter, the triatomic  $\text{SeO}_2$  molecule. About 100 bands in the region  $\lambda$  4700 to  $\lambda$  3200 are analysed as belonging to two new systems of  $\text{SeO}_2$  molecule arising out of transitions from the deformation vibrational levels of the upper states to symmetric vibrational levels of the lower states. The following are the vibrational constants of the two systems.

	0,0,0	Sym. vib. frequency of lower state	Def. vib. frequency of upper state
System -I.	32145 $\text{cm}^{-1}$	910.5 $\text{cm}^{-1}$	182 $\text{cm}^{-1}$
System -II.	32052 $\text{cm}^{-1}$	911.5 $\text{cm}^{-1}$	182 $\text{cm}^{-1}$

Bands below  $\lambda$  3200 down to  $\lambda$  2750 are found to belong to a part of the B - X system of  $\text{SeO}_2$  molecule observed previously in absorption.

## INTRODUCTION

In our recent investigation on the spectra of the dioxides of selenium and tellurium, it has been found that the emission of pure  $\text{SeO}_2$  vapour excited in electrical discharges revealed a characteristic band spectrum consisting of a number of new bands in the visible and near ultraviolet region. The origin and nature of these new bands have been discussed in this paper.

## EXPERIMENTAL

Selenium dioxide employed in the present investigation is a white powder which sublimes at  $315^\circ\text{C}$ . The substance was perfectly dehydrated before it was introduced into the discharge tube. Spectra were excited by an oscillator of approximately 50 Watt output power at 10 m.c.s. frequency and in an uncondensed discharge from a 10 KV transformer. The oscillator discharge tube was an ordinary pyrex glass tube of 30 cm. in length and 20 mm in diameter. One end of the tube was drawn into an adaptor and was connected to a system of high vacuum pumps. The other flat end was closed by a quartz window. The electrodes drawn directly across the tank circuit of the oscillator, were wrapped

\*National Research Fellow.

round the discharge tube. A flowing vapour of the substance was maintained inside the tube by continuous evacuation and by occasional heating with Bunsen flame.

In the case of transformer discharge experiments, a similar discharge tube was employed but provided with two side limbs at 10 cm apart fused with tungsten electrodes to which the high tension of 10KV was applied. In both these discharges the colour of the emission free from usual impurities is deep blue.

Spectra were photographed on Hilger Medium Quartz, Fuess, Hilger's Quartz Littrow and Glass Littrow spectrographs and were recorded on Ilford Special Rapid plates. The times of exposures were of 5 to 10 minutes duration on the low dispersion instruments and of 20 to 30 minutes duration on the high dispersion instruments.

#### RESULTS

The emission of  $\text{SeO}_2$  vapour excited in different electrical discharges revealed a characteristic spectrum of a number of bands in the region  $\lambda 4700$ — $\lambda 2700$ . Plate XIV, Fig. 1(a) and (b) are the reproductions of the spectra photographed on the medium quartz instrument. The band heads in the region  $\lambda 4700$ — $\lambda 3200$  (strip-a) appear diffuse and those below  $\lambda 3200$  down to  $\lambda 2700$  (strip-b) are sharp and red degraded. Each of these diffuse bands when photographed on high dispersion Littrow spectrographs, was resolved into a number of component heads of different intensities which might correspond probably to the isotopic effect of selenium in the  $\text{SeO}_2$  molecule. About 100 band heads in the region  $\lambda 4700$ — $\lambda 3200$  were measured on a number of high dispersion plates and the accuracy of the band head data was found to be within the limits of 2 to 3  $\text{cm}^{-1}$ .

The wavelength data of these new bands were compared with the band head data of the well known spectra of the diatomic  $\text{SeO}$  and  $\text{Se}_2$  molecules excited under similar conditions. They totally disagree and the spectra of the three molecules appear entirely different from each other. On the other hand, the new bands do not appear to possess the characteristic rotational structure, even when photographed on the high dispersion instruments, which should be the case if they belong to the diatomic  $\text{SeO}$  molecule. On the basis of this experimental evidence, the 100 bands in the region  $\lambda 4700$ — $\lambda 3200$  obtained in the present investigation, could tentatively be assigned to the triatomic emitter  $\text{SeO}_2$  molecule. The sharp red degraded bands in the region below  $\lambda 3200$  to  $\lambda 2700$  were found to belong to a part of the previously known *B-X* system of  $\text{SeO}_2$  observed in absorption by Duchesne and Rosen (1941).

#### ANALYSIS OF THE BANDS

Already three systems—namely, A, B and C, are observed (Choong Shin Piaw, 1938; Duchesne and Rosen, 1947) in absorption of  $\text{SeO}_2$  vapour in which B and C

TABLE I  
Vibrational analysis of system I

$v_1'$	$v_2''$	0	1	2	3	4	5	6	7	8	9	10	11	12	13
0.	32145	31234	30352	29426	28535	27645	26762	25883	25010	24144	23289	—	21599	—	—
1.	32326	31416	30511	29614	28713	27833	26946	26068	25195	24323	23470	22617	—	—	—
2.	—	—	30695	29798	28889	28007	27125	26252	25370	24501	23651	22795	22795	—	—
3.	—	—	—	29975	29068	28184	27301	26410	25547	24681	23822	—	—	—	—
4.	—	—	—	30148	29248	28366	27471	26592	25728	24860	23992	—	—	—	—
$\Delta G(v_2')$		910.5	903.5	900	900	884	884	880	871	868	857	845.5			

TABLE II  
Vibrational analysis of system II

$v_1'$	$v_2''$	0	1	2	3	4	5	6	7	8	9	10	11	12	13
0.	32052	31143	30226	29339	28446	27552	26668	25790	24919	24054	23200	22356	21520	—	—
1.	32234	—	30423	29523	28626	27732	26848	25973	25097	24238	23379	22537	21703	—	—
2.	—	31409	30601	29699	28804	27913	27032	26152	25277	24412	23558	22710	21882	21053	—
3.	—	—	30779	—	28982	28089	27213	26327	25456	24589	23736	22888	—	—	—
4.	—	—	—	—	29161	28270	—	26503	25633	24754	23910	—	—	—	—
$\Delta G(v_2')$		909	902.5	900	895	893	881	880	873	867	853	845.5	833	829	—

occurring in the regions  $\lambda 3400$ — $\lambda 2200$  and  $\lambda 4500$ — $\lambda 3400$  respectively, are more extensive. There are possibilities that the present emission bands in the region  $\lambda 4700$ — $\lambda 3200$ , might either belong to system C or form an extension of system B. No agreement was found between the wave-length data of these emission bands and the absorption bands of C-X system occurring in this region. Attempts made to extend the analysis of B-X system to include the present emission bands yielded no satisfactory analysis. The emission bands above  $\lambda 3200$  appear diffuse whereas the bands below  $\lambda 3400$  belonging to the B-X system are sharp and red degraded. As such, the series of emission bands in the region  $\lambda 4700$ — $\lambda 3200$  cannot be attributed to either of the two systems B and C and are to be considered as forming one or more new systems of  $\text{SeO}_2$  molecule.

The whole series of new bands in the region  $\lambda 4700$ — $\lambda 3200$  are analysed as belonging to two new overlapping systems to each of which every alternate band belongs. These two systems are designated here as Systems I and II and their vibrational analyses are presented in Tables I and II.

In both the systems, several characteristic long lower state progressions are developed. Some of these prominent progressions are marked in Plate XIV, Fig. 1(a) & (b). An average difference of  $910 \text{ cm}^{-1}$  is observed between the successive bands near origin of the system in each progression of the two systems. This frequency of  $910 \text{ cm}^{-1}$  can be identified with or can be considered as a similar one to the previously known symmetric vibrational frequency  $\omega''_2 = 910 \text{ cm}^{-1}$  for the ground state of  $\text{SeO}_2$  molecule derived from the absorption work of C-X system by Duchesne and Rosen (1947)

For each system, only four upper state progressions are formed with a characteristic difference of about  $180 \text{ cm}^{-1}$  between the successive bands. The low value of this frequency in each system suggests that this has to be identified as the deformation vibrational frequency of the corresponding excited states of  $\text{SeO}_2$  molecule. Thus, the transitions observed in the two systems are from the vibrational levels of the upper states with deformation frequency  $\omega'_1 = 182 \text{ cm}^{-1}$  to the vibrational levels of lower states with symmetric frequency  $\omega''_2 = 910 \text{ cm}^{-1}$ .

The vibrational constants for the two emission systems as obtained from the analysis are as follows.

	$\nu_{0,0-0}$ $\text{cm}^{-1}$	Symmetric vib. frequency of the lower state $\omega''_2$	$X''_2\omega''_2$	Def. vib. frequency of the upper state. $\omega'_1$
System I	32145	$910.5 \text{ cm}^{-1}$	$3.0 \text{ cm}^{-1}$	$182 \text{ cm}^{-1}$
System II	32052	$911.5 \text{ cm}^{-1}$	$2.5 \text{ cm}^{-1}$	$182 \text{ cm}^{-1}$

Since, the corresponding average  $\Delta G(v''_2)$  values of the lower state progressions are almost equal in the two systems, they might be considered of having a common

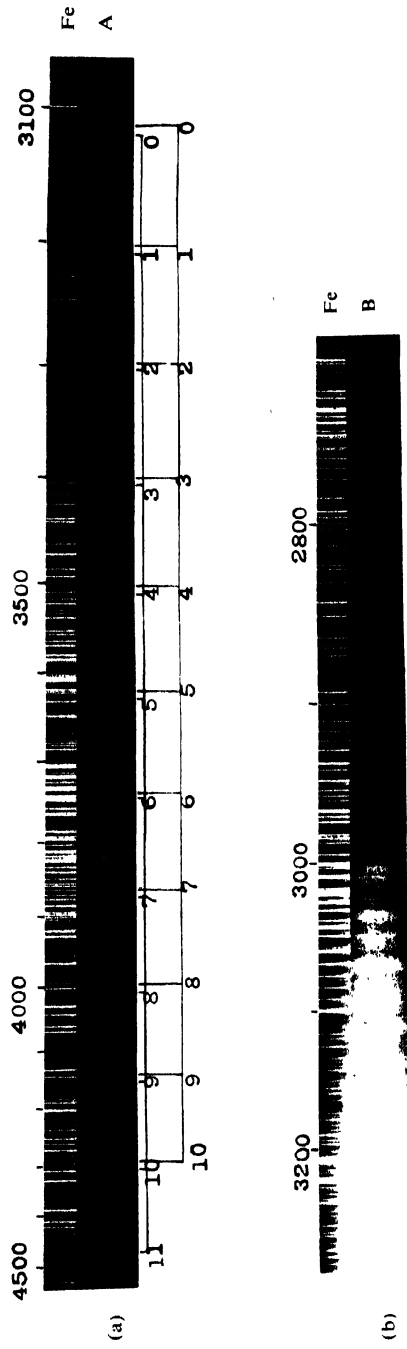


Fig. 1 (a) Emission spectrum of FeO<sub>2</sub> Vapour (  $\lambda$  4500 –  $\lambda$  3200 ).  
(b) Emission spectrum of FeO<sub>2</sub> Vapour (  $\lambda$  3200 –  $\lambda$  2700 ).





lower state. However, it is difficult to conclude whether this common lower state is the same as the normal state of SeO<sub>2</sub> molecule, since these bands are not observed in absorption.

ACKNOWLEDGMENTS

The authors wish to express their grateful thanks to Dr. P. T. Rao and Prof. K. R. Rao for their kind interest in this work.

REFERENCES

- Choong Shin Piaw, 1938., *Ann. Phys.*, **10**, 191.  
Duchesne and Rosen, 1941, *Physica*, **8**, 540.  
Duchesne and Rosen, 1947, *J. Chem. Phys.*, **15**, 633.

# THE SHAPE OF THE TARGET MOLECULE AND THE DIFFUSION DISTANCE OF RADICALS FORMED BY IONIZING RADIATION

S. B. BHATTACHARJEE AND N. N. DAS GUPTA

BIOPHYSICS DIVISION,

SAHA INSTITUTE OF NUCLEAR PHYSICS,

CALCUTTA-9, INDIA.

**ABSTRACT.** The increased sensitivity of any micro-organism, when irradiated in wet condition, is explained by the radical formation in the film of water surrounding the vital molecules and the diffusion of these radicals to the vital molecules causing their inactivation. This diffusion distance can be obtained from a measurement of the doses of radiation for inactivation in the dry and wet conditions. This distance is a function of the shape of the vital molecule, the number of effective radicals per primary ionization and the ratio of dry to wet irradiation doses. In this paper is reported a simple method for estimation of this diffusion distance for an ellipsoidal target of any axial ratio for any measured value of dry and wet irradiation doses.

## INTRODUCTION

Biological material is more sensitive to radiation in the wet than in the dry state of irradiation. This additional inactivation of biological samples, when irradiated in hydrated condition, is due to the formation of radicals in the water surrounding the vital molecules, some of which subsequently diffuse to these and inactivate them (Zirkle and Tobias, 1953; Hutchinson, 1957; Hutchinson and Ross 1959; Hutchinson and Norcross, 1960). The diffusion distance in the different cases has been estimated on the assumption of a spherical target. In a recent paper Hutchinson and Arena (1960) have calculated the diffusion distance in the case of irradiation of DNA *in vivo*. They assumed the model of a right cylinder.

In the present report, a simple theory has been developed for estimation of the diffusion distance for the general case of ellipsoidal target molecule. This method enables one to determine the diffusion distance for any measured values of dry and wet irradiation doses, for any axial ratio and for different probabilities of inactivation by radical formation.

This theory has been used to calculate the diffusion distance from the experimental data on dry and wet inactivation of different enzymes as presented by previous workers.

# ANALYSIS OF INDIRECT EFFECT

If the inactivation is due to a single-hit type of process the survival ratio  $S = N/N_0$  after dose of  $D$  rads is given by

$$S = \exp(-I\sigma V) \quad \dots (1)$$

where  $I$  is the number of primary ions per cc of unit density material produced by the dose  $D$  rads and  $V$  is the volume of a target molecule responsible for inactivation. Assuming that 1 rad of energy absorption releases  $5.68 \times 10^{11} \sigma$  primary ions per cc of the target material of density  $\sigma$ , the total target volume  $V$  is given by

$$V = \frac{1}{D_d \times 5.7 \times 10^{11} \sigma} \text{ cc} = \frac{1.76 \times 10^{12} \text{ \AA}^3}{D_d \sigma} \quad \dots (2)$$

where  $D_d$  is the dose of radiation giving 37 per cent survival in the dry condition.

If the target molecule be assumed as an ellipsoid of revolution with the semi-axes  $a$  and  $b$ , the axis of revolution being the  $b$  axis, the volume  $V$  is given by

$$V = \frac{4\pi}{3} ab^2 = 4.18pb^3 \text{ \AA}^3 \quad \dots (3)$$

where  $p = a/b. \quad \dots (4)$

Combining Eqs. (2) and (3), the dimensions of the target molecule is given by

$$b = \frac{7.5 \times 10^3}{(D_d p \sigma)^{1/3}} \text{ \AA} \quad \dots (5)$$

If  $\sigma$  be assumed as 1.33 for protein

$$b = \frac{6.81 \times 10^3}{(D_d p)^{1/3}} \text{ \AA} \quad \dots (5a)$$

The effect of hydration is to increase the target dimensions by an additional thickness of water, from which the radicals can diffuse to the target and inactivate it. If it is assumed that in the wet condition of irradiation, each target molecule is surrounded by an uniform layer of water of thickness  $\rho$  \AA, then the volume of this water film is given by

$$v_w = \frac{4\pi}{3} [(a+\rho)(b+\rho)^2 - ab^2] = \frac{4\pi}{3} [\rho^3 + \rho^2 b(2+p) + \rho b^2(1+2p)]$$

Replacing  $b$  from Eq. 5(a)

$$v_w = \frac{4\pi}{3} [\rho^3 + 6.81 \times 10^3 \cdot \frac{2+p}{p^{1/3}} \cdot \frac{1}{D_d^{1/3}} \rho^2 + 4.63 \times 10^7 \cdot \frac{1+2p}{p^{2/3}} \cdot \frac{1}{D_d^{2/3}} \rho] \quad \dots (6)$$

If  $Y$  is the number of radicals formed per primary ionization in water and  $q$  is the probability of reaction between the radicals and the target molecules, then increase in the reaction probability per primary ionization, due to the presence of this water layer, is given by

$$\Delta V = \frac{4\pi}{3} Yq \left[ \rho^3 + 6.81 \times 10^3 \cdot \frac{2+p}{p^{1/3}} \cdot \frac{1}{D_d^{1/3}} \rho^2 + 4.63 \times 10^7 \cdot \frac{(1+2p)}{p^{2/3}} \cdot \frac{1}{D_d^{2/3}} \rho \right] \quad \dots \quad (7)$$

Due to this increase in the sensitive volume, the 37 per cent survival dose in the wet condition is smaller than that in the dry condition and the surviving fraction  $S$  is given by

$$S = \exp - I \left[ V\sigma + \frac{4\pi}{3} Yq \left( \rho^3 + 6.81 \times 10^3 \cdot \frac{2+p}{p^{1/3}} \cdot \frac{1}{D_d^{1/3}} \cdot \rho^2 + 4.63 \times 10^7 \cdot \frac{1+2p}{p^{2/3}} \cdot \frac{1}{D_d^{2/3}} \cdot \rho \right) \right] \quad \dots \quad (8)$$

where  $I$  is the total number of primary ionizations per cc of unit density material and  $\sigma = 1.33$ .

If  $D_w$  and  $D_d$  be the 37 per cent survival doses in the wet and in the dry conditions respectively then from Eq. (2)

$$\Delta V = 1.76 \times 10^{12} \left[ \frac{1}{D_w} - \frac{1}{D_d} \right] \quad \dots \quad (9)$$

$$= \frac{1.76 \times 10^{12}}{D_d} (K-1) \quad \dots \quad (10)$$

where

$$D_d = KD_w$$

Equating (7) and (10) and rearranging terms we obtain

$$\begin{aligned} \rho^3 + 6.81 \times 10^3 \cdot \frac{2+p}{p^{1/3}} \cdot \frac{1}{D_d^{1/3}} \cdot \rho^2 + 4.63 \times 10^7 \cdot \frac{1+2p}{p^{2/3}} \cdot \frac{1}{D_d^{2/3}} \cdot \rho \\ = \frac{4.2 \times 10^{11}}{(D_d Yq)} \cdot (K-1) \quad \dots \quad (11) \end{aligned}$$

$$\text{or } x^3 + 6.81 \times 10^3 \cdot \frac{2+p}{p^{1/3}} \cdot x^2 + 4.63 \times 10^7 \cdot \frac{1+2p}{p^{2/3}} \cdot x - \frac{4.2 \times 10^{11}}{Yq} (K-1) = 0 \quad \dots \quad (12)$$

where

$$x = D_d^{1/3} \rho \quad \dots \quad (13)$$

This is a general expression giving the values of  $x$  as a function of the ratio of the dry to the wet dose ( $K$ ), the shape factor of the target molecule ( $p$ ) and the probability of inactivation by radical formation per primary ionization ( $Yq$ ).

This equation may be solved and  $x$  obtained for any particular values of  $K$ ,  $p$  and  $Yq$ .  $\rho$  can then be directly obtained by using Eq. (13) from  $X$  and  $D_{s7}$  in the dry condition. For quick estimation of  $x$  under different specified conditions, the charts, given in Figs. 1 and 2, have been prepared.

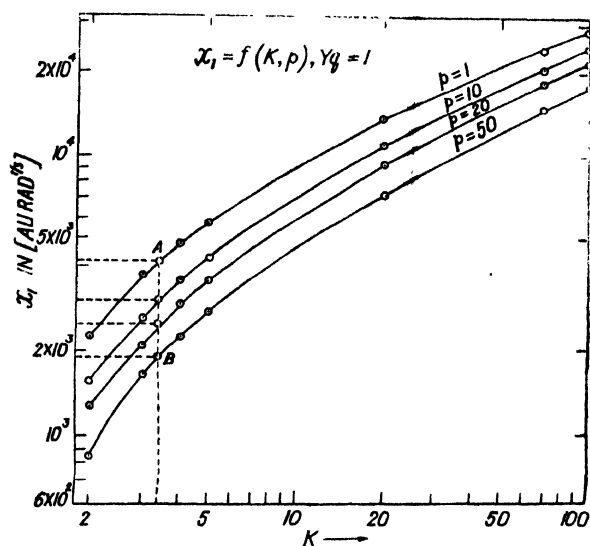


Fig. 1. Variation of  $x_1$  with  $K$ , for different values of  $p$ .

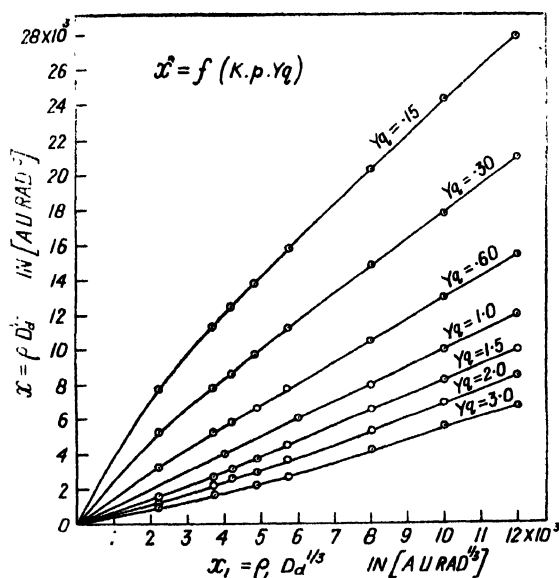


Fig. 2. Variation of  $x$  with  $x_1$  for different values of  $Yq$ .

## ILLUSTRATION

The diffusion distance may be obtained by successive approximations with the help of Figs. 1 and 2. Fig. 1 gives the approximate values of  $x = x_1$  for different values of  $K$  and  $p$  when  $Yq = 1$  i.e., the graph is a plot of the equation

$$x_1^3 + 6.81 \times 10^3 \cdot \frac{2+p}{p^{1/3}} \cdot x_1^2 + 4.63 \times 10^7 \cdot \frac{1+2p}{p^{2/3}} \cdot x_1 - 4.2 \times 10^{11}(K-1) = 0 \quad (14)$$

With the help of this graph,  $x_1$  can be obtained for any experimentally measured values of dry and wet doses, when the number of effective radicals formed per primary ionization  $Yq$  is assumed to be unity. For example, if the dry dose is 20 kilorads and the wet dose 6 kilorads i.e.,  $K = 3.3$ , the values of  $x_1$  are found to be  $4.2 \times 10^3$ ,  $3.0 \times 10^3$ ,  $2.50 \times 10^3$  and  $1.88 \times 10^3$  for  $p = 1, 10, 20$  and  $50$  respectively as shown by the dotted line  $AB$ .

Fig. 2 plots the values of  $x$  as a function of  $x_1$ , for different values of  $Yq$  i.e.- it gives the changes in the values of  $x_1$  to  $x$ , as the probability of inactivation per primary ionization changes. It is seen from this curve that in the above example, the values of  $x_1$ , obtained previously, change to  $x = 3.2 \times 10^3$ ,  $2.2 \times 10^3$ ,  $1.8 \times 10^3$  and  $1.4 \times 10^3$  respectively as  $Yq$  changes from 1 to 1.5. Thus with the help of the graphs given in Figs. 1 and 2, one can obtain the value of  $x = D_d^{1/3}p$  for any combination of  $p$  and  $Yq$ .

## DISCUSSIONS

The method of estimation of diffusion distance developed here is of a very general nature and may be applied to any ellipsoidal target molecule of arbitrary shape and any assumed value of the reaction probability  $Yq$  per primary ionization. If the vital molecule is spherical, diffusion distance can be obtained by assuming  $p = 1$ .

In the case of inactivation of the enzymes various workers (Rajewsky *et al.*, 1957, Hutchinson, 1960) have assumed spherical model. The diffusion distance calculated from the present method given in column 8 of Table I. Column 7 of the Table I gives the value of diffusion distance obtained previously. Inactivation of DNA *in vivo*, has been investigated by Hutchinson *et al.* (1960) who, showed that  $D_{37}$  for the transforming principle in pneumococcus cells was about 3 megarads. Asymmetry of the molecule for the transforming activity was found to be about 40 and diffusion distance calculated from the cylindrical model was 8–10 A.U. The present method gives diffusion distance under this condition as 8 A.U.

The values calculated from the present method seem to be slightly less than those deduced previously. This slight difference is due to the fact that the expression used previously for the calculation of  $\rho$  was  $\Delta V = 4\pi Yq(\rho b^2 + \rho^2 b)$ . For  $p = 1$ , the general expression (7) differs from this by a term involving  $\rho^3$ .

This difference arises from the fact that here an average thickness of water film  $\rho$  has been assumed around the vital molecule, thus defining a zone in which all radicals formed has equal probability of inactivating the vital molecule. Absence of  $\rho^3$  term in the expression used previously increased the value of diffusion distance in the case of Invertase, ADH, CoA, Cytochrome C. However in the case of TP, the method used considered the  $\rho^3$  term and the agreement between the two values is therefore excellent.

# ACKNOWLEDGMENTS

This work was carried out under the financial sponsorship of the Council of Scientific and Industrial Research. One of the authors (S.B.B.) is indebted to C.S.I.R. for a Senior Research Fellowship.

TABLE I

Diffusion distances from the *in Vivo* radiation inactivation of molecules

Sample	D <sub>37</sub> in mega-rads.		K	$\rho$	Yq per ionization	Previous in AU	$\rho$ Present in AU	Ref.
	Wet	Dry						
TP (DNA)	1.2	3	2.5	40	1.5	8-10	8	H and A (1960)
Invertase	6	12	2	1	0.15	38	33	
Alcohol dehydrogenase	1.3	28	21	1	2.79	31	25	H (1960)
Co-enzyme A	3	200	67	1	2.70	35	25	
Cytochrome C	1	54	54	1	0.3	150	105	R. G and P (1957)

# REFERENCES

- Hutchinson, F. (1957), *Radiation Research*, **7**, 473-483.  
Hutchinson, F. and Ross, D.A. (1959), *Radiation Research*, **10**, 477-489.  
Hutchinson, F. and Norcross, C., (1960), *Radiation Research*, **12**, 13-19.  
Hutchinson, F. and Arena, J., (1960), *Radiation Research*, **13**, 137-147.  
Hutchinson, F., (1960), *Ann. Naturalist.*, **94**, 59-70.  
Rajowsky, B., Gerber, G. and Pauly, H., (1957), *In Advances in Radiobiology* (G. C. Hevesy, A. G. Forsberg and J. D. Abbatt, Edts.) pp. 25-32, Oliver and Boyd, Edinburgh.  
Zirkle, R. E. and Tobias, C. A. (1953), *Arch. Biochem. and Biophys.*, **47**, 282-306.

# STUDIES IN K-CAPTURE POSITRON BRANCHING RATIOS- $^{58}\text{Co}$ \*

M. K. RAMASWAMY†

DEPARTMENT OF PHYSICS, THE JOHNS HOPKINS UNIVERSITY  
BALTIMORE 18, MARYLAND (USA)

(Received March 18, 1960)

**ABSTRACT.** One of the methods of determining the Fierz term in Gamow-Teller-transitions is by means of precise determinations of  $K/\beta^+$  ratio. With this in mind the amount of positron emission in the decay of  $\text{Co } 58$  has been measured using coincidence scintillation methods. The measured value is  $0.151 \pm 0.005$ . This leads to a  $K/\beta^+$  ratio of  $5.08 \pm 0.17$  to the 0.810 MeV level in  $\text{Fe}^{58}$ . On the assumption that the beta transition is pure Gamow-Teller, the Fierz term is computed to be  $-0.004 \pm 0.014$ .

## GENERAL INTRODUCTION

### a. *The interaction in beta decay*

The central problem in the theory of beta-decay has been the determination of the nature of the interaction responsible for this decay. In general the interaction can be a linear combination of five types, namely, scalar (S), vector (V), tensor (T), axial vector (A) and pseudoscalar (P), all satisfying the requirement of relativistic invariance. Beta-Decay can be classified as allowed or forbidden depending on the change in angular momenta and parities of the nuclear states involved. The selection rules permit a further distinction between transitions as Fermi or Gamow-Teller. The selection rules are :

Allowed	$\Delta J = 0$	Fermi
	No	
	$\Delta J = 0, \pm 1$	Gamow-Teller
	No $0 \rightarrow 0$	
First forbidden	$\Delta J = 0, \pm 1, \pm 2$	Gamow-Teller
	Yes	
	$0, \pm 1$	Fermi

and so on.

The Fermi transitions involve only the interactions  $S$  and  $V$ , and the interactions  $A$  and  $T$  characterize Gamow-Teller transitions. A transition allowed

\*Supported in part by the U.S. Atomic Energy Commission

†On leave from University of Mysore, India

Present Address : Dept. of Physics, The Ohio State University, Columbus, Ohio (USA)



by both types of selection rules should therefore involve  $S$ ,  $V$ ,  $A$ ,  $T$  and perhaps  $P$ . There is strong evidence that the  $P$  interaction is unimportant. The fact that transitions obeying both kinds of selection rules are observed indicates that the beta-interaction is an admixture of both Fermi and Gamow-Teller types. It remains to determine the ratio of these interaction strengths. A study of the angular correlation between the electron and the neutrino in an allowed pure transition can be used to distinguish which of the interactions  $S$  or  $V$ , or  $A$  or  $T$  is predominant. It is now established from such experiments [Hermansfeldt, (1957, 1958), Alford (1954), Burman (1959)] that the Fermi interaction is mostly  $V$  and the Gamow-Teller interaction mostly  $A$ . The neutron decay (mixed transition) combined with the  $O^{14}$  decay (pure Fermi transition) leads to the determination of the relative strengths of Fermi and Gamow-Teller interactions. The recent Russian measurement (Sosnovski, 1959) of  $11.7 \pm 0.4$ , min. for the half life of neutron leads to  $(C_{GT}/C_F)^2 = 1.42 \pm 0.08$ .

Considering only pure transitions, Fermi or Gamow-Teller one can expect interference between the two types  $S$  and  $V$ , or  $A$  and  $T$ . The possible existence of such terms was first pointed out by Fierz (1937) and hence these terms are called Fierz interference terms. It is the principal objective of the present work to make an estimate of this effect in Gamow-Teller transitions. Such interference is possible in the electron-neutrino angular correlation expression, but because of the difficulties involved in such experiments these terms are often neglected. Interference between  $A$  and  $V$  in a mixed transition can also occur, but we will not concern ourselves with this here, nor will we treat forbidden transitions.

#### b. *Fierz interference*

The general expression for the energy distribution of electrons (positrons) in an allowed transition can be written as (Gerhart, 1958)

$$N(W) dW = [2\pi^3]^{-1} p W (W_0 - W)^2 F(Z, W) \xi (1 \pm 2b/W) dW$$

$$\text{where } \xi = \frac{1}{2} [1 + |k|^2 (|C_S|^2 + |C_S'|^2) + (|C_V|^2 + |C_V'|^2) + 4 \operatorname{Re} \{ C_A C_T^* + C_A' C_T'^* \}]$$

$$\text{and } \xi b = \pm \gamma [ \frac{1}{2} |k|^2 \operatorname{Re} \{ C_S C_V'^* + C_S' C_V^* \} + 4 \operatorname{Re} \{ C_A C_T^* + C_A' C_T'^* \} ]$$

Here the  $+$  sign refers to electron, and  $-$  to positron emission. The other symbols are explained as follows.

$pW(W_0 - W)^2$  is the statistical weight factor which determines, in the absence of the coulomb field, the sharing of energy between the electron and the neutrino.

$F(Z, W)$  is the coulomb field factor which represents the effect of nuclear charge on the emitted electron

$p$  is the momentum of the electron

$W$  is the energy of the electron in relativistic units

$W_0$  is the maximum energy of the electron or positron

$$k = f1/f\beta$$

where  $f1$  = the scalar matrix element

$f\beta$  = the vector matrix element

$k = 1$  only if the motion of the nucleons is non-relativistic, since in this case  $\beta = \gamma_4 = 1$ .

Putting  $k = 1$  we get

$$b = \gamma \left[ \frac{R_s(C'_S C'_{V'}^* + C'_S C'_{V'}^*)}{(|C'_S|^2 + |C'_S|^2 + |C'_{V'}|^2 + |C'_{V'}|^2)} |f1|^2 + R_s(C_A C_T^* \right. \\ \left. + (|C'_A|^2 + |C'_T|^2 + |C'_A|^2 + |C'_T|^2) |f\sigma|^2 \right]$$

is called the Fierz interference term. Here  $\gamma = \sqrt{1 - (\alpha Z)^2} \approx 1$  represents the screening effect due to the atomic electrons.

$C_i = S, V, A, T$  = is the coupling constant for parity conserving interaction

$C'_i = S, V, A, T$  = is the coupling constant for parity non-conserving interaction.

The complex conjugation on the coupling constants represents the possibility of time reversal non-invariance in the beta-decay process.

An immediate consequence of  $b \neq 0$  is that the spectral shape of an allowed transition will deviate from the statistical shape because of the inverse dependence on  $W$  through  $b$ . One way of seeing this deviation experimentally is to plot the form factor

$N(W)/F(Z, W) pW(W_0 - W)^2$  as a function of  $W$ . From this kind of analysis the limits set on  $b_{GT}$  are  $-0.09 \leq b_{GT} \leq 0.20$ . Because of the weak dependence on  $W$  such deviations are rather hard to detect. Further the analysis has so far been generally restricted to Gamow-Teller transitions only. Recently, Daniel (1958) has applied this method to estimate the Fierz term in the decay of  $N^{13}$  ( $1/2^- \rightarrow 1/2^-$ ). He obtained  $b_F = 0.14$  using the  $O^{14}$   $ft$  value to evaluate the Fermi part of the matrix element.

Integrating expression (1) over the allowed spectrum, we obtain

$$(2) \quad 2\pi^3 (ft^{-1}) \ln 2 = \xi + \xi b \langle W^{-1} \rangle \quad (2)$$

where  $f = \int_1^{W_0} F(Z, W) pW(W_0 - W)^2 dW$  is the so-called Fermi function and

$f^{-1} \int_1^{W_0} F(Z, W) p(W_0 - W)^2 dW = \langle W^{-1} \rangle$  is the expectation value of  $W^{-1}$  over the allowed spectrum.

Thus a consequence of  $b \neq 0$  is that the  $ft$  values will depend on  $W^{-1}$ . From a plot of  $2\pi^3 [ft|1|^2]^{-1} \ln 2$  vs  $2\gamma' [1|^2] < W^{-1} >$  which should give a straight line provided  $k = 1$  and the matrix elements remain the same (Gerhart (1958) finds from an analysis of data for 0 0, No (Fermi) transitions — O<sup>14</sup>, Al<sup>26</sup> and Cl<sup>34</sup>, that

$$b_F = \gamma \frac{\text{Re}(C_S C_V^* + C_S' C_V'^*)}{|C_S|^2 + |C_S'|^2 + |C_V|^2 + |\bar{C}_V'|^2} = 0.00 \pm 0.12$$

the chief uncertainty being due to the assumption regarding  $k$ . (Recently Altman and MacDonald (1958) have considered the effect of coulomb and relativistic corrections to the evaluation of the Fierz term and conclude that the corrections are within experimental uncertainties.) The matrix elements were evaluated by Gerhart on the basis of charge independence of nuclear forces.

Another fruitful approach for the evaluation of  $b$  has been the method of *K*-capture to positron branching ratios first exploited by Sherr and Miller (1954). In the following section we will describe the information that can be derived from a study of  $K/\beta^+$  ratios and in particular about the Fierz term.

#### c. *K*-Capture positron branching ratios

The study of the shapes of beta-spectra together with the  $ft$  values and the shell model (to determine parities) has been very useful in classifying transitions as to the order of forbiddenness. When, however, between two nuclear states enough energy is available both for *K*-capture and positron emission, a useful quantity that can be measured is the *K*-capture positron branching ratio. In fact, it was one of the early triumphs of the Fermi theory of beta-decay that the *K*-capture mode of decay was observed as predicted. A measurement of the  $K/\beta^+$  ratio can be used to find the energy difference between two nuclear states if it is known otherwise that the transition is allowed. However, it is observed (Zweifel, 1957) that all allowed shaped transitions (most first-forbidden transitions) have allowed branching ratios also. Thus it is not possible to determine whether an allowed shape transition is indeed allowed, without a knowledge of the parity change. However, the  $K/\beta^+$  ratio does show a detectable change for unique first forbidden and higher transitions intensified with increasing order of forbiddenness (Brysk, 1958). These latter transitions can probably be much more easily identified on the basis of the shape of the positron spectrum and life-time. In such cases  $K/\beta^+$  ratios can only serve as an additional check on the assignment. However, the chief virtue of measurement of  $K/\beta^+$  ratio for supposedly pure transitions is that it lends itself to the estimation of small-order effects in beta-decay such as the Fierz term. Consider a pure transition, say, a Gamow-Teller transition. Then for this transition the probability for positron emission is

$$P_+ = \frac{1}{2\pi^3} \int_0^{W_0} F(Z, W) p W (W_0 - W)^2 \xi (1 - 2b/W) dW$$

where the various quantities have already been defined. (Note that the terms involving  $C_S$  and  $C_V$  are set equal to zero.)

The probability for  $K$ -capture to the same state can be written as

$$P_K = \frac{1}{4\pi^2} (W_0 + W_k)^2 g_k^2(R) \xi(1+2b)$$

where  $g_k^2(R) = \frac{1+\gamma}{2\Gamma(2\gamma+1)} R^{2\gamma-2} (2\alpha Z_{eff})^{2\gamma+1}$  is the Dirac radial function,

$W_0$  = total energy available for the transition in  $m_0c^2$  units,

$$W_K = \gamma \simeq \sqrt{1-\alpha^2 Z^2}$$

So that the ratio of  $K$ -capture to positron emission becomes

$$P_K/P_+ = \frac{(1/4\pi^2)(W_0 + W_k)^2 g_k^2(R) \xi(1+2b)}{(1/2\pi^3) \int_{W_0}^{W_0+W_k} F(Z, W) p W (W_0 - W)^2 dW \xi(1-2b/W)} = R \quad \dots (1)$$

If the Fierz interference term were zero, then putting  $b = 0$ , we get

$$(P_K/P_+)_{b=0} = \frac{(1/4\pi^2)(W_0 + W_k)^2 g_k^2(R)}{(1/2\pi^3) \int_{W_0}^{W_0+W_k} F(Z, W) p W (W_0 - W)^2 dW} = R_0 \quad \dots (2)$$

Dividing Eq. (2) by (1), we obtain

$$R/R_0 = \frac{1+2b}{1-2b\langle W^{-1} \rangle} \text{ where } \langle W^{-1} \rangle \text{ has already been defined.}$$

$$b = \frac{R/R_0 - 1}{2[1 + R/R_0 \langle W^{-1} \rangle]}$$

Thus a measurement of  $R$  can be used to evaluate  $b$ . It should be noted that the matrix elements cancel out in the ratio.

Before comparing the theoretical  $K/\beta^+$  ratio with the observed value, correction for the finite size of the nucleus and screening of the positron and the bound  $K$ -electron have to be made. Further, if the measured quantity is the total electron-capture, then correction for capture from higher shells has to be made to obtain the  $K$ -capture alone.

For allowed transitions the finite size correction has been shown to be negligible (Zweifel, 1957). The screening correction, on the other hand, is not insigni-

ficant. Recently Perlman, Welker and Wolfsberg (1958) have evaluated the effect of screening on the positron wave function and have given in graphical form the ratio of screened to unscreened values. For most  $Z$  values of interest the screening on the  $K$ -electron is taken into account by putting  $Z_{\text{effective}} = Z_K - 0.3$ . Zweifel (1957) has evaluated the deviation of the actual  $Z_{\text{eff}}$  from this Slater screening. Regarding correction for capture from higher shells, only  $L$ -capture is important for most cases of interest. (At high  $Z$ ,  $M$ -capture also becomes important.) Correction for  $L$ -capture is obtained by using  $L/K$  ratios given in graphical form by Rose and Jackson (1949).

We have applied the  $K/\beta^+$  ratio technique for the decays of  $\text{Ga}^{68}$ ,  $\text{Co}^{58}$  and  $\text{Na}^{22}$ , all pure Gamow-Teller emitters, to obtain the Fierz interference term. The results on  $\text{Ga}^{68}$  have been reported (Ramaswamy, 1959a) briefly at the Cambridge meeting of the American Physical Society, and published elsewhere (Ramaswamy, 1959b).

#### INTRODUCTION

72 day  $\text{Co}^{58}$  decays by electron capture and positron emission to the 0.810 MeV level in  $\text{Fe}^{58}$  followed by a gamma-ray of this energy to the ground state. Besides, there is a weak electron-capture branch (2%) to the second excited state at 1.63 MeV. This level de-excites itself predominantly by the emission of a gamma ray of 0.820 MeV to the 0.810 MeV level and partly by the emission of a gamma ray of 1.63 MeV to the ground state of  $\text{Fe}^{58}$ . The decay scheme as given by Frauenfelder *et al.* (1956) is reproduced in Fig. 4. The end-point of the positron spectrum is measured to be  $0.472 \pm 0.006$  MeV (King, 1954). No positron emission to the  $0^+$  ground state of  $\text{Fe}^{58}$  has been observed. The spin of 0.810 MeV level is  $2^+$  from systematics of even-even nuclei (Scharff-Goldhaber, 1953). The spin of the second excited state at 1.63 MeV has been assigned  $2^+$  from angular correlation studies. This is consistent with the presence of a cross-over gamma transition to the  $0^+$  ground state. The decay of  $\text{Co}^{58}$  to the  $2^+$  states in  $\text{Fe}^{58}$  and the absence of transition to the  $0^+$  ground state suggest a spin of  $2^+$  or  $3^+$  for  $\text{Co}^{58}$ . The spin has been directly measured to be 2 by Dobrov and Jeffries (1957) by means of paramagnetic resonance experiments. The assignment of  $2^+$  to  $\text{Co}^{58}$  makes the beta transition to the 0.810 MeV level allowed by both Gamow-Teller and Fermi selection rules ( $\Delta J = 0, \text{No}$ ). However, recent nuclear orientation experiments of Dagley *et al.* (1958) have shown that the angular distribution of the 0.810 MeV gamma ray is consistent only with the beta transition being pure Gamow-Teller, the amount of Fermi admixture being  $0.005 \pm 0.003$ . Thus the measurement of electron capture to positron branching ratio to the 0.810 MeV level becomes of obvious interest from the point of view of determining the Fierz term.

Good *et al.* (1946) and Cook and Tomnovec (1956) have measured the ratio of total electron capture to positron emission in the decay of  $\text{Co}^{58}$  to be  $5.9 \pm 0.2$ .

When account is taken of the weak electron capture branching to the 1.63 MeV level, the  $K/\beta^+$  ratio to the 0.810 MeV level becomes  $5.8 \pm 0.2$ . This result was obtained by comparison of the intensities of the annihilation radiation and the 0.81 MeV gamma ray, and by a knowledge of the efficiencies. After the work to be described on Co-58 had been completed and briefly published by the author (Ramaswamy, 1958), the work of Konijn *et al.* (1958) on the same subject has come to attention. By using beta-gamma coincidence technique these workers determined the  $\epsilon/\beta^+$  ratio to be  $5.67 \pm 0.14$ .

Neglecting the weak electron-capture branch ( $\sim 2\%$ ) to the 1.63 MeV level for the moment, the fraction of positrons in the decay of Co-58 can be expressed as  $f_+ = \beta/2c\sigma$ , where  $c$  is the singles counting rate for the 0.810 gamma ray,  $\beta$  is the coincidence rate between the 0.810 MeV gamma ray and the annihilation radiation, and  $\sigma$  is the efficiency for detecting the annihilation radiation. The value of  $f_+$  when corrected for the presence of the weak branch will give the desired  $\epsilon/\beta^+$  ratio to the 0.810 MeV level.

#### EXPERIMENTAL

Through the courtesy of Dr. R. W. Hayward of the National Bureau of Standards, Co-58 source was made available for studies. Unfortunately this source contained an appreciable Co-60 impurity. Co-58 was evaporated onto a 0.0003" mylar foil and sealed with cellophane. The sandwich was then squeezed between two lucite slabs each 1.3 mm thick and 1 cm square. The whole assembly was then sealed with black tape. Thus the positrons from Co-58 (0.470 MeV) were completely stopped. The 0.810 MeV gamma ray was detected in a 2" cube NaI(Tl) crystal and the annihilation radiation was detected in a  $1\frac{1}{2} \times 1$ " NaI(Tl) crystal. Source to detector distance of 1" to  $1\frac{1}{2}$ " was used. A typical singles gamma spectrum measured in the 2" cube crystal is shown in Fig. 2. Besides the annihilation radiation and the 0.810 MeV gamma ray belonging to Co-58, gamma rays at 1.17 and 1.33 MeV are also prominently seen. The 1.63 MeV gamma ray of Co-58 is too weak to be seen, and no effort was made to observe it. In order to determine the number of counts in the 0.810 MeV photopeak, it is necessary to subtract the Compton background due to Co-60 gamma rays. In order to do this a pure Co-60 source was substituted and its spectrum was carefully normalized to that of Co-58, 60. The dotted curve in Fig. 2 shows the normalized spectrum. For the coincidence measurements a single channel analyzer was set on the photopeak of the annihilation radiation and the spectrum in coincidence was obtained by gating the 20-channel analyzer with the annihilation radiation. The coincidence spectrum thus obtained is shown in Fig. 3. It is observed that the coincident 0.810 MeV gamma ray is superposed on a rather high background due to Co-60. In order to estimate and subtract this background, a coincidence spectrum was taken by replacing Co-58 by Co-60 and the spectrum normalized to the Co-58 spectrum. The resulting background was thus subtracted.

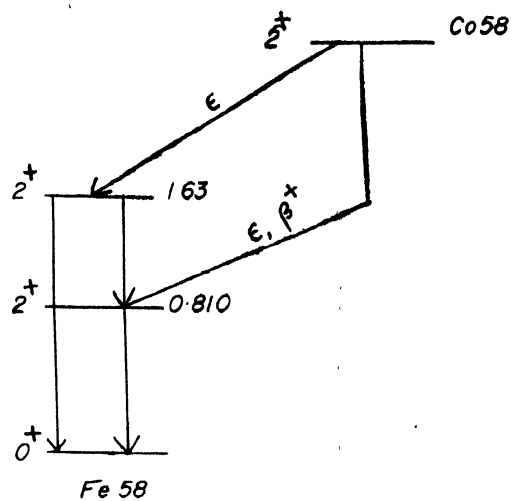


Fig. 1,

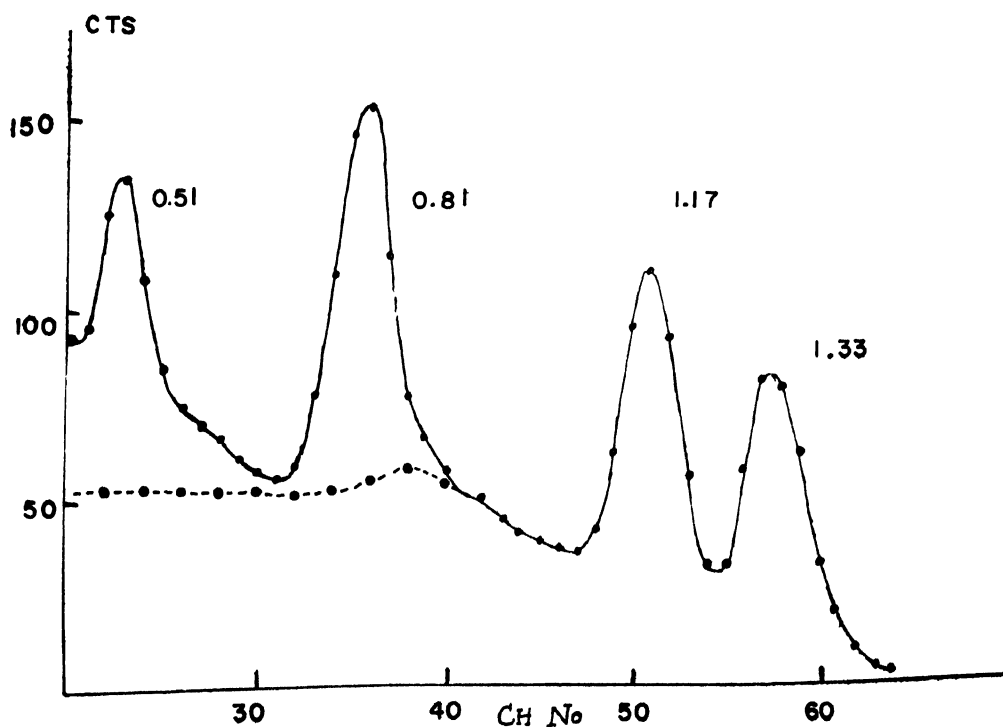


Fig. 2.

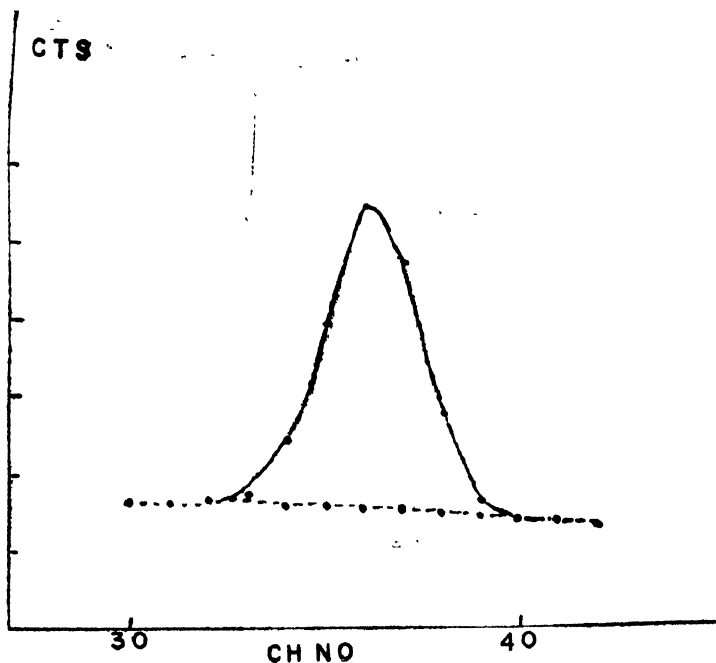


Fig. 3.

In order to check on the reliability of this procedure, the 0.810 MeV gamma ray was measured in triple coincidence with the two annihilation quanta. From this it was concluded that the background had been correctly estimated. The accidentals were about 10 per cent of true coincidences in the doubles spectrum.

In order to determine  $\sigma$ , the efficiency for detecting annihilation radiation initially a calibrated  $\text{Na}^{22}$  source (accurate to 3%) was used. By measuring the area under the photopeak and knowing the source strength one could compute the efficiency. A more accurate efficiency determination was made as follows: A  $\text{N}^{13}$  source (a pure positron emitter of 10 minutes half life) was produced by bombarding a 2 mil polyethylene foil for 10 minutes with 1 MeV deuterons at the Johns Hopkins University Van de Graaff generator through the courtesy of O.N. Rask. After the bombardment the foil was cut into a tiny piece approximating the dimensions of the Co-58 source and sandwiched between two freshly cleaved NaI(Tl) crystals 1.2 mm thick and 1 cm square, and mounted in the same geometry as the Co-58 source. The beta spectrum observed in this system is shown in Fig. 4. The energy calibration of the counter was made after the  $\text{N}^{13}$  source was dead by using external gamma ray sources of  $\text{Co}^{57}$  (0.123 MeV),  $\text{Cs}^{137}$  (0.661 MeV) and  $\text{Na}^{22}$  (1.28 MeV). A Fermi plot of the spectrum is shown in Fig. 5. It has an end-point of  $1.16 \pm 0.05$  MeV, in good agreement with the value of 1.20 MeV (Scharff-Goldhaber, 1953). By following the decay of the activity for 3 half-lives, it was concluded that no impurities were present. Under the conditions of the bombardment, no other impurities were likely to be formed.



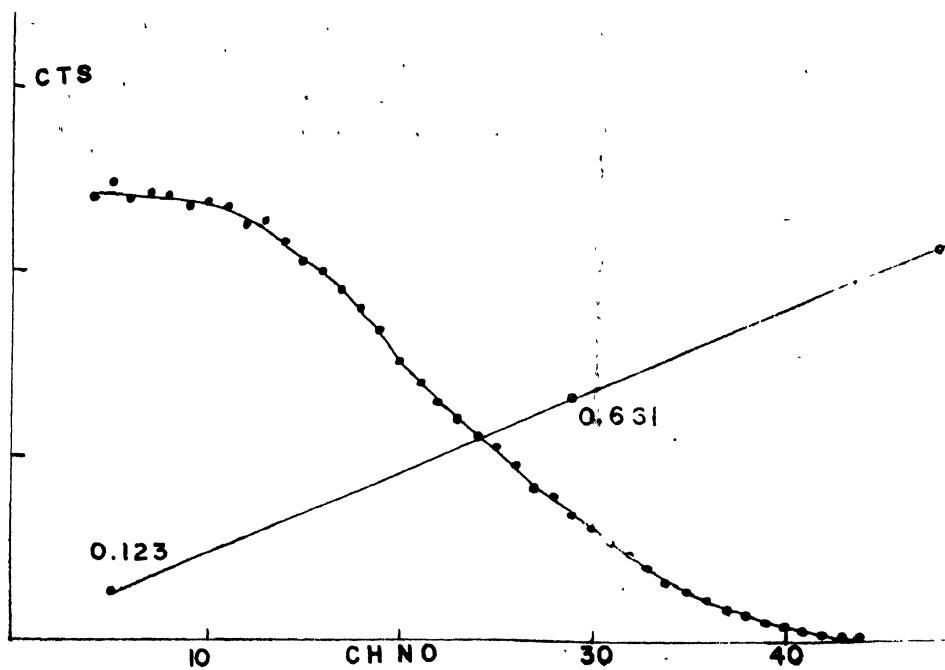


Fig. 4.

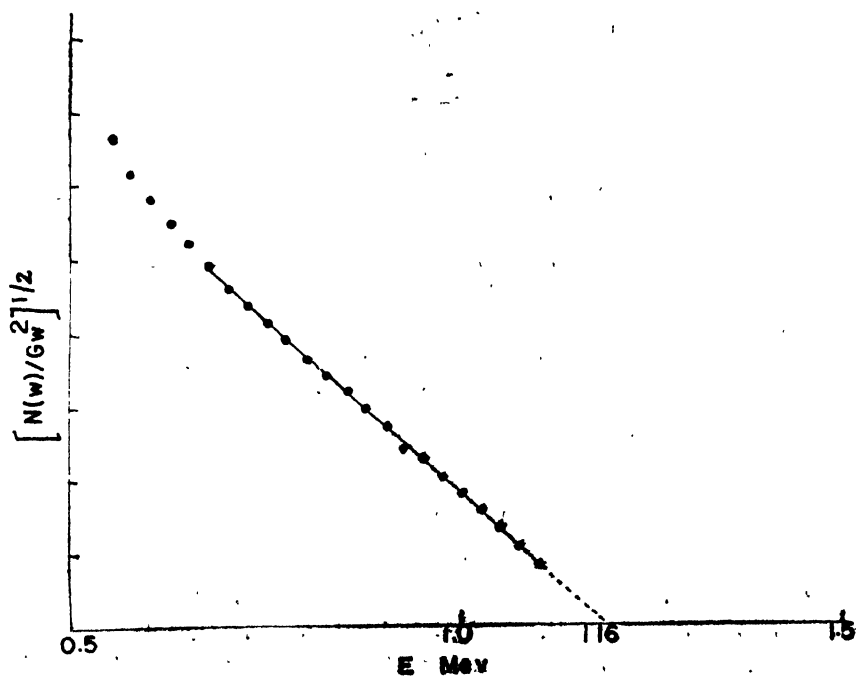


Fig. 5.

The beta-spectrum was measured in coincidence with the annihilation radiation photopeak which was detected by the same  $1\frac{1}{2}'' \times 1''$  NaI counter whose efficiency was to be determined. A portion of the beta spectrum is shown in Fig. 6. The efficiency for detecting the annihilation radiation is simply the ratio of the beta-spectrum in coincidence and in singles when corrected for decay.

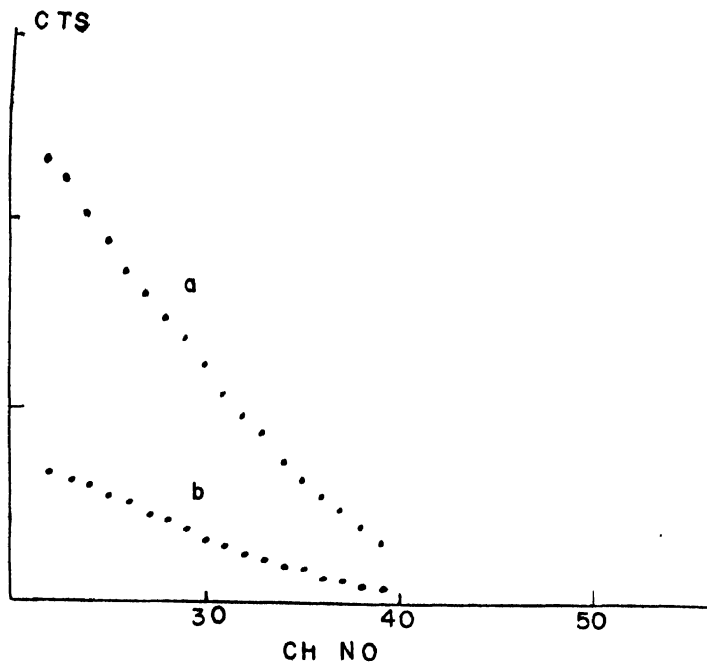


Fig. 6.

Further, since the crystal source was mounted on a light pipe, a correction for the absorption of the 0.511 MeV gamma ray has to be made. This is of the order of 3.7 %. Since the positrons from  $\text{Co}^{58}$  (0.470 MeV) and those from  $\text{N}^{13}$  (1.2 MeV) have different ranges in lucite and NaI respectively used to annihilate them, one might think that a correction for solid angle has to be made. However, the range of 0.470 MeV positrons of  $\text{Co}^{58}$  in lucite is 1.4 mm and that of 1.2 MeV positrons of  $\text{N}^{13}$  in NaI (Tl) is 1.16 mm. The actual thickness used to annihilate the positrons were 1.3 and 1.2 mm respectively. A source to detector distance of 25 mm was used. In view of these circumstances the solid angle correction is less than 1%.

## RESULTS

Table I lists the results obtained. The uncorrected  $f_+$  is  $0.147 \pm 0.005$ . Referring to the  $\text{Co}^{58}$  decay scheme (Fig. 1), it is seen that  $1\frac{1}{2}\%$  of the 0.810 MeV gamma rays arise from the 1.63 MeV level, and another  $1\frac{1}{2}\%$  arise from cascading to the ground state. The uncorrected  $f_+$  has therefore to be multiplied by 0.03 to get the corrected value of  $f_+$ . In order to obtain the amount of elec-

tron-capture to the 0.810 MeV level, it should be noticed that 2% of the Co-58 transitions lead to the 1.63 MeV level. Hence  $\epsilon = 0.98 - 0.151 \pm 0.005$ . Thus the  $\epsilon/\beta^+$  ratio to the 0.810 MeV level is computed to be  $5.49 \pm 0.18$ . The error introduced in the value of 2% for the branching is very small.

# DISCUSSION

The  $\epsilon/\beta^+$  ratio computed above has to be corrected for 8%  $L$ -capture to give (Gerhart, 1958) the value  $K/\beta^+$  ratio. The value so obtained is  $5.08 \pm 0.17$ . The theoretical value is  $5.15 \pm 0.24$  corresponding to maximum beta energy of  $0.472 \pm 0.006$  MeV. Thus our value is in excellent agreement both with theory and with previous measurements. As before, the Fierz term is computed from the expression

$$b = \frac{R/R_0 - 1}{2[1 + R/R_0 \langle W^{-1} \rangle]}$$

For Co-58  $\langle W^{-1} \rangle = 0.76$  corresponding to  $W_0 = 1.924$ .

$$b = -0.004 \pm 0.014$$

TABLE I

Summary of results on Co<sup>58</sup>

(For symbols see text)

$$c = 91.00 \pm 1.12 \text{ cps}$$

$$\beta = 0.242 \pm 0.003$$

$\sigma$ : (a) from Na<sup>22</sup>

Source strength =  $N_0$  = no. of positrons/min =  $(3.16 \pm 0.10) \times 10^5 \beta^+/\text{min}$

$a$  = no. of cts in the 0.511 photopeak =  $47.0 \pm 0.0$  cps

$$\sigma = a/N_0 = (8.92 \pm 0.33) \times 10^{-3}$$

(b) from N<sup>13</sup>

$$\Delta\beta_{0.5} = 358.0 \pm 6.0 \text{ cpm}$$

$$N\beta = 23200 \pm 150 \text{ cpm}$$

$$\sigma = \frac{1}{2} \frac{N\beta_{0.5}}{N\beta} = (9.02 \pm 0.18) \times 10^{-3}$$

$$f_+ \text{ (uncorrected)} = \beta/2c\sigma = 0.147 \pm 0.005$$

$$f_+ \text{ (corrected)} = (0.147 \pm 0.005) / 1.03 = 0.151 \pm 0.005$$

$$\epsilon = 0.980 - f_+ = 0.829 \pm 0.005$$

$$\epsilon/\beta^+ = \frac{0.829 \pm 0.005}{0.151 \pm 0.005} = 5.49 \pm 0.18$$

$$L/K = 0.08$$

$$K/\beta^+ = 5.08 \pm 0.17$$

# CONCLUSIONS

The fraction of Co-58 decays by positron emission has been measured by coincidence methods using NaI crystals. The value is  $0.151 \pm 0.005$ . This value leads to a  $K/\beta^+$  ratio of  $5.08 \pm 0.17$  for the beta transition to the 0.810 MeV level

The theoretical ratio is  $5.15 \pm 0.24$ . The Fierz term is computed to be  $-0.004 \pm 0.014$ . It is rather striking that the theoretical value of  $K/\beta^+$  ratio has a larger error than the measured value.

It follows then that the Fierz interference term is extremely small. Unfortunately Co-58 is not the best case, since a small admixture to Fermi component in the beta transition may invalidate the conclusions reached so far. However, if it turns out, as is likely, that the Fermi component is zero, then it may be worth while to measure the end-point of the positron spectrum more accurately. The smallness of the Fierz term has been conclusively shown from  $\text{Na}^{22}$  decay (Ramaswamy, 1959c)

#### ACKNOWLEDGMENTS

The author wishes to express his deep appreciation to Prof. L. Madansky for valuable suggestions and discussions.

#### REFERENCES

- Alford, W. P., and Hamilton, D. R., 1954, *Phys. Rev.* **95**, 1351.  
 Altman, A. and MacDonald, W. M. 1958, *Phys. Rev. Lett.* **1**, 458.  
 Brysk, H. and Rose, M. E. 1958, *Rev. Mod. Phys.* **30**, 1169.  
 Burman, Hermannsfeldt, Allen and Braid, 1959, *Phys. Rev. Lett.* **2**, 9.  
 Cook, C. S. and Tomnovec, F. 1956, *Bull. Am. Phys. Soc.* **2**, 3, 357.  
 Dagley, Grace, Hill and Sowter, 1958, *Phil. Mag.* **3**, 489  
 Daniel, H. and Schmidt-Rohr, U. 1958, *Nuclear Phys.* **7**, 516.  
 Dobrov, W. and Jeffries, C. D. 1957, *Phys. Rev.* **108**, 60.  
 Fierz, M. 1937, *Zeit. Physik*, **105**, 553.  
 Frauenfelder, LeVine, Rossi and Singer, 1956, *Phys. Rev.* **103**, 352.  
 Gerhart, J. B. 1958, *Phys. Rev.* **109**, 897.  
 Good, Peaslee and Deutsch. 1946, *Phys. Rev.* **69**, 313.  
 Hermannsfeldt, Stahelin, Maxson and Allen, 1957, *Phys. Rev.* **107**, 641.  
 Hermannsfeldt, Burman, Stahelin, Allen and Braid, 1958, *Phys. Rev. Lett.* **1**, 61.  
 King, R. W., 1954, *Rev. Mod. Phys.* **26**, 327.  
 Konijn, Van Nooijen, Hagedoorn and Wapstra, 1958, *Physica*, **24**, 931.  
 Perlman, Welker and Wolrsberg, 1958, *Phys. Rev.* **110**, 381.  
 Ramaswamy, M. K., 1959a, *Bull. Am. Phys. Soc.* **2**, 4, 151.  
 Ramaswamy, M. K., 1959b, *Nuclear Phys.* **10**, 205.  
 Ramaswamy, M. K., 1959c, *Ind. J. Phys.*, **33**, 285.  
 Ramaswamy, M. K. 1958, *Bull. Am. Phys. Soc.* **2**, 3, 357.  
 Rose, M. E. and Jackson, J., 1949, *Phys. rev.* **76**, 1540.  
 Scharff-Goldhaber, G., 1953, *Phys. Rev.* **90**, 587.  
 Sherr, R., and Miller, R.H., 1954, *Phys. Rev.* **93**, 1076.  
 Zweifel, P. F. 1957, Proc. Rehovoth Conf., North-Holland Publishing Co. p. 300  
 Sosnovski, A. N., and Spivak, P. E., 1959, *JETP. Apr.*

# SCATTERING OF ELECTRON BY EXCITED HELIUM ATOM

MRS. TARA BHATTACHARYYA

DEPARTMENT OF THEORETICAL PHYSICS,

INDIAN ASSOCIATION FOR THE CULTIVATION OF SCIENCE, JADAVPUR, CALCUTTA-32

(Received September 21, 1961)

**ABSTRACT.** Born's first approximation formula has been applied here to calculate the differential cross section of scattering of an electron by an excited helium atom. It is found that the cross section of scattering of electrons of 700 eV energy by excited He atom is very nearly the same as that by screened He atom; the cross section of scattering of the same by bare He nucleus is slightly greater than both of them. However, the experimental cross section for ordinary He is considerably larger than these three theoretical results at angles above  $80^\circ$ , whereas at angles below  $70^\circ$ , the experimental values are less than all the theoretical values.

## INTRODUCTION

Various models have been proposed to take into account the screening effect of the two electrons surrounding the nuclear charge. To calculate the above screening, Hylleraas (1929) has taken the wave function of the Schrödinger equation to be a product of two wave functions in the  $1s$  state with  $Z = \frac{27}{8}$ ,  $Z$  being the nuclear charge value.

Huzinaga (1960), on the other hand, has taken symmetrized product of two wave functions in  $1s$  state with two different  $Z$  values.

In the present paper we propose to study the problem of scattering of electrons if the target atoms are already excited. In actual experimental conditions, the target atoms are also excited by inelastic collisions, so that there is always a certain fraction of the number of atoms which are in excited states; it is worth while to see how the scattering is effected by the excited states of the target atoms. Here we are considering one of the electrons to be in its  $1s$  state and the other in  $2s$  state.

## MATHEMATICAL RESULTS

The potential function of atom having two electrons is given by

$$V = -e^2 \int_{\tau_1=0}^{\infty} \int_{\tau_2=0}^{\infty} \psi^* \left\{ \frac{2}{r} - \frac{1}{|r-r_1|} - \frac{1}{|r-r_2|} \right\} \psi d\tau_1 d\tau_2 \quad \dots (1)$$

where the co-ordinates of the two electrons of the atom are denoted by  $r_1$  and

$r_2$  and  $r$  is the co-ordinate of the incident electron with the nucleus as the origin.  $\psi$  is the wave function of the system and is taken to be

$$\psi = \frac{N}{\sqrt{2}} \{R_1(r_1) R_2(r_2) + R_1(r_2) R_2(r_1)\}$$

where

$$R_1 = \left( \frac{Z_1}{a_0} \right)^3 \frac{1}{2} e^{-\frac{Z_1 r}{a_0}}$$

$$R_2 = \left( \frac{Z_2}{2a_0} \right)^3 \left( 2 - \frac{Z_2 r}{a_0} \right) e^{-\frac{Z_2 r}{a_0}}$$

and the normalization factor  $N$  is given by

$$N^2 = \frac{1}{4\pi^2 \left\{ 1 + 8Z_1^3 Z_2^3 \left( \frac{2}{2Z_1 + Z_2} \right)^8 (Z_1 + Z_2)^2 \right\}}$$

Substituting (2) in (1) we obtain for  $V$  the following expression

$$\begin{aligned} V = & -(4\pi)^2 N^2 e^2 \left[ \frac{2}{r} \left\{ 8Z_1^3 Z_2^3 \left( \frac{2}{2Z_1 + Z_2} \right)^8 (Z_1 - Z_2) \right\} \right. \\ & + \left( \frac{1}{r} + \frac{Z_1}{a_0} \right) e^{-\frac{2Z_1 r}{a_0}} + \left( \frac{1}{r} + \frac{3Z_2}{4a_0} + \frac{1}{4} \frac{Z_2^2}{a_0^2} r + \frac{1}{8} \frac{Z_2^3}{a_0^3} r^2 \right) e^{-\frac{Z_2 r}{a_0}} \\ & + e^{-\frac{r}{2a_0}(2Z_1 + Z_2)} \left\{ \frac{4Z_1^3 Z_2^3}{a_0^3} \left( \frac{2}{2Z_1 + Z_2} \right)^4 (Z_1 - Z_2) \right\} \left\{ \frac{2(Z_1 - Z_2)}{2Z_1 + Z_2} r^2 \right. \\ & \left. \left. - \frac{4Z_2 a_0 r}{(2Z_1 + Z_2)^2} + \frac{8a_0^2(2Z_1 - 3Z_2)}{(2Z_1 + Z_2)^3} - \frac{8(Z_1 - Z_2)(2a_0)^3}{r} \frac{1}{(2Z_1 + Z_2)^4} \right\} \right] \quad \dots (3) \end{aligned}$$

To calculate the differential scattering cross section  $\sigma(\theta)$  which is  $|f(\theta)|^2$  we apply the Born approximation method in which  $f(\theta)$  is given by

$$f(\theta) = -\frac{8\pi^2 m}{h^2} \int_0^\infty \frac{\sin kr}{hr} V(r) r^2 dr \quad \dots (4)$$

Substituting the value of  $V$  from Eq. (3) in Eq. (4) we obtain

$$f(\theta) = \frac{2me^2}{\hbar^2 k^2} \left\{ 1 + 8Z_1^3 Z_2^3 \left( \frac{2}{2Z_1 + Z_2} \right)^8 (Z_1 - Z_2)^2 \right\} \\ \times \left[ 16Z_1^3 Z_2^3 \left( \frac{2}{2Z_1 + Z_2} \right)^8 (Z_1 - Z_2)^2 \right. \\ + \frac{k^2 a_0^2 (k^2 a_0^2 + 8Z_1^2)}{(4Z_1^2 + k^2 a_0^2)^2} + \frac{k^2 a_0^2}{(Z_2^2 + k^2 a_0^2)^4} \{ 7Z_2^3 + 4Z_2^4 a_0^2 k^2 \\ + 4Z_2^2 a_0^4 k^4 + a_0^6 k^6 \} + \frac{4Z_1^3 Z_2^3}{a_0^3} \left( \frac{2}{2Z_1 + Z_2} \right)^4 (Z_1 - Z_2)(2a_0)^4 R \left. \right] \quad \dots \quad (5)$$

where  $R = 4\{2(2Z_1 + Z_2)^3 k a_0 - 8(2Z_1 + Z_2)k^3 a_0^3\} \{64Z_1^4 - 16Z_1^3 Z_2$

$$+ 120Z_1^2 Z_2^2 - 76Z_1 Z_2^3 - 14Z_2^4 + 32Z_1^3 k^2 a_0^2 - 8Z_2^2 k^2 a_0^2\} \\ + 2k a_0 (32Z_1^2 + 40Z_1^2 Z_2 + 8Z_1 Z_2^2) \{ (2Z_1 + Z_2)^4 - 24(Z_2 + 2Z_1)k^2 a_0^2 + 16k^4 a_0^4 \}$$

If we put  $Z_1 = 2$ ,  $Z_2 = 1$ , we get

$$f(\theta) = \frac{2a_0}{k^2 a_0^2} \left\{ 1 + 64 \left( \frac{2}{5} \right)^8 \right\} \left[ 128 \left( \frac{2}{5} \right)^8 + \frac{k^2 a_0^2 (32 + k^2 a_0^2)}{(16 + k^2 a_0^2)^2} \right. \\ \left. + \frac{k^2 a_0^2}{(1 + k^2 a_0^2)^4} \{ (7 + 4k^2 a_0^2 + 4k^4 a_0^4 + k^6 a_0^6) \} \right]$$

In the above we have neglected the contribution of the last term of the expression (5) as it is very small compared with those of the other terms.

#### DISCUSSIONS

In the table below we have given the numerical values of the differential cross section at different scattering angles for the incident electron energy of 700 ev. For comparison we also give similar values of the differential cross section when the screening due to the electrons is completely neglected. In the third column the experimental values (Hughes, Mac Millan and Webb, 1932) are added.

TABLE I  
Energy 700 ev  
 $|f(\theta)|^2$  in units of  $10^{-20} \text{ cm}^2$

$\theta$	Present result	Coulomb field	Experimental values
57°	17.19	20.25	15.5
72°	8.4	8.8	8.12
87°	4.46	4.7	5.10
102°	2.37	2.88	3.97
117°	1.97	2.00	3.56
132°	1.48	1.53	3.44
147°	0.9	1.25	1.54

From the above table we find that the present theoretical cross section of scattering of electrons of 700 ev energy by excited He atoms is considerably

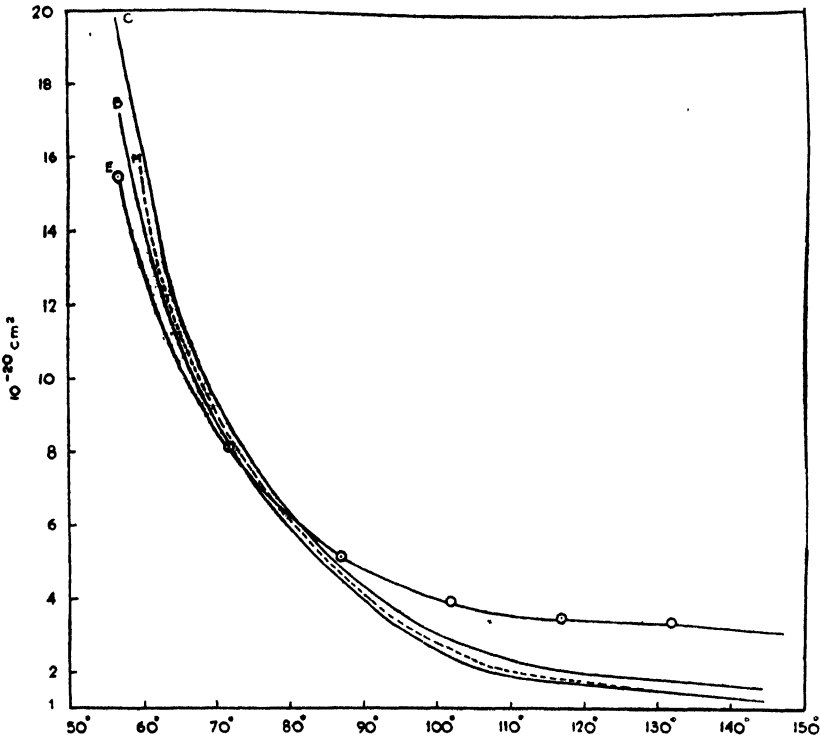


Fig. 1. Differential scattering cross section is plotted against angles in degrees. The curves marked E, B, M and C represent respectively the experimental results and the theoretical results of Bhattacharyya, Mukherji and of coulomb scattering of the bare nucleus.



lower than the experimental cross section of scattering by ordinary He, at large angles of scattering. The theoretical cross section of scattering by screened He atoms in the ground state calculated by the method of Born's first approximation (Mukherjee, 1961) is given in the graph and found to be very nearly the same as the scattering cross section by excited He atoms at angles above  $90^\circ$ , and slightly larger at angle below  $90^\circ$ . The cross section of scattering by bare nucleus calculated by the first Born approximation method is larger than both the theoretical cross sections either by ordinary He atoms or by excited He atoms; this shows that the influence of screening is not so appreciable at this energy of the incident electron. Moreover, the fact that the cross section of scattering even by bare nucleus calculated in the first Born approximation is much lower than the experimental findings at angles greater than  $80^\circ$ , seems to indicate the inadequacy of the first Born approximation and the necessity of taking into account higher order terms of Born series.

#### ACKNOWLEDGEMENT

The author expresses her deep sense of gratitude to Prof. D. Basu for suggesting the problem and for his helpful guidance throughout the progress of the work.

#### REFERENCES

- Hylleraas, E.A., 1929, *Z. Physik*, **54**, 347.
- Huzinaga, S., 1960, *Prog. Theo. Phys.* **23**, 562.
- Huges, A.L., Mc Millan, J.H. and Webb, G.M., 1932, *Phys. Rev.* **58**, 154.
- Mukherjee, S. C., 1961, *Ind. J. Phys.* **35**, 333.

# ON THE SINGLET→TRIPLET ABSORPTION IN A FEW POLYSUBSTITUTED BENZENES IN THE VAPOUR STATE\*

J. K. ROY

OPTICS DEPARTMENT,

INDIAN ASSOCIATION FOR THE CULTIVATION OF SCIENCE,  
CALCUTTA-32

(Received November 13, 1961)

**ABSTRACT.** The absorption spectra in the near ultraviolet region of ortho-, meta- and parafluorotoluene, *m*-chlorotoluene, 2, 4-dichlorotoluene and 3, 4-dichlorotoluene in the vapour state at the room temperature and with a path length equivalent to about 7 mm of the liquids have been investigated and compared with those due to equivalent path lengths of the liquids. In the case of 2, 4-dichlorotoluene and 3, 4-dichlorotoluene the spectra have also been photographed with the vapours at about 205°C using a high dispersion spectrograph.

It has been observed that these vapours exhibit continuous absorption starting at different points in the region lying between 26000  $\text{cm}^{-1}$  and 32000  $\text{cm}^{-1}$  and increasing towards longer wavelengths. When the vapours are liquefied the region of absorption shifts towards longer wavelengths, the shift being larger for ortho compounds than for the para compounds, but the long wavelength limit in the spectra of the isomeric molecules in liquid state are almost identical. It has been found that the spectra due to the vapours at different temperatures are identical. These results have been discussed.

## INTRODUCTION

The absorption spectra of some substituted benzene and toluene compounds in the vapour state at the saturation vapour pressure of the substances at the room temperature and with a path length of about 18.90 metres were studied recently by Sirkar and Roy (1960) and by Roy (1961). They observed weak continuous structureless absorption spectrum in the near ultraviolet region at large distances on the long wavelength side of the region of absorption due to singlet→singlet transition. They assigned this continuous absorption to singlet→triplet transition in the molecules. It was further observed that the continuous absorption increases considerably in some cases when equivalent path lengths of the substances in the liquid state are used. It was concluded that the increase is due to perturbation by the surrounding molecules of the same kind in the liquid state.

In the previous experiments long path of the vapours at low pressures at the room temperature was used in order to obtain sufficient path lengths of the vapour equivalent to that of the liquid without change of temperature. It was not known whether the continuous absorption spectrum attributed to singlet→triplet transi-

\*Communicated by Professor S. C. Sirkar

tion in the molecules is affected by temperature and pressure. It was, therefore, thought worthwhile to study the influence of temperature on the absorption due to the vapour. For this purpose the absorption spectra in the near ultraviolet region in two dihalogen substituted toluenes in the vapour state at the saturation pressures at the boiling points of the liquids and with path lengths of 140 cm have been investigated and compared with those due to equivalent path lengths of the substances in the vapour and liquid states at the room temperature.

The influence of heavy atoms as substituents in the benzene or naphthalene molecule on the singlet→triplet absorption spectrum was investigated by previous authors (McClure, Blake and Hanst, 1954) but it was not definitely known how such an influence changes with the change in position of the substituents in the ring. To find out such changes the absorption spectra of a few halogen substituted toluenes in the vapour state at the saturation pressures at the room temperature have been investigated using a path length about 18.90 metres and compared with the spectra due to the liquids with equivalent path lengths.

#### EXPERIMENTAL

The substances selected for the present investigation are ortho-, meta- and parafluorotoluene, metachlorotoluene, 2,4-dichlorotoluene and 3,4-dichlorotoluene. Orthofluorotoluene of chemically pure quality was obtained from Dr. Theodor Schuchardt, Germany, meta- and parafluorotoluene from Eastman Kodak Co., U.S.A. and metachlorotoluene, 2,4-dichlorotoluene and 3,4-dichlorotoluene from Fisher Scientific Company, U.S.A. The colourless samples were distilled several times under reduced pressure before being used in the present investigation.

The experimental arrangement for recording the ultraviolet absorption spectra of the substances at the room temperature was the same as that employed in the previous investigations (Sirkar and Roy, 1960; Roy, 1961). The absorption spectra of the substances in the vapour state were photographed first by filling the 18.90 metres long absorption cell with the vapours of the compounds at the saturation pressures at about 24°C. The pressures measured with a differential manometer were found to be about 60 mm, 50 mm and 45 mm of Hg in the cases of the fluorotoluenes, metachlorotoluene and dihalogenated toluenes respectively. The equivalent path lengths of the liquids were 7.4 mm, 6.5 mm and 6.4 mm respectively. In each case an empty cell of length equal to equivalent path length for the liquid was first placed in the path of the beam while the absorption spectrum due to the vapour was recorded with a cell of length 1890 cm. The long cell was then evacuated and the short cell was filled with the pure liquid and the absorption spectrum of the liquid was photographed by the side of the spectrum due to the vapour. An Adam Hilger medium quartz spectrograph giving a dispersion of about 22 Å/mm in the 3500 Å region was used for this purpose.

The absorption spectra of the substances in the vapour state at temperatures near about the boiling points of the liquids were studied in the cases of 2, 4-dichlorotoluene and 3,4-dichlorotoluene using a 140 cm long Pyrex glass cell fitted with quartz windows. The cell was placed inside a long cylindrical heater and was heated to a temperature slightly above the boiling point of the liquid and another heater was used to heat the liquid contained in a bulb attached through a side tube to the long cell. The temperature of the bulb was raised to the boiling point of the liquid and was kept constant during the experiment. The corresponding path length for the liquid was 7.6 mm in each case. After photographing the absorption spectrum of the vapour, that due to the liquid at the room temperature was photographed on the same film using a cell 7.6 mm long and the same time of exposure. The continuous spectrum due to the incident light was also photographed in order to compare the absorption spectrum of the vapour with the spectrum of the incident light. A Hilger E. 476 automatic quartz spectrograph giving a dispersion of about 8 Å/mm in the 3500 Å region was used for photographing the spectra of the vapours at high temperature (205°C). Agfa Isopan films backed by metal plates were used to photograph the spectra. Iron arc spectrum was photographed on each spectrogram as comparison. Microphotometric records of the spectrograms were obtained with a self-recording microphotometer made by Kipp and Zonen. The wave lengths in the continuous absorption spectra were measured by drawing a sharp line across the spectrogram in the position of a known iron line in the adjacent iron arc spectrum and comparing the microphotometric record of the iron arc spectrum with that of the absorption spectrum.

## RESULTS AND DISCUSSION

The microphotometric records of the absorption spectra due to pure ortho-fluorotoluene and parafluorotoluene in the liquid and vapour states at room temperature are reproduced in Figs. 1(a)–1(d), those due to pure 2, 4- and 3, 4-dichlorotoluene are reproduced in Figs. 2(a)–2(d). The records due to pure *m*-fluorotoluene and *m*-chlorotoluene are reproduced in Figs. 3(a)–3(d) respectively. The microphotometric records of the absorption spectra due to pure 2, 4- and 3, 4-dichlorotoluene at the high temperature are shown in Figs. 4(a), (b) and 5(a), (b) respectively. The reference line in the records has the wave length 4046Å.

It can be seen from Figs. 1, 2, 3 and 4 that the vapours of the substances show continuous absorption in the region 3600 Å–3300Å and its strength increases rapidly towards shorter wavelengths starting from the long wavelength limit. The position of the long wavelength limit is slightly different for the different compounds. Also the relative positions of the substituents has some influence on the strength of the S→T absorption, as can be seen from a comparison of the records due to ortho- and parafluorotoluene in Figs. 1(a), 1(b), 1(c) and 1(d) and those due to 2, 4-dichlorotoluene and 3, 4-dichlorotoluene shown in Figs. 2(a), 2(b), 2(c) and 2(d). It appears that in the vapour state the strength of absorption

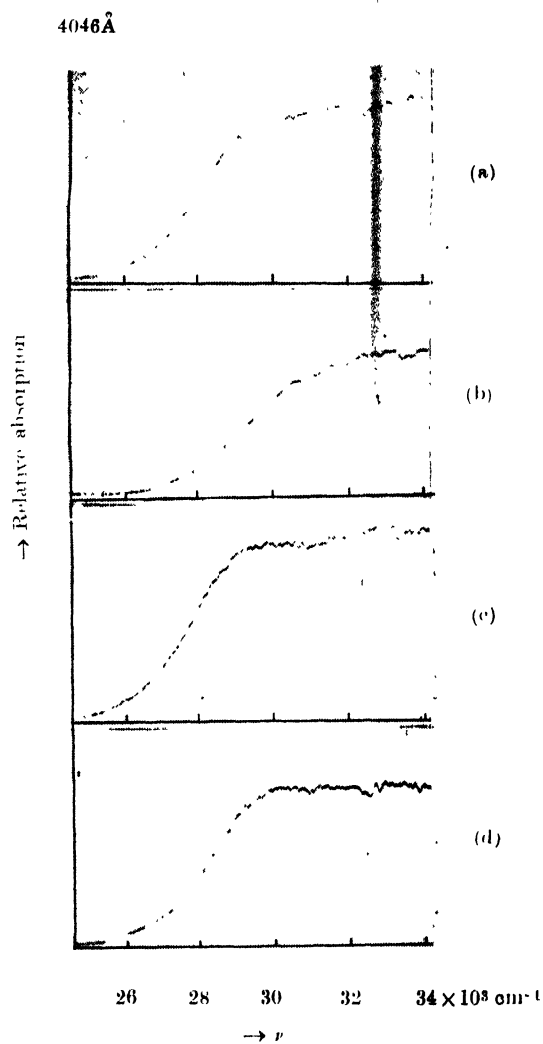


Fig. 1 (a) *o*-Fluorotoluene (liquid)  
 (b) *o*-Fluorotoluene (vapour)  
 (c) *p*-Fluorotoluene (liquid)  
 (d) *p*-Fluorotoluene (vapour)

4016 Å

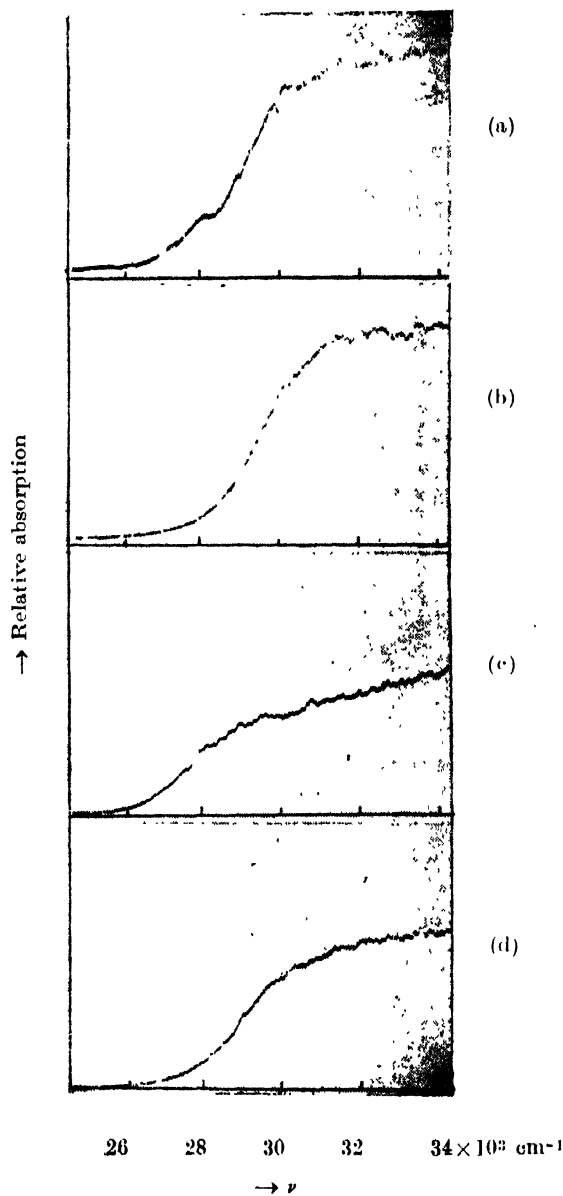


Fig. 2 (a) 2,4-Dichlorotoluene (liquid)  
(b) 2,4-Dichlorotoluene (vapour)  
(c) 3,4-Dichlorotoluene (liquid)  
(d) 3,4-Dichlorotoluene (vapour)

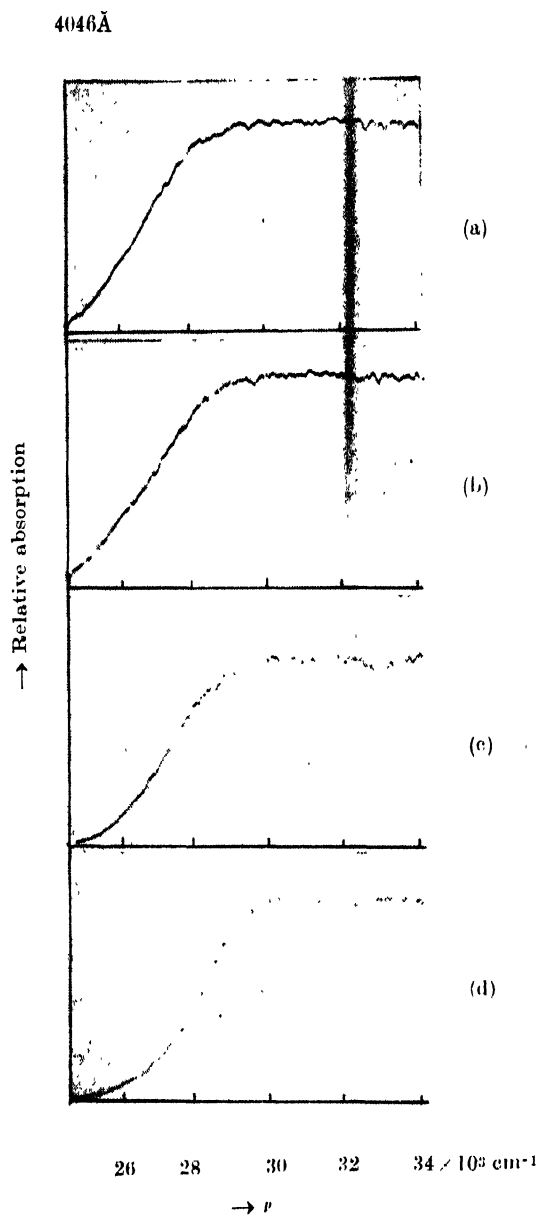


Fig. 3 (a) *m*-Fluorotoluene (liquid)  
 (b) *m*-Fluorotoluene (vapour)  
 (c) *m*-Chlorotoluene (liquid)  
 (d) *m*-Chlorotoluene (vapour)

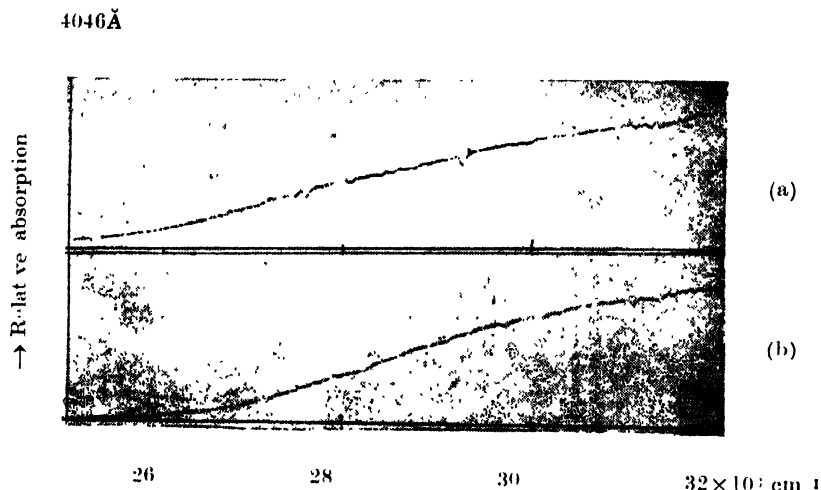


Fig. 4. (a) 2,4-Dichlorotoluene (liquid) at 30°C.  
(b) 2,4-Dichlorotoluene (vapour) at 205°C

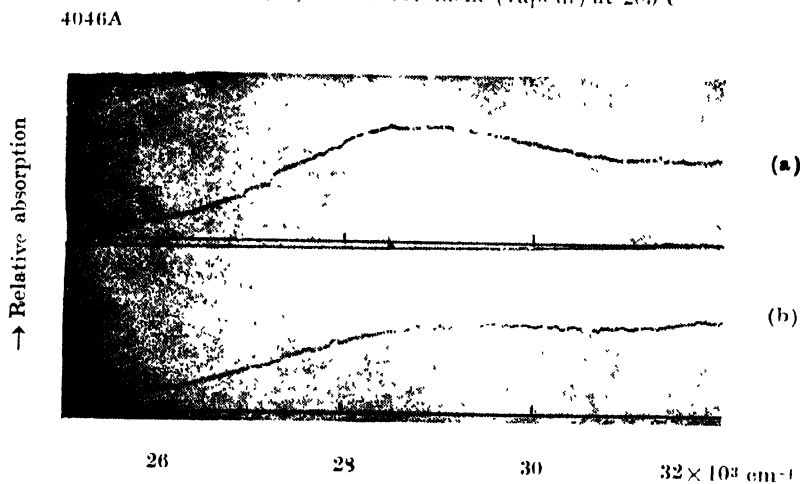


Fig. 5. (a) 3,4-Dichlorotoluene (liquid) at 30°C.  
(b) 3,4-Dichlorotoluene (vapour) at 205°C

at about  $30,000 \text{ cm}^{-1}$  is larger in the case of *p*-fluorotoluene than in the case of the ortho compound, but the increase in the strength due to intermolecular field in the liquid is larger in the latter case than in the former case. Fig. 2 on the other hand shows that absorption due to the 2,4- and 3, 4-dichlorotoluene in the vapour state is almost identical in respect of position and strength, but the increase due to intermolecular field in the liquid is larger in the latter case.

It would be interesting to find out how far the strengths of absorption in the vapours of the different substituted benzene molecules can be explained with the help of vector diagrams which were used by Platt (1951) to explain the singlet→



singlet systems of such compounds. It was shown by Platt that the transition moments due to the substituents ( $\text{CH}_3$  and halogen atoms) have the same sign in the case of singlet→singlet transition. Assuming this to be true for the singlet→triplet transition also, it can be seen from the vector diagrams for trisubstituted benzenes that the resultant transition moments for 2, 4-dichlorotoluene and 3, 4-dichlorotoluene are exactly the same. The curves in Figs. 2(b) and 2(d) show that the strengths of absorption and positions of the region of absorption in the vapours of the two compounds are the same. Again, the vector diagrams for disubstituted benzenes show that the transition moment of the para substituted compound should be larger than that of the ortho substituted compound. The curves in Figs. 1(b) and 1(d) show that the experimental results agree with those deduced from the vector diagrams. Figs. 3(b) and 3(d) also show that the heavier atom chlorine produces a larger transition moment than the lighter substituent atom fluorine both situated at the meta position.

It appears from these results that the substituent atoms make the forbidden transition to the triplet state allowed, but the upper triplet state becomes very broad and diffuse. Probably the perturbation due to the substituent atoms changes the nature of coupling between the spin and orbital angular momentum so that the resultant spin is not quantised and this may explain the continuous nature of the upper state.

It can be seen from the curves reproduced in all the figures that the region of absorption shifts towards longer wavelengths as the vapour is liquefied, the shift being different for the different compounds. It is remarkable, however, that the long wavelength limits for the curves due to isomeric molecules with the same substituents are exactly the same. This shows that the perturbation due to the heavy substituent atom in the neighbouring molecule is responsible for the shift of the spectrum. As this effect is exhibited mostly by polar molecules it may not be unlikely that formation of loose dimers takes place in the liquid state and the shift may be partly due to such bond-formation.

Fig. 4 shows that curves due to 2, 4-dichlorotoluene in the vapour state at  $205^\circ\text{C}$  and in the liquid state at  $30^\circ\text{C}$ . A comparison of the curve due to the vapour at  $205^\circ\text{C}$ , Fig. 4(b) with that due to the vapour at  $30^\circ\text{C}$  reproduced in Fig. 2(b) shows that the curves are identical. This shows that temperature and pressure have very little influence on the absorption.

The microphotometric records of the spectra due to 3,4-dichloro-toluene in the liquid state at  $30^\circ\text{C}$  and in the vapour state at  $205^\circ\text{C}$  photographed with the high dispersion spectrograph and reproduced in Fig. 5 show that in both the curves there is a tendency for the formation of a very broad maximum. The centre of the maximum is at about  $29200\text{ cm}^{-1}$  in the case of the vapour. The maximum is more prominent in the case of the liquid and its centre shifts to about  $28500\text{ cm}^{-1}$ . Such a phenomenon is not exhibited by 2,4-dichlorotoluene. This may

be due to overlapping of the singlet→triplet and singlet→singlet systems in the latter case.

It is thus evident from the results for the compounds mentioned above that the absorption due to singlet→triplet transition is continuous with a maximum in some cases and the perturbation due to heavy atoms in the neighbouring molecules always shifts the region of absorption towards longer wavelengths.

#### ACKNOWLEDGMENT

The author is highly indebted to Professor S. C. Sirkar, D.Sc., F.N.I. for his kind interest and for guidance throughout the progress of the work.

#### REFERENCES

- McClure, D. S., Blake, N. W. and Hanst, P. L., 1954, *J. Chem. Phys.*, **22**, 255.  
Platt, J. R., 1951, *J. Chem. Phys.*, **19**, 263.  
Roy, J. K., 1961, *Ind. J. Phys.*, **35**, 143.  
Sirkar, S. C. and Roy, J. K., 1960, *Ind. J. Phys.*, **34**, 581.

# AMPLITUDE OF THERMAL VIBRATIONS IN PCl<sub>3</sub>, AsCl<sub>3</sub> AND SbCl<sub>3</sub> MOLECULES

T. A. HARIHARAN

DEPARTMENT OF PHYSICS,

KARNATAKA REGIONAL ENGINEERING COLLEGE,

SURATHKAL S. K. (MYSORE STATE)

(Received August 18, 1961)

**ABSTRACT.** The root mean square amplitudes of vibration of the bond distances during the totally symmetric stretching vibrations have been calculated for the molecules PCl<sub>3</sub>, AsCl<sub>3</sub>, SbCl<sub>3</sub> at a temperature of 300° K. The necessary potential and kinetic energy matrices were worked out using symmetry coordinates corresponding to the two species of vibrations in each case.

## INTRODUCTION

The determination of the mean square amplitudes of thermal vibrations of atoms in crystals is of considerable importance in the X-ray crystal structure analysis (James, 1948; Lonsdale, 1948; Cribier, 1953 and Cochran, 1954). In the particular case of molecular crystals Cruickshank (1956) and Higgs (1953, 1955) have shown that the vibrational spectra of the constituent molecules and the normal co-ordinate analysis can be used to determine the contribution to the mean square amplitude of thermal motions of atoms from internal molecular vibrations. In the case of free molecules, accurate interpretation of the precise electron diffraction data makes it necessary to take into account the mean square amplitude of thermal vibrations of the atoms. A simple procedure for calculating these amplitudes has been developed by Morino *et al* (1953) and applied successfully to the molecules C<sub>2</sub>F<sub>4</sub> and CH<sub>2</sub>F<sub>2</sub>. The present investigation follows a similar procedure to calculate the mean amplitudes for the molecules PCl<sub>3</sub>, AsCl<sub>3</sub> and SbCl<sub>3</sub> and the results are presented here.

## METHOD OF CALCULATION

The mean square amplitude of thermal vibrations in molecules is given by the well known formula

$$\langle Q_n^2 \rangle = \frac{h}{8\pi^2\nu_n} \coth \frac{h\nu_n}{2kT}$$

where,  $Q_n$  represents the normal coordinate.

$\nu_n$  the frequency.

$T$  the absolute temperature.

and  $k$  the Boltzmann constant.

By making use of appropriate transformation matrices we can determine the mean square amplitudes corresponding to the internal coordinates rather than the normal coordinates. These matrices can be obtained once the proper Wilson's  $G$  and  $F$  matrices for the molecular vibrations are determined. A simplified procedure has been used by Morino *et al* (1953) and this lies in the approximate expansion of the coth function as

$$\coth x = \frac{1}{x} + \frac{x}{4}$$

This of course involves slight error from the actual expansion but is applicable to frequencies less than  $1200 \text{ cm}^{-1}$ .

The final relation for the amplitudes corresponding to the internal coordinates  $R$  is given by

$$R_i^2 = -kT(F^{-1})_{ii} + \frac{h^2}{64\pi^2 kT} G_{ii}$$

$$(F^{-1})_{ii} = \frac{F_{ii}'}{\det F}$$

$F$  and  $G$  correspond to the Wilson's potential and kinetic energy matrices. Symmetry coordinates can also be used with the appropriate transformation matrices.

The molecules  $\text{PCl}_3$ ,  $\text{AsCl}_3$  and  $\text{SbCl}_3$  are known to have a pyramidal structure and they belong to the point group  $C_{3v}$ . The vibrational spectra of these have been obtained by several investigators and fairly accurate assignment of the observed frequencies is available. A normal coordinate analysis has been carried out by Howard and Wilson (1934) using four force constants.

In the present case the Wilson's  $F$  and  $G$  matrices are calculated using a valence force potential function containing all the interaction terms. These are given below :

#### 1) $\text{PCl}_3$

For  $A_1$  type vibrations

$$G \rightarrow \begin{vmatrix} 2.898 \times 10^{22} & -1.456 \times 10^{30} \\ & 2.416 \times 10^{38} \end{vmatrix} \quad F \rightarrow \begin{vmatrix} 2.67 \times 10^5 & 3.15 \times 10^{-3} \\ & 5.384 \times 10^{-11} \end{vmatrix}$$

For  $E$  type vibrations.

$$G \rightarrow \begin{vmatrix} 4.01 \times 10^{22} & 1.403 \times 10^{30} \\ & 1.7995 \times 10^{38} \end{vmatrix} \quad F \rightarrow \begin{vmatrix} 1.83 \times 10^5 & -4.696 \times 10^{-5} \\ & 1.24 \times 10^{-11} \end{vmatrix}$$

2)  $\text{AsCl}_3$ For  $A_1$  type vibrations.

$$G \rightarrow \begin{array}{c} 2.14 \times 10^{22} \\ -5.145 \times 10^{29} \\ 1.1154 \times 10^{38} \end{array} \quad F \rightarrow \begin{array}{c} 2.39 \times 10^5 \\ 2.57 \times 10^{-3} \\ 4.32 \times 10^{-11} \end{array}$$

For  $E$  type vibrations.

$$G \rightarrow \begin{array}{c} 2.682 \times 10^{22} \\ 5.729 \times 10^{29} \\ 1.1669 \times 10^{38} \end{array} \quad F \rightarrow \begin{array}{c} 1.82 \times 10^5 \\ -1.021 \times 10^{-4} \\ 8.511 \times 10^{-12} \end{array}$$

3)  $\text{SbCl}_3$ For  $A_1$  type vibrations.

$$G \rightarrow \begin{array}{c} 2.0209 \times 10^{22} \\ -3.302 \times 10^{29} \\ 8.34 \times 10^{37} \end{array} \quad F \rightarrow \begin{array}{c} 2.07 \times 10^5 \\ 1.949 \times 10^{-3} \\ 3.2 \times 10^{-11} \end{array}$$

For  $E$  type vibrations.

$$G \rightarrow \begin{array}{c} 2.2773 \times 10^{22} \\ 2.961 \times 10^{29} \\ 8.444 \times 10^{37} \end{array} \quad F \rightarrow \begin{array}{c} 1.59 \times 10^5 \\ 3.48 \times 10^{-5} \\ 7.947 \times 10^{-12} \end{array}$$

Symmetry coordinates were used to derive the above matrices. Making use of proper transformation matrices the root mean square amplitudes of the bond distances during the totally symmetric stretching vibrations at a temperature of 300°K were obtained and the values are given in the following Table together with the interatomic distances.

Molecule	Bond distance in Å units	Root mean square amplitude in Å units
$\text{PCl}_3$	2	0.075
$\text{AsCl}_3$	2.16	0.0718
$\text{SbCl}_3$	2.325	0.0709

It has to be mentioned that the values of the root mean square amplitudes obtained here may depend on the actual potential energy function used apart from the slight error introduced because of the approximate expansion of the coth function. In order to avoid large discrepancies, a potential energy function containing all interaction terms is used in the calculations.

## REFERENCES

- Cochran, 1954, *Acta Cryst.*, **7**, 503.  
 Cribier, 1953, *Acta Cryst.*, **6**, 293.  
 Cruickshank, 1956, *Acta Cryst.*, **9**, 747, 754, 757, 1005.  
 Higgs, 1953, *Acta Cryst.*, **6**, 232.  
 Higgs, 1955, *Acta Cryst.*, **8**, 99.  
 Howard, and Wilson, 1934, *J. Chem. Phys.*, **2**, 630.  
 James, R. W., 1948, *Optical Properties of Diffraction of X-rays*.  
 Lonsdale, K., 1948, *Acta Cryst.*, **1**, 142.  
 Morino, 1953, *J. Chem. Phys.*, **21**, 1927.

# Letters to the Editor

*The Board of Editors will not hold itself responsible for opinions expressed in the letters published in this section. The notes containing reports of new work communicated for this section should not contain many figures and should not exceed 500 words in length. The contributions must reach the Assistant Editor not later than the 15th of the second month preceding that of the issue in which the letter is to appear. No proof will be sent to the authors.*

9

## REFINED MOLECULAR STRUCTURE OF NAPHTHAZARIN

P. SRIVASTAVA

INDIAN ASSOCIATION FOR THE CULTIVATION OF SCIENCE, CALCUTTA-32.

(Received July 27, 1961)

Approximate structure of naphthazarin  $C_{10}H_4O_2(OH)_2$ , form II, (Borgen, 1956), belonging to the space group,  $P2_1$ , has already been determined at room temperature by Srivastava (1958, 1960) and by Billy (1958). The present communication deals with the refinement of its molecular structure by employing the low temperature Weissenberg technique and difference synthesis and least square method.

A single crystal of naphthazarin was subjected to a low temperature of  $-140^\circ\text{C}$  and the Weissenberg photographs along  $a$ - and  $b$ -axis were taken in a semicylindrical camera of diameter 5.75 cm. The unit cell parameters at  $-140^\circ\text{C}$  and  $+30^\circ\text{C}$  (room temperature) are given below :-

	at $-140^\circ\text{C}$	at $+30^\circ\text{C}$
$a$	$7.70 \pm 0.01 \text{ \AA}$	$7.90 \pm 0.01 \text{ \AA}$
$b$	$7.27 \pm 0.01 \text{ \AA}$	$7.27 \pm 0.01 \text{ \AA}$
$c$	$16.52 \pm 0.02 \text{ \AA}$	$16.91 \pm 0.02 \text{ \AA}$
$\beta$	$123^\circ 30' \pm 5'$	$124^\circ 38' \pm 5'$

The  $b$ -axis has been found to remain unchanged in this temperature range.

The final atomic co-ordinates of the asymmetric unit are given in Table I. The electron-density projection on the plane (010) has been shown in Fig. 1. The difference map clearly indicates the position of hydrogen atoms in the molecule. Isotropic form of temperature parameter was used for individual atoms and the discrepancy factor  $R$  was found to be 0.11 (without including the hydrogen atoms). In case of the unobserved planes, half the minimum observed value of the structure factor was taken in the calculation of  $R$ .

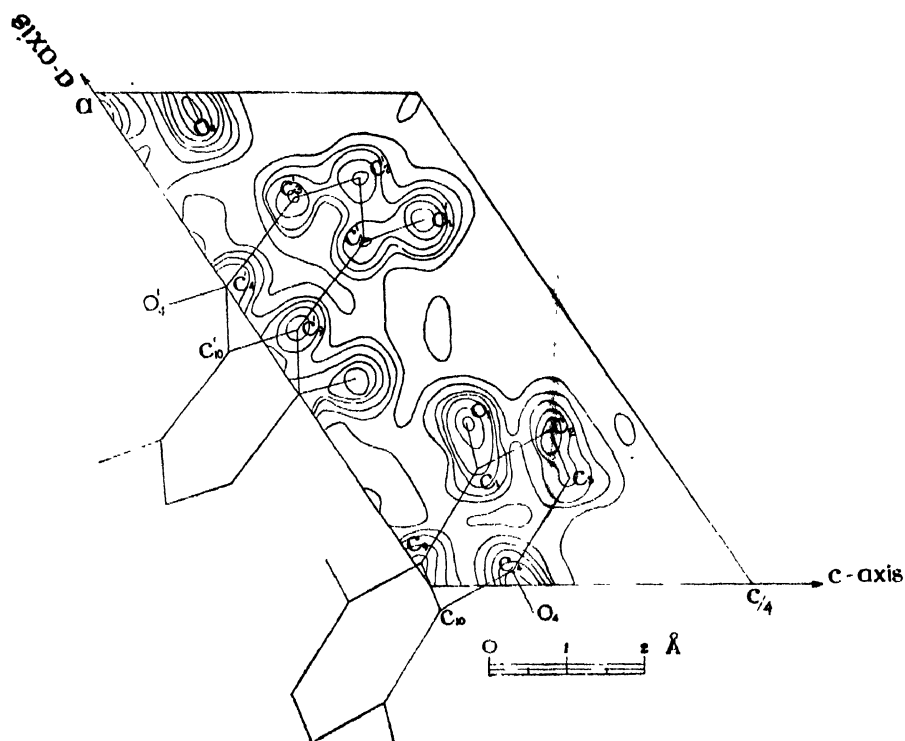


Fig. 1. Electron density projection along [010].

TABLE I

Atomic co-ordinates at  $-140^{\circ}\text{C}$ .

Molecule at 0,0,0				Molecule at $a/2,0,0$			
	X	Y	Z		X	Y	Z
	Å	Å	Å		Å	Å	Å
C <sub>1</sub>	1.8250	0.9000	1.6250	C' <sub>1</sub>	5.3875	-0.5000	2.1500
C <sub>2</sub>	2.4250	-0.0250	2.8875	C' <sub>2</sub>	6.3750	0.6500	2.6500
C <sub>3</sub>	1.6750	-1.2625	2.7250	C' <sub>3</sub>	6.0750	1.7375	1.6375
C <sub>4</sub>	0.2250	-1.5375	1.1750	C' <sub>4</sub>	4.6875	1.6875	0.0000
C <sub>5</sub>	0.3750	0.6250	0.0875	C' <sub>5</sub>	4.0125	-0.5375	0.5250
O <sub>1</sub>	2.5750	2.0250	1.9000	O' <sub>1</sub>	5.7250	-1.4625	3.1250
O <sub>4</sub>	-0.4250	-2.6875	1.0750	O' <sub>4</sub>	4.4500	2.7000	-0.8750

The refined structure of naphthazarin is being published in detail elsewhere.

The author is thankful to Prof B. N. Srivastava, D.Sc., F.N.I., for his keen interest throughout the progress of this work. He also expresses his sincere thanks to Dr. B. V. R. Murty, D.Phil and Dr. S. K. Dutta, Ph.D., for their valuable criticisms and suggestions and to Mr. A. S. Trivedi, M.Sc., for his help in calculations. The award of the C.S.I.R. Research Fellowship is also gratefully acknowledged.

## REFERENCES

- Billy, C., 1958, *Comp. Rend.* **247**, 1019.  
Borgen, O., 1956, *Acta Chem. Scandinavica*, **10**, 867.  
Srivastava, P., 1958, *Zeit. f. Kristallogr.*, **111**, 77.  
Srivastava, P., 1960, *Ind. J. Phys.*, **34**, 291.



# ON THE OPTICAL ABSORPTION SPECTRA OF $\text{Ni}^{2+} \cdot 6\text{H}_2\text{O}$ COMPLEX IN CRYSTALS

A. S. CHAKRAVARTY AND R. CHATTERJEE

DEPARTMENT OF MAGNETISM,

INDIAN ASSOCIATION FOR THE CULTIVATION OF SCIENCE,

JADAVPUR, CALCUTTA-32.

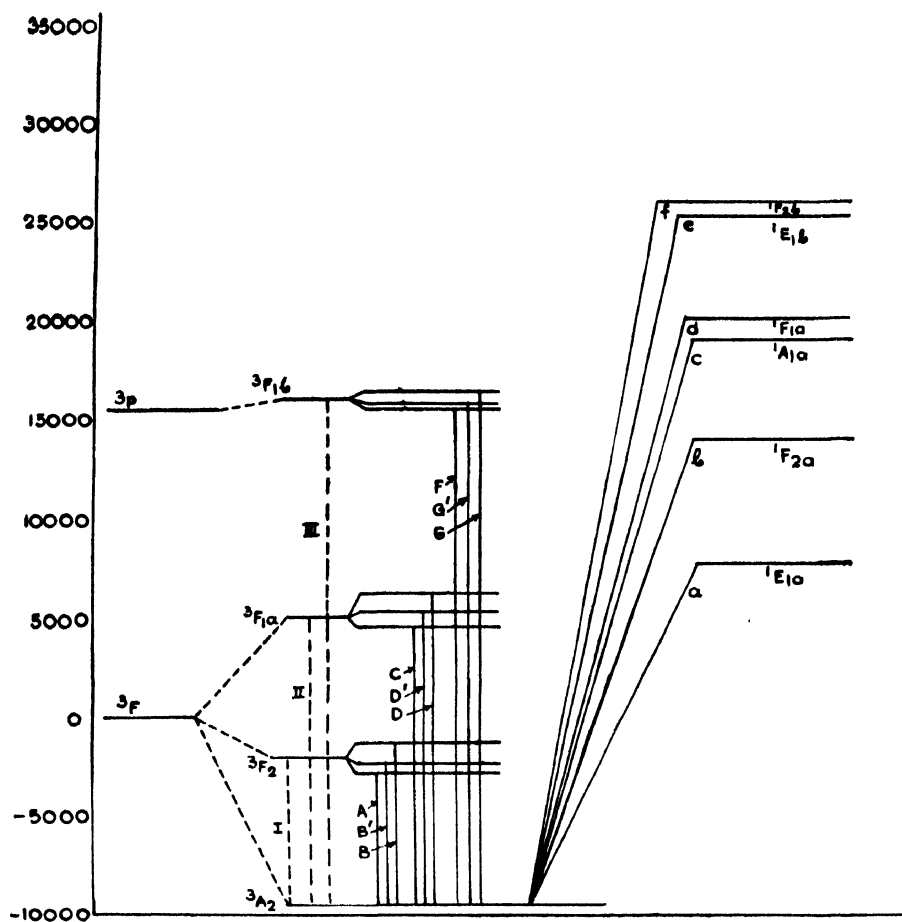
(Received August 7, 1961)

In crystalline electric field of symmetry  $O_h$ , the  $^3F$  groundstate of the  $\text{Ni}^{2+}$  ion is split into three components  $^3A_2$ ,  $^3F_2$ ,  $^3F_{1a}$  with successively increasing energy. In considering the absorption spectra, the transitions to the upper  $^3P$  level as also the forbidden transition to the singlets  $^1D$ ,  $^1G$  and  $^1S$  with low transition probabilities should be taken into account. All these transitions have energies of the order of  $10^4 \text{ cm}^{-1}$  and since they take place only in combination with suitable vibrational transitions, the intensities of the light absorptions must be lower than if they had been due to pure electronic transitions. The three main transitions  $^3A_2 \rightarrow ^3F_2$ ,  $^3A_2 \rightarrow ^3F_{1a}$  and  $^3A_2 \rightarrow ^3F_{1b}$  ( $^3P$ ) give rise to broad bands called hereafter I, II and III over which the other weaker lines are superimposed.

For the aqueous solutions of several hydrated salts of  $\text{Ni}^{2+}$ , Dreisch *et al.* (1937, 1939) found that the peak of band I lies at  $8300 \text{ cm}^{-1}$ , peak of band II at  $14100 \text{ cm}^{-1}$  and peak of band III at  $25000 \text{ cm}^{-1}$ . This has been confirmed by Hartmann and Muller's (1958) observation of the absorption spectra of  $\text{NiSO}_4 \cdot 6\text{H}_2\text{O}$  and  $\text{NiSO}_4 \cdot 7\text{H}_2\text{O}$  crystals. Hartmann and Muller (1958; cf. Mookherjee *et al.* 1960) have been able to resolve the bands II and III into several peaks, e.g., band II into three peaks *C*, *D*, *E* of more or less the same intensity and *a* of much smaller intensity; band III into two peaks *F*, *G* of nearly the same intensity as the peaks of II, and three other *b*, *c* and *d* of much smaller intensity. They obtained further two more very weak peaks *e*, *f* near  $39000 \text{ cm}^{-1}$ . They could apparently explain all these peaks *except E*, on the basis of the splitting of the different states of the  $\text{Ni}^{2+}$  ion caused by a small tetragonal field superimposed upon cubic field (Fig. 1.).

Since the intensity of this band *E* is almost equal to the transitions from other Stark levels, it cannot be due to any intercombination between terms of different multiplicity (Orgel 1955). Contention of Ballhausen (1955) and Hartmann and Muller (1958) that the occurrence of this band is due to (L.S.) coupling effect has been also contradicted by Jorgensen (1958). On the other hand, Mookherjee

*et al* (1960) have shown that the observed anisotropy of  $\text{Ni}^{2+}$  ion :  $K_{\perp} - K_{\parallel} = 354 \times 10^{-6}$ , assuming a tetragonal field, does not agree with the splitting  $C \rightarrow D \approx 300$



Energy level diagram of  $\text{Ni}(\text{H}_2\text{O})_6^{2+}$  ion under cubic and orthorhombic field.  
(Not drawn to scale)

$\text{cm}^{-1}$  but with the splitting  $C \rightarrow E \approx 1300 \text{ cm}^{-1}$ . In that case the peak *D* remains unexplained. Paramagnetic resonance studies of several salts of  $\text{Ni}^{2+}$  by Griffiths and Owen (1952) show that the electric field in all these salts has really an orthorhombic symmetry. We have therefore assumed an orthorhombic field in all these salts and been able to prove that all the three peaks *C*, *D* and *E* are really due to transitions from ground  $3A_2$  level to the three components of the level  $3F_{1a}$  split up by the orthorhombic field.

We have neglected the effect of the spin-orbit interaction, which being a second order effect, is not so important in the case of optical absorption of  $\text{Ni}^{2+}$ ,

$6\text{H}_2\text{O}$  complex and the inclusion of this in the Hamiltonian would unnecessarily complicate the present calculations, meant to explain the existing experimental facts, as far as they go.

Following the method of Van Vleck (1932), and Schlapp and Penney (1932), Tanabe and Sugano (1954), Pryce and Runciman (1958) and taking into consideration all the energy states as already mentioned, we have calculated the energy levels of  $\text{Ni}^{2+}$ ,  $6\text{H}_2\text{O}$  with the following cubic and orthorhombic field parameters (Table 1), and compared them with the experimental values obtained by the aforementioned authors. All things considered the fit is much better than that obtained by Hartmann and Muller. Authors have also worked out a complete theory of the susceptibility of  $\text{Ni}^{2+}$  ion in an orthorhombic field which will be discussed in a future communication.

The authors are grateful to Prof. A Bose, D.Sc., F.N.I., for suggesting the problem and helpful criticism of the work.

TABLE I

Cubic field parameter  $D_q = 810 \text{ cm}^{-1}$

Orthorhombic field parameters  $\sigma = -70 \text{ cm}^{-1}$ ,  $\delta = 20 \text{ cm}^{-1}$

Racah parameters  $B = 1030 \text{ cm}^{-1}$   $C = 4850 \text{ cm}^{-1}$

Splittings	Calculated values $\times 10^{-3} \text{ cm}^{-1}$ .	Experimental values $\times 10^{-3} \text{ cm}^{-1}$ .
${}^3\text{A}_2 ({}^3\text{F}) \rightarrow {}^3\text{F}_2 ({}^3\text{F})$	7.957 (A) 8.010 (B') 1 8.097 (B)	8.300
$\rightarrow {}^3\text{F}_{1a} ({}^3\text{F})$	14.130 (C) 14.405 (D) II 15.423 (E)	13.900 14.200 15.200
$\rightarrow {}^1\text{E}_{1a} ({}^1\text{D}^1\text{G})$	17.230 (a)	17.500
$\rightarrow {}^3\text{F}_{2a} ({}^1\text{D}^1\text{G})$	24.811 (b)	23.900
$\rightarrow {}^3\text{F}_{1b} ({}^3\text{P})$	25.030 (F) 25.080 (G') III 25.120 (G)	25.400
$\rightarrow {}^1\text{A}_{1a} ({}^1\text{D}^1\text{G})$	26.941 (c)	26.900
$\rightarrow {}^1\text{F}_1 ({}^1\text{D}^1\text{G})$	30.160 (d)	30.050
$\rightarrow {}^1\text{E}_{1b} ({}^1\text{D}^1\text{G})$	35.879 (e)	
$\rightarrow {}^1\text{F}_{2b} ({}^1\text{D}^1\text{G})$	36.399 (f)	39.000
$\rightarrow {}^1\text{A}_{1b} ({}^1\text{S})$	67.929 (g)	—

## REFERENCES

- Ballhausen, C. J., 1955, *C. J. Kgl. Danske Videnskab., Selskab, Mat, fgs. Medd.* No. 8  
29.
- Draisch., Th. and Kallscheuer, O., 1939, *Z. Phys. Chem.*, B45, 19.
- Griffiths, J. H. and Owen, J., 1952, *Proc. Roy. Soc., A*, **213**, 451.
- Hartmann, H. and Muller, H., 1958, *Disc. Farad. Soc.* **26**, 49.
- Jorgensen, C. K., 1958, *Disc. Farad. Soc.*, **26**, 90.
- Mookherji, A. and Chhonkar, N. S., 1960, *Ind. J. Phys.*, **43**, 363.
- Orgol, L. E., 1955, *J. Chem. Phys.*, **28**, 1004.
- Pryce, M. H. L. and Runcimann, W. A., 1958, *Disc. Farad. Soc.*, **26**, 34.
- Schalpp, R. and Peunoy, W. G., 1932, *Phys. Rev.*, **42**, 666.
- Tanabe, Y. and Sugano, S., 1954, *Proc. Phys. Soc. Japan*, **9**, 753, 766.
- Van Vleck, J. H., 1932, *Phys. Rev.*, **41**, 208.